Title 40 CFR Part 191
Compliance Certification
Application
for the
Waste Isolation Pilot Plant

Appendix GCR

(M)

United States Department of Energy
Waste Isolation Pilot Plant

Carlsbad Area Office
Carlsbad, New Mexico

Geological Characterization Report

Geological Characterization Report, Waste Isolation Pilot Plant (WIPP) Site, Southeastern New Mexico

Volume I

August 1978

**Dennis W. Powers, Steven J. Lambert, Sue-Ellen Shaffer,
Leslie R. Hill, Wendell D. Weart, Editors**

Sandia Laboratories

Issued by Sandia Laboratories, operated for the United States
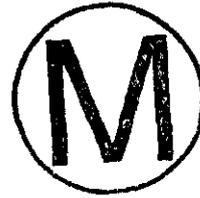Department of Energy by Sandia Corporation.

GEOLOGICAL CHARACTERIZATION REPORT
WASTE ISOLATION PILOT PLANT (WIPP) SITE,
SOUTHEASTERN NEW MEXICO

SAND78-1596

VOLUME I

Dennis W. Powers, Steven J. Lambert, Sue-Ellen Shaffer,
Leslie R. Hill, Wendell D. Weart, Editors

Department 4510
Waste Management Technology
Sandia Laboratories
Albuquerque, New Mexico   87185

AUGUST, 1978
PRINTED DECEMBER, 1978

PREFACE

The Geological Characterization Report (GCR) for the WIPP site presents, in one document, a compilation of geologic information available to August, 1978, which is judged to be relevant to studies for the WIPP. As such, commonly available documents are summarized as appropriate while other documents may be presented more fully. In some instances, the information presented may be preliminary or may reflect continuing studies not yet complete. The Geological Characterization Report certainly should not be construed as the final word on the WIPP geology. Furthermore, specific judgements of how the geologic information affects the WIPP are restricted since the document is intended as a source of information. However, recommendations may be made on the basis of the document. The Geological Characterization Report for the WIPP site is neither a Preliminary Safety Analysis Report nor an Environmental Impact Statement; these documents, when prepared, should be consulted for appropriate discussion of safety analysis and environmental impact. The Geological Characterization Report of the WIPP site is a unique document and at this time is not required by regulatory process.

The Geological Characterization Report (GCR) for the WIPP has been created through the efforts of many individuals who are to be acknowledged for their contributions; little of the material presented, however, is original material created solely for the Geological Characterization Report. At Sandia Laboratories, principal contributors to the writing of the GCR are, in alphabetical order: G.E. Barr, B.M. Butcher, R.G. Dosch, L.R. Hill, S.J. Lambert, D.W. Powers, S.E. Shaffer, W. Wawersik, and W.D. Weart. Bechtel Corporation provided basic summaries for many chapters; the principal participants were: D. Dale, C. Farrell, V. Howes, J. Litehiser, D. Roberts, R. Sayer. In particular, J. Litehiser provided the analysis of seismic risk in Chapter 5. G.B. Griswold of Tecolote Corporation summarized resources in Chapter 8. F.H. Dove of NUS summarized hydrology in Chapter 6.

Editorial and review comments were solicited on a working copy and received from independent agencies with personnel familiar with the geology of southeastern New Mexico, particularly the New Mexico Bureau of Mines and Mineral Resources. An internal review at Sandia Laboratories of a working copy of the entire document also resulted in detailed comments. Those review comments were incorporated as appropriate into this draft copy. As usual, some of the suggestions were not followed for various reasons. The draft copy received review and comment by the WIPP Panel (Committee on Radioactive Waste Management, National Research Council) of the National Academy of Science, the Office of Nuclear Waste Isolation (ONWI) and various subcontractors, and by Westinghouse as a contractor to DOE. Major parts of the draft were reviewed by members of the Special Projects Branch, USGS. These comments have resulted in some revision of the final copy, as seemed appropriate. The editors assume responsibility for the contents of this report.

The editors and writers acknowledge the enormous volume of accumulated data and interpretations which provide the background for the Geological Characterization Report; referencing of authors is intended to reflect this background and to properly attribute material.

The Report is primarily intended for use by those with a technical background in earth sciences. However, the text should also be generally readable without all of this background by referral to the American Geological Institute Glossary of Geology (1974).

GEOLOGICAL CHARACTERIZATION REPORT
TABLE OF CONTENTS

APPENDICES

Chapter 2

Figures:

Tables:

Chapter 3

Figures:

Table:

Chapter 4

Figures:

Table:

Chapter 5

Figures:

Tables:

Chapter 6

Chapter 7

Figures:

Tables:

Chapter 8

Figures:

Tables:

GCR CHAPTER 1

EXECUTIVE SUMMARY

This Executive Summary presents, in condensed form, geotechnical information relevant to the Waste Isolation Pilot Plant (WIPP) in southeastern New Mexico. The presentation of material follows the Geological Characterization Report (GCR) chapter organization, beginning with Chapter 2, INTRODUCTION. Figures and a reference list are not included in the Executive Summary; where desired the reader must examine the figure and reference list following each Chapter.

INTRODUCTION   (Chapter 2)

The Introduction provides an overview of the purpose of the WIPP, the purpose of the Geological Characterization Report, the site selection criteria, the events leading to studies in New Mexico, status of studies, and the techniques employed during geological characterization.

The purpose of the Waste Isolation Pilot Plant (WIPP) is to demonstrate the technology for the disposal of the transuranic (TRU) waste resulting from this nation's past and current defense programs. It is anticipated that the WIPP will be converted to a repository after successful demonstration of this technology and assessment of safety of a repository for southeastern New Mexico. In addition, the WIPP is to provide a research facility to examine, on a large scale, the interactions between bedded salt and high-level radioactive waste. A Department of Energy (DOE) Task Force (DOE/ER-0004/D, 1978) has recommended that WIPP also be used to demonstrate surface and subsurface methods of handling, storing and disposing of up to 1,000 canisters of spent reactor fuel. A decision on implementing this recommendation has not been made at this time.

If this site is accepted by the DOE, the schedule calls for the initiation of facility construction in early 1981; completion is to be late 1985, and the first waste to be accepted in 1986. The TRU waste would be readily retrievable for a five to ten year period of initial

operation. All HLW for experiments would be retrieved upon completion of the experiments. The conceptual design of WIPP facilities is complete. DOE has expressed an intent to request licensing of the WIPP by the Nuclear Regulatory Commission (NRC), but this issue is not yet resolved.

Interest in disposal of radioactive waste in geologic media may be traced back to a 1957 committee report by the National Academy of Sciences - National Research Council, that recommended guidelines for permanent disposal of radioactive waste in geological media. Recommendations fell into two categories: burial in bedded salt deposits or in deep sedimentary basins (perhaps 4000 - 5000 m deep).

Salt became the leading candidate as a disposal medium, and from 1957 until the 1970's most disposal studies in the U.S. concentrated on bedded salt. In the mid-1960's, Oak Ridge National Laboratories (ORNL) conducted a successful in situ experimental program called "Project Salt Vault" in a salt mine near Lyons, Kansas. A subsequent plan to establish a federal repository near Lyons was withdrawn due to both technical and political objections.

Subsequent evaluation of salt basins in the United States by ORNL and the USGS led in 1974 to field investigations of Permian salt deposits of the Delaware Basin in southeastern New Mexico to determine if the geologic setting was adequate for a radioactive waste repository. Permian evaporite deposits consist of the Castile Formation which is interbedded halite and anhydrite, the Salado Formation which consists principally of halite and the Rustler Formation which is mostly anhydrite but contains halite, dolomite, and siltstone.

In 1975, the AEC (later Energy Research and Development Administration (ERDA) and now Department of Energy (DOE)) assigned responsibility for site evaluation and conceptual design for this project in New Mexico to Sandia Laboratories of Albuquerque, New Mexico. The project in New Mexico is now known as the Waste Isolation Pilot Plant (WIPP).

Preliminary site selection criteria were general in nature. (Most areas are not well enough known to allow application of precise criteria.) After Sandia Laboratories determined in 1975 that the first preliminary study area originally selected by ORNL was geologically unsuitable, site selection factors were refined specifically for and applied to the Delaware Basin in New Mexico to define the present study area. The major siting factors employed in southeastern New Mexico are that the repository salt beds should be: (a) relatively pure; (b) several hundred feet thick; (c) between depths of 1000 and 3000 feet; (d) located where groundwater dissolutioning is relatively limited; (e) at least one mile from boreholes that completely penetrate the evaporite section, (f) generally located to avoid private land; (g) located where strata are relatively flat; and (h) located to minimize conflicts with mineral resources. Data from hundreds of borehole geophysical logs and more than fifteen hundred miles of existing seismic reflection lines from petroleum companies were analyzed and considered along with hydrologic data and available information on natural resources to narrow the area of search. A relatively restrictive criterion was the requirement the repository be one mile or more to the nearest borehole penetrating the complete evaporite section. Existing studies of borehole dissolution indicated one mile is sufficient, though perhaps not necessary, to ensure repository integrity.

Geologic studies for the WIPP fall into three different phases: preliminary site selection activities, geological characterization, and studies of long-range geologic processes affecting a repository. Preliminary site selection activities are complete now, and geological characterization is nearing completion with this report. Studies of long-range processes are becoming the focus of geotechnical programs; some of these latter studies are already underway. These studies, which will be oriented toward geologic processes and rates, will mostly be completed before conversion of the WIPP to a permanent repository for defense waste; these studies plus operation should provide further refinement to criteria for conversion of the WIPP.

Many standard petroleum and mineral industry techniques have been used to characterize the WIPP site. Considerable reliance has been placed on the combination of geophysical techniques corroborated by borehole information. The geophysical techniques most widely used to characterize the WIPP site include seismic reflection and resistivity. By summer, 1978, about 75 line miles of new seismic reflection data were obtained and over 9000 resistivity measurements had been made and analyzed. Twenty-one boreholes were drilled to evaluate potash, 14 hydrologic test holes were drilled and four potash holes were converted for hydrologic studies of the aquifers above the Salado Formation. Ten stratigraphic test boreholes have been drilled on or around the WIPP site as of early August, 1978, and two other holes have been drilled well away from the WIPP site to study dissolution processes. Two of these holes were drilled through the salt to test deep aquifers and to acquire geologic data.

Most of the WIPP geologic studies to date advanced geological characterization. Geologic studies will continue in order to permit a better quantification of the rates of geologic processes in and near the WIPP site and to develop a more thorough understanding of the geologic phenomena of interest (see Chapter 10).

REGIONAL GEOLOGY   (Chapter 3)

Regional Geology provides a broad assessment of the surface and subsurface environment of the area within a radius of about 200 miles of the proposed WIPP Site. The discussion comprises a synthesis of the available data pertaining to the physiography and geomorphology, stratigraphy and lithology, structure, tectonic development and geologic history of this region. Such information is necessary to understand the geological processes that need to be understood for assessment of long-term safety of a repository in the Delaware Basin of southeastern New Mexico. The paragraphs below present a brief summary of this information.

The WIPP site is located within the Pecos Valley section of the southern Great Plains physiographic province, a broad highland belt which slopes gently eastward from the Rocky Mountains and Basin and Range province to the Central Lowlands province. The Pecos Valley section itself is dominated by the Pecos River valley, a long north-south trough from 5 to 30 miles wide and as much as 1,000 feet deep, which exhibits an uneven rock and alluvium-covered floor marked by widespread solution subsidence features resulting from dissolution within the underlying Upper Permian Ochoan rocks. The section is bordered on the east by the Llano Estacado, the virtually uneroded fluviatile plain of the High Plains section, and on the west by the Sacramento and Guadalupe Mountains area of the Sacramento section.

The principal geomorphic features with bearing on the site area include the Pecos River drainage system, the Mescalero Plain, karst topography and wind erosion "blow-outs." The Pecos River system has evolved from the south, cutting headward through the Ogallala sediments to capture what is now the upper Pecos and becoming entrenched sometime after the Middle Pleistocene. The system at present receives almost all the surface and subsurface drainage of the region; most of its tributaries are intermittent, due to the contemporary semi-arid climate. Most of the ground surface east of the Pecos River valley comprises the Mescalero Plain, a poorly drained surface covered by gravels, eolian sand and caliche, which has developed since Early to Middle Pleistocene time. The surface of the region exhibits karst topography containing superficial sinkholes, dolines, solution-subsidence troughs, and related features, formed as a result of both surface erosion and subsurface solutioning activity.

The WIPP site lies on a caliche and sand covered drainage divide separating two major and perhaps still developing solution-erosional features, Nash Draw on the west and San Simon Swale to the east. This prevailing erosional pattern is expected to continue in the future, with most local erosion occurring in the draw and swale areas. The site is located west of the local drainage divide.

The stratigraphic section present in the site region includes Precambrian through Triassic rocks, overlain by outliers of possible Cretaceous age, and widespread Late Tertiary through Holocene sediments.

Metasediments and granitic-volcanic igneous materials constitute the majority of the regional basement, cropping out in isolated areas to the west and north. The granitic rocks range in age from about 1,400 million years in the north to about 1,000 million years in the south and are overlain in places by younger Precanibrain volcanic terrains. The surface of the Precambrian reflects the Late Paleozoic platform and basin structural configuration of the area.

The Paleozoic section comprises up to 20,000 feet of Upper Cambrian sandstones through Upper Permian evaporites and redbeds. The Ordovician, Silurian and Devonian rocks are primarily carbonates with lesser sands, shales and cherts which were deposited in shallow, rather calm shelf areas of broadly subsiding areas of the Tobosa Basin, with some minor influence from uplifted areas such as the ancestral Central Basin Platform. The Mississippian sequence consists of locally cherty limestones overlain by silty and sandy shales, truncated against adjacent emerging uplands. Post-Mississippian orogeny caused uplift, tilting and erosion; producing a massive section of Lower Pennsylvanian continental sediments, interbedded with dark limestones, particularly toward the top of the section. Late in the Pennsylvanian, a basin, basin margin, and shelf configuration, which endured through the Permian, developed, resulting in deposition of dark shales, clastics and some limestones and bioclastics forming a series of reefs along the basin margins, and shallow-water limestones and clastics on the adjacent shelves. Upon filling of the basins in the Late Permian, a sequence of evaporites totalling 4000-5000 feet in thickness was deposited during recurrent retreats of shallow seas restricted by the encircling Guadalupian reefs. The Castile Formation consists of anyhdrite interlaminated with calcite and halite overlain by the Salado Formation, which is primarily halite with lesser clastics, anhydrite and a suite of salts. The Rustler Formation overlying the Salado is composed of anhydrite, gypsum and

lesser salt with carbonates and clastics. The top of the Paleozoic is marked by the thin Dewey Lake Redbeds.

The Mesozoic sequence is represented by only the Upper Triassic Dockum Group of terrigenous redbeds, which in many places are truncated or removed by erosion, and by scattered patches of Cretaceous limestone and sandstones.

The lower Cenozoic section is missing from the region due to erosion and/or non-deposition, and the widespread Late Miocene-Pliocene Ogallala clastics represent the earliest deposition of the section. The Ogallala is capped by a dense, resistant layer of caliche, which probably started to form during the Late Pliocene. Quaternary deposits occur only locally and consist of the Middle Pleistocene to Holocene terrace, channel and playa deposits as well as windblown sands.

The major structural framework of the region is provided by the large-scale basins and platforms of late Paleozoic age and by Cenozoic features primarily associated with Basin and Range tectonics.

The principal late Paleozoic features of the area consisted of the western extent of the Tobosa and later the Permian Basin and its border lands. These elements include the Delaware Basin, Central Basin Platform, Midland Basin, the Northwestern Shelf, Pedernal Uplift, Matador Arch, Val Verde Basin and Diablo Platform.

The site is located in the northern portion of the Delaware Basin, a broad, oval-shaped asymmetrical trough with a northerly trend and southward plunge and a structural relief of more than 20,000 feet on top of the Precambrian. Deformation of the basin rocks is minor, those formations older than Late Permian are only gently downwarped. Deep-seated faults, some reflecting Precambrian faults, occur in the basin, as do folds, joint sets, and a number of smaller, probably solution-related structures originating in the Upper Permian evaporites. The basin was defined by early Pennsylvanian time, and major structural

adjustment occurred from Late Pennsylvanian to Early Permian time. By
the Late Permian, this episode of tectonic activity ended in the basin;
regional eastward tilting occurred later, in the Cenozoic.

The Central Basin Platform, a northward-trending feature, separated from
the Delaware Basin to its west by a zone of major normal faulting,
represents a broad uplift of Precambrian to Pennsylvanian rocks, within
which movement took place periodically, probably from the Precambrian
until the late Paleozoic when the basin became structurally stable.

North and northwest of the Delaware Basin lies the Northwestern Shelf,
which was well-developed before Permian time and may have originated in
the Early Paleozoic, when it formed the margin of the Tobosa Basin. A
number of flexures, arches, and faults which have been identified on the
shelf had probably ceased tectonic activity in Tertiary time.

The Diablo Platform, forming the southwestern border of the Delaware
Basin, experienced primary deformation in the late Paleozoic in the form
of uplift, folding and faulting. Deformation also occurred here during
late Tertiary time through block faulting and buckling. Recent uplift
along its eastern side suggests continuing tectonic development in the
area. The remainder of the previously listed late Paleozoic structural
elements of the area are only remotely related to the site area.

Late Tertiary Basin and Range tectonics produced the Sacramento,
Guadalupe and Delaware Mountains bordering the region on the west. These
uplifts are generally eastward-tilted fault blocks bordered on the west
by complex normal fault systems forming short, steep westward slopes and
backslopes dipping gently eastward. Tectonic activity began in this area
during Mississippian to Early Permian time in the form of fault systems,
followed by the major Basin and Range tectonics. Small fault scarps in
recent alluvium along the western edge of these ranges, as well as some
seismic activity, suggest that structural development here may still be
taking place.

Post-Precambrian igneous activity in the region consists of Tertiary intrusives and Tertiary to Quaternary volcanic terrains located on the north, west and south of the site area. Only minor igneous activity, in the form of dikes and possibly sills, is known to have occurred within the Delaware Basin.

The closest such igneous feature to the site is a near-vertical trachyte or lamprophyre dike or series of en echelon dikes trending about N50°E for perhaps 75 miles into New Mexico from near the Texas-New Mexico border southwest of Carlsbad Caverns, passing about 9 miles northwest of the site. Evidence for the dike's existence consists of exposures in two mines, cuttings from several drill holes, aeromagnetic indications and surface exposures some 42 miles southwest of the site in the Yeso Hills. This dike has been dated as mid-Tertiary and intrudes only the Late Permian Salado and underlying formations.

The principal Tertiary igneous features of the area beyond the Delaware Basin include several intrusive bodies within the Delaware Mountains, widespread occurrences further south in the Trans-Pecos region and several areas well to the north of the basin, in the form of the eastward-trending El Camino del Diablo and Railroad Mountain dikes (near Roswell) and the stocks of the Capitan and Sierra Blanca Mountains. Quaternary volcanic and related extrusive terrains are present west of the site region, well within the Basin and Range province.

The geologic history of the region is recorded in igneous and metasedimentary rocks as old as about 1,400 million years which indicate a complex Precambrian history of mountain-building, igneous events, metamorphism and erosional cycles. Probably before Paleozoic time, erosion had reduced the area to a nearly level plain.

The early to middle Paleozoic Era was characterized by generally mild epeirogenic movements and carbonate deposition interrupted by only minor clastic sedimentation. The oldest sediments in the region are the Late Cambrian and perhaps Early Ordovician Bliss sandstones. Following Early

Ordovician time, a broad sag, the Tobosa Basin, formed and began
deepening. Shelf depositions of clastics continued, derived partly from
the ancestral Central Basin Platform, and carbonates deposited in shallow
waters. By Late Ordovician time, the Marathon Ouachita geosyncline to
the south of the area began subsiding, but until the Middle
Mississippian, only mild tectonic activity continued, with several
periods of minor folding and perhaps some faulting, the basin subsiding,
the Pedernal landmass to the north emergent and some regional erosion
occurring.

From late in Mississippian time through the Pennsylvanian, regional
tectonic activity accelerated, folding up the Central Basin Platform,
Matador Arch and the Ancestral Rockies, producing massive deposition of
clastics. The Tobosa Basin was definitively split into the rapidly
subsiding Delaware, Midland and Val Verde Basins. Throughout the
Permian, sedimentation was continous in the basins, climaxing in the
development of massive reefs, and, following stabilization in the Late
Permian, in the deposition of a thick sequence of evaporites. By the end
of the period, the area was slightly emergent, and a thin sheet of
redbeds covered the evaporites.

Since the close of the Permian, the basin area has been relatively stable
tectonically, and the Mesozoic through Cenozoic eras have been
characterized by erosion, with only relatively minor deposition of
terrestrial materials. During the Triassic, a broad flood plain sediment
surface developed, followed late in the period by fluvial clastic
deposition and formation of a rolling topography. Sometime during the
Cretaceous, submergence occurred, and thin limestone and clastics
collected in intermittent, shallow seas. During the Jurassic and perhaps
as early as the Triassic, subsurface dissolution of the Upper Permian
evaporites began. The close of the Mesozoic was marked by the Laramide
orogeny and uplift of the Rocky Mountains, with mild tectonic and igneous
activity to the west and north of the site area. Throughout most of the
Tertiary, erosion dominated, until deposition of the Ogallala late in the
era. Mid to late Tertiary Basin and Range uplift of the Sacramento and

Guadalupe-Delaware Mountains was accompanied by regional uplift and east-southeastward tilting. Upon this gently sloping surface the Miocene-Pliocene Ogallala fan deposits accumulated, and a resistant caliche caprock began to form. During Quaternary time, the present landscape has developed through processes of surface erosion and dissolution of the Upper Permian evaporites, accompanied by terrace and stream valley deposition and eolian activity.

The regional geology shows that the northern Delaware Basin has been a part of large structures reacting slowly to tectonic and climatic processes. About 300 million years of Paleozoic geologic history indicate a downwarping basin on a grand scale. The last 200 million years are characterized by slow uplift relative to surroundings resulting in some erosion and dissolution of rocks in the Delaware Basin. Dramatic geologic events such as faults and volcanic activity have not occurred in the northern Delaware Basin where the WIPP site is located. The nearest events of this type are occurring west of the Guadalupe Mountains about 70 miles southwest of the WIPP site. The regional geology does not indicate that any dramatic changes in geologic processes or rates have recently occurred at the WIPP site.

SITE GEOLOGY   (Chapter 4)

Much investigative effort has been expended to define subsurface geologic conditions at the WIPP site. These studies not only provide detailed information regarding mining conditions at the repository levels, but also furnish a basis for an assessment of the level of protection or safeguard against possible modes of containment failure at the site, in the context of the long-term isolation requirements of radioactive waste. Information for geologic investigations conducted by the U.S. Geological Survey and reported in several open-file reports by that agency, as well as details of salt deformation investigated by other consultants, have done much to define the general geologic conditions in the vicinity of the WIPP site and have been freely utilized in assembling Chapter 4 of the GCR. Detailed site-specific exploration techniques include seismic

reflection, resistivity, gravity and magnetic surveys, borehole
exploration including coring, geophysical logging and hydrologic testing,
and reconnaissance geologic mapping. From data thus obtained a series of
structure contour and isopach maps were constructed which are presented
and discussed in section 4.3 and 4.4 A continuously cored stratigraphic
test hole, ERDA-9, has been drilled to a depth of 2,875 feet below ground
surface near the center of the WIPP site and provides much detail on
geologic properties at and above the WIPP repository levels.

The surface of the WIPP site is a slightly hummocky plain sloping gently
southwest at about 50 feet per mile; elevations range at the site from
about 3300 to 3600 feet above sea level. There are no permanent drainage
courses in the site area. Any intermittent runoff drains west into Nash
Draw, a broad swale of about 150 feet of relief leading southwest toward
the Pecos River. A declivity marking the east edge of Nash Draw in the
site area, known as Livingston Ridge, is located about 4 miles west of
the center of the site. Nash Draw, now partly filled with Pleistocene
sediments, has evolved both by surface erosion and by subsurface
dissolution of salt, presumably during wetter intervals in the geologic
past.

Recent windblown sand and partly stabilized sand dunes blanket most of
the site area. A hard, resistant duricrust or caliche (Mescalero
caliche) is typically present beneath the sand blanket and has developed
upon the surface of the underlying Pleistocene fluvial (Gatuna)
deposits. The fluvial deposits are tentatively assigned a Kansan age and
the caliche formed upon them a Yarmouth (interglacial) age; that is, the
caliche formed starting approximately 500,000 years ago. At some places,
the caliche is fractured and drapes into Nash Draw along Livingston
Ridge, indicating that some erosion and dissolution has taken place in
Nash Draw since the caliche was formed, presumably during wetter climatic
intervals associated with Illinoian and Wisconsin glaciations. Increased
erosion from runoff, should the climate of the region become more humid
in the future, would be expected to occur in the existing drainage
courses, leaving the drainage patterns relatively unaltered.

The proposed WIPP underground storage facilities are to be placed near the middle of a 3,600-foot-thick sequence of relatively pure evaporite strata containing primarily rock salt and anhydrite, lying between depths of about 500 and 4,100 feet beneath ground surface. The formation richest in rock salt, the Salado Formation, is nearly 2,000 feet thick and contains the relatively pure salt layers in which the two proposed underground storage levels are to be constructed, at a depth near 2,120 feet for the upper level and near 2,670 feet for the lower. The storage horizons are well isolated from the hydrologic environment by adjacent evaporite strata. A thickness of at least 1,300 feet of undisturbed evaporite rock, primarily rock salt, overlies the upper storage horizon and about an equivalent thickness of anhydrite and rock salt intervenes between the lower storage horizon and the next adjacent underlying non-evaporite formation. The salt deposits of the Castile and Salado Formations at the WIPP site were formed about 225 million years ago and have remained isolated from dissolution since about that time.

The total thickness of the sedimentary pile resting on top of Precambrian basement beneath the WIPP site is about 18,000 feet of Ordovician to Recent strata. Following is a brief summary of the stratigraphy, proceeding from the surface down to the basement. Beneath a thin but persistent veneer of windblown sand at the site are sediments representing Pleistocene, Upper Triassic, and uppermost Permian strata, all of which occur above the evaporite sequence. Sandstone of the Pleistocene Gatuna Formation, capped by Mescalero caliche also developed in Pleistocene time, is only a few tens of feet thick at the site and is of interest primarily for the geochronologic and paleoclimatic implications of its presence. Between the Pleistocene deposits and the evaporite sequence is a 500-foot-thick succession of nonmarine redbeds of Late Triassic Age (Santa Rosa sandstone) and marine redbeds of latest Permian age (Dewey Lake Redbeds). This redbed sequence thins westward and thickens eastward, having been beveled westward by several post-Late Triassic erosional episodes; the thickness of redbed deposits remaining above the evaporite sequence is crudely proportional to the degree to which the underlying salt horizons have been protected from surficial processes leading to erosion and dissolution.

At the center of the site all but the uppermost 50 feet of the 18,000 feet of strata are of Paleozoic age, the marine Dewey Lake Redbeds being the topmost Paleozoic rocks. The Permian section alone, about 12,800 feet thick, constitutes over two-thirds of the sedimentary pile. The Permian section is divided into four series, the three lowest of which (Wolfcampian, Leonardian and Guadalupian) contain thick clastic sequences, and the uppermost of which (Ochoan) is represented by the Castile, Salado, Rustler, and Dewey Lake (in ascending order).

The Rustler, which lies over the Salado, contains the largest percentage of clastic material of the three evaporite formations, yet where its original thickness of around 450 feet has been protected from salt dissolution, about 70 percent of the formation is composed of evaporite minerals, more than half of which is halides. Beneath the Los Medanos site the Rustler has been leached of most of its rock salt, with the result that 310 feet of the formation was encountered at ERDA-9 at the center of the site. This implies that up to 140 feet of rock salt have been removed and that the overlying strata have subsided accordingly; it does not, however, imply that dissolution and subsidence is presently active or even that it has recently occurred. The uppermost occurrence of halite in the Rustler Formation was encountered at a depth of about 760 feet (about 100 feet above the base of the formation). Between this level and the upper level storage zone of the proposed WIPP facility over 1,300 feet of undisturbed evaporite rock, primarily Salado rock salt, intervene.

The 2,000-foot thickness of the salt-rich Salado Formation is divided into three members by the recognition of a middle member referred to as the McNutt potash zone, which is the interval within the Salado that contains all of the potential reserves of potash, or potassium minerals commercially mined in the Carlsbad district west of the site. The lowest member of the Salado, beneath the McNutt potash member, is the member that contains the nearly pure halite chosen for the proposed facility. The Castile Formation beneath the Salado contains highly pure beds of halite but, unlike the Salado, also contains much massive anhydrite.

The rest of the Permian section beneath the evaporite sequence, together with the subjacent Pennsylvanian and possibly Late Mississippian sections, contain dominantly clastic rocks that represent deposition during the time in which the Delaware Basin existed as a distinct structural entity. Much of these pre-evaporite, basinal sediments, which total about 11,000 feet in thickness beneath the site, have been targeted for petroleum exploration at one point or another in the Delaware Basin and contain nearly all of the region's known potential reserve of hydrocarbons.

The remainder of the Paleozoic section (Mississippian down through the Ordovician) consists of about 3,000 feet of mainly carbonate strata deposited in shallow-water or shelf conditions over a period of long-sustained crustal stability.

The underlying crystalline basement is believed to be a granitic terrane, formed about 1,300 million years ago. The only other igneous rocks that are known in the site area are known only in the subsurface and occur as lamprophyre (basaltic) dike rock intruded into evaporite beds along a single northeast dike trend that approaches no closer than about 9 miles northwest of the center of the proposed WIPP site.

With regard to subsurface geologic structure at the site, all of the Permian and older strata exhibit a gentle, regional homoclinal dip to the east or southeast, reflecting the presence of the Delaware Basin tectonic structure. No surface faulting is known. A general summary and assessment of structure in the site area was provided by C.L. Jones in an open-file report issued by the U.S. Geological Survey in 1973. Jones stated,

> "The structure of the Los Medanos area is basically simple and the
> rocks are, for the most part, only slightly deformed. Nevertheless,
> the rocks have been tilted, warped, eroded, and subroded, (ed. note:
> subjected to subsurface removal by dissolution), and discrete
> structural features can be recognized. These include: (1)
> structural features of regional extent related to Permian
> sedimentation, (2) intraformational folds of limited extent related

to "down-the-dip" movement of salt under the influence of gravity and weight of overburden and (3) subsidence folds related to warping and settling of rocks to conform with the general shape and topography of the surface of salt in areas of subrosion...

"On the basis of available geological information, the salt deposits of Los Medanos area seem in many ways to constitute a suitable receptacle for use in a pilot-plant repository for radioactive wastes. The deposits have thick seams of rock salt at moderate depths, they have a substantial cover of well-consolidated rocks, and they have escaped almost completely undamaged long periods of erosion. The deposits are only slightly structurally deformed, and they are located in an area that has had a long history of tectonic stability."

Information developed in the succeeding five years of investigations do not significantly alter that assessment relative to the structural and tectonic conditions present at the Los Medanos site. Based on exploration accomplished to date, a series of structure contour and isopach maps are presented for rocks ranging in age from Devonian to Pleistocene. This and other information indicate that active tectonic faulting and warping of rocks in the site vicinity seems to have predated Permian evaporite deposition; certain minor faulting within the thick Permian section appears to have occurred contemporaneously with sedimentation and may be ascribed to compaction. Deformation related to salt flowage has occurred primarily in the Castile Formation beneath the Salado, and has locally modified the regional easterly gradient to 80 to 100 feet per mile at the level of the storage horizons near the base of the Salado. Areas in the vicinity of the site in which artesian brine reservoirs have been encountered are associated with thickened salt sections and salt-flow anticlines in the Castile, but no such major structural features are recognizable within the limits of the WIPP storage facility on any of the Salado horizons contoured. The site appears to be in a slight structural saddle, a condition considered to be favorable for site selection. Dissolution of bedded salt at the site has been restricted to horizons within the Rustler Formation; there is no evidence that the resulting settlement produced any significant

structural irregularities or collapse features in the overlying strata within the area of the Los Medanos site. Investigations are continuing to further define the extent to which salt deformation in the Castile may have affected the structural configuration within the lower part of the Salado where excavation of the remote handling (RH) and contact handling (CH) levels is presently planned. These investigations will permit a more detailed assessment of the optimum layout, design and construction method of the storage facility.

The geologic history of the Los Medanos site may be organized into three main phases occurring subsequent to the original establishment of a granitic basement intrusive complex between about one billion and 1.4 billion years ago, forming the cratonic crust beneath the site. The first phase, of at least 500 million years duration, was a time of uplift and erosion of all pre-existing Precambrian sedimentary and metamorphic rocks which may have once been deposited or formed in the site area, eventually exposing the deep-seated igneous rocks.

The second phase, which corresponds to the Paleozoic Era, was characterized by an almost continuous marine submergence lasting about 225 million years, wherein shelf and shallow basin sediments slowly accumulated. It culminated in a comparatively rapid accumulation of over 13,000 feet of Permian sediment within a relatively brief period lasting 50 to 55 million years, toward the end of which time thick evaporite beds, mainly rock salt, were deposited. This rapid Permian deposition was presaged in Late Mississippian time by tectonic activity that differentially upwarped elements of the craton, such as the Central Basin Platform, thereby defining the Delaware Basin as a tectonic feature for the first time. During Pennsylvanian time, repeated marginal faulting caused periodic uplift of bordering platforms and some warping within the basin. By early Permian time, this tectonic activity apparently died out as basin subsidence and sedimentation accelerated. Eventually the Permian sea became shallow and briny, at first characterized by extensive reef development, but eventually in Ochoan time by a vast brine flat in

which thick evaporite deposits formed, burying the earlier reef masses. The final event of the long, nearly continuous accumulation of marine sediment of the second phase was deposition of a blanket of marine or brackish tidal flat redbeds over the evaporite strata.

Uplift and subaerial conditions next occurred at the site in the third and final phase, and persisted some 225 million years to the present, with the exception of a brief marine inundation in about the middle of that span of time. Periods of terrestrial deposition alternated with erosional episodes, so that a series of nonmarine deposits separated by angular unconformities blanket the evaporite beds at the site. These angular unconformities represent intervals during which the salt beds at the WIPP site were tilted and subjected to potential dissolution. At least four erosional episodes separated by depositional intervals are recognized: (1) Early Triassic time in which the Dewey Lake Redbeds were tilted and eroded to a slight angular unconformity before deposition of the Upper Triassic Dockum Group; (2) Jurassic-Early Cretaceous time in which the Dockum Group was tilted and eroded to a wedge before marine inundation in Washitan time (latest Early Cretaceous); (3) a Late Cretaceous through mid-Tertiary erosional interval when the region was again tilted and the Triassic Dockum Group of sediments was bevelled for a second time; and (4) a post-Ogallala (post-Pliocene) uplift and erosion in early Pleistocene time, prior to deposition of the (Kansan?) Gatuna Formation took place. Subsequent to deposition of the Gatuna, there probably were intervals corresponding to the later Illinoisian and Wisconsin glaciations during which accelerated erosion in these wetter times occurred in the area of the WIPP site.

Each period of tilting, which accompanied renewed erosion as outlined above, afforded an opportunity for salt flow by plastic deformation along the imposed gradient and salt deformation as the salt impinged against reef abutments or responded to uneven, differential sediment loading or erosional unloading; therefore there may have been several episodes of salt deformation of this type. To the extent that some "deep dissolution" features are recognized today in salt at depths of several

thousand feet below the surface, it seems likely that subsurface
dissolution of salt could have been initiated at comparable depths
beneath the surface as soon as Early Triassic time. It is reasonable to
assume that episodes of active dissolution occurred during the Jurassic
and Late Cretaceous-mid Tertiary erosional intervals, as well as during
the several pluvial periods corresponding to Pleistocene glacial stages.
Any attempt at reconstructing past history of salt dissolution in the Los
Medanos area as an approach to predicting the future course of salt
erosion must contend with the likelihood of the existence of times of
greatly accelerated dissolution of salt in the geologic past interspersed
with intervals of much lesser activity. The evidence available today
indicates little if any change in erosion rates at the WIPP site in the
recent geologic past. Detailed mapping studies are underway which will
contribute to information on dissolution rates at various times in the
geologic history of the site.

The discussion of the site geology defines the present conditions of the
site which must be known to establish the WIPP. These conditions relate
mostly to physical characteristics such as thickness, depth, extent,
purity, and structure of the evaporites (as well as some of the
surrounding beds). In addition, baseline conditions regarding the
processes of dissolution and erosion as they affect the immediate site
have been determined. Thus the baseline geological conditions at the
site are presented so that judgement of the site relative to the present
criteria may be undertaken and so that continuing studies will focus on
geologic processes important to assessment of repository safety.

The site geomorphology indicates tectonic stability at the site for the
last 500,000 years or more. The local stratigraphy is continuous with
the regional stratigraphy. Local minor structures exist within the
evaporite beds, but no severe displacements or brine or gas have been
encountered. Potential repository zones at depths of 2730-2620 feet and
2176-2074 feet have been chosen on the combined basis of purity, depth,
thickness, mutual separation, and depth below the potash zone.

SEISMOLOGY   (Chapter 5)

Regional seismicity of the Los Medanos site is discussed in two separate
time intervals suggested by the type and quality of information available
for each interval.   These intervals are before 1962 (non-instrumental)
and from 1962 to the present (instrumental).

Before 1962 almost all data on earthquakes within 300 kilometers of the
site are based on collection, cataloging, and consideration of
non-instrumental reports.   These data indicate that twenty earthquakes
with maximum reported intensities between III and VIII on the Modified
Mercalli Scale have occurred within a 300 kilometer radius of the site
region from 1923 to 1960.   There have been no earthquakes of epicentral
intensity V or greater within about 200 kilometers of the site in this
period.   The closest reported shocks are two intensity IV events at
Carlsbad in 1923 and 1949.   The strongest reported earthquake to occur
within 300 kilometers is the intensity VIII Valentine, Texas event of
lugust 16, 1931 at a distance of approximately 210 kilometers.

Between 1962 and 1972 inclusive, a general instrumental survey of the
site region shows 38 earthquakes with magnitudes ranging from 1.2 to 4.6
(Richter scale).   The seismicity pattern of these instrumentally located
events is very similar to pre-instrumental data except that a number of
earthquakes occur on the Central Basin Platform in the later data set.
The closest reported shock between 1962 and 1972 was a magnitude 2.8
event on July 26, 1972 about 40 kilometers northwest of the site.   The
largest event in this period is the magnitude 4.6 earthquake almost 300
kilometers to the southwest.

Three investigations of a more local and temporally restricted nature
have impact on the Los Medanos site.   These involve earthquakes recorded
at a seismographic station installed near the site itself, events
recorded at an array of seismographic stations installed on the Central
Basin Platform near Kermit, Texas, and three earthquakes recorded
regionally and found to have occurred near the site.

At the beginning of April, 1974 a vertical, single-component, continuously recording seismograph station (with letter designation CLN) was installed very near the site. During the latest available reporting period, April, 1974 to October, 1977, 291 events identifiable as local and regional earthquakes have been recorded and locations for 75 of the 291 events have been obtained. The seismicity pattern suggested is very similar to that of the general 1962-1972 instrumental survey. Approximately one-half of all located events in the CLN data set occur on the Central Basin Platform while most of the rest occur to the west and southwest of the site in the Rio Grande Rift Zone. There is also a scattering of earthquakes in the High Plains physiographic province of the site. Included is a magnitude 3.6 event on November 28, 1974 at about 40 kilometers to the northwest, which was close to the July 26, 1972 earthquake mentioned above.

Instrumental studies show earthquake activity in the Central Basin Platform at a higher level than expected. Primarily for this reason, the Kermit, Texas seismographic station array was established in late 1975 to more closely monitor this activity. During the latest available reporting period for this array (November, 1975 to July, 1977), 407 local events have been detected and 135 located with array data. Of the located events 56 were in the interior of the array while the rest have been peripheral to it. Earthquakes with magnitudes calculated both using Kermit array data and regional seismographic station and CLN data show that Kermit magnitudes are almost one unit higher. This inconsistency remains unresolved at this time.

As a result of general survey and specialized seismic instrumental studies in the Los Medanos site region there is little doubt that the Central Basin Platform has been seismically active since at least mid-1964, and that during this time it has been the most active seismic area within 300 kilometers of the site in terms of number of events. The basic conclusion from all instrumental data is that seismic activity is equally likely to occur anywhere along the Central Basin Platform structure without particular regard to small scale structural details

such as pre-Permian buried faults. Attempts have been made to relate this seismicity to secondary oil recovery operations in the area. Although both spatial and temporal coincidences of Central Basin Platform seismicity with secondary recovery projects are highly suggestive of a close relationship, this has not been satisfactorily established at this time.

Questions of the tectonism and seismic activity very near or at the site are of great interest. For this reason the most important seismic events instrumentally recorded are those closest to the site: July 26, 1972, and November 28, 1974, magnitudes 2.8 and 3.6, respectively; and a later shock on January 28, 1978, with only preliminary data yet available. If these events are an indication of normal background seismicity in the immediate site area, they might cause a re-evaluation of previous estimates of seismic risk at the Los Medanos site (Sanford and Toppozada, 1974). At the time of the first two events rockfalls and surface ground cracking were reported at the National Potash Company Eddy Co. Mine. To see if mine collapse at this mine was responsible for both events, an analysis was run to see if both epicenters could be made coincident with each other. Such a coincidence would be a strong indication of a rock fall origin for both events. At this time the best available analysis indicates that these small events did not both occur at the Eddy Co. Mine and thus they cannot both have been caused by a very localized non-tectonic source there. The third shock is located, in a very preliminary fashion, north of the station an estimated 17 km.

Using all the information developed above on regional seismicity and some additional simple assumptions about regional tectonism a preliminary analysis of risk from vibratory ground motion at the surface is derived in a way useful to seismic design characterization at the site during its active phase of development and use. The results of this analysis are that the 1000 year acceleration is less than or equal to 0.06 g and the 10,000-year acceleration is less than or equal to 0.1 g for all models tried. Probabilities at which higher acceleration levels occur depend almost exclusively on the assumptions made about the seismic potential of the immediate site area.

In addition to its use to determine risk as a function of vibratory ground motion level, regional seismicity is also considered as an indicator of longer-term tectonic processes. Natural regional seismicity should be consistent with the geologic indicators of tectonic processes unless the tectonic setting is changing. Regional stress patterns, as implied by focal mechanism solutions for regional earthquakes and in site measurements, and regional tectonism, as implied by earthquake recurrence statistics, are both considered. Although other explanations cannot be precluded, it seems that the most reasonable interpretation of the seismic implications to tectonism at this time are: (1) Observed geologic and seismic data are in general agreement in the Rio Grande rift zone to the west and southwest of the site where the largest historic earthquakes within 300 kilometers of the site have occurred. Future significant earthquakes can be expected there. (2) The current level of seismic activity on the Central Basin Platform is probably related to fluid injection for secondary recovery of oil. (3) The lack of geologic indications of natural recent tectonic activity for the High Plains province of the site can probably be reconciled with the seismic data by assuming a maximum magnitude limit of the earthquakes that have occurred here.

The importance of seismicity information over the immediate future is to provide a data base for design of facilities for the operational time of the WIPP. Seismicity information also serves as an indicator of the tectonic situation in assessing the WIPP site for a repository.

HYDROLOGY (Chapter 6)

Chapter 6 contains an assessment of surface and groundwater resources in and surrounding the proposed WIPP site and a status report of current hydrogeologic investigations in the local site area. The water resource assessment incorporates the published results of regional and local hydrologic studies supported by universities and state and federal agencies since the late 1930's. Present studies of the proposed site and

adjacent area are directed toward a more quantitative evaluation of the salt dissolution process, the hydrogeologic parameters affecting groundwater movement, and the major elements of surface and groundwater quality as related to water resource use and local ecology. The collection of hydrologic data is projected to continue for several years to provide site-specific information for a detailed safety analysis of the WIPP. Because of the relationship to hydrologic processes, dissolution activity is also summarized within this chapter.

The only major stream near the site is the Pecos River which flows southeasterly through Carlsbad. At its closest point, the river is approximately 14 miles southwest of the WIPP site. Several reservoirs, located on the Pecos upstream of the site, regulate river flow. The maximum recorded flood on the Pecos River occurred on August 23, 1966, with a discharge of 120,000 cfs and a maximum water surface elevation near Malaga of approximately 2938 feet. The minimum surface elevation of the site is more than 310 feet above this historic flood level.

Climatological records show that mean annual precipitation at the site is approximately 12 inches per year. The maximum daily precipitation recorded at Carlsbad was 5.12 inches in August 1916, and the maximum daily snowfall was 10 inches in December 1923. Winter storms in the area occur as a result of fronts moving from the west while summer storms, generally the most severe, occur as thunderstorms from moist air moving northwest from the Gulf of Mexico.

Surface drainage patterns at the site are undeveloped. Infiltration rates are high because of the sandy, gravelly soils that cover the region. However, the nearest groundwater is more than 50 feet below the land surface. Aided by the low relative humidity (typically 36% during daylight hours) and high mean annual temperature ($61^{\circ}F$), most infiltration escapes the soil through evaporation and transpiration.

Important aquifers of the region include the San Andres Formation, a major source for irrigation waters in the Roswell Basin and other areas

to the north and northwest of the site region. Potable water is present in the Capitan aquifer southwest of the community of Carlsbad and is the primary source of municipal water in the local area. Other important aquifers of the region include the Ogallala Formation to the east of the proposed site, and unconsolidated alluvium along the Pecos River.

Groundwater within the Delaware Basin is predominantly of poor quality with total dissolved solids concentrations typically in excess of 3,000 ppm. The only large quantities of potable groundwater are found in aquifers west of and along the Pecos River. To the west, the formations of the basin crop out, and the soluble salts have been leached from the Ochoan evaporites. From recharge areas west of the Pecos River, groundwater in the Delaware Basin moves eastward. From the site area, water in hydrologic units above the salt moves generally southwest to the Pecos. These shallow units, or those cut by the Pecos River, discharge to the river, either directly or to alluvium of the river channel. Although a local hydraulic connection between the river and the Capitan aquifer may occur near Carlsbad, groundwater flow in the reef formation is severely restricted near the Eddy-Lea county line. Groundwater in formations older than the Capitan is not directly affected by the river, is present under confined conditions, and flows eastward. The aquifer of most significance to the proposed site in these older formations is the Bell Canyon Formation.

Water-bearing strata in the local site area at elevations above the proposed repository include the Santa Rosa Sandstone and the Culebra and Magenta members of the Rustler Formation. Hydrologic units below the repository elevation include the Bell Canyon Formation of the Delaware Mountain Group. Hydrologic test results to date show the average head elevations of the potentiometric surfaces from these aquifers are 3200 feet for the Santa Rosa Sandstone, 3150 feet for the composite Rustler Formation, and 3350 feet for the Delaware Mountain Group (equivalent "fresh-water" elevation). The thick halite beds of the Salado Formation are isolated from circulating groundwaters by confining layers of low hydraulic conductivity, directly above and below the salt formation.

In the vicinity of the proposed site, potable groundwater is not present, except in small, isolated, near-surface perched pockets. Thus, it would appear that the proposed repository is favorably situated in relation to groundwater circulation and occurrence. Detailed investigations of groundwater hydrology at the proposed site have been conducted and are continuing. The data will provide a basis for more quantitative determinations regarding the continued isolation of the proposed repository from groundwater circulation.

A shallow salt dissolution zone occurs in Nash Draw at the contact between the Salado and Rustler Formations. The dissolution area ranges in width from 2 to 10 miles and has a length of approximately 30 miles. The brine solution flows southwesterly and discharges into the Pecos River at Malaga Bend. The average rate of vertical dissolution has been estimated to be between 0.33 and 0.5 feet per 1,000 years, and the average rate for lateral dissolution has been estimated to be between 6 and 8 miles per million years. Dissolution of salt at the top of the Salado occurs about 2 miles west of the center of the site. Eastward across the site salt is present in the Rustler at progressively higher levels, indicating that the salt has not been dissolved out of the Rustler and that the Salado has not been attacked by dissolution.

Future measurements obtained from the hydrologic test programs and analyses of the test data will be used to refine bounding calculations, such as estimates of groundwater travel times, and to provide a more detailed description of the physical system and system dynamics. The use of computer models as predictive tools is expected to be closely coordinated with timely observations from an established monitoring network. The predictive results and the real time measurements will aid in the continued assessment of repository isolation from dissolution and groundwater circulation. The retardation of radioisotopes within the hydrologic system (Chapter 9.3), when coupled with the hydrologic model,

will allow realistic calculations of radioisotope transport for postulated failure scenarios.

GEOCHEMISTRY   (Chapter 7)

Chapter 7 of this WIPP Geological Characterization Report discusses geochemical properties of geologic materials from Southeastern New Mexico. Geochemistry includes accounts of mineralogy and petrology of evaporites and the associated non-evaporites, volatile constituents of the Salado Formation, fluid inclusions in evaporite minerals, ground water chemistry, and age-dating of evaporites and ground waters.

Megascopic, microscopic and x-ray diffraction examination of the Permian (Ochoan) evaporite section showed the three most common minerals of the Salado Formation to be halite, anhydrite and polyhalite. In addition, there are the potassic and magnesic minerals sylvite, kainite, kieserite, langbeinite, loeweite and bloedite in the McNutt Potash Zone of the Salado Formation. Marker beds throughout the Salado Formation (mostly anhydrite and polyhalite) occur at intervals of a few tens of meters, are on the order of 10 to 100 cm thick, and are laterally traceable in core holes adjacent to the center of this investigation. The McNutt Potash Zone varies laterally in mineralogy, and contains "clay partings" typically at the top of each individual ore zone. Silicate minerals in the Salado Formation are quartz, illite, feldspar, chlorite, talc, serpentine, and several varieties of expandable clay, including saponite, illite-saponite and chlorite-saponite. In rock salt, the contribution of silicates is 0.004 to 2.5 weight percent in the lower part of the Salado (>2400 ft. depth in ERDA No. 9), 0.009 to 5 weight percent in the middle Salado (2000 - 2400 ft. depth), and 0.003 to 21% in the McNutt Potash Zone (above 1,650 ft. depth).

Petrographic textures reveal that significant portions of the evaporites have preserved their original depositional textures, indicating no

post-depositional recrystallization or other sorts of alteration. Other
portions have undergone extensive recrystallization to non-primary
evaporite minerals such as sylvite and polyhalite, which do not
precipitate from sea water in normal evaporation. Textures of bedded
anhydrite in the Castile Formation below the Salado Formation show a
finely laminated arrangement of evaporite and detrital materials in
alternating laminae, implying an original depositional form.
Petrographic relationships of minerals in the McNutt Potash Zone show
that at no time were these minerals in equilibrium with a solution only
of sodium chloride, also precluding the possibility of large incursions
of surface-derived water in the geologic past.

Amounts and compositions of volatile constituents in the evaporite
minerals were determined by heating rock samples to $600^{\circ}C$, recording
mass loss, and in some cases analyzing the effluent in a gas
chromatograph/mass spectrometer. Except for samples rich in hydrous
minerals (polyhalites, clay partings, potash zones), the vast majority of
rock salt contains less than 0.5 weight percent total volatiles.

The most abundant volatile constituent in that 0.5% or less is water.
Next most abundant is nitrogen, followed by CO_2. Traces of
hydrocarbons and fluorides from drilling operations were detected as
contaminants in the core.

In addition to fluid inclusions in halite, (see below), the minerals
thought to be sources of volatiles in the Salado Formation include clays
and polyhalite, and traces of gypsum, magnesite, carnallite, celestite,
glauconite, and kainite. The typical volatile content in Salado salt is
3 to 30 times less than that in the Hutchinson (Kansas) rock salt. An
additional contributor to the less than 0.5 total weight percent may be
traces of hydrated iron oxides, which account for the red-orange to
red-violet colors in some accumulations of polyhalite, sylvite,
carnallite and halite in the evaporite section.

Fluid inclusions have been studied in core samples from nineteen horizons above and below the levels of the proposed repository in Salado salt beds. The techniques used include mainly petrography, freezing stage, heating stage, crushing stage and decrepitation tests. The purpose was to determine those inclusion parameters that might be pertinent to an understanding of the origin and geological history of these salt beds.

Four general types of inclusions were found in these samples: type A - extremely abundant but minute primary liquid inclusions, with or without a tiny vacuum bubble, outlining primary growth features; type B - much larger liquid inclusions, trapped during several stages of recrystallization of the primary salt, some with a small vacuum bubble and/or unidentified daughter crystals; type C - scarce large liquid inclusions with large and variable gas bubbles under pressure, presumably from fracturing and refilling of type B inclusions; and type D - empty (i.e., gas) inclusions, found principally along grain boundaries, that have leaked and hence have lost their liquid contents.

The total weight percent of liquid as fluid inclusions in these 19 samples, as measured, ranged from 0.1 to 1.7%, mostly as type B inclusions; the amount of liquid in these same samples in situ was larger, since many of the largest inclusions, that are the major contributors to the total percentage, and the intergranular fluids, have been drained during the boring and sample preparation. The temperatures at which these inclusions were trapped were generally in the range of 25-45°C. The brines in them are never simple saturated NaCl solutions, or even NaCl-KCl solutions; freezing temperatures indicate that they must contain considerable amounts of other ions such as Mg and Ca.

When the host crystal is uniaxially stressed, the geometries of the inclusion walls show visible changes within several minutes, possibly due to solution and redeposition, as well as deformation. Internal fracturing of the inclusion walls, but generally without leakage, occurs on freezing.

The distribution of primary type A inclusions provides evidence that they have not moved visibly (i.e., less than a few micrometers at most) in that fraction of the 225 million years between original deposition and the present that these samples have been in the small but finite normal-geothermal gradient.

Subsurface samples of water from various rock types in the Delaware Basin of Southeastern New Mexico and West Texas have been analyzed for their solute contents and $^{18}O/^{16}O$ and D/H ratios. Saturated brines (total dissolved solids greater than 300,000 mg/l) were found in one well in the Bell Canyon Formation, two wells in the Castile and in potash mine seeps in the Salado. According to Cl/Br ratios (between 430 and 900), all the waters have derived their dominant solute (NaCl) from nearby rocks. Potash mine seeps and saline Capitan waters contain solutes corresponding to common primary evaporite mineral assemblages, (halite-anhydrite-kainite-carnallite-bischofite) indicative of simple uptake of dissolved solids. Bell Canyon and Morrow brines contain less magnesium but more calcium than primary evaporite assemblages, and have participated in ion exchange reactions. Stable isotope measurements indicate that Santa Rosa, Rustler and Capitan waters are meteoric, while Salado, Bell Canyon, Morrow and one of the Castile waters (ERDA No. 6) have undergone episodes of low-temperature isotopic exchange with oxygen- and hydrogen-bearing minerals. Isotopically the Carlsbad Caverns hydrologic system is unique to the Guadalupe Mountains, unrelated to the Delaware Basin as a whole.

The ERDA No. 6 occurrence of saturated $NaCl-Na_2SO_4$ brine and H_2S-rich gas (55% CO_2, 28% H_2S, 15% CH_4, 1.5% N_2 and 0.5% C_2H_6 by weight) in the Castile represents a biogenically-produced sulfide-sulfate disequilibrium. The brine's Na_2SO_4 content may have arisen by rock/fluid ion exchange involving a replacement of magnesium by sodium in the solution. None of the saline groundwaters were found to be original evaporite mother-liquors or products of partial evaporation.

Rb-Sr geochronologic study of the bedded salt deposits from the Salado Formation has been undertaken to age date the last episode of evaporite

crystallization or recrystallization, and to test their feasibility for alkali and alkaline earth retention.

Whole rock samples (i.e., water soluble plus insoluble material) are typically unsuited for Rb-Sr isochron work due to the low Rb/Sr ratio; however, several of these samples do indicate the R_o (i.e., $^{87}Sr/^{86}Sr$ at T=0) value to be about 0.708, thus indicating that large amounts of brine, typically enriched in ^{87}Sr, have not been generated in the sample area since evaporite formation some 235 ± 10 m.y. ago.

The water soluble fraction of evaporite samples yields an apparent isochron date of 206 m.y. with $R_o = 0.7084$ while clay minerals (less than two micron size) yield 325 m.y. with $R_o = 0.7123$. A composite of the water soluble fractions and clay minerals yields a date of 204 m.y. with $R_o = 0.7137$. This 204 m.y. date is interpreted as a minimum date due to the high R_o value; but it does suffice to indicate that the evaporite-clay mineral assemblages apparently have remained closed to widespread alkali-alkaline earth migration since about the time the evaporites were formed.

Regional exploration of bedded salt for a radioactive waste repository in the Delaware Basin included boreholes into the evaporites and associated rocks. One such hole, ERDA No. 6, encountered an accumulation of saturated $NaCl-Na_2SO_4$ brine accompanied by H_2S-rich gas. This fluid and fluids from other boreholes elsewhere in the area have been characterized geochemically according to solute content, $^{18}O/^{16}O$ and D/H ratios and natural actinide content. Deviations from the equilibrium $^{234}U/^{238}U$ activity ratio (α) of 1.0 were found in all water samples. These deviations are used to affirm the isolation of ERDA No. 6 and to establish bounds on the age of the ERDA No. 6 fluid.

A mathematical model for the age of ERDA No. 6 water intrusion was formulated in terms of the following variables: initial α -value (α_0) of the brine precursor waters, zero order kinetic rate constants of leaching of ^{234}Th and ^{238}U from the rocks, and degree of leaching of

[234]Th from the rocks. The model allows calculation of α-values of brines as a function of time, leach rate and α_0. Various combinations of α_0's, leach fractions and leach rates indicate that the leach rate must be low. If no leaching is assumed and the α_0 is the highest known α from the nearby Capitan Reef (α_0 = 5.2 at present), the fluid is older than 880,000 years. ERDA No. 6 brine has undergone more profound rock/fluid interactions, reflected in its solutes and stable isotopes, compared with younger meteoric Capitan waters.

The geochemistry of the proposed WIPP site shows that the mineralogy of most of the rock salt is relatively simple. The evaporites have been recrystallized, resulting in some mineral assemblages different from those precipitated from original sea-water-like solutions at one time present in the Delaware Basin. The last episode of such recrystallization took place more than 204 million years ago. The recrystallization resulted in evaporite mineral assemblages which apparently have reached thermodynamic equilibrium. The nature, distribution, geochronology and composition of fluid inclusions, clay minerals, and isolated accumulations of aqueous solutions in the evaporites show no evidence of movement of surface-derived water through the WIPP evaporites (at depths greater than 1000 feet) since their deposition in the Permian Period.

RESOURCES   (Chapter 8)

Potash salts and natural gas are the two resources of economic significance under the WIPP site. Other minerals present are halite (salt), gypsum, and caliche, but deposits of similar (if not better) quality exist in the surrounding areas. Other economic minerals and elements, including lithium, uranium, sulfur and metalliferous deposits, could exist in a geologic setting like that of the WIPP, but none appears to be present.

Potassium salts occur in a variety of mineral types, but only sylvite (KCl) and langbeinite ($K_2Mg_2(SO_4)_3$) are mined in the Carlsbad

Potash Mining District, which is the largest domestic source of potash, accounting for approximately 80% of U.S. production. The U.S. is a net importer of potassic fertilizers. The U.S. Bureau of Mines has judged that a langbeinite deposit located in the northeast quadrant of the WIPP site could be profitably mined using today's technology at the current market price for the refined product. The deposit extends beyond the bounds of the WIPP site, but about 49 million tons of langbeinite averaging on the order of 9% K_2O, lie inside the WIPP withdrawal area. Several deposits of sylvite are present, but none meet today's economic conditions; to meet them would require the market price for refined sylvite to increase from $43 to $52 or more per ton.

Natural gas accompanied with some distillate and oil with associated gas are being produced from various beds in the Delaware Basin. One particular formation, the Morrow of Pennsylvanian age, is a consistent producer in this region, and the exploration risk ("wildcatting") is justifiable in much of the western half of the site. About 37 billion cubic feet of natural gas accompanied by about 0.5 million barrels of distillate are estimated to be economically recoverable from beneath the WIPP site.

The studies also included estimation of total resources under the site, not just the resources that could be considered economic today. The U.S. Geological Survey estimates that there are 353.3 million tons of sylvite and langbeinite mineralization under the WIPP site of sufficient quality to require competitive bidding for mineral rights. The WIPP site accounts for about 7% of the potash resources that the USGS believes to be present in the Carlsbad area. Langbeinite is probably the most significant mineral resource under the WIPP site. It is a specialized agricultural fertilizer that finds its use on crops that need potassium but cannot tolerate additional chlorine. Langbeinite adds potassium but is a sulfate. Southeast New Mexico is the only economic source for this particular mineral in the free world. Langbeinite equivalent is produced from potassium and magnesium sulfates from brine lakes. A report is in preparation for DOE which will estimate the fraction of the Carlsbad district's langbeinite resources within the WIPP site.

The New Mexico Bureau of Mines and Mineral Resources studied a large area surrounding the site area, and in its judgement the total hydrocarbon resource in that area is 37.5 million barrels of crude oil, 490 billion cubic feet of natural gas, and 7.33 million barrels of distillate. While these are large quantities, they represent only about 1% of the hydrocarbon resources for southeast New Mexico.

SPECIAL STUDIES OF REPOSITORY ROCKS   (Chapter 9)

Special studies are being conducted to address issues of particular interest because the site is being evaluated for the isolation of radioactive wastes. Rocks from the WIPP site were tested in four broad areas: (1) petrography (2) physical properties (density, moisture content, resistivity), (3) thermo-mechanical properties (quasi-static and creep parameters), and 4) radionuclide sorption. Because of a scarcity of core, only those tests deemed necessary for early design were conducted. Testing at specified temperature and creep rates is continuing.

Physical properties representative of rock salt found in the WIPP horizons are summarized in the following table:

Property	Average Value* (Range)
Density	2.18 grams/cm^3
Porosity	0.5 percent (0.1-0.8)
Moisture Loss to 300°C	0.4 weight per cent (0-1.0)
Resistivity	58,100 ohm-meters (4,900-230,000)
Gas Permeability	$< 0.05 \times 10^{-6}$ darcy
Compressional Wave Velocity	4.5 km/sec (4.42-4.62)
Thermal Conductivity	5.75 w/m°K

*Except for moisture loss, values are given at 25°C
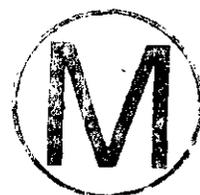
Rock salt properties are both time and temperature dependent; as a result, mechanical properties must be generated at a specific loading rate and temperature. Parameters defining the mechanical behavior at different load conditions must be inferred with considerable caution and with proper regard for the time dependent nature of the material. Quasi-static experiments were carried out at particular loading rates, e.g. 30 psi/min.

Quasi-static Properties of WIPP Rock Salt at 23 ^{o}C

Unconfined Strength	2,450 to 3,700 psi
Secant Modulus	2×10^6 psi
Principal Strain Ratio	0.25-0.35
Strain at failure:	

confining pressure	strain at failure
0 psi	2.5-6.0%
500 psi	17-20%
3,000 psi	> 20%

Tensile Strength	220 psi
Initial Yield Stress	$(\sigma_1 - \sigma_3) \approx 100$ psi

Preliminary Creep Properties

Steady State Creep Rate ($\dot{\varepsilon}$)

At 23°C:	$(\sigma_1 - \sigma_3) = 1000$ psi	$\dot{\varepsilon} = 10^{-10}$ sec^{-1}
At 130°C:	$(\sigma_1 - \sigma_3) = 2000$ psi	$\dot{\varepsilon} = 10^{-7}$ sec^{-1}

Results analyzed to date indicate that WIPP salt may undergo both transient and steady-state creep. However the latter is a tentative observation as occurrence of steady-state creep is uncommon. Indeed, if steady state creep occurs under loading conditions expected in the WIPP,

design calculations should consider creep in detail. This most likely will be of concern if elevated temperatures are involved. Although present considerations of steady-state creep are incomplete, it appears that steady-state creep rates range from 10^{-10} to 10^{-7} /sec. The transient creep results indicate that pressure, principal stress difference and temperatures are strongly coupled. Furthermore, of these three, temperature appears to have the most dramatic effect on the creep rate.

Data from the petrographic and physical properties studies show the WIPP horizon rock salt has low moisture content (less than 0.5%), is essentially impermeable (less than 5×10^{-8} darcy) and has a high thermal conductivity (about 5.75 watts/m$^{\circ}$K). These properties, along with the studies of fabric and fracture, indicate that this rock salt is ideally suited from a physical standpoint for the storage of heat producing radioactive wastes.

It has been shown that rock salt can experience large creep strains (greater than 25%) prior to loss of load bearing capacity. Gradual creep is an acceptable feature in the design of underground openings in rock salt as it allows the structure to close without a reduction in bearing strength. As long as allowances for creep are incorporated into design and the shape of the opening does not create large shear stresses, the WIPP rock salt can be expected to sustain stable openings.

A survey of the potential of geological media from the vicinity of the WIPP site in southeastern New Mexico for retardation of radionuclide migration in an aqueous carrier was conducted. The survey included the measurement of sorption coefficients (Kd) for twelve radionuclides between three natural water simulants and ten samples from various geological strata.

The nuclides included ^{137}Cs, ^{85}Sr, ^{131}I, ^{99}Tc, ^{125}Sb, ^{144}Ce, ^{152}Eu, ^{153}Gd, ^{106}Ru, ^{243}Am, ^{244}Cm, and ^{238}Pu. The compositions of the simulant solutions were those expected of water in contact with halite

deposits in the area and in a typical groundwater found in the Delaware Basin. The geological samples were obtained from potential aquifers above and below the proposed repository horizons and from bedded salt deposits in the repository horizons.

In brine solutions, Tc and I were not significantly adsorbed by any of the minerals and Cs and Sr showed minimal adsorption (Kd's < 1). The lanthanide and actinide Kd's were typically > 10^3 and Ru and Sb Kd's varied in the range of 25 to > 10^3. In the groundwater simulant, Tc and I showed the same behavior, but the Kd's of the other nuclides were generally higher.

Some initial parametric studies involving pH, trace organic constituents in the simulant solutions, and radionuclide concentrations were carried out. Differences in the observed Kd's can result from varying one or more of these solution parameters.

The WIPP site rocks, including rock salt, show an affinity for radionuclide sorption ($K_d > 0$). Even small values of K_d ($0 < K_d < 1$) are effective in retarding the movement of radionuclides in groundwaters.

It is not anticipated that results of these special studies will be pivotal in site selection; rather, they are being performed to provide additional confidence in geologic isolation in bedded salt.

CONTINUING STUDIES (Chapter 10)

Although much detailed information has been reported here as a result of site selection and characterization, there remain a number of programs which have not come to completion, or in some cases, have not begun. These pending programs are aimed at refining and supplementing information gathered to increase the confidence to be placed in factors relating to site selection. Furthermore, some kinds of information remain to be gathered to support laboratory and in-situ experiments and long-term safety assessment.

In regional geology, paleoclimatic studies based on detailed geologic mapping, geomorphology studies, microfossils, and age-dating are planned to provide a history of past climatic changes and to help assess the possible effects of future changes. Tectonic studies, involving examination of LANDSAT photos and accompanying field evaluation, first-order levelling surveys, and seismic monitoring of structural features adjacent to the Delaware Basin will continue to provide an account of the dynamic forces which might affect the Basin.

Continuing studies in site geology are aimed at expanding the details of site characterization for the purpose of refining site-specific safety assessment modeling scenarios for the repository. Geologic mapping is being undertaken to establish the local geomorphologic stability. High resolution aeromagnetic surveys will be implemented to provide greater confidence that possible geologic anomalies such as breccia pipes and igneous dikes have been identified and may be examined and sampled in detail.

Seismological studies will continue to document and evaluate the seismicity of the region due to various sources (mining, secondary hydrocarbon recovery, tectonic activity). The data will assure the appropriate seismic risk has been assumed in facility design and will further the safety assessment in general.

Hydrological studies will continue to expand the area around the site for which the groundwater behavior is characterized. In addition to hydrologic monitoring points near site center and periphery, a system of points will be established in nearby Nash Draw to evaluate the relationships among groundwater movement, evaporite dissolution and resulting subsidence. Also, investigations of "breccia pipes" will be undertaken to improve our understanding of why, how and when these features developed. The hydrologic monitoring system will provide the basis for development of a regional groundwater model to be used in safety assessment, and will be evaluated as a monitoring tool for repository-induced changes in the groundwater system.

Continuing studies in geochemistry are designed to support other investigations (such as the examination of dissolution products), provide detailed characterization of geologic materials to be used in in-situ and laboratory experimental programs (such as waste-rock interactions) and to contribute towards our understanding of the nature of Ochoan evaporites in general. These studies include mineralogy, petrology, volatile and fluid inclusion analyses, major, minor and trace element analyses in rocks and fluids, age-dating, stable isotopes, and examination of dike-evaporite interactions as a partial analogue of waste-evaporite interactions.

There are no continuing studies of resources planned at the WIPP site.

Continuing special studies of rock properties include long-term creep analyses in various temperature regimes, micromechanics of rock deformation, migration of volatiles, and mechanistic studies of radionuclide sorption on rocks. Some of these special studies are designed to provide an understanding about differences in mineralogy, grain size, volatile content and rock fabric which are to be found at different in-situ test horizons. The physical properties of the various horizons will be examined with these variations in mind. Non-salt horizons, which may be significant in the development of refined models for calculation of repository effects, will also be tested.

Continuing studies of radionuclide sorption include measurements of dynamic sorption from fluids flowing through columns of WIPP rocks in laboratory environments. In addition, parametric studies will continue to determine changes in sorption which accompany changes in mineralogy, pH, oxidation state, radionuclide concentration, and concentrations of organic contaminants. The rates at which sorption takes place and the differences between the processes of sorption and desorption will be investigated.

INTRODUCTION

The purpose of this chapter is to provide introductory information concerning the function of the WIPP and to discuss the site selection criteria and factors affecting the criteria; the criteria and factors are specific to the WIPP and to the Delaware Basin of southeastern New Mexico. In addition, some of the site exploration techniques are briefly mentioned here as background to further discussion of geological characterization.

2.1 THE PURPOSE OF WIPP

The purpose of the WIPP should be understood clearly as it is distinct from that of several other projects for the disposal of radioactive waste. The WIPP will demonstrate disposal technology for the transuranic (TRU) waste resulting from this nation's defense programs of over 30 years. After a period (5-10 years) of limited (pilot) operation it is anticipated that the WIPP will be converted to a full-scale repository for permanent disposal of defense TRU waste. Secondly, the WIPP is to provide a research facility to examine, on a large scale, the interactions between bedded salt and high-level radioactive waste. These interactions will involve physical and chemical phenomena resulting from thermal and radiation fluxes. A DOE Task Force (DOE/ER-0004/D, 1978) has recommended that WIPP also be used to demonstrate surface and subsurface methods of handling, storing and disposing of up to 1,000 canisters of spent reactor fuel; however, a decision on this recommendation has not been made at this time.

If the site is accepted by the DOE, the schedule calls for the initiation of facility construction in 1981; completion is to be about 1985, and the first waste to be accepted in 1986. The conceptual design of facilities is complete. The Draft Environmental Impact Statement and this Geological Characterization Report for DOE are presently scheduled for completion in late 1978. DOE has expressed an intent to request

licensing of the WIPP by the Nuclear Regulatory Commission (NRC), but
this policy is presently under discussion between the DOE and Congress.

2.2   PURPOSE OF GEOLOGICAL CHARACTERIZATION REPORT (GCR)

The purpose of the GCR is to provide an account of the known geotechnical
information considered relevant to site selection (see Section 2.3) for
the proposed WIPP site. The GCR presents background information as well
as information regarding factors related to selection criteria; for the
most part, specific judgements regarding the suitability of the site are
not made. Those judgements and recommendations are the function of other
processes and documents. The GCR is neither a Preliminary Safety
Analysis Report nor an Environmental Impact Statement; these documents,
when prepared, should be consulted for appropriate discussion of safety
analysis and environmental impact. The GCR is intended as a source
document on the geology of the WIPP site for individuals, groups, or
agencies seeking basic information. Therefore, rather extensive
reference lists of reports and documents are provided at the end of
chapters for the reader who may desire extended detail concerning
particular geotechnical subjects discussed in this report. The GCR is
not intended to present primary source material, and the instances of
reporting original data or information in this document have been limited.

2.3   SITE SELECTION

Within this document, "site selection" primarily refers to the activities
whereby the Los Medanos (or other) area is evaluated, on geotechnical
grounds, as to whether it is an acceptable location for the WIPP.
"Preliminary site selection" may be used here or elsewhere as a
description of the activities which result in selecting a site for
characterization; the characterization of such a site establishes
technical grounds for the more specific site location of the WIPP. "Site
selection" has also been described as that action which results when all
technical aspects of establishing a repository site have been satisfied.
For the WIPP studies, this latter action is termed "site confirmation";

the criteria for "site confirmation," which means conversion to a repository, will in part be developed through operation of the WIPP as a demonstration facility. Because of unforeseen geological occurrences or enhanced understanding of geological processes, final satisfaction regarding the geological suitability of the site for a repository may not develop until significant portions of the underground workings are explored and studies of geological processes finished. Site selection here refers to the position that most, if not all, of the extant geological characteristics are favorable to the WIPP; the rates of some geological processes may require further examination to reduce that uncertainty with regard to specific detailed effects on a repository. Site selection for the WIPP is not to be interpreted as a guarantee that a repository will be established.

2.3.1   History of WIPP Site Selection Effort

The sequence of events which has culminated in the WIPP site selection activities in the Delaware Basin of southeast New Mexico began in 1955 when the Atomic Energy Commission (AEC) requested the National Academy of Science (NAS) to examine the issue of permanent disposal of radioactive wastes. The Academy's Committee on Waste Management issued a report (NAS/NRC Report) in 1957 in which they stated, "The most promising method of disposal of high-level waste at the present time seems to be in salt deposits." This recommendation initiated several years of research, directed by Oak Ridge National Laboratory (ORNL), on the phenomena associated with disposal of radioactive waste in salt. In 1961 (NAS/NRC Meeting Minutes, December, 1961), the NAS waste management committee reaffirmed its position on the use of salt beds for disposal commenting that "Experience both in the field and in the laboratory on the disposal of wastes in salt have been very productive and well conceived; plans for the future are very promising." Pierce and Rich (1962) reported on salt deposits in the United States that might be suitable for disposal of radioactive wastes. The Delaware Basin was one of these areas discussed. The ORNL research was expanded to include a large-scale field program in which simulated waste (irradiated fuel elements), supplemented

by electric heaters, was placed in salt beds for observation of the resulting phenomena. This experiment, called Project Salt Vault (Bradshaw and McClain, 1971), was conducted in an existing salt mine at Lyons, Kansas, from 1963 to 1967. Results from this program were favorable, and no unacceptable phenomena occurred which would rule out salt as a repository medium. The NAS committee again reviewed and endorsed the NAS position regarding disposal in salt (NAS/NRC Report, 1966). In June, 1970, the Lyons site was tentatively selected by the AEC as the location for a radioactive waste repository. The concept and location were conditionally endorsed by the NAS committee in November, 1970 (NAS/NRC, 1970). Conceptual design for a facility accommodating both transuranic (TRU) and high-level waste (HLW) was completed in 1971. During 1971, as plans for the repository proceeded, two technical problems arose. The first involved the presence of a large number of existing boreholes in the vicinity of the repository which penetrated through the salt beds into underlying aquifers. There was concern that not all these holes could be adequately plugged and that not all such drill holes were on record and identified. This prospect meant that borehole dissolutioning and eventual breaching of the repository could not be ruled out. The second concern related to the solution mining being carried on by the American Salt Mining Company about three miles from the proposed repository but only 1700 feet from an extension of the Carey Salt Mine which was to contain the repository. The revelation that large volumes of water were unaccountably "lost" in the hydraulic fracturing and solution mining was regarded as illustrating a mechanism threatening to the repository site. This site was opposed by the Director of the Kansas Geologic Survey and political opposition within the state increased. By early 1972, the proposal for a repository at Lyons was abandoned and a much expanded search for a suitable repository site was commenced. Other potential sites in the state were identified by the Kansas Geological Survey, and the United States Geological Survey (USGS) examined potential salt sites in other areas of the United States.

After a nationwide search for a suitable repository site (Pierce and Rich, 1962; Anderson et al., 1973; Bachman and Johnson, 1973; Hite and

Lohman, 1973; Jones et al., 1973; Mytton, 1973; Ekren et al., 1974), the USGS and ORNL selected the Permian Basin in New Mexico as best satisfying their site selection guidelines. Four locations within this area were examined in more detail (Brokaw et al, 1972; Jones et al, 1973; Jones, 1974a; Jones, 1974b), and a location in the Los Medanos area, about 30 miles east of Carlsbad, New Mexico, was chosen for exploratory work. One of the most restrictive site selection criteria, primarily because of the Lyons experience, was avoidance of drill holes penetrating through the salt within two miles of the repository border. This criterion caused the potential site to be shifted twice within the Los Medanos area as oil/gas wells were drilled in the vicinity. The eventual site selected by ORNL was located on the Eddy-Lea county line, 30 miles due east of Carlsbad, New Mexico.

Field investigations began at this site in March, 1974, with the drilling of core holes AEC 7 (3,918 feet deep) and AEC 8 (3,028 feet deep) at the northeast and southwest corners of the 1 1/2 by 2 mile rectangular site. The data from these holes was considered satisfactory by ORNL, but further work at the site was suspended in May, 1974. This suspension was due in part to a shift in AEC waste management emphasis to retrievable surface storage facilities (RSSF) and in part to a reluctance at the commission level to ask for land withdrawal to set aside the necessary area for the repository and its protective "buffer" zones.

Sandia received program funding to continue field investigations in southeastern New Mexico on March 31, 1975. Geologic investigations resumed at the ORNL site in May, 1975. Extensive review sessions with ORNL and the USGS covered past efforts in site selection. Studies conducted by the USGS and ORNL consultants on regional geology, seismicity, hydrology and solutioning of salt were re-evaluated. Sandia concurred that the northern Delaware Basin seemed appropriate for siting a waste repository.

In the opinions of both ORNL and USGS, the two core holes, AEC 7 and 8, indicated acceptable subsurface geology at the ORNL site. The first

Sandia task, therefore, was to confirm this by additional drilling and geophysical investigations. Core hole ERDA 6 was initiated in May, 1975, at the northwest corner of the ORNL site. ERDA 6 encountered unexpected subsurface geology. Formation contacts were much higher than anticipated, and salt and anhydrite beds exhibited severe distortion with dips up to 75 degrees. Sections of the upper Castile Formation were missing, and the fractured anhydrite encountered at a depth of 2710 feet contained a pocket of pressurized brine. The unpredictability of the detailed geology at this site was not compatible with Sandia requirements for the pilot plant; therefore, site selection activities were expanded. Reconsideration of site selection guidelines in light of the results of continuing studies and exploration in southeast New Mexico led to the adoption of additional guidelines and some modification of the original guidelines. Evaluation of oil company seismic and drilling data and the resultant structural contours on the Castile Formation confirmed deformation of Castile salt beds in a band about five miles wide paralleling the Capitan Reef front. Since this deformation and the distortion of the geologic units encountered in ERDA 6 was believed due to gravity-induced buckling of salt beds abutting against the Capitan Reef, an additional site selection factor was established requiring a site area to be at least six miles from the reef front.

The proximity of boreholes penetrating the salt formations, another site selection criterion, was re-evaluated during this period. Analytical studies and field research conducted for ORNL after the Lyons, Kansas, borehole problems allowed a more quantitative judgement (Snow and Chang, 1975; Walters, 1975). In the Los Medanos area, a requirement to separate the repository from boreholes penetrating through the salt by one mile seemed quite conservative and was adopted. This buffer would assure more than a quarter million years of isolation using very conservative flow assumptions. While improved borehole plugging and study of the consequences of an unplugged hole may make such holes acceptable even closer to the repository, neither has yet been demonstrated.

The New Mexico portion of the Delaware Basin was re-examined by both the USGS and Sandia in late 1975. On November 14, 1975, the USGS recommended an area about seven miles southwest of the ORNL site for further examination. Sandia had independently selected the same area as showing the most promise for a repository site. Considerable geologic data were available in this region from oil/gas wells and from shallow drill holes used to explore for potash. In a regional study, the USGS found that initial dissolution of Salado salt, the formation of interest, was sufficiently distant from the proposed site that dissolution would pose little, if any, threat to the WIPP. The three-square mile repository could be located to avoid the known potash area (KPA) and to be at least one mile from all boreholes penetrating through the salt. No private (fee) land and less than three sections of state land were present in the potential withdrawal area. A stratigraphic core hole, ERDA 9, was started in parallel with geophysical studies of the area. ERDA 9, drilled in the center of the area under study, revealed the expected geology and indicated the desired flat bedding (dips are about 75 feet/mile). Physical properties of the salt beds were found to be satisfactory; beds at depths of about 2100 and 2600 feet were selected as appropriate for TRU and heat-generating wastes respectively. Consequently, an extensive program of site evaluation and laboratory investigation was begun and is continuing as of the date of this report (August, 1978). Sufficient information has now been developed to allow the site to be adequately characterized for site selection purposes.

2.3.2 General Location and Land Requirements of WIPP Facility

Figure 2-1 shows the general location of the Los Medanos site within the regional geographic setting. The nearest town is Loving, New Mexico, (population about 1100) 18 miles west-southwest of the site. Carlsbad, New Mexico, (population about 25,000) is 26 miles west of the site, and Carlsbad Caverns National Park is about 40 miles to the southwest.

Figure 2-2 is a diagram of the WIPP site showing proposed land use controls around the limits of the underground facilities (Zone II).

Engineering studies had indicated that approximately 3 square miles were desired for ultimate development of underground facilities at the WIPP site, necessitating the restriction of land use within an equivalent area of land at ground surface. *Administrative control of additional land* (Table 2-1) will also be required beyond the boundary of the excavated area to protect the repository: a mile-wide restricted zone around the repository in which, for the present, no underground mining, excavation, or through-going boreholes will be considered (Zone III); and an additional mile-wide buffer zone in which limited (i.e. subject to control and regulation by DOE) underground mining and deep drilling will be allowed (Zone IV). "Hydrofracing" and other injection methods of hydrocarbon recovery, and any kind of solution mining, would be prohibited. This zonation is shown in Figure 2-2, (which also indicates the corresponding total acreage of restricted land needed for the WIPP site). On the surface, only the plant site itself (Zone I) will exclude land access.

The irregular pattern of the outer boundary of the WIPP site (Figure 2-2) originated from a desire to conform to the Bureau of Land Management's (BLM) land subdivision system and to exclude private land and producing wells. The WIPP program plan calls for the entire area within this boundary to be brought under control of the DOE. The inner boundaries that define restricted areas are polygonal, designed to minimize the area to be withdrawn while achieving optimum conformance to the siting criteria.

2.3.3   General Considerations and Requirements of Underground
         Storage Facilities for Radioactive Waste

Neglecting consideration of surface restrictions and land use conflicts for the purposes of this report, geotechnical siting requirements for an underground radioactive waste repository are ultimately determined by: 1) the physical (including thermal), chemical and radioactive interactions between the waste and the surrounding media, 2) the type of rock chosen in which to place the repository, and 3) the level of

assurance desired against failure of the containment. While WIPP is anticipated to be a repository for defense transuranic waste, Sandia was also requested to consider possible future options for high-level waste in its site selection studies of bedded salt in the Delaware Basin. For WIPP, the desired goal is complete isolation of waste with negligible consequence in the event of containment failure for the total duration of time in which the radioactivity of the waste could constitute a potential hazard to the biosphere or humans in general.

These unprecedented long storage requirements, which embrace a small but significant interval of geologic time, call for a careful characterization of long-term hydrologic, geologic and climatic processes, potentially affecting stability and survival of the underground facility, in order that appropriate siting criteria may be specified. These and other considerations in the long-term management of radioactive wastes have been defined and discussed in ORNL reports by Gera and Jacobs (1972) where they identify geologic processes relevant to waste disposal and discuss the suitability of various geologic media for radioactive waste storage. Claiborne and Gera (1974) describe and evaluate potential mechanisms of containment failure and of hydrologic release of contaminants from the bedded salt deposits in the southeastern New Mexico area. The conclusions and recommendation of these studies, which are not repeated here, have been utilized as guidelines in formulating siting criteria employed in the selection of candidate site locations in the Delaware Basin area of southeastern New Mexico. Regarding the overall danger of contamination from properly sited underground waste storage facilities, however, it is appropriate for proper perspective to repeat the observation of Claiborne and Gera (1974, p.4) that

> "the conditions required for a serious release of activity to the biosphere from a repository in bedded salt tend to approach the bizarre and have considerably less credibility than the 'maximum credible accident' assumed for nuclear power plant safety analyses."

2.3.4 Initial Screening Criteria and Selection of the Original (ORNL) Site in the Delaware Basin

Preliminary site screening studies for an underground waste isolation storage facility in the Delaware Basin were initiated jointly in 1972 by ORNL and the USGS for the AEC. Guidelines developed at that time were mostly contained in the ORNL report by Gera and Jacobs (1972) and in ORNL-TM-4219, which, however, did not address conditions in the southeastern New Mexico area specifically. Geologic information was assembled by the USGS for use in evaluating the suitability of various areas in the Delaware Basin for disposal of radioactive wastes; this information appeared in open-file form in the report by Brokaw, et al. (1972). Additional data by Bachman, et al. (1972) appeared as an ORNL report.

Large-scale (Stage I) site screening criteria (ORNL-TM-4219) were developed and were employed in an initial selection of a site at the Lea-Eddy County boundary, about 7 miles northeast of the present WIPP site. In addition to the usual geologic standards some technical criteria which were applied by ORNL were as follows (Griswold, 1977, p.12):

A two-mile radius from any boring through the Ochoan evaporites down into the Delaware, or deeper formations.

No active mining within five miles.

Salt of high purity at depths of less than 3,000 ft.

A minimum depth to suitable salt of 1,000 ft.

Avoidance of obvious mineral resources to the extent possible.

The maximum depth indicated was solely a mine engineering criterion dictated by the viscous flow potential of salt at pressures exerted by the lithostatic loading and at temperatures imposed by the expected geothermal gradient coupled with the maximum thermal flux of the stored waste; the minimum depth was that considered adequate to insure against disinterment by erosion.

Figure 2-3 shows the results of this initial screening process. A two-mile radius from deep wells proved to be the most restrictive criterion; on the figure the shaded areas indicate land, more than two miles from deep wells, also satisfying the depth and mineral resource exclusion criteria. The site initially selected by this method is also indicated.

Cores from AEC Nos. 7 and 8 intercepted leasable grades of potash; ERDA No. 6 cores did not. However, at ERDA No. 6, evidence of complex evaporite structure and the encounter of an artesian flow of brine were sufficient evidence that this original site was unsuitable and that more information would be needed to define additional criteria to be used in selection of acceptable alternate sites.

2.3.5 Site Selection and Evaluation Criteria for the Los Medanos Site

When the initial Delaware Basin repository study area was shown to be unacceptable, Sandia undertook the task of locating a satisfactory site in the New Mexico portion of the Delaware Basin. By late 1975 a more complete understanding of the geology of the basin and of potential repository failure mechanisms permitted a reformulation of siting criteria and site selection factors. These criteria and factors were developed rather specifically for the Delaware Basin in southeastern New Mexico, and are neither generic criteria for bedded salt nor generic criteria for all rock types.

Some of the specific studies contributing to this effort include the following: Claiborne and Gera (1974) considered potential failure modes of bedded salt containment in the Delaware Basin; Bachman and Johnson (1973), Jones (1973), Bachman (1974) and Piper (1973) reported on geologic and hydrologic conditions in the Permian Basin region and in the Delaware Basin in particular; Jones (1975) discussed potash deposits; and Foster (1974) and Netherland, Sewell and Associates (1975) investigated hydrocarbon resources. Reports on dissolutioning associated with unplugged boreholes (Snow and Chang, 1975; Walters, 1975; Pader, 1973)

were also available. The selection of additional alternate sites made in November, 1975, utilized this information. Two factors which received careful attention because of the experience gained in locating and evaluating the original site were the existence of salt flow structures and associated brine pockets and the dissolution potential of man-made penetrations through the evaporites.

Siting factors were formulated to eliminate from further consideration areas of possible severe structural deformation or complexity of the salt beds. Geologic evidence (Jones, 1973) indicated the tendency for greater structural complexity to occur in salt beds adjacent to the Capitan reef front. Substantial salt deformation resulting in displacement and fracturing of anyhdrite beds was encountered in ERDA-6. Structural contouring of the Castile Formation, based on petroleum drilling and seismic reflection data, indicate this distortion of salt is most severe in a belt, about five miles wide, paralleling the reef front. Accordingly, a belt with a width of six miles basinward from the Capitan reef was eliminated from eligible areas. This also served to avoid any possible dissolution hazards which might be associated with the reef. Known locations of artesian brine flow appeared to be related to anticlinal features in the subsurface; therefore, the avoidance of pronounced anticlinal structures in salt was adopted as a selection factor.

The extent of deep drilling, resulting from hydrocarbon exploration in the Delaware Basin, indicated that a careful evaluation of the required separation from boreholes be performed. Desirable regions could be excluded from consideration if this factor was unduly restrictive. The two mile separation distance established after the Lyons, Kansas, experiences, was modified to one mile based on studies by Snow and Chang (1975), Walters (1975), and Fader (1973). These studies improved prospects for assuring plugging of boreholes, and the hydrologic conditions expected in the acceptable portions of the Delaware Basin all indicate that a one-mile buffer zone is amply conservative against potential borehole dissolution (Griswold, 1977, p. 12). Figure 2-4 shows

areas that are more than one mile from boreholes penetrating into the
Delaware Mountain Group. Avoiding these boreholes would also result in
avoiding existing oil or gas fields.

In addition to the salt anticline and borehole restrictions already
mentioned as assuming a primary role in narrowing the choice of
acceptable sites, several other aspects proved to be significant for the
northern portion of the Delaware Basin. Proximity to the dissolution
front at the top of the Salado Formation and the existence of local
solution features were prime considerations.

Although open joints, fractures or faults are not expected to occur in
salt, intrusions in the form of igneous dikes which pass through the salt
beds are known to exist locally in the Delaware Basin. The proximity of
such a feature might be cause for rejection of a site for geologic,
hydrologic and engineering reasons. Shown in Figure 2-5 are areas where
undesirable structure, such as salt deformation, brine-flow anticlines,
or dike trends, are known or presumed to occur; the dike trend is
magnetically expressed and is defined by magnetic survey methods.

Candidate sites should be located in areas affording adequate long-term
protection against encroachment of salt dissolution. Surface dissolution
was assumed to be related to downward percolation of meteoric water and
removal through Nash Draw and the Pecos drainage system. In addition,
evidence of possible dissolution in salt over the Capitan reef aquifer is
known in such places as San Simon Sink. Dissolution fronts, or
boundaries at which salt has been or is being dissolved from the
enclosing rock material, had been recognized at various horizons in the
evaporite sequence of the Delaware Basin. Rates of dissolution were
estimated by Bachman (1974), and longevity of Salado salt was diagrammed
by Jones (1973, Figure 7). These observations were translated into
appropriate avoidance criteria. Dissolution of salt in the Rustler
Formation was not considered to be a significant hazard to a repository
located in the lower part of the Salado; however, areas that exhibit
extensive salt dissolution at the top of the Salado would be rejected.

For conservatism, sites that would be in, or within a mile of, areas of
known dissolution at the top of the Salado were considered less
desirable. Figure 2-6 displays areas where dissolution at the top of
Salado was indicated to occur, based on studies current at that time.

The interception of commercial grades of potash by holes AEC-7 and AEC-8
and the known occurrences of potash nearby highlighted the necessity of
evaluating the potential of this resource to assess possible resource
conflict. Areas of potash mineralization meeting minimum grade and
thickness criteria, termed the "potash enclave" by Aguilar et al. (1976),
would be avoided to the extent possible by the three square mile core of
the site. Regarding possible conflict with hydrocarbon reserves, the
avoidance of deep drill holes automatically insures that a potential site
would not be located over an existing oil or gas field. To minimize the
possibility of siting over areas having favorable potential for discovery
of additional hydrocarbon reserves, oil and gas trends in the subsurface
beneath a possible site location would be considered in siting the
repository. The locations of such trends are shown in Figure 2-7.

Finally, with regard to land ownership, the land withdrawn should be
federally owned to the extent possible to expedite site exploration and
land withdrawal. Potash lease rights would be avoided by Zones I and II
to the extent feasible.

2.3.6 Site Selection: Criteria and Factors

Two principal stages are involved in establishing a nuclear waste
repository. The first stage, outlined mainly in the previous section
(2.3.5), involves preliminary site selection of the most desirable site
from among the potentially acceptable study areas. This selection is
based on application of criteria and selection factors to the existing
knowledge and general reconnaissance information available for the
areas. Specific and detailed studies are not conducted at this stage.
The second stage is to determine the characteristics and processes
affecting a site or sites sufficiently well to allow confirmation of a

site for a repository. It is possible that this detailed study will reveal that some factors are less than ideal. It is unlikely (and unnecessary) that a site will be ideal with respect to all selection factors. Similarly, it is unnecessary and, indeed, impossible to prove that the "best" site has been selected. The extent of investigation in stage two is such that all prospective sites cannot be examined in this detail. Rather it is sufficient to establish that an adequate, safe, and acceptable site has been identified. This knowledge requires that potential failure modes and hazards be recognized and that siting factors take them into consideration.

For the WIPP, the facility demonstration and additional studies of processes and underground geology will lead to further development of criteria for a repository and subsequent assessment of the safety of the WIPP site as a repository. Thus, at least for WIPP, it is necessary to refine criteria, through operation and continued study, sufficient for confirmation as a repository.

For site selection of the Los Medanos site the following criteria and the factors which address those criteria are listed. In most cases, the nature of the factor desired can be indicated but not quantitatively specified a priori since the acceptable combinations of factors under the multiple barrier concept is so large. Many of the desired factors are just that - desired. They are sufficient but may not be necessary for long-term repository safety. The general relationship of factors to WIPP studies is indicated by referring to principal chapters containing information about particular factors.

    Geology Criterion: The geology of the site will be such that the repository will not be breached by natural phenomena while the waste poses a significant hazard to man. The geology must also permit safe operation of the WIPP.

Factors: Topography - Must permit access for transportation.
Effect on inducing salt flow during excavation must be
considered. Surface water flow and future inundation
must be evaluated. (See 3.2, 4.2)

Depth - Repository horizons should be deeper than 1000
feet to assure erosion and consequences of surficial
phenomena are not a major concern. Depth of suitable
horizons will not exceed 3000 feet to limit rate of
salt deformation around the excavations. (See 3.3,
4.3, 9.2)

Thickness - Total thickness of the salt deposits
should be several hundred feet to buffer thermal and
mechanical effects. The desired thickness for the
repository bed is 20 feet or more to mitigate the
thermal and mechanical effects at non-halite units.
(See 4.3.2, 9.2)

Lateral Extent - The distance to structural or
dissolution boundaries must be adequate to provide for
future site integrity. For the Los Medanos area a
distance of five miles to the Capitan reef and one
mile to regional Salado dissolution have been
established. (See 3.3, 4.3, 6.3)

Lithology - Purity of the salt beds is desirable to
reduce the brine content of the salt. Pending further
investigations, three percent brine is established as
a desirable upper limit for the heat-producing waste
horizon. Additional geochemical interactions must be
considered if significant chemical or mineralogical
impurities are present. (See 4.3, 7.2, 7.3, 7.4, 7.5,
7.6)

Stratigraphy - Continuity of beds, character of
inter-bedding and nature of beds over- and underlying
the salt are important considerations in construction
of the facility and in assessment of possible failure
scenarios. (See 3.3, 3.4, 4.3, 4.4)

Structure - Relatively flat bedding ($< 3°$) is
desirable for operational purposes. Steep anticlines
and major faults are to be avoided. (See 3.4, 4.4)

Erosion - While the depth factor reduces concern for
erosion it is desirable to avoid features which would
tend to localize and/or accelerate erosion. (See
3.2.3, 3.6, 4.2, 4.5, 6.2)

Hydrology Criterion: The hydrology of the site must provide high
confidence that natural dissolution will not breach the
site while the waste poses a significant hazard to man.
Accidental penetrations should not result in undue hazards
to mankind.

Factors: Surface Water - Present and future run-off patterns,
flooding potential, etc., should not endanger the
penetrations into the repository while these openings
are unplugged. (See 6.2)

Aquifers - For WIPP, the over- and underlying aquifers
represent a secondary barrier if the salt is
breached. Consequently low permeability and
transmissivity are desirable but not mandatory.
Accurate knowledge of aquifer parameters is important
to construction, decommissioning and realistic
calculation of the consequences of failure scenarios.
(See 6.3)

Dissolution - Regional and/or local dissolution must
not breach the repository while the wastes represent a
significant hazard to man. While there are various
suggestions for the time a repository should remain
isolated from the biosphere, 250,000 years (ten
half-lives of ^{239}Pu) is one period which may be
sufficient for evaluating the WIPP site. (See 6.3.6)

Subsidence - Subsidence due to dissolution of salt
will be avoided when the subsidence adversely affects
the repository beds or unduly accelerates the rate of

dissolution to the jeopardy of long-term integrity of
the repository. (See 6.3.6, 10.6)

Hydrologic Transport - For the WIPP, this is a
secondary factor which must be evaluated to allow
quantitative calculations of the consequences of
various failure scenarios. Slow transport of isotopes
is acceptable if more critical factors have been
satisfied. (See 6.3, 9.3. 10.6)

Climatic Fluctuations - Possible pluvial cycles must
be considered when estimating the effects of the above
factors. (See 3.6, 4.5, Chapter 6, 10.3)

Man-made Penetrations - The effect of drill-holes and
mining operations on the site selection must be
evaluated in considerations of dissolution.

Tectonic Stability Criterion: Natural tectonic processes must not
result in a breach of the site while the wastes represent a
significant hazard to man and should not require extreme
precautions during the operational period of the repository.

Factors: Seismic Activity - The frequency and magnitude of
seismic activity impacts facility design and safety of
operation. Low levels of seismicity are desirable but
facility design can accommodate higher levels as
well. (See Chapter 5, 10.5)

Faulting/Fracturing - While open faults, fractures or
joints are not expected in salt, the more brittle
units within and surrounding the salt may support such
features which can enhance dissolution and hydrologic
transport. Major faults and pronounced linear
structural trends should be avoided. (See 3.4, 4.4)

Salt Flow/Anticlines - Major deformation of salt beds
by flow can fracture brittle rock and create porosity
for brine accumulations. Major anticlines resulting
from salt flow should be avoided or evaluated to check
on brine presence and anhydrite fracturing. (See 4.4)

Diapirism - An extreme result of salt flow, this
feature will be avoided for WIPP siting. (See 4.4)

Regional Stability - Areas of pronounced regional uplift or subsidence should be avoided since such behavior makes anticipation of future dissolution, erosion and salt flow more uncertain. (See 3.4, 4.4, 10.3.2)

Igneous Activity - Areas of active or recent volcanism or igneous intrusion should be avoided to minimize these hazards to the repository. (See 3.5)

Geothermal Gradient - Abnormally high geothermal gradients should be avoided to allow construction in salt at 3000 feet. High gradients may also be indicative of recent igneous or tectonic activity. (See 4.4.1)

Physico-chemical Compatibility: The repository medium must not interact with the waste in ways which create unacceptable operational or long term hazards.

Factors: Fluid Content - The repository bed containing high level waste should not contain more than three percent brine. The limit for TRU waste has not been established, but the same value used for HLW is acceptable. (See 7.5, 10.7.8)

Thermal Properties - No major natural thermal barriers should exist closer than 20 feet to avoid undesirable temperature rises. (See 4.3, 9.2.3)

Mechanical Properties - The medium must safely support excavation of openings even while thermally loaded. Clay seams and zones of unusual structural weakness should be avoided in selection of the repository horizon. (See 9.2.4)

Chemical Properties/Mineralogy - Beds of unusual composition and/or containing minerals with bound water should not occur within 20 feet of the waste horizon. This will lessen the uncertainties with regard to thermally driven geochemical interactions. (See 4.3, 7.2, 7.3, 7.4, 7.5)

Radiation Effects - While no unacceptably deleterious effects are postulated, these phenomena are best quantified in halite and thus the purer rock salt beds are desired for high- level waste. (See 9.3)

Permeability - Salt has very low permeability and only the inter-beds and surrounding media are considered for siting with respect to this factor. Low permeability is desirable, but quantitative limits need not be specified for site selection. (Salt permeability to gases may be important in establishing waste acceptance criteria.) (See 9.2.3)

Nuclide Mobility - This is a secondary factor in siting since confinement by the salt and isolation from water is the basic isolation premise. Ion sorption must be determined to allow quantification of safety analyses and to indicate whether engineered barriers (clay) would be beneficial. (See 9.3)

Economic/Social Compatibility Criterion - The site must be operable at reasonable economic cost and should not create unacceptable impact on natural resources or the biological/sociological environment.

Factors: Natural Resources - Unavoidable conflict of the repository with actual or potential resources will be minimized to the extent possible. (See Chapter 8)

Man-made Penetrations - Boreholes or shafts which penetrate through the salt into underlying aquifers shall be avoided within one mile of the repository. Existing mining activity, unrelated to the repository, should not be present within two miles of the repository. Future, controlled mining, will be allowable up to one mile from the repository. Future studies may permit still closer mining and drilling if properly controlled. (See 2.3, Chapter 4)

Transportation - Transportation should be capable of
ready development. Avoidance of population centers by
transportation routes is not a factor in WIPP siting.
(Not addressed in GCR)

Accessibility - The site should be readily accessible
for transportation and utilities. (Not specifically
addressed in GCR; see Chapter 2 figures)

Land Jurisdiction - Siting will be on federally
controlled land to the extent possible. (Not
specifically addressed in GCR; see Chapter 2 and 8
figures)

Population Density - Proximity to population centers
and rural habitats will be considered in siting. Low
population density in the immediate site area is
desirable. (Not addressed in GCR)

Ecological Effects - Major impacts on ecology due to
construction and operation should not occur.
Archaeological and historical features of significance
should be preserved. (Not addressed in GCR)

Sociological Impacts - Demographic and economic
effects should not result in unacceptable sociological
impacts. (Not addressed in GCR)

One may summarize the WIPP siting criteria having the greatest impact as
follows:

Avoidance of land within one mile of any boring through the Ochoan
evaporites and into the Delaware or deeper formations.

Salt of high purity at a depth between 1000 and 3,000 ft.

Avoidance of areas where dissolution had advanced to the top of
Salado or deeper levels, by establishing a distance of one mile or
more from dissolution fronts at the top of Salado.

Avoidance of possible salt deformation in a belt 6 miles wide
basinward from the Capitan reef.

Avoidance of pronounced known anticlinal structures.

Avoidance of known oil and gas trends.

Avoidance of the known potash enclave above the repository and
minimizing conflict with the known enclave in the buffer zone.

Minimize existing potash lease rights in Zones I and II.

Minimize state and private land in Zones I through IV.

These criteria were applied to all areas within the Delaware Basin in New
Mexico. Figure 2-8 illustrates result of application of the expanded set
of criteria. Two alternate sites survived the constraints imposed by the
site selection criteria.

2.3.7   Preferred Preliminary Site Selection

Since only two alternate sites in the New Mexico part of the Delaware
Basin withstood the set of revised Stage II siting criteria, the
preliminary selection of a preferred site was fairly straightforward.
Alternate I, now known as the Los Medanos site, appeared to be the
preferred site. Alternate II was considered less desirable because it
was restricted in size, the acceptable salt zones were deeper, and the
high-purity salt lying between the Cowden anhydrite (in the lower Salado
Formation) and the Castile was thought to be absent. The top of the
Salado was about 800 feet deep at Los Medanos versus 1500 feet at
Alternate II. Other factors that favored the selection were:

Structural interpretation of what seismic data was then available to
Sandia indicated the Los Medanos site would be in a synclinal area
unfavorable for oil and gas acccumulation.

Similarly, if the site were in a syncline, geopressured brine
reservoirs would be less likely.

The Alternate II area lay adjacent to the Double X and Triple X
shallow oil fields where water flooding for secondary recovery could
occur.

No seismic exploration data whatsoever was available to Sandia on the
Alternate II area, and only partial coverage at Los Medanos.

Sandia Laboratories selected the Los Medanos alternate as the best
candidate area in early December, 1975. Figure 2-9 illustrates how the
siting criteria apply to the Los Medanos site.

Geological characterization activities were then expanded to focus on
obtaining subsurface data at the Los Medanos site. A descriptive summary
of these programs is given in Section 2.5.

2.4 STATUS OF STUDIES

In review, geologic studies for the WIPP fall naturally into three
different phases: preliminary site selection activities, geological
characterization, and studies of long-range geologic processes affecting
a repository. Preliminary site selection activities are complete now;
these consisted primarily of national and regional studies over the past
fifteen years, and resulted in selection of the WIPP study area for
geological characterization. The work of geological characterization
should be considered to have begun with the drilling of ERDA 9 and the
initiation of seismic reflection work on the site. That geological
characterization, which is primarily oriented to provide specific data
concerning the present geology of the site, will be virtually complete in
1978 when this Geological Characterization Report is submitted to DOE;
much basic information has been gathered indicating no major technical
problems with the site as it is now understood. Studies of long-term

processes which might affect a repository or have an effect on safety analyses will be the major geotechnical activity for the WIPP project after 1978, although some of these activities are already underway. These studies will concern the age of significant features and the rates and processes which produce those features. The information so gained will be useful in increasing the confidence in evaluation of the safety of a repository when a decision is necessary regarding conversion of the WIPP to a repository.

2.5   EXPLORATION TECHNIQUES

Much of the geological characterization of the WIPP study area is done using exploration geophysics and boreholes. About 75 line miles of new seismic reflection data and 9000 resistivity measurements were collected and 47 drillholes completed to support WIPP geological characterization to date (August, 1978). For convenience, the boreholes are listed in Table 2-2 according to primary objective. Twelve geologic exploratory holes (two by ORNL and ten by Sandia Labs) have been drilled to date in support of this program (Table 2-2A); three holes were drilled at the old study area, two are located off the WIPP site, and seven were drilled on the WIPP site. ERDA 9 is located at the center of the present study area (Figure 2-10). These boreholes were extensively logged, cored, and drill-stem tested in the evaporite section. The cores form the basis for several continuing laboratory studies that are important to an understanding of the physical and chemical phenomena associated with the WIPP and contribute to general knowledge about the formation of evaporites. Two of the exploratory boreholes have been drilled well outside the immediate site to obtain dissolution and paleoclimate data. Twenty-one holes (Table 2-2B) were drilled in conformance with industry standards to obtain core from the potash zones to supplement more than 30 existing industry holes for evaluation of potash resources within the WIPP study area by the USGS and the U.S. Bureau of Mines (Figure 2-11). When that evaluation is complete, others may use the core for studies of potash ore formation. Fourteen hydrologic holes (Table 2-2C) have been drilled and four potash holes converted to hydrologic monitoring to

provide a total of eighteen holes now dedicated to hydrologic studies. Hydrologic tests of the Bell Canyon Formation underlying the evaporites have also been conducted in two of the exploratory boreholes, one northeast and one south of the site. Except for ERDA 9, none of the boreholes within Zones I, II, or III penetrate as deep as the repository horizons. Future holes will sample repository horizons within these zones.

Seismic reflection data available from petroleum companies and 26 line miles initially obtained strictly for the study area (Figure 2-12), were collected using standard techniques for the petroleum industry. The data are excellent for interpreting deeper structure, but are not as useful for showing reflectors in the upper 3000 feet. In 1977, about 48 line miles of new data (Figure 2-13) were collected using shorter spacings for geophones, higher frequencies from vibroseis units, and higher rates of data sampling. These data show much improved reflections from, and better resolution in, the shallow section of interest. Resistivity has also been extensively used as a characterization tool. Field tests indicated that resistivity could detect certain types of solution features; more than 9,000 measurements have been taken in the study area to search for such features (Figure 2-14). Additional measurements of resistivity using expander arrays have been made to study resistivity changes with depth and to help interpret the detailed measurements (Figure 2-15). Analysis of geophysical data for the geological characterization was nearly complete by Summer, 1978. One resistivity anomaly was drilled to determine the cause of the anomaly and consequences, if any, for the WIPP. This anomaly did not result from dissolution phenomena. Further detailed geophysical investigation of the site, using techniques previously described for better resolution of shallow horizons, is now underway (Summer, 1978) for the primary purpose of providing detailed engineering information.

A variety of studies to continue geological characterization and contribute to long-range assessments are under way. Studies directed primarily toward geochemistry include water chemistry and stable isotope

studies of surface and subsurface water of the Delaware Basin; fluid inclusion studies of the evaporite beds; chemical and mineralogic effects of an igneous intrusion into the evaporite section; Rb/Sr dating of potash ores; and sorptive capacities of evaporites and associated rocks for various radionuclides. The dissolution history for the area and the local paleoclimate are being investigated through analysis of a core taken from a sink in nearby San Simon Swale. Field investigations of the climatic history and stability of the Pecos River drainage are beginning, and caliche studies will form a significant part of this effort. Studies of LANDSAT images will conclude in 1979. In addition, the first 200 km of the first-order level line from Carlsbad to El Paso, Texas, has been resurveyed to examine regional tectonic movements associated with the West Texas salt flats graben and trans-Pecos volcanic area. A first-order level line has also been established from Carlsbad east to the WIPP site through Nash Draw for future assessment of tectonic, erosion, solutioning, and subsidence phenomena. Further assessment of basin tectonics may be derived through measurements of in situ stress. These long-range studies will continue until sufficient data are available to permit reasonable and confident assessment of the risks involved in having a repository in bedded salt in southeastern New Mexico. These studies, plus the successful operation of the WIPP as a demonstration facility, are essential for the development of criteria for the conversion of the WIPP to a repository.

2.6 SUMMARY

Bedded salt has been a leading candidate as a rock type for the storage of radioactive waste; a combination of technical factors has led to the examination of the Delaware Basin in southeastern New Mexico as a location for the WIPP. Through preliminary site selection and partial site characterization of an early site near the WIPP, site selection criteria and factors which are rather specific to southeastern New Mexico were refined, and a new preliminary site was selected. Chapter 2 contains the description of the criteria and factors used in this process as an introduction to the geological characterization of the WIPP site

which is presented in the following chapters. The geological techniques used in the characterization of the WIPP site are a combination of well-tested conventional techniques supported by state of the art tools. Multiple, supporting techniques are used where appropriate. Continuing geological studies will increase the data base for assessment of the WIPP as a repository and allow refinement of criteria for conversion to a repository.

2.6   REFERENCES

Aguilar, P.C., Cheeseman, R.J., and Sandell, E.T., Jr., 1976, Preliminary map showing distribution of potash resources, Carlsbad mining district, Eddy and Lea Counties, New Mexico: U.S. Geol. Surv., Open-file Map 76-554.

Anderson, R.E., Eargle, D.H., and Davis, B.O., 1973, Geology and Hydrologic Summary of Salt Domes in Gulf Coast Region of Texas, Louisiana, Mississippi, and Alabama: U.S. Geol. Surv. Open-file report 4339-2.

Bachman, G.O., 1974, Geologic processes and Cenozoic history related to salt dissolution in southeastern New Mexico: U.S. Geol. Surv. Open-file report 74-194.

Bachman, G.O., and Johnson, R.B., 1973, Stability of salt in the Permian salt basin of Kansas, Oklahoma, Texas and New Mexico: U.S. Geol. Surv. Open-file report 4339-4.

Bachman, G.O., Johnson, R.B., and Swenson, R.A., 1972, Stability of bedded salt in the Permian basin, Colorado, Kansas, Oklahoma, Texas and New Mexico: in Oak Ridge National Laboratory Pilot Plant Repository Staff, Alternative geologic formations for the disposal of radioactive wastes, ORNL Report 72-6-42.

Bradshaw, R.L. and McClain, W.C. (eds.), 1971, Project Salt vault: Demonstration of the disposal of high-activity solidified wastes in underground salt mines: Oak Ridge National Laboratory, Oak Ridge, Tennessee, ORNL-4555.

Brokaw, A.L., Jones, C.L., Cooley, M.E., and Hayes, W.H., 1972, Geology and hydrology of the Carlsbad potash area, Eddy and Lea Counties, New Mexico: U.S. Geol. Surv. Open-file report 4339-1.

Claiborne, H.C., and Gera, F., 1974, Potential containment failure mechanisms and their consequences at a radioactive waste repository in bedded salt in New Mexico: Oak Ridge National Laboratory ORNL-TM-4369.

Department of Energy, 1978, Draft Report of Task Force for Review of Nuclear Waste Management: DOE/ER-0004/D.

Ekren, E.B., et al, 1974, Geologic and hydrologic considerations for various concepts of high-level radioactive waste disposal in conterminous United States: U.S. Geol. Surv. Open-file report 74-158.

Fader, S. W., 1973, Land subsidence caused by dissolution of salt near Four Wells in central Kansas: U.S. Geol. Surv. Administrative Report for AEC.

Foster, R.W., 1974, Oil and gas potential of a proposed site for the disposal of high-level radioactive waste: Oak Ridge National Laboratories Open-file report, Contract No. AF(40-1)-4423.

Gera, F., and Jacobs, D.G., 1972, Considerations in the long-termed management of high-level radioactive wastes: Oak Ridge National Laboratory, ORNL-4762.

Griswold, G.B., 1977, Site selection and evaluation studies of the Waste Isolation Pilot Plant (WIPP), Los Medanos, Eddy County, New Mexico: Sandia Laboratories Report SAND-77-0946.

Hite, R. J., and Lohman, S. W., 1973, Geologic Appraisal of Paradox Basin Salt Deposits for Waste Emplacement: U.S. Geol. Surv. Open-file report 4339-6.

Jones, C. L., 1973, Salt deposits of Los Medanos area, Eddy and Lea Counties, New Mexico, with sections on Ground water hydrology, by M.E. Cooley and Surficial geology, by G. O. Bachman: U.S. Geol. Surv. Open-file report 4339-7.

Jones, C.L., 1974a, Salt Deposits of the Mescalero Plains Area, Chaves County, New Mexico: U.S. Geol. Surv. Open-file report 74-190.

Jones, C. L., 1974b, Salt deposits of the Clovis-Portales area, east-central New Mexico: U.S. Geol. Surv. Open-file report 74-60.

Jones, C.L., 1975, Potash resources in part of Los Medanos area of Eddy and Lea Counties, New Mexico: U.S. Geol. Surv. Open-file report 75-407.

Mytton, James W., 1973, Two salt structures in Arizona; The Supai Salt Basin and the Luke Salt Body: U.S. Geol. Surv. Open-file report 4339-3.

NAS/NRC 1957 Disposal of Radioactive Wastes on Land, 1957, National Academy of Sciences - National Research Council, Washington, D.C., Publ. 519.

NAS/NRC, 1961, "Minutes of the Meeting of December 7-8, 1961," National Academy of Sciences - National Research Council, Division of Earth Sciences, Committee on Geologic Aspects of Radioactive Waste Disposal Advisory to the U. S. Atomic Energy Commission.

NAS/NRC, 1966, "Report to the U.S. Atomic Energy Commission," NAS-NRC, Division of Earth Sciences, Committee on Geologic Aspects of Radioactive Waste Disposal.

NAS/NRC, 1970, "Report by the Committee on Radioactive Waste Management," Disposal of solid radioactive wastes in bedded salt deposits.

Netherland, Sewell and Associates, 1974, Evaluation of hydrocarbon potential, AEC study area, southeast New Mexico: Report submitted to ORNL by Netherland, Sewell and Associates.

ORNL-TM-4219, 1973, Site Selection Factors for the Bedded Salt Pilot Plant. Staff of the ORNL Salt Mine Repository Project.

Pierce, W.G., and Rich, E.I., 1962, Summary of rock salt deposits in the United States as possible storage sites for radioactive waste materials: U.S. Geol. Surv. Bull. 1148.

Piper, A.M., 1973, Subrosion in and about the four-township study area near Carlsbad, New Mexico: ORNL Subcontract 3745.

Snow, R.H., and Chang, D.S., 1975, Prediction of cavity growth by solution of salt around boreholes, with appendix: Union Carbide Corporation IITRI C6313-14.

Vine, J.D., 1963, Surface geology of the Nash Draw Quadrangle, Eddy County, New Mexico: U.S. Geol. Surv. Bull. 1141-B.

Walters, R. F., 1975, Salt Dissolution in oil and gas test holes in Central Kansas: ORNL Contract No. 78X-38283V.
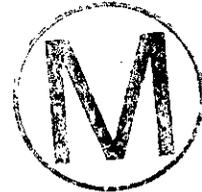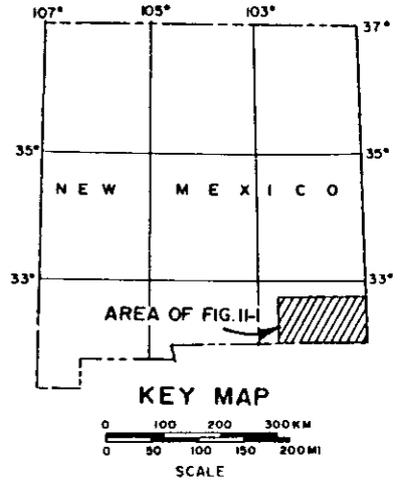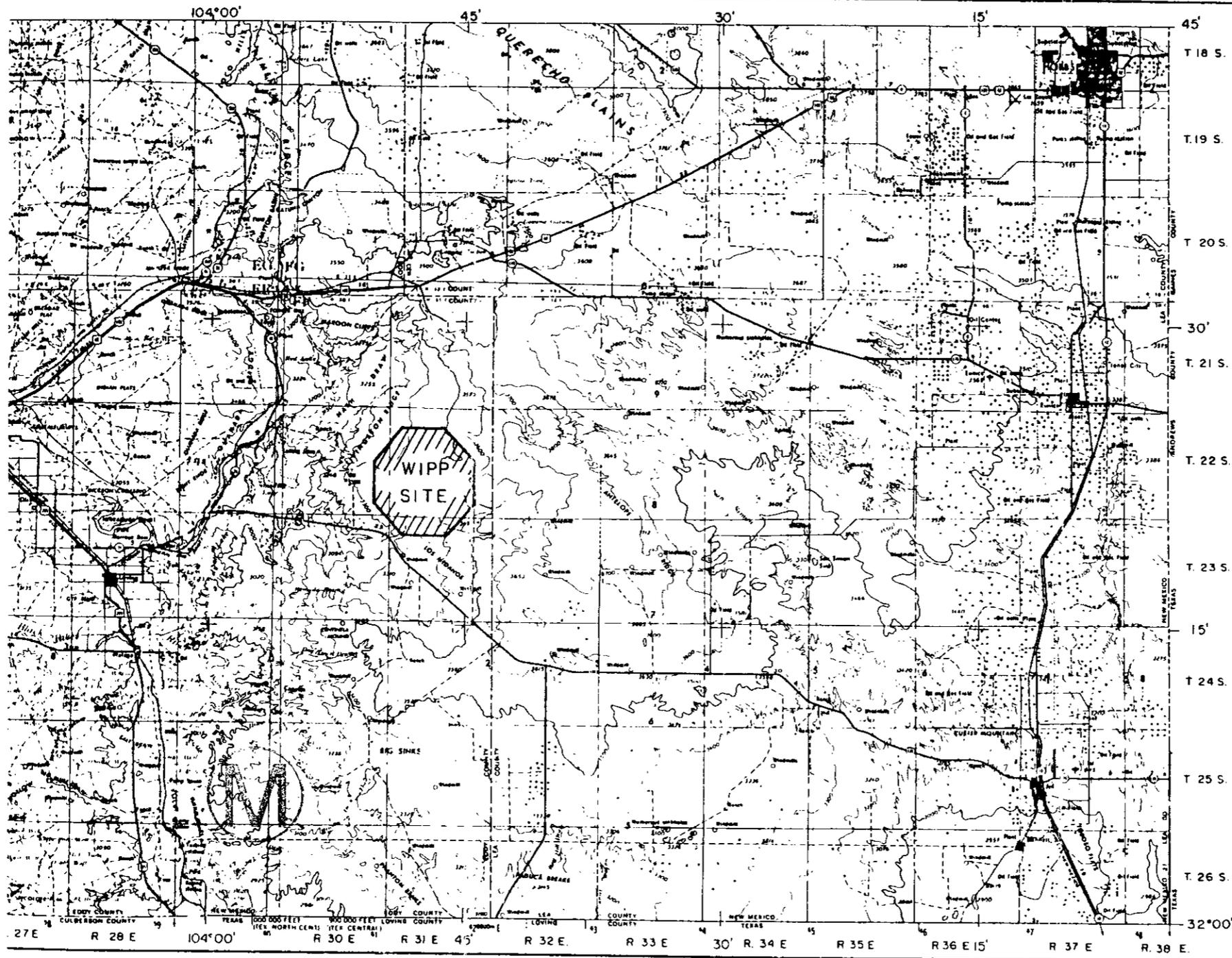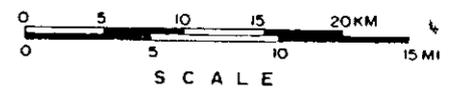
GEOGRAPHIC LOCATION MAP

FIGURE 2-1

34	35	36	31	32	33	34	35	36	31
3	2	1	6	5	4	3	2	1	6
10	11	12	7	8	9	10	11	12	7
15	14	13	18	17	16	15	14	13	18
22	23	24	19	20	21	22	23	24	19
27	26	25	30	29	28	27	26	25	30
34	35	36	31	32	33	34	35	36	31
3	2	1	6	5	4	3	2	1	6
10	11	12	7	8	9	10	11	12	7
15	14	13	18	17	16	15	14	13	18

ZONE IV

ZONE III

ZONE II

ZONE I

EDDY COUNTY

LEA COUNTY

T. 22 S.

T. 23 S.

R. 30 E.   R. 31 E.   R. 32 E.

N

ZONE ACREAGE

ZONE I — 60-100 (surface facilities)

ZONE II — 1860 (underground repository)

ZONE III — 6230 (no mining or drilling)

ZONE IV — 10,810 (DOE-controlled mining and drilling)

1   0   1   2   3
SCALE IN MILES

M

WIPP SITE ZONATION

FIGURE 2-2

APPLICATION OF
PRELIMINARY SITE
SCREENING CRITERIA BY ORNL

FIGURE 2-3
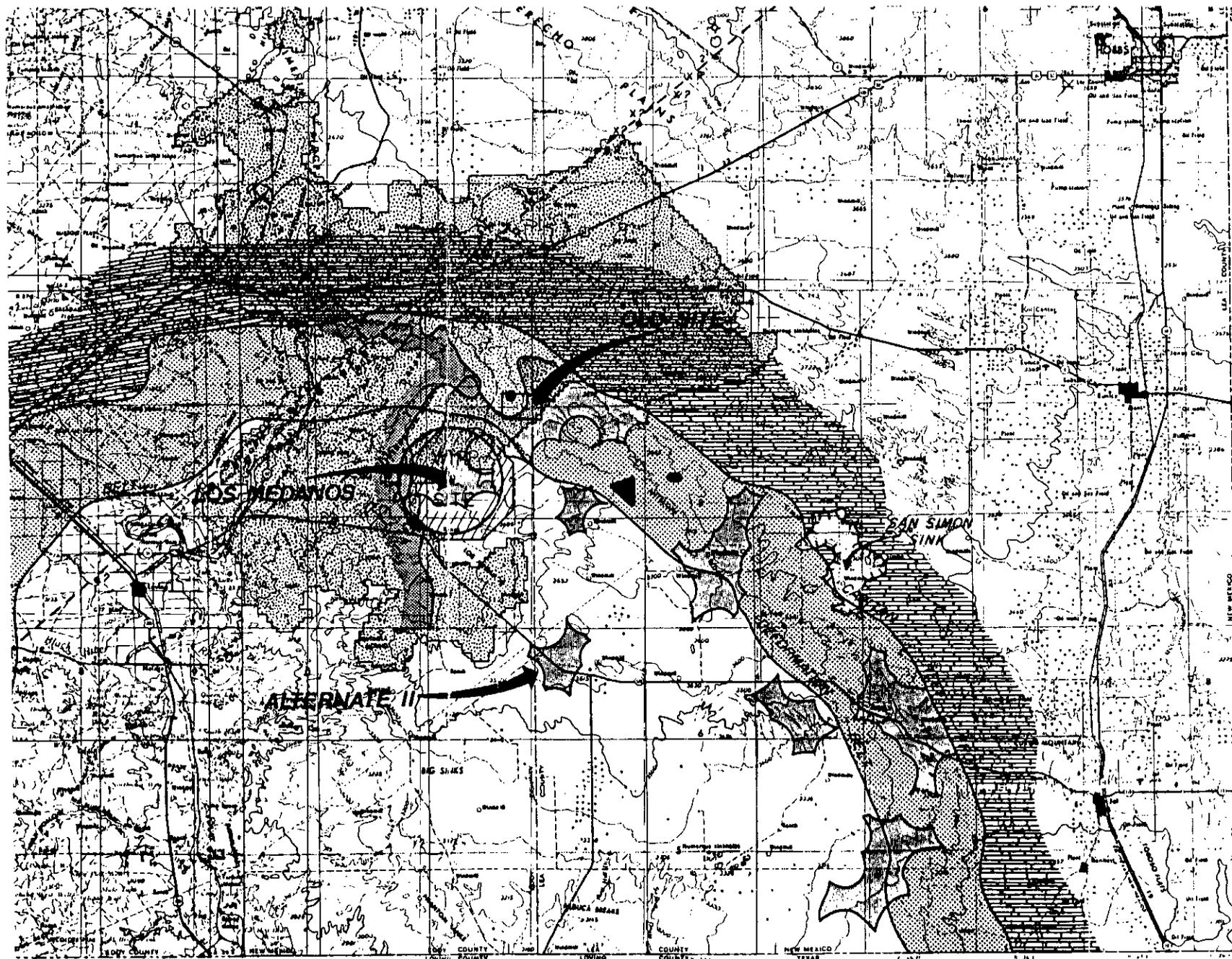
EXPLANATION

AREAS MORE THAN ONE MILE FROM DEEP DRILL HOLES

CAPITAN REEF FRONT

DEFORMATION BELT
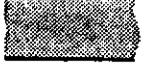
DISSOLUTION FRONT AT TOP OF SALADO

KNOWN POTASH ENCLAVE

ARTESIAN BRINE FLOW (1, 2 OR 3 WELLS)

DIKE TREND SYMBOLS

△ Outcrop of Dike
✧ Well Intercept of Dike
● Airborne Magnetic Response - 1960
X Airborne Magnetic Response - 1963-64

SCALE

REFERENCE:

GRISWOLD, 1977

SUMMARY OF APPLICATION OF SITE SELECTION CRITERIA BY SANDIA

FIGURE 2-4
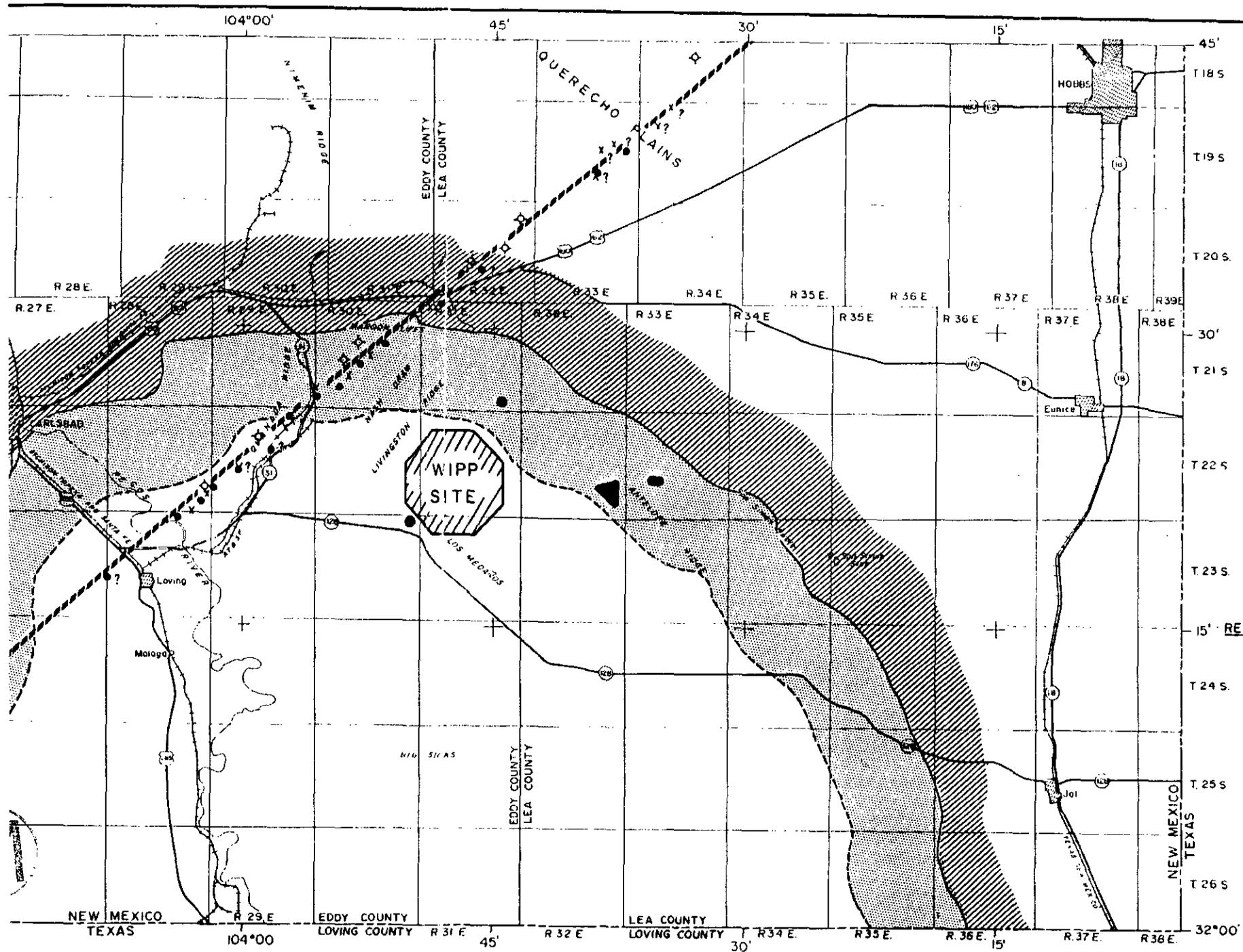
EXPLANATION

CAPITAN REEF FRONT
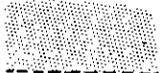
DEFORMATION BELT

ARTESIAN BRINE FLOW

DIKE TREND

△ Outcrop of Dike
✧ Well Intercept of Dike
● Airborne Magnetic Response - 1960
✕ Airborne Magnetic Response - 1963-64

REFERENCE:

GRISWOLD, 1977, FIGURE I

SCALE
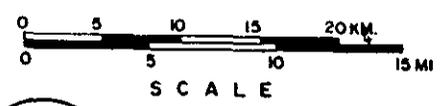
AREAS OF UNFAVORABLE
GEOLOGIC STRUCTURE

FIGURE 2-5
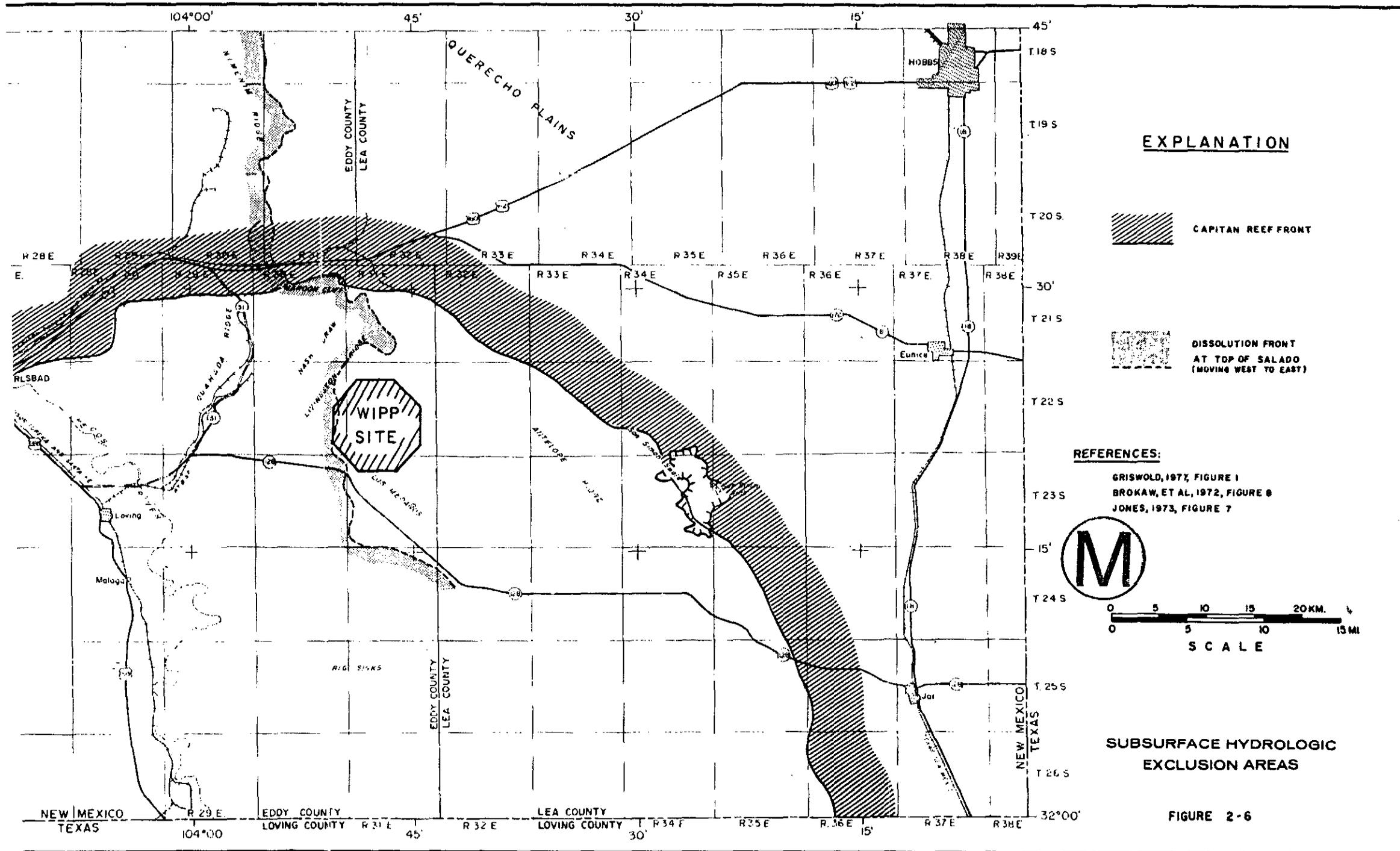
EXPLANATION

CAPITAN REEF FRONT
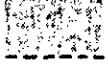
DISSOLUTION FRONT
AT TOP OF SALADO
(MOVING WEST TO EAST)

REFERENCES:

GRISWOLD, 1977, FIGURE 1
BROKAW, ET AL, 1972, FIGURE 8
JONES, 1973, FIGURE 7

SCALE

SUBSURFACE HYDROLOGIC
EXCLUSION AREAS

FIGURE 2-6
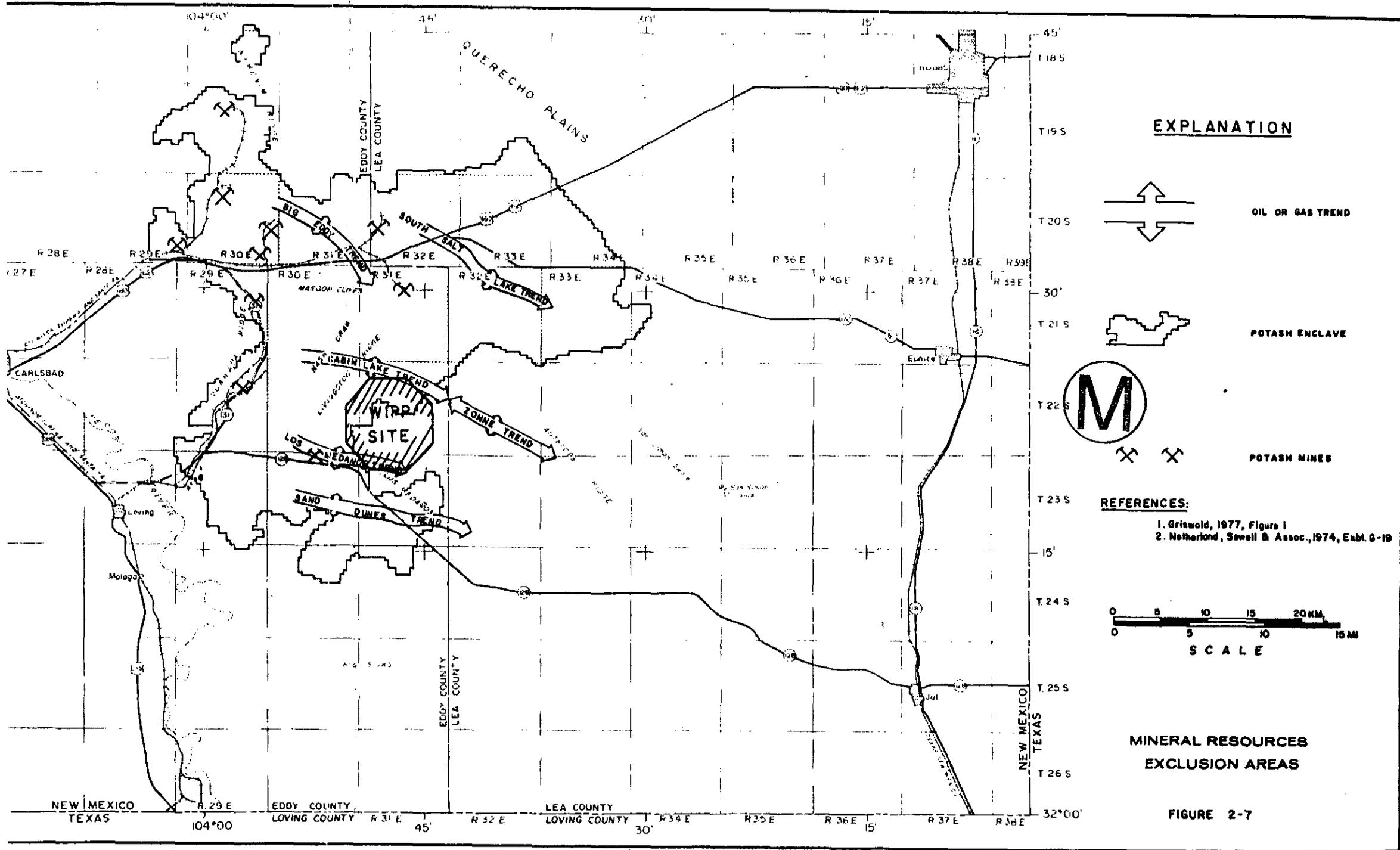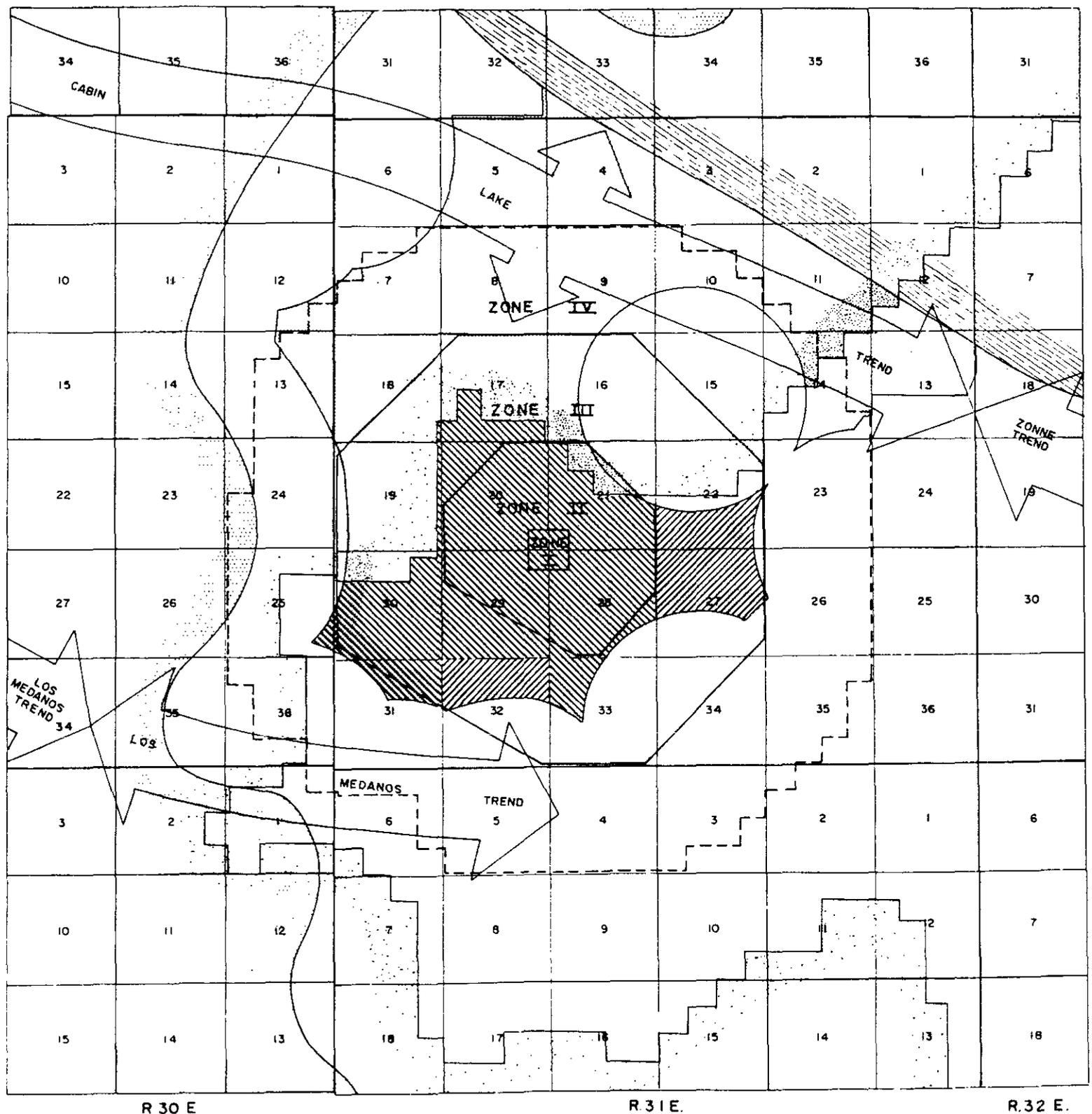
EXPLANATION
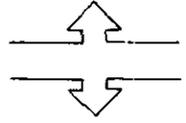
⇕ OIL OR GAS TREND

⬡ POTASH ENCLAVE

Ⓜ

⚒ ⚒ POTASH MINES

REFERENCES:
1. Griswold, 1977, Figure 1
2. Netherland, Sewell & Assoc., 1974, Exht. G-19

SCALE

**MINERAL RESOURCES
EXCLUSION AREAS**

FIGURE 2-7

EXPLANATION

CAPITAN REEF FRONT

AREAS MORE THAN ONE
MILE FROM DEEP DRILL
HOLES

M

REFERENCE:

GRISWOLD, 1977

DEEP DRILL-HOLE
EXCLUSION AREAS
FIGURE 2-8

SELECTION OF PREFERRED SITE

FIGURE 2-9
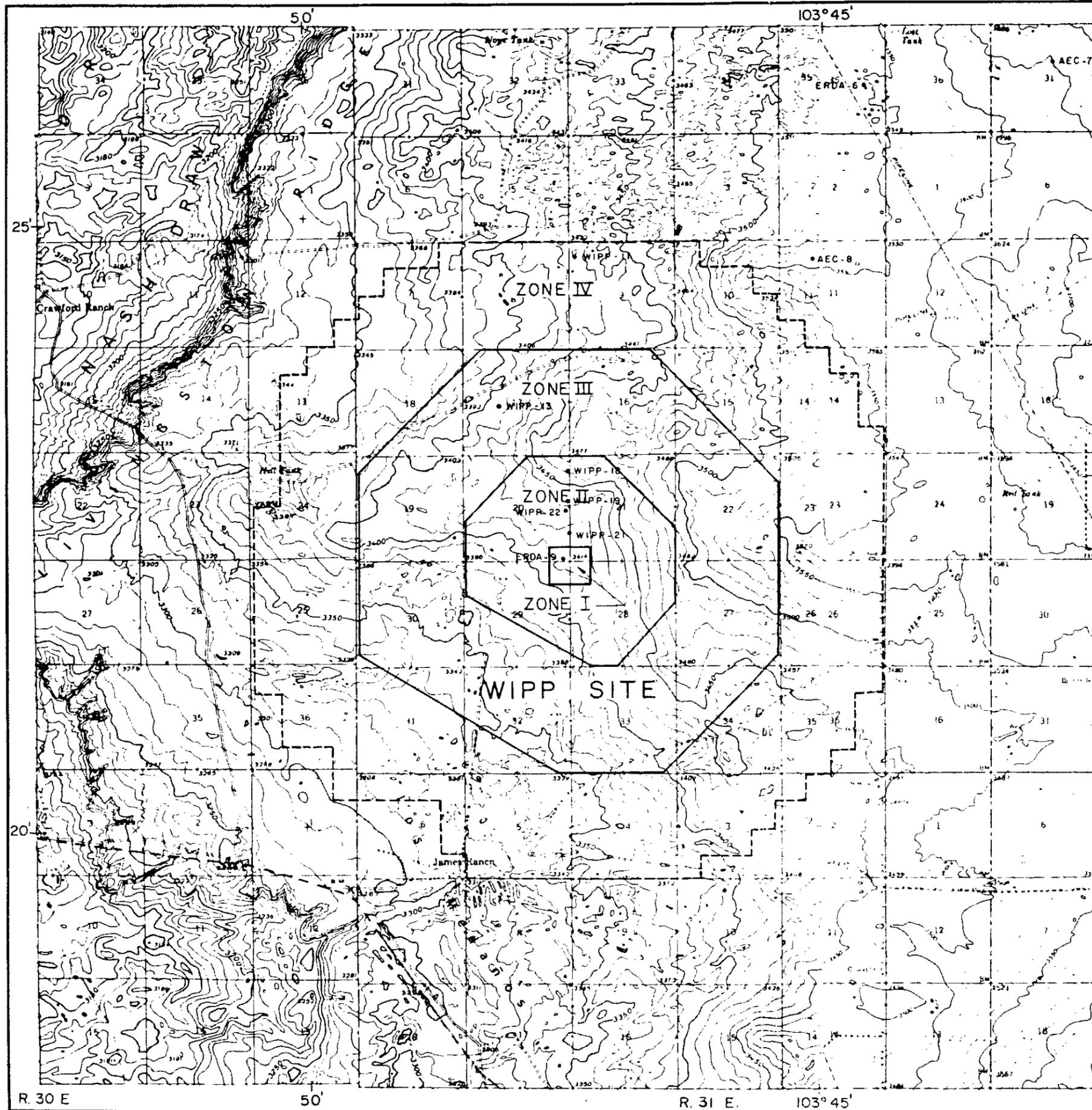
REFERENCE:

U.S.G.S. 15 minute quadrangles: Nash Draw,
N.Mex.,1965 and Hat Mesa, N.Mex.,1972.

SCALE
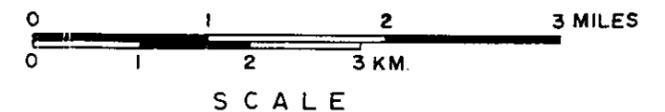
WIPP SITE STRATIGRAPHIC HOLES

FIGURE 2-10
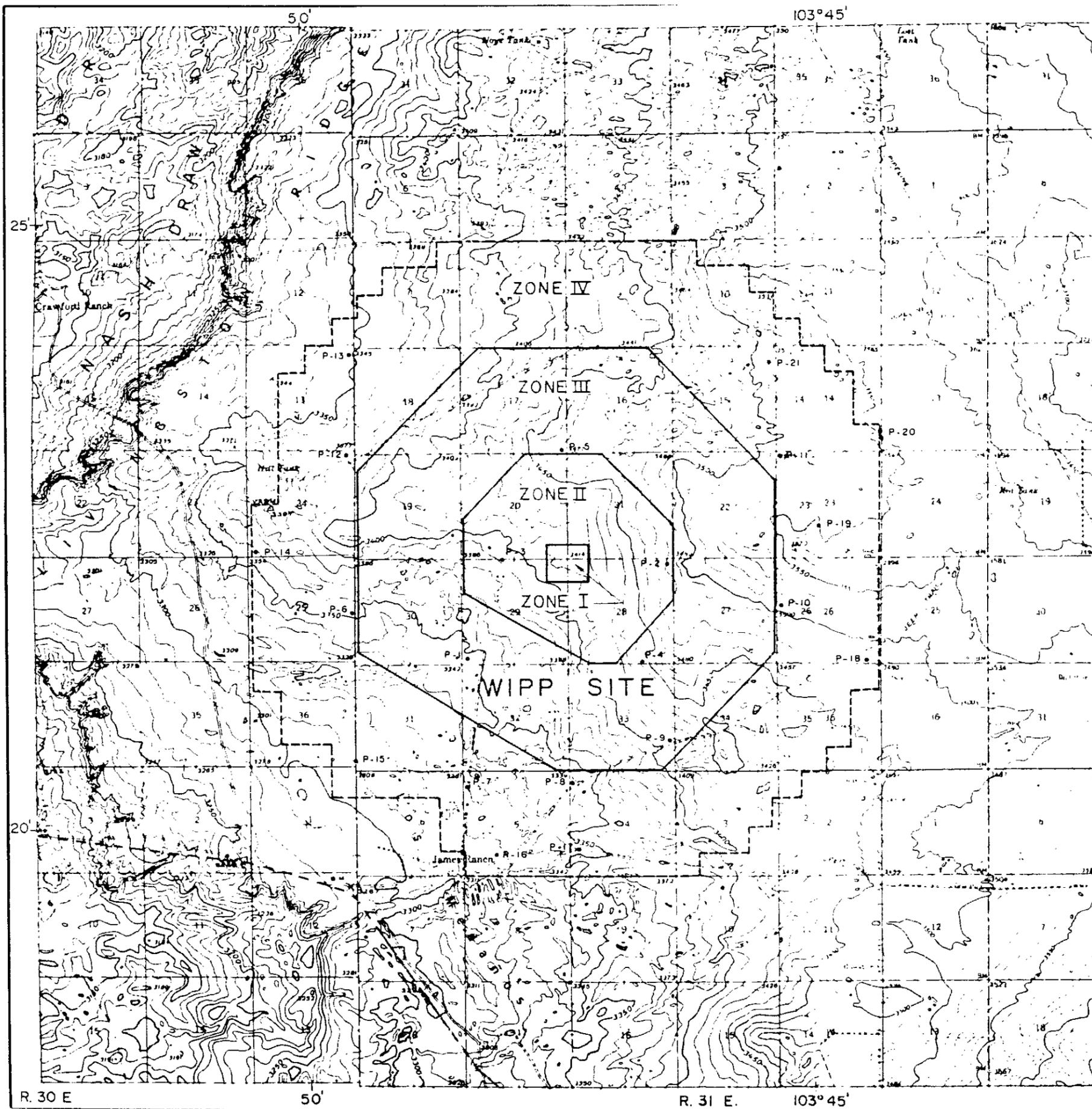
REFERENCE:

U.S.G.S. 15 minute quadrangles: Nash Draw, N. Mex., 1965 and Hat Mesa, N. Mex., 1972.

SCALE
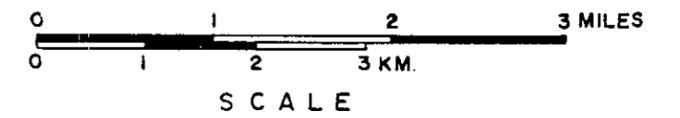
WIPP SITE POTASH DRILLING BY ERDA, 1976

FIGURE 2-11

ZONE IV

ZONE III

ZONE II

ZONE I

WIPP SITE
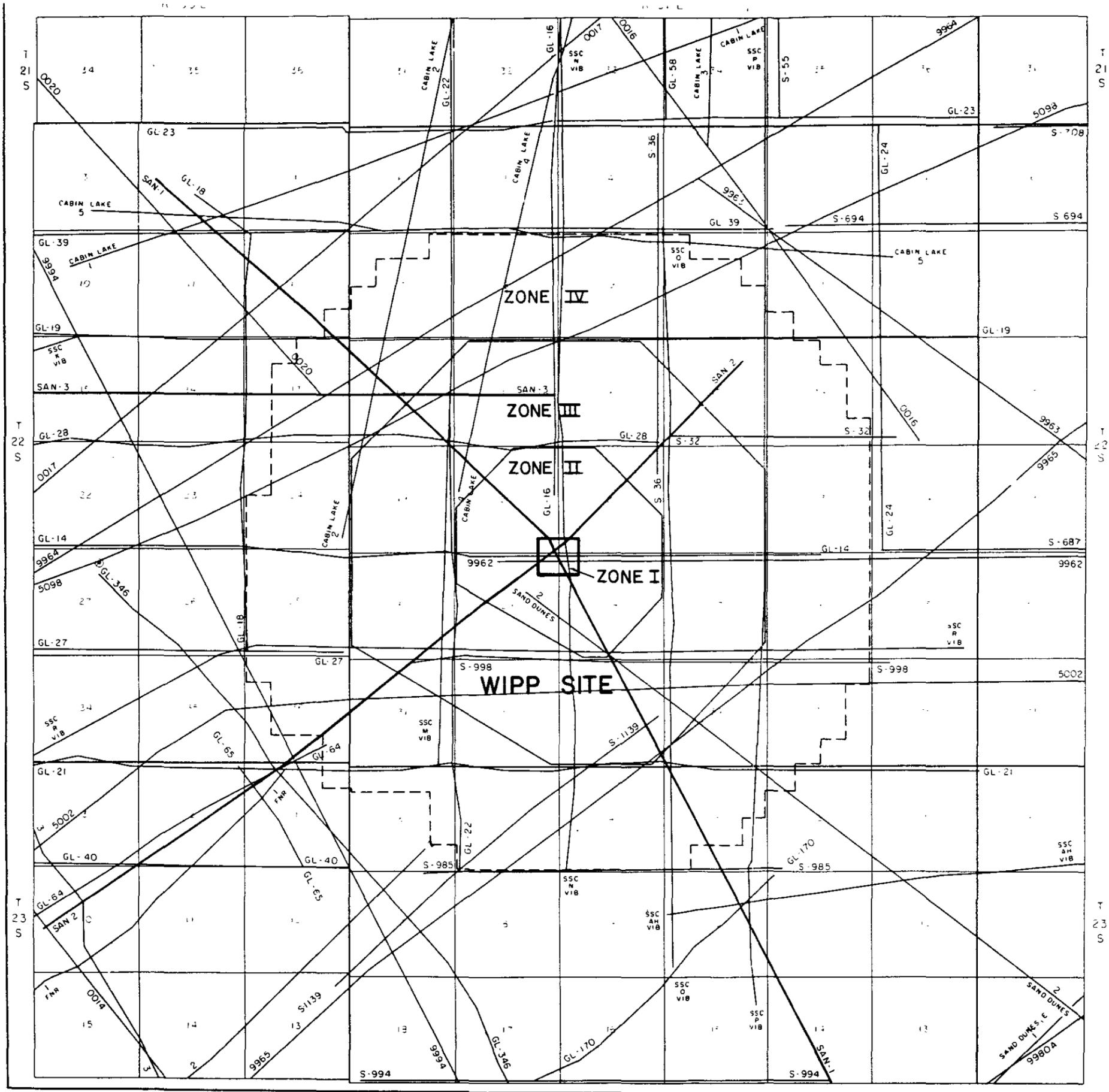
INDUSTRY SEISMIC REFLECTION LINES
PLUS SANDIA REFLECTION LINES
(SAN. — 1, 2, 3) FROM 1976

FIGURE 2-12

REFERENCE:

U.S.G.S. 15 minute quadrangles: Nash Draw,
N. Mex., 1965 and Hat Mesa, N. Mex., 1972.

SCALE

SEISMIC REFECTION LINES FOR

SEISMIC PROGRAM, 1977
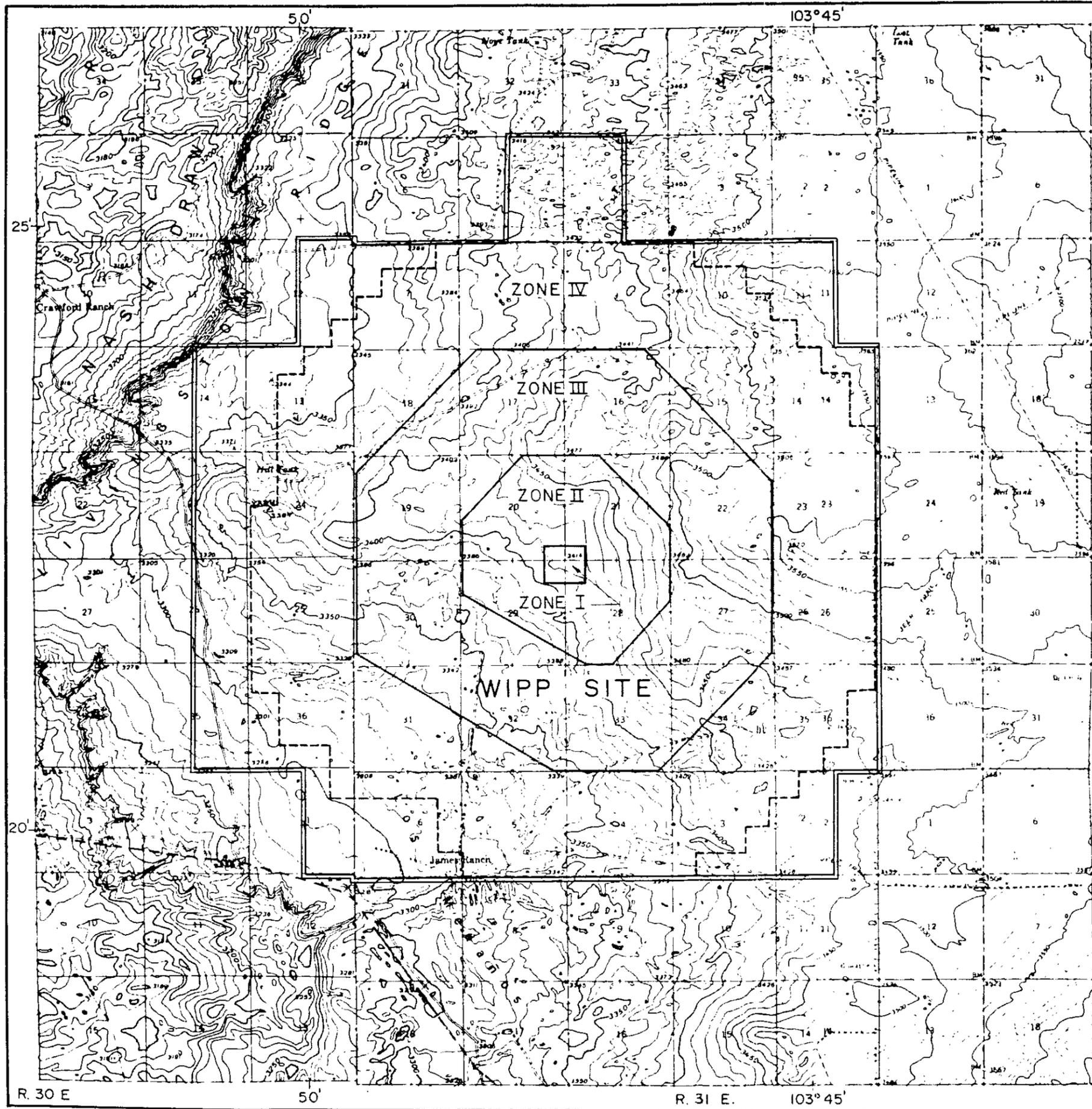
FIGURE 2-13

EXPLANATION:

=== Outer Boundary of Resistivity
Measurement Area

REFERENCE:

U.S.G.S. 15 minute quadrangles: Nash Draw,
N. Mex., 1965 and Hat Mesa, N. Mex., 1972.

SCALE
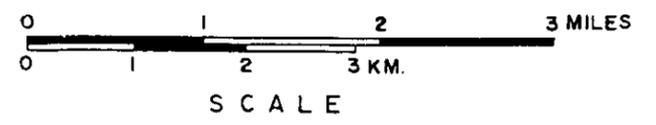
PROFILE LOCATION MAP
OF
GRADIENT ARRAY RESISTIVITY

FIGURE 2-14

M
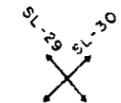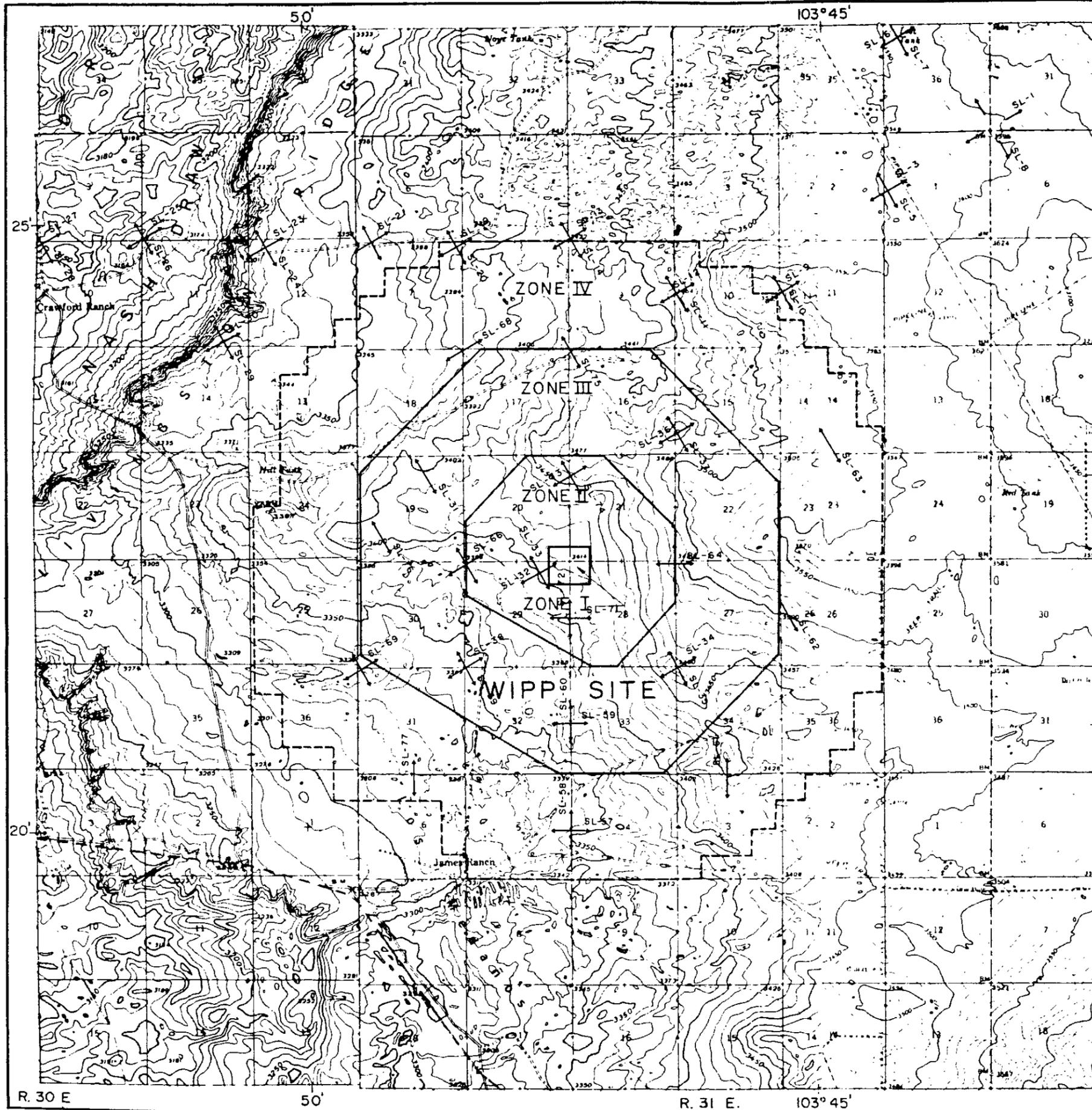
SL-29 SL-30 ✕ Schlumberger Array Soundings with Line No. and Direction

REFERENCE:

U.S.G.S. 15 minute quadrangles: Nash Draw, N.Mex.,1965 and Hat Mesa, N.Mex.,1972.

0   1   2   3 MILES
0   1   2   3 KM.

SCALE
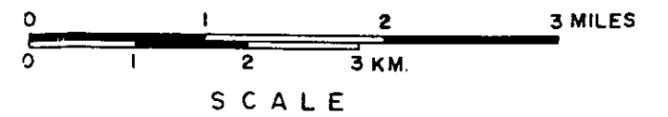
LOCATION MAP
FOR
RESISTIVITY SOUNDINGS

FIGURE 2-15

TABLE 2-1

<u>WIPP SITE CONTROL ZONES</u>

Zone	Area Description	Surface Use and Activity Control	Approximate Acreage
I	Surface Exclusion Area	All non-WIPP activities excluded (security fenced area).	60(to 100)
II	Underground Storage Limits	Restricted; land use same as Zone III. Must be free of prior lease rights.	1,860
III	Restricted Buffer Zone	Drilling & mining operations prohibited. Current livestock grazing activities permitted. Other future activities subject to approval and regulation under ERDA authority.	6,230
IV	Controlled Use Buffer Zone	Drilling and mining operations permitted but restricted in conformance with ERDA specifications. Solution mining, well injection recovery methods prohibited. Other activities as specified for Zone III.	10,810

TOTALS   18,960
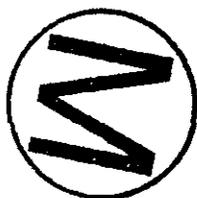
TABLE 2-2

A. GEOLOGIC EXPLORATORY HOLES
(Figure 2-10)

Designation	Location	Date	Purpose
AEC 7	21/32/31	3/74	ORNL Stratigraphic--Old Site
AEC 8	22/31/11	4/74, 6/76	ORNL Stratigraphic--Old Site
			Sandia--Deep Hydrology--Old Site
ERDA 6	21/31/35	6/75	Stratigraphic--Old Site
ERDA 9	22/31/20	4/76	Stratigraphic--WIPP Site
ERDA 10*	23/30/34	8/77	Deep Dissolution--Off Site
WIPP 11	22/31/9	2/78	Stratigraphic--WIPP Site
WIPP 13	22/31/17	7/78	Stratigraphic--WIPP Site
WIPP 15*	23/35/18	3/78	Paleoclimate--Off Site
WIPP 18	22/31/20	2/78	Stratigraphic--WIPP Site
WIPP 19	22/31/20	4/78	Stratigraphic--WIPP Site
WIPP 21	22/31/20	5/78	Stratigraphic--WIPP Site
WIPP 22	22/31/20	5/78	Stratigraphic--WIPP Site

* not shown on Figure 2-10

B. ERDA POTASH HOLES
(Figure 2-11)

Designation	Location	Date
P1	22/31/29	8/76
P2	22/31/21	8/76
P3	22/31/20	8/76
P4	22/31/28	8/76
P5	22/31/17	9/76
P6	22/31/30	9/76
P7	23/31/5	9/76
P8	23/31/4	9/76
P10	22/31/26	9/76
P11	22/31/23	9/76
P12	22/30/24	9/76
P13	22/31/18	9/76
P14	22/30/24	9/76
P15	22/31/21	8/76
P16	23/31/5	9/76
P17	23/31/4	10/76
P18	22/31/26	10/76
P19	22/31/23	10/76
P20	22/31/14	10/76
P21	22/31/15	10/76
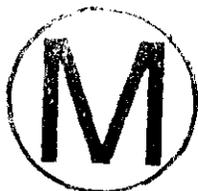
TABLE 2-2 (Continued)

C. HYDROLOGIC TEST HOLES
(See Figure 6.3-5)

Designation	Location	Date	Purpose
H1	22/31/29	5/76	Rustler, Top Salado Hydro
H2a	22/31/29	2/77	Magenta
H2b	22/31/29	2/77	Culebra
H2c	22/31/29	2/77	Top Salado
H3	22/31/29	7/76	Rustler, Top Salado Hydro
H4a*	22/31/5	5/78	Magenta
H4b*	22/31/5	5/78	Culebra
H4c*	22/31/5	4/78	Top Salado
H5a*	22/31/15	6/78	Magenta
H5b*	22/31/15	6/78	Culebra
H5c*	22/31/15	5/78	Top Salado
H6a*	22/31/18	7/78	Magenta
H6b*	22/31/18	6/78	Culebra
H6c*	22/31/18	6/78	Top Salado

* Holes being drilled at time of report
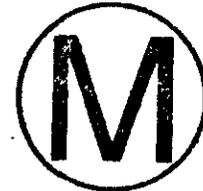
3.1   INTRODUCTION

This chapter considers the physiography and geomorphology, stratigraphy
and lithology, structure and tectonics, igneous activity, and geologic
history of the southeast New Mexico-west Texas area within a radius of
about 200 miles of the proposed WIPP site. The information presented in
the discussion below has been derived from previously available published
and unpublished sources, including well-known reference texts, U.S.
Geological Survey publications and open-file reports, Roswell Geological
Society and New Mexico State Bureau of Mines and Mineral Resources
materials, journal articles, and reports prepared under contract to
Sandia Labs. A study of LANDSAT imagery was also conducted to examine
lineaments as well as physiographic and structural features.

Section 3.2 presents a general description of the physiographic
divisions, illustrated in Figure 3.2-1, which lie within approximately
200 miles of the site, followed by a more detailed study of the origin
and development of those geomorphic features having significance to the
site and by a consideration of relative erosion rates estimated for the
future in the area surrounding the site.

Section 3.3 summarizes the major rock types and stratigraphic
nomenclature by which the Precambrian basement and overlying sedimentary
section are characterized within an area roughly bounded by the
Sacramento Mountains on the northwest, and by Texas' Midland and Val
Verde basins on the south and southeast. Generalized cross sections,
depicting the entire stratigraphic section present in the area (Figure
3.3-2) and a study of Permian reef relationships (Figure 3.3-4) as well
as correlations of the Precambrian rocks, (Figure 3.3-1) and Permian
section (Figure 3.3-3) supplement the discussion.

Section 3.4 describes the major structural elements comprising the southeast New Mexico-west Texas region and summarizes the history of their tectonic development. The features discussed include the major subsurface basins and platforms of Late Paleozoic origin, which together have produced the essential structural framework of the area, and large-scale Cenozoic features, which generally possess surficial structural expression, as well as the more important smaller structures occurring within the boundaries of these elements. The structures considered in this section are displayed in Figure 3.4-1, and a basement contour structure map (Figure 3.4-2) demonstrates the basic structural configuration of the region.

The major occurrences of igneous activity within the site region are described in Section 3.5. As demonstrated in Figure 3.5-1, this igneous activity has been generally limited to the area west and south of the proposed WIPP site, in the form of Tertiary intrusive bodies and volcanic terrains. The igneous feature nearest to the site, a northeast-trending dike located about nine miles northwest of the site, is discussed separately in this section and is illustrated in Figure 3.5-2.

Section 3.6 presents a synthesis of the major events which have affected the site region, as these have been determined from lithologic and structural data available in the area. A schematic visualization of the regional geologic history, as correlated with the geologic time scale, is provided in Figure 3.6-1.

3.2   REGIONAL PHYSIOGRAPHY AND GEOMORPHOLOGY

Figure 3.2-1 presents the major physiographic units which encompass the southeast New Mexico-west Texas region. The discussion below includes a general description of the physiographic sections, as defined by Fenneman (1931), which lie within a radius of about 200 miles of the proposed WIPP site. This is followed by a more detailed description of the development of the major nearer site landforms.

3.2.1 Physiographic Setting

The proposed WIPP site is located within the eastern part of the Pecos
Valley section of the southern Great Plains physiographic province. The
Great Plains physiographic province comprises a broad highland belt
sloping gradually eastward from the Rocky Mountains and Basin and Range
province to the Central Lowlands province. The Great Plains province in
turn represents the western extent of the Interior Plains major
physiographic division (Fenneman, 1931).

Pecos Valley Physiographic Section The Pecos Valley section consists of
the Pecos and upper Canadian valleys, which together form a long
north-south trough carved from what was once part of the High Plains
section on the east, but whose axis now lies 500 to 1,000 feet below the
High Plains surface -- the Llano Estacado. The Guadalupe and Sacramento
mountains of the Basin and Range physiographic province flank the Pecos
Valley section to the west.

The topography of the Pecos Valley section varies from flat plains and
lowlands to rugged canyon lands. Except where covered by alluvium, much
of the land surface has an uneven rock floor, which results from the
erosion of the moderately resistant limestones, sandstones, shales and
gypsum to form scarps, cuestas, terraces, side canyons and some mesas of
limited extent. The valleys of the Pecos River in the vicinity of the
Delaware Basin exhibit a characteristic lowland topography marked by
widespread solution-subsidence features, which have resulted from
dissolution within the Upper Permian Ochoan rocks (see the karst
topography discussion below).

The land surface generally slopes gently eastward, reflecting the
attitude of the underlying rock strata. The average elevations within
the section range from over 6,000 feet above sea level in the northwest
and about 5,000 feet in the north to 4,000 feet on the east and 2,000
feet to the south (Fenneman, 1931).

The Pecos Valley section is drained primarily by the Pecos River which
lies slightly to the west of the center of the Pecos trough and flows in
a southeast to southward direction through most of the length of the
section. The extreme northeastern portion of the section is also drained
by a short segment of the generally eastward-flowing Canadian River.
Owing to the desert character of the area, most of the tributaries of
these major streams flow only intermittently, and some creeks drain into
local depressions, where the water evaporates or percolates into the
underlying sediments.

The Canadian River has cut much more deeply into the surrounding land
than has the Pecos River, thereby producing a much greater relief in the
far nothern portion of the section than is present to the south.

The northern portion of the Pecos River, north of Roswell, has cut a
valley in places as deep as 1,000 feet below the surrounding land surface
and from 5 to 30 miles wide. The central portion of the river, from
about 50 miles north of Roswell to near the New Mexico-Texas border,
flows through an alluvial valley of comparable width but much reduced
relief and is underlain by as much as 250 feet of alluvium near
Carlsbad. The southern part of the Pecos, just north of the Edwards
Plateau, flows across an alluvial plain, called the Toyah Basin, which is
similar to that further north and comprises most of the west Texas
portion of the Pecos Valley section (Fenneman, 1931). The genesis and
development of the Pecos River system are discussed in Section 3.2.2,
below.

The immediate valley of the Pecos River is bordered on the east by almost
continuous bluffs, beyond which the eastward-dipping rock strata lie at
or near the surface for a distance of several miles. A sloping
alluvium-mantled plain extends eastward from this rocky belt to the
westward face of the Llano Estacado (Fenneman, 1931).

High Plains Physiographic Section East of the Pecos Valley section lies
the High Plains section of the Great Plains physiographic province,

extending from South Dakota on the north to near the Rio Grande (river) in Texas. The High Plains are remnants of a former great fluviatile plain, which stretched from the mountains on the west to the Central Lowlands on the east. The portion of the High Plains east of the Pecos valley is known as the Llano Estacado and comprises approximately 20,000 mi^2 of almost completely flat plain, which has undergone very little dissection. Northward, the land is more dissected, and the original flat surface is still preserved only along stream divides.

The High Plains originated through deposition of the Late Tertiary Ogallala Formation, resulting in more than 500 feet of silts with lesser gravels and sand. The deposits were laid down in alluvial fans by overloaded streams flowing eastward from the Rocky Mountain area over an irregular erosional surface. By the end of the time of formation of the Ogallala, the High Plains surface was probably continous across the area of the present Pecos River drainage to the back slope of the Sacramento Mountains (Bachman, 1976) (also see Section 3.6.5). In many areas, the nearly flat surface which resulted was later cemented by a hard caliche layer. The almost perfect preservation of the orginal topography in the Llano Estacado area is due to a combination of the porous nature of the sediments, the protection afforded by the caliche, and the relatively arid climate of the region (Fenneman, 1931).

The few, generally insignificant topographic features present in the High Plains section consist mainly of depressions derived from a variety of origins, such as dissolution with subsidence, blowout activity, buffalo wallowing or differential compaction of the Tertiary sediments. Ponding of water occurs in these depressions following rain storms, and a few maintain permanent pools (Thornbury, 1965). Sand dunes also occur in scattered locations throughout the section, generally fringing the leeward sides of streams (Fenneman, 1931).

Edwards Plateau Physiographic Section   The Llano Estacado merges southward into the Edwards Plateau section of the Great Plains province by the gradual thinning and disappearance of the Ogallala Formation. It

comprises a wedge-shaped portion of west Texas, and then extends across the Rio Grande into Mexico. The Edwards Plateau is bounded on all sides by an escarpment, except for two small areas, where it merges with the Llano Estacado on the northwest and where it terminates against the mountains of the Mexican Highlands on the west. The northern edge of the plateau, bounding the Central Texas Section, is formed by an eroded and deeply notched southward-retreating escarpment, and the southern boundary is marked by a line of faulting and local folds, which produces an escarpment up to 1,000 feet high (Fenneman, 1931).

The Edwards Plateau ranges in elevation from 3,000 feet on the north at its border with the Llano Estacado and 4,000 feet at the foot of the mountains on the west to 2,200 feet along its southern margin and 1,000 feet at the southeast corner.

The surface of the Edwards Plateau is underlain by a single resistant layer of limestone dipping gently to the south and east, which has encouraged the development of rather flat-lying terrain and bold escarpments. In the eastern part of the plateau, where rainfall is greatest, the plateau is narrow and highly cut by the dissection moving inward from the margins. West of the 100th meridian, the plateau becomes a drier, broad area covered by a plain much like the Llano Estacado. The wide, shallow valleys that have formed in this part of the section generally carry runoff only during rain storms. However, the Pecos River and Rio Grande have cut canyons across the section as deep as 1,000 feet. And on all sides where escarpments exist, the dissected edges carry outflowing streams.

Other surface features on the plateau are limited and generally restricted to erosion or dissolution-type structures. Some shallow sinkholes exist in areas where dissolution of the underlying limestone has caused a collapse of the land surface (Fenneman, 1931).

Sacramento Physiographic Section   West of the Pecos section lies the Sacramento section of the Basin and Range physiographic province,

comprising a narrow, north-south strip approximately 300 miles long and
less than 70 miles wide (Fenneman, 1931). The section is bordered on the
west and south by the Rio Grande depression (Thornbury, 1965) and Mexican
Highlands and on the east by the Great Plains province. The northeastern
boundary of the Sacramento section is formed by the eastward escarpment
of the Glorieta mesa, an intricately carved divide of horizontal strata.
Farther south, the Capitan escarpment marks the boundary of the two
provinces along the southeast side of the Guadalupe Mountains and is
exposed for a distance of some 45 miles between Carlsbad and El Capitan
Peak (Thornbury, 1965).

Topographically, the section is characterized by two major basinal areas,
called bolsons, located at the north and south ends of the section, and
by a series of intervening mountain ranges (Thornbury, 1965).

The Estancia Valley, or Sandoval Bolson, forms the central feature of the
north part of the section, and is bordered on the east by the Glorieta
Mesa and Pedernal Hills, on the west by the Sandia and Manzano Mountains,
and on the south by the elevated Chupadera Mesa. The Estancia Valley,
primarily composed of a group of salt basins and dunes or low hills, was
the site of an extensive lake during Pleistocene time (Thornbury, 1965),
which is now reduced to several small salt lakes.

Southeastward from the Estancia Valley and Pedernal Hills lie a series of
mountain ranges, many of which are bordered on the west by bold scarps
and on the east by gently dipping slopes extending toward the Pecos
Valley. Sierra Blanca, the highest of the mountain ranges, reaches an
elevation of approximately 12,000 feet above sea level. The other ranges
attain maximum elevations of from 8,000 to 10,000 feet (Fenneman, 1931).

At the south end of the Sacramento section is a second large bolson known
as the Salt Basin, situated west of the Guadalupe and Delaware Mountains
and east of the Sierra Diablo or Diablo Plateau. The Salt Basin is a
large down-faulted block with an average floor elevation of about 3,600
feet above sea level. The floor lies some 800 feet below the basin rim

(Thornbury, 1965). The basin covers an area approximately 150 miles long and from 8 to 20 miles wide, rising on both north and south ends to merge into rocky plateaus (Fenneman, 1931). The floor of the basin is covered almost entirely by unconsolidated Cenozoic sediments, with rocky outcrops limited primarily to the margins of the basin (Thornbury, 1965). The LANDSAT color composite of this vicinity shows that the surface sediments are sandy, with a series of salt lakes present in the center of the Salt Basin. Evidence of two Pleistocene lake phases in the basin have been described by King (1948), but their time of formation during the Pleistocene is uncertain.

<u>Mexican Highland Physiographic Section</u> West and south of the Sacramento section lies the vast Mexican Highland section of the Basin and Range physiographic province. This section extends southeastward from Nevada and the Colorado Plateau far into Mexico, where it has its maximum development. The eastern boundary in New Mexio is unclear but is defined as extending east of the Rio Grande to about longitude 106°W, where alternating basins and ranges give way to the faulted and sloping plateaus of the Sacramento section (Fenneman, 1931).

The Mexican Highland section consists of almost equal areas of mountains and plains or basins. In the eastern portion of the section, the mountains generally trend north-south, while in the west they trend northwestward. Of the intermountain area, about half is bolson, and the rest drains or slopes toward the major rivers, such as the Rio Grande. The following discussion considers further only the large-scale features within the eastern part of the section.

The Mexico Highlands mountain ranges of Texas and New Mexico can be grouped into three or more north-south lines from 10 to 50 miles apart and are dominantly Great Basin type, in common with those of the western half of the section. Faulting and related deformation as well as volcanic activity have formed these ranges since Late Tertiary times.

Between the eastern mountain ranges lie generally continuous, flat-floored troughs separated by divides into bolsons or drainage basins (Fenneman, 1931). The two major basins here are the Hueco and Tularosa, on the north, which together mark the eastern border of the section in New Mexico and Texas. They form a trough about 30 to 40 miles wide and 125 miles long, interrupted at the Texas border by a low divide separating the two basins. These basins are grabens in general configuration, bordered on both east and west by fault-bounded mountain ranges. The floors of the basins are relatively flat and slope southward from an elevation of about 4,500 feet at the north end of the Tularosa Basin to 3,500 feet at the south end of the Hueco Basin. The Tularosa Basin exhibits centripetal drainage marked by arroyos and a great salt marsh flanked by the gypsum dunes of White Sands monument.

The northern end of the Tularosa Basin is bordered by Chupadera Mesa averaging 7,000 feet elevation and underlain by gently eastward-dipping Permian strata, which have been dissected almost to maturity (Fenneman, 1931).

3.2.2   Major Geomorphic Features in the Site Vicinity   The geomorphic development of the major land forms which constitute the near-site setting are discussed in this section. These features include the Pecos River drainage system, the Mescalero Plain and associated deposits, karst topography and blowouts. In general, these geomorphic features as considered below are located within the Pecos Valley physiographic section.

Pecos River Drainage System   The Pecos River, 20 miles west of the site, is the only major, perennial stream in the Eddy and Lea Counties area of southeastern New Mexico. It receives almost all of the surface drainage in this region and a large part of the subsurface drainage. The Pecos originates in the southern Rocky Mountains of north-central New Mexico and flows south and southeastward to join the Rio Grande in west Texas (Kottlowski, et al., 1965). The dimensions of the contemporary river valley are stated above in Section 3.2.1 under the Pecos Valley section.

According to King (1948), the Pecos River apparently had its origin to the south, in the Edwards Plateau, as a short tributary of the Rio Grande River. As the Pecos worked its way northward, eroding the Ogallala sediments in the process, it captured the westward-flowing streams of the present upper Pecos valley, thereby reversing their drainage direction. This stream piracy was facilitated by the underlying poorly resistant Permian rocks (Thornbury, 1965).

Bachman (1973, 1974) has expressed the opinion, in accordance with Lee (1925) and Morgan (1942), that the present course of the Pecos was formed, at least in part, through the coalesence of trains of solution sinks (see Karst Topography below, for discussion of solution-sink development). Bachman cites as evidence for this theory many places along the course of the river in southeast New Mexico where the river follows broad meanders, although the floodplain as a whole is unusually narrow or nonexistent, as well as locations adjacent to the Pecos where intermittant tributaries follow seimcircular collapse valleys. Bachman concludes that the river became entrenched in its present position by a combination of this solution-subsidence, headward cutting, and piracy.

The age of entrenchment of the Pecos River is somewhat uncertain. Thornbury (1965) has stated that the age of the piracy which constituted part of the entrenchment process is rather definitely dated as post-Pliocene and is assumed to have taken place in the early Pleistocene. Bachman (1974) has stated that it is not possible to precisely date the entrenchment of the ancestral Pecos River in southern New Mexico. But Bachman has observed (1976) that the Pecos entrenched itself near its present channel along the toes of pediments east of the Sacramento Mountains sometime after middle Pleistocene, which would place the establishment of the present course at a later date.

Since entrenchment, the river has carved a valley in which a variety of subsidence features have developed through dissolution processes which are probably still active in the valley today.

Mescalero Plain   East of the Pecos River to about longitude 104°W lies
an extensive, gently sloping pediment surface known as the Mescalero
Plain (Thornbury, 1965), which extends from the vicinity of Fort Sumner
in northern New Mexico to south of the Mexico-Texas border (Bachman,
1974).   The surface of the plain rises eastward from about 150 feet above
the Pecos River to as much as 400 feet above the river at the base of the
Llano Estacado (Bachman, 1973; Kelley, 1971).   The average elevations
range from about 3,800 to 4,100 feet above sea level in northwestern Lea
County near Mescalero Ridge to about 3,100 feet in southeastern Eddy
County, south of Big Sinks (Bachman, 1973).

Although termed a "plain", the area includes many low mesas, bluffs and
wide draws.   Locally the surface has been dissected by intermittent
streams, but in general the area is poorly drained and contains numerous
playa pans and smaller sinks (Brokaw, et al., 1972; Kelley, 1971).   The
surface of the plain is covered widely with gravels and sands, often
cemented with caliche.   As much as 5 to 10 feet, and locally more, of
these materials are exposed along the edges of the long irregular mesas
of the area (Kelley, 1971).

The Mescalero Plain is very obvious on LANDSAT imagery.   The surface
materials of the plain are generally darker in color and exhibit more
vegetation and higher moisture content than sandy areas.

The Mescalero Plain probably formed during a period of tectonic stability
after deposition of the Gatuna Formation in the Early to Middle
Pleistocene and has been modified both during and after its formation by
solution-subsidence features, discussed below (Bachman, 1976).   The
widely distributed gravel deposits have probably been derived from
erosion of the Ogallala Formation in the Llano Estacado, to the east
(Kelley, 1971).   The development and distribution of caliche and sand
dune deposits, both of which overlie extensive portions of the
pre-caliche Mescalero surface in southeast New Mexico, are discussed
separately in the following paragraphs.

1) <u>Mescalero Caliche</u>

The deposits of the Mescalero Plain are generally covered by the calcareous, cemented remnant of an extensive soil profile known as the Mescalero caliche (see Section 3.3.4). The caliche forms a resistant caprock which averages 3 to 5 feet thick and is generally less than 10 feet thick. It consists of a basal earthy to firm, nodular calcareous deposit and an upper well-cemented laminar caprock (Bachman, 1976). In places, the caliche has weathered to a ledge that overhangs less resistant deposits. The caliche is generally thin; it is locally absent over the solution depressions of the plain, and in areas of collapse may be nearly vertical. Caliche may also be locally absent due to erosion on nondeposition. Because of the generally uniform covering by the erosion-resistant caliche, it is probable that these irregular surfaces result from subsurface solutioning and subsidence of the underlying sediments, primarily after the caliche caprock formed.

Although the genesis of the Mescalero caliche is uncertain, it is thought to be a process dependent upon climatic conditions involving certain ranges of both temperature and rainfall, in which carbonate movement is produced within the soil profile, resulting in the reworking and cementing of the soil constituents into a cohesive, calcareous mass. This caliche formed during a period of stable, semiarid climatic conditions which have been tentatively correlated with the Yarmouthian interglacial stage of the middle Pleistocene (Bachman, 1974, 1976).

2) <u>Eolian Sand</u>

Eolian sand covers much of the Mescalero Plain in southeastern New Mexico and is known locally as the Mescalero sand (Vine, 1963). This sand generally forms two distinct types of deposits - sheetlike stretches of surficial sand, which vary in thickness from about 5 to 15 feet (Bachman, 1973; Vine, 1963), and dunes, having a maximum thickness of about 60 feet (Hendrickson & Jones, 1952).

The eolian sand deposits of the Mescalero Plain have probably been derived from a widespread source of fine-grained sediments. Bachman (1974) suggests that most of this sand originated from the Ogallala Formation, although local sources, such as blowouts, have also been a source of some dune materials. There is litle evidence to indicate that much sand has been derived from the Pecos River (Bachman, 1973, 1974, 1976).

Except where the sand is stabilized by vegetation, it is continually blown about to form transverse dune ridges and barchan dune areas separated by broad flats. The orientation of the dune ridges is not uniform throughout the area, with the long dimension of the ridges apparently reflecting the direction of the strongest prevailing winds at the time of their formation (Vine, 1963) (also see Section 3.6.5).

At least two periods of eolian sand emplacement have occurred since the formation of the Mescalero Plain in Pleistocene time and are evidenced in some places by two distinct layers of sand. The lower deposit consists of a semiconsolidated somewhat clayey sand, as much as 1.5 feet thick, overlain by as much as 20 to 25 feet of loose surficial sand forming the contemporary sheet and dune formations (Bachman, 1976).

Karst Topography The land surface in southeastern New Mexico locally exhibits a karst topography, characterized by geomorphic features such as sinkholes, linear depressions (called solution-subsidence troughs by Olive, 1957), domes (including one known "breccia pipe"), "castiles" and collapsed outliers (Anderson, 1978). Many of these features show up on LANDSAT imagery as ponds and other water-filled depressions concentrated particularly near Roswell and also between the Pecos River and Mescalero Ridge. These features have resulted from the dissolution of salts and other soluble materials within the upper Permian Ochoan Series (see Section 3.3.2), particularly in the Rustler and the Upper Salado. The water required for the dissolution process has come into contact with the soluble materials either by surface exposure, following erosional removal of the protective mantle of younger sediments such as the Ogallala and
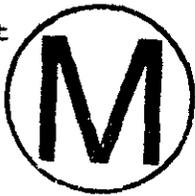
caliche, or at depth, by means of the downward percolation of local surface water or by contact by means of fracture systems between the Ochoan rocks and underlying regional aquifers, which have been exposed along basin margins by the Cenozoic regional uplift, tilting and erosion. These solution processes have been followed by collapse of the insoluble strata into the voids left behind by the dissolution (Bachman, 1974).

Development of karst features may have occurred in southeastern New Mexico as early as Triassic or Jurassic time, when the area was above sea level and probably undergoing extensive erosion which exposed the soluble materials. Bachman (1976) surmised that some dissolution of Permian salts and gypsum probably took place in the western part of the Delaware Basin during Jurassic time, before resubmergence in the Cretaceous. Extensive regional erosion also took place during the early Tertiary, presumably with accompanying renewed dissolution activity, although no sedimentary records of that period are preserved today. The earliest and most widespread basis for relative dating of solution-collapse features in the area is the Mescalero caliche, of Middle Pleistocene time. If, as is generally believed the caliche was derived from a soil profile, it could not have formed on the irregular and, in places, very steep slopes of today. Additionally, the fracturing and slumping of the Mescalero caliche along the widely occurring depressions of the area indicates collapse after Mescalero time. Some of the major collapse features here, such as Nash Draw, Clayton Basin and Crow Flats, exhibit evidence of several intervals of dissolution and subsidence activity. For example, Crow Flats, a large feature 15 miles east of Artesia, contains evidence for at least 3 such episodes, ranging in time from after Triassic and before Pleistocene Gatuna deposition, during or after Gatuna time and after Mescalero time (Bachman, 1976). Notwithstanding this evidence of long term dissolution history, Anderson (1978) believes that many of the deep-seated dissolution features formed during the most recent and most extensive period of salt removal following the Cenozoic erosion and exposure of the evaporites. Much of this activity is suggested to have occurred during the past few million years; dissolution has apparently progressed from west to east and from south to north across the Delaware Basin.

1)   Principal Types of Solution - Subsidence Features

a)   Sinkholes

Sinkholes form a category of features represented by thin or missing
sections of halite in the Castile or by surficial depressions. Thin or
missing halite in the Castile may be determined on the basis of borehole
geophysical logs (see Anderson, 1978); the data may not assuredly
represent dissolution at depth. Sinkholes designated on the basis of one
borehole should also be viewed with caution. Similar data might be
obtained in an area with some salt deformation. For the purposes of
building a working hypothesis of deep dissolution, Anderson (1978) took
these data as possible indications of deep dissolution.

Many of the sinkholes present in the northern Delaware Basin area
developed as deep-seated features originating in the Castile Formation.
These sinks are often expressed as thin or missing sections of the
"Halite I" and "Halite II" salt of the Castile, and to a lesser extent of
smaller salt beds above these units, and resulting structural depression
of the overlying stratigraphic units. At least 100 deep-seated sinks are
estimated to exist presently in the New Mexico portion of the basin.
Around the margin of the basin, a number of these deep-seated sinks
appear to be associated with anticlinal structures in the salt; in the
mid-basin area, these sinks occur as both isolated features and in
association with salt anticlines (Anderson, 1978). In addition to these
deep-seated features, there are many sinks present in the area which are
associated with active near-surface dissolution, such as those along the
Pecos River and in Nash Draw (Anderson, 1978).

Compound sinkholes, resulting from coalescing collapse sinks, are common
along the Pecos River valley south of Roswell. Many of these sinks have
collapsed within historic time (Bachman, 1974). As discussed above,
Bachman (1974) has suggested that the course of the Pecos River southward
from Carlsbad to near the New Mexico-Texas border lies within a major
belt of such collapse sinks. Bachman has also described similar

developments along the east side of the Pecos River southeast of
Carlsbad, where a linear scarp is believed to have formed as the result
of a collapse structure which is now occupied by the river.

b)   Dolines

Dolines are very common features in southeastern New Mexico, forming on
limestone bedrock and caliche surfaces. Dolines are defined as
relatively shallow solution sinks that develop on the surface beneath the
soil mantle without physically disturbing the underlying rocks or being
underlain by subsurface solution cavities (Bachman, 1974).

c)   Solution-Subsidence Troughs

Narrow, linear, generally northeast-trending depressions that vary in
width from a few hundred feet to a mile and in length from one-half mile
to 10 miles in southeastern New Mexico have been termed
solution-subsidence troughs by Olive (1957), who proposes that these
troughs result from the subsidence of near-surface material which fills
voids dissolved by water flowing in underground channels. According to
Thornbury (1965), these troughs are particularly common west of the Pecos
in areas underlain by the Castile Formation and extend eastward, parallel
to the regional dip as a result of dissolution along eastward-trending
joint systems that parallel the regional dip.

Bachman and Johnson (1973) also describe linear features occurring in
areas generally underlain by the Ogallala, to the north and northeast of
the site, and suggest that at least some of these depressions may be the
result of alternate leaching and wind deflation (Judson, 1950; Price,
1958). These features appear on LANDSAT imagery as alternating linear
strips of vegetation and white to gray soil, trending NW-SE. They are
most prominent north of Hobbs, north of San Simon Sink, and at scattered
locations on the Mescalero Plain. The leaching may have been produced by
the chemical action of plant growth on the caliche surface between
longitudinal sand dunes where small amounts of ground water were able to

collect during periods of eolian quiescence; later periods of eolian activity removed these leached sediments from between the dunes. The swales left behind by this leaching activity mark the location of former longitudinal dune fields which have been displaced or removed by continued eolian activity. The effect of these linear features has been to provide depressions in which surface runoff collects and serves as sources of ground water recharge. Solutioning and erosion along these lineaments may have also opened conduits to the subsurface and contributed to a more rapid dissolution of the underlying soluble rocks (Bachman and Johnson, 1973).

d)   Breccia Pipes and Domes

Various domal structures, having diameters of from several hundred to several thousand feet, occur in southeastern New Mexico, particularly along and east of the Pecos River, and are associated with areas of relatively recent surface salt dissolution (Anderson, 1978). Although they have been termed "breccia pipes," these features have no relationship whatsoever to volcanic activity. Many of the domes have been breached by erosion to reveal brecciated cores of stratigraphically displaced Gatuna, Rustler, and Triassic beds. These features are also characterized by doming-related deformation of rocks as young as the Mescalero caliche (Vine, 1960). The depth to which these breccia pipes extend is not known; one pipe is known to reach as deep as the McNutt member of the Salado Formation, as evidenced by underground exposures in the Mississippi Chemical Company potash mine (Griswold, 1977).

Anderson (1978) hypothesized that breccia pipes originate from the dissolution of salt at depth by waters circulating along intersecting joint sets in adjacent brittle rocks. Subsequent collapse of insolubles into the cavity forms a rubble breccia chimney, which sometimes penetrates to the ground surface. The only known breccia pipe (located in the Mississippi Chemical Corporation mine in Nash Draw) is observed to be well-cemented by fine-grained material with no perceptible open space. There is no evidence of removal of soluble material from the

evaporites adjacent to the feature in the mine. This particular feature is expressed at the surface by a dome with a collapsed center. The doming of this brecciated core takes place at a later time. Vine (1960) has suggested three possible mechanisms for this later deformation: the erosion of the rock surrounding the core of the sink; the upward flow of salt into the sink; an increase in volume of rock as anhydrite is altered to gypsum in the brecciated core. Anderson (1978) expressed the opinion that the doming has been produced by regional near-surface dissolution removing the salt from around the pipes and producing a sagging of the beds around the pipes. As a result of the doming process, the rock strata surrounding the dome at the surface generally dip away from the breccia pipe core (Vine, 1960). Underground, in the Mississippi Chemical mine, beds adjacent to the breccia pipe dip down toward the breccia pipe at about 10-20°.

The age of the breccia pipe formation in this area has not been determined. Mescalero caliche, of Middle Pleistocene age, is present on the flanks of breccia pipes and lying at steeper angles than those at which the caliche probably originally formed. This may indicate that the breccia pipes are younger than the Mid-Pleistocene. It is also possible, however, that the breccia pipes predate the caliche and that later subsurface removal of salt by dissolution produced greater amounts of downdrop away from the more resistant breccia pipes, resulting in the slopes present today. (Continuing studies of these features are addressed in Chapter 10.)

Despite the fact that the breccia pipes which have been recognized are generally expressed topographically as domes, it has been surmised that others may have no surficial expression and have therefore gone undetected to the present time. Geophysical exploration has been used to explore for pipes without surficial expression. Electrical resistivity surveys have shown that the breccia core of the known pipe has a much lower resistivity than does the surrounding undisturbed strata (Elliot, 1976). Continuity of seismic reflections are lost when similar geomorphic features are crossed by survey lines (Griswold, 1977).

e)   Collapsed Outliers and "Castiles"

Outliers of the Rustler Formation, separated from the main outcrop area through erosional processes, as described by Anderson (1978), are circular to elongate or irregular collapse features consisting mostly of the Culebra dolomite. They occur where the salt has been completely dissolved from the evaporites.

Limestone buttes, called Castiles, occur west and south of the collapsed outliers, primarily in Texas, in the lower part of the Castile Formation outcrop area. These features consist of biogenic calcite which has replaced the gypsum or anhydrite of the Castile Formation, and some exhibit collapse structures with brecciated cores. These buttes are similar in size and distribution to the collapsed outliers (Anderson, 1978).

2)   Major Near-Site Features

Major geomorphic features which have formed in the area of the proposed WIPP site as a result of sinkhole formation and related solution-subsidence mechanisms include Nash Draw and San Simon Swale (see Figure 2-1 for their location and topographic configurations). These features and their specific development are discussed separately, below.

a)   Nash Draw

Approximately 5 miles northwest of the proposed WIPP site is a prominent geomorphic feature, known as Nash Draw, which Vine (1960) described as "a sinuous depression about 4 miles wide and 18 miles long." Its surface structural expression is similar to that of a breached anticline plunging gently northward, with the older Rustler Formation exposed in its center and the younger Dewey Lake redbeds and Santa Rosa Sandstone exposed along its flanks. However, well records in the area indicate that the bedrock underlying the draw exhibits a gentle homoclinal configuration. Accordingly, Nash Draw has been identified as an undrained physiographic

depression, which has probably developed as a result of regional and differential dissolution of the anhydrite, gypsum and halite beds of the Rustler and upper Salado Formations (Vine, 1963).

According to Vine (1963), dissolution on top of the massive salt in the Salado has produced a rather uniform lowering of the land surface in Nash Draw, but its surficial structural features have been produced and greatly modified by differential solution of the more soluble portions of the Rustler Formation. While the bedrock in the northern part of Nash Draw is generally covered by eolian sand, caliche and alluvium, the central and southern portions of the draw contain exposures of Rustler that has been highly deformed primarily as a result of large-scale collapse following solution of the Rustler and Salado. This dissolution activity has also produced numerous individual sinkholes in Nash Draw, which vary in configuration from circular features a few tens or hundreds of feet across to irregular or arcuate features up to more than a mile across. Many of the larger depressions in the area of Nash Draw, including the basin at its southwestern extent which contains Salt Lake, have probably formed through the coalescing of several smaller solution depressions or sinks. Some such places, where several depressions tend to line up may also indicate the location of subterranean cavernous water courses (Vine, 1963).

The age of the earliest solution activity that produced Nash Draw is uncertain. It is thought that some of the deep-seated solution in the Delaware Basin area had occurred by the middle part of the Mesozic, but that a substantial amount of this process has taken place since the Late Tertiary regional tilting of this area. Within Nash Draw, the formation of a large number of the individual solution features has resulted in the deformation of rock units as young as the Pleistocene Mescalero caliche, which indicates that Quaternary dissolution of the Salado and Rustler Formations is of primary importance in the geomorphic history of Nash Draw. Assuming that this disturbed caliche originally lay at an elevation corresponding to that of the adjacent Mescalero Plain, then at least 100 to 150 feet of local warping and depression has occurred in

Nash Draw within relatively recent time (Vine, 1963). Bachman (1974)
estimated that at one place in Nash Draw a surface lowering of
approximately 180 feet, almost wholly the result of solutioning and
subsidence, has occurred in the past 600,000 years.

b)   San Simon Swale

San Simon Swale is one of a series of large deep-dissolution depressions
filled with Cenozoic sediments, lying above the inner margin of the
Capitan reef along the eastern side of the Delaware Basin (Anderson,
1978). Situated approximately 20 miles east of the proposed WIPP site,
San Simon Swale forms a southeasterly-trending depression approximately
25 miles long and from 2 to 6 miles in width. Much of the surface of the
swale is at present covered by eolian sand, which masks the relief. Of
particular interest within San Simon Swale is a compound collapse feature
called San Simon Sink, which occupies an area about 2 miles long and 1
mile wide at the southeastern end of the swale (Bachman and Johnson,
1973).

San Simon Swale originated from a combination of surface stream erosion
and solution-subsidence (Bachman & Johnson, 1973). During the
Pleistocene, a major tributary of the Pecos River is thought to have
flowed southeastward through what is now San Simon Swale to join the
Pecos in western Texas. The initial course of this tributary was
determined as it eroded its way through the caliche caprock of the
Ogallala Formation (Bachman and Johnson, 1973). The dissolution and
subsequent removal of these beds resulted in the formation of numerous
sinkholes, some of which coalesced to form, at least in part, the
depression now known as San Simon Swale (Bachman and Johnson, 1973). The
swale has been lowered at least 180 to 200 feet below its original
surface, in view of lake deposits in the sink encountered during
preliminary WIPP studies. Current drilling operations reveal a thickness
of over 600 feet of post-Ogallala sediments underlying the present floor
of the swale.

Within San Simon Swale, the San Simon Sink formed as a secondary collapse structure, probably during the Pleistocene. Numerous ring fractures around the sink indicate that it has had a long history of successive collapse events since its initial formation (Bachman and Johnson, 1973). The most recent of these events is reported to have occurred in the 1930's (Nicholson and Clebsch, 1961). It is therefore assumed that salt dissolution in the underlying formation is continuing here and it is thought by some that the resulting brine is being carried in a southeasterly direction toward Texas (Bachman and Johnson, 1973).

On the basis of written communication from C.L. Jones of the U.S. Geological Survey, Bachman (1973) reported that over 500 feet of Cenozoic sediments have thus far been deposited in San Simon Sink. Nicholson and Clebsch (1961) have estimated that alluvium is presently being deposited in the sink at a rate of about 1 foot in 5 years. Recently acquired core (WIPP 15) from San Simon Sink has been analyzed in a preliminary way (Anderson, 1978) showing about 545 feet of fill on top of Triassic sediments. Dates on the fill have not yet been obtained.

Blowouts Some of the basins which are present in southeastern New Mexico have been formed by processes other than the previously described mechanisms of dissolution and collapse. The most conspicuous of these basins in the area of the proposed WIPP site are named Williams Sink, Laguna Gatuna and Laguna Plata, all of which are situated approximately 15 miles to the north of the site.

These features, termed blowouts, have formed through the removal of loose sand deposits by wind erosion. During the rainy season, many of the depressions which have resulted are partially filled with water. The floors of the blowouts are mantled with clay and saline deposits, and many blowouts are surrounded by eolian sand. Dune fields commonly develop along the northeastern and eastern leeward margins of these depressions (Bachman, 1974).

3.2.3   Erosion Rate- Significance of Geomorphic Developments to Site

This section provides a short review of the degree to which the major
surface and subsurface processes discussed in the previous section have
affected the land surface in the vicinity of the site and discusses to
what extent these activities may be predictive of future geomorphic
modifications in this area.

The resistant Mescalero caliche covers most of the land surface in the
vicinity of the site and underlies the site itself. Where present, the
caliche provides an indication that no significant erosion of the surface
in these areas has occurred since the formation of the caliche in
Mid-Pleistocene time.

The major areas of relief which have developed since this time have
probably been produced to a large extent from subsurface dissolution and
subsidence. The two major features of significance to the site,
originating from these processes, are Nash Draw and San Simon Swale. In
Nash Draw the surface has been lowered at least 100 feet by dissolution,
and locally as much as 180 feet, within approximately the past half
million years. Bachman (1974) also cited one location within the draw
where the lowering of the ground surface appears to have exceeeded the
rate of salt removal, indicating a surface erosion of about 40 feet in
addition to solution activities. San Simon Swale, a product of surface
erosion as well as solution-subsidence, lies at its lowest point some 180
to 200 feet below the surrounding land surface (Claiborne and Gera,
1974), and may have undergone a total subsidence of about 750 feet. No
age has yet been obtained from the sediments obtained during recent
drilling. (See Chapter 10, Continuing Studies.)

Wind erosion has produced other depressions in the area, with a resultant
buildup of material in the same vicinity. However, these features are
generally of only minor dimensions and are local in extent (Claiborne and
Gera, 1974).

These observations should not be considered as constants for rates of erosion which would hold true for the future. But in providing a general indication of the surface modification in the vicinity of the WIPP site, they do indicate the pattern of continuing geomorphic development of the area. Variations in climatic conditions give rise to variations in rates of denudation and also in rates of subsurface dissolution. The nature of the ground surface is also of major importance in terms of its vulnerability to erosional processes.

The site is located west of and near a drainage divide between Nash Draw and San Simon Swale, where it appears that very little dissolution or surface erosion has occurred since Early Pleistocene time, as evidenced by the relatively undisturbed nature of the Mescalero caliche there, which has also served as a protective layer for the underlying soluble rock units. Contouring studies, too, indicate that this area has been a drainage divide between San Simon Swale and Nash Draw at least since Mid-Pleistocene time (Bachman, 1976). Although erosion here has been minimal under the present semiarid climatic conditions, if more humid conditions should develop in the future, an accelerated erosion of the caliche is reasonable to expect. However, with increased rainfall, it is also expected that Nash Draw and San Simon Swale will be exposed to more erosive stress, since most of the runoff will probably flow out of the immediate area along these depressions.

3.3 REGIONAL STRATIGRAPHY AND LITHOLOGY

3.3.1 Precambrian Rocks

Metasediments and granitic igneous materials consititute the majority of the basement rock of the southeast New Mexico – west Texas region. These Precambrian rocks crop out in only a few localities, in the western part of the region, such as the Nigger Ed Canyon area of the Sacramento Mountains (Pray, 1954), in the core of the Pajarito Mountain dome (Kelley, 1971) and in the Bent Dome, east of Tularosa (Bachman, 1960). Data on the Precambrian underlying the Delaware Basin and further east

and south across the Central Basin Platform into southwest Texas have been obtained principally through oil company records; hundreds of wells have been drilled in this area, particularly on the Central Basin Platform. Little data are available from the basin areas, where most wells penetrate only to the Upper and Middle Paleozoic sections.

The configuration of the Precambrian basement surface reflects the late Paleozoic structural framework of the region (see Figure 3.4-2). The surface is deepest along the northern axial portion of the Delaware Basin, where it reaches a depth of about 20,000 feet below sea level. The basement surface rises to the east, north and west of the Delaware Basin. On the northeast, into Otero and Chaves Counties, the basement rises fairly uniformly to more than 4,000 feet above sea level; on the east, the surface rises rapidly on the Central Basin Platform to elevations of between -5,000 and -4,000 feet (Cohee, et al., 1962; Foster and Stipp, 1961). Well data suggest that a number of post-Precambrian faults break the profile of the basement surface throughout the region. A notable example of this occurs along the west margin of the uplifted Central Basin Platform, where a vertical offset of perhaps more than 5,000 feet is present along the south portion of a large normal fault system.

The Precambrian sections which have been examined display a complex association of metasedimentary, sedimentary, metavolcanic, volcanic and plutonic rock types, suggesting a history of repeated orogenic activity interspersed with erosional episodes. Muehlberger, et al. (1967) have classified the Precambrian rocks of the region into a number of terranes of various age and lithology. A modified version of their geological map, Figure 3.3-1, presents the distribution of the major Precambrian rock types of the area.

Outcrops of probably Late Precambrian age slightly metamorphosed siltstones, shales and fine-grained quartz sandstone with associated intrusive sills are found in the vicinity of Nigger Ed Canyon in the Sacramento Mountains. The majority of the sills are diabase, and some are markedly porphyritic (Pray, 1954, 1961).

In the subsurface, similar Precambrian diabase and incipiently
metamorphased clastics, including quartzite, siltstone and impure
limestone, comprise a broad band which extends from southern Otero County
northward for over 200 miles to southeastern Guadalupe Country.
Muehlberger, et al. (1967) have termed these rocks the DeBaca terrane.
In the Franklin Mountains at the extreme western tip of Texas, these
metasediments attain a known thickness of almost 4,000 feet (Harbour,
1960). The rocks are underlain, at least in part, by rhyolites of the
Panhandle volcanic terrane, discussed below, and are overlain in the
Franklin Mountains by up to 1,000 feet of rhyolite (Harbour, 1960) dated
at 900 million years.

To the east of the Sacramento Mountains on the Northwestern Shelf, an
approximately 2-square-mile outcrop of Precambrian rock is exposed in the
core of Pajarito Mountain dome. These rocks, radiometrically dated as
1,270 million years old, consist of hornblende, syenite, hornblende
syenite gneiss, and some diabase, locally intruded by leucocratic syenite
and hornblende syenite pegmatite (Kelley, 1971). Granitics apparently
underlie most of the south-central parts of New Mexico and large areas in
Eddy and Lea Counties (Foster & Stipp, 1961), extending at least as far
west as the Guadalupe Mountains as well as south and southeastward into
Texas (Flawn 1954: Muehlberger et al. 1967). These rocks, named the
Chaves granitic terrane, are largely granite, granodiorite,
compositionally equivalent gneiss and lesser amounts of metasedimentary
and metaigneous rocks. Granite comprises about 80 percent of the samples
studied. Foliation in these rocks is generally faint, but is enhanced by
some shearing (Muehlberger et al., 1967). Wasserberg et al. (1962) dated
the granitics in this area as between 1,250 and 1,400 million years in
the north and as young as 1,090 million years to the south. These
granitics appear to predate the sedimentary Precambrian rocks to the west
(Foster & Stipp, 1961).

Younger volcanics, which appear to have been extruded and deposited as a
relatively thin layer above the granitics, are present in at least parts
of Chaves, Lea, Roosevelt, Curry and Quay counties as well as near the

south border of New Mexico west of the Brokeoff Mountains and eastward in the Texas Panhandle (Foster & Stipp, 1961; Muehlberger, 1967). These rocks, known as the Panhandle volcanics, are primarily rhyolitic flows and tuffs and pyroclastics with subordinate trachytic and andesitic types. The volcanics are mostly undeformed and unmetamorphosed. Rb-Sr dating of these rocks yields an average age of 1,140 ± 50 million years (Muehlberger et al., 1967).

Gabbro and diabase or basalt, commonly showing intergranular ophitic to subophitic textures, underlies parts of Roosevelt and southern Curry Counties and extends eastward into Texas. These rocks, termed the Swisher diabasic terrane, intrude the volcanics, and, although their age is uncertain, are considered Precambrian (Muehlberger et al., 1967; Flawn, 1954). According to Flawn (1954, 1956), these rocks appear to be a great stratiform body occupying a major basement syncline, although no large positive gravity or magnetic anomaly is present over this region.

Clastics of Late Precambrian age crop out near Van Horn, Texas. These deposits are part of an alluvial fan which is overlain by the Bliss sandstone (McGowan and Groat, 1971). Elsewhere, including the Guadalupe Mountains, these rocks have been studied through well cuttings.

3.3.2 Paleozoic Rocks
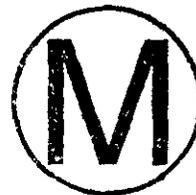
Cambrian Rocks

Very little is known about the existence or nature of any Cambrian sediments underlying the Delaware and Val Verde Basins area of southeast New Mexico-west Texas, partly because the great thickness of the overlying section in this region and partly because the belief that the Ordovician Ellenburger is the deepest potential reservoir formation has discouraged deeper drilling (Vertrees et al., 1959).

Basal Paleozoic clastics were named the Bliss Sandstone by Richardson (1904) for exposures in the Franklin Mountains. They range in thickness from 0 feet to the north to about 375 feet toward the south. The Bliss unconformably overlies the Precambrian and in most places is conformably overlain by the El Paso Group (Hayes, 1964). According to Harbour (1960), the Bliss is probably a beach or near-shore deposit of the sea in which the overlying El Paso Limestone accumulated.

In its type locality and in most areas east of longitude 107°W, the Bliss generally consists of over 90% sandstone that is thin-bedded and jointed. Subordinate, thin interbeds of siltstone or shale and rare thin beds of sandy limestone or dolomite are present. Dark siltstone grains, cemented by glauconite and hematite, combine to produce a dark color (Hayes, 1975; Harbour, 1972).

In the Sacramento Mountains of southeastern New Mexico, the Bliss Sandstone is exposed in the vicinity of Nigger Ed Canyon. A 10° angular unconformity separates it from the underlying Precambrian. The Bliss in this area contains 110 feet of quartz sandstone, minor dolomitic sandstone, sandy dolomite, brown-weathering sandstone interbeds in the upper third of the section. Abundant glauconite is present in some of the strata. In general, this section is similar to that at the type locality near El Paso (Pray 1954, 1961). Farther southeast in the subsurface at the Guadalupe Mountains area, the Bliss consists of less than 30 feet of light gray to white, poorly sorted, coarse-grained quartz sandstone at the base and top, separated by gray, fine-to-medium grained, sandy dolomite (Hayes, 1964).

Most investigators consider the Bliss Sandstone to be diachronous, ranging in age from Late Cambrian through Early Ordovician, becoming younger from west to east, as determined from faunal evidence and lithologic correlations (Hayes, 1975). The Bliss of the Sacramento Mountain area has been dated as Cambrian by the Residue Research Laboratory of Midland (Roswell Geological Society, 1953). However, Flower (1953) has indicated that the formation is time-transgressive and

contains both Late Cambrian and Early Ordovician fauna in New Mexico (Harbour, 1972). The evidence indicates that in its easternmost localities, the entire Bliss is of Early Ordovician age (Hayes, 1975). Hayes reported in 1964 that it is very likely that the Bliss in the subsurface of the Guadalupe Mountains area is entirely Ordovician. Foster (1974) also considers that the Bliss sediments of the southeastern New Mexico Delaware Basin area probably correlates only with the Ordovician part of the unit as defined in Texas.

Ordovician Rocks   The Lower Ordovician section is composed mainly of carbonates deposited in a shallow sea with a relatively calm shelf environment (see Figure 3.3-2). In 1904 Richardson named exposures in the Franklin Mountains the El Paso Limestone (Hayes, 1975). Cloud and Barnes (1948) named exposures in western and central Texas the Ellenburger Group, and this name is commonly applied to subsurface rocks in the Permian Basin. Some workers have subdivided these rocks into formational groupings that are recognizable over much of the region. For discussion of nomenclature and detailed stratigraphy, refer to Hayes (1975).

Where the El Paso crops out in the Sacramento Mountains escarpment, it is composed of up to about 420 feet of light-to-olive-gray, very fine-to medium-grained dolomite. Thin to medium beds predominate, chert nodules occur sporadically, and interbeds of dolomitic quartz sandstone are common toward the base, derived from erosion of rocks to the east. In the Sacramento Mountain area, at least, the El Paso appears to be either time-transitional with the Bliss Sandstone or separated from it by a minor disconformity (Pray, 1961). To the southeast, in the subsurface of the Guadalupe Mountains, the El Paso comprises from 520 to 550 feet of gray, fine-to medium-grained, crystalline, siliceous dolomite with some sand near the base and top and some light-colored aphanitic chert. Eastward in the Delaware Basin over 700 feet of El Paso or Ellenburger has been encountered. In the New Mexico portion of the basin, the formation is almost entirely a light-gray to gray crystalline dolomite with small amounts of sandstone; much chert is present in some localities

near the top of the section (Haigler, 1962). South and southeastward in the west Texas Delaware-Val Verde Basin area, the Ellenburger reaches a maximum thickness of at least 1,600 feet and is composed almost entirely of limestone and dolomite (Vertrees et al., 1959). Its limestones are light-gray and dominantly sublithographic, becoming purer upward; the dolomites range from coarse-grained pale rocks, generally near the bottom to finer-grained, more brightly colored ones above (Cloud and Barnes, 1946).

Middle Ordovician sediments comprising the Simpson Group are recognized in the subsurface from the Guadalupe Mountains area through the Delaware Basin and east into Texas. The Simpson thins rapidly to the west at an average rate of about 10 feet per mile (Hayes, 1964), wedging out near Artesia, New Mexico. To the north, it extends to the latitude of Roswell and elsewhere is truncated by erosional unconformities. Where the Simpson, or equivalent, is encountered within the New Mexico portion of the Delaware Basin, it ranges in thickness from less than 200 feet to 1,850 feet in southern Lea County (Nicholson & Clebsch, 1961). In the basin, the Simpson consists of 3 main layers of limestone, alternating with thinner green, brown and black shale, black shale with rounded quartz grain inclusions, and sandstone (Haigler, 1962). Towards the south and southeast, the formation thickens considerably, reaching a maximum of at least 2,250 feet before wedging out in the Marathon Mountains region. Shaly facies predominate towards the south. In the Delaware-Val Verde region, the sandstones and some of the carbonate members are potential oil and gas reservoirs (Vertrees et al., 1959).

In the subsurface of the Permian Basin, the Simpson is overlain conformably by carbonates of the Montoya Group, assigned to the Middle and Late Ordovician by Hayes (1975). At the type locality in the Franklin Mountains, the Montoya ranges in thickness from about 140 to 250 feet, averaging about 200 to 225 feet, and consists of a lower olive gray to dark gray cliff-forming dolomite with a thin, very coarse-grained quartz sandstone at the base and an upper, lighter colored cherty and finer-grained, slope-forming dolomite. The top of the group is marked by

a zone of bedded chert (Bachman and Myers, 1969). Eastward in the north part of the Delaware Basin, the Montoya ranges from about 280 to 440 feet in thickness and consists of medium-to dark-gray dolomite with minor amounts of dark gray limestone and chert (Haigler, 1962). Where it occurs on the Central Basin Platform, the Montoya is a cherty limestone about 150 feet thick. To the south, the Montoya is composed of primarily chert and dolomite, reaching a maximum thickness of 600 feet (Vertrees et al., 1959).

The uppermost rocks of Ordovician age in the area consist of a generally light-gray, thin-bedded dolomite with some marl. It had been included by Darton (1917, 1928) as the lower part of the Fusselman, but having been recognized by Kelley and Silver (1952) as Ordovician, it was removed from the Fusselman and renamed the Cutter Formation. Pray (1954) called it the Valmont, where he encountered it in the Sacramento Mountains. Now, however, these beds have been established as the Cutter Member of the Montoya Dolomite (Harbour, 1972; Bachman and Myers, 1969).

Silurian Rocks   The Silurian of the southeast New Mexico - west Texas areas consists of the Fusselman limestone and the carbonates and shales of an "Upper Silurian" unit, both of which were deposited in a broad subsiding area named the Tobosa Basin.

The Fusselman rests unconformably on the Late Ordovician Montoya and ranges in thickness from 0 to 1,000 feet in part of southern New Mexico and west Texas, and thins westward and northward into an erosional wedge (Hayes, 1975). It is composed of a massively-bedded, clean, light-colored dolomite and locally limestone. The limestone facies is dominant to the southeast; a thicker dolomite facies is dominant to the north and west. The Fusselman has been dated as Middle Silurian and possibly also Early Silurian in age (McGlasson, 1968; Hayes, 1975; Pray 1958).

In the Sacramento Mountain area, the sequence overlying the Montoya has been divided by Pray (1953, 1954, 1961) into two units. The lower member, which he termed the Valmont, is composed mostly of light gray, very finely textured dolomite ranging in thickness from 150 to 225 feet. The upper part of the sequence in the Sacramento area, recognized by Pray (1954) as Silurian, comprises a medium to finely crystalline, light to medium gray, cherty dolomite not exceeding 100 feet. As identified in the subsurface of the Guadalupe Mountains, the Fusselman ranges from 580 feet to about 740 feet of white to light gray, coarse to medium crystalline dolomite, which contrasts sharply with the darker, fine-grained underlying Montoya (Hayes, 1964). In the Delaware Basin, the Fusselman is a light-colored dolomite containing abundant chert and two thick limestone intervals. It reaches its maximum thickness in southern Lea Country. Eastward across the Central Basin Platform, the Fusselman is represented by a coarse-grained crystalline glauconitic limestone and dolomite 180 to 200 feet thick (Nicholson & Clebsch, 1961).

The subsurface unit informally called the "Upper Silurian" consists of a shaly facies to the southeast and much thicker carbonate facies to the north and west. The unit is more restricted areally than is the underlying Fusselman, pinching out northward and westward across north-central Eddy and Lea Counties. The carbonate facies predominates in the New Mexico portion of the Delaware Basin and includes both limestones and dolomites, reaching over 1,500 feet in thickness (McGlasson, 1969). On the Central Basin Platform, it consists of 180 feet of green, gray, and black shales interbedded with dense limestones (Nicholson & Clebsch, 1961). Southward into Texas, the shaly facies is composed of bright green to dark brown shales and white to brown calcilutites with a maximum thickness of 300 feet (McGlasson, 1968).

Devonian Rocks Lower to Middle Devonian rocks are known only from subsurface exploration, and only in the southeastern corner of Lea County, New Mexico. Called the "Devonian" rock unit by McGlasson (1965), these rocks are more restricted in area than the "Upper Silurian" and range in thickness from zero to 1,000 feet in the vicinity of Crane

County, Texas. The unit is composed primarily of chert in the southwest, grading northeastward into dark siliceous micrite and light-colored calcarenite. After deposition, the unit underwent considerable diagenetic alteration.

In the western part of the region, along the Sacramento Mountain escarpment, a unit dated as upper Middle Devonian, the Onate, has been recognized (Pray, 1954, 1961). It consists largely of dark gray to olive gray, very fine-grained dolomite mixed with coarse silt to very fine quartz sand, with minor shale, increasing to the south. Small, irregular chert or silicified dolomite nodules several inches long are distinctive lithologic features of the upper part of the formation in the central and northern parts of the escarpment. To the west the Onate forms beds generally less than 1 foot thick and rarely thicker than 2 feet but is as much as 60 feet thick in the central escarpment area, thinning northward and southward.

Upper Devonian rocks in the subsurface of the southeast New Mexico area constitute the Woodford shale, portions of which are also variously known as the Percha shale and Canutillo Formation. These rocks are described by McGlasson (1968) as extending from eastern Chaves and southern Roosevelt Counties in New Mexico, southward and eastward through western Texas and ranging in thickness from zero to approximately 700 feet near the southeast corner of Lea County, with an average of 200 feet elsewhere (Vertrees et al., 1959). The Woodford is a dark brown to black, fissile, bituminous, spore-bearing shale which becomes arenaceous northward and contains black chert to the south and west (McGlasson, 1968).

Across the Central Basin Platform, the rocks correlative to the Woodford in age consist of interbedded, calcareous chert and siliceous limestone, reaching a maximum thickness of 980 feet (Nicholson & Clebsch, 1961). Westward in the northern Delaware Basin, the unit decreases to less than about 200 feet thick and is an organic pyritic shale. In the Guadalupe Mountain area, the unit comprises less than 100 feet of dark gray, locally silty shale, with a few feet of dark or medium gray chert at its

base (Hayes, 1964). At the northwestern limit of the unit in the Sacramento Mountains, the lower Upper Devonian section has been called the Sly Gap Formation and consists of up to 50 feet of calcareous, yellow-gray to dark gray shale with irregular nodular limestone becoming predominant upward. This unit is absent in the south half of the escarpment, where the Upper Devonian is represented by a dark gray noncalcareous shale, considered equivalent of the Percha shale and recognized southward as the Woodford (Pray, 1954).

The Woodford and equivalent units are transgressive and lie unconformably on an erosional surface formed on the rocks of the older Devonian section through the Ordovician Montoya Group. According to McGlasson (1968), the upper portion of the Woodford deposition probably was deposited in Early Mississippian time. At its upper limit, the Woodford is conformably overlain by limestones and sandstones of the Early Mississippian.

Mississippian Rocks Mississippian rocks throughout most of the southeast New Mexico-west Texas area consist of limestones overlain by shales, which together attain a maximum thickness of some 2,400 feet, truncated by erosional unconformities (Vertrees et al., 1959). Rocks of definite Mississippian age appear to be absent across the Central Basin Platform (Nicholson & Chelbsch, 1961).

The Lower Mississippian Kinderhookian-Osagian series is represented in southeast New Mexico and west Texas by a limestone unit (Roswell Geol. Soc. 1958). It is 365 feet thick in the Guadalupe Mountains and 220 to 320 feet in the northern Delaware Basin, thickening to the southeast and thinning to the west (Haigler, 1961). The limestone is light gray to brown, finely crystalline and commonly cherty, with a basal dark gray organic-rich shale unit. The limestone partially grades to shale southeastward from the northern margin of the Delaware Basin (Brokaw et al., 1972; Haigler, 1962). The northwestern face of the Sacramento Mountains contains exposed units of equivalent age, but detailed correlation with the foregoing surface data from the rest of the area is unreliable (Haigler, 1962). The Kinderhookian here is represented by up

to 60 feet of Caballero limestone and calcareous shales. The overlying Osagian series Lake Valley Formation, which attains a thickness of about 400 feet in the northern and central Sacramento Mountains, is composed of 6 members whose dominant lithology is limestone containing various amounts of chert and argillaceous and biohermal materials (Pray, 1954).

The Upper Mississippian rocks in the subsurface of southeast New Mexico, apart from the Sacramento area, consist of black, brown and gray shale much of which is silty, variously named the Barnett, Chester or Meramec (Brokaw et al., 1972; Haigler, 1962). Near the north and west edges of the Delaware Basin, and in the Guadalupe Mountains, gray limestone beds occur at the top of the Mississippian shale, with some interspersed thin sandstone beds. To the east and south, in the central portion of the Delaware Basin, the unit consists of between 250 and 320 feet of primarily a black argillaceous shale with a dark gray to black calcareous shale of shaly limestone comprising approximately the lower 100 feet of section (Haigler, 1962). Equivalent age rocks in the western part of the region have been defined as the Rancheria and Helms Formations of Meramacian and Chesterian age, respectively. The Rancheria, whose type locality is north of El Paso, Texas, closely resembles the Lower Mississippian limestones of the southeast New Mexico area. (For detailed description, refer to Harbour, 1972). The Rancheria is up to 400 feet thick in the Franklin Mountains and 300 feet at the south end of the Sacramento Mountains, thinning northward, and is composed of gray argillaceous and silty thin-bedded limestone with minor shales and massive crinoidal limestone strata. Its basal contact is an angular unconformity with the underlying Lake Valley and Caballero. The Helms, of latest Mississippian age, which reaches a maximum of 230 feet in the Franklin Mountains and only 60 feet northward in the Sacramento Mountains, consists of thin-bedded, argillaceous limestone and yellow to gray calcareous interbedded shales with lesser limestones (Harbour, 1972; Pray, 1954).

<u>Pennsylvanian Rocks</u> Post-Mississippian orogeny uplifted and tilted much of the southeast New Mexico-west Texas basinal areas, eroding the exposed rocks and, upon subsequent Pennsylvanian deposition, producing a major angular unconformity called the Springer hiatus (McGlasson, 1968). Relatively rapid, almost continual deposition in most of the region resulted in a thick Pennsylvanian carbonate section, with large volumes of terrigenous clastics in some places. The Pennsylvanian in places is thicker than the entire underlying Paleozoic section (Pray, 1954). Total thickness of the Pennsylvanian section varies from about 3,000 feet in the Sacramento Mountains, near 2,500 feet in the northern Delaware Basin, and between 1,650 and 2,700 feet in southern Lea County along the Central Basin Platform.

The rocks of Pennsylvanian age were derived from a variety of different sources and deposited in increasingly active structural settings. As a result, the lithology of the section is highly variable, both horizontally and vertically, and correlations on the basis of mappable rock units are difficult to make (Pray, 1961; Oriel et al., 1967). Although a variety of schemes have thus been utilized to subdivide the Pennsylvanian section of the area, the following discussion employs the common usage of Morrowan through Virgilian stages as a framework for consideration of the dominant lithologies and several formations identified in this region.

1) <u>Morrowan Series</u> Of the stages present in New Mexico, the basal Pennsylvanian Morrowan rocks occupy the smallest area and contain, in the central and northern portions of the Delaware Basin, the largest proportion of clastic material. These rocks, which mark the initiation of a major transgression climaxing in the Virgilian, attain a thickness of about 1,250 feet in the Permian Basin area and wedge out northward in southeast New Mexico (Meyer, 1968). The Morrowan rocks in New Mexico consist largely of limestone and shaly limestone; fine-grained sediments predominate (Bachman, 1975).

In the Sacramento Mountains, at the northwest extent of the area, the basal Pennsylvanian strata were deposited on a surface of at least 100 feet of local relief, the lowest parts of which were filled with coarse sandstone or cobble conglomerates derived from Mississippian cherts. The percentage of shales and dark limestones increase upwards into the Atokan. These rocks have been called the basal part of the Gobbler formation by Pray (1954). Southward across the Guadalupe Mountains area of the Northwest Shelf, the Morrowan consists of from 230 to over 400 feet of fine to coarse-grained, poorly sorted, locally conglomeratic quartz sandstone, mottled medium gray oolitic limestone and medium to dark gray shale, which resemble the lower Gobbler as well as the rocks of central to northern New Mexico, called the Sandia Formation (Hayes, 1964). Fine-grained detrital sediments trend southeasterly from the Pedernal Uplift into the western Delaware Basin. Within the Delaware Basin, the Morrowan is composed primarily of brown to gray argillaceous limestones and gray quartzose sandstones with dark gray to black shale. Across the Central Basin Platform into Texas, the basal Pennsylvanian unit is a black shale (Nicholson & Clebsch, 1961; Bachman, 1975).

2) Atokan Series The Early-Middle Pennsylvanian rocks, assigned to the Atokan or Derryan Stage, consist of dark-colored sandstones, shales and limestones, which attain a maximum thickness of about 1,000 feet. These rocks were deposited over the entire area, with the exception of the Pedernal Uplift to the north (Meyer, 1968).

Interbedded shales and dark limestone constitute the top of the 200 to 500 foot section of the lower Pennsylvanian Atokan deposition to the northwest in the Sacramento Mountains (Pray, 1954). Southward into the northern Delaware Basin, the unit consists of gray to brown and black, fine-grained to dense limestone and chert and dark gray to black shale with minor sandstone. In the southern Delaware and Val Verde Basins region, the Atokan rocks consist mainly of sandstones and shales in the lower part and carbonate rocks in the upper part, reaching about 1,000 feet in thickness (Vertrees et al., 1959). The top of the Atokan section is transitional, and is placed at the change from dominantly terrigenous, detrital rocks below to predominantly carbonates above (Bachman, 1975).

3) **Desmoinesian Series** Upper-Middle Pennsylvanian Desmoinesian rocks
are predominantly carbonates, and attain a maximum thickness of about
1,000 feet in the Delaware and Lucero Basins and in northwestern New
Mexico (Bachman, 1975). Sedimentation during this time was primarily
influenced by reef and adjacent shelf and basinal deposition within the
areas of the Permian Basin and Orogrande Basin to the west. Also known
as the Strawn, the unit is the only readily identifiable Pennsylvanian
rock found widespread over the southeast New Mexico-west Texas area
(Vertrees et al., 1959).

The Desmoinesian rocks of the Sacramento Mountain area constitute up to
1,000 feet of contrasting facies: a shelf limestone or reef, consisting
almost entirely of cherty calcilutites, and a deltaic facies of equal
thickness but smaller lateral extent, composed of quartz sandstones,
subgraywackes, shales and minor limestones (Pray, 1954). Southward and
eastward, in the Permian Basin area, the Desmoinesian strata were
deposited in a variety of environments from back-reef lagoon, to reef, to
deep marine basin - a spectrum which lasted from this time through most
of the Permian (Meyer, 1968). Within the Delaware Basin, these rocks are
typically dark brown, fine-grained cherty limestones, the lower part of
which may contain interbeds of gray shale and gray to white,
medium-grained angular quartz sandstone (Meyer, 1966). Reef facies of
the Desmoinesian also extend south and eastward into the Val Verde
Basin. The limestones of the Desmoinesian within both the Delaware and
Val Verde Basins are known for their numerous stratigraphic traps, and
have been attractive for oil and gas exploration (Vertrees et al.,
1959). Desmoinesian limestones also occur across the Central Basin
Platform into Texas.

4) **Missourian Series** The Missourian rocks of the late Lower
Pennsylvanian age constitute up to 1,000 feet of mostly clastic
sediments, such as interbedded arkose and arkosic sandstone, as well as
mudstone and limestone, deposited in environments similar to those of
Desmoinesian time (Meyer, 1968; Bachman, 1975).

On the northwest, as much as 500 feet of thin-bedded, argillaceous
limestone and shale of the Missourian overlie the shelf limestone and
deltaic deposits of the Desmoinesian. Most of these rocks reflect
basinal deposition, but locally there was cyclic deposition in turbulent
shallow waters (Pray, 1954). To the south, Missourian rocks are
identified generally only in the deeper parts of the Permian Basin area.
Within the New Mexico portion of the Delaware Basin, the Missourian rocks
consist of dark gray shales and limestones, quartz sandstone, and some
chert, ranging in thickness from zero to 1,250 feet (Meyer, 1966).
Toward the Val Verde Basin near the Texas-New Mexico border and across
the Central Basin Platform, the unit grades into a dark gray,
non-fossiliferous shale (Vertrees et al., 1959). The absence of datable
materials in this unit has made its correlation as Upper Pennsylvanian
difficult to verify.

5) <u>Virgilian Series</u> The uppermost Pennsylvania section is similar to
that of the Missourian but contains, in addition to carbonates, some
continental shales, coarser clastics and evaporites.

Over most of the area to the northwest, algal reefs up to 100 feet thick
formed. The Virgilian deposition grades upwards into more uniformly
bedded, light-colored limestone with interbedded shale and minor
sandstones. At the top of the section, red shales and limestone
conglomerates repeat cyclically with nonred shales and massive nodular
limestone, indicating fluctuations in depth and gradual transition to
final emergence of the northwestern area. The Upper Pennsylvanian units
of this area were named the Holder Formation by Pray (1959). Within the
Permian Basin proper, over 1,000 feet of Virgilian limestones and shales
were concurrently deposited. Southward over the Northwestern Shelf and
eastern side of the Central Basin Platform and northeastward of the
Horseshoe Atoll, the series is represented by limestone. Toward the
Eastern shelf, the unit consists of both mudstone and limestone with some
interbedded sand (Oriel et al., 1967). Reefs formed along the northern
margin of the Delaware Basin (Meyer, 1968), while within the basin up to
1,000 feet of brown to tan, fine-grained limestone, black to brown shale
and white, fine-to coarse-grained subangular quartz sandstone were
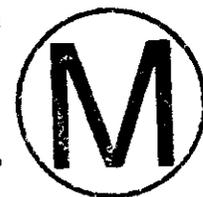
deposited (Meyer, 1966). Southward in the deeper part of the basin, dark nonfossiliferous shale, similar to the underlying Missourian, continued to be deposited.

Permian Rocks. In many parts of the southeast New Mexico area, the lower boundary of the Permian is difficult to determine except on the basis of fusilinids, because the Permian rocks are underlain by lithologically similar Pennsylvanian rocks. In the Delaware and Val Verde Basins, the boundary is located below several hundred feet of dark gray mudstone unit. No lithologic basis of recognizing the boundary is apparent on the Northwestern Shelf, along the east margin of the Central Basin Platform, or in the area of the Horseshoe Atoll (in the northern Midland Basin). Only in the structurally positive areas where Pennsylvanian rocks are missing, as in many locations on the Central Basin Platform, is the base of the Permian clear. In other places, such as the Sierra Diablo, an angular unconformity separates the Permian from underlying units. Ages of basin rocks to the base of the Permian are usually assigned through fusilinids interpretation but it is sometimes difficult because of the scarcity of fossils (Oriel et al., 1967). The thickness of the Permian sediments equals or exceeds the total thickness of the underlying Paleozoic systems. Details are presented in the discussions of each series below. Figure 3.3-2 provides a schematic illustration of the subsurface distribution and relative thicknesses of the Permian.

Most of the major structural elements that influenced Permian sedimentation in the area were well developed late in Pennsylvanian to very early in the Permian; thus, marked differences in lithology occur from the Northwestern shelf region, through the Delaware Basin and across the Central Basin Platform into the Midland Basin, and the stratigraphic nomenclature differs from place to place. In general, the units of the basins contain a much higher proportion of clastics than do the adjacent shelf areas, and the basin carbonates are much less dolomitized than are the shelf carbonates. The rock units along the basin margins are partially dolomitized, and contain less clastics than equivalent shelf units. In common practice, the different facies of the region have been

related to each other by time-stratigraphic units. The provincial series names used in New Mexico and Texas are, from oldest to youngest, the Wolfcampian, Leonardian, Guadalupian and Ochoan (Oriel et al., 1967). Figure 3.3-3 presents a summary and correlation of the major Permian formations of the region which are discussed below.

1) Wolfcampian Series The Wolfcampian series consists primarily of limestones and dolomites. A few reefs are present on the shelves; dark gray shales, sandstones, and conglomerates are present in the basins. The basinal sediments of the Delaware, Midland and Val Verde were probably deposited under stagnant, reducing, deep-water conditions, while the limestone on the Northwestern and Eastern shelf and Central Basin Platform were deposited in relatively shallow and well-aerated water. The series thickens southward from generally less than 1,000 feet over the shelf areas and 1,500 feet in the subsurface of the Guadalupe Mountains area of the Northwestern Shelf, to somewhat less than 5,000 feet in the Midland Basin, 7,500 feet in the central Delaware Basin, and over 15,000 feet southward in the eastern half of the Val Verde Basin (Oriel et al., 1967). The name Hueco limestone has been applied to the rocks of the basal Permian in the region; however, some workers prefer to restrict this term to the Northwestern shelf and northernmost Delaware Basin (Hayes, 1964).

On the Northwestern Shelf, the Wolfcampian is subdivided into two cherty limestone units separated by interbedded limestones and red, green and gray mudstones, which thicken northward and become sandy. Along the shelf margins, medium to dark-gray mudstone layers intertongue with the limestone (Oriel et al., 1967).

Within the northern Delaware Basin, the Wolfcamp consists of about equal parts of gray, black or brown shale and fine, crystalline, rarely cherty, brown limestone with a few thin beds of micaceous and calcareous sandstone (Hayes, 1964). Southward, in the deeper parts of the basin, it consists primarily of dark shale with brown sand and some coarser clastics. Here the absence of index fossils precludes satisfactory lower

time boundary detection. Within the Delaware Basin, both the sandstone and carbonate facies have been recognized as potential oil and gas reservoirs. Southward, in the Val Verde Basin, sandstones interbedded within the shales of the Wolfcampian are established as a commercial gas reservoir (Vertrees et al., 1959).

Eastward, over the Central Basin Platform, the Wolfcampian consists chiefly of limestone with a basal unit of as much as 440 feet of red and green shale and conglomerate (Nicholson & Clebsch, 1961). The Wolfcampian within the Midland Basin is similar to that of the Delaware Basin, except for the presence of an upper zone of dark argillaceous, locally cherty limestone and interbedded dark mudstone. The lower part of the section consists of dark mudstone with thin units of fine-grained, argillaceous sandstone and fossiliferous limestone, which increase in thickness north and west along the basin periphery (Oriel et al., 1967).

2)   Leonardian Series The Leonardian series of the Lower Permian is represented by a highly variable group of facies consisting of limestone and dolomite, with mudstones, sandstones and some chert. Clastics are dominant in the lower parts of the basins, while calcareous deposits dominate the margin and shelf areas. The series was deposited under mostly marine conditions, but some strata formed in restricted or marginal environments. The Leonardian rocks are over 4,000 feet thick in two north-trending belts along the east and west margins of the Delaware Basin and in the south-central part of the Midland Basin. In the Val Verde Basin, thicknesses average 2,000 to 3,000 feet. On the shelf north and west of the Delaware Basin along the oil-producing Abo reef trend, thicknesses are over 3,500 feet. On the Eastern Shelf, the Leonardian is less than 2,000 feet. Minimum thicknesses in the area are about 800 feet (Vertrees et al., 1959; Oriel et al., 1967).

The Bone Spring Limestone represents the basin facies of the Leonardian in the Delaware Basin and northwest end of the Val Verde Basin, and consists of a dominantly dark-gray, thin-bedded, argillaceous limestone, a gray to buff, very fine-grained sandstone in three separate zones, and

a black shale with some chert nodules and beds. The base is a sandstone member which may be Wolfcampian, and the top is placed above a black shale with dark gray limestone. Deep water conditions with poor circulation probably characterized these basin settings (Oriel et al., 1967).

Eastward, in the Midland Basin, the Leonardian rocks have been assigned to formations different from those in the Delaware, but the rock types, dominantly black shales and limestones, are similar. The section—known as the upper Wichita Group, the Clear Fork Group and the lower part of the Pease River Group at the top—consists of mudstone with lesser sandstone and limestone at the base, two fine-grained sandstone members divided by dark calcareous mudstone and a muddy limestone, that may be time-correlative with two of the three sandstone layers of the Bone Spring. Above this zone, limestone and dolomite predominate, with lenses of mudstone and sandstone; the top of the unit is primarily carbonate.

At the margins of the basins, these basin units grade laterally into limestones. Around the perimeter of the Delaware Basin, the lower part of the Bone Spring Limestone grades into thick-bedded gray limestone overlapping unconformably on the Hueco Limestone (King, 1965). The middle and upper part of the Bone Spring grades into the shelf-margin dolomite of the Victorio Peak, which is correlative with the Yeso of the shelf. The Victorio Peak is a light-gray, thick-bedded fossiliferous limestone containing some chert and sandstone and made up of small, discontinuous or patch reefs and a limestone bank. Unconformably overlying the Victorio Peak of Leonardian to Guadalupian age, is the Cutoff shale consisting of as much as 150 feet of a thin-bedded, platy gray to black limestone, black siliceous or sandy mudstone, and thin-bedded, fine-grained sandstone (Hayes, 1964). In the Midland Basin, the unit grades laterally north and westward into almost pure limestone and dolomite along the peripheries of the Central Basin Platform and Northern Shelf (Oriel et al., 1967).
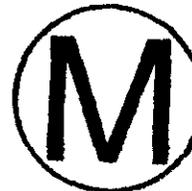
Away from the Delaware Basin onto the shelves and Central Basin Platform areas, the Leonardian series grades laterally from the Bone Spring and Victorio Peak a into light-colored dolomite, almost 3,000 feet thick, with a few sandstone units. The lower portion of the dolomite has been called the Wichita Group on the Central Basin Platform and the Abo Formation in central eastern New Mexico, which grades northward into red mudstone, sandstone and anhydrite. The Yeso overlies the Abo in central eastern New Mexico, and consists of medium to light gray, fine-crystalline dolomite with lesser sandstones and siltstones (Hayes, 1964). Somewhat below the middle of the Leonardian shelf dolomite on the Central Basin Platform, is a thin but extensive sandstone bed called the Tubb, Fullerton or Drinkard, which serves as a regional marker. The name "Clear Fork Group" is sometimes applied to the section of dolomite encompassing this bed on the Central Basin Platform, and is roughly age-equivalent with the Yeso. The upper limit of the Leonardian on the shelves is formed by a unit consisting of two sandstone layers separated by dolomite. On the northwest shelf, this unit is called the Glorieta; on the Central Basin Platform, it is called the San Angelo (Oriel et al., 1967; King, 1948; Hayes, 1964).

3) Guadalupian Series

The Guadalupian Series in the southeastern New Mexico region encompasses three distinct depositional settings, closely related to structural elements: clastic sedimentation in the Delaware Basin and on the Eastern shelf, carbonate reefs along the margins, and mixed carbonate and evaporite deposition on platforms and shelves other than the Eastern Shelf. The series is over 5,500 feet thick in the Delaware Basin, and gradually thins northward on the Northwestern Shelf to less than 3,000 feet. It thins southeastward from less than 2,000 feet to 1,400 feet at the south end of the Central Basin Platform. Maximum thicknesses in the Midland and Val Verde Basins are about 3,500 feet (Oriel et al., 1967).

a) Basin Facies

The basin facies of the Guadalupian, known as the Delaware Mountain Group, is composed mainly of light gray, very fine-grained sandstone and

siltstone separated by gray shale and a few thin light gray to gray limestone and dolomite members with minor evaporites, indicating frequent relative sea level changes. The Delaware Mountain sandstones produce oil and gas and are important exploration objectives (Vertrees et al., 1959). The Group has been subdivided into three formations from oldest to youngest—the Brushy Canyon, the Cherry Canyon, and Bell Canyon—each of which are up to 1,000 feet in thickness. The Brushy Canyon differs from the upper two formations in that its sandstones are coarser grained with minimal amounts of sediments other than sandstone, and its structural features are indicative of deposition in agitated water. Harms (1974) discusses the Brushy Canyon and proposes density currents as the origin of the formation rather than turbidity currents. This formation terminates northward against the Bone Spring flexure at the basin margin. The Cherry Canyon and Bell Canyon are fine-grained sandstone to siltstone and very finely laminated. The sandstone tongue of the Cherry Canyon disconformably overlies the Cutoff Shale as a shelfward extension of the lower fourth of the Cherry Canyon Formation. Along the reef facies area, the tongue averages 200 to 300 feet thick and, where described in Last Chance Canyon of the Guadalupe Mountains, consists of moderately resistant, indistinctively bedded, grayish-orange, very fine-grained, well-sorted quartz sandstone with scattered chert nodules and silicified megafossils. The upper 25 to 30 feet of the unit is transitional shelfward into an overlying dolomite tongue of the San Andres Limestone (Hayes, 1964) (Also see Figure 3.3-3). The upper Cherry Canyon and the Bell Canyon grade into reef facies at the margin of the basin.

b)   Reef Facies

The Guadalupian reef facies consists of the Goat Seep Dolomite and the overlying Capitan Limestone. A generalized cross-section through the reef facies, Figure 3.3-4, demonstrates the relationships between the various Guadalupian units along the reef margins.

Gradationally overlying the sandstone tongue of the Cherry Canyon Formation is the Goat Seep Dolomite. The Goat Seep was a reef, which grew primarily upward and formed a barrier around a considerable portion of the western side of the Delaware Basin. King (1948) originally extended the name Goat Seep to include the shelfward-lying thin-bedded limestones and interbedded sandstones, but Newell et al., (1953) restricted the formation to the massive "reef and forereef talus facies" of the basin margin, a designation maintained by Hayes (1964). The lowerportion of the Goat Seep is thick-bedded, and the upper portion is a massive light gray, fine-crystalline to saccharoidal, in places very porous, dolomite.

The overlying Capitan Limestone is a light colored, fossiliferous and vuggy limestone and breccia which reaches a maximum vertical thickness of about 2,000 feet in McKittrick Canyon of the Guadalupe Mountains, and is at least 6 times as broad as thick, reaching a width of from 10 to 14 miles along the Northwestern Shelf. It apparently formed primarily by oblique or horizontal basinward growth (Newell, et al., 1972; Hayes, 1964; Hiss, 1976). The Capitan virtually encircles the Delaware Basin. It extends from the west side of the Guadalupe Mountains northward and eastward as a bold escarpment which gradually descends to the hills in the vicinity of Carlsbad, where it is overlain by younger rocks (Dunham, 1972). The buried reef front trends northeastward to eastward from there across the Eddy-Lea County line, turns southward to parallel the length of the Central Basin Platform, and then turns west and crops out in the Glass Mountains (Hiss, 1976; Kelley, 1971). The Capitan grades laterally basinward into the Bell Canyon Formation and possibly into the lowermost beds of the Castile; onto the Northwestern Shelf the Capitan grades laterally into the Seven Rivers, Yates, and Tansill Formations of the Artesia Group (Hayes, 1964) (Also see Figure 3.3-3).

The limits of the Capitan described by Crandall (1929) and Lang (1937) have been used by most of the more recent workers, including King (1948), Adams and Frenzell (1950), Newell, et al., (1957), Hayes (1964), and Kelley (1971) and are followed in this report. For a different interpretation, see Dunham (1972).

Hayes (1964) recognizes two units as comprising the Capitan Limestone, a massive member and a breccia member, which grade into each other both laterally and vertically. The massive member forms nearly vertical, smooth-weathering cliffs and ranges in thickness from about 250 to 270 feet averaging 400 feet along its Guadalupe Mountains portion. This member is composed primarily of light to yellowish gray, fine-textured, fossiliferous limestone with virtually no discernible bedding planes. Isolated aggregates of coarsely crystalline calcite are common, and some dolomite, sandstone dikes, and isolated sandstone pockets occur. Solution and recrystallization, weathering, and the very small size of the fossils have made the organic content difficult to recognize in the field. Newell, et al., (1953), however, have identified 115 species of fossils within the formation, including fusulinids, sponges, corals, crinoids, bryozoans, brachiopods, and mollusks; in total volume, stromatolites are probably most important in the construction of this rock unit (Hayes, 1964).

The breccia member, which generally forms more easily eroded uneven slopes, consists of thick beds dipping basinward at 20 to 30 degrees or more on the west side of the Delaware Basin. Most of this member is composed of microbreccia derived from the massive member and from the Artesia Group and also contains coarse, angular cobbles and boulders of limestone and dolomite from these sources. The breccia attains a maximum vertical thickness of about 1,750 feet and averages 1,250 feet and as such comprises about two-thirds of the bulk of the Capitan (Hayes, 1964).

Although it has been generally agreed that the Capitan Formation represents a "geologic reef," (a thick, laterally restricted mass of pure or largely pure carbonate, according to Dunham, 1972), investigators of the Capitan have over the years proposed different interpretations as to its genesis and environment of formation.

Crandall et al. (1929) published the barrier reef hypothesis, according to which reef-building, sediment-binding organisms grew practically at sea level on a reef which developed rapidly enough, despite erosion, to

maintain a nearly vertical front, overriding its own debris. Newell, et al., (1953) concurred with Crandall, based on their detailed petrological work on the reef constituents, and a number of recent investigators, such as Hayes (1964), Boyd (1955), Adams (1944), and Adams and Rhodes (1960) have generally followed this interpretation.

A second alternative was advocated by King (1948) and named by Dunham (1972) the "uninterrupted slope hypothesis." King used it to explain his findings in the southern Guadalupe Mountains which seemed to indicate facies change due to change in slope as the shelf descended to the Delaware Basin. Dunham (1972) pointed out, however, that King studied only portions of the structure. Had he gone farther northwestward, his findings would have corroborated Lang (1937), who proposed a third hypothesis, that of the marginal mound.

According to the marginal mound alternative, supported elaborately by Dunham (1972), organisms produced carbonate particulate sediment upon a broad topographic high which was at different times a sandy shoal or an island bordered by sand and mud flats. The sediment was cemented during the island stages of development. Achauer (1969) has advocated a somewhat similar view that the Capitan represents an ancestral organic bank, rather than a classical barrier reef.

c)   Back-Reef or Shelf Facies
The thick massively-bedded limestones along the margins of the basins grade shelfward into thin-bedded dolomites. On the Northwestern and Eastern Shelves and southward along the Central Basin Platform, the Guadalupian includes the San Andres Limestone and overlying Artesia Group (also identified eastward on the Central Basin Platform as the Whitehorse Group by Nicholson and Clebsch, 1961). This group includes from base to top the Grayburg, Queen, Seven Rivers, Yates and Tansill Formations (Hayes, 1964). These shelf units are also recognized in the Midland Basin area. There is some disagreement as to whether the Lower Guadalupian there is missing or greatly resembles the upper Leonardian (Hendrickson & Jones, 1952; Oriel et al., 1967).

In the western part of the Delaware Basin, parallel to the reef front, facies encountered in a shelfward direction are: 1) dolomitized coquin and calcarenite, 2) pisolites, 3) fine-grained dolomite, 4) evaporites, and 5) terrigenous red detritus (Newell et al., 1953). This general succession of facies is also described by Dunham (1972) in the vicinity of the Capitan Escarpment. Hayes (1964) presents a comprehensive discussion of the Guadalupian shelf rocks.

The San Andres is partly time-correlative with the basinal Brushy Canyon; at its base it may be upper Leonardian, and at its top it interfingers with the base of the Cherry Canyon. The San Andres is mainly dolomite with minor limestone near its base and some chert, sandstone and reddish mudstone (Oriel et al., 1967; Kelley, 1971). It extends shelfward much farther than the Artesia Group before grading into evaporites and detrital materials. The San Andres thins eastward across the Midland Basin, and detrital and evaporite contents increase progressively to the east.

The Artesia Group ranges in thickness from about 880 feet to over 1,500 feet. In the shelf and Central Basin Platform areas, it is separated from the underlying San Andres by an unconformity, according to Nicholson and Clebsch (1961). The basal Grayburg and Queen Formations are time-correlative with the marginal Goat Seep Reef and basinal Cherry Canyon Formation. To the south, they consist of dolomites and sandstone; they grade northward into gypsum, mudstones and dolomite (Kelley, 1971). The Queen Formation is distinguished from the underlying Grayburg by its much greater abundance of clastics and red mudstones. The Seven Rivers, Yates and Tansill Formations are all correlative with the Capitan Limestone at the margin, and with the Bell Canyon in the Delaware Basin. To the south, they all resemble the lower two formations of the Group, except for the presence of gypsum and limestone in the Yates. Toward the north, gypsum and anhydrite increase in the Tansill, and siltstone and dolomite increase in both the Yates and Tansill.

Ochoan Series

The Late Permian Ochoan series consists primarily of evaporites that were deposited during recurrent retreats of a shallow sea restricted by the Guadalupian reefs. The lower three formations in the series, the Castile, Salado and Rustler, comprise what is perhaps the thickest and most extensive evaporite rock sequence in North America (Oriel et al. 1967). They are overlain by the Dewey Lake Redbeds, which may be either Permian or Triassic in age. Within the Ochoan, halite is dominant on the shelf north of the Delaware Basin, where the Salado Formation makes up the bulk of the unit; total thickness of salt is greatest, however, in the Delaware Basin, but the presence of the Castile Formation in the basin reduces the proportion of halite there. The proportion of carbonates to other rock types increases southwestward and southward, and the proportion of detrital rocks increases eastward and northeastward (Oriel et al., 1967). The total thickness of the Ochoan ranges from slightly more than 5,000 feet in the center of the Delaware Basin and 4,000 feet in a north trending belt through the basin, to about 1,500 feet in the Midland Basin and 1,000 feet on the shelves. Irregular thinning occurs near the basin margins as a result of erosion and leaching of the more soluble beds (Oriel et al., 1967; Nicholson & Clebsch, 1961).

The Castile Formation is confined to the Delaware Basin and was deposited upon the Bell Canyon, in "apparent conformity," according to Kelley (1971), but unconformably, according to Nicholson and Clebsch (1961), and is laterally bounded by the Capitan limestone reef. The Castile is generally of uniform thickness, up to about 2,000 feet, throughout the basin. The formation consists primarily of massive anhydrite, limestone interlaminated with anhydrite, and halite in beds as thick as several hundred feet (Vine, 1963). In the lower to middle portion of the sequence, banded light gray anhydrite is interlaminated with brown bituminous limestone on a scale of millimeters. Two very extensive layers of fairly pure halite averaging 200 to 350 feet thick persist throughout the northern Delaware Basin. Several smaller tongues of halite are also present through the unit. Towards the basin margins, the

Castile thins abruptly. The basal part of the banded portion grades reefward into laminated limestone and the upper part into massive anhydrite. The top of the Castile is light-gray massive anhydrite, grading into the basal part of the overlying Salado by wedging of thin anhydrite tongues northeastward into salt (Jones, 1954; Brokaw et al., 1972).

The Salado Formation extends from the Delaware Basin area beyond the limits of the Castile and across most of the Permian basin, including the Midland Basin, the Northwestern Shelf and the Central Basin Platform. The complete Salado is present only in the subsurface of this area, and is represented at the surface only by a solution residue. Its thickness varies because of leaching, but it is generally up to 2,000 feet near the northern Delaware Basin, thinning northward over the Capitan reef to 700 to 1,200 feet and thinner farther north and east. In the shelf and platform areas, it rests unconformably on the Artesia, or Whitehorse, Group (Brokaw et al., 1972; Nicholson & Clebsch, 1961).

The Salado is mainly halite, some of which is argillaceous, red mudstones, sandstone, siltstone, abundant anhydrite and a suite of salts including polyhalite, kieserite, glauberite, sylvite, carnallite, langbeinite, kainite and leonite. Beds locally rich in sylvite, KCl, and other soluble potassium minerals constitute valuable potash ores (Vine, 1963). The principle lithologic materials occur in cyclic sequences 2 to 30 feet thick consisting of a detrital layer, a relatively thin sulfate layer chiefly composed of anhydrite and polyhalite, and a thicker halite zone, overlain by a mixed halite-detrital layer, all with gradational contacts. The potash ores occur near the middle of the formation in irregularly lenticular to tabular bodies (Brokaw et al., 1972; Oriel et al., 1967). The upper part of the Salado is locally characterized by a leached zone from which the halite has been removed, and is largely unconsolidated reddish-gray to brown silt and clay with varying amounts of brecciated gray or red gypsum (Vine, 1963).

The Rustler Formation ranges in thickness from 90 to about 400 feet, and overlies the Salado in the Permian Basin area. In the central part of the Permian Basin, the Rustler conformably overlies the Salado, but in other places, as along the west and north margins of the Delaware Basin, it truncates the Salado by a marked unconformity (J. A. Adams, 1944; Nicholson and Clebsch, 1961). In outcrop, the Rustler appears as calcareous sandstone, fine grained dolomites and gypsum. The subsurface Rustler consists primarily of anhydrite or gypsum and subordinate salt, with lesser amounts of dolomite, limestone, siltstone and sandstone. Within the Delaware Basin, the limestone and dolomite increase to the south and southeast.

Vine (1963) has described the Rustler in the northern part of the Delaware Basin. Here, the lower part of the Rustler consists of over 100 feet of siltstone and very fine-grained sandstone with interbeds of gypsum or anhydrite. Next above is the Culebra dolomite, about 30 feet of uniformly microcystalline gray dolomite or dolomitic limestone with numerous small, generally unconnected, nearly spherical cavities. Overlying the Culebra is the Tamarisk member, about 115 feet of anhydrite with local gypsum and a 5 foot thick siltstone bed some 20 feet from its base. The Magenta member, above the Tamarisk, consists of about 20 feet of thin, wavy, lenticular laminae of dolomite and anhydrite (or gypsum). The uppermost member of the formation is the Forty-niner, consisting of up to 65 feet of anhydrite (or broken gypsum in outcrops) with a bed of massive siltstone near the base. According to Jones et al., (1960), the siltstone represents insoluble residue from a bed of halite present in the subsurface to the east.

The top of the Rustler has been placed at the top of the first persistent anhydrite bed penetrated by oil and gas tests and provides a clear marker for structural correlations (Oriel et al., 1967).

Overlying the Rustler in apparent conformable relationship is a sequence of redbeds, up to about 600 feet thick, which represents deposition of terrigenous materials in shallow water remaining in the basin areas over

the older evaporate sequence (Mercer & Orr, 1977; Oriel et al., 1967).
On the basis of physical stratigraphy, the unit has been traditionally
assigned a Permian age (Oriel et al., 1967). No fossils have been
found. Although several names (e.g. the Pierce Canyon) have been
proposed for this unit, the term Dewey Lake Redbeds, as defined in west
Texas (Page and Adams, 1940), is generally used throughout the area
(Nicholson & Clebsch, 1961).

The Dewey Lake consists of a series of micaceous, orange to red sandy
siltstones, sandstones and some mudstone. Gypsum commonly forms cement,
secondary crystals and veins. The lower 10 feet of the sequence contains
a widely distributed zone of coarse, frosted quartz grains.

The top of the redbed unit is marked by an erosion surface, upon which
younger units were deposited with a slight angular discordance. In some
places, the Dewey Lake has been removed by later erosion, and rocks of
Cretaceous or Cenozoic age rest on the Rustler or Salado (Oriel et al.,
1967).

3.3.3   Mesozoic Rocks

Triassic Rocks Unconformably overlying the rocks of Late Permian age is
the Upper Triassic Dockum Group of red beds, composed of up to 1,500 feet
of moderate-reddish-brown to yellow-brown conglomeratic sandstones,
siltstones and shales (Brokaw et al., 1972). The sediments of this group
display characteristics of rapid deposition from a local source, in their
poorly rounded sand grains and micaceous minor constituents. This group
has been subdivided into two formations, the Santa Rosa Sandstone and
overlying Chinle Formation; however, because of poor exposures and
lithologic similarities between the sandstones of the two units, the
distinction cannot be made throughout the entire southeast New Mexico
area (Nicholson & Clebsch, 1961).

The Santa Rosa is a fine-to-coarse-grained sandstone, generally red but containing white, gray, and greenish to lavender sands and some minor reddish-brown mudstones and conglomerate. The unit is commonly cross-stratified and ranges in thickness from about 140 to over 300 feet (Kelley, 1971; Nicholson & Clebsch, 1961).

The upper portion of the Dockum Group, the Chinle Formation, ranges in thickness from zero to almost 1,300 feet, thickest to the east, near the Texas-New Mexico border, and entirely absent in the west, where it has been removed by post-Mesozoic erosion. The Chinle is a reddish-brown to greenish-gray shaly mudstone with interbedded lenses of conglomerate and thin, gray to reddish-brown sandstone and siltstone (Mercer & Orr, 1977; Nicholson & Clebsch, 1961).

Jurassic Rocks No record of Jurassic deposition has been shown to exist in the southeast New Mexico region.

Cretaceous Rocks Kelley (1971) described three formations, identified as Cretaceous, which crop out to the north and northwest, in the Sierra Blanca and Capitan area, named the Dakota Sandstone, Mancos Shale and Mesaverde formation. The Dakota is comprised of up to 150 feet of sandstone, conglomerate, and beach shale. The overlying Mancos is up to 700 feet of dark shales, siltstone and local thin sandstone and limestone. The Mesaverde Formation comprises from 500 to 1,500 feet of light-colored to maroon coarse clastics and mudstones, and coal. These deposits reflect subsidence of the area during the Cretaceous to a shallow marine and floodplain environment. An outlier of Cretaceous rocks is also present on the crest of the Sacramento Mountains. Here, a pebble-bearing quartz sandstone 150 feet thick is overlain by a shale containing fossils of late Early to early Late Cretaceous age (Pray & Allen, 1956).

Further south on the Northwestern Shelf, there are no definite Cretaceous age outcrops, but solution cavities on the surface of the Castile southeast of the Guadalupe Mountains contain pebbles of limestone and

sandstone with fossils of early Washita age. At several places along the top of the Reef Escarpment, low areas on the ridge and joints in the Permian Tansill formation contain conglomeratic quartz sandstone which closely resembles the Cretaceous deposits in the Sacamento Mountains (Hayes, 1964).

To the southeast, in the Lea County area, only several exposures of Cretaceous rocks are known. A gravel pit east of Eunice contains large slump blocks, up to 5 feet thick and 20 feet long, of massive, highly fossiliferous, white to buff sandstone containing some sand and shaly partings along the bedding planes (Nicholson and Clebsch, 1961; Ash and Clebsch, 1961). This rock and the Comanche limestone of Early Cretaceous age are strikingly similar, so are believed by Ash and Clebsch (1961) to be equivalent. Another outcrop of Cretaceous rocks at North Lake consists of dark gray siltstone and thin interbedded stringers of light brown crystalline to light gray, fine-grained limestone. According to fossil and lithologic similarities, the rocks at North Lake are correlated with the Early Cretaceous Tucumcari shale (Ash & Clebsch, 1961). In the subsurface of Lea County, 5 feet or more of yellow, blue, or gray clay or shale encountered by drilling and consistent with the description of the rock at North Lake constitute the major evidence for the subsurface presence of Cretaceous outliers in the area. Based on some 8,000 water-well logs and seismic shotholes, Ash and Clebsch (1961) have determined that in the subsurface Cretaceous rocks are generally continuous in the northeastern portion of Lea County, but further west and south, only scattered, discontinuous occurrences have been encountered.

Rocks of Cretaceous age were deposited over the southeast New Mexico area but have been almost entirely removed by erosion. Now only scattered patches or reworked pockets of limestone and sandstones of probable Early and Mid-Cretaceous age are present in the area; Cretaceous rocks have also been identified here in the subsurface through drilling (Bachman, 1976; Hayes, 1964; Nicholson and Clebsch, 1961).

3.3.4   Cenozoic Rocks

Tertiary Rocks. Following Cretaceous deposition, widespread uplift and
erosion occurred throughout the region, and the earliest Cenozoic
deposits for which there is record, the Ogallala, were depositied in Late
Tertiary Miocene to Pliocene time.

The Ogallala Formation underlies the High Plains of eastern New Mexico
and west Texas. Although there are no confirmed remnants of the Ogallala
west of easternmost Eddy County, isolated gravels to the west in the
Pecos Valley and Guadalupe Mountains have been interpreted as belonging
to this formation (Mercer and Orr, 1977). The Ogallala was deposited on
an irregular, broadly sloping pediment or complex alluvial fan surface by
southeastward flowing streams under rapidly changing conditions (Bachman,
1976).

The Ogallala in the region is up to 400 feet thick (Bachman, 1976) and
consists of a yellowish-gray semi-consolidated, fine-to medium-grained,
calcarous sand containing some silt, clay, and gravel. In many places, a
basal gravel deposited within stream beds is also encountered. Some beds
of well consolidated silica-cemented conglomeratic sandstone from one to
three feet thick also occur within the formation.   As a result of
intertonguing, lensing and pinching out of the beds caused by the varying
depositional conditions there are no consistent marker beds within the
Ogalalla (Nicholson and Clebsch, 1961; Bachman, 1973).

The Ogallala is capped by a dense layer of brecciated and pisolitic
caliche ranging in thickness from a few feet to as much as 60 feet. At
the surface it is a well indurated calcium carbonate, but below the
surface, it becomes softer and more porous and grades into the underlying
sands. This capping was formed in post-Ogallala time and before the
extensive Pleistocene erosion of the area, probably during the Late
Pliocene. The caliche accumulated within the zone of illuviation of a
pedocal "climax soil," which developed on the depositional surface of the

Ogallala (Nicholson and Clebsch, 1961; Bachman, 1976). (Pedogenic caliche formation in southern New Mexico is described in detail by Gile, et al., (1966).)

Quaternary Rocks Following Pliocene time, erosion removed much of the Ogallala as well as some of the older materials, and stream systems became entrenched. Periodic deposition also occurred in the southeastern New Mexico area during the Pleistocene and Holocene, leaving behind the Gatuna Formation, caliche, terrace, channel and playa deposits and windblown sand.

The Gatuna, of Pleistocene age, unconformably overlies rocks as old as Permian and Triassic and consists of up to several hundred feet of reddish-brown friable sandstone, siltstone and cherty and siliceous conglomerate, but locally also includes gypsum, gray shale and claystone. Remnants of the formation are discontinuous and may have been deposited in local depressions such as stream channels and solution subsidence areas (Bachman, 1973; Vine, 1963).

Unconformably above the Gatuna and older deposits throughout southeastern New Mexico, there formed a fairly continuous mantle of caliche called the Mescalero. It is a sandy light gray to white deposit composed of a lower nodular calcareous zone and upper dense laminar caprock and ranges in thickness from 3 to 10 feet. According to Bachman (1973), the caliche is the remnant of an extensive soil profile.

Late Pleistocene to Holocene terrace and channel deposits are preserved in the western part of the area, particularly along the Pecos River and the Guadalupe Mountains area. Channel deposits consist of silt and sand to boulders. Within the Guadalupe Mountains area, deposits are generally limestone cobbles and boulders. Three terraces are commonly recognized in the area: the Blackdom, Orchard Park and Lakewood. The Blackdom and Orchard Park have been dated as Pleistocene while the Lakewood may be of Holocene age. The deposits of the Blackdom terrace are generally coarser than those of the younger terraces, but the two Pleistocene terraces are

similar in composition, consisting of limestone-porphyry conglomerates capped by caliche. The younger Lakewood terrace contains river conglomerates and pond, marsh, and lake silts (Bachman, 1973; Hendrickson and Jones, 1952).

Playa and shallow lake deposits are present in the area in many small shallow depressions, particularly east of the Pecos River. In most of these depressions, lakes formed after heavy runoff and evaporated rapidly, but some contain generally perennial lakes, the largest of which is Laguna Grande de la Sal, in Nash Draw. The playa deposits consist of alluvium, reworked eolian sands, silt and clay. Around some of the standing lakes, gypsum, carbonate minerals, and some halite have been deposited. These deposits date from the Late Pleistocene to Holocene time (Hendrickson and Jones, 1952, Vine, 1963).

Windblown sands mantle much of the surface east of the Pecos River for 20 to 30 miles eastward to the Mescalero ridge and south to the Texas border. The sand is very erratic in both thickness and distribution, and appears to be fairly uniform, fine-grained light brown to pale reddish-brown quartz. Many of the grains are rounded and frosted. Some of the sand rests in coppice dune fields where the sand is as thick as 25 feet. Most of the sand has been stablized by mesquite, bunchgrass and other vegetation.

3.4   REGIONAL STRUCTURE AND TECTONICS

The major tectonic structures of the region are displayed in Figure 3.4-1. Most of the large-scale elements that provide the structural framework of the area were developed in the Late Paleozoic, principally from Late Pennsylvanian to Early Permian time. These include the Delaware Basin, the Central Basin Platform, the Midland Basin, and the Northwestern Shelf of the western extent of the Permian Basin, the Pedernal Uplift, the Matador Arch, the Val Verde Basin, and the Diablo Platform, as well as secondary features such as the Huapache Monocline and Artesia-Vacuum Arch and the northeast-trending buckles and smaller

fold systems believed to be expressions of basement faulting. Middle to Late Tertiary Basin and Range-related doming and faulting produced the remainder of the major tectonic features in the area, including the Guadalupe, Delaware, and Sacramento Mountains, and associated west-bounding faults, as well as a gentle regional east to southeastward tilt which affected the entire region under consideration.

The WIPP site lies near the western margin of the region of the Western Interior known as the Permian Basin, which comprises a series of sedimentary basins in which halite and associated salts accumulated during Permian time and where Permian rocks have reached their maximum development. The region extends about 520 miles from the Amarillo uplift on the north to the Marathon thrust belt on the south and some 300 miles westward, from west-central Texas to the Diablo Platform and the present Sacramento and Guadalupe Mountains (Hills, 1963).

The formation of a depositional basin in the west Texas-southeast New Mexico area began following Lower Ordovician Canadian time, when a broad sag, named the Tobosa Basin by Galley (1958), developed. Several periods of minor folding and perhaps some faulting occurred in the Tobosa Basin area prior to Pennsylvanian time. There was some erosion, but a general tectonic stability prevailed until the Late Mississippian to Late Pennsylvanian-Early Permian time. Tectonic activity accelerated in the area coincident with the Marathon disturbance, and the sag was split into two rapidly subsiding basins--Midland to the east, and Delaware on the west--by the final uplift of the median ridge, the Central Basin Platform (Foster, 1974). Continuing basin and platform development occurred throughout the Permian Basin through Permian time. Stabilization of the basins followed, during which time evaporites were deposited. Since Permian time, the Permian Salt Basin has been relatively stable tectonically (Bachman & Johnson, 1973); thus, the large structural features of the Permian Basin are reflected only indirectly in the Mesozoic and Cenozoic rocks (Nicholson & Clebsch, 1961).

The structure of each of the major tectonic units of the Permian Basin in the site region is described below, followed by discussion of the larger *secondary features and younger Tertiary Basin and Range-related* structures.

3.4.1.   Delaware Basin

The site is located within the northern portion of the Delaware Basin, which, during most of Permian time, was a deep-water embayment extending into what is now southeastern New Mexico and western Texas.   The Delaware Basin is a broad, oval-shaped asymmetrical trough with a northerly trend and southward plunge, as reflected on the top of the Precambrian (Figure 3.4-2).   Its axis lies in central Lea County, New Mexico, roughly paralleling the Central Basin Platform.   The eastern slope of the trough rises rapidly to the platform, while the western slope is much gentler (Figure 3.3-2).   The basin comprises an area of about 12,000 mi^2 and measures roughly 75 to 100 miles east to west and 135 to 160 miles north to south.   The Delaware Basin is nearly surrounded by the large horseshoe-shaped Capitan limestone that extends from Carlsbad on the northwest and opens to the south in Texas, between the Davis and Glass Mountains.   However, the structural boundaries of the basin encompass a larger area to the north, beyond the Capitan reef front, into which the older and deeper lying basin sediments (e.g. the Delaware Mountain Group and Bone Spring) extend.   The Delaware Basin represents the area of maximum subsidence of the Permian Basin, with more than 20,000 feet of structural relief, on the Precambrian (See Figure 3.4-2), and it is also here that the Permian section is thickest, with some 13,000 feet of Permian strata present in southeast New Mexico (Oriel, et al., 1967)

Regional structural deformation of the Delaware Basin rocks is relatively minor.   The sediments older than Late Permian are gently downwarped as a result of concurrent basinal development.   The Late Permian Ochoan rocks and Triassic rocks do not reflect this basinwide warping; their major structural feature is the regional eastward slope (Brokaw, et al., 1972).

There are no known active faults within the northern Delaware Basin study area of the WIPP site. Deep-seated faults, which may be partly of tectonic origin, do occur within the older sediments of the Delaware Basin. Some of these faults probably originated from the rapid Pennsylvanian-Early Permian subsidence of the basin, during which widespread block faulting occurred within the basin (Adams, 1965). Others are pre-Permian and basement structures which are reflected in the overlying beds. An example of this type of intrabasin feature is the Bell Lake fault, recognized by Haigler (1962, 1972), which has a displacement of about 500 feet in the Precambrian. The structure is reflected upwards through the Pennsylvanian Section and Foster's (1974) map. It shows as a north-south high with closure on the south. Closure is also indicated on the Bone Springs map. Whether this structural representation results from continued movement of the Bell Lake fault system up to that time or is only an effect of compaction is not known (Foster, 1974). A complex series of faults with several thousand feet of offset marks the boundary between the Delaware Basin and Central Basin Platform. These faults were involved in the development of the basin and are considered to have been inactive after Permian time. They are discussed in more detail in the following section.

Two sets of joints, with strikes to the northwest and northeast, have been recognized within the basin. The northeasterly set appears to be better developed and penetrates the lower anhydrite of the Castile Formation along the western margin of the basin, where the formation is exposed. This set also controlled the emplacement of replacement limestone within the evaporites (Anderson, 1978).

Other structures within the Delaware Basin include flexures, some of which formed during Early to Mid-Permian basinal downwarping and deposition of the Bone Spring and Delaware Mountain Groups (Pray, 1954), and minor scattered folding of the younger beds (U.S. Bureau of Mines, 1977). Evidence of anticlinal structures as well as an unusual type of fracturing and microfolding within the Castile anhydrite has been cited by Anderson and Powers (1978) and Anderson, et al., (1972), as evidence

of salt movement. C. L. Jones (unpub.) has described a deformation zone encircling the inner margin of the basin and extending inward about 5 miles, as well as a number of similar structures in the interior of the basin, which, according to Anderson and Powers (1978), may be salt anticlines. These features may have formed as a result of differential stress from unloading related to salt dissolution (Anderson, 1978). Scattered small domes, various collapse structures due to salt and/or gypsum dissolution (including domal structures with collapsed centers, known colloquially as breccia pipes), limestone buttes (Castiles), collapsed outliers, and deep-seated sinks can be found in the evaporite sections (Vine, 1960; Anderson, 1978). Stipp (1954) also identified brecciation in the beds of the Wolfcampian and Leonardian rocks, which he attributed to adjustment in the basin in response to sedimentation and structural forces.

The tectonic development of the Delaware Basin, as reflected in the structures discussed in this section, may be summarized as follows. The Delaware Basin was defined by early Pennsylvanian time and major structural adjustment took place in Late Pennsylvanian to Early Permian time. Regional subsidence in conjunction with broad arching, folding, and faulting occurred until Late Permian time, when the basin's history as an active structural feature ended (Brokaw, et al., 1972). Regional uplift and deposition of continental red beds in Triassic time was followed by continued emergent conditions, resulting in erosion or nondeposition. Mid-Cenozoic to Late Cenozoic regional eastward tilting of the basin much later shifted the deepest part of the Basin to its present position close to and paralleling the Central Basin Platform (Stipp, 1954). Since then, the only structural developments in the basin have been related to hydration and solutioning of the Late Paleozoic sediments.

3.4.2 Central Basin Platform

The Central Basin Platform is a subsurface feature (see Figure 3.3-2) which represents an ancient broad uplift of Precambrian and Cambrian to

Pennsylvanian rocks separating the Delaware and Midland Basins at the southern extreme of the Permian Basin in southeastern New Mexico and southwest Texas. The platform extends in a north-northwest trend for about 200 miles to the south flank of the Matador Arch (Bachman and Johnson, 1973). The Central Basin Platform may represent a zone of structural weakness along which movements took place periodically at least into Late Paleozoic time. Displacement within and along the margins of the platform appears to have been along large, high-angle normal or reverse faults, which trend north to northwest and break Early Permian and older rocks; all faults predate the salt deposits of the adjacent basins (Bachman and Johnson, 1973). According to Hills (1970), these faults may have been involved in considerable lateral as well as vertical movement.

The platform itself is a horst. In the structurally higher parts of the platform identified by Foster (1974) as the Hobbs and Eunice blocks, the Precambrian surface is from 4,000 to 7,000 feet below sea level, while the adjacent Monument-Jal block stands at 6,500 to 11,500 feet below sea level. The fault system separating the Hobbs and Eunice blocks from the Monument-Jal block has a displacement of about 1,000 feet in the north to possibly 4,000 feet west of Eunice. The fault bounding the Monument-Jal block extends about 50 miles southward, into Texas, with an inferred displacement of 1,500 feet at the north to over 6,000 feet west of Jal. The aeromagnetic map of the Carlsbad area (U.S.G.S., 1973) provides fairly good definition of the trend of the major features of the Central Basin Platform (Foster, 1974).

The maximum structural relief east-west between the Central Basin Platform and the Delaware Basin is remarkably uniform, at about 9,000 feet (Foster, 1974). Complex fault systems form the boundary between these two structural units. Hills (1970) indicated a fault in approximately this location and termed it the West Platform fault. According to Haigler (1962), this fault system has a relief about equivalent to that of the Huapache monocline bordering the west side of the Delaware Basin.

The Central Basin Platform has been more intensely deformed than has the Delaware Basin or shelf areas (Brokaw, et al., 1972). The tectonic development of the Central Basin Platform may have begun in Precambrian time, and it appears to have been a high during Early Ordovician time. The platform was unstable during late Devonian time but was generally an area of stability thoughout early to Mid-Paleozoic time. In latest Mississippian or early Pennsylvanian time, the area was deformed to an elevated emergent fold belt, trending north-northwest. After submergence and deposition in Middle and part of Late Pennsylvanian time, renewed orogeny further elevated the area and sharpened, compressed, and faulted the folds (Hills, 1963). The complex fault system bordering the platform on the west formed either in Late Pennsylvanian or Early Permian time, according to Haigler (1962), and contributed as well to the structural development of the Delaware Basin. Claiborne and Gera (1974) also identify the subsurface faults outlying the Central Basin Platform as no younger than Permian age, since the Permian and younger beds in the area are unfaulted. Over the faulted platforms, the sedimentary formations were broadly arched, and concurrently eroded, in places to the Precambrian basement. Subsidence followed, and upper Wolfcampian-through Guadalupian-age carbonates were deposited on the roots of the earlier mountain ranges. Since filling of the Midland and Delaware Basins in Late Permian time, the platform has been structurally stable (Brokaw, et al., 1972). Recent seismic activity there is being studied to determine its relationship to secondary oil recovery operations (see Section 5.). The Central Basin Platform is probably not naturally active at the present time, in view of the lack of fault scarps to match the seismic activity (Sanford, 1978).

3.4.3   Midland Basin

The Midland Basin, situated to the east of the Central Basin Platform, is similar in most respects to the Delaware Basin but shallower, having experienced less structural development. The Midland Basin extends some 200 miles along a north to northwest trend to the Matador Arch vicinity. Its shape is much more symmetric than is the Delaware Basin, and its

relief is only 4,000 to 5,000 feet. Extensive major faulting occurred before the deposition of Late Permian salt in the southern part of the basin and on its west flank in proximity to the Central Basin Platform (Bachman & Johnson, 1973). As is the case with the Delaware Basin, general tectonic stability has prevailed in the Midland Basin since Permian time.

3.4.4   Matador Arch

The Matador Arch is a narrow east-west trending Paleozoic highland of irregular relief and outline underlain by Precambrian granitic rocks. The uplift extends for some 300 miles across the Permian Basin, from west of Wichita Falls, continuing westward, north of Lubbock and entering New Mexico in southern Roosevelt County. Its western limits are uncertain, but some have supposed a connection with the Capitan Mountains to the west, by way of the intrusive igneous Railroad Mountain and Camino del Diablo dikes that parallel the trend of the Matador arch in eastern New Mexico (Stipp, 1960). The Matador Arch provides structural division between the Delaware and Midland Basins to the south and the Hardeman, Palo Duro, and Tucumcari Basins in the northern part of the Permian Basin.

The Precambrian structural framework of the Matador Arch itself is probably not a continuous ridge, but a series of prominences which may be the roots of a chain of islands or hills existent during Precambrian and Early Paleozoic times. The only large tectonic structures on the Matador Arch consist of strong faults and folds that trend obliquely across the uplift in a northwest direction (Eardley, 1962). These faults are present only on the southern flank of the arch, near its western extremity and break only the Precambrian basement rocks (Bachman and Johnson, 1973). The history of the major tectonic development and activity of the Matador can thus be considered to have ended by early Paleozoic time.

3.4.5   Pedernal Uplift

The Pedernal Uplift represents a southward extension of the Rocky Mountains in south-central New Mexico about midway between the Rio Grande and Pecos Rivers. The boundaries of the uplift are not very well defined but in general trend north-south from the eastern side of the Sacramento Mountains in Otero County, apparently continuously to northern Torrance County (Eardley, 1962). The uplift is named for Pedernal Mountain in Torrance County, which is considered to be a remnant and the southernmost exposure of the Ancestral Rockies.

Together with the Permian Basin, the Pedernal landmass strongly influenced the depositional and structural patterns of the region. The Pedernal Uplift appears to have been a wide and not particularly emergent area connecting southward with the Diablo Uplift, and existed, according to Thompson (1942), and Pray (1961), from Early Pennsylvanian time until well after the beginning of Permian time. Within the confines of the Uplift, red shales, sandstones, variegated shales, and limestones of Permian age rest directly on igneous and metamorphic rocks of Precambrian age (Eardley, 1962). In structure, the uplift may have been a broad upwarp in some places and fault-bounded blocks in others. The uplift was probably sharpest on the west with the possible exception of the southeastern edge along the buried Huapache zone (Kelley, 1971).

There is some disagreement as to the time of initial uplift of the Pedernal. According to Stipp (1960), the uplift apparently rose in Late Mississippian or Early Pennsylvanian concurrently with the Central Basin Platform, and was subsequently eroded down to its Precambrian core. Kelley (1971) states that the Pedernal began its rise in Late Pennsylvanian time. According to Bachman (1975), the earliest indication of Ancestral Rocky Mountain building in New Mexico occurred during the Middle Pennsylvanian Desmoinesian time but the Ancestral Rocky Mountain-Pedernal Uplift activity accelerated and was extended southward into New Mexico during Late Pennsylvanian Missourian time, and the uplift reached its maximum in New Mexico during the Virgilian, with accompanying

major faulting occurring along the west side of the Pedernal Uplift. Acceleration of uplift continued through Wolfcampian time, denuding the rocks well into the Precambrian core. Some broad arching and erosion had taken place before the basal Artesia was deposited, followed by renewed rise during and following Salado deposition. Post-Triassic to pre-Dakota time saw renewed rise of the Pedernal Uplift. Structural development ended with a slight uplift and tilting of the Pedernal towards the north during Late Jurassic to Early Cretaceous time (Kelley, 1971).

3.4.6 Diablo Platform

The Diablo Platform is a northwest-trending, structurally positive area southwest of the Delaware Basin, extending southeastward from the Cornudas Mountains at the New Mexico-Texas border and terminating with the Marathon Uplift area and Ouachita tectonic belt to the southeast. The platform is a horst with an average elevation of 1,200 meters above sea level and is bounded on the east, south, and west by grabens. At its northern extent and closest approach to the site, the platform is bordered on the east by the Salt Flat graben (Barker, et al., 1977). (See Figure 3.4-1).

The Diablo Platform experienced primary deformation in Late Pennsylvanian or Early Permian time, but topographic relief and the presence of coarse detritus favor Early Permian for the major portion of the activity. Deformation consisted of uplift, folding, and faulting. The uplift was greater on the south than the north, in the Carrizo Mountain-Van Horn area, where subsequent erosion exposed Precambrian rocks. Faulting is also known to have occurred in post-Permian rocks along the northeast margin of the platform. The Late Cenozoic Basin and Range activity affected the Diablo platform through prominent block faulting and buckling. Major movement in this area was on northwest-trending faults along the northeast margin of the Diablo Platform. Late Cenozoic regional uplift concurrently affected the platform (Oriel, et al., 1967). Oliver (1977) reports several centimeters of relative uplift of the eastern Diablo Plateau and western Salt Basin between 1934 and 1958.

Releveling of this first-order line by the National Geodetic Survey in 1977 for the WIPP indicates only millimeters of relative uplift during the period 1934-1958 and about 5 centimeters of downwarping from 1958-1977 relative to the 1958 line. Further studies of this area are indicated in Chapter 10.

3.4.7 Val Verde Basin

The Val Verde Basin was a deep Early Permian depositional basin at the southwestern extent of the Permian Basin area. The Val Verde Basin trends east-southeast towards the Delaware Basin, adjacent to the north rim of the Ouachita tectonic belt.

The Val Verde Basin attained its major structural definition in Late Paleozoic time. The southeastern part of the south margin of the trough may have been established early in Pennsylvanian time. During Upper-Middle Pennsylvanian Desmoinesian time, the Val Verde area was a fairly stable foreland. But near the beginning of Permian time, the Val Verde trough was abruptly deepened and its north side irregularly steepened opposite the Marathon salient of the south rimming structural belt. Large-scale faulting believed to be of Pennsylvanian age has been recognized, through drilling, along the north flank of the trough; sagging along these zones of weakness during the Early Permian deepening of the trough is probable, according to Vinson (1959), Hester and Holland (1959) and Oriel et al., (1967). The large-scale rapid downwarping that occurred in earliest Permian time caused Permian rocks to accumulate here to a thickness exceeding 17,000 feet, the greatest accumulation of Permian rocks to be found in the Permian Basin. By the Mid-Permian there was a marked decrease in deformation, and a shelf formed across part of the area. Permian rocks here were later warped, possibly in Early Triassic time and eroded (Oriel et al., 1967).

3.4.8   Huapache Flexure

The Huapache Flexure is a long, narrow, northwest-trending monoclinal structure along the eastern slope of the Guadalupe Mountains on the west border of the Delaware Basin. The monocline extends from parallel to the Guadalupe Ridge anticline on the south, northward across the Capitan Reef escarpment, where it is offset to the west. Similar offset occurs farther north as it crosses the folds along the shelf margin. The monocline terminates at the north end of the Guadalupe uplift.

The Huapache flexure is marked by tonal and textured differences on LANDSAT imagery. On the southwest side of the mapped flexure line, the terrain is more dissected, has more vegetation, and from the visible shadows appears to be topographically much higher than the area to the northeast.

The width of the flexure ranges from 0.5 to 2.5 miles. The Precambrian structural relief ranges from 300 to 400 feet in the north to as much as 1,000 feet in the south, just north of Guadalupe Ridge. In the Delaware Basin, the structural relief on the Precambrian along the monocline is from 300 to 600 feet. The maximum dip along the flexure is about 15 degrees to the east, and above and below the structure, dips are from 3 to 5 degrees (Kelley, 1971).

Although the Huapache structure has the configuration of a monocline at the surface, there is evidence that it overlies a thrust fault or series of faults in the Precambrian basement and Paleozoic sedimentary section, and so represents the draping of sediments over a fault or fault zone (Stipp, 1960; Hayes, 1964). Haigler (1962) interpreted the results of drilling as indicating a displacement of as much as 5,400 feet along an underlying fault.

According to Claiborne and Gera (1974), the age of inception of the Huapache was Pennsylvanian; according to Haigler (1962), it was late Pennsylvanian to Permian, contributing to the final structural

development of the Delaware Basin. Hayes (1964) has indicated that the Huapache thrust faulting must have been post-Mississippian in age, since Mississippian rocks show no lithologic change across the zone but are vertically displaced as much as 4,000 to 6,000 feet, with a much higher Pennsylvanian section east of the zone (also see Meyer, 1966). According to Hayes, the zone was apparently intermittently active through all or most of Pennsylvanian time, into Early Permian. The Guadalupian San Andres Limestone, however, is not ruptured; thus, the faulting must have been pre-Guadalupian. According to Kelley (1971), too, movement ceased in Leonardian time. Since then, deposition of sediments above the fault trace has produced the low eastward-dipping flexure configuration exposed today. Although no major activity has occurred here since the Mid-Permian, Hayes (1964) believes that inasmuch as the monocline affects rocks of Late Guadalupian age, it appears that minor post-Guadalupian, probably Tertiary, movement has taken place along the old zone of weakness.

3.4.9   The Northwestern Shelf

North and northwestward of the Delaware Basin is a large platform area. Some investigators have taken the southward front of the platform to be delineated by the Capitan Reef Escarpment. Here the dips of the beds average about 20° to the southeast (Hendrickson & Jones, 1952).

The Northwestern Shelf was well developed before the onset of Permian time, as shown by the abundance of shelf limestones, including numerous reefs of Virgilian age, along its present trend. This tectonic element may have originated in early Paleozoic time, when it formed the margin of the early Tobosa Basin (Galley, 1958, Oriel, et al., 1967).

A number of flexures, arches, and buried fault systems have been identified in this area, several of the largest and best known of which are discussed below. The consensus is that tectonic activity along the individual structures had ceased in Tertiary time, and since then, only broad regional monoclinal flexing has occurred. Other than minor

surficial effects due to solution and hydration of evaporates, the entire southern part of the shelf appears to have been stable in Quaternary time (Brokaw, et al., 1972).

Folds A belt from 6 to 9 miles wide of sharply flexured folds lies just back of the Capitan Reef front, extending in long arcs convex to the west and parallel to the shelf margin for a distance of about 65 miles eastward to the Central Basin Platform. These symmetrical and parallel folds termed the Carlsbad folds by Kelley (1971), average about 1.5 miles apart from crest to crest and have an average fold amplitude of about 100 feet (Motts, 1972). Kelley (1971) describes their shape as "domical uplifts," circular to elliptical, with average dimensions of 1.5 by 3 miles. These folds are partly expressed in the present topography. Shelf domes, consisting of biohermal cores covered by shelf beds, are superimposed on the folds, which suggests to Motts (1972) that the folds may have been topographically positive features during the time of Capitan Reef. Brokaw, et al., (1972) dates these folds as of early Tertiary or perhaps older age. According to Hayes (1964), they are presumed to be Laramide in age, since they post date the Permian rocks and antedate the development of Carlsbad Cavern in early and middle Tertiary.

Another arcuate fold belt, called the Waterhole Anticlinorium, is present about 12 miles west of Carlsbad and extends for about 20 miles with a width of 1 to 2 miles. The feature consists of a narrow, closely spaced set of 3 synclines alternating with 3 anticlines. Structural relief on the folds is from 200 to 400 feet. The axes of the anticlines are sharper than those of the synclines, and locally, their axial planes appear to be faults (Kelley, 1971). Like the Carlsbad folds, this system has been dated as early Tertiary or older (Brokaw et al., 1972).

The Cenozoic folds that parallel the reef escarpment on its northwest may be indirectly related to the older Bone Spring Monocline, which formed a broad southeast-dipping fold along the basinward edge of the Victorio Peak Limestone in the Late Leonardian-Early Guadalupian time. The

monocline is exposed only in the south end of the Guadalupe Mountains in Texas but is presumed to continue northeastward into New Mexico, forming the southeast flank of the 15 to 20 mile-wide Bone Springs Arch. The arch was virtually buried in Brushy Canyon time, but near the end of San Andres time the flexure was rejuvenated and produced an accentuated northwest margin for the Delaware Basin. This had a great effect on later Permian deposition and may have controlled the position of the Capitan limestone (Hayes, 1964).

Numerous other local fold structures have been identified on the shelf area, a good number of which are described by Kelley (1971), by Motts (1972), and by Hayes (1964). Many of these folds have north to northwesterly curving axes and structural closure of up to 100 feet or more. According to Motts (1972), the size of some of these features, such as the McKittrick anticline and adjacent Dark Canyon syncline, as well as their possible influence upon the orientation of the Capitan reef, suggests that they may reflect deeper flexures or faults in the basement. Some of these features have been dated: Motts (1972) has found evidence that the McKittrick anticline and Dark Canyon syncline were a topographic high and low, respectively, during Guadalupian time.

Faults The most prominent area of fault-like structures on the shelf north of the Delaware Basin is the zone of straight northeast-trending shears extending from several miles north of Artesia northwestward toward the Sacramento Uplift and Capitan Mountains. The major structures of this group, such as the Y-O, Six-Mile Hill, and Border Hills Buckles, are exposed for from 35 to 80 miles along strike and spaced at distances of 8 to 20 miles. Movement along these features has involved folding, faulting along strike, and overthrusting, and along the strike of these buckles the nature of deformation may change markedly over a short distance. These features are visible on LANDSAT imagery to varying degrees. The Border Hills Buckle appears as a very obvious scarp and adjacent depression which is visible along its entire length, whereas there are no obvious scarps or depressions along the mapped trace of the Six-Mile Hill Buckle, although some stream offsets are aligned along its

trend, and the Y-O fault is marked only by portions of 3 streams which follow the fault line a short distance. Evidence exists that movement on these zones was initiated in Carboniferous or earlier times and may have been basically right lateral (Brokaw et al., 1972 and Kelley, 1971).

Kelley (1971) has described two faults, named the Barrera and Carlsbad, fronting the reef escarpment 32 kilometers and 16 kilometers southwest of Carlsbad and having "late Tertiary with possible Quarternary movement." However, many other geologists who have investigated the area are not convinced that the linear features seen on aerial photos are actually faults. (Claiborne and Gera, 1974).

Artesia-Vacuum Trend The Artesia-Vacuum trend is a long, low, east-trending arch in Permian rocks, which extends eastward from a little south of the town of Artesia, in Eddy County, New Mexico, for a distance of about 75 miles, roughly paralleling the Carlsbad folds. The trend represents slightly warped Permian strata in an eastward-plunging anticline (Stipp, 1960). The arch is almost completely covered by post-Permian beds, except for a short stretch near Chalk Bluff Draw where the plunging south limb is seen dipping southeastward at about 4 degrees. This feature has been dated as either Early Permian or pre-Permian, and, according to Brokaw et al. (1972), is largely or wholly the product of differential compaction over the Abo reef of Early Permian age.

3.4.10   Sacramento Mountains

The Sacramento Mountains constitute an uplift area to the west of the Northwestern Shelf and form the local eastern border of the Basin and Range province. The uplift extends for a distance of over 45 miles in a north to slightly northeast direction, and most of the structures within the range also exhibit a northerly trend. The overall structure of the Sacramento Mountains is a tilted fault block, with a regional dip to the east of about 1 degree. The eastern flank of the mountains is character-ized by its simple, undeformed eastward dip of 100 to 140 ft/mi. Greater
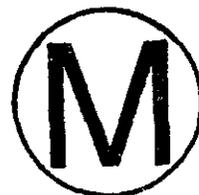
uplift along the central crestal zone has produced dips of several degrees in the strata on the north and south ends of the range. The Sacramento uplift is separated from the Tularosa Basin on the west by one or more normal faults involving several thousand feet of displacement (Stipp, 1960).

The Sacramento Mountains have developed through several periods of tectonic activity, probably beginning in Late Pennsylvanian and early Wolfcampian time. Pre-Permian strata of the range are deformed by folding and faulting during this time, and many of the internal structures of the Sacramento Mountains formed then. Some further deformation occurred during Mesozoic or early Cenozoic time (Pray, 1959).Cretaceous strata, strongly folded and faulted and intruded by dikes and sills, occur extensively in the northern Sacramento Mountains, especially between the towns of Capitan and Carrizozo. Here the structure suggests a depressed synclinal block greatly affected by igneous activity (Stipp, 1960).

Late Cenozoic Basin and Range faulting, which produced uplift and tilting, gave the Sacramento Mountains their present configuration. The dominant location of this activity has been the large fault zone at the western base of the uplift in the Tularosa Basin, and the uplift appears to be still in progress (Pray, 1959).

3.4.11   Guadalupe-Delaware Mountains Uplift

The Guadalupe-Delaware Uplift is a gently northeastward-tilting fault block extending northwestward for some 110 miles, from the Diablo Platform area near Van Horn, Texas, to east of Pinon, New Mexico. In New Mexico, the western boundary of the uplift is a great fault scarp produced by a system of nearly en echelon, normal faults of Late Cenozoic age, along which the displacement ranges from 2,000 to 4,000 feet (Kelley, 1971; Hayes, 1964). The eastern margin is formed largely by erosional conformance to the Late Paleozic to Tertiary Huapache Monocline, and the southeast margin of the range coincides with the Reef

Escarpment, which, according to Hayes (1964) may have resulted partly from Cenozoic rejuvenation of the Late Paleozoic Bone Spring Monocline. Using the Huapache Monocline as the east boundary, the uplift is about 11 miles wide in its southern part, tapering northward to about 3 miles (Kelley, 1971). The Guadalupe Mountains lie within the Sacramento section of the Basin and Range province and are structurally part of the Northwestern Shelf (Brokaw, et al., 1972).

In cross section, the mountains have a cuesta-like or asymmetric profile, with the fault scarp forming a short, steep western slope and a backslope dipping gently eastward at generally less than 3o or about 200 ft/mi. The beds usually dip more steeply than the land surface, thus exposing progressively younger rocks to the east and southeast (Hendrickson & Jones, 1952).

The principal structural elements within the Guadalupe Mountains area have been described in detail by Hayes (1964), Boyd (1958), and King (1948). These include the Huapache and Bone Springs Flexures and the folds which parallel the Reef Escarpment (refer to Section 3.4.8). The only faults along the eastern periphery of the uplift, paralleling the reef, are short normal faults of very small displacement, which probably originated as tension joints (Hayes, 1964). The major faulting in the area is located to the west of the Guadalupe Mountains Uplift, where many closely spaced faults trend north to northwest. Hayes (1964) describes those in the New Mexico portion of the area in three groups: those along the Guadalupe Mountains scarp north of Stone Canyon, those parallel to the Shattuck Valley scarp south of Stone Canyon, and those in and north of the Brokeoff Mountains. Along the Guadalupe Escarpment are numerous, closely spaced, high-angle normal faults paralleling the scarp and generally downthrown on the west. From high on the scarp westward into Big Dog Canyon, the faults decrease in dip to as low as 60 degrees and increase in displacement from rarely over 100 feet on the east to about 800 feet in the canyon, low on the scarp. The faults south of Stone Canyon are separated from those to the north by an unfaulted monocline some 1 1/2 miles wide. Most of the displacement on the scarp here is

along a large fault high on the scarp having a displacement of as much as 800 feet, and an arcuarte trace convex to the east; adjacent to its trace are a number of small strike faults (Hayes, 1964; see also King, 1948; Boyd, 1958). West of the Guadalupe Mountains is a graben area occupied by a complex north-northwestward trending zone of Late Cenozoic faults in and adjacent to the Brokeoff Mountains. Most of the faults are high angle and normal and are downthrown to the east, except for several in the north that form grabens and horsts. Stratigraphic displacements here range from a few feet to about 600 feet (Hayes, 1964).

Evidence has been presented by King (1948) that tectonic deformation was occurring in the southern Guadalupe area before Middle Permian time and produced the Bone Spring Flexure, which possibly governed the location of the Delaware Basin. Hayes (1964) describes a fault zone in the Guadalupe Mountains that may have trended southeastward into the western edge of the Delaware Basin and may have been active during Mississippian to Early Permian time. Like the Sacramento Uplift, though, the Guadalupe-Delaware Mountains are primarily a Late Cenozoic structural feature, uplifted and tilted eastward by the Basin and Range tectonic activity.

King (1948) dated most of the major normal faulting of the Guadalupe Mountains area as Late Pliocene to Early Pleistocene. He did note, however, that some renewed movement along pre-existent faults probably took place in the Early Pleistocene, as evidenced by dissection of probable early Pleistocene deposits due to change in base level. But he found no evidence for younger movements in the Delaware or Guadalupe Mountains.

There is evidence, though, that development of the uplift may still be continuing at a reduced rate today. Kelley (1971) reports that during his work a small scarp in the alluvial fans along the northeastern end of the Guadalupe Fault Scarp, in T20S, R17E was found, indicating some slight Holocene uplift. More recent field investigations in the Salt Basin graben region adjacent to the Guadalupe Mountains in Texas have identified over 100 Quaternary-age normal, en echelan, and discontinuous

fault scarps and photolineaments with displacments of as much as 18 feet, which appear to be controlled by preexisting structural zones of weakness. The orientation of the scarps, the proximity of recurring seismic activity, and the youthfulness of offset surfaces suggest that these scarps have a tectonic origin and are maintained by intermittent activity which is in some places younger than 1,000 years old and probably continuing (Goetz, 1977). Such data would thus indicate some ongoing Holocene structural development of the eastern extent of the Basin and Range elements in the Southeast New Mexico west-Texas region.

3.5 REGIONAL IGNEOUS ACTIVITY

Large-scale post-Precambrian igneous activity in the southeast New Mexico-west Texas area consists of Early to mid-Tertiary intrusive bodies and Tertiary to Quaternary volcanic terrains located well to the north, west, and south of the site area. Figure 3.5-1 presents the regional distribution of known igneous features. Within the northern Delaware Basin, only minor igneous activity, in the form of one or more Tertiary dikes and possibly associated sills, is known to have occurred. This section discusses the igneous features known to exist within about 100 miles of the WIPP site and considers in particular detail the near-site intrusives within the northern Delaware Basin.

3.5.1 Near-site Activity

The outcrops of igneous dike-related material nearest to the WIPP site are located about 42 miles southwest of the site, in the Yeso Hills. Subsurface samples of intrusive igneous rock within about 9 miles of the site have also been obtained from drill holes and from two underground potash mining operations, located some 10 miles apart in the Salado Formation. Aeromagnetic investigations have also indicated the presence of magnetically responsive, perhaps igneous, materials in this area. Whether all these occurrences represent parts of one dike or en enchelon dikes, they together produce a very linear trend striking approximately N50° E for a distance in excess of 75 miles. This trend extends from a

point near the Texas-New Mexico border southeast of Carlsbad Caverns at least to the northeasterly most well intercept, some 30 miles northeast of the site (Elliot, 1976b; Claiborne and Gera, 1974). The location of the intercepts and magnetic indications and the dike trace they suggest are plotted on Figure 3.5-2.

The outcrops in the Yeso Hills consist of rectilinear patches of rust-colored, earthy material studded with occasional sharp, small fragments of a dark, fine-grained igneous rock that represent the surface expression of three parallel, en enchelon dikes within the outcropping Castile gypsum. The dikes trend east northeast and vary in width up to about 20 feet and in length up to about one-half mile (Pratt, 1954). These outcrops are separated by a distance of about 27 miles from the nearest subsurface dike intercepts or definite magnetic response along strike to the northeast.

Intercepts of intrusive igneous material have been reported from at least 9 drill holes within the northern Delaware Basin along the trend indicated above (See Table 3.5-I). These intercepts have generally been multiple in each well or drill hole. For instance, the Stanolind U.S. Duncan #1 is reported to have 8 intercepts which range in depth of location from 470 to 13,300 feet. Several petroleum exploration geologists have interpreted the occurrences to represent a series of sill-like intrusions (Elliot, 1976b), a theory which may be supported by magnetic data discussed below.

Dike exposures have also been observed in the underground workings of the International Minerals and Chemical Corporation mine, located approximately 9-1/2 miles northwest of the proposed WIPP site, and in the Hobbs Plant mine of the Kerr-McGee Chemical Corporation, some 10-1/2 miles north of the site (See Table 3.5-1). The dike exposures in these mines are intruded into the Upper Permian Salado Formation. These intrusives are nearly vertical and usually only a few inches to a foot thick, but thicken to approximately 15 feet wide at their widest observed point, in the Kerr McGee mine. No displacement exists between the salt

beds on the two sides of the dike and, in one of the mines, the end of
the dike can be observed (Claiborne & Gera, 1974), indicating a
discontinuous, segmented character.

Airborne magnetic surveys of the region, performed by the U.S. Geological
Survey, have been utilized to help determine the position of the dike
material and its genetic relationship to the surrounding rock strata.
These surveys show magnetic indications of a dike-like structure
extending southwestward from a point approximately 30 miles northeast of
the WIPP site to near the Pecos River. The width of the magnetic anomaly
so indicated varies from several miles at its base, at a depth of about
12,000 to 13,000 feet, near the Precambrian basement to a very thin trace
at its upper extremity near the ground surface. Elliot (1976b) noted
that an aeromagnetic response indicating such an apparent single, broad
anomaly may be produced by a series of dikes which have a broad base and
pinch out vertically. The feature under consideration may thus represent
"a multiplicity of en echelon dikes forming a swarm, which rise generally
vertically from the basement and pinch out in an upward direction
(Elliot, 1976b)". According to this interpretation, one of these dikes
extends upward above the other dikes, penetrating units as young as the
Salado Formation, and is encountered in the outcrops and subsurface
intercepts. The multiple showings from one drill hole are, according to
this interpretation, thought to represent small sill-like projections
which extend outward horizontally from the main vertical dike source.

The dike or series of dike-related features indicated by the above lines
of evidence has a similar appearance, composition, and structure wherever
it has been encountered in the subsurface. The dike rock is a
medium-gray to grayish-black, fine-grained porphyritic material
identified as lamprophyre by Jones (1973). The groundmass of the rock
consists of orthoclase with accessory biotite, which is partially altered
to vermiculite, and minor amounts of ilmenite, apatite, anatase and
pyrite. The rock also contains corroded andesine phenocrysts and
pseudomorphs of siderite and antigorite after pyroxene. Amygdules as
large as 2 mm in diameter, filled with halite, siderite, calcite, and
natrolite are dispersed through the dike rock.

Nearly vertical and subhorizontal fissures are present throughout the dike and are usually filled with halite, with local polyhalite, anhydrite and minor amounts of pyrite, dolomite, quartz and crystalline hydrocarbons. The dike has a rather poorly-developed flow structure and a chilled border. The halite of the adjacent intruded beds has been recrystallized as much as 3/4 inch along the dike contact, and, in places, contains methane and other gases under pressure. Where the termination of the intrusive mass is observed, a vein of polyhalite, also containing minor amounts of pyrite, dolomite, and crystalline hydrocarbons, extends upward into the adjacent salt, indicating that some migration of fluids along the dike must have taken place following intrusion. Later recrystallization and plastic flowage have, however, healed any permeable zones which may have formed at the time of the intrusion and flowing water is not now present where the dike is observable (Claiborne & Gera, 1974).

Specimens of the dike material from the Yeso Hills were classified by Peter H. Masson (reported in Pratt, 1954) as an alkali trachyte and as a soda trachyte of porphyritic texture with principal minerals of anorthoclase, albite, chlorite, ilmenite, and magnetite. The rocks are severely altered, and the walls of the dikes are not clearly defined. Both specimens examined were vesicular, indicating a surface environment of cooling and crystallization. Calcite and gypsum often line the vesicles as secondary deposits (Pratt, 1954).

The emplacement of the lamprophyre dikes probably occurred during mid-Tertiary time, approximately 30 million years ago. Urry (1936) dated the intrusives at 30 +1.5 m.y., from drill hole cuttings of the Texas Co. No. 1 Moore well, located about 12 miles north of the WIPP site. More recent K/Ar whole-rock dating by the U.S. Geological Survey, Denver, has determined an age for a sample (#J-1-71(M75)) of this dike of about 34.8+0.8 million years (recalculated for recent change in measured decay constant) (C. L. Jones, personal communication).

The span of time thus indicated since intrusion has been ample to provide for complete cooling of even the largest of these intrusive bodies, and at the present time there is no evidence of magnetic masses unusually close to the surface in the area.

These dike indications may represent part of an en echelon dike arrays extending northeastward for almost 80 miles from the Gypsum Hills in southern Eddy County, near the New Mexico—Texas state line, to the Vacuum oil field south of Buckeye in central Lea County, New Mexico.

The northeast trend of all these dikes generally coincides with the orientation of several tectonic lineaments in the area and also parallels the trend of crevasses and joints in the carbonate rock of the Capitan and Tansill Formation near Carlsbad Caverns. These fractures are filled with Early Cretaceous sandstones and conglomerates. Thus, the emplacement of the magmatic material may have been facilitated by earlier patterns of structural weakness, which developed in response to regional stresses operative previous to Cenozoic time. The date of the dikes, however, suggests that their development may have been related events which were precursors to the later Basin and Range tectonism of Mid-to-late Tertiary time.

3.5.2 Guadalupe-Delaware Mountains Area Activity

King (1948) described several occurrences of igneous material in the Guadalupe—Delaware Mountain area. He identified one small intrusive plug, about 15 miles southwest of the Yeso Hills dikes, located within the Delaware Mountains in a ravine one-half mile north of Lamar Canyon, 1-1/2 miles east of its junction with Cherry Canyon. This plug forms a low ridge several hundred feet long and cuts sandstones within the Guadalupian-age Bell Canyon Formation. These sandstones have been tilted, baked, and silicified, according to King, for about 10 feet from the edge of the plug. The intrusive rock itself he described as "light gray and aphanitic, probably a trachyte." Pratt (1954) later examined this reported plug and similar outcrops in the area. He found no igneous

rock or any tilted or baked sandstones, only evidence of intense
silicification of the sandstones within low parallel ridges oriented
north northwest. Pratt, however, interpreted these features to be
evidence of underlying intrusive dikes, as did King. Pratt futher stated
that the dikes formed part of the siliceous mantle of an underlying
igneous intrusion.

Seven miles to the east southeast of these chalcedony-like ridges, within
the Magnolia Petroleum Company's Homer Cowden No. 1 well, a body of
igneous rock has been intercepted at depths from 8,730 feet to 9,140 feet
(Pratt, 1954). The feature is oriented parallel to the trend of the
hypothesized dikes of Lamar Canyon and is interpreted as a sill. Pratt
(1954) suggests that "the source of this intrusion may also be the source
of the solutions which so intensely silicified the conspicuous outcrops"
in the Delaware Mountains, described above. The "sill" is composed of
extremely porous, light gray and holocrystalline rock with prominent
black needles of a ferromagnesian mineral, which has been analyzed by
Peter T. Flawn as a "lenco syendiorite," otherwise possibly termed a
monzonite (Pratt, 1954).

King (1948) has postulated the existence of a third buried intrusive,
located in the Guadalupe Mountains of Texas, approximately 1-1/2 miles
south of the Otero-Eddy county line, on the northeast slope of Lost
Peak. His hypothesis is based on the observation that the Carlsbad
limestone here, at the Calumet and Texas mine, "has been replaced by
copper, lead, zinc, and iron minerals, which probably emanated from an
igneous source beneath (King, 1948)."

The age of the igneous intrusive activity in the Guadalupe-Delaware
Mountains region has been conjectured by King (1948) as Early Tertiary or
somewhat younger, representing the northern extension of a vast number of
intrusives related to the intense Trans-Pecos Davis Mountain activity.
Unlike the region further south, however, little remains of these records
in the Guadalupe Mountains area, and only minor igneous activity occurred
here (King, 1948). Pratt (1954), in agreement with King's dating work,

has stated that the Delaware Mountain materials he investigated "may reasonably be presumed to be of Tertiary age." He based this judgement on the assumption that these rocks are similar in composition to the generally alkalic igneous rocks identified by Flawn (1952) as comprising the Tertiary intrusives of the west Texas-eastern New Mexico area.

3.5.3   Trans-Pecos Magmatic Province

The Trans-Pecos "magmatic province" comprises a vast area of both intrusive and extrusive igneous outcrop terrains of Tertiary age situated east of the Rio Grande River and west and south of the Guadalupe-Delaware Mountains, approaching within about 90 miles of the WIPP site at the northern extent of the province. The magmatic province extends a distance of about 225 miles from the Diablo Plateau-Cornudas Mountains outcrops near the New Mexico-Texas border, southeastward through the Davis Mountains volcanic area and associated intrusives to the southern tip of Texas (see Figure 3.5-I). The entire province contains in excess of 200 intrusive bodies having outcrops exceeding about 1/2 square mile each in surface area (Barker, 1977) in addition to the approximately 6,000 square-mile region of volcanic outcrop terrain of the Davis Mountains area (from Cohee, et al., 1962). According to King (1948), this magmatic province was developed during Early Tertiary time, when great sheets of lava spread over the Davis Mountains and adjacent areas, across a surface of Cretaceous and older rocks. Both the lavas and sedimentary rocks were then intruded by a host of small to large intrusive masses, some of which were far removed from the Davis Mountains region. Barker (1977) has determined that the magmatic activity in the Trans-Pecos province occurred during the interval from 43 to 16 million years before present. Those intrusives which lie closest to the site are discussed further, below.

Within the northern portion of the Diablo Plateau, some 22 intrusive igneous bodies are exposed along a north northwest trending belt. The northernmost of these igneous outcrops occurs within the Cornudas Mountains, which are centered approximately 105 miles west-southwest of the proposed WIPP site, on the Texas-New Mexico border.

These intrusions, known collectively as the Cornudas Group, generally consist of a central group of plugs, surrounded by sills and laccoliths. The materials composing these intrusions have been classified as nepheline syenites, phonolites, or quartz-bearing syenites. The older rocks are generally fine to coarse-grained, equigranular to porphyritic, with only weakly and locally developed flow structure. The younger rocks of the group are fine-grained, microporphyritic and vesicular, with strongly developed flow structure. Abundant autoliths of alkalic igneous material are contained within several of the intrusions of the Cornudas Mountains (Barker, et al., 1977).

K-Ar dating of biotite in igneous rock samples from the Cornudas Group yields an age of approximately 31 to 37 m.y. for the time of intrusion. The intrusives were emplaced in sedimentary rocks which range in age from Early Permian to Cretaceous (Barker, et al., 1977).

3.5.4   El Camino del Diablo and Railroad Mountain Dikes

The east-west trending El Camino del Diablo and Railroad Mountain dikes are the igneous features nearest to the WIPP site on the north, beyond the limits of the Delaware Basin. The outcrop areas of both dikes are covered by a thin veneer of gravel, caliche, and alluvium (Kelley, 1971), and neither have much expression on LANDSAT imagery.

The southernmost of the two dikes, El Camino del Diablo, is located approximately 67 miles north of the WIPP site. The dike can be traced on the surface for about 25 miles (Kelley, 1971) from the caliche-capped plains east of the Pecos River eastward until it disappears under the Mescalero sands. The dike varies in width from some 32 feet on the west to about 47 feet at its easternmost outcrop. Although it exhibits very little topographic expression, in places along its trace the dike is marked by a slight depression produced by a greater erosion of the dike than of the surrounding country rock. The intrusive material is an extensively altered, fine-grained, slightly porphyritic, bluish-gray rock displaying typical diabasic texture and is composed of augite and

magnetite in a matrix of lath-shaped feldspar crystals. Since the composition is intermediate between an andesite and basalt, the rock has been classified as an "augite-andesite" (Semmes, 1920). Bordering the dike are contact zones from one to 12 feet wide, which consist primarily of a mere baking of the country rock with no appreciable mineralization.

The Railroad Mountain Dike parallels the Camino del Diablo Dike 13 miles 6o the north and extends a distance of about 30 miles from the eastern side of the Pecos River eastward into the Mescalero sands. The width of the dike is remarkably constant, measuring at most about 100 feet, which suggested to Semmes (1920) that the exposed portion represents only a fraction of the entire intrusion (Kelley, 1971; Semmes, 1920). In contrast with the Camino del Diablo Dike, this dike forms a ridge, which in places reaches as high as 60 to 80 feet. On LANDSAT imagery, it has its most pronounced expression as it approaches the Matador uplift region to the east. The dike material is a massive, dense, dark-blue, medium-grained granitoid rock composed of pyroxene and olivine with considerable magnetite in a felt-like mass of interlocking lath-shaped plagioclase crystals. The rock may thus be classified as an olivine gabbro, of more basic nature than most of the other intrusives of the region. Almost no secondary alteration has occurred, which accounts for the dike's prominent ridge-like expression (Semmes, 1920). The contact zone between the dike and host rock displays a slight baking but little mineralization and is, at most, several feet wide.

Both the Railroad Mountain and El Camino del Diablo Dikes have been classified as Tertiary in age by Cohee (1962) and have intruded rocks as young as the Triassic Santa Rosa Sandstone (Kelley, 1971). Semmes (1920) considered the dikes to have been Eocene or younger in age and possibly as young as Middle to Late Tertiary, representing later stages in Tertiary igneous activity, when the basaltic intrusives and extrusives of the area originated. The generic relationship of the dikes to other features in the region is unclear, but airborne magnetic surveys indicate that both of the dikes "nose out" to both east and west (Elliot, 1976b).

This would seem to preclude the dikes being direct extensions of either the Capitan stock activity, to the west (see section 3.5.5, below), or of the Matador Arch (section 3.4.4) to the east.

3.5.5   Capitan and Sierra Blanca Mountains Region

The Capitan intrusive is located within the Capitan Mountains region approximately 117 miles northwest of the WIPP site. The feature is about 21 miles long and from 3.5 to 5 miles wide, with an above ground volume of about 20 cubic miles (Kelley, 1971; Semmes, 1920). There is some controversy regarding the nature of the intrusion, due to the fact that it has characteristics of both a laccolith and a stock. Typical of a laccolith, there is evidence of a concordant roof along most of the summit, but the structural and stratigraphic discordances, including observed uplift and structural nosing, favor its designation as a stock. In any case, the intrusion has penetrated units as young as the Rio Bonito member of the San Andres Formation and the Yeso Formation, of Middle Permian Leonardian age. Along the eastern end of the mountain, the Yeso beds stand almost vertically near the contact (Kelley, 1971). "Mesaverde beds" of Cretaceous age show thermal alteration as well according to Kelley (1971).

The Capitan intrusive is remarkably uniform for its size in both composition and texture. It is a medium- to fine-grained, slightly porphyritic rock, classified by Kelley (1971) as a leucoratic quartz syenite. The Capitan intrusive has been designated as Tertiary in age by Cohee (1962); Semmes (1920) suggested that it may be of Early Tertiary age, in concurrence with Lindgren, et al. (1910), who considered all of the quartz-bearing monzonitic and dioritic intrusives of this area to be Early Tertiary. Semmes (1920) considered these acidic intrusives to represent an early stage in igneous activity, preceeding the more basic, less extrusive diorities and gabbros of later Tertiary time.

Immediately west and southwest of the Capitan intrusive, underlying and cropping out in the Sierra Blanca Mountains, are the Sierra Blanca volcanics, dikes, and stocks.

The Sierra Blanca volcanics crop out in an area of some 200 square miles;
Thompson (1966) believes that the field was once as large as 750 square
miles prior to intrusion by the stocks and Late Tertiary erosion. The
volcanics consist of massive, purplish-brown, andesitic breccias, flow,
and tuffs overlain by trachtye breccia and have a recorded thickness of as
much as 3,340 feet. These volcanics are thought to be of Early to
Mid-Tertiary age (Kelley, 1971; Thompson, 1966).

Some 200 dikes occur in swarms oriented generally radially with respect to
the Sierra Blanca stocks and in a great swarm 7 miles wide and 22 miles
long, trending north northeastward from Ruidoso to east of Patos
Mountain. The dikes are generally traceable for less than one mile and
range in thickness from one foot to 60 or 70 feet. They vary in
composition from a few occurrences of syenite porphyry to diabasic,
although 60 to 70 percent of the dikes are basic (Kelley, 1971). Since
the dikes intrude the Sierra Blanca volcanics, they post-date them, and
may be Mid-Tertiary in age.

3.5.6 Conclusions

The data presented above indicate that, within some 100 miles of the WIPP
site, no igneous activity has taken place since the early part of Basin
and Range tectonism, which began in the mid-Tertiary. In the near-site
vicinity, the closest igneous feature to the site is a lamprophyre dike or
series of en echelon dikes, which approaches no nearer than about nine
miles from the site; no associated igneous bodies have been found to
approach or underlie the site itself. The dike has been dated as
approximately 35 m.y. old and has long since completely solidified and
cooled. Younger intrusive and extrusive features are situated far to the
west of the site, beyond the area of discussion, and are associated with
the regions of more recent Basin and Range tectonism. Thus, judging from
the pattern of the structural development of the northern Delaware Basin
area, further igneous activity is not expected in the near-site region.

3.6   REGIONAL GEOLOGIC HISTORY

Figure 3.6-1 presents a summary of the major geologic events which have affected the southeast New Mexico-west Texas area as have been determined from the rock types and structural relationships for which evidence remains and has been uncovered.

3.6.1   Precambrian

Very little is known about the Precambrian history of the southeast New Mexico-west Texas area. The Precambrian rocks penetrated in the Guadalupe Mountain and Sacramento uplift regions in southern Lea County and in west Texas, consist of plutonic granitics and metamorphics, which suggest that the region has a complex Precambrian history of mountain building, metamorphism, and erosional cycles (Nicholson & Clebsch, 1961; Hayes, 1964; Kelley, 1971). According to Flawn (1956), the Precambrian granitics encountered in the southern part of this area comprise a generally stable mass, called the Texas Craton, which extended northward from Texas into southeastern New Mexico. Muehlberger, et al. (1967), however, have demonstrated that these materials comprise part of a much more complicated basement surface representing a variety of environments involving intrusive and extrusive igneous activity as well as metamorphism of sediments.

The ages suggested for the Precambrian rocks encountered in this region are all fairly ancient. In the core of the Pajarito Mountain dome, southeast of the Sacramento uplift, the metamorphics have a radiometric date of 1,270 million years (Kelley, 1971). The granitics and metamorphics of the Guadalupe Mountain area are probably somewhat less than one billion years old (Hayes, 1964), while slightly greater ages have been indicated for the Precambrian rocks of the Texas Craton. Wasserberg, et al. (1962) determined ages of 1,250 to 1,400 million years in the northern part of the area and a younger 1,090 million years terrain to the south, suggesting progressively younger metamorphic events from north to south in this region during the Precambrian.

There is no record of the latest Precambrian or of most of the Cambrian time in this region; however, about one billion years before present the area was reduced to a nearly level plain upon which the Paleozoic rocks were later deposited (Hayes, 1964).

3.6.2   Early and Middle Paleozoic

During most of the Paleozoic Era, from at least Late Cambrian until near the close of the Mississippian Period, the eastern New Mexico-western Texas area was part of a broad, low-lying, generally stable region named the Tobosa Basin by Galley (1958). The shallow basins of the area formed northern arms of the Ouachita trough, which shoaled on the north in south-central New Mexico and merged southward with the Ouachita-Marathon geosyncline, connecting with the open sea in the vicinity of the present Gulf Coast or coast of southern California (Brokaw, et al., 1972; Hills, 1972). During the early Paleozoic there seem to have been no well-marked platforms within the basin. However, lines of weakness along strike-slip faults in the basement probably were present (Hills, 1970). Along these faults later vertical movement took place (Hills, 1972).

For a span of about 180 million years, until Late Mississippian time, almost continuous deposition occurred in this area under conditions of general tectonic stability in shallow seas periodically transgressing from the south. Shelf-type carbonate deposition predominated but was interrupted by shale sedimentation during Middle Ordovician, Late Devonian, and Early Mississippian. The total section of these sediments is about 2,500 feet, from the base of the Bliss Sandstone to the top of the Helms Shale, in the Guadalupe Uplift-southeastern New Mexico area (Hayes, 1964).

The chief events which characterized each period of the Early through Middle Paleozoic are summarized below.

Cambrian-Ordovician. No rock record older than Late Cambrian age has been uncovered in the southeastern New Mexico area (Hayes, 1964). The Bliss

Sandstone near El Paso, Texas, provides evidence of clastic sedimentation in that area during part of the Late Cambrian. After the Precambrian rocks had been uplifted and deeply eroded, a sea advanced over the region from the west or southwest and the Bliss sandstone was deposited; the abundant quartz grains in the Bliss were probably derived from reworking of sedimentary debris on the eroded Precambrian surface (Harbour, 1972; Bachman and Meyers, 1969).

During Early Ordovician time, the sea in which the Bliss was deposited continued to transgress eastward and extended at least as far north as Roswell. During this time, the carbonates and clastics known as the El Paso Formation in New Mexico and the Ellenburger in west Texas were deposited in shallow seas containing abundant marine life (Bachman, 1969). These sediments thickened southeastward from a thin layer lapping onto a positive area of Precambrian basement then present in northern New Mexico and Colorado to a massive deposit over 2,000 feet thick in Texas, at the edge of what may have been the continental shelf (Eardley, 1962). At this time, the ancestral Central Basin Platform was a granitic upland or island chain which provided clastics to the early Ordovician shelf and adjacent shallow basin deposits.

During the Ordovician, the Marathon-Ouachita geosyncline bounding the Tobosa Basin area on the south began subsiding (McGlasson, 1968). In Mid-Ordovician time, a broad and gently emergent peninsula, extending southeastward through Texas, rose, and the region was also tilted southward. To the north, the shales, sandstones, and sandy limestones of the Simpson Group were deposited above the El Paso--Ellenburger, wedging out north at the latitude of Roswell, west around Artesia and east around the Central Basin Platform. Southward, toward the deepening basin regions, the deposits thickened and became predominantly shaly. In Middle to Late Ordovician time, fewer clastics were provided to the area, and the carbonates, and fine-grained calcareous muds of the Montoya Group were deposited in shallower, calmer seas than earlier, that moved northward over the tilted surface of the El Paso Formation. At the close of Montoya time, a gentle southward tilting occurred (Bachman, 1969).

Silurian-Devonian. During Silurian and Devonian time, the Pedernal
Landmass, to the northwest, and the Texas Peninsula, to the south, were
land areas of low relief. The Tobosa Basin between these two areas,
joined southward with the Marathon-Ouachita geosyncline. There is no
evidence of major tectonic activity during this time in west Texas or
southeast New Mexico. However, mild epeirogenic movements did occur, and
the Tobosa Basin was gently subsiding throughout the period, becoming also
more restricted areally. To the south, the Ouachita-Marathon geosyncline
reached its maximum depth.

During Early Silurian time, most of the Tobosa Basin was emergent but
low-lying. By the Middle Silurian, the sea returned, perhaps
transgressing from the south and southeast, and broad, shallow areas
developed around the northern, eastern, and western margins of the Tobosa
Basin, upon which the thick Fusselman dolomites and limestones were
deposited conformably in a marine environment atop the Montoya Group in
clear, well-circulating water (McGlasson, 1968; Harbour, 1972; Bachman,
1969). At this time, the basin waters reached their furthest extent into
New Mexico. Minor fluctuations of sea level within this shallow area of
deposition produced a karst topography on the surface of the periodically
exposed carbonates. During Late Silurian time, southward tilting occurred
once more, and the sea regressed. Within the deeper areas to the south
into Texas, a sediment-starved condition developed, resulting in
deposition of micrites and green shales. Around the Tobosa Basin rim,
carbonates continued to form (McGlasson, 1968).

The shallow sea continued to retreat from the New Mexico area through
Early and Middle Devonian time. In Early Devonian, the shoreline had
retreated, producing a carbonate plain of low relief. The depositional
basin had an asymmetrical shape, with the deepest water to the west, in
which cherts and silicious limestones were deposited. By the late Middle
Devonian, mild uplift and southward tilting had occurred, and most of the
Tobosa Basin was exposed to erosional processes; the only deep water lay
to the south, where the basin plunged into the Marathon-Ouachita
geosyncline. In Late Devonian time, the area was again submerged as

shallow seas spread across southern New Mexico, and the dark heavily clastic Woodford shales were deposited in a nearshore environment (Bachman 1969), overlapping all of the previous Devonian and Silurian deposits (McGlasson, 1968). Woodford deposition continued into Mississippian time.

Mississippian. Subsidence of the Tobosa Basin continued into Mississippian time. The Texas peninsula to the south and the Pedernal landmass to the northwest were mildly positive features and remained so until the Middle Mississippian (McGlasson, 1968).

In Early Mississippian time, a new paleogeographic regime began to develop in this region. The ancient Tobosa Basin began deepening on either side of a medial zone, later to become the Central Basin Platform, that was bounded by Precambrian basement faults. Shelf deposition continued along the margins of the basinal areas.

Toward Late Mississippian time, regional tectonic activity accelerated in the Tobosa Basin area, folding up the medial zone along its ancient lines of weakness. By the end of the period, erosion had probably exposed Precambrian rocks in the cores of the larger anticlines (Hills, 1963). Meanwhile, deep, broad basins, the forerunners of the Delaware and Midland Basins, formed to the east and west of the median upland area. Broad carbonate shelves developed around the margins of these basins, while black shale sedimentation occurred in their deep central portions. The black shale deposition was probably slow, much of it taking place during times of slight sea level sinking (Hills, 1972). Toward the south end of the basins, deposition of the shale and sandstone of the Tesnus Formation continued from Late Mississippian into the beginning of Pennsylvanian time, the clastics apparently being derived from highlands on the southeast which were rising in the earliest activity of the Ouachita orogeny (Flawn, 1961).

To the north of the basins, the Matador Arch was upfolded in the latest Mississippian and rapidly eroded to expose its Precambrian core. At the same time, orogenic forces raised the Ancestral Rocky Mountains to the

west, in a general north-south trend through central New Mexico (Stipp, 1960), producing a regional southward tilt which resulted in widespread erosion, exposing progressively older rocks toward the north.

By the close of the Mississippian Period, most of northeast New Mexico formed a low hilly area of Precambrian rocks, rimmed on the north and east by outcrops of Lower Ordovician dolomites and on the south by the uplifted former site of the Tobosa basin.

3.6.3   Late Paleozoic

Pennsylvanian. Following Mississippian time, the entire region was invaded by the sea from the south and east, and, particularly near the uplifted areas, tremendous thicknesses of Pennsylvanian rocks were deposited unconformably over the tilted bedrock strata, which ranged in age from Mississippian in the south to Precambrian northward in central New Mexico (Hills, 1963; Meyer, 1968). The tectonic processes initiated near the close of the Mississippian, including uplift and erosion of mountains in the Ouachita-Marathon area, of the mountain range separating the early Delaware and Midland Basin areas, and of the Matador Arch and Ancestral Rockies, continued into early Pennsylvanian, providing clastic materials to the adjacent basins. This tectonic activity also involved vertical movement along the ancient strike slip faults, with some new faulting taking place in the recently deposited early Pennsylvanian rocks (Hills, 1972; Stipp, 1960).

The basal Pennsylvanian rocks, the Morrowan, occupied the smallest area, wedging out northward, and contained the greatest proportion of coarse clastic material of the Pennsylvanian section. Along the edges of the platforms, especially in the eastern basin, strong reef and bank growth also occurred during the beginning of the Pennsylvanian. At the same time, submarine tectonism began in the Guadalupe Mountains area, continuing intermittently through the period, elevating the southeastern part of the area relative to the northeast along the northwest-trending Huapache thrust zone (Hayes, 1964).

Lower Middle Pennsylvanian Atokan strata were deposited over most of the southeastern New Mexico area except for the then-positive Pedernal uplift. During this time, anticlinal folds developed north of the Delaware Basin area on the Northwestern Shelf, and the Central Basin Platform range was uplifted as a fault block and eroded. By Desmoinesian time in upper Middle Pennsylvanian, deposition in the Permian basin region consisted primarily of limestones. The environmental setting consisted of a back-reef (lagoon), reef, and basin or open sea, a situation which persisted from this time through Late Pennsylvanian and much of Permian time (Meyer, 1968).

During most of the Late Pennsylvanian, depositional conditions in the Permian Basin were similar to those of Desmoinesian time. The sea encroached farther than before onto the rising Pedernal landmass, followed by a regression beginning in the northwest. To the northeast, the land was intermittently emergent. And southward, in Texas, the Ouachita-Marathon disturbance folding and uplift was being followed by strong northward thrusting, which continued into early Permian time (Hills, 1963). Ensuing erosion from these areas provided an abundance of clastics to the Late Pennsylvanian deposits. The Central Basin Platform, emergent throughout most of the Pennsylvanian, began to subside and received a sequence of Late Pennsylvanian sediments (Nicholson & Clebsch, 1961). Meanwhile, reef banks continued to form, especially along the northwestern edge of the Delaware Basin.

Toward the close of Pennsylvanian time, tectonic activity had virtually ceased, and mixed continental and marine sediments were deposited in the lower areas, nearly obscuring the irregular sea bottom caused by the earlier tectonism (Hayes, 1964).

At the end of Pennsylvanian time the entire region subsided, and the major features of the Permian Basin became firmly established. The rapidly eroding range of the Central Basin Platform separated the Delaware and Midland Basins which were rimmed to the north by a broad shelf area. By this time, the Delaware and Midland Basins were probably both

topographically and structurally deep; only the northern part of the Midland Basin remained a relatively shallow platform, upon which the Horseshoe Atoll grew (Oriel et al., 1967). The Central Basin Platform and shelf areas were subsiding more slowly than was the Delaware Basin and consequently received a lesser thickness of sediments, which were lithologically distinct from the deeper water deposits of the basin (Nicholson & Clebsch, 1961).

Permian. Through Early Permian Wolfcampian time, sedimentation was continuous in most of the basin areas of southeast New Mexico and west Texas, with shales deposited in the low areas and limestone on the shelves (Hills, 1972). The regression in the northwest which had commenced in the Late Pennsylvanian became pronounced, and the acceleration of the rise of the Pedernal uplift through Early Permian resulted in its denudation well into the Precambrian basement rocks. Southward, the Delaware and Midland Basins and the Val Verde Trough were rapidly sinking, at a rate exceeding that of deposition, a situation which favored shales and other stagnant-water deposits to form there (Oriel et al., 1967). The deepening of these basins, as well as uplift elsewhere, was encouraged by the development of major normal fault zones towards late Wolfcampian time (Meyer, 1968), along the north and west sides of the Diablo Platform, on the southeast side of the Pedernal Uplift, and along the periodically emergent Central Basin Platform, where strong submarine relief was produced. Around the perimeter of the Delaware Basin, the Abo reef developed, along with back-reef lagoons into which muds and carbonates accumulated. Along the south border of the Permian Basin region, the final northward thrusting of the Ouchita-Marathon structural belt occurred, causing Late Pennsylvanian and Early Permian strata to be overridden and a large volume of detritus to pour into the Val Verde trough (Hills, 1963; Oriel, et al, 1967). Following the close of this activity, the rest of Permian time was marked by regional tectonic stability in which depositional basins separated by platform areas passed through maturity.

Through Middle Permian time, restriction of marine circulation, coupled with eustatic withdrawal of the sea in a southwest direction, resulted in the development of high reefs and carbonate banks, behind which evaporites, ranging from dolomites, sulfates, and chlorides to potash minerals, were deposited in highly saline, shallow lagoons (Hills, 1972).

Early in lower Middle Permian Leonardian time, movement on a line along the Delaware Basin margin, the later Bone Spring monoclinal structure, accompanied by continued subsidence of the basin, produced a more definite northwest margin of the basin, the development of which resulted in deposition of a great submarine bank that formed a barrier to free circulation of the sea water. The gray carbonates of the Victorio Peak formation represent patch reefs which built upward and southwards across earlier deposits as the basin margin regressed. Similar carbonate reefs and banks formed along the margins of the Midland Basin as well as on the Central Basin Platform, overlying the old medial mountain range (Hills, 1972). Within the deep basin areas the black limestones and shales of the Bone Spring were deposited, and on the broad back-reef lagoonal shelf north and northeast of the basin, the Yeso gypsum and limestone or dolomite and clastics were laid down. Northwestward, the entire area including the Pedernal was gradually overlapped by sediments, and, by latest Leonardian time, all but a few of the highest Precambrian peaks were buried (Kelley, 1971).

At the end of Leonardian time and into the Guadalupian, pronounced differential movement occurred along the Delaware Basin margin, and a broad, southeastward-dipping fold, the Bone Spring Arch, was elevated, forming a barrier 15 to 20 miles wide between the basin and the Northwestern Shelf area (Hayes, 1964). In a marked regression, the seas withdrew, and were nearly restricted to the Delaware Basin (King, 1942).

As Guadalupian time opened, the arching and limited evaporitic conditions resulted in deposition of clastics in the basins and limestone on the shelf areas (Kelley, 1971; Hayes, 1964).

By the mid-Guadalupian, slight rejuvenation of the Bone Spring arch led to growth of lime-bank deposits upon the arch, which provided the foundation for a barrier reef, the Goat Seep. As the Delaware Basin continued to deepen, the reef grew primarily upwards, in consequence, restricting circulation, thus producing sediment-starved conditions within the basin and leading to the precipitation of calcium sulfate shelfward for a distance of 15 to 25 miles. (Oriel et al., 1967; Hayes, 1964). Eastward, the Midland Basin gradually filled and became favorable for evaporite deposition, in common with the adjacent shelves and Central Basin Platform.

Late Guadalupian time brought gradual subsidence of the shelf and even greater downwarping of the Delaware Basin, while renewed reef growth occurred at great pace around the periphery of the Delaware Basin. The Capitan Limestone began to grow upward and basinward in oblique fashion from the top of the Goat Seep dolomite, resulting in a wide barrier which even at its narrowest point was six times as wide as it was high (Hayes, 1964; Newell et al., 1972). Most investigators consider the Capitan to have been a true barrier reef. Achauer (1969), however, believes that it originated as a linear organic belt, instead, since he finds no coincidence between the topographic and lithologic break produced by it, and Dunham (1972) hypothesizes that the structure represents a marginal mound. In any case, as the structure grew, deposition in the basin proceeded more slowly than on the shelf and did not keep pace with the sinking of the basin, so that by the close of the period, the sea bottom in the Delaware Basin was about 1,500 feet below the adjacent reef and lagoon floor to the northwest. The reefs and banks eventually grew almost continually around the periphery of the Delaware Basin, and by the close of Guadalupian time, access of water to and from the open ocean was sharply restricted, the seas of the shelf area evaporated, and the water of the Delaware Basin itself became highly saline, thus halting the reef growth.

The Delaware Basin was essentially an evaporating pan by the beginning of Late Permian Ochoan time. Many hundreds of feet of Castile evaporites, containing anhydrite and limestone laminae at the bottom and a few beds of

halite, were deposited in the basin, with apparently little in the reef
and back-reef areas. By the latest Castile time, the basin had filled
such that a thin tongue of anhydrite extended northward across the reef to
the shelf. Saline waters then spread from the Delaware Basin over the
shelf, the Central Basin Platform and Midland Basin areas, and extensive
salt deposition occurred, resulting in the predominantly halite Salado
Formation. From this time on, the old Permian Basin structures, notably
the Central Basin Platform, became progressively more deeply buried by
Late Permian sediments and no longer constituted depositional barriers.
Periodically, clastics swept into the area from the north and northwest,
increasing towards the end of Salado time, as the Pedernal Landmass
underwent renewed uplift. At the same time, the sea freshened somewhat,
probably from the south, judging from the presence of more soluble salts
northward, in New Mexico. Halite deposition decreased while anhydrite
became dominant, along with an increase in carbonate muds during Rustler
Formation deposition (Hayes, 1964; Brokaw et al., 1972). Broad
epeirogenic uplift at the close of Permian time caused the seas to
withdraw, and the continental fine sands and silts of the Dewey Lake
Redbeds were deposited in a thin layer on broad mudflats over the former
seabed (Brokaw et al., 1972; Kelley, 1971). As terrestrial conditions
developed across the New Mexico-west Texas area, erosion became the
dominant geologic process.

3.6.4   Mesozoic Rocks

Triassic. During most of Triassic time, the southeast New Mexico area was
emergent and subject to erosion, and by late Triassic the entire area,
including the Pedernal, must have been reduced to a great peneplain
(Kelley, 1971). In Late Triassic time, a broad floodplain basin formed on
the site of the Permian Basin over a large area and beyond the borders of
the Delaware Basin. This was an interior basin draining toward the
northwest into other interior basins (Hills, 1963, Brokaw, et al., 1972).
Source areas to the north provided fluvial sands, muds, and gravels to the
basin, forming the Dockum Group red beds that included the Santa Rosa
Sandstone and finer-grained Chinle Formation.

The nearly conformable relationship which exists between these Upper Triassic strata and the Permian Dewey Lake Redbeds indicates continued regional tectonic stability through Triassic time (Oriel, et al., 1967). It is possible that some dissolution of soluble Permian rocks occurred during the general emergence of Triassic time. Bachman and Johnson (1973) state that during this period, sinkholes may have formed in parts of the Pecos Valley due to removal of salts (Gorman & Robeck, 1946). And Bachman (1974) describes a Late Triassic karst topography in the vicinity of Santa Rosa, New Mexico. However, direct evidence for this Triassic dissolution and collapse has not been found in southeastern New Mexico (Bachman, 1974).

Jurassic. During Jurassic time, the southeast New Mexico area was uplifted above sea level so that the Triassic and perhaps Permian rocks in the western part of the Delaware Basin and westward were eroded away. Some dissolution of Permian salt deposits probably occurred here at this time. The period of exposure, which generally affected the entire Permian Basin, may have been 50 million years; however, the surface relief was probably low, and erosion was not deep. This is the first of three erosional cycles which have incised the Triassic rocks of the area (Nicholson & Clebsch, 1961; Bachman, 1974).

During Jurassic time, continental rocks were laid down to the north, in central and northern New Mexico, derived from the sediments being stripped from the eroding basin area in southeastern New Mexico. South of the basins, in western Texas and northern Mexico, marine conditions prevailed during at least part of the time (Bachman, 1974). By Late Jurassic Entrada and Morrison time, seas again encroached on the north, covering southeast Colorado and northeastern New Mexico. And from the Late Jurassic into the Early Cretaceous, a slight tilt involving uplift took place in the northern part of the former basins region, accompanied by widespread erosional stripping across the area (Hills, 1963; Kelley, 1971).

Cretaceous. By the early part of Cretaceous time, the west Texas-southeast New Mexico area comprised a rolling topography of Triassic rocks with beds from Precambrian to Permian exposed on the uplifts and on

the Diablo Platform. The geography evolved from that of interior basins with highlands in the north and east to a general gulfward slope with highlands in the west and evidence of only slight tectonic activity (Hills, 1963; Kelley, 1971).

During Cretaceous time, a large part of the western interior of North America became submerged beneath epicontinental seas. By late in the Early Cretaceous, the southeast New Mexico area had subsided slightly, and shallow shelf seas advanced over the area from the south and remained until early in Late Cretaceous time, when the seas probably withdrew for the last time, leaving behind a thin deposit of fossiliferous limestone and coarse sandstone and conglomerate (Hayes, 1964; Nicholson & Clebsch, 1961). Isolated slump blocks of limestone and shale in Lea County east of Eunice, in the Pecos River drainage, in the Sacramento and Guadalupe Mountains and perhaps on the crest of the reef escarpment are the only remaining evidence of the sea's advance in the southeast New Mexico area (Hayes, 1964; Bachman, 1973).

There is no record of most of the Late Cretaceous in the area. The land surface was probably slightly above sea level, and the region was dry land by the close of Cretaceous time (Bachman & Johnson, 1973).

3.6.5 Cenozoic

Early Tertiary. The Mesozoic Era came to a close with the Laramide revolution and uplift of the Rocky Mountains. Late in the Cretaceous or very early in the Tertiary Period, the entire region from north of the Guadalupe Mountains through southeast New Mexico was elevated by broad epeirogenic uplift and tilted slightly to the northeast. Mild tectonism affected the Guadalupe area of the Northwestern Shelf, producing small igneous dikes, fold systems, and setting the stage for the ancestral northeast flowing drainage system (Hayes, 1964). Igneous activity also occurred to the northwest in the Sierra Blanca and Capitan Mountains (Bachman, 1974). In general, however, most of the area southwest of the Pedernal Uplift and Matador Arch was not subject to such tectonic forces.

According to Hills (1963), these ancient positive elements formed
buttresses which transmitted and distributed the orogenic forces on the
east, and this protected the basins on the southeast from folding.

The dominant process in southeast New Mexico from Late Cretaceous until
Late Tertiary, notwithstanding the minor tectonism, was erosion. No Early
or Middle Tertiary rocks are represented in the Permian Basin. The
Cretaceous and Triassic rocks of the area underwent intense erosion to
form a surface of low relief, sloping gently east and southeast (Bachman,
1974; Brokaw, et al., 1972). In the Lea County area of southeast New
Mexico, the entire sequence of Cretaceous rocks, particularly to the west,
was stripped off, except for small remnants, and the Triassic rocks were
subjected to a second cycle of erosion (Nicholson & Clebsch, 1961). By
Late Tertiary Miocene time, erosion had again exposed the Permian rocks to
dissolution, notably in the vicinity of San Simon Swale (Bachman, 1974).

Late Tertiary (Miocene-Pliocene). In Late Tertiary time, regional uplift
and east-to-southeastward tilting occurred throughout southeastern New
Mexico into Texas, as Basin and Range tectonic activity commenced to the
west, producing the western escarpments of the Delaware, Guadalupe, and
Sacramento Mountains. The western section of the Permian evaporites was
elevated, and exposed to dissolution and subsidence, particularly in the
vicinity of the Pecos River divide, which created new patterns of
groundwater movement (Bachman, 1973; Mercer & Orr, 1977). Erosional
forces carved a pediment-like surface, down which streams flowing eastward
from the Rocky Mountains deposited an extensive blanket of gravel, sand,
and related deposits in coalescing fans, which comprise the Ogallala
Formation. Deposition of the Ogallala began about 12 million years ago,
in Miocene time. The Ogallala represents the first preserved sedimentary
record in the vicinity of the Delaware Basin since Cretaceous deposition
(Bachman, 1974). The Ogallala formed a thick mantle throughout the
Permian Basin, producing the even surface of the High Plains, called the
Llano Estacado in western Texas and eastern New Mexico. Locally, eolian
activity played a part in deposition, and periodically, widespread soils
formed (Frye, 1970).

Ogallala deposition ended about 4 million years ago, in Pliocene time, with regional warping and uplift. Eolian activity reworked the sediments, producing a widespread soil profile across the Great Plains. A caliche zone formed within the soil complex and constitutes the carbonate "caprock" of today (Mercer & Orr, 1977; Bachman & Johnson, 1973). The caliche caprock has since undergone a complex history of brecciation, solution, and recementation (Bachman, 1973).

Pleistocene-Holocene. During the Late Pliocene and Early Pleistocene, the major part of the faulting and uplift of the Guadalupe Mountains occurred (Hayes, 1964). Concurrently to the east, fields of great longitudinal dunes formed atop the Ogallala surface of the southern Great Plains as a result of desert conditions with westerly to northwesterly prevailing winds. Since this time, erosion has exceeded deposition in the Permian salt basin area. Etching and thinning of the caliche caprock between the dunes created series of parallel swales. Erosion and coalescence of subsided areas removed Ogallala sediments, and in places also eroded the Triassic rocks a third time and entrenched the Pecos and San Simon drainages (Nicholson Clebsch, 1961; Mercer & Orr, 1977). Also during early to Middle Pleistocene time, Nash Draw, Clayton Basin, and probably San Simon Swale underwent extensive subsidence and partial filling (Bachman, 1973). Local sink holes and other solution features began to form at this time.

The most humid climate and the greatest erosion occurred during the Middle Pleistocene. The western escarpment of the High Plains underwent severe erosion, followed by a period of aggradation in the valley areas, during which the mostly locally-derived pebbles and other coarse debris of the Gatuna Formation filled the depressions and mantled the slopes (Brokaw, et al., 1972). During this time of heavy precipitation and stream flow, major salt dissolution is assumed to have occurred within the Delaware basin (Bachman, 1974). After Gatuna time, but still during the Middle Pleistocene, the region became more stable and semi-arid, and the Mescalero caliche formed on the ground surface.

During the Late Pleistocene, there were intermittent episodes of caliche formation and renewed periods of high rainfall accompanied by erosion and salt dissolution, which produced local subsidence and deposition of fluvial and lacustrine sediments.

From Late Pleistocene through Holocene time, the climate has remained variable although becoming more arid. The detrital materials have been reworked by winds from the west and southwest, giving rise to the vast deposits of dune sand that now cover large parts of southeast New Mexico east of the Pecos River (Nicholson & Clebsch, 1961; Bachman, 1973). Some slight uplift is also probably still occurring along the western escarpments of the Basin and Range structures, such as the Guadalupe Mountains. Renewed periodic downcutting by streams and subsurface solution with resultant subsidence, have continued to the present, accompanied by intermittant local accumulations of pediment and terrace alluvium and playa deposits. Most of the recent erosion has been confined to the Pecos Valley, and solution and subsidence have occurred at a slower rate than during the earlier Pleistocene time (Bachman, 1973).

3.7 SUMMARY

The regional geology of SENM is the source of much information germane to long-term safety; knowledge of the regional geology also permits preliminary site selection and general evaluation of the consistency of site geology with regional geology.

The regional geology and geological history may first be divided into three major intervals of about .5 billion years each. This period from about 1.5 to 1.0 billion years ago is represented by metamorphosed rocks of various sedimentary to igneous origins. The time from about 1.0 to .5 billion years ago is not known to be represented by rocks through most of the region; erosion is assumed to be the dominant geological process during this time. The last interval, from about .5 billion years ago to the present, shows more complexity in the rock record. From about 500 to

100 million years ago, SENM shows a rock record of mostly marine sediments deposited in a basin that became shallower as time passed. About 225 million years ago the marine environment became quite restricted, resulting in deposition of about 4000 feet of evaporites in which it is proposed to dispose of radioactive waste. The lack of rock record in much of the region from about 100 million years to about 4 million years ago imply that erosion has been dominant. Fluvial sediments and caliche developed within the last 4 million years suggest some change in base level but considerable stability.

The list of important structural events in the region include metamonolusm and relative uplift during the Precambrian, downwarping through much of the Paleozoic, some downwarping and uplift during the Mesozoic, and some uplift during the Cenozoic. Specific structural features include basin and range type faulting more than 70 miles west of the site and about 1o eastward tilting of the Delaware Basin; both of these features are believed to be about mid-Cenozoic in age. The Central Basin Platform to the east of the site has probably not been active since the Permian (see also Chapter 5).

Thus the regional geology furnishes evidence of tectonic and geologic stability that will be used for assessing the safety of a repository at the WIPP site.

3.8 REFERENCES

Achauer, C.W., 1969, Origin of Capitan Formation, Guadalupe Mountains, New Mexico and Texas: Am. Assoc. Pet. Geol. Bull., v. 53, no. 11, p. 2314-2323.

Adams, J.E., 1944, Upper Permian Ochoan Series of Delaware Basin, west Texas and southeast New Mexico: Am. Assoc. Pet. Geol. Bull., vol. 28, no. 11, p. 1596-1625.

Adams, J.E., 1965, Stratigraphic-Tectonic Development of Delaware Basin: Am. Assoc. Pet. Geol. Bull. , v. 49, no. 11 p 2140-2148.

Adams, J.E., and Frenzel, H.N., 1950, Capitan barrier reef, Texas and New Mexico: Journal Geology, v. 58, no. 4, 289-312.

Adams, J.E., and Rhodes, M.L., 1960, Dolomitization by seepage refluxion: Am. Assoc. of Pet. Geol. Bull., v. 44, no. 12, p. 1912-1920.

Anderson, R.Y., 1978, Report to Sandia Laboratories on deep dissolution of salt, northern Delaware Basin, New Mexico.

Anderson, R.Y., Dean, W.E., Kirkland, D.N., and Snider, H.I., 1972, Permian Castile varved evaporite sequence, west Texas and New Mexico: Geol. Soc. Am. Bull., v. 83, p. 59-86.

Anderson, R.Y., and Powers, D., in press, Salt anticlines in the Castile-Salado evaporite sequence, northern Delaware Basin, New Mexico: New Mexico Bureau of Mines and Mineral Resources, Circ. 159.

Ash, S.R. and Clebsch, A.C., 1961, Cretaceous Rocks in Lea County, New Mexico: U.S. Geol. Surv. Prof. Paper 424-D, p. 139-142.

Bachman, G.O., 1960, Southwestern edge of late Paleozoic Landmass in New Mexico: U.S. Geol. Surv. Prof. Paper 400b, p. 239-241.

Bachman, G.O., 1973, Surficial features and late Cenozoic history in southeastern New Mexico: U.S. Geol. Surv. Open-file report.

Bachman, G.O., 1974, Geologic processes and Cenozoic history related to salt dissolution in southeastern New Mexico: U.S. Geol. Surv. Open-file report 74-194.

Bachman, G.O., 1975, New Mexico: in McKee and Crosby, et al., Paleotectonic Investigations of the Pennsylvanian System in the United States, U.S. Geol. Surv. Prof. Paper 853L, p. 233-244.

Bachman, G.O., 1976, Cenozoic Deposits of Southeastern New Mexico and an Outline of the History of Evaporite Dissolution: U.S. Geol. Surv. Journal of Research, v. 4, no. 2, p. 135-149.

Bachman, G.O., and Johnson, R., 1973, Stability of salt in the Permian salt basin of Kansas, Oklahoma, Texas and New Mexico: U.S. Geol. Surv. Open file report 4339-4.

Bachman, G.O. and Myers, D.A., 1968, Geology of the Bear Peak area, Dona Ana County, New Mexico: U.S. Geol. Surv. Bulletin 1271C, p.1-46.

Barker, D.S., 1977, "Northern Trans-Pecos Magmatic Province: Introduction and Comparison with the Kenya Rift", Geol. Soc. Am. Bull., v. 88, no. 10, p. 1421-1427.

Barker, D.S., Lang, L.E., Hoops, G.K., Hodges, F.N., 1977, Petrology and RB-Sr isotope geochemistry of intrusives in the Diablo Plateau, northern Trans-Pecos magmatic province, Texas and New Mexico: Geol. Soc. Am. Bull., v. 88, p. 1437-1446

Boyd, D.W., 1955, San Andres Formation in the Brokeoff Mountains, Southeastern New Mexico (abs.): Geol. Soc. Am. Bull. v. 66, no. 12, pt. 2, p. 1533.

Brokaw, A.L., Jones, C.L., Cooley, M.E., and Hays, W.H., 1972, Geology and hydrology of the Carlsbad potash area, Eddy and Lea Counties, New Mexico, U.S. Geol. Surv. Open-file report 4339-1.

Claiborne, H.C. and Gera, F., 1974: Potential containment failure mechanisms and their consequences at a radioactive waste depository in bedded salt in New Mexico: ORNL-TM-4639.

Cloud, P.E., Jr., and Barnes, V.E., 1948, The Ellenburger Group of Central Texas: Texas Univ. Bur. Econ. Geol. Publ. 4621.

Cohee, G.V. (Chairman), 1962, Tectonic Map of the United States: U.S. Geol. Surv. and Am. Assoc. Pet. Geol.

Crandall, K.H., 1929, Permian stratigraphy of southeastern New Mexico and adjacent parts of western Texas: Am. Assoc. of Pet. Geol. Bull., v. 13, p. 927-944.

Darton, N.H., 1917, A comparison of Paleozoic sections in southern New Mexico: U.S. Geol. Surv. Prof. Paper 108-C, p. 31-55.

Darton, N.H., 1928, Red beds and associated formations in New Mexico, with an outline of the geology of the state, U.S. Geol. Surv. Bull. 794.

Dickey, R.I., 1940, Geologic Section from Fisher County thru Andrews County, Texas to Eddy County, New Mexico: Am. Assoc. Pet. Geol. Bull., v. 24, No. 1.

Dunham, R.J., 1972, Capitan Reef, New Mexico and Texas: Facts and questions to aid interpretation and group discussion: Permian Basin Section, Soc. Econ. Paleontologists and Mineralogists Pub. 72-14.

Eardley, A.J., 1962, Structural geology of North America: Harper & Row, New York.

Elliot, C.L., 1976a, A Laboratory Investigation of Magnetic Physical Properties of Igneous Dike Samples from Kerr-McGee Hobbs Plant, Section 32, T 20 S, R 32 E, and Surface Outcrop, Section 31, T 26 S, R 25 E, Elliot and Geophysical Company, Tucson, Arizona, p. 1-7.

Elliot, C.L., 1976b, A Preliminary Geophysical Study of a Trachyte Dike in Close Proximity to the Proposed Los Medanos Nuclear Waste Disposal Site, Eddy and Lea Counties, New Mexico, Elliot Geophysical Company, Tucson, Arizona, p. 1-19.

Elliot, C.L., 1976c., An experimental detailed resistivity survey of known or suspected breccia pipes and sinkholes, Eddy County, New Mexico. Report written under Sandia contract.

Fenneman, N.M., 1931, Physiography of Western United States, New York, McGraw-Hill Book Company, Inc., p. 11-25, 47-54, 379-395.

Flawn, P.T., 1952, Significance of alkalic igneous rocks in wells in west Texas and southeast New Mexico: Am. Assoc. Pet. Geol. Bull., v. 36, no. 7, p. 1457-1461.

Flawn, P.T., 1954, Summary of basement rocks in west-central Texas: San Angelo Geological Society, Cambrian Field Trip--Llano Area, p. 74-77.

Flawn, P.T., 1956, New study of Texas' basement rocks: Oil and Gas Journal, v. 54, no. 59.

Flawn, P.T., 1961, The Marathon area, in The Ouachita System: Texas Univ. Pub. 6120. p. 49-58.

Flower, R.H., 1953, Age of Bliss sandstone, New Mexico: Am. Assoc. Pet. Geol. Bull., v. 37, No. 8, p. 2054-2055.

Foster, R.W. and Stipp, T.F., 1961, Preliminary geologic and relief Map of the Precambrian rocks of New Mexico: New Mexico Bureau of Mines and Mineral Resources, Circular 67.

Foster, R.W., 1974, Oil and Gas potential of a proposed site for the disposal of high-level radioactive waste, New Mexico Bureau of Mines and Mineral Resources, New Mexico Institute of Mining and Technology: Oak Ridge Nat'l Laboratories, Open-file report.

Frye, J.C., 1970, The Ogallala formation; a review: in Ogallala Aquifer Symposium, p. 5-14, Int. Cent. Arid Semi-arid Land Stud., Lubbock, TX.

Galley, J.E., 1958, Oil and geology in the Permian Basin of Texas and New Mexico in Weeks, L.G., ed., Habitat of oil - a symposium: p. 395-446.

Gile, L.H., Peterson, F.F., and Grossman, R.B., 1966, Morphological and genetic sequences of carbonate accumulations in desert soils: Soil Science, v. 101, p. 347-360.

Goetz, L.K., 1977, Quaternary faulting in Salt Basin Graben, west Texas: M.A. thesis, University of Texas at Austin.

Gorman, J.M., and Robeck, R.C., 1946, U.S. Geol. Surv. Oil and Gas Inv. Preliminary Map 44.

Griswold, G.B., 1977, Site Selection and Evaluation Studies of the Waste Isolation Pilot Plant (WIPP), Los Medanos, Eddy County, N.M., Sandia Laboratories Report 77-0946, Albuquerque, N.M., p. 11, 33, 43.

Haigler, L., 1962, Geologic notes on the Delaware Basin: New Mexico Bureau of Mines & Mineral Resources, Socorro, N.M., Circular 63.

Harbour, R.L., 1960, Precambrian rocks of North Franklin Mountains, Texas: Am. Assoc. of Pet. Geol. Bull., v. 44, no. 11, p. 1785-1792.

Harbour, R.L., 1972, Geology of northern Franklin Mountains, Texas and New Mexico: U.S. Geol. Surv. Bull. 1298.

Harms, J.C., 1974, Brushy Canyon Formation, Texas: a deep water density current deposit: Geol. Soc. Am. Bull. v. 85, p. 1763-1784.

Hayes, P.T., 1964, Geology of the Guadalupe Mountains, New Mexico: U.S. Geol. Surv. Prof. Paper No. 446.

Hayes, P.T., 1975, Cambrian and Ordovician rocks of southern Arizona and New Mexico and westernmost Texas: U.S. Geol. Surv. Prof. Paper 446.

Hendrickson, G.E. and Jones, R.S., 1952, Geology and ground water resources of Eddy County, New Mexico: New Mexico Bureau of Mines and Mineral Resources, Ground Water Report 3.

Hester, R.J., and Holland, R.R., 1959, Structure of the Puckett Field, Pecos County, Texas, in West Texas Geological Soc. Guidebook, p. 87-92.

Hills, J.M., 1963, Late Paleozoic tectonics and mountain ranges, western Texas to southern Colorado: Am. Assoc. Pet. Bull., v. 47, No. 9, p. 1709-1725.

Hills, J.M., 1968, Permian Basin Field area, west Texas and southeastern New Mexico, in Int'l Conf. on Saline Deposits, 1962: Geol. Soc. Am. Special Paper 88, p. 17-27.

Hills, J.M., 1970, Late Paleozoic structural directions in southern Permian Basin, west Texas and southeastern New Mexico: Am. Assoc. Pet. Geol. Bull. v. 54, no. 10, p. 1809-1827.

Hills, J.M., 1972, Late Paleozoic sedimentation in west Texas Permian basin: Am. Assoc. Pet. Geol. Bull., v. 56, no. 12.

Hiss, W.I., 1976, Structure of the Permian Guadalupian Capitan aquifer, southeast New Mexico and west Texas: New Mexico Bureau of Mines and Mineral Resources, Resource map 6.

Jones, C.L., 1954, The occurrence and distribution of potassium minerals in southeastern New Mexico: in, New Mexico Geol. Soc. Guidebook 5th Field Conf., Southeastern New Mexico 1954, p. 107-112.

Jones, C.L., 1960, Thickness, character and structures of Upper permian evaporites in part of Eddy County, New Mexico: U.S. Geol. Surv. TEM-1033.

Jones, C.L., 1973, Salt Deposits of Los Medanos Area, Eddy and Lea Counties, New Mexico, U.S. Geol. Surv. Open-file report 4339-7, p. 29-30.

Jones, C.L., and Madsen, B.M., 1959, Observations on Igneous Intrusions in Late Permian Evaporites, Southeastern New Mexico: (abs.), Geol. Soc. Am. Bull., v. 70, no. 12, pt. 2, p. 1625-1626.

Judson, S.S., Jr., 1950, depressions of the northern portion of the southern High Plains of eastern New Mexico: Geol. Soc. Am. Bull., v. 61, no. 3, p. 253-274.

Kelley, V.C., 1971, Geology of the Pecos County, southeastern New Mexico: New Mexico Bureau of Mines and Mineral Resources, Memoir 24, 75 p.

King, P.B., 1942, Permian of west Texas and southeastern New Mexico: Am. Assoc. Pet. Geol. Bull., v. 26, p. 535-763.

King, P.B., 1948, Geology of the southern Guadalupe Mountains, Texas: U.S. Geol. Surv. Prof. Paper 215.

King, P. B., 1965, Geology of the Sierra Diablo region, west Texas: U.S.G.S., Prof. Paper 480.

Kottlowski, F.E., Cooley, M.E., and Ruhe, R.V., 1965, Quaternary Geology of the Southwest: in The Quaternary of the United States Wright, H.E., Jr., and Frey, David G., (eds.), Princeton, New Jersey, Princeton University Press, p. 290-291.

Lang, W.B., 1937, The Permian formations of the Pecos Valley of New Mexico and Texas: Am. Assoc. Pet. Geol. Bull., v. 21, p. 833-898.

Lee, W.T., 1925, Erosion by Solution and Fill, U.S. Geol. Survey Bull. 760-C, p. 107-121.

McGlasson, E.H., 1968, The Siluro-Devonian of west Texas and southeast New Mexico: West Texas Geological Society-Delaware Basin Exploration Guidebook, Pub. 68-55, p. 35-44.

McGlasson, E.H., The Siluro-Devonian of West Texas and southeastern New Mexico in border stratigraphy symposium: New Mexico State Bureau Mines Mineral Resources, Circ. 104, p. 26-37.

McGowan, J.H. and Groat, C.G., 1971, Van Horn Sandstone, West Texas: An alluvial fan model for mineral exploration: Bureau of Economic Geology, Univ. Texas at Austin, Report of Investigations, no. 72.

McKee, E.D. and Oriel, S.S., et al., 1967, Paleotectonic maps of the Permian System: U.S. Geol. Surv. Misc. Geologic Investigations Map I-450.

Mercer, J.W., and Orr, B.R., 1977, Review and analysis of hydrogeologic conditions near the site of a potential nuclear waste laboratory, Eddy and Lea Counties, New Mexico: U.S. Geol. Surv. Open-file report 77-123.

Meyer, R.F., 1966, Geology of Pennsylvanian and Wolfcampian rocks in southeast New Mexico: New Mexico Bureau of Mines and Mineral Resources, Memoir 17.

Meyer, R.F., 1968, Geology of Pennsylvanian and Wolcampian rocks in southeastern New Mexico (abs.): University of Kansas manuscript.

Morgan, A.M., 1942, Solution Phenomena in New Mexico, in Symposium on Relations of Geology to the Ground Water Problems of the Southwest: Am. Geophys. Union Trans., 23rd An. Mtg., Pt. 1, p. 27-35.

Motts, E.S, 1972, Geology and paleoenvironments of the northern segment, Capitan shelf, New Mexico and west Texas: Geol. Soc. Am. Bull., v. 83, p. 701-722.

Muehlberger, W.R. et al., 1967, Basement rocks in continental interior of United States: Am. Assoc. Pet. Geol. Bull., v. 51, no. 12, p. 2366-2371.

Olive, W.W., 1957, Solution-Subsidence Troughs Castile Formation of Gypsum Plain, Texas and New Mexico: Geol. Soc. Am. Bull., v. 68, p. 351-358.

Muehlberger, W.R., Denison, R.E., and Lidiak, E.G., 1967, Basement rocks in continental interior of United States: Am. Assoc. Pet. Geol. Bull., v. 51, No. 12, p. 2366-2371.

Newell, N.D., Rigby, J.K., Fischer, A.G., Whiteman, A.J., Hickox, J.E., and Bradley, J.S., 1953, The Permian Reef complex of the Guadalupe Mountains region Texas and New Mexico--A Study in Paleoecology: San Francisco, W. H. Freeman & Co., 236 p.

Newell, N.D., Rigby, J.K., Fischer, A.G., Whiteman, A.J., Hickox, J.E., and Bradley, J.S., 1972, The Permian Reef complex of the Guadalupe Mountains region Texas and New Mexico: Hafner Publishing Co., New York.

Nicholson, A., Jr., and Clebsch, A., Jr., 1961, Geology and ground-water conditions in southern Lea County, New Mexico: U.S. Geol Surv. and New Mexico Bureau of Mines and Mineral Resources, Ground-water Report 6.

Olive, W.W., 1957, Solution-Subsidence Troughs in the Castile Formation of Gypsum Plain, Texas and New Mexico: Geol. Soc. Am. Bull., v. 68, p. 351-358.

Oliver, J., 1977, Recent vertical crustal movements, The eastern United States: quarterly progress report for period Sept. 1, 1976 - Jan 1, 1977 to U.S.N.R.C., Cornell University.

Oriel, S.S., Myers, D.A., and Crosby, E.J., 1967, West Texas Permian basin region, in Paleotectonic Investigations of the Permian System in the United States: U.S. Geol. Surv. Prof. Paper 515, p. 21-60.

Page, L.R., and Adams, J.E., 1940, Stratigraphy, eastern Midland Basin, Texas: Am. Assoc. Pet. Geol. Bull., v. 24, no. 1, 52-64.

Pratt, W.E., 1954, Evidences of Igneous Activity in the Northwestern Part of the Delaware Basin: in New Mexico Geol. Soc. Guidebook of Southeastern New Mexico Fifth Field Conference, p. 143-147.

Pray, L.C., 1953, Upper Ordovician and Silurian Stratigraphy of Sacramento Mountains, Otero County, New Mexico: Am. Assoc. Pet. Geol. Bull., v. 37, no. 8, p. 1894-1918.

Pray, L.C., 1954, Outline of the stratigraphy and structure of the Sacramento Mountain Escarpment: in Fifth Field Conference, Southeastern New Mexico, New Mexico Geological Society, p. 92-106.

Pray, L.C., 1958, Stratigraphic Section, Montoya Group and Fusselman Formation, Franklin Mountains, Texas: in West Texas Geol. Soc. Guidebook, 1958 Field Trip Franklin and Hueco Mountains, Texas, p. 30-37.

Pray, L.C., 1959, Stratigraphic and structual features of the Sacramento Mountain escarpment, New Mexico: in Guidebook for Joint Field Conference in the Sacramento Mountain of Otero County, New Mexico, Alamogordo, N.M., Permian Basin section of Economic Paleontologists and Mineralgists and Roswell Geological Society.

Pray, L.C. and Allen, J.E., 1956, Outlier of Dakota (?) strata, southeastern New Mexico: Am. Assoc. Pet. Geol. Bull., v. 40, no. 11, p. 2735-2740.

Pray, L.C., 1961, Geology of the Sacramento Mountains escarpment, Otero County, New Mexico. New Mexico Bureau of Mines and Mineral Resources, Bull. 35.

Price, W.A., 1958, Sedimentology and Quaternary Geomorphology of South Texas: Gulf Coast Assoc. Geol. Soc. Trans., v. 8, p. 41-75.

Richardson, G.B., 1904, Report of a reconnaisance in Trans-Pecos Texas North of the Texas and Pacific Railway: Univ. Texas Bull. 23.

Roswell Geological Society, 1958, North-south stratigraphic cross-section; Delaware Basin-Northwest Shelf: Roswell Geological Society.

Sanford, A.R. and Toppozada, T.R., 1974, Seismicity of proposed radioactive waste disposal site in southeastern New Mexico: New Mexico Bureau of Mines and Mineral Resources, Circular 143.

Sanford, A.R., Sandford, S., Caravella, F., Merritt. L., Sheldon, J., Ward, R., 1978, Seismic Studies of the Los Medanos Area in Southeastern New Mexico: Report to Sandia Laboratories.

Semmes, D.R., 1920, Notes on the Tertiary Intrusives of the Lower Pecos Valley, New Mexico: Am. Jour. Sci., 4th Ser. v. 50, p. 415-430.

Silver, B.A. and Todd, R.G., 1969, Permian cyclic strata, northern Midland and Delaware basins, west Texas and southeast New Mexico: Am. Assoc. Pet. Geol. Bull., v. 53, no. 11 p. 2223-2251.

Stipp, T.F. (ed), 1954, Guidebook of southeastern New Mexico, Fifth Field Conference, New Mexico Geological Society.

Stipp, T.F., 1960, Major structural features and geologic history of southeastern New Mexico, the oil and gas fields of Southeastern New Mexico: Supplement: A symposium.

Stipp, T.F., and Haigler, L.B., 1956, Preliminary Structure Contour Map of a Part of Southeastern New Mexico Showing Oil and Gas Development: U.S. Geol. Surv. Oil and Gas Inv. Map OM-177 (1957).

Thompson, T.B., 1966, Geology of the Sierra Blanca, Lincoln and Otero Counties, New Mexico: Univ. N. Mex. Ph.D. dissertation, p. 47.

Thornbury, W.D., 1965, Regional Geomorphology of the United States: New York, John Wiley & Sons, Inc., p. 289-290, 300-310, 315-317, 498-501.

United States Bureau of Mines, 1977, Valuation of potash occurrences within the Waste Isolation Pilot Plant site in southeastern New Mexico: U.S. Dept. of Interior.

U.S. Geol. Surv., 1973, Aeromagnetic Map of the Carlsbad area, New Mexico and Texas: U.S. Geol. Surv. Geophysical Investigations, Map GP-861.

Urry, W.E., 1936, Post-Keweenawan Time Scale: National Research Council Rept. Comm. on Measurement of Geologic Time 1935-1936, Exh. 2, p. 35-40.

Vertrees, C.D., Atchison, C.H., and Evans, G.L., 1959, Paleozoic geology of the Delaware and Val Verde basins, in Geology of the Val Verde basin and field trip guidebook: West Texas Geological Society, p. 64-73.

Vine, J.D., 1960, Recent Domal Structures in Southeastern New Mexico Am. Assoc. Pet. Geol. Bull., v. 44, no. 12, p. 1903-1911.

Vine, J.D., 1976, Breccia Pipes and Burial Metamorphism in Permian evaporites of the Delaware Basin, New Mexico: Geol. Soc. Am. Abstracts, v. 8 No. 6.

Vine, J.D., 1963, Surface geology of the Nash Draw Quadrangle, Eddy County, New Mexico: U.S. Geol. Surv. Bull. 1141-B, U.S.G.S.

Vinson, M.G., 1959, Brown-Basset Field, Terrel County: in West Texas Geol. Soc. Guidebook, November 1959, field trip, p. 85-86.

Wasserberg, G.J., Wetherill, G.W., Silver, L.T., and Flawn, P.T., 1962, A study of the ages of the Precambrian of Texas: Journal of Geophysical Research, v. 57, No. 10, p. 4021-4046.
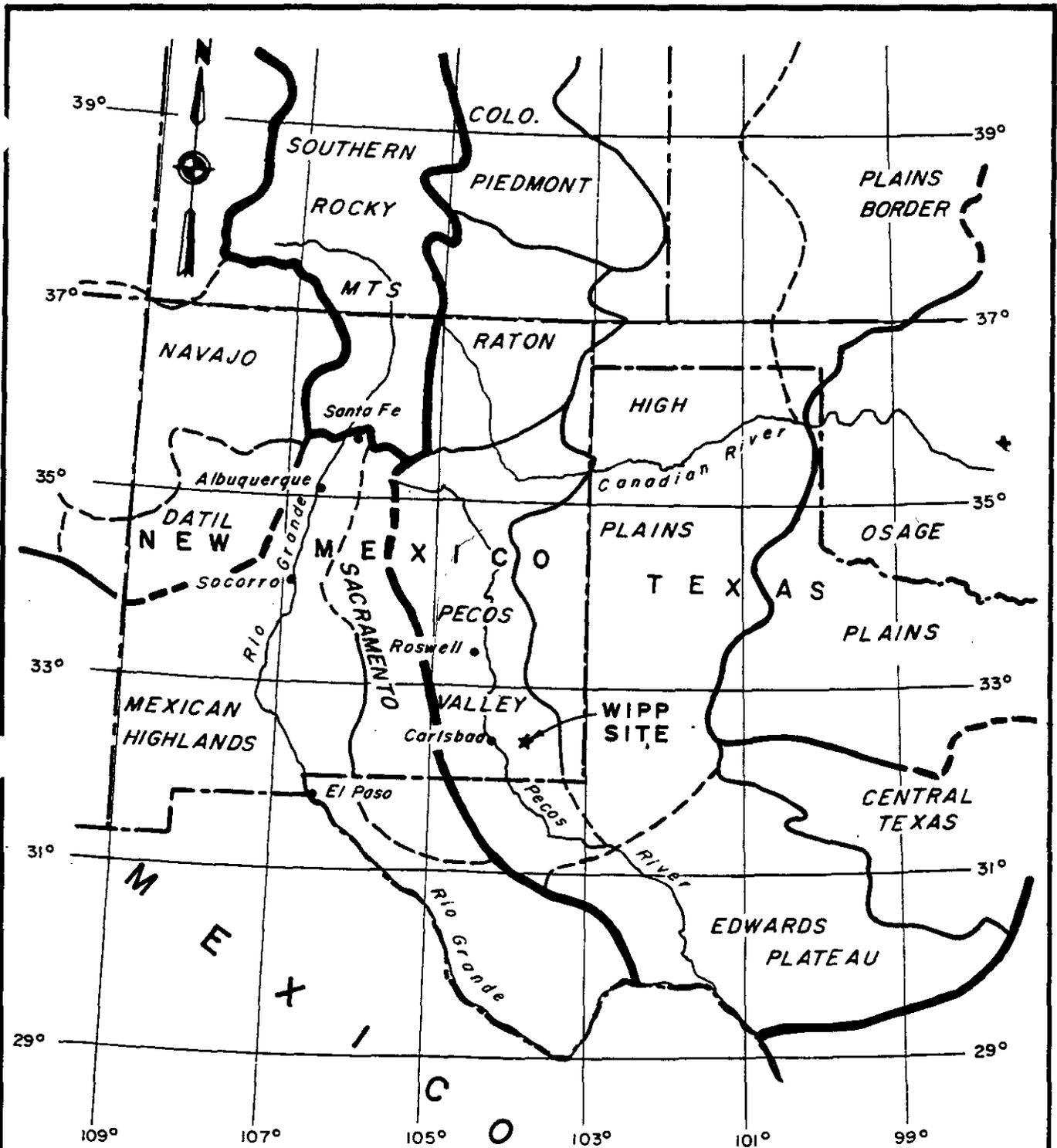
EXPLANATION

━ ━ ■ ■ Boundary of major
          physiographic division

━ ━ ─ ─ Boundary of physiographic province

─ ─ ─ ─ Boundary of physiographic section

SCALE

0   100   200   300 KM
0   50   100   150   200 MI

M
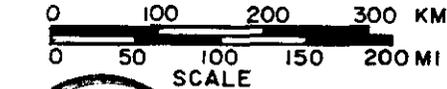
PHYSIOGRAPHIC SECTIONS

REFERENCE:

Fenneman, N.M., and D.W. Johnson, 1946.

FIGURE 3.2-1

EXPLANATION

CH: Chaves granitic terrane

PV: Panhandle volcanic terrane

SD: Swisher diabasic terrane

DB: De Baca terrane

TM: Tillman metasedimentary group

GN: Older gneiss and granite

AG: Amarillo granite terrane

TOR: Older metasedimentary and meta-igneous rocks

SG: Sierra Grande granite terrane

WP: Cambrian igneous rocks: Wichita Province

FM: Fisher metasedimentary terrane

— — — — County boundary

— · — · — State boundary

— · · — · · — International boundary

REFERENCE:

Muehlberger, et al. (1967)
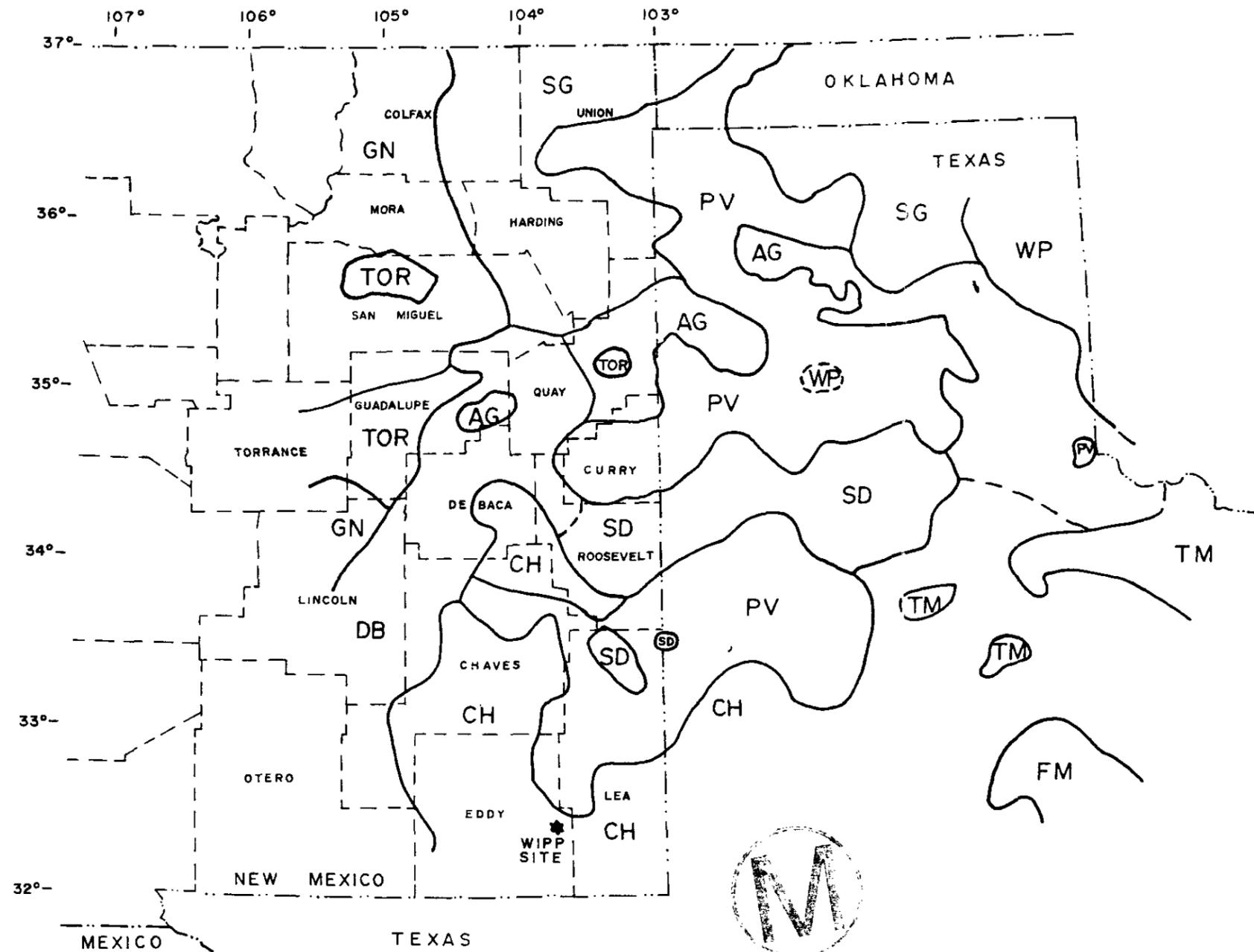
25 0 25 50 75 miles

PRECAMBRIAN ROCKS OF TEXAS PANHANDLE

AND EASTERN NEW MEXICO

FIGURE 3.3-1
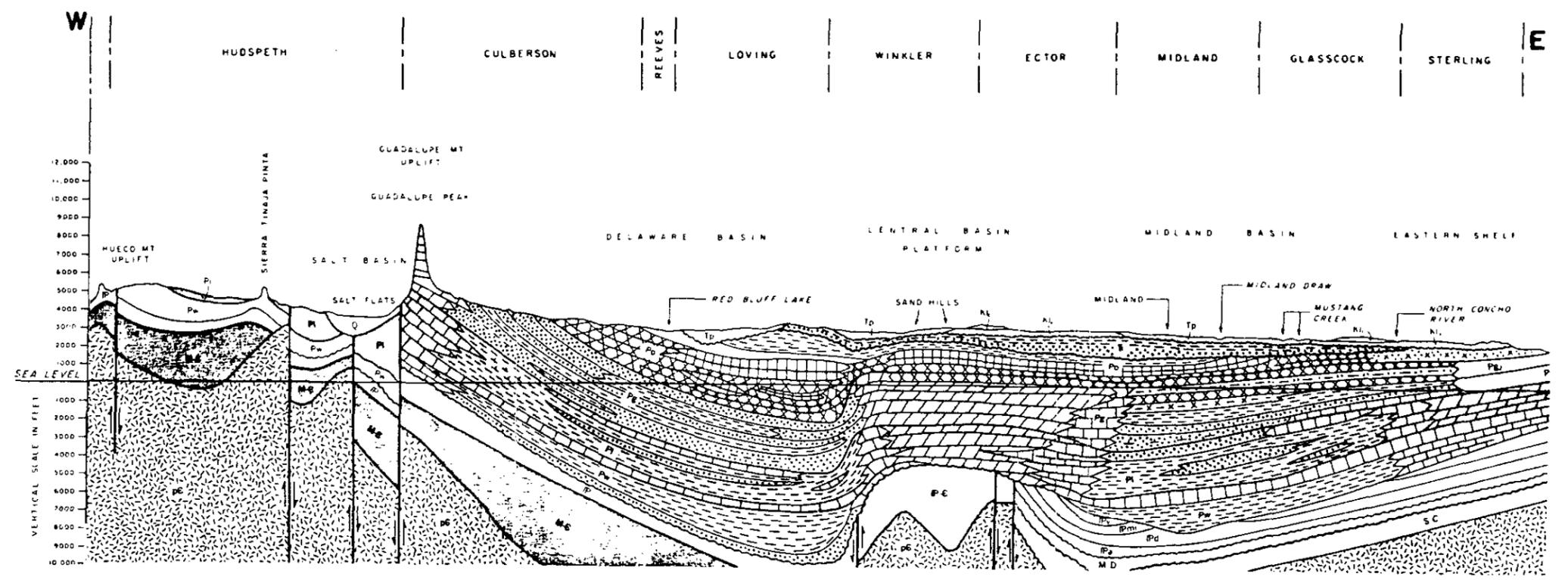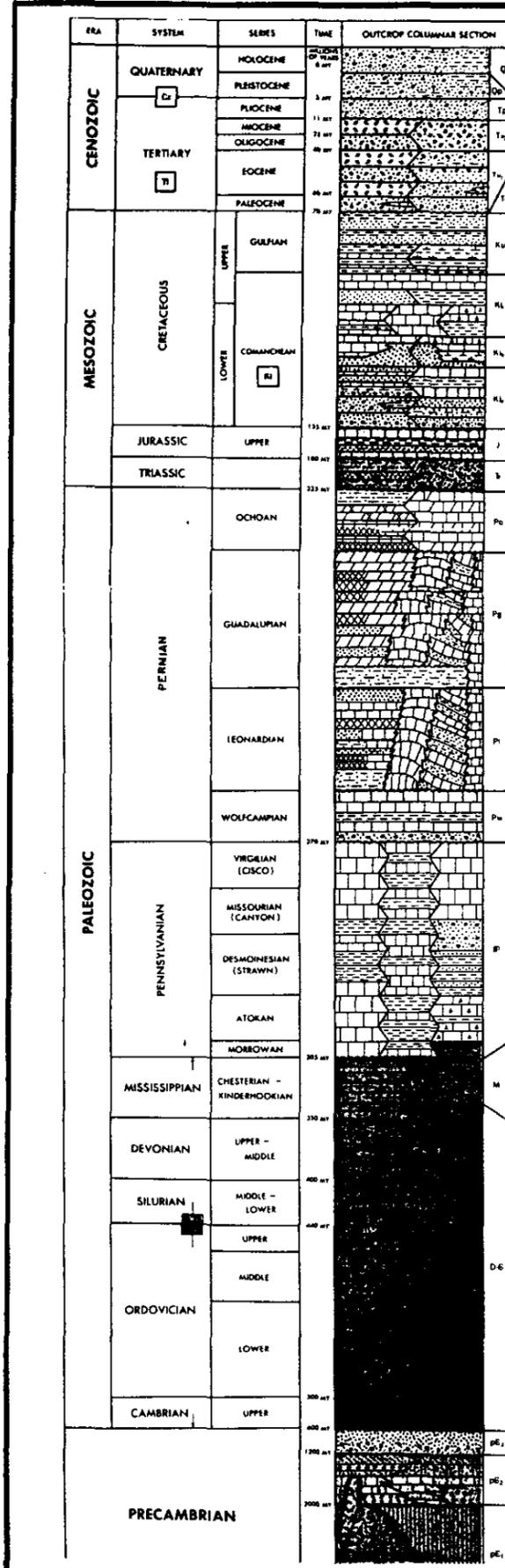
15

WEST–EAST CROSS SECTION
NEW MEXICO – TEXAS BORDER

REFERENCE: From Geological Highway Map of Texas, 1973

FIGURE 3.3-2

STRATIGRAPHIC CORRELATIONS PERMIAN SYSTEM SOUTHEAST NEW MEXICO

West Texas provincial series	International series	Central eastern New Mexico	Guadalupe Mountains (back-reef facies)	Guadalupe Mountains (reef facies)	Delaware basin (fore-reef facies)	Central Basin platform	Midland basin
Ochoa		Dewey Lake Redbeds / Rustler Formation / Salado Formation	Dewey Lake Redbeds / Rustler Formation / Salado Formation	Dewey Lake Redbeds / Rustler Formation / Salado Formation	Dewey Lake Redbeds / Rustler Formation / Salado Formation / Castile Formation	Dewey Lake Redbeds / Rustler Formation / Salado Formation	Dewey Lake Redbeds / Rustler Formation / Salado Formation
Guadalupe	Upper Permian	Artesia Group: Tansill Formation / Yates Formation / Seven Rivers Formation / Queen Formation / Grayburg Formation; San Andres Limestone	Artesia Group: Tansill Formation / Yates Formation / Seven Rivers Formation / Queen Formation / Grayburg Formation; San Andres Limestone; Cutoff Shale	Tansill Formation / Limestone / Capitan Limestone / Goat Seep Limestone; Sandstone tongue of Cherry Canyon Fm; Brushy Canyon Fm; Victorio Peak Ls	Bell Canyon Formation / Cherry Canyon Formation / Brushy Canyon Formation; Victorio Peak Ls	Artesia Group: Tansill Formation / Yates Formation / Seven Rivers Formation / Queen Formation / Grayburg Formation; San Andres Limestone: Upper member / Lower cherty member	Artesia Group: Tansill Formation / Yates Formation / Seven Rivers Formation / Queen Formation / Grayburg Formation; San Andres Limestone; Sandstone and mudstone
Leonard	Lower Permian	"Glorieta Sandstone"; Victorio Peak Limestone; Yeso Formation; "Abo Formation"	Victorio Peak Limestone; Bone Spring Limestone	Victorio Peak Limestone; Bone Spring Limestone	Bone Spring Limestone	"Glorieta Sandstone"; (Clear Fork Group) (upper part); Fullerton or Tubb Sand; Clear Fork, Group (lower part); "Abo Formation" / "Wichita Group"	"Glorieta Sandstone"; Clear Fork Group; Spraberry Sandstone; Mudstone
Wolfcamp		Hueco Limestone; Limestone and dark mudstone	Third Bone Spring sand; Limestone and dark mudstone	Third Bone Spring sand; Limestone and dark mudstone	Third Bone Spring sand; Limestone and dark mudstone	Hueco Limestone; Limestone	Wichita Group: Dean Sandstone; Mudstone, limestone, and sandstone

REFERENCE:

U.S.G.S. Prof. Paper 515, Table 1, 1967.

MISSING SECTION

FIGURE 3.3-3

Stratigraphic summary of the Guadalupe, Leonard, and adjacent series of the Permian System in the Southern Guadalupe Mountains. The Delaware basin area is to the right and the shelf or platform area is to to the left. Rock facies are greatly generalized.

REFERENCE:

Adapted from E.D. McKee, et al. (1967).

(Originally compiled from P.B. King (1942, 1948)).

CROSS SECTION OF

CAPITAN REEF AREA

FIGURE 3.3-4

MAJOR REGIONAL STRUCTURES

FIGURE 3.4-1
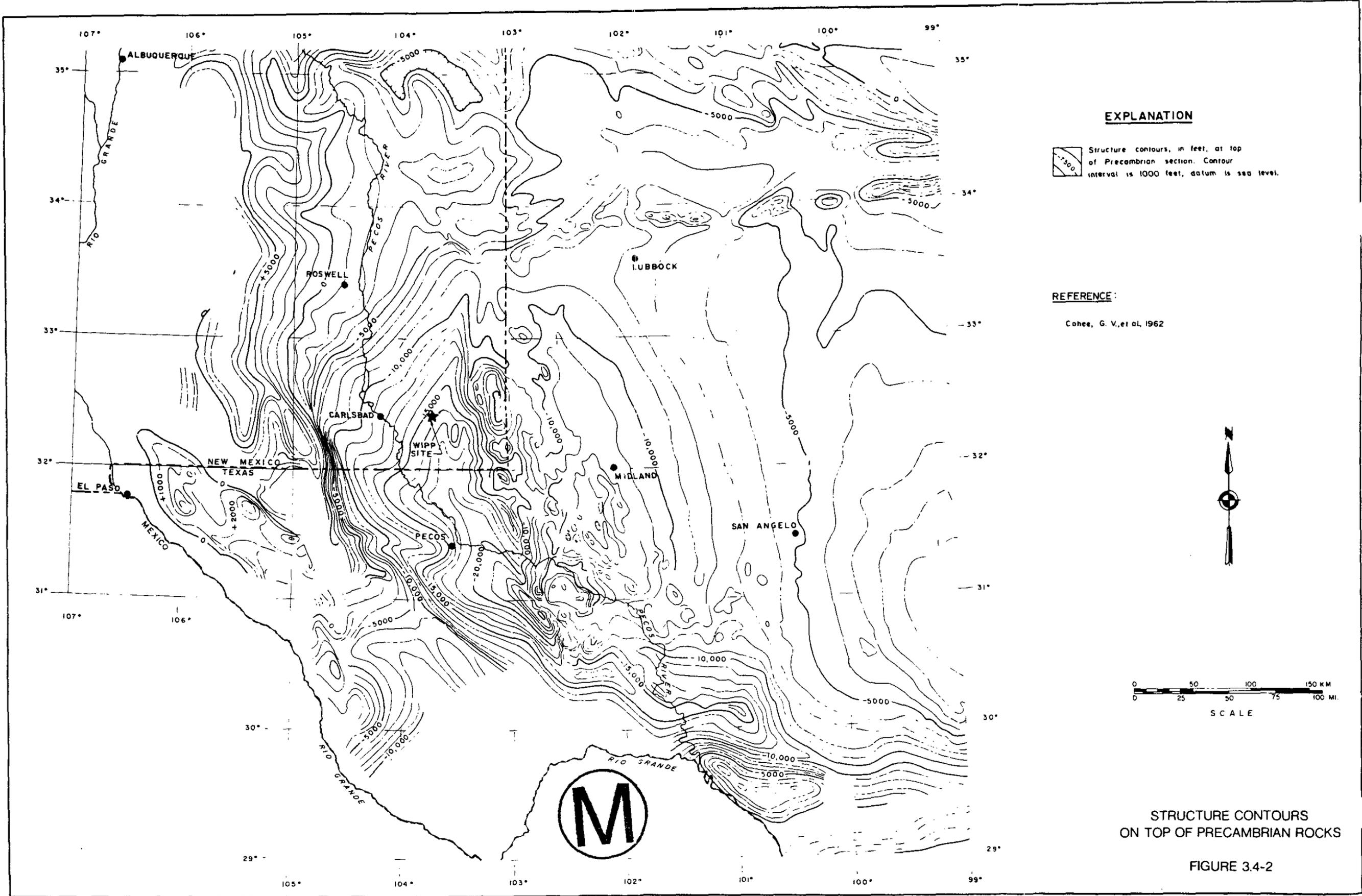
EXPLANATION

Structure contours, in feet, at top of Precambrian section. Contour interval is 1000 feet, datum is sea level.

REFERENCE:

Cohee, G. V., et al, 1962
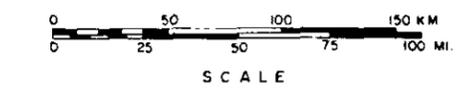
STRUCTURE CONTOURS
ON TOP OF PRECAMBRIAN ROCKS

FIGURE 3.4-2

SCALE
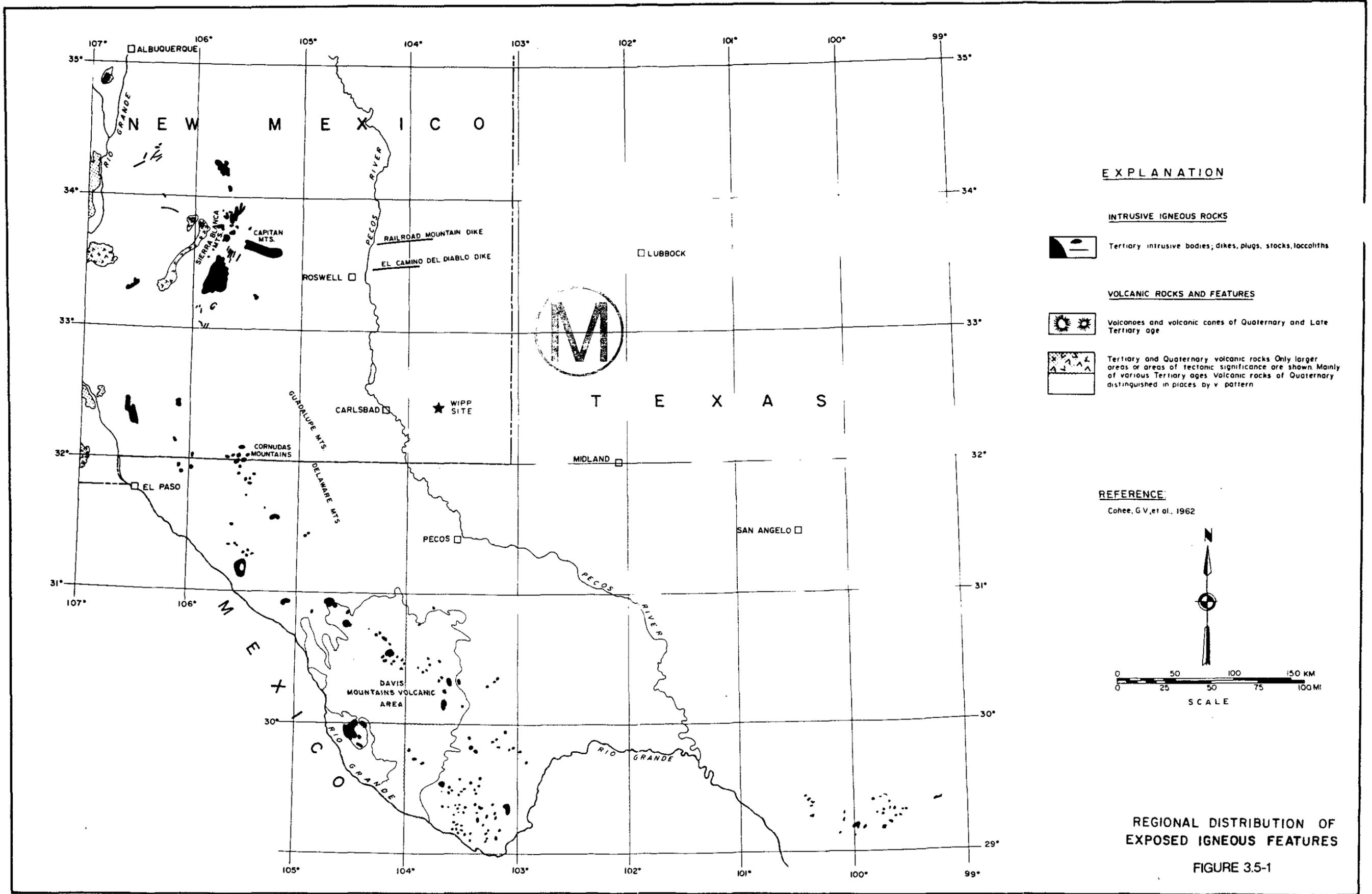
EXPLANATION

INTRUSIVE IGNEOUS ROCKS

Tertiary intrusive bodies; dikes, plugs, stocks, laccoliths

VOLCANIC ROCKS AND FEATURES

Volcanoes and volcanic cones of Quaternary and Late Tertiary age

Tertiary and Quaternary volcanic rocks Only larger areas or areas of tectonic significance are shown Mainly of various Tertiary ages Volcanic rocks of Quaternary distinguished in places by v pattern

REFERENCE:

Cohee, G V, et al., 1962

SCALE
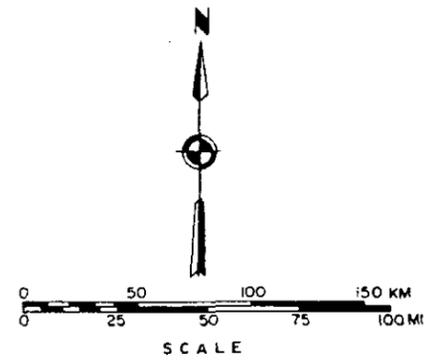
REGIONAL DISTRIBUTION OF
EXPOSED IGNEOUS FEATURES
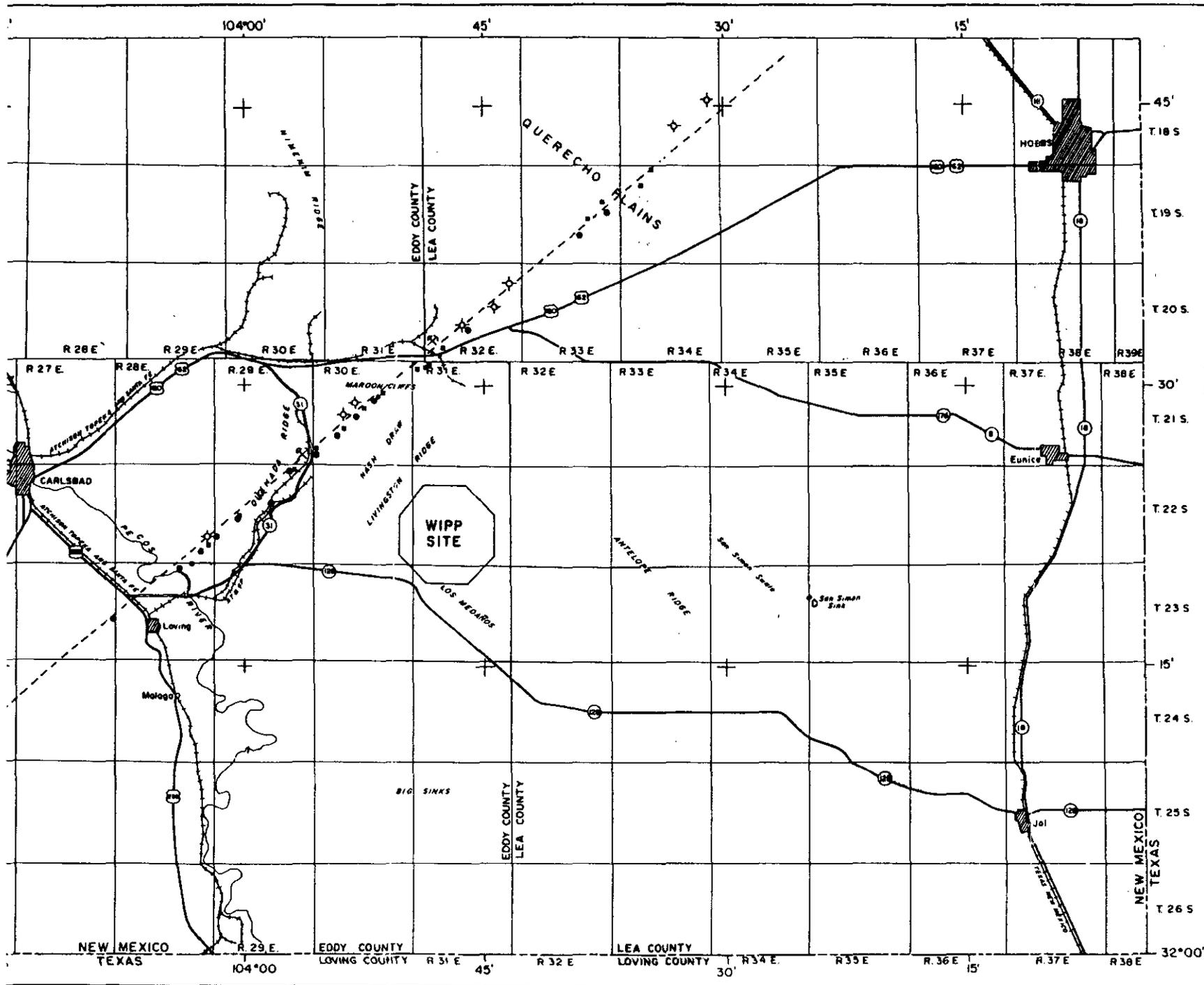
FIGURE 3.5-1

EVIDENCE OF NEAR-SITE DIKE

FIGURE 3.5-2

MAJOR GEOLOGIC EVENTS – SOUTHEAST NEW MEXICO REGION

ERAS	PERIODS	EPOCHS	MILLIONS OF YEARS		MAJOR GEOLOGIC EVENTS
			DURATION	BEFORE THE PRESENT	
CENOZOIC	Quaternary	Holocene	To Present		— Eolian and erosional/solution activity. Development of present landscape.
		Pleistocene	1,000,000	1,000,000	
	Tertiary	Pliocene	12,000,000		— Deposition of Ogallala fan sediments. Formation of caliche caprock.
		Miocene	12,000,000		— Regional uplift and east-southeastward tilting; Basin-Range uplift of Sacramento and Guadalupe - Delaware Mountains.
		Oligocene	11,000,000		
		Eocene	22,000,000		— Erosion dominant. No Early to Mid-Tertiary rocks present.
		Paleocene	5,000,000	63,000,000	— Laramide "revolution." Uplift of Rocky Mountains. Mild tectonism and igneous activity to west and north.
MESOZOIC	Cretaceous		72,000,000		— Submergence. Intermittant shallow seas. Thin limestone and clastics deposited.
	Jurassic		46,000,000		— Emergent conditions. Erosion. Formation of rolling topography. — Deposition of fluvial clastics.
	Triassic		49,000,000	230,000,000	— Erosion. Broad flood plain pediment surface develops.
PALEOZOIC	Permian		50,000,000		— Deposition of evaporite sequence followed by continental redbeds. — Sedimentation continuous in Delaware, Midland, Val Verde basins and shelf areas.
	Pennsylvanian		30,000,000		— Massive deposition of clastics. Shelf, margin, basin pattern of deposition develops.
	Mississippian		35,000,000		— Regional tectonic activity accelerates, folding up Central Basin platform, Matador arch, Ancestral Rockies. Regional Erosion. Deep, broad basins to east and west of platform develop.
	Devonian		60,000,000		— Renewed submergence. — Shallow sea retreats from New Mexico. Erosion. — Mild epeirogenic movements. Tobosa basin subsiding. Pedernal landmass and Texas peninsula emergent, until Middle Mississippian.
	Silurian		20,000,000		— Marathon — Ouachita geosyncline, to south, begins subsiding.
	Ordovician		75,000,000		— Deepening of Tobosa basin area; shelf deposition of clastics, derived partly from ancestral Central Basin platform, and carbonates.
	Cambrian		100,000,000		— Clastic sedimentation — Bliss sandstone.
PRECAMBRIAN				600,000,000	— Erosion to a nearly level plain. — Mountain - building, igneous activity, metamorphism, erosional cycles.

MAJOR GEOLOGIC EVENTS –
SOUTHEAST NEW MEXICO

FIGURE 3.6-1

TABLE 3.5-I
REPORTED DIKE INTERCEPTS OR SURFACE EXPOSURES

WELL OR DRILL HOLE NAME	LOCATION	INTERCEPT DEPTHS IN FEET
Humble Oil & Refining; State "BO"#3	SE 1/4 Sec. 12, T18S-R34E	8745
Continental; Forest #1	Sec. 22, T18S-R34E	7210-8640
International Minerals Corp.; ConcDale #95	NW 1/4 Sec. 12, T20S-R32E	2239
Noranda; HB-10	SW 1/4 Sec. 14, T20S-R32E	1700
Texaco; Moore #1	SW 1/4 Sec. 21, T20S-R32E	2115
Kerr-McGee; Mine	Sec. 31, T20S-R32E	1530
Perry R. Bass; Big Eddy #44	SE 1/4 Sec. 25, T22S-R28E	12120-13330
Stanolind; U.S. Duncan #1	SW 1/4 Sec. 30, T21S-R30E	470-2710(8 Intercepts)
International Minerals Corp.; Mine	Sec. 36, T21S-R29E	790
H & W Drilling; Danford #1	SE 1/4 Sec. 9, T22S-R29E	2210
Perry R. Bass; Big Eddy #43	SE 1/4 Sec. 25, T22S-R28E	940-2050
Outcrop	Sec. 31, T25S-R25E	Surface
Outcrop	Sec. 11, T26S-R24E	Surface
Amoco; Teledyne Gas #1	Sec. 13, T23S-R28E	Rumor?
Unknown	Sec. 25, T22S-R28E	1880-1900 (γ Ray Response)

Reference: C. L. Elliot (1976 b), Table I.

4.1 INTRODUCTION

This chapter is a detailed review of the geologic characteristics of the
Waste Isolation Pilot Plant (WIPP) repository site and its environs,
including discussions of geomorphology, stratigraphy, structure, and
tectonics.   In keeping with the concept of underground placement of the
radioactive wastes, subsurface geologic conditions are emphasized.
Structure contour and isopach maps are presented and discussed.   Par-
ticular effort has been made throughout the text to relate site-specific
aspects to regional geologic conditions.   A final section on geologic
history reviews the geologic origin and development of the WIPP site.

The available literature, including maps and reports on file with federal
and state agencies, has been consulted.   Results of field and research
investigations carried out specifically to define site geologic
conditions have been integrated into the discussion and the investigative
reports referenced.   Detailed descriptions of the various exploration
programs and investigations may be found in Chapter 2.

4.1.1 Area of Study

The area to be considered in detail in this chapter on site geology is
shown in Figure 4.1-1.   It represents a 10-by-10-mile square area
centered on the site, including all of Township 22 South, Range 31 East
and parts of the adjacent townships in eastern Eddy and western Lea
Counties in the southeastern corner of New Mexico.   In many instances,
however, the topics under discussion were judged to require consideration
of areas more distantly removed or to benefit from a somewhat broader
focus, so that Figure 4.1-1 should not be construed as a limitation of
the area considered or discussed.

Also shown in Figure 4.1-1 is the outline of the WIPP site itself, locating land-use restriction zones. Zone I is the area of the surface facilities. The roughly octagonal Zone II represents the underground area which would be mined if a fully developed (3 square miles) repository were developed here. No drill hole extending through the salt beds to deeper strata occurs within one mile of the Zone II boundary. Other zones represent levels of land-use restriction and are discussed elsewhere in this report (for example, see Table 2-1). The outer boundary of Zone IV defines the area of the WIPP site. The term "Los Medanos" is also frequently used to refer to the WIPP site area, as for instance in the site selection process to distinguish the WIPP site from other alternate sites in the same region (see Chapter 2). Griswold (1977) defined the 10-by-10-mile square of Figure 4.1-1 as the "Los Medanos site"; however, for the purpose of this report, it seems more appropriate to use the term "Los Medanos" to refer to the general vicinity of the WIPP site, roughly corresponding to the sand- and dune-mantled area bearing that name and within which the site occurs.

4.2.1   Sources of Data

Much of the information specific to the Los Medanos area and to the WIPP site is available from various agencies commissioned to carry out special technical studies. In assembling these descriptions, free recourse has been made to what is available in the open literature, particularly to the numerous open-file reports released by the U.S. Geological Survey. Much useful information on surficial stratigraphy of the Los Medanos area is provided by Vine (1963) and by Bachman (1974; also in Jones, 1973); both have provided surficial geologic maps of parts of the area. Valuable compilations of stratigraphy and structure of the Ochoan evaporite sequence have been assembled by Jones (1972, 1973, 1975), by Brokaw et al. (1972), by Anderson et al. (1972), and by Anderson (1978). Permian Basin geology in general is extensively discussed in King (1948) and in McKee et al. (1967a, 1967b). Pennsylvanian studies are presented for the Los Medanos area by Foster (1974) and regionally by Meyer (1966). Much of the available information regarding pre-Pennsylvanian

stratigraphy is reviewed in Foster (1974), who presents numerous reference sections and isopach and structure contour maps for these deeply buried strata.

A series of subsurface structure contour and isopach maps has been prepared specifically for the WIPP site by Griswold (1977) and most are incorporated into this chapter. The data base for these maps is furnished by available well and borehole information supplemented by specially contracted seismic reflection surveys. The location of all boreholes and seismic reflection profiles used in the subsurface studies reported herein are shown in Figure 4.1-2 and listed in Table 4.1-1.

A glance at the depths of holes listed in Table 4.1-1 shows the paucity of data available for horizons deeper than about two thousand feet. With the possible exception of oil or gas fields where deep holes are clustered, well spacing is typically such that minor faulting probably would not be delineated; only the smoothed trend of local depressions and arches is outlined. The detection of minor faulting and other local structural detail is generally possible only through the use of deep seismic reflection techniques, supplemented by deep well control where available. Horizons which most efficiently reflect seismic wave energy are the most logical targets for detailed study of deep structures. Beneath the site, horizons which are found to be good reflectors include top of the Silurian carbonate sequence, top of Morrow limestone (lower part of Pennsylvanian rocks), and top of Delaware sand (below base of Castile). Although many hundreds of miles of seismic reflection profiling have been carried out in the Delaware Basin, nearly all of it is privately owned by industry sources and the record profiles are not subject to disclosure. Accordingly, Sandia Laboratories engaged the services of G.J. Long and Associates, Inc., of Houston, Texas and Permian Exploration Company of Roswell, New Mexico, to carry out a program of seismic reflection profiling across the WIPP site, supplemented by any oil industry data which was made accessible for examination. Over 1,500 miles of private seismic data were examined and about 70 miles of new

seismic data have been obtained by Sandia. (For further information on seismic reflection profiling and well data control used in the exploration for deep structure at the site, refer to Section 2.5).

Data regarding structural detail of bedded salt in the Delaware Basin, in contrast to deeper horizons, are not generally available in the form of seismic reflection surveys of the type normally used in subsurface exploration, nor do petroleum exploration companies generally pick stratigraphic markers above the Delaware, as there is no commercial hydrocarbon interest in these relatively shallow strata. Perhaps the lack of early recognition of the character of deformation within the bedded salt sequence is accounted for by the petroleum industry's disinterest in non-petroliferous strata. The intensive exploration drilling for potash deposits by commercial mining interests, however, has provided a means of obtaining at least some general outline of deformation features within the evaporite sequence down through the McNutt potash zone of the Salado that would not otherwise have been available. In addition, mine workings have provided supplementary detail in localized areas. Within the site exclusion area, additional potash exploratory holes have been drilled under contract to Sandia Laboratories. Because commercial potash exploration is targeted to the McNutt member of the Salado Formation, shallower strata have generally not been extensively logged and sampled, with the result that details of structure in the Rustler Formation and Dewey Lake Redbeds were not well recorded. The holes drilled under contract to Sandia Laboratories to determine the extent of potash reserves in the site area were logged through these upper formations by wireline geophysical methods and are the source of much of the shallow subsurface data near the WIPP site. Figures 4.4-11 through 4.4-15 are constructed from these data.

Nothwithstanding the apparent wealth of drill hole data in the area, it should be emphasized that well data necessarily represent an incomplete sampling and extrapolation from such data will be imprecise to an extent dependent on the well spacing, the complexity of the subsurface structure, and the level of detail desired. Well picks probably will not

record absolute maxima or minima of sharper crests and troughs, and certain smaller features could remain undetected. Other techniques such as seismic reflection aid in finding smaller structures.

4.2 SITE PHYSIOGRAPHY AND SURFICIAL GEOLOGY

4.2.1   Site Physiography

The proposed WIPP site is located on the eastern edge of the Pecos Valley section of the southern Great Plains physiographic province (Figure 3.2-1). The land surface within the area of the site is a monotonous, semi-arid, eolian plain sloping gently to the west and southwest (Figure 4.2-1a), its surface made somewhat hummocky by an abundance of sand ridges and dunes. Figure 4.2-2 is a topographic map of the area in the vicinity of the site (from Nash Draw and Hat Mesa 15-minute topographic quadrangle maps). Also shown on this figure are the boundary zones of the WIPP site as discussed in Section 4.1, extending a maximum distance of about 3 miles from the geographic center of the site. Within these boundaries, elevations range from 3,570 feet in the east to 3,250 feet in the western part of the site. The average slope from east to west is 50 feet per mile (Griswold, 1977).

In the vicinity of the site, Livingston Ridge is perhaps the most prominent physiographic feature. Located about a mile beyond the northwestern border of the WIPP site, it is a northeast-southwest trending, west facing escarpment about 75 feet high marking the east edge of Nash Draw. Nash Draw, the nearest drainage course of any significance in the vicinity of the site, is a shallow, 5-mile-wide valley open to the southwest. Elevations within Nash Draw, which descend from about 3,300 feet at its northeast head to 2,945 feet at Salt Lake, near the Pecos River, are generally 200 to 300 feet lower than the surrounding terrain and may reflect substantial subsurface dissolution of salt from the Rustler and Salado Formations and accompanying subsidence of overlying materials. Livingston Ridge marks the approximate boundary, therefore, between terrain that has undergone erosion and/or solution collapse and

terrain that has not been so affected, and may be considered to indicate the approximate position east of which significant dissolution of the underlying Salado Formation has not occurred (refer to Chapter 6 and Section 3.2 for further discussion).

East of the site, the nearest major drainage course is the southeast-trending San Simon Swale, some 15 miles or more distant (a more regional topographic map is shown in Figure 2-1). It, too, most likely owes part of its decreased elevation to subsurface dissolution. Between Sam Simon Swale and the WIPP site, a broad, low mesa named "The Divide" occurs about 6 miles east of the site, rising about 100 feet above the surrounding terrain and attaining an elevation of about 3,800 feet, and, as such, marks a local boundary between general southwest drainage toward Nash Draw and general southeast drainage toward San Simon Swale. The Divide is capped by the Ogallala Formation, and overlying caprock caliche upon which have formed small, elongate depressions similar to those found developed on the Ogallala of the High Plains, proper, farther east (refer to Regional Geomorphology, Section 3.2, for additional discussion of these features).

Surface drainage in the site area is intermittent; the nearest perennial stream is the Pecos River, more than 15 miles south-west of the center of the site. Surface runoff in the site area finds its way to the Pecos River via Nash Draw; discharge of shallow groundwater is likewise believed to be controlled by the Pecos River (refer to hydrology sections 6.2.5 and 6.3). Although basins like Nash Draw may have evolved partly through active subsurface dissolution of thick, buried salt deposits, there is no evidence available at present to evaluate differences in rates of dissolution which may have prevailed under different climatic conditions. That the site is in a natural divide between drainage basins indicates that it is protected from serious flooding and erosion from heavy runoff. Should the climate of the region become more humid in the future, any perennial streams which might then arise would be expected to follow the present basins, and Nash Draw and San Simon Swale would undergo the greatest amount of erosion from this increased humidity, leaving the divide area relatively intact (Bachman, 1974).

Because of the presence in Nash Draw and elsewhere in the Delaware Basin of extensive subsidence which appears to be caused by subsurface dissolution of salt, much attention has been focused on the search for geomorphic indications of possible subsidence features in the vicinity of the site. One feature that has attracted some attention is described by Griswold (1977) as a shallow sink about 8 miles north of the site in the southeast part of Section 9, T. 21 S., R. 31 E. (pictured in Figure 4.2-1b). The feature is very subdued, about 1,000 feet in diameter and 30 feet deep. Resistivity studies conducted by Elliot (1976) indicate very shallow surficial fill within the feature and no. disturbance of underlying beds, indicating a probable surface rather than subsurface origin. This type of feature is common in southeastern New Mexico and is not necessarily indicative of an origin tied to subsurface subsidence. On the other hand, recent resistivity surveys conducted over the surficial sand cover within the WIPP site area (Elliot, 1977e) have disclosed a resistivity anomaly in section 17, T. 22 S., R. 31 E., within the limits of the Zone II exclusion area. The anomaly bears some resemblance in character to the pattern observed over a known sink, a so-called salt "breccia pipe" (Elliot 1977a). Recent drilling (WIPP 13) has shown this resistivity anomaly is not caused by dissolutioning but by lower than average resistivity in the Dewey Lake Redbeds.

4.2.2   Site Surficial Geology

Most of the site area is covered by blanket eolian sand or, especially on the north, east, and southeast, by partially stabilized sand dunes. Active sand dunes are located in the southern portion of the site (Figure 4.2-3). The sand, of Holocene age ("Mescalero sand"), forms a thin, persistent veneer no more than a few meters thick (except where dunes occur) that is believed to have been swept westward from the High Plains, where the inferred source material, the sandy Ogallala Formation, is abundant. The widespread sand cover is readily apparent on the surficial geologic map of the site area, Figure 4.2-4, which is compiled from maps prepared by Vine (1963) and Bachman (1974).

Not at all apparent from the map, however, is the general occurrence of a
hard, caliche layer up to 10 feet thick immediately beneath the eolian
sand blanket. The relatively high resistance of the caliche to erosion
has protected the more erodable underlying strata from dissection and
exposure. It is recognized over a regionally broad area and has been
termed the "Mescalero caliche". Caliche may form pedogenically over
geologic time at or near the surface through capillary rise of
carbonate-laden water in the vadose zone followed by precipitation of
solute upon evaporation of pore water (Brown, 1956). The youngest
formation on which the Mescalero caliche has formed is the Pleistocene
Gatuna Formation, of presumed Kansan age (Bachman, 1974). Bachman (1974)
indicates that the formation of the Mescalero caliche probably dates back
to the Yarmouth interglacial stage, or approximately 500,000 years ago.
That such a thick, areally extensive, and continuous caliche had accreted
implies past stable climatic and geomorphic conditions over the
considerable time period required for its formation. The relevance of
this type of paleoenvironmental indicator to the stability of present
climatic conditions and to possible future climatic variablility, and the
implications regarding the long-term integrity of the WIPP repository,
are presently being pursued by Bachman (see Chapter 10).

On the surficial geologic map (Figure 4.2-4) exposures of the Mescalero
caliche are indicated. These occur where the eolian cover is very thin
or removed entirely, mostly near the edge of Nash Draw, into which much
of the nearby loose sand may have been swept. Along Livingston Ridge,
the Mescalero caliche is draped inward into Nash Draw and is present over
much of the north half of the valley, indicating that at least some
subsidence or lateral backwasting along Nash Draw has occurred subsequent
to the formation of the caliche, presumably during the more humid glacial
stages (Illinoian or Wisconsin) of Pleistocene time.

Within Nash Draw, and the WIPP site area, the Triassic Santa Rosa
Sandstone, the Ochoan Dewey Lake Redbeds, and more than half of the
Rustler Formation are sporadically exposed. Field descriptions of these
formations are included in Section 4.3.
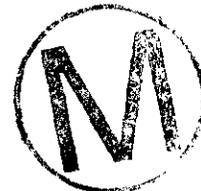
The overall geology and structure of the WIPP site is quite simple. It is characterized by a persistent, gentle homoclinal dip toward the east of 50 to 200 feet per mile (2 degrees or less), depending upon depth. Successively older rocks are seen to occur toward the west, the result of erosional bevelling of the gently eastward-dipping strata. Additional information regarding erosional history of the WIPP site is presented in section 4.5; details of the site structure and stratigraphy are discussed in the following sections.

4.3   SITE STRATIGRAPHY AND LITHOLOGY

The following paragraphs briefly summarize the stratigraphic sequence at the WIPP site; systematic description of the various lithologic units commences in Section 4.3.1.

The proposed WIPP underground storage facilities are to be placed near the middle of a 3,600-foot-thick sequence of relatively pure evaporite strata containing primarily rock salt and anhydrite, lying between depths of about 500 and 4,100 feet beneath ground surface. The formation richest in rock salt, the Salado Formation, is nearly 2,000 feet thick. The Salado contains the relatively pure salt layers in which the two proposed underground storage levels are to be constructed, at a depth near 2,120 feet for the upper level and near 2,670 feet for the lower. The storage horizons are well isolated from the enviroment by adjacent evaporite strata. A thickness of at least 1,300 feet of undisturbed evaporite, primarily rock salt, overlies the upper storage horizon, and about an equivalent thickness of anhydrite and rock salt intervenes between the lower storage horizon and the next adjacent underlying non-evaporite formation. The salt deposits were formed at least 225 million years ago and have apparently remained isolated since that time.

The total thickness of the sediments resting on Precambrian basement beneath the surface of the proposed WIPP facility is about 18,000 feet of Ordovician to Recent strata. Depicted in Figure 4.3-1 is a generalized stratigraphic section of the site, showing the vertical sequence of major
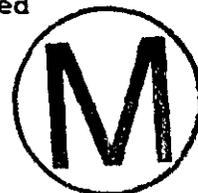
units and their relative thicknesses. More detail, but still of a generalized nature, is provided in Figure 4.3-2, Site Geologic Column, which shows simplified graphic and descriptive lithologies of the major units known or inferred to occur beneath the site and gives the geologic classification of rock units used in this report. Following is a brief summary of the stratigraphy, proceeding from the surface down to basement.

Beneath a thin but persistent veneer of windblown sand at the site are sediments representing Pleistocene, Upper Triassic, and uppermost Permian strata, all of which occur above the evaporite sequence. Sandstone of the Pleistocene Gatuna Formation, capped by Mescalero caliche, also developed in Pleistocene time, is only a few tens of feet thick at the site and is of interest primarily for the geochronologic and paleoclimatic implications of its presence; it was deposited, and much of the caliche on its surface believed to have developed, half a million years ago (Kansan-Yarmouth time) (Bachman, 1974). Between the Pleistocene sandstone and the evaporite sequence is a 500-foot-thick succession of nonmarine redbeds of Late Triassic age (Santa Rosa Sandstone) and marine redbeds of latest Permian age (Dewey Lake Redbeds). This redbed sequence thins westward and thickens eastward, having been beveled to the west by one or more post-Late Triassic erosional episodes; the thickness of redbed deposits remaining above the evaporite sequence is crudely proportional to the degree to which the underlying salt horizons have been protected from surficial processes leading to erosion and dissolution.

At the center of the site, all but the uppermost 50 feet of the 18,000 feet of strata are of Paleozoic age, the marine Dewey Lake Redbeds being the topmost of the Paleozoic rocks. The Permian section alone, about 12,800 feet thick, constitutes over two-thirds of the sedimentary column. The Permian section is divided into four series, the three lowest of which (Wolfcampian, Leonardian, and Guadalupian) contain thick clastic sequences, and the uppermost of which, the Ochoan Series, contains the evaporite formations, which are in descending order the

Rustler, Salado, and Castile Formations. (The topmost Ochoan formation, the Dewey Lake Redbeds, is not part of the evaporite sequence but represents a return of clastic, normal marine deposition.)

The Rustler, which overlies the Salado, contains the largest percentage of clastic material of the three evaporite formations. However, where its original thickness of around 450 feet has been protected from salt dissolution, about 70 percent of the formation is composed of evaporite beds, including about 40 percent rock salt. Beneath the WIPP site, the Rustler has been leached of most of its rock salt in the geologic past. At ERDA-9, 310 feet of the formation was encountered, which implies that up to 150 feet of rock salt has been removed and that the overlying strata have subsided accordingly. It does not, however, imply that dissolution and subsidence is necessarily presently active or even that it has recently occurred. At ERDA 9 halite was logged in the lower 100 feet of the Rustler. Over 1,300 feet of undisturbed evaporite rock, primarily Salado rock salt, occur above the upper level storage zone of the proposed WIPP facility.

The 2,000-foot thickness of the salt-rich Salado Formation is divided into three members by the recognition of a middle member referred to as the McNutt potash zone, which is the interval within the Salado that contains the potential reserves of potash minerals mined in the Carlsbad District west of the site. The lowest member of the Salado, beneath the McNutt potash member, is the member that contains the nearly pure halite which is proposed for the WIPP facility. The Castile Formation beneath the Salado also contains nearly pure beds of halite but, unlike the Salado, also contains massive anhydrite beds.

The rest of the Permian section beneath the evaporite sequence, together with the subjacent Pennsylvanian and possibly Late Mississippian sections, contain dominantly clastic rocks that represent deposition during the time in which the Delaware Basin existed as a distinct structural entity. These pre-evaporite, basinal sediments, which total about 11,000 feet in thickness beneath the site, have been targeted for

petroleum exploration at one point or another throughout the Delaware Basin. They contain nearly all of the region's known potential reserve of hydrocarbons.

The remainder of the Paleozoic section (Mississippian down through the Ordovician) consists of about 3,000 feet of mainly carbonate strata deposited in shallow-water or shelf conditions over a period of long-sustained crustal stability.

The underlying crystalline basement is believed to be a granitic terrane, formed about 1,300 million years ago. The only other igneous rocks known in the area occur as a lamprophyre dike rock intruded into the evaporite beds along a single northeast dike trend that approaches no closer than about 8 miles northwest of the center of the proposed WIPP site.

Brief descriptions of the various stratigraphic units are provided in the following sections, in order of deposition from oldest to youngest, with emphasis on the evaporite beds, particularly the Salado Formation.

4.3.1   Precambrian Eonothem

Few holes in the near vicinity of the WIPP site have penetrated entirely through the Paleozoic section. The nearest such holes are the Richardson and Bass No. 1 Cobb-Federal, approximately 13 miles north-northwest of the center of the site, and the Texas No. 1 Richards, 12-1/2 miles to the north-northeast. Inferences about the nature of basement rock lying beneath the site have been gleaned from these wells and others more distantly removed.

Crystalline basement rocks beneath the Mesozoic and Paleozic sedimentary pile near the proposed site are believed to be either granitic igneous rock or metamorphosed granites and rhyolites. The basement surface here is at a depth of approximately 17,900 feet (Foster and Stipp, 1961); a slightly greater depth (approximately 18,200 feet) has been inferred by independent consultants (Sipes et al., 1976). The basement rocks occur

within what has been considered by Flawn (1954, 1956) to be part of a regional Precambrian granitic terrane constituting the Texas craton. A later investigation (Muehlberger et al., 1967), which reclassified the rocks within the Texas foreland or craton, among other areas, suggests that the basement rocks in the area near the site belong to the Chaves granitic terrane, composed largely of granite, granodiorite, and equivalent gneisses, with a minor amount of other metamorphic rocks included. Measured radiometric dates for basement rocks in the area range between 1,140 to 1,350 million years (Foster, 1974; Muehlberger et al., 1967); the Chaves terrane is defined to include the 1,350 m.y.-old granitic basement rocks.

4.3.2   Paleozoic Erathem

Cambrian System. No Cambrian strata are recognized in the subsurface in the vicinity of the WIPP site. Basal conglomerate and sandstone resting on the Precambrian of southeastern New Mexico are sometimes called Bliss sandstone, which is partly Late Cambrian and partly Early Ordovician in age, but such rocks in this area probably correlate only with the Ordovician part of the Bliss (Foster, 1974) and are here considered a member of the Ellenburger Group.

Ordovician System. In the Los Medanos area, the Paleozoic section begins with an estimated 1,290 feet of Ordovician rocks beneath the center of the site (Foster, 1974), assuming an even gradient between widely spaced well control points. In ascending order the sequence includes the Ellenburger, Simpson, and Montoya Groups, representing Lower, Middle, and Upper Ordovician strata, respectively.

Detail of the local stratigraphy of the Ordovician is based on samples and a radioactivity log from the Texas No. 1 Richards well, 12-1/2 miles north-northeast of the site. The Ellenburger Group there consists of at least 300 feet of dolomite with some chert; included is a basal member of sandstone and conglomerate about 75 feet thick. The top of the Ellenburger may be at a depth of as much as 17,800 feet beneath the
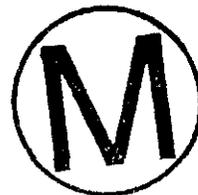
center of the site (Netherland, Sewell, 1974). Overlying the Ellenburger
dolomite is a sequence of alternating limestone and green or gray shale
members, with several sandstone units occurring in the upper half of the
sequence. The Upper Ordovician Montoya Group is almost entirely
carbonate rock. At the Texas 1 Richards well, the lower half of the
Montoya is limestone and the upper half dolomite, chert being fairly
common, particularly in the middle of the section; whereas 14 miles south
of the site the Montoya has been logged as mostly limestone and sandy
limestone. Some intermediate lithology is therefore to be expected
beneath the WIPP site.

In the Texas 1 Richards reference section the Ordovician rocks total 975
feet in thickness; however, the section thickens in a south to southeast
direction at a rate estimated to be 25 to 40 feet per mile (Foster,
1974), most of which is due to the thickening of the Ellenburger and
Simpson groups in that direction. It is likely that the Ellenburger and
Simpson are each between 400 and 500 feet thick in the site area.

Silurian System. Lying above the dolomite of the Ordovician Montoya
Group is additional carbonate rock of Silurian, or perhaps
Siluro-Devonian age. Near the site it consists entirely of light-colored
dolomite with appreciable chert, except for two prominent intervals of
limestone, one about 100 feet thick near the middle of the section and
one about 200 feet thick near the top (Foster, 1974). The basal contact
is apparently disconformable in this area.

The relatively homogenous lithology of the Silurian carbonate sequence in
the subsurface of southeastern New Mexico has thus far precluded its
formal separation into formational units. McGlasson (1968), however, has
suggested that the lower part is correlative with the Fusselman Formation
of Early and Middle Silurian age, and that the upper part, generally
referred to as "Upper Silurian" strata, may be correlative with the
Henryhouse Formation of partly late Middle and partly Late Silurian age.
McGlasson (1968) also shows that no Devonian carbonate rocks were
deposited in New Mexico, except in the extreme southwest corner of Lea

County. Nevertheless, common oil-field usage refers to these carbonates as "Siluro-Devonian" carbonates (Foster, 1974). Probably most if not all of the post-Montoya, pre-Woodford carbonate strata beneath the WIPP site is Silurian in age, according to McGlasson's studies. Isopach maps (Foster, 1974) indicate the total thickness of the Silurian or "Siluro-Devonian" carbonates at the site to be about 1,140 feet. The sequence thins westward relatively uniformly at a rate of about 25-50 feet per mile toward a landmass emergent during Silurian time.

The marked contrast in lithology between the Silurian carbonate and the overlying Devonian shale is believed to provide a good seismic reflecting horizon. Structure contour maps on top of "Siluro-Devonian lime" indicate that the top of Silurian, equivalent to base of Devonian, is at a depth of about 15,850 feet beneath the center of the WIPP site (elev. minus 12,450 feet) (Netherland, Sewell, 1974).

Devonian System. The Devonian system is represented by a distinctive unit of organic, pyritic black shale which unconformably overlies the Silurian carbonate sequence. McGlasson (1968) correlates it with the Upper Devonian Woodford Shale of Oklahoma and describes it as a "dark brown to black, fissile, bituminous, spore-bearing shale". He shows that it is a transgressive unit which overlaps successively older units to the northwest (McGlasson, 1968). Beneath the center of the site it is indicated to be about 175 feet thick, thickening gradually southeastward (Foster, 1974). Haigler and Cunningham (1972) show the top of undifferentiated Silurian and Devonian rocks at an elevation of slightly above minus 12,300 feet MSL at the center of the WIPP site. The uppermost portion of the Woodford Shale in the Delaware Basin is reported to be actually of earliest Mississippian age (McGlasson, 1968).

Mississippian System. Rocks of the Mississippian System at the site include a series of limestones referred to simply as "Mississippian limestone," and an overlying shale interval called the Barnett shale. At the Texas 1 Richards locality, the limestone is light-yellowish brown, locally cherty, with some minor gray shale, contrasting with brown,

locally silty shale of the Barnett. Like the top of Silurian carbonate, the top of Mississippian carbonate most likely affords a good reflecting horizon; structure contour maps indicate that it is about 15,150 feet below Zone I at the site (elev. minus 11,750 feet) (Netherland, Sewell, 1974). Total thickness of the carbonate appears to be about 480 feet at the site, gradually thickening northward. The overlying black shale is about 175 feet thick.

Stratigraphic relations between subsurface Mississippian strata in southeastern New Mexico and formational units defined in other areas are unclear. On the basis of the local fauna, the carbonate sequence in the Delaware Basin is assigned to the Lower Mississippian (Foster, 1974). Lithologically it is similar to the Rancheria Formation in the Franklin Mountains. At or near the site, deposition of the Barnett Shale corresponds for the most part to Late Mississippian time.

Pennsylvanian System. Approximately 2,200 feet of Pennsylvanian strata occur in the subsurface at the WIPP site (Foster, 1974). The section consists of alternating members of sandstone, shale, and limestone, and rests unconformably on the underlying Barnett Shale.

Unlike most of the earlier Paleozoic strata, the Pennsylvanian strata in the Delaware Basin, and some of the Lower Permian strata as well, are characterized by relatively numerous changes in lithology vertically in the section and by an abundance of lateral facies changes along time-equivalent horizons. Lithologic units traceable over broad areas in the subsurface generally cannot be assumed to represent time-stratigraphic units under these conditions. Attempts to construct a basin-wide geologic history for Pennsylvanian time and to develop regional correlations based on time equivalence are greatly complicated by these lithologic changes. These complexities have spawned efforts such as those of Meyer (1966) to develop a method for placing surface outcrop and subsurface strata into a formal Pennsylvanian time-stratigraphic framework. As defined by this approach, the Lower Pennsylvanian Series includes rocks assigned to the Morrowan Stage, the

Middle Pennsylvanian Series to rocks assigned to the Atokan (or Derryan) and Desmoinesian Stages, and the Upper Pennsylvanian Series to rocks assigned to the Missourian and Virgilian Stages.

In the Delaware Basin, local subsurface stratigraphic units have sometimes been informally defined, or extended on the basis of lithology and are therefore, strictly speaking, lithostratigraphic and not time-stratigraphic units. Thus, rocks considered part of, for example, the "Morrow" or the Morrow Series on the basis of subsurface lithologies may not necessarily all be encompassed within or represent all of the time of the Morrowan Stage as formally defined. Although the Pennsylvanian section is herein described by reference to lithologies recorded in nearby wells, for the reasons stated the section at the site cannot from the nature of data available be positively correlated with formal stage names or with Lower, Middle, or Upper Pennsylvanian Series. Nevertheless, the designations of Morrowan, Atokan, Desmoinesian, and Missourian-Virgilian rocks for the respective Bend, Strawn, and Canyon-Cisco rock units have frequently been used with modifications for some time (Thompson, 1942; Haigler, 1962, p. 7-8, Netherland-Sewell, 1974, exbt. G-2; see also Meyer, 1966, p. 11). The bipartite classification of Lower Pennsylvanian for Morrowan and Atoka and Upper Pennsylvanian for Strawn has also been employed (e.g., Sipes et al., 1976).

Foster (1974), in his description of Pennsylvanian subsurface lithologies in the vicinity of the site, adopted the usage of Morrow, Atoka and Strawn, which denote from deepest to shallowest the respective principal oil and gas producing zones in Pennsylvanian rocks of the Delaware Basin. He noted that the "overlying rocks of Missourian and Virgilian ages are present... but following the common oil-field usage (they) are included in the Wolfcamp sequence". Hence, "... it appears that the top of (Meyer's) Desmoinesian Stage is the same as the top of the Strawn..." (Foster, 1974). This usage is followed in this chapter in the interest of its adaptability to existing commercial exploratory data. Reference sections are provided by Foster for Pennsylvanian strata some distance

north and south of the site (his Figures 12 and 36, respectively). Sipes, et al. (1976) show "picks" on Pennsylvanian units in the Clayton W. Williams Jr., Badger Unit Federal well about 2 miles northeast of the center of the site, and they present down-hole logs on this and other exploration holes in the vicinity of the site as well.

Morrowan rocks near the site consist mostly of fine- to coarse-grained sandstone with varying amounts of dark gray shale. Some limestone, generally as a series of relatively thin beds with shale and sandstone, typically occurs in the upper part of the sequence and is often separately identified. The Morrow sand is a known hydrocarbon producer of oil and gas in this part of the Delaware Basin, particularly from fields in the area north of the site (refer to Section 8.3.2). Foster (1974) shows areal distribution of sand lithologies in this zone.

The Atoka rocks are principally limestone, becoming cherty toward the middle of the section, and alternating with varying amounts of medium- to dark-gray shale. Sandstones are subordinate. The Atoka is considered to have locally significant hydrocarbon potential in this part of the Delaware Basin, as in the Los Medanos field which is southwest of and nearest to the WIPP site.

The lower part of the Strawn (regionally the Desmoinesian) is dominated by light gray to white, medium- to coarse-grained sandstone, locally conglomeratic in the site area. In its upper part, the Strawn is dominantly limestone, apparently with a minor amount of chert but becoming more abundant northeastward in the immediate vicinity of the site (Foster, 1974). Thin beds of dark gray and brown shale are present throughout the section.

Records of the apparent thickness of the Morrow, Atoka and Strawn vary considerably from area to area simply because there is no completely agreed-upon way of selecting "picks" on down-hole logs and seismic reflection data. In some oil fields, "picks" above the Morrow include

Atoka (or Bend), Strawn, Missourian, and Virgilian. According to Foster (1974), "in well completion reports the top of the Strawn is picked fairly consistently," but selections for the top of Morrow and Atoka may differ significantly, and generally the Canyon and Cisco are not distinguished in this part of basin. Sipes et al. (1976) show the top of Strawn at elevation minus 9,400 feet msl beneath the center of the WIPP site. The "picks" they show in the C.W. Williams Jr., Badger Unit Federal well two miles northeast of ERDA 9 yield thicknesses of 1,224, 607, and 257 feet for the Morrow, Atoka, and Strawn rocks, respectively, for a total thickness of 2,088 feet for the Pennsylvanian. Presumably, one or more units thicken southwestward slightly to attain the 2,200-foot value that Foster shows at the center of the site, a value which specifically excludes at least some Missourian-Virgilian strata. Probably the value of approximately 2,500 feet shown by Meyer (1966, Figure 48) is more truly representative of the total accumulation of strata beneath the site during Pennsylvanian time.
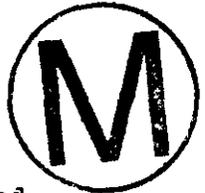
Permian Rocks. As much as 13,000 feet of Permian strata were deposited within the area of the Delaware Basin, which constitutes the most complete succession of the Permian in North America (Brokaw et al., 1972). The entire Permian section beneath the WIPP site averages about 12,800 feet in thickness, over two-thirds that of the entire sedimentary column, or over twice as thick as all of the earlier Paleozoic formations combined (about 5,200 feet). Of this total, about 3,600 to 3,800 feet of thick, relatively pure evaporite beds (primarily salt and anhydrite) occur in the upper part of the sequence, in which the proposed waste isolation facility is to be constructed.

Because the Permian in the Delaware Basin and surrounding region has long been the subject of intensive exploration and study by both commercial and non-commercial interests, its subsurface and surface stratigraphy have become a relatively well understood aspect of a classic study area (e.g., King, 1942, 1948; Adams, 1944, Newell et al., 1953; McKee et al., 1967a, 1967b; Anderson et al., 1972; Brokaw et al., 1972; Jones, 1973).

Even so, problems in stratigraphic nomenclature still abound,
particularly with regard to the more deeply buried basin sediments of the
Lower Permian within the Delaware Basin.

Permian rocks are divided into four series (Adams et al., 1939), two of
which (Wolfcampian and Leonardian) are equated with Lower Permian time
and two (Guadalupian and Ochoan) with Upper Permian. The well-known
massive reef deposits bordering the Delaware Basin were built up mainly
during Guadalupian time; massive evaporite deposits were formed only
during Ochoan time, between 225 and 250 million years b.p. (before
present). Regional correlations of the Permian are shown in Figure 3.3-3.

1) Wolfcampian Series

"Apparently sedimentation in the Permian Basin was continuous from
Pennsylvanian time throughout Wolfcampian" (Meyer, 1966, p. 1); "major
tectonic elements of Early Permian time in west Texas and southeastern
New Mexico were inherited from the Pennsylvanian and continued to grow"
(Oriel et al., 1967, p. 37). These regional generalities suggest the
difficulty that has been experienced, at least basinward from shelves, in
identifying the base of the Wolfcamp strata. An arbitrary convention in
exploration practice in the Delaware Basin is to use the top of the
Strawn to mark the top of the Pennsylvanian. If any Pennsylvanian strata
are present above the Strawn, they are very similar to the overlying
Wolfcampian Series and attempts have not normally been made to
distinguish the two in the subsurface.

In the site area, the Strawn is overlain by a thick sequence of
interbedded, dark-colored limestone and shale, including considerable
dolomite. Sandstone is insignificant. No formational status has yet
been designated for this interval; informally the sequence is sometimes
called "Wolfcamp formation". It is known to markedly thicken southward
with increasing shale and sand content toward the Val Verde trough, where
extremely thick Wolfcampian strata are known. Toward the north, it thins
and gains limestone content, suggesting a shelf margin facies. Foster
(1974) indicates that at the WIPP site the shale content probably nearly

equals that of the carbonate. Isopachs presented in Foster (1974) indicate slightly less than 1,400 feet of Wolfcampian strata beneath the site, whereas Meyer (1966) shows between 1,000 and 1,100 feet; the latter value excludes some rocks above the Strawn. A regional map by McKee et al., (1967a) appears to indicate nearly 2,000 feet. The nearest "pick", in the Badger Unit Federal Well, indicates 1,493 feet of Wolfcampian strata, 2 miles northeast of the center of site (Sipes et al., 1976). These differing values reflect the uncertainties in identifying lower and upper limits of subsurface Wolfcampian strata in the Delaware Basin.

2) Leonardian Series.

The Leonardian series of the Lower Permian Series is represented by basinal sandy equivalents of the Bone Springs Limestone, which was originally defined for a shelf and bank facies of the unit at the margin of the Delaware Basin. Both the name "Bone Spring" and "Bone Springs" have been used in the past, and both usages are found in the current literature. Originally defined as Bone Springs by Blanchard and Davis (1929), King (1948, p. 13) changed it to Bone Spring "to agree with the geographic term" of the type locality, which "is in the lower course of Bone Canyon below Bone Spring..." The U.S.G.S. Lexicon (Keroher et al., 1966) also gives Bone Spring Limestone, but states that it is "named for Bone Springs Canyon...," citing Blanchard and Davis (1929).

Conditions favoring significant buildup of reef and bank limestone at the edge of the Delaware Basin existed in Leonardian time (Victorio Peak Limestone), but development of by far the most extensive of these limestones occurred subsequently in Guadalupian time. Within the basin in the vicinity of the WIPP site, the Bone Springs interval thickens markedly and consists of alternating units of sandstone and dark-colored limestone, with a thick, slightly cherty limestone at the top. Three laterally persistent, very fine to fine-grained sandstone units are recognized as the first, second, and third Bone Springs sands. Shale is a minor constituent of the Bone Springs strata, but the limestone beds are commonly argillaceous.

Foster (1974) shows the WIPP site to be near a local center of maximum thickness of Bone Springs strata, about 3,500 feet. The unit becomes thinner to the east and northeast. The Badger Unit Federal well is indicated to have penetrated 3,427 feet of Bone Springs rocks.

3) Guadalupian Series.

The Delaware Mountain Group includes all basin facies rocks of Guadalupian age in the Delaware Basin, which at the site are composed mostly of sandstones interbedded with some dark shales and a few thin-bedded limestones. A dramatic facies change takes place about 10 miles north of the site, where the basin facies terminates abruptly against massive reef limestones. Because these reef limestones almost completely encircle the Delaware Basin, they seem to conveniently demark the structural limits of the basin, although earlier basin sediments of the Delaware Group extend some distance beneath, or behind, the latest and most massive of the reefs, represented by the Capitan Limestone. North of the site, these reefs are buried by later sediments but become progressively less deeply buried toward the west; west of Carlsbad they surface and form a bold escarpment that defines the eastern boundary of the Guadalupe Mountains, for which the Guadalupian Series was named.

During their earlier development, the reefs at first built upward at the margin of the basin, but during later development progressed outward into the basin as well. Thus, successively older formations of the basin facies of the Delaware Mountain Group have greater areal extent beyond the Delaware Basin as defined by the uppermost part of the Capitan reef. Like modern reefs, the lateral development of these Guadalupian reefs was accompanied by an appreciable vertical buildup of material, in some cases exceeding 1,000 feet, such that sediments being contemporaneously deposited in the basin now appear structurally to be correspondingly lower in the section, where in actuality they are time-stratigraphic equivalents. By the same token, the evaporitic materials (Ochoan evaporites) that later filled the basin now appear to some extent to be laterally equivalent to the reef masses. These stratigraphic relationships are especially well portrayed by Haigler (1962) and King (1948).

A thickness of 3,944 feet of Delaware Mountain Group strata is recorded 2 miles northeast of the center of the WIPP site. Surface mapping at the margins of the basin led to the recognition there of three formations; namely, in ascending order, the Brushy Canyon, Cherry Canyon, and Bell Canyon Formations. Generally, petroleum exploration practice in the Delaware Basin has been not to attempt to define these formations in the subsurface. However, Foster (1974) provides a reference section showing stratigraphic positions of the formations of the Delaware Mountain Group in the Shell No. 1 James Ranch well about 3 miles southwest of the site, and Sipes et al. (1976) give similar "picks" in the Clayton W. Williams, Jr., well to the northeast of the area. Foster shows 3,970 feet of Delaware Mountain strata.

The Shell No. 1 James Ranch well lithologies indicate that the Brushy Canyon Formation is 1,540 feet thick and consists of mostly fine-grained, gray to brown sandstone with minor brown shale and dolomite. The Cherry Canyon Formation consists of 1,070 feet of sandstone similar to that in the Brushy Canyon Formation, interbedded with shale, dolomite, and some limestone. The Bell Canyon Formation, 1,180 feet thick, also consists mostly of fine-grained sandstone, but has a greater percentage of limestone, the result of closer proximity to the shelf-margin carbonates. A limestone member at the top of the Bell Canyon Formation, known as the Lamar limestone, is recognizable over a considerable part of the Delaware Basin. Basinwide the sands of all three formations are targets for hydrocarbon exploration. The top of the Delaware beneath the center of the site is contoured by Sipes et al. (1976) at minus 650 feet (depth 4,065 feet). It is overlain by evaporites of the Castile Formation.

4) Ochoan Series.

The Ochoan Series "includes perhaps the thickest and most extensive evaporite rock sequence in North America" (Oriel et al., 1967). It also contains, within the Salado Formation east of Carlsbad, extensive potash evaporite deposits which contain 65 percent of presently exploitable potash resources available within the United States (Jones, 1975).

All of the salt deposits and other evaporites of the Los Medanos area are restricted to the Ochoan rocks, of Late Permian age. The Ochoan rocks are entirely of marine origin, but have two unlike parts--a thick lower section of evaporite and a thin upper section of red beds (Jones, 1973). The lower section includes, in ascending order, the Castile, Salado, and Rustler Formations; the upper section is made up of the Dewey Lake Redbeds. Together the four formations have a maximum thickness of 3,600 feet, slightly more than 3,000 feet of which are evaporite beds of the lower three formations, which are composed dominantly of anhydrite and rock salt with minor amounts of gypsum, potassium evaporite minerals, carbonate rock, and fine-grained clastic material.

At the WIPP site, the Ochoan rocks are about 3,900 to 4,000 feet thick, of which 3,600 to 3,800 feet, or about 90 percent, are the evaporite sequence. Of the three evaporite formations, roughly one-half the total thickness belongs to the Salado. Both the underlying Castile and overlying Rustler are richer in anhydrite and poorer in rock salt than the Salado, and they provide this salt-rich formation with considerable protection from fluids which might be present in adjacent rocks (Jones, 1973). Jones (1972) provides lithologic percentages of the complete Ochoan evaporite sequence (Castile-Rustler), obtained from exploratory potash drilling, as follows: 59 percent halite and associated potash deposits; 33 percent anhydrite and gypsum, with glauberite and polyhalite; 6 percent carbonate rock (limestone, dolomite, magnesite) and 2 percent clastic rock (clays and silts).

Considered broadly, the evaporites represent a transitional zone between underlying reef and normal marine limestones (Guadalupian beds) and the overlying Dewey Lake which was deposited under brackish or restricted marine conditions (Jones, 1968). The floor of the Delaware Basin in early Ochoan time is generally estimated to have been at least 1,200 feet below the top of the Capitan reef, which almost completely encircled it, restricting southern access to the open sea and setting the stage for deposition of evaporites within the basin (Brokaw, et al., 1972).

Castile Formation

The Castile Formation is almost completely confined within the limits of the Delaware Basin (Oriel et al., 1967), the only evaporite formation so restricted. It gradationally overlies the Bell Canyon Formation (Brokaw et al., 1972).

Lithologically, the Castile is the least complex of the evaporite formations, being composed chiefly of anhydrite with a few interbeds of rock salt. Limestone is present in secondary amounts; clastic materials (siltstone, shale, sandstone) are notably absent. A lithologic summary by Jones (1972) lists 59 percent anhydrite and other sulfates, 30 percent halite and other chlorides, 11 percent limestone, dolomite, and magnesite, and no clastic rock for the Castile Formation, based on data from exploratory drilling. The rock is sparingly bituminous and yields a fetid odor. It has a faint to conspicuous lamination or banded structure involving a color change, a difference in texture, or a rhythmic alternation of bituminous calcite and anhydrite, bitumen and anhydrite, or anhydrite and halite in layers a fraction of a millimeter to a few centimeters thick. The color of the rock ranges from white to dark gray, becoming darker with increasing depth below the top of the formation (Jones, 1975).

In the subsurface, the Castile Formation, to use Jones' description, is readily divisible into three informal members by a salt-rich zone 200-400 feet above the base: a lower member composed chiefly of anhydrite, a middle member composed chiefly of rock salt, and an upper member composed chiefly of anhydrite. The three members are discrete, readily distinguished lithologic units that are laterally persistent over wide sections of the Delaware Basin. Near the margin of the basin, however, they merge into a single wedge-like mass of anhydrite that rapidly thins to a narrow tongue and extends across the basin margin for a few miles before thinning out in the southern part of the Northwestern Shelf.

As described by Jones (1973), the lower member of the Castile Formation is a well-stratified evaporite consisting of laminae of gray anhydrite and brownish-gray limestone in regular, rhythmic alternation. Some beds of laminated dark-gray and brownish-gray limestones, a few inches to several feet thick, are present at wide intervals in the lower and middle parts of the member, and there are a few thicker beds of massive gray anhydrite at long intervals. The member is 200-240 feet thick south of the site, but it thickens northward and reaches a thickness of at least 400 feet before merging with other members of the Castile to form a single unbroken mass of anhydrite adjacent to the Capitan reef mass.

The middle member of the Castile Formation, a salt-rich, tabular zone that forms a widespread, lithologically distinct stratigraphic marker, is 500-700 feet thick in the southern part of the Carlsbad potash area, but thickens northward and attains thicknesses of 800-1000 feet along a broad 2 to 3-mile-wide belt of deformation within the evaporite sequence paralleling the margin of the Delaware Basin (refer to Section 4.3.2.7). The member is predominantly rock salt, but it contains thin to thick layers of interlaminated anhydrite-limestone rock. The thickest of these layers averages about 100 feet, and it divides the member into two almost equally thick salt beds. The upper bed includes several interlaminated anhydrite-limestone layers, some of which are 2-5 feet thick, whereas the lower bed has none. This member terminates northward by grading laterally into, and intertonguing with, anhydrite.

The upper member of the Castile Formation exhibits greater lithologic complexity and is composed chiefly of anhydrite interlaminated and interbedded with calcitic limestone and, to a lesser extent, with massive anhydrite, rock salt, and carbonate rock, including both magnesite and dolomite. It contains a northward-thinning tongue of magnesitic anhydrite that overlaps the Capitan Limestone along the margin of the Delaware Basin and extends a few miles into the northwest shelf. Though 600-700 feet thick some distance south of the site, the upper member thins rapidly northward to as little as 170 feet near the margin of the basin. The nature of this northward reduction in thickness is, as

subsurface studies in the Carlsbad potash area and elsewhere in the Delaware Basin have shown, due both to a lateral gradation and to an intertonguing, or pinching out, of individual anhydrite beds at the top of the Castile into the rock-salt beds of the overlying Salado Formation, resulting in a northward stratigraphic descent of identifiable Castile anhydrite. These relationships demonstrate that the contact between the Castile Formation and the overlying Salado Formation is conformable and gradational; nevertheless, the contact at any particular location is generally rather sharply definable as the horizon at which dominant anhydrite below gives way to rock salt above.

A somewhat different classification scheme of the Castile Formation has been established by R.Y. Anderson and his co-workers. Working in the central and southern part of the basin with thin sections of cores obtained through special drilling arrangements made with industry operators, Anderson et al. (1972) divided the Castile into three separate halite members and four anhydrite members across the width of the Delaware Basin. Furthermore, they traced individual laminae in the anhydrite members over distances as great as 113 km. Each anhydrite-calcite couplet is believed to represent an annual varve, the nature of the evaporite precipitation being controlled by changes in the partial pressure of carbon dioxide in the Castile brine sea as the growth of brine algae waxed and waned with the seasons. Some 250,000 varve couplets are inferred, by representative counts, beginning below the Lamar limestone in the Bell Canyon and ending in the lower part of the Salado (Anderson et al., 1972).

Toward the northern part of the Delaware Basin, the upper halite and anhydrite units appear to converge and cannot be traced basinwide as major units. In the site area two lower anhydrite members (AI, AII) and two halite members (HI, HII) are recognized as basinwide equivalents of units identified elsewhere; a more heterogeneous upper unit, principally anhydrite, corresponds to the position of Anhydrite IV but may not be stratigraphically equivalent to it (Anderson et al., 1972; Anderson and Powers, 1978; Anderson, 1978). These anhydrite and halite members are

identified on Figure 4.3-2. Thicknesses are taken from isopach maps which appear in Anderson et al. (1972) and Anderson, (1978). Thus, the lower anhydrite (Anhydrite-I) member is indicated to be nearly 250 feet thick in the vicinity of the WIPP site; Halite-I, about 330 feet thick; Anhydrite-II, 100 feet thick; and Halite-II, 210 feet thick. The remainder of the total thickness of the formation is occupied by the upper anhydrite described by Jones (1973), as quoted above. Jones' middle halite unit is equivalent to Anderson's Halite-I plus Anhydrite-II plus Halite-II sequence; Anderson has simply subdivided the sequence based on the presence of a middle anhydrite member (Anhydrite-II) that Jones also recognized (see above). Both Jones and Anderson recognize that here the upper anhydrite unit does not display the varved interlaminations comparable to those observed in the lower anhydrite units.

The only major disagreement between Anderson and Jones appears to center around the nature of the Castile-Salado contact. Jones asserts that the contact is conformable and laterally intertongues (see discussion above), whereas Anderson believes an unconformity exists. Anderson (1978) cites as evidence for this the presence of some dissolution breccia near the top of the Castile, suggesting a period of non-deposition or even subaerial erosion. Furthermore, Halite-III is missing over the northern part of the basin, which could be explained by a local erosional episode there. Anderson also notes that the basal infra-Cowden salt of the Salado Formation (see below) does not occur to the south and is thickest wherever the Halite-III member is absent. This controversy has not been resolved to date; whether or not significant dissolution took place during deposition of the Castile and Salado evaporite sequence could have important implications regarding models invoked to estimate past and present rates of salt dissolution in the Delaware Basin.

Because no drill hole within Zones I-III of the WIPP site has made a complete penetration of the Castile, the thickness of the Castile beneath the repository must be estimated. Beneath the site, the base of the Castile is indicated by structure contours in Figure 10 of Jones (1972)

to be at an elevation of about minus 680 feet MSL at the center of the site; Sipes, et al. (1976) show it at minus 650 feet MSL. Since ERDA-9 intersected the top of Castile at elevation 579 feet above sea level, the Castile is indicated to be about 1,230-1,260 feet thick at the site, or approximately 1,250 feet thick. Drill hole AEC-8 encountered 1,333 feet of Castile in section 11, about 4 miles northeast of ERDA-9 (Griswold, 1977, Table III).

b) Salado Formation. The Salado Formation contains the thick salt beds in which the contemplated WIPP repository would be constructed. It is one of the principal deposits of halite on the North American continent (Brokaw, et al., 1972, p. 21), and it contains the Carlsbad potash enclave, the principal producer of potash in the United States.

As of the date of this report, one core hole, ERDA No. 9, has been drilled through the Salado at the location of the proposed repository. A schematic section of that hole, including general lithology, location of marker beds, position of halite zones in which the repository will be located, and well construction data, is given in Figure 4.3-3a. The detailed lithologic log is included as Figure 4.3-3b of this report. Details of the numerous down-hole logs performed, mineralogical and geochemical determinations made, and rock mechanics tests conducted are not discussed here but are given in Chapters 7 and 9 of this report, to which the reader is referred.

At the ERDA-9 location at the center of the site, the base of the Salado is 2824 feet and the top 848 feet below ground surface (elevations 590 and 2,566 feet above sea level, respectively), for a total thickness of 1,976 feet. The proposed contact handling (CH) zone halite interval, containing halite of relatively high purity, is between elevations 1,250 and 1,352 feet, and the remote handling (RH) zone, high-purity halite interval between elevations 696 and 806 feet. (Ground surface elevation at the ERDA-9 hole location is given as 3414.70 feet MSL).

Variations in the thickness of the Salado in the vicinity of the WIPP
site are on the order of 300 feet (1,700 to 2,000 feet), based on results
of the AEC and ERDA test holes (Griswold, 1977, Table III). Thicker
sections of the Salado (over 2,300 feet) are known where it may have been
affected by deformation due to salt flow. West of the site in the Nash
Draw area the thickness of the formation locally and erratically
decreases owing to local solution and removal of rock salt in the upper
part of the formation (Vine, 1963; Jones, 1973). These variations are
illustrated by a subregional isopach map of the Salado Formation
presented by Brokaw et al. (1972).

As discussed by Brokaw et al. (1972),

> "In exposures of the Salado Formation along the west side of the
> Carlsbad potash area (10 or more miles west of the site), all the
> salt has been removed by solution and the anhydrite and polyhalite
> have been altered to gypsum. The alternation of the evaporite rocks
> extends to depths ranging from 260 feet to almost 1,600 feet below
> the surface and is responsible for a fourfold to sixfold reduction
> in the thickness of that part of the Salado and for a change in
> composition from dominantly rock salt in the subsurface to
> dominantly gypsum in the outcrop. The contact between the two
> highly dissimilar parts of the formation, known locally as the 'base
> of leached zone' and also as the 'top of salt', is highly irregular,
> with many closed depressions and isolated pinnacles. The contact
> dips generally eastward but rises in stratigraphic position from the
> base of the Salado near the west side of the potash area to the top
> of the formation near the Eddy-Lea County line at the east side of
> the area."

Figure 8 of Brokaw, et al. (1972) shows the location of the contact at
the top of the Salado, or in other words the easternmost extent of
dissolution in the Salado, to be located about 1 mile from the east edge
of Range 30 E.; that is, about 2 miles west of the center of the WIPP.
Additional discussion of solutioning is discussed in Section 6.3.7 of
this report.

Broadly considered, the Salado is characterized by a predominance of rock
salt compared to a predominance of anhydrite in the Castile and by
typically thinner bedding or interbedding of lithologic units. Unlike
the Castile, the Salado as well as the overlying Rustler extends over and
beyond the confining Capitan reef masses to the north and east, in effect

overfilling the ancient basin formed by the reefs. The Salado sea was, in general, even more saline than the sea of Castile time. Lacking a shield of carbonate reefs, it received, however, considerable fine clastic sediment. Consequently, its halite deposits are generally less pure than those of the Castile (Brokaw et al., 1972), although thick intervals of highly pure halite are known in the lower half of the Salado Formation.

A detailed description of the overall lithology and member units has been provided by Jones (1973), who studied data from the numerous potash exploratory holes drilled in the Los Medanos area. The remainder of this section incorporates Jones' description, modified where appropriate by discussion of more recent data from ERDA-9.

The Salado Formation is composed of rock salt, anhydrite, and potassium rocks with varying amounts of other evaporites and fine-grained rocks. Rock salt constitutes about 85-90 percent of the formation except in the western part of the area where percolating ground water has dissolved and removed some of it. The next most abundant rock in the formation is anhydrite. The remainder of the formation is chiefly polyhalite and other potassium and magnesium-bearing minerals with minor amounts of sandstone, and claystone.

The rock salt in the Salado is composed of halite and clayey halite in discrete layers ranging from an inch to several feet in thickness. The two rock types differ primarily in that the halite is free of detrital debris and the clayey halite characteristically contains this debris in significant but typically small amounts. The detritus is chiefly quartz and clay, including illite, chlorite, and a corrensite-type of swelling, regular mixed-layered clay mineral (Grim et al., 1960). In general, the detritus-bearing clayey halite is mostly brown and tan; it is moderately crystalline but somewhat porous with a scattering of small cavities or vugs filled with clay and other detritus, and it either lies between seams of claystone or has a layer of halite below and a seam of claystone

above. The halite is typically reddish orange but its color grades to amber, gray, and white. It is generally somewhat more coarsely crystalline than the clayey halite.

Common to both the halite and the clayey halite in the rock salt of the Salado are traces to very minor amounts of polyhalite and anhydrite. Locally, glauberite is present in small amounts, and there are several potassium and magnesium minerals, including sylvite, carnallite, kieserite, and several other exotic evaporite minerals that occur in small to large amounts in seams of rock salt in the middle and upper parts of the formation. Other constituents of the halite and clayey halite include traces to very minor amounts of brine and gas that fill microscopic to very small cubic and rectangular cavities in grains of halite and other evaporite minerals. Less common, but more notable in other respects, are much larger cavities or pockets that contain halite-saturated brine and nitrogenous gas confined under presure sufficient to produce "blow-outs" when encountered during drilling operations.

The seams of anhydrite and polyhalite, which alternate with rock salt in all sections of the Salado, are very persistent but highly variable in composition (Jones, 1954; Jones, 1972). Lateral replacement of anhydrite by polyhalite is common, and nearly all seams show one or more stages of replacement between an initial slight development of polyhalite in the lower and upper parts of the seam to complete replacement of anhydrite by polyhalite. Locally, anhydrite and polyhalite give way laterally to glauberite, and polyhalite in the middle and upper parts of the Salado is replaced by hartsalz consisting of a coarsely crystalline mixture of anhydrite, kieserite, and carnallite.

Close examination of the Salado in drill cores and geophysical logs of boreholes in the Los Medanos area and vicinity reveals that rock sequences show a regular order of succession. A typical sequence, repeated many times between the base and top of the formation, involves a change from claystone upward through anhydrite or polyhalite and halite

to clayey halite capped by claystone. In other sequences the change is from halite to clayey halite capped by claystone. Boundaries between individual members of a rock sequence are gradational, but those along the lower and upper sides of the individual sequences are corrosion surfaces that form sharp, clear-cut breaks in the evaporite section but, nevertheless, are laterally persistent and convergent northward. The rock sequences represent a fundamental sedimentation unit or evaporite cycle, and they are believed to record discrete periods of influx and subsequent precipitation of calcium sulfate and soldium chloride during evaporation of sea water or an initially dilute brine. The ubiquitous claystone is thought to be a residue concentrated during dissolution of clayey halite by inflowing sea water or dilute brine.

The Salado Formation is divided into three members (Figure 4.3-3), but more subtle divisions can be made, for the beds are very persistent. In fact, the persistence of individual beds is the prime basis for the system of numbering individual seams of anhydrite and polyhalite which was introduced by geologists of the United States Geological Survey (USGS), such as Jones (1960) and is widely used by mining companies in the Carlsbad potash field. The numbers used in the USGS system to designate some seams of anhydrite and polyhalite in selected parts of the three members of the Salado are shown on Figure 4.3-3, and on Figures 4 and 6 of Jones (1973).

The threefold division of the Salado used herein includes: an unnamed lower member, a middle member known locally as the McNutt potash zone, and an unnamed upper member. The three members are about equally rich in rock salt, anhydrite, polyhalite, and fine-grained clastic rocks, and they are generally similar in all but one major respect. The lower and upper members are generally lacking or poor in sylvite, carnallite, and other potassium- and magnesium-bearing minerals, while the McNutt potash zone is generally rich in these minerals and accounts for the large and extensive deposits in the potash field.

Lower Member. Located below Marker Bed 126, the lower member of the Salado is the rock unit in which it is proposed to place both levels of the repository. As shown in Figure 4.3-3, the CH-zone is defined as the interval between Marker Beds 137 and 139 near the middle of the lower member, 560 feet above the base of the Salado. The RH-zone is in a zone devoid of nearby polyhalite marker beds, beneath a prominent anhydrite bed known as the "Cowden anhydrite." The top of the RH-zone is 344 feet below the base of the CH-zone; its base is 106 feet above the base of the Salado. The choice of zone intervals was made on the basis of combined purity, depth, thickness, mutual separation, and depth below the potash zone (Griswold, 1977).

The Cowden anhydrite identified above forms a distinctive, areally extensive bed of anhydrite about 20 feet thick below which is a salt bed of exceptional purity. This thick salt bed lying below the Cowden and above the Castile-Salado contact is sometimes referred to as the "Infra-Cowden", a sub-member located at the base of the Salado as shown in Figure 4.3-3. It is 296 feet thick at ERDA-9.

Lithologic details of each of the three members in the site area are provided by Jones (1973). The lower member of the Salado Formation is almost entirely made up of alternating thick seams of rock salt and thinner seams of anhydrite and polyhalite. Magnesite in thin bands, laminae, and ragged knots form a carbonate-rich zone in the lower part of most anhydrite and polyhalite seams. Seams and partings of claystone underlie the anhydrite and polyhalite seams, and claystone caps layers of clayey halite in the rock salt. There are also a few beds of very-fine-grained halitic sandstone, a few inches to a foot or so thick, near the base and top of the member. Insofar as has been determined by drilling, the member is completely free of carnallite and other hydrous potassium and magnesium evaporite minerals in all parts of the Los Medanos area, but the upper part contains traces to small amounts of these minerals several miles to the north of the area.

The lower member is 1,195 feet thick as recorded in ERDA-9. The member thins to 430 feet near the northeast corner of the area; in this instance the decrease of thickness seems to be due to beds missing at the corrosion surfaces that truncate individual rock sequences, as well as to thinning of all beds northeastward. Southward, the lower 240-300 feet of the member (that is, the Infra-Cowden) grades, according to Jones (1973), by intertonguing into the upper part of the Castile Formation, and the thickness of the member decreases to between 785 and 950. Anderson (1978) disagrees with the concept of an intertonguing lithofacies relationship between the Infra-Cowden salt and Castile anhydrite. He asserts that the Infra-Cowden wedges out southward and that the top of the Castile is unconformable with the Salado because of dissolution at or near the top of Castile prior to Salado deposition (refer to discussion above). Anderson (1978) presents an isopach map showing distribution of Infra-Cowden salt across the northern part of the Delaware Basin.

McNutt Potash Zone. The McNutt potash zone, located between the Vaca Triste halitic sandstone and the 126-marker bed, is another salt-rich member of the Salado Formation. However, unlike other members of the Salado, the McNutt may contain potassic rocks rich in sylvite, langbeinite, and hydrous evaporite minerals. The potassic rocks occur at short to long intervals in seams of rock salt scattered through nearly all parts of the McNutt zone. They are the obvious lithologic feature by which the NcNutt is distinguished, yet they are absent locally and, at best, probably comprise only 3 to 5 percent of the member in the most potassium-rich sections of the Los Medanos area.

Apart from the potassic rocks, the McNutt presents virtually the same aspect as other members of the Salado. Thick seams of rock salt alternate with thinner seams of anhydrite and polyhalite. There are partings of claystone beneath most anhydrite and

polyhalite seams and above layers of clayey halite. A bed of very-fine-grained halitic sandstone, the Vaca Triste, a foot or so thick, occurs in clayey halite at the top of the member.

The McNutt potash zone is 369 feet thick at ERDA-9, decreasing in thickness to the northeast. This decrease is similar in nature to that observed for the lower member. As a rule, where the member is thinnest it seems to be more thinly bedded and to have fewer beds.

Upper member. The upper member of the Salado, located above the Vaca Triste marker, consists of rock salt, minor anhydrite and polyhalite, and two persistent beds of very-fine-grained halitic sandstone, which are, respectively, 30-40 feet and 110-115 feet below the top of the unit. Claystone underlies seams of anhydrite and polyhalite, and coats the upper surfaces of clayey halite layers in the rock salt. Most parts of the upper member are generally free of hydrous evaporite minerals, but, nevertheless, some intervals of rock salt and other rocks in the upper 130 to 180 feet of the unit commonly contain traces to very small amounts of carnallite and kieserite.

Of particular interest is the occurrence of carnallite at the top of the upper member. The carnallite forms a major deposit of potassic rock that extends over a wide section in the northern part of the Los Medanos area and much of the region immediately to the north. The deposit is the only one known to occur in the upper member of the Salado, but is not restricted to the unit. It extends irregularly upward into sandstone of the overlying Rustler Formation.

At the WIPP site, the upper member of the Salado Formation is 512 feet thick (ERDA-9), becoming thinner (between 430 to 480 feet) farther north. This thinning northward seems to be partly depositional and partly erosional, for the member is more thinly bedded in the north and contains fewer beds. Many seams of anhydrite, polyhalite, and other evaporites are only about

three-fourths as thick as at the south end of the area. Beds of halite and clayey halite are missing beneath many of the corrosion surfaces that separate rock sequences in the unit.

Several miles west of the site in the Nash Draw area, variations in thickness of the upper member are fairly complex and large. The complexity and thickness of the member are believed to reflect a combination of geologic factors involving mostly (1) gradual thinning northward in response to changes in deposition patterns during the Ochoan Epoch, and (2) rapid thinning westward in response to change in dissolution patterns during the Pleistocene and earlier parts of the Cenozoic Era. In contrast to the modest northward thinning, the westward thinning of the member toward Nash Draw involves as much as a fourfold reduction in thickness in a distance of 4 to 6 miles, and the member is as thin as 150 to 170 feet at places along the west side of the area. This small thickness is considered to include the residue or remnants of at least a 450- to 500-foot-thick section of rock from which soluble salts have been leached by percolating ground water. The section of rock from which salts have been leached decreases in thickness eastward and feathers out in the area immediately east of Nash Draw. Insofar as can be determined from drilling records, the feather-edge of the residual materials marks the easternmost extent of dissolution of the upper member of the Salado Formation at any time. Apparently the regime here is highly stabilized and of long duration, with very little or practically no dissolution since the Pleistocene, or perhaps earlier. Estimates prepared by Bachman and Johnson (1973) indicate that the rate of salt removal during dissolution may amount to as much as 0.5 foot per 1,000 years. This rate suggests that roughly 1 million years would be required to reduce 450 to 500 feet of the upper member to an insoluble residual debris, and that dissolution in the western part of Los Medanos area has a long history extending back at least as far as mid-Pleistocene time. Other considerations, however, suggest that its history is even longer and may have begun by the mid-Tertiary (Bachman, 1976).

In all parts of the Los Medanos area, where the upper member of the Salado is thinned by dissolution, the section of rock between the upper surface of salt and the upper surface of the formation is composed of clay with crudely interlayered seams of broken and shattered gypsum and fine-grained sandstone. The clay is considered to be a subsurface residue concentrated through dissolution of clayey halite and other clay-bearing evaporites by percolating ground water. The gypsum is clearly the hydrated remnant of anhydrite and polyhalite seams, for it commonly contains ragged and embayed masses of anhydrite and polyhalite, and also grades laterally into anhydrite and polyhalite. The clay, gypsum, and sandstone comprise a fairly distinct residual unit that thins out eastward by grading into, and intertonguing with, rock salt and the other precursory rocks from which it originated. The residual unit thickens westward and crops out locally along the Pecos River west of the Los Medanos area. The unit is generally assigned by geologists mapping areas along the Pecos River to the lower member of the Rustler Formation, but this practice should be discontinued, for the clayey residue is clearly part of the Salado Formation.

Isopach maps of intervals in the upper member and in the McNutt potash zone are shown in Figures 4.3-4 through 4.3-7 referenced to the marker beds indicated. The same gradual northward decrease in thickness at the rate of about 10 to 15 feet per mile is exhibited by all four intervals contoured. It is significant that pronounced westward thinning of the Salado, which would be related to dissolution of salt from the Salado toward the Nash Draw area, is evidenced only in the uppermost interval (figure 4.3-7), and then only in Range 31 E., a mile or more west of the proposed WIPP repository boundary. The onset of westward thinning of the Salado Formation as defined by these isopach countours delimits a "suberosion" front at the top of the Salado (Griswold, 1977; Brokaw, et al., 1972; Jones, 1973) or the leading edge of a wedge of dissolution in the Salado progressing from west to east. This indicates that, insofar as can be detected by isopach patterns,

leaching of salt at the top of the Salado Formation by dissolution activity centered in the Nash Draw area has not occurred closer than approximately 1 mile west of the proposed WIPP repository.

In the Los Medanos area, the Salado Formation is overlain conformably by the Rustler Formation. The contact between the two formations is rather sharply defined as the horizon at which dominant rock salt below gives way to a 35- to 55-foot-thick unit of fine-grained sandstone that is generally dolomitic in the basal few feet.

Rustler Formation. The Rustler Formation, the uppermost or last of the three Ochoan evaporite formations, contains the least quantity of rock salt and the largest proportion of clastic material in this evaporite sequence. It was deposited in the last stages of the saline Permian sea that inundated the Delaware Basin, and is very largely coextensive with the Salado in this area (Brokaw et al., 1972). Jones (1972) lists lithologic percentages in the Rustler, presumably from areas in the Delaware Basin where Rustler salt has not been leached, as follows: 43 percent rock salt and other halides, 30 percent anhydrite, polyhalite, gypsum, and other sulfates, 17 percent clastic rocks, and 10 percent dolomite, limestone, and magnesite.

Shallowest of the evaporites to be exposed in the site area, the Rustler Formation crops out locally about 5 miles west of the center of the site, beyond the Livingston Ridge escarpment which forms the east edge of Nash Draw (refer to Figure 4.2-4, Surficial Geologic Map) Generally it is covered by alluvial material, sand dunes, or collapse debris.

The following descriptions of the Rustler are given by Jones (1973). As typically exposed in outcrop, the Rustler is a broken and somewhat jumbled mass of gypsum with minor dolomite and a few crude seams of virtually unconsolidated sands and clays. The outcrops in Nash Draw are decidedly poor for any study that requires precise information on the lithology, thickness, or specific chemical or physical properties of the
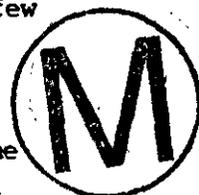
formation, and, as previously noted by Vine (1963), it is impossible to piece together a meaningful stratigraphic section from study or mapping of outcrops. Exposed rocks are porous, friable, and loose-textured, and all are strongly jointed, cavernous, and locally brecciated. Stratification is obscured or completely obliterated, and the attitude of bedding can rarely be determined with any degreee of confidence. The considerable deformation attests to the removal of much soluble material by percolating ground water and to the altered nature of the debris exposed in outcrop.

Two areally persistent beds of dolomite in the Rustler serve as important marker beds. The lowermost of the two dolomite beds, normally 100-150 feet above the base of the formation, is known as the Culebra Dolomite member. The upper bed, 200-250 feet above the base, is the Magenta Dolomite member. They were named and described by Adams (1944). Clastic rocks, consisting of thin to thick beds of sandstone and claystone, make up the remainder of the less soluble part of the formation.

In the subsurface, proceeding eastward across the WIPP site and into Lea County, all the gypsum in the Rustler gives way to anhydrite and minor polyhalite, and the sands and clays grade into sandy and clayey rock salt. In western Lea County at depths of 900-1,000 feet, the Rustler is largely an alternation of thick seams of rock salt and anydrite. A persistent seam of polyhalite occurs near the middle of the formation, and, insofar as has been determined, it is the only hydrous evaporite rock of any great extent or major importance in the stratigraphy of the formation.

With the eastward, down-dip change in composition from gypsum to anhydrite and rock salt, the thickness of the Rustler also changes rather significantly. The thickness ranges between 280 and 300 feet near the Nash Draw outcrop , but increases eastward to 490 feet about 10 miles southeast of the site and to 385 feet about 10 miles to the northeast. The increase ranges in amount between 105 and 160 feet and provides a crude measure of the minimum thickness of rock salt that is missing in

the area of outcrop. The difference in formation thickness between the southeast and northeast corners of the area is probably depositional in origin, for the formation is more thickly bedded in the southeast where it is thickest (Jones, 1973). These relationships are shown on a Rustler isopach map in Brokaw, et al. (1972).

In the immediate site area, the Rustler is lithologically divisible into a sandy lower part and an anhydritic upper part (Jones, 1975). The sandy lower part, 92 to 125 feet thick, is dominantly very fine-grained, silty sandstone, with less abundant anhydrite and rock salt; the sandstone is halitic and light to dark gray in its lower section and reddish brown and salt-free in its upper section. The anhydritic upper part of the formation, 200 to 227 feet thick, is largely gray anhydrite, with a few interbeds of reddish-brown clay and gray dolomite. The anhydrite is in fairly massive beds which have gypsiferous rinds along their lower and upper sides.

At the proposed WIPP site, ERDA-9 encountered 310 feet of Rustler commencing at a depth of 550 feet (refer to Figure 4.3-3). The Culebra and Magenta members were both encountered and measured at 26 and 24 feet thick, respectively. The thickness of the formation as a whole would indicate that much of the halite originally contained in the formation has been leached away, particularly in the upper part of the formation. The detailed well record of ERDA-9 (Griswold, 1977) shows that clayey halite was encountered in the Rustler below the Culebra dolomite, about 100 feet above the base of the formation. Between this position downward to the proposed upper level CH-storage zone, over 1300 feet of undisturbed evaporite rock, primarily Salado rock salt, intervene.

An isopach map of the Rustler Formation is shown in Figure 4.3-8. The closely spaced contours at the east edge of the site are a measure of the increasing amount of salt remaining in the Rustler in the eastward direction. The formation increases in thickness eastward and southeastward by about 180 feet over a distance of about 2.7 miles, or over 65 feet per mile. As with the Salado Formation, these contours can be used to postulate a dissolution front in the Rustler.

The Rustler Formation is separated from the overlying Dewey Lake Redbeds by a sharp lithologic break, an abrupt change from gray anhydrite to reddish-brown mudstone. The anhydrite below the break is free of sand and clay, and it ranges erratically in thickness from 18 to 32 feet. There is no indication of northward thinning, such as that common to most, if not all, rock units in the Rustler and underlying Salado Formations, and it would appear that the contact between the Rustler and Dewey Lake is an unconformity. The discordance and hiatus is probably not very great.

Dewey Lake Redbeds. The Dewey Lake Redbeds are the uppermost of the Late Permian Ochoan Series of formations and represent as well the top of the Paleozoic in the Delaware Basin. The term "Dewey Lake" is synonymous with the term "Pierce Canyon" originally proposed by Lang (1935) and applied to the redbeds in the Nash Draw area by Vine (1963). Actually the assignment of the Dewey Lake to the Permian Ochoan sequence is somewhat arbitrary, being based on certain lithologic details and stratigraphic aspects, rather than any definitely demonstrable affinity. Like the underlying Ochoan evaporites, the Dewey Lake appears to lack fossils despite its marine origin. Bachman (in Jones, 1973), while acknowledging the customary age assignment of the formation, nevertheless feels "that the Dewey Lake of southeastern New Mexico may actually be Triassic in age." He does not state, however, whether he believes it might be of Early or Late Triassic age.

The Dewey Lake crops out in places along the west edge of Nash Draw where partial thicknesses are exposed (refer to Surficial Geologic Map, Figure 4.2-4), but generally the formation is mantled by dune sand and caliche. Beneath the surficial cover, however, the Dewey Lake occupies a broad band between the center of the WIPP site and Nash Draw. It is bounded on the west by gypsiferous residue of the uppermost anhydrite seam in the Rustler Formation and on the east by coarse-grained clastic rocks of the Santa Rosa Sandstone of Late Triassic age. The latter contact occurs approximately across the center of the WIPP site.

The Dewey Lake is differentiated from other formations by its lithology, distinctive reddish-orange to reddish-brown color, and sedimentary structures. The formation consists almost entirely of an alternation of siltstone and very-fine-grained sandstone beds a few inches to several feet thick, but there are a few beds of claystone in its lower and upper parts. Individual beds are persistent, and the formation is readily separable on well log records into several sequences alternately richer or poorer in sandstone. Surficially, most rock is evenly and thinly bedded, liberally sprinkled with greenish-gray spots, and irregularly intruded by horizontal and criss-crossing veins of fibrous selenite. Some beds are structureless, whereas others are either horizontally laminated or cross-laminated. Many bedding surfaces carry shallow current or oscillation ripple marks. Silt-filled mud cracks occur at the top of many mudstone layers, and there are small chips and flattened pellets of mudstone in the basal part of many siltstone and sandstone layers (Jones, 1975).
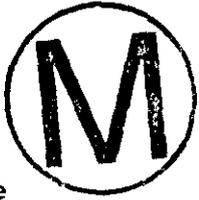
According to Vine (1963), the Dewey Lake Redbeds represent the beginning of continuous deposition of detrital sediment following the long period of predominantly evaporite deposition in the Delaware Basin and adjacent shelf areas of southeastern New Mexico. However, the abrupt change in lithology does not necessarily signify a sudden tectonic or eustatic movement, but only a gradual decrease in the salinity or depth of the water plus a new source for the detrital sediments which were deposited.

Certain general features of the Dewey Lake are especially noteworthy. The lithology and color appear to be remarkably uniform. Viewed from the distance of a few feet, the stratification nearly always appears to be parallel, even though small-scale cross-lamination may be seen on close inspection. The small grain size, together with the minute scale of primary sedimentary structures, such as cross-lamination in sets less than 1 cm thick and oscillation ripple marks less than 1 inch from crest to crest, suggests that the silt was deposited in extremely shallow water extending over a broad flat. Lenses of medium-scale, cross-laminated, fine-grained sandstone or siltstone in the upper part of the Dewey Lake

probably indicate a gradual change toward fluvial deposition near the end
of Dewey Lake time. The deposit undoubtedly blanketed the Delaware Basin
and part of the shelf area to the north, but the source of the sediment
is unknown.

The ERDA-9 well records a thickness of 487 feet of Dewey Lake strata.
The thickness varies greatly across the area, however, from about 550
feet a few miles southeast of the site to 100 feet a few miles to the
southwest (refer to isopach map, Figure 4.3-9). Normally in this area,
the Dewey Lake ranges betwen 500 and 560 feet in thickness, thinning to
the northwest. This northwestward thinning is attributed to pre-Late
Triassic erosion after the redbeds had been tilted southeastward (Jones,
1973, p. 25). Locally, however, where the Dewey Lake forms the surface
of either pre-late Tertiary terrain or Quaternary terrain, erosion later
than Triassic has cut through the Dewey Lake, producing the steepened
isopach gradients. In Figure 4.3-9 the gradients of 20 to 40 feet per
mile observable in the eastern half of the map reflect pre-Late Triassic
erosional thinning, while the steeper dips of up to 150 feet per mile to
the west represent later dissection, apparently related to the origin and
development of Nash Draw. A geologic section given by Jones (1973,
Figure 3) illustrates the effect of this later dissection on the Dewey
Lake surface.

4.3.3 Mesozoic Erathem

Triassic System. Triassic rocks in the northern part of the Delaware
Basin are all Late Triassic in age and are included in the Dockum Group.
The Dockum is entirely of continental origin and consists of the
dominantly fine sediments of broad flood plains and coarse alluvial
debris deposited over a very broad area extended beyond the borders of
the Delaware Basin. It surfaces the pre-Tertiary terrane at and east of
the WIPP site. Local subdivisions of the Dockum Group are the Santa Rosa
Sandstone (Darton, 1922) and the Chinle Formation.

1) Santa Rosa Sandstone

The Santa Rosa Sandstone rests unconformably with sharp lithologic contact on the underlying Dewey Lake Redbeds. Vine (1963), based on outcrop observation, called this contact a disconformity (that is, parallel beds on either side of the contact representing a time-rock gap), but Jones (1973) considers it "an angular unconformity of low angle." Corresponding to an interval between the end of Permian time and the start of Late Triassic time, this unconformity represents a break in deposition perhaps longer than had previously occurred in the region since Mississippian time or even earlier, assuming the assignment of the Dewey Lake Redbeds to the Permian is valid.

At the site, the Santa Rosa occurs as an erosional wedge pinching out westward just beyond the center of the site; a thickness of only 9 feet of Santa Rosa Sandstone was recorded at ERDA-9. Eastward the formation forms the pre-Gatuna surface (See Figure 2 in Jones, 1973) but is blanketed by such an extensive veneer of Upper Tertiary alluvial deposits and caliche, and Recent dune sand, that the nearest extensive outcrops occur about 7 miles to the north (Vine, 1963).

The wedge of Santa Rosa thickens relatively rapidly eastward at the rate of up to 150 feet per mile, attaining a maximum thickness of 250 feet over a distance of only two or three miles, thereafter maintaining a more uniform profile (refer to isopach map of the Santa Rosa, Figure 4.3-10). Sections compiled by Jones (1973) indicate a relatively uniform thickness of the Santa Rosa on the order of 250 feet at least as far as several miles east of the Lea County boundary. The steepened wedge effect of the Santa Rosa across the site area is undoubtedly due to the post-Late Triassic, pre-Gatuna erosion that cut downward into the Dewey Lake surface, which is discussed above (compare Figure 4.3-9).

The Santa Rosa Sandstone consists, for the most part, of cross-stratified, medium- to coarse-grained, gray to yellow-brown sandstone, but includes both conglomerate and reddish-brown mudstone. In

outcrop it has been observed by Vine (1963) to consist of large-scale, trough-type, cross-bedded, pale-red sandstone and conglomerate lenses, 3 to 15 feet thick, separated by thin partings of moderate reddish-brown siltstone and silty claystone. The conglomerate lenses contain both silty dolomite pebbles and chert or quartz pebbles. The sandstone is characteristically poorly sorted. The formation differs from the underlying Dewey Lake Redbeds by being coarser grained, less well sorted, and by having beds that are thicker and more lenticular. Fossil plant impressions, carbonaceous plant fragments, and fossil reptile bones and teeth thought to be from phytosaurs characterize some of the beds. Clay is a relatively minor constitutent in most of the Santa Rosa Sandstone. Secondary dolomite is the most abundant cement, and it probably constitutes at least 10 percent of the rock.

The Santa Rosa Sandstone represents a change in the environment of deposition as compared with the Dewey Lake Redbeds. The large-scale trough-type crossbedding probably indicates a fluvial environment. The lack of sorting, arkosic composition, and angularity of the grains suggests rapid deposition by streams descending from a predominantly crystalline terrain (Vine, 1963).

2)   Chinle Formation

The Chinle Formation, though not present at the WIPP site itself, occurs at about the Lea County line 5 miles to the east, where it forms the subcrop surface of pre-Tertiary rock, as shown by Jones (1973). Like the Santa Rosa Sandstone at the site, in profile the Chinle is seen to wedge out from the east at the Lea County line, beveled by pre-Gatuna erosion. Farther east, the Chinle appears not to attain a thickness in excess of 100 feet as shown by Jones (1973). Northward, however, it achieves a thickness of about 800 feet near the Hat Mesa gas field, about 11 miles northeast of the site, where the Chinle is blanketed by Late Tertiary Ogallala Formation (Jones, 1973). These relationships plus the areal distribution of Ogallala remnants indicate that post-Chinle, pre-Ogallala erosion occurred subsequent to an eastward to northward tilting of at

least the northern part of the Delaware Basin, resulting in a greater amount of Chinle sediments removed progressively southward and eastward. Later, one or more erosional episodes beveled a westward-sloping surface on post-Ogallala terrain.

In lithology, the Chinle is dominantly reddish-brown shaly mudstone interspersed with some greenish-gray mudstone and minor lenses of sandstone and conglomerate, deposited in a floodplain or alluvial environment basically similar to that of the Santa Rosa. Its contact with the underlying Santa Rosa Sandstone is conformable and is at the change from sandstone of the Santa Rosa to shaly mudstone of the Chinle. It is overlain unconformably by the Ogallala Formation of Late Tertiary age.

Post-Triassic Rocks of Mesozoic Age. No Mesozoic rocks later than the Chinle strata are known to exist in the WIPP site area. According to Jones (1973), there are good reasons to infer from paleogeology and other considerations that the Jurassic Period was a time of erosion and removal of the Dockum. Some rocks of Cretaceous age, though absent from the site area, almost certainly were deposited by Early Cretaceous seas which advanced northward across southeastern New Mexico. Small outliers, crevasse deposits, and other remnants of Lower Cretaceous rocks are found lying unconformably on the Capitan, Tansill, and Castile Formations near Carlsbad Caverns (Hayes, 1964; Lang, 1937), on the Salado Formation near Black River Village, on the Rustler Formation a few miles northeast of Carlsbad, New Mexico, and on the Chinle Formation at many places to the north and east of the WIPP site area (Ash and Clebsch, 1961).

4.3.4   Cenozoic Erathem

Tertiary System. No Early or Middle Tertiary sedimentary rocks are known to be present in the region. A lamprophyre dike, the only igneous rock later than Precambrian age known in the region, is observed to intrude the Salado Formation at the Kerr-McGee potash mine, about ten miles north of the center of the WIPP site (refer to Figure 3.5-2). Part of a

northeast-southwest dike trend of regional extent, the closest approach
of which is at least eight miles northwest of the center of the site, the
dike is not exposed at the surface east of the Pecos River. A
radiometric date of 30 million years for the lamprophyre has been in the
record for some time (Urry, 1936); an Oligocene or mid-Tertiary age for
emplacement is therefore indicated. Further discussion of this dike
trend, including an account of more recent investigations conducted, is
included in Regional Geology, Section 3.5.1.

In Late Tertiary time extensive alluvial fans carried sandy and gravelly
material eastward over a broad erosional plain that had developed in the
region by Late Miocene time. The sediments accumulated during this
alluviation, which lasted until Late Pliocene time, constitute the
Ogallala Formation. The youngest fauna present in the Ogallala Formation
is of Kimball age. This fauna may be as old as 4.6 million years
(Bachman, 1974).

Only one area occupied by the Ogallala is present within 10 miles of the
site, namely, a relatively thin erosional remnant capping The Divide
located between 6 and 9 miles east-northeast of the center of the site
(refer to Figure 4.2-4, Surficial Geologic Map). A geologic map by
Bachman (in Jones, 1973) indicates that the Ogallala at the Divide is
restricted to elevations above 3750 feet, where it is about 25 feet thick
and includes about 10 feet of conglomeratic sandstone at the base
overlain by about 15 feet of caliche. Pebbles of rounded quartzite and
chert as much as 1-1/2 inches in diameter are present in lenticular beds
(Bachman, 1974).

Special attention has been given to the caliche developed on the Ogallala
by Bachman (in Jones, 1973), who suggests that it may be distinct in
origin from caliche observed elsewhere in the area. Based on field
examination, he finds that

> "Caliche of the Ogallala Formation is a distinctive travertine-like
> calcium carbonate. It is dense, light gray to white, and composed
> of concentrically laminated fragments that range from less than
> one-half inch to more than 2 inches in diameter. Space between

these fragments is filled with structureless or, in places, laminated limestone. The weathered surface appears algal or pisolitic in places. However, these concentric laminae probably are not the result of organic activity but indicate repeated generations of inorganic solution and reprecipitation. The caliche is sandy and has been precipitated in porous spaces between sand grains; therefore, individual sand grains appear to float in the caliche. The Ogallala caliche probably formed as a part of a soil profile that developed on the High Plains surface either during or after deposition of the Ogallala Formation."

In the High Plains to the east of The Divide, longitudinal depressions in the Ogallala caliche are interpreted to be interdunal swales caused by solution etching of Ogallala caliche where it was not protected by Pleistocene sand dunes (Bachman, 1976).

Quaternary System

1)   Pleistocene Series

a)   Gatuna Formation

The only Pleistocene deposit at the proposed WIPP site which has been assigned a formal stratigraphic name is the Gatuna Formation. In the immediate area, the Gatuna forms a thin blanket, locally absent, ranging in thickness from zero to slightly more than 30 feet (refer to Figure 4.3-11, Gatuna Isopach Map); at ERDA-9, 27 feet of Gatuna were recognized. In spite of its shallow depth below the surface, however, the Gatuna crops out only rarely, being for the most part obscured by a thin but persistent veneer of caliche and surficial sand. The nearest mapped outcrops occur along the west-facing slope of Livingston Ridge at the edge of Nash Draw (about four miles northwest of the center of the site; see Figure 4.2-4, Surficial Geologic Map) where they were mapped by Vine (1963), and to the southeast of the site as mapped by Bachman (1974). In Nash Draw itself the Gatuna locally exceeds 100 feet in thickness and fills sinkholes previously formed by dissolution of salt and other evaporites. It has alluviated most drainage valleys of an ancient Pecos system, of which Nash Draw was a part. Though the Gatuna is predominantly a fine-grained, reddish or brownish friable sandstone,

conglomerate lenses and blankets are common regionally. It is the
pebbles in the conglomerate which have proved most useful in providing
evidence relating to geologic history, age, and provenance of the
formation.

Bachman (1974) discusses age, lithology, and paleoclimatic implications
of the Gatuna at some length. Generally, the Gatuna was stream-laid
under pluvial conditions. In some areas having fine-grained materials in
the lower part of thicker sections, the Gatuna first filled collapsed
basins and extensive sinks; in other areas, such as in the southern part
of Nash Draw, gypsum-rich clays and silts in the section suggest
deposition in areas then undergoing sinking and collapse. Based on
examination of pebble clasts in Gatuna gravels of the Pecos River
northwest of the site in Chaves and northern Eddy Counties (refer to
Regional Geology and Regional Geomorphology sections for additional
discussion of these gravels), Bachman concludes that the Gatuna was
deposited in a much wetter climate than present. There is no indication
that modern drainage is carrying clasts of the size and quantity
preserved in Gatuna stream deposits. The discovery of Ogallala pisolitic
debris (i.e., pebbles of Ogallala caprock caliche) in the Gatuna
demonstrates that the Gatuna is Pleistocene rather than Pliocene in age.
Futhermore, on the basis of the many stream and pond deposits in the
Gatuna and the evidence for widespread solution and collapse, Gatuna time
represents the most humid Pleistocene stage in southeastern New Mexico.
Regional considerations lead Bachman to assign a tentative Kansan age to
the Gatuna, or approximately an age of 600,000 years (Bachman, 1974).

b)   Mescalero Caliche
Beneath an obscuring cover of wind-blown sand, much if not all of the
site area, excluding some depressions and drainages such as Nash Draw,
are covered by a hard, resistant caliche crust. It is very extensive to
the north in Chaves County on the Mescalero plain between the Pecos River
and the Llano Estacado and is informally called the Mescalero caliche.
Though generally less than 10 feet thick in the site area, its resistance
to weathering in the dry climate has effectively prevented natural

exposure of older strata and has allowed it to form extensive surfaces that can themselves be mapped in definite stratigraphic sequence with other deposits.

Vine (1963) provides a detailed account of caliche as he observed its occurrence in the Nash Draw quadrangle. He states,

> "Caliche is a near-surface accumulation of calcareous and clastic material that forms a resistant mantle. It is characterized by an excess of calcareous material over that required to cement the clastic grains, with the result that the grains appear to float in the matrix. In many areas the caliche is characteristically brecciated and recemented. In addition to sand and calcareous material, pebbles are locally abundant, and silica in the form of chalcedony or opal also forms part of the cementing matrix. Other soluble minerals, including gypsum, are probably locally present. Where the top surface of caliche has long been exposed to weathering, it almost invariably has a very hard dense limestone surface that could easily be misinterpreted as an outcrop of massive limestone similar to those in some older formations. Close inspection, however, generally reveals sand grains, chalcedony, and brecciation. Commonly the dense layer at the top is only 1 or 2 feet thick, and the rock becomes more friable and shows a greater proportion of sand grains to matrix within a few feet of the surface. The less calcareous zone in turn grades downward within 5 or 10 feet into the underlying bedrock, which generally is broken into angular fragments recemented with calcareous material. (Note: five feet of caliche were encountered at ERDA-9.) In many areas caliche has concentric lamination or colloform structure resembling calcareous algal structures. The widespread mantle of caliche has much the same composition throughout the area regardless of whether the underlying bedrock is red sandstone and siltstone from the Gatuna Formation, Santa Rosa Sandstone, and Pierce Canyon (=Dewey Lake) Redbeds, or gypsum from the Rustler Formation."

Bachman (1974) shows a regional structure contour map of the Mescalero caliche. He confirms Vine's recognition of an upper dense zone over an earthy-to-firm nodular calcareous deposit, and notes that it is the upper dense caprock that is prominently laminated. The character of the laminae indicates that the Mescalero caliche arose through successive cycles of dissolution and reprecipitation of the matrix, and that this occurred during an interval of tectonic stability that followed deposition of the Gatuna Formation--that is, in the semiarid environment that followed the moist conditions of Gatuna time. Based on regional geomorphic considerations, Bachman correlates the formation of the
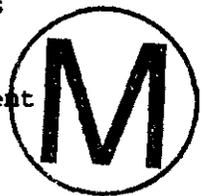
Mescalero caliche with the Yarmouthian interglacial stage, or mid-Pleistocene time, about 500,000 years ago. Brown (1956) reached generally similar conclusions on the origin of caliche he studied on the Llano Estacado of the Texas panhandle, where he found that "the caliche, with interruptions, apparently has been forming continuously since its inception in the Pliocene, and its multiple occurrence is a reflection of climatic variations in the Pliocene and Pleistocene". Noting that the Mescalero caliche dips abruptly into Nash Draw along Livingston Ridge, Bachman (1974; also in Jones, 1973) concludes that Nash Draw was subjected to subsidence after the formation of the caliche, presumably during the more pluvial conditions of the subsequent Illinoian or Wisconsin glaciations.

2)   Recent Deposits

Deposits of Recent age in the vicinity of the WIPP site include windblown sand, alluvium, and playa lake deposits.

The most prevalent deposit by far is the windblown sand which covers nearly all of the area of the WIPP site itself. The sand, locally known as the Mescalero sand (Vine, 1963), occurs either as a sheet deposit resting on caliche or as tracts of conspicuous dune fields (Los Medanos). In the former case, the sand is probably no more than 10 to 15 feet thick on the average; in the latter, the sand may attain 100 feet in thickness locally. At many places the sand consists of two parts: a compacted, slightly clayey moderate-brown eolian sand up to 1-1/2 feet thick, overlain by loose, windblown light-brown to light yellowish-gray sand. The sand dunes appear to be relatively inactive at present, partly stabilized by sparse plant cover. The widespread deposits of windblown sand are indicative of a large source of fine sand as well as of the extreme fluctuations of climate that have occurred during Pleistocene time. There is very little evidence that much sand has been derived from the Pecos River. Bachman (1974) suggests that most sand has been derived from deposits of the Ogallala Formation. During humid intervals in Pleistocene time the sand has been eroded from the Ogallala, and during arid intervals the wind has moved this sand across the Mescalero plain.

Deposits of alluvium are mapped by Vine (1963) generally in belts 1/4 to
3/4 of a mile wide along the base of declivities into Nash Draw, as along
the base of Livingston Ridge, and locally in smaller depressions (refer
to Figure 4.2-4, Surficial Geologic Map). These deposits are similar to
sheet wash or small alluvial fans, and Vine considers them analogous to
pediment or bolson deposits.

Playa deposits occur in mudflats, and consist of eolian sand and alluvium
reworked by shallow-lake waters. Vine (1963) shows these areas clustered
mostly within Nash Draw, where the occasional runoff accumulates. The
nearest playas are mostly small, circular areas about 5 miles west of the
center of the site filling in the bottoms of sinkhole depressions
adjacent to Nash Draw.

4.4   SITE STRUCTURE AND TECTONICS

4.4.1   Tectonic and Structural Setting of Los Medanos Site

Relation of Site Structure to Regional Tectonics. The single dominating
tectonic feature in the region around the proposed WIPP site is the
Delaware Basin, the locus of unusually thick and rapid sedimentation in
Permian time. Beneath the site, for example, about 15,000 feet of
Pennsylvanian and Permian clastics, limy clastics, and evaporites
accumulated. The basin was marginal to an orogenic belt located farther
southwest (the Diablo Platform) which was tectonically active in Late
Pennsylvanian and Permian time. The basin evolved by downwarp of
Precambrian basement terrane of the Texas foreland, a granitic craton.
South of the New Mexico border in Texas, the Delaware Basin in Late
Pennsylvanian time was trough-like and received much of its sediment from
a bordering mobile orogenic belt (Marathon system), in the manner of a
molasse trough or exogeosyncline; in New Mexico, however, the northern
part of the Delaware Basin received sediment from intracratonic highs
located both to the west (Huapache flexure) and to the east (Central
Basin Platform) and assumed more the character of an intracratonic basin
in which subsidence was accomplished mainly by downwarping of the craton

without major marginal faulting and without subsequent folding or compressive tectonic deformation, although buried normal faults of fairly large displacement are known at the margins of the Central Basin Platform. The Central Basin Platform, located approximately along the New Mexico—Texas border east of the site, may be viewed as a medial, arched horst, now deeply buried by later sedimentary deposits, which separated and partly isolated the Delaware Basin from its eastern counterpart, the Midland Basin, during Late Pennsylvanian and Early Permian time; later in Permian time these basins constituted part of the broad Permian Basin (refer to Sections 3.4 and 3.6; see Figure 1 of Bachman and Johnson (1973) for the extent of the Permian salt basin).

In the Delaware Basin toward the close of Permian time, as much as 4,000 feet of evaporite beds, dominantly rock salt, accumulated, during which time differential subsidence ceased and stable cratonic conditions returned to the area. Later, Triassic redbeds mantled the region. In mid to late Tertiary time, rifting and tensional faulting occurred in the Basin and Range region of New Mexico as far east as the Sacramento and Delaware Mountain anticlinal structures west of the Delaware Basin, and southeast along the Diablo Platform to the Big Bend area of Texas, but did not occur within the Delaware Basin itself. The basin was, however, tilted gently one or more times between Late Triassic and Pliocene time, producing a general net eastward tilt of about 2 degrees. The Late Permian Ochoan rocks and the Triassic rocks exposed in the basin today do not reflect basinwide warping; the major structual feature of these deposits is merely the regional eastward slope produced after Triassic time (Bachman and Johnson, 1973).

Tectonic and Nontectonic Mechanisms at the Site. At the site, stresses associated with the origin and development of the Permian Delaware Basin have deformed the pre-existing rocks or contemporaneous sediments in different ways. Specifically, these stresses included the nontectonic downward pressure imposed by the weight of rapidly deposited sediment and the tectonic stress arising from within the earth's crust and transmitted through the basement rocks to the sedimentary pile. The tectonic stress

would have been most effectively imposed upon those rocks of the sedimentary pile that had already undergone lithification and were therefore mechanically coupled with the basement rocks. Stress imposed by sedimentary loading would have been most effectively absorbed by subjacent materials that were the least lithified and therefore the most compressible and capable of adjusting to differential sediment loads. Each mechanism would have produced different kinds of structures and caused different types of faulting in the rocks beneath the basin. The temperatures measured and heat flow calculated for AEC 8 (Mansure and Reiter, 1977) show evidence of normal geothermal gradients.

The presence of thick salt beds profoundly affects the type of deformation which occurs in the salt itself and which is imposed upon rocks and sediment lying above the salt, inasmuch as thick salt is known to deform plastically and to behave as a viscous medium over extended periods of time. This behavior is promoted by high overburden pressures and increased temperatures. Under favorable conditions, even slight tilting of the beds or lateral differences in lithostatic pressure are sufficient to initiate long-term viscous flow of salt. Salt deformation is therefore quite different in mechanism and manifestation than the deformation of the enclosing rock materials. As a result, deformational features exhibited by rocks and sediments lying above thick salt would normally be expected to have little or no mechanical relationship to structures in rocks occurring beneath the salt, because the intervening salt effectively decouples the two rock masses. Rocks overlying salt would be expected to display local structures that are generated by mass flow of salt. In addition, because shallow salt is susceptible to dissolution by unsaturated ground water, sediments above shallow salt where active solutioning had occurred could be expected to exhibit karst and collapse features, or to have internal irregularity and chaotic structure brought about by uneven subsidence or upward stoping following removal of significant thicknesses of salt in the subsurface. It should be emphasized, however, that at the WIPP site, evaporite dissolution has been restricted to salt beds of the Rustler Formation. No evidence has been obtained to date to indicate that this relatively small amount of dissolution of Rustler salt has resulted in significant differential

subsidence in the site area. In contrast, the potential for subsidence structures to occur has been realized in areas such as Nash Draw, where partial dissolution of Salado evaporite beds has taken place.

It is concluded on the basis of the preceding discussion that the nature of the origin and development of possible structural features in the rocks which occur in the Los Medanos area is spatially related to the position of these rocks in the geologic column relative to the position of thick bedded salt. Accordingly, the following description of geologic structure at the WIPP site is organized into separate discussions of deep structure (i.e., structure in rocks underlying Ochoan salt), salt deformation, and shallow structure.

4.4.2   Deep Structures

Subregional Structure of Pre-Evaporite Rocks. A variety of structure contour maps covering an area within about a 25-mile radius of the WIPP site has been prepared, generally from well data. Foster (1974) provides seven such subregional maps from top of Precambrian to top of Bell Canyon (base of Castile); Sipes et al. (1976) show somewhat more structural detail on top of Devonian, Morrow, Atokan, Strawn, and Delaware strata (their exhibits 11,10, 9, and 8, respectively, the first two of which incorporate seismic reflection profile interpretations). Netherland, Sewell and Associates (1974) present generalized structure contour maps of a slightly different area on eleven horizons, from Ellenburger to top of Bell Canyon (their Figures G-6 through G-16).

Structure contour maps express a homoclinal regional dip toward the southeast to east on all pre-Ochoan Paleozoic strata, reflecting the presence of the Delaware Basin downwarp. Gradients on all pre-Permian horizons are similar in magnitude and direction, decreasing from about 150 feet per mile southeasterly in the lower Paleozoic to about 100 feet per mile at the top of the Pennsylvanian. The nearest fault large enough to be indicated by subsurface well control is a north-trending fault shown by Foster (1974) about 15-20 miles east and southeast of the WIPP

site, and referred to as the "Bell Lake fault." It has a length of about
15 miles and a displacement of about 500 feet. Located west of the
central axis of the Delaware Basin, it nevertheless appears to be
structurally related by orientation and displacement (upthrown to the
east) to the west-bounding fault of the Central Basin Platform farther
east, as is shown on the regional structure contour map of Haigler and
Cunningham (1972). The fault is not indicated to offset Permian strata
(Foster, 1974), but contours of Wolfcamp and Bone Springs strata in the
lower part of the Permian section are deflected in the area of the
fault. Permian structure contour maps indicate a difference in gradient
and direction of horizons compared to earlier strata. This indicates
significant tectonic activity in the basin in Late Pennsylvanian and
Early Permian time, which was the major period of structural adjustment
in the Delaware Basin (Foster, 1974). Permian strata beneath the Ochoan
Series slope east-southeast at about 50 feet per mile (Foster, 1974),
markedly less than pre-Permian strata.

Site-Specific Interpretations. In the immediate site area seismic
reflection data can be utilized as an adjunct to well control in
preparing more detailed structure contour interpretations. Figures 4.4-1
thru 4.4-3 contour horizons at, respectively, the top of the Silurian
(Siluro-Devonian carbonate, refer to Section 4.3.2), top of Morrow, and
near the top of the Delaware. Seismic profile lines are indicated and
well control points are shown. Structural interpretation of seismic
reflection profiles has been furnished by G.J. Long and Associates, Inc.
(1977). (Additional seismic profiling has been performed (G.J. Long,
1977b) or is presently being undertaken as part of a continuing program
by Sandia Laboratories to delineate subsurface structures at the WIPP
site. These additional data will be presented and discussed when the
analyses are completed.)

In general, Figures 4.4-1 through 4.4-3 reveal the existence of minor
faulting and secondary warping (swells and saddles) in Paleozoic strata
below the evaporite beds. Comparing Figure 4.4-1 with 4.4-2, a pattern
of generally north-northeast-trending faults has been interpreted,

oriented roughly parallel to regional strike and typically upthrown to the east. Small, subdued dome-like features and complementary saddles spaced several miles apart and with crest-to-trough amplitude of several hundred feet are superimposed on the regional gradient and appear to persist in position through both horizons. In the Silurian, for example, several small arches of up to 300 feet of relief are aligned in an east-southeast or west-northwest anticlinal trend passing just north of the Zone II exclusion area (Figure 4.4-1). In the Morrow a similar east-west trend in about the same location is defined by more subdued structural gradients and highs of lower amplitude (Figure 4.4-2). This trend is identified as the "Cabin Lake" trend by Netherland, Sewell and Assoc. (1974); see also Figure 2-7 of this report. On both horizons a domal feature is evident beyond the southwest edge of the site. This feature, which Netherland, Sewell (1974) indicate is at the east edge of the "Los Medanos" trend, is presumably responsible for the gas production of the Los Medanos field, the nearest hydrocarbon field to the site. Between these two anticlinal trends, a northwest-trending saddle is defined, located beneath the southwestern edge of the site.

The north-northeast-trending faults inferred in Figures 4.4-1 and 4.4-2 are, as interpreted from seismic reflection records, of greater intensity in the Devonian, being traceable over distances exceeding ten miles and having displacements of up to 400 feet (Figure 4.4-1). Faulting of the Morrow (Figure 4.4-2), some 2,500 feet higher stratigraphically, is roughly correlative with the deeper displacements, but seems to dissipate into discontinuous segments of generally smaller displacement.

Small-scale structures interpreted on the Delaware Mountain Group, roughly 9,500 feet above the Morrow horizon, show little or no correlation with deeper features (refer to Figure 4.4-3). The north-northeast-trending faulting is no longer apparent; instead, seismic reflection studies (G.J. Long, 1977a) indicate short (less than 5 miles in length), discontinuous northwest-trending offsets of small displacement (less than 50 feet) passing beneath the northeast half of the site; refer to Figure 4.4-3. The fact that the faults are not

detected at greater depths suggests a shallow-seated origin. Warping in the Delaware Mountain Group appears to be much more subdued than in the Morrow; structure contours lack closure around irregularities, and trends in the Delaware Mountain Group appear to be unrelated to Morrow and deeper trends. One feature of note shown (Figure 4.4-3) is a shallow, northwest-trending saddle of not more than 100 feet of structural relief, located beneath the center of the site; the presence of such structural lows is considered to be a favorable site selection criterion (refer to Section 2).

The contrasting structural characteristics between the Delaware and pre-Permian horizons suggest different origins. All strata from the Pennsylvanian on down have been deformed in continuity, with intensity of deformation increasing with depth. Tectonic deformation apparently occurred in Late Pennsylvanian or Early Permian time and established the local structural elements of all pre-Permian rocks. The "rootless" character of at least some of the normal faulting in the Permian suggests that these are shallow-seated features. Considering the unusually rapid rate of accumulation of material in Permian time (about 13,000 feet), it seems reasonable to presume a predisposition for the occurrence of contemporaneous sedimentary deformation brought about by such factors as gravity creep, compaction during diagenesis, differential sedimentary loading and rates of dewatering, and differential subsidence. Such deformation has been documented along "growth faults" in the Gulf Coast basin (Murray, 1961, p. 137; Fisher and McGowen, 1967, Figure 3; Bishop, 1973; Bruce, 1973). Contemporaneous faults of this type may have been initiated during deposition of thick pre-Ochoan clastic sequences. Conceivably, further movement might have been promoted by mass movement of salt subsequent to evaporite deposition, which shifted overburden loads over possibly still compressible sedimentary material.

Figures 4.4-4 and 4.4-5 show southwest-northeast and northwest-southeast sections, respectively, across the proposed WIPP site area, adapted from Griswold (1977). The overwhelming thickness of Permian pre-evaporite strata relative to earlier deposition is graphically displayed. Faults
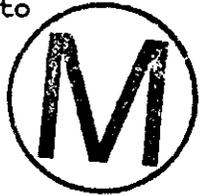
arising in the basement offset Pennsylvanian strata but do not propagate through the lowest Permian series, the Wolfcampian. The regional dip of the Delaware Basin is most evident in Figure 4.4-5.

4.4.3 Salt Deformation

For the purpose of this discussion, detailed description of deformational features within the salt beneath the site and in the northern part of the Delaware Basin is restricted to consideration of structure displayed by the Castile and Salado Formations even though the Rustler is normally considered part of the evaporite sequence. At the site and in the vicinity of the site, the Rustler has been leached of much of its salt with the result that most of its structure is surficial in origin and is included in the discussion of site surficial structure, Section 4.4.4.

Of previous studies available in the literature on the northern part of the Delaware Basin, the papers by Brokaw et al. (1972), Anderson et al. (1972), Jones (1973) and Anderson (1978) are most relevant to salt deformation in the area of the proposed WIPP site.

Subregional Structure of Evaporite Beds. Throughout the northern Delaware Basin, the general uniformity in direction and amount of the gentle southeastward homoclinal dip is practically the only structural feature that is common to all levels of the evaporite section (Jones, 1973). Superimposed on this homocline is a rather complex system of flow features variably developed relative to both areal location and stratigraphic position, features attributable to mass migration of salt.

Features that are of subregional significance, and that appear to have a fundamental role in the development of salt deformation, include the Capitan reef front. It formed a steep, submarine prominence or wall 1,000 to 1,500 feet high isolating the deep water of the early Castile brine sea from the rest of the Permian inland sea (refer to Sections 4.3.2 and 3.6). Figure 10 of Jones (1973), a structure contour map on the base of the Castile Formation, graphically depicts the structural

relationship of reef and basin in the site area. Immediately basinward
of these buried reef masses, which are located 8 miles north of the WIPP
site, is a northwest-southeast-trending structural trough paralleling the
base of the reef and descending in elevation, or plunging,
southeastward. The most intense deformation in the evaporite sequence
seems to be spatially related to this trough; not only is the trough
expressed within the salt layers, but the top of the clastic Delaware
Mountain Group (Bell Canyon Formation) is also depressed. Subregional
geologic sections constructed by Jones across Nash Draw and Livingston
Ridge (Brokaw, et al., 1972, Jones, 1973,) illustrate the general
configuration of reef, trough, and deformation within the evaporite
sequence in the site area. Jones' (1973) assessment of these particular
features is pertinent:

> "At intermediate and other levels in the (evaporite)
> section, the structure is generally more uneven than at
> the base of the Castile Formation, and minor folds are
> somewhat more prominent. Salt and anhydrite in the middle
> member of the Castile are crumpled in sharp
> intraformational folds that appear to die out
> northwestward up the dip and to become more pronounced
> southeastward down the dip. Spatially the
> intraformational folding of the salt and anhydrite appears
> to be confined to a single long northwestwardly-trending
> belt, about 3-4 miles wide, that more or less coincides in
> trend and extent with the prominent southeastwardly
> plunging trough at the base of the Castile. The folding
> has resulted in some buckling and downwarping of rocks in
> the Salado Formation, and it has uplifted the Salado and
> other rocks as young as the Chinle Formation in a fairly
> broad arch that trends northwestward across the area. The
> exact age of the deformation is unknown; it can be dated
> only very broadly as post-Late Triassic to pre-Pliocene.
> Specific considerations concerning minimum thickness of
> overburden required to initiate salt movement suggest that
> the deformation may have occurred during or shortly after
> the period of regional tilting that followed the
> deposition of Cretaceous rocks. The deformation almost
> certainly had to occur before any great thickness of
> Cretaceous rocks was removed by erosion."

Subsequent studies by Anderson (1978) and Anderson and Powers (1978) have
supplied some detail on the character of the salt deformation recognized
by Jones. Apparently the only part of the Castile that has not been

involved in significant plastic flow deformation is the lower or basal anhydrite, Anhydrite I (refer to site stratigraphy, section 4.3.2 for discussion of Castile stratigraphy). On the other hand, the lowest thick Castile salt member, Halite I, has undergone severalfold increases in thickness in some areas. Anderson (1978) presents a basinwide isopach map of the lower Castile Halite-I unit which shows an increase of thickness from a normal value of about 300-350 feet, as occurs in the area of the proposed WIPP site, to a value of 1,200 feet at the ERDA-6 location 5 miles north-northeast of the site. The isopach lines at this location define an elongate, sharply thickened bulge of the Halite-I unit, the long axis of which is about 12 miles long and is oriented parallel to, and on the basin side of, the buried Capitan reef front. Anderson's isopach map also shows numerous similar, slightly smaller elongate bulges, their long axes all about 3-1/2 times the length of their shorter ones, contained within a belt about 5 miles wide paralleling the basin side of the reef front. Since the anhydrite unit (Anhydrite I) underlying this deformed salt is not significantly deformed and does not itself rest on deformed rocks (Jones, 1973), the tops of these large salt mounds or bulges define what may be termed salt anticlines. These are not anticlines in the usual sense of the term because the top and base of the unit have totally dissimilar profiles; piercement associated with the term salt anticline is not generally present. This belt of salt anticlines, then, is the northwestward-trending belt of intraformational salt deformation recognized by Jones as occurring within the Castile and affecting strata above the Castile.

Structural detail within the large salt anticline located about 5 miles northeast of the center of the proposed WIPP site has been provided by cores recovered from the ERDA-6 hole drilled near the center of the anticline (Anderson and Powers, 1978). Stratigraphic interpretation made by Anderson and Powers from study of the core indicates that the middle anhydrite bed which overlies the salt has indeed been pushed up by the rising salt but has apparently acted as a semirigid confining blanket that was stretched upward like a flexible sheath; whether the anhydrite bed everywhere remained intact or was in places fully ruptured and

detached by extension is not known. What is displayed in the core is that most of the anhydrite, which actually consists of finely interlaminated calcite and anhydrite, was stretched by extensional microfracturing of the calcite laminae and in-filling of the fractures by mobilized calcium sulfate, which presumably was derived by diffusion or creep from adjacent anhydrite laminate. The process seems closely analogous to boudinage in metamorphic rocks, and could be viewed as a microboudinage structure brought about by the properties of finely laminated calcite and anhydrite when subjected to high shear stress under sufficient confining pressure.

Anderson and Powers (1978) find that Halite-I salt, together with streched Anhydrite II or middle anhydrite, have in their upward migration pushed aside both the overlying upper salt (Halite II) and upper anhydrite (Anhydrite III) beds in the manner of an intrusion, since the stratigraphy in the ERDA-6 hole passes directly from Infra-Cowden salt to Anhydrite II. The authors show that the overlying Salado beds, though not breached by the intrusion, are arched over it. It is therefore evident that the arching effect in beds of the Salado and even younger rocks referred to by Jones (1973) along the belt of deformation is in at least some cases due to the presence beneath these anticlines of a salt core which arose from the lower part of the Castile and partly intruded the overlying rocks.

In .addition to revealing the cores of many of the salt anticlines in the northwest-southeast belt of deformation described above, the subregional Halite-I isopach map (Anderson, 1978) shows numerous, sharply defined localized depressions at locations where the Halite-I salt is entirely missing from the section. In the central part of the basin, these "deep-seated sinks", as Anderson calls them, do not have obvious surface expression, and are not clearly related to shallower dissolution features--such as collapsed and uncollapsed domes, dissolution fronts, castiles, and collapsed outliers--which have been described and

documented elsewhere in the Delaware Basin region. Many of these isopachous depressions, some of which are defined by a single data point, may possibly be attributed to "deep dissolution" processes (Anderson, 1978), presumably acting from near, or perhaps below, the base of the salt section. A few appear, however, to originate within the Castile in salt zones above the lower halite. Anderson (1978) has proposed that some of them may have propagated vertically upward in the evaporite section to form known cylinders or chimneys of dissolved and collapsed debris. Alternatively, halite flow from adjacent regions into anticlines may account for these paired features as illustrated in Anderson and Powers (1978). (For description of these features in the Delaware Basin subregion and a discussion of their origin and development, refer to regional geomorphology, regional structure, and subsurface hydrology, Sections 3.2, 3.4, and 6.3).

Unlike the belt of salt anticlines having cores of Halite-I salt, the distribution of the localized pockets of missing, or greatly reduced thickness of, Halite I and higher Castile or Infra-Cowden halite that Anderson classifies as "deep sinks" is not confined to a belt above or adjacent to the Capitan reef but includes mid-basin areas as well, as illustrated by Figure 16 of Anderson (1978). The nearest of these deep mid-basin features to the proposed WIPP site as disclosed by the various halite isopach maps of Anderson (1978) occurs about 5 miles southeast of the site at the Eddy-Lea County line. This particular feature is not indicated to originate within the Halite-I zone of the Castile; rather, it appears to be a feature in the infra-Cowden salt (Anderson, 1978, Figure 7); compare this report, Figure 4.4-7, and refer to the section immediately following for additonal detail on the near-site structure.

It is not yet clear whether all or even some of these deeply buried mid-basin "sinks" identified by Anderson have a hydrologic origin subsequent to diagenesis and salt deformation. If they do, they may well be related to other collapse features in the Delaware Basin region as simply one manifestation of the same general process being seen at different levels of exhumation by erosion (Anderson, 1978, p. 58-59).

The concept that these diverse solution structures are being exhumed by present-day erosion suggests that the conditions of their formation in the geologic past may not be·present today in kind or to the same degree.

The nature of the deformation in the middle and upper part of the salt sequence above the Halite-I zone is recorded by the subregional halite isopach and structure contour maps of Anderson (1978) and Brokaw et al. (1972). The salt isopachs of Anderson (1978, Figures 4 through 10) clearly show that no other salt member of the evaporite sequence has experienced local flow deformation as severe as the Halite-I zone, nor are the "deep sinks" apparently as prevalent in the middle and upper part as they are near the base of the Castile. The Halite-II member of the Castile mirrors the same thickness trends exhibited by the Halite-I bed, but in a much muted manner. The infra-Cowden salt is the highest salt of the Castile-Salado sequence to exhibit marked thickening along the trend of the buried Capitan reef; it is also the lowest, or first, major salt bed to overtop and extend beyond the confines of the reef margin in this part of the basin. Even though no appreciable thickening of Salado salt above the infra-Cowden is apparent over the Capitan reef margin (Anderson, 1978), structure contours at the base of the Salado Formation (= top of Castile) (Jones, 1973) and on the 124-marker bed within the McNutt potash zone (Anderson, 1978) document that the Salado is indeed arched along the basinward edge of the reef and confirm that the salt deformation which occurs at depth around this margin had imposed an anticlinal structure on overlying strata, much as Jones (1973) described (also compare Brokaw et al., 1972 with Jones, 1973).

The evidence presented in this section regarding the subsurface structure of Castile and Salado halite beds and the spatial relationship of deformation structures with the bounding Capitan reef margin suggests that viscous flow of salt was initiated by post-depositional regional tilting and that the Capitan reef acted as a dam or abutment obstructing the eastward subsurface viscous flow of the lower part of the salt section which impinged against it. The salt piled up slightly, as a rug might when gently pushed against a wall, until lithostatic equilibrium

was attained with the superjacent rock mass. That larger, more dramatic salt plumes were not formed in the Delaware Basin, as they are known to occur in the Gulf Coast basin, for example, may be attributed to several factors. Two of these factors are the gentleness of the regional tilt and perhaps a relatively shallow depth of burial of salt. This would have resulted in lower lithostatic pressures and relatively higher viscosity of salt and hence greater resistance to migration. Evidence from structures nearer the site (e.g., WIPP 11, as discussed in the next section) indicates that the redbeds overlying the Salado are not always involved in the structure. This implies that some of the structures may be Permian in age.

No conclusive evidence establishing the exact time of regional tilting of the Delaware Basin has yet been found, except that it occurred after Chinle deposition (Late Triassic time) and before Ogallala time (uppermost Miocene). King (1948) has proposed that regional tilting took place in early to mid-Tertiary, concomitant with known Basin and Range faulting that occurred in the region west of the Delaware Basin, with relative upthrow of the Guadalupe and Delaware Mountains. Certain relations of Cretaceous strata, as described and discussed in section 4.5 on geologic history, and the long time span between Triassic and Late Cenozoic, suggest that there may have been earlier episodes of moderate regional tilting, of which the present eastward tilt is merely the resultant vector summation.

Geologic Structure of Salt at the Site. Within the context of the subregional relationships of deformation in the Castile-Salado evaporite sequence described and discussed in the previous sub-section, geologic structural features in the salt lying beneath the WIPP site may now be reviewed. Figures 4.4-6 through 4.4-10 show, respectively, structure contours on top of Castile, on the 124-marker bed of the Salado (within the McNutt potash zone in the middle part of the Salado), on top of the Vaca Triste member (top of McNutt), on the 103-marker bed, and on top of the Salado. Geological sections across the site area are shown on Figures 4.4-4 and 4.4-5. Gross structure of all evaporite horizons

reflects the regional easterly homoclinal dip of 50 to 100 feet per
mile. Salt deformation has modified this homocline to a variable extent,
generally more so in the Castile than in the Salado, inasmuch as the
lower halite beds of the Castile appear to have been the most mobile
(refer to subsection 4.3.3).

Seismic reflection surveys performed at the site (G.J. Long, 1977a,
1977b) were designed in part to record the relatively shallow Castile
horizons (for description of the seismic survey programs refer to Section
2.4); survey lines are shown on Figure 4.4-6 along with the well control
points. A reflecting horizon tentatively identified on the seismic
records as the top of Castile (located about 100 feet below the base of
the RH-zone) is contoured on Figure 4.4-6, which also shows preliminary
structural interpretations made from the seismic records. The contours
of Figure 4.4-6 indicate that the easterly regional dip of the Castile is
modified by a broad, northwesterly-trending ridge and saddle
configuration, with crest-to-trough separation of 2 to 3 miles and total
structural relief of up to 400 feet. According to this interpretation,
the normal gradient of bedding in this part of the Delaware Basin (about
100 feet per mile or 1 to 2 degrees to the east/southeast) may be
significantly greater and different in direction locally at the top of
Castile, directly beneath the proposed WIPP underground Facility.
Specifically, Figure 4.4-6, G.J. Long's preliminary interpretation of
structure on the presumed top of Castile about 100 feet beneath the
proposed RH-Zone level, indicates as drawn that local gradients may be as
great as 400 feet per mile (about 4 1/2 degrees) to the south and
southwest.

Northeast of the site, G.J. Long (December, 1977) shows a domal feature
in section 36, T. 31 S., R. 22 E of about 500 feet of structural relief
(Figure 4.4-6). ERDA-6, which was drilled in section 35 just west of the
crest of this feature, encountered a geopressured (artesian) brine
reservoir in the Castile. Studies of the ERDA-6 core establish that the
doming in this area is due to a salt anticline with a core of mobilized
Halite-I salt (Anderson and Powers, 1978); refer to Figure 4.4-4. This

dome is located within the belt of salt deformation flanking the Capitan reef (refer to Section 4.4.3.1 and Chapter 2, Figure 2-4) where such occurrences are to be expected. Artesian brine flow was also encountered by Belco No. 1 Hudson-Federal over a similar domal feature southwest of the site in the Los Medanos gas field area (Section 1, T. 23 S., R. 30 E)., although no salt-cored anticline of the type encountered at ERDA-6 is known to occur there.

The origin of the inferred northwest-trending structural ridge at the top of the Castile at the northeast edge of the Zone-II exclusion area has not yet been determined; it may be a depositional structure, or it may reflect possible past deformation by salt in underlying halite units. The steepness of the southward gradient suggests possible offset of one or more anhydrite beds as G.J. Long (1977b) has proposed. By contrast, a deep seismic reflection profile running southwest-northeast across the center of the site (Sandia Line 2, G.J. Long, 1977a; compare Figure 4.4-4) detected no anomalies at and below the lower part of the Castile across the trend of the ridge, whereas a significant anomaly is apparent in the same profile at the lower Castile-upper Delaware levels across the Los Medanos gas field southwest of the site (refer to Figure 4.4-4).

The more recent seismic investigation (G.J. Long, 1977b) also defined an area of poor data quality to the north of the site. From the ERDA-6 anomaly westward into Range 30 E. and southward into section 17 at the north edge of the the site, the quality and continuity of data as viewed on the seismic records deteriorate. This suggests the possibility of increased structural disturbance in this area, presumably caused, if real, by some form of previous salt deformation. Deterioration of the seismic record can also be brought about by anomalous or irregular transmission characteristics of the overlying medium. For example, near-surface structural disturbance, such as might be caused by dissolution in the Rustler, or the presence of an anomalously rigid near-surface layer such as caliche could change the quality of the seismic record (Dobrin, et al., 1954). A salt anticline at the northwest corner of Section 9, T22S, R31E, was suspected on the basis of seismic reflection data; drilling (WIPP 11) confirmed the structure was present

in the Castile. WIPP 11 did not show any brine or gas though drilled to the lower anhydrite of the Castile Formation. This confirms that anticlinal structures within the evaporites are not always associated with brine and gas. The apparent non-involvement of the redbeds in the structure may be interpreted, as noted in the previous section, as indicating a Permian age for this structure.

At the present time, while these seismic reflection records are undergoing further study and review, additional seismic reflection surveys are being undertaken in conjunction with exploratory drilling at critical locations. The results of these further investigations are to be reported at a later date.

Figure 4.4-7 presents 10-foot structural contours on the base of the 124-marker bed of the Salado, which is the deepest and most consistently reported horizon in the potash exploration grid. Figure 4.3-3 provides a stratigraphic orientation for the 124 bed, which is in the lower part of the McNutt, or middle Salado; at ERDA-9, the 124 marker is 470 and 1,020 feet, respectively, above the CH- and RH-level mining horizons selected for waste disposal. A uniform, gentle eastward regional gradient of 80 to 100 feet per mile across the repository is evident; there is no suggestion of a northwest-southeast ridge for the Castile (Figure 4.4-6). Two anticlines, or domal structures, are present, one centered near the ERDA-6 locality and the other at the Los Medanos gas field. At both structures, and only at these structures in the map area, exploratory drilling encountered artesian brine reservoirs in the Castile. No such structures are indicated by the 124-marker bed contours to be present within the site exclusion area.

The comparison of Figures 4.4-6 through 4.4-8 to each other indicates that structural disturbance is present within the Castile that is not reflected upward to any great extent. Structural relief on the upper beds is a fraction of that of the Castile. The inferred faulting at depth has not been confirmed by drilling, seismic data and drilling in the area indicates salt remains in the Castile rather than disappearing as any consequence of the faulting.

Two depressions in the 124-marker bed are indicated to occur near the site (Figure 4.4-7). In Lea County in section 31 at the east edge of the map there is a depression with probably less than 100 feet of closure; this is the same feature identified by Anderson (1978) as a possible "deep sink", and apparently is related to a greatly reduced or missing section of the Infra-Cowden (Anderson, 1978, Figure 7). It is nearly 4 miles from the edge of the Zone-II exclusion area. A second depression of the 124-marker bed horizon is centered about a mile north of Zone-II exclusion area, at the southwest corner of section 9. A single-hole anomaly with 50 feet structural closure, it is not reflected by any isopach anomalies in the Salado (Figures 4.3-4 through 4.3-7), nor does it correspond to any evident structural feature higher in the Salado (compare figures 4.4-8 thru 4-4-10). Salt isopach maps of Anderson (1978) indicate no anomaly at this location, nor does the recent seismic reflection work by Long (1977b) show subsurface disturbance of horizons near this point. These negative indications suggest the feature might have developed contemporaneously with depostion and is not significant to the WIPP site. Nevertheless, results obtained from exploratory drilling will be noted and applied if relevant. Higher levels within the Salado are contoured in Figures 4.4-8 and 4.4-9 (refer to Figure 4.3-3 for location in section). Within the area contoured on these Figures, which is somewhat less than the area covered by Figures 4.4-7 and 4.4-10, the two maps are virtually identical in configuration and gradient and exhibit no significant structural features other than the regional gradient.

Structure contours on top of the Salado, or at the contact between the Salado and the Rustler, are displayed in Figure 4.4-10. It should be recalled (Section 4.1) that there is less data control for the top of the Salado than for deeper horizons in the Salado, because potash industry exploration practice normally includes coring and geophysical wireline logging only for horizons below the top of the Salado. Reliable control for top of the Salado is therefore provided mainly by those potash exploratory holes commissioned by DOE. Outlined by contours on Figure 4.4-10, the same domal feature associated with the salt-cored anticline

and brine reservoir encountered by ERDA-6 is still in evidence. The change from regular contours in Range 31 E. to a more irregular configuration in Range 30 E. is due to dissolution at the top of Salado, and is also reflected in the upper Salado isopach map (Figure 4.3-7). (Refer to Section 6.3 for a discussion of dissolution processes in the site area.). A 70-foot depression is apparently recorded by an industrial potash hole (Hole F-91) a mile northeast of the Zone-II exclusion boundary; two similar but smaller features occur a couple of miles farther northwest. Since there is no geophysical or core record available for hole F-91 at the top of the Salado, it may well be that the first encounter of Salado salt is simply not recognizable in the record for this particular hole.

Assuming the record is accurate, however, it is not known at this time whether the apparent depression is a feature of sedimentary origin, although the horizon is a contact zone between two formations, or whether the feature is related to post-depositional solution processes. It should be noted that this apparent depression is about a mile east of, and structurally about 700 feet higher than, a similar depression contoured on the 124-marker bed (Figure 4.4-7, discussed above). However, no such anomalies have been detected on intervening horizons in the Salado (Figures 4.4-8 and 4.4-9). Furthermore, a line connecting the two apparent depressions would have a maximum slope of less than 8 degrees. The available evidence therefore indicates that it is unlikely that there is a physical continuation of this assumed depression at the top of the Salado to horizons lower in the evaporite sequence. On the other hand, there is an approximate spatial coincidence of this depression with a shallow (less than 30 feet of relief) topographic depression at ground surface containing mapped playa deposits (Figure 4.2-4). Resistivity profiles (Elliot, 1977) indicate only minor surficial disturbance attributable to shallow basin fill with no indication of probable subsurface collapse structure.

Preliminary interpretation of seismic reflection data (Long, 1977b) near the top of the Salado indicated the possibility of faulting, with a possible displacement of 100-250 feet, less than one mile north of ERDA 9. Consequently four holes (WIPP 18, 19, 21, 22) were drilled bracketing the possible location of the faulting (see Figure 2-10) to validate the interpretation. The resulting borehole data shows no apparent faulting in this region. The data collected by seismic reflection for that particular seismic program are not apparently useful for primary interpretation of the stratigraphy at the top of the Salado. Revision of field parameters in future surveys may permit more secure interpretation of data for such shallow reflectors.

A preliminary assessment of the proposed WIPP site relative to structural features presently indicated in the Salado and Castile salt formation enclosing the selected CH- and RH-storage levels can now be stated. *Structure contour maps of various horizons in the Salado Formation indicate a uniform easterly regional structural gradient of about 80 to 100 feet per mile across the limits of the proposed storage facility,* with little indication of the presence of any significant structural anomalies. Plastic deformation and buckling associated with salt migration or flowage has apparently not occurred in the Salado in the geologic past to the extent that it has in the lower levels of the underlying Castile Formation. Areas in the region in which artesian brine reservoirs have been encountered are associated with thickened salt sections and salt-cored anticlines in the Castile. However, a thickened salt section and salt cored anticline was drilled in WIPP 11 (Sec. 9, T. 22 S. R. 31 E.) without encountering fluids. Further, the occurrence of these reservoirs appears to be correlative with consistent structural highs, delimited by structure contours of successive horizons in the overlying Salado Formation. No such structural features are recognizable within the limits of the WIPP storage facility on any of the Salado horizons contoured; in fact, the site, if anything, appears to be in a slight structural saddle.

Among aspects needing further investigation, perhaps the most significant is a determination of the extent to which the upper levels of the Castile closest to the repository levels have been deformed by any salt deformation that may have taken place in the lower halite units of the Castile. There is no suggestion here of deformation of the type associated with artesian brine reservoirs. Seismic reflection techniques suggest, however, that a certain amount of flexure occurs in the upper levels of the Castile beneath the proposed limits of the repository, which could possibly affect local structural gradients in the lower part of the Salado. Faulting on the Castile reflector has also been inferred. Investigations are in progress to further define and delimit structural configurations near the top of the Castile and the extent to which these structures may be reflected within the lower part of the Salado where excavation of the RH- and CH-levels is presently planned. This knowledge will permit a more detailed assessment relative to the location, design and construction of the storage facility but is not believed necessary for a general qualification of the site area.

4.4.4   Shallow Structure

As discussed in Section 4.4.1, in the Los Medanos area a distinction may conveniently be made between structural features exhibited by rocks occurring above unleached salt beds and structural features of all other strata. The distinction may be made because rocks above the Salado at the site have at one time or another in the geologic past been subject to weathering processes and hence might display secondary structures related to surficial dissolution and subsidence that would not have been imposed upon deeper strata. Accordingly, shallow structures at the WIPP site have a potential for greater irregularity and complexity than those which occur at depth. "Shallow structure" is here defined to include the Rustler Formation which extends to a depth of about 850 feet beneath the center of the site (refer to Figure 4.3-3). Figures 4.4-11 through 4.4-15 are structure contour maps on Rustler and higher strata, constructed from the data obtained from wireline geophysical logging of holes drilled at the WIPP site to assess potash reserve potential.

Shallow Subsurface Structure. Structure contours on top of the Culebra
Dolomite member of the Rustler Formation are shown on Figure 4.4-11
(refer to Figure 4.3-3 for location in site geologic column). The
Culebra is the most productive aquifer in the Rustler Formation. The
closely spaced contours in the southwestern quadrant of the map define a
slope of about 80 feet per mile eastward (compare Figure 4.4-9). The
wider spacing of contours in the eastern half of the map is anomalous
with respect to regional structure and marks the increasing amount of
halite preserved progressively eastward in the Rustler below the Culebra
member. A similar configuration is evident on top of the Rustler, Figure
4.4-12: again the regional gradient appears in the southwestern
quadrant, while an anomalously gentle eastward gradient, in some places
even reversed, signifies thickening due to an increasing content of salt
preserved from dissolution (see Figure 6.3-7). Virtually the same
pattern is observed with respect to the structure contours of the Magenta
Dolomite member (Griswold, 1977). Isopachs of the Rustler (Figure 4.3-8)
show the gradient and amount of eastward thickening. A broad, shallow
depression with 30 to 40 feet of closure near hole P-11 appears near the
northeast corner of the site on both the Magenta and the top of Rustler
levels, but not on the Culebra. Possibly it represents an area of
greater dissolution in the upper part of the Rustler, since Rustler
isopachs show the Rustler is not thickening eastward at this particular
location (Figure 4.3-8)

The area in Figures 4.4-11 and 4.4.-12 wherein the regional gradient is
reflected by the Rustler structure contours identifies the area where the
Rustler has been leached of most of its salt, and hence presumably where
maximum settlement of overlying rocks has occurred, assuming, of course,
that no dissolution took place prior to deposition of overlying Dewey
Lake strata. Jones (1973) supplies a subregional structure contour map
of the Dewey Lake-Rustler contact and recognizes that the unevenness it
shows is due to the added complexities of subsidence (Jones, 1973). A
low resolution seismic reflection survey conducted at the site (C.B.
Reynolds, 1976) suggests the presence in the Rustler of more localized
and higher amplitude irregularities than would necessarily be defined by

data points in Figure 4.4-12. However, the known top-of-Rustler data points from potash exploration shown on Figure 4.4-12 are in nearly complete disagreement with elevations of this horizon interpreted from the shallow seismic data (Reynolds, 1976). It would appear that the reflections of horizons in the Rustler obtained by this shallow survey method are not of sufficient quality to provide a basis for making structural interpretations. The subsurface data collected to date indicate that the dissolution of salt in the Rustler has not been accompanied by the development of highly irregular subsidence structures in the overlying strata at the WIPP site.

Proceeding higher in the section, the top of Dewey Lake Redbeds (Figure 4.4-13) is the first horizon that does not reveal the eastward gradient of the Delaware Basin that all lower horizons show. The Dewey Lake surface across the site area is undulatory, possibly reflecting to some extent original undulations in the uncomformable Dewey Lake-Santa Rosa contact mentioned by Jones (1973). A broad depression near hole P-11 with about 50 feet of closure is in the same location as a similar depression on the underlying Rustler surface (Figure 4.4-12). Subregional structure contours of Jones (1973) indicate considerable irregularity of the Dewey Lake surface as is also suggested by Figure 4.4-13, but overall the surface slopes northeastward. Isopachs of the Dewey Lake Redbeds (Figure 4.3-9) disclose that the west-trending slope of the Dewey Lake surface at the west edge of Figure 4.4-13 is the result of the Late Tertiary erosion which is associated with the development of Nash Draw and which completely truncates the Dewey Lake in Nash Draw itself (Brokaw, et al., 1972). Continuation of this erosion surface to the east across higher strata is quite obvious in Figure 4.4-14, contoured on the surface of the Santa Rosa Sandstone. Structure contours of the Gatuna surface (below Mescalero caliche) (refer to Figure 4.4-15) show virtually the same configuration as does the Santa Rosa surface on the east and the Dewey Lake surface on the west, indicating that the thin Gatuna veneer was deposited over these surfaces after erosion occurred.

Surficial Structures. Extensive surficial deposits of dense sand all but
preclude the observation of surface geologic structure at the WIPP site
(Figure 4.2-4; refer to maps by Bachman in Jones, 1973, and by Vine,
1963). The nearest measurements of bedding orientation appearing on
Bachman's map are at the edge of The Divide, some 6 miles northeast of
the center of the proposed WIPP site. The Nash Draw geologic quadrangle
map by Vine (1963) shows no such measurements, for Vine recognized that
dissolution of salt in rocks beneath Nash Draw had caused widespread
slumping of the surface rocks. Thus, they are not indicative of original
structures. He documents places where not only salt but considerable
gypsum has been dissolved. In Nash Draw the Magenta and Culebra dolomite
members of the Rustler are observed in contact, whereas normally, when
leached of salt only, they are separated by 120 feet of gypsum (Vine,
1963). In mapping the overlying Dewey Lake Redbeds, he noted that,
        "exposures of the redbeds are commonly tilted or draped into simple
        structures as a result of the collapse and swelling that accompanies
        solution and hydration of the underlying evaporite rocks. Some
        exposures...along the margin of Nash Draw show a downwarping into
        the topographic depression that is presumably the result of removal
        of soluble rocks. For this reason, strike and dip readings, even on
        the very apparent parallel stratification of the redbeds, do not
        necessarily reflect the structure of older rocks" (Vine, 1963).

Jones (1973) affirms that "it is impossible to piece together a
meaningful stratigraphic section from study or mapping of outcrops" in
Nash Draw. "The (exposed) rocks are porous, friable, and loose-textured,
and all are strongly jointed, cavernous, and locally brecciated.
Stratification is obscured or completely obliterated, and the attitude of
bedding can rarely be determined with any degree of confidence" (Jones,
1973, refer also to discussion of Rustler stratigraphy, Section 4.3.2).
It should be emphasized that this surface evidence of jumbled structure
is restricted to Nash Draw and has not been described for the area
between Livingston Ridge and the WIPP site.

No surface faults have been mapped within 5 miles of the center of the
WIPP site; faults that are mapped at the surface are distant and are
plainly related to collapse features. Bachman's (1976) mapping east of
the WIPP site shows no surface faults. The nearest faults mapped by Vine
(1963) involve Rustler offsets in Nash Draw about 9 miles southwest of
the site in section 18, T. 23 S., R. 30 E. Although he recognized these
faults as being produced by karst processes, involving areas of circular
or semicircular rock deformation up to a few thousand feet in diameter,
he was unsure of how to account for the fact that some were positive

topographic features or domes (Vine, 1960; Vine, 1963). Anderson (1978) believes that they may be the eroded remnants of former caverns in salt whose roofs had collapsed; the collapsed debris then remained as the upper part of the surrounding salt was partially dissolved and carried away (refer to regional geomorphology, Section 3.2).

Livingston Ridge, 4 miles northwest of the site, marks the edge of Nash Draw, a broad swale developed by a combination of erosional and dissolution processes. Bachman (1974) mapped occurrences of caliche in the region around the WIPP site, and noted the structural relationship of the caliche to depressions such as Nash Draw (refer to structure contour map of the Mescalero caliche in Bachman, 1976). He concludes that,

> "major solution and collapse preceded and followed the accumulation of the Mescalero caliche in Nash Draw..." (Bachman,1976). "The Mescalero caliche probably formed on an undulatory stable surface. ...Along Livingston, Quehada, and Nimenim Ridges...the caliche dips abruptly into the adjacent depressions. The crowding of contours, the presence of fractures, and the uniform thickness of the caliche along these ridges indicate that Nash Draw Draw and Clayton Basin were subjected to collapse after the formation of the Mescalero caliche. On the other hand... the uniform spacing of the contours in the area of the Divide between Livingston and Antelope Ridges suggest that this surface...approaches its original slope" (Bachman, 1974).

Thus, surface mapping and structural interpretations have found no evidence of any anomalous structure in the vicinity of the WIPP site east of Nash Draw that might be indicative of significant differential subsidence of underlying strata. Such surface features and structural relationships that are exposed in the area reveal no indication of any surface faulting at the WIPP site.

In summary, surface and shallow subsurface structure in the vicinity of the WIPP site has presumably been modified to some extent by loss from dissolution of 100-200 feet of salt originally present in the Rustler Formation. The resulting subsidence and settlement would not be expected to have progressed in a perfectly constant and uniform manner over an area of several square miles. On the other hand, there is no indication of the presence of the types of chaotic structure encountered in the Rustler in Nash Draw, as described by Jones (1973) and by Vine (1963).

In the Nash Draw area, the widespread collapse structures observed are due to extensive dissolution in the Salado rather than in the Rustler alone. Further, the successive erosional stripping of Santa Rosa, Dewey, and Rustler strata westward into Nash Draw, coupled with the general eastward regional dip of the evaporite strata, indicates that the amount of overburden above the level of dissolution actually was much less in Nash Draw than it presently is east of Livingston Ridge. Thus the potential for significant differential subsidence to have occurred beneath the Los Medanos site seems to have been minimized by the restriction of salt dissolution to beds within the Rustler and by the relatively high overburden pressure which would have tended to provide more uniform settlement as salt was being removed. Stratigraphic data from potash holes drilled in the site area indicate no major irregularities in horizons above the Salado (Figures 4.4-10 through 4.4-15).

4.4.5   Summary and Conclusions

Jones (1973) concludes that:

> "The structure of the Los Medanos area is basically simple and the rocks are, for the most part, only slightly deformed. Nevertheless, the rocks have been tilted, warped, eroded, and subroded (i.e., subjected to subsurface solution), and discrete structural features can be recognized. These include: (1) structural features of regional extent related to Permian sedimentation, (2) intra-formational folds of limited extent related to "down-the-dip" movement of salt under the influence of gravity and weight of overburden, and (3) subsidence folds related to warping and settling of rocks to comform with the general shape and topography of the surface of salt in areas of subrosion...

> "On the basis of available geological information, the salt deposits of (the) Los Medanos area seem in many ways to constitute a suitable receptacle for use in a pilot-plant repository for radioactive wastes. The deposits have thick seams of rock salt at moderate depths, they have escaped almost completely undamaged from long periods of erosion. The deposits are only slightly structurally deformed, and they are located in an area that has had a long history of tectonic stability."

Information that has been developed in the succeeding five years of investigations has little altered that assessment relative to the

structural and tectonic conditions present at the WIPP site. Based on exploration accomplished to date, a series of structure contour and isopach maps is presented for rocks ranging in age from Devonian to Pleistocene. This and other information indicates that tectonic faulting and warping of rocks in the site vicinity seems to be restricted to Pennsylvanian and older rocks and to have predated Permian evaporite deposition; certain minor faulting within the thick Permian section appears to have occurred contemporaneously with sedimentation. Deformation related to salt flowage has occurred primarily in the Castile Formation beneath the Salado, and has perhaps modified the regional easterly gradient to 80 to 100 feet per mile to some extent at the level of the storage horizons near the base of the Salado. Areas in the vicinity of the site in which artesian brine reservoirs have been encountered are associated with thickened salt sections and salt-cored anticlines in the Castile, but no such structural features are recognizable within the limits of the WIPP storage facility on any of the Salado horizons contoured. The site, if anything, appears to be in a slight structural saddle, a condition considered to be a favorable criterion for site selection. Dissolution of bedded salt beneath the site has been resticted to horizons within the Rustler Formation; there is no evidence that the resulting settlement produced any significant structural irregularities or collapse features in the overlying strata within the area of the WIPP site. Investigations are continuing to further define the extent to which salt deformation in the Castile may have affected the structural configuration within the lower part of the Salado where excavation of the RH- and CH- levels is presently planned. These investigations will permit a more detailed assessment of the optimum location, design, and construction method of the storage facility.

4.5   Site Geologic History

Three main phases characterize the geologic history of the WIPP site subsequent to the original establishment of a granitic basement intrusive complex between a billion and a half-billion years ago, forming the cratonic crust beneath the site. The first phase, of at least 500

million years' duration, was a time of uplift and erosion of all pre-existing Precambrian sedimentary and metamorphic rocks which may have once been deposited or formed in the site area, eventually exposing the deep-seated igneous rocks. The second phase was characterized by an almost continuous marine submergence lasting about 225 million years, wherein shelf and shallow basin sediments slowly accumulated. This depositional phase culminated in a comparatively rapid accumulation of over 13,000 feet of sediment within a relatively brief period lasting 50 to 75 million years, toward the end of which time thick evaporite beds, mainly rock salt, were deposited. Uplift and subaerial conditions next returned to the site in the third and final phase, and have persisted some 225 million years to the present, with the exception of a brief marine inundation in the middle of that span of time. Periods of terrestrial deposition alternated with erosional episodes, so that a series of nonmarine deposits separated by unconformities blanket the evaporite beds at the site.

Since the first phase mentioned above really reflects the absence of any evidence in the geologic record at the site for specific events which may have occurred during the latter part of Precambrian time, the following review of site geologic history considers only post-Precambrian events. Additional discussion of geologic history in a regional context is contained in Section 3.6. The reader is referred to Figure 4.3-2 for stratigraphic orientation.

The Precambrian basement terrane, exhumed during the vast erosional regime of late Precambrian time, was first submerged at the start of Ordovician time, with deposition of the basal Bliss Sandstone. From Ordovician time through Pennsylvanian time in the southeastern part of New Mexico where the site is located, marine sediments accumulated slowly but continuously. Shelf and shallow basin deposition progressed marginally to or within broad, nearly flat subsiding basin areas of the Tobosa Basin that formed northern arms of the Ouachita trough (Brokaw et al., 1972).

The dominantly carbonate section (dolomite and limestone) from Ordovician through Mississippian time (a span of roughly 180 million years) indicates stable shelf and gently subsiding shallow basin environments. A sandy clastic sequence in mid-Ordovician time (Simpson Group) may perhaps signify mild uplift of a landmass ancestral to the Central Basin Platform. Although an Ordovician-Silurian unconformity has been recognized elsewhere in the region (refer to Section 3.5), none is evident in the site area. The first significant post-Cambrian emergence or marine regression occurred during the Early and Middle Devonian, but the area apparently was a broad plain never elevated much above sea level. Marine waters reinvaded the area in Late Devonian time, accompanied by unconformable deposition of distinctive black shale (Woodford Shale), followed by a return to carbonate accumulation in Early Mississippian time. Continued subsidence of the area was accompanied by deep-water deposition of dark, silty shale (Barnett).

The end of Mississipian time heralded significant regional warping and tectonic activity. Major faulting accompanied upwarp of positive tectonic elements in the region, including the Central Basin Platform area (refer to Section 3.6). These positive land masses provided a more abundant supply of clastic detritus which was carried into adjacent marine basins and deposited on moderately warped, tilted surfaces. At about this time, the tectonic framework of the Delaware Basin began development. The site area received sandy Lower Pennsylvanian Morrowan sediment and more or less continuously accumulated sediment over the remainder of the period as repeated basin margin faulting caused periodic, strong uplift of the bordering platforms and some warping within the basin. By the end of Pennsylvanian time, differential tectonic upwarp had ceased (refer to Section 3.6).

At the WIPP site, sedimentation was continuous from Pennsylvanian into Early Permian time. In contrast to Pennsylvanian deposition, however, the Delaware Basin subsided at a greatly accelerated pace during Permian time, partly by downwarp and partly by downfaulting along pre-existing basin margin faults. Perhaps the previous Pennsylvanian tectonic

activity had predisposed the Delaware Basin to more rapid downwarping; at any rate, a thickness of about 9,000 feet of Wolfcampian, Leonardian, and Guadalupian sediment was deposited over little more time than had been required for about 2,500 feet of Pennsylvanian strata to accumulate. The sequence tended to progress from shale to basin limestone to sand, possibly related to encroachment of the basin margin reef deposits, as the central part of the basin continued to subside more rapidly than the shelf areas. Although basin margin reef buildup was active in both Leonardian (Bone Springs) and Guadalupian (Delaware Mountain) time, it was not until the latter part of Guadalupian time that continuous, massive reefs, accreting rapidly to keep pace with continued basin subsidence, virtually encircled the basin. This process culminated with the formation of the massive Capitan reef limestone, which approaches to within 9 miles of the site and delimited the Delaware Basin at that time. Although for many millions of years previous to this time, various lesser reef deposits had been encroaching inward upon the basin, the Capitan reef defined a more restricted area of the Delaware Basin than was ever the case previously. At the WIPP site, the basin facies equivalent to the Capitan reef is the Bell Canyon Formation, mostly siliceous sandstone in lithology. When the Capitan reef eventually encircled the basin at the close of Guadalupian time, the top of Bell Canyon was 1,000 to 1,500 feet lower in elevation than its facies equivalent high on top of the reef only a few miles away. At this time the reef had closed off free access of the open sea to the Delaware Basin, setting the stage for the ensuing precipitation of the Ochoan evaporites.

As the seawater in the salt basin of Castile time evaporated to brine, precipitation of anhydrite and limestone, followed by anhydrite and finally salt (halite) occurred. Several major incursions of seawater must have refilled the basin, for there are a number of thick, laminated anhydrite-calcite beds separated by thick salt members. Because this salt basin was shielded from clastic sediment deposition by high bounding reefs, the Castile evaporites tend to be the most chemically pure of the Ochoan evaporites. Eventually the Castile evaporites filled the basin

enclave to the level of the top of the sheltering reef masses. The Salado salt then extended over the top of the still subsiding reefs, burying them and extending outward into the Permian Basin. Although the region continued to subside, reef organisms could not survive in the briny environment, and burial of the reefs by the Salado resulted in the final disappearance of the Delaware Basin as a paleogeomorphic entity.

The Salado, inasmuch as it formed in a broad, regionally extensive brine basin not bounded by protective reefs, was more susceptible to clastic influx, and therefore its halite deposits are generally somewhat less pure than those of the Castile. Nearly 2,000 feet of mostly rock salt accumulated before an increase of clastic influx accompanied by a decrease in salinity caused deposition of Rustler lithologies to occur (anhydrite more dominant with significant thicknesses of clastic rocks). Finally in a shallowing sea or on marginal mudflats, the Dewey Lake Redbeds were deposited as subsidence gradually ended, covering the salt beds with a thick clastic blanket. This was the final episode, about 225 million years ago, of a remarkable accumulation of marine deposits which had been first laid down in Ordovician time.

No Lower Triassic strata occur at the WIPP site, nor are they known in the region (refer to Section 3.6.4). It was a time of general regional epeirogenic uplift and erosion; only a slight angular unconformity is present between Dewey Lake strata and overlying strata (Jones, 1973). According to Bachman (1974), "it is possible that some dissolution of Permian soluble rocks occurred in the periods of uplift during Triassic time", but direct evidence of this has not been found in southeastern New Mexico. Isopachs of the Dewey Lake where it is covered by Upper Triassic rocks indicate a thickness of about 500 feet. Furthermore, Jones (1973) indicates the pre-Upper Triassic Dewey Lake thickness decreases northwestward. Although the actual original protective thickness of the Dewey Lake westward across Nash Draw and over to the Pecos is now indeterminate due to later removal by erosion, it is interesting to speculate whether some dissolution features and processes presently observed there may not have had their beginning in Early Triassic time, over 200 million years ago.

In Late Triassic time inland basin streams laid down floodplain deposits of the Santa Rosa and Chinle Formations, the first record of non-marine deposition in the area. The total original thickness of Late Triassic deposition is not known, because of an erosional surface on the Triassic of the region. The first erosion to have acted upon the Triassic rocks lasted from the close of Triassic time to Late Early Cretaceous, a period which may have lasted as long as 90 million years. In latest Early Cretaceous time (Washita, about 100 m.y.b.p), a shallow sea transgressed across the site area and deposited an unknown thickness of marine sediments. Later erosion removed all but slumped or sunken residual fragments of a presumably once extensive Cretaceous cover.

These Late Triassic-Early Cretaceous relationships hold important implications for the history of both salt dissolution and salt deformation in the Delaware Basin. As Bachman (1974), has stated,

> "In central and southeastern New Mexico where Triassic rocks are
> preserved they are overstepped by rocks of Cretaceous age. In
> general, these Cretaceous rocks rest on progressively older rocks
> toward the south and southwest. After cutting across the wedge edge
> of Triassic rocks, the Cretaceous rocks rest on Permian or older
> strata at many places in southern New Mexico."

By plotting locations of these small Cretaceous outliers and noting the age of rocks on which they occur, Bachman (1976) reconstructed an approximation of the Jurassic erosion surface, showing where Permian rocks were unprotected by Triassic cover and exposed to erosion sometime during the Jurassic-Early Cretaceous erosional interval. The sketch shows that Permian rocks along the western edge of the Delaware Basin were exposed to the atmosphere and presumably eroded during Jurassic time. "Probably some dissolution of Permian salt and gypsum occurred in the western part of the Delaware Basin at this time" (Bachman, 1976). To the extent that "deep dissolution" features are recognized today in salt at depths of several thousand feet below the surface (Anderson, 1978), it seems quite likely that similar features would have been present and developing at comparable depths during the Jurassic erosion 100-190 million years ago. Further, considerable dissolution effects could have been initiated or accelerated during the Cretaceous at times preceding or

subsequent to Washitan submergence, particularly in view of the humid or even tropical conditions known to have characterized the Cretaceous in North America.

A second aspect of the above-described Triassic-Early Cretaceous relationships relates to the history of salt deformation at the WIPP site. Prior to Cretaceous submergence, Jurassic erosion had bevelled the blanket of Upper Triassic Dockum sediments to a wedge that pinched out westward across the Delaware Basin. Evidently, eastward regional tilting had occurred, at least by the end of Jurassic erosion. Since this tilt would have involved the underlying salt beds, some salt flow and deformation may have occurred at this time. Deformation may even have continued during the time in which the region was submerged by the Cretaceous marine incursion and was later covered by an unknown thickness of marine strata.

Although the duration of the Cretaceous epicontinental marine transgression is not precisely known for this area, probably early in late Cretaceous time the sea withdrew; during the remainder of Late Cretaceous time the area was probably of low relief and only slightly above sea level (Hayes, 1964). No early or middle Tertiary deposits are known in the site area, so that geologic events near the site over the 60 million years after the end of Cretaceous time and the beginning of Pliocene time are poorly known. Major uplift probably took place concurrent with the Laramide orogeny that occurred farther north and west. "Probably late in the Cretaceous Period or very early in the Tertiary Period the entire region was elevated by broad epirogenic uplift and was tilted slightly to the northeast" (Hayes, 1964). The Cretaceous rocks were eroded to expose Triassic rocks in the eastern half of the Delaware Basin and Permian rocks in the western half of the basin. This erosion again subjected Permian salt to further dissolution (Bachman, 1974), and produced a second erosional truncation of Late Triassic Dockum sediments (Jones, 1973). In Oligocene time (35 m.y.b.p.), lamprophyre

(basaltic) dikes were intruded in the subsurface along a northeast-southwest dike trend which occurs about 8 miles northwest of the site; this is the only post-Precambrian igneous rock known in the New Mexico part of the Delaware basin.

By Late Miocene time conditions became less arid and eastward-flowing alluvial distributories began to deposit sandy and gravelly sediment over an irregular erosion surface. Deposition of these sediments, referred to as the Ogallala Formation, began as early as 12 million years ago and ended before the close of Pliocene time, perhaps as early as 4 million years ago (Bachman and Johnson, 1973). The nearest Ogallala occurrence is at The Divide, 6 or more miles northeast of the site, where its maximum thickness is only 27 feet, which is considered to represent an original, or depositional, thickness (Bachman, 1974).

It is not known whether any Ogallala sediments were ever deposited at or west of the site, or to what extent dissolution subsidence features were geomorphically expressed in Nash Draw and southwestward within the Delaware Basin by the time the erosional plain associated with Ogallala deposition had developed. Bachman (1976) states that, "by the end of Ogallala time the High Plains surface was probably continuous westward across the present Pecos River drainage to the backslope of the Sacramento Mountains" in the region north of the Delaware Basin but that "the Ogallala Formation may not have been deposited in the Pecos depression southward from Carlsbad.... Although some form of major drainage may have been present in the vicinity of the modern Pecos River during pre-Ogallala time, (Bachman's) work does not support an interpretation of thick Ogallala fill southwest of The Divide" (Bachman, 1974). Nevertheless, Bachman (1976) believes "much of the lowering of the Pecos River Valley has occurred as a result of dissolution of evaporites in the underlying Permian rocks since Ogallala time."

When Ogallala deposition ceased in Late Pliocene time, the region around the site was tectonically stable and the climate was arid to semiarid: during this time a caliche caprock developed on the Ogallala surface.

Renewed erosion took place during early Pleistocene time following Basin-and-Range tectonic activity and rejuvenation of the Rocky Mountains. At the site the effect of this uplift and increased rainfall was to cause a renewal of erosional and dissolutional activity. Active stream erosion in the site area caused a third erosional surface to be incised into the Late Triassic sediments; in Nash Draw, this erosion cut deep into the Dewey Lake Redbeds at the same time that Nash Draw was actively collapsing due to subsurface dissolution. Eventually these channels and sinks were filled with the Gatuna Formation, which was derived from reworked Ogallala and older sediments, and a veneer of Gatuna material was deposited across the Los Medanos Mid-Pleistocene surface. Bachman considers that this erosion and deposition occurred "during the most humid climatic conditions that have existed in the area since Ogallala time" (Bachman, 1974), and tentatively correlates the Gatuna deposition with Kansan time, which ended approximately 600,000 years ago.

After deposition of the Gatuna Formation, a caliche (Mescalero caliche) caprock formed on the Gatuna surface in a semiarid environment during an interval of climatic and tectonic stability (Bachman, 1974). Regional climatic considerations lead Bachman to assign a mid-Pleistocene age for the Mescalero caliche, which he tentatively correlates with the Yarmouth interglacial stage, or about 600,000 years before the present (refer to Section 4.3.2).

Since the formation of the Mescalero caliche some half a million years ago, little geological activity has occurred at the WIPP site. In the Pecos Valley a number of Pleistocene surfaces can be identified which provide some clue to the evolution of the regional drainage system (refer to Regional Geomorphology, section 3.2.2.1). At the edge of Nash Draw along Livingston Ridge, the Mescalero caliche is fractured and draped into the draw, indicating that Nash Draw was subjected to some dissolution and subsidence in the half million years subsequent to formation of the caliche, presumably during the more pluvial periods of Illinoian or Wisconsinan glaciations. Similar evidence exists along

other slopes and in sinks within and adjacent to Nash Draw, but is not observed away from Nash Draw in the direction of the site. Perhaps the most obvious activity at the site has been the formation of a nearly continuous cover of windblown sand and sand dunes in Late Pleistocene and Recent time, believed to have been supplied from the east rather than from the Pecos area to the west. The sand apparently was eroded from the Ogallala in wet climatic intervals and was blown westward across the area during dry intervals.

4.6   SUMMARY

Investigations of the site geology for the WIPP define the geology as it is presently known for determination of the general suitability of the site. Many of the factors in Chapter 2 are addressed here in Chapter 4. The ultimate acceptability of the site for a repository may only come after the detailed geology of the site is known from underground workings.

The site physiography and geomorphology shows the site to have been relatively stable through the last 500,000 years or more. The development of the Mescalero caliche, and the lack of developed drainage are indicative. Localized sinks or basins are surficial.

Site stratigraphy and lithology including the evaporites shows continuity from the regional setting. The evaporites at the site are about 3500' thick, and include the Castile Formation, Salado Formation and Rustler Formation from bottom to top. The subsurface structure at the WIPP site within the evaporites is salt deformation three miles north of the site center and possibly also one mile north. The structure three miles north involves deformation of the Castile and lower Salado; drilling (WIPP 11) showed the deformation to be upward bulging of salt, but no severe displacements and no brine or gas were encountered. The structure one mile north appears to be smaller, and is of concern mainly for design of underground workings. It is being investigated further for this purpose. Within the site structure contours on evaporite horizons show areas with slight closure; the range of precision of data from industry

sources and natural variability can probably account for these features though slight deformation or dissolution could also be invoked. No surficial faults are known at the WIPP site.

The potential repository zones are located in the Salado Formation at depths from 2730' to 2620' (remote handling) and 2176' to 2074' (contact handling). These beds are chosen on the combined basis of purity, depth, thickness, mutual separation, and depth below the potash zone.

The geological history of the site is encompassed in the geological history of the region.
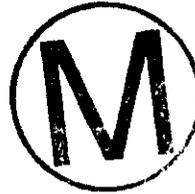
4.7 REFERENCES

Adams, J.E., 1944, Upper Permian Series of Delaware Basin, west Texas and southeastern New Mexico: Am. Assoc. Pet. Geol. Bull., v. 28, p. 1592-1625.

Adams, J.E., et al., 1939, Standard Permian section of North America: Am. Assoc. Pet. Geol. Bull., v. 23, p. 1673-1681.

Anderson, R.Y., 1978, Report to Sandia Laboratories on deep dissolution of salt, northern Delaware Basin, New Mexico: Sandia Laboratories, Albuquerque, New Mexico.

Anderson, R.Y., and Powers, D.W., 1978, Salt anticlines in the Castile-Salado evaporite sequence, northern Delaware Basin, New Mexico: (preprint), New Mexico Bureau Mines and Mineral Resources, Circ. 159 (in press).

Anderson, R.Y. et al., 1972, Permian Castile varved evaporite sequence, west Texas and New Mexico: Geol. Soc. Am. Bull., v. 83, p. 59-86.

Ash, S.R., and Clebsch, A.C., 1961, Cretaceous rocks in Lea County, New Mexico: U.S. Geol. Surv., Prof. Paper 424-D, p. 139-D142.

Bachman, G.O., 1974, Geologic processes and Cenozoic history related to salt dissolution in southeastern New Mexico: U.S. Geol. Surv., Open-file report 74-194.

Bachman, G.O., 1976, Cenozoic deposits of southeastern New Mexico and an outline of the history of evaporite dissolution: U.S. Geol. Surv., Journal of Research, v. 4, no. 2, p. 135-149.

Bachman G.O., and Johnson, R.B., 1973, Stability of salt in Permian salt basin of Kansas, Oklahoma, Texas and New Mexico: U.S. Geol. Surv. Open-file Report 4339-4.

Bishop, W.F., 1973, Late Jurassic contemporaneous faults in north Louisiana and south Arkansas: Am. Assoc. Pet. Geol. Bull., v. 57, p. 858-877.

Blanchard, W.G., Jr., and Davis, M.J., 1929, Permian stratigraphy and structure of parts of southeastern New Mexico and southwestern Texas: Am. Assoc. Pet. Geol. Bull., v. 13, p. 957-995.

Brokaw, A.L., Jones, C.L., Cooley, M.E., and Hays, W.H., 1972, Geology and hydrology of the Carlsbad potash area, Eddy and Lea Counties, New Mexico: U.S. Geol. Surv. Open-file report 4339-1.

Brown, C.N., 1956, The origin of caliche on the northeastern Llano Estacado, Texas: Jour. Geology, v. 64, p. 1-15

Bruce, C.H., 1973, Pressured shale and related sediment deformation mechanism for development of regional contemporaneous faults: Am. Assoc. Pet. Geol. Bull., v. 57, p. 878-886.

Darton, N.H., 1922, Geologic structure of parts of New Mexico: U.S. Geol. Surv. Bull. 726-E, p. 173-275.

Dobrin, M.B., Lawrence, P.L., and Sengbush, R.L., 1954, Surface and near-surface waves in the Delaware Basin: Geophysics, v. 19, p. 695-715.

Elliot, C.L., 1976a, A Laboratory investigation of magnetic physical properties of igneous dike samples from Kerr-McGee Hobbs plant, section 31, T. 20., R. 32 E. and surface outcrop, section 31, T. 26 S., R. 25 E.: Report submitted to Sandia Laboratories, Albuquerque, New Mexico, dated December 1, 1976.

Elliot, C.L., 1976b, A preliminary geophysical study of a trachyte dike in close proximity to the proposed Los Medanos nuclear waste disposal site, Eddy and Lea Counties, New Mexico, dated December 10, 1976.

Elliot, C.L., 1976c, An experimental detailed resistivity survey of known or suspected breccia pipes and sinkholes: report submitted to Sandia Laboratories, Albuquerque, New Mexico.

Elliot, C.L., 1977a, Experimental resistivity soundings near a known breccia pipe, Weaver area, Eddy County, New Mexico: Report submitted to Sandia Laboratories, Albuquerque, New Mexico.

Elliot, C.L., 1977b, Evaluation of the proposed Los Medanos nuclear waste desposal site by means of electrical resistivity surveys, Eddy and Lea Counties, New Mexico: Report (in two volumes) submitted to Sandia Laboratories, Albuquerque, New Mexico.

Fisher, W.L., and McGowen, J.H., 1967, Depositional systems in the Wilcox Group of Texas and their relationship to occurrence of oil and gas: Gulf Coast Assoc. Geol. Soc. Trans., v. 17, p. 105-125; see also Univ. Texas Bur. Econ. Geology, Geol. Circ. 67-4.

Flawn, P.T., 1954, Summary of southeast New Mexico basement rocks, in New Mexico Geol, Soc. 5th Field Conf.: Guidebook of southeastern New Mexico, p. 114-116.

Flawn, P.T., 1956, Basement rocks of Texas and southeast New Mexico: Univ. Texas Bur. Econ. Geol. Pub. 5605.

Foster, R.W., 1974, Oil and gas potential of a proposed site for the disposal of high-level radioactive waste: Oak Ridge National Laboratory, Open-file report (Contract No. AF(40-1)-4423).

Foster, R.W., and Stipp, T.F., 1961, Preliminary geologic and relief map of the Precambrian rocks of New Mexico: New Mexico Bureau of Mines and Mineral Resorces, Circ. 57.

Grim, R.E., Droste, J.B., and Bradley, W.F., 1960, A mixed-layer clay mineral associated with an evaporite: in Swineford, Ada (ed.), Clays and clay minerals, v. 8, Proc. 8th Natl. Conf. Clays and Clay Minerals, p. 228-236.

Griswold, G.B., 1977, Site selection and evaluation studies of the Waste Isolation Pilot Plant (W.I.P.P.), Los Medanos, Eddy County, New Mexico: Sandia Laboratories Rept. SAND-77-0946, Albuquerque, New Mexico.

Haigler, L.B., 1962, Geologic notes on the Delaware Basin: New Mexico Bureau of Mines and Mineral Resources, Circ. 63.

Haigler, L.B., and Cunningham, R.R., 1972, Structure contour map on top of the undifferentiated Silurian and Devonian rocks in southeastern New Mexico: U.S. Geol. Surv. Map OM-218.

Hayes, P.T., 1964, Geology of the Guadalupe Mountains, New Mexico: U.S. Geol. Surv. Prof. Paper 446.

Hills, J.M., 1942, Rhythm of Permian seas, a paleogeographic study: Am. Assoc. Pet. Geol. Bull., v. 26, p. 217-225.

Jones, C.L., 1954, The occurrence and distribution of potassium minerals in southeastern New Mexico: New Mex. Geol. Soc., 5th Field Conf., Guidebook of southeastern New Mexico, p. 107-112.

Jones, C.L., 1968, Some geologic and petrographic features of Upper Permian evaporites in southeastern New Mexico: Geol. Soc. Am. Special Paper No. 88, p. 538-539.

Jones, C.L., 1972, Permian basin potash deposits, southwestern United States, in Geology of Saline deposits: UNESCO, Earth Sci. Ser, No. 7, p. 191-201 (reprinted in Brokaw, et al., 1972, Geology and hydrology of the Carlsbad potash area, Eddy and Lea Counties, New Mexico: U.S. Geol. Survey Open-file report, 4339-1, Appendix A)

Jones, C.L., 1973, Salt deposits of Los Medanos area, Eddy and Lea Counties, New Mexico: U.S. Geol. Surv., Open-file report, 4339-7.

Jones, C.L., 1975, Potash resources in part of Los Medanos area of Eddy and Lea Counties, New Mexico: U.S. Geol. Survey, Open-file report, 75-407.

Jones, C.L., Bowles, C.G., and Bell, K.G., 1960, Experimental drill hole logging in potash deposits of the Carlsbad district, New Mexico: U.S. Geol. Surv. Open-file report, 60-84.

Keroher, G.C., et al., 1966, Lexicon of geologic names of the United States for 1936-1960: U.S. Geol. Surv. Bull. 1200.

King, P.B., 1942, Permian of west Texas and southeastern New Mexico: Am. Assoc. Pet. Geol. Bull., v. 26, p. 535-763.

King. P.B., 1948, Geology of the southern Guadalupe Mountains, Texas: U.S. Geol. Surv., Prof. Paper 215.

Lang, W.B., 1935, Upper Permian formation of Delaware Basin of Texas and New Mexico: Am. Assoc. Pet. Geol. Bull., v. 19, p. 262-276.

Lang, W. B., 1937, The Permian formations of the Pecos Valley of New Mexico and Texas: Am. Assoc. Pet. Geol. Bull., v. 21, no. 7, p. 833-898.

Long, G.J., and Associates, Inc., 1977a, Final report, Waste Isolation Pilot Plant (WIPP), Los Medanos area, Eddy and Lea Counties, New Mexico: Report submitted to Sandia Laboratories, Albuquerque, New Mexico.

Long, G.J., and Associates, Inc., 1977b, Letter report from J.L. Hern of G.J. Long and Associates, Houston, Tex,. to W.D. Weart of Sandia Laboratories, Albuquerque, New Mexico.

Mansure, A., and Reiter, M., 1977, An accurate equilibrium temperature log in AEC #8, a drill test in the vicinity of the Carlsbad disposal site: New Mexico Bureau Mines and Mineral Resources, Open-file report #80.

McGlasson, E.H., 1968, Siluro-Devonian of west Texas and southeastern New Mexico: New Mexico Bureau Mines and Mineral Resources, Circ. 10, p. 26-37.

McKee, E.D., and Oriel, S.S., et al., 1967a, Paleotectonic investigations of the Permian System in the United States: U.S. Geol. Surv. Prof. Paper 515.

McKee, E.D., and Oriel, S.S., et al., 1967b, Paleotectonic maps of the Permian System: U.S. Geol. Surv. Misc. Geologic Investigations Map I-450.

Meyer, R.F., 1966, Geology of Pennsylvanian and Wolfcampian rock in southeast New Mexico: New Mexico Bureau Mines and Mineral Resources, Memoir 17.

Muehlberger, W.R., Denison, R.E., and Lidiak, E.G., 1967, Basement rocks in continental interior of United States: Am. Assoc. Pet. Geol. Bull., v. 51, p. 2351-2380.

Murray, G.E., 1961, Geology of the Atlantic and Gulf coastal province of North America: Harper Bros., New York.

Netherland, Sewell and Associates, 1974, Evaluation of hydrocarbon potential, AEC study area, southeast New Mexico, based on geological and engineering studies as of May, 1974: report submitted to Oak Ridge National Laboratory, Oak Ridge, Tennesee, dated June 11, 1974.

Newell, N.D., Rigby, J.K. Fischer, A.G., Whiteman, A.J., Hickox, J.E., and Bradley, J.S., 1953, The Permian reef complex of the Guadalupe Mountains region, Texas and New Mexico -- A study in paleoecology: W.H. Freeman & Co., San Francisco, 236p.

Oriel, S.S., Myers, D.A., and Crosby, E.J., 1967, West Texas Permian Basin region, Chapter C, in McKee, E.D., et al., Paleotectonic Investigations of the Permian System of the United States: U.S. Geol. Surv. Prof. Paper 515-C, p. 21-60.

Reynolds, C.B., and Associates, 1976, Summary and final report, shallow seismic reflection survey, Phases I and II, Los Medanos area, Eddy County, New Mexico: Report submitted to Sandia Laboratories, Albuquerque, New Mexico, undated.

Sipes, Williamson and Aycock, Inc., 1976, Hydrocarbon evalution, proposed southeastern New Mexico radioactive material storage site, Eddy County, New Mexico: Report submitted to Sandia Laboratories, Albuquerque, New Mexico, dated September 1, 1976.

Vine, J.D., 1960, Recent domal structures in southeastern New Mexico: Am. Assoc. Pet. Geol. Bull., v. 44, no. 12, p. 1903-1911.

Vine, J.D., 1963, Surface geology of the Nash Draw quadrangle, Eddy County, New Mexico: U.S. Geol. Surv. Bull. 1141-B.

Thompson, M.L., 1942, Pennsylvanian system in New Mexico: New Mexico School of Mines, Bull. 17.

Urry, W.E., 1936. Post-Keweenawan time scale: Nat. Res. Council Comm. on Measurement of Geologic Time, 1935-1936: Rept. Exbt. 2, p. 35-40.

T. 21 S.

T. 22 S.

T. 23 S.

34	35	36	31	32	33	34	35	36	31
3	2	1	6	5	4	3	2	1	6
10	11	12	7	8	9	10	11	12	7
15	14	13	18	17	16	15	14	13	18
22	23	24	19	20	21	22	23	24	19
27	26	25	30	29	28	27	26	25	30
34	35	36	31	32	33	34	35	36	31
3	2	1	6	5	4	3	2	1	6
10	11	12	7	8	9	10	11	12	7
15	14	13	18	17	16	15	14	13	18

ZONE IV

ZONE III

ZONE II

ZONE I

LEA COUNTY
EDDY COUNTY

R 30 E.

R 31 E.

R. 32 E.

N

ZONE ACREAGE

ZONE I – 60-100 (surface facilities)

ZONE II – 1860 (underground repository)

ZONE III – 6230 (no mining or drilling)

ZONE IV – 10,810 (DOE-controlled mining and drilling)

SCALE IN MILES

1   0   1   2   3

M

WIPP SITE ZONATION

FIGURE 4.1-1

FIGURE 4.1-2

SITE EXPLORATION
DRILL HOLES AND SEISMIC REFLECTION LINES

NOTE:
1. Additional drill hole data are listed in Table 4.1-1
2. All seismic profiling shown was performed under contract to Sandia Laboratories for the WIPP Site.

Area of planned underground potash mining

Location of underground potash mines

.... Seismic reflection survey lines

⊛ Hydrocarbon producer (past or present)

◉ Drill holes penetrating Delaware and deeper horizons

● Shallow drill holes (bottoming above the Delaware)

EXPLANATION

REFERENCES:
Griswold, 1977, figure 4.
G. J. Long & Associates, May, 1977
G. J. Long & Associates, Dec., 1977

SCALE IN MILES
0   1   2   3

FIGURE 4.2-1

SITE PHYSIOGRAPHIC FEATURES

A) Air view northwest across WIPP Site, showing general terrain. Drill rig at right is near center of site, working on ERDA-9. Rig at left is set up on hole H-1.

B) Shallow depression eight miles north of site. Diameter about 1000 feet and relief about 30 feet. Investigation of this feature has found no indication of subsurface subsidence or collapse.
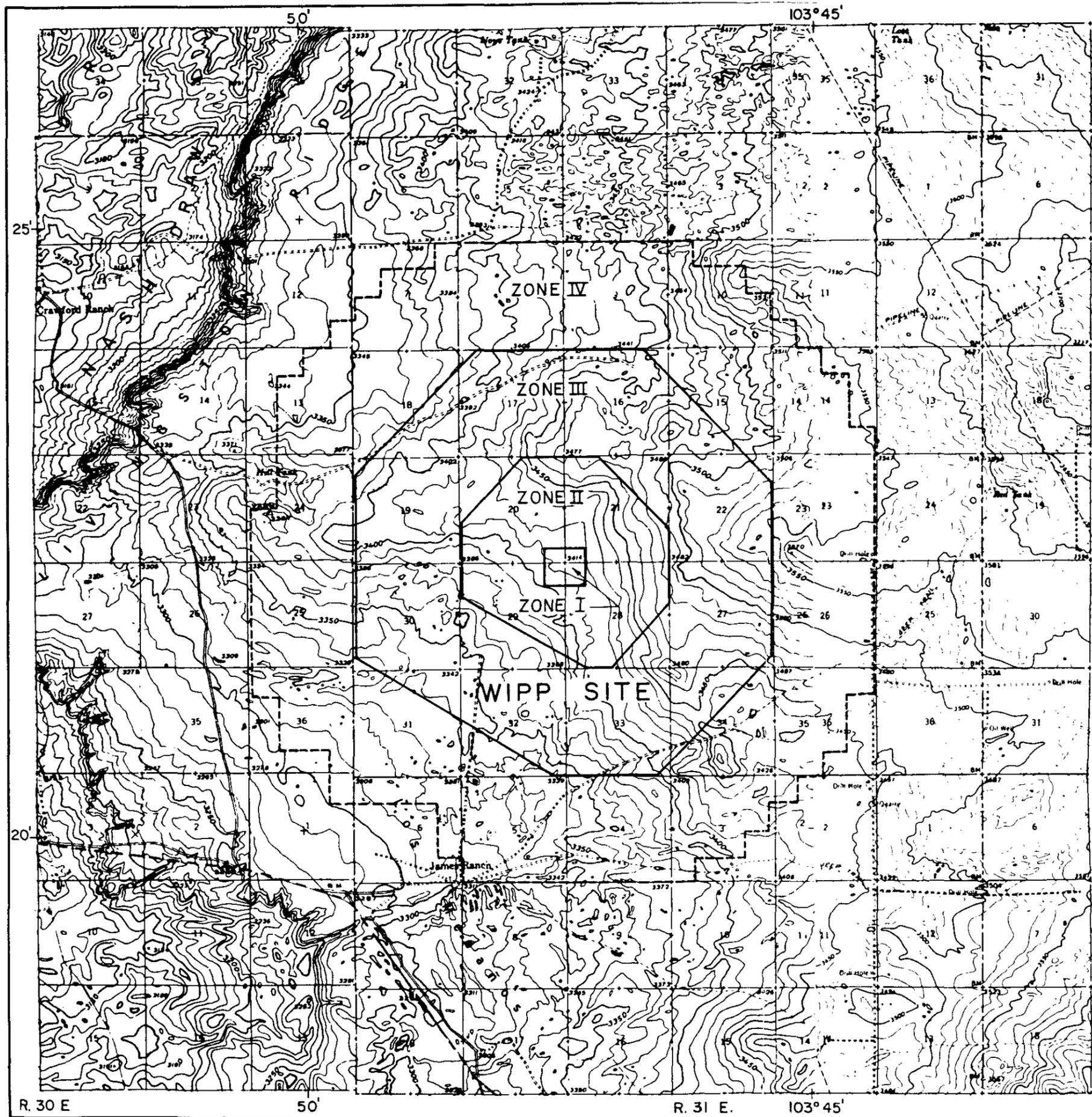
REFERENCE:

U.S.G.S. 15 minute quadrangles: Nash Draw, N.Mex.,1965 and Hat Mesa, N.Mex.,1972.
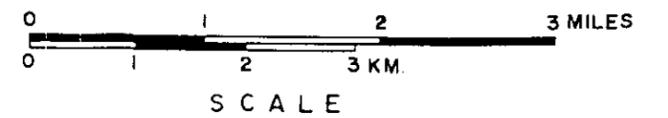
SITE TOPOGRAPHIC MAP

FIGURE 4.2-2

Active sand dunes at James Ranch. Location is 3 miles south
of center of site. Viewed southeast.

ACTIVE DUNES NEAR SITE

FIGURE 4.2-3
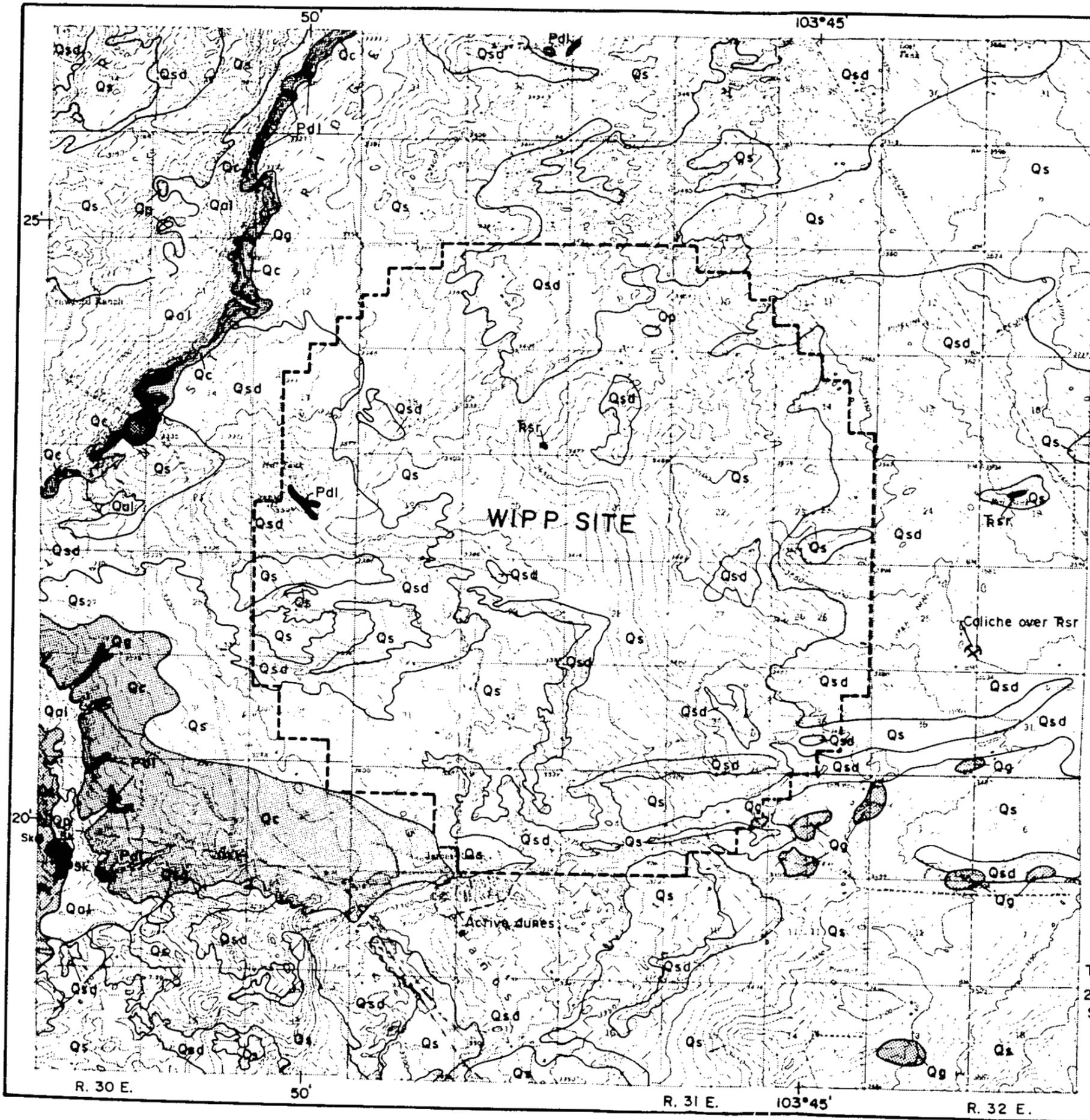
EXPLANATION

SAND – Eolian sand plains (Mescalero sand). Qsd, conspicuous dunes, generally stabilized or partly stabilized.

ALLUVIUM – Sand and silt, locally conglomeratic, deposited on gentle slopes and depressions. Qp, playa deposits of sand and silt in shallow intermittent ponds or lakes.

CALICHE – Limestone (Mescalero caliche), dense to travertine-like, with included sand grains and rock fragments. Has been assigned to Yarmouth interglacial stage.

GATUNA FORMATION – Gravel, sand, silt and clay deposited as alluvium; dominantly reddish-orange, grading to pink, gray or yellow. Has been assigned to Kansan glacial stage.

SANTA ROSA SANDSTONE – Conglomeratic sandstone, moderate reddish-brown to light brown, poorly sorted, cross-bedded; interbedded locally with moderate reddish-brown claystone and siltstone.

DEWEY LAKE REDBEDS – Fine sandstone and siltstone, moderate reddish-orange to reddish-brown, conspicuous thin laminae generally less than 1/4 inch thick, locally clayey and with light greenish-gray partings.

RUSTLER FORMATION – White, massive gypsum.

SK • Sinkhole

⚒ Quarry

REFERENCES: Compiled from geologic maps by Vine (1963) and Bachman (1974).

SCALE

SURFICIAL GEOLOGIC MAP

FIGURE 4.2-4

SW   NE

SKELLY No. I FORTY-
NINER RIDGE UNIT

SHELL No. I JAMES
RANCH UNIT

WIPP SITE AREA
ZONE IV

C.W. WILLIAMS No. I
BADGER UNIT
FEDERAL

PHILLIPS No. I
HAT MESA

PHILLIPS No. I
ETZ FEDERAL

HORIZONTAL SCALE

VERTICAL EXAGGERATION, 8 TIMES

GENERALIZED SITE STRATIGRAPHIC SECTION

FIGURE 4.3-1

LOCATION MAP

EDDY COUNTY
LEA COUNTY

REFERENCE:
Netherland, Sewell & Associates, 1974, Exbt. G-18

FIGURE 4.3-2

SITE GEOLOGIC COLUMN
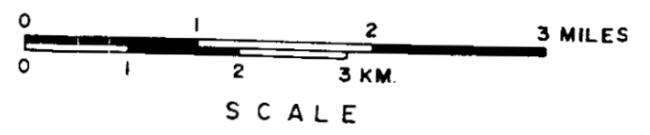
EXPLANATION

LITHOLOGIC SYMBOLS

- Sandstone
- Mudstone; siltstone; silty and sandy shale.
- Shale
- Limestone
- Dolomite
- Cherty limestone and dolomite
- Shaly limestone
- Anhydrite (or gypsum)
- Interlaminated anhydrite-calcite
- Halite (rock salt)
- Granitic rocks

REFERENCES:

1. Anderson, 1978
2. Anderson, et al, 1972
3. Brokaw, et al, 1972
4. Foster, 1974
5. Griswold, 1977
6. Meyer, 1966
7. Sipes, Williamson and Aycock, 1976

NOTE:

For complete citations, refer to reference list for chapter 4.

VERTICAL SCALE OF SECTION IN FEET

(scale: 0, 300, 600, 1200, 1800, 2400, 3000)

ERA	SYSTEM	SERIES	FORMATION	GRAPHIC LOG	APPROX DEPTH TO CONTACT AT SITE	PRINCIPAL LITHOLOGY	APPROX THICKNESS (feet)
CENOZOIC		RECENT	Surficial sand		10	BLANKET SAND AND DUNE SAND; SOME ALLUVIUM INCLUDED	0-100
	QUATERNARY	PLEISTOCENE (Kansan?)	Mescalero caliche & Gatuna Fm.		40	PALE REDDISH BROWN, FINE-GRAINED FRIABLE SANDSTONE, CAPPED BY 5-10 FT. HARD, WHITE CRYSTALLINE CALICHE (LIMESTONE) CRUST.	0-35
MESOZOIC	TRIASSIC	UPPER TRIAS.	Santa Rosa Sandstone		50	PALE RED TO GRAY, CROSS-BEDDED, NON MARINE, MEDIUM TO COARSE-GRAINED FRIABLE SANDSTONE; PINCHES OUT ACROSS SITE.	0-250
PALEOZOIC	PERMIAN	OCHOAN	Dewey Lake Redbeds		540	UNIFORM DARK RED-BROWN MARINE MUDSTONE AND SILTSTONE WITH INTERBEDDED VERY FINE-GRAINED SANDSTONE; THINS WESTWARD	100-550
			Rustler		850	GRAY, GYPSIFEROUS ANHYDRITE WITH SILTSTONE INTERBEDS IN UPPER PART; REDDISH BROWN SILTSTONE OR VERY FINE SILTY SANDSTONE IN LOWER PART, HALITIC NEAR BASE. CONTAINS 2 DOLOMITE MARKER BEDS, MAGENTA (M) IN UPPER PART AND CULEBRA (C) IN LOWER PART. THICKENS EASTWARD DUE TO INCREASING CONTENT OF UNDISSOLVED ROCK SALT.	275-425
			Salado		CH ZONE	MAINLY ROCK SALT (85-90%) WITH MINOR INTERBEDDED ANHYDRITE, POLYHALITE AND CLAYEY TO SILTY CLASTICS. TRACE OF POTASH MINERALS IN MC NUTT ZONE. THE MINOR INTERBEDS ARE THIN AND OCCUR IN COMPLEXLY ALTERNATING SEQUENCES. THICKEST NON-HALITE BED IS THE COWDEN ANHYDRITE (CA), 17 FT. THICK. MULTIPLE ANHYDRITE INTERBEDS ARE MOST COMMON IMMEDIATELY BELOW THE COWDEN AND IMMEDIATELY ABOVE BASE OF SALADO.	1750-2000
					RH ZONE 2825		
			Castile		4075±	THICK MASSIVE UNITS OF FINELY INTERLAMINATED ("VARVED") ANHYDRITE CALCITE ALTERNATING WITH THICK HALITE (ROCK SALT) UNITS CONTAINING THINLY INTERBEDDED ANHYDRITE. TOP ANHYDRITE UNIT LACKS CALCITE INTERLAMINATIONS.	1250±
		GUADALUPIAN	Bell Canyon (Delaware sand) (DELAWARE MOUNTAIN GROUP)		5100±	MOSTLY LIGHT GRAY FINE-GRAINED SANDSTONE WITH VARYING AMOUNT OF SILTY AND SHALY INTERBEDS AND IMPURITIES. CONTAINS CONSIDERABLE LIMESTONE INTERBEDS AND LIME RICH INTERVALS. TOP UNIT IS LAMAR LIMESTONE MEMBER, A PERSISTENT SHALY LIMESTONE OR LIMY SHALE.	1000±
			Cherry Canyon		6200±	MOSTLY GRAY TO BROWN, FINE TO VERY FINE GRAINED SANDSTONE SIMILAR TO BRUSHY CANYON, INTERBEDDED WITH SHALE, DOLOMITE AND SOME LIMESTONE.	1100±
			Brushy Canyon		8000±	PREDOMINANTLY FINE-GRAINED, GRAY TO BROWN SANDSTONE INTERBEDDED WITH MINOR BROWN SHALE AND DOLOMITE.	1800±
		LEONARDIAN	Bone Springs (First sand / 2nd sand / Third sand)		11400±	THICK, PARTLY CHERTY BASIN LIMESTONE SEQUENCE IN UPPER PART UNDERLAIN BY ALTERNATING UNITS OF FINE TO VERY FINE-GRAINED SANDSTONE AND LIMESTONE. SHALE IS NOT COMMON BUT THE LIMESTONES ARE COMMONLY ARGILLACEOUS.	3400±
		WOLFCAMPIAN	"Wolfcamp"		12800±	DARK-COLORED BASIN LIMESTONE AND DOLOMITE WITH INTERBEDDED SHALE; SANDSTONE IS SCARCE. SHALE AND CARBONATE CONTENT ROUGHLY EQUAL. MAY CONTAIN A FEW HUNDRED FEET OF LITHOLOGICALLY SIMILAR UPPER PENNSYLVANIAN STRATA (CISCO AND CANYON EQUIVALENTS).	1400±
	PENNSYLVANIAN	DESMOINESIAN? DERRYAN?	Strawn		13100±	DOMINANTLY LIMESTONE WITH SOME CHERT AND INTERBEDDED SHALE IN UPPER PART; DOMINANTLY LIGHT GRAY, MEDIUM TO CONGLOMERATIC SAND IN LOWER PART.	300±
			Atoka		13800±	PRINCIPALLY LIMESTONE, CHERTY IN MIDDLE PART, ALTERNATING WITH DARK SHALE.	650±
		MORROWAN?	Morrow		15000±	MOSTLY FINE TO COARSE OR CONGLOMERATIC SANDSTONE WITH DARK GRAY SHALE. SOMEWHAT LIMY SEQUENCE NEAR TOP INTERBEDDED WITH SANDSTONE IS REFERRED TO AS "MORROW LIME".	1250
	MISSISSIPPIAN	UPPER MISS.	Barnett Shale			(UNCONFORMITY)	
		LOWER MISS.			15600±	LIGHT YELLOWISH BROWN, LOCALLY CHERTY LIMESTONE OVERLAIN BY DARK BROWN SHALE (BARNETT).	650±
	DEVONIAN	UPPER DEV.	Woodford Shale		15800±	BLACK, ORGANIC SHALE; PYRITIC. (UNCONFORMITY)	175
	SILURIAN				16900±	LIGHT-COLORED, CHERTY DOLOMITE; CONTAINS TWO LIMESTONE INTERVALS IN UPPER HALF OF SECTION.	1180
	ORDOVICIAN		MONTOYA GROUP			CHERTY LIMESTONE AND DOLOMITE.	1300±
			SIMPSON GROUP			ALTERNATING BEDS OF LIMESTONE AND GRAY OR GREEN SHALE, WITH MINOR SANDSTONE UNITS.	
			ELLENBURGER GROUP		18200±	CHERTY DOLOMITE, INCLUDES BASAL SANDSTONE MEMBER. (UNCONFORMITY)	
	PRECAMBRIAN					IGNEOUS INTRUSIVE TERRANE (AGE 1.2-1.4 BILLION YEARS)	

ERDA-9

DUNE SAND AND CALICHE
GATUNA
SANTA ROSA

DEWEY LAKE

27'
54'

850'

608'   MAGENTA MEMBER
632'
RUSTLER
714'   CULEBRA MEMBER
740'

860'   860'

1038'   M.B. 103
1050'   UPPER MEMBER

1362'   VACA TRISTE M.B.
1372'

MC NUTT MEMBER

1644'   M.B. 124
1650'

1741'   M.B. 126   SALADO

2040'
2050'   M.B. 136
2073'   M.B. 137
2074'
2176'   M.B. 139   LOWER MEMBER
2180'
2240'   M.B. 140
2250'
2320'   M.B. 141
2330'
2377'   M.B. 142
2381'
2450'   M.B. 143
2455'
2497'   M.B. 144
2505'
2540'   COWDEN ANHYDRITE
2550'
2620'   INFRA-COWDEN

2730'

2836'

CASTILE

EXPLANATION

Sand and Sandstone

Mudstone and Siltstone

Anhydrite

Rock Salt

Dolomite

Storage zones

Drill Stem Test Interval

Cement grout
Bottom of casing

Marker bed zones

NOTES:

1. All rocks below Santa Rosa are Permian in age.

2. All depths given are measured from Kelly bushing reference point (See note 4).

3. Ground surface elevation is 3414.70 feet, MSL

4. Kelly bushing elevation is 3426.25 feet, MSL

5. MB = Marker Bed

REFERENCE:

Griswold, 1977, fig. 19

GENERALIZED ERDA-9 STRATIGRAPHY

FIGURE 4.3-3 A

KEY PLAN
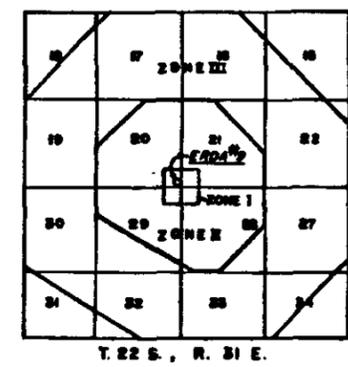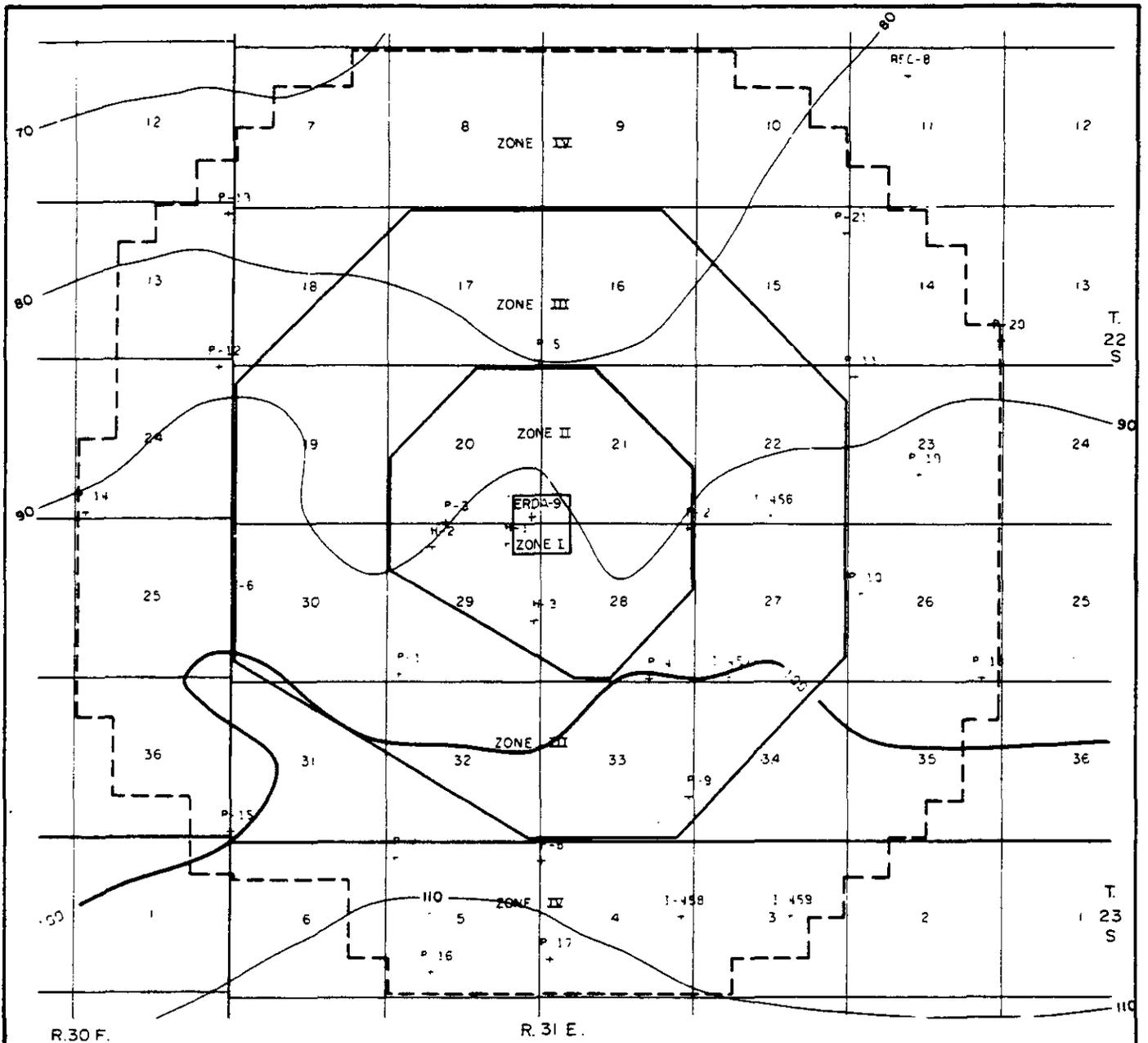
T. 22 S., R. 31 E.

N

ZONE IV

ZONE III

ZONE II

ERDA-9
ZONE I

ZONE III

ZONE IV

12 7 8 9 10 11 12

13 18 17 16 15 14 13

24 19 20 21 22 23 24

25 30 29 28 27 26 25

36 31 32 33 34 35 36

1 6 5 4 3 2

70 80 90 100 110

80 90 110

REC-8

P-19 P-21

P-12 P-20

P-14

P-6

P-15

P-8

P-16 P-17

P-9

P-1

P-18 P-10

P-3 P-2

H-2 H-3

456

458 459

T. 22 S

T. 23 S

R.30 E.   R.31 E.

SCALE IN MILES

0   1   2   3

CONTOUR INTERVAL - 10 FEET

W

N

REFERENCE:

Griswold, 1977, figure 11

ISOPACH MAP

124 TO 126 MARKER BEDS

FIGURE 4.3-4

CONTOUR INTERVAL -10 FEET

SCALE IN MILES

0   1   2   3
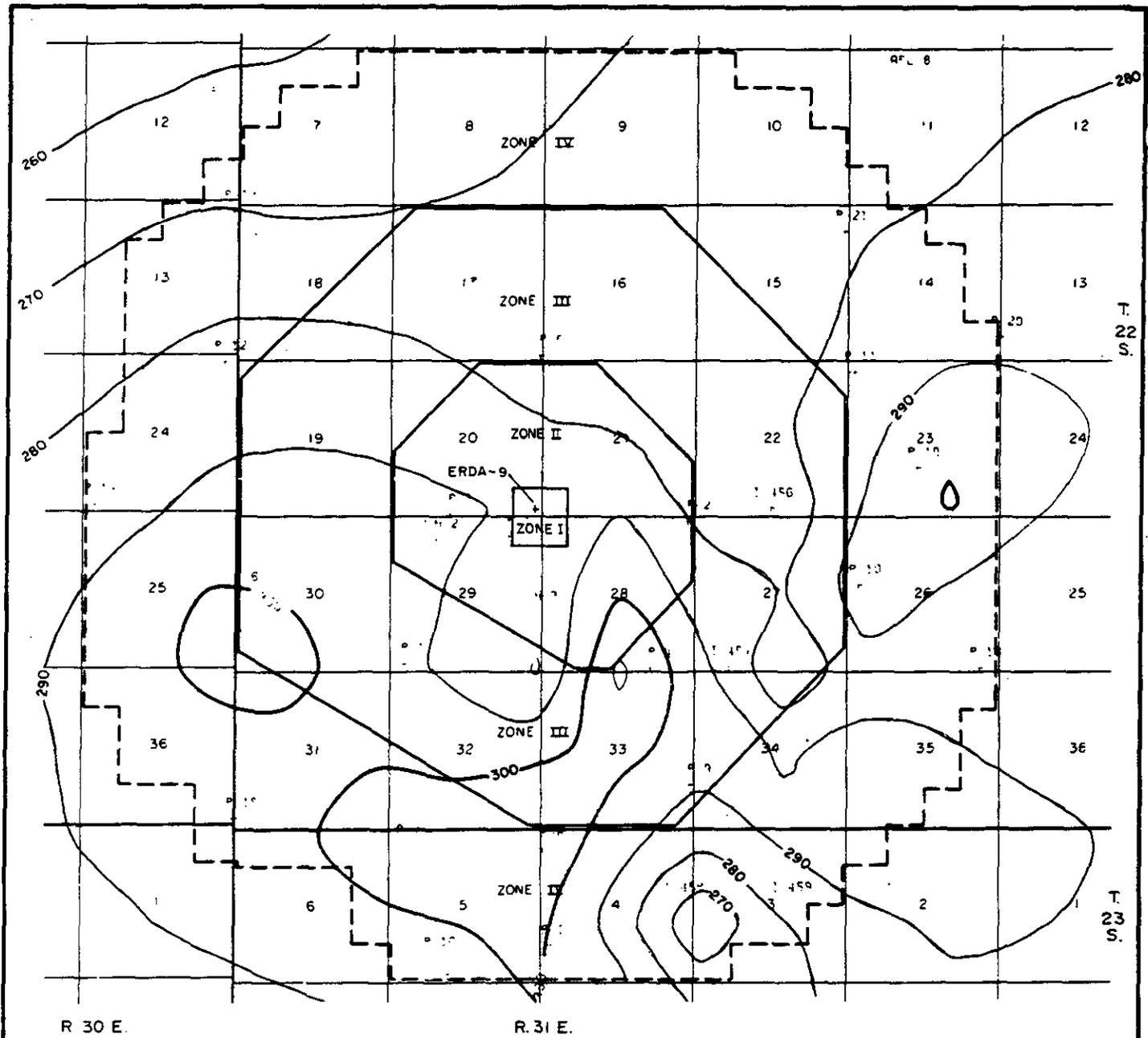
ISOPACH MAP VACA TRISTE

TO 124-MARKER BEDS

FIGURE 4.3-5

REFERENCE:

Griswold, 1977, figure 11

CONTOUR INTERVAL - 10 FEET

SCALE IN MILES

ISOPACH MAP 103 TO
VACA TRISTE MARKER BEDS

FIGURE 4.3-6

REFERENCE:

Griswold, 1977, figure II

CONTOUR INTERVAL - 10 FEET

SCALE IN MILES

ISOPACH MAP   TOP OF SALADO
TO 103-MARKER BED

REFERENCE:

Griswold, 1977, figure 11
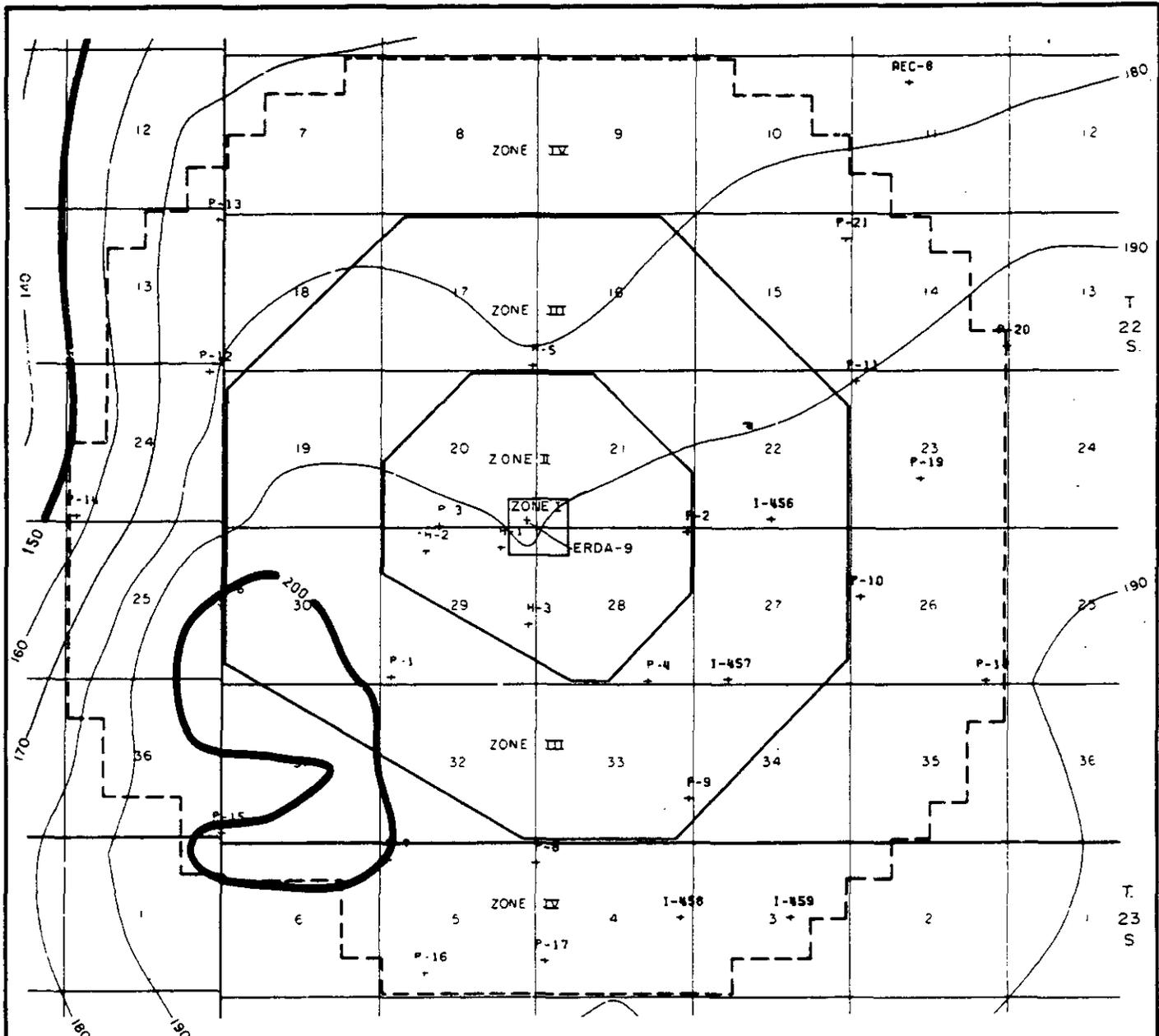
FIGURE 4.3-7
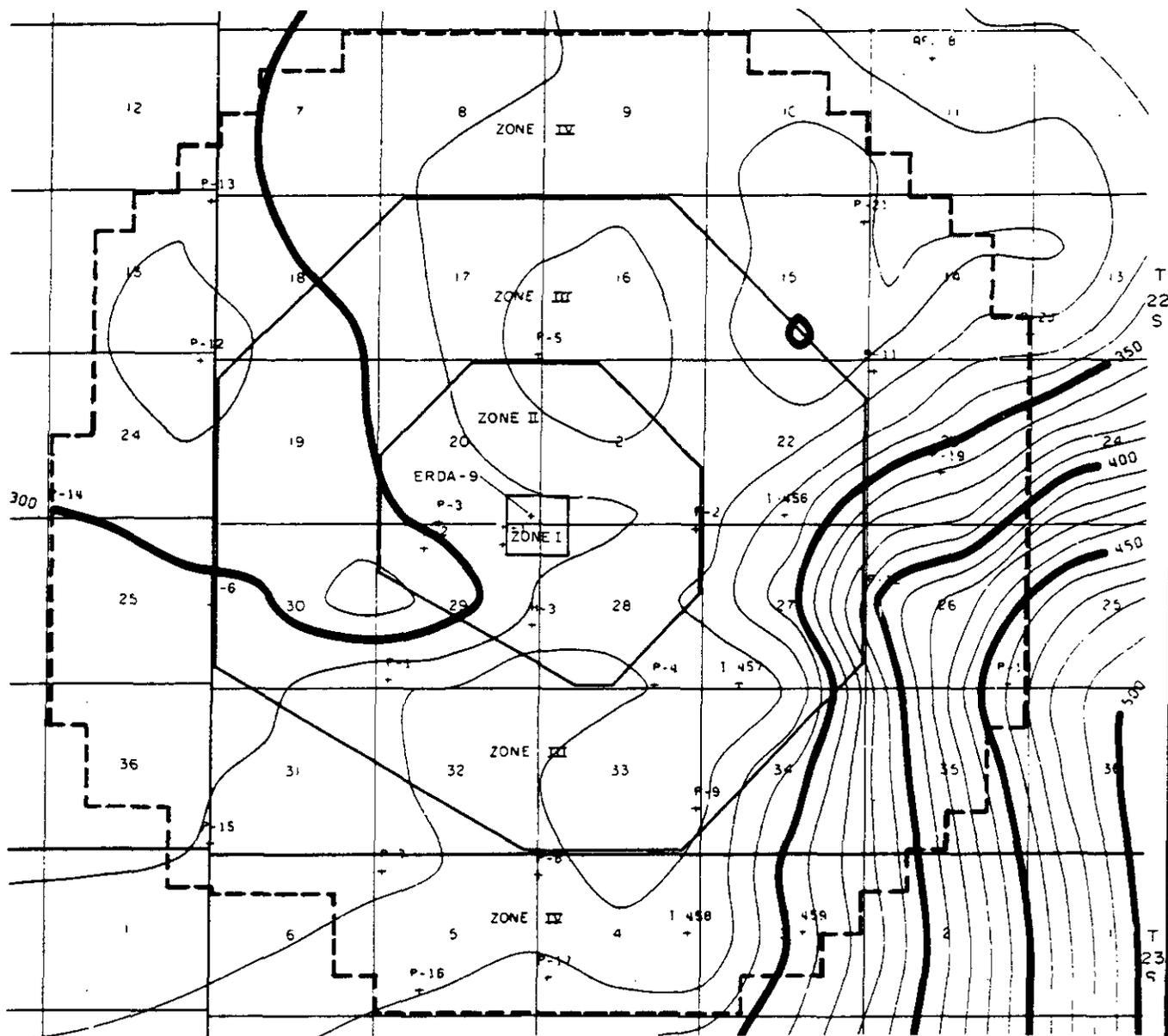
R 30 E.

R. 31 E.

CONTOUR INTERVAL – 10 FEET

SCALE IN MILES

ISOPACH MAP
RUSTLER FORMATION

REFERENCE:

Griswold, 1977, figure 10
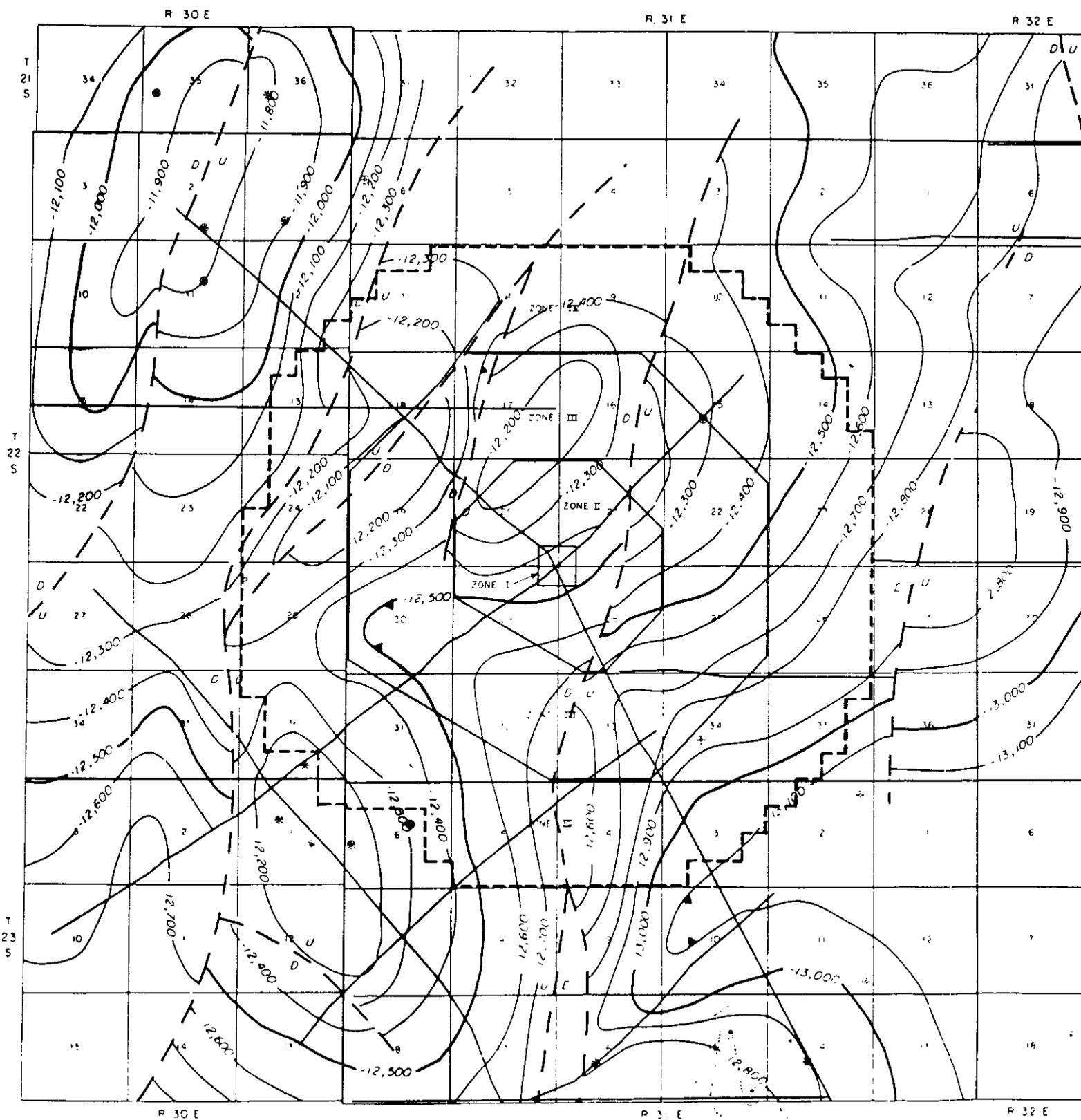
FIGURE 4.3-8

R. 30 E.　　　　　　　　　R. 31 E.

SCALE IN MILES

0　　1　　2　　3

CONTOUR INTERVAL – 10 FEET

N

ISOPACH MAP

DEWEY LAKE REDBEDS

REFERENCE:

Griswold, 1977, figure 10

FIGURE 4.3-9

R.30 E.   R.31 E.

SCALE IN MILES

0   1   2   3

CONTOUR INTERVAL - 10 FEET

REFERENCE:

Griswold, 1977, figure 10

ISOPACH MAP
SANTA ROSA SANDSTONE

FIGURE 4.3-10

CONTOUR INTERVAL – 10 FEET

REFERENCE:

Griswold, 1977, figure 10

ISOPACH MAP

GATUNA FORMATION

FIGURE 4.3-11

SCALE IN MILES

STRUCTURE CONTOURS
ON TOP OF SILURIAN

FIGURE 4.4-1
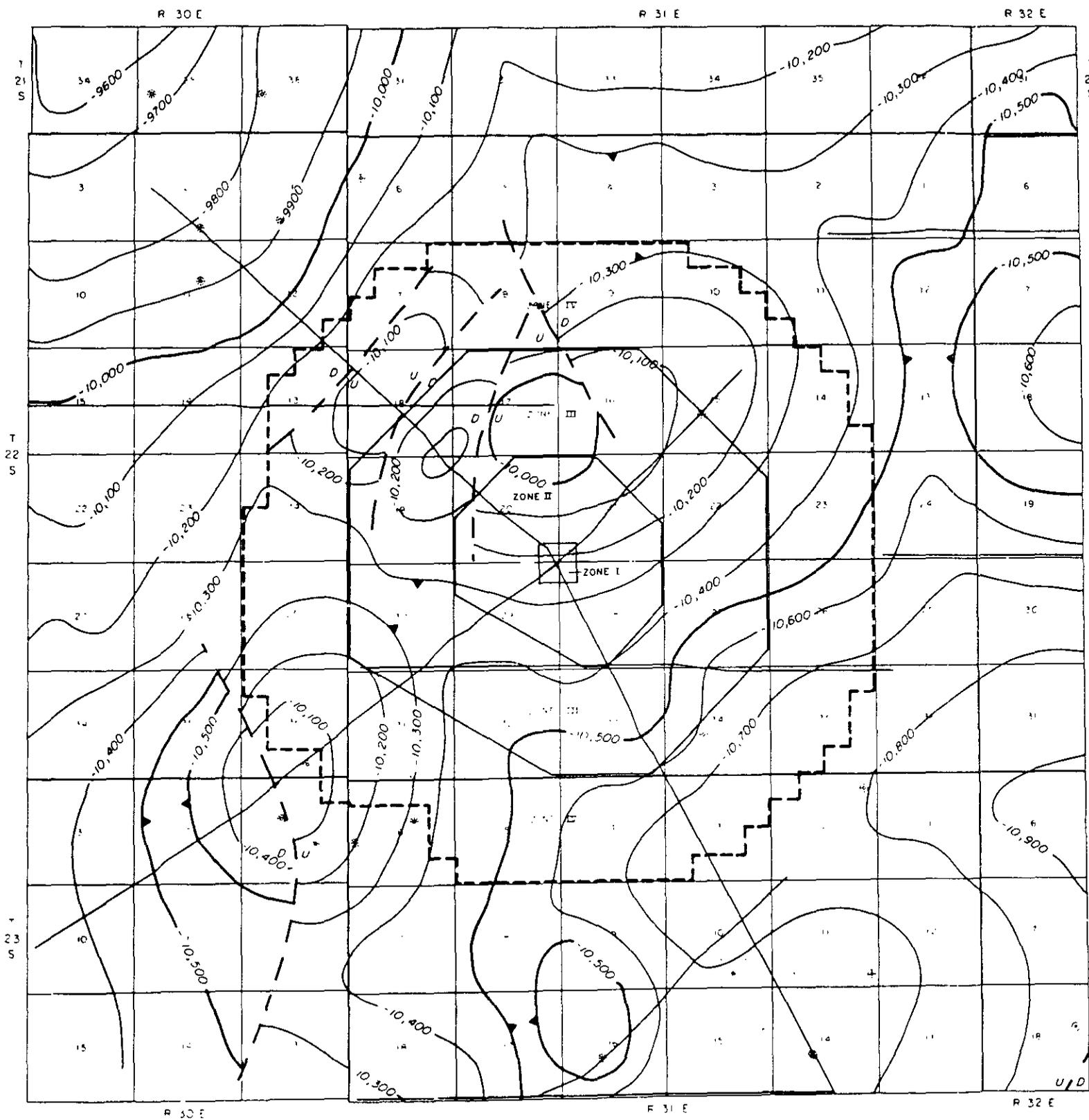
EXPLANATION

Seismic reflection
profile lines

Inferred faults
U – Upthrown side
D – Downthrown side

⊗ Well – Dry and Abandoned
◉ Completed Well – Producing Gas
● Completed Well – Producing Oil

Contour interval – 100 feet
Datum is mean sea level

REFERENCE
Griswold, 1977, figure 17

SCALE IN MILES

EXPLANATION

Seismic reflection
profile lines.

Inferred faults.
U-Upthrown side
D-Downthrown side

⊗ Well - Dry and Abandoned
◉ Completed Well - Producing Gas
● Completed Well - Producing Oil

Contour interval - 100 feet
Datum is mean sea level

REFERENCE:

Griswold, 1977, figure 16.

SCALE IN MILES

STRUCTURE CONTOURS
ON TOP OF
MORROW LIMESTONE

FIGURE 4.4-2
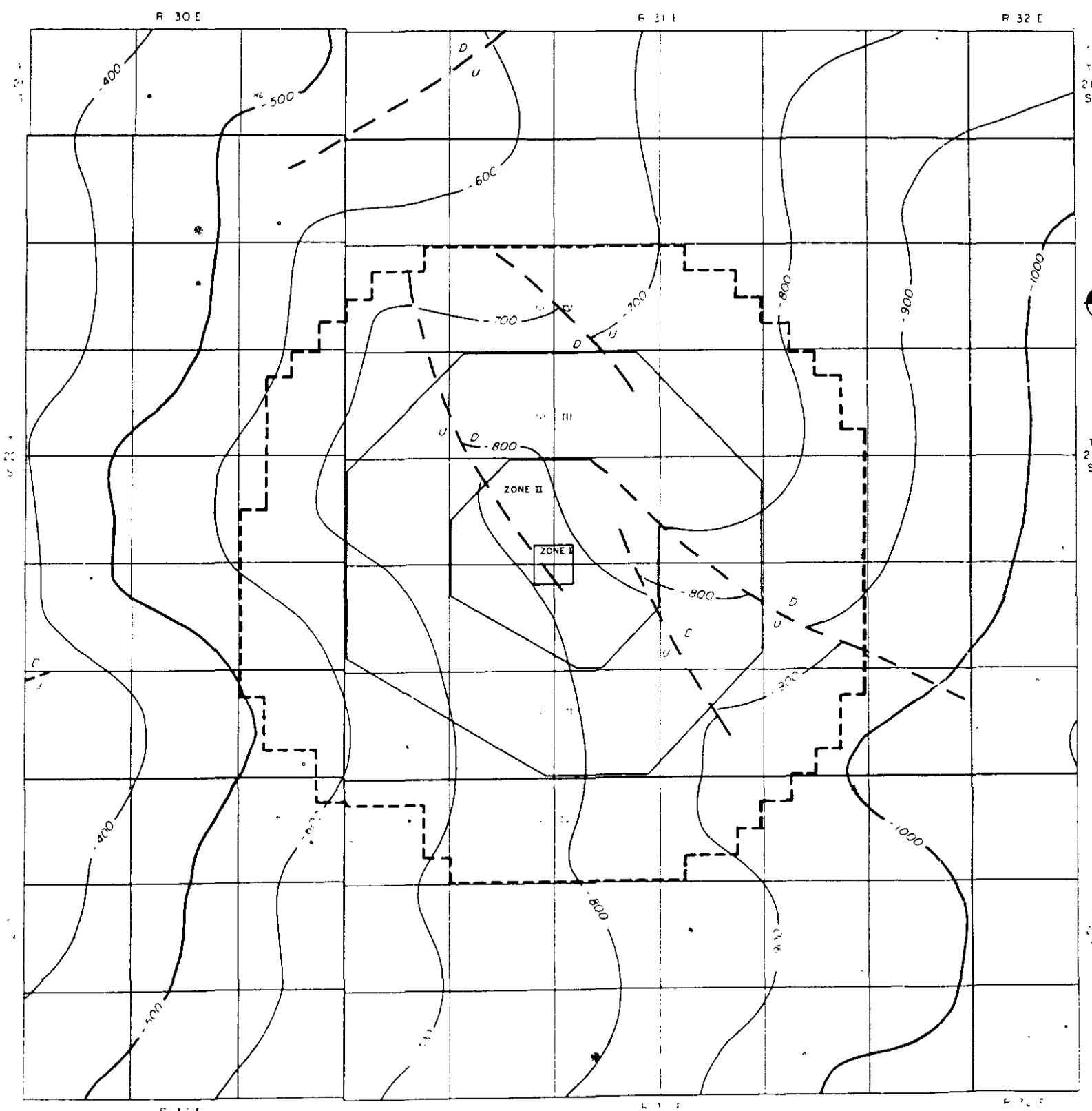
EXPLANATION

Possible faults.
U — Upthrown side
D — Downthrown side

⊗ Well-Dry and Abandoned
⊙ Completed Well- Producing Gas
● Completed Well - Producing Oil

Contour interval - 100 feet
Datum is mean sea level

REFERENCE:

Griswold, 1977, figure 15

SCALE IN MILES

STRUCTURE CONTOURS
ON TOP OF
DELAWARE SANDSTONE

FIGURE 4.4-3
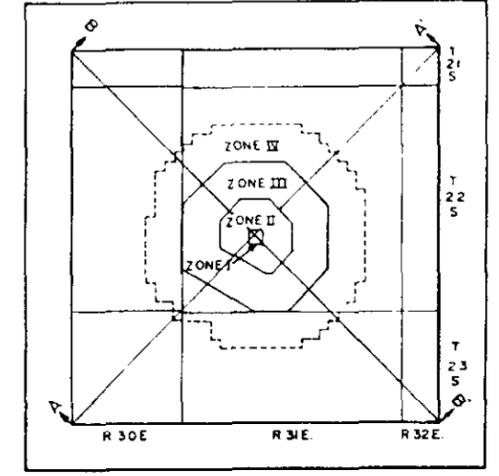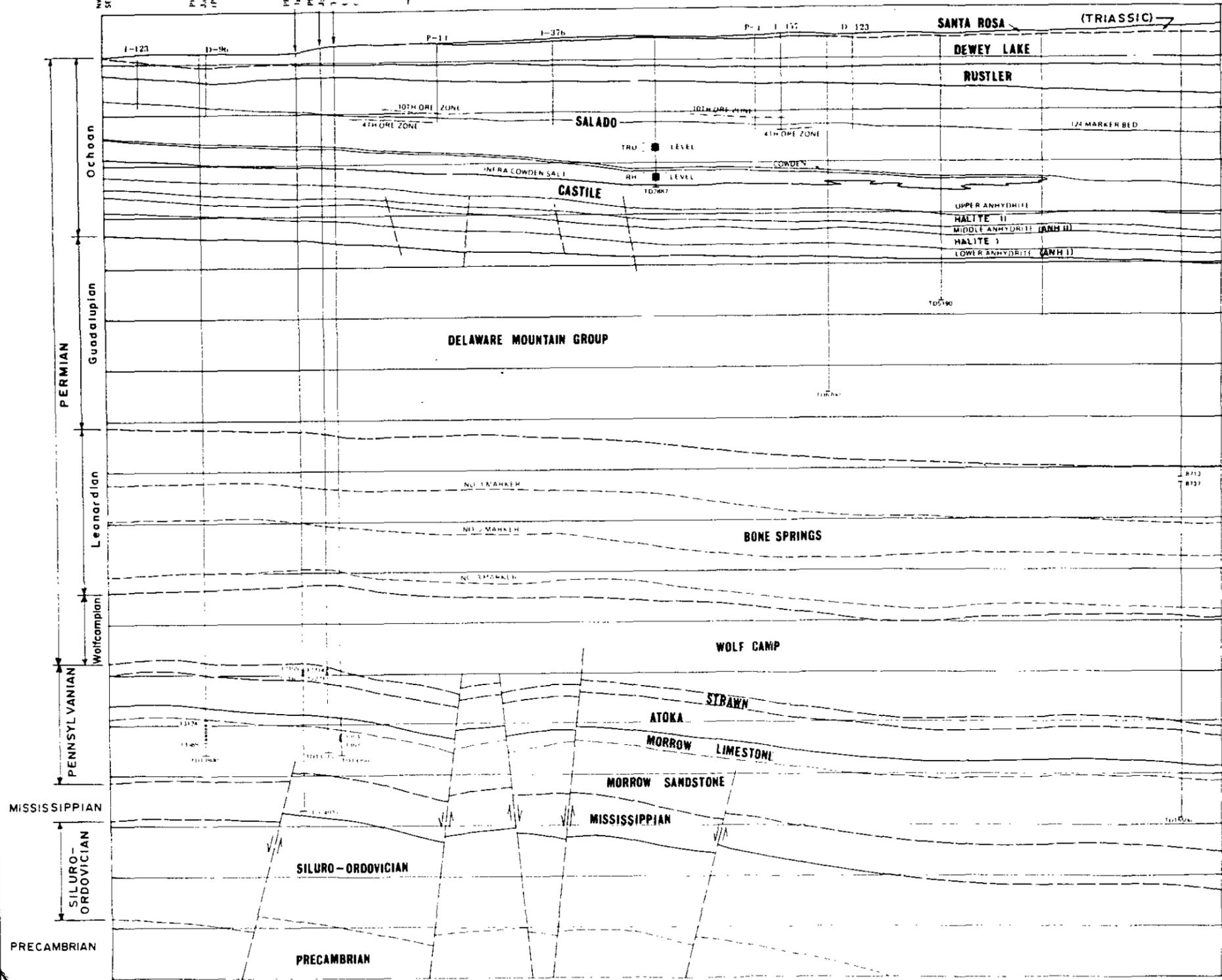
SITE GEOLOGIC SECTION A-A'

FIGURE 4.4-4

SITE GEOLOGIC SECTION B-B'

FIGURE 4.4-5
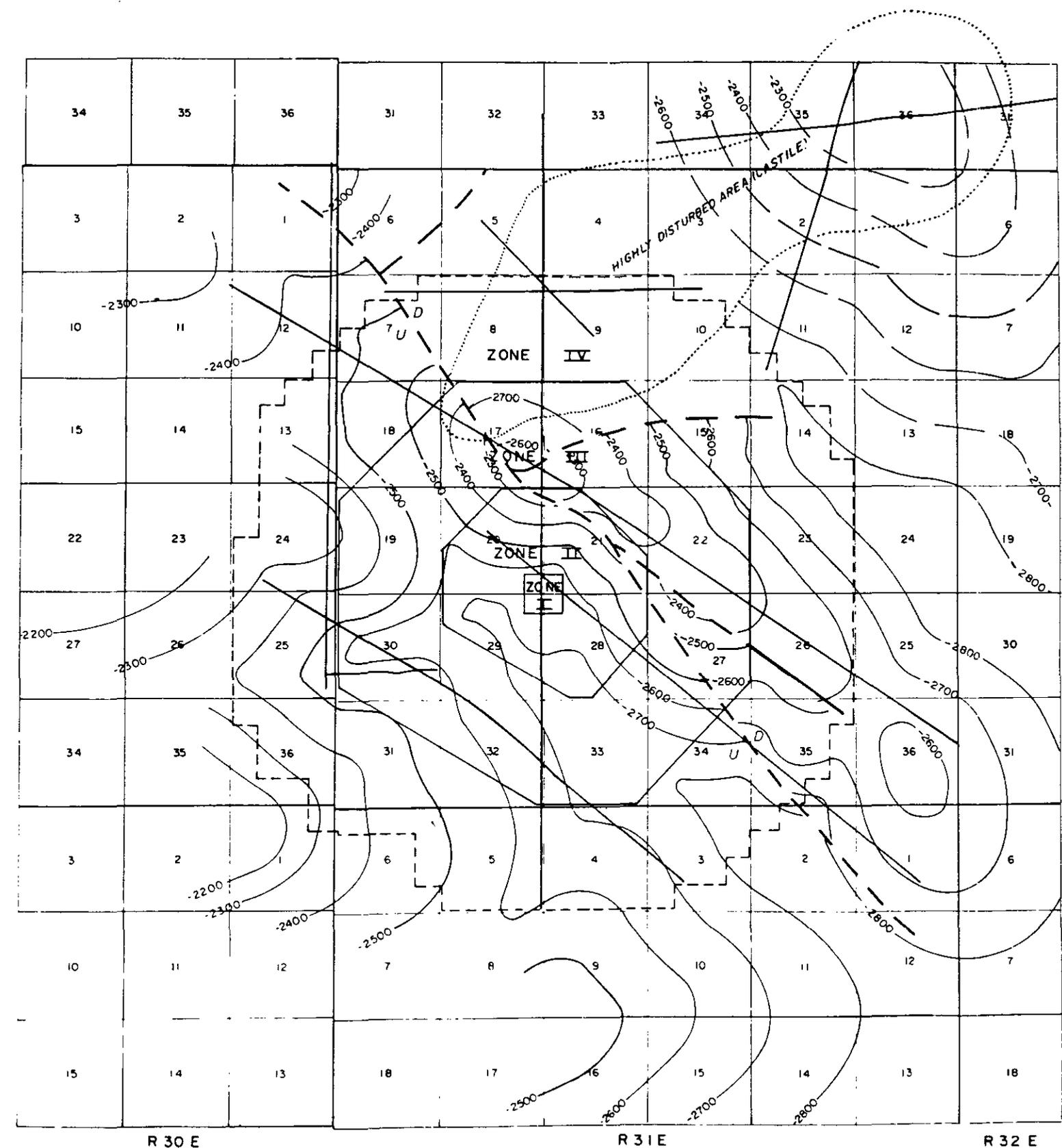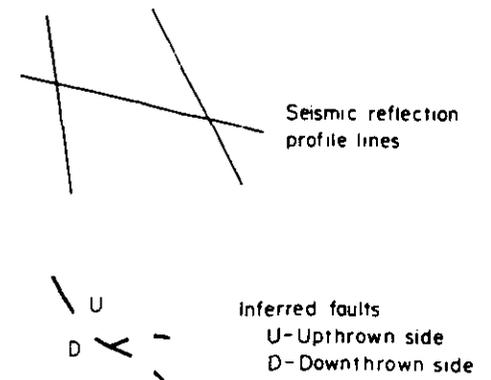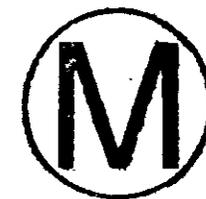
STRUCTURE CONTOURS
ON TOP OF CASTILE

FIGURE 4.4-6
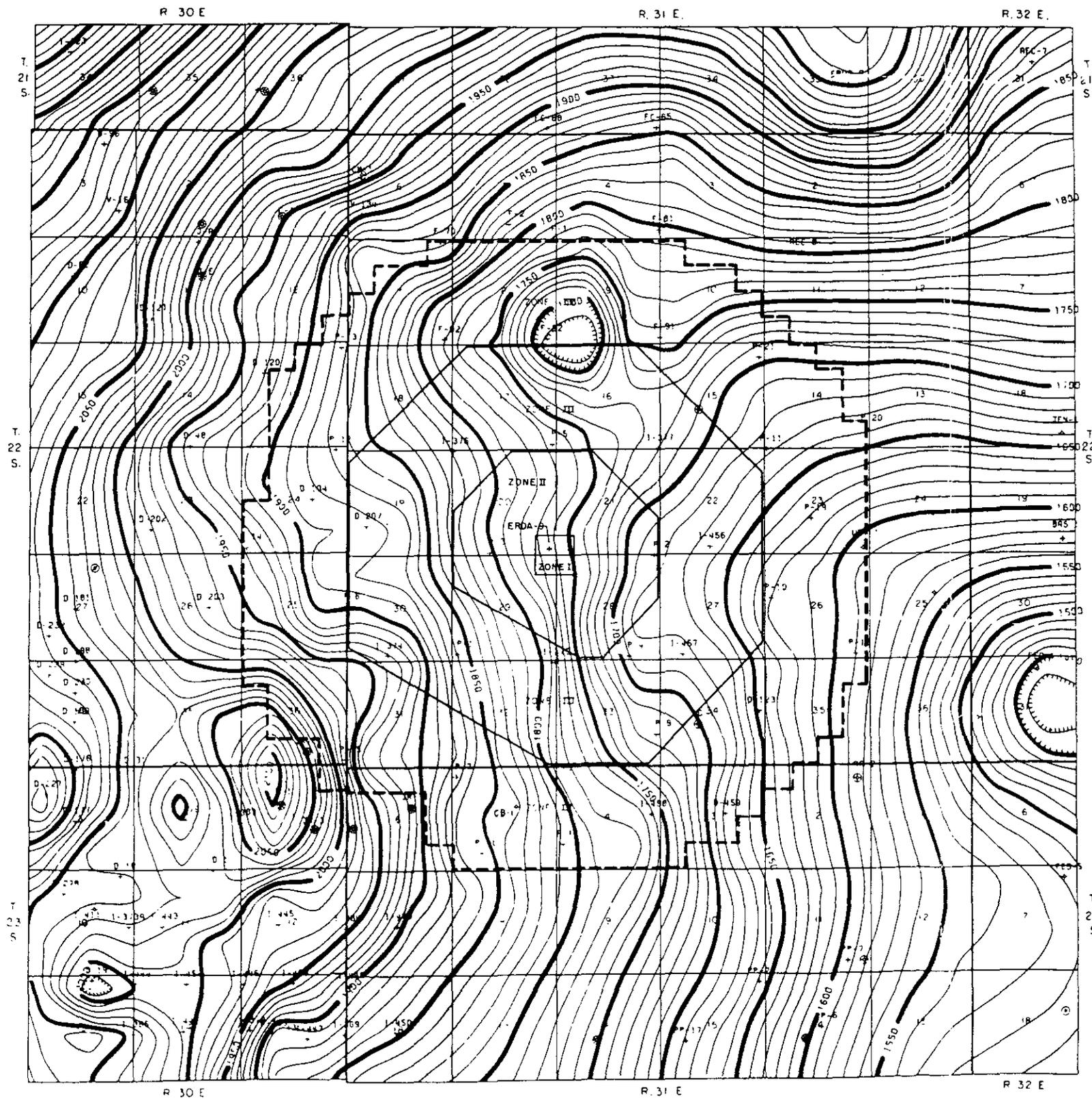
Note:
Borehole sources of data are shown.

REFERENCE
Griswold, 1977, figure 13

Contour interval, 10 feet

SCALE IN MILES

STRUCTURE CONTOURS
ON 124-MARKER BED

FIGURE 4.4-7
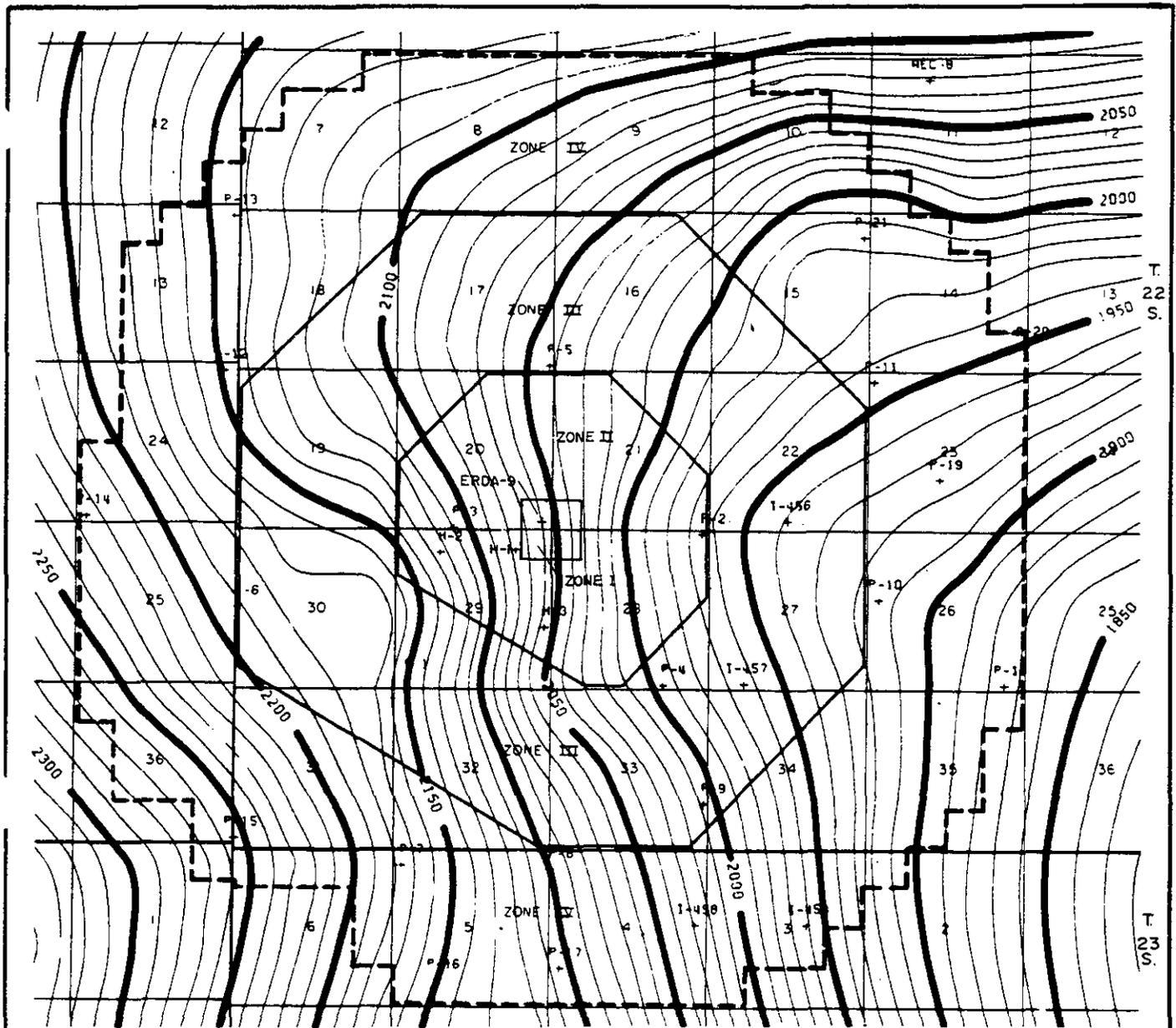
R. 30 E.   R. 31 E.

0   1   2   3
SCALE IN MILES

Contour interval, 10 feet

Note:
Borehole sources of data are shown.

REFERENCE:

Griswold, 1977, figure 9

STRUCTURE CONTOURS
ON TOP OF
VACA TRISTE MARKER BED

FIGURE 4.4-8
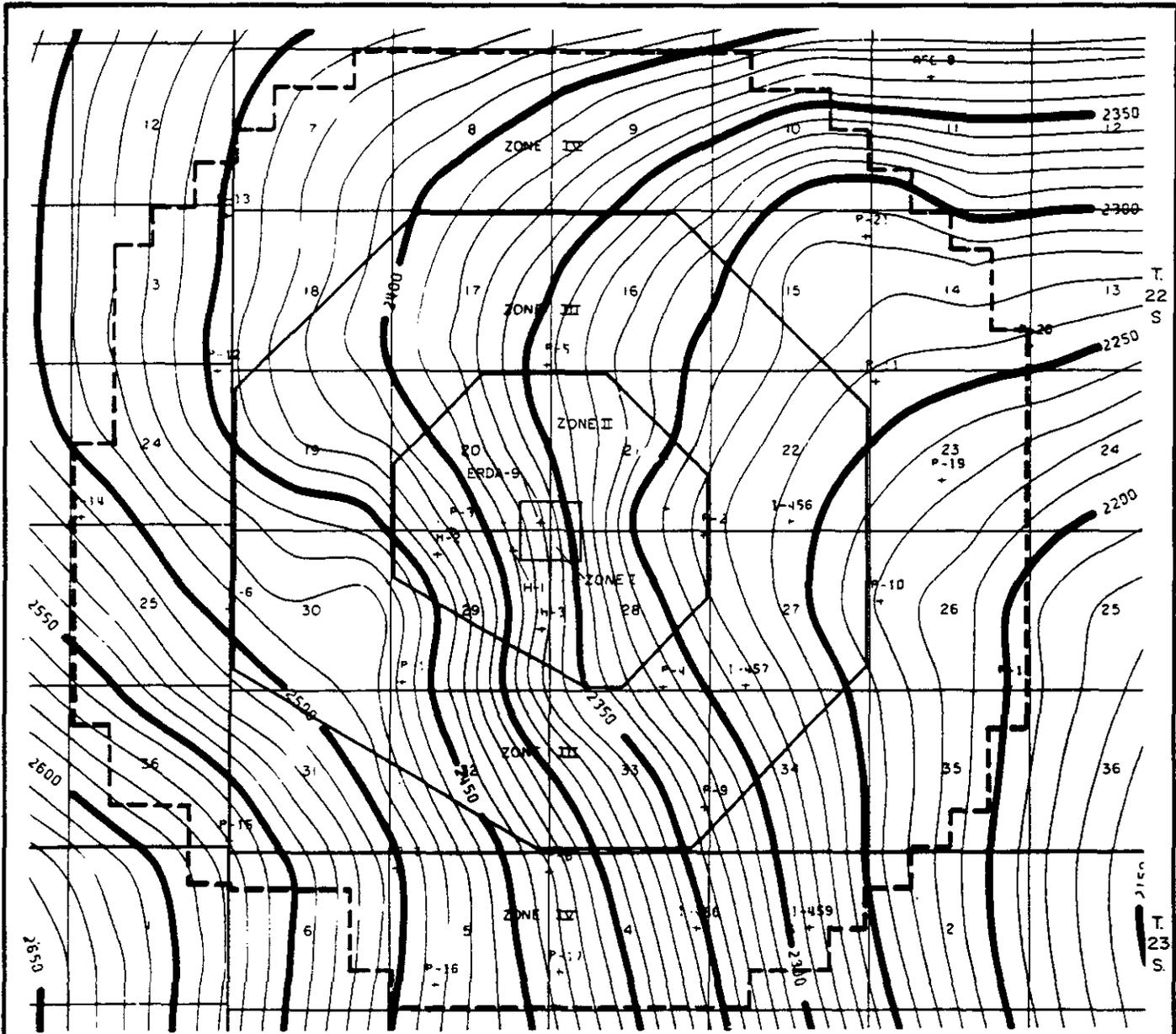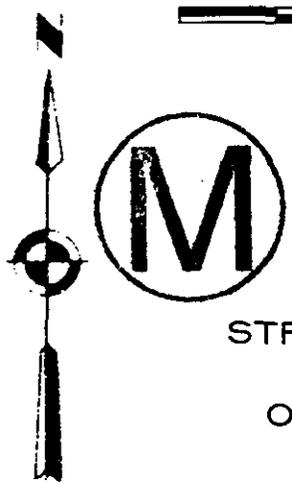
STRUCTURE CONTOURS

ON 103 MARKER BED
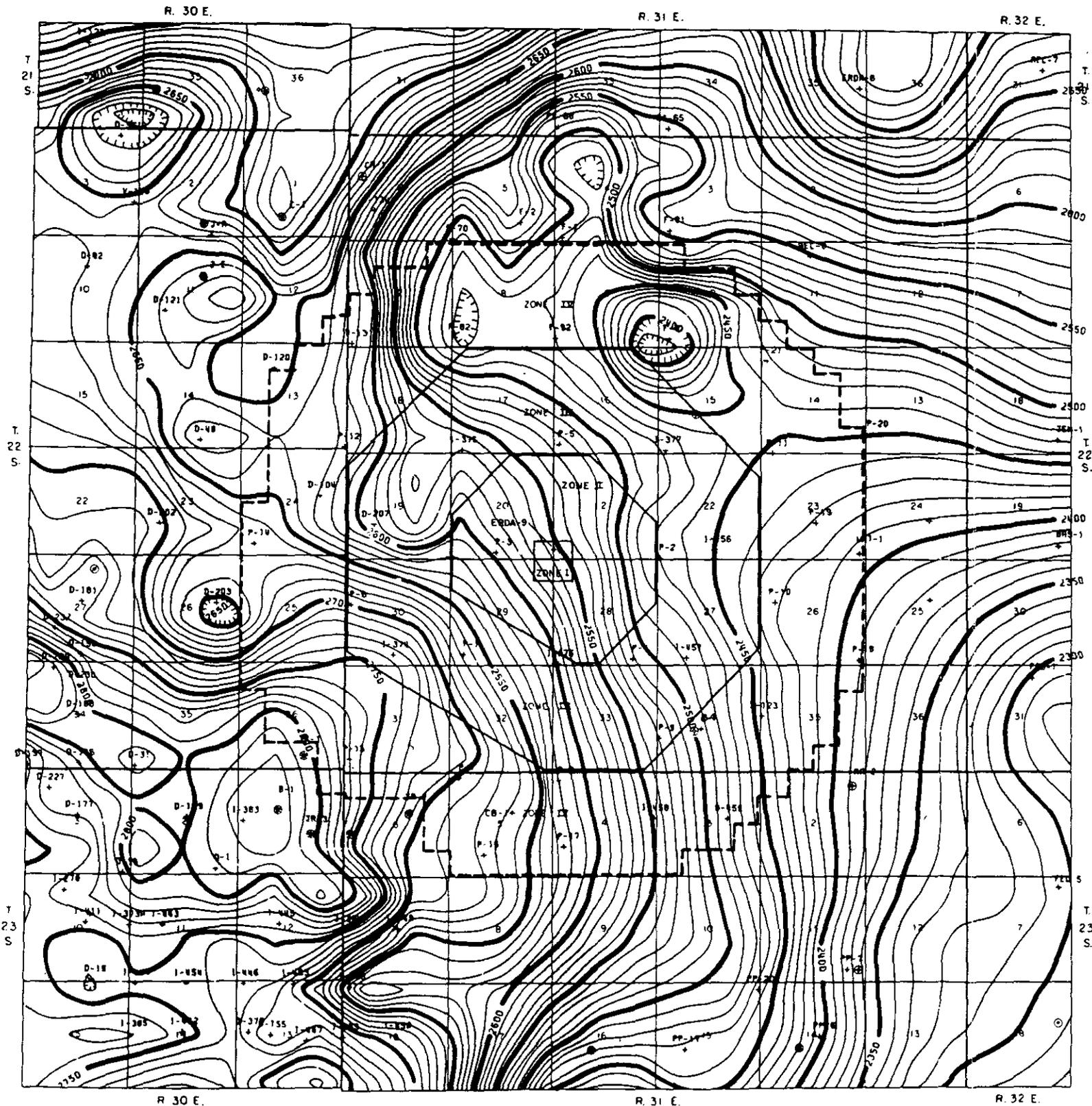
FIGURE 4.4-9

Contour interval, 10 feet

Note:
Borehole sources of data are shown.

SCALE IN MILES

REFERENCE:

Griswold, 1977, figure 9

R. 30 E.

R. 31 E.

SCALE IN MILES

STRUCTURE CONTOURS
ON TOP OF
SALADO FORMATION

FIGURE 4.4-10
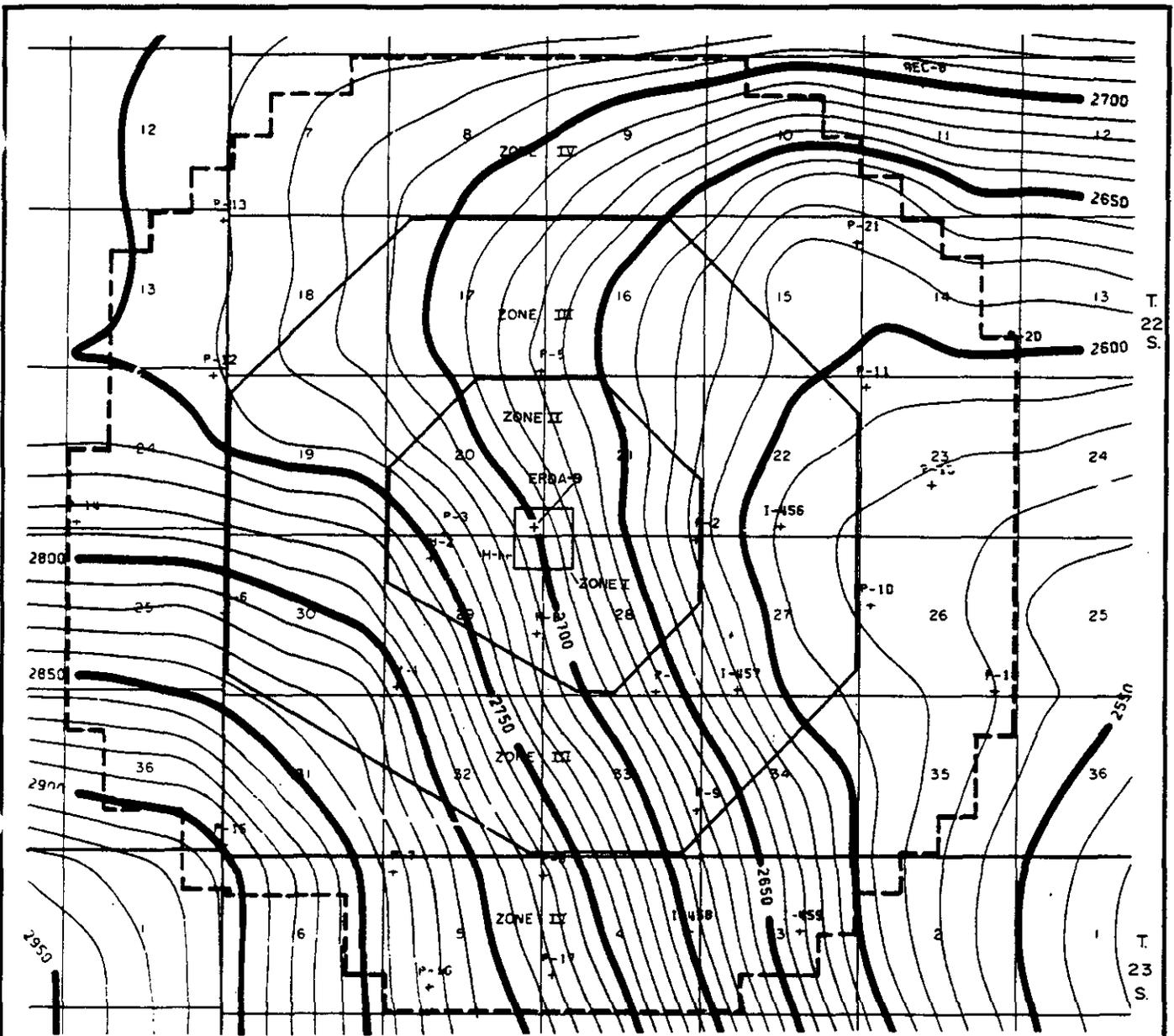
Contour interval, 10 feet

Note:
Borehole sources of data are shown.

REFERENCE:

Griswold, 1977, figure 9

SCALE IN MILES

STRUCTURE CONTOURS
ON TOP OF
CULEBRA DOLOMITE MEMBER

FIGURE 4.4-11
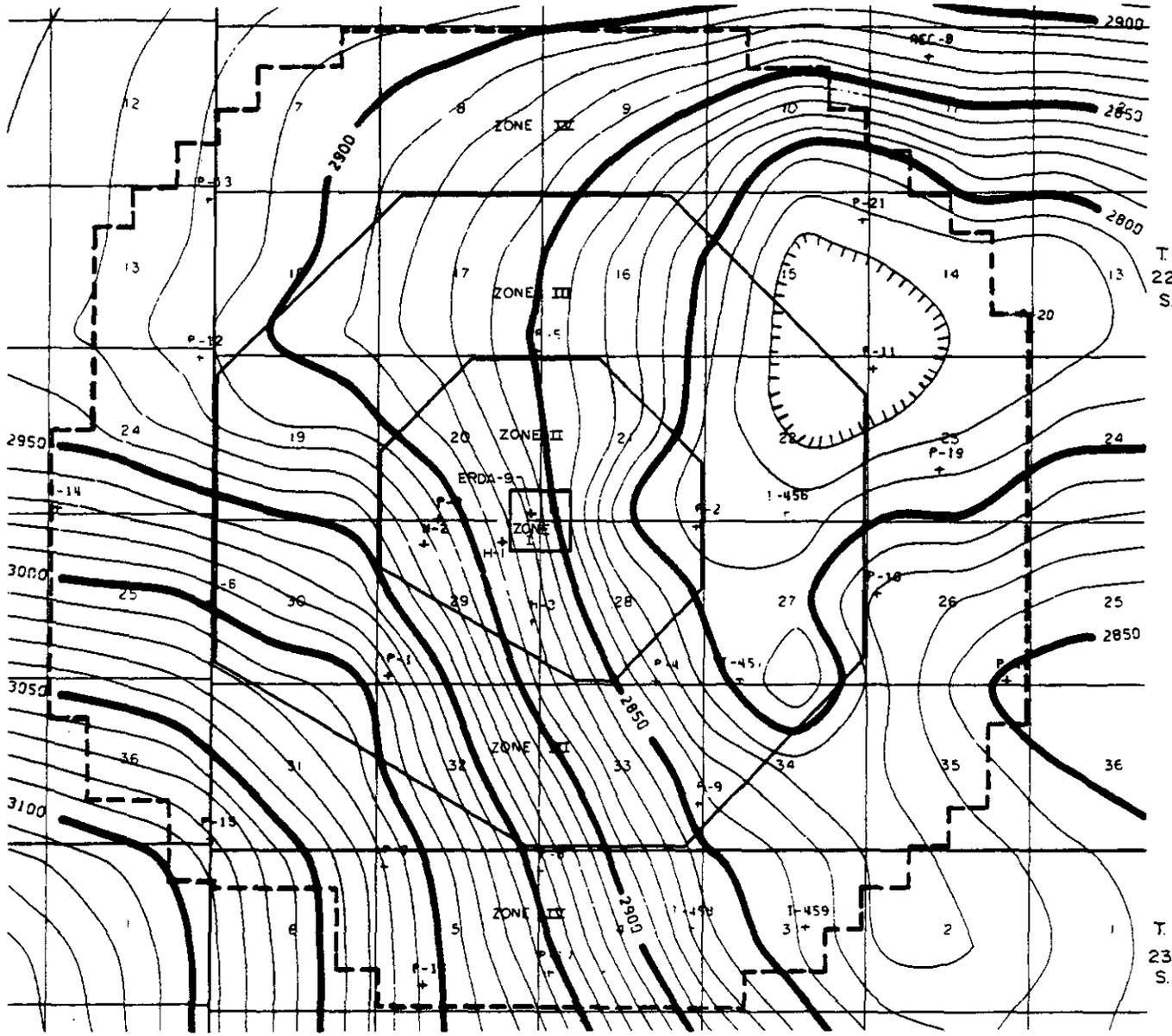
R. 30 E.

R. 31 E.

T. 22 S.

T. 23 S.

Contour interval, 10 feet

Note:
Borehole sources of data are shown.

0   1   2   3
SCALE IN MILES

REFERENCE:

Griswold, 1977, figure 8

STRUCTURE CONTOURS
ON TOP OF
RUSTLER FORMATION

FIGURE 4.4-12
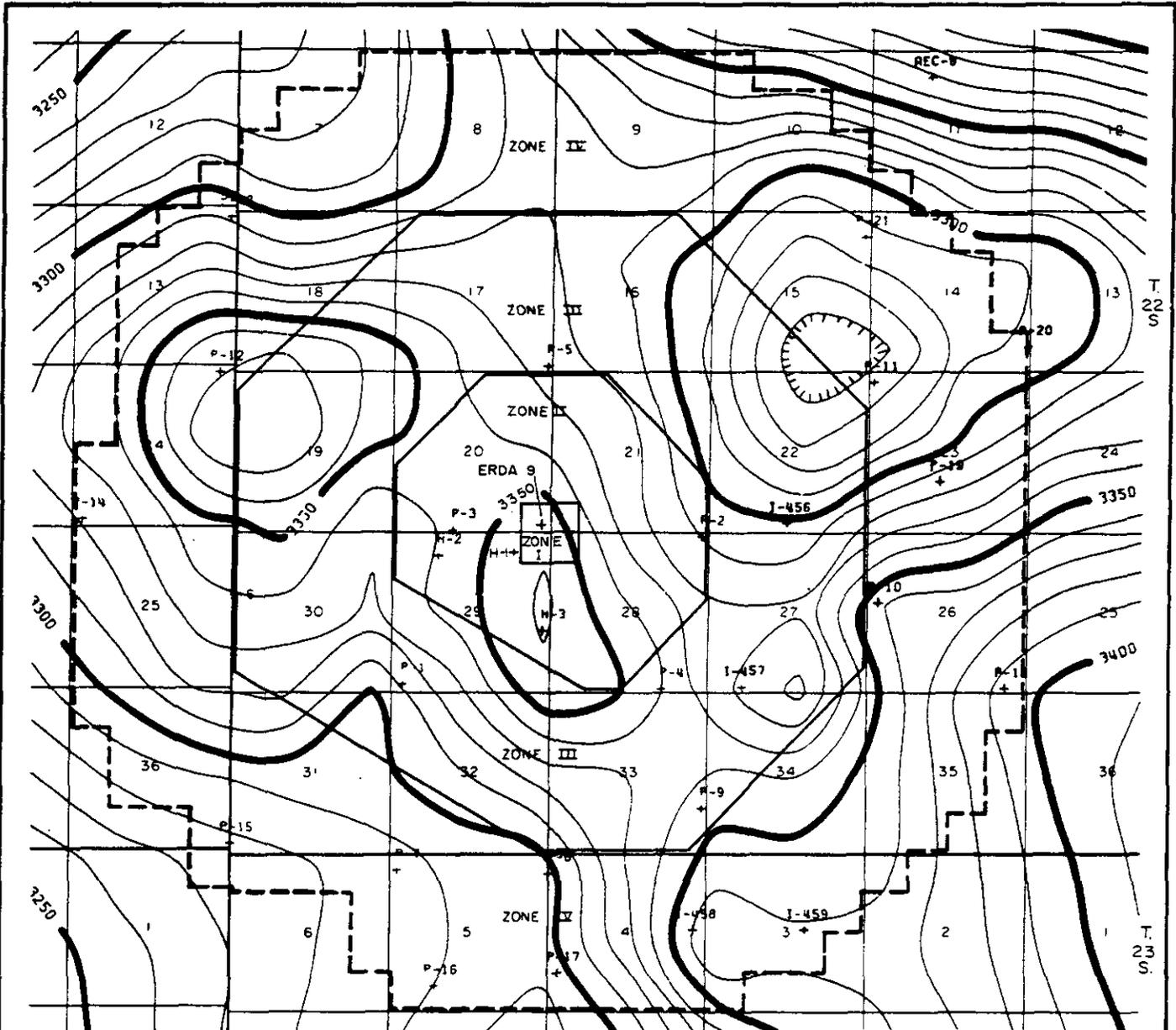
Contour interval, 10 feet

Note:
Borehole sources of data are shown.

N

SCALE IN MILES

0   1   2   3

REFERENCE:

Griswold, 1977, figure 8

STRUCTURE CONTOURS
ON TOP OF
DEWEY LAKE REDBEDS
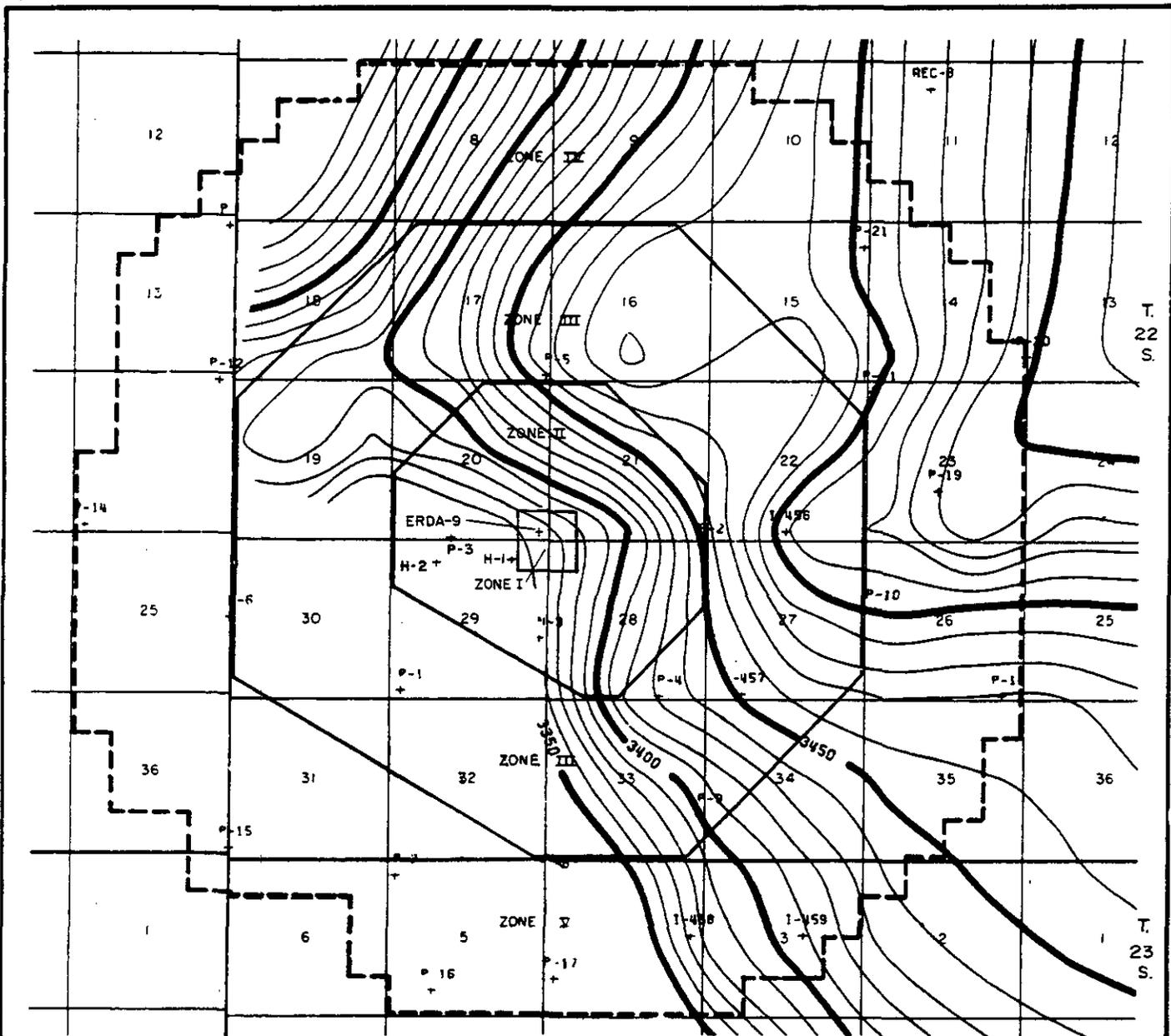
FIGURE 4.4-13

Contour interval, 10 feet

Note:
Borehole sources of data are shown.

REFERENCE:

Griswold, 1977, figure 8

SCALE IN MILES

STRUCTURE CONTOURS
ON TOP OF
SANTA ROSA SANDSTONE

FIGURE 4.4-14

Contour interval, 10 feet
Note:
Borehole sources of data are shown.

SCALE IN MILES

REFERENCE:

Griswold, 1977, figure 8

STRUCTURE CONTOURS
ON TOP OF
GATUNA FORMATION

FIGURE 4.4-15

TABLE 4.1-1

HOLE NO.	T/R/S	COLLAR ELEVATION	SALADO ELEVATION	BASE 124 ELEVATION	TOTAL DEPTH	HOLE NO.	T/R/S	COLLAR ELEVATION	SALADO ELEVATION	BASE 124 ELEVATION	TOTAL DEPTH
I-123	21/30/34	3170	2182	1382	1880	P-4	22/31/28	3441	2511	1688	1857
W-7	21/31/31	3333	2743	2046	N/A	P-1	22/31/29	3446	2668	1859	1591
FC-63	21/31/32	3409	2719	1997	1483	P-6	22/31/30	3554	2695	1892	1573
FC-68	21/31/32	3430	2510	1881	1644	I-374	22/31/30	3340	2735	1931	1538
F-52	21/31/34	3485	2625	1970	1623	P-15	22/31/31	3310	2768	1957	1465
FC-65	21/31/34	3465	2645	1851	1869	P-9	22/31/33	3406	2528	1714	1796
FC-69	21/31/34	3461	2632	1952	1562	I-375	22/31/33	3390	2600	1788	1746
ERDA-6	21/31/35	3536	2721	1999	2775	D-123	22/31/34	3432	2444	1644	1880
AEC-7	21/32/31	3662	2664	1874	3918	G-1	22/31/34	3450	2495	1708	4475
C-1	22/30/1	3357	2727	1954	13950	JEN-1	22/32/18	3896	2471	1664	4898
D-96	22/30/3	3189	2609	2133	1210	BAS-1	22/32/19	3820	2378	1578	4802
V-188	22/30/3	3170	2660	2108	1173	FED-1	22/32/31	3627	2294	1447	4777
D-82	22/30/10	3149	2669	2102	1135	B-1	23/30/1	3290	2825	2115	14312
D-121	22/30/11	3202	2642	2045	1266	I-383	23/30/1	3272	2832	2061	1307
J-A	22/30/11	3191	2673	2014	14923	JR-3	23/30/1	3288	2806	2041	15692
J-E	22/30/11	3220	2626	1991	13950	D-1	23/30/2	3241	2809	2032	1310
D-120	22/30/13	3338	2654	1930	1500	D-31	23/30/2	3244	2812	2036	1314
D-48	22/30/14	3337	2627	1937	1524	D-179	23/30/2	3244	2794	1997	1350
D-202	22/30/23	3323	2703	1981	1443	D-176	23/30/3	3197	2782	2078	1223
D-104	22/30/24	3388	2629	1883	1596	D-177	23/30/3	3151	2741	2088	1188
P-12	22/30/24	3376	2627	1867	1598	D-197	23/30/3	3141	2731	2110	1138
P-14	22/30/24	3358	2671	1939	1545	D-227	23/30/3	3246	2818	N/A	1073
D-203	22/30/26	3317	2647	1965	1443	D-18	23/30/10	3190	2806	2040	1265
D-181	22/30/27	3288	2748	2039	1345	I-278	23/30/10	3120	2780	2035	1217
D-198	22/30/27	3258	2748	2069	1302	I-373A	23/30/10	3140	2785	2036	1242
D-229	22/30/27	3218	2825	2068	1266	I-411	23/30/10	3128	2753	2041	1206
D-232	22/30/27	3258	N/A	2063	1221	I-443	23/30/11	3185	2770	2028	1270
D-36	22/30/34	N/A	N/A	N/A	N/A	I-445	23/30/12	3235	2765	1988	1385
D-180	22/30/34	3210	2790	2083	1230	D-TS5	23/30/13	3210	2685	1848	1495
D-188	22/30/34	N/A	N/A	N/A	N/A	PP-19	23/30/13	N/A	N/A	N/A	N/A
D-230	22/30/34	3231	2821	2067	1195	I-370	23/30/13	3220	2740	1988	1341
JR-1	22/30/36	3308	2802	2037	17555	I-446	23/30/13	3210	2730	1978	1345
D-160	22/30/36	N/A	N/A	N/A	N/A	I-447	23/30/13	3250	2741	1891	1480
F-81	22/31/3	3471	2851	1797	1735	I-453	23/30/13	3240	2730	1963	1405
F-2	22/31/5	3404	2629	1818	1690	I-385	23/30/14	3185	2770	2046	1238
CM-1	22/31/6	3376	2688	1961	14050	I-442	23/30/14	3170	2755	2007	1275
V-134	22/31/6	3363	2622	1898	1563	I-444	23/30/14	3130	2745	2003	1240
F-70	22/31/7	3388	2490	1867	1603	I-454	23/30/14	3170	2735	2000	1300
F-82	22/31/8	3382	2472	1781	1684	D-19	23/30/15	3149	2727	1957	1369
F-92	22/31/8	3420	2470	1688	1818	I-440	23/30/15	N/A	N/A	N/A	N/A
F-1	22/31/9	3422	2482	1781	1747	AA-2	23/31/2	3453	2383	1583	5190
F-91	22/31/10	3460	2390	1755	1788	I-459	23/31/3	3418	2482	1679	1855
AEC-8	22/31/11	3542	2548	1801	4910	I-458	23/31/4	3385	2549	1762	1750
P-20	22/31/14	3553	2450	1662	1995	P-8	23/31/4	3336	2621	1791	1860
P-21	22/31/15	3510	2467	1705	1915	P-17	23/31/4	3340	2625	1805	1860
P-5	22/31/17	3472	2525	1767	1830	P-7	23/31/5	3332	2702	1873	1575
P-13	22/31/18	3345	2624	1874	1576	P-16	23/31/5	3323	2677	1853	1585
D-207	22/31/19	3406	2595	1886	1613	CB-1	23/31/5	3320	2662	1845	4190
ERDA-9	22/31/20	3415	2555	1765	2890	JR-7	23/31/6	3319	2713	1920	14590
I-376	22/31/20	3410	2570	1819	1702	I-384	23/31/7	3290	2790	1984	1438
P-3	22/31/20	3382	2596	1803	1676	I-449	23/31/7	3310	2680	1906	1515
I-377	22/31/22	3490	2476	1720	1876	PP-7	23/31/11	3485	2375	1593	2033
I-456	22/31/22	3520	2451	1867	1975	PP-6	23/31/14	3485	2405	1594	2079
P-11	22/31/23	3506	2448	1673	1940	PP-17	23/31/15	3418	2468	1689	1920
P-19	22/31/23	3546	2429	1629	2000	PP-20	23/31/15	3429	2469	1880	1910
WRT-1	22/31/23	3595	2406	1596	4766	I-369	23/31/18	3280	2715	1871	1538
P-10	22/31/26	3508	2422	1820	2009	I-448	23/31/18	3290	2625	1900	1510
P-18	22/31/26	3479	2391	1590	1993	I-450	23/31/18	3300	2690	1854	1570
I-457	22/31/27	3460	2480	1683	1885	FED-5	23/32/7	3539	N/A	N/A	4712
P-2	22/31/28	3478	2470	1683	1895						

P—ERDA POTASH HOLE
V—U.S. POTASH CO. (MISSISSIPPI POTASH)
D DTS DUVAL CORP.
I—INTERNATIONAL MINERALS
PP—PERMIAN POTASH
F—FC —KERR McGEE
N/A—NOT AVAILABLE

4.2

5.1   INTRODUCTION

The study of the Los Medanos site region's seismicity is of interest for
two reasons. First, it forms the primary basis for the analysis and
selection of reasonably expected vibratory ground motion for use in
aseismic design; second, when considered along with the geology and
tectonic history of the region, it provides some indication of current
and long-term tectonic stability. In this chapter both aspects of the
regional seismicity are discussed.

In Section 5.2 the temporal and geographic distribution of observed
earthquakes in the site region are discussed. The regional seismicity is
considered in two separate time intervals suggested by the type and
quality of information available during each interval. These intervals
are: before 1962, and from 1962 to the present. In the post-1962
period, several specialized instrumental studies are considered in
addition to a more general regional instrumental survey.

Using the information developed on regional seismicity, and some
additional simple assumptions about regional tectonism, a preliminary
analysis of probabilistic vibratory ground motion at the ground surface
is derived in Section 5.3 in a way that is useful for seismic design
characterization at the site during its active phase of development and
use. This analysis shows that short-term accelerations during the
operational phase are likely to be very modest. Probabilities at which
higher acceleration levels occur depend almost exclusively on the
assumptions made about the seismic capabilities of the immediate site
area.

Finally, in Section 5.4, regional seismicity is considered as an
indicator of long-term tectonic processes. Regional stress patterns, as
implied by focal mechanism solutions for regional earthquakes and in-situ
stress measurements, and regional tectonism, as implied by earthquake

recurrence statistics, are both considered. Several tentative
conclusions are reached as a result of this study and are outlined at the
conclusion of this chapter.

5.2 SEISMICITY

In this section the temporal and geographic distribution characteristics
of observed earthquakes in the site region are discussed. Detailed
discussion is restricted to earthquakes within 300 kilometers (about 186
miles) of the Los Medanos site in view of historical analysis by Sanford
and Toppozada (1974).

As always, in studying any single earthquake or group of earthquakes, it
is important to note the date of occurrence in relation to the state of
the art of seismology at the time. The certainty with which fundamental
properties of earthquakes, such as size and location, can be determined
largely depends on the availability and quality of instrumental data.
Prior to 1960, nearly all information on the strengths and distribution
of earthquakes in New Mexico was determined without the aid of
instruments (Sanford, 1965). Therefore, inferences which may be drawn
from pre-1960 seismicity studies are fundamentally different and more
speculative than instrumentally derived parameters.

Instrumental studies of earthquakes in New Mexico began in June 1960 when
high magnification seismographs were placed in operation by the New
Mexico Institute of Mines and Technology at Socorro, and by the Atomic
Energy Commission at Sandia Base near Albuquerque (Sanford et al.,
1972). These two stations provided some information on locations and
strengths of earthquakes in central New Mexico, but accurate information
about locations throughout the state was not available until the
beginning of 1962, when additional high-gain stations went into operation
in New Mexico and bordering states (Las Cruces, N.M.; Payson, Arizona;
Ft. Sill, Oklahoma). Also at this time the United States Coast and
Geodetic Survey (U.S.C.G.S.) established a regular reporting station at
Albuquerque. Instrumental seismology for the state of New Mexico as a
whole dates from this time.

In this discussion the format of a previous study by Sanford and Toppozada (1974) is followed. Regional seismicity of the Los Medanos site area is considered in two distinct time frames in accordance with the types of data available. Preinstrumental data, roughly that before 1962 in the site area, is treated first; a separate study of the later period for which seismograph records exist follows in several separate subsections.

Two very recent investigations of seismicity on a much more local scale affect the Los Medanos site. One involves recordings made on a continuously operating, vertical component, high frequency system installed and operated at the site itself by personnel from the New Mexico Institute of Mining and Technology at Socorro. The principal objective of this station, which has gathered data for most of the interval April 5, 1974, to October 29, 1977, and which continues to function, has been to determine if seismic activity is occurring at or near the proposed nuclear waste repository at such a low level that it might not be adequately detected by more standard instrumental data surveys (Sanford et al., 1976a). The other recent study is one designed to investigate in detail local small magnitude seismicity in and near the Central Basin Platform of west Texas. To this end, a seismic array centered near Kermit, Texas, has been installed. Initial operation of this array began in early November 1975, and some preliminary conclusions have been reached at this time (Hays, 1977; Rogers and Malkiel, 1978). Both of these recent study efforts will be discussed in separate subsections of this report.

In a final subsection, two small earthquakes important to the question of background seismicity level in the immediate site area are discussed.

5.2.1   Preinstrumental Data - Regional

Most historic earthquakes in New Mexico cataloged before seismic instrumentation occur in the Rio Grande Valley area between Albuquerque and Socorro. About half the earthquakes of Modified Mercalli Intensity V

or greater in New Mexico between 1868 and 1973 are in this region. In conformity with previous studies (Sanford and Toppozada, 1974; Sanford et al., 1978) these events are not considered to be of immediate concern for this study and will not be discussed further. As will be seen, the area within roughly 200 kilometers of the site has experienced only low intensity earthquakes prior to the first availability of seismographic data in 1961; there have been a few modestly damaging earthquakes during the same interval between 200 and 300 kilometers from the site. The area up to 300 kilometers from the site is defined as the site region in the following discussions.

Figure 5.2-1 shows locations of earthquakes occurring before 1961 that have been assigned epicenters within 300 kilometers of the site. Table 5.2-1 lists the events shown on Figure 5.2-1. Intensities appearing in this table, and anywhere in this section, are Modified Mercalli intensities (Wood and Neumann, 1931).

The primary source used was Sanford and Toppozada (1974), although some supplemental descriptive material was obtained from Neumann and Bodle (1932), Neumann (1932, 1938, and 1940), Murphy and Ulrich (1951), Murphy and Cloud (1954 and 1957), Northrop and Sanford (1972), and Coffman and Von Hake (1973). An abridged version of the Modified Mercalli Intensity Scale of 1931 may be found in Table 5.2-2. In the descriptions below, intensities in parentheses were assigned by Sanford and Toppozada (1974) based only on their personal evaluation of the data.

> 1923, Mar. 7 El Paso, Texas V Felt in Sierra Blanca (166 kilometers to SE), Columbus (130 kilometers to W), Alamogordo (135 kilometers to N). Newspaper accounts suggest epicenter in northern Chihuahua. (Sanford and Toppozada, 1974).

> 1926, July 17 Hope and Lake Arthur, N.M. III Earth sounds heard in NE direction at Hope; windows rattled at Lake Arthur. (Sanford and Toppozada, 1974).

1930, Oct. 4 Duran, N.M. IV A moderate shock felt by many.
Rolling motion, rumbling sound, rattled windows. No damage.
(Neumann and Bodle, 1932).

1931, Aug. 16 Valentine, Texas VIII At Valentine, the point of
maximum destruction, all types of buildings, especially adobe, were
heavily damaged; many chimneys fell. There were some cracks in the
ground, and tombstones rotated both clockwise and counterclockwise.
While people were panic-stricken, there were no fatalities and only
a few minor casualties. There were cracked walls and damaged
chimneys in several towns in Brewster, Jeff Davis, Culberson, and
Presidio Counties. Some rockslides occurred in the mountains.
There were rumbling and roaring sounds. This earthquake would have
been severe in a densely populated region. (Coffman and Von Hake,
1973).

1931, Aug. 16 Valentine, Texas (V) Strong aftershock of intensity
VIII event.

1931 Aug. 18 West Texas V at Alpine, Pecos, Lobo, and Valentine;
IV at Carlsbad, N. Mex. This was preceded by a lighter shock on the
same day. Recorded at Tucson. (Neumann, 1932).

1931, Aug. 19 Valentine, Texas (V) Strong aftershock of intensity
VIII event.

1931, Oct. 2 El Paso, Texas III "To-day", El Paso, Texas.
Feeble. (Neumann, 1932).

1931, Nov. 3 Valentine, Texas (V) West Texas. Felt at
Valentine. Aftershock of August 16 earthquake. Recorded at Tucson.

1935, Dec. 20 Clovis, New Mexico III-V Two Shocks. A tile wall
in a creamery was cracked. Another report of wall paper being split
(AP news item). (Northrop and Sanford, 1972).

1936, Jan. 8 Carlsbad, N.M.? (IV) Felt by few; press reports some property damage (Neumann, 1938). Newspaper account indicates this earthquake was probably centered near Ruidoso, N.M. (Sanford and Toppozada, 1974).

1936, Aug. 8 El Paso, Texas (III) Weak shock not felt elsewhere (Neumann, 1938).

1936, Oct. 15 El Paso, Texas (III) "Earth tremor" shortly before noon. No details. (Neumann, 1938).

1937, Mar. 31 El Paso, Texas (V) Slight. Felt by many. (Neumann, 1940).

1937, Sept. 30 Ft. Stanton, N.M. V Slight. Awakened many. (Neumann, 1940).

1943, Dec. 27 Tularosa, N.M. IV Rattled windows. (Sanford and Toppozada, 1974).

1949, Feb. 2 Carlsbad, N.M. IV Press reported two distinct shocks which were felt by several. A few people were frightened. Windows, doors, and dishes rattled; houses seemed to shudder momentarily. (Murphy and Ulrich, 1951).

1949, May 23 East Vaughn, N.M. VI Felt over an area of only about 1300 square miles. "Results of a questionnaire coverage indicated the felt area to be a 20-mile strip connecting Pastura with Vaughn and East Vaughn. Maximum intensity VI at the last named place where a few things fell from shelves, loose objects rattled and buildings creaked. Deep rumbling and grinding sounds were heard before and during shock" (Murphy and Ulrich, 1951). Many people were awakened and many were frightened. One person felt the shock while driving a car 20 miles southeast of Vaughn on the highway to Roswell. (Northrup and Sanford, 1972).

1952, May 22 Dog Canyon, New Mexico (about 70 miles northwest of Carlsbad). IV Felt by two in ranch house. Windows, doors, and dishes rattled; house creaked. (Murphy and Cloud, 1954).

1955, Jan 27 Valentine, Texas IV Felt by many. Houses shook (Murphy and Cloud, 1957).

As can be seen from the above data, there have been no earthquakes of epicentral intensity V or greater recorded as occurring within about 200 kilometers of the Los Medanos site when noninstrumental data alone is considered. The strongest earthquake reported to occur within 300 kilometers of the site was the Valentine, Texas event of August 16, 1931. The reported maximum intensity for this shock was VIII on the Modified Mercalli scale (Table 5.2-2). Reports of earthquake intensity for a wide area have been compiled into several isoseismal maps (Neumann, 1932; Sellards, 1933). Intensities in these maps are based on the Rossi-Forel scale which was subsequently abandoned for the Modified Mercalli Scale of 1931. Sanford and Toppozada (1974) have assigned Modified Mercalli intensities on the basis of descriptions of the earthquake effects for this event and plotted the isoseismal map shown in Figure 5.2-2. According to this map the intensity at the site was probably no greater than V. This is the largest known historical site intensity.

Close to the source, the isoseismals are elongated northwest-southeast conforming to the structural grain of the region. Further from the epicenter, the earthquake had higher intensities to the east than west due to lower topographic relief to the east (Sanford and Toppozada, 1974), differences in attenuation, or some other reason. The data to the southwest, in Mexico, are particularly sparse.

Two instrumental locations have been published for this earthquake. The U.S.C.G.S. (Neumann, 1932) places the epicenter at 29.9°N and 104.2°W with an origin time of 11:40:15 GMT. Byerly (1934), who made a detailed instrumental investigation of this earthquake, found the epicenter to be

at 30.9°N and 104.2°W with an origin time of 11:40:21 GMT. Byerly's epicenter, 110 kilometers north of the U.S.C.G.S. epicenter is closer to the region of highest reported intensities and may for this reason be considered the more accurate of the two. Although neither is particularly close to Valentine, Texas, the USCGS and Byerly epicenters bracket this area of max reported intensity fairly well. For the purposes of Figure 5.2-1 and Table 5.2-1, Valentine, Texas, has been adopted for the location of the main earthquake and its aftershocks in agreement with the work of Sanford and Toppozada (1974).

The area over which an earthquake is perceptible can be used to estimate its magnitude (Slemmons et al., 1965; Wiegel, 1970), although this relationship is an empirical one different for different regions of the United States. If a felt area of 4.5×10^5 mi^2 is accepted (1.15 x 10^6 km^2) as reported by the U.S.C.G.S. (Neumann, 1932) and a magnitude-felt area formula for the central United States and Rocky Mountain region is used (Wiegel, 1970), a magnitude of about 6.4 is calculated for the Valentine, Texas, earthquake. This result appears reasonable and is compatible with the maximum intensity reported for the shock (Sanford and Toppozada, 1974). It is also in good agreement with the estimate of magnitude for this event calculated at Pasadena (Gutenberg and Richter, 1954).

Other earthquakes within 300 kilometers of the site were probably not perceptible or resulted in low intensities in the site area.

5.2.2   Instrumental Data--Regional

As mentioned above instrumental studies of earthquakes in New Mexico began in June 1960 when high-magnification seismographs were placed in operation on the campus of the New Mexico Institute of Mining and Technology at Socorro and by the Atomic Energy Commission at Sandia Base near Albuquerque (Sanford et al., 1972). Most of the early seismic research at Socorro was concentrated on near shocks (Sanford and Holmes, 1961, 1962; Sanford, 1963) because of this initial station distribution

and because information from other stations located in New Mexico and adjacent states was not available in sufficient quantity for a study of the seismicity of the entire state. This situation changed about the beginning of 1962 when stations at Albuquerque and Las Cruces, New Mexico; Payson, Arizona; and Ft. Sill, Oklahoma; began continuous operation.

Detailed reports on the instrumental seismicity of New Mexico as a whole have appeared in a number of publications, principally Sanford (1965), Sanford and Cash (1969), and Toppozada and Sanford (1972). Collectively, these papers cover the interval January 1, 1962, through June 30, 1971. The study of instrumental seismicity in this area, as in any other, evolved over this 11 year period. Not only did more data become available as more seismograph stations began operation, but these data were processed in increasingly sophisticated ways. The ways regional earthquakes have been located and analyzed during this period are summarized below. For a more complete discussion, the reader is referred to the original reports; both those mentioned above and Sanford et al. (1972), Sanford and Toppozada (1974), Sanford (1976a), Sanford (1976b), and Sanford et al. (1976b).

The method used to initially locate the earthquakes during the period January 1, 1962, through June 30, 1964 (Sanford, 1965) was based on the procedure described by Richter (1958). This is an arc intersection procedure where: 1) a trial origin time is estimated from measured S-P intervals, 2) a depth is selected, either 5 kilometers or 10 kilometers, 3) station-epicenter distance is calculated from the P-O (origin time) intervals and a T-D curve (in this instance a graph relating travel time to distance for each of the two depths of focus) and 4) the epicenter is determined from the intersection of the arcs whose radii have just been calculated in step 3) above. If no satisfactory intersection occurs, the process is repeated after adjustment of the origin time estimate. The time-distance curves used by Sanford (1965) in this process were based on a simple crustal model close to the average of those found for the region in previous studies (Tatel and Tuve, 1955; Stewart and Pakiser, 1962;

Romney et al., 1962). The crustal model adopted consisted of a single 39 kilometers thick layer with a P-wave velocity of 6.0 km/sec overlying a half-space with a P-wave velocity of 8.0 km/sec. The two T-D curves, one for a depth of focus of 5 kilometers and one for a 10 kilometers focal depth, were calculated using this model.

For earthquakes occurring between July 1, 1964, and December 31, 1967, a slightly different format was used to present the data (Sanford and Cash, 1969). Whenever available, origin times and epicentral coordinates were taken directly from U.S.C.G.S. reports. Two types of data distributed by the U.S.C.G.S. were consulted; the Monthly Summary series, or where these were not yet published, as for the period October 1966 through December 1967, the Preliminary Determination of Epicenters reports. A majority of the New Mexico earthquakes listed in this period were not located by the U.S.C.G.S., however. When this was the case, events were located precisely as outlined above for the earthquakes of January 1962 through June 1964.

Finally, for initial location of those shocks occurring from January 1968 to June 1971, inclusive, the procedure adopted was identical to that of the previous reporting period except that for those earthquakes located by the New Mexico Institute of Mining and Technology a focal depth of 8 kilometers was used to construct the T-D curves (Toppozada and Sanford, 1972).

The method of assigning magnitudes to the earthquakes of New Mexico has also undergone some evolution. From the start the idea has been to calculate a close analog to the Richter local magnitude (M_L). Magnitude can be expressed by the equation $M_L = \log A - \log A_o$, where A is the maximum trace amplitude (almost always the crustal shear wave, Sg, for local and regional New Mexico earthquakes, Sanford, personal communication, 1978) in millimeters on the seismogram and A_o is the corresponding trace amplitude for a calibration earthquake selected as the standard. The numbers obtained for M_L are dependent on the magnification and frequency response of the seismograph used, and on the

selection of the standard shock. The original Richter scale is based on the Wood-Anderson seismograph, an instrument which records horizontal motion, whose natural period is 0.8 second, and whose static magnification and damping are 2800 and 0.8 critical, respectively. Furthermore, the standard or zero magnitude event is defined such that it would produce a trace deflection of one thousandth of a millimeter when recorded by a Wood-Anderson seismograph at a distance of 100 kilometers.

The direct application of the Richter scale to New Mexico earthquakes was impossible, because none of the available data came from Wood-Anderson seismographs. As an initial best estimate, Sanford (1965) decided to rate the shocks on the basis of the amplitude a Wood-Anderson instrument would produce had it recorded these shocks; that is, maximum trace deflections were first converted to ground displacements, which in turn, were converted to equivalent Wood-Anderson trace amplitudes using the known response characteristics of this instrument. An attempt was made to consider response differences between the actual recording seismograph and the Wood-Anderson seismograph as a function of frequency. The Richter values for A_o were adopted with no attempt to consider possible source or wave transmission differences between those earthquakes occurring in California, where the Richter Scale was developed, and those occurring in New Mexico. Most of the magnitudes were calculated from the maximum SH (or horizontally polarized shear wave) ground motions reported by the station at Las Cruces. When no SH amplitude information was available from the Las Cruces station, magnitude was assigned on the basis of the maximum SV ground motion at Albuquerque. The relation between SV (or vertically polarized shear wave) motion at Albuquerque and magnitude was established from data on shocks detected by both the Las Cruces and Albuquerque stations (Sanford, 1965). This initial attempt to assign magnitudes to New Mexico earthquakes was never intended to be completely accurate but rather to serve as rough indications of the relative strengths of shocks.

Slightly different procedures were followed for magnitudes calculated for
the two later reporting periods of July 1964 to December 1967 and January
1968 to June 1971. In these periods three magnitudes are listed: 1)
U.S.C.G.S., 2) Albuquerque, and 3) Socorro. Magnitudes assigned by the
U.S.C.G.S. (or its later administrative equivalents, such as the National
Oceanic and Atmospheric Administration) are body wave magnitudes (m_b)
based on the maximum amplitude of the initial P phase. Magnitudes
calculated from Albuquerque and Socorro seismograms are based on the
amplitudes of the S phases as noted above. For Albuquerque, the maximum
SH ground motion was converted to an equivalent Wood-Anderson trace
amplitude and the previous procedure was used to obtain an estimate of
the equivalent Richter magnitude. A similar procedure was used for
Socorro magnitudes, except that for these computations it was necessary
to substitute maximum SV motion for maximum SH motion. Checks at the
Socorro station indicate SH averages about 1.5 times as large as SV.
*This correction factor was included in the Socorro magnitudes
computations.*

Since the initial publication of the 1962-1972 instrumental data
(Sanford, 1965; Sanford and Cash, 1969; Toppozada and Sanford, 1972)
several additional studies have been undertaken to partially rework this
data. Two of these, Sanford and Toppozada (1974) and Sanford et al.
(1978), are of particular interest since they deal almost exclusively
with earthquakes within 300 kilometers of the Los Medanos site. Sanford
and Toppozada (1974) list a total of 34 earthquakes in this area. Of
these, 12 appeared in the previously discussed studies, 13 represented
new locations by the New Mexico Institute of Mining and Technology not
previously published, and the remaining events were taken directly from
U.S. Department of Commerce reports, either the Seismological Bulletin or
Earthquake Data Reports. An updated version of this listing is presented
in Sanford et al (1978). In this update four shocks have been added to
the Sanford and Toppozada (1974) tabulation: February 11, 1964; March 3,
1964; October 20, 1964; July 26, 1972. The last of these is most
noteworthy because of its proximity to the site. This event will be
considered in greater detail in a later subsection. The October 20, 1964

earthquake is included here in conformity with Sanford et al (1978) even though this event apparently falls slightly beyond the 300 kilometers circle specified as the region of interest.

The most significant difference between the 1978 and all previous tabulations is in the magnitudes assigned to the individual earthquakes. The shocks listed in Sanford et al. (1978) have local magnitudes (M_L) substantially lower than those published earlier by the New Mexico Institute of Mining and Technology or the U.S.C.G.S. These revised magnitudes came about because in calculating local magnitudes for single earthquakes, it was noticed that a systematic increase in calculated magnitude occurred with increasing distance from the earthquake. This strongly suggested that more efficient transmission of the phase producing maximum trace amplitude was occurring in New Mexico than would be indicated by an uncritical use of the A_o standard earthquake amplitude attenuation factor of Richter (1958). Therefore, a correction factor for attenuation differences, as well as another correction factor for individual station effects, has been incorporated in the latest magnitude calculations.

Listed in Table 5.2-3 and shown in Figure 5.2-1 are the 38 earthquakes as they appear in Sanford et al. (1978). These data represent the latest and best estimate of all significant parameters associated with those earthquakes occurring within 300 kilometers of the Los Medanos site for the interval January 1, 1961, through December 31, 1972.

5.2.3   Specialized Instrumental Studies—Station CLN

With the publication of Sanford and Toppozada (1974), the first phase of the investigation of southeastern New Mexico seismicity ended. This early phase was concerned with the estimation of seismicity in the Los Medanos area based on careful evaluation of available geologic and seismic data. In early 1974 the emphasis changed. Since at that time no data were available from a station very near the site area itself, it was decided that acquisition of new instrumental data from such a station

would be of immediate value. With the installation of a high-gain
seismograph in the site area, the question of the occurrence of low level
seismic activity at or near the proposed waste repository could be more
meaningfully addressed. Therefore, at the beginning of April, 1974, a
single component (vertical) high-gain, continuously recording seismograph
station (given the letter designation CLN by the U.S. Geological Survey)
was installed in a shack located in a caliche pit very near the proposed
nuclear waste disposal site. Analysis and interpretation of the data
collected by this station may be found in Sanford et al (1976a),
Caravella and Sanford (1977) and Sanford et al (1978). In this section
the findings presented in these publications will be briefly discussed.

The essential elements of station CLN are a short-period, vertical
seismometer (Earth Sciences Ranger SD 211), an amplifier (Astrodata 120),
a film recorder (Earth Sciences RF 220), and a WWVB radio receiver
(Specific Products--T60). The recording rate is 1 mm/sec, a speed that
can produce high-resolution seismograms of small local and regional
earthquakes. At this recording rate, the seismograph requires a film
change every three weeks. Otherwise, the station is self-sufficient.
Five minutes of the WWVB coded time signal is placed on the record every
two hours to assure excellent time control. The ground displacement
response of the seismograph has varied slightly over its operating
lifetime as the free period and percent critical damping of the
seismometer changed. These changes are summarized in Sanford et al.
(1978). However, the magnification response of the system has remained
essentially constant within the frequency range 4 to 30 Hz. The peak
magnification is near 455 thousand times when a factor of 12 for record
enlargement during photographic processing is included. This peak occurs
near 22 Hz.

For most of the time since the station went into operation on April 5,
1974, the seismograph has performed as expected, except for the changes
in response characteristics already mentioned. However, there were times
when no records were obtained and when the station was without time
signals. Table 5.2-4 lists these periods and the reasons for the breaks

in service. From April 5, 1974, to October 29, 1977, the total reporting period considered in this subsection, the station was in operation 83 percent of the time.

During the April 1974 to October 1977 period, 291 events identifiable as local and regional earthquakes (Sg - Pg $\leq$ 81 seconds, where Sg and Pg are the crustal shear-wave and compressional-wave arrival times) were recorded at station CLN. For a complete list of these events see Sanford et al. (1978, Table 3). For each earthquake the date, arrival time (GMT), and character, whether impulsive or of several phases, are given. The Sg phase amplitudes (from which magnitudes are determined) are also listed. With the aid of additional arrival times from other regional seismograph stations, epicenters for 75 of these 291 events were obtained. This group of 75 events may be further subdivided into those which are fairly well located (49) and those for which only tentative epicentral locations may be given (26). Table 5.2-5 lists the origin times, locations, and magnitudes (and seismograph stations used) for the seismic events whose epicenters are reasonably well known. A map of these epicenters is shown in Figure 5.2-3. Table 5.2-6 lists the remaining events for which there are insufficient data to allow exact locations. For many earthquakes in Table 5.2-6 two epicenters are possible because readings are presently available from only two stations. In this case, the epicenter is listed that is most compatible with the locations of the well-determined events.

Figure 5.2-4 shows histograms of the number of recorded earthquakes versus the Sg-Pg interval in seconds. The upper histogram represents the complete data set at station CLN for all those events whose Sg-Pg interval is less than or equal to 40 seconds. Major peaks in the histogram occur at Sg-Pg intervals of 8 to 13 seconds, 22 to 24 seconds, and 31 to 36 seconds. The middle histogram shows those events in the CLN data set which occurred during local day-time hours (12:00-02:00 GMT), and the bottom histogram those during the local nighttime hours (02:00-12:00 GMT). The similarity in shape of the middle and bottom histograms suggest that explosions from any small number of specific

sources have been largely eliminated from the data set. However, the disproportionate number of events during the day-time hours (7.62 X 10^{-3}/hour) compared to the nighttime hours (5.14 X 10^{-3}/hour) does not rule out the possibility that some cultural sources still exist in the data set.

Because a substantial fraction of the shocks within each of the prominent peaks of the histogram in Figure 5.2-4 are located, speculation on the epicenters for the other shocks is possible. All of the located shocks within the Sg-Pg distance range of 8 to 13 seconds have epicenters within the area from 31.7° to 32.3°N and from 102.8° to 103.2°W. These coordinates bracket a section of the Central Basin Platform centered roughly on the southeastern corner of New Mexico. All of the evidence suggests that all shocks with Sg-Pg times from 8 to 13 seconds are generated within this section of the Center Basin Platform.

Nearly all of the located shocks with Sg-Pg intervals between 22 and 24 seconds have epicenters within the area from 31.5° to 31.85°N and from 102.2° to 102.8°W. The region defined by these coordinates is centered on a section of the Central Basin Platform located about 50 kilometers southeast of the southeastern corner of New Mexico. Most unlocated shocks with Sg-Pg intervals from 22 to 24 seconds are believed to originate from this section of the Central Basin Platform.

The known epicenters for shocks with Sg-Pg intervals from 31 to 36 seconds indicate a number of tectonically active regions are contributing to this peak in the histogram. Notable among these is a region centered on Valentine, Texas, the site of a strong earthquake in 1931 (Sanford and Toppozada, 1974), and much of the Tularosa Basin.

5.2.4   Specialized Instrumental Studies--Central Basin Platform

The first earthquake to be located in the Central Basin Platform from instrumental data occurred on February 3, 1965. This event attracted little attention at first although it was recorded at a number of

regional stations (Socorro, New Mexico; Lubbock, Texas; Ft. Sill, Oklahoma; Vernal, Utah; Las Cruces, New Mexico; El Paso, Texas; and Albuquerque, New Mexico) and was located by the New Mexico Institute of Mining and Technology (Sanford and Cash, 1969). It was not, for example, listed in the Preliminary Determination of Epicenters reports of the U.S.C.G.S.

To learn more about the seismicity of the Central Basin Platform in conjunction with their study of southeastern New Mexico earthquake risk, Sanford and Toppozada (1974) examined the total available record from station FOTX, a Long Range Seismic Measurements (LRSM) station near Ft. Stockton, Texas, in operation from June 21, 1964 to April 12, 1965. Apparently, this is the only high-magnification station (350-400 thousand times at 1 Hz) to have operated for any substantial period within 120 kilometers of the Central Basin Platform before installation of station CLN in 1974. FOTX was in operation at the time of the February 3, 1965 earthquake on the Central Basin Platform. Based on this examination a number of earthquakes believed to have originated in the Central Basin Platform were found including two occurring before the February 3, 1965 event. Prior to examination of the FOTX records these two events on November 8 and 21, 1964 were unknown. All events located by Sanford and Toppozada in the Central Basin Platform during the operation of FOTX - and based primarily on readings from this station - are listed in Table 5.2-7.

The studies by Sanford and Toppozada (1974) suggested earthquake activity on the Central Basin Platform at a level higher than expected, but were not conclusive because of the very small amount of instrumental data available close to this area. About all that could be said at that time was that eight significant earthquakes (see Table 5.2-8) had occurred near the Central Basin Platform between November 1964 and September 1971 ranging in magnitude (new revised estimates as discussed in Section 5.2.2) from 2.5 M_L to 3.2 M_L; that one of these events, August 14, 1966, had an associated maximum intensity of VI on the Modified Mercalli scale; and that a number of smaller earthquakes had apparently occurred

at about the same location during the operating lifetime of station
FOTX. The basis for this latter supposition was that all of the measured
Sg-Pg intervals on the FOTX seismograms yielded an epicentral distance
corresponding to the distance between the FOTX station and the area of
activity on the Central Basin Platform. In addition, for some of the
stronger shocks, arrival times were available from the Las Cruces station
(LCN). The difference between P arrival times at LCN and FOTX was the
same (34.7 plus or minus 0.5 sec) for the unlocated shocks as for the
located events in November 1964 and February 1965. Thus, it is
reasonably certain that the Central Basin Platform has been seismically
active since mid-1964. Since the activity rate was roughly the same at
the end as at the beginning of the 10-month period for which FOTX records
were available, it can be supposed that earthquakes also occurred before
mid-1964. If such activity had occurred, it probably would not have been
detected on the regional seismograph stations then in existence.

The instrumental coverage of this part of the country has improved
markedly in the past several years. The first important improvement took
place in the spring of 1974 when station CLN was installed by personnel
of the New Mexico Institute of Mining and Technology. Data recorded by
this station between April 1974 and the end of October 1977 has already
been discussed in detail in subsection 5.2.3. However, it should be
mentioned that of the 49 earthquakes recorded during this period by CLN
and enough other regional stations to allow accurate location (Sanford et
al., 1978), 24 of them occurred within the active parts of the Central
Basin Platform. Of the 26 less well located earthquakes of Table 5.2-6
and Figure 5.2-3, 13 of them are thought to belong to the Central Basin
Platform area. Thus, for the period of operation of station CLN through
October 1977 (which represents the last records so far analyzed from this
station) nearly half of the events located within 300 kilometers of the
Los Medanos site have occurred within the Central Basin Platform

The most recent advancement in the instrumental coverage of the Central
Basin Platform area took place with the initiation of operation of the

Kermit, Texas, seismic array in November 1975. The remainder of this subsection is concerned with discussions of the operation and preliminary findings of this array.

Based on the seismicity information developed by Sanford and Toppozada (1974) the Central Basin Platform was instrumented with an array of seismograph stations encompassing the largest historical events discussed above. The purpose of this array is to study, in some detail, the seismicity of this region which is of interest both because it is important to the evaluation of seismic risk at the Los Medanos site and because secondary petroleum recovery projects have been active in this area for a period roughly coincident with its known seismic activity. It is hoped that ultimately such a study will answer questions fundamental to an evaluation of the implications of Central Basin Platform earthquakes to the tectonism, not only of the platform, but of surrounding regions. Evaluation of the Kermit, Texas, array data has not yet progressed to this point, but some preliminary discussion is possible at this time. The treatment below is largely abstracted from Hays (1977) and Rogers and Malkiel (1978).

The Kermit seismic network currently consists of 10 self-contained radio telemetry systems placed in a grid pattern covering 2200 square kilometers. Each field station is equipped with a single component vertical seismometer and accompanying amplifier-transmitter equipment. The seismometers are Mark Products L-4C's with a natural period of one second and 67 percent critical damping. Typical magnifications range from 25 to 50K near 1 Hz increasing 6dB/octave to 10 Hz. A receiver station is centrally located at the Winkler County Airport at distances from individual stations ranging from 12 to 40 kilometers. The current locations of the 10 array stations are shown in Figure 5.2-5 taken from Rogers and Malkiel (1978). Those stations designated by a three symbol code followed by an "A" represent second locations for these instruments. The moves were usually made to diminish background noise levels or improve foundation conditions. The initial location of these stations may be found in Hays (1977). In general, the effect of unfavorable surface

geology and high cultural noise in this area has posed problems that have resulted in less than optimum station gain for a micro-earthquake study (Rogers and Malkiel, 1978).

Once the signals are placed on the phone lines, recording and timing take place at the National Earthquake Information Center (NEIC) in Golden, Colorado. Signals from the individual stations are put on film (in a 20 channel Develocorder microfilm recorder) and the highest quality station (KT7, see Figure 5.2-5) is simultaneously recorded on a Helicorder visible recorder to provide rapid identification of events of interest. Film recording speed is 3 cm/min and optical enlargement of 20 times permits resolution of plus or minus 0.01 seconds for impulsive arrivals. Direct recording of station WWV also insures correct absolute timing.

The average level of detection within the array is given as magnitude $M_{LD}=2.0$, where M_{LD} is a magnitude determined from the coda length as discussed in Lee and Lahr (1972). This represents a relatively low array sensitivity due to the surface geology and unfavorable operating environment as previously mentioned. Detection threshold for individual stations varies from a high of M_{LD} = 2.5 in oil fields with sandy surface conditions to a low of M_{LD} = 0.5 along the west edge of the array where low levels of pumping, and caliche "bedrock", allow higher gains to be used. In the discussion below, M_L will be used for M_{LD} wherever the Rogers and Malkiel (1978) data are referenced.

During the current reporting period (November 1975 through July 1977) 407 events have been detected of which 135 have been well enough recorded to be located. These earthquake locations were determined using the hypocenter location program HYPO71 (Lee and Lahr, 1972) and a four layer over a half-space crustal model developed by Stewart and Pakiser (1962) for eastern New Mexico.

Of the 135 located events, 56 occurred within the area of the array. these earthquakes are shown in Figure 5.2-6 and listed in Table 5.2-9. Of these 56 earthquakes, 22 have been located using the readings from only

three stations. This is inadequate to allow hypocentral depth to behave
as an unknown in the formal location algorithm so that for all these
events an assigned depth of 5 kilometers is used (denoted 5.00* in Table
5.2-9). For an additional 14 events, locations have been accomplished
using only four stations. In this case the hypocenter may be fixed
deterministically but no redundancy in possible locations exists to allow
some estimate of the uncertainty in the formal location. Thus, of the 56
internal, and presumably best located, earthquakes of Table 5.2-9 only 20
are available with an estimate of both depth and hypocentral uncertainty,
at least in a formal sense.

An interesting independent estimate of the accuracy with which events have
been recently characterized in the Central Basin Platform is provided by a
comparison of earthquakes common to both Tables 5.2-9 and 5.2-5. There
are only four such events. The majority of those earthquakes appearing in
both the Sanford et al. (1978) and Rogers and Malkiel (1978) "well
located" data sets are somewhat peripheral to the Kermit array as will be
seen below. The location and origin time agreement is very good;
differences averaging 0.04 degree and 0.6 seconds respectively. Such
modest differences can probably be easily explained by minor model
differences and, in the case of the Sanford et al. (1978) data set, focal
depth assumptions. However, estimates of local magnitude, M_L, differ
significantly. The four events under consideration average over 0.9
magnitude units higher in the Rogers and Malkiel data set than that of
Sanford et al. This point is worth keeping in mind.

Table 5.2-10 lists those earthquakes occurring on the periphery of the
Kermit array with locations that use readings from at least five array
stations. This does not necessarily imply that these events are well
located. In fact, many are given a low location quality factor by Rogers
and Malkiel (1978). Indeed, these authors do not plot the formal
hypocentral positions for earthquakes occurring outside the boundaries of
the array but instead outline zones in which these events apparently lie.
These zones are meant only to be indicative of the general area where
earthquakes appear to be occurring. Both the zone boundaries and formal
locations are shown in Figure 5.2-6.

The events listed in Table 5.2-10 may be compared with those in Table 5.2-5 in a manner similar to that discussed above in connection with Table 5.2-9. Of the 51 earthquakes around the periphery of the Kermit, Texas, array as determined by array station readings, 15 also appear in Table 5.2-5. The average origin time difference is greater in this case, being 1.9 sec., and a larger epicenter location difference of 0.1 degree is also present. Again, the most interesting differences are in local magnitude, M_L. As before, the Kermit array data set shows magnitudes consistently higher (in this case 0.84 units higher) than the New Mexico Institute of Mining and Technology values as they appear in Sanford et al. (1978).

Solely to present consistent-looking plots, events listed in Tables 5.2-9 and 5.2-10 and shown in Figure 5.2-6 have been scaled to circumvent this magnitude disparity. That is, the symbol used for a particular earthquake epicenter of magnitude M_L in Figure 5.2-6 is the same as would have been used for a magnitude $M_L-0.85$ in previous epicenter plots.

All available data through mid-1977 for the Central Basin Platform have now been considered. It is clear that continuing effort in this area will improve the understanding of this seismicity. Before outlining the speculations that have been made based on information to date, it seems appropriate here to briefly summarize this seismicity in very general terms.

There is little doubt that the Central Basin Platform has been seismically active since at least mid-1964. Its activity before this time will likely remain speculative. There is no evidence of historical felt reports for events felt in this area similar to the epicentral intensity = VI earthquake of August 14, 1966, even though local histories and newspapers have now been searched specifically for any such reference (Sanford and Toppozada, 1974). Conclusions as to the lack of previous seismic activity on this basis, however, must be tempered somewhat by the knowledge that this part of western Texas has never had a large population.

Since the first instrumental detection of events in the Central Basin
Platform region, the number of recorded earthquakes has been largely a
function of the number and sophistication of the seismograph stations
available to record them. With the startups of station CLN in 1974, and,
more important, with the Kermit array, large numbers of small earthquakes
are now being noted that previously would have completely escaped notice.
It is now clear that, at least for the last several years and probably for
the last decade, the Central Basin Platform has been the most seismically
active area within 300 kilometers of the Los Medanos site in terms of
number of events.

It is worthwhile here to put the Central Basin Platform activity into
perspective. Even though some events near magnitude 0 are recorded
(Rogers and Malkiel, 1978), fewer than ten detected events are reported
for many months during the operation of the Kermit array. This rate is
relatively low compared with the activity rates of some of the more active
areas in the eastern U.S. such as Blue Mt. Lake, New York (Sbar et al.,
1972), or southeastern Missouri (Stauder et al., 1976). The largest known
earthquake to occur in the Central Basin Platform had, by the most recent
estimate, a magnitude of less than 3-1/4. It is very difficult to believe
that any event very much larger than this (say $M_L \geq 5$) could have
escaped instrumental notice during the past 50 years or so. The
Valentine, Texas, earthquake of 1931, to the south, for example, had an
epicentral intensity of VIII on the Modified Mercalli Scale and was
recorded worldwide (Byerly, 1934). The magnitude of this event has been
estimated to be 6.4 based on the felt area (Sanford and Toppozada, 1974).
The I_o=VI event of August 1966, where I_o is epicentral intensity, has
recently been assigned a magnitude somewhat less than 3. In short, the
Central Basin Platform has exhibited some activity since mid-1964, but
this activity has been of small magnitude. There is no evidence to
suggest that moderate or large magnitude events occurred before mid-1964.
Within limits imposed by general regional and worldwide seismographic
capabilities, there is no evidence to allow a determination of the small
magnitude earthquake activity in this area before 1964.

In the remaining discussion, the causes and implications of the Central Basin Platform seismicity, as best these have been determined, are considered. This discussion is speculative since the definitive evidence critical to a unique view of either the causes or implications of these earthquakes does not yet exist. Figure 5.2-6 shows the 107 earthquakes of Tables 5.2-9 and 5.2-10, as well as the approximate boundaries of the Central Basin Platform and a series of pre-Permian faults inferred from drilling. These faults, which are all deeply buried, are taken from 1:9600 scale maps provided by Geomap Corporation to Rogers and Malkiel (1978). From a comparison of fault and epicenter locations it is clearly not possible to associate the earthquakes with known faulting although an alignment of epicenters in the southwest corner of the array appears to occur on a short fault segment. Other events or groups of events appear equally likely to occur in the vicinity of faults as not. In a very general sense, however, it appears that both the eastern and western boundaries are active (Rogers and Malkiel, 1978). The basic conclusion from all instrumental data is that seismic activity is equally likely to occur anywhere along the Central Basin Platform structure as asserted by Sanford et al. (1978) without particular regard to small scale structural details such as individual pre-Permian faults.

Attempts have also been made to relate Central Basin Platform seismicity to secondary oil recovery operations in the area. Both the spatial and temporal association of Central Basin Platform seismicity with secondary recovery projects at oilfields in the area are very suggestive of some cause and effect relationship.

Shurbet (1969) was the first to suggest that seismic activity on the Central Basin Platform is related to water injection for secondary recovery of oil. His suggestion was based on the clearly established association between earthquakes and waste injection into crystalline bedrock at the Rocky Mountain Arsenal near Denver (Healy et al., 1968). Subsequently, a direct association between earthquakes and fluid injection for secondary recovery of oil was established at the Rangely field in northwestern Colorado (Healy et al., 1972). As the fluid pressure builds

up during injection, the effective stress across pre-existing fractures diminishes with an associated decrease in frictional resistance to sliding.

There appears to be a correlation between the number of active waterflood projects and the first known occurrence of earthquakes in 1964. Although waterflood projects began in this area as early as 1944, the number of projects began to increase considerably in the mid-1960's and, on the average, injection pressures have also increased with time (Rogers and Malkiel, 1978). A study of the number of active secondary recovery projects versus time in this area shows a rapid increase in the early 1960's, a peak in 1968, and relative constancy since that time. The increase in secondary recovery activity occurs prior to, but in rough conjunction with, the first occurrence of earthquakes in the area. During the period of operation of the Kermit array, the largest earthquakes recorded have occurred in the vicinity of the Keystone unitized oil field. The Dollarhide unitized field, although outside the boundaries of the array, appears to be one of the most seismically active areas. Other areas of seismic activity occur, however, that are not within the major oil field boundaries, and major secondary recovery fields exist that apparently are not seismically active. Although the evidence is not conclusive, based on this seismicity pattern and the absence of recent geologic faulting within the Central Basin Platform it is believed that the best working hypothesis at this time is that earthquakes are associated with the release of low level residual stress by secondary recovery operations. It is neither proved nor precluded by a consideration of current best estimates of regional stress regime (Hays, 1977) as discussed in a later subsection.

5.2.5 The Events of July 26, 1972 and November 28, 1974

Questions on the tectonism and seismic activity very near or at the site are of great interest. For this reason the single most important seismic event to occur since installation of station CLN at the Los Medanos site has been the earthquake at 03:35:20 GMT on November 28, 1974 (see Table 5.2-5 and Figure 5.2-3). This earthquake, whose most recently estimated

magnitude is 3.6 (Sanford et al., 1978), had an epicenter about 40 kilometers northwest of station CLN. If it is an indication of normal background seismicity in the immediate site area, this event might cause a reevaluation of previous estimates of seismic risk at the Los Medanos site by Sanford and Toppozada (1974) who considered the likely principal sources of site vibratory ground motion to be a major earthquake to the west, no closer than approximately 115 kilometers, and a moderate earthquake in the Central Basin Platform. Because of its potential importance, this event has attracted considerable notice. It was prominently mentioned in two studies (Sanford et al., 1976a; Sanford et al., 1978) and was the main topic of another (Caravella and Sanford, 1977).

As may be seen from Table 5.2-5 the event of November 28, 1974 has been located by the New Mexico Institute of Mining and Technology at about 32.6°N, 104.1°W by using phase readings from six stations. An independent location by the U.S. Geological Survey places this earthquake at 32.3°N, 104.1°W. Both solutions give a virtually identical origin time. At the time of this earthquake, a rockfall and considerable ground cracking were reported at the National Potash Co. Eddy County Mine. The location of this rockfall was 32.55°N, 104.04°W and it occurred within about one minute of the calculated earthquake origin time. In view of this rather remarkable coincidence the question naturally arose as to the cause and effect relationship of the rockfall to the recorded seismic event. The issue was whether the source of this event could be related to a non-tectonic cause such as mine collapse at the Eddy County Mine or if it should be considered a more normal release of accumulated strain energy. Clearly the epicentral uncertainty grossly implied by the two different formal solutions found by the New Mexico Insitute of Mining and Technology and the U.S. Geological Survey allowed actual spatial coincidence of rockfall and seismic disturbance. Therefore it was decided that a more careful location effort would be worthwhile.

As information was being collected for this redetermination effort, it was discovered that a previous rockfall had occurred at the National Potash Co. Eddy County Mine on July 26, 1972. A check of past seismograph

records revealed that a seismic event had been recorded at a number of
regional seismograph stations, too. A subsequent location using these
readings put this event at 32.6°N, 104.1°W and assigned a magnitude of
M_L=2.8 (see Table 5.2-3). Thus this event, although weaker, was found
to be located very near the November 28, 1974 event, and study of the
individual station records indicated that its coda was of nearly identical
character to the later event. Since more records were available for the
earlier event, it was decided that a detailed relocation effort would be
attempted for it first. The question of the nature of its source was
still of primary concern.

The relocation method is described thoroughly in Caravella and Sanford
(1977) and will only be outlined here. The origin time was picked by
extrapolation to the S-P interval equal zero intercept of a straight line
fit of S-P versus P data. Such a procedure, using data from all six
stations recording the July 26, 1972 event (LUB, SNM, ALQ, JCT, TUC, and
GOL) yielded an origin time of $04:35:40.4;\pm$ about 3.3 seconds at the 95
percent confidence level. A similar linear regression using only the
first five S-P intervals yielded an origin time of $04:35:43.9 \pm$ about 2.8
seconds at the same confidence level. Ultimately, the five interval
origin time was selected because a better location was obtained with it.

To develop a velocity model to use in the relocation effort the following
procedure was adopted: seismic wave arrival times from the underground
nuclear explosion GNOME were noted. This explosion, which was detonated
at 19:00:00 GMT on December 10, 1961, at 32.264°N, 103.866°W (located
about 35 km south of the National Potash Co. Eddy County Mine) was
recorded by many of the stations noted above (see Romney et al., 1962).
From these arrival times, crustal and subcrustal velocities were developed
over the ray paths from GNOME to each individual station. In essence,
each station was modeled as being underlain by two layers over a half
space. The velocity and thickness of the upper layer were assumed known
from independent sources (Reddy, 1966; Romney et al., 1962; Wilson et al.,
1969; Major, 1975; Shurbet, 1975; Toppozada and Sanford, 1976) and the
velocity (and implied critical incidence angles) of the lower (and main)

crustal layer was then found by an iterative technique for each station independently. Subcrustal velocities could then be similarly found. Corrected crustal velocities (layer two) determined in this way ranged from 6.31 km/sec to 6.02 km/sec. Thus lateral inhomogeneity is built into the model.

Using the station-dependent model and the preferred origin time, 95 percent confidence interval arcs were drawn from each station. The results are shown in Figure 5.2-7. As can be seen, the intersecting arcs so constructed define a rather large area of approximately 1900 km^2. Although the Eddy County Mine lies very near this area, other locations within the same area have the same formal likelihood of being the epicentral location.

The November 28, 1974, seismic event was not relocated in the same way. Instead, another fundamental question was asked. That is, could the two events, July 1972 and November 1974, have occurred at the same focus based on existing seismographic evidence. The test applied is that if the events had the same hypocenter, the differences in arrival times of specific phases at common stations should be the same for all stations. As may be seen from Table 5.2-11 this is not the case for the limited data set available.

The difference between the smallest and largest time difference is 1.4 sec. Caravella and Sanford (1977) believe this is too large to be explained by reading errors. The time differences indicate, under this conclusion, that the two events did not have the same hypocenter, even though location uncertainties are such that either of them might, by itself, have occurred at the rockfall site. The time differences can be explained by locating the hypocenter of the November 28, 1974 event about 10 kilometers northwest or southwest of the July 26, 1972 shock (Caravella and Sanford, 1977). At this time, then, best available analysis indicates that both of these small events did not occur at the Eddy County Mine and cannot both be caused by some nontectonic source at that location. In the seismic risk analysis of the next section, therefore, some background earthquake activity in the immediate site area is considered.

5.3   SEISMIC RISK ANALYSIS

In this section, a broad characterization of the site region's seismicity is developed in a way useful for making conservative earthquake-resistant design decisions. This risk analysis is intended to be applicable only to vibratory ground motion resistant design of surface facilities on good foundations. Generalization of the results of this analysis to less idealized conditions, such as design of subsurface facilities for shaking during an earthquake or allowance for poor surface foundation conditions (should they be encountered), may be accomplished at a later time without altering the import of the original analysis. However, it must be emphasized that in this section the risk formally presented is intended to be a meaningful and conservative estimate of proper design values for short-term features of the facility. "Short-term" as used here means time periods on the order of decades. Specifically, it is not believed that any results presented here can be simply extrapolated to periods of tens or hundreds of thousands of years even though formal extrapolations of this kind are possible. This is not a severe handicap in this case. Although the lifetime of the repository will be longer than the limits of applicablility of this risk analysis, the length of time for which vibratory ground motion will be of concern is much shorter (during surface facilities use) and, in fact, falls well within the intent of this analysis.

There are a number of ways to characterize site seismicity in a way useful for rational design against the effects of earthquake associated ground shaking. One measure of the proper design value is the maximum historical site intensity which can be estimated from the historical earthquake record and some intensity attenuation law, whether this law is explicitly or only implicitly considered. As noted in the previous section, the maximum historical intensity at the Los Medanos site is estimated to be less than or equal to V on the Modified Mercalli Intensity Scale (Wood and Neumann, 1931). This characterization of earthquake design motion has the great advantage of being simple and straightforward. It is not, however, generally used for important structures or facilities because it does not

provide a basis for estimating whether future events will result in site intensities exceeding the maximum historical site intensity. This is a serious drawback for areas with a relatively short historic record such as the United States, and especially its western half.

To construct seismic design values for a particular site that go beyond a simple interpretation of a maximum historical measure of ground motion, something more than historical seismicity must be considered. Therefore, the geology of a region is often used in several ways to supplement historic earthquake data. There are several studies that attempt to present a seismic zonation of the United States using both seismic and geologic arguments. The stated intent of one of these (Richter, 1959) is to present a seismic regionalization showing the maximum reasonably expectable intensity during future earthquakes on ground of prevailing character. The Los Medanos site is in a region of intensity VIII according to this study. Algermissen 1969) has developed a Seismic Risk Map that has been closely associated with editions of the Uniform Building Code since 1970 (Uniform Building Code, 1970, 1973, and 1976) and by this association is most directly applicable to an estimate of proper design of structures with lifetimes measured in decades. The Los Medanos site intensity is shown to be V and/or VI in this zonation. Both these seismic risk maps, which were considered for the site region by Sanford and Toppozada (1974), are based on essentially the same data. The differences are due to varying interpretations and intent. That the interpretations are not really very far apart is indicated by a statement by Richter (1959) that an individual structure intended for a lifetime of the order of 30 years might within that life be exposed to shaking of no more than one scale degree below that mapped. Thus, over several decades, the Los Medanos site might reasonably be subjected to shaking at around the V to VII intensity level according to both Richter and Algermissen.

Although based on both historical seismicity and large scale geologic features, the seismic regionalization maps of Richter and Algermissen do not explicitly consider frequency of occurrence of damaging earthquakes. More fundamentally, the subjective decisions implicit in any

characterization of future earthquake ground motion are largely concealed and not subject to scrutiny. Any shifts of emphasis or new geologic or seismic information are, therefore, very difficult to incorporate into such zonations. In recent years, several procedures have been developed that allow formal determination of earthquake design parameters to be made (Cornell, 1968; Cornell and Vanmarke, 1969), and a number of studies incorporating these procedures have been performed (e.g., Cornell and Merz, 1975: Shah et al., 1975; Algermissen and Perkins, 1976). In typical seismic hazard analyses of this kind, the definition of seismicity is made by using geologic and tectonic data as well as observed earthquake locations. The region of study is divided into seismic sources within which future events are considered equally likely to occur at any location. For each seismic source area the rate of occurrence of events above a chosen threshold level is estimated, using the observed frequency of historical events. The sizes of successive events in each source are assumed to be independent and exponentially distributed; the slope of the log-number versus frequency relationship is estimated from the relative frequency of different sizes of events observed in the historical data. This slope, often termed the b value (Richter, 1958), is determined either for each seismic source individually or for all sources in the region jointly. Finally, the maximum possible size of events for each source is determined, using judgment and the historical record (McGuire, 1977).

It is clear from this description that all assumptions, no matter what the level of subjectivity employed in making them, must be made explicit. In addition, this method of determining site-specific earthquake risk may be used for a wide range of geologic and seismic assumptions. In this section, the method of Cornell (1968) will be applied to the question of risk as a function of ground shaking at some prescribed level at the Los Medanos site. Input parameters at each stage of the development will be taken from current best information available in the literature. These input parameters are discussed below in some detail following a general discussion of the mechanics of the Cornell method itself. Finally, several curves showing probablility of maximum ground surface acceleration versus acceleration level, will be presented and discussed for several

different assumptions about the individual source area capabilities. The conclusions that may be drawn from these curves will be considered. It is believed that the data, treated in this way, may be used to arrive at a general preliminary statement of risk from vibratory ground motion that is applicable at the site during its active phase of development and use.

5.3.1   The Method of Cornell

Cornell (1968) developed a method to produce relationships between ground motion parameters, such as peak ground displacement or maximum ground acceleration, and their average return period. The data used include best estimates of average activity levels for various potential sources of earthquakes. Arbitrary geographical relationships are allowed between these potential sources and the site. Cornell provides a technique for integrating the individual influences of these sources into the probability distribution of the ground motion parameter and the average return period then follows directly. The potential sources are modeled geometrically in such a way as to permit a solution of closed analytical form.

In this Section, a calculation is made of the probability that a random peak ground acceleration "A" will exceed a given value "a" once an event of magnitude greater than some threshold level has occurred. Before the method can be used, a geometric model or characterization of the potential earthquake sources must be made. Cornell develops the necessary formulation for point, line, and annular area sources. The geological structure and seismic history of the Los Medanos site do not imply that linear or point source models are appropriate, so use of the technique begins with an approximation of the source regions (Algermissen and Perkins, 1976) by annular segments (see Fig. 5.3-5). As discussed in the next subsection, the annular segments are in all cases believed conservative approximations of the source regions.

Let acceleration be related to Richter magnitude M and hypocentral distance R (in kilometers) by the equation:

$$a = b_1 \exp(b_2 M) R^{-b_3}$$

where a is in units of cm/sec^2 and the values of the constants (b_1, b_2, b_3) are discussed in a later subsection. Then if M and R are assumed to be probabilistically independent within the source areas, the probability of an acceleration A exceeding a given value a can be expressed as:

$$P\left[A \geq a\right] = 1 - F_M(m) = P\left[M \leq (\ln a + b_3 \ln R - \ln b_1)/b_2\right]$$

where F(m) is a distribution function of earthquake magnitudes, which can be calculated using a recurrence relation of the form (Gutenberg and Richter, 1942):

$$\log N = \underline{a} - \underline{b}M$$

where $\underline{a}$ and $\underline{b}$ are constants.

To find the proportion of events having magnitudes in the range $m_0 < M < m$ the number of such events ($N_{m_0} - N_m$) is divided by the total total number of events with magnitude greater than m_0

$$F_M(m) = (N_{m_0} - N_m)/N_{m_0} = 1 - \exp\left[-B(m - m_0)\right]$$

where $m_0 < m \infty$ and B is used to denote the constant $b\ln 10$. However, it is desirable to impose an upper limit on the magnitude of an event that may occur in a given source area, i.e., to specify that $m_0 \leq m \leq m_1$. Our cumulative distribution function must now satisfy the boundary condition $F_M(m \geq m_1) = 1$ so:

$$F_M(m) = C\left[1 - \exp\left[-B(m - m_0)\right]\right]$$

where C is a constant such that

$$C = 1/\left[1 - \exp\left[-B(m_1 - m_o)\right]\right] \equiv 1/(1 - k_{m_1})$$

In this case, the probability expression may be rewritten as

$$P\left[A \geq a\right] = 1 - F_M(m) = \left[-k_{m_1} = \exp\left[-B(m - m_o)\right]\right]/(1 - k_{m_1})$$

where $k_{m_1} = \exp\left[-B(m_1 - m_o)\right]$. For values of m less than m_o, $\left[P A \geq a\right] = 1$ while for values of $m > m_1$, $P\left[A \geq a\right] = 0$.

Aside from the limits on the range of r due to the inner and outer radii of the annular segment, it is important to note that the condition m_o m m_1 also places limits on the range over which the above probability is valid. Specifically, the condition on m implies, for a given acceleration value a, that:

$$\left[\exp(b_2 m_o/b_3)\right](b_1/a)^{1/b_3} \leq r \leq \left[\exp(b_2 m_1/b_3)\right](b_1/a)^{1/b_3}$$

The lower boundary value of r may be thought of as the distance from the site within which any event of magnitude m or greater will result in an acceleration of a or greater. In other words, the probability is unity that for values of r less than the cutoff value a random acceleration A will exceed the chosen a. The upper boundary is the maximum radius from the site at which an event of magnitude m could have a nonzero probability of causing an acceleration a, given an attenuation law of the proper form. A schematic representation of these limits on r, for a given a, over which the above probability is valid is shown in Figure 5.3-1 (top).

In order to find the cumulative distribution $F_M(m)$ for all possible values of the focal distance and their relative likelihoods, integration over the annular area under consideration is performed:

$$P[A \geq a]_{annular\ area} = \frac{1}{2\pi} \int_0^{2\pi} \int_d^{r_o} P[A \geq a] \cdot f_{R,\Theta}(r,\theta)\ drd\theta$$

where $f_{R,\Theta}$ (r,Θ) is the probability density function of R, Θ the coordinates of a random focal position within the annulus (see Fig. 5.3-1bottom). Assuming that $f_{R,\Theta}$ (r,Θ) is independent of Θ, the probability of the source falling within the annular area bounded by X (Fig. 5.1-1bottom) is just the ratio of this area to the total area or

$$F_{R,\Theta}(r,\theta) = \pi(X^2 - \Delta^2)/\pi(\ell^2 - \Delta^2) = (r^2 - h^2 - \Delta^2)/(\ell^2 - \Delta^2)$$

so then

$$f_{R,\Theta}(r,\theta) = \frac{d}{dr} F_{R,\Theta} = 2r/(\ell^2 - \Delta^2)$$

Substituting the expression for $f_{R,\Theta}$ (r,Θ) into the probability equation and integrating, an expression is found of the form:

$$P[A \geq a]_{ann.} = \frac{2}{\ell^2 - \Delta^2} (1 - k_{m_1})^{-1} [Da^{-B/b_2} (\frac{1}{(\gamma-1)d^{\gamma-1}} [1 - (\frac{r_0}{d})^{-(\gamma-1)}]) - \frac{k_{m_1}}{2}(r_0^2 - d^2)]$$

where

$$D = b_1^{B/b_2} \exp(Bm_o) \quad : \quad \gamma = Bb_3/b_2) - 1$$

The question of the random number of occurrences in any time period is next considered. It is assumed that for the magnitudes of interest the occurrence of any event is Poissonian, that earthquakes have equal likelihood of occurring anywhere within the source area considered, and that the average occurrence rate, ν per year, is constant in time. The above three assumptions, particularly that of Poissonian distribution of events, are fundamental.

It may then be shown that the probability that $A_{max}(t)$, the maximum value attained by A over a time of t years, will be less than or equal to a is:

$$P\left[A_{max}(t) \leq a\right] = \exp(-p\nu t)$$

where p is the annular area probability, $\left[P\; A \ge a\right]_{ann.}$, calculated above and $\quad$ is the average occurrence rate..

The risk or annual probability that A_{max} will <u>exceed</u> a is

$$1 - P\left[A_{max}(t=1) \le a\right] = 1 - \exp(-p\nu)$$

Sources near the Los Medanos site will be modelled by angular segments of an annulus. In this case, a simple modification of p in the above exponential is required but the method is otherwise the same.

The average return period, T, of an acceleration equal to or greater than a is defined as the reciprocal of $P\left[A_{max} \ge a\right]$, that is:

$$T(years) = 1/P\left[A_{max} \ge a\right]$$

Tables of values of annual risk (and average return period) versus values of a can be constructed for each source area near and surrounding the site. The risk at the site arising from all such sources may then be found by combining the results above in the following way: Consider source areas A, B, and C to be independent in a statistical sense. Then, where $P^{ABC}\left[A_{max} \le a\right]$ is the familiar probability that the maximum value of A, the peak ground acceleration arising from composite source area ABC, is less than a at the site, is

$$P^{ABC}\left[A_{max} \le a\right] = P^{A}\left[A_{max} \le a\right] \bullet P^{B}\left[A_{max} \le a\right] \bullet P^{C}\left[A_{max} \le a\right]$$

If it is assumed that all the sources are modeled by annular segments (i.e., not a combination of annular and line sources), then the composite probability of <u>exceeding</u> a in terms of the probability results for the individual areas can be written as

$$P^{ABC}\left[A_{max} \ge a\right] = 1 - P^{ABC}\left[A_{max} \le a\right]$$

or:

$$P^{ABC}[A_{max} \geq a] = 1 - [(1 - P^A[A_{max} \geq a]) \cdot (1 - P^B[A_{max} \geq a]) \cdot (1 - P[A_{max} \geq a])]$$

This equation is the desired formula for combining the previous probability results into a composite curve for "risk" which takes into account influences of all the various source areas near the site.

Thus, given certain input parameters, and estimates of average activity rates for potential sources of earthquakes, Cornell's method offers the means by which to make a quantitative estimate of the seismic risk at a site. Subject to certain fundamental assumptions stated above, the results can be expressed in a form that is easily applied and interpreted.

In the next subsection, the values used for input parameters such as constants of attenuation, and average seismic activity rates for individual source areas, will be discussed. The choice of annular segments approximating the source areas surrounding the site will also be discussed in some detail.

5.3.2   Input Parameters

The first input parameters that must be considered are those having to do with acceleration attenuation as a function of earthquake magnitude and epicentral distance. An unmodified use of Cornell's (1968) hazard analysis method requires, as seen above, a law of the form

$$a = b_1 \exp(b_2 M) R^{-b_3}$$

where a is acceleration in cm/sec^2, M is earthquake magnitude, and R is distance in kilometers. A number of relationships of the above form exist in the literature (Esteva and Rosenblueth, 1964; Seed, et al., 1968; Orphal and Lahoud, 1974). In all these studies, however, the constants b_1, b_2, and b_3 are found for data collected exclusively, or almost exclusively in the western part of the United States and are

therefore applicable there. Recently, several reasons have emerged, both theoretical and empirical, that indicate fundamental differences in acceleration attenuation in the central part of the U.S. For example, it has been demonstrated that the attenuation of body waves (Evernden, 1967) and surface waves (Mitchell, 1973; Nuttli, 1973a) is appreciably lower east of the Rocky Mountains than west. This serves to explain the much larger areas of perceptibility and of damage for central United States earthquakes than for west coast earthquakes of the same magnitude. It is also the source of the reluctance here to use previously published attenuation constants uncritically for this study. With particular reference to attenuation of acceleration, Nuttli (1973b) found that in the central United States the acceleration values of greatest engineering significance may be related to the vector resultants of the vertical and horizontal components of the sustained maximum surface-wave motion rather than to isolated peaks. This is true for ground motion at some distance from the source and for a wide range of magnitudes. The amplitude and shape of the attenuation curve for surface waves (Lg) in the frequency range of interest is known (Nuttli, 1973b) so that the accelerations associated with the Sg/Lg part of the earthquake ground motion coda may be plotted as a function of frequency and epicentral distance (see Nuttli, 1973c, Figure 8) for an event of a given magnitude.

The site area is very close to the western margin of the region of interest in Nuttli's studies so that it is not immediately clear that central United States attenuation laws are more pertinent than their western counterparts. It is believed, however, that there are several reasons for adopting a central United States formula. First, the site geology seems appropriate. The site is near the western boundary of the High Plains physiographic province (Sanford et al., 1976b) which extends eastward well into that part of the continental United States considered the "central U.S." by Nuttli (1973c). Second, there are features of the time histories recorded in the site region that are suggestive of kinship with central United States records. For example, the maximum record motions are almost always in the Sg part of the coda (Sanford, personal communication, 1978) in analogy to central United States Sg/Lg motion.

This feature has the interesting implication that magnitude scales are most naturally developed for this wave in the site region. Third, as mentioned in subsection 5.2.2, recent revision in the method of magnitude determination of events in the source region by stations in this region has been made necessary by the realization that peak record amplitudes have not attenuated with distance as quickly as implied by the uncritical use of Richter's (1958) standard earthquake ground amplitude values. Finally, the observation made by Sanford and Toppozada (1974) that the Valentine, Texas isoseismals apparently encompass more area to the east than to the west of the source is an indication on a very graphic level that attenuation is less in that direction. All these observations, although not rigorously indicative, are at least suggestive of acceleration attenuation in the site region similar to that found appropriate for the central region of the country. For these reasons, it was decided to use such a law for this seismic hazard analysis.

Algermissen and Perkins (1976) found that east of 105°W longitude the Schnabel and Seed (1973) curve developed from western United States data was consistent at about the magnitude 7.6 level with the similarly defined acceleration attenuation curve suggested by Nuttli (1973c) for the central United States out to distances of about 50 kilometers. Beyond this distance, the Nuttli curve attenuates at a slower rate (see Algermissen and Perkins, 1976, Figure 3). Curves applicable to other magnitudes are drawn by Algermissen and Perkins (1976) tangent to the Schnabel and Seed curves, but taking the same general shape as the Nuttli curve. These curves are shown in Figure 5.3-2 for magnitudes of 4.2, 5.2, 5.6, 6.6, 7.6, and 8.5. It is clear that these curves will not fit a single attenuation law of the form desired for simple application of Cornell's (1968) method as discussed in the previous subsection. Such a form requires not only a constant slope for all distances but a constant line spacing for equal magnitude intervals. Neither of these requirements is met by the acceleration attenuation curves taken from Algermissen and Perkins. The task then is to find proper coefficients for a Cornell type attenuation law such that the predicted acceleration so derived for a given magnitude and distance will be conservative

relative to the plotted values taken from Algermissen and Perkins. After some experimentation, the coefficients b_1=17, b_2=0.92, b_3=1.0 were selected (Bickers, 1978). Curves using these values are also shown in Figure 5.3-2 for the same suite of magnitudes. As can be seen from this figure, the model equation with the above constants yields higher accelerations for all values of magnitude and distance than the corresponding Algermissen and Perkins curves and is most closely matched to these curves in the region 10 kilometers < R < 300 kilometers and 5 < M <6. This adopted attenuation law, therefore, represents a conservative compromise between the estimated curves of previous authors and the required form of Cornell.

The next feature needed for hazard curve development for the site is some idealization of the regional seismic source areas. Whatever configuration is ultimately chosen for the geometry and location of the source regions affecting the site, the fundamental data are basically regional seismicity and geology. These features of the southeastern New Mexico region have already been evaluated in the literature (Algermissen and Perkins, 1976) with precisely the intent of developing an estimate of maximum acceleration in rock in a probabilistic format. Therefore, it was decided to investigate the feasibility of using these same source zones in the slightly different context of the current hazard evaluation.

As originally defined, the probabilistic estimate of maximum acceleration determined by Algermissen and Perkins (1976) was based primarily on the seismic record; geologic data, primarily distribution of faults, was employed only to a minor extent. In particular, the general principle used by these authors in the construction of seismic source zones was that future earthquake occurrences are assumed to have the same general time rate characteristics as the earthquakes in the past in the same overall region, but that future earthquakes in a particular area might occur over somewhat more extended areas than indicated by historical data. In practice, the seismic source zones were drawn using the following guidelines:

1) Areas of seismicity where shocks of maximum Modified Mercalli intensity V or greater have occurred were considered source zones. (Note that intensity and magnitude are deterministically related by the formula (Gutenberg and Richter, 1942) $M_c = 1.3 + 0.6I_o$ where "M_c is the magnitude corresponding to I_o" (Algermissen and Perkins, 1976). Thus $I_o = V$ is equivalent to $M_c = 4.3$). For any given zone the average distance from the epicenters to the boundary was chosen to be approximately the average separation distance for earthquakes of the maximum intensity found there, when these were sufficiently numerous to establish such a distance. If the maximum intensity earthquake in a source area only occurred once or twice (as in the case of source areas in and near southeastern New Mexico), the distance between earthquakes of the second largest intensity was used.

2) Some zones such as described above were extended to include adjacent areas where evidence of Holocene faulting is present. This type of extension was used in the Great Plains and Southern Rocky Mountains where epicentral clusters could be associated with faults appearing on the tectonic maps of the United States.

3) From 2) above, areas of known Quaternary faulting are generally within source zones, if the faulting is associated with at least low-level historical seismicity. Except as noted above, Quaternary or older faulting not associated with historical earthquakes of Modified Mercalli intensities greater than V or magnitudes greater than 4.0 was not included within source areas.

Using these principles, the seismic source zones of interest to the calculation of hazard at the site as drawn by Algermissen and Perkins are shown in Figure 5.3-3. As seen below, independent studies of regional Quaternary faulting and the more detailed seismicity studies of the last several years do not seriously imply the modification of these source area boundaries with one conceptual exception involving small earthquakes within the immediate site area. This observation is most directly supported by considering the historical seismicity through 1972 as shown

in Figure 5.2-1 in conjunction with the three earthquake source zones of
Algermissen and Perkins as shown in Figure 5.3-3. To aid this
comparison, the epicenters of the former figure have been drafted on to
Figure 5.3-3. It is clear from this superposition that the large
majority of significant historical seismicity conforms well with the
zonation presented. The location of the Valentine, Texas, earthquake and
its aftershocks (if these are formally constrained to share the location
of the main event in this sequence), apparently lie slightly to the east
of the boundary of the southernmost seismic source zone if the Byerly
(1934) location is used. It should be noted, however, that the
instrumental location is not well constrained by the data available at
the time of Byerly's study and, in particular, the epicentral uncertainty
is such that a more southerly or westerly location is equally likely.
For example, as may be seen from Figure 5.3-2 both the U.S.C.G.S.
instrumental location for this event and the town of Valentine, Texas
itself are within the source zone as drawn by Algermissen and Perkins.
For the purposes of this risk analysis, the Valentine earthquake and its
aftershocks are assumed to have occurred within the southernmost seismic
source zone of Algermissen and Perkins.

Of more immediate concern is the scattered residual small magnitude
seismicity occurring throughout the site area which cannot be associated
with any of the source zones as drawn in Figure 5.3-3. This problem was
recognized by Algermissen and Perkins (1976). These authors treated
these isolated earthquakes which could not be associated with known
faults or tectonic features as seismic background and the same shall be
done here. On a nationwide basis these events could have an intensity of
VII or less on the Modified Mercalli Scale and were assumed capable of
happening over broad areas of the midwest; however they produced
acceleration levels below the lowest acceleration contour on their map,
because this contour represented the 0.04g level with a 90-percent
probability of not being exceeded in a 50-year period (Algermissen and
Perkins, 1976). Since acceleration levels for much longer time intervals
are of interest in this study, some more explicit treatment of these
random events will be necessary, and some explicit source zone including

the site must be considered. This is the conceptual modification of the Algermissen and Perkins study mentioned above.

A simple calculation is adequate to show that it is not necessary to consider any source zone other than the four already mentioned--the three of Figure 5.3-3 and an additional one including the site. The next closest source zone of Algermissen and Perkins is approximately 300 kilometers away from the site and all others are even farther away. Using this distance, the attenuation law considered above and (for the moment) an arbitrary maximum magnitude 7.5 earthquake, the maximum acceleration at the site is slightly less than 0.06g. Thus, such a source zone cannot contribute anything to site accelerations higher than this at any probability level. Furthermore, as will be more forcibly indicated in the next subsection where some actual hazard curves will be discussed, the contributions to probabilities of occurrence from distance source zones even at lower acceleration levels are insignificant when compared to the contributions from the closer zones.

An independent estimate of the appropriateness of the source zones as drawn in Figure 5.3-3 can be obtained from a consideration of faults offsetting Quaternary geomorphic surfaces. This is an independent estimate in the sense that no episode of surface faulting associated with historic seismicity is known in the site region. Nevertheless, Quaternary faulting has often been used as an indicator of the seismic activity of an area over a longer time span than is furnished by the historical seismicity record (e.g. Allen et al., 1965). Sanford and Toppozada (1974) have made an investigation of fault scarps within 300 kilometers of the disposal site, exclusive of the Permian Basin in which the site lies. This investigation consisted primarily of a literature search supplemented by limited reconnaissance of aerial photographs. The study was restricted to fault scarps offsetting Quaternary alluvial surfaces because these are the only fault displacements whose age can be estimated with any certainty. The authors note that tectonic movements in the area may have occurred during the Quaternary along faults cutting older rocks, but detection of recent offsets along such faults are nearly

impossible. Bachman and Johnson (1973) have completed a detailed investigation of the surface features in the Permian Basin which indicates recent fault scarps of a tectonic nature do not exist in this area. Since completion of the Sanford and Toppozada (1974) study, further studies on the existence or nature of fault scarps in the general site region have been actively pursued by Dr. Muehlberger and his students of the University of Texas, Austin (Sanford et al., 1978). To date, the most recent data are consistent with the picture derived from the earlier studies. That is, the Rio Grande Rift and southern Basin and Range provinces have abundant geologic evidence - primarily recent fault scarps - of recent crustal movements (Sanford et al., 1972; Muehlberger et al, 1978) whereas the High Plains, which is the physiographic province of the Permian Salt Basin in the site area, does not. The closest known Quaternary offset is about 125Km from the site.

Shown in Figure 5.3-4 are the faults noted by Sanford and Toppozada (1974) and Muehlberger et al. (1978) superimposed on the Algermissen and Perkins source zones. The references used in construction of these fault traces are Talmage (1934), Reiche (1938), Kelley (1971), Dake and Nelson (1933), King (1948, 1965), Kottlowski (1960), Kottlowski and Foster (1960), and Pray (1961). Also shown is the eastern boundary of the area of investigation of Sanford and Toppozada, that is, the western boundary of the Permian Basin.

It is clear that the Quaternary faults are completely contained within the two western seismic source zones of Algermissen and Perkins. These two zones may be combined under the name "southern Basin and Range--Rio Grande Rift" source zone since they include the parts of those provinces significant to the evaluation of probabilistic acceleration at the site. The reason for combining the two original zones is implied by a comparison of Figures 5.3-3 and 5.3-4. Although the historical seismicity has been of a higher level in the more southerly of the two zones (Algermissen and Perkins assign a maximum intensity of VIII to this southerly zone to correspond to the Valentine, Texas, earthquake and one of only V to the northern zone), the Quaternary fault offset strongly

suggests that to insure conservatism this pattern should be considered a happenstance of the short historical earthquake record. Thus for the purposes of this analysis, the seismic capabilities of the southern zone will be shared by the region to its north. Although only epicenters of earthquakes occurring prior to 1973 are shown in Figure 5.3-3, the implications of more recent activity as they affect the southern Basin and Range—Rio Grande Rift source zone (which will be referred to only as the Rio Grande Rift source zone in the following discussion for brevity) are similar. For example, Figures 5.2-3 and 5.2-4 show that the known epicenters for shocks between April 1974 and November 1977 with Sg-Pg intervals at station CLN from 31 to 36 seconds occur in apparently historically active regions, notably centered around Valentine, Texas and much of the Tularosa Basin. That is, they occur precisely in the Rio Grande Rift source zone as defined above.

One important implication of these studies is that the easternmost of the three Algermissen and Perkins source zones, that corresponding to the post-1964 seismic activity around Wink, Texas, on the Central Basin Platform, is based on seismic evidence alone. This activity was discussed in detail in subsection 5.2.4. For the purposes of specifying a conservative source zone geometry, the only geometrical issue with regard to the Central Basin Platform source zone, then, is the closest approach of the Central Basin Platform relative to the source zone used to model it. Shown in Figure 5.3-4 is an outline of the buried Central Basin Platform as it appears in Rogers and Malkiel (1978). It may be easily seen that the closest approach to the site of the Algermissen and Perkins Central Basin Platform seismic source zone implies its use is adequate. Therefore, this zone, as drawn, will be used for the model to be developed. The general model will consist of three source zones:

1) The Rio Grande Rift zone drawn by combining the western source zones as discussed above.

2) The Central Basin Platform zone as shown in Figure 5.3-4.

3) A site source zone centered at the site and with a radius to be specified below.

There are two purely geometrical issues to be resolved. The first involves specifying a focal depth for the events in each of the source zones. The second is really an exercise in adapting the irregular zones, as shown, to Cornell's method much as it was necessary to adapt the form of the attenuation law.

There is little doubt that the focal depths of earthquakes in the site region should be considered shallow. As we saw in subsection 5.2.2, early instrumental locations were achieved using an arc intersection method employing travel-time-distance curves calculated from a given crustal model and the assumption that focal depths were either 5 kilometers, 10 kilometers, or for later calculations, 8 kilometers. Good epicentral locations could generally be obtained under these assumptions. Confidence in calculated or assumed focal depths is greatly increased, of course, if at least one recording station is situated not much farther away from the epicenter than the focal depth. This situation is not generally realized for New Mexico region earthquakes but several specialized studies for which this criterion has been satisfied are suggestive. For an approximately two-year period beginning in June 1960, several hundred natural microearthquakes having S-P intervals of less than 2.3 seconds were recorded by high-magnification seismographs west of Socorro, New Mexico (Sanford and Holmes, 1962). Rather detailed studies of the depths of these events indicated hypocenters ranging from 2.7 to 6.3 kilometers. More recently, and nearer to the site, preliminary data from the Kermit, Texas, array indicate focal depths ranging from very near the surface down to about 10 kilometers although only about 20 percent of the events are located at depths greater than about 3.7 kilometers (Rogers and Malkiel, 1978). For the formal instrumental location procedure with array data, an initial trial hypocenter at 5 kilometers depth is used by these authors.

Within the range discussed – that is, focal depths of from 0 to 10 kilometers – the issue of selecting a proper depth for the probabilistic acceleration analysis at this site is clearly important only in the site source zone itself. For example, the difference in hypocentral distance – the distance to be used in the acceleration attenuation formula – for a closest approach event in the Central Basin Platform is only 1.93 kilometers in this depth range assuming that the closest approach of this source zone is 25 kilometers as is indicated by Figures 5.3-3 or 5.3-4. This is clearly the greatest difference of this kind outside the site source zone. Within the site source zone the selection of focal depth can be, formally, very important simply because the form of the attenuation law used asymptotically approaches infinite acceleration at very small distances. This is certainly not mechanically realistic and is not the intent of the empirical fitting process to an attenuation law of this form. There is some empirical evidence that the rate of increase of peak acceleration with decreasing hypocentral distance becomes less as the zone of energy release is approached. This is the case for example, for the Parkfield and San Fernando, California earthquakes of 1966 and 1971, respectively (see Page et al., 1972, Figures 4 and 6). Some empirical acceleration attenuation curves make use of this property in extrapolating to the vicinity of energy release. Most importantly for our purposes here, the attentuation curves of Schnabel and Seed (1973) are constructed in this manner and it is these curves that form the basis for near-source acceleration as a function of magnitude used by Algermissen and Perkins (1976). Since it is the intent here to follow these authors insofar as conservatism allows, it was decided to use a focal depth of 5 kilometers in all source zones of this study including that of the site. For smaller hypocentral distances, the form of the attenuation law adopted here deviates significantly from that suggested by Algermissen and Perkins in such a way as to severely exaggerate the importance of very small but very close shocks in the estimation of probabilistic acceleration at the site pertinent to design. This may be seen from Figure 5.3-2.

The manner in which the irregular source zone geometry of Figures 5.3-3 and 5.3-4 may be adapted to the method of Cornell (1968) is shown in Figure 5.3-5. As has been implied above, the seismicity of the site region is, at best, poorly related to observed faults - whether observed Quaternary faults do not occur, as in the case of the Central Basin Platform source zone (Rogers and Malkiel, 1978) or whether they do, as in the case of the Rio Grande Rift source zone (Sanford et al, 1972). Since the boundaries of the latter zone are so drawn as to be as close or closer than known recent faults, conservatism is served by allowing the largest earthquake postulated for specific faults within the region to occur randomly throughout the region. For these two reasons, lack of apparent fault control and additional conservatism, areal source zones were used (see subsection 5.3.1). Thus the object is to approximate the given source zones by a series of annular segments. This is done in such a way that total source zone area is conserved, and such that excluded area of the Algermissen and Perkins zones is replaced by annular areas closer to the source. Finally, closest approach distances are conserved. These criteria are followed in construction of the pattern in Figure 5.3-5. The site source region is drawn to be centered at the site and to include all area not already in another source zone. The radius of this site source zone will be determined by magnitude restrictions.

With the attenuation law and geometry defined for this hazard analysis, the question of the right recurrence formulas for each source zone is next addressed. A number of empirically fitted curves of the form $\log N = a - bM$ have been published for the site region in a broad sense (Sanford and Holmes, 1962; Algermissen, 1969). As before, N is the number of earthquakes of magnitude greater than or equal to M in some area and over some time period. The constants a and b are determined by fitting the data, usually in a least squares procedure. Although data for any time period may be used, all the formulas considered explicitly here will be normalized to one year. In addition, all formulas will be normalized to source areas of 10^5 square kilometers for ease of comparison. For these broad regional studies, b values around 1.0 have been found.

Several studies published recently regarding the immediate site region are not in good agreement with the previous results. For example, graphs of magnitude versus number of earthquakes for events within 300 kilometers of the site exclusive of shocks from the Central Basin Platform and aftershocks of the 1931 Valentine, Texas earthquake yield recurrence formulas of the form

$$\log N = 1.65 - 0.6M_L \quad \text{per yr per } 10^5 \text{ km}^2$$

using instrumental data only, and

$$\log N = 1.27 - 0.6M_L \quad \text{per yr per } 10^5 \text{ km}^2$$
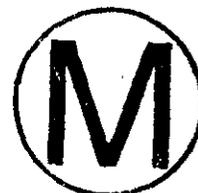
using both historical and instrumental data (Sanford and Toppozada, 1974). Because the numbers of shocks used to establish the linear portions of these curves is very small (16 and 25, respectively), and the total time intervals over which data were collected is very short (11 and 50 years, respectively), an error in the slope (or b value) is quite possible. In fact, a certain dissatisfaction with these results on the part of Sanford and Toppozada is indicated by their development of alternate curves somewhat arbitrarily defined to have a slope of 1.0 instead of 0.6. Algermissen and Perkins (1976) calculate recurrence curves for a number of their source zones. For example, for source zone 45 (as defined in either Figure 5.3-3 or 5.3-4) they find the equivalent of

$$\log N = 0.53 - 0.52 \, M_C \quad \text{per yr per } 10^5 \text{ km}^2$$

while for source zone 43, no formula is found, presumably for lack of data. Clearly, the difficulties of finding meaningful recurrence relations for such a short and areally restrictive interval in a region of low seismicity are formidable. Another problem is also implied by the last two equations. Magnitude M_C in the Algermissen and Perkins

formulation is somewhat vaguely defined, as mentioned above, as the magnitude corresponding to I_O in the equation:

$$M_C = 1.3 + 0.6 \ I_O$$

where I_O is maximum intensity on the Modified Mercalli Scale. There seems to be no rigorous and straightforward way to relate this magnitude to the M_L of Sanford and Toppozada. Even the definition of M_L, upon which development of recurrence curves is fundamentally dependent, has been revised in the past few years as was seen in subsection 5.2.2

Fortunately, recent work (Sanford et al., 1976b) allows a preliminary treatment of the data that circumvents the worst of these problems. This recent study is based on eleven years of instrumental seismicity data which have been reinterpreted with respect to magnitude. In addition, recurrence formulas are computed for broad physiographic regions of New Mexico vastly increasing the data base. The criterion used in this current hazard analysis will be to use the Sanford et al. (1976b) recurrence formula for the physiographic province in which an individual source zone occurs with the value scaled down to reflect area differences. For example, Sanford et al. (1976b) find

$$\log N = 2.4 - 1.0 \ M_L \quad \text{per yr per } 10^5 \text{ km}^2$$

for the High Plains province where the site is located, and

$$\log N = 2.5 - 1.0 \ M_L \quad \text{per yr per } 10^5 \text{ km}^2$$

for the Basin and Range - Rio Grande Rift region. The area of the High Plains province of interest for this analysis is approximately 3.4 x 10^4 km^2 surrounding the site but exclusive of part of the Central Basin Platform. Thus the proper recurrence formula becomes

$$\log N = 1.93 - M_L \quad \text{Site source zone}$$

Similarly, the part of the Southern Basin and Range – Rio Grande Rift region of interest has been referred to in the above discussion as the Rio Grange Rift source zone and had an area of about 1.15×10^5 km^2. The proper recurrence formula becomes

$$logN = 2.56 - 1.0 M_L \quad \text{Rio Grande Rift source zone}$$

This leaves only the Central Basin Platform which is essentially a special case. Although the above two formulas were developed for areas near 2×10^5 km^2 in extent with the increase in confidence therefrom derived, this cannot be done for the Central Basin Platform source zone because it is unique and very limited in area. It, therefore, cannot be treated as simply a scaled-down version of some broader region. Although recent work using data from the Kermit array (Rogers and Malkiel, 1978) is available for this source zone, it was decided to use the recurrence formulation of Sanford et al., (1978) for this hazard analysis both for consistency in approach and because this treatment is the only one to calculate a recurrence formula for this source zone using revised magnitude estimates. Based on the seismicity detected in the Central Basin Platform since the installation of station CLN in April 1975, the cumulative number of shocks versus magnitude may be expressed as

$$logN = 3.84 - 0.9 M_L \quad \text{per yr per } 10^5 \text{ } km^2$$

Assuming that the active portion of the Central Basin Platform had an area of 8×10^3 km^2 during this period (Sanford et al, 1978) the proper recurrence relation becomes:

$$logN = 2.74 - 0.9 M_L \quad \text{Central Basin Platform source zone}$$

These are the recurrence relationships used in the current hazard analysis for the site.

One feature of several of these recurrence formulas is apparent: that is, they are very similar when normalized to equal source areas. This is

somewhat surprising in that the geologic indications of recent tectonism
vary from source zone to source zone. One way in which the seismic and
geologic data may be reconciled is to impose some upper limit on the
magnitude of the earthquake that can occur in the geologically quiet
areas that is less than the maximum magnitude event that can occur in
source zones with evidence of Quaternary tectonism in the form of fault
offset. This will be discussed in a later section but is mentioned here
as a preface to the final aspect of source region characterization
necessary to perform a hazard analysis: that is, maximum magnitude event
within each source zone.

It is clear that a simple consideration of maximum historical magnitude
within each of the three source zones as specified above will not be
adequate to assure conservatism. This is particularly true of the
northern part of the Rio Grande Rift source zone (Zone 43 of Algermissen
and Perkins, 1976) where a maximum historical intensity of only V is
known. As discussed above, the fault scarps in this area, particularly
along the margins of the San Andres and Sacramento Mountains, indicate
the strong possiblity that major earthquakes have occurred in this region
within the past 5×10^5 years. The length of the faulting in these two
areas (about 60 to 100 kilometers) suggests earthquakes comparable in
strength to the Sonoran earthquake of 1887 (Sanford and Toppozada,
1974). This major earthquake (M=7.8) produced 80 kilometers of fault
scarp with a maximum displacement of about 8.5 m extending southward from
the U.S. - Mexico border at about 109°W longitude. Sanford and
Toppozada (1974) assume that a similar event is possible in the future
west of a line in good agreement with the eastern boundary of the Rio
Grande Rift zone as shown in Figure 5.3-5. This eclipses the more
southerly Valentine, Texas, earthquake whose magnitude has been variously
estimated to be 6.1 (Algermissen and Perkins, 1976) and 6.4 (Sanford and
Toppozada, 1974). For the purposes of this analysis, a maximum magnitude
event of 7.5 will be assumed able to occur anywhere within the Rio Grande
Rift source zone in general agreement with Sanford and Toppozada.

Selection of maximum magnitude events for the site source zone and the
Central Basin Platform source zone is more difficult. Algermissen and
Perkins (1976) assign a maximum historical intensity of VI to the Central
Basin Platform. This is presumably the earthquake of August 14, 1966
which has been assigned this intensity in United States Earthquakes, 1966
(Von Hake and Cloud, 1968). On the basis of this intensity and the
empirical relationship of Gutenberg and Richter (1942):

$$M = 1.3 + 0.6 \, I_o$$

a maximum magnitude event of 4.9 has been selected for the Central Basin
Platform by Algermissen and Perkins (1976) as appropriate for their
probabilistic acceleration analysis. The magnitude scale was designed to
give some indication of the elastic energy released at the earthquake
source, and in this context, the 4.9 value above is almost certainly an
exaggeration of the energy really released during this particular
earthquake. This conclusion is based on both macroseismic and
instrumental evidence. For example, one of the descriptions of this
shock was, "Like a stick of dynamite being detonated several hundred feet
away" (Von Hake and Cloud, 1968). This and a general consideration of
felt effects are consistent with the contention that this earthquake has
been assigned a relatively high epicentral intensity primarily because it
occurred very near a population center. In addition, several magnitudes
have been published for this earthquake (U.S.C.G.S. - 3.4; Sanford et al.
1978 - 2.8) which are substantially lower than the 4.9 value used by
Algermissen and Perkins.

The maximum instrumental magnitude for an event in the Central Basin
Platform source zone is open to some debate because of the apparently
different application of magnitude scale by various agencies for this
region. The largest earthquake in this region before installation of
station CLN had a magnitude less than 3.25 according to the most recent
calculations at New Mexico Institute of Mining and Technology (Sanford et
al., 1978). Between 1974 and October 1977, during the operation period
of CLN for which data is currently available, a number of earthquakes

have been located by Sanford and his colleagues, none of which have been assigned magnitudes greater than 3.2. In the Rogers and Malkiel (1978) study of data from the recently established Kermit array, events with magnitudes approaching 4 are listed. However, as was stated in subsection 5.2.4, a direct comparison of magnitudes for earthquakes listed in both the New Mexico Institute of Mining and Technology and Kermit array data sets shows that events are routinely assigned magnitudes almost one unit higher in the latter listing. Therefore, the maximum historical magnitude earthquake in the Central Basin Platform Source Zone is still a matter for conjecture although some value between 3.0 and 4.0 is most likely.

The features of this source zone that might bear on its possible maximum magnitude are the lack of recent geologic evidence of tectonism, and the high activity rate which may or may not be directly associated with secondary oil recovery efforts. Sanford and Toppozada (1974) conjecture that the maximum magnitude might be 6.0 for this source zone, and in this study of hazard their example will be followed for one set of calculations. Because this value may be exceptionally conservative, an alternate maximum magnitude of 5.0 is also considered.

With regard to the site source zone, there is even less indication that significant magnitude events are reasonably likely. There is no Quaternary fault offset (Bachman and Johnson, 1973) and seismic activity is low. However, recent studies (Caravella and Sanford, 1977) have shown that some level of background seismicity must currently be considered for the site area if conservatism is to be served. Apparently, an earthquake which may be tectonic in origin and with a magnitude of 3.5 has occurred within the site source zone itself (see subsection 5.2.5). Two maximum magnitudes were considered in the hazard analysis of this section: 4.5, that is the maximum historical event plus one magnitude unit; and 5.0, a rather ad hoc attempt to consider additional conservatism in general agreement with the size of a random event possible in the central United States and not associated with a particular source zone (Algermissen and Perkins, 1976).

All the parameters necessary to perform a probabilistic acceleration hazard calculation for the Los Medanos site after the method of Cornell (1968) have now been presented and discussed. In the next subsection the results of these calculations are considered.

5.3.3   Results

The basic results are shown in Figures 5.3-6 and 5.3-7. These are plots of the probabilities that the maximum annual acceleration will exceed some specified acceleration versus the specified acceleration. For example, in Figure 5.3-6, Curve 1, which shows the contribution to risk at the site due to earthquakes in the Rio Grande Rift source zone as shown in Figure 5.3-5, indicates that the probability that the maximum acceleration at the site from this source zone in any one year will exceed 0.05g is approximately 1.8×10^{-5} or 1.8 in one hundred thousand. Probabilities are similarly found for other values of acceleration.

In both Figures 5.3-6 and 5.3-7, six curves are shown. Curve 1 is the same in both figures and represents the probabilistic maximum acceleration distribution for the Rio Grande Rift source zone as described above. Curves 2 and 2' are also the same in both figures, representing the risk from the site source zone when its maximum magnitude is 5.0 and 4.5, respectively. Curve 3 in each figure is the risk distribution from earthquakes in the Central Basin Platform source zone. In Figure 5.3-6, the maximum magnitude event in this zone is assumed to be 6.0 while in Figure 5.3-7 it is given a value of 5.0. Finally, curves 4 and 4' are the total probabilistic maximum accelerations at the site from all source areas combined. For example, Curve 4 in Figure 5.3-6 is the risk at the site assuming the geometric and recurrence properties, and the acceleration attenuation, of the last subsection and a maximum magnitude of 6.0 in the Central Basin Platform source zone and 5.0 in the site source zone.

Probabilities for accelerations below 0.03g have not been calculated. This is because of a feature of the method used. For a given source geometry and minimum magnitude, the lower limit of validity of probabilistic acceleration is fixed (see Figure 5.3-1top) such that $a \geq a'$.

$$a' = 17 \exp 0.92 \, m_o \, d^{-1}$$

where m_o is the minimum magnitude and d is minimum distance to any source zone. For the worst case, d = 5 km. The value for m_o, 2.4, is the same for all source zones and is derived from an estimate of the smallest earthquakes recorded uniformly throughout the state of New Mexico (Sanford et al., 1978). Substituting these values into the above expression results in a' = 30.9 cm/sec^2 or a' = 0.03g.

There are several interesting features that may be derived from a comparison of the four curves, 4 and 4' in both Figures 5.3-6 and 5.3-7. First, it may be noted that in spite of the greater conservatism exercised in the selection of model parameters for this study than in the Algermissen and Perkins (1976) study--on which so much of the current risk evaluation depends--the basic conclusion of Algermissen and Perkins that the site is in an area with less than one chance in ten that an acceleration of 0.04g will be exceeded in any 50 year period is in very good agreement with the results shown in Figures 5.3-6 and 5.3-7. To see this it may be noted that the return period for the Algermissen and Perkins study is about 475 years. For the slightly more conservative curves of Figure 5.3-6, the maximum accelerations at this return period are around 0.045g while in Figure 5.3-7 they are 0.035g.

Secondly, it is interesting to note that under the assumptions of the previous section the significance of the Rio Grande Rift source zone to the total risk at the site is relatively small at all acceleration levels. Because of the earthquake recurrence relationships for the various source zones, this will be true at lower acceleration levels no matter what assumptions are made about the maximum magnitudes in the site

and Central Basin Platform source zones. At higher acceleration levels, this will be true unless the lowest maximum magnitude proper for the site source zone is lower than the 4.5 value considered here. Although probabilities are low at all site acceleration levels from the Rio Grande Rift source zone, the maximum acceleration at the site from a 7.5 shock at a distance of 115 kilometers using the attenuation law of subsection 5.3.2 is 0.15g. This is slightly greater than the 0.1g acceleration assumed to be the maximum at the site in previous studies (Sanford and Toppozada, 1974).

In the case of the Central Basin Platform source zone, a comparison of the two figures shows an interesting phenomenon. For the case where 6.0 is the maximum magnitude event, probabilities are largely controlled by earthquakes in this source zone up to accelerations of around 0.1g. For higher accelerations, the site source zone is more important. If 5.0 is a better maximum magnitude shock in the Central Basin Platform, its significance as a source of risk is completely eclipsed by the site source zone itself at all acceleration levels.

Perhaps the most universal feature of all four total risk curves is their dominance by the site source zone at higher accelerations. If the probabilities at which these higher acceleration levels occur are thought to be of interest, it is the assumptions that are made about the immediate site area that are most critical.

It is believed that the presentation in this section gives the broadest possible assessment of seismic risk at the site in a way that shows explicitly the assumptions used and, to a small extent at least, the effect of varying some of these assumptions. Acceleration is not the only parameter of design significance, of course, so that a plot of its probability is not the whole story even if such a plot is completely accurate.

5.4   SEISMOLOGICAL DATA AND SITE REGION TECTONISM

In previous sections the historical record of seismicity in the site
region has been explored as well as the way this record, when combined
with very general geologic arguments, can be used to estimate risk levels
attached to various possible seismic design acceleration values. In this
section the extent to which this seismological data may be used to draw
inferences of a longer term nature is considered. The interval over
which seismological data can be collected is still very brief; the total
available earthquake record, and especially that fraction of it
representing the period of instrumental observation, covers a period of
time that is very short compared to the total geologic time scale. Thus,
a comparison of the regional tectonism derived from a study of geologic
processes and structures, with that derived from a study of earthquakes,
involves a question of consistency: that is, are the characteristics of
regional earthquakes consistent with known geologic structures and the
large-scale stresses thought to have been active in their evolution?

Implicit in this concept of tectonics is the definition of tectonic
earthquake that is used in this section. The subject of tectonics as it
is used here is structural geology. Tectonic earthquakes are those
believed to be associated with faulting. This is taken to exclude minor
shocks due to less important causes (Richter, 1958). As mentioned in
subsections 5.2.4 and 5.2.5 it is not clear that the detected earthquakes
in either the site source zone or the Central Basin Platform are tectonic
under this definition. There seem to be few geologic structures in
either area that would lead one to expect significant tectonism either
now or for vast times in the past. Nevertheless, conservatism suggests
that these events should be considered tectonic at this stage of our
knowledge, and this assumption was made for the seismic risk analysis of
the previous section.

Seismology, in the context of tectonism, will be considered below under
two general headings: implications about the regional stress regime from
focal mechanism solutions, and implications about regional activity from

historic recurrence statistics. Although earthquakes are sometimes used
to delineate specific active structures in a way important to discussions
of regional tectonism this will not be attempted here, primarily because
even in areas with recent faulting, such as occur in the southern Basin
and Range province, or in areas with sophisticated seismic array location
capabilities as in the Central Basin Platform, the known earthquakes are
simply not well correlated with specific geologic structures on a
detailed scale.

The ultimate association of seismic and geologic processes is derived
from the observation that the structural behavior of an element of the
earth's crust is often associated with the release of elastic strain
energy in the form of earthquakes. The nature of this association
itself, however, may be far from simple. This is especially true of
small earthquakes whose characteristics are derived from processes taking
place in a very small volume of a crust that, in this context, must be
considered very inhomogeneous. As was seen in Section 5.2, the latest
calculations show that only one instrumentally located earthquake within
300 kilometers of the site (the Valentine, Texas, event) has exceeded
magnitude 4.6. Similarly, within 300 kilometers of the site but outside
the Rio Grande Rift source zone as defined in Section 5.3 no earthquake
has exceeded magnitude 3.5. This should be kept in mind throughout this
section. It may also be noted that most empirical experience in relating
tectonic features to seismicity, or vice versa, has been gathered in
regions that are much more active than the site region. This too was
mentioned in Section 5.2 and is made very clear by comparing earthquake
recurrence statistics for the site region with similar statistics for an
area such as California. The picture presented by a comparison of
seismologic with structural geologic data appears confused for the site
region. At least these two data sources are not consistent in the same
way or to the same degree that is found in other regions characterized by
larger historical earthquakes. It is premature to attempt a
reconciliation here, if indeed one is necessary, so that in this section
existing evidence (although often only preliminary) is outlined and
briefly discussed.

5.4.1· Regional Stress Orientation

The catalog of published crustal stress measurements in the Los Medanos
region is a short one. It consists of three focal mechanism solutions
and one in situ hydrofracture determination. Another in-situ stress
measurement was quoted recently in connection with west Texas studies
(Rogers and Malkiel, 1978), but this measurement is some distance to the
east, on the Llano uplift. In this very limited data collection, there
is little agreement, and none should necessarily be expected since the
measurements come from different structural blocks.

The earliest indication of the stress regime for a point within the
general Los Medanos site region (when defined as it has been in this
chapter as within 300 kilometers of the site) comes from an analysis of
first motion polarities from the Valentine, Texas, earthquake of August
16, 1931. In his study of this event Byerly (1934), carefully noted the
polarity, azimuth, and epicentral distances of waves at all stations
recording this earthquake. He concluded that the observed polarity
pattern could be explained by normal movement on a shallow fault striking
$N35^{O}W$, and dipping very steeply to the west. He also noted that
certain stations did not fit this pattern and attributed most of these
discrepancies to difficulties in observing the true first arrival, which
was apparently lost in the noise at these stations. Fortunately, all
polarity readings were listed in Byerly's paper for this earthquake,
which was recorded at distances ranging from 5.8^{O} to 104.8^{O}.
Applying the recent techniques of stereographic projection to Byerly's
data, Sanford and Toppozada (1974) obtained an independent but very
similar solution shown in Figure 5.4-1a. This solution indicates
predominantly dip-slip motion along a normal fault striking $N40^{O}W$ and
dipping 74° southwest, or motion of a similar nature on a fault
striking $N19^{O}W$ and dipping 18° northeast. The first possibility is
preferred because of the structural fabric of the epicentral region with
which it is consistent. The inconsistent polarity readings are those
noted previously by Byerly. It is worth mentioning that the regional
stresses implied by this solution (P-axis or axis of maximum compressive

stress striking N51°E and plunging 62° to the northeast and T-axis or axis of least compressive stress striking S61°W and plunging 28° to the southwest) are the only ones for this region that are incontrovertibly of some tectonic significance.

The remaining two focal mechanism solutions available at this time for the site region have been very recently determined from data recorded at the Kermit array. One solution is a composite of data from three small earthquakes that occurred within a 7-day period in January 1976 and is reproduced from Rogers and Malkiel (1978) in Figure 5.4-1b. The other solution is from a single earthquake on April 26, 1977, in the same area as the other three near array station KT5 (see Figure 5.2-5) and is reproduced, also from Rogers and Malkiel, in Figure 5.4-1c. These are the only events occurring during array operation that have produced a sufficient number of clear first motion polarities to allow focal mechanism solutions.

The earthquakes from which the composite solution of Fig. 5.4-1bottom was derived occurred on January 19, 22, and 25, 1976 and had U.S.G.S. assigned magnitudes of 3.47, 2.83, and 3.92, respectively. It has already been noted in Section 5.2 that these magnitudes appear to be almost a unit larger than those most recently calculated for shocks in this area by Sanford and his colleagues at the New Mexico Institute of Mining and Technology. The preferred fault plane, based on the geologic structure of the Central Basin Platform, strikes N19°W and dips to the west at 53°. The sense of fault motion is that of normal faulting. Similarity to the solution for the Valentine earthquake is clear. The data for the April 1977 event do not fit this type of solution and do not permit a unique mechanism to be obtained. Normal, thrust, and strike-slip mechanism are possible. The normal solution shown in Figure 5.4-1c is the only one considered by Rogers and Malkiel to be relatively consistent with the composite mechanism and the regional tectonics.

The tectonic significance of these last two focal mechanisms is confused by their occurrence in an area where both active fluid withdrawal and

injection are taking place. This confusion is apparently not lessened by considering the in situ stress data. Hydrofracture data from a well in Howard County, Texas to the east (Fraser and Pettit, 1962) indicate a tension axis that trends south-southeast. Overcoring data from Hooker and Johnson (1969) even further to the east in Burnet County, Texas, on the Llano uplift show reversion to a southwest trend for the tension axis. According to Rogers and Malkiel (1978), both the Howard and Burnet County data show a horizontal axis of maximum compression. This is in disagreement with the focal mechanisms, for which the greatest compressive stress is steeply plunging. Also, von Schonfeldt et al. (1973) have indicated that the greatest principal stress in this area is a vertically oriented, overburden induced compressive stress because hydrofracture experiments generally produce vertical fractures in Texas, except in some shallow wells (Hays, 1977). In the face of such a variety of interpretations, it is premature to speculate on the significance, or lack of it, of these data. Any such speculation will have to wait on the collection of new data or additional analysis of existing information.

5.4.2   Tectonism and Earthquake Recurrence Relations

In Section 5.2 the seismicity of the Los Medanos site region was studied. It was noted that most of the activity of recent years had occurred in the Central Basin Platform in two particular areas located such that Sg-Pg intervals at station CLN very near the site were 8 to 13 seconds and 22 to 24 seconds (Sanford, et al. 1978). Another group of epicenters for shocks with Sg-Pg intervals from 31 to 36 seconds were found by these authors to occur in several tectonically active regions to the southwest and west of the site—notably near Valentine, Texas, and in much of the Tularosa Basin. These three Sg-Pg intervals account for the most important peaks on the histogram appearing in Figure 5.2-5. Earthquakes at other distances contribute a general background occurrence level also apparent in this histogram. At least some of these events are known to have occurred in the general site region and not in association with either the Central Basin Platform or the Rio Grande Rift source

zones of the previous section. This characterization of the regional seismicity is interesting because there is abundant geologic evidence for recent tectonic activity for the source zones to the west and none for the Central Basin Platform.

This situation can be described more quantitatively by considering earthquake recurrence statistics. Relations of the form logN=a-bM for the three source zones of Section 5.3 have already been shown. These formulas, taken from Sanford et al. (1976b) and Sanford et al. (1978) may be normalized to equal time intervals and areas for comparison (assuming such a comparison is meaningful) to give:

$$\log N = 2.5 - M_L \quad \text{Rio Grande Rift zone}$$

$$\log N = 2.4 - M_L \quad \text{High Plains Province}$$

$$\log N = 3.84 - 0.9 \ M_L \quad \text{Central Basin Platform}$$
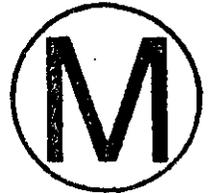
where in each case the formulas give the number of occurrences, N, of events with magnitude M_L or greater per year in a $10^5 \ km^2$ area. It is clear that if these relations truly indicated some measure of tectonic activity in effect for a long time period the relative tectonic importance of these areas would be in conflict with that implied by the geologic data. This is particularly true for the Central Basin Platform activity.

Several explanations have been offered to resolve this conflict (Sanford et al., 1978). One is that a recent change in regional stress may be responsible. In this view, the tectonic implications of very recent seismicity are preferred to those of the geologic record. The other extreme possibility is that the observed recent seismicity, especially in the Central Basin Platform, has little bearing on tectonism in the sense normally used in connection with magnitude recurrence relations. Thus, the geologic implications to past and recent (and, by extrapolation, future) tectonism are preferred to those of recent seismicity. Finally,

there is an intermediate position which attempts reconciliation of both the geologic and seismic data by prescribing some particular mode of crustal behavior in the High Plains physiographic province and the Central Basin Platform. The only explicit property of this mode of behavior is that large magnitude earthquakes do not occur; hence, extrapolation of the recurrence formulas above to large magnitudes is fundamentally inaccurate.

The first possibility, that the regional geology of the High Plains province and Central Basin Platform is in essence misleading, is the least satisfactory. There does not seem to be any implication of recent regional stress changes in the more active areas of New Mexico. Sanford et al. (1972) performed calculations comparing the implications to tectonic activity of recent fault offset in the Rio Grande Rift (where recent is defined as less than 4×10^5 years old) with similar implications from recurrence statistics both from historical earthquakes and from microearthquake studies (Sanford and Singh, 1968). These calculations show that if the fault scarps are less than 4×10^4 years old, the seismicity obtained is compatible with the historical earthquake activity in the Socorro region. If the age span of the fault scarps is increased to about 2×10^5 years, the seismicity becomes close to that indicated by the microearthquake studies. It may also be noted here that the focal mechanism solution obtained for the Valentine, Texas, earthquake is consistent with the sense of fault motion implied by the geologic structure of that area.

Using similar types of arguments some limits can be placed on how recently the change in stress postulated for the High Plains province and the Central Basin Platform must have taken place. Consider that part of the High Plains province designated as the site source zone in Section 5.3. Then the recurrence relation is, after Sanford et al. (1976b):

$$\log N = 1.93 - M_L$$

The use of this formula in an uncritical way leads to the conclusion that an earthquake of magnitude greater than or equal to 7.0 should occur in this zone on the average of once in about 10^5 years. Such an earthquake would certainly leave physical evidence of fault offset. If the High Plains province of New Mexico is taken as a whole, a similar earthquake would be expected on the average of once in slightly over 2 x 10^4 years. Assuming that earthquake occurrence is distributed as a Poisson process, it can be concluded that an earthquake of magnitude 7.0 or greater has a 63 percent likelihood of occurring in a given 2 x 10^4 year period and that it has a 90 percent likelihood of occurring in a given 2 x 10^5 year period. Nevertheless, no evidence is known of fault offset suggesting earthquakes of this size anywhere in the High Plains during comparable or longer time periods. Thus, if there have been changes in regional stress that are responsible for the observed conflict between geologic and seismic data, these changes probably have taken place more recently than within the last 2 X 10^4 to 2 X 10^5 years.

A similar calculation may be applied to the Central Basin Platform. In this case on the basis of seismic evidence the recurrence interval for a magnitude 7.0 earthquake is about 3500 years. As in the High Plains, there is no geologic evidence for such an earthquake. Thus, the geologic and seismic evidence appear to contradict one another unless the current seismicity is the result of a tectonic stress change that took place within the last several thousands or tens of thousands of years. The implications of recurrence intervals for large earthquakes developed from short term seismic data should not form the basis for rationally discarding contradicting geologic evidence.

The second possibility as it is presented here applies only to the Central Basin Platform. That is, the recurrence statistics for earthquakes in this small area are not related to tectonism in the usual sense of this concept and should not be used for tectonic implications of long time intervals. The principal support for this view is outlined in Sanford and Toppozada (1974). Basically, it has been postulated that the earthquakes on the Central Basin Platform are related to massive fluid

injection for secondary recovery of oil. Both the spatial and temporal association of this seismicity with these secondary recovery projects are very suggestive. This has already been discussed in greater detail in subsection 5.2.4 and will not be repeated here. The wide variety of hypotheses regarding the stress field in the area of the Central Basin Platform neither preclude nor prove any causal relationship between the earthquakes and secondary recovery operations (Hays, 1977), but, the widely observed phenomenon of increased seismic activity during fluid injection (Healy et al., 1968; Healy et al., 1972) argues strongly against the uncritical extrapolation of short term magnitude recurrence formulas under the present conditions.

The third possibility, that the geologic and seismic data are not really in conflict, is the most satisfying from a philosophical viewpoint. It is certainly simpler to derive meaningful conclusions about the physical properties of a system that is not changing than about one that is. It has already been mentioned that such consistency exists for the Rio Grande Rift, at least in gross terms. A similar reconciliation might be possible for the High Plains province or the Central Basin Platform by restricting the maximum magnitude of an earthquake that can occur in either the High Plains physiographic province or the Central Basin Platform.

The simplest restriction that can be applied to the magnitude of shallow seismic events that have occurred in the past is imposed by the size or absence of observed faulting. An argument of this type has been used above in considering the questions of recent stress regime changes. In very general terms, it is believed that where recent geologic faulting exists, even in the absence of observed large magnitude earthquakes, conservatism requires that such seismic activity should be anticipated (Allen et al., 1965; Sanford et al., 1972); that is, to a high level of confidence, large recent faults in an area imply large magnitude earthquakes must be considered there. The converse argument, that large magnitude shallow earthquakes always produce episodes of large scale shallow faulting is even more widely believed. This assertion appears so

absolute because the definitions of "large" earthquake and "large-scale" faulting have been left purposely vague. A more empirically useful statement might be that the largest recent fault offsets (in terms of both fault length and fault displacement) that are found in an area under a given set of geologic conditions and after an adequate search impose an upper limit on the magnitudes of past earthquakes.

The general relation between magnitude of shallow-focus earthquakes and size or volume of the deformed region and the length and amount of displacement of activated surface faults has long been recognized (Tsuboi, 1956; Richter, 1958). Tocher (1958) developed an early empirical relation between magnitude and fault length, and between magnitude and the product of fault length and maximum displacement. Many subsequent refinements have been formulated by adding additional data points (Iida, 1959 and 1965), applying the method to specific areas, as for southern California (Albee and Smith, 1966), and by refining the source data either for the western United States (Bonilla, 1967 and 1970; Bonilla and Buchanan, 1970) or for the world (Ambraseys and Tchalenko, 1968; Bonilla and Buchanan, 1970). Various dislocation models have been proposed by seismologists (Aki, 1967; Brune, 1968; Chinnery, 1969; King and Knopoff, 1968 and 1969; Press, 1967; and Wyss and Brune, 1968) one of which (King and Knopoff, 1968) was used by Sanford et al. (1972) in connection with fault offset-magnitude comparisons in the Rio Grande Rift as discussed above. A recent recompilation and reconsideration of fault offset data has been performed by Slemmons (1977). He finds, for North America data and faulting of all types that

$$\log D = -4.47 + 0.67M$$

$$\log L = 1.61 + 0.44M$$

where both D (fault displacement) and L (fault length) are in meters. Using these formulas, fault lengths of 6.46, 10.72, 17.78, 29.51, 48.98, and 81.28 kilometers are found for magnitudes from 5.0 to 7.5 in half magnitude increments. The respective displacements are 0.08, 0.16, 0.35,

0.77, 1.66, and 3.59 meters. Thus, if an area has been mapped so well that no fault of length about 18 kilometers and maximum displacement of about 1/3 meter could escape notice in strata of a given age, then it could be maintained that no event of magnitude greater than or equal to 6.0 had occurred in that area in the time since formation of the strata. Explicit statements of the kind necessary about the minimum observable fault are not generally available in the literature. If it is assumed that the conclusion of Bachman and Johnson (1973), that no recent fault scarps of a tectonic nature exist in the Permian Basin, is applicable at the scale of the minimum observable fault associated with a magnitude 6.0 earthquake, then the conflict between the geologic and seismic recurrence data is resolved. That is, the recurrence data may not be extrapolated beyond magnitude 6.0. Arguments of this type, although they are clearly over-simplified and depend on relationships between magnitude and fault offset derived from widely scattered data, are of interest at least for purposes of comparison with similiar studies made in other areas.

A more complete treatment of this type would have to address the issue of regional deformation. This involves not only the offset associated with a single earthquake but the deformation implied by summing the effects of all earthquakes. If total strain energy released as seismic waves is calculated from the magnitude recurrence relations, estimates of total available strain energy and total implied steady state deformation may be derived. These are both dependent on the maximum magnitude event allowed, since significant strain and most of the energy are associated with the larger events (Richter 1958). Thus, general deformation rates may be derived as a function of maximum magnitudes, and observed deformation rates may be used to infer an acceptable maximum magnitude for the region over which deformation is observed. Unfortunately, application of this type of analysis is subject to more complication and uncertainty than a simple fault argument. It seems clear, however, that deformation of a type that would be associated with accumulation and release of elastic strain energy has not been very important in the Permian Basin for very long periods of time.

Although other explanations cannot be precluded, it seems that the most reasonable interpretations of seismic implications to tectonism at this time are:

1) Observed geologic and seismic data are in general agreement in the Rio Grande Rift and Southern Basin and Range zones and that future significant earthquakes can be expected there.

2) The current level of activity on the Central Basin Platform is probably related to fluid injection for secondary recovery of oil. This fluid injection makes it unwise to question the geologic data of the area solely on the basis of this high seismic activity level (see Chapter 10).

3) The geologic data, principally the lack of recent geologic faulting, and the seismic data for the High Plains province, in which the site lies, can probably be reconciled by imposing a maximum magnitude limit on the earthquakes that may occur here.

5.5 SUMMARY

Non-instrumental and regional instrumental studies of earthquakes prior to 1972 in southeastern New Mexico indicate that the most significant sources of earthquakes were the Central Basin Platform region near Kermit, Texas, and the area about 200 km or more west and southwest of the site (Rio Grande Rift Zone). The strongest earthquake reported to occur within 300 km is the intensity VIII Valentine, Texas, event of August 16, 1931, at a distance of approximately 210 km. The closest shock (as of 1972) reported from these studies was a magnitude 2.8 event on July 26, 1972, about 40 km northwest of the site. The record from regional studies of events west and southwest of the WIPP site 200 km or more is consistent with the record of Quaternary faulting in that area.

Instrumental studies near the WIPP site since 1974 and near Kermit, Texas, since late 1975 have recorded additional evidence of the seismic activity for the site and region. The pattern obtained from near the site is similar to that from regional studies; about one-half of the located events in the data set occur on the Central Basin Platform while most of the rest occur to the west and southwest of the site in the Rio Grande Rift Zone. The data set also includes three events within about 40 km of the WIPP site since 1972. Two events have been assigned magnitudes of 2.8 and 3.6; the third event (from 1978) has only preliminary data available.

Data reported for the Central Basin Platform from the Kermit, Texas, array continue to show that location as the most active seismic area within 300 km of the site in terms of number of events. The largest earthquake known to occur in the Central Basin Platform had, by the most recent estimate, a magnitude of less than 3-1/4. The activity appears equally likely to occur anywhere along the Central Basin Platform structure without particular regard to small scale structural details such as pre-Permian buried faults. The spatial and temporal coincidence of this seismicity with secondary petroleum recovery projects suggest a close relationship, but this has not yet been satisfactorily established. The lack of known Quaternary faults from the seismically active region of the Central Basin Platform is suggestive that large magnitude earthquakes are not occuring or have not occurred within the recent geologic past in the area.

Analysis of the regional and local seismic data indicate that the 1000 year acceleration is less than or equal to 0.06 g and the 10,000 year acceleration is less than or equal to 0.1 g for all models tried. Probabilities at which higher acceleration levels occur depend almost exclusively on the assumptions made about the seismic potential of the immediate site area.

5.6 REFERENCES

Aki, K., 1967, Scaling law of seismic spectrum: Jour. Geophysical Res., v. 72, p. 1217-1231.

Albee, A.L. and Smith, J.L., 1966, Earthquake characteristics and fault activity in southern California: Engineering Geology in Southern California, R. Lung and R. Proctor, eds., Associated Engineering Geologists, Glendale, Calif., p. 9-33.

Algermissen, S.T., 1969, Seismic risk studies in the United States: Fourth World Conf. on Earthquake Engineering, Santiago, Chile, p. 14-27.

Algermissen, S.T., and Perkins, D.M., 1976, A probabilistic estimate of maximum ground acceleration in the contiguous United States: U.S. Geol. Surv. Open-file report 76-416, p. 1-45.

Allen, C.R., St. Amand, P., Richter, C.F., and Nordquist, J.M., 1965, Relationship between seismicity and geologic structure in the southern California region: Seismol. Soc. Am. Bull., v. 55, p. 753-797.

Ambraseys, N. and Tchalenko, J., 1968, Documentation of faulting associated with earthquakes, Part I: Unpublished Manuscript, Dept. of Civil Eng., Imperial College of Science, London.

Bachman, G.O., and Johnson, R.B., 1973, Stability of Salt in the Permian Salt Basin of Kansas, Oklahoma, Texas, and New Mexico: U.S. Geol. Surv. Open-file report, 4339-4.

Bickers, G., 1978, "WIPP acceleration attenuation curves": Bechtel Interoffice Memorandum, dated Jan. 30, to J. Litehiser.

Bonilla, M.G., 1967, Historic surface faulting in continental United States and adjacent parts of Mexico: U.S. Geol. Surv. Open-file report.

Bonilla, M.G., 1970, Surface faulting and related effects in earthquake engineering: Earthquake Engineering, Prentice-Hall, Englewood Cliffs, p. 47-74.

Bonilla, M.G., and Buchanan, J.M., 1970, Interim report on worldwide historic surface faulting: U.S. Geol. Surv. Open-file report.

Brune, J.N., 1968, Seismic moment, seismicity and the rate of slip along major fault zones: Jour. Geophysical Res., v. 73, p. 777-784.

Byerly, P., 1934, The Texas earthquake of August 16, 1932: Seismol. Soc. Am. Bull., v. 24, p. 81-89.

Caravella, F.J., and Sanford, A.R., 1977, An analysis of earthquakes north of the Los Medanos site on July 26, 1972 and November 28, 1974: New Mexico Institute of Mining and Technology, Report to Sandia Laboratories, Contract No. 03-6223/GTK.

Chinnery, M.A., 1969, Earthquake magnitude and source parameters: Seismol. Soc. Am. Bull., v. 59, p. 1969-1982.

Coffman, J.L., and von Hake, C.A., (eds.), 1973, Earthquake history of the United States, U.S. Dept. Commerce, Publication 41-1, Revised edition (through 1970), Nat. Oceanographic and Atmospheric Admin., Washington, D.C.

Cornell, C.A., 1968, Engineering seismic risk analysis: Seismol. Soc. Am. Bull., v. 58, p. 1583-1606.

Cornell, C.A., and Merz, H.A., 1975, Seismic risk analysis of Boston: Jour. Struct. Dov., Am. Soc. Civil Eng., v. 10, p. 2027-2043.

Cornell, C.A., and Vanmarke, E.H., 1969, The major influences on seismic risk: Fourth World Conf. on Earthquake Engineering, Santiago, Chile, p. 69-83.

Dake, C.L., and Nelson, L.A., 1933, Post-Bolson faulting in New Mexico: Science, v. 78, p. 168-169.

Esteva, L., and Rosenblueth, E., 1964, Espectros de Temblores a Distancias Moderas y Grandes: Bol. Soc. Mex. Ing. Sism, v.2, p. 1-18.

Evernden, J.F., 1967, Magnitude determination at regional and near-regional distances in the United States: Seismol. Soc. Am. Bull., v. 57, p. 591-639.

Fraser, C.D., and Pettit, B.E., 1962, Results of a field test to determine the type of induced formation fracture: Jour. Petrol. Tech., v. 14, p. 463-466.

Gutenberg, B., and Richter, C.F., 1942, Earthquake magnitude, intensity, energy, and acceleration: Seismol. Soc. Am. Bull., v. 32, p. 163-191.

Gutenberg, B., and Richter, C.F., 1954, Seismicity of the Earth and Associated Phenomena: Princeton Univ. Press, p. 1-310.

Hays, W.W., 1977, Progress report on the Central Basin Platform seismic study - April 1, 1976 through November 15, 1976: Report to ERDA and Sandia Laboratories.

Healy, J.H., Rayleigh, C.B., Brodehoeft, J.C., and Byerlee, J.D., 1972, Seismic activity related to fluid injection (abs.): Society of Exploration Geophysicists, 42nd Annual Meeting, Program, p. 15.

Healy, J.H., Rubey, W.W, Griggs, O.T., and Rayleigh, C.V., 1968, The Denver earthquakes: Science, V. 161, p. 1301-1310.

Hooker, V.B., and Johnson, C.F., 1969, Near-surface horizontal stresses, including the effects of rock anistropy: U.S. Bur. Mines Rept. of Inv. 7224, p. 1-29.

Iida, K., 1959, Earthquake energy and earthquake fault: Nagoya Univ., Jour. Earth Science, v. 7, p. 98-107.

Iida, K., 1965, Earthquake magnitude, earthquake fault and source dimensions: Nagoya Univ., Jour. Earth Science, v. 13, p. 115-132.

Kelley, V.C., 1971, Geology of Pecos country, southeastern New Mexico: New Mexico Bureau Mines and Mineral Resources, Mem. 24, p. 1-69.

King, C.Y. and Knopoff, L., 1968, Stress drop in earthquakes: Seismol. Soc. Am. Bull., v. 58, p. 249-257.

King, C.Y. and Knopoff, L., 1969, A magnitude-engergy relation for large earthquakes: Seismol. Soc. Am. Bull., v. 59, p. 269-273.

King, P.B., 1948, Geology of the southern Guadalupe Mountains, Texas: U.S. Geol. Surv. Prof. Paper 215.

King, P.B., 1965, Geology of the Sierra Diablo region, Texas: U.S.Geol. Surv. Prof. Paper 480, p. 1-179.

Kottlowski, F.E., 1960, Reconnaissance geologic map of Las Cruces thirty-minute quadrangle: New Mexico Bureau Mines and Mineral Resources, Geol. Map 14.

Kottlowski, F.E., and Foster, R.W., 1960, Road log - second day - Las Cruces to Hembrillo Canyon in San Andres Mountains: Roswell Geol. Soc. Guidebook, p. 34-74.

Lee, W.H.K., and Lahr, J.C., 1972, HYP071 - A computer program for determining hypocenter, magnitude, and first motion pattern of local earthquakes: U.S. Geol. Surv. Open-file report, p. 1-100.

McGuire, R.K., 1977, Effects of uncertainty in seismicity on estimates of seismic hazard for the east coast of the United States: Siesmol. Soc. Am. Bull., v. 67, p. 827-848.

Major, M., 1975, Private communication cited in Caravella and Sanford, 1977.

Mitchell, B.J., 1973, Radiation and attenuation of Rayleigh waves from the southeastern Missouri earthquake of October 21, 1965: Jour. Geophys. Research, v. 78, p. 886-899.

Muehlberger, W.R., Belcher, R.C., and Goetz, L,K., 1978, Quaternary faulting in Trans-Pecos Texas: Geology, v. 6, p. 337-340.

Murphy, L.M., and Cloud, W.K., 1954, United States earthquakes 1952: U.S. Dept. Commerce, Coast and Geodetic Survey, Washington, D.C.

Murphy, L.M. and Cloud, W.K., 1957, United States earthquakes 1955: U.S. Dept. Commerce, Coast and Geodetic Survey, Washington, D.C.

Murphy, L.M., and Ulrich, F.P., 1951, United States earthquakes 1951, United States earthquakes 1949: U.S. Dept. Commerce, Coast and Geodetic Survey, Washington, D.C.

Neumann, R., 1932, United States earthquakes 1931: U.S. Dept. Commerce, Coast and Geodetic Survey, Washington, D.C.

Neumann, F., 1938, United States earthquakes 1936: U.S. Dept. Commerce, Coast and Geodetic Survey, Washington, D.C.

Neumann, F., 1940, United States earthquakes 1937: U.S. Dept. Commerce, Coast and Geodetic Survey, Washington, D.C.

Neumann, F., and Bodle, R.R., 1932, United States earthquakes 1930: U.S. Dept. Commerce, Coast and Geodetic Survey, Washington, D.C.

Northrop, S.A., and Sanford, A.R., 1972, Earthquakes of northeastern New Mexico and the Texas Panhandle, in Guidebook of Eastern-central New Mexico: New Mexico Geol. Soc. 23rd Field Conf., p. 148-160.

Nuttli, O.W., 1973a, Seismic wave attenuation and magnitude relations for eastern North America: Jour. Geophys. Research, v. 78, p. 876-885.

Nuttli, O.W., 1973b, The Mississippi Valley earthquakes of 1811 and 1812 - intensities, ground motion and magnitudes: Seismol. Soc. Am. Bull., v. 63, p. 227-248.

Nuttli, O.W., 1973c, Design earthquakes for the central United States: Misc. Paper S-73-1, U.S. Army Waterways Experiment Station, Vicksburg, Mississippi, p. 1-45.

Orphal, D.L., and Lahoud, J.A., 1974, Prediction of peak ground motion from earthquakes: Seismol. Soc. Am. Bull., v. 64, p. 1563-1574.

Page, R.A., Boore, D.M., Joyner, W.B., and Coulter, H.W., 1972, Ground motion values for use in the seismic design of the Trans-Alaska pipeline system: U.S.G.S. Circular 672, p. 1-23.

Pray, L.C., 1961, Geology of the Sacramento Mountains escarpment, Otero County, New Mexico: New Mexico Bureau Mines and Mineral Resources, Bull. 35, p. 1-133.

Press, F., 1967, Dimensions of the source region for small shallow earthquakes: Proceedings, VESIAC Conf. on the Source Mechanism of Shallow Seismic Events, VESIAC Rept. 7885-1-X, p. 155-164.

Reddy, R.S., 1966, Crustal structure in New Mexico: M.S. Thesis, New Mexico Institute of Mining and Technology, Socorro, New Mexico, p. 1-45.

Reiche, P. 1938, Recent fault scarps, Organ Mountain destrict, New Mexico: Am. Jour. Sci., v. 36, p. 400-444.

Richter, C.F., 1958, Elementary Seismology: W.H. Freeman & Co., San Francisco, 768 p.

Richter, C.F., 1959, Seismic regionalizaton: Seismol. Soc. Am. Bull., v. 49, p. 123-162.

Rogers, A.M., and Malkiel, A., 1978, A study of earthquakes in the Permian Basin, Texas - New Mexico: draft of a U.S. Geol. Surv. report for open-file.

Romney, C., Brooks, B.G., Mansfield, R.H., Cardes, D.S., Jordan, J.N., and Gordon, D.W., 1962, Travel times and amplitudes of principal body phases recorded from GNOME: Seismol. Soc. Am. Bull., v. 52, p. 1057-1074.

Sanford, A.R., 1963, Seismic activity near Socorro: N. Mex. Geol. Soc., Guidebook, Fourteenth field conference, The Socorro Region, p. 146-151.

Sanford, A.R., 1965, An instrumental study of New Mexico earthquakes: New Mexico Bureau of Mines and Mineral Resources, Circ. 78, p. 1-12.

Sanford, A.R., 1976a, Seismicity of the Los Alamos region based on seismological data: Los Alamos Scientific Laboratory, LA-6416-MS Informal Report, p. 1-9.

Sanford, A.R., 1976b, Seismicity of the Tualarosa Basin: in, A Preliminary Economic Feasibility Study for Establishment of an Energy-Water Complex in the Tularosa Basin, WRRI Report No. 068, New Mexico Water Resources Research Institute, New Mexico State University, Las Cruces, New Mexico p. 84-93.

Sanford, A.R., Budding, A.J., Hoffman, J.P., Alptekin, O.S., Rush, C.A., and Toppozada, T.R., 1972, Seismicity of the Rio Grande Rift in New Mexico: New Mexico Bureau Mines and Mineral Resources, Circ. 120, p. 1-19.

Sanford, A.R., and Cash, D.J., 1969, An instrumental study of New Mexico earthquakes July 1, 1964, through Dec. 31, 1967: New Mexico Bureau Mines and Mineral Resources, Circ. 102, p 1-7.

Sanford, A.R., and Holmes, C.R., 1961, Note on the July 1960 earthquakes in central New Mexico: Seismol. Soc. America Bull., v. 51, p. 311-314.

Sanford, A.R., and Holmes, C.R., 1962, Microearthquakes near Socorro, New Mexico: Jour. Geophys. Res., v. 67, p. 449-4459.

Sanford, A.R., Johansen, S.J., Caravella, F.J., and Ward, R.M., 1976a, A report on seismic recording at the Los Medanos area of southeastern New Mexico, 1974-1975: New Mexico Institute of Mining and Technology, Oak Ridge Operations Contract No. AT-(40-1)-4582.
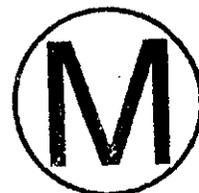
Sanford, A.R., Sandford, S., Caravella, F.J., Merritt, L., Sheldon, J., and Ward, R.M., 1978, A report on seismic studies of the Los Medanos area in southeastern New Mexico: New Mexico Institute of Mining and Technology, Report to Sandia Laboratories, Contract No. 03-6233.

Sanford, A.R., and Singh, S., 1968, Minimum recording times for determining short term seismicity from microearthquake activity: Seismol. Soc. Am. Bull., v. 58, p. 639-644.

Sanford, A.R., and Toppoazda, T.R., 1974, Seismicity of proposed radioactive waste isolation disposal site in southeastern New Mexico: New Mexico Bureau Mines and Mineral Resources, Circ. 143, p. 1-15.

Sanford, A.R., Toppozada, T.R., Ward, R.M., and Wallace, T.C., 1976b, The seismicity of New Mexico 1962 through 1972: Geol. Soc. Am. Abstracts With Programs v. 8, p. 625.

Sbar, M.L., Armbruster, J., and Aggerwal, Y.P., 1972, The Adirondack, New York, earthquake swarm of 1971 and tectonic implications: Seismol. Soc. Am. Bull. v. 62, p. 1303-1318.

Schnabel, P.B., and Seed, H.B., 1973, Accelerations in rock for earthquakes in the western United States: Seismol. Soc. Am. Bull., v. 63, p. 501-516.

Seed, H.B., Idriss, I.M., and Kiefer, R.W., 1968, Characteristics of rock motions during earthquakes: Earthquake Eng. Res. Center, Rept. no. 68-5.

Sellards, E.H., 1933, The Valentine, Texas, earthquake: Univ. Tex. Bull. no. 3201, p. 113-138.

Shah, H.C. Mortgat, C.P., Kiremidjian, A., and Zsutty, T.C., 1975, A study of seismic risk for Nicaragua: Rept. 11, Dept. of Civil Eng., Stanford Univ., Stanford, California.

Shurbet, D.H., 1969, Increased seismicity in Texas: Texas Jour. Sci., v. 21, p. 37-41.

Shurbet, D.H., 1975, Private communication cited in Caravella and Sanford, 1977.

Slemmons, D.B., 1977, Faults and earthquake magnitude: U.S. Army Engineer Waterways Experiment Station, Miscellaneous Paper s-73-1.

Slemmons, D.B., Jones A.E., and Gimlett, J.I., 1965, Catalog of Nevada earthquakes, 1852-1960: Seismol. Soc. Am. Bull., v. 55, p. 537-583.

Stauder, W., Kramer, M., Fisher, C., Shaefer, S., and Morrissey, S.T., 1976, Seismic characteristics of southeast Missouri as indicated by a regional telemetered microearthquake array: Seismol. Soc. Am. Bull., v. 66, p. 1953-1964.

Stewart, S.W., and Pakiser, L.C., 1962, Crustal structure in eastern New Mexico interpreted from the GNOME explosion: Seismol. Soc. Am. Bull., v. 52, p. 1017-1030.

Talmage, S.B., 1934, Scarps in Tularosa valley, New Mexico: Science, v. 79, p. 181-183.

Tatel, H.E., and Tuve, M.A., 1955, Seismic exploration of a continental crust: Geol. Soc. Am., Spec. Paper 62, p. 35-50.

Tocher, D., 1958, Earthquake energy and ground breakage: Seismol. Soc. Am. Bull., v. 48, p. 147-153.

Toppozada, T.R., and Sanford, A.R., 1972, Instrumental study of New Mexico earthquakes January 1968 through June 1971: New Mexico Bureau Mines and Mineral Resources, Circ. 126, p. 1-6.

Toppozada, T.R., and Sanford, A.R., 1976, Crustal structure in central New Mexico interpreted from the Gasbuggy explosion: Seismol. Soc. Am. Bull., v. 66, p. 877-886.

Tusboi, C., 1956, Earthquake energy, earthquake volume, aftershock area, and strength of the earth's crust: Physics of the Earth Jour. (Tokyo), v. 4, p. 63-66.

Uniform Building Code, 1970, 1973, 1976 editions, International Conference of Building Officials, Whittier, California.

Von Hake, C.A., 1975, Earthquake history of New Mexico: Earthquake Info. Bull, v. 7, No. 3, p. 23-26.

Van Hake, C., and Cloud, W.K., 1968, United States earthquakes 1966: U.S. Dept. Commerce, Coast and Geodetic Survey, Washington, D.C.

Von Schonfeldt, H.A., Kehle, R.O., and Gray, K.E., 1973, Mapping of stress field in the upper earth's crust of the United States: Final Tech. Rept. to U.S. Geol. Surv. under Contract No. 14-08-0001-122278, p. 1-40.

Wiegel, R.L., (ed.), 1970, Earthquake Engineering: Prentice-Hall Inc., Englewood Cliffs, N.J., p. 1-518.

Wilson, E.D., Moore, R.T., and Cooper, J.R., 1969, Geologic Map of Arizona: Arizona Bureau of Mines, Tucson, Arizona, Scale 1:500,000.

Wood, H.O., and Neumann, F., 1931, Modified Mercalli intensity scale of 1931: Seismol. Soc. Am. Bull., v. 21, p. 277-283.

Wyss, M. and Brune, J.N., 1968, Seismic movement, stress, and source dimensions for earthquakes in the California - Nevada region: Jour. Geophysical Res., v. 73, p. 4681-4694.

EXPLANATION

Locations of earthquakes within 300 km of the repository site. Locations shown with square symbols are based on reports of felt earthquakes prior to 1961. Epicenters shown with circles were deter_mined instrumentally and cover the period 1961 through 1972. In the Central Basin Platform and Chihuahua areas where crowding occurs some epicenters are slightly offset for drafting convenience. The true epicenters are listed in Tables 5.2-1 and 5.2-3.

Local Magnitude

Symbol	Magnitude
∘	< 1.5
○	1.51 – 2.0
○	2.01 – 2.5
○	2.51 – 3.0
○	3.01 – 3.5
○	3.51 – 4.0
○	4.01 – 4.5
○	4.51 – 5.0

Maximum Intensity

Symbol	Intensity
□	III
□	IV
□	V
□	VI
□	VII
□	VIII

SCALE

REFERENCE:

SANFORD AND TOPPOZADA (1974)

REGIONAL SEISMICITY 1923–1972

FIGURE 5.2-1

13

EXPLANATION

Isoseismal map for the Valentine, Texas earthquake of August 16, 1931 (after Sanford and Toppozada, 1974). Intensities are in the Modified Mercalli scale of 1931 (see Table 5.2-2). Also shown are the instrumental epicenters for this earthquake as determined by the U.S.C.G.S. (Neumann, 1932) and Byerly (1934).
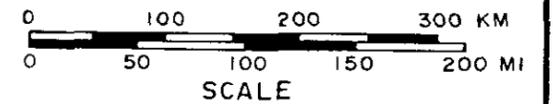
VALENTINE, TEXAS EARTHQUAKE ISOSEISMALS

FIGURE 5.2-2
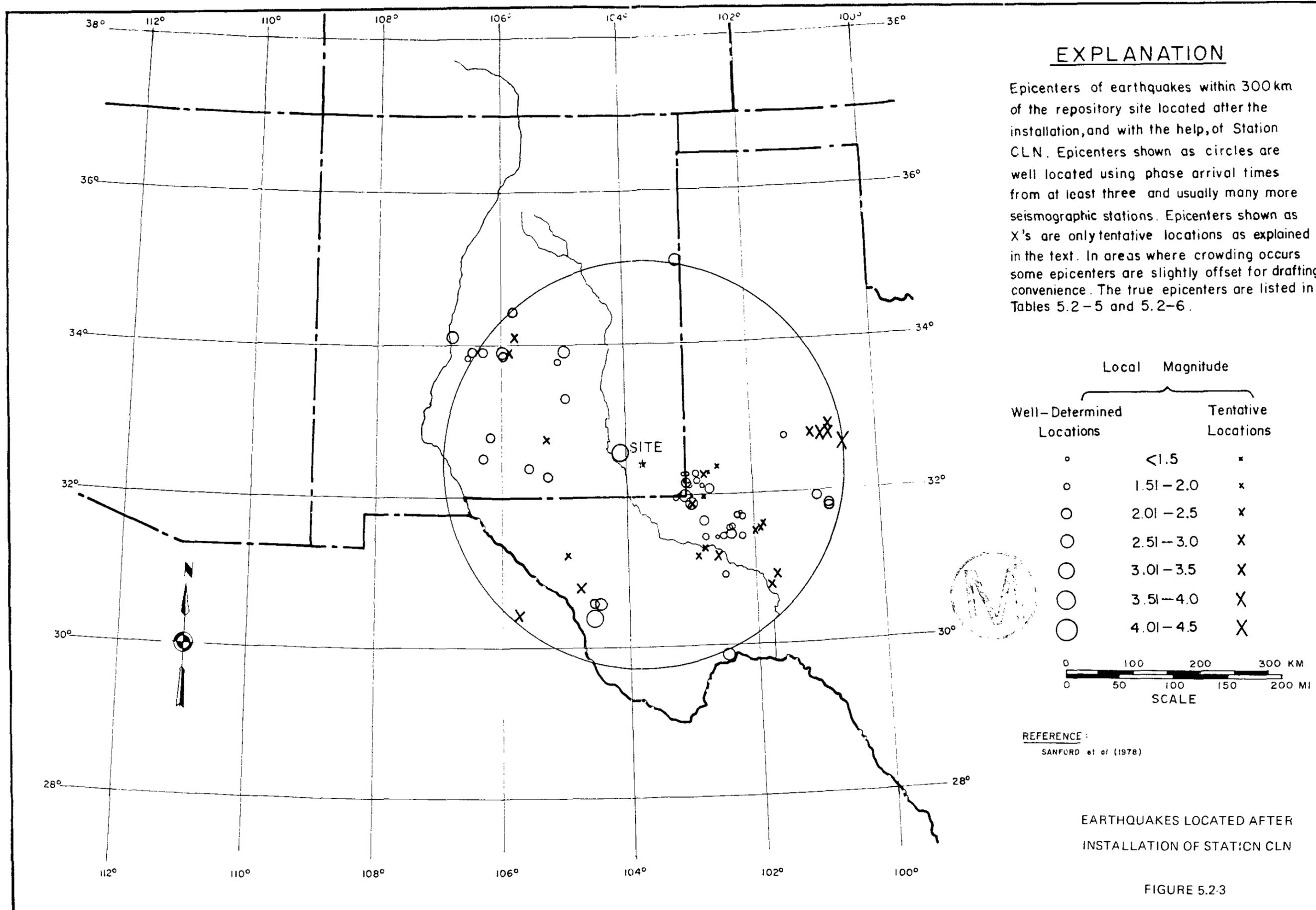
EXPLANATION

Epicenters of earthquakes within 300 km of the repository site located after the installation, and with the help, of Station CLN. Epicenters shown as circles are well located using phase arrival times from at least three and usually many more seismographic stations. Epicenters shown as X's are only tentative locations as explained in the text. In areas where crowding occurs some epicenters are slightly offset for drafting convenience. The true epicenters are listed in Tables 5.2−5 and 5.2−6.

Local Magnitude

Well−Determined Locations		Tentative Locations
∘	<1.5	.
∘	1.51−2.0	x
O	2.01−2.5	X
O	2.51−3.0	X
O	3.01−3.5	X
O	3.51−4.0	X
O	4.01−4.5	X

0   100   200   300 KM
0   50   100   150   200 MI
SCALE

REFERENCE :
SANFORD et al (1978)

EARTHQUAKES LOCATED AFTER

INSTALLATION OF STATION CLN

FIGURE 5.2-3

45

The three histograms show "Number of seismic events" versus "Sg – Pg Interval (seconds)":

Top frame: 00:00–24:00 GMT, Total seismic events – 206

Middle frame: 12:00–02:00 GMT local day-time, Total seismic events – 139

Bottom frame: 02:00–12:00 GMT local night-time, Total seismic events – 67
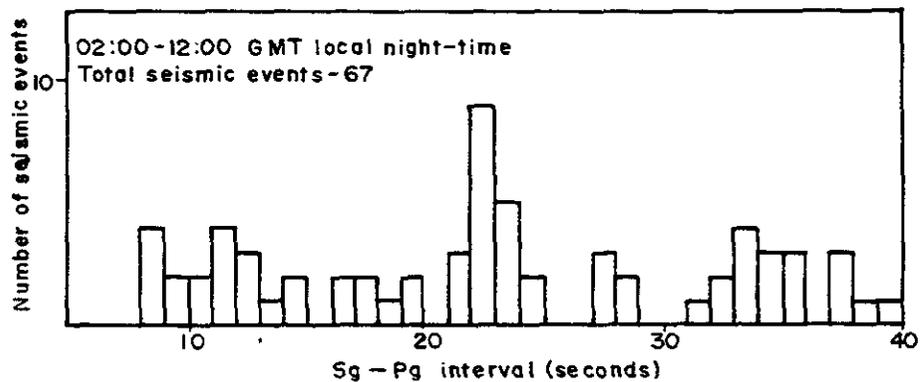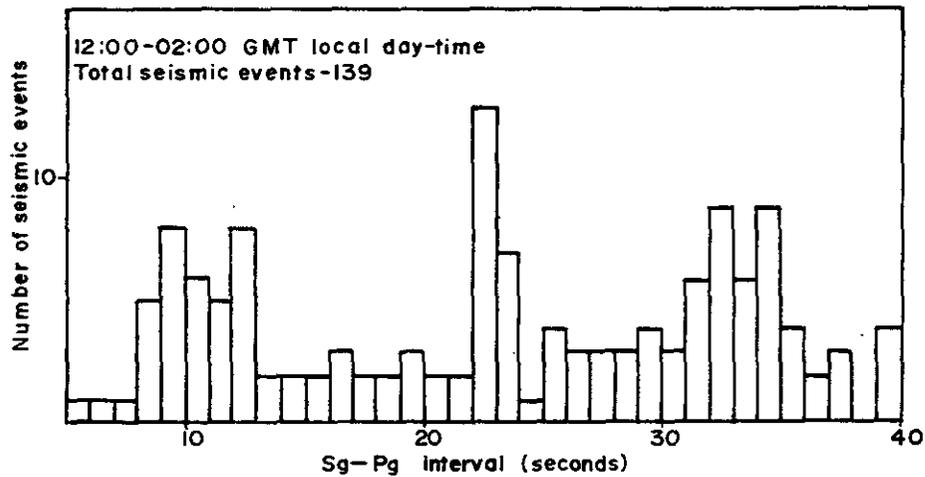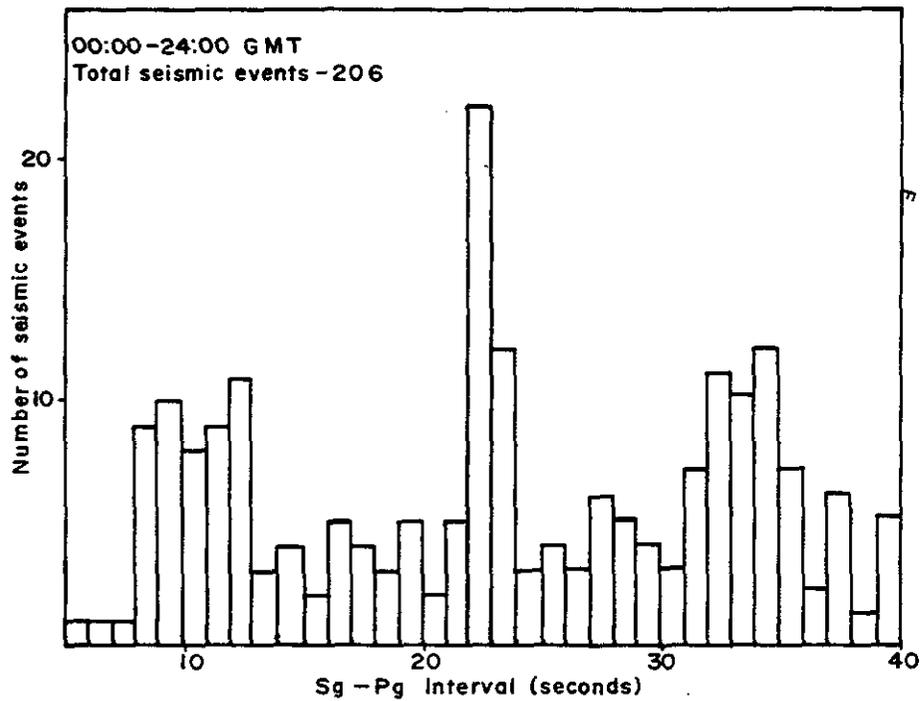
<u>EXPLANATION</u>

Histograms of the number of earthquakes versus Sg-Pg interval for data collected at station CLN from April 5, 1974 to October 29, 1977. Total number of events in top frame is separated into two subsets in the lower frames.

<u>REFERENCE:</u>

Sanford et al., 1978

EVENT-DISTANCE HISTOGRAMS

FIGURE 5.2-4
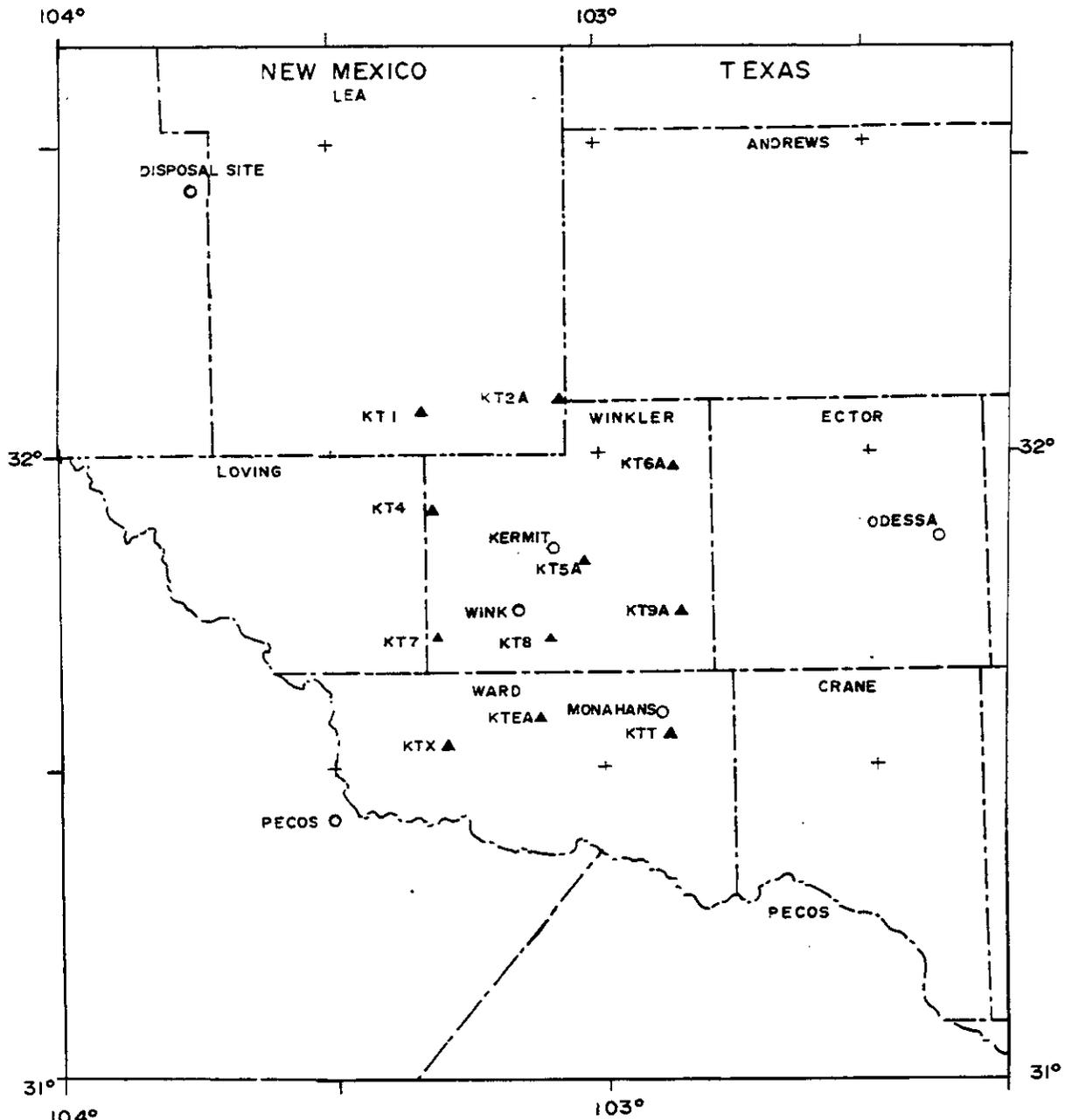
EXPLANATION

Current seismograph station locations in the Kermit array shown in relation to surrounding cultural features (from Rogers and Malkiel, 1978). Stations with an addended A have been moved from their original sites.
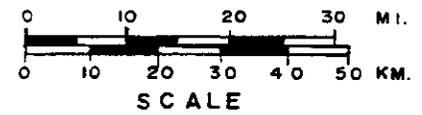
KERMIT ARRAY CONFIGURATION

FIGURE 5.2-5
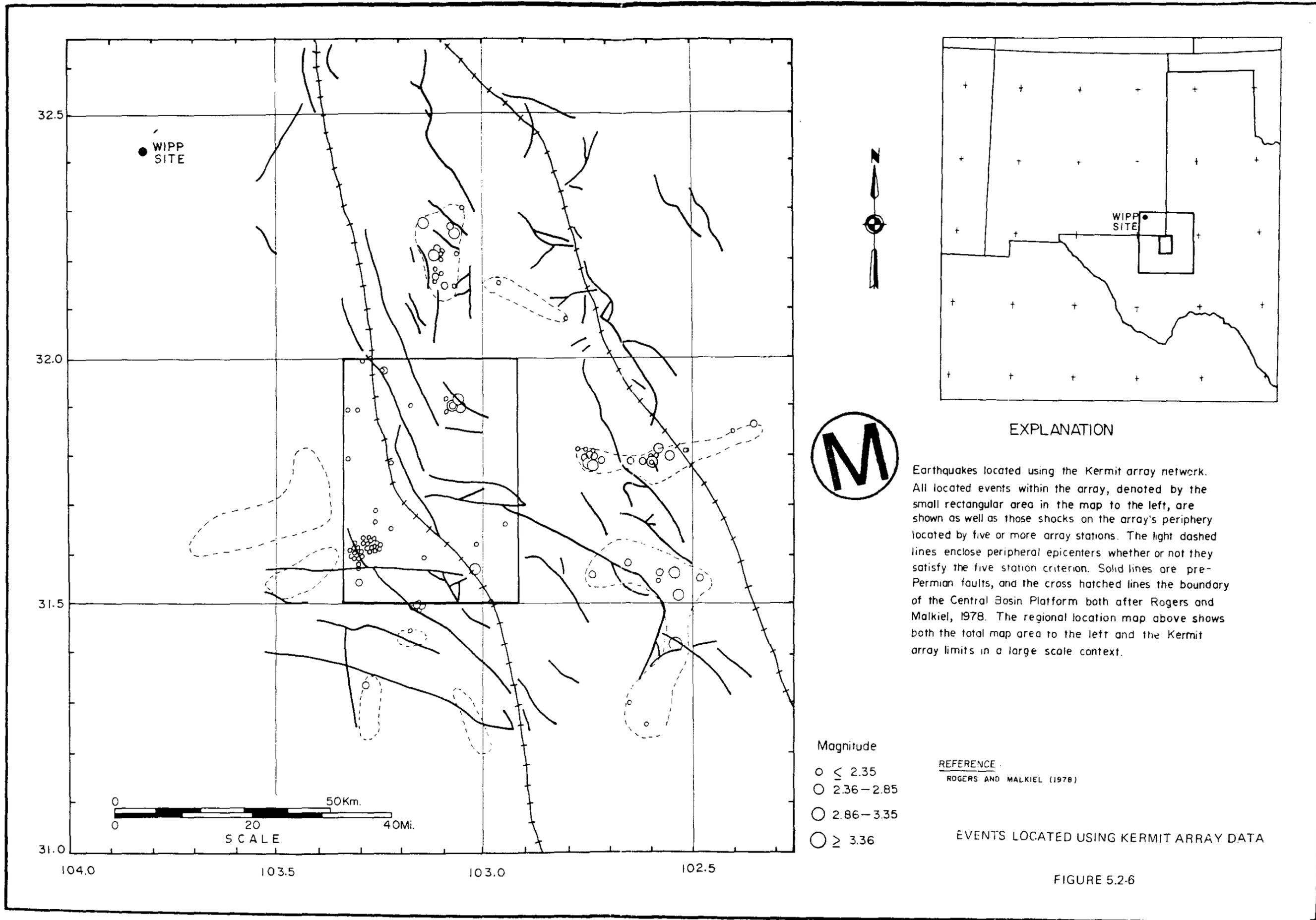
EXPLANATION

Earthquakes located using the Kermit array network. All located events within the array, denoted by the small rectangular area in the map to the left, are shown as well as those shocks on the array's periphery located by five or more array stations. The light dashed lines enclose peripheral epicenters whether or not they satisfy the five station criterion. Solid lines are pre-Permian faults, and the cross hatched lines the boundary of the Central Basin Platform both after Rogers and Malkiel, 1978. The regional location map above shows both the total map area to the left and the Kermit array limits in a large scale context.

Magnitude

○ ≤ 2.35
○ 2.36 − 2.85
○ 2.86 − 3.35
○ ≥ 3.36

REFERENCE
ROGERS AND MALKIEL (1978)

EVENTS LOCATED USING KERMIT ARRAY DATA

FIGURE 5.2-6

Origin time
04:35:40.9

NPM

GOL

Origin time
04:35:46.6

ALQ

LUB

SNM

TUC
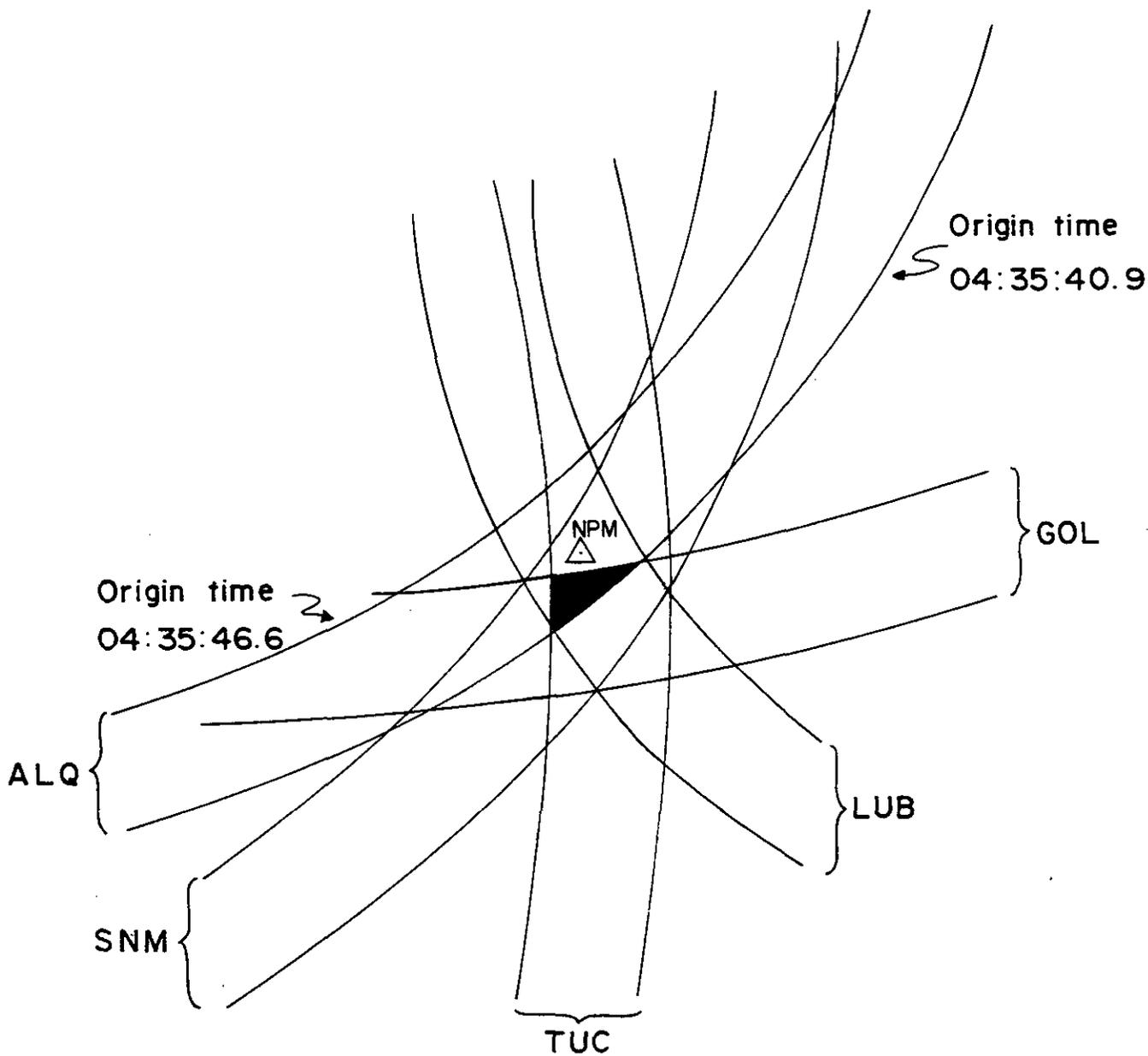
EXPLANATION

The area defined by arc intersections
using the 95% confidence intervals for
the origin time. NPM is the National
Potash Company Eddy County Mine
location. All arcs shown are for
Pg waves. Actual area of mutual
intersection is shaded.

REFERENCE: Caravella and Sanford, 1977.
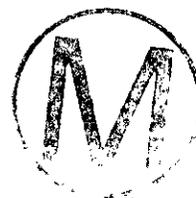
LOCATION UNCERTAINTY

FOR THE JULY 26, 1972 EVENT

FIGURE 5.2-7

$$r = \left[\exp\left(b_2 m / b_3\right)\right]\left(b_1 / a\right)^{1/b_3}$$

(See section 5.3.1 for symbol discussion)
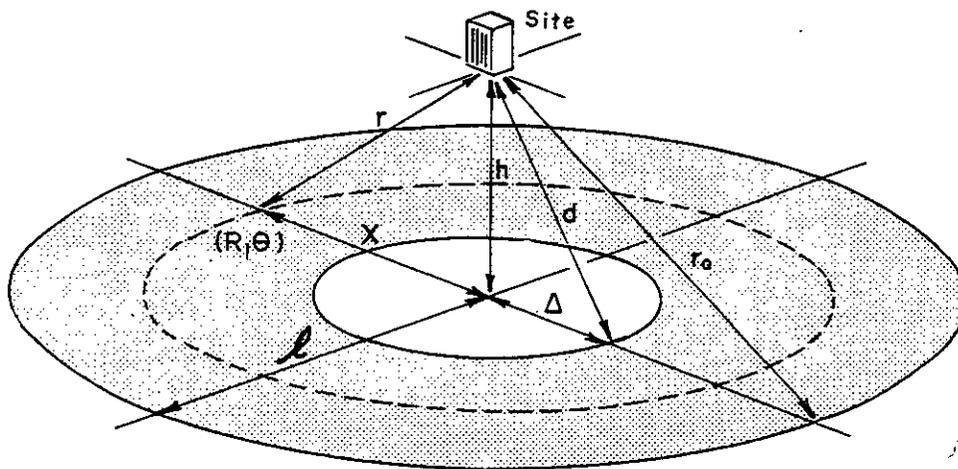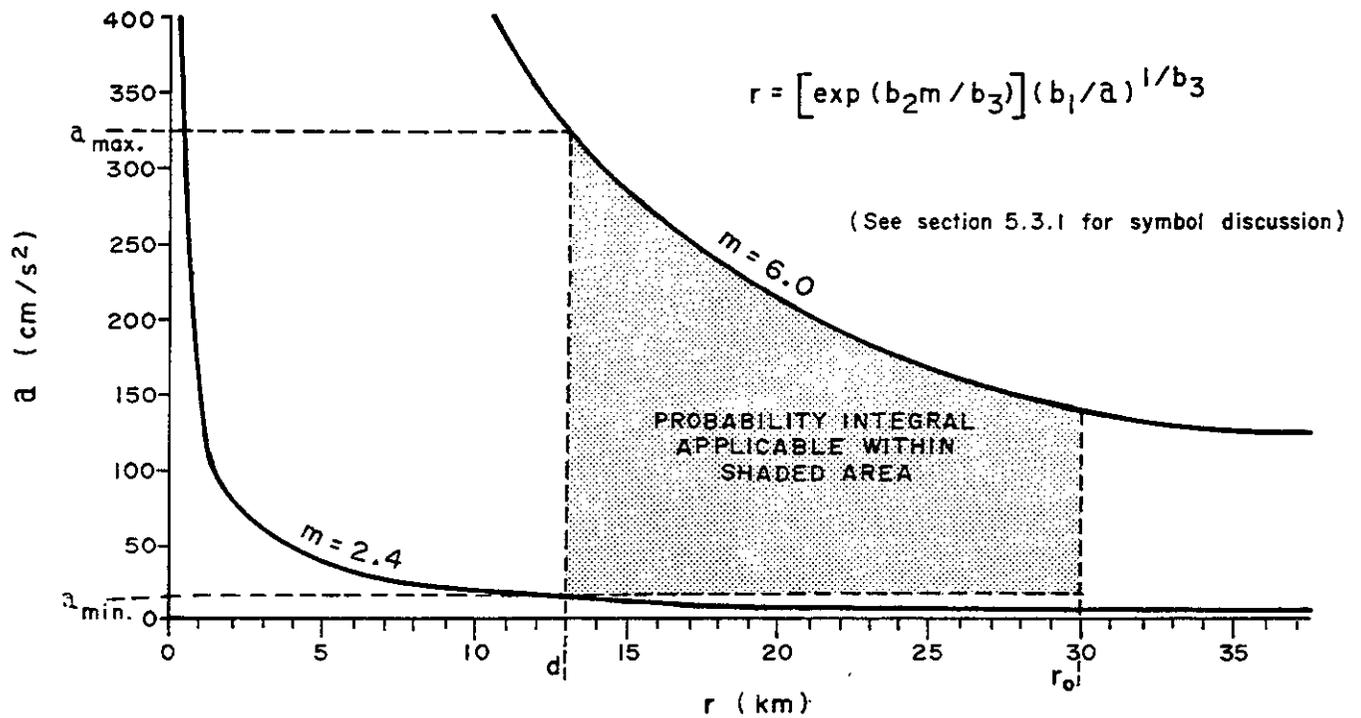
EXPLANATION

TOP - geometric and attenuation law constraints

on limits of integration for the annular area

probability integral. The shaded region represents

values over which the probability is valid.

BOTTOM - schematic of annular source area

showing variables of integration.

(After Cornell, 1968).

PARAMETERS FOR THE DETERMINATION

OF PROBABILISTIC ACCELERATION

FIGURE 5.3-1
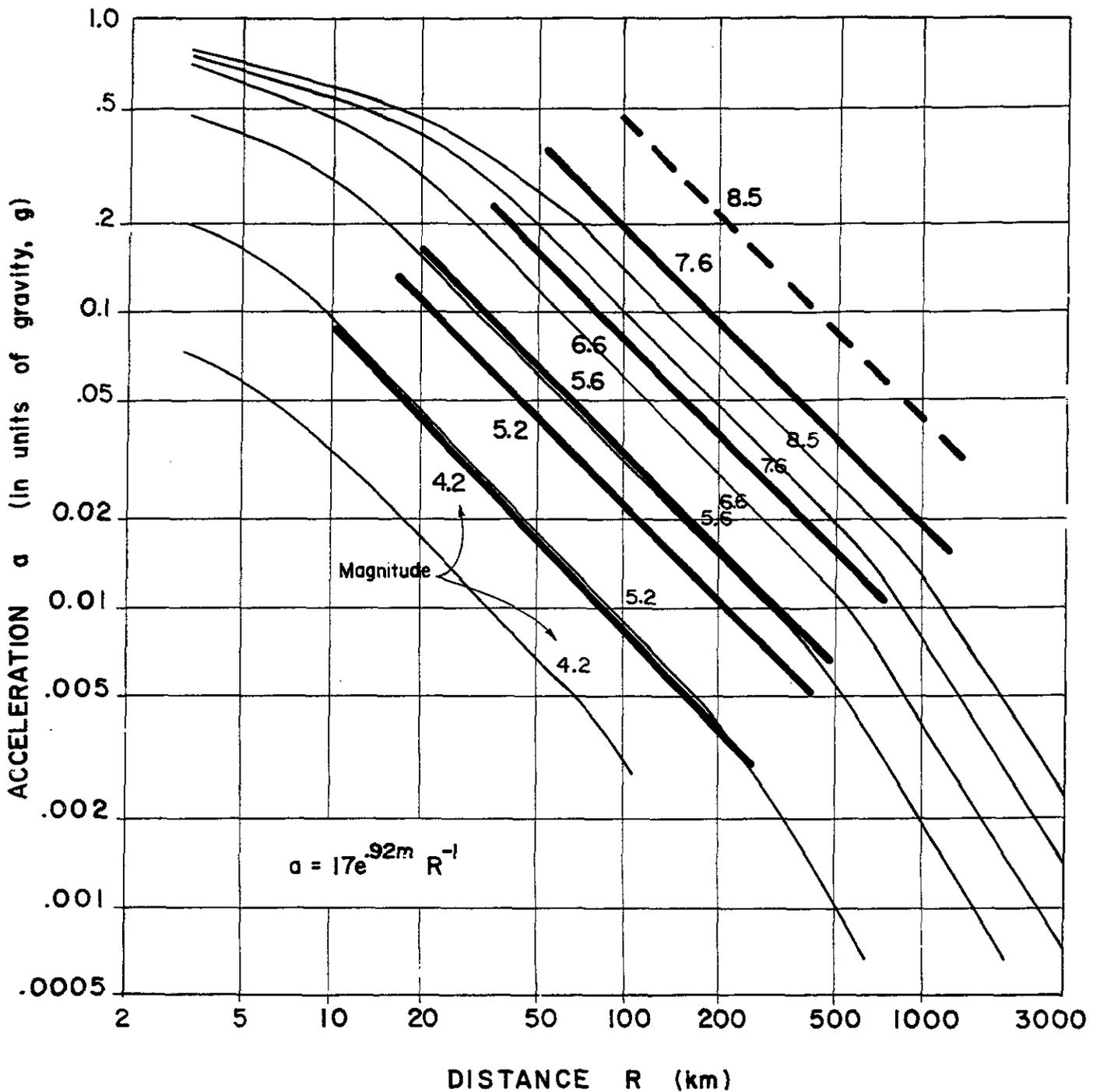
EXPLANATION

Comparison of acceleration attenuation curves for areas of the United States *east* *of* *105°W* *longitude* after Algermissen and Perkins (1976) (light lines) with those used in the site hazard analysis of this report (heavy lines). The equation for the recommended attenuation curves is shown in the inset.
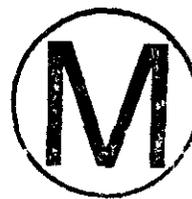
RECOMMENDED ATTENUATION CURVES

FIGURE 5.3-2

SEISMIC SOURCE ZONES

FIGURE 5.3-3

STRUCTURAL FEATURES IN THE SITE REGION

FIGURE 5.3-4

Annular segment source zones used in the seismic risk study. These source zones approximate the irregular polygon zones of Figure 5.3-3 which are also shown in dashed lines.

SITE SOURCE ZONE

CENTRAL BASIN PLATFORM SOURCE ZONE

RIO GRANDE

RIFT

SOURCE

ZONE

SCALE

0 100 200 300 KM

0 50 100 150 200 MI

ANNULAR SEGMENT APPROXIMATION OF SOURCE ZONES

FIGURE 5.3-5

49
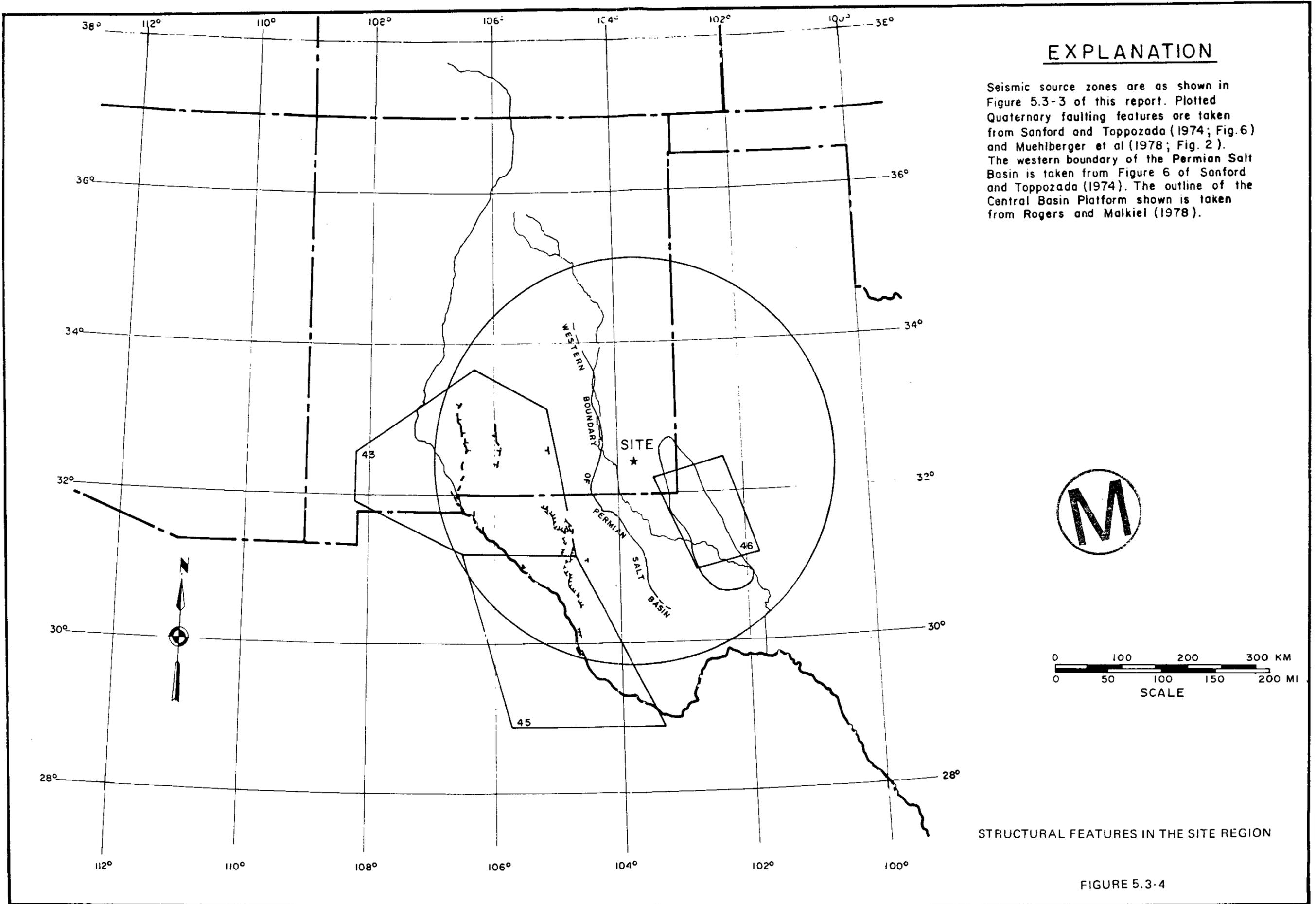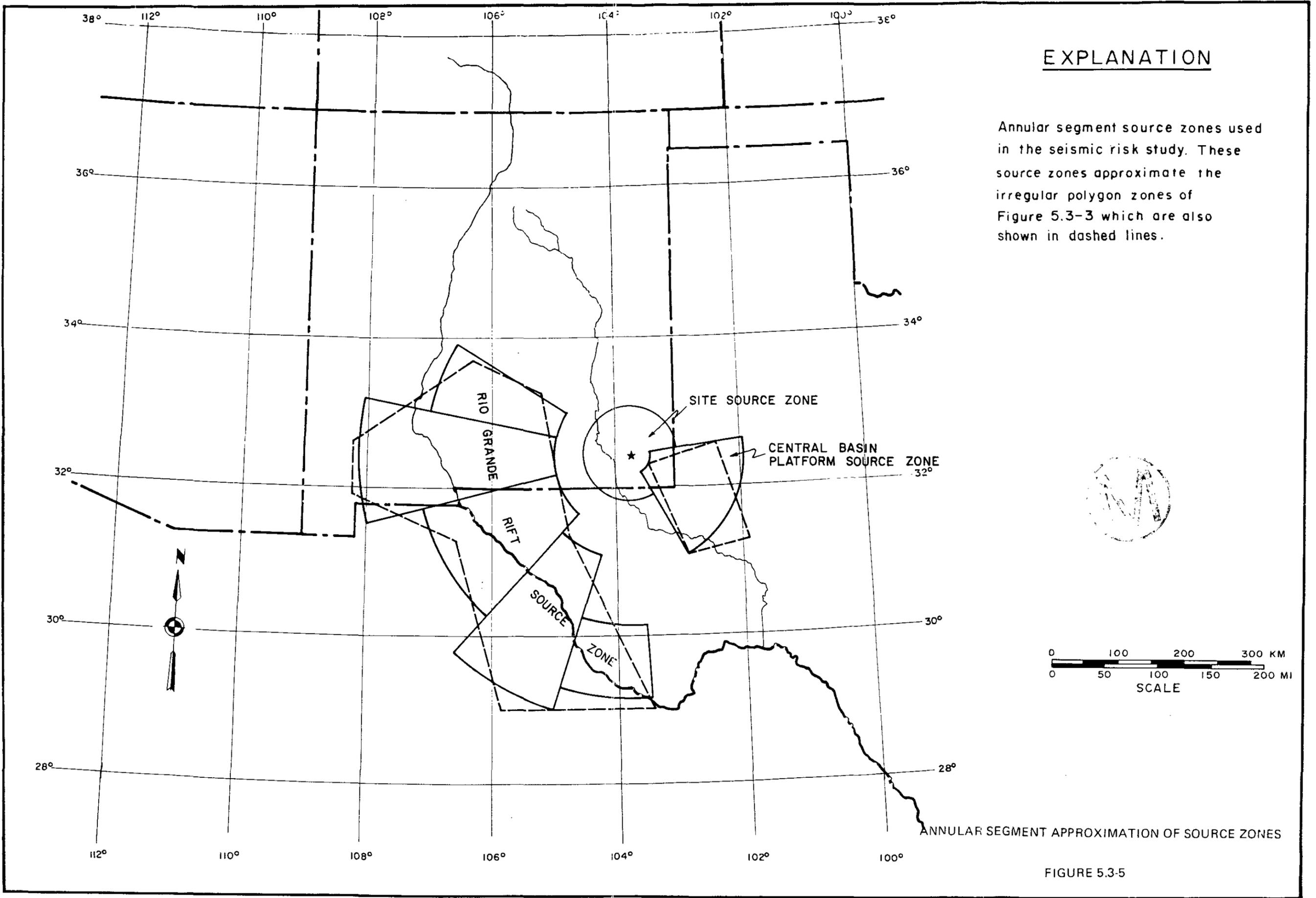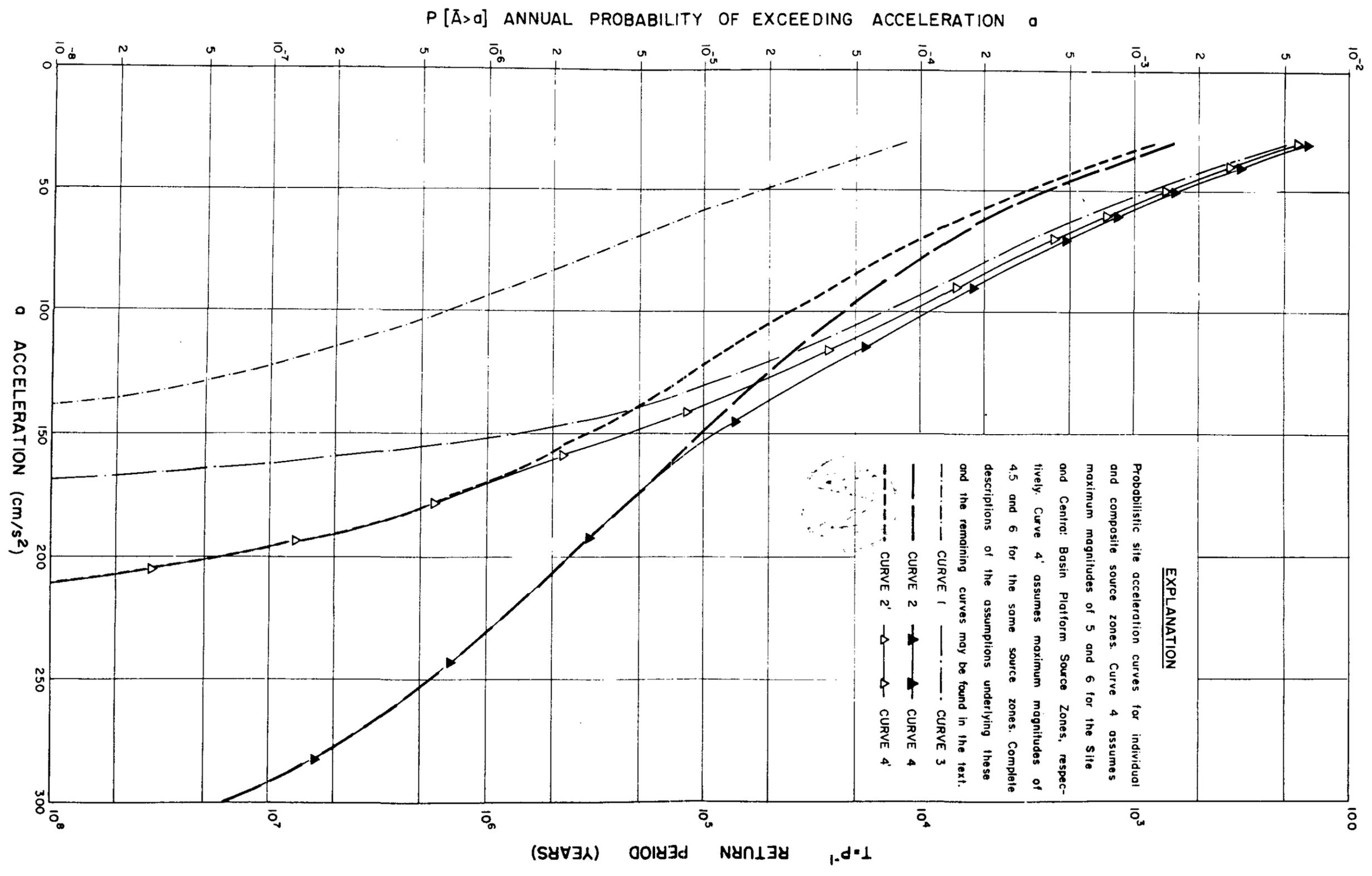
ACCELERATION PROBABILITY CURVES — SET 1

FIGURE 5.3.6

P [Ã>a] ANNUAL PROBABILITY OF EXCEEDING ACCELERATION a

a ACCELERATION (cm/s²)

T=P⁻¹ RETURN PERIOD (YEARS)

EXPLANATION

Probabilistic site acceleration curves for individual and composite source zones. Curve 4 assumes maximum magnitudes of 5 and 6 for the Site and Central Basin Platform Source Zones, respectively. Curve 4' assumes maximum magnitudes of 4.5 and 6 for the same source zones. Complete descriptions of the assumptions underlying these and the remaining curves may be found in the text.

————— CURVE 1
————— CURVE 2
————— CURVE 2'
—·—·— CURVE 3
————— CURVE 4
————— CURVE 4'

FIGURE 5.3.7

ACCELERATION PROBABILITY CURVES — SET 2

EXPLANATION

Probabilistic site acceleration curves for individual and composite source zones. Curve 4 assumes a maximum magnitude of 5 for both the site and the Central Basin Platform Source Zones. Curve 4' assumes maximum magnitudes of 4.5 and 5 respectively, for the same source zones. Complete descriptions of the assumptions underlying these and the remaining curves may be found in the text.

— · — · — CURVE 1

— · · — CURVE 3

————— CURVE 2 ▶

— — — CURVE 2' ▽

— · · — CURVE 4 ▶

— — — CURVE 4' ▽

a   b   c

EXPLANATION

Plots of lower focal hemisphere projections of P-wave polarities for a) the August 16, 1931 Valentine, Texas earthquake, b) a composite solution for three small earthquakes on the Central Basin Platform which occurred in January, 1976, and c) one possible solution for an earthquake in the same area of the CBP ocurring on April 26, 1977. P is the maximum and T the minimum compressive stress axes for each solution.

REGIONAL FOCAL MECHANISM SOLUTIONS

FIGURE 5.4-1

Table 5.2-1
EARTHQUAKES OCCURRING BEFORE 1961 AND
CENTERED WITHIN 300 KILOMETERS OF THE SITE

DATE Yr/Mo/Day	ORIGIN TIME (GMT)	LOCATION	INTENSITY	DISTANCE (km)
23/03/07	04:03	El Paso, Tex.	V	260
26/07/17	22:00	Hope and Lake Arthur, N.M.	III	90
30/10/04	03:25	34.5°N 105.4°W	(IV)	280
31/08/16	11:40	Valentine, Tex.	VIII	210
31/08/16	19:33	Valentine, Tex.	(V)	210
31/08/18	19:36	Valentine, Tex.	V	210
31/08/19	01:36	Valentine, Tex.	(V)	210
31/10/02	?	El Paso, Tex.	(III)	260
31/11/03	14:50	29.9°N 104.2°W	(V)	295
35/12/20	05:30	34.4°N 103.2°W	III-IV	230
36/01/08	06:46	Carlsbad, N.M.	(IV)	40
36/08/08	01:40	El Paso, Tex.	(III)	260
36/10/15	~18:00	El Paso, Tex	(III)	260
37/03/31	22:45	El Paso, Tex.	(IV)	260
37/09/30	06:15	Ft. Stanton, N.M.	(V)	200
43/12/27	04:00	Tularosa, N.M.	IV	220
49/02/02	23:00	Carlsbad, N.M.	(IV)	40
49/05/23	07:22	34.6°N 105.2°W	IV	280
52/05/22	04:20	Dog Canyon, N.M.	IV	158
55/01/27	00:37	Valentine, Tex.	IV	210

Table 5.2-2   page 1 of 1

MODIFIED MERCALLI INTENSITY SCALE OF 1931

[Abridged]

I. Not felt except by a very few under especially favorable circumstances. (I Rossi-Forel scale.)

II. Felt only by a few persons at rest, especially on upper floors of buildings. Delicately suspended objects may swing. (I to II Rossi-Forel scale.)

III. Felt quite noticeably indoors, especially on upper floors of buildings, but many people do not recognize it as an earthquake. Standing motor cars may rock slightly. Vibration like passing of truck. Duration estimated. (III Rossi-Forel scale.)

IV. During the day felt indoors by many, outdoors by few. At night some awakened. Dishes, windows, doors disturbed; walls make cracking sound. Sensation like heavy truck striking building. Standing motor cars rock noticeably. (IV to V Rossi-Forel scale.)

V. Felt by nearly everyone; many awakened. Some dishes, windows, etc., broken; a few instances of cracked plaster; unstable objects overturned. Disturbance of trees, poles, and other tall objects sometimes noticed. Pendulum clocks may stop. (V to VI Rossi-Forel scale.)

VI. Felt by all; many frightened and run outdoors. Some heavy furniture moved; a few instances of fallen plaster or damaged chimneys. Damage slight. (VI to VII Rossi-Forel scale.)

VII. Everybody runs outdoors. Damage negligible in buildings of good design and construction; slight to moderate in well-built ordinary structures; considerable in poorly built or badly designed structures; some chimneys broken. Noticed by persons driving motor cars. (VIII Rossi-Forel scale.)

VIII. Damage slight in specially designed structures; considerable in ordinary substantial buildings with partial collapse; great in poorly built structures. Panel walls thrown out of frame structures. Fall of chimneys, factory stacks, columns, monuments, walls. Heavy furniture overturned. Sand and mud ejected in small amounts. Changes in well water. Disturbs persons driving motor cars. (VIII+ to IX Rossi-Forel scale.)

IX. Damage considerable in specially designed structures; well-designed frame structures thrown out of plumb; great in substantial buildings, with partial collapse. Buildings shifted off foundations. Ground cracked conspicuously. Underground pipes broken. (IX+Rossi-Forel scale.)

X. Some well-built wooden structures destroyed; most masonry and frame structures destroyed with foundations; ground badly cracked. Rails bent. Landslides considerable from river banks and steep slopes. Shifted sand and mud. Water splashed (slopped) over banks. (X Rossi-Forel scale.)

XI. Few, if any (masonry), structures remain standing. Bridges destroyed, Broad fissures in ground. Underground pipe lines completely out of service. Earth slumps and land slips in soft ground. Rails bent greatly.

XII. Damage total. Waves seen on ground surfaces. Lines of sight and level distorted. Objects thrown upward into the air.

Table 5.2-3   Page 2 of 2

INSTRUMENTALLY LOCATED EARTHQUAKES WITHIN 300 KM
OF THE LOS MEDANOS SITE: 1962-1972

DATE Yr/Mo/Day	ORIGIN TIME GMT	LOCATION Lat N/Long W		MAGNITUDE M_L
69 May 12	08:26:18	32.0	106.4	3.0
69 May 12	08:49:16	32.0	106.4	2.6
69 Jun 1	17:18:24	34.2	105.2	2.0
69 Jun 8	11:36:02	34.2	105.2	2.4
69 Oct 19	11:51:34	30.8	105.7	2.8
71 Jul 30	01:45:50	31.7	103.1	3.1
71 Jul 31	14:53:48	31.6	103.1	3.2
71 Sep 24	01:01:54	31.6	103.2	3.0
72 Feb 27	15:50:04	32.9	106.0	2.3
72 Jul 26	04:35:44	32.6	104.1	2.8
72 Dec 9	05:58:39	31.7	106.4	2.2
72 Dec 10	14:37:50	31.7	106.5	2.2
72 Dec 10	14:58:02	31.7	106.5	1.8

Table 5.2-3   Page 1 of 2

INSTRUMENTALLY LOCATED EARTHQUAKES WITHIN 300 KM
OF THE LOS MEDANOS SITE: 1962-1972

DATE Yr/Mo/Day	ORIGIN TIME GMT	LOCATION Lat N/Long W		MAGNITUDE M_L
62 Mar 3	18:16:47	33.8	106.4	1.2
62 Mar 6	09:59:10	31.1	104.6	3.0
64 Feb 11	09:24:10	34.4	103.7	2.5
64 Mar 3	01:26:27	35.0	103.6	2.2
64 Jun 18	20:20:18	33.1	106.1	1.2
64 Jun 19	05:28:39	33.1	106.0	1.7
64 Oct 20	00:53:00	30.7	106.8	3.1
64 Nov 8	09:26:00	31.9	103.0	2.7
64 Nov 21	11:21:24	31.9	103.0	2.5
65 Feb 3	19:59:32	31.9	103.0	3.0
65 Apr 13	09:35:46	30.3	105.0	2.5
65 Aug 30	05:17:30	31.9	103.0	2.6
66 Aug 14	15:25:47	31.9	103.0	2.8
66 Aug 17	18:47:21	30.7	105.5	2.9
66 Aug 19	04:15:44	30.3	105.6	4.6
66 Aug 19	08:38:21	30.3	105.6	3.6
66 Sep 17	21:30:13	34.9	103.7	2.2
66 Nov 26	20:05:41	30.9	105.4	2.6
66 Nov 28	02:20:57	30.4	105.4	3.3
66 Dec 5	10:10:37	30.4	105.4	3.3
67 Sep 29	03:52:48	32.3	106.9	2.0
68 Mar 9	21:54:26	32.7	106.0	2.9
68 Mar 23	11:53:39	32.7	106.0	2.3
68 May 2	02:56:44	33.0	105.3	2.6
68 Aug 22	02:22:26	34.3	105.8	2.1

Table 5.2-4

INTERRUPTIONS IN OPERATION OF SEISMOGRAPH STATION CLN.

From		To		Cause
Time	Date	Time	Date	
Records were not obtained for the following periods:				
08:34	April 29, 1974	20:39	May 1, 1974	Recorder ran out of film.
13:13	May 18, 1974	07:03	May 19, 1974	Developing error.
07:18	May 31, 1974	13:32	June 12, 1974	Operating error changing film.
03:31	June 20, 1974	15:47	June 25, 1974	Developing error.
08:08	Sept 1, 1974	07:05	Sept. 2, 1974	Ran out of film.
17:09	Sept. 27, 1974	21:35	Sept. 28, 1974	Ran out of film.
03:23	Dec. 24, 1974	19:20	Jan. 5, 1975	Film broke.
07:37	May 28, 1975	18:08	June 7, 1975	Galvanometer light burned out.
20:23	June 21, 1975	18:20	July 4, 1975	Film broke.
17:50	Oct. 12, 1975	19:16	Oct. 26, 1975	Programmer-chronometer removed for repair.
19:31	Nov. 8, 1975	23:22	Jan. 12, 1976	Loss of power from thermal-electric generator.
12:40	Nov. 20, 1976	19:35	Jan. 17, 1977	Failure of voltage regulator on thermal-electric generator.
19:35	May 23, 1977	18:49	June 4, 1977	Film advance inoperative.
19:18	Sept. 13, 1977	18:20	Sept. 17, 1977	Film advance inoperative.
22:20	Oct. 6, 1977	18:47	Oct. 8, 1977	Film advance inoperative.
Station was operating without internal time for the following periods:				
22:01	May 1, 1974	07:18	May 31, 1974	Programmer-chronometer malfunction.
23:55	Aug. 18, 1974	23:55	Sept. 1, 1974	" " "
22:30	Nov. 28, 1974	03:23	Dec. 24, 1974	" " "

Table 5.2-5
WELL DETERMINED EPICENTRAL LOCATIONS
FOR
EARTHQUAKES AFTER INSTALLATION OF STATION CLN

DATE Yr/Mo/Day	ORIGIN TIME	LOCATION Lat°N/Long°W		DISTANCE to CLN (km)	CLN MAGNITUDE
74/08/26	07:33:22.0	34.4	105.8	305.9	2.4
74/09/26	23:44:08.5	32.8	106.2	235.8	2.4
74/10/15	10:07:57.9	33.9	106.5	316.9	2.3
74/11/01	10:45:49.6	33.8	106.6	314.9	2.0
74/11/12	02:31:57.3	31.9	100.8	288.9	2.5
74/11/12	07:14:28.5	31.9	100.8	273.7	2.2
74/11/21	16:22:58.6	32.5	106.3	240.3	2.4
74/11/21	18:59:05.8	32.1	102.7	105.7	2.1
74/11/22	08:54:05.1	32.8	101.5	213.6	2.0
74/11/22	14:11:13.2	33.8	105.1	211.7	1.9
74/11/28	03:35:20.5	32.6	104.1	43.1	3.6
75/02/02	20:39:22.6	35.1	103.1	317.3	2.7
75/07/25	08:11:40.0	29.9	102.5	309.8	2.8
75/08/01	07:27:47.3	30.4	104.6	239.3	3.9
75/10/10	11:16:55.9	33.3	105.0	160.4	2.1
76/01/10	01:49:57.0	31.7	102.8	123.4	2.1
76/01/14	07:01:31.5	34.1	106.8	353.7	2.6
76/01/19	04:03:30.4	31.9	103.0	93.8	2.4
76/01/22	07:21:57.8	31.9	103.0	89.1	2.0
76/01/25	04:48:27.5	32.0	103.1	80.2	2.9
76/01/28	07:37:48.5	32.0	101.0	262.9	2.4
76/03/18	23:07:04.8	32.2	102.9	77.9	1.6
76/03/20	16:15:58.0	32.2	103.1	63.8	1.4
76/03/27	22:25:22.0	32.2	103.1	64.1	1.8

Table 5.2-5 (Continued)

DATE Yr/Mo/Day	ORIGIN TIME	LOCATION Lat°N/Long°W		DISTANCE to CLN (km)	CLN MAGNITUDE
76/04/01	14:46:58.0	33.9	106.0	275.5	2.6
76/04/06	18:09:00.2	33.9	105.0	208.6	2.7
76/04/18	03:48:18.5	33.9	106.0	271.2	2.1
76/04/21	08:40:05.5	32.3	102.9	81.4	1.7
76/05/03	06:52:59.0	32.4	105.6	182.4	2.4
76/05/06	17:18:23.8	32.0	103.2	71.9	1.8
76/05/21	13:17:35.0	32.3	105.3	149.0	2.2
76/06/15	02:19:58.3	31.6	102.4	158.4	1.7
76/06/15	08:50:20.0	31.5	102.4	164.0	2.1
76/08/10	09:03:11.6	31.8	102.2	158.0	1.4
76/08/10	10:15:13.8	31.8	102.2	166.0	1.7
76/08/25	01:27:48.5	31.5	102.5	156.3	1.8
76/08/26	15:22:12.7	31.8	102.2	160.8	1.7
76/08/30	11:51:25.2	31.5	102.6	145.9	1.4
76/08/30	13:07:47.5	33.9	106.3	297.8	2.3
76/08/31	12:46:22.4	31.5	102.8	130.6	1.9
76/09/05	10:39:45.7	32.2	102.8	93.8	1.4
76/09/17	02:47:46.9	32.2	103.1	62.7	2.1
76/09/19	10:40:46.4	30.6	104.5	222.9	3.0
76/10/14	11:02:59.7	32.3	103.1	63.9	0.9
76/10/22	05:06:11.8	31.5	102.2	176.2	2.0
76/10/23	12:51:36.9	31.6	102.4	161.6	1.6
76/11/03	23:24:14.7	31.0	102.5	199.3	1.8
77/01/29	09:40:43.5	30.6	104.6	220.0	2.1
77/02/10	01:22:49.4	32.3	103.1	60.2	1.0

Ⓜ

Table 5.2-6
TENTATIVE EPICENTRAL LOCATIONS FOR
EARTHQUAKES AFTER INSTALLATION OF STATION CLN

DATE Yr/Mo/Day	ORIGIN TIME	LOCATION Lat°N/Long°W		DISTANCE TO CLN (km)	CLN MAGNITUDE
74/08/17	07:35:18	30.4	105.8	300	3.5
76/03/20	12:42:20	31.2	105.0	180	2.3
76/04/01	14:40:26	34.1	105.8	280	2.8
76/04/01	14:51:17	33.9	105.9	270	2.8
76/05/04	15:05:40	32.0	103.2	70	1.9
76/05/08	11:46:38	32.0	102.8	100	1.8
76/05/11	23:04:38	32.3	102.8	90	1.9
76/05/26	11:52:26	32.4	102.6	110	1.7
76/06/14	23:29:50	31.6	101.9	200	2.3
76/06/16	14:05:12	31.6	101.9	200	2.3
76/08/05	22:23:29	30.8	101.8	260	3.0
76/08/25	01:21:01	32.8	101.1	260	2.8
76/09/10	23:17:48	30.9	101.7	260	2.8
76/10/13	19:11:06	32.0	103.0	90	1.5
77/03/14	10:10:22	32.9	100.8	290	3.5
77/03/19	21:27:49	31.3	102.8	160	2.2
77/03/20	07:54:05	32.3	102.8	90	2.3
77/04/12	23:18:27	31.2	102.6	170	2.9
77/04/16	06:44:22	31.2	102.9	160	2.1
77/04/17	21:47:07	31.5	102.0	190	2.1
77/04/26	09:03:05	31.9	103.0	100	2.6
77/06/07	23:01:17	32.7	100.6	300	4.5
77/06/08	00:51:29	32.8	100.8	280	4.0
77/06/17	03:37:05	32.8	100.9	270	3.9
77/08/03	02:11:48	32.8	105.3	150	2.5
77/08/21	03:01:16	30.8	104.8	210	3.4

Table 5.2-7

page 1 of 1

Central Basin Platform earthquakes recorded at Ft. Stockton Station (FOTX)
from June 21, 1964 through April 12, 1965*

Date Yr/Mo/Day	FOTX-P Arrival Time GMT	FOTX-S-P Interval Secs.	LC-P Arrival Time GMT
64/06/22	07:07:47	14	07:08:22
64/07/13	12:20:03	14	
64/07/13	16:18:17	14	
64/07/19	02:34:16	13	
64/08/14	14:56:37	14	14:57:11
64/09/07	13:42:36	14	13:43:10
64/09/08	22:06:20	15	
64/09/11	12:33:08	14	
64/11/08	09:26:19	S**	09:26:53
64/11/16	02:06:05	15	
64/11/17	08:05:14	14	
64/11/18	10:20:30	14	
64/11/19	11:39:59	14	
64/11/19	11:40:30	14	
64/11/21	11:21:42	S**	11:22:17
64/11/23	03:30:18	14	
64/11/25	23:18:43	14	
64/11/26	00:03:13	14	
64/11/27	16:29:53	14	16:30:28
64/11/28	23:46:55	14	
64/12/01	20:59:50	13	
64/12/01	06:49:47	13	
64/12/05	23:09:43	14	
64/12/07	06:24:12	14	
64/12/07	06:31:40	14	
64/12/08	17:16:02	14	
64/12/13	19:19:19	13	
64/12/14	15:20:26	14	
64/12/26	00:08:29	14	
65/01/08	14:01:13	14	
65/01/12	20:35:19	14	
65/01/12	20:49:38	14	
64/01/21	11:51:51	14	
65/02/02	09:59:19	13	
65/02/03	19:59:52	S**	20:00:27
65/03/08	21:00:01	14	
65/03/09	03:46:18	14	
65/04/02	07:30:58	14	

* Listing of shocks restricted to events whose maximum peak to peak amplitudes exceeded 20 mm.

** Earthquake too strong on the seismogram to read S-P interval

Table 5.2-8
EARTHQUAKES IN THE CBP LOCATED WITH
REGIONAL STATIONS BETWEEN 1962-1972

DATE Yr/Mo/Day	ORIGIN TIME (GMT)	LOCATION Lat°N/Long°W		MAGNITUDE
64/11/08	09:26:00	31.9	103.0	2.7
64/11/21	11:21:24	31.9	103.0	2.5
65/02/03	19:59:32	31.9	103.0	3.0
65/08/30	05:17:30	31.9	103.0	2.6
66/08/14	15:25:47	31.9	103.0	2.8
71/07/30	01:45:50	31.7	103.1	3.1
71/07/31	14:53:48	31.6	103.1	3.2
71/09/24	01:01:54	31.6	103.2	3.0

Table 5.2-9   Page 1 of 3
EARTHQUAKES LOCATED WITHIN THE
KERMIT ARRAY NOV 75-JUL 77

Date	Origin time	Lat N	Long W	Depth	M_L	#Sta
1976						
Jan 19	04:03:30.4	31.91	103.07	0.12	3.47	6
22	07:21:57.0	31.90	103.08	0.01	2.83	9
25	04:48:27.7	31.90	103.08	0.89	3.92	9
Feb 25	22:22:59.4	31.78	103.23	0.03	-	4
May 03	08:00:40.1	31.99	103.29	5.56	1.96	5
03	11:27:41.8	32.00	103.27	6.54	2.00	5
04	15:05:39.1	31.97	103.24	0.16	2.32	5
06	17:18:23.6	31.97	103.23	6.88	2.59	6
08	11:46:41.8	31.90	103.18	1.17	1.90	6
27	21:16:06.9	31.89	103.30	5.00*	1.60	3
28	16:15:23.6	31.89	103.32	5.00*	1.49	3
Jun 18	16:51:18.4	31.79	103.32	5.00*	1.68	3
Aug 05	18:53:09.2	31.57	103.02	9.29	3.01	4
Sep 05	16:10:27.7	31.61	103.31	5.00*	2.24	3
10	19:18:43.4	31.91	103.09	5.00*	2.25	3
Nov 04	23:27:54.0	31.67	103.26	0.12	1.74	4
05	22:55:30.4	31.65	103.22	5.00*	1.63	3
06	22:30:23.6	31.68	103.26	0.16	1.64	4
Dec 18	18:27:45.7	31.62	103.02	0.17	2.26	6
24	07:34:53.3	31.61	103.30	5.00*	1.45	3
25	12:58:34.9	31.63	103.29	0.41	1.18	4
26	12:15:04.6	31.63	103.26	0.00	1.17	4

Table 5.2-9   Page 2 of 3
EARTHQUAKES LOCATED WITHIN THE
KERMIT ARRAY NOV 75-JUL 77

Date	Origin time	Lat N	Long W	Depth	M_L	# Sta
1977						
Jan 08	20:20:27.2	31.50	102.98	5.00*	1.95	3
14	13:33:33.4	31.60	103.31	5.00*	1.12	3
18	04:39:59.5	31.61	103.27	0.52	0.25	4
20	23:01:01.2	31.61	103.27	5.00*	1.75	3
Mar 12	00:05:23.8	31.62	103.29	5.00*	1.90	3
24	10:31:36.3	31.61	103.27	3.93	0.81	4
24	21:13:10.4	31.67	102.95	2.65	1.77	4
29	00:35:34.9	31.62	103.27	3.43	1.67	5
Apr 03	13:48:09.2	31.49	103.17	0.12	2.36	5
03	14:24:07.1	31.49	103.17	0.04	2.43	6
04	00:44:05.3	31.48	103.17	0.29	2.37	5
04	04:35:56.8	31.50	103.17	0.41	2.11	6
04	04:47:29.9	31.49	103.17	0.17	1.77	5
04	21:40:16.3	31.59	103.31	5.00*	1.68	3
04	22:55:54.0	31.59	103.30	5.00*	1.77	3
05	19:23:03.2	31.58	103.30	5.00*	1.60	3
06	23:22:30.9	31.59	103.31	5.00*	1.66	3
07	18:56:55.6	31.59	103.30	5.00*	1.67	3
07	22:32:29.3	31.60	103.30	5.00*	1.78	3
09	09:44:39.5	31.62	103.28	4.12	0.64	4
09	11:04:14.2	31.62	103.27	1.80	0.56	4
16	01:21:11.4	31.61	103.30	5.00*	0.51	3
16	06:44:22.0	31.62	103.26	3.91	1.26	4
16	14:38:39.6	31.61	103.25	0.34	0.52	7
17	20:52:38.3	31.63	103.31	5.00*	0.63	3

Table 5.2-9   Page 3 of 3
EARTHQUAKES LOCATED WITHIN THE
KERMIT ARRAY NOV 75-JUL 77

Date	Origin time	Lat N	Long W	Depth	M_L	# Sta
18	18:08:24.1	31.61	103.27	6.63	2.14	7
20	12:59:58.7	31.61	103.31	5.00*	0.74	3
23	18:58:46.7	31.59	103.14	0.01	0.69	4
26	09:03:07.3	31.90	103.07	4.02	3.10	8
26	09:05:50.4	31.89	103.09	2.67	1.06	5
May 19	04:25:30.6	31.62	103.26	0.20	1.00	4
Jun 09	11:37:35.4	31.61	103.26	5.00*	1.33	3
29	23:59:46.6	31.54	103.30	0.14	2.76	5
Jul 25	17:45:48.1	31.57	103.30	5.00*	1.27	3

* Focal depths constrained to 5 km

Table 5.2-10   Page 1 of 3
EARTHQUAKES LOCATED AROUND THE PERIPHERY OF THE
KERMIT ARRAY BY 5 OR MORE ARRAY STATIONS

Date	Origin time	Lat N	Long W	Depth	M_L	# Sta
1976						
Mar 15	02:30:48.3	32.15	102.96	0.12	1.56	5
20	16:15:55.5	32.30	103.05	0.35	1.70	5
27	22:25:21.0	32.21	103.10	0.06	1.49	9
Apr 12	08:02:35.9	32.17	103.11	0.45	2.38	5
21	08:40:07.4	32.21	103.10	0.25	2.53	6
May 01	11:13:40.8	32.27	103.14	9.92	3.04	8
Jun 15	02:20:00.5	31.58	102.65	0.76	2.39	7
15	08:50:20.9	31.55	102.48	6.85	2.67	13
Aug 10	09:03:12.2	31.86	102.35	0.14	2.39	7
10	10:15:18.2	31.80	102.55	0.55	2.87	9
25	01:27:49.3	31.56	102.58	3.89	2.79	9
26	15:22:17.7	31.79	102.59	0.75	3.03	11
31	12:46:21.1	31.56	102.73	7.84	2.78	9
Sep 05	10:39:49.4	32.16	103.11	0.18	1.68	5
17	02:47:45.4	32.21	103.10	0.20	2.98	10
17	03:56:28.9	31.42	102.54	1.66	3.44	7
19	10:23:24.4	32.14	103.09	7.29	2.41	6
Oct 14	11:03:00.1	32.21	103.07	2.74	2.32	6
22	05:06:15.9	31.57	102.54	3.03	2.94	7
25	00:27:04.2	31.81	102.58	6.59	2.95	7
25	10:52:27.3	31.85	102.40	0.17	2.15	5
26	10:44:44.1	31.33	103.28	0.46	2.81	7
Dec 12	23:00:14.0	31.52	102.53	7.59	3.21	11
12	23:25:56.0	31.55	102.58	0.13	2.33	7
19	21:26:16.0	31.79	102.64	0.25	2.61	5

Table 5.2-10   Page 2 of 3
EARTHQUAKES LOCATED AROUND THE PERIPHERY OF THE
KERMIT ARRAY BY 5 OR MORE ARRAY STATIONS

Date		Origin time	Lat N	Long W	Depth	M_L	# Sta
	19	23:54:22.7	32.18	103.11	1.48	2.26	6
	19	23:56:46.5	32.26	103.08	1.04	2.85	6
1977							
Feb	10	01:22:50.5	32.17	103.10	2.04	2.03	6
	18	14:10:36.8	32.20	103.10	3.89	1.17	5
Mar	05	22:56:10.0	31.30	102.65	2.14	2.35	9
	17	15:14:13.3	32.14	103.07	2.21	0.95	6
	20	07:54:08.0	32.21	103.10	0.99	2.22	8
	23	11:02:51.8	31.81	102.51	4.69	1.93	6
Apr	04	01:47:50.4	31.44	103.18	3.96	2.11	5
	07	05:45:39.4	32.24	103.17	1.53	2.91	7
	12	23:18:26.4	31.26	102.61	0.21	2.24	9
	25	10:12:51.1	32.08	102.80	5.94	1.35	6
	28	12:54:36.9	31.81	102.51	0.46	2.16	7
	28	12:55:40.5	31.79	102.59	4.21	2.17	7
	28	12:57:20.3	31.80	102.59	4.77	1.73	7
	28	15:22:37.7	31.79	102.61	3.14	2.46	8
	29	03:09:40.4	31.80	102.58	1.25	1.73	6
Jul	11	12:31:55.7	31.79	102.73	2.93	2.74	10
	11	13:29:49.8	31.79	102.73	2.49	2.19	9
	12	17:06:06.3	31.79	102.71	4.86	2.44	9
	18	12:37:30.6	31.80	102.74	0.97	2.90	8
	22	04:01:10.1	31.80	102.73	3.42	3.35	8
	22	04:18:10.5	31.80	102.73	2.30	2.50	7
	22	04:36:51.0	31.81	102.75	0.38	1.67	6

Table 5.2-10   Page 3 of 3
EARTHQUAKES LOCATED AROUND THE PERIPHERY OF THE
KERMIT ARRAY BY 5 OR MORE ARRAY STATIONS

Date	Origin time	Lat N	Long W	Depth	M_L	# Sta
24	09:23:00.5	31.80	102.73	2.04	2.49	10
26	02:01:09.3	31.81	102.77	0.27	1.45	9

Table 5.2-11   Page 1 of 1

DIFFERENCES IN ARRIVAL TIMES BETWEEN THE EARTHQUAKES ON

JULY 26, 1972 AND NOVEMBER 28, 1974

Station	Phase	Earthquake on July 26, 1972	Earthquake on Nov. 28, 1974	ΔT
LUB	Pn	04:36:20.3	03:35:58.25	22.05
ALQ	Pn	04:36:36.8	03:36:13.35	23.45
SNM	Pg	04:36:36.9	03:36:13.85	23.05

SAND 78-1596

UNLIMITED RELEASE

Geological Characterization Report, Waste Isolation Pilot Plant (WIPP) Site, Southeastern New Mexico

Volume II

August 1978

Dennis W. Powers, Steven J. Lambert, Sue-Ellen Shaffer,
Leslie R. Hill, Wendell D. Weart, Editors

Sandia Laboratories

GEOLOGICAL CHARACTERIZATION REPORT
WASTE ISOLATION PILOT PLANT (WIPP) SITE,
SOUTHEASTERN NEW MEXICO

SAND78-1596

VOLUME II

Dennis W. Powers, Steven J. Lambert, Sue-Ellen Shaffer,
Leslie R. Hill, Wendell D. Weart, Editors

Department 4510
Waste Management Technology
Sandia Laboratories
Albuquerque, New Mexico 87185

AUGUST, 1978
PRINTED DECEMBER, 1978

GEOLOGICAL CHARACTERIZATION REPORT

TABLE OF CONTENTS

VOLUME II

PAGE

APPENDICES

6.1   INTRODUCTION

The location of the proposed WIPP site is within the surface water
boundaries of the Rio Grande Water Resources Region and the groundwater
boundaries of the Unglaciated Central region of the Permian Basin. In
addition, the site lies within the boundaries of the Delaware Basin, a
portion of the Unglaciated Central region that includes some of the least
productive aquifers in the United States. The Delaware Basin is
characterized by a semiarid climate with low rainfall and runoff, high
evaporation, and frequent strong winds. The proposed site contains
neither perennial streams nor surface water impoundment, and the water
bearing strata beneath the site do not yield large quantities of water to
wells. Shallow wells in the local area are generally used only for
watering livestock and typically produce non-potable groundwater with
total dissolved solids (TDS) concentrations in excess of 3,000 parts per
million (ppm).

Hydrologic studies of the water resources surrounding the site have been
supported by universities and state and federal agencies since the late
1930's (Robinson and Lang, 1938; Theis and Sayre, 1942; Hendrickson and
Jones, 1952; Bjorklund and Motts, 1959; Nicholson and Clebsch, 1961;
Brokaw et al., 1972; Hiss, 1975a). The early studies were primarily
concerned with the control of water quality in the Pecos River for
agricultural usage downstream from the brine discharge at Malaga Bend
(Robinson and Lang, 1938; Hale et al., 1954). The first investigations
of hydrogeologic parameters describing the occurrence and flow of
groundwater in close proximity to the proposed WIPP location began in the
late 1950's with Project Gnome (Cooper, 1962; Gard, 1968; Cooper, 1971).

Hydrologic studies at the site and adjacent site areas have concentrated
on defining the hydrogeology and associated salt dissolution phenomena
(Griswold, 1977; Lambert and Mercer, 1977; Mercer and Orr, 1977; Mercer
and Orr, 1978; Anderson, 1978). These investigations are directed toward
a more quantitative evaluation of the salt dissolution process, the

hydrogeologic parameters affecting groundwater movement, and the major elements of surface and groundwater quality affecting water resource use and local ecology. The collection of hydrologic data is projected to continue for several years to provide site-specific information for a detailed safety analysis of the WIPP.

Hydrologic test results to date have been used to make bounding calculations of hypothetical occurrences based upon simplifying assumptions of the physical system. Future measurements obtained from the experimental programs and analysis of the test data will be used to refine the initial bounding calculations and to provide a more detailed description of the physical system and system dynamics. The use of computer models as predictive tools is expected to be closely coordinated with current test results from an established monitoring network. Compatible chemical tracers will be injected directly into the groundwater system as a test of the predictive computer results. Also, the use of chemical tracers during construction phases of the WIPP may provide an early indication of leaky borehole plugs or faulty repository seals, if any, far in advance of radionuclide concentrations in the groundwater system.

6.2 SURFACE WATER HYDROLOGY

The area proposed for the Waste Isolation Pilot Plant (WIPP), located in southeastern Eddy County, New Mexico, lies at an average elevation of 3410 feet above mean sea level (MSL) in the Northern Chihuahuan Desert. Although the area belongs to the drainage basin of the Pecos River, surface drainage patterns at the site are not well defined. Preliminary studies indicated that areal requirements for the surface facilities, underground storage, and safety considerations during the operation of the repository would be as shown in Table 6.2-1 (see also Table 2.1).

6.2.1 Surface Water Features

The Rio Grande Water Resources Region, which includes the Pecos River basin, is an area of 88,968 square miles. The Pecos River basin has a

total drainage area of about 44,535 square miles (approximately 20,500 square miles of which do not contribute to river flow), a maximum basin width of about 130 miles, and an overall length of about 500 miles before combining with the Rio Grande River. The Pecos is generally perennial, except in the reach below Anton Chico and in the reach between Fort Sumner and Roswell, where the low flows percolate into the stream bed. About 60 percent of the annual flow occurs between April and September.

The Pecos River is located west of the site and flows southeast through Carlsbad. At the closest point (river mile 430), the Pecos River is approximately 14 miles west of the WIPP site center. The total drainage area of the river at this location is 19,000 sq. miles. A few small unnamed creeks and draws constitute all tributaries flowing westward of the Pecos River within 20 miles north or south of the site. From the west, the Black River (drainage area of 400 square miles) joins the Pecos at a point approximately 16 miles southwest of the site near river mile 436. The Delaware River (drainage area of 700 square miles) joins the Pecos near river mile 446, and a number of small unnamed creeks and draws join at various points along this reach. Pecos River flow in this reach is regulated by storage in Lake Sumner (river mile 401.9), Lake McMillan (river mile 404.2), Lake Avalon (river mile 407.2) and several other smaller upstream dams that divert water for irrigation. The salient features of the five existing dams on the Pecos River in a reach extending 25 miles upstream and 25 miles downstream of the WIPP site are listed in Table 6.2-2. The approximate slope of the Pecos riverbed in the vicinity of the WIPP site is 4.5 ft/mile (U.S.G.S. Topographic Maps NI 13-11 & NI 13-12).

There are no major lakes or ponds within 10 miles of the WIPP site center. Laguna Gatuna, Laguna Tonto, Laguna Plata and Laguna Toston are lakes located to the north more than 10 miles from the site. All these lakes are at or above elevation 3,450 feet. Therefore, surface runoff from the site would not flow toward any of the lakes to the north. To the west and northwest, Red Lake, Lindsey Lake, Salt Lake, and a few unnamed ponds are located more than 10 miles from the site, between elevations 3,000 and 3,300 feet (U.S.G.S. Topo. Maps, 1:250,000).

Surface water and groundwater withdrawals in the Pecos River basin are listed in Table 6.2-3.

6.2.2 Precipitation Patterns

The nearest station to the WIPP site for which climatological records are available is located at Carlsbad, about 26 miles west of the site, at an elevation of 3,120 feet MSL (U.S. Weather Bureau, 1961). Over a period of more than 71 years (NOAA, 1977), the annual precipitation at Carlsbad ranged from 2.95 inches to 33.94 inches. The average annual precipitation over a period of 30 years (1931-1960) was 12.43 inches (U.S. Weather Bureau, 1961). The average annual precipitation from 1951 to 1974 was 9.78 inches at Artesia (elevation 3320 feet), which is about 48 miles northwest of the WIPP site. At Hobbs (elevation 3615 feet), which is about 44 miles northeast of the site, the average annual precipitation for the period 1951-1974 was 14.29 inches. Interpolation of precipitation data for Carlsbad, Artesia and Hobbs indicates that the average annual precipitation at the site should be approximately 12 inches, which is nearly equal to the average annual precipitation at Carlsbad. Therefore, the precipitation patterns at Carlsbad are assumed to be representative of the conditions at the WIPP site.

Maximum, average, and minimum monthly precipitation at Carlsbad over a period of 30 years (1931-1960) are given in Table 6.2-4. The maximum monthly precipitation, 12.28 inches, occurred in May. With the exception of May and August, when the record minimum monthly precipitation were 0.18 and 0.01 inch, respectively, the record minimum precipitation for all other months has been 0.00 inch. The maximum daily precipitation since 1905 occurred in August, 1916, and was 5.12 inches.

The maximum daily and monthly snowfalls at Carlsbad since 1905 have been 10 inches (December, 1923) and 17.8 inches (February, 1905), respectively (U.S. Weather Bureau, 1961).

In general, summer rain is more abundant than that of other seasons and is caused by thunderstorms generated by the southeasterly circulation of moist air from the Gulf of Mexico. Approximately 75 percent of the total annual precipitation occurs from April through September. Winter rainfall is least abundant and is caused mainly by frontal activity associated with the movement of the Pacific storms across the country from west to east (NOAA, 1977).

6.2.3 Drainage

The site is located between elevations 3,250 and 3,570 feet MSL (Griswold, 1977). General ground slope in the vicinity is approximately 39 feet/mile from the northeast to southwest. Average ground slope from north to south is approximately 13 feet/mile. A topographic and surface water divide (Antelope Ridge) exists approximately 8 miles east of the site center and 4 miles from the exterior boundary of Zone IV (Refer to Table 6.2-1).

In general, the surface in the site vicinity is hummocky and covered by sand dunes. The local slope is poorly defined, and rain collects in pools between sand dunes and evaporates, is transpired, or sinks into the sand. Surface runoff from an area of about 10 sq. miles to the northeast, along with that from the site area, drains through a number of small draws which terminate in unnamed ponds to the southwest. Runoff is typically 0.1 to 0.2 inches annually.

6.2.4 Floods

Historically, floods for the Pecos River are reported to have occurred in 1904, 1905, 1915, 1916, 1919, 1937, 1941, 1942, and 1966 (NOAA, 1977). The earliest flood for which discharge information is available occurred on October 2, 1904, following the failure of Avalon Dam. During this flood, the flow at Avalon gaging station (river mile 406.3) exceeded 90,000 cfs. The corresponding river stage is not available. The river stage at Red Bluff (river mile 459.8) is reported to have reached 28 feet

(gage datum of 2850.05 feet) during this flood. Another major flood occurred on August 7, 1916, when the discharge at Carlsbad Station (river mile 419.1) reached 70,000 cfs.

A third major flood occurred in September, 1919, when the river stage at Malaga gaging station (river mile 432.2) was recorded as 29.4 feet (gage datum of 2895.64 feet). The corresponding discharge was 40,400 cfs. The highest flood of record (through 1976) for the Pecos River occurred on August 23, 1966, when the discharge and stage at Malaga were 120,000 cfs and 42.1 feet, respectively (U.S. Geological Survey, 1976). The minimum surface elevation of the site is more than 310 feet above this maximum historic flood level.

6.2.5 Evaporation and Transpiration

In New Mexico, potential evaporation is much greater than the average annual precipitation. In the southeastern valleys, evaporation from a class A pan is on the order of 110 inches per year. During the warm months, May through October, evaporation in the southeast portion of the state is approximately 73 inches.

The record high temperature at Carlsbad is $112^{O}F$ (June, 1902). The record low temperature at this station is $7^{O}F$ (January, 1911). The maximum, average and minimum monthly temperatures at this station over a period of 30 years (1931-1960) are given in Table 6.2-5 (U.S. Weather Bureau, 1961). June, July and August are the warmest (average temperature of $80.7^{O}F$) while December and January are the coldest months of the year (average temperature of $44.3^{O}F$).

In this type of desert climate, more than 90 percent of all infiltrated water evaporates or transpires. The high rate of evapotranspiration is aided by the frequent winds, the low relative humidity (typically 36 percent during daylight hours), and the high mean annual temperature $(61^{O}F)$.

6.2.6 Infiltration

Soils at the site are generally comprised of sands extending to a depth of as much as 25 feet. Actual sand dunes cover a good portion of the site area. With pervious sand on the surface, infiltration rates are high and probably similar to the 1.6 inch-per-hour intake rate of Harkey Sand Loam (75 percent sand) near Carlsbad (Blaney and Hanson, 1965). Groundwater in the area of the site is more than 50 feet below surface elevations. Because the surface sands are underlain by a caliche layer about 2 to 8 feet thick, percolation of rainfall through the sands to the nearest groundwater would be only a portion of the total infiltration. Most infiltration will return to the atmosphere by evapotranspiration.

6.2.7 Surface Water Quality

Water quality in the Pecos River basin is affected by mineral pollution from natural sources and from irrigation return flows. Springs near the headwaters of the basin below Colonias, New Mexico, are estimated to discharge approximately 707 tons per day of dissolved solids into the Pecos River. Below Lake McMillan, springs flowing into the river are usually submerged and difficult to sample; however, dissolved solids concentrations between 3350 and 4000 ppm have been measured in springs that could be sampled. The chemical quality of these mineral discharges indicates the nonpotable character of the ground water in contributing source beds. Inflow of concentrated brine solutions at Malaga Bend increases the chloride content of the Pecos River by an estimated 370 tons per day (see account by Swenson in Bachman and Johnson, 1973). Time-weighted averages of water quality parameters for three sampling stations on the Pecos River between Carlsbad and Malaga Bend are shown in Table 6.2-6. In general, natural spring flows and irrigation return flows progressively concentrate salts downstream. Further downstream at Red Bluff Reservoir, the water is useable occasionally during high flow periods.

6.3 GROUND WATER HYDROLOGY

Detailed investigations of ground water conditions at the proposed site
are being conducted to identify the presence of ground water, to measure
ground water quality, and to determine hydraulic conductivity and other
characteristics of the stratified rocks. The data will provide a basis
for assessment of the continued isolation of the proposed repository from
ground water circulation. The thick halite beds of the Salado Formation
at the WIPP site are isolated from circulating ground water by beds of
low hydraulic conductivity, both above and below the formation. In the
vicinity of the proposed site, fresh or potable ground water is not
present except in small, isolated, near-surface perched bodies.

Investigations to evaluate the transport of radionuclides by ground water
flow in the southeastern New Mexico portion of the Delaware Basin were
made by the Water Resources Division of the U.S. Geological Survey for
Project Gnome in the late 1950's. Since that time, several studies have
been carried out by individual consultants, the U.S. Geological Survey,
Oak Ridge National Laboratories, and Sandia Laboratories. These studies
have been directed to the specific task of providing a better
understanding of the relationship between the proposed waste repository
and ground water movement. The following is a description of ground
water occurrence and flow as understood from the studies completed to
date. Ground water is first described on a regional basis, then the
results of site specific studies are reviewed, and, finally, dissolution
of salt evaporites is discussed.

6.3.1 Regional Ground Water Conditions

Ground water within the Delaware Basin is predominantly of poor quality,
with total dissolved solids concentrations in excess of 3,000 ppm. The
only large quantities of potable ground water are found in aquifers west
of and along the Pecos River. To the west in the Guadalupe Mountains,
many rock units of the basin crop out, and the soluble salts have been
leached from the Ochoan evaporites.

Important aquifers of the region are the San Andres Limestone and the Capitan Limestone and related reef limestones. The San Andres is a major source for irrigation waters in the Roswell basin, and other areas to the north and northwest of the site. The Capitan aquifer southwest of the community of Carlsbad is the primary source of municipal water. An important aquifer in the region east of the proposed site is the Ogallala Formation. Unconsolidated alluvium along the Pecos River yields large amounts of relatively fresh ground water in some areas, although it is commonly of marginal quality for drinking purposes.

From the outcrop areas west of the Pecos River, ground water moves eastward. The shallow aquifers, those cut by the Pecos River, discharge to the river, either directly or to alluvium of the river channel. The Capitan aquifer is the oldest permeable formation that may have contact with the river. Ground water in permeable formations older than the Capitan is not directly affected by the river, is present under confined conditions, and migrates eastward into the Delaware Basin.

East of the Pecos River, thick beds of evaporites are present at depth, and brines are common in the underlying permeable formations. Ground water in any of the rock units east of the river in Eddy County is of brackish quality, at best. Fresh meteorically-derived ground water does not flush out the poor quality waters in these aquifers. Consequently, the major utilization of ground water in the central and eastern Delaware Basin is for oil-field flooding. The predominant source of the ground water is the Capitan aquifer.

The shallow aquifers east of the Pecos River are limited in extent, are low yielding, and usually contain water of poor quality. Recharge to these shallow aquifers is presumed to be from precipitation on outcrop areas or from overlying formations, and migration of the water generally follows surface drainage patterns, eventually reaching the Pecos River.

In discussing ground water occurrences in relation to the proposed repository, it is convenient to relate them to the Salado Formation because the Salado and its associated evaporite formations have very low hydraulic conductivities and form a barrier to vertical flow (see Table 9.2.3-1). Aquifers stratigraphically below the Salado are widespread and contain large quantities of brine under confined conditions. Aquifers present above the Salado in the proposed site area are either limited in extent or very low-yielding. This upper ground water is of poor quality (TDS concentrations greater than 3,000 ppm) and occurs under unconfined, as well as confined, conditions.

6.3.2 Hydrology of Rocks Underlying the Salado Formation

The halite beds of the Salado Formation that are proposed for the repository are underlain by thick anhydrite and salt beds of the Castile Formation. They act as an aquiclude, separating the Salado from the underlying sandstones of the Delaware Mountain Group. The sandstones are present at a depth of about 4,200 feet in the site area. The hydraulic conductivity of the sandstones of the Delaware Mountain Group, associated with the relatively high hydraulic conductivity of the shelf-margin facies (the Capitan Limestone) and the shelf facies (which includes the San Andres Limestone) make this group the most important hydrologic system underlying the Salado. The hydrology of these Guadalupian-age rocks has been investigated in detail by Hiss (1975a).

Considerable information derived from hydrocarbon exploration in the *basin is available on the hydrologic properties of the formations* underlying the Permian evaporites. As reported by Lambert and Mercer (1977), the Delaware Mountain Group is the uppermost of the oil- and gas-producing horizons, which extend to the Ellenburger Group at a depth of about 18,000 feet. Several zones are encountered that contain water, oil, and/or gas that are under sufficient pressure to maintain a potentiometric surface at an elevation above that of the Salado Formation. Some of the zones have sufficient hydraulic conductivity to allow flow rates of several hundred barrels per day. In addition to the

Delaware Mountain Group, the Atoka zone at a depth of about 13,150 feet, and the Strawn (Desmoinesian) zone at about 12,900 feet are other oil and gas production zones that are considered deep aquifers by Lambert and Mercer (1977).

Deep Hydrologic Units. The hydrologic parameters of pre-Guadalupian zones are not as well defined, nor are they as hydrologically significant to the proposed repository as the Guadalupian-age rocks. Nevertheless, a review of them is presented, based primarily on McNeal's (1965) analysis of hydrodynamics of the Permian Basin. He described the potentiometric surfaces of seven zones, using elevations of outcrops where cut by a stream or body of water, static water levels in cable tool holes or water wells, and formation pressures converted to potentiometric surface elevations. McNeal prepared maps showing the regional potentiometric surfaces in terms of fresh water, using density differences of the various brine concentrations and depths of the nearby wells. The three deep hydrologic units reviewed are the Ellenburger Group, the Devonian zone, and the Mississippian- Pennsylvanian zone.

1) Ellenburger Group. The Ellenburger Group consists mainly of chert-bearing limestones and dolomites. It is a widespread unit, covering some 100,000 square miles in southeastern New Mexico and northwestern Texas (McNeal, 1965, Figure 1). The unit is estimated to be 350 feet thick at the proposed site (Lambert and Mercer, 1977) and as much as 1000 feet thick elsewhere in the region. The potentiometric surface compiled by McNeal for the Ellenburger indicates an altitude range from 4,200 feet MSL southwest of the site to less than 1,400 feet MSL in central Texas. In the vicinity of the WIPP site, the ground surface elevation is about 3200 feet MSL. The average gradient of the potentiometric surface is about 8 feet per mile in an easterly direction. Water in the Ellenburger is a brine solution, with a dissolved solids range of 50,000 ppm to more than 200,000 ppm. No water production data are available for this group.

2) <u>Devonian Zone</u>. McNeal's potentiometric surface for the Devonian hydrodynamic zone ranges in altitude from 4,000 feet MSL in the vicinity of the Glass Mountains to 3,200 MSL feet along the Lea County - Texas line. In the Midland Basin, there are nearly hydrostatic conditions at an elevation range of 2,800 to 3,200 feet MSL. A high potentiometric nose extending across southeast Eddy County indicates a potentiometric surface at the proposed site of about 3,700 feet MSL. Salinity of the formation water is less than 50,000 ppm in most of southeast New Mexico. In west Texas, salinity reaches 200,000 ppm in one area.

The Devonian, as inferred from McNeal's potentiometric map, extends throughout southeast New Mexico and northwest Texas. He has included Silurian data in the eastern (Texas) subcrop area. The potentiometric surface generally slopes to the east, and the average gradient appears to be about 7 feet per mile.

3) <u>Mississippian-Pennsylvanian Zone</u>. Mississippian rocks are thin and few data are available on the occurrence of fluids under the Delaware Basin. McNeal (1965) delineated a potentiometric surface for the Mississippian zone of West Texas, but has not extended it into New Mexico.

There are three water-bearing zones in Pennsylvanian age rocks. In ascending order they are the Morrow, the Atoka, and the Strawn (Desmoinesian). Lambert and Mercer (1977, p. III-2) report that the Morrow may be a high pressure, low capacity reservoir with water-production rates ranging from 10 to 20 barrels per day. The Atoka also may be an overpressured reservoir with enough head to yield fluid columns of 3375 to 6552 feet MSL at gradients of 0.47 psi per foot. The water is produced from gas wells at rates ranging from 21.6 barrels per day to as much as 214.4 barrels per day (Texas American's Todd Federal Well No. 1).

Lambert and Mercer (1977) report that several wells have been drill stem tested in the Desmoinesian age Strawn zone and several others have been completed as oil wells. On five drill stem tests, the calculated heads

ranged from 3350 to 6203 feet MSL. Water production was reported to be as much as 416 barrels per day in one drill-stem test, and one well (Phillip's James "E" No. 1) produced an average of 106 barrels per day. A potentiometric surface of the Strawn zone is presented by McNeal (1964, Figure 4), but the only area in the Delaware Basin for which data were available was in the southwestern part of Eddy County. Elevation of levels in that area range from 3,200 feet to 3,800 feet MSL. The gradient is easterly at about 20 feet per mile.

Bone Spring Formation. According to Lambert and Mercer (1977), the Bone Spring Formation (Leonardian Series) can be considered an aquiclude. They report that bottom-hole pressure data from the majority of seven wells tested had insufficient heads to prevent downward movement of shallower water. They suggest the pressure data indicate the formation has a low capacity and contains reservoirs of limited volume.

Guadalupian Age Rocks. The most important aquifers of the Delaware Basin are part of a hydrologic system that incorporates rocks of Guadalupian age. The system comprises three interconnected aquifer groups; the shelf aquifers (including the San Andres Limestone and the Artesia Group), the Capitan aquifer (including primarily the reef deposits - Capitan and Goat Seep Limestones), and the basin aquifers (sands of the Delaware Mountain Group). These aquifers are depositionally juxtaposed, but are distinguished in most areas by contrasting hydraulic conductivities, water salinities, and potentiometric levels. Along the north and northwest interface, hydraulic conductivity of the shelf aquifer, although lower, is near the hydraulic conductivity of the Capitan aquifer. The basin aquifers have the lowest values of hydraulic conductivity, and the Capitan is a discharge point for ground water flows in them. Recharge to these basin aquifers probably occurs in outcrop areas along the west flank of the Delaware Basin. Ground water then moves generally eastward, downdip in the tilted beds. Data on aquifer characteristics, compiled by Hiss (1975a), are summarized in Table 6.3-1. Hydrologic, lithologic, and physical properties of the formations in which these aquifers occur are discussed below.

1) <u>Delaware Mountain Group Aquifer</u>. The Delaware Mountain Group includes, in ascending order, the Brushy Canyon, Cherry Canyon, and Bell Canyon Formations and comprises the basin facies of the system. The combined thickness of these formations ranges from less than 2,000 feet in the southern part of the Delaware Basin to more than 4,000 feet in southwestern Lea and eastern Eddy Counties, New Mexico (Hiss, 1975a).

The Brushy Canyon Formation is as much as 1,000 feet thick and consists chiefly of sandstone with limestone lenses and occasional conglomerate at the base. No wells are known to be extracting water from this formation in Eddy County (Hendrickson and Jones, 1952).

The Cherry Canyon Formation is also as much as 1,000 feet thick and consists of thin-bedded, fine-grained sandstone and some persistent limestone beds. The lower one-fourth of the formation persists as a sandstone tongue striking northwestward into the Guadalupe Mountains which may yield water to some wells and springs in that area (Hendrickson and Jones, 1952).

The Bell Canyon Formation ranges in thickness from 670 to 1,040 feet and consists mainly of sandstone and thin beds of limestone (King, 1948). The formation interfingers to the northwest with the reef limestone of the Capitan Formation, providing the potential hydrologic interconnection of the Guadalupian Age rocks. Large springs near the base of the reef escarpment west of the Pecos River are probably supplied by ground water moving through the upper beds of the Bell Canyon Formation (Hendrickson and Jones, 1952).

An average hydraulic conductivity of 0.016 ft/d (feet per day) and a porosity of 15.65 percent were determined by Hiss (1975a) from analyses of approximately 4,500 samples of rock core cut from the Delaware Mountain Group in Eddy and Lea Counties, New Mexico, and Ward and Winkler Counties, Texas. Hiss also computed a similar hydraulic conductivity from productivity indexes (approximately equivalent to specific

capacities) obtained from an oil company for two wells in the El Mar field located on the boundary between Lea County, New Mexico, and Loving County, Texas.

Hiss (1975a) indicated that similar values of hydraulic conductivity were reported by earlier writers for much of the same part of the Delaware Basin.

Hiss compiled a potentiometric surface map of the Delaware Mountain Group, of which the northern Delaware Basin portion is shown in Figure 6.3-1. The data used by Hiss in compiling the map were taken at different times over a period of about 25 years between the late 1940's and early 1970's. However, he believes the contours are representative of conditions during the period 1960 and 1970. Although some local changes to the potentiometric surface are due to oil and water withdrawals during that period, no data suggest that the regional directional trend has changed. The potentiometric surface data for the brines have been corrected to "fresh-water" density, indicating a potentiometric elevation of 3350 feet MSL in the vicinity of the proposed WIPP site. The hydraulic gradient in the northern portion of the basin dips northeasterly at approximately 15 feet per mile.

Quality of the water in the Delaware Mountain Group is generally poor. An isochlor map compiled by Hiss (1975a, Figure 26) shows a chloride-ion concentration range from 50,000 to 150,000 ppm in the east half of the Delaware Basin. Concentration diminishes to approximately 1,000 ppm southward in the vicinity of the Glass Mountains and northwestward in the vicinity of the Guadalupe Mountains. These are outcrop areas where the Guadalupian Age rocks probably have been recharged by precipitation. However, analyses of water samples taken from the hydrologic system in the vicinity of the repository site indicate that the brine solutions do not contain oxygen and hydrogen isotopes in ratios characteristic of meteoric waters. The relative proportions of O^{18}/O^{16}, and deuterium/ hydrogen ratios have probably been altered through interaction with the rock of the formation (Lambert, 1978; see also Chapter 7 of this report).

According to Hiss, recharge to the basin aquifers is through precipitation on the outcrops in the Guadalupe, Delaware, Apache, and Glass Mountains, and from downward leakage through the younger rocks in areas where the overlying soluble Ochoan evaporites have been removed. The potentiometric surface (Figure 6.3-1) indicates water moves north and northeastward, and discharge is to the overlying Capitan and shelf aquifers.

2) Capitan Aquifer. The Capitan Limestone and the underlying Goat Seep Limestone constitute the main body of the Capitan aquifer, which is the reef facies of the Guadalupian rocks. Hiss (1975a) describes the aquifer as a long continuous unit that extends in an arcuate strip along the north and east margins of the basin, with exposures in the Guadalupe and Glass Mountains, as well as the Delaware and Apache Mountains. The thickness of the aquifer ranges from a few hundred to more than 2,000 feet, and the average width is approximately 10 miles (Hiss, 1975a, Figure 11). It is one of the most important aquifers of the region and is a major control in the hydrologic system (Mercer and Orr, 1977).

Relatively few aquifer tests have been performed to measure the hydraulic conductivity of the Capitan aquifer. The data compiled by Hiss (1975a) are summarized in Table 6.3-1. Hiss calculated that the hydraulic conductivity of the Capitan aquifer along the western margin of the Central Basin Platform in Texas and New Mexico ranges from 1 to 25 ft/d and estimated that for most of southern Lea County and for about 15 miles east of the Pecos River valley from Carlsbad it is about 5.0 ft/d. Although Hiss was unable to conduct any aquifer tests in the area west of the Pecos River, he concluded that high production wells, the presence of caverns, and high porosity suggest that the hydraulic conductivity of the Capitan is higher west of the river than east of the river. The hydraulic conductivity is probably very high, as well, in the Glass Mountains, because of numerous small caverns (Hiss, 1975a). The coefficient of transmissivity of the Capitan aquifer along the northern and eastern margins of the Delaware Basin is estimated by Hiss to range from 10,000 ft^2/d (square feet per day) in thick sections to less than 500 ft^2/d in the vicinity of eroded, thin sections of the reef.

The Capitan aquifer receives some recharge by direct infiltration on outcrops in the Guadalupe and Glass Mountains, and probably more by percolation of discharge from the basin and shelf aquifers along the north and east margins of the basin. Water-table conditions exist in the aquifer west of the Pecos River and in the Glass Mountains, but to the north of the Glass Mountains and east of Carlsbad water in the aquifer is confined. Hiss believes that water entering the Capitan aquifer in the Guadalupe Mountains moves northeastward toward Carlsbad where most of the water discharges into the Pecos and Carlsbad Springs. The Pecos River controls the movement of ground water in the Capitan aquifer in the vicinity of Carlsbad, and east to the ground-water divide near the Eddy-Lea County line (figure 6.3-1).

Hiss (1975a) believes that a deep submarine canyon cut into the Capitan Limestone is present near the Eddy-Lea county line, and a hydraulic restriction is formed to constrain the eastward movement of water in the aquifer from the vicinity of the Pecos River. Apparently there is little movement of water between the Pecos River and the Eddy - Lea County line. East of the hydraulic restriction, the potentiometric surface declines with an eastward gradient. Hydrographs of observation wells, established by the U. S. Geological survey in the Capitan aquifer from Carlsbad east and south to the Texas - New Mexico state line have recorded these water level differences. Water levels during the years 1967 through 1972 indicate that from Carlsbad eastward to near the Eddy - Lea County line, the potentiometric surface has remained nearly constant, responding to minor fluctuations of the Pecos River. East of the county line, water levels declined more than 100 feet, at a constant rate, during those 6 years (Hiss, 1975a, Figure 24). The eastward gradient and decline in potentiometric surface are caused primarily by the large withdrawals of water for oil-field water flooding in eastern New Mexico and western Texas (Mercer and Orr, 1977). These withdrawals are apparently the primary discharge from the aquifer at the present time. The similar potentiometric heads and directions of movement of the Capitan and shelf aquifers along the northeast and east sides of the basin (Figure 6.3-1) suggest some discharge from the shelf aquifer also

occurs. In analyzing potentiometric data prior to 1950, when large extractions of water from the Capitan had not developed, Hiss (1975a), concluded that discharge at the time was east, into the shelf aquifers.

Water of good quality, although hard, is available in the Capitan aquifer in the area west of Carlsbad (Hendrickson and Jones, 1952), and apparently in the Glass Mountains. However, in the major portion of the aquifer, east of the Pecos River, quality is poor. Chloride-ion concentration increases from 200 ppm just west of Carlsbad to as much as 23,000 ppm east of the community. Along the east flank of the basin, salinity of Capitan water is significantly lower than that in the adjacent shelf and basin aquifers, ranging from about 1,100 to 5,000 ppm in most wells (Hiss, 1975a, Figure 26).

3)   Shelf Aquifers.

The shelf aquifers do not have a direct impact on hydrologic conditions underlying the proposed site because the Capitan aquifer is a hydrologic boundary. Nevertheless, they are in close hydraulic connection with that aquifer, and would apparently accept some discharge from the Capitan, should the extensive pumping from the Capitan be discontinued.

The lowermost unit of the Guadalupian age shelf or "back-reef" facies, known as the San Andres Limestone, extends over much of southeast New Mexico and into northwest Texas. The average thickness of the unit is about 1500 feet. Overlying the San Andres are formations of the Artesia Group. Strata in these formations that yield significant quantities of water are the shelf aquifers. The contact between the Capitan and shelf aquifers is gradational and difficult to differentiate in some areas. In the Pecos River Valley between Carlsbad and Roswell, and to the west of that area, the shelf aquifers are quite porous and yield large quantities of potable water to wells (Hendrickson and Jones 1952). The hydraulic conductivity of the aquifers east of the river and in the Central Basin Platform are significantly less than those to the west, and water quality is poor (Hiss, 1975a).

Measurements of hydraulic conductivity and porosity of core samples of
the shelf aquifers were collected by Hiss (1975a) and the data are
summarized in Table 6.3-1. It can be seen that the hydraulic
conductivities in this area are at least one order of magnitude less than
hydraulic conductivities of the Capitan aquifer. Potentiometric levels
of the shelf aquifer, shown on Figure 6.3-1, are similar to those of the
Capitan aquifer along the east side of the Delaware Basin. In the
vicinity of Carlsbad, however, the levels are as much as 200 feet higher
than those of the Capitan, suggesting poor interconnection between
aquifers in that area.

The major areas of recharge to the shelf aquifers are probably north and
west of Carlsbad in the Guadalupe mountains and areas west of the Roswell
basin. Water in the shelf aquifers to the north moves either
southwestward to the Pecos River, or southeastward onto the Central Basin
Platform. Water quality in the shelf aquifers varies considerably from
one area to another, but is generally poor east of the Pecos River.
Chloride-ion concentrations in excess of 150,000 ppm are indicated by
Hiss (1975a, Figure 26) north of the Capitan aquifer and along the east
flank of the Delaware Basin. However, a narrow band of better quality
water (salinity less than 10,000 ppm) in the San Andres Limestone is
indicated to the northeast, between the shelf and the Central Basin
Platform.

Castile Formation. The Castile Formation overlies the Delaware Mountain
Group and consists predominantly of anhydrite with halite interbeds, and
subordinate limestone. Its thickness ranges from 1,300 to 2,000 feet
over most of the Delaware Basin. In most of the basin hydraulic
conductivity of the Castile is very low so that this formation acts as a
confining layer for the underlying Delaware Mountain Group (Mercer and
Orr, 1977). However, west of the Pecos River, the salt beds have been
removed, hydraulic conductivity of the residuum is higher and water is
available to wells (Bjorklund and Motts, 1959).

In the central Delaware Basin, isolated pockets of brine and associated
hydrogen-sulfide gas have been encountered by various oil companies in

the Castile, and also in the Sandia Laboratories exploratory hole, ERDA-6 (Mercer and Orr, 1977). High-pressured brines encountered in three oil wells east of the proposed site reportedly have had flow rates as high as 20,000 barrels per day. These brines are present near the top of the formation, suggesting a brine zone, but since no other wells have encountered brines, the zone is apparently not continuous (Rose, 1977). Brine from ERDA-6 further suggests a long isolation time on the order of one million years for that pocket (Barr, Lambert and Carter, 1978).

Salado Formation. Massive beds of halite of the Salado Formation are the intended host rock for the WIPP repository. The formation extends more than 100 miles both north and east of the Delaware Basin and underlies an area of approximately 25,000 square miles (Pierce and Rich, 1962). Formation thickness in the Los Medanos area is 1,976 feet, as measured at ERDA-9, and the depth to the top is 848 feet.

Porosity of the halite is very low and interconnected pores are virtually non-existent. Lack of open fractures is assured because of the high plasticity of the material. As a result, hydraulic conductivity of the beds is effectively zero. As reported by C. L. Jones (1973), microscopic to very small angular cavities in grains of halite contain very minor amounts of brine and gas. Less common are much larger cavities or pockets in the halite beds that contain halite-saturated brine and nitrogenous gas confined under pressure sufficient to produce a "blow-out" when encountered during drilling. Nevertheless, the brine pockets do not appear to be interconnected, but seem to be isolated fluid bodies within the rock.

Because halite is quite soluble, it would readily dissolve if the beds came in contact with circulating, unsaturated solutions. West of the proposed site, where the Salado rises to the surface, progressively less halite is present as a result of leaching by percolating ground water. Where exposures existed, all of the salt has been removed (see Section 4.3.2.).

As discussed in Section 4.3.2., removal of salt from the Salado Formation
in the western portion of the basin where it is exposed, or near the
surface, has formed a residuum of clay, gypsum and sand. In the Carlsbad
area along the Pecos River and to the west, Bjorklund and Motts (1959)
report that these clays are dense, and are referred to as "red beds".
They suggested that the residue has slowed ground-water infiltration and
subsequent salt removal.

Underlying Nash Draw, a salt dissolution zone is present in the residuum
at the contact between the Salado and the overlying Rustler Formation.
As reported by Mercer and Orr (1977), the dissolution zone extends from
the recharge area north of Nash Draw to its termination in the vicinity
of Malaga Bend. Water penetrates the overlying units through fractures
and solution zones in the recharge area and moves southward along the top
salt, and discharges into the Pecos River at Malaga Bend (Figure 6.3-2).
The dissolved solids content of the brine at the river has been reported
to be in excess of 300,000 ppm. Theis and Sayre (1942) calculated the
discharge from the brine aquifer into the Pecos River at Malaga Bend to
be about 200 gpm. Hale (in Hale, Hughes, and Cox, 1954) calculated a
value of transmissivity of 8,000 ft^2/d from aquifer tests in the area
between Malaga Bend and Laguna Grande de la Sal. Apparently, as salt has
been progressively leached from the overlying beds, the residuum has
developed a base of low hydraulic conductivity, preventing further
downward leaching, and the dissolution zone has developed along the same
structural control as Nash Draw (Robinson and Lang, 1938).

6.3.3 Hydrology of Rocks Overlying the Salado Formation

Nearly all of the water bearing formations overlying the Salado in the
Delaware Basin are of materials with low hydraulic conductivity and which
contain limited amounts of poor-quality water. The major hydrologic unit
in the area that yields moderate quantities of marginal-quality water to
wells is the alluvium of the Pecos River valley. Information on the
hydraulic characteristics of these water bearing formations is limited,
and only regional descriptions of potentiometric levels and hydraulic
conductivity can be established.
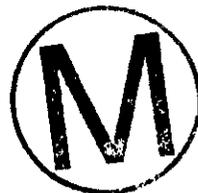
Rustler Formation   The Rustler Formation extends laterally beyond the
limits of the Salado Formation and consists of interbedded anhydrite,
dolomite, siltstones, clays, and halite.   Two dolomite beds in the
formation are water-bearing units, other than the Rustler-Salado contact,
discussed above.   The thickness of the dolomite beds ranges from 20 to 30
feet; these beds are areally extensive.   The Magenta Dolomite is a finely
crystalline, dense dolomite, and the Culebra Dolomite is vuggy and
commonly associated with some anhydrite.   The Magenta transmits only
minor amounts of water and is not considered an important aquifer
(Lambert and Mercer, 1977).

Although the Culebra Dolomite is areally persistent, yields of water vary
considerably from place to place.   Cooper and Glanzman (1971) suggested
that the variability of yields is related to the size and number of
fractures and openings in the dolomite, which in turn, could be related
to its depth.   In the northern part of Nash Draw, the dolomite is near
the surface and is reported to yield as much as 700 gpm.   East of Nash
Draw, where the dolomite is covered with Triassic and younger rocks,
yields are typically at least two orders of magnitude less.

Measurements of the hydraulic properties of the Culebra in the region are
scarce, primarily originating from studies related to Project Gnome
investigations (Cooper and Glanzman, 1971).   Aquifer-performance tests in
holes drilled for Project Gnome studies indicate a transmissivity of 460
ft^2/d, an average hydraulic conductivity of 16 ft/d, a storage
coefficient of about 10^{-4}, and an average effective porosity of 10
percent.

Mercer and Orr (1977) prepared a map of the potentiometric surface from
water levels measured in wells open to the Rustler Formation in the north
portion of the Delaware Basin (Figure 6.3-2).   The data were taken from
several sources and represent a composite of the Culebra and Magenta
dolomites, or other zones.   However, it is believed that most wells are
open to the Culebra dolomite bed because it is the most consistently
producing rock in the vicinity.

These data indicate that water in the Rustler Formation moves west and southwestward across the Lea - Eddy County line, and southeastward from the community of Carlsbad toward Nash Draw, and the Pecos River to the south. Only the Magenta is exposed locally on the flanks of Nash Draw, and both the Culebra and the Magenta form the floor of wide sections of Nash Draw in the vicinity of Laguna Grande de la Sal.

A single water well in Lea County is reportedly deep enough to have reached Permian beds (Nicholson and Clebsch, 1961); otherwise no additional information is available on occurrence of water in the Rustler Formation in the area.

The Dewey Lake Redbeds. The youngest formation in the Ochoan Series, the Dewey Lake Redbeds, consists of orange-red siltstone with some mudstone and sandstone. This formation has been removed from the western and southern parts of the Delaware Basin by post-Permian erosion but is present in the subsurface throughout most of the site area. The thickness of the formation varies from about 200 feet to as much as 600 feet (Hiss, 1975a).

The Dewey Lake Redbeds are not an aquifer, although some permeable sand lenses are present and yield small quantities of water to a few wells. Regionally, the beds act as an aquiclude, restricting water at the surface from percolating downward to more permeable units in the underlying Rustler Formation.

Dockum Group. The Dockum Group consists of three formations. In ascending order, they are, 1) the Tecovas Formation, which consists of up to 300 feet of red shale, siltstone, and fine-grained sandstone, 2) the Santa Rosa Sandstone, which is composed of 100 to 650 feet of red, brown, and gray sandstone, and 3) the Chinle Formation equivalent, which consists of up to 1,300 feet of red, maroon, and purple shales and siltstones with lenses of fine-grained red-to-gray sandstone (Hiss, 1975a). The group is present only as a thin wedge in Eddy County, thickening to the east in Lea County and in Texas.

Both the Chinle Formation equilvalent and the Tecovas Formation are present only as thin, isolated remnants in southeastern New Mexico, primarily in Lea County. The few wells drilled into these formations yield small quantities of poor-quality water (Hiss, 1975a). In contrast, the Tecovas and Chinle are not considered aquifers in the Delaware Basin. The Santa Rosa Sandstone is a principal aquifer in several areas, particularly in Winkler and Ward Counties, Texas (Hiss, 1975a). It produces both fresh and saline water, depending on location. The westernmost extent of the Santa Rosa Sandstone is just into Eddy County, as shown in Figure 6.3-3. Water levels in wells open to the Santa Rosa Sandstone, reported by several sources, are the basis of the potentiometric surface by Mercer and Orr (1977) shown in Figure 6.3-3. Wells completed in the Santa Rosa Sandstone have low yields with specific capacities of 0.14-0.2 gpm per foot of drawdown (Nicholson and Clebsch, 1961); the formation porosity is about 13 percent.

Ground water recharge to the Santa Rosa Formation is from precipitation on the outcrop and percolation through sand dunes and the overlying Ogallala Formation to the east (Nicholson and Clebsch, 1961). Movement is generally southwest, but additional recharge apparently occurs along the potentiometric high that trends southwest along the eastern side of Eddy County. Discharge is to underlying formations at the edge of outcrops and reportedly downward through collapse zones such as San Simon Swale.

Ogallala Formation. The High Plains (Llano Estacado) region south of the Canadian River is mantled by the Ogallala Formation, which consists of Pleistocene sediments from 0 to 500 feet thick. South of Mescalero Ridge in Lea County the formation becomes discontinuous, and there are no definite remnants of the Ogallala west of easternmost Eddy County. Recharge to the Ogallala is by direct precipitation on the outcrop and by percolation through overlying sand dunes and alluvium. Nicholson and Clebsch (1961) reported that the saturated thickness of the Ogallala ranges from 25 to 175 feet. This variability can be attributed to the very irregular Triassic surface that underlies it. Movement of water in

the Ogallala is controlled to a great extent by the generally southeastward slope of the underlying Triassic red beds (Mercer and Orr, 1977).

Quaternary Deposits The Gatuna Formation is the oldest known Quaternary formation in the area and fills channels and steep-walled valleys cut primarily into the Dewey Lake red beds and Rustler Formation. In the type section and in the vicinity of Nash Draw where the Gatuna is readily recognizable, it is overlain by an extensive caliche zone that marks the Mescalero surface (Bachman, 1974). East of Nash Draw, there are few outcrops of the formation.

The Gatuna Formation yields limited amounts of water to wells where the water is in isolated gravel and sand lenses. Yields of one to five gpm are small but are usually sufficient for stock and domestic use. Ground water from the Gatuna probably percolates downward into Triassic sandstone or the Rustler Formation (Mercer and Orr, 1977).

Younger quaternary deposits are represented by alluvium. The most extensive alluvial deposits are along the west side of the Pecos River north of Malaga. Isolated patches of alluvium, however, occur along the Pecos to the south. In some areas the thickness is nearly 300 feet, and yields are reported to be as much as 3,000 gpm (Hendrickson and Jones, 1952). The source of water is primarily underflow from west of the Pecos River augmented by leakage from canals and from irrigation return flow.

Alluvium east of the Pecos River is restricted to relatively small closed depressions. Nash Draw and Clayton Basin contain Quaternary alluvium, and, in places such as Laguna Grande de la Sal, contain lake or playa deposits. The thickest alluvial deposits occur within San Simon Swale where they are in excess of 500 feet. Ground water present in the San Simon alluvium may be derived from discharge from the Santa Rosa Sandstone (Mercer and Orr, 1977). The lake and playa deposits often yield some water, although it is generally highly mineralized.

6.3.4 Regional Ground Water Use

Ground water is used in the region for irrigation, municipal supplies, rural domestic supplies, stock watering, a few industrial purposes, and for secondary oil recovery (usually referred to as "oil field flooding"). In southeastern New Mexico and western Texas almost all the ground water produced is used for this latter category. The Capitan aquifer is the largest source, but supplies are also taken from the Santa Rosa Sandstone and the Rustler Formation (Hiss, 1975a).

Demand for water throughout the region has increased steadily over the past three decades and is expected to continue into the 1980's. Production from the Capitan aquifer alone increased from approximately 80,000 acre-feet in 1950 to about 700,000 acre-feet in 1970 (Hiss, 1975a, Figure 38). The increase has been fairly linear over the 20 year period. Most of the increased demand has been for oil-field flooding which began in the early 1950's. The largest amount of pumping for this purpose is in Ward and Winkler Counties, Texas, and is primarily extracted from the Capitan aquifer. The other major source is the San Andres Limestone. According to Hiss (1975a), the cumulative total of *water produced from these aquifers for the period 1920-1969, in thousands of acre-feet, is as follows:*

	Eddy County	Lea County	West Texas	Total
Industrial	65.4	-	-	65.4
Irrigation	151.0	-	223.7	374.7
Municipal	162.0	-	-	162.0
Secondary Recovery	0.6	2.8	293.0	296.4
TOTAL	379.0	2.8	516.7	898.5

Listed below (in acre-feet) is a summary of usage in Eddy County for the year 1949 (Hendrikson and Jones, 1952) and in Lea County for the year 1954 (Nicholson and Clebsch, 1961). It is reasonable to assume that the quantities reported for industrial, irrigation, municipal, and rural use

have increased a moderate amount. The quantity listed for secondary recovery has increased moderately in southeastern New Mexico and dramatically in west Texas, as noted above.

	Eddy County (1949)	Lea County (1954)
Industrial	4,000	2,710
Irrigation	130,000	2,600
Secondary Recovery	0	40
Rural Domestic/Stock	2,000	450
TOTAL	141,000	6,350
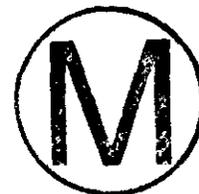
Occurrence of large quantities of potable ground water is restricted to west of the Pecos River, and most of this water is extracted from the Capitan aquifer. Hiss (1975a) reported that the municipal water supplies for the communities of Carlsbad and White's City are obtained from wells completed in the Capitan aquifer. Hiss also reported that water pumped from the Capitan aquifer is used to irrigate about 2,300 acres of farmland in the Pecos River valley, the immediate vicinity of Carlsbad.

In addition, water pumped from the Capitan aquifer at Carlsbad is transported by pipeline to a potash refining plant located about 18 miles east of Carlsbad. Approximately 3,740 acre-feet of water per year was used to refine potash ore during the period 1965-1969.

Oil Field Secondary Recovery. In the early 1950's, the petroleum companies operating in the region initiated a process to recover crude oil that could no longer move to wells under existing reservoir pressure. This secondary recovery technique is one in which water is injected under pressure into the oil-bearing formation to drive the residual oil to the pumping wells. Injection may be into existing depleted wells or into wells constructed specifically for this purpose.

According to Hiss (1975a, Table 15), a cumulative total of nearly 300,000 acre-feet of water has been produced from the Capitan aquifer for

secondary recovery versus a total of about 725,000 acre-feet actually used in the flooding process. The difference of 425,000 acre-feet has been supplied from other sources including the San Andres Limestone and the Ogallala and Rustler Formations. The major areas of extraction for this use are in Ward and Winkler Counties, Texas.

Ground Water Utilization East of the Pecos River, Southeast New Mexico. In this area, small amounts of ground water are used for rural domestic supplies, stock watering, gasoline plants, and gas stripping. The Rustler Formation, the Santa Rosa Sandstone, and the Artesia Group are the principal hydrologic units pumped for those purposes. In the Nash Draw area, relatively large quantities of ground water have been taken from the Rustler Formation for use in potash refining. In the past, considerable amounts were pumped for irrigation in Lea County, but this has apparently been discontinued (Nicholson and Clebsch, 1961).

Gasoline plants use a considerable amount of water for their cooling and boiler systems. Nicholson and Clebsch (1961) report that in Lea County a total of 2400 acre-feet of ground water was used for this purpose in 1959. Gas stripping plants in the area also use water for extracting hydrogen sulfide and carbon dioxide from residual gas. Nicholson and Clebsch (1961) estimated that 150 acre-feet per year is used for this purpose.

In 1972, Cooley (1973, Table 4) inventoried the existing and abandoned wells in a nine-township block in east-central Eddy and west-central Lea Counties, New Mexico. Most of these wells are of low yields and are used mainly for domestic supplies and stock watering. Table 6.3-2 is extracted from the Cooley survey; well locations are shown on Figure 6.3-4.

6.3.5 Ground-Water Occurrence at the Proposed Site

The wells in the vicinity of the site (Figure 6.3-4) indicate that ground water above the Salado Formation is found only in limited quantities, and

is commonly of such poor quality, that it is not usable. Where the quality is marginal, it is utilized for watering stock, and is considered a valuable resource (Nicholson and Clebsch, 1961). Below the Castile Formation, at considerable depth, the Bell Canyon Formation might yield large quantities of water, but it would be brine. Although these units are technically regarded as aquifers, in the following discussion, only the hydrologic characteristics of fluid-bearing zones underlying the proposed site will be described. These zones are not identified as aquifers because an aquifer readily yields good quality water to wells.

Fluid-bearing Zones. The hydrologic exploration at the proposed site performed by the U. S. Geological Survey to date has been directed primarily to the fluid-bearing rocks of the Rustler Formation, and to the Rustler-Salado contact zone. They directly overlie the Salado salt and furnish a potential, although remote avenue for salt dissolution and radionuclide transport (Mercer and Orr, 1978). Additionally, brines in the sands of the underlying Bell Canyon Formation have been tested. These fluids are under sufficient head to allow them to reach the Salado salt. Because the brines are undersaturated, they could dissolve the salt. However, to reach the Salado, these fluids would have to first penetrate the Castile Formation. Permeabilities (or lack of permeability) of the Castile and Salado Formations at the site have been determined by drill-stem tests in two exploratory holes: ERDA No. 9 and AEC No. 8. The tests, summarized by Lambert and Mercer, 1977, Tables 1 and 2, indicate that the two formations are extremely tight. The tests gave no indication of fluid content in either formation.

Other zones that were briefly tested include zones in the Dewey Lake red beds where circulation was lost during drilling, or where hydraulic conductivity was believed to be measurable. However, no appreciable amounts of fluid were encountered (Mercer and Orr, 1978).

When the exploration and testing were completed, Mercer and Orr (1978) made several conclusions concerning the occurrence of fluids in the rocks. These include the following:

Monitoring of fluid-bearing zones in the Rustler Formation indicate that stabilized heads decrease with depth; consequently, potential fluid movement would be downward in rocks above the salt. However, the large head differences between fluid-bearing units within the Rustler indicate little or no vertical connection.

Head distribution determined for the Culebra dolomite indicates fluid movement to the southeast across the site. Gradients range from 7 to 120 ft/mi and vary as a function of hydraulic conductivity.

Head distribution within the Magenta dolomite has been determined only in three holes and indicates fluid movement to the southwest. The hydraulic gradient is 50 ft/mi.

Fluids in the Culebra and Magenta are expected to move primarily along fracture systems, and measurements of the effective porosities and hydraulic conductivities in low-yielding fractured rocks are very difficult to obtain.

Brines were found at some locations along the Rustler-Salado contact, but extremely low yields were measured.

Although evaluation of the testing of Bell Canyon sands is not complete, preliminary results at AEC-8 indicate the potentiometric surface, corrected to fresh-water density, is higher than similarily corrected levels of fluid zones in the Rustler Formation.

Hydrologic Testing. The geologic and geophysical exploration performed at the site provides a detailed understanding of the stratigraphy and structure of the underlying formations. This work was described in previous sections. In coordination with the exploratory drilling, a program of hydrologic testing and monitoring was established. As a result, considerable data on the occurrence of ground water have been collected. The ground-water studies are continuing and the data collected will further our understanding of the site conditions.

In addition to continued monitoring of the existing observation wells, long-term pumping tests to measure vertical connection between zones, and other tests have been planned. Also, some hydrologic information is available from the recently completed ERDA 10 test hole, located approximately 8.5 miles southwest of the proposed site.

One of the major problems faced in this program is the difficulty of measuring hydrologic parameters in materials of extremely low hydraulic conductivity in the field. Thorough testing of even the more permeable zones, such as the Culebra Dolomite, requires long periods of time, as well as close control of the interval being tested. To collect a sufficient quantity of water from these materials for proper water quality sampling requires long periods of time. Recovery of water levels in observation wells to static conditions is very slow; levels in some of the wells on site had not stabilized after more than 12 months of monitoring. Nevertheless, the data collected are sufficient to provide a good measure of the hydraulic characteristics and an understanding of ground-water occurrence at the proposed site. Hydrologic test data as of August, 1978, are available from 9 exploratory holes within the proposed land withdrawal boundary, and from the hole designated AEC 8, which is just outside the boundary, as shown on Figure 6.3-5. The U. S. Geological Survey Water Resources Division has been directing the testing program. A summary of drilling and testing operations is given for each hole in Section 6.4. A full description of the testing program and the data collected is presented in Mercer and Orr, 1978. The following discussion is extracted from that report.

The objectives of the program have been to determine the static head or reservoir pressure, the water-yielding potential (i.e., hydraulic conductivity and transmissivity) of the rock strata, and the chemistry of formation waters. These hydrologic tests are made in the exploratory test holes both during drilling and after the hole has been drilled to total depth.

Five of the test holes were specifically designed for hydrologic testing (H-1, H-2 complex, and H-3); the others were drilled for other purposes as well (potash mineral evaluation and/or geologic exploration) but were adapted for hydrologic testing. After drilling and testing wells H-1 and H-3, triangular arrays H-4, H-5, and H-6 complexes were designed similar to the H-2 complex but with a 100-foot well spacing. The additional sets of triangular arrays (H-4, H-5, and H-6) have been completed recently and testing has started.

The H-series test holes were drilled with air and detergent to avoid the undesirable mudcake that occurs when drilling with gel. This method also allows detection of fluid-producing zones that are encountered during drilling. When detected, some of these zones were tested before completion of drilling for a preliminary estimate of yield. On completion of drilling, geophysical logging was performed in all holes. These logs provided detailed information on lithologic changes, formational characterstics, potential zones of water yield, and borehole diameter changes. These data are used to select intervals to be tested, as well as provide information on hole conditions in the selection of packer seats.

Following logging, each potential zone of water yield was isolated with packers, and a drill-stem test (DST) was conducted. The DST is a temporary well completion designed to furnish hydrologic data, such as representative samples of formation fluid, undisturbed formation pressures, and indications of the formation permeablity, and/or transmissivity. The standard DST, as used in oil-field exploration, was run in test holes AEC 8 and ERDA 9, but in the other tests the procedures were modified. The modification most commonly made was in the method of recording formation pressures. In the standard DST, pressures are recorded throughout the test by a Bourdon-tube pressure recording gage (pressure bomb) located near the bottom of the drill string. Data from this pressure bomb cannot be retrieved until after completion of the test. In the modification DST used in these investigations, the fluid was initially removed from the tubing, and the stabilizing fluid levels
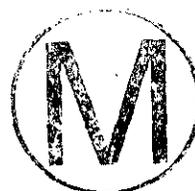
were measured in the drill string. This modification allowed for continuous monitoring throughout the test. Additionally, pressure-monitoring devices were placed above and below packers to determine the degree of isolation of the zone from the rest of the borehole.

The test zones were bailed or swabbed until temperature, conductivity, and density of fluid in the casing stabilized to assure that the fluid was representative of formation fluid. Samples were then collected, treated according to standard U. S. Geological Survey techniques, and chemically analyzed for the major and trace elements and for radiochemistry. Results of these analyses are listed in Table 6.3-3. The geochemistry of these fluids is discussed in Chapter 7.

During the bailing, the volume and rate of fluid withdrawal were monitored. The rate of recovery following withdrawal was measured, and yields from test zones were then calculated. The results of these tests are summarized in Table 6.3-4.

After all potential water zones were tested in the open hole, casing was installed and grouted in all holes except ERDA 9. Selected intervals were perforated for monitoring potentiometric levels, and provision was made for long-term hydrologic testing. Radioactive tracer tests were conducted in some of the holes after they had been cased and perforated to examine the cement-bond for leaks between casing and the borehole wall. These tests also yielded some information on vertical distribution of permeability across the test interval. The perforated zones were then tested for yield by bailing or swabbing, as was done in the open hole, and results are summarized in Table 6.3-4.

When the testing of the cased holes was completed, the holes were prepared as multiple observation wells. The holes are used to monitor potentiometric levels of two separate zones with the use of packers and inner tubing. In some wells, a third zone was perforated, but a bridge plug was set above it, and the zone is not available for periodic

monitoring. Figure 6.3-6 illustrates the method of completing the wells, and Table 6.3-5 indicates the zones monitored at each observation well.

Periodic monitoring of the fluid levels in the wells began after completion of testing. Because of the low yield of the zones tested, considerable time is required after bailing for the recovery of fluid to reach a stabilized level. Most levels had stabilized by October 1977, as indicated in Table 6.3-6. These levels provide a measure of the potentiometric surfaces of the monitored zones, and an indication of hydraulic gradients.

Bell Canyon Formation. During the WIPP hydrologic testing program, cores were taken in the Bell Canyon Formation in exploratory hole AEC 8. Analyses of these cores indicated the presence of two sandstone units whose permeabilities were higher than those of the surrounding rocks. These units are referred to as the lower sand and upper sand; their depths are, respectively, 4,844 to 4,860 feet, and 4,821 to 4,827 feet.

Hydrologic testing of the two sand units was made only in cased, perforated zones. There was no open-hole testing. These tests included formation pressure testing, fluid level monitoring, aquifer yields, recovery rates, water sampling, and geophysical logs. Radioactive tracer logs were also run on this hole. Analysis of the data had not been completed at the time of the report by Mercer and Orr (1978).

After the fluid in the casing had been removed by swabbing to a depth of approximately 4,200 feet, the lower sand yielded 31 gallons of fluid in 166 minutes (average 0.2 gpm), recovering to a depth of 4,095 feet. The zone was then shut-in, and a static formation pressure of 2,037 lbs/in^2 was reached in 44-1/2 hrs. The upper sand was not tested for yield. Static formation pressure was 2,044 lbs/in^2 after 57 hours.

Samples collected from the two sand units indicate that these units contain dense brines. For example, the upper sand contains 189,000 ppm of total dissolved solids, 175,000 ppm of which is sodium chloride

(Mercer and Orr, 1978, p. 80). The major constituents from the analyses are listed in Table 6.3-3. Density of the brines of each zone was determined to be 1.11 gm/cm3 for the upper sand, and 1.12 gm/cm3 for the lower sand. These values were used to correct static heads to fresh-water equivalents (Table 6.3-6).

Rustler-Salado Contact. The contact zone between the Rustler and Salado Formations was tested in holes H-1, H-2c, H-3, P-14, P-15, P-17, and P-18.

Both open-hole and cased-hole tests were run on the Rustler-Salado contact in H-1 and H-3, and cased hole tests were run in H-2c, P-14, P-15, P-17, and P-18. Without exception, all tests showed very low yields, typically producing a few gallons per day in the cased holes and only slightly more in the open holes (Table 6.3-4). A yield of 9.1 gallons in a 20-hour period (in H-1) was the highest yield recorded. Based on the collected data, Mercer and Orr (1978, p. 83) calculated transmissivities from the yield data, ranging from 10^{-1} ft^2/day (in P-14) to 10^{-4} ft^2/day (in P-18). Recovery rates in the monitoring wells are so slow that the level had not stabilized in P-18, after 4 months (Table 6.3-6).

Samples were taken from all of the test wells except P-18. Analyses of these samples show that the fluid in the Rustler-Salado contact zone is a saturated brine containing more than 300,000 ppm total dissolved solids (Table 6.3-3).

Culebra Dolomite. The Culebra dolomite was tested in holes H-1, H-2b, H-2c, H-3, P-14, P-15, P-17, and P-18. Logs of these holes indicate that the thickness of this unit is about 28 feet and that its depth ranges from 410 to 940 feet below ground level.

Both open-hole and cased-hole tests were run in the Culebra in H-1 and H-3, and cased hole tests were run in H-2c, P-14, P-15, P-17, and P-18. Yields varied considerably. At P-14, 720 gallons of fluid were bailed with no noticable drawdown, while P-18 produced only 16 gallons of fluid

in 33 days of monitoring. Preliminary transmissivity values calculated
by Mercer and Orr (1978) also reflect the variability with values of 140
ft^2/day at P-14, 10^{-1} ft^2/day at H-1, and 10^{-4} ft^2/day at P-18.

Mercer and Orr (1978) reported that fluids in the Culebra have a total
dissolved solid range of 23,700 to 118,300 ppm, and a sodium chloride
range of 17,900 to 89,200 ppm. The major constituents of samples taken
from the Culebra are listed in Table 6.3-3.

Magenta Dolomite. The Magenta Dolomite was tested only in H-1, H-2a, and
H-3. In these holes the Magenta is 25 feet thick and the top of the unit
is 502 feet below ground level.

Both open-hole and cased-hole modified drill stem tests were run on the
Magenta in H-1 and H-3; well number H-2a was constructed as an
observation well for the Magenta. The open-hole drill-stem test on the
Magenta in H-1 produced only 13 gallons of fluid in 13 hours. A
subsequent swabbing of the permeable zone produced 107 gallons of fluid,
which indicated higher productivity than the DST displayed. In the
cased-hole test, the Magenta zone was bailed constantly until a pumping
level of 424 feet (depth) was attained. After bailing was stopped, the
fluid level recovered to a depth of 340 feet in 33 days. In H-3, an open
hole drill-stem test produced 23 gallons of fluid in 38 hours, but 442
gallons were swabbed from the hole after the DST was discontinued. In
the cased hole test, 1 hour of bailing produced 6 feet of drawdown, and
recovery was from 405 to 401 feet in 33 days of monitoring. Preliminary
transmissivity values computed by Mercer and Orr (1978) range from 40
ft^2/d to less than 1 ft^2/d.

The quality of the Magenta fluids is poor (Table 6.3-3), with a total
dissolved solids range of 10,300 to 29,700 ppm. The sodium chloride
range is from 6800 to 24,300 ppm.

Salt-Residue Zone. Rocks of the Rustler Formation in which halite beds
have been removed by leaching--salt-residue zones--were considered to be

areas for possible fluid retention. A potential zone was identified from geophysical logging and drill stem tests performed in H-1 and H-3. Results show that very little fluid now exists in those zones. In H-1, the suspected zone yielded 11.2 gallons of fluid in 12 hours of monitoring.

6.3.6   Dissolution of Salt in the Permian Evaporites

Features apparently caused by solution and/or subsidence are common in southeastern New Mexico. The extensive karst plain of the Llano Estacado (the High Plains or Caprock region) indicate the prominence or rock solution as a geologic process. Depressions near the WIPP site range from small features no more than a few meters in diameter to large features such as Laguna Grande de la Sal (Salt Lake), 11 miles to the west-southwest of the WIPP site, and Laguna Plata and Laguna Gatuna, 14 miles to the north. Not all depressions in the region, however, have been formed by solution and collapse. Some have been formed by wind action, and others are the result of solution or etching of the caliche. Salt Lake does appear to occupy an area of coalesced collapse dissolution sinks, but Laguna Plata and Laguna Gatuna appear to have formed as solution blowouts in windborne sand deposits.

A report to Sandia Laboratories by R. Y. Anderson was prepared in early 1978. This report served to assemble and summarize available data regarding the dissolution of evaporites in the Delaware Basin. The Anderson (1978) report also proposed a set of working hypotheses for the origin of various dissolution features, in order to guide future Sandia investigations of evaporite dissolution relevant to the potential integrity of the WIPP horizons and adjacent evaporites. In the text that follows, an attempt is made to distinguish available data from working hypothesis, whenever Anderson (1978) is cited.

It has been estimated that as much as 50 percent of the original salt of the Delaware Basin evaporites has been removed (Anderson, 1978) either by surface erosion or by subsurface dissolution and transport by ground

water. These processes have been in progress intermittently through more
than 100 million years (Bachman, 1974). At least four erosional periods,
in which the removal of salt could have been accomplished, can be
recognized. These include: 1) Early Triassic time, 2) Jurassic through
Early Cretaceous time, 3) a Late Cretaceous through mid-Tertiary period,
and 4) post-Ogallala uplift and erosion.

Of the processes which accomplished the removal, two types of salt
dissolution have been recognized in the Delaware Basin. The more
familiar dissolution is the removal of salt by waters percolating
downward from above (primarily from precipitation falling directly on the
ground surface above the salt). The percolating water removes soluble
salts, leaving behind a residuum of insoluble material that is referred
to as a leached zone (Vine, 1963). The shallow dissolution beneath Nash
Draw is such a zone and is apparently the route of lateral migration of
the leached salts that discharge into the Pecos River.

A second type of salt dissolution has been recognized as having dissolved
salt from somewhere within the body of evaporites, generally resulting in
the collapse and lowering of the overlying stratigraphic units. Anderson
(1978) recognized the resulting insoluble residue as a blanket
dissolution breccia which occurs to the west of the present salt edge in
the basin. In addition, deep dissolution phenomena within the evaporites
may have developed more localized collapse features that have been
recognized around the margin of the basin and within the basin (Maley and
Huffington, 1953). The origin of these deep dissolution features and
breccias is more problematical than the origin of surface dissolution and
the rates of dissolution more difficult to assess. Source of the water
to dissolve the salt is hypothetically assumed to be aquifers underlying
the salt beds, communicating through fracture systems in the intervening
anhydrite beds.

Shallow Dissolution. The depth of shallow dissolution in the evaporites
(base of leached zone) is highly irregular, but is usually less than 300
feet in the vicinity of the proposed site (see Section 4.3.2). It is

developed in the western part of the Delaware Basin where the evaporites
are exposed, or near the surface. For example, in Nash Draw, where the
Rustler Formation is exposed, leaching extends into the Salado, and the
permeable residuum contains brine (Vine, 1963). It appears that
percolating ground waters move laterally toward Nash Draw, eventually
discharging to the Pecos River after becoming saturated with salt.

East of Nash Draw, down dip into the basin, the evaporite formations
become progressively deeper, and the present-day top of salt becomes
progressively higher in the stratigraphic section. The top of salt is at
the top of the Salado Formation about 2 miles west of the center of the
proposed site, and becomes progressively higher in the Rustler Formation
across the site (Figure 6.3-7, also see Figure 2-6).

Jones (1972) reported the solution front in the Salado Formation to be
between 2 and 3 miles west of the center of the site. Bachman (1974)
described a thinning of the upper member of the Salado Formation to the
west and north that he attributed to a combination of thinning inherent
in the original deposition processes and thinning due to subrosion
"during the middle and late Cenozoic. West of the line marked "edge of
Salado salt" in Figure 6.3-8, there is almost a fourfold reduction in
thickness of the upper member of the Salado Formation to as little as
150-170 feet in some places. This is the residue of a 500-foot thick
section from which the soluble portions have been leached by circulating
ground water. Wherever the upper member of the Salado has been thinned
by dissolution, the section of rock between the upper surface of the
remaining salt and the top of the formation consists of clay with crudely
interlayered seams of broken gypsum (from rehydration of anhydrite) and
fine-grained sandstone.

As dissolution progresses and the salts are carried away, voids develop
and the residual layer is weakened until it is no longer able to support
the overlying material. Slumping of the residue and the associated
collapse of the roof can extend to surface elevations, resulting in a

topographic sink. The distinctive pitted topography that results is
termed karst. Such topography, in which surface drainage is poorly
defined, is extensive in southeastern New Mexico.

Bachman (1974) reported that dolines (that are believed to develop into
shallow sinks on the rock surface beneath the soil mantle) are very
common, and suggested that the course of the Pecos River southward from
Carlsbad to the proximity of the New Mexico-Texas state line lies in a
major belt of collapsed sinks. For example, along the east side of the
Pecos River, southeast of Carlsbad at Malaga Bend, a linear scarp is
believed to have formed along a collapse structure that is now occupied
by the river. Other major collapse features mentioned by Bachman include
Clayton Basin and Nash Draw. Bachman believes that these features formed
as coalescing sinks, probably during Pleistocene time.

Another large depression cited by Bachman is San Simon Sink, located 22
miles east of the proposed site. Shallow dissolution is a factor in the
development of this sink, which is apparently still in process. The last
recorded collapse in San Simon Sink occurred approximately 40 years ago
(Nicholson and Clebsch, 1961). Many sinks along the Pecos River Valley
have collapsed in historic time (Bachman, 1974). As recently as 1973 a
small collapse sink formed at Lake Arthur, N.M., about 50 miles (80 km)
north of Carlsbad.

Deep Dissolution. Large, deep dissolution features filled with Cenozoic
sediments overlying the inner margin of the Capitan reef (Figure 6.3-8)
were recognized by some of the first geologists working in the Delaware
Basin (Maley and Huffington, 1953). The source of water to dissolve the
salt was assumed to be the Capitan aquifer.

The extent of large-scale dissolution structures is shown on Figure
6.3-8. The dissolution wedges were identified through varve correlation
across the basin in the Castile Formation and recognition of dissolution
breccia beds in the western part of the basin (Anderson et al., 1972).
These studies suggest that deep dissolution wedges in the Castile

Formation occurred in the lower Salado and upper Castile salt beds (Anderson, 1978). The position of the eastern margin of the western wedge coincides with the location of dissolution features containing deep Cenozoic fill (Figure 6.3-8). The development of these features and the wedge was apparently a complex process. It probably included initial wedge development adjacent to the reef, similar to that seen in the eastern wedge (Anderson 1978), and later combined with shallow dissolution.

The most prominent small-scale, (less than 1 mile across) dissolution features in the vicinity of the Delaware Basin have been described by Vine (1960) as "domal karst features". The subsurface projection of one of these (dome "C") was encountered at the level of the McNutt potash zone by Mississippi Chemical Corporation. It was found to be a chimney in the Salado Formation filled with clay-cemented brecciated rock belonging to strata above the 7th ore zone. There are other erosion-breached domes similar to Vine's dome "C" in the vicinity of Nash Draw. The subsurface expression of the domes, if any, is virtually unknown. A chimney containing cemented rubble (incorrectly termed a "breccia pipe") was encountered in commercial exploratory drilling within the proximity of a low circular hill near the Wills-Weaver Mine, but this chimney was not associated with a breached-dome at the surface. Recent geophysical surveys of the region have revealed that some of these hills, including the "Weaver Pipe" and dome "C", are associated with resistivity lows. Both Vine (1960) and Anderson (1978) have proposed mechanisms for origin of these features, all of which remain to be tested by field investigations of their subsurface structure and composition (see Chapter 10). These mechanisms involve various combinations of differential solution, hydration of anhydrite to gypsum, and salt intrusion. An attempt to reconcile these mechanisms and apply them to the origin of domes near Queen Lake southwest of Nash Draw was made by Reddy (1961).

Anderson believes that the dissolution giving rise to these features is an ongoing process. The proposed site is in an area of the Delaware Basin that is free of regional deep dissolution, but localized features

are present in the vicinity. Nevertheless, the extensive investigation carried out at and near the proposed site, including exploratory holes, ERDA-10, ERDA-11, ERDA-9, and AEC-8, indicate that deep dissolution is not taking place there. ERDA 10 was located and drilled specifically to evaluate the suggestion of Anderson that the absence of Halite III in the Castile south of the WIPP site was due to deep dissolution. Examination of the core revealed no apparent solution residue or collapse breccia; the recently collected data indicate nondeposition rather than dissolution since this was the nearest probable location of regional deep dissolution, its absence implies a lack of threat to the WIPP site from this phenomenon.

Rates of Dissolution. It is evident that dissolution is an active process, and can be expected to continue in the future. The potential hazard to the proposed site by continued dissolution in nearby places such as Nash Draw, 7 to 8 miles west of the site, can be evaluated if the rates of dissolution are known. In relation to human activity, the rate of dissolution is almost immeasureably slow. However, in terms of geologic processes, an attempt to estimate the rate is not altogether impractical. As stated by Bachman (1974): "Active geologic processes have not changed since the close of Tertiary Ogallala time, about 3-4 m.y. (million years) ago. However, the rates of these processes have varied considerably. It is assumed that the rates of these processes will continue to vary and that prediction of future events can be made by assuming that the extremes of past conditions will not be exceeded in the future."

With this in mind, Bachman analyzed the rate of dissolution in Nash Draw since the development of the Mescalero caliche, estimated to be 600,000 years ago. The following summarizes his analysis (Bachman, 1974):

Collapse of the Mescalero caliche along the margins of Nash Draw indicates that this depression has formed, at least in part, since the deposition of the caliche.

Along Livingstone Ridge on the east side of Nash Draw, the Mescalero caliche is undeformed at elevations above 3,300 feet. It dips steeply into the depression along the ridge and occurs at elevations of 3,200 feet, and less, within the depression. Along Quahada Ridge on the west side of Nash Draw the Mescalero is likewise undeformed at elevations about 3,300 feet, but it dips steeply into Nash Draw and occurs as collapsed fractured masses within the depression (NE 1/4 sec. 1, T. 22 S., R. 29 E.).

A cross section through potash exploratory holes in Nash Draw indicates the approximate extent of salt dissolution in the Salado Formation since Mescalero time (Figure 6.3-9).

Nash Draw appears to have subsided between Livingstone and Quahada Ridges as much as 180 feet since Mescalero time. At one locality the surface of Nash Draw is 180 feet below the projected altitude of the Mescalero caliche (See figure 6.3-9). However, the interval between the top of the Salado Formation and the top of marker bed 124 at the same location is 420 feet, or 330 feet less than at Livingston Ridge where relatively little Salado salt has been removed. It is therefore interpreted that about 150 feet of Salado salt was removed before Mescalero time and about 180 feet has been removed since Mescalero time. At another locality, Nash Draw subsided approximatley 160 feet below the projected elevation of the Mescalero caliche while about 120 feet of Salado salt was being removed. There is a discrepancy here of about 40 feet that could be explained by surficial erosion.

Thus, in the area of Nash Draw that subsided 180 feet, the average rate of vertical dissolution over the 600,000 years was about 0.33 feet per 1000 years (Bachman, 1974).

These conclusions are based on the available geologic evidence, but the assumption should not be made that this rate of dissolution is a constant for the region. At least two other factors must be considered in this interpretation, but geologic information is not currently available to permit evaluation of them. The factors are:

Dissolution and subsidence rates probably have not been constant in Nash Draw during the past 600,000 years. A major part of this subsidence may have occurred during periods of high humidity in late Pleistocene (Wisconsin time).

The subsidence in Nash Draw, whenever it occurred in the Pleistocene, is not an average rate for the region. In the area of "the Divide," between Antelope and Livingstone Ridges, the Mescalero caliche is relatively undisturbed and probably no dissolution has occurred there since Mescalero time.

Calculations have also been made of the removal of salt from the Rustler and Salado Formations in Nash Draw based on the rates of discharge of dissolved sodium chloride and calcium sulfate into the Pecos River by brine seeps at Malaga Bend. Active dissolution of halite from the upper part of the Salado Formation occurs in the solution breccia zone at the base of the Rustler Formation in Nash Draw (Brokaw et al. 1972). The brine solution is believed to be recharged by aquifers in the Rustler and above, and its discharge is thought to be primarily at the Malaga Bend brine seeps and the salt lakes in Nash Draw. Piper (1973) calculated that the salts discharged into the Pecos River between Malaga Bend and a point 6 miles (10 km) downstream amount to 310,000 tons (2.8 x 10^8 kg) of NaCl and 170 tons (1.5 x 10^8 kg) of $CaSO_4$ each year. This is equivalent to a loss of 0.16 vertical feet of salt section per thousand years, a rate of the same order of magnitude as that calculated from the subsidence of Nash Draw.

An alternative approach of estimating vertical dissolution was used by F.A. Swenson (Bachman and Johnson 1973). He investigated the tonnage of salt dissolved and discharged by springs and streams along the east flank of the basin and found the maximum tonnage for the many subbasins to be 955 tons per square mile of drainage area each year. If the discharge continued at that rate it would mean a vertical dissolution of about 0.5 foot of salt in 1,000 years, provided the dissolution was distributed evenly over the area drained.

A rate of lateral shallow dissolution of salt in the western part of the Delaware Basin has been estimated to be about 6 to 8 miles per million years horizontally (Bachman and Johnson 1973). These estimates were based on the assumption that the salt-bearing Salado Formation extended to the Capitan reef escarpment on the western edge of the basin at the end of Ogallala time. It is now recognized that dissolution of this salt could have occurred at previous times in the past, and the average rate of salt removal by shallow dissolution is believed to be much slower than those estimates which establish an upper bound.

As stated previously, it is estimated that about 50 percent of the original volume of salt has been removed from the Basin. In considering the rate at which the salt was removed, it is generally recognized that much of the erosion and dissolution probably occurred since the beginning of Cenozoic time. This is a period of major uplift and erosion. Anderson pointed out (1978) that the dissolution features are closely associated with Cenozoic and postuplift hydrologic and structural controls. Nevertheless, as early as Jurassic time the basin was tilted and the western portion shown on Figure 6.3-8 was exposed and subject to erosion (Bachman, 1976). The hydrologic and structural conditions were apparently similar at that time to those of the Cenozoic, and the Jurassic climate is recognized to have been wet. Thus, it seems quite likely that the deep dissolution and erosional processes of salt removal could have been significantly accelerated during the Jurassic period.

The rate of deep dissolution is difficult to assess, and Anderson (1978) does not believe that estimates can be made with any degree of confidence, considering the available data. He suggests that if it is assumed that 1) deep dissolution progresses at a constant rate, and 2) that significant dissolution did not begin until after stripping of the Ogallala Formation from the basin (3-4 million years ago), projection of that rate would imply all of the lower Salado salt would be removed in about another million years. However, he does not believe the assumptions are valid.

Deep dissolution, as hypothesized by Anderson, would seem to have been a significant geologic process in Jurassic time, as well as in the Cenozoic. It is apparent that further study of these factors is needed to fully assess the impact on the proposed site. Sandia Laboratories and the U.S. Geological Survey are currently performing studies to provide data which should aid in this evaluation (see Chapter 10).

6.4 HYDROLOGY DRILLING AND TESTING SUMMARY

6.4.1 HOLE NO. H-1

LOCATION: T.22 S., R.31 E., Sec. 29

ELEVATION: 3,403.2 feet (ground level)

DEPTH DRILLED: 848 feet

DATE COMPLETED: June 9, 1976

DRILLING CONTRACTOR: Sonora Drilling Co., Carlsbad, N. Mexico

DRILLING METHOD: Auger 18 inch hole (0-40 feet)
Rotary 7.88 inch hole with air-air/mist (40-731 feet)
Core 4.75 inch hole with air mist (731-842 feet)
Ream 9.88 inch hole (40-848 feet)

CASING RECORD: 10.75 inch O.D. steel surface pipe, (0-40 feet) cemented to surface
7 inch O.D. steel casing (0-848 feet), cemented to surface (cement plug to 797 feet, drilled to 831 feet)

GEOPHYSICAL LOGS: Differential Temperatures
BHC Acoustic
Compensated Densilog
Dual-Laterolog

Micro-Laterolog
Compensated Neutron-Gamma
Sperry-Sun Magnetic Survey
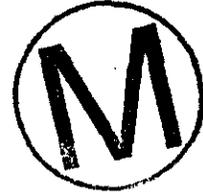
HYDROLOGIC TESTING (OPEN HOLE):

A. 699-842 feet: DST, of Rustler-Salado Contact, 9.1 gallons of water *in 20 hours*

B. 667-699 feet: DST of Culebra Dolomite, 10.6 gallons of water in 11.5 hours

C. 626-667 feet: DST, of suspected salt residue, 11.2 gallons of water in 12 hours.

D. 562-592: DST of Magenta Dolomite, 13 gallons of water in 13.5 hours; after hole was drilled to 592 feet inflow of 490 gpd was observed.

HYDROLOGIC TESTING (CASED HOLE):

E. 803-837 feet: Perforated zone, Rustler-Salado contact, water level rose from 826.5 to 811 (25 gallons) in 33 days.

F. 675-703 feet: Perforated zone, Culebra Dolomite, fluid level rose from 665 to 406 (416 gallons) in nine days.

G. Tracer, ^{131}I, no annulus leaks, no flow in 694-703 interval, major loss in 675-694 interval, tracer injection rate of 8 gpm, total 1634 gal. injected.

H. 562-590 feet: Perforated zone, Magenta Dolomite, after bailing, water rose from 424.5 to 340.7 feet in 33 days (53 gallons), could not bail below 424 feet.

I. Culebra water level stable at 390 feet depth.   (October 1977)

J. Magenta water level stable at 249 feet depth.   (October 1977)

DRILLING & TESTING SUMMARY

6.4.2 HOLE NO. H-2a

LOCATION: T.22 S., R.31, E., Sec. 29

ELEVATION: 3,377.1 feet (ground level)

DEPTH DRILLED: 563 feet

DATE COMPLETED: February 19, 1977

DRILLING CONTRACTOR: Pennsylvania drilling Co., Carlsbad, N. Mexico

DRILLING METHOD: Auger 18 inch hole (0-33 feet)
Rotary 8.75 inch hole with air-air/mist (33-513 feet)
Core 4.75 inch hole with air/mist (513-563 feet)
(cut 2.25 inch diameter core)

CASING RECORD: 10.75 inch O.D. steel casing (C-33 feet) cemented to
surface
6.63 inch O.D. steel casing, (0-511 feet), cemented to surface

Geophysical Logs: None. Available from H2C, 90 feet away.

HYDROLOGIC TESTING:

A. 0-188 feet: Stopped drilling after encountering wet zone at 185
feet; interval produced no appreciable fluid in 5 hours

B.   513-563 feet: Open hole, Magenta Dolomite, water rose from 556.8 to 538.7 in one day (22 gallons).

C. Magenta static level at 249 feet, October, 1977

DRILLING & TESTING SUMMARY

6.4.3   HOLE NO. H-2b

LOCATION: T.22 S., R. 31 E., Sec 29

ELEVATION: 3,377.1 feet (ground level)

DEPTH DRILLED: 661 feet

DATE COMPLETED: February 12, 1977

DRILLING CONTRACTOR: Pennsylvania Drilling Co., Carlsbad, N. Mexico

DRILLING METHOD: Auger 18 inch hole (0-33 feet)
Rotary 8.75 feet hole with air-air/mist (33-611 feet)
Core 4.75 inch hole with air/mist (611-661 feet) (cut 2.25 inch diameter core)

CASING RECORD: 10.75 inch O.D. steel casing (0-33 feet) cemented to surface
6.63 inch O.D. steel casing, (0-609 feet)., cemented to surface

Geophysical Logs: None. Available from H2C, 75 feet away.

HYDROLOGIC TESTING:

A.   611-661 feet: Open hole, Culebra cored interval, water rose from 636.9 to 458.0 feet in one day (260 gallons). Level stable at 352 feet (February 1977)

B.   Hole # H-2c was bailed from the Culebra while monitoring H-2b in the Culebra. First response in H2b was detected 50 minutes after bailing of H2C started.

C.   510-538 feet: Perforated zone, Magenta Dolomite, water rose from 560 to 420 feet in one day (210 gallons).

D. Well constructed for monitoring at Culebra Dolomite via tubing and Magenta via annulus. Culebra static level at 351 feet, Magenta static level at 292 feet (perforations may be blocked).

DRILLING & TESTING SUMMARY

6.4.4   HOLE NO. H-2c

LOCATION: T.22 S., R.31 E., Sec 29

ELEVATION: 3,377.1 feet (ground level)

DEPTH DRILLED: 795 feet

DATE COMPLETED: February 5, 1977

DRILLING METHOD: Auger 18 inch hole (0-33 feet)
Rotary 8.75 inch hole with air/mist (33-743 feet)
Core 4.75 inch hole with air/mist (743-795 feet)
(cut 2.25 inch diameter core)

CASING RECORD: 10.75 inch steel casing (0-33 feet) cemented to surface
6.63 inch O.D. steel casing, (0-742 feet), cemented to surface.

Geophysical Logs: Compensated Densilog
Dual-Laterolog
BHC Acoustilog
Micro-Laterolog

Compensated Neutron-Gamma

4-Arm Caliper

USGS Lithologic-log

HYDROLOGIC TESTING:

A.   743-795 feet: Open hole, Rustler-Salado cored interval produced 14 gallons in 18 days.

B.   624-652 feet: Culebra perforated zone, water rose from 656.4 to 446.6 in one day (310 gallons). Static level at 352 feet. (March 1977)

C. Tracer ^{131}I, no flow below 642 in casing, fluid loss zone was between 631 and 644, especially 640-644 where core indicates pitted and fractured dolomite, tracer injection rate was 8 gpm, total 697 gal. injected.

D. Dual completion monitoring (Rustler-Salado via tubing and Culebra via annulus) shows Culebra stable at 355 feet (October 1977) and Rustler-Salado still recovering at 34 feet per month. (June 1978)

DRILLING AND TESTING SUMMARY

6.4.5 HOLE NO. H-3

LOCATION: T.22 S., R.31 E., Sec. 29

ELEVATION: 3,388.7 feet (ground level)

DEPTH DRILLED: 894 feet

DATE COMPLETED: August 12, 1976

DRILLING CONTRACTOR: Pennsylvania Drilling Co., Carlsbad, New Mexico
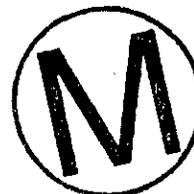
DRILLING METHOD: Auger 18 inch hole (0-38 feet)

Rotary 7.88 inch hole with air-air/mist (38-894 feet)

Ream 8.75 inch hole (38-894 feet)

CASING RECORD: 10.75 inch O.D. steel surface pipe (0-38 feet) cemented to surface.
6.63 inch O.D. steel casing, (0-891 feet), cemented to surface (cement plug to 804 feet drilled to 864 feet)

Geophysical Logs: Compensated Densilog
Micro-Laterolog
Dual-Laterolog
BHC Acoustilog
Compensated Neutron-Gamma
Differential Temperature

HYDROLOGIC TESTING (OPEN HOLE)

A. 800-868 feet: DST, Rustler-Salado contact, produced 1.8 gallons of water in 16.5 hours;

B. 672-703 feet: DST, Culebra, produced 2.1 gallons of water in 21.5 hours.

C. 703-780 feet: DST, salt residue, 2 gallons of water in 26 hours.

D. 558-608 feet: DST, Magenta, 23 gallons after 37.5 hours. after developing operation via swabbing.

HYDROLOGIC TESTING (CASED HOLE)

E. 813-837 feet: Perforated Rustler-Salado contact; produced 37 gallons in 32 days.

F.   675-703 feet: Perforated Culebra, bailed hole and monitored, recovery was up to 410 from an initial level of 550 feet (200 gallons in 8 days).

G.   Tracer ^{131}I, showed no flow below 696 feet; major fluid losses in intervals 684-692 and 692-695; tracer injection rate was 8 gpm, total injected 450 gal.

H.   562-590 feet: Perforated Magenta, bailed 360 gallons in one hour with 6 feet of drawdown.

I.   Dual-completion monitoring (Culebra via tubing and Magenta via annulus)   indicate Culebra static level at 404.5 and Magenta static level at 245.1 as of October 1977.

DRILLING & TESTING SUMMARY

6.4.6   HOLE NO. P-14

LOCATION: T.22 S., R.30 E., Sec. 24

ELEVATION: 3,358.1 feet (ground level)

DEPTH DRILLED: 1,545 feet.

DATE COMPLETED: October 3, 1976

DRILLING CONTRACTOR: Boyles Brothers Drilling Co., Las Cruces, New Mexico

DRILLING METHOD: Rotary 8.75 inch hole with air (0-20 feet)
Rotary 7.88 inch hole with air-air/mist (20-784 feet)
Rotary with air/mist (784-1,168 feet)
Core with brine mud (1,168-1,545 feet)

CASING RECORD: 8.63 inch O.D. steel casing (0-20 feet)

4.50 inch O.D. steel casing, (0-775 feet) cemented to surface, hole

plugged back from 1,345 feet to 759 feet with cement.

Geophysical Logs: Gamma

Gamma-Gamma

Neutron

Caliper

HYDROLOGIC TESTING (CASED HOLE)

A.   676-700 feet: Perforated Rustler-Salado, fluid level rose from 730

to 620 feet in one day (75 gallons).

B.   573-601 feet: Perforated Culebra, bailed 720 gallons of water in

three hours with no drawdown.

C.   Tracer ^{131}I, showed 63 percent fluid loss in interval 583-590,

remaining loss in interval 573-583; no loss below 590 feet.   Injection

rate 7 gpm.   Total injected 1634 gal.

D.   Dual-completion monitoring (Rustler-Salado via tubing and Culebra via

annulus); Rustler-Salado stabilized at 386 feet, Culebra stabilized at

324 feet (October 1977)

DRILLING & TESTING SUMMARY

6.4.7   HOLE NO. P-15

LOCATION: T.22 S., R.31 E., Sec. 31

ELEVATION: 3,309.7 feet (ground level)

DEPTH DRILLED: 1,465 feet

DATE COMPLETED: October 14, 1976

DRILLING CONTRACTOR: Boyles Brothers Drilling Co., Las Cruces, New Mexico.

DRILLING METHOD: Rotary 8.75 inch hole with air (0-20 feet)
Rotary 7.88 inch hole with air-air/mist (20-515 feet)
Core 4.75 inch hole with air/mist (515-600 feet) (cut 2.25 inch diameter core)
Ream 7.88 inch hole with air/mist (515-637 feet)
Rotary 5 inch hole with air/mist (637-1,038 feet)
Core with brine mud (1,038-1,465 feet)

CASING RECORD: 8.63 inch O.D. steel casing (0-20 feet)
4.50 inch O.D. steel casing, (0-635 feet), cemented to surface, hole plugged back from 1,465 to 600 feet with cement, cement drilled out to 620 feet.

Geophysical Logs: Gamma
Gamma-Gamma
Neutron
Caliper
Spectralog
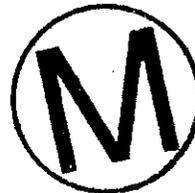
HYDROLOGIC TESTING:

A.   532-556 feet: Perforated Rustler-Salado contact, fluid rise from 618 to 497 in 42 days (81 gallons).

B.   410-438 feet: perforated Culebra, fluid rose from 496 to 420 feet in one day (50 gallons); 125 gallons in 33 days

C.   Dual Completion monitoring (Rustler-Salado via tubing and Culebra via annulus) shows Rustler-Salado static level at 324 feet and Culebra at 308 feet as of October, 1977.

DRILLING AND TESTING SUMMARY

6.4.8 HOLE NO. P-17

LOCATION: T.23 S., R.31 E., Sec. 4

ELEVATION: 3,339.5 feet (ground level)

DEPTH DRILLED: 1,660 feet

DATE COMPLETED: October 26, 1976

DRILLING CONTRACTOR: Boyles Brothers Drilling Co., Las Cruces, New Mexico.

DRILLING METHOD: Rotary 8.75 inch hole with air (0-20 feet)
Rotary 7.88 inch hole with air-air/mist (20-755 feet)
Rotary with air/mist (755-1,220 feet)
Core with brine mud (1,220-1,660 feet)

CASING: 8.63 inch O.D. steel casing (0-20 feet)
4.50 inch O.D. steel casing, (0-751 feet), cemented to surface, hole plugged back from 1,660 feet to 720 feet with cement, cement drilled out to 731 feet.

Geophysical Logs: Gamma
Gamma-Gamma
Neutron
Caliper

HYDROLOGIC TESTING (CASED HOLE)

A.   702-726 feet: Perforated Rustler-Salado contact; fluid rose from 726 to 622 feet (71 gallons in 73 days).

B. 558-586 feet: Perforated Culebra, single packer set at 683 feet, bailed and monitored for 29 days with fluid rise from 622 to 372 feet.

C. Dual Completion monitoring (Rustler-Salado via tubing and Culebra via annulus) indicates fluctuating levels; problem could be leaking bridge packer or communication in cemented annulus.

DRILLING & TESTING SUMMARY

6.4.9 HOLE NO. P-18

LOCATION: T.22 S., R.31 E., Sec. 26

ELEVATON: 3,478.7 feet (ground level)

DEPTH DRILLED: 1,998 feet

DATE COMPLETED: November 5, 1976

DRILLING CONTRACTOR: Pennylsvania Drilling Co., Carlsbad, New Mexico.

DRILLING METHOD: Rotary 8.75 inch hole with brine mud (0-18 feet)
Rotary 7.88 inch hole with brine mud (18-1139 feet) to casing depth.
Rotary with brine mud (1,139-1,630 feet)
Core with brine mud (1,630-1,998 feet)

CASING RECORD: 8.63 inch O.D. steel casing (0-18 feet)
4.50 inch O.D. steel casing, (0-1, 138 feet), cemented to surface, hole plugged back from 1,998 feet to 1,125 feet with cement.

Geophysical Logs: Gamma
Gamma-Gamma
Neutron
Caliper

HYDROLOGIC TESTING (CASED HOLE)

A.   1076-1100 feet: Perforated Rustler-Salado contact, fluid rise from 1123 to 1073 feet in 73 days (34 gallons)

B.   912-940 feet: Perforated Culebra, bailed and monitored recovery for 33 days with fluid rise from 1045 to 1022 feet (16 gallons).

C.   Dual completion (Rustler-Salado via tubing, Culebra via annulus) indicated Rustler-Salado at 755 feet and still recovering as of October, 1977.

DRILLING & TESTING SUMMARY

6.4.10   HOLE NO. AEC-8

LOCATION: T.22 S., R.31 E., Sec. 11

ELEVATION: 3,531.9 feet (ground level)

DEPTH DRILLED: 3,019 feet (1974), deepened to 4,910 feet (1976)

DATE COMPLETED: August 5, 1976

DRILLING CONTRACTOR: Sonora Drilling Co., Carlsbad, New Mexico

DRILLING METHOD: Core, ream, rotary 7.88 inch hole with brine mud (31-3,019 feet)
Core, ream, rotary 7.88 inch hole with brine mud (3,018.5-4,910.5 feet)

CASING RECORD: 8.63 feet O.D. steel casing (0-874 feet), cemented to surface.
5.50 inch O.D. steel casing, (0-4,907 feet), cemented to 880 feet.

Geophysical Logs; Compensated Neutron

Micro-Laterlog

Dual-Laterolog

Gamma

HYDROLOGIC TESTING (CASED HOLE)

A. 4,844-4,860 feet: Perforated lower sand lense of Bell Canyon Formation; fluid level rose from 4126 feet to 4095 feet in 166 minutes (31 gallons).

B. 4,832 - 4,910 feet: Production packer with sentry monitoring device showed formational pressure of 2037 lbs/ in^2 reached in 44.5 hours; fluid density was 1.11 g/cm^3.

C. Tracer ^{131}I, along with temperature logs, indicated major fluid loss in interval 4839 to 4860 feet; minor communication down casing to 4870 feet; tracer injection rate was 14 gpm. Total injected 2289 gal.

D. 4,821-4,827 feet: Perforated upper sand lense of Bell Canyon Formation; single packer set at 4835 feet; swabbed fluid to 2600 feet; pressure monitor installed at 4805 feet; shut-in pressure recovered to 2037 lbs/in^2 in 57 hours, fluid density was 1.12 gm/cm^3,

E. Tracer ^{131}I, showed no upward or downward communication; injection rate at tracer was 11 gpm. Total injected 300 gal. Injection was occurring uniformly in the lower 4 feet of perforations.

F. Dual completion monitoring (lowering sand via tubing and upper sand via annulus) indicate lower sand stablized at 615 feet and upper sand at 560 feet as of November, 1977.

6.5 SUMMARY

The proposed site contains neither perennial streams nor surface water impoundment, and the water bearing strata above and below the evaporite section do not yield large quantities of water to wells. At its closest point, the Pecos River is approximately 14 miles southwest of the WIPP site. Water bearing strata in the local site area at stratigraphic horizons above the proposed repository include the Santa Rosa Sandstone and the Culebra and Magenta members of the Rustler Formation. Hydrologic units below the repository horizons include the Bell Canyon Formation of the Delaware Mountain Group. Ground water velocities vary with porosity, hydraulic conductivity, and head gradient but are typically 0.3 ft/d in the Santa Rosa Sandstone, 0.5 ft/d in the Rustler Formation, and 0.0006 ft/d in the Bell Canyon Formation. Shallow wells in the local area are generally used only for watering livestock and typically produce nonpotable ground water with total solute concentrations in excess of 3,000 ppm.

Natural potentiometric levels of fluids from rocks above and below the evaporites at the WIPP site (from the Rustler and Bell Canyon Formations, respectively) are comparable (about 2950 to 3050 above mean sea level). The head differential between upper and lower units varies within about 200 feet on the periphery of the site, the sign and magnitude of the differential depending upon precise geographic location.

Gentle eastward tilting of the Delaware Basin resulting in the exposure of the Salado Formation to near-surface waters has given rise to the removal of a wedge-shaped mass of soluble salts between the Guadalupe escarpment (30 miles due west of the site), where there remains no rock salt, and a point about 3 miles due west of the site center, where the Salado Formation is intact.

The proposed site is in an area of the Delaware Basin that is free of regional deep dissolution, but localized shallow features are present in the vicinity. A shallow salt dissolution zone (called the "brine aquifer") occurs in Nash Draw at the contact between the Salado and

Rustler Formations. This local shallow dissolution area ranges in width from 2 to 10 miles and has a length of approximately 30 miles. The brine solution flows southwesterly at a rate of about 0.2 ft/d and discharges into the Pecos River at Malaga Bend. The average rate of vertical dissolution has been estimated to be between 0.33 and 0.5 feet per 1,000 years, and the average rate for lateral dissolution has been estimated to be between 6 and 8 miles per million years.

Climatological records show that mean annual precipitation of the site is approximately 12 inches per year. Aided by the low relative humidity (typically 36% during daylight hours) and high mean annual temperature (61°F), most of the annual precipitation returns to the atmosphere through evaporation and transpiration. Runoff is typically 0.1 to 0.2 inches annually.
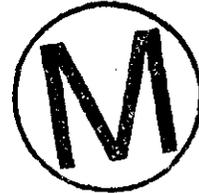
6.6 REFERENCES

Anderson, R.Y., Dean, W.E., Kirkland, D.N., and Snider, H.I., 1972, Permian Castile varved evaporite sequence West Texas and New Mexico: Geol. Soc. Amer. Bull. v. 83, p. 59-86.

Anderson, R. Y., 1978, Report to Sandia Laboratories on deep dissolution of salt, northern Delaware Basin, New Mexico, January 1978, 98pp.

Anderson, R.Y., and Powers, D. W. (in press). Salt anticlines in the Castile-Salado evaporite sequence, Northern Delaware Basin, New Mexico, Symposium on the Ochoan rocks of southeastern New Mexico and West Texas, Cir. 159, New Mexico Bureau of Mines and Mineral Resources.

Bachman, G.O., and Johnson, R., 1973, Stability of salt in the Permian Salt Basin of Kansa, Oklahoma, Texas and New Mexico: U.S. Geol. Survey Open-file report 4339-4.

Bachman, G.O., 1974, Geologic processes and Cenozoic history related to salt dissolution in southeastern New Mexico: U.S. Geol. Survey Open-file report 74-194.

Bachman, G. O., 1976, Cenozoic deposits of southeastern New Mexico and an outline of the history of evaporite dissolution: U.S. Geol. Survey, Jour. Research v. 4, No. 2, p. 135-149.

Barr, G.E., Lambert, S.J., and Carter, J.A., 1978, Uranium isotope disequilibrium in groundwaters of southeastern New Mexico and implications regarding age-dating of waters. SAND77-1779. IAEA-SM-228/32, Sandia Laboratories, Albuquerque, New Mexico.

Bjorklund, L. J. and Motts, W. S., 1959, Geology and water resources of Carlsbad area, New Mexico: U.S. Geol. Survey Open-file report 59-9.

Blaney, H.F., and Hanson, E.G., 1965, Consumptive use and water requirements in New Mexico: New Mexico state engineer, technical report 32.

Brokaw, Arnold L., Jones, C.L., Cooley, M.E., and Hays, W.H., 1972, Geology and hydrology of the Carlsbad potash area, Eddy and Lea Counties, New Mexico: U.S. Geol. Survey Open-file report 4339-1.

Cooper, J.B., 1962, Ground-water investigations of the Project Gnome area, Eddy and Lea Counties, New Mexico: U.S. Geol. Survey Report REI-802.

Cooper, J. B., and Glanzman, V. M., 1971, Geohydrology of project Gnome site, Eddy County, New Mexico: U.S. Geol. Survey, Prof. Paper 712-A, 24 p.

Gard, L.M., Jr., 1968, Geologic studies, Project Gnome, Eddy County, New Mexico: U.S. Geol. Survey Prof. Paper 589.

Griswold, G. B., 1977, Site selection and valuation studies of the Waste Isolation Pilot Plant (WIPP), Los Medanos, Eddy County, New Mexico: SAND77-0946 Sandia Laboratories, Albuquerque, New Mexico.

Hale, W. E., Hughes, L.S., and Cox, E.R., 1954, Possible improvement of quality of water of the Pecos River by diversion of brine of Malaga Bend, Eddy County, New Mexico: Report of the Pecos River Commission, New Mexico and Texas with U.S. Geol. Survey Water Resources Division.

Hendrickson, G. E., and Jones, R. J., 1952, Geology and ground water resources of Eddy County, New Mexico: New Mexico Bureau of Mines and Mineral Resources, Ground-Water Report 3.

Hiss, W.L., 1975a, Stratigraphy and ground-water hydrology of the Capitan Aquifer, southeastern New Mexico and western Texas, unpublished Ph.D. thesis, University of Colorado, Boulder, Colorado.

Hiss, W.L., 1975b, Thickness of the Permian Guadalupian Capitan aquifer, southeast New Mexico and west Texas: New Mexico Bureau of Mines and Mineral Resources, Resource Map 5.

Hiss, W.L., 1975c, Chloride-ion concentration in ground water in Permian Guadalupian rocks, southeast New Mexico and west Texas: New Mexico Bureau of Mines and Mineral Resources, Resource Map 5.

Hiss, W. L., 1976a, Structure of the Permian Ochoan Rustler Formation, southeast New Mexico and West Texas: New Mexico Bureau of Mines and Mineral Resources, Resource Map 7, 1976.

Hiss, W.L., 1976b, Structure of the Permian Guadalupian Capitan Aquifer southeast New Mexico and west Texas: New Mexico Bureau of Mines and Mineral Resources, Resource Map 6.

Jones, C. L., Cooley, M.E., and Bachman, G.O., 1973, Salt deposits of Los Medanos area, Eddy and Lea Counties, New Mexico, U.S. Geol. Survey Open-file report 4339-7.

Kelley, V.C., 1971, Geology of the Pecos country, southeastern New Mexico New Mexico Bureau of Mines and Mineral Resources, Memoir 24.

King, P. B., 1948, Geology of the southern Guadalupe Mountains, Texas: U.S. Geol. Survey Prof. Paper 215.

Lambert, S.J., 1977, The geochemistry of Delaware Basin groundwaters, Sandia Laboratories Report, Albuquerque, New Mexico, SAND77-0420. Report also in New Mexico Bureau of Mines and Mineral Resources, Circ. 159 (1978 - in press).

Lambert, S. J. and Mercer, J. W., 1977, Hydrologic investigations of the Los Medanos area, southeastern New Mexico, 1977: SAND77-1401, Sandia Laboratories, Albuquerque, New Mexico.

Lohman, S.⁻., 1972, Definitions of selected ground-water terms--revisions and conceptual refinements: U.S. Geol. Survey Water Supply Paper 1988.

Maley, V. C., and Huffington, R. M., 1953, Cenozic fill and evaporite solution in the Delaware Basin, Texas and New Mexico: Geol. Soc. Amer. Bull. v. 64, pp 539-546..

McNeal, R. P., 1965, Hydrodynamics of the Permian Basin Fluids, in subsurface environments symposium: Amer. Assoc. of Petrol. Geologists Memoir No. 4, p. 308-326.

Mercer, J.W., (to be published), Hydrologic tests and observations in the potash-hydro holes P-14, P-15, P-17, and P-18, U.S. Geol. Survey.

Mercer, J.W., and Orr, B. R., 1977, Review and analysis of hydrogeologic conditions near the site of a potential nuclear waste laboratory, Eddy and Lee Counties, New Mexico, U.S. Geol. Survey Open-file report 77-123.

Mercer, J. W., and Orr. B. R., 1978, Geohydrology of the proposed Waste Isolation Pilot Plant, southeastern New Mexico: U.S. Geol. Survey report submitted to DOE (preliminary).

Motts, W.S., 1957, Geology and ground water resources of the Carlsbad area, New Mexico, unpublished Ph.D. Thesis, University of Illinois (Urbana).

Nicholson, Alexander, Jr., and Clebsch, A., Jr., 1961, Geology and ground-water conditions in southern Lea County, New Mexico: Ground-water Report 6, New Mexico Bureau of Mines and Mineral Resources.

NOAA Environmental Data Service, 1977, Climatography of the United States, No. 60, Climate of New Mexico: U.S. Dept. of Commerce, March 1977.

Pettigrew, Richard R. and Assoc., 1977, WIPP conceptual design report (soils and foundation investigation): Prepared for Sandia Laboratories Albuquerque, New Mexico.

Pierce, W. G. and Rich, E. I., 1962, Summary of rock salt deposits in the United States as possible storage sites for radioactive waste materials: U.S. Geol. Survey Bull. 1148, 33-35P.

Piper, A.M., 1973. Subrosion in and about the four-township study area near Carlsbad, New Mexico, ORNL subcontract 3745, Oak Ridge National Laboratory, Oak Ridge, TN.

Reddy, G. R., 1961, Geology of the Queen Lake domes near Malaga, Eddy County, New Mexico: unpublished M.S. Thesis, Univ. of New Mexico.

Robinson, T. W., and Lang, W. G., 1938, Geology and ground water conditions of the Pecos River Valley in the vicinity of Laguna Grande de la Sal, New Mexico, with special reference to the salt content of the river water. N. Mex. State Engineer 12th and 13th Bienn. Repts., p. 77-100.

Rose, Walter, 1977, Development of a conceptual model to explain brine flowage into wells drilled thru the Salado-Castile Formation. Contact in locations such as the ERDA #6 site near Carlsbad in southeastern New Mexico: Report to Sandia Laboratories.

Theis, C.V., and Sayre, A.N., 1942, Geology and ground water, in (U.S.) National Resources Planning Board, 1942, Pecos River Joint Investigation-Reports of the participating agencies: Washington, U.S. Govt. Printing Office, P. 27-38.

U.S. Department of Agriculture, Soil Conservation Service, 1971, Soil survey of Eddy area, New Mexico, U.S. Government Printing Office, Washington, D.C.

U.S. Department of Agriculture, Soil Conservation Service, 1974, Soil survey of Lea area, New Mexico, U.S. Government Printing Office, Washington, D.C.

U.S. Department of Commerce, Weather Bureau, 1952, Mean number of thunderstorm days in the United States, Technical paper No. 19.

U.S. Department of Commerce, Weather Bureau, 1955, Rainfall intensity-duration-frequency curves. Technical paper No. 25.

U. S. Department of Commerce, Weather Bureau, 1969, Severe local storm occurrences, 1955-1967. Technical Memorandum WBTM FCST 12.

U.S. Department of Commerce, Weather Bureau, 1961, Climatological Survey Station, Carlsbad, New Mexico.

U.S. Department of Commerce and U.S. Department of Army, Weather Bureau and corps of Engineers, 1976, Hydrometeorological report No. 33, seasonal variation of the probable maximum precipitation east of the 105th meridian.

U.S. Department of the Interior, 1975, Preliminary regional environmental analysis record potash leasing in southeastern New Mexico: Bureau of Land Management, New Mexico State Office.

U.S. Geological Survey, 1976, Water resources data for New Mexico, water year 1976: U.S. Geol. Survey Water-Data Report NM-76-1.

U.S. Geological Survey Topographic maps, 15 minute series (1:62,500) for Nash Draw and Hat Mesa, New Mexico.

U. S. Geological Survey Topographic Maps, (1:250,000), NI 13-11 (Carlsbad) and NI 13-12 (Hobbs), New Mexico.

Vine, J. D., 1960, Recent domal structures in southeastern New Mexico: Amer. Assoc. Petrol. Geol. Bull., v. 44, no. 12, p. 1903-1911.

Vine, J. D., 1963, Surface geology of the Nash Draw quadrangle, Eddy County, New Mexico: U.S. Geol. Survey Bull. 1141-B.

Wolfe, H.G., editor, 1977a. An environmental baseline study of the Los Medanos Waste Isolation Pilot Plant (WIPP) project area of New Mexico: a progress report: SAND77-7017, Sandia Laboratories, Albuquerque, New Mexico.

Wolfe, H.G., editor, 1977b. An environmental baseline study of the Los Medanos Waste Isolation Pilot Plant (WIPP) project area of New Mexico: a progress report. An addendum: SAND77-7018, Sandia Laboratories, Albuquerque, New Mexico.

POTENTIOMETRIC SURFACE
OF THE GUADALUPIAN
AQUIFER SYSTEM

FIGURE 6.3-1
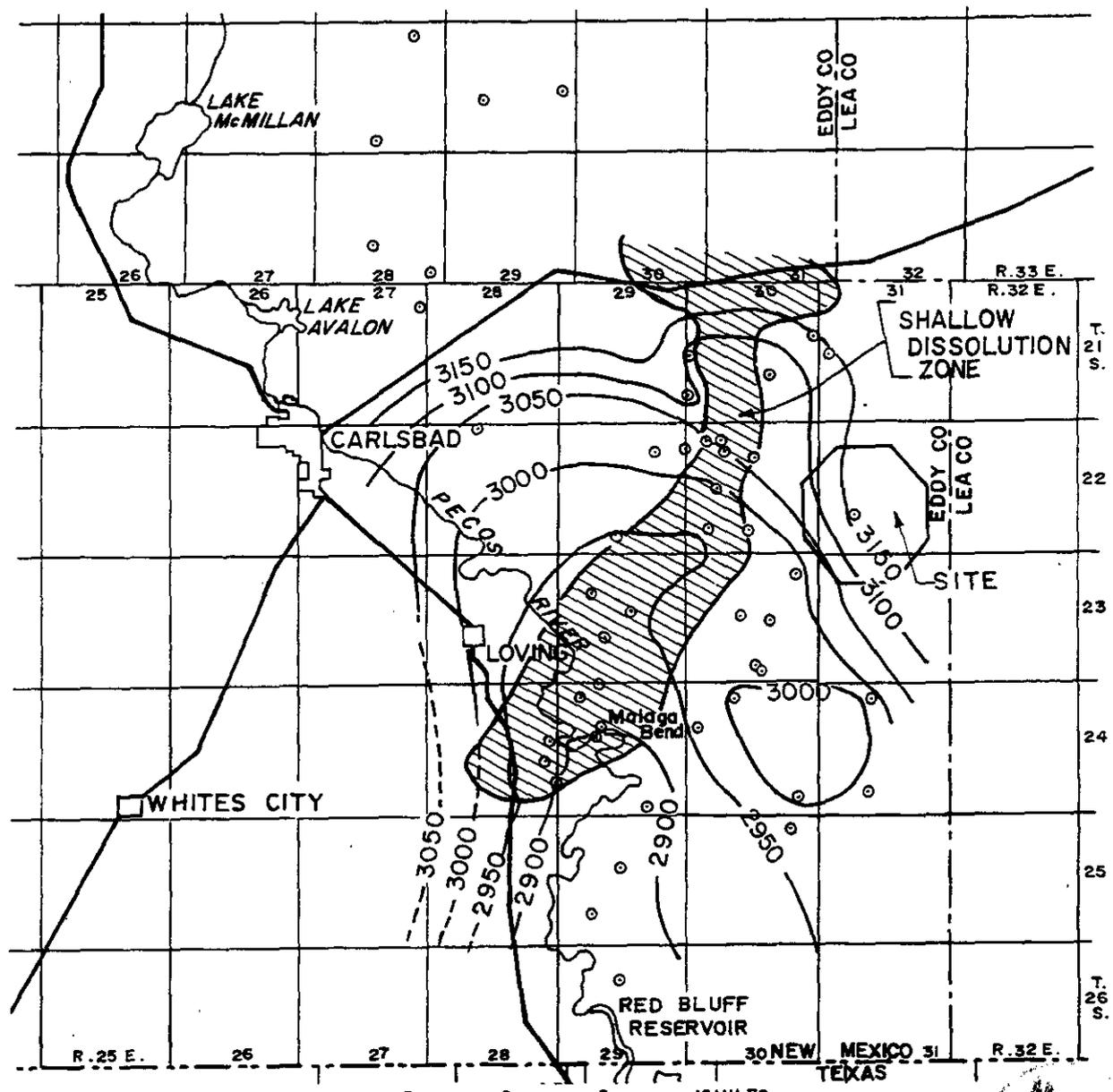
EXPLANATION

⊙ Well or exploratory hole open to the Rustler Formation

3000 -- Potentiometric elevation contour based on water levels measured
in wells, 1952-1973. Dashed where approximately located.
Datum is mean sea level.

Reference: Figures 5 & 6, U.S.G.S. Open File Rpt. 77-123, 1977

POTENTIOMETRIC SURFACE
RUSTLER FORMATION AND AREAL
EXTENT OF SHALLOW DISSOLUTION ZONE

FIGURE 6.3-2
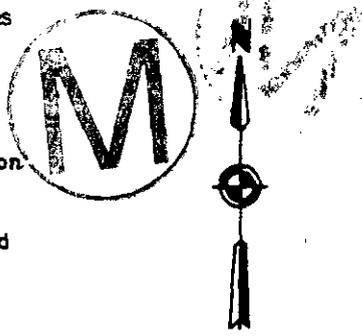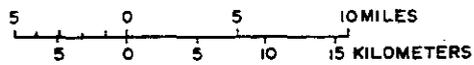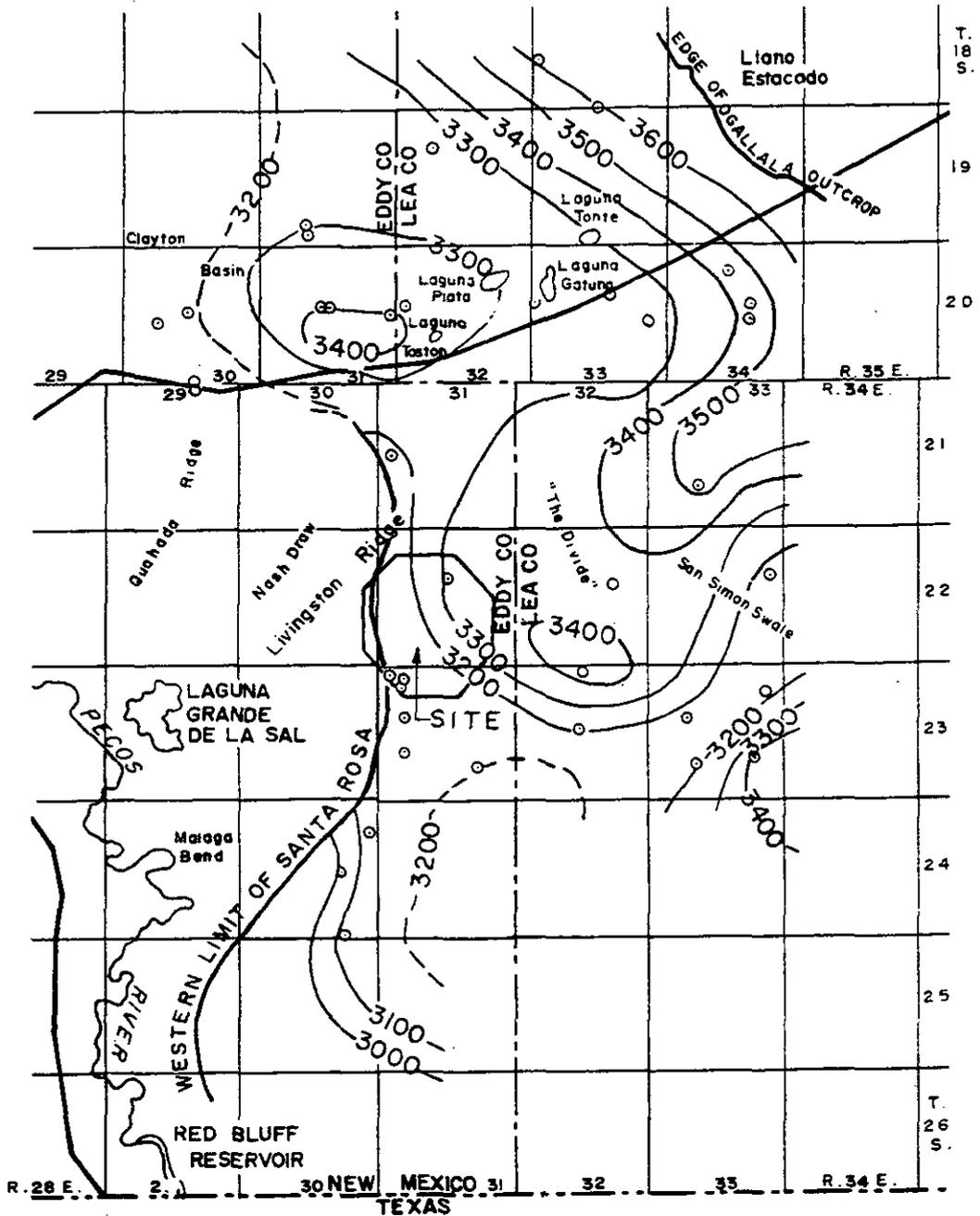
EXPLANATION

⊙ Well open to Triassic rocks

◠ Potentiometric elevation contour, based on water levels
measuerd in wells, 1952 –1973. Dashed where approximately
located. Datum is mean sea level.

POTENTIOMETRIC SURFACE
SANTA ROSA SANDSTONE

Reference:
Mercer and Orr, 1977, figure 7.

FIGURE 6.3-3
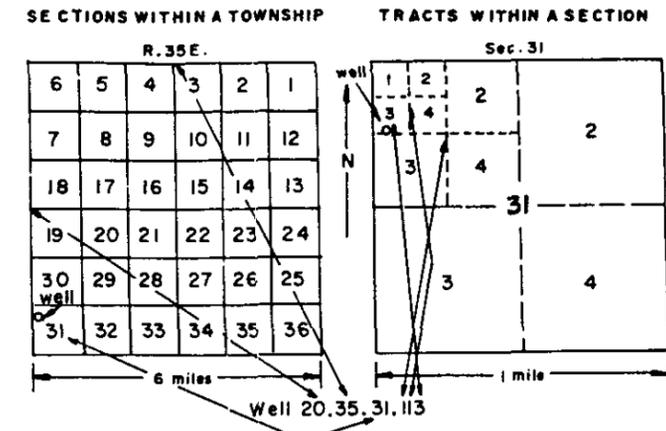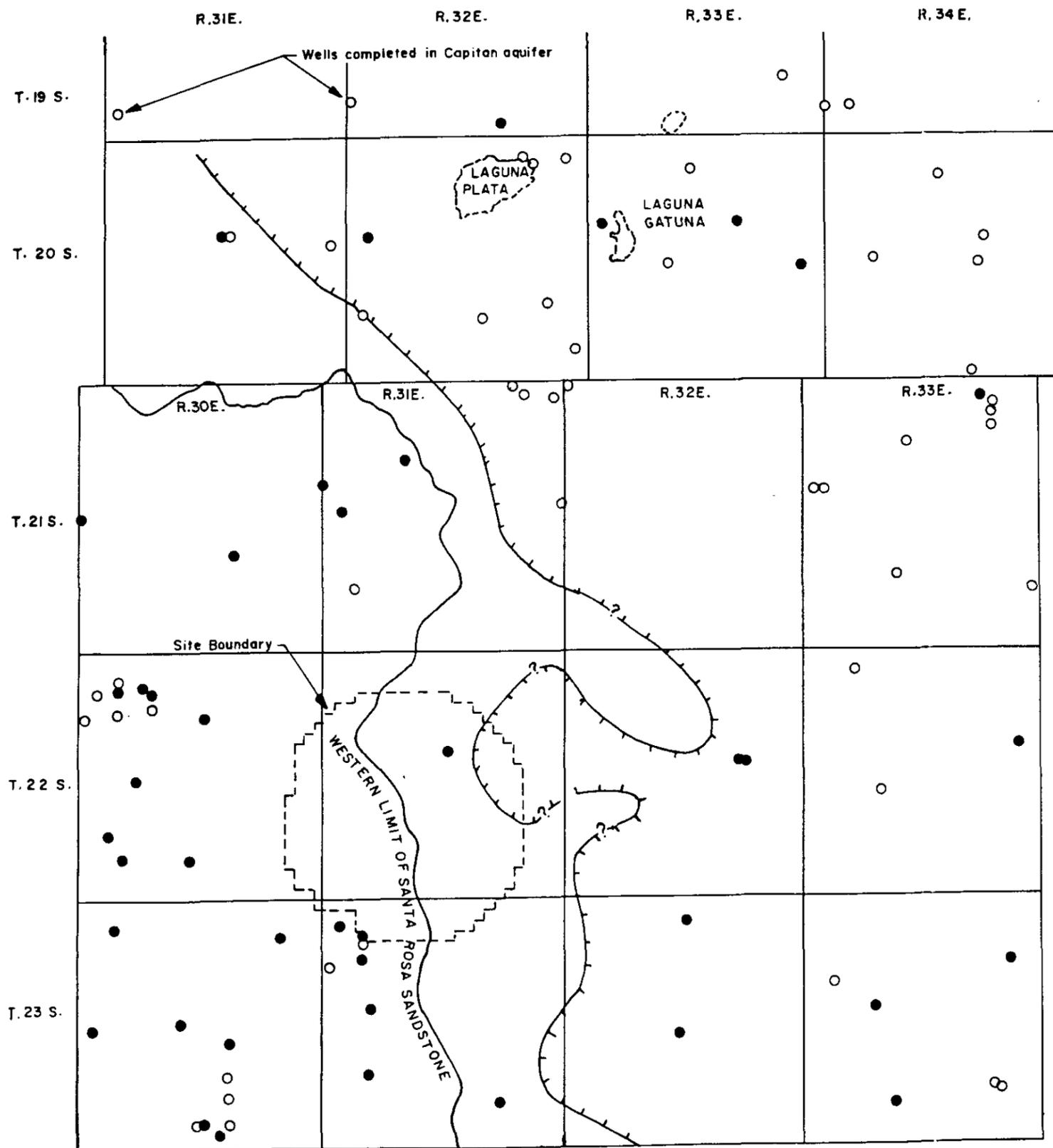
WELL-NUMBERING SYSTEM

The well number consists of four parts separated by periods. The first part is the township number, the second part is the range number, and the third part is the section number. The fourth part of the number consists of three digits which denote the particular 10-acre tract within the section in which the well is located.

EXPLANATION

⊥⊥⊥⊥ Approximate western limit of occurrence of ground water in the Santa Rosa Sandstone.

○ Water well completed in surficial deposits or upper sandstone beds of the Chinle Formation.

● Water well completed in lower sandstone beds of the Chinle Formation, Santa Rosa Sandstone, Dewey Lake Redbeds, or Rustler Formation.

NOTE:
See Table 6.3—2 for descriptions of wells.

Reference: USGS Open File Report 4339-7, Jones, C.L., et al, 1973

SCALE IN MILES
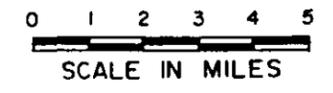
WATER WELL SURVEY

FIGURE 6.3-4

R.30 E.   R.31 E.

PROPOSED LAND
WITHDRAWAL
BOUNDARY

●AEC NO.8

LOS

PIPELINE

ERDA NO. 9

A

●P14   P3●   ●P2
        H1●
    H2
P6●   CONTROL ZONE
        BOUNDARIES

●H3   27

SEE DETAIL   MEDAÑOS   A'
                    ●P18

36   31   36

●P15

6   1

●P17

T.22 S.

T.23 S.

DETAIL
(H2 Configuration)

H2C
75'   90'
H2B●   N
50'
    H2A

SCALE IN MILES
0   1   2
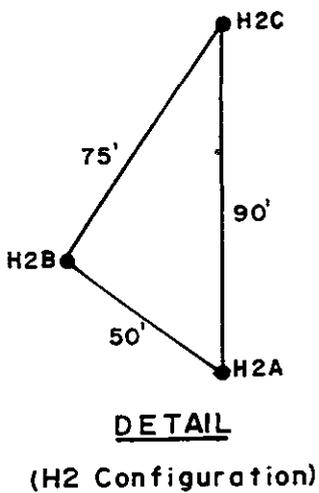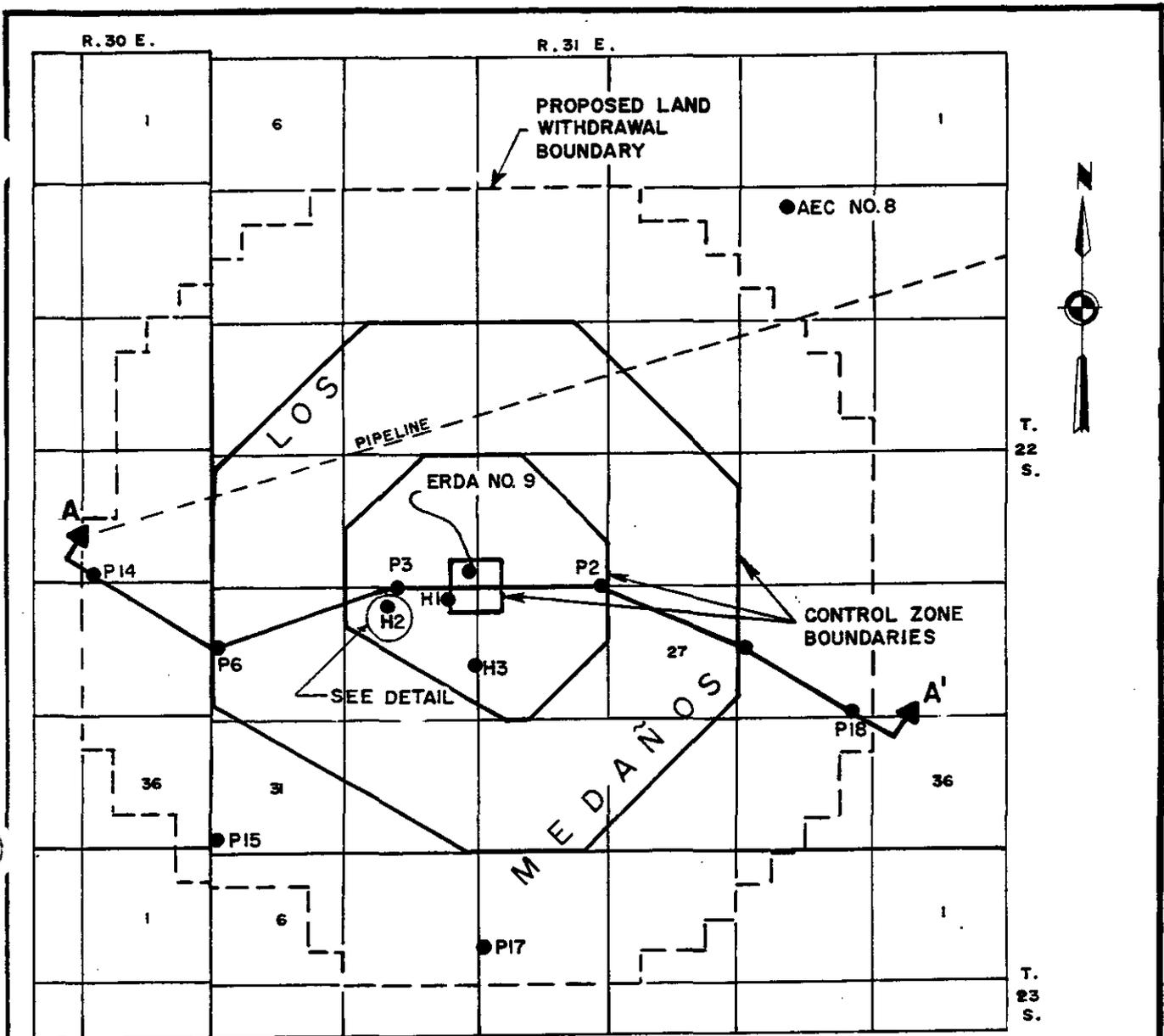
See figure 6.3-7 for
Section A-A'

HYDROLOGIC TEST HOLES

FIGURE 6.3-5

DEPTHS IN FEET

Elevation of Ground Surface 3388.7 ft.

0

22 — Dune sand & Gatuna Formation

DEWEY LAKE

10 3/4 inch ∅ casing to 38 ft.

6 5/8 inch ∅ casing to 894 ft.

Cement grout

REDBEDS

2 inch ∅ tubing to production packer (652 ft.)

502

RUSTLER

Perforated interval, 564-592 ft. (3-1/2 inch jet shots per foot)

Magenta Dolomite (560-584)

Inflatable production packer at 652 ft.

Culebra Dolomite (670-694)

Perforated interval, 675-703 ft. (3-1/2 inch jet shots per foot)

Top of Salt @ 718

FORMATION

Inflatable bridge plug at 795 ft.

820

Perforated interval, 813-837 ft. (3-1/2 inch jet shots per foot)

SALADO

FORMATION

Top cement plug 864 ft.

Status October 1977:

Total depth drilled : 894 ft.
Diameter of drilled hole : 9 7/8 inch
Monitoring Culebra through tubing
Monitoring Magenta in annulus
Contact zone not accessible (bridge plug)

CONSTRUCTION OF OBSERVATION WELL

FIGURE 6.3-6
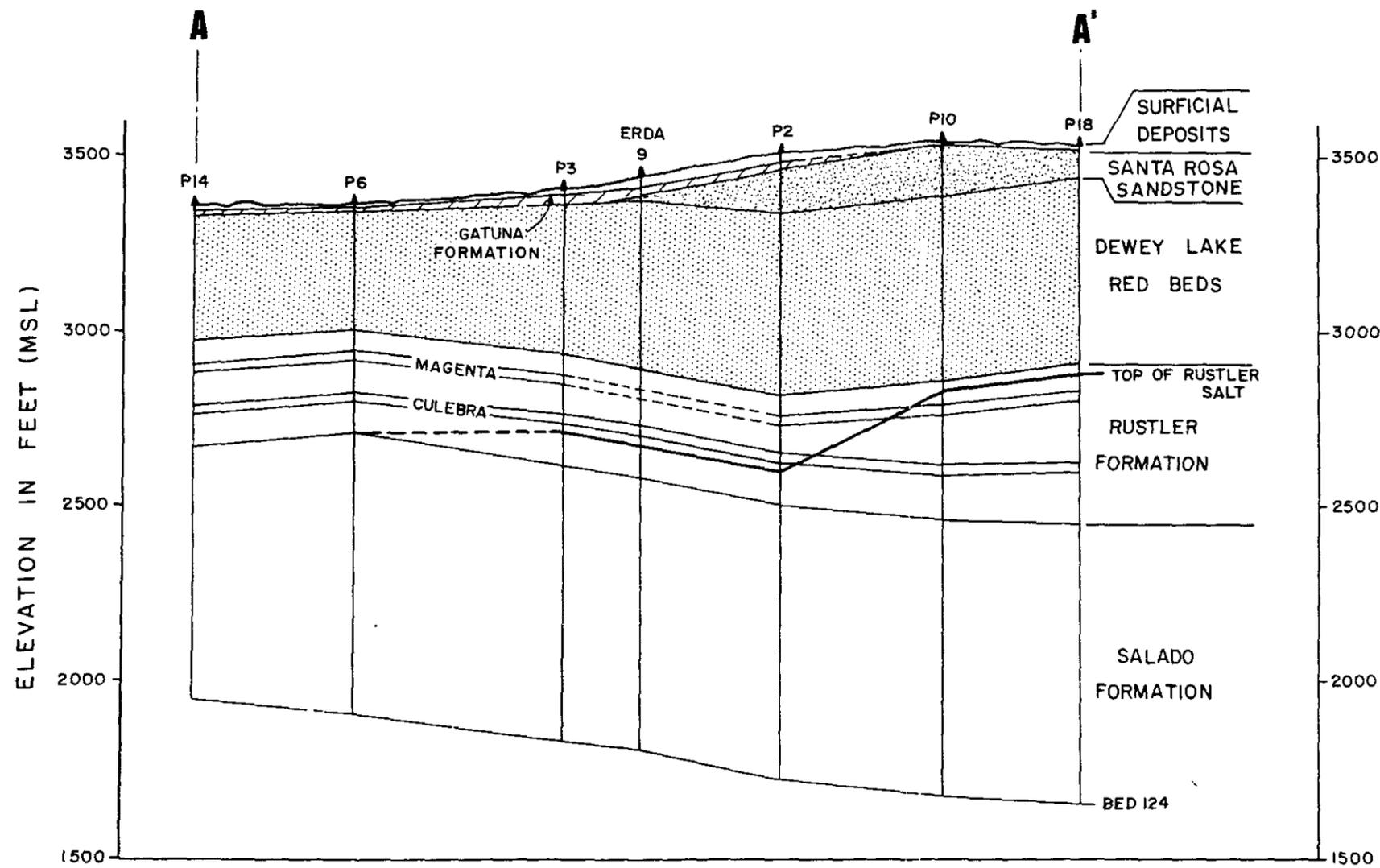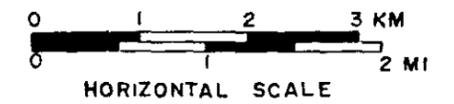
GEOLOGIC SECTION
THROUGH THE LOS MEDANOS AREA

FIGURE 6.3-7

EXPLANATION

- DISSOLUTION WEDGE
- EXTENT OF CENOZOIC FILL
- DEEP CENOZOIC FILL
- AREA SUBJECT TO EROSION DURING JURASSIC TIME (BACHMAN 1976)

Reference: Based on Figure 1 from Anderson, 1978

DISSOLUTION FEATURES AND EXTENT OF EROSION IN DELAWARE BASIN

FIGURE 6.3-8

RELATIONSHIP OF
NASH DRAW TO DISSOLUTION
IN SALADO FORMATION

FIGURE 6.3-9

Reference: Fig. II, USGS Open File
Report 74-194, 1974

Table 6.2-1.   AREAL REQUIREMENTS OF THE WIPP SITE

Zone	Zone Use	Approximate Acreage
I	Surface Facilities	60-(100)
II	Underground Storage	1,860
III	1-mile wide zone surrounding Zone II No mining or drilling.	6,230
IV	1-mile wide zone surrounding Zone III. Mining and drilling in conformance with ERDA specifications are allowed.	10,810
	TOTAL	18,960
		29.6 square miles

TABLE 6.2-2

SALIENT FEATURES OF MAJOR DAMS UPSTREAM AND

DOWNSTREAM FROM WIPP SITE

Name of Reservoir	River	Drainage Area (sq. mi.)	Type of Dam	Year Completed	Height (ft.)	Max. Storage Capacity (AF)	Purpose
Sumner	Pecos	4,390	earth	1937	143	258,500	Irrigation
McMillan	Pecos	16,990	earth	1908	40	66,600	Irrigation
Avalon	Pecos	18,070	earth	1907	40	36,600	Irrigation
Red Bluff	Pecos	20,720	earth	1937	98	405,000	Irrigation & Hydro-power
Two Rivers	Rio Hondo Rocky Arroyo	963 64	earth earth	1963 1963	93 116	262,221	Flood Control

TABLE 6.2-3

WATER USE DATA FOR THE PECOS BASIN

Use category	Surface-water and groundwater withdrawals (mgd) 1975[a]
Agriculture	1546
Steam-electricity	12
Manufacturing	0
Domestic	47
Commercial	8
Mining	151
Public lands	4
Fish hatcheries	3
Total	1771
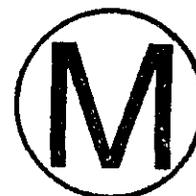
SOURCE: U.S. Water Resources Council, Second National Assessment of Water and Related Land Resources, in press.

[a]The total groundwater withdrawal for 1975 was 1079 mgd.

TABLE NO. 6.2-4

PRECIPITATION AT CARLSBAD, N.M. (in inches)

Period of Record   1931-1960

MONTH	JAN.	FEB.	MARCH	APRIL	MAY	JUNE	JULY	AUG.	SEPT.	OCT.	NOV.	DEC.	ANNUAL
Max. Precip	2.31	1.93	4.27	3.99	12.28	6.24	5.48	4.41	7.36	6.13	1.55	2.12	33.94
Av. Precip.	0.44	0.37	0.46	0.54	1.76	1.33	1.56	1.60	1.94	1.61	0.35	0.47	12.43
Min. Precip.	0	0	0	0	0.18	0	0	0.01	0	0	0	0	4.40

SOURCE: U. S. Weather Bureau, 1961.

)   )   )

TABLE NO. 6.2-5

TEMPERATURES AT CARLSBAD, N.M. (in °F)

Period of Record   1931-1960

MONTH	JAN.	FEB.	MARCH	APRIL	MAY	JUNE	JULY	AUG.	SEPT.	OCT.	NOV.	DEC.	ANNUAL
Max. Temp	50.4	54.8	61.2	69.1	74.6	83.6	84.2	84.6	80.6	70.8	57.4	52.6	66.3
Av. Temp.	43.8	48.4	54.8	63.3	71.4	79.8	81.4	80.8	74.2	64.1	51.5	44.7	63.2
Min. Temp.	35.2	43.6	47.8	60.1	68.4	73.4	77.4	76.7	70.2	58.2	45.8	37.5	60.3

SOURCE: U. S. Weather Bureau, 1961.

TABLE NO. 6.2-6

WATER QUALITY PARAMETERS (TIME-WEIGHTED AVERAGE)
FOR SAMPLING STATIONS ON THE PECOS RIVER,
OCTOBER, 1975, TO SEPTEMBER, 1976

Station No.	Discharge (cfs)	pH	Dissolved-solids concentration (mg/1)				
			Total	Chloride	Sulfate	Sodium	Calcium
08405000 (Carlsbad)	12	7.7	2,500	531	1100	322	334
08406500 (Near Malaga)	26	7.7	5,390	1690	1820	1030	524
08407000 (Pierce Canyon Crossing)	28	7.5	13,900	6500	2280	4020	551

SOURCE: U. W. Geological Survey, Water-Data Report NM-76-1.

TABLE NO. 6.3-1 AQUIFER CHARACTERISTICS OF THE GUADALUPIAN AGE ROCKS (ADAPTED FROM HISS, 1976, TABLES 6 AND 7)

Geologic Unit	Avg. Hydraulic Conductivity (ft/day)	Average Porosity (%)	No. of samples or tests	
			Conductivity	Porosity
Rock Core Analysis				
Tansill Fm.	0.006	4.23	399	381
Yates Fm.	0.026	9.74	11,287	11,387
Seven River Fm.	0.140	6.56	4,367	4,485
Queen Fm.	0.029	7.79	7,324	7,648
Grayburg Fm.	0.032	7.15	1,971	1,973
Grayburg-San Andres (Und.)	0.033	5.76	7,062	7,313
Glorieta Sandstone	0.027	9.16	3,128	3,115
Delaware Mt. Gp.	0.016	15.65	4,549	4,493
Pumping Tests (San Andres)				
T.20S, R.38E, Sec. 7	0.20		(Drawdown Test)	
Same well as above	0.20		(Recovery Test)	
T.22S, R.37E, Sec. 29	0.30		(Drawdown Test)	
Pumping Tests (Capitan)				
T.21S, R27E, Sec. 5	2.4		(Recovery Test)	
T.21S, R.28E, Sec. 30	16.0		(Recovery Test)	
T.21S, R.34E, Sec. 24	3.0		(Specific Capacity)	
T.21S, R34E, Sec. 14	1.7		(Specific Capacity)	
Same Well	1.9		(Drawdown Test)	
Same Well	1.4		(Recovery Test)	
T.24S, R36E, Sec 4	24.0		(Drawdown Test)	
T.24S, R36E, Sec. 16	7.4		(Specific Capacity)	
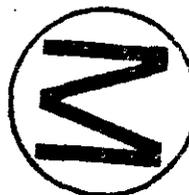
TABLE 6.3-2 -- Records of Wells in the Los Medanos Area, New Mexico
(Adapted from Cooley, 1972, Table 4)

Location Number	Altitude Above Mean Sea Level (feet)	Depth of Well (feet)	Diameter of Well Casing (inches)	Depth Below Land Surface (feet)	Date of Measurement	Geologic Source	Use and Remarks
19.32.34.434	3560	260	--	Dry	9-22-72	QTs, Trc, Trsr(?)	Unused; 3 wells at this locality; no access for entering casing in the other 2 wells.
19.33.26.244	3609	--	6	90.58	9-25-72	QTs, Trc(?)	Electric Submersible; stock.
26.244a	3609	101	--	90.93	9-25-72	QTs, Trc(?)	--
19.34.31.131	3620	53	6	Dry	9-25-72	QTs	Unused; 2 ft. of water in bottom of hole--probably does not represent true water level.
31.232	3632	120R	6	--	9-25-72	QTs, Trc(?)	Windmill; stock; "Hardin Well," no access to enter casing.
20.31.13.412	3440	30	6	1.12	9-18-72	QTs	Unused.
15.130	3460	105	6	62.10	9-18-72	QTs(?), Trsr	Unused.
15.130a	3460	79	6	63.39	9-18-72	QTs(?), Trsr	Unused; 5 wells at this location of which only 1 is an operating well.
15.130b	--	--	--	--	--	QTs(?), Trsr	Windmill; stock.
20.32. 1.312	3510	20	6	Dry	9-22-72	QTs	Unused; deepest of 4 wells at this location, all wells are dry.
24.333	3555	67	5	37.67	9-11-72	QTs	Unused
24.333a	3555	--	--	--	--	QTs(?)	Windmill; stock.
27.144	3545	30	--	23.67	9-18-72	QTs	Unused; no casing present.
36.214	3585	--	--	P43.88	9-18-72	QTs	Windmill; stock; 3 wells at this location at Bingham ranch, well pumping estimated at 2 gallons per minute.

TABLE 6.3-2 (continued)-- Records of Wells in the Los Medanos Area, New Mexico

Location Number	Altitude Above Mean Sea Level (feet)	Depth of Well (feet)	Diameter of Well Casing (inches)	Depth Below Land Surface (feet)	Date of Measure- ment	Geologic Source	Use and Remarks
20.33. 4.432	3555	4		Dry	9-22-72	QTs	Unused.
18.123	3521	249	6.5	245.58	9-25-72	Trc	Unused.
21.111	3536	49	6	36.90	9-25-72	QTs	Unused.
24.124	3630	680	12	405.15	9-22-72	Trc, Trsr(?)	Windmill; stock; "West Windmill," watersand at about 300 feet as reported by driller.
20.34. 4.444	3633	200	8	P174.08	10-2-72	Trc	Windmill; stock; "Robert's Well," old oil test drilled before 1930.
14.133	3648	230		190.25	10-2-72	Trc	Windmill; stock.
17.334	3640	220(?)	8	P129.68	10-2-72	Trc	Windmill; stock; "City Service Well," possibly oil test.
22.224	3655	220	12	196.49	10-2-72	Trc	Windmill; stock; "North Well," old oil test
34.432	3770	96	6	89.50	10-2-72	QTs	Windmill; stock.
21.30.18.333	3220	156	6	129.54	9-25-72	Pru	Unused.
22.423	3180	130	6	111.50	9-25-72	Pru	Unused.
21.31. 1.131	3580	30R	6	20.80	9-18-72	QTs	Windmill; domestic & in stock; at Campbell Ranch. "Grave Well."
1.241	3600	--	--	--	--	--	
2.221	3570	35	--	29.80	9-18-72	QTs	Windmill; stock.
7.331	3350	367	14	192.10	9-14-72	Pru, Prc (?)	Unused.
13.244	3600	68	6	Dry	9-13-72	QTs, Trc	Unused.
18.411	3310	--	6	158.32	9-14-72	Pru	Windmill; stock; "New Well."
30.421	3300	176	6	Dry	9-25-72	Pru	Unused.

Location Number	Altitude Above Mean Sea Level (feet)	Depth of Well (feet)	Diameter of Well Casing (inches)	Depth Below Land Surface (feet)	Date of Measurement	Geologic Source	Use and Remarks
21.32. 6.111	3598	54R	--	44.00R	9-18-72	QTs	Windmill; domestic & stock; at Allred Ranch; 2 wells at this location.
21.33. 2.231	3810	1150R	--	--	9-22-72	Trsr	Unused; could not pass tape below 550 feet in 1972.
2.420	3770	94	6	79.58	9-22-72	QTs	Windmill; stock.
4.434	3805	147	--	129.66	10-2-72	QTs(?), Trc	Unused.
4.434a	3805	127	--	Dry	10-2-72	QTs(?), Trc	Unused.
18.114	3890	150	--	140.75	9-12-72	QTs	Windmill; stock.
18.114a	3890	175	--	142.88	9-12-72	QTs	Unused.
18.123	3855	--	--	--	9-12-72	QTs(?)	Windmill; stock.
18.123a	3855	145	8	117.30	9-12-72	QTs	Unused.
18.131	3895	11	--	Dry	9-12-72	QTs	Unused.
25.421	3670	67	--	56.58	9-22-72	QTs	Windmill; stock; "West Well."
28.124	3688	210	8	179.00	9-22-72	Trc	Windmill; stock; "Standard Wells," 3 wells at this location.
22.30. 5.431	3120	225	14	53.25	9-19-72	Pru, Prc(?)	Unused.
6.444	3140	176	22	92.40	9-19-72	Pru	Unused.
7.244	3110	58	12	Dry	9-19-72	Pru	Unused.
10.311	3135	68	6	63.70	9-12-72	Pru	Unused; at Crawford Ranch.
20.120	3076	10	5	Dry	9-19-72	QTs, Pru	Unused.
32.111	3010	35	6	32.70	9-19-72	Pru	Unused.
22.31.15.130	3460	--	--	144.07	9-12-72	Trsr(?) Pdl	Windmill; stock.
15.130a	3460	--	--	145.50	9-12-72	Trsr(?) Pdl	Unused.

)))

TABLE 6.3-2 (continued)-- Records of Wells in the Los Medanos Area, New Mexico

Location Number	Altitude Above Mean Sea Level (feet)	Depth of Well (feet)	Diameter of Well Casing (inches)	Depth Below Land Surface (feet)	Date of Measurement	Geologic Source	Use and Remarks
22.32.14.323	3717	380	--	367.80	9-13-72	Trsr	Jenson Jack; stock; "Comanche Wells."
14.324	3720	380(?)	--	370.40	9-13-72	Trsr	Windmill; stock; "Comanche Wells."
22.33. 5.321	3650	10	6	0.0	9-22-72		Windmill; stock; well on edge of Dagger Lake.
13.231	3515	490	6	388.05	9-21-72	Trc	Windmill; stock; "Roger's Well."
13.231a	3515	400	6	388.05	9-21-72	Trc	Windmill; stock.
20.244	3602	--	--	--	--		Unable to locate well in 1972.
23.30. 2.444a	3250	315	7	257.73	9-20-72	Prc	Windmill; stock; "Little Windmill," well 444 destroyed.
6.424	2980	--	6	0.0	9-20-72	--	Unused; "Nash Well," area flooded by lake.
19.123	3045	--	7	68.55	9-20-72	Prc	Windmill; stock.
21.122	3165	--	5	--	9-20-72	Pru, Prc(?)	Windmill; stock; "Indian Well," no access for water level measurement.
		204	5	179.25	4-6-59	Pru, Prc(?)	
22.234	3210	244	--	227.32	9-20-72	Pru, Prc(?)	Unused.
33.244	3438	696	--	--	--	Pru, Prc	Abandoned; at Gnome Site, plugged 6-25-69, USGS No. 5.
34.133	3413	518	--	433.91	9-25-72	Pru, Prc	Observation; at Gnome Site, USGS No. 4.
				433.67	12-12-61	Pru, Prc	
34.133a	3413	--	--	427.03	9-25-72	Pru, Prc	Unused; at Gnome Site, USGS No. 8.
34.234	3401	568	6	415.70	4-14-62	Pru, Prc	Observation; at Gnome Site, USGS No. 6, drld to 1499' & plugged back to 568'.
34.234a	3402	563	6	418.10	4-16-62	Pru, Prc	Observation; at Gnome Site, USGS No. 7, drld to 1507' & plugged back to 563'.
34.324	3426	567	--	441.67	9-25-72	Pru, Prc	Observation; at Gnome Site, USGS No. 1.
				442.40	9-22-60	Pru, Prc	

Location Number	Altitude Above Mean Sea Level (feet)	Depth of Well (feet)	Diameter of Well Casing (inches)	Depth Below Land Surface (feet)	Date of Measurement	Geologic Source	Use and Remarks
23.31. 6.320	3300	213	8	144.72	2-4-59	Pdl	Windmill; domestic.
6.320a	3300	400R	--	--	--	Pdl, Pru	Windmill; domestic; tape will not pass 222' in 1972.
6.444	3310	--	6	106.35	9-20-72	Pdl	Windmill; domestic.
7.240a	3315	--	6	62.27	9-20-72	Pdl	Windmill; stock.
17.310	3305	--	--	--	9-20-72	Pdl, Pru	Windmill; stock.
26.340	3451	--	6	250.47	9-20-72	Pdl	Windmill; stock.
29.113	3335	--	4	139.90	9-20-72	Pdl	Windmill; stock.
23.32. 3.311	3660	550R	8	--	9-13-72	Trsr	Windmill; stock.
3.311a	3660	--	10	204.18	9-13-72	Trsr	Unused.
21.241a	3680	515	--	480.75	9-21-72	Trsr	Windmill; stock.
		550	6	510.00R	4-13-59	Trsr	
23.33.12.312	3530	388	12	351.45	9-21-72	Trsr	Windmill; stock; "Allred Well."
17.423	3702	650(?)	8	504.40	9-21-72	Trc(?), Trsr	Submersible; stock "Graham Wells."
26.421	3645	173	6	165.15	9-21-72	Trc	Windmill; stock; "Tip Top Wells."
26.421a	3645	189	6	P184.00	9-21-72	Trc	Windmill; stock; "Tip Top Wells."
28.334	3675	544(?)	--	500.00R	11-27-53	Trc(?), Trsr	Windmill; stock & domestic; at Brinninstool Ranch, 2 wells at this location, tape will not pass 220' in either well.

Explanations

(1) Geologic source: QTs, surficial deposits; Trc, sandstone beds in the Chinle Formation; Trsr, Santa Rosa Sandstone; Pdl, Dewey Lake Redbeds; Pru, Rustler Formation above Culebra Dolomite Member, including Magenta Dolomite Members; Prc, Culebra Dolomite Member of Rustler Formation.

(2) Altitute: From topograhical maps.

(3) Depth of well: All depths of wells were obtained in 1972; all depths to water in the wells measured in 1972 or before are listed; R, reported depth; P, pumping level; < , than.
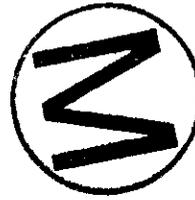
TABLE 6.3-3: Water Quality Data (from Table 2, Mercer and Orr, 1978)
reported in parts per million

Monitor Well	Date of Sample	pH Units	Temperature (Celsius)	Calcium (Ca)	Magnesium (Mg)	Sodium (Na)	Potassium (K)	Bicarbonate (HCO$_3$)	Carbonate (CO$_3$)	Sulfate (SO$_4$)
Magenta Dolomite										
H-1	5/10/77	7.2	22.0	1,000	460	6,200	840	93	0	3,600
H-2a	2/22/77	8.6	22.0	820	170	2,700	81	74	0	2,400
H-3	5/10/77	8.0	22.5	1,200	480	9,300	250	51	0	3,400
Culebra Dolomite										
H-1	3/17/77	7.3	22.5	820	1,800	29,000	5,600	100	0	11,000
H-2b	2/22/77	8.4	21.5	690	160	2,100	91	59	5	3,000
H-2c	3/16/77	8.1	20.5	680	120	3,600	120	62	0	3,200
H-3	3/17/77	7.4	21.5	1,500	670	19,000	630	115	0	5,700
P-14	3/14/77	6.0	21.5	3,100	760	7,600	600	357	0	1,400
P-15	5/10/77	10.2	21.5	770	63	6,900	1,700	63	24	3,200
P-17	5/10/77	7.4	22.5	1,700	1,600	30,000	120	77	0	5,000
P-18	5/10/77	7.2	24.5	5,600	16,000	9,200	6,200	310	0	980
Rustler-Salado Contact										
H-1	2/22/77	7.9	21.0	13,000	30,000	56,000	17,000	675	0	520
H-2c	2/23/77	5.9	20.5	9,200	25,000	66,000	9,100	199	0	1,300
H-3	2/24/77	7.6	21.5	18,000	25,000	59,000	14,000	467	0	370
P-14	2/24/77	7.2	24.5	570	1,200	120,000	1,300	222	0	10,000
Delaware Sand										
AEC-8	9/22/77	6.0	30.0	10,000	2,500	55,000	860	420	0	240

Table 6.3-3 Continued

Monitor Well	Chloride (Cl)	Fluoride (F)	Silica (SiO$_2$)	Dissolved Solids (Sum of constitents)	Nitrate* +Nitrate (N)	Ortho* Phosphorus (P)	Boron* (B)	Iron* (Fe)	Manganese* (Mn)
Magenta Dolomite									
H-1	10,000	2.0	1.7	22,200	0.04	0.03	3.3	0.22	0.95
H-2a	4,100	-	6.0	10,300	0.04	0.01	0.22	0.06	< 0.05
H-3	15,000	1.8	6.4	29,700	0.08	0.04	13.0	0.04	0.22
Culebra Dolomite									
H-1	49,000	0.8	0.6	97,300	0.03	0.00	18.0	0.79	2.8
H-2b	2,800	2.0	1.7	8,890	0.01	0.03	9.5	0.02	0.2
H-2c	4,700	1.6	3.5	12,500	0.16	0.00	10.0	0.11	0.14
H-3	29,600	0.5	1.2	57,200	0.07	0.00	20.0	0.05	0.12
P-14	20,000	0.9	33	33,700	0.01	0.02	0.7	17	0.5
P-15	11,000	1.2	1.6	23,700	0.04	0.03	4.7	0.1	0.02
P-17	54,000	1.5	1.0	92,500	0.06	0.11	1.7	1.2	3.0
P-18	80,000	1.2	1.0	118,000	0.81	0.40	100.0	0.54	4.5
Rustler-Salado Contact									
H-1	210,000	-	0.0	327,000	0.29	0.00	110	1.5	52
H-2c	200,000	-	2.0	311,000	1.1	0.00	150	2.5	78
H-3	210,000	-	1.0	327,000	0.77	0.00	1.9	1.5	3.8
P-14	180,000	-	2.0	313,000	0.34	0.08	1.7	2.1	3.4
Delaware Sand									
AEC-8	120,000	1.2	3.6	189,000	0.11	0.05	53	23	14.0

* Due to sampling conditions, analyses of NO_3^{-1}, PO_4^{-3}, BO_3^{-3}, Fe^{+2}, and Mn^{+2} are probably no more precise than $\pm 15\%$. The others have a precision of about $\pm 5\%$.

TABLE 6.3-4 Fluid Yield From Test Zones
(gallons per day)

Hole No.	Test Interval (depth in ft)	Magenta Dolomite	Culebra Dolomite	Salt Residue Zone in Rustler Fm.	Rustler-Salado Contact	Bell Canyon Sand
Open hole, drill stem tests (1)						
H-1	562 - 592	23.1				
	626 - 667			22.4		
	667 - 669		22.1			
	669 - 842				10.9	
H-3	558 - 608	14.1				
	672 - 703		2.3			
	703 - 780			1.8		
	800 - 868				2.6	
Open hole, bailing tests (2)						
H-2a	513 - 563	27				
H-2b	611 - 661		260			
H-2c	743 - 795				0.8[3]	
Cased hole with perforated interval, bailing tests (2)						
H-1	562 - 590	66				
	675 - 703		46[4]			
	803 - 827				1.0[5]	
H-2b	510 - 538	210				
H-2c	624 - 652		310			

TABLE 6.3-4 (continued) Fluid Yield From Test Zones
(gallons per day)

Hole No.	Test Interval (depth in ft)	Magenta Dolomite	Culebra Dolomite	Salt Residue Zone in Rustler Fm.	Rustler-Salado Contact	Bell Canyon Sand
		Cased hole with perforated interval, bailing tests (2)				
H-3	562 - 590	(8640)[6]				
	675 - 703		200			
	813 - 837				$11/32d$[8]	
P-14	573 - 601		(5760)[7]			
	676 - 700				75	
P-15	410 - 438		50		$2.0/42d$[8]	
P-17	558 - 586		170			
	702 - 726				$1.0/72d$[8]	
P-18	912 - 940			$0.5/33d$[8]		
	1076 - 1100				$0.5/73d$[8]	
AEC-8	4844 - 4860					269[9]

NOTES:

(1) Inflows measured over periods ranging from 11.5 to 37.5 hours.
(2) Inflows monotired for periods ranging from 8 days to 217 days. Rate based on inflow during first 24 hours.
(3) Inflow of 14 gallons in 18 days (no other data).
(4) Inflow of 416 gallons in 9 days (no other data).
(5) Average trend after 33 days recovery.
(6) Bailed 360 gallons in 1 hour with 6 feet of drawdown.
(7) Bailed 720 gallons in 3 hours with no drawdown.
(8) Early measurements inconclusive; inflow for period of days (d) indicated.
(9) Recovery measured for only 2.8 hours.

TABLE NO. 6.3-5

OBSERVATION WELLS - MONITORING ZONES

WELL NO. (GROUND ELEV.)	ZONE TESTED	ACCESSIBLE DEPTH	INTERVALS ELEV.
H-1	Magenta	562-590	2841-2813
(3403)	Culebra	675-703	2728-2700
	Rustler-Salado	803-827	2600-2576
H-2a	Magenta	No tests except levels	
H-2b	Culebra	510-538	2867-2839
H-2c	Culebra	624-652	2753-2725
(3377)	Rustler-Salado	743-795	2634-2582
H-3	Magenta	562-590	2837-2799
(3389)	Culebra	675-703	2714-2686
	Rustler-Salado	813-837	2576-2552
P-14	Culebra	573-601	2785-2757
(3358)	Rustler-Salado	676-700	2682-2658
P-15	Culebra	410-438	2900-2872
(3310)	Rustler-Salado	532-556	2778-2754
P-17	Culebra	558-586	2782-2754
(3340)	Rustler-Salado	702-726	2638-2614
P-18	Culebra	912-940	2567-2539
(3479)	Rustler-Salado	1076-1100	2403-2379
AEC-8	Bell Canyon (Upper)	4821-4827	[1289-1295]*
(3532)	Bell Canyon (Lower)	4844-4860	[1312-1328]*

*Elevations in brackets are below mean sea level; all other elevations are above msl. All depths and elevations are given in feet.

TABLE NO. 6.3-6

POTENTIOMETRIC LEVELS
OCTOBER 1977
(Elevation in Feet)

Observation Well	Ground Surface Elevation	Magenta Dolomite	Culebra Dolomite	Rustler-Salado Contact	Delaware Sands "Upper"	"Lower"
H-1	3,403	3,154	3,013	Not Monitored[1]		
H-2a	3,377	3,128	Not Penetrated	Not Penetrated		
H-2b	3,377	3,081	3,026	Not Penetrated		
H-2c	3,377	Not Screened	3,021	34'/Month[2]		
H-3	3,389	3,141	2,984	Not Monitored[1]		
P-14	3,358	Not Screened	3,034	2,970		
P-15	3,310	Not Screened	3,002	2,975		
P-17	3,340	Not Screened	2,968	2,970		
P-18	3,479	Not Screened	8'/month[2]	40'/month[2]		
AEC-8	3,532	Not Screened	Not Screened	Not Screened	2,927	2,933

NOTES:

[1]The Rustler-Salado contact is accessible, but is temporarily off.

[2]Recovery Rate: Level in tubing had not reached static level in October, 197__
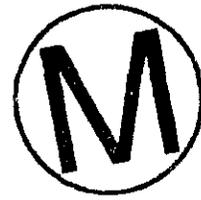
7.1 INTRODUCTION

In the context of this Geological Characterization Report, "geochemistry" is taken here to include a description of chemical properties of geologic media presently found in the surface and subsurface environments of southeastern New Mexico in general, and of the proposed WIPP withdrawal area in particular. "Chemical properties of geologic media" might be extended to include a description of present understanding of chemical processes which have taken or are taking place in southeastern New Mexico rocks. This geochemistry chapter of the WIPP Geological Characterization Report does not consider any aspect of artificially-introduced material, temperature, pressure, or any other physico-chemical condition not native to the rocks of southeastern New Mexico. These as-yet hypothetical considerations belong in the realm of interactions between radioactive waste and rock, a subject of the experimental programs initiated as part of the WIPP studies that are not yet completed. Early experimental results of radionuclide interactions with southeast New Mexico rocks and fluids are reported in Chapter 9.

A substantial fraction of this chapter consists of original source material, never before published in any format aside from reports of investigations resulting from research contracts. Much of this material is, however, in the process of being recast so as to be suitable for presentation in various professional forums. Some material has already been so presented.

Information contained herein was offered if the work involved was at a suitable stage of completion so as to allow conclusions to be drawn. Some subjects of investigation related to geochemistry require several years more investigation, even for final site characterization, and are discussed in Chapter 10, "Continuing Studies." Subjects of the present chapter are those which provide background data of relevance to (1)

experimental programs involving radioactive waste and its interaction with geomedia, (2) borehole plugging, (3) the intrinsic physico-chemical stability of southeastern New Mexico rocks in the geologic past, and (4) safety assessment, which is described in other major documents relating to the proposed WIPP. These data include mineralogy, volatile constituents of rocks, the constitution, origin and history of liquids and gases found in rocks, and the lengths of time which have passed since the latest episodes of thermodynamic instability resulting in rock/fluid interactions.

In the absence of a satisfactory theoretically-formulated mathematical model which can accurately predict phase equilibria among complex evaporite minerals, an empirical approach, based on observed assemblages, is adopted here. Such modelling is beyond the scope of this document.

It will be noted that volatile contents of evaporites were determined by three different methods: static heating (Section 7.5.3), thermogravimetric analysis (Section 7.5.2) and counting of fluid inclusions (Section 7.6). Each set of data was collected for a different geochemical purpose, but results from all techniques show comparable amounts of volatile constituents in the evaporites. The most accurate results, however, are probably those derived from static heating.

7.2 THE MINERALOGY OF DELAWARE BASIN EVAPORITES AND RELATED ROCKS OF THE LOS MEDANOS AREA

7.2.1 Introduction

The foregoing sections on geology and stratigraphy have briefly mentioned generalized mineralogies of Delaware Basin rocks of the Los Medanos area. Here it becomes of interest to present a more thorough exposition of mineralogies. This is done for a variety of reasons: (1) mineralogies affect properties of rocks important to physical aspects of mining, (2) soluble minerals in rocks potentially give rise to solutions which can interact with waste and its containers, and (3) minerals in

rocks have various degrees of sorptive affinities for radionuclides and can serve to decrease their mobility. While this section is devoted mainly to an account of the minerals found in the main Ochoan evaporite section (Castile and Salado Formations), mineralogies of some Guadalupian rocks and some rocks above the main evaporite section are included. This information is particularly useful to the consideration of radionuclide mobility in rocks containing substantially more fluid than the evaporites, and is of fundamental importance to in situ experiments involving waste-rock interactions. Also, investigations of fluid inclusions, sources of volatiles, groundwater geochemistry and age-dating of rocks and waters are closely related to mineralogy.

7.2.2   Previous Work

Southeastern New Mexico evaporites have been economically important for many years because they contain the well-known McNutt Potash Zone in the middle part of the Salado Formation. Descriptions of mineralogies of the McNutt and adjacent portions of the Salado have been given in several previous reports covering much of the Permian Basin, and environs of southeastern New Mexico (Brokaw et al., 1972; Jones, 1973; Jones, 1974a; Jones, 1974b; Jones, 1975). A detailed review of the economic mineralogy of the McNutt Potash Zone underlying Los Medanos appears in Chapter 8 of this report. This section on mineralogy has been developed as background critical to mine design, waste-rock-fluid interactions, and other aspects of geochemistry, such as age-dating and radionuclide migration.

7.2.3   Overview of Evaporite Mineralogy

X-ray powder diffraction examination of 50 core samples from ERDA #9 in the center of the study area (Figure 4.1-2) has been completed. Only qualitative information was obtained from these preliminary cores in order to assess mineralogical variations among selected horizons.

As-received cores were crushed and ground to bulk powder to provide a representative sample of that zone, x-ray specimen mounts weres scanned

at 1°/min on a diffractometer equipped with copper x-ray source, graphite monochrometer and scintillation detector.

Eight minerals were identified in the 50 samples:

1. anhydrite $CaSO_4$

2. clay $Al_2Si_4O_{10}(OH)_2$ xH_2O

3. halite $NaCl$

4. loeweite $Na_{12}Mg_7(SO_4)_{13}$ $15H_2O$

5. magnesite $MgCO_3$

6. polyhalite $K_2Ca_2Mg(SO_4)_4$ $2H_2O$

7. quartz SiO_2

8. sylvite KCl

Their occurrence is given qualitatively in Table 7.1 with a corresponding graphical distribution shown in Figure 7.1. Trace amounts of the potassium minerals sylvite and polyhalite were found in the proposed TRU horizon (2034-2110'), and the high-level horizon (2594-2692') was void of potash.

7.2.4 Mineralogy of Fluid-Bearing Zones in the Rustler Formation and Delaware Mountain Group

Mineralogies of certain fluid-bearing rocks above and below the main evaporite sequence have been determined as background information for radionuclide sorption studies.

Magenta Member, Rustler Formation (AEC No. 8). The Magenta member of the Rustler Formation is largely ferroan dolomite, probably containing minor ankerite which gives rise to the reddish color in weathered outcrops. This rock also contains detrital quartz, and gypsum forms as crystals, filling the vugs in the dolomite, which can be up to several cm across.

Culebra Member, Rustler Formation (AEC No. 8). Like the Magenta, the Culebra member is largely dolomite, with traces of detrital quartz. In addition, small amounts of calcite are found.

Bell Canyon Sandstone (AEC No. 8). The Bell Canyon Formation is the uppermost unit in the Delaware Mountain Group immediately underneath the main evaporite sequence. It is mostly detrital quartz and major feldspar with a matrix of kaolinite and chlorite cemented with calcite and minor amounts of dolomite.

Cherry Canyon Sandstone (Pine Springs Outcrop). Although the Cherry Canyon Formation was not sampled in any WIPP exploratory borehole, its stratigraphic position directly underneath the Bell Canyon made it of interest in preliminary radionuclide sorption measurements. The detrital component is largely quartz, and the cement is mostly dolomite. Minor amounts of albite and microcline contribute to the detrital component, and minor amounts of gypsum and calcite are found in the cement.

7.3   DETAILED CHEMISTRY AND MINERALOGY OF SOLUBLE AND INSOLUBLE
        COMPONENTS OF THE SALADO FORMATION

7.3.1   Introduction
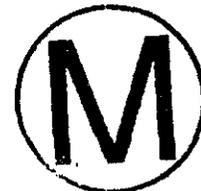
While this section deals primarily with results obtained from cores from AEC No. 7 and AEC No. 8, exploratory holes three miles northeast of the present study area (Figure 4.1-2), these holes provided material of sufficient lithologic similarity to ERDA No. 9 so as to be of value. The analytical strategy employs a normative-type calculation, in which mineralogical compositions are derived mathematically from bulk chemical compositions. The results of those calculations then can be compared to mineralogies determined petrographically or by x-ray diffraction. This section serves as fundamental background information for the chapters on silicate mineralogy and sources of volatile components within the evaporites.

7.3.2   Materials and Methods

Sample Preparation and Handling. The core samples as received were halved and one-half was retained while the remaining half was crushed and ground. The ground sample was size-distributed as shown in Table 7.2.

The samples were all double-wrapped for storage in plastic bags due to their hygroscopic nature. A portion of the crushed sample weighing approximately 20 grams was accurately weighed and dried in an oven at $70^{\circ}C$ for two hours to determine weight loss. The dried sample was then added to 200 ml of distilled water, stirred for 1 hour, and filtered. The filtered material was dried and weighed to determine the insoluble portion of the sample while the filtrate contained the soluble portion of the sample.

Analysis of Soluble Portion. The elements potassium, calcium, magnesium, silicon, iron, aluminum, and strontium were analyzed by standard atomic absorption methods using a Perkin-Elmer 403 Atomic Absorption Spectrophotometer. Sodium, typically difficult to analyze precisely, was analyzed using an Orion Specific Ion Sodium electrode and an Orion Research Model 801 pH meter. Sulfate was determined gravimetrically as barium sulfate; chloride was determined volumetrically by titrating with mercuric nitrate (Vogel, 1961)

Analysis of Insoluble Portion. The insoluble portion was separately analyzed only if the insoluble percentage was greater than 0.5% of the total sample weight. Samples containing less than 0.5% insolubles did not provide sufficient material for analysis, and it was deemed that even a major constituent in such a small percentage of the total would not contribute significantly to the sample behavior. A portion of the water-insoluble material weighing about 100 mg was dissolved in HF, using the following procedure in a teflon-lined high pressure bomb (Bernas, 1968; 1973) obtained from Parr Instruments. Nitric acid (1 ml) was added

to wet the sample and 3 ml of 50% HF were added. The bomb was assembled
and placed in a 70°C oven for 2 hours. The contents of the bomb were
quantitatively transferred to a polypropylene beaker containing 2.8 g of
boric acid and about 30-40 ml deionized water. The boric acid was
allowed to dissolve with stirring and the solution diluted to 100 ml in a
volumetric flask and stored in a polyethylene bottle. A solution
containing all of the matrix material was prepared for use in making
standards for the atomic absorption spectrophotometer. All analyses were
performed as described in the preceding section. Samples were tested for
the presence of carbonates using concentrated HCl but only occasionally
was a trace amount detected.

Thermal Analysis. Samples analyzed for weight loss upon heating were
ground so that greater than 90% of the sample was smaller than 100 mesh.
Each sample was dried for at least 3 days at 65°C in a thermostatically
regulated oven. This temperature was chosen to avoid the long-term
dehydration of gypsum described elsewhere in this report. Low
temperature weight loss (70°C for 2 hours) was used to measure
absorbed water. This weight loss is probably higher than for rock
distant from the sample collection point owing to absorption of drilling
water. Samples of 100 mg weight were heated for differential thermal
analysis (DTA) using a Fisher 200A DTA apparatus at a rate of 10°C/min
from 25°C to 500°C.

Thermogravimetric analysis was carried out with a Fisher 100A TGA
apparatus and a Cahn Model R6 electrobalance at a rate of 5°C/min from
60°C to 500°C using 100 mg of sample material. A few samples were
heated to 800°C and are described elsewhere in this subsection.

Results of Analyses. Whole-rock chemical analyses, soluble-insoluble
fractions, and weight losses upon heating are presented in Appendix 7.A.
These analyses are converted to relative numbers of moles of components
by multiplying weight percents by appropriate values of 1000/molecular
weight. The results are listed in Appendix 7.B. If the insoluble
fraction of a sample exceeds 0.5 weight percent, separate calculations
are provided for both the soluble and insoluble fractions of the sample.

7.3.3   Results and Discussion

Distribution of Mineral Phases. Chemical analyses may be used to
estimate, semiquantitatively, the amounts of constituent minerals present
in a rock. This is accomplished by distributing the quantitatively
determined chemical components among mineral phases known qualitatively
to be present in the rock. The method was as follows:

The distribution of the total number of moles (Nt) of a given
chemical component (c) among the various mineral phases (p) present
in a rock is described by the equation

$$Nt,c \ = \ \Sigma \ (Np) \ (Nc,p)$$

where:

Nt, c = the total number of moles of the component c in the rock

Np = the total number of moles of each of the mineral phases p in the
rock,

Nc,p = the number of moles of the component c in one mole of phase p.

This equation is simply a statement of conservation of mass, indicating
that the total amount of a given chemical component must be distributed
among the minerals containing that component; this distribution is
controlled by the specific chemical compositions of the minerals.
An expression of the form of the above equation may be written for each
of the components present in a rock sample. For a given rock, one of
three conditions are possible for the set of simultaneous equations
describing the distribution of all components in that rock:

1)   if the number of equations (1 for each component) is equal to
the number of unknowns (the moles of each of the phases), an
exact solution to the equations may be determined.

2)   if the number of components exceeds the number of phases (more
equations than unknowns) the system is overdetermined and a
solution to the equations may be evaluated by a method such as
least squares regression.

3)   if the number of components is less than the number of phases
(more unknowns than equations), the system is indeterminate.

If either of the first two criteria are met, the chemical composition of
the rock can be employed to calculate the quantitative amounts of
minerals known, qualitatively, to be present.

An important assumption for the treatment described above is that the
chemical composition of all mineral phases is known. This is necessary
in order to define $N_{c,p}$ for all phases in the mass balance equations. If
a mineral of variable composition is present in a rock sample (i.e., a
solid solution), an additional variable is introduced to the set of
equations; that is, the composition of the solid solution. This
additional variable may change a set of N equations and N unknowns
(condition 1 above) to an indeterminate set containing N + 1 unknowns.
If such is the case, it is necessary to employ some additional analytical
technique to determine the actual composition of the unknown. On the
other hand, if the solid solution is present in a rock meeting condition
2 above, it will suffice to simply introduce two values of N_p for the
phase; in other words, an unknown for the number of moles of each of the
pure end-members of the solid solution present. The composition of the
mineral is then defined by the relative number of moles of each of the
end-members present.

Qualitative mineralogy may be carried out by a variety of methods such as
x-ray diffraction and thin-section analysis in addition to
straight-forward examination. The chemical data obtained during this
study have been used to attempt to estimate relative amounts of minerals
present in the various samples. With only a few exceptions, the rocks
are made up essentially of halite, and other mineral phases are present
in comparatively minor or trace amounts.

Samples from the Carlsbad boreholes consist of two chemically distinct
fractions: (1) water-soluble chlorides and sulfates of sodium,
potassium, calcium, and magnesium, and (2) water-insoluble silicates of
potassium, magnesium, and aluminum with quartz and iron oxide. Minerals
of the first group generally contain stoichiometric compositions, whereas
those of the second group exhibit extensive compositional variation. In

the case of the soluble portion, sodium occurs mainly with chloride as halite, while the other cations combine in various proportions with sulfate (and only occasionally chloride) forming minerals such as polyhalite, anhydrite, and kainite. These sulfates are of importance because they contain hydrate water which may be released upon heating. Silicates also undergo dehydration at elevated temperatures, but generally much higher temperatures are required than for the soluble salts because the water must be derived through destruction of hydroxyl groups. Compositions of minerals from these two classes are listed in Table 7.3.

Recognizing that soluble potassium, calcium, and magnesium are combined with sulfate, a semiquantitative estimate of various sulfate phases may be made by plotting the relative numbers of moles of the cations on triangular composition diagrams. The compositions of various stoichiometric mineral phases in the sulfate group are shown on such a diagram in Figure 7.2. No sulfate of potassium alone is common in nature, so sylvite is placed at the potassium apex of the triangle. Also shown on this diagram are the chloride and chloride-sulfate of potassium and magnesium. Not shown on Figure 7.2 are the soluble sulfates containing sodium. After plotting a given sample composition in terms of relative numbers of moles of soluble K_2O, CaO, and MgO, the total number of moles of these cations is compared to the number of moles of sulfate determined analytically; if the two are equal, then the minerals in the rock are estimated using the location of the sample on the diagram. If the cation sum is greater than available sulfate, an appropriate amount of chloride is added to make up the charge balance. Relative amounts of chloride and sulfate are then used in conjunction with the cations to determine appropriate amounts of carnallite, kainite and/or sylvite. If on the other hand, cations are deficient relative to sulfate, then sodium is added to the sulfate group to form bloedite, glaserite and/or glauberite.

The addition of sodium or chloride must be compatible with the relative amounts of these two components in the analysis. Generally, these are

present in such large amounts that a small error in their contents provides sufficient amounts for addition to the potassium-calcium-magnesium-sulfate fraction. In many instances, it is found that when it is necessary to do such addition, the appropriate component (sodium or chloride) is present in excess of the other necessary to form halite. Where such addition is not compatible with the chemical analysis, examination must be made of the insoluble portion of the sample. Where anhydrite-gypsum is present in significant amounts in a sample, the relatively low solubility of $CaSO_4$ (and possibly polyhalite) causes this phase to appear in both the soluble and insoluble fractions.

Minerals of the insoluble fraction consist of quartz, iron oxide, and a variety of clay minerals which are difficult to identify due to fine-grain-size and compositional variability. Iron probably occurs chiefly as either hematite (much of the halite is tinted orange) or an equivalent hydrated form although it may substitute for aluminum to a minor extent in clay minerals.

According to our chemical analyses, the remainder of the insoluble fraction is made up of the components K_2O, Al_2O_3, MgO, and SiO_2. Because the first three of these generally occur combined with the fourth, potential mineralogy of the samples may be evaluated by comparing insoluble analyses to mineral compositions plotted on the compositonal triangle K_2O-Al_2O_3-MgO shown in Figure 7.3. On this diagram, mixed-layer solid solution among potassium and magnesium montmorillonites and seawater-illite is indicated by the shaded area between these three endmember components. It should be noted that the chlorite composition plotted on Figure 7.3 is that which has been observed in present day seawater sediments and evaporites. Relative proportions and amounts of minerals occurring in a given sample are evaluated by distributing potassium, aluminum, and magnesium along appropriate limiting phase compositions. Silica is then distributed among these phases according to stoichiometry, and any excess occurring in the sample analysis is considered to be free quartz.

Halite is by far the most abundant mineral in the soluble fractions of the samples. In only a few cases is halite a minor or trace constituent. Polyhalite and anhydrite/gypsum are accessory minerals in most samples, and in two of these, $CaSO_4$, is a major component. In normative calculations for sulfate deficient samples, kainite and carnallite are included, whereas thenardite, glaserite, bloedite, and kieserite appear in sulfate-excess and balanced samples. These phases are rarely present in more than trace amounts and are calculated to occur in such small quantities as to be insignificant in terms of contributions to hydrate water. Sample 8-1652 (i.e., 1652 feet depth in AEC No. 8) is significantly different from other soluble material in that it is calculated to contain relatively large amounts of the soluble salts sylvite, polyhalite, leonite, and glaserite. The drilling log reports loss of mud at this point, so it is uncertain as to whether a rock is of exotic mineralogy, or one from which certain cations have been leached by moving drilling mud, or one which has exhibited the incongruent solubility of polyhalite, leaving a sample of abnormal chemistry.

Most of the insoluble analyses plot within the triangle bounded by the phases Mg chlorite-K feldspar-talc on Figure 7.3. These minerals are recognized to occur in evaporite sequences which have undergone mild diagenesis (P < 100 atm, T < 100°C), forming as a result of interaction of brine with amorphous aluminosilicate detrital material (Braitsch, 1971). The only other phases calculated to occur in the insoluble fraction are mixed-layer illite-montmorillonite, quartz, and iron oxide. It should be noted that the presence of the mixed layer silicate as well as chlorite and talc may be difficult to establish if they occur in very fine grain size. None of the observed silicate phases undergo dehydration below 500°C, according to the DTA.

Effects of Heating Samples. A number of different responses to heating were exhibited by the samples. Heating to 70°C was designed to measure absorbed water recognizing that gypsum dehydrates, according to thermochemical data, at about 70°C. In normal differential thermal analysis, gypsum undergoes stepwise dehydration to hemihydrite and

anhydrite at about 150° and 185°C, respectively. Kopp, (University of Tennessee, pers. comm.) has observed that gypsum dehydrates upon fine grinding and prolonged heating at 70°C, hence the observed DTA breakdown is probably a result of kinetic factors. Consequently, samples analyzed using thermogravimetric analysis were powdered and placed in an oven at 70°C for several days prior to analysis of weight loss at elevated temperatures. Samples 7-1171 and 8-2563 both contain major $CaSO_4$, but only the latter showed gypsum-type dehydration. This appears to indicate that sample 7-1171 actually contained anhydrite whereas sample 8-2563 contained gypsum since only 8-2563 showed significant weight loss at 70°C but both analyses summed to near 100%.

Essentially isothermal dehydration was observed over a continuum of temperatures from 100° to 500°C for a large number of samples. In addition, weight loss over a 50° to 100°C span in temperature was observed for most samples, but generally at temperatures above 300°C. These two types of weight loss probably indicate single-mineral dehydration for isothermal loss, and dehydration as a result of mineral-mineral chemical interaction for the weight loss occurring over a large temperature span. Such solid interaction is demonstrated by sample 8-1953 which contains both anhydrite and polyhalite but minimal bloedite. Figure 7.4 shows the DTA curves for pure polyhalite and gypsum. Comparison of these two curves to that of sample 8-1953 shows the 325°C exotherm of polyhalite to be lacking while the lower temperature endotherms of gypsum are present. We suggest the missing polyhalite endotherm is a result of chemical interaction between polyhalite and anhydrite somewhere between 200° and 325°C. Such interaction among evaporite minerals should probably be investigated in some detail in terms of retention of hydrate H_2O.

A few samples were heated to 800°C to get an indication of how much weight might be lost from samples at high temperatures (>500°C). Of the nine samples examined under these "extreme" conditions, four began gaining weight at about 700°C. One sample increased in weight by about 15% between 725° and 800°C. This gain in weight is not a result of

oxidation of iron (eg. Fe^{+2} in chlorite) since sample 8-2050 did not contain any iron. That the gain in weight may be caused by formation of an extremely hygroscopic phase at high temperatures as a result of solid-solid chemical interaction upon heating. Whether or not such a phase forms would undoubtedly depend upon the initial mineralogy of the rock to provide the correct reactant phases since not all sample exhibited this weight gain. The water necessary for this rehydration is probably a result of the fact that the testing laboratory is cooled during the summer months (the analyses were run in early June) by evaporation which results in high relative humidity.

A composite histogram of weight loss of all samples at elevated temperatures is shown in Figure 7.5. The distribution appears to be log-normal with the maximum density near 0.25% weight loss upon heating $500^{O}C$. Over half of the samples (56%) show weight loss of 0.5% or less, and only 15 samples exceed 1%. Figures 7.6A and 7.6B are plots of sample weight loss vs depth for the two drill holes. Samples showing more than 1% weight loss upon heating are scattered throughout the depth range but are generally separated by more than one hundred feet of low-water-loss material. There is a broad correlation between higher weight loss and increasing insoluble content of sample, but no clearcut relationship is seen between weight loss and silica content. It is concluded that high temperature weight loss is contributed by both silicate and sulfate minerals. It can be stated in general, however, that samples showing less than 1% weight loss contain less than 10 wt % insoluble material.

7.3.4   Conclusion

Most of the samples showed very little water loss between 200° and $300^{O}C$ and there were only small water losses at temperatures $200^{O}C$ and $300^{O}C$. As can be seen by examining the data, there are several zones where there is essentially no change in sample behavior with heating to moderate temperatures. These areas show good potential as burial sites for nuclear waste.

7.4   DETAILED PETROLOGY AND SILICATE MINERALOGY OF SOME PERMIAN BASIN
       ROCKS

7.4.1 Introduction

The purpose of this section is to describe and evaluate the petrologic,
mineralogic and geochemical properties of designated core samples,
primarily from the ERDA – 9 drill hole and various grab samples exposed
in mines and at the surface, in connection with the WIPP (Waste Isolation
Pilot Plant) site evaluation.

ERDA – 9 penetrates the Mescalero Caliche, Gatuna Formation Santa Rosa
Sandstone, Dewey Lake Red Beds, Rustler Formation, Salado Formation and
the uppermost 50 feet of the Castile Formation (Figure 4.3-3). Primary
interest is focused on selected intervals within the Salado and uppermost
Castile Formations.

The general problems under study are: 1) the genesis of the dominantly
evaporite succession with associated silicates and 2) the extent of
post-depositional alteration of these sediments. The basic approach (and
analytical method) is broadly threefold. First, detailed study of the
occurrence and mineralogy of silicates, particularly clay minerals, in
the evaporite succession (disaggregation, size fractionation, x-ray
diffractometry). Second, bulk chemical analysis of whole rock, water
soluble, acid insoluble, and clay size fraction (x-ray fluorescence,
atomic absorbtion spectroscopy, other rapid procedures). Third,
macroscopic and microscopic petrography (handspecimen and microscope
mineral identification, description of form, texture and lithology of
mineral associations, and x-ray diffractometry of bulk samples).

7.4.2 Procedure

After core intervals were selected for study, cores were cut lengthwise,
mostly in the form of 1/2, less commonly 1/4, of the core. Criteria for
selection and additional procedures for analysis of these samples are

described in the following sections on the silicate mineralogy, geochemistry and petrography.

7.4.3 Silicate Mineralogy and Geochemistry

Systematic logging of ERDA - 9 core and accompanying gross mineralogy have been described in Chapter 4. This section is focused on selected segments of the core and examination of the paragenesis of minor constituents, namely the silicate minerals, their composition, and their interpretation in terms of depositional and postdepositional phenomena.

Silicate mineralogy and geochemistry have not been comprehensively studied within the Ochoan rocks and the Permian Basin. Adams (1969) has reported briefly on the occurrences of talc in argillaceous rocks as a part of this extensive study of bromine distribution throughout the section; specialized clay mineral determinations by Grim et al. (1961) and Fournier (1961) have been undertaken on a limited number of samples and with minimal regard to their detailed stratigraphic setting and geneses.

In an effort to provide substantially more complete understanding of the silicates associated with the Permian evaporites, some 70 samples of the ERDA - 9 core ranging from 300 feet below the Salado-Rustler contact (1163.3 foot depth) down to a few tens of feet below the Salado-Castile contact (2867.6 foot depth) were selected. The following criteria were used in the selection: (1) representation of major lithologies; (2) detailed representation of an apparent "cycle" of evaporite deposition which occurs repeatedly through the Salado Formation section; (3) representation of intervals under consideration for waste storage sites; (4) detailed representation of selected polyhalite-anhydrite occurrences toward interpreting the genesis of the unusually abundant polyhalite; and (5) representation of the sequences which may provide data for interpreting postdepositional solution and recrystallization phenomena. In Table 7.4, we list the samples by depth, gross lithology, and stratigraphic position, as well as by character of data obtained; Table 7.5 provides a cross-listing for relating sample number to depth.

Sample Preparation and Analysis. The core was split and one split
rebagged for future reference. One to 10 cm segments of the remaining
half were selected for analysis (petrographic, mineralogic, and/or
chemical) and sectioned off. A 1 cm slab of this was retained for
petrographic examination; the remainder was coarsely crushed and a split
retained for whole rock analysis. The larger fraction of the sample was
leached with excess demineralized water to dissolve the halite host.
This was repeatedly centrifuged, decanted, and rewashed to remove all
traces of dissolved halite from the residue. The residue was dried,
reweighed, and a split suspended in boiling EDTA solution in order to
separate the "acid-soluble" salts (sulfate and carbonate minerals)
following the procedure of Bodine and Fernalld (1973). Again, after
repeated centrifuging, decanting and washing to remove EDTA and to
dissolve solid components from the insoluble residue, the suspension was
dried and reweighed. Table 7.6 depicts the quantities of sample residues
insoluble in water and EDTA. A split of this fraction was resuspended in
water, thoroughly disaggregated with an ultrasonic probe, and separated
into the > 2 μm and < 2 μm (effective spherical diameter) fractions by
timed gravity settling. Oriented diffractometer mounts of the fine
fraction were prepared by pipetting several drops of each suspension onto
glass slides and air-drying. Smear (paste) mounts and mounts using the
conventional commercial powder mounts were used for the < 2 μm insoluble
fraction as well as for the other fractions. In addition, pellet or
uniformly compressed mounts or "briquettes" of these fractions prepared
for x-ray fluoresence were also used for diffraction.

Where sufficient sample was available, normal procedure for the silicate
fraction included: (1) diffraction data for the whole EDTA-insoluble
fraction using the briquettes or paste mounts; (2) oriented (sedimented)
clay-size mounts on glass which were air-dried, glycol saturated, heated
to 300°C, and heated to 500°C. Conventional x-ray diffractometer
traces were obtained at a scanning speed of 2°2θ/min with Cu-radiation
and a curved crystal monochromator.

X-ray fluorescence work involved briquette mounts using the vacuum-path Norelco fluorescence goniometer with quartz and gypsum analyzing crystals. In this study, standard regression procedures are used along with matrix evaluation for calculating abundances from the raw data. However, at this time the data can only be reported in terms of a unit-slope regression from one standard. Because of the severe errors such a procedure may induce, only "semi-quantitative" chemical results are claimed for this report.

Silicate Mineralogy. The following silicate minerals have been identified in the course of this study; their distribution is given in Table 7.7.

Quartz - Quartz occurs throughout the entire interval of the stratigraphic section analyzed; however, it does not occur in every sample. Quartz is generally fine-grained ($<10\mu$m), subhedral to anhedral, and readily identified in diffraction traces by its very strong peak at 3.34$\overset{\circ}{A}$ and moderate peak at 4.26 $\overset{\circ}{A}$; interference by the micas and mica-clays with the former and by potash feldspar for the latter only rarely preclude its ready identification.

Illite (mica-clay) - Illite also occurs throughout much of the stratigraphic interval. It is readily observable in diffraction traces with its strong 10$\overset{\circ}{A}$ and 3.34$\overset{\circ}{A}$ peaks and its moderate 5.0$\overset{\circ}{A}$ peak (001, 003, and 003 respectively). All illites observed in the core are dioctahedral as based upon (060) $< 1.52\overset{\circ}{A}$ and (001, 002, and 003) <1.0, 5.1, and 3.44 $\overset{\circ}{A}$ respectively. Many of the illites contain recognizable but small quantities of interlayered smectite, presumably saponite or other trioctahedral varieties, based on the slight asymmetry of the (001) reflection.

Feldspar - Feldspar occurs frequently, but generally in small quantities, throughout the section and its identification is based principally on one or more diffraction maxima in the 3.17 - 3.30$\overset{\circ}{A}$ range. Unfortunately, its abundance is usually low and when coupled with the presence of other

minerals its diffraction maxima for resolving its composition and its thermal character are not interpretable; both plagioclase and K-feldspar have, on occasion, been recognized.

Chlorite - Chlorite is commonly a minor constituent and its presence is often difficult to establish. With a 14 Å periodicity its maxima can be masked by smectities, various interlayered species, and by the 7 Å minerals, kaolinite and serpentine. In glycol saturated specimens, the 14 Å peak from expandable clays can be removed and at $500^{\circ}C$ the 7 Å peak from kaolinite is lost. Even so with only a small amount present in such an assemblage it can remain undetected.

Talc - Talc is rare throughout the core. It is common in the ore zones (Adams, 1969) but appears to be nearly absent from the other lithologies. Talc is identified by very sharp, strong reflections at 9.5 and 3.15 Å (001 and 003); the former is quite distinct from the broad reflection at 9.0 - 9.7 from a regular interlayered chlorite-saponite (corrensite).

Serpentine - Serpentine, like talc, is relatively rare in the section and is confined to the lowermost interval (below 2820.3 and at or below the Salado-Castile contact) in rock salt and anhydrite. Serpentine is identified by strong peaks at $\sim$7.3 Å and $\sim$3.6 Å (001 and 002 respectively for a single-layered variety). These maxima are noticeably greater than the 7.0 - 7.2 Å and 3.5 - 3.65 Å reflections attributable to chlorite. In our samples, these larger spacings are characteristically sharp and are not accompanied by the odd (00) reflections of the 14 Å minerals.

Expandable Clays - Expandable clays, the smectities, vermiculites, and mixed-layer clays containing either of these constituents, are the dominant clays of the section and are ubiquitous (Table 7.8). We have recognized at least four such clays; however, their definitive identity has not yet been resolved.

a. Saponite (e.g. JS-CS-9 at 1466.9') expands to >16Å with glycol
    saturation and collapses to < 14Å upon heating, (further heating
    would yield an ~9.5Å peak).

b. (?) Illite-saponite (e.g. JL-CS-2 at 1440.5' JL-CS-10 at 1325.3')
    with an air-dried maximum at 10.2 - 10.3Å, glycol saturation at
    10.0Å and with or without a less intense shoulder or separate peak
    at 11.3 - 12.1Å, and collapsing to 9.8Å at 300°C. We have not
    ruled out a mixed-layer talc saponite identification for this
    phase.

c. Chlorite-saponite (e.g. MB-CS-21 at 1404.6' and MB-CS-32 at
    2541.5') exhibits a 14Å peak expanding to 15.5Å with glycol
    saturation and collapse to <14Å upon heating. The
    chlorite-vermiculite phase described by Fournier (1961) and Grim
    et al. (1961) is probably this chlorite-saponite; the expansion
    with glycol is too great for this to be a chlorite-vermiculite.
    In some cases the interlaying is random; in others it is regular
    and produces a distinct superlattice peak (~29Å); in most there is
    some regularity with a slight shoulder present in the 25-30° 2θ
    present (these shoulder "maxima" are exceedingly difficult to plot
    precisely and all contain ±0.3-0.5° 2θ definition).

Nearly all of the diffraction data in Table 7.8 can be assigned to one of
these three clay phases, yet data from several samples are not yet
resolved, e.g. MG-CS-13 at 2518.3. It should be noted that smectities
are smectite-bearing mixed-layer clays which commonly appear to be
"stripped" by the EDTA-dissolution of nonsilicates; they commonly show
12-13.8Å air-dried spacings. However, suspending these clays in $MgCl_2$
or NaCl solutions and then rewashing and redrying restores the
appropriate 14-15Å spacing.

In Appendix 7.C, we present a number of the diffraction diagrams
illustrating these silicate assemblages.

Distribution of Clay Materials. Some general but tentative observations
regarding these minerals throughout the section are:

(1) Serpentine appears to be restricted to the lower
40 feet of the analyzed section; it most commonly occurs in
anhydrite and associated rock salt.

(2) Talc is not restricted to assemblages from bitterns as suggested
by Adams (1969).

(3) Interlayered illite-saponite (or talc-saponite) appears to be
resricted to polyhalite lithologies or adjacent anhydrite. It
appears to be absent from clay beds and associated rock salts and
from the polyhalite-free remainder of the section.

(4) Expandable clays appear to show somewhat less relative abundance
in clay beds (1244.8, 1247.2, 1328.6, 1441.7, and 1468.1 ft.) than
in the silicate assemblages from the evaporite rocks.

(5) Furthermore, the mixed-layered clay species in each of these clay
seams consists solely of the well developed regularly
interstratified chlorite-saponite (corrensite).

7.4.4 Mineralogy of Duval Mine Samples

Several samples of wall-rock were taken from the 4th ore zone
(langbeinite level) of the Duval Nash Draw potash mine, about 5 miles
west-by-southwest from the study area. These samples include a dark
brown clay parting (the DV-4 series) taken from the upper boundary of the
4th ore zone.

Untreated oriented powders were scanned from 2 to 60 degrees two theta.
The untreated slide was glycolated by vapor-soaking on a rack in a
container filled partially with ethylene glycol. An additional oriented
powder was heated at 450°C. Both the glycolated and the heated
specimens were scanned from 2 to 3 degrees two theta.

Whole rock samples were analyzed by loading a small amount of randomly oriented rock powder in a Norelco powder holder. This powder was scanned from 5 to 80 degrees two theta and the resulting diffractogram compared to values compiled in the Joint Committee on Powder Diffraction Standards file to determine bulk mineralogic composition. Mineralogic abundances noted were estimates based on comparative peak intensities.

All samples x-rayed (both clays and whole rocks) were scanned with Ni-filtered CuKα radiation. A time constant of two seconds was used with a scintillation counter detector and pulse height analyzer. The goniometer slit system consisted of a divergent and anti-scatter slit of 1 degree and a 0.003 inch receiving slit.

The results for Duval Mine samples appear in Table 7.9. For comparison, "dirty salt" from about 2100 feet depth in ERDA No. 9 has about 8% by weight insolubles.

7.4.5 <u>Chemical Composition</u>

Since appropriate regressions for each component based on several standards have not yet been calculated and matrix effect corrections have not yet been made, the analyses in Table 7.10 must be considered as only semiquantitative. In most cases, most totals are between 85 and 98%; perfectly reasonable totals with the remainder being chiefly water. A few totals exceed 100% and a few others are less than 85%; these are unquestionably in error. These data, however, do illustrate a number of important relations and are compatible with the mineralogic data.

Thus for example, those analyses with high alkali content (JS-CS-2 at 1440.5', JC-CS-6 at 1441.5, MB-CS-27 at 2067.0, MB-CS-31 at 2512.5, MB-CS-13 at 2518.3, MB-CS-10 at 2705.8, and MB-CS-36 at 2758.4) show substantial feldspar with or without abundant mica-clay.

In general, the chemical data support the mineralogic determinations. The silicate fractions are extraordinarily high in MgO (~20-30 wt % MgO)

and correspondingly low in CaO ($\sim$1 wt % CaO); Al_2O_3 is low ($\sim$8-12 wt % Al_2O_3) for clay mineral assemblages. Thus, except for illite, our clays are trioctahedral with only chlorite containing appreciable Al_2O_3.

7.4.6 Petrography

Petrographic analysis, both macroscopic and microscopic, is used in three ways: first, determination of the mineralogy of samples; second, given the mineralogy of a sample, description of lithology; third, the primary utility of petrographic analysis in this study, description of the texture of the sample. Texture refers to grain or crystal size, shape (habit or form), orientation, relationships (such as nature of contacts between crystals or grains) among different minerals and lithologies.

Macroscopic Petrography.

Sample Preparation and Procedures - Slabs, approximately 1 cm thick, were cut lengthwise using a band saw, from the 1/2 or 1/4 core samples. One face of a remaining core sample was then polished using a sander with various grit sandpapers. The sample was not to be used for silicate mineralogy-geochemistry analysis in order to avoid contamination. The polishing enhanced textural detail. Faces were also polished on some slabs.

Samples were selected from the core in which mineralogy based on macroscopic identification was obscure or uncertain for x-ray diffractometry of the bulk sample. Conventional diffractometry methods, as described previously, were used.

Macroscopic Petrographic Description - The mineralogy, lithology and texture in the polished sections of all the core intervals selected were described. Appendix 7.D is a brief extract from 54 pages of sketches accompanied by textural descriptions of these core intervals. Table 7.11 is a summary of the gross lithology reported largely as macroscopic

mineral identification and core footage. Table 7.11 indicates that
macroscopic mineral identifications are generally reliable, especially
for coarse-grained minerals, but visual estimation of the relative
minerals abundances are less reliable. Estimates of relative abundances
based on x-ray diffraction analysis are regarded as "semi-quantitative"
and maybe in error, but it is still more reliable because of its greater
precision, if not accuracy, compared to visual estimation.

Plates 7.1 through 7.6 are photographs of polished faces of cores or
slabs illustrating typical textures. Plate 7.1 shows a variety of shapes
of halite in anhydrite. The occurrence as beds or laminae or irregular
lenses is inferred to be primary because halite and anhydrite can
precipitate jointly or alternately from evaporating seawater. The
apparent swallow-tail form of halite in laminated anhydrite is a problem
because no primary occurrence of this form of halite is known. The
swallow-tail form can occur as a twinned crystal of gypsum, but
coprecipitation of gypsum and anhydrite is thermodynamically impossible.
One interpretation is primary precipitation of calcium sulfate only as
gypsum in the form of rapidly growing swallow-tail twins and finely
crystalline aggregates. Then post-depositional alteration of the finely
crystalline aggregates to anhydrite takes place, and the twinned crystals
alter either directly to halite or first to anhydrite which then alters
to halite, with preservation of the primary swallow-tail forms. This
interpretation is favored by the almost exclusive dominance of gypsum
rather than anhydrite as the primary precipitate in modern environments
and lab experiments. Controversial thermodynamic analyses also favor
gypsum as the primary precipitate, even metastably.

Plate 7.2 also illustrates occurrence of halite in well laminated
anhydrite. This is interpreted as primary coprecipitation of halite and
gypsum with these textures followed by post-depositional alteration of
gypsum to anhydrite with preservation of primary texture.

Plate 7.3 illustrates an occurrence of halite and polyhalite. The
triclinic crystal system of polyhalite is unlikely to produce a
rectangular outline in cross section whereas the cubic habit of halite or

the orthogonal morphology of anhydrite would. Thus, the rectangular outline of the polyhalite body suggests post-depositional alteration of anhydrite, (to a lesser extent of halite) to polyhalite as does the occurrence of most polyhalite in irregular masses among halite masses. Thermodynamic and experimental considerations as well as observation of modern evaporites indicate that polyhalite does not precipitate from evaporating seawater.

Plate 7.4 illustrates coarse, relatively pure halite with anhedral, granular texture. The halite contains small crystals of anhydrite, probably a post-depositional alteration product of a primary coprecipitate of halite and gypsum.

Plate 7.5 illustrates another texture of halite in anhydrite with traces of magnesite. As previously indicated, it is believed to result from primary co-precipitation of halite and gypsum with post-depositional alteration of gypsum to anhydrite with preservation of primary texture. Magnesite is not known to precipitate from evaporating seawater but calcite does, suggesting post-depositional alteration of a primary (probably calcium) carbonate to magnesium carbonate.

Plate 7.6 illustrates textures in a dominantly anhydrite rock. The occurrence of the swallow-tail form near the stratigraphic top of the specimen as well as previously related discussions suggest primary precipitation of gypsum followed by post-depositional alteration of anhydrite, which could occur shortly after deposition, with preservation of primary textures.

Microscopic Petrography.

Sample Preparation and Procedure - The 1 cm thick slabs were converted to standard and oversize thin sections following conventional procedures (with the following exceptions) to minimize chemical alteration of the sample. Fluid in contact with the sample was a pure vegetable cooking

oil. Temperatures during the thin sectioning process did not exceed $30^\circ C$. Samples were put in dessication jars during impregnation to minimize contact of fluid acetone with the sample.

Microscopic Petrographic Description - Plates 7.7 through 7.12B are photomicrographs of thin sections of rock samples from the Permian Basin of southeast New Mexico. The samples are not from ERDA-9 core but are representative of mineralogies, lithologies and textures commonly encountered in the core.

Plate 7.7 is a photomicrograph of relatively finely crystalline euhedral to subhedral halite. The crystal form, relative clarity (although containing very fine crystals of anhydrite) and occurrence of fluid inclusions as both negative crystals and subspherical forms all suggest little post-depositional alteration with the exception of alteration of primary gypsum to anhydrite.

In Plate 7.8 also dominantly of halite (typical of the rock in Plate 7.4), there is a startling contrast to the texture in Plate 7.7. Crystals in Plate 7.8 are anhedral to subhedral, cloudy, coarser and devoid of fluid inclusions (the apparent void in the lower left was produced by plucking of a cleavage fragment from the specimen during sectioning). Because the texture shown in Plate 7.7 is regarded as indicative of little post-depositional alteration, the texture in Plate 7.8 is considered as indicative of extensive alteration, greater than that required for the postulated gypsum to anhydrite alteration which is also postulated for very fine crystals of anhydrite within the halite in Plate 7.8. These contrasting textures are also apparent in thin sections of carbonate rocks. Bathurst, (1975, especially Chapter 12), deals with recognition of chemically precipitated calcite (analogous to Plate 7.7) versus calcite post-depositionally altered from argonite or some other form of pre-existing calcite (analogous to Plate 7.8). Bathurst uses and builds upon terminology and concepts of the causes and processes of these alterations developed by Folk (1965).

Plate 7.9 shows an occurrence of halite with sylvite. The irregular bodies and irregular contacts of the sylvite (as well as the anhedral nature of the halite and bodies of intimately mixed halite and sylvite) are interpreted to be the product of post-depositional alteration. This interpretation is also favored by the fact that sylvite does not occur as a primary precipitate in the marine evaporite succession.

Plates 7.10A and 7.10B show the irregular and gradational nature of the contact between polyhalite and halite and the concentration of opaques, probably hematite, along the contact. These observations and those discussed under Plate 7.3 are interpreted to be products of post-depositional alteration of either anhydrite or halite to polyhalite.

Plate 7.11 shows the microscopic texture typical of many laminated or banded anhydrites of the Castile and Salado Formations. Neither x-ray diffractometry nor staining techniques have been used to determine the mineralogy of the carbonate. This texture is interpreted as annual varves by Anderson et al. (1972).

Plate 7.12A and 7.12B show dominately massive anhydrite, typical of much of the unlaminated anhydrite in the Salado Formation but atypically cut by a veinlet of gypsum. The rock sample was taken from outcrop and the gypsum veinlet is interpreted to have been produced by alteration of anhydrite to gypsum during uplift and exposure.

The petrographic descriptions and interpretations generally agree with those in the classic and relevant report of Schaller and Henderson (1932).

7.4.7 Interpretations and Tentative Conclusions

1. All of the samples discussed under macroscopic and microscopic petrography exhibit mineralogy, lithology and textures which are indicative of post-depositional alteration of the sediments (dated at 204 million years in Section 7.8). It is believed that fluids

migrating through the sediments are responsible for most of these alterations. Interestingly, the alteration of primary gypsum to anhydrite would liberate abundant volumes of fluid.

2. The abundance of polyhalite and the atypical mineral assemblages (sylvite-langbeinite vs kainite/carnallite-kieserite) of the ore zones suggest either drastic recrystallization or a former primary evaporite depositional environment. The areal extent of the Ochoan rocks and their great thickness coupled with paleogeographic evidence and the marine character of the underlying Permian strata appear to preclude the second alternative. Further evidence of the post-depositional origin of the present assemblage includes the low and highly variable bromine values in the Salado Formation rock salts (Holser, 1966; Adams, 1969). Age dates on K-bearing salts, discussed later in this chapter, further suggest recrystallization shortly after deposition.

3. The general mineralogy and chemistry of the EDTA-insoluble (silicate) fractions of the evaporite beds throughout the Salado and uppermost Castile Formations preclude their detrital origin.

4. The silicate assemblages and their chemistry further supports the hypothesis of post-depositional alteration of these rocks — at least throughout much of the Salado Formation.

   a. The predominance of smectites (saponite) and trioctahedral smectite-bearing clays suggest relatively immature assemblages. The silicate assemblages of the Zechstein (Permian) of Germany are almost entirely nonsmectitic except for the well-crystallized, well-ordered regular interstratified chlorite-(smectite/vermiculite) mineral corrensite (Fuchtbauer and Goldschmidt, 1969). The Haselgebrige (Permo-triassic) of the Austrian alps similarly contains no smectites nor even smectite-bearing mixed-layered clays (Bodine, 1971), and the same is true for the Silurian salts of New York (Bodine and Standaert, 1977). The development of the unusual illite-saponite/talc/ saponite phase with polyhalite suggests immaturity of the silicate

phase with respect to the evaporite phase. Any further phase changes that would take place in the silicate appear to be kinetically inhibited.

b. The variability of the clay assemblages and their lack of correlation with major evaporite lithologies bespeaks strongly of recrystallization accompanying migrating post-depositional pore fluids. Except for the unusual 10.3 Å phase with polyhalite, the only other lithic correlations are: (1) reasonably well crystallized corrensite as the only expandable clay in the discreet clay seams and (2) the occurrence of serpentine in the uppermost Castile Formation. The former is tentatively attributed to the "closed system" nature of the impermeable salzton beds; they were not subject to the attacks by a variety of migrating pore fluids of different composition. The latter relates to the vertical distance between K-Mg-bearing salt beds and the Castile Formation, which essentially comes in contact only with less mobile fluids in equilibrium with halite-anhydrite.

c. It is very tentatively suggested that many of the salzton seams formed through accumulation of silicate debris included in salts which have been dissolved; their association with the soluble K-Mg salt ore zones and with the extensive polyhalite replacement of anhydrite beds appears remarkable and may provide the geometry for the "plumbing system" in which migrating pore fluids circulated. It is also recognized that some of the salzton beds may well represent recrystallized detrital accumulations during periods of no evaporite deposition as suggested by Adams (1969). If migrating groundwaters do flow in some such controlled pattern, ore mineral distribution in each ore zone should reflect this, i.e. remnants of the primary carnallite-kieserite farthest from the source of the brines, enveloped by langbeinite and langbeinite-sylvite assemblages, in turn enveloped by langbeinite and langbeinite-sylvite assemblages, in turn enveloped by sylvite, and finally by barren halite. Similarly polyhalite

crystallization should be at a maximum under the
langbeinite-sylvite assemblage within a given "cell" and would
likely decrease both away from and toward the lateral pore fluid
source.

In summary, substantial evidence has been accumulated that there has been
extensive salt recrystallization, most noticeably within the McNutt ore
zone.   This is considerably less noticeable in the lower Salado and
Castile Formations, but may simply reflect the far simpler evaporite
mineralogy and persistence of substantially more homogeneous compositions
within the pore fluids.

Preliminary computer modeling does, for example, substantiate that a
typical primary marine evaporite salt assemblage of
carnallite-kieserite-halite can, when under continued attack by migrating
halite-gypsum saturated pore fluids flowing down dip in a hypothetical
cell, generate a progression of salt facies with remnants of the primary
assemblages farthest from the source.   Toward the source, the following
succession of assemblages would be found: langbeinite-carnallite-halite
(or langbeinite-kieserite-halite) then langbeinite-halite, then
langbeinite-sylvite-halite facies, then sylvite-halite, culminating
toward the source in a barren halite facies.   At the same time, the K-Mg
rich pore fluids which were generated through ore mineral dissolution and
alteration would no longer be in equilibrium with anhydrite; anhydrite
would alter to polyhalite until the solution chemistry reached the
polyhalite-anhydrite equilibrium composition.   The precise thermodynamic
conditions and mineralogic reactions which governed these alterations are
not known; however, the age of this recrystallization of evaporites has
been determined to be in excess of 204 million years.   For more details
regarding this recrystallization which closely followed deposition, the
reader is referred to Section 7.8.

7.5 VOLATILES AND FLUID INCLUSIONS IN MINERALS OF THE SALADO FORMATION

7.5.1 Introduction

Sources of liquids and gases native to the evaporites must be
considered. One source is the intergranular fluid to be found in the
pore spaces between mineral crystals and lithic fragments. These fluids
are discussed in detail in a subsequent section (7.7). Another fluid
source is the water of crystallization chemically bound in hydrous
minerals. Yet a third source is fluid inclusions inside the mineral
crystals themselves, which can behave as separate micro-geochemical
systems.

Data presented in the overview Section 7.5.2, and Section 7.5.3 result
from heating bulk rock samples to recover all types of fluid. In the
major portion of the Salado, the total recovered amounted to less than
0.5 weight percent of the rock. As discussed in the overview section, it
was possible to separately identify: (1) loosely-bound volatiles, (2)
chemically-bound volatiles, and (3) fluid inclusions.

The sections on mineral sources of water and on fluid inclusions endeavor
to place the data in the context of the mineralogy of the rocks serving
as hosts for the volatiles. It will be noted that geochemistry in the
context of the mineralogy is a pervasive theme in all parts of the
geochemistry section of this report. This is true for the sections which
follow on groundwater geochemistry and radiometric age-dating also. It
will also be noted that the characterization of geochemical properties of
solutions in the Salado confirm the qualitative measurements of fluid
inclusion solute contents.

This chapter contains considerable data which will assist in the
anticipation of short and long term physico-chemical conditions likely to
arise during the experiments involving heat-producing radioactive wastes.

7.5.2 Overview of Volatile Contents of Evaporites

Themogravimetric analyses of 35 selected core samples from ERDA No. 9
were made. These were many of the same samples which were qualitatively
examined for mineralogy by x-ray diffraction (refer to Section 7.2.3).

These analyses were made by suspending powdered samples from a
microbalance while dry nitrogen flowed above the sample. The samples
were heated by 5°C/minute until the temperature reached 500°C and
were held there until gas evolution had ceased. A hygrometer was
inserted downstream to register qualitatively whenever moisture was
evolved.

The as-received salt core specimens were massive pieces approximately 4
inches in diameter and 1-2 inches thick. No attempt was made to obtain
homogenized samples by powdering the entire piece. Instead nuggets were
chiseled from the center of the specimen. The nuggets were crushed and
ground to a powder just prior to the weighing and transferring to the
microbalance system. A maximum of ten minutes elapsed between the start
of crushing and the start of analysis. Thus, the possible loss or gain
of moisture prior to testing was minimized. Powdered samples were
necessary to minimize decrepitation.

The complete test results are presented in Table 7.12. Figure 7.7
illustrates the typical kinds of weight-loss curves observed. About half
the specimens showed 0.5% weight-loss (curve A). Curve B is common with
the rapid weight-loss occurring sometimes at 300° and sometimes above
400°C. Some samples show two stages. Only two samples followed curve
C, where weight-loss was observed from the beginning of the run. The
weight-loss curves for all samples are filed and are available for
inspections.

Replicate runs were made in several cases, predominantly those which
showed the larger weight-losses, and good agreement, i.e. within 5%, was
observed.

All mass-loss is not due solely to water. Only the weight-loss below 300°C can be attributed largely to water; the weight-loss at higher temperatures is in part due to decomposition of carbonates or other volatile-bearing minerals.

Results were correlated with the x-ray diffraction results previously reported in an effort to identify which minerals may be decomposing. No definite conclusions could be reached so selected samples were analyzed for the evolved gases by gas chromatography/mass spectrometry. In particular, this was done for the samples 2302.6, 2516.3, 2658.5, 2786.5 and 2821.0.

The highest weight-loss was experienced by sample 2302.6. Its total ion chromatogram (Appendix 7.E) shows data channel numbers calibrated approximately in terms of temperature. Conspicious peaks occur at 100°C, 250°C and 300°C. Detailed mass spectra are given for 50°C, 100°C, 150°C, 200°C and 250°C; the most prominent mass peak is 18, corresponding to water. At higher temperatures, mass 14 (monoatomic nitrogen) becomes abundant. Even at lower temperatures, mass 28 (diatomic nitrogen) is present.

Sets of peaks separated by 12 mass units, corresponding to carbon, (95, 83, 71; 81, 69, 57, 45) probably represent fragments of hydrocarbons present in the diesel oil which was the lubricant used to core the hole. The contribution of mass 44 (CO_2) to the spectrum is a minimum at 200°C and rises again at higher temperatures. The low-temperature contribution is again probably due to the contaminant diesel oil.

At the highest temperatures, the mass peaks 15, 16, and 17 (CH_3, CH_4, O, OH) are accentuated along with 14, 18, and 28 (N, H_2O and N_2). All the individual ion chromatrograms for mass numbers 14, 18, 19, 20 and 44 have coincidental peaks at about 25°C and 300°C. Water and carbon dioxide are almost continuously evolved over the entire temperature range, but the coincidence of all the peaks for N, H_2O, F(?) and CO_2 (mass peaks 14, 18, 19, and 44, respectively) implies that evolution of

these components at 250°C and 300°C is related to a common source. Since halite decrepitates, releasing its fluid inclusions at about 250°C, those inclusions appear to be the most probable source of volatiles evolved at 250°C. Similarly since polyhalite dehydrates at a temperature slightly above 300°C, fluid inclusions in that mineral might be also released at that temperature (see Section 7.3). A detailed treatment of fluid inclusions appears in a subsequent discussion.

Mass numbers 32, 48, 64 and 80 have sharp coincidental chromatogram peaks at channel 517. These mass numbers most probably represent O_2, SO^{+2}, (possibly O_3 made inside the mass spectrometer) SO_2 and SO_3 released from the sudden decomposition of a sulfate. Similarly mass 36 (HCl) is released in major quantity at this point. All these phenomena occur at a slightly lower temperature than the main 200°C event, and their relationship with that event possibly indicates the presence of a very volatile sulfate phase rapidly decomposing when the halite fluid inclusions begin to rupture. Daughter crystals of gypsum in halite fluid inclusions would indicate a high concentration of sulfate in the inclusions (see subsequent discussion) and such a solution might give rise to the observed sulfur species in the mass spectrum.

The sample with the next greatest total mass loss (2786.5, 3.64%) is considered next. Many of the same features of the chromatograms in Appendix 7.E are observed here as in the previous sample. The main difference is the appearance of a large hump of many volatiles (H_2O, F, N_2, O_2) released at less than 100°C. This is consistent with the occurrence of clay minerals which can absorb various volatiles at surface and interlayer sites. Volatiles would be expected to be weakly bound at these sites. The same hump as before appears at 250°C, incorporating N, H_2O, HF(?), N_2, O_2, HCl, CO_2 and SO^{+2}, but only the postulated SO_2 species appears to be catastrophically released and is probably a product of ionization in the mass spectrometer.

A hump incorporating N, H_2O, HF, N_2, O_2, HCl, CO_2 and SO^{+2} occurs substantially below $300^{\circ}C$. This peak probably corresponds to release of water and other volatiles born of OH and fluid inclusions in the clay minerals, when the clays decompose upon dehydration.

Sample 2516.3 (2.15% mass loss) was unusual in that it contained magnesite. As is seen in the chromatograms in Appendix 7.E, the loss of H_2O and N_2 from various sources provides most of the pattern, which was not sampled at a temperature greater than about $240^{\circ}C$. There is almost a continuum of absorbed O_2 released. The most significant feature of this sample is the high-temperature loss of CO_2, presumably from the decomposition of magnesite.

Finally, the most abundant-type sample is considered: those which have mass losses less than 0.5%. These are characteristic of most of the main evaporite section and contain very little other than halite and anhydrite. Typical examples of these rocks are samples 2658.5 and 2821.0 (Appendix 7.E). The main difference between these two is the apparent larger number of types of volatile sites in the shallower sample. Absorbed N, H_2O, N_2, and O_2 form a large, broad hump at low temperature, with catastrophic release (of fluid inclusions?) of H_2O, N_2, HCl, and CO_2 at higher temperature in 2821.0. In 2658.5, the catastrophic release of H_2O, N_2, HCl, and CO_2 (with possibly some SO^{+2}) appears to occur in smaller episodes as various sets of fluid inclusions are ruptured at higher temperature.

7.5.3 Mineral Sources of Water in the Salado Evaporite Sequence

Introduction. The purpose of this section is to describe the mineralogy and petrologic characteristics of samples taken from two coreholes of the Salado salt from the boreholes AEC Nos. 7 and 8 in Lea and Eddy Counties, near Carlsbad, New Mexico, and the degree to which the evaporite rocks present would dehydrate if subjected to the heat generated by containers of radioactive wastes (radwaste). In a previous study, (Fallis, 1973) the general characteristics of evaporite deposits and their minerals were

described and a detailed mineralogic and petrologic study of two cores from the Hutchinson Salt near Lyons, Kansas, was made. The results at that time indicated that water losses ranging from 0.4 to 19.0 weight % might be anticipated if the surrounding rocks were heated to 100°C.

Sample splits corresponding to ones in this section were also discussed in Section 7.3. A comparison of those results and these is presented in the following section.

Sampling and Sample Preparation. Segments of the original 4 inch (10.2 cm) cores were split in half, lengthwise, for chemical analysis and weight loss determination by thermogravimetric analysis (previous section). Eighty-three samples (coded by core number and depth) arrived wrapped in plastic to reduce the possibility of absorption of moisture during shipping and handling. Core AEC-7 was drilled in Lea County, New Mexico, and core AEC-8 in Eddy County, New Mexico.

Throughout the sample preparation, care was taken to not expose any of the samples to water; however, since it was necessary to cut, grind and sieve various portions of the samples, it was not possible to completely protect them from exposure to moisture in the air. During those periods when samples were not actively being worked upon, they were kept in plastic bags, tightly-stoppered bottles, etc.

Since several different analyses were to be made, it was necessary to obtain representative sample splits which would correspond to each other as closely as possible. A more complete discussion of sample preparation is given in the thesis by Combs. However, for convenience, a brief summary of the methods used in sample preparation is given below:

1. A representative segment of each core sample was chosen and removed by sawing the original core (normal to the axis of the core) with a dry blade, masonry-type saw. This new segment was typically about three inches (8 cm) long.

2. Next, a slice was cut from each core segment (parallel to the axis
    of the core) with the approximate dimensions 3 x 2 x 1/2 inches (8
    x 5 x 1 cm) for use in preparing the thin sections. The sections
    were prepared by Fred Roberts Petrographic Section Service,
    Monterey Park, California. They were cut using oil rather than
    water and mounted with an epoxy cement which was not heated.

3. About one-half of the remainder of each core segment was crushed
    and sieved, and representative portions selected to be analyzed by
    x-ray diffraction, x-ray spectroscopy and by static heating
    methods for water loss determination. (Later, some additional
    separations were made and portions of the samples selected for
    bromine analysis using x-ray spectrocopy. These procedures will
    be described briefly in the following sections.)

Analytical Methods Used in This Study. Several different kinds of
analyses were performed on the samples received. The methods used
include static weight loss determinations (water loss), mineralogical and
petrological analysis, and some chemical analyses using x-ray spectrocopy.

The weight loss determinations were made in essentially the same manner
as for samples studied from Lyons, Kansas, and which was reported
previously (Fallis, 1973). Splits of the several samples (sample size
generally ranged from 1.5 to 2.0 gms and in the 60 to 120 mesh size
fraction) were heated to $102\pm5^{O}C$ for periods ranging from 2 to 42
days. The results of repeated analyses indicated that the precision of
weight loss determinations was generally $\pm$ 0.1 to 0.2%. When new sample
splits were used, the "precision" dropped to approximately $\pm$ 0.2 to
0.3%. Some data concerning precision are presented in Appendix 7.F.

In addition to the weight loss determinations performed near $100^{O}C$,
weight loss determinations were also made for several samples which had
been heated to 170 ± 5° (for 2 days) and $300\pm10^{O}C$ for (2 to 3 days).
The results of the weight loss analyses are reported in Appendix 7.G and
discussed in the following section.
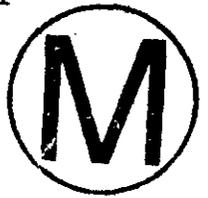
Mineralogical and petrological analyses were made using x-ray diffraction and standard petrological techniques. A summary of important mineralogical and petrological data is given in Appendix 7.H and discussed following the next section. The chemical analyses were made using two variants of the x-ray spectrographic method, x-ray fluorescence analysis (wave length dispersive) and x-ray emission spectroscopy (non-dispersive). The chemical analyses were made primarily for bromine, which can be used to aid in the interpretation of the origin of evaporite deposits, and semi-quantitative analyses were made for chlorine, sulfur and iron.

Weight Losses for Cores, AEC NO. 7 and 8. Weight loss data for the samples studied are tabulated in Appendix 7.G and illustrated in Figure 7.8. In general, the weight losses are much less than those found for samples from the site at Lyons, Kansas. The range of weight loss values at $102 \pm 5^{\circ}C$ for the Carlsbad samples (Salado salt), Cores Nos.7 and 8 was from 0.0 to 3.5% with the majority of samples showing losses less than 0.5%, while the Hutchinson salt, Cores Nos. 1 and 2 was from 0.5 to 19.0%, and most of the samples showed weight losses from 1 to 5%. A plot of approximate range of water loss at $102 \pm 5^{\circ}C$ to be expected at various depths is shown in Figure 7.9. This is based on data from both Lyons, Kansas and Carlsbad, New Mexico sites.

Based on the results of the various heat treatments, the following conclusions can be drawn concerning the behaviour of the samples from Carlsbad:

1. Samples consisting almost entirely of halite and/or anhydrite show weight losses (up to $300^{\circ}C$) which are typically less than 0.5% and probably less than 0.3%. The final total loss will depend on the amounts of clay minerals and minor hydrated evaporite minerals, such as polyhalite, which are present.

2. Larger water losses (>1% at $102 \pm 5^{\circ}C$) are generally associated with the presence of clay minerals (and/or gypsum) in more than trace amounts. The exact losses will depend on

the kinds and amounts of clays present, the temperatures to which they are heated and the length of time for which they are heated.

3. At some temperatures between 170° and $300^\circ C$, polyhalite, which is a common accessory mineral constituent in some parts of the Salado salt, will start to break down. It can contribute water to the extent of about 6% of its weight in the rock being heated.

4. Although present in only minor amounts (or absent) in the samples that were analyzed, there are other evaporite minerals such as carnallite, kainite, leonite, etc., near the potash ore zones (the McNutt potash zone at approximately 1600' to 1800').

The weight losses determined in Section 7.3 are compared with these in Appendix 7.G. It should be noted that the earlier data were determined by thermogravimetric analysis; hence, weight losses were not determined at any fixed temperatures but at the actual temperatures at which the decompositions were detected. In order to make the data more comparable, the previous data were rearranged and weight losses taking place within certain temperature ranges were combined. The reader is referred to Section 7.3 for the specific temperatures at which weight losses occurred. It should also be noted that the two sets of data are not directly comparable, since the weight losses of this section were accomplished by heating under static heating conditions for periods of 2 or more days, while the previous data were obtained under dynamic conditions (much more rapid heating). As a general rule, the decomposition temperature of any given mineral will be higher under conditions of dynamic heating rather than static heating.

Even so, there is generally good agreement between the two sets of data which were obtained by different investigators using different techniques. Most minor discrepancies can be explained on the basis of

differences in the methods of analysis. Only a few real discrepancies seem to exist (such as for sample at 1697 in Core #7). This is to be expected since each group rceived different halves of the core and since Section 7.3 involved sample splits of the entire core segment while this work involved only a sample split corresponding to the portion of the core used in preparing the thin section. Since there are both vertical and lateral variations in mineral content within the cores, samples might occasionally have been analyzed which were mineralogically different.

The rocks being considered at the proposed WIPP site, New Mexico, appear to be much more favorable than those from Lyons, Kansas. Even so, some mineral water is still present and is apt to be released during the period when the rocks are heated by the waste containers. It will be important to determine the maximum temperatures to be reached, the volume of rock which will be heated, and the probable maximum volume of water which will be released.

Mineralogy and Petrology of Cores No. 7 and 8. In some respects the mineralogy and petrology of the core samples from Carlsbad are similar to those of the core samples from Lyons. Both cores were taken through evaporite sequences and hence encountered sedimentary sequences containing typical saline minerals such as halite, anhydrite and polyhalite. In addition, clay minerals, magnesite, gypsum, quartz, feldspar, carnallite, celestite (?), glauconite and kainite (?), were detected in smaller amounts. The presence of any of the other less common evaporite minerals in the samples studied is uncertain. In general, they only occur in such small amounts and/or such fine grain sizes that positive identification was not possible using the diffractometer and petrographic miscroscope. In Section 7.3 it was noted that several of these less common minerals are apparently present in many of the samples analyzed. Readers of this section should be aware that the analyses are based on the actual minerals observed (modal analysis) in thin section as supplemented by X-ray diffraction while the analyses presented in Section 7.3 were done by computer manipulation of the chemical analyses determined for each sample (normative analysis). Such

normative analyses can be quite useful, especialy when working with very

fine grained or glassy materials. However, it should be noted that

normative analyses may generate mineral assemblages which do not agree

with the actual minerals present, as was pointed out in section 7.3.

Summaries of the mineralogic and petrologic features of the individual

samples studies are presented in Appendix 7.H. For the reader's

convenience, some general comments about the mineralogy and petrology of

these samples are presented below. An excellent study of the mineralogy

and petrology of the rocks in this region is given by Schaller and

Henderson, 1932. Brief description of the major minerals noted in the

Carlsbad samples follow.

Halite. Most of the halite is colorless and shows excellent cubic

cleavage. These features, coupled with less low relief and isotropic

optical character, make its identification easy. Sometimes the halite is

colored red or orange by minute inclusions of hematite (or other iron

oxides) or other minerals such as polyhalite. The grain size showed a

wide range, from less than 1 mm (fine grained), to greater than 1 cm

(coarse grained). Grains between 1 mm and 1 cm are considered to be

medium grained.

Because halite fractures and cleaves so readily, it is difficult to

determine whether the numerous breaks observed in thin sections were

already present at depth or whether they developed during the coring

operation, shipping, handling, thin section preparation, etc. More

fractures are noted at the outer margins of each of the thin sections.

However, some of them must have occurred prior to the taking of the core

because they are filled (at least in part) with other minerals,

petroliferous material, etc. In several cases fracture zones could be

traced across the entire width of a thin section.

Inclusions (liquid, solid and gas) are common in the halite. During the

preparation of some samples hydrogen sulfide (gas) was released. In many

cases the inclusions are oriented with respect to the cubic crystal

planes. These oriented inclusions appear to represent hopper crystals which grew at the water surface in times of quiet water and are inferred to represent deposition from shallow water.

Intergrowths of relatively well-formed, cubic crystals of halite with clay and silt-size minerals are likewise inferred to represent very shallow conditions, perhaps even subaerial exposure for brief period.

"Patches" (regular to irregular, more or less equidimensional areas) and "stringers" (regular to irregular areas which are generally elongated in one direction) of anhydrite, polyhalite, clay and silt-sized minerals are common in halite. Sometimes these patches and stringers follow grain boundaries, but often they cut across grains. Where they follow grain boundaries, they may represent (nearly) simultaneous growth of the halite crystals and smaller amounts of the other mineral phase(s). Where they cut across grains, they presumably represent deposition of the minerals along zones of weakness or along which solutions passed. Enough of this latter material is present to demonstrate that there were opportunities for solutions to migrate through these relatively impermeable rocks, even though it is not possible to determine just how far the solutions actually traveled.

Anhydrite. Anhydrite was recognized on the basis of its relatively high birefringence, differences in relief upon rotation and cleavages at right angles. Normally, anhydrite shows parallel extinction, too, but because of twinning, replacement phenomena, etc., this characteristic was not always useful.

Anhydrite occurs in three major types. "Primary" anhydrite, which is commonly bedded, is very fine grained (much less than 1 mm) and somewhat fibrous in character. It also occurs in coarser-grained crystals and twinned crystals (sometimes over 1 cm long). At least some of these larger crystals appear to be pseudomorphs (replacement) after previously-existing gypsum crystals. Sometimes, very small amounts of questionable gypsum are noted nearby, perhaps as a result of partial

rehydration of the anhydrite. Finally, there are more or less isolated crystals and crystal clusters of anhydrite which occur in patches and stringers within the halite or are intergranular with halite. These may be associated with polyhalite and/or clay and silt-sized minerals. This type of anhydrite is thought to be authigenic (formed in place from fluids contained in the pores of the rock or passing through the rock).

Anhydrite can be replaced by polyhalite if fluids containing potassium, magnesium and additional sulfate ions are present. Many examples of this replacement were observed.

A few examples of bedded, nodular anhydrite were observed. The nodules may have originally been composed of gypsum which was later replaced by anhydrite. The origin of such bedded nodules is thought by some workers to represent depositions in very shallow water which was periodically exposed (Sabkha facies).

Polyhalite. Polyhalite was recognized on the basis of its relatively low birefringence, inclined extinction and complex twinning. (Unfortunately in some fine-grained material and/or mixtures, polyhalite and anhydrite can be confused because their optical properties of relief and birefringence are almost the same in certain orientations).

Much of the polyhalite observed is rather fine grained (much less than 1 mm in size for the individual cyrstallites) and often fibrous. However, some larger crystals are numerous, isolated crystals and crystal clusters were observed. Polyhalite is often reddish due to iron oxide inclusions, but this is not universally true.

Some of the polyhalite appeared to be a bedded form associated primarily with halite and lesser anhydrite. Polyhalite also is found replacing anhydrite and associated with nearby patches and stringers of clay and silt-sized minerals. Whether the clay, etc., provided some of the ions necessary for formation of polyhalite or just acted as a pathway for solutions passing through the rock cannot be determined.

Minor Minerals. Minor minerals were identified on the basis of their optical properties and X-ray diffraction analyses, which were occasionally aided by information contained in the well logs for the cores. Just a few brief comments for each mineral are given here.

Clay minerals. Overall, much less clay is present in the samples from Carlsbad than was present in the Lyons samples. X-ray diffraction peaks attributed to clay minerals were noted in nine samples from Core #7 and in fourteen samples from Core #8. Based on the X-ray patterns and peaks noted at approximately 7, 10, 11.5, 14 and 15 angstroms, major clay minerals present include illite, chlorite, mixed-layer clays and possibly some kaolinite.

Magnesite. Although well-crystallized magnesite was not detected in thin sections, some very fine-grained, relatively high birefringent phase was noted in some thin sections and magnesite peaks were detected in some thin sections and magnesite peaks were detected in a number of X-ray patterns. Schaller and Henderson (1932) stated that many of the clays in the samples they studied were magnesitic. The common association of polyhalite with clay and silt-sized minerals may be due in part to the magnesium ions in the magnesitic shales and clays.

Gypsum. Gypsum is monoclinic and in thin section has low birefringence and low, negative relief. Twins ("swallowtail") are fairly common. Well-crystallized gypsum was detected in only one thin section among the samples studied. In addition, several of the sections contained small amounts of questionable gypsum in association with anhydrite and/or polyhalite. However, the amounts present were much less than 1% and could not be confirmed by X-ray diffraction.

Quartz and feldspar. These minerals are present in two forms, as detrital (silt and very fine sand-sized) material deposited along with the clays, and also as authigenic minerals which formed in or near patches and stringers of clay and silt-sized minerals.

Sylvite. A few thin sections contain small amounts of sylvite which was recognized on the basis of its distinctive reddish purple color (due to iron oxide inclusions) and lower relief than halite. Most of the sylvite observed was associated with polyhalite as well as with halite. There were no samples from the sylvinite (mixed halite and sylvite) zones. Adams (1967) reported that not all sylvite is colored; however, in the thin sections studied, the distinctive color was useful in locating the small amounts present.

Carnallite. Only one section contains detectable carnallite. This mineral was suspected on the basis of nearby carnallite as noted in the well log. Its high negative relief and "metallic" luster due to inclusions were used to confirm its presence.

Celestite (?). In two or three thin sections some isolated spear-shaped crystals and clusters of crystals with relatively high relief were noted. Although no positive identification could be made, it is suspected that these are celestite, which is the most common strontium mineral present in evaporite deposits.

Glauconite. A few greenish, rounded grains of glauconite were noted, generally associated with the clay and silt-sized minerals. Not enough of this material was present to attempt to determine its origin or source.

Kainite(?). Kainite (?) was observed in only one thin section. It is a monoclinic mineral with moderate birefringence and negative relief.

Summary and conclusions. The results of this study indicate that the Salado Salt in the samples received is composed primarily of fine to coarse-grained halite with polyhalite, anhydrite, and clay minerals. Other minerals detected in small amounts include gypsum, magnesite, quartz, feldspar, sylvite, carnallite, celestite (?), glauconite, and kainite(?). It should be noted that the samples received for analysis were selected from halite-rich zones in most cases; hence, some of the rarer evaporite minerals such as kieserite, langbeinite, leonite,

bischofite, etc., noted by Schaller and Henderson (1932) were not detected either because they were absent from the specimens analyzed or present in amounts too small (or too fine grained) to identify.

There is much petrographic evidence that the Salado salt was deposited in rather shallow water and may have been exposed subaerially at times. This evidence includes the presence of numerous hopper crystals (which can develop at the air-water interface of quiet, shallow seas) and the intergrowth of euhedral grains of halite with clay and silt-sized minerals, anhydrite, and polyhalite. The latter texture can develop in an exposed, mud-flat type environment. Previous workers, such as Anderson, et al. (1972), have concluded that the underlying, Castile Formation was deposited in deep water, perhaps as much as 2100' (650 m) deep. Hence, there must have been a major change in environmental conditions between the deposition of Castile and that of the Salado.

Petrographic evidence also suggests that local fluids native to the Salado have been able to move through the Salado salt (during recrystallization) along beds and seams of clay and silt, and to a lesser degree along fractures (see Section 7.8). These paths are now marked by entrapped fluid inclusions, zones of altered minerals and zones along which new minerals have been deposited.

Water loss determinations for over eighty samples from cores #7 and #8, indicate a range of water loss (upon heating to $102\pm5^{\circ}C$) from 0.0 to 3.5%, which is considerably below the water losses for samples from Lyons, Kansas. It whould be noted that the samples from the Lyons site came from much shallower depths than those from the Carlsbad area. In the section on weight losses, the ranges of dehydration to be anticipated with respect to depth are shown graphically. It appears that the ranges determined for the relatively shallow Lyons site merge with the ranges determined for the deeper Carlsbad site.

Most of the dehydration water at relatively low temperatures (near $100^{\circ}C$) appears to come from clay minerals, although gypsum may make a

contribution for samples taken at shallow depths. At higher temperatures, polyhalite will start to contribute to the dehydration of water. This dehydration takes place somewhere between 170° and $300^{O}C$. Pure polyhalite rock can lose up to 6% water. In general, the purer halite beds have weight losses below 0.3 to 0.5%.

As far as can be determined from the samples available for study, the rock units present in the Salado salt seem to release much less water when dehydrated than do the rocks of the Hutchinson salt from Lyons. Hence, the site near Carlsbad would seem to be more favorable (in so far as dehydration water goes) than Lyons. However, these rocks are not totally without water, and most units will lose from 0.0 to 0.3% water when heated and some units may lose up to 3.5% water.

Finally, it was noted during the preparaton of some of the samples that H_2S (and possibly some natural gas) was released when the samples were crushed. No H_2S was detected mass spectrometrically (previous section), which probably attests to a sensitivity of the human nose for H_2S that is unapproachable even with the most sophisticated available instrumentation.

7.6 FLUID INCLUSIONS IN CORE SAMPLES FROM ERDA NO. 9

7.6.1 Introduction

Fluid inclusions in the host rock are of interest to several aspects of nuclear waste disposal. First, determination of their origin and nature may provide insight into the complex sequence of processes and events from original deposition of the salt through to the present; such insight may well be of value in site evaluation. Second, fluid inclusions provide one source of water (and other volatiles) that would certainly aid in the corrosion and eventual breach of the waste containers, and subsequent leaching of the waste itself. Third, fluid inclusions, and their reaction under the thermal pulse from hot wastes, could have an effect on important physical properties of the hot host rock, such as deformation rates and particularly melting.

7.6.2 Samples Studied

Most samples studied were taken from ERDA core No. 9, and came from the following footage intervals:

From	To
1799.0	1799.5
1902.0	1902.3
2065.0	2065.4
2095.1	2095.5
2272.4	2272.7
2391.0	2391.3
2611.5	2611.8
2658.7	2659.0
2760.0	2760.2
2820.8	2821.2
2058.8	2059.0
2070.4	2070.6
2606.5	2606.9
2617.2	2617.7
2626.7	2627.0
2659.0	2659.2
2665.0	2665.1
2692.4	2692.6
2699.8	2700.0

In addition to the above "representative" samples, four nonrepresentative samples from ERDA No.9 were selected because they contained plainly visible large inclusions, suitable for special tests:

2061.2 – 2061.6

2064.5 – 2065.0

2614.7 – 2615.0

2518.5 – 2619.0

In order to test certain sample preparation and inclusion extraction procedures with no loss of important core, two pieces of core from AEC 8 were also picked:

$$2059.5 - 2059.8$$
$$2462.0 - 2462.9$$

In the Kerr-McGee potash mine, Lea County, New Mexico, northwest of the WIPP site a 4-m igneous dike has cut potash ore beds. As this represents a natural simulation of some of the heat effects of canister storage, it is instructive to examine the fluid inclusions in samples taken at measured distances from this dike:

MB-77-8   White halite 1-2 cm from dike
MB-76-3   Barren salt 0.2 m from dike
MB-76-4   "Ore" horizon 2.5 m from dike
MB-76-5   "Ore" -21 m from dike

Of these samples, the field evidence indicates that only MB-77-8 has been molten. The others show some mineralogical effects of the heating, but as sedimentary structures are preserved, they have presumably not melted (M. Bodine, personal communication).

7.6.3   Sample Preparation

Sections. A thick slice was cut from each sample using a diamond saw and ethyl alcohol lubricant. One side was fine ground with an alcohol slurry of abrasive (1200 grit), ultrasonically cleaned in alcohol, mounted on glass with cold-setting epoxy resin, and cured in 16 hrs. at room temperature. The section was then ground down on a lap, using an alcohol slurry, to 3-8 mm thickness (depending on opacity) and then polished by finer abrasives, ending with either 1200 grit or 0.3 μm Al_2O_3. Plates with fine-ground surfaces were examined using a matching silicone oil or saturated brine and coverglass. Coarse cleavages could be examined directly, without polishing.

A small section (~ 2 X 4 cm) was cut first, perpendicular to the core axis (when nature of sample permitted orienting), then one or more larger plates (5 X 8 cm) were cut parallel with the core axis.

Coarse water-soluble residues. 100- to 150- gram samples were dissolved in tap water at room temperature with frequent stirring. The solution was decanted frequently to remove dissolved salts and finely divided solids such as clays.

7.6.4   Methods of study

Petrographic Examination. All slides and preparations were examained with the petrographic microscope, but phases present other than halite were not determined due to the short time available and the redundancy with extensive mineralogical work by others. Most examination time was spent on finding and characterizing the nature, size, frequency and distribution of the fluid inclusions.

Considerable time was spent determining the volume of fluid inclusions in the plates, through counts of representative portions. This determination was based on measurements with a graduated ocular (calibrated with a stage micrometer) and several assumptions. First, the inclusions were considered to be cubes (based on observation); one edge was measured and then the volume calculated. Larger inclusions ($\sim$ 1mm edge length) that were obviously not cubes were estimated from the summation of a series of smaller cubes. Second, since bubbles were very rare (only about 0.1% of the inclusions), and small ($\sim$ 1% of inclusion volume), they were ignored. Third, most inclusions in these samples were of one or the other of two types (essentially the same as the types "A" and "B" discussed in a later section on Results), and any given small portion of salt contained only one type. As the bulk of the sample in any plate could be characterized easily into these two types the approximate volume percent of the samples for each type could be estimated. A $\sim$ 500 mm^3 volume of the plate was then selected from each type, visually estimated to be representative of that type in that plate, and the volume percent of inclusions determined in it by measurement and counting, using a transparent grid template at 500X. The total volume percent of inclusions was then calculated from the weighted average. The weight percent of inclusion fluid was calculated, assuming the salt to have a density of 2.2 and the brine to be 1.3 g/cm^3. Large numbers of very tiny inclusions were estimated from counts and estimates of small

but visually representative volumes. Although the relative errors involved in this step are large, the total contribution by these small inclusions, even though they are extremely abundant, was very small. Most of the fluid found was present as a small number of large inclusions that could be measured more accurately. All inclusions over 200 μm (edge length) in the count volume were measured. The overall measurement error in volume percent of inclusions present is believed to be on the order of ±5% of the value stated for a given plate. Other variables, particularly rare, still larger, centimeter-sized inclusions that were opened during coring or sample preparation (and hence not counted), and the large difference between different plates from the same sample, introduced much larger errors.

Heating Stage. The liquid in inclusions trapped as homogenous fluid at above surface temperature shrinks on cooling, forming a bubble that provides a measure of the amount of differential shrinkage of liquid and host crystal. As the bubbles in the inclusions were small, relatively little heating was needed to cause homogenization. Hence a new heating stage was set up, consisting of a bath of silicone oil with an electric · immersion heater and thermometer. Temperature equilibration was achieved through convection and frequent stirring. The individual runs were approximately 2-3 hrs. in length. Many inclusions that had no bubble as received developed one on cooling the silicone to $\sim -6^{\circ}C$ with solid CO_2. On subsequent heating this bubble would decrease in volume but persist as a very small bubble at room temperature. Heating was done on the stage of a low power binocular microscope, since the inclusions were large and scattered.

Freezing stage. The depression of the freezing point of the fluid in an inclusion (i.e., the "freezing temperature") is a function of the composition of the fluid. Using this techique under the microscope can permit a quick measure of the salinity of 10^{-10} g of fluid, a far smaller sample than can be measured by any other method. Metastable supercooling is common, so most inclusions had to be cooled to very low temperatures (three hours in CO_2-acetone at -78° or even LN_2 at $-196^{\circ}C$) to cause freezing. Subsequent slow warming of the sample while

surrounded by rapidly circulating refrigerated acetone of known temperature under the microscope permits recording the temperature of disappearance of the various solid phases formed on freezing (salts, hydrates, and ice), under equilibrium conditions.

If an inclusion is frozen completely to a mixture of solids, with no liquid, it becomes rather opaque. On warming, the first melting wets the crystal interfaces, suddenly making the mass more translucent, and permitting recrystallization to coarser crystals with time. This is called the "first melting temperature." It ranges from $-21^{\circ}C$ for pure NaCl solutions to $-51^{\circ}C$ for $CaCl_2$ solutions.

Crushing stage. If a host crystal containing an inclusion with a bubble is surrounded by a fluid and gradually crushed while under the microscope so that the behavior of the bubble can be observed, the presence of noncondensable gas in the bubble, and its pressure, can be determined. The test is only crudely quantitative in terms of pressure (based on the volume precent expansion), but it is extremely sensitive as a detector of small amounts of gas. Less than one billion molecules of gas can be detected readily. Numerous cleavage fragments of salt containing various types of inclusions were crushed on several models of crushing stages to determine the amount and pressure of any noncondensable gases present.

Coarse water-soluble residues. These were studied in oil immersion mounts in hopes that some of these phases were sufficiently coarse to contain fluid inclusions that would provide data on their conditions of formation.

Decrepitation. A portion of the core weighing approximately 100 g was split out with a rock splitter; where possible the outside core surface was avoided, due to the probability of physical deformation and resultant leakage of incluions. This piece was wrapped loosely in aluminum foil, weighed, and heated to the run temperature ($150-250^{\circ}C$) over a period of 8 hours to avoid thermal shock, held at run temperature for 3-4 days, cooled and reweighed to determine weight loss. Following this the homogenization temperature range was redetermined for a series of

inclusions that appeared, on petrographic examination, to be representative. Crushing tests were also repeated on the heated samples to detect the presence of noncondensable gases under pressure.

7.6.5 Results of Petrographic Examination

Inclusions type A. This is the most abundant type by far. It consists of slightly rounded cubic cavities (Plates 7.13 and 7.14) filled with liquid and generally no other phase, except for rare tiny vacuum (shrinkage) bubbles that comprise ~ 1% by volume of those inclusions having bubbles. Only about 0.1% of the inclusions have bubbles, usually the larger inclusions only, but there are exceptions (see below). Type A inclusions occur as dense irregularly shaped clouds of randomly distributed but crystallographically oriented inclusions (e.g., Plate 7.16). In such dense arrays, individual inclusions are rarely over 20μ m on an edge (Plate 7.18), few are >5 μ m, and most are in the range 0.5-2.0 μ m, with the highest concentrations in the smallest sizes (Plate 7.19). Estimates of the maximum number of such inclusions, based on counts of representative volumes, show about one inclusion per 100 μ m^3, or 10^{10} per cm^3. If these are assumed to average one μ m^3 in volume, such cloudy halite would contain about one volume percent of fluid.

In addition to these irregular clouds, abundant type A inclusions occur in crystallographically arranged (cubic) planes and zones in the host halite, frequently with parallel inclusion-free zones (Plates 7.13 and 7.14).

In some zones type A inclusions grade into more sparsely distributed but larger inclusions (< 100 μ m), as seen in Plates 7.14 and 23-24. These coarser inclusions may represent incipient recrystallization of the host. The distinction between these larger type A inclusions and type B (next section) may seem inexact, but actually there is little overlap.

Inclusion type B. Type B inclusions, although far less abundant than type A, carry most of the inclusion fluid in these samples, since they are much larger ($\geq$ 100 μ m to several millimeters). Although large, many have no bubble as found (Plate 7.20), but may develop one if cooled slightly ($\sim$ -7°C) and warmed back to room temperature. They are generally irregular if large ($\geq$ 500 μ m) and are more nearly euhedral negative cubes if smaller (Plates 7.15 and 7.17). They occur as single isolated inclusions in otherwise almost optically clear halite, and as dense groups of many inclusions, in part interconnected with tubular extensions (Plate 7.15).

The host halite for type B inclusions may occasionally have cloudy wisps of type A inclusions, but they are never immediately adjacent to a large inclusion (Plates 7.15 and 7.17). These features suggest that salt originally containing only clouds of "primary" type A inclusions has been partly or completely recrystallized to form coarser crystals of clear salt with type B inclusions. This interpretation is supported by the grain size of the host salt, which is almost always coarser in those parts of a sample containing type B inclusions (see Table 7.13 in next section on weight percent of fluid). The boundary between cloudy primary and clear recrystallized salt is sometimes curved (Plate 7.16). If it were straight, it might not be possible to distinguish it from a primary growth zone boundary between fast cloudy and slow clear growth. Most areas of type A occur as irregular masses within single crystals of mainly recrystallized halite (Plates 7.15 and 7.17).

Relatively few samples, particularly sample 1902.2, show birefringent crystals of an unidentified phase inside what appear otherwise to be type B inclusions. These are equant to bladed crystals of moderately high birefringence ($\sim$ 0.06) and moderate index of refraction (but well above that of the surrounding brine). Many are twinned (Plates 7.25 and 7.26), and when prismatic or bladed, the extinction positions are strongly inclined to the crystal elongation. As the distribution of these crystals is irregular, and as a similar birefringent phase occurs in some of the same samples (Plate 7.27) the occurrence in the inclusions might be interpreted as accidental trapping of solids present at the time of

trapping of the inclusions. All 10 inclusions in one group in sample 1902.2 (Plate 7.27) contain these crystals, in roughly the same amount (estimated at ~ 5% by volume), thus suggesting that they are true daughter crystals, formed by precipitation from the trapped fluid. Another plane of inclusions in this same sample, only 400 µ m away, contains only liquid (Plate 7.28) so it is concluded that the fluids present during recrystallization changed in composition with time.

Inclusions Type C. This type is similar to type B in size, shape, and occurrence, but rarer, and differs only in containing a relatively larger gas bubble, of variable volume, but > 1% by vol. (Plate 7.29). A larger gas bubble can originiate by several processes -- leakage, necking down, higher temperature of trapping, or primary gas. The gas bubbles in these inclusions are found to be under pressure (see "Results of crushing stage studies"), so it is believed that such inclusions have trapped a mixture of gas and liquid (i.e., primary gas). In some (e.g., Plate 7.30), such inclusions have apparently formed by a refilling of an earlier type B inclusion with a gas-liquid mixture along a crack.

Inclusion Type D. This type occurs in curving planes outlining some of the individual crystal boundaries (Plates 7.31 and 7.32). It was probably full of fluid under natural conditions, but as the grain boundary permitted leakage and desiccation, these are now full of gas (presumably air).

7.6.6   Weight Percent of Fluid

A summary of the results of measurements of the volume percent of fluid in the inclusions is given in Table 7.13. In calculating these volumes some simplifying assumptions had to be made, in addition to those mentioned in Section 7.6.5. For simplicity the host salt volume counted was categorized as type A or B on the basis of the maxiumum size of inclusions it contained. If these were ≤ 1 mm, it was called type A. This division is not the same as given in the descriptions of type A and B inclusions, where ~ 100 µ m inclusions are considered as probably indicative of recrystallization, but this has little effect on the results, since on the average, over 90% of the fluid is present as type B

inclusions > 1mm in about 30% of the volume of the salt. Table 7.13
shows that these samples now contain a total of from 0.17 to 2.86% fluid
by volume, and average 0.61. These values correspond to 0.1 to 1.7
weight percent fluid as extremes, and average 0.36 weight percent. These
results are compatible with those reported in Sections 7.5.2 and 7.5.3.

These values have a measurement error of about ± 5% of the amount found.
Much larger, however, is the variability introduced by the samples
themselves. Thus three parallel plates were cut at ∼ 3-cm intervals
through samples 2272, and yielded 1.23, 0.36, and 0.20 volume percent
fluid.

Even more important to consider is the bias inherent in these
measurements due to substantial and unpreventable loss of inclusions.
Examination of the cores showed some centimeter-sized cavities, the sites
of former fluid inclusions. No inclusion this size could possibly be
included in our count since the plates counted had to be <1 cm in
thickness to be translucent. In addition, in situ all natural
intergranular porosity in these salt beds was possibly full of fluids.
The type D inclusions found represent probably only a trivial part of the
total in situ water content present as such "imperfectly sealed fluid
inclusion." Large scale in situ porosity tests would be needed to
evaluate this variable.

7.6.7   Results of Heating Stage Studies

Only 35 inclusions were run, as listed in Table 7.14. These are mostly
from type B inclusions. Some of these inclusions had to be cooled to
below room temperature to nucleate a bubble before the run (Plates 7.20,
33 and 34). Why some very tiny inclusions have vapor bubbles (Plate
7.36), yet many large ones have persisted metastably as stretched liquid
(i.e., one phase) is puzzling. The data are too sparsely distributed to
determine whether the range of values (20.4 to 45.5°C) represents a
real difference between samples. One group of inclusions in sample 2821
with birefringent daughter crystals showed no change in the crystals on
heating to 24.5°C.

7.6.8   Results of Freezing Stage Studies

Inclusions in NaCl have a special type of behavior on freezing, as a
result of reaction of the water of the inclusions with the walls to form
the new incongruently-melting phase hydrohalite ($NaCl.2H_2O$), at
temperatures below $+0.15^\circ C$. As a result, the inclusion enlarges and
becomes full of birefingent crystals upon being held at low
temperatures. Evidence of this expansion remains on warming to room
temperature. Furthermore, the volume resulting from expansion to form
ice is frequently larger than the original volume of the inclusion, and
the inclusion's walls crack to relieve the pressure (Plate 7.35).

The freezing data are summarized in Table 7.15. If the solution present
is simply NaCl and H_2O, the last crystal of hydrohalite will melt at
$+0.15^\circ C$, assuming equilibrium has been obtained (which is an extremely
slow process for this phase). Although only relatively few large type B
inclusions were run, many smaller type A inclusions were also watched at
the same time. None were found to have either first melting at -21° or
freezing at $+0.15^\circ C$, so none consist of essentially pure NaCl
solutions. Much hydrohalite formed in these inclusions, but as there
were birefringent crystals (generally with birefringence less than that
of hydrohalite) that persisted well above $+0.15^\circ C$, the last solid is a
phase other than hydrohalite, and the solutions must contain significant
quantities of materials other than NaCl (Plate 7.37). This is also very
evident from the first melting temperatures.

7.6.9   Results of Crushing Stage Studies

Bubbles in types B and D inclusions from several samples were examined on
the crushing stage. All disappeared immediately on opening, indicating
that they consist of water vapor (at $\sim$ 20 mm pressure), and hence
collapse at one atmosphere. The bubbles in several type C inclusions
showed considerable expansion, however, indicating gas under pressure.
Thus the bubble in the inclusions shown in Plate 7.38 expanded 270% by
volume on opening (Plate 7.39), indicating that nearly three atmospheres
of noncondensable gas is present. The composition of this gas is unknown
at present.

A previously unrecorded inclusion deformation phenomenon was also observed in some inclusions that were in a sample that was under uniaxial stress on the crushing stage at room temperature but had not been broken to release the inclusions. These inclusions developed a scalloped pattern along the corners (Plate 7.40), presumably due to solution at points of stress concentration and redeposition elsewhere. This pattern developed over a relatively few minutes at effectively constant stress. At least some volume change occurred in this process, since the bubble in the inclusion disappeared at constant temperature.

7.6.10 Results of Study of Coarse Water-Insoluble Residues

The weight percent of such residues ranged from 0.005% (sample 2391 to 0.3% (sample 2821). Unfortunately, however, although there were a variety of phases present in the residues, none of the crystals contained visible fluid inclusions. Some samples emitted a petroliferous odor and showed oily films on the water surface during leaching; it is not known whether these represent contamination from the oil-based drilling mud used in part of the coring, or natural oil in the samples (as is present in other salt deposits, as integranular films and inclusions). No oil inclusions were seen in this work.

7.6.11 Decrepitation Tests

These tests were run only on the last nine samples of the first 19. A summary of the test data and results is given in Table 7.16. On examination of the material after the decrepitation tests, several general features were evident. The nature of the test is such that systematic inclusion counts before and after the test on the same sample are impossible. It was obvious that although most of the larger inclusions had decrepitated, and were empty, many small inclusions ($\leq$ ~ 100 μ m) had not. These small inclusions appear perfectly normal in distribution, but almost all had developed appreciable vapor bubbles (Plate 7.41), with a vapor/liquid ratio that is obviously higher after heating than that present in two-phase inclusions before heating. Only the 150°C sample still had inclusions without bubbles; a few 10-20 μ m one-phase liquid inclusions were found there. All three samples showed some "steam" inclusions - cubic negative crystals with fillets of liquid

in the corners. No gas under pressure was found in any of the heated
inclusions. In most cases, the weight losses increase with increasing
run temperature; the several exceptions are probably a result of
nonhomogeneous distribution of inclusion in the sample aliquots taken.

Homogenization temperatures were determined on two-phase inclusions
remaining in the samples after the decrepitation tests. The results are
given in Table 7.17, along with the volume percent of vapor phase,
estimated from measurements of bubble diameters.

7.6.12   Study of Suite of Samples from Kerr-McGee

The three samples closest to the lamprophyre dike (See Chapter 3) yielded
usable inclusions. (Sample MB-76-5 was too fine grained and opaque to be
usable by the sample preparation techniques used here, and will not be
considered futher in this report.) In all three samples about 15% of the
small inclusions ($< \sim 20$ μm) were without bubbles as received. Most
inclusions in all three samples were normal, two-phase inclusions with a
small bubble. Homogenization temperatures were determined on a
representative group of these two-phase inclusions in each, with results
as shown in Table 7.18.

Freezing runs were made on inclusions in two of these samples. In both
cases the first melting temperatures were well below that of a pure
NaCl-H_2O system ($< -28^{\circ}C$ for MB-77-8 and $< -31.0^{\circ}C$ for MB-76-4).
On warming, the last solid phase to dissolve in both samples was an
unidentified phase, presumably a hydrate other than $NaCl\cdot2H_2O$. This
dissolved at +11 to +18°C (MB-77-8) and at +4 to +7.2°C (MB-76-4).

One 75-μm inclusion was found in MB-77-8 that yielded an entirely
different freezing behavior. This inclusion contains a single homogenous
fluid at room temperature, presumed to be gas (Plate 7.43a). On cooling
to the range -70 to -75°C this inclusion develops a number of grains of
an unidentified solid (Plate 7.43f). On warming to about -68°C, a
liquid/vapor meniscus becomes visible (Plate 7.43e), with solid grains

still present. The last of these grains disappears at $\sim -56^\circ$C (Plate
7.43d); on further warming the liquid/gas meniscus becomes faint (Plate
7.43c) and the two homogenize, by expansion of the liquid, at -20.9°C
(Plate 7.43b). This behavior is difficult to interpret in terms of
composition. CO_2 has its triple point at -56°C, in exact agreement
with the disappearance of the solid phase at -56°C observed here, but
obviously the inclusions cannot contain just CO_2, as there is liquid
present at a lower temperature. The nature of the mixture of gases can
only be guessed at this time.

The crushing tests in the Kerr-McGee mine samples were most revealing.
The normal, small-bubble inclusions contain a vacuum bubble (i.e., water
vapor at ~ 20 mm presure). Many inclusions that either had a very large
bubble or appeared to contain gas only, from all three samples, were
found to contain either vacuum (Plates 7.44 and 7.45), or a partial
vacuum (Plates 7.46 and 7.47). These are probably from the trapping of
bubbles of steam, with or without some noncondensable gas and brine. All
three samples also contained a few inclusions with gas under greater than
atmospheric pressure. These inclusions were one-phase as first observed,
and except under special circumstances, it is not possible to distinguish
between a vacuum, dense gas, or even liquid, in such single inclusions.
It is only on crushing, when these inclusions formed bubbles of
noncondensable gas in the surrounding fluid, that the internal pressure
became evident. By measuring the size of the inclusions before crushing,
and the diameter of the bubbles evolved, we obtain a crude measure of the
internal pressure, assuming each unit volume expansion corresponds to one
bar pressure. In a few inclusions, the contents changed to a two-phase,
liquid + vapor system during the expansion (Plate 7.48), but usually the
pressure release was too sudden to reveal if there was a transient
two-phase condition. The volume expansion varies for different
inclusions, from 30- to 40-fold (Plates 7.49 and 7.50) to a maxiumum of
perhaps 100-fold (Plate 7.51). As the immersion medium used is an oil in
which methane is probably readily soluble, this gas is more likely CO_2,
since the bubbles dissolve in the oil very slowly.

Interpretation of the data from the Kerr-McGee mine samples is difficult at this time. The presence of an inclusion filled with a dense CO_2-rich (?) gas in sample MB-77-8, (in halite that was probably molten at the time of intrusion of the dike) is not unexpected, since there is a small amount (0.2-2%) of magnesite in the adjoining rock (M. Bodine, personal communication). The dike shows no evidence of carbonate alteration, however, and there is a problem in explaining the presence of inclusions of low-temperature, gas-free brine, apparently pure steam, and dense CO_2 in the same sample. Formation of these types at different times is obviously required, but there is no other indication of differences in conditions or time of origin.

The temperature at which the dense gas inclusion was trapped is of interest. Although the melting point of pure NaCl is 800^OC, other materials present here in the potash ore zone (such as KCl) will lower this temperature. If we assume that the gas inclusion contains pure CO_2, the -21^OC homogenization indicates a filling density of about 1.03 g/cm^3 (Roedder, 1965). Combining this with the estimate of confining pressure of ~ 38 MPa (380 bars) yields an obviously erroneous "trapping temperature" of 0^OC. The several inconsistencies and difficulties in interpretation of the data from the Kerr-McGee samples cannot be resolved until additional studies are made.

7.6.13   Discussion

Geological Significance. Several aspects are evident from these various results. First, the fluids in all the inclusions, both type A in primary salt crystals and type B in recrystallized salt, are strongly saline brines, with significant amounts of other salts present in addition to NaCl. These brines differ from one inclusion to another, indicating that a range of fluids has been present at various times in these beds, but no inclusions with simple NaCl solutions were found, as are found in other salt beds and as might be expected if pure salt beds have been fractured in the presence of meteroically-derived (fresh) ground water. The original deposition of salt occurred from highly-concentrated brines, and

presumably all waters that have passed through these samples since have had dissolved in them amounts of other minerals in addition to NaCl. Such fluids have caused extensive recrystallization of the salt, and presumably other mineralogical changes, so that little of the original salt texture remains. Second, at some stage in this recrystallization, gas-liquid mixtures were present in the pores of these beds. Third, this recrystallization occurred at near-surface temperatures $(20-45^\circ C)$. Fourth, the movement of these fluids must have been slow, as the evidence of extensive inclusion metastability indicates very clean solutions, free from the solid nuclei present in most fast-moving near-surface waters.

The fluids from which the salt crystals making up these beds originally crystallized were exceedingly saline brines with much material other than NaCl in solution, as shown by the freezing data on primary inclusions in hopper salt. These hopper crystals appear to have grown on the surface and then to have sunk, as described by Dellwig (1955). All but about 1% of this original hopper salt texture has been eliminated by recrystallization at some unknown later time, yielding coarser, clearer crystals of salt, and presumably gross changes in the mineral assemblage other than halite. Some of the clear salt surrounding the chevron structures may represent crystallization of these hopper nuclei on the bottom of the basin, but most is believed to be from recrystallization. This recrystallization occurred in the presence of exceedingly saline brines and with much material other than NaCl in solution. The brine may have been composed essentially of fluids from the primary fluid inclusions, released during the recrystallization. It was trapped as large inclusions in the recrystallized salt and comprised the bulk of the liquid now present in the samples as studied in the laboratory. Although the salt beds now appear dry to the eye, the samples contain 0.1 to 1.7 weight % fluid as examined, and may contain more in situ. At some stage or stages early in the history of these beds, the fluids present in these rocks varied in composition. (See section 7.7) A very few were saturated with organic gases such as methane and actually contained bubbles of a separate gas phase. Others contained additional salts in solution, resulting in the precipitation of various crystalline solids

from the liquid within inclusions in halite. The relative time sequence
of these various fluids is not known, and most inclusions have neither
methane nor crystalline solids. The latest episode of any
recrystallization has been dated at 204 million years, slightly younger
than Permian.

Homogenization temperatures of inclusions in recrystallized salt range
from 20.4 to 45.5^{O}C. During burial, creep from recrystallization in a
salt bed with intergranular films of solution should result in the
hydrostatic pressure on fluids (during trapping in a crystal) being
essentially equal to the lithostatic pressure. If an overburden of 5000
ft. (1524 m) is assumed to have been present during the recrystalliza-
tion, the maxiumum pressure (lithostatic) would have been ~ 38 MPa
(380 bars). There are no PVT data on the specific fluids present in the
inclusions, but if the data on a 25-percent NaCl solution are used, this
pressure would suggest a maximum pressure correction of 36°C (Potter,
1977), and hence trapping (i.e., recrystallization) temperatures of
56-82°C. However, the true pressure correction may be lower,
particularly since the fluids are more saline than 25-percent NaCl. Thus
there is a drop of 12°C in the pressure correction on changing from
20-percent NaCl to 25-percent NaCl.

The presence of smooth planes of primary hopper salt inclusions of
various sizes, separated by planes of inclusion-free salt, with the plane
orientation horizontal, proves that these minute inclusions have not
moved measurably since deposition, although they have been in a
geothermal gradient presumably similar to that of the present for about
225 m.y.

The widespread occurrence of metastable phenomena in these inclusions,
even in some large ones, suggests that fluid flow in the past through
these beds has been very slow. Also, the fact that all inclusions that
have been frozen prove to contain bitterns, and none was found with just
NaCl-H$_2$O solution, proves that at no time during the history of these
samples did ground water, saturated only with respect to NaCl, ever
penetrate into these particular samples.

Nuclear Waste Disposal Significance. The most signficant aspects at this stage in the study are as follows: First, the amount of fluid water solution now present in the samples as fluid inclusions averages 0.36 weight percent. Second, although noncondensable gases are present under pressure in some inclusions, the total amount is very small. Third, the inclusions change dimensions signficantly within minutes at room temperatures when the host crystal is subjected to uniaxial stress; this might suggest more rapid movement of inclusions in a thermal gradient if simultaneously under stress, as in mine pillars. Fourth, and possibly most significantly, the distribution of primary inclusions indicates that they have not moved visibly (i.e., less than a few micrometers at most), in the 225 million years since they formed, yet they have been in the small but finite geothermal gradient all this time. All fluid inclusions can be expected to move when placed in a thermal gradient. Since there is usually a thermal coefficient of solubility, material will dissolve on one wall and precipitate on the other. The rate of movement is a complex function of numerous variables (including inclusion size), but the temperature coefficient of solubility is probably the most limiting parameter in the case of NaCl. In the pure system $NaCl-H_2O$, the solubility change per 100g H_2O is low, only $0.03gm/^{\circ}C$ in the range of $0-100^{\circ}C$. This increases by approximately a factor of two at the elevated temperatures expected near the wastes. This coefficient is comparable in the $NaCl-MgCl_2-H_2O$ system.

All these aspects will now be treated in expanded detail.

Amount of Water in the Beds. Although this is the most important single datum that might be obtained from inclusion studies, fluid inclusion counting can provide only approximate values. The nature of the samples and the necessary sample preparation are such that there is a bias toward low values built into these data. Superimposed on this uncertainty in accuracy is poor precision in the measurement, due to variability of the sample material. For example, adjacent slabs of the same sample showed a five-fold range. It is probable that precisely calibrated neutron logs, reflecting the amount of hydrogen in the beds, give a more accurate

evaluation of the total water present, since they would effectively integrate over a much larger sample and would include the effects of the liquid-filled intergranular cavities which these tests miss.

One important aspect of the inclusions on the properties of the salt is the effect of the constitutents present on the lowering of the temperature of melting, and on the amount of liquid present at any given temperature. In this connection it is important to note that the inclusions' fluid is not water, but a strong bittern with probably significant quantities of magnesium ions. This will certainly affect the temperature coefficient of solubility of NaCl in these liquids, and will have important effects on the vapor pressure of these liquids (see below).

Corrosive Gases in the Inclusions. Although gas analyses by mass spectrometry are still to be made on the inclusion fluids, it is evident from the crushing studies that the inclusions in these samples, at least, contain very little noncondensable gases. Although hydrogen sulfide was found as an important constituent of gases in a gas pocket in another drill hole, (ERDA-No. 6, Section 7.7), there can be very little, if any, in these inclusions. The human nose is a rather sensitive detector of H_2S, ordinarily responding to a minimum of $\sim 10^{-10}$ g. No odor of H_2S was detected during preparation of these samples, when relatively large volumes of inclusion liquid were exposed to the air. Gases such as HCl formed within the inclusions or by reactions of inclusion fluids with other minerals during heating, and under intense gamma radiation, may be a much more important cause for corrosion than those now present in the inclusions.

Effects of Water on Physical Properties of the Salt. The intergranular porosity in these salt beds, in situ, possibly contains some aqueous solution. Such fluids will tend to be squeezed out of the salt beds over geological time as recrystallization along grain boundaries and other processes permit compaction, just as the residual water in a sandstone is eliminated during the formation of a quartzite. Such flow will occur, however, only if there is an escape route for the fluid to take. As

pointed out very aptly by Baar (1977), there is much evidence from high pressure fluid pockets that salt rocks in situ are generally impermeable at depths exceeding about 300 m. It may well be that under such conditions, which preclude further "dewatering", the fluid in these intergranular films is still able to migrate short distances, enough to permit it to coalesce into "pockets", perhaps at points of slightly reduced pressure, just as a plastic shale will flow to the crest of folds in firmer rocks. These "pockets" might be represented in part as the short-lived seeps observed in potash mines.

Even if the intergranular liquid were to be removed completely, yielding a polycrystalline texture with salt crystals in true contact with each other, there is no driving force to remove the fluid inclusions from within the individual halite crystals. If such a salt bed is deformed to the point of rupture of salt crystals, any inclusions along the rupture will provide water to "lubricate" the fracture and hence lower the apparent strength of the rock. Although one might expect that a new fracture would preferentially follow planes of inclusions, as from the healing of former fractures, Gerlach and Heller (1966) have shown that the salt recrystallized in the vicinity of such a healed fracture is actually stronger than the adjacent unrecrystallized salt, and new fractures could not be made through the inclusions. Actually, most of the fluid in inclusions in the Carlsbad salt is in large, apparently randomly arrayed inclusions in recrystallized salt, and examination of fractures through such samples suggests that cracks induced in the laboratory experiments reported here have preferentially taken routes through such inclusions.

One example of the surprising effects of inclusion fluids on the properties of salt crystals is found in the behavior of fluid inclusions in single crystals of salt under uniaxial stress (Plate 7.40). Under these conditions, fluid inclusions visibly change shape, and volume, within a few minutes, at room temperature. This is a new inclusion phenomenon, never reported before.

Evidence of Previous Solution Movement in These Beds. The fluid inclusion evidence obtained so far on solution movements is encouraging in that it indicates at most only very slow movement, and suggests that part of the fluids now present in these beds may even be nearly Permian in age. The lack of any pure $NaCl-H_2O$ inclusions also argues against any previous sudden inrush of groundwater that could be trapped as inclusions in halite before it had time to acquire a full complement of other salts.

Movement of Inclusions in a Thermal Gradient. All fluid inclusions should move when the host crystal is placed in a thermal gradient. The nature and rate of such movement has been the subject of numerous studies, since it is of consequence in the chemical industry. Wilcox (1968) summarizes this extensive work (citing 111 references). Similar migration of inclusions is also an important cause for degradation of laser crystals grown at high temperatures by the Czochralski technique (Hopkins et al., 1976). Most liquid inclusions move up the thermal gradient, but if the vapor bubble is large relative to the liquid, and particularly if boiling occurs, the movement may be in the reverse direction (Wilcox, 1969; Anthony and Cline, 1972; Chen and Wilcox, 1972). The rate of movement is independent of inclusion size in many systems, but strongly (and directly) dependent on inclusion size in others (Wilcox, 1969); there may be a threshold size below which no movement occurs (~ 10 μ m in KCl; Anthony and Cline, 1971a). Large inclusions may break up during movement (Wilcox, 1968; Anthony and Cline, 1973). Many factors may affect the rate of migration, even in a given host, including gravity, composition, surface tension, inclusion shape, crystal anisotropy and imperfections, presence of a foreign gas, etc. In salt, since the thermal coefficient of solubility is small at surface temperatures, but increases greatly with increase in temperature, the rate of movement in a given gradient can be expected to increase with increase in ambient temperature. Higher ambient temperature also increases the travel rate by increasing the solubility, the diffusion coefficient, and the interface kinetics, and the increase in rate was found to be particularly striking in NaCl (Wilcox, 1968, p. 20). The

fact that the inclusions in Carlsbad salt have not moved measurably during geological time in the geothermal gradient is perhaps an indication of exceedingly slow rate, or perhaps a result of a very weak driving force.

Accurate prediction of behavior of _in situ_ inclusions in the thermal gradient around a canister in salt cannot be obtained at this time, as there are too many uncontrolled variables. Since most inclusions at Carlsbad contain no bubble or only a very small bubble, they will move toward the canister, as was shown to occur at Project Salt Vault (Holdoway, 1974). The rate of this movement will depend most particularly on the inclusion size, the ambient temperature of the grain, the temperature gradient, and the temperature coefficient of solubility of NaCl in the particular inclusion fluid involved. The average distance that an inclusion must travel before it intersects a grain boundary will vary with the grain size of the salt, but seldom would be over 1 cm.

What can be expected when the inclusion reaches a grain boundary? Anthony and Cline (1971b) showed that grain boundaries in crystal aggregates tend to trap migrating droplets, but Anthony and Sigsbee (1971) showed that gas bubbles (10-50 μm) migrating in polycrystalline camphor could cross grain boundaries. However, migrating bubbles were observed to drag grain boundaries when the bubble concentration on the grain boundary was large. In Project Salt Vault, Holdoway (1974) says only that "little migration across grain boundaries appears to have occurred." Obviously, if a grain boundary is very tight, a large inclusion could cross it without effect. But if the grain boundary is composed of different material, the fluid could spread out along it as a film. Any such film should act as an inclusion, with material diffusing across it away from the heat source.

The behavior of an inclusion migrating to the wall of an open cavity (e.g., that holding the canister) will be different. On contacting the cavity, Anthony and Cline (1974) and Wilcox (1968, 1969) have shown that

some evaporation occurs, a vapor bubble forms, the inclusion seals itself, and now that it has a large bubble, it reverses direction and moves back the way it came, this time going down the gradient.

Decrepitation Release of Liquid Inclusions. In view of the expected slow migration rates of liquid inclusions in the thermal gradients established by the canisters, it seems probable that release of inclusion fluid by decrepitation will be an important process. An individual inclusion, if it is assumed to have rigid walls, to contain 25-percent NaCl solution, and to homogenize at 40°C, will develop 70.0 MPa (700 bars) internal pressure when heated to 100°C, and 200 MPa (2000 bars) at 200°C (Potter, 1977). However, salt cannot stand such internal pressures without yielding. Even a strong, hard mineral such as quartz starts to decrepitate when the internal pressure in its fluid inclusion reaches 80 $\pm$ 3 MPs (800 $\pm$ 3 bars) (Khetchikov and Samoilovich, 1970), and halite can be expected to decrepitate when the internal (inclusion) pressure reaches four times the yield stress for monolithic halite, under no confining stress (Cline and Anthony, 1971).

When Carlsbad halites were heated, some of the inclusions decrepitated in part causing the samples to fragment, and yielding an average weight loss of 0.13% (150°C), 0.22% (200°C), and 0.73% (250°C). This means that this much volatiles left the system. More inclusion fluid may well have been exposed, and merely lost water until its concentration of salts was such that the vapor pressure of H_2O at that temperature was less than one atmosphere. Salts in solutions in these brines (including materials other than NaCl as well) have effects on the vapor presure and hence on any vapor transport.

In addition to those inclusions that decrepitated, however, many inclusions remain sealed as liquid inclusions in the sample after heating, albeit in a changed form. These have permanently deformed their walls to form a larger chamber, and now have a much larger shrinkage bubble, proportional to the amount of expansion. (Why some decrepitate and others expand is at present unanswered; residual stresses in the host

crystal may be involved.) This expansion phenomenon is not new - it has been reported at various times in the past. It is the net result of several volume changes during heating of the inclusion. On heating, the host salt expands, enlarging the cavity as well. This effect is small, yielding a cavity volume increase of only 1.2% from 40 to $140^{\circ}C$. The fluid in the inclusion dissolves more salt from the walls on heating; the net volume effect of this (generally a decrease; i.e., an increase in cavity volume) will vary widely with the composition of the solution. Thermal expansion of the brine would develop high pressures if the walls were rigid, but instead, in the presence of liquid, the inclusion walls frequently just expand. The amount of expansion is roughly proportional to the temperature of heating, i.e., the inclusion fluid streches the walls until its internal pressure drops just below that needed to cause further stretching at that temperature. Nucleation of a vapor phase may even occur (Geguzin and Dzyba, 1973), in which case loss of water to the expanding vapor phase also helps to limit the expansion. Some of the thermodynamic variables of the process have been modeled by Cline and Anthony (1971) for the pure halite system.

7.7   THE GEOCHEMISTRY OF DELAWARE BASIN GROUNDWATERS IN RELATION TO
         THEIR HOST ROCKS

7.7.1 Introduction

Geochemical studies of waters found in Permian and younger rocks of the Delaware Basin (Southeast New Mexico, West Texas) have assumed a new importance in recent years. This began in 1975 when Sandia Laboratories, in cooperation with the United States Energy Research and Development Administration undertook studies of the suitability of Delaware Basin evaporite deposits for the long-term storage of radioactive wastes generated by the national nuclear defense program.

In particular, three aspects of fluid geochemistry have bearing on an understanding of the geology of the area:

1. Rock history - the relationships between dissolution features and nearby fluids which may have dissolved evaporites.

2. Fluid history - evidence of rock/fluid interactions preserved in fluid chemistry, indicating the complexities of fluid movement.

3. Fluid origins - the ultimate sources of fluids which have participated or have potential for participating in dissolution of evaporites.

Many of the waters considered here were bailed from preexisting wells with the assistance of the United States Geological Survey, between December, 1975, and June, 1976. In addition, boreholes for subsurface exploration of Los Medanos (the ERDA study area) tapped some fluid producing zones. These holes include ERDA No. 6,. which at a depth of 2711 feet produced saturated brine associated with H_2S-rich gas from the Castile Formation. In this hole, stratigraphic marker beds were found several hundred feet above their expected positions (Anderson and Powers, 1978). Nine holes penetrating the Rustler Formation have facilited hydrological testing and sampling of Rustler waters. Finally, samples of waters were collected from pools in Carlsbad Caverns. Table 7.19 is an inventory of water samples, together with their collection locations. New Mexico locations are given in Figure 7.10, showing their distribution with respect to the Capitan Limestone.

Three geochemical approaches will be followed in this subchapter. Each approach will consider a few examples of various "types" of water:

1. Solute chemistry - dissolved solids content.

2. Thermodynamics - equilibia and non-equilibria of a fluid-gas system.

3. Stable isotope ratios - variations in deuterium and oxygen - 18 content.

7.7.2 Data

Analytical results for the 29 waters are given in Table 7.20. Solute
analyses are expressed in mg/l, performed according to APHA (1971)
methods, with modifications by Collins (1975). Analyses by Martin Water
Laboratories have a precision of about $\pm$ 5 to 10%; others $\pm$ 3% (Table
7.19).

Stable isotope analyses were made according to Epstein and Mayeda (1953)
and Bigeleisen et al (1952), and are reported in " δ " notation as
deviation of the D/H or $^{18}O/^{16}O$ ratio from the corresponding ratio of
Standard Mean Ocean Water (SMOW) (Craig, 1961b, Epstein and Mayeda,
1953), in parts per thousand (‰, "per mille") for example:

$$\delta D = \frac{(D/H)\ \text{sample} - (D/H)\,\text{SMOW}}{(D/H)\ \text{SMOW}}\ X\ 1000$$

The precision of $\delta\ ^{18}O$ values is better than $\pm$ 0.1‰ and that of δ D
is better than $\pm$ 1‰ .

Solutes. In this discussion "fresh water" is taken to contain less than
3000 mg/l total dissolved solids (TDS), and is potable at least to local
cattle. "Brackish water" refers to TDS contents between 3000 and 30000
mg/l. Brines are waters containing more than 30000 mg/l TDS. According
to these definitions, number 1, probably 18 and 26 through 29 (Table
7.19) are fresh waters, found in the Capitan and Santa Rosa Formations.
Numbers 2, 6, 11, 17, 22, 24 and probably 19 through 21 are brackish, and
include most Rustler waters, one Capitan and one Castile. The fresh and
brackish waters contain the solutes expected to be found in carbonate and
anhydritic or gypsiferous aquifers. All the other waters are brines, and
include the Salado, Morrow, Delaware (Bell Canyon) waters, two Castile,
one Capitan, and even two Rustler waters; these Rustler samples came from
the Culebra dolomite member, adjacent to halite-bearing parts of the
Rustler Formation.

Brines are treated in the most detail here, since their presence has implications regarding either their representation of original evaporite mother-liquors, or their solutes having been derived through rock-water interaction. Their geochemical complexity cannot be understood from solute chemistry alone, and a brine occurrence in a particular rock unit does not necessarily imply that the brine has interacted with its host rock.

The chloride/bromide ratios, where obtainable, of all the brines were between 430 and 900, compared to 292 for modern sea water (Collins, 1975). If the Permian Basin water had a Cl/Br ratio similar to that of sea water, as suggested by Holser (1963) for fluid inclusions in Kansas salt, then these Delaware Basin brines do not contain "original" Permian water as a major component. Since halite crystallizing from sea water selectively excludes bromide from the NaCl lattice, halite has a Cl/Br greater than 300 (Adams, 1969), as would brine resulting from the dissolution of halite. Hence, the sodium chloride in these brines has been dissolved from rocks, but not necessarily the rocks in which the brines were found.

Rather than discuss abundances of individual ions in brine solutions, it is more instructive to consider solute ions combined as solids which might be expected to precipitate from solution upon complete evaporation. Following the crystallization sequences compiled by Braitsch (1971), not only some similarities will be noted between the resulting normative mineral assemblages, but also some significant differences. Waters 16, 9, and 14 (Salado, Bell Canyon, Castile) will be presented as examples.

Water from the Duval Mine Vent Hole is similar to the other potash mine seeps (Numbers 3, 4 and 5) all of which are saturated solutions. Table 7.21 shows the relative proportions of minerals expected to precipitate from this solution. This assemblage is similar to that expected to precipitate from sea water, even though the relative proportions are different (note the overwhelming preponderance of carnallite). In view

of the incongruent dissolution of polyhalite resulting in a calcium-poor solution, this brine is what one would expect for water which has dissolved a potash deposit. Note the presence of normative borax, an evaporite mineral not commonly reported in the Carlsbad potash district (cf. Jones, 1975).

Waters from the more saline portions of the Capitan aquifer (numbers 11, 12 and 13) contain the normative assemblage dolomite-anhydrite-kainite(or carnallite)-halite±sylvite, in various proportions, and are also indicative of solutes obtained by dissolution of adjacent evaporites.

Water number 9, from the Bell Canyon Formation, is examined in Table 7.22. The solution is calcium-rich, as indicated by the less common minerals tachyhydrite and antarcticite. These two minerals are not known to precipitate from sea water, and together with a magnesium deficit distinguish this water from a simple solution of primary evaporites. Graf et al. (1966), have given attention to the origin of calcium chloride waters, and emphasized shale ultrafiltration as an explanation. Other possibilities include diagenetic reactions in which magnesium in solution displaces calcium in carbonates to form dolomite, or in which Mg-rich sheet silicates are formed, having given up more easily replaceable cations such as Na and Ca (Grim, 1968), which were present in the original minerals (kandites and smectities). Mg-rich sheet silicates are present in the Ochoan evaporites overlying the Bell Canyon (see subsection 7.4). Since brine number 9 is a saturated solution, and since calcite, not dolomite is the prevalent carbonate mineral of the Bell Canyon, neither dolomitization nor shale ultrafiltration (which tends also to produce a low-Ca water, which has not yet been found) appears to be a satisfactory model for the in situ evolution of Bell Canyon brine. The sulfate deficiency could have arisen from biogenic degradation of sulfate. The most likely explanation for the in situ Ca-enrichment is ion exchange. This brine probably did not originate in the Bell Canyon, but its solutes probably came from nearby evaporites.

Waters 8 and 10 have a much lower TDS content than does 9, but otherwise yield most of the same minerals. The high strontium content of all three could be taken to indicate that these waters have indeed participated in the recrystallization of carbonates, but probably not within the Delaware Mountain Group of sandstones, which includes the Bell Canyon Formation. According to the Sr/Ca studies of Oxburgh et al. (1959), this solution would have been in equilibrium with a calcite containing about 4000 ppm Sr, a value too high for most natural calcites and dolomites. The Sr in solution could easily have come from the diagenetic alteration of aragonite outside the Bell Canyon.

On July 30, 1975, borehole ERDA No. 6 produced saturated brine (number 14, Table 7.19) and H_2S-rich gas (0.16 cubic feet STP per gallon) from a fractured, gray, laminated Castile anhydrite unit 2711 feet below the surface. Similar phenomena in the Castile have been reported by oil companies, but with an order of magnitude more gas. The analysis of one other such brine (Shell Bootleg, number 15 in Table 7.19) is given in Table 7.20, and is quite similar to the ERDA No. 6 brine. The solutes are resolved in Table 7.23, and aside from thenardite and LiCl (resulting from an almost economic concentration of lithium) are similar to the case of the dissolved potash deposit. Na_2SO_4 has been previously reported in subsurface brines (Reeves, 1963), and thenardite is known to precipitate from local surface lakes. Lithium is a common component of evaporites formed near igneous rocks, but the nearest igneous rock is several kilometers away (Calzia and Hiss, 1978). The brine is sodium-rich and magnesium poor. Once again in terms of ion exchange, a loss of evaporite-derived magnesium into silicates, which give up sodium, appears to be the mechanism here, although this need not have taken place in the Castile. Such like processes may account both for magnesium depletion in the solution and the formation of magnesium silicates in the evaporite sequence.

Thermodynamics. The ERDA No. 6 gas and brine are the only fluids which lend themselves to multiphase thermodynamic considerations. The gas amounted to 1.22 liters (STP) per liter of liquid, and consisted of
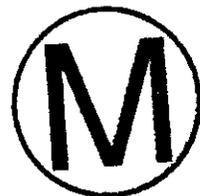
55% CO_2, 28% H_2S, 15% CH_4, 1.5 N_2 and 0.5% C_2H_6, determined

mass spectrometrically. The H_2S is not saturated in the solution, even

in the light of the salting-out effect of high TDS content (Randall and

Failey, 1927), and amounts only to 0.02 molal. In order to examine the

role of sulfur in this system (the only multivalent element common to

both liquid and gas phases) a predominance area diagram (cf. Garrels and

Christ, 1965), was constructed for the system S-O-H with the variables pH

and oxygen partial pressure, and with total sulfur equal to 0.36 molal

(approximating the sulfate and H_2S in solution). The resulting diagram

is Figure 7.11, for the field-temperature of 25°C. The field-measured

pH is 6.3, and samples of the brine containing dissolved H_2S were

observed to precipitate elemental sulfur upon standing at atmospheric

conditions. The diagram shows that at pH 6.3, the sulfur field occurs

between the sulfate and H_2S fields. Thus, the diagram correctly

predicts the oxidation of H_2S to sulfur, and the sulfate and H_2S

cannot be in thermodynamic equilibrium with one another at pH < 7.

Unfortunately, the oxidation potential was not measured, and the precise

position of the ERDA No. 6 system on the diagram is not known. The most

probable origin of the H_2S is biogenic reduction of sulfate, an ion

abundant in the surrounding rocks as anhydrite as well as in solution.

Kuznetsov et al (1963), have indicated that bacteria such as

Desulfovibrio aestuarii can exist in saturated NaCl solutions, although

their activity is inhibited by bivalent cations, which are not prevalent

in the ERDA No. 6 brine.

Stable Isotopes. Analysis of water samples for their $^{18}O/^{16}O$ and D/H

ratios has been found to be a useful method of identifying the source of

water molecules, and to some degree identifying the types of interactions

the water has undergone in the presence of other phases.

Figure 7.12 is a δ D versus δ ^{18}O plot for Delaware Basin

groundwaters. Most of the earth's meteoric waters have isotopic

compositions which fall between the lines described by the equations:
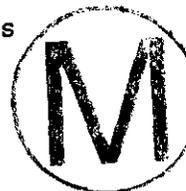
$$\delta D = 8 \ \delta \ {}^{18}O + 5 \ \text{(Epstein et al., 1965; 1970)}$$

and

$$\delta D = 8 \ \delta \ {}^{18}O + 10 \ \text{(Craig, 1961a)}.$$
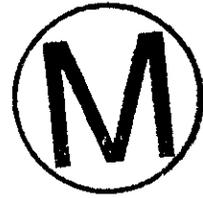
These lines are included in Figure 7.12, and the area between them is labelled "Meteoric Field."

Most of the points in Figure 7.12 lie in or near the meteoric field. Except for Carlsbad Caverns, a $\delta \ {}^{18}O$ value of $-7\%_o$ and a δD value of $-50 \ \%_o$ appears to be a good approximation to local meteoric water in the Delaware Basin. The Caverns are part of the hydrologic system independent of the rest of the Capitan. Their enrichment in D and ${}^{18}O$ reflects the water's origin from air mass conditions different from those which produce other Basin rains.

Bracketing the cluster of meteoric points are two dashed lines whose intervening field is labelled "evaporation." This field is the trajectory of isotopic compositions that the meteoric waters would follow during evaporation. The trajectory slope is 5, according to Craig et al. (1963). The few points that lie in or near the evaporation field (4 Rustler and 1 Castile) may indeed have suffered partial evaporation prior to infiltration, but definitely originated as metoric water.

The dashed line through the origin, also of slope 5, is the trajectory of isotopic compositions of evaporating sea water. This line is also valid for the evaporation of warm-climate coastal meteoric waters ($\delta \ {}^{18}O \approx -2\%_o$, $\delta D \approx -10\%_o$, as indicated by the intersection of this line with the meteoric field. Such waters were postulated by Holser (1963; 1966) to have been potential contributors to the Delaware Basin. The figure shows that the waters of positive $\delta \ {}^{18}O$ values are not the products of partial evaporation either of Delaware Basin water or of modern meteoric water. This conclusion is the same as that drawn from the Cl/Br ratios.

The environments in which the Salado, Morrow and Delaware (Bell Canyon) waters were found involved a rock/water ratio that was very large, as deduced from the low productivity of these reservoirs. Consequently, any interaction involving isotopic exchange between these waters and host rocks would tend to alter the isotopic composition of the water toward δ D and δ^{18}O values consistent with equilibrium isotopic fractionation between water and minerals in the rock. Calcite in the Bell Canyon Sandstone had a δ^{18}O value of +25.1‰, a value only slightly less than typical marine carbonate. This implies only minor isotopic alteration of easily exchanged carbonate oxygen in the rock through the action of water, and indicates lack of calcite-water isotopic equilibrium in the Bell Canyon. The oxygen and hydrogen in clay minerals are known to be readily exchangeable with water (O'Neil and Kharaka, 1976). The Delaware, Morrow and Salado waters have isotopic compositions that are suggestive of at least partial isotopic exchange between local meteoric waters and clay minerals in the sediments, in which the mineral/water ratio was very large (cf. Savin and Epstein, 1970) for at least several thousand years. Other mineral sources of exchangeable oxygen and hydrogen are fluid inclusions, whose stable isotopes have yet to be studied, and the water of crystallization of many evaporite minerals. The potash seep waters may have interacted with hydrous minerals. However, gypsum-water is the only such mineral-water system for which the ^{18}O/^{16}O and D/H fractionation factors are known.

None of the waters have resulted directly from the dehydration of gypsum to form anhydrite. If ERDA No. 6 were such a water, the point marked "G" in Figure 7.12 would be the isotopic composition of the water from which that gypsum precipitated (using the gypsum-water fractionation factors of Fontes and Gonfiantini, 1967). "G" is not consistent with evaporating Delaware Basin water, whose anticipated δ D - δ^{18}O trajectory was discussed above. The isotopic composition of ERDA No. 6 brine is consistent with an approach to isotopic equilibrium between water and clay minerals, not necessarily in the Castile. Its isotopic exchange, together with its history of cation exchange, has resulted in a brine whose history appears to be similar to that of oil field brines of Alberta and the Gulf Coast (cf. Clayton et al., 1966).

7.7.3 Summary

Many types of rock/fluid interactions are evident in the geochemistry of groundwaters found in the Delaware Basin. It is not possible to completely characterize these interactions from solutes or stable isotopes alone, nor through a study of water alone without a similar study of rock. In addition to fresh and brackish waters, which have acquired solutes from their host rocks, the brines have here illustrated three examples of various types of rock/fluid interactions:

1. dissolution of evaporites (saline Capitan waters).

2. dissolution of evaporites with isotopic exchange between fluid and rock (Salado potash seeps).

3. dissolution of evaporites, isotopic exchange, and cationic exchange (Delaware, Morrow and ERDA No. 6 waters).

The latter two types indicate more profound interaction than the first, since these involve changes in the water molecules themselves.

No original Permian waters could be identified. If much of the evaporite section has been recrystallized, as Holser (1963) suggests, not even the fluid inclusions are expected to preserve such waters.

7.8 RUBIDIUM-STRONTIUM SYSTEMATICS OF THE SALADO FORMATION, SOUTHEASTERN NEW MEXICO

7.8.1 Introduction

One of the important reasons for studying bedded salt deposits for a radioactive waste repository is to determine their intrinsic geological stability and to understand the behavior of alkali and alkaline earths in such a system assuming leakage of isotopes such as ^{90}Sr and ^{137}Cs.

If it can be demonstrated that such isotopes are likely to be retained at or very near the possible leakage area, then the potential danger of such leakage is minimized. Alternately, if it is found that there has been widespread migration of alkali and alkaline earth elements in the prospective storage sites, then these sites may be unfavorable for retention of ^{90}Sr, ^{137}Cs, etc. assuming leakage occurs. Furthermore, if the latest episode of diagenetic evaporite recrystallization can be dated, arguments can be made for the geochemical requilibration of the evaporite assemblage into a thermodynamically stable configuration, reducing the liklihood of such events in the future.

To address this problem the WIPP study area and nearby sites were chosen for investigation, utilizing the well-established Rb-Sr geochronologic method of age determinations. This method is especially well suited for . addressing alkali and alkaline earth retention and/or migration because of the species involved and its simplicity. Because of geochemical similarities (ionic radii, ionization potential, charge) Rb can be used as an analogue for Cs, and ^{90}Sr will behave as any other Sr isotope. Hence the Rb-Sr ages will allow, in theory, meaningful interpretation of the stability of the Salado Formation in terms of Rb and Sr retention and/or migration.

The basic age equation is:

$$T = \frac{(^{87}Sr/^{86}Sr)_m - (^{87}Sr/^{86}Sr)_o}{(^{87}Rb/^{86}Sr)_m \ (\lambda)}$$

where:

T = age in years

$(^{87}Sr/^{86}Sr)_m$ = measured isotopic ratio normalized to $(^{86}Sr/^{88}Sr) = 0.1194$ (the average abundance ratio in the earth)

$(^{87}Sr/^{86}Sr)_o$ = initial isotopic ratio before $^{87}Rb \ (\beta^-) \ ^{87}Sr$ radiogenic decay (R_o) occurs.

$$(^{87}Rb/^{86}Sr)_m = \text{measured isotopic ratio}$$
$$\text{(calculated from Rb/Sr ratio)}.$$

$$(\lambda) \qquad = \text{decay constant for } ^{87}Rb$$
$$= 1.42 \times 10^{-11}/y.$$

The $(^{87}Sr/^{86}Sr)_m$ term is the sum of
$$(^{*87 + 87}N)_{Sr}/^{86}Sr$$

where *87 and ^{87}N refer to radiogenic and normal mass 87 respectively.

The initial ratio $(^{87}Sr/^{86}Sr)_o$ can either be assumed, determined by measurements on Rb-free phases formed at T =0, or determined by extrapolation from an isochron (i.e. line of slope $e^{T\lambda}-1$ along which all samples of the same age and initial ratio but with different Rb/Sr ratios will fall; see Faure and Powell, 1972). The last of these choices is considered the most reliable due to natural variations of the initial ratios in nature, even from supposedly uniform, Rb-free, reservoirs.

7.8.2 Previous Work

K-Ar dating of evaporites has been shown by numerous investigators to be extremely risky (see discussion in Faure, 1977) due to loss of radiogenic ^{40}Ar by diffusion and other processes. Some K-Ar ages have beeen attempted for salts from the WIPP study area at Los Medanos (Shell Dev. Co.; 1973). For sylvites, minimum dates from 18 ± 8 to 74 ± 8 m.y. were obtained while two langbeinite-sylvite mixtures yielded nearly identical dates of 137 ± 8 and 147 ± 8 m.y. Only one very pure langbeinite (18%K) yielded a date of 245 ± 10 m.y.; this date is in excellent agreement with the 225-240 m.y. age range assigned to the Late Permian evaporites of the Castile and Salado formations.

The only other officially reported work is that by E. L. Tremba (1973; unpub. Ph.D. dissertation) in which he reports widely scattered data for evaporites from the Los Medanos area. Tremba's (1973) work was not directed toward problems of local alkali or alkaline earth migration, however, and composite samples were commonly taken which would, in

effect, mask any such local effects. He reports two model Rb-Sr dates of 241 $\pm$ 23 m.y. and 208 $\pm$ 8 m.y. respectively for (1) a K-ore zone from the Saunders Mine and (2) two separate aliquots of a water-soluble K-ore. An initial ratio of 0.7077 was used in both cases. For water soluble samples from mine faces within the Saunders Mine, Tremba reports a 129 $\pm$ 5 m.y. isochron but, without adequate justification, one point (#3SS) is omitted from the isochron calculation. As a model age for this one point yields an apparent model date of 330 m.y. (R_O = 0.708), then the significance of the 129 $\pm$ 8 m.y. date, based on only 4 of 5 samples, is difficult to interpret.

Similarly, five samples from Tremba's core 184, first ore zone, yield an apparent isochron date of 120 $\pm$ 28 m.y. but with an extremely high initial ratio of 0.7226 $\pm$ 0.0092. The argument is made that the two 120 to 129 m.y. isochrons can be explained by some type of Cretaceous "rehomogenization event". This interpretation can be criticized because 27 low-K samples from core 184 yield a mean $(^{87}Sr/^{86}Sr)_m$ = 0.7077 $\pm$ 0.0001; and any hypothesized rehomogenization event must explain how selective parts of the core can be affected whereas others are not. For example, Tremba argues that recrystallization involving polyhalite may have taken place at approximately 120 m.y. ago at which time the initial ratio was increased by rehomogenization to above 0.72; yet the data in Table 7.24 yield at least one sample (ERDA-9, 1759.1-1759.8) with $^{87}Sr/^{86}Sr_m$ = 0.7064. Furthermore, if one uses the individual points for Tremba's 129 m.y. isochron and assumes an initial ratio of 0.7077 (based on his data), a range in model dates results from about 185 m.y. to 100 m.y. (not counting sample EV-13 with a very low $^{87}Rb/^{86}Sr$ ratio). The reason for this apparent scatter is unanswered by Tremba's work.

7.8.3 Analytical Procedure

Sample Preparation. Samples studied thus far have been core segments from WIPP exploratory holes. The core segments were about four inches in diameter and ranged in length from 4 to 12 inches. These samples first

were trimmed by air saw to remove all outer surfaces that may have contacted drilling brines or been otherwise contaminated. Only the remaining prism of rock was retained for analysis; the outer portions were stored for possible use in the future.

Enough of the remaining inner portions were ground to -100 mesh to produce approximately 200 g of rock powder. About 30 g of this powder was quartered out and saved for whole rock analysis.

Separation of Water-Insoluble From Water-Soluble Material. The concentration of water-insoluble residue in a sample was determined during the separation of the soluble from the insoluble material. Approximately 60 g of powdered sample, weighed to the nearest 0.01 g, was placed in a 250 ml glass centrifuge tube together with about 175 ml of distilled and deionized H_2O. The bottle was then capped and the mixture shaken vigorously for about 3 minutes, centrifuged for 15 minutes and decanted into S and S 576 filter paper. This procedure was repeated with 175 ml of H_2O followed by a third leaching of 150 ml of H_2O.

The resulting solution was transferred into a Pyrex 600 ml beaker, which was placed on a $150^{\circ}C$ hotplate until no more liquid remained. The salt residue was then quantitatively removed from the beaker, weighed, and stored for analysis.

Separation of the < 2 Micron Fraction. The < 2 micron fraction was separated from the insoluble residue remaining from the above procedure. The insoluble residue was repeatedly washed and centrifuged until a disperson of the clay-sized material was obtained. The washed slurry was then put into 1000 ml cylinders for gravity settling. The length of time necessary for settling was calculated from the equation noted by Folk (1968). Fractions finer than 2 microns were siphoned off after the proper length of time had passed. A portion of the < 2 micron fraction was used for oriented slides (for x-ray diffraction analysis); the remainder was dried, ground to -100 mesh and used for Rb-Sr isotopic and other geochemical analyses.

X-ray Diffraction Analysis of Clay and Evaporite Minerals. Thus far, identification of clay minerals has been based solely on x-ray diffractograms, obtained from a Norelco wide range diffractometer. Untreated oriented powders were scanned from 2 to 60 degrees two theta. The untreated slide was glycolated by vapor-soaking on a rack in a container filled partially with ethylene glycol. An additional oriented powder was heated to 450°C. Both the glycolated and the heated specimens were scanned from 2 to 30 degrees two theta.

Whole rock samples were analyzed by loading a small amount of randomly oriented rock powder in a Norelco powder holder. This powder was scanned from 5 to 80 degrees two theta and the resulting diffractogram compared to values compiled in the Joint Committee on Powder Diffraction Standards file to determine bulk mineralogic composition. Mineralogic abundances noted were estimates based on comparative peak intensities.
All samples x-rayed (both clays and whole rocks) were scanned with Ni-filtered CuK radiation. A time constant of two seconds was used with a scintillation counter detector and pulse height analyzer. The goniometer slit system consisted of a divergent and anti-scatter slit of 1 degree and a 0.003 inch receiving slit.

Rb-Sr Isotopic Analysis. Procedures for the dissolution of samples for Rb-Sr isotopic analyses varied dependent on the samples mineralogic composition. All samples were first weighed accurately and placed into a 100 ml teflon evaporating dish; the amount of sample to be dissolved was determined to ensure at least 10 mg Sr and Rb would be in solution. The sample was then spiked with ^{84}Sr and ^{87}Rb solutions. Samples which contained silicate minerals were dissolved with 30 ml reagent grade HF and 3 ml vycor distilled $HClO_4$ on a hot plate. Samples containing only water soluble material were dissolved with 50 ml of distilled and deionized H_2O and 10 ml of vycor distilled 6N HCl. Samples containing large amounts of sulfate minerals were first dissolved in aqua regia and then treated with HF and $HClO_4$.

After complete dissolution of the powder and evaporation of all HF and $HClO_4$, the samples were digested with 25 ml of H_2O and 25 ml of HCl.

The mixture was then reduced to about 5 ml by slow evaporation and allowed to cool overnight. After cooling the solution was filtered through S and S #576 filter paper and loaded onto the top of a chromatography column charged with sulfonated polystyrene, a chromatographic grade cation exchange resin.

The column was washed with 2N HCl repeatedly while the effluent was flame tested for cationic composition. Rb and Sr fractions were collected at the appropriate intervals indicated by the flame test. The collected fractions were subsequently dried, redissolved and transferred to precleaned quartz microvials. The microvials, containing the samples, were fused, cooled and stored for mass spectrometric analysis.

All Rb and Sr concentrations were determined by standard isotope dilution techniques. All Rb and Sr isotopic ratios were measured using a 23 inch, 90 degree sector, solid source, single filament Nuclide mass spectrometer equipped with an electrometer and strip-chart recorder.

7.8.4 Results

Samples for the present study were provided from Sandia Laboratories drill cores AEC-8, ERDA--6, and ERDA 9 drill cores. Samples were studied for their Rb-Sr systematics by mass spectrometer and (Table 7.24, 7.25), mineralogy by x-ray diffraction (Table 7.26). Additional geochemical studies are planned (i.e., rare earth elements, by instrumental neutron activation analysis).

Samples have been divided into whole rocks, water soluble portions, and the minus-two micron fractions. This approach varies significantly from Tremba's (1973) approach in that he worked with water soluble and total water insoluble fractions; the latter were not treated for separation of authigenic from allogenic fraction. This will be discussed later.

Whole rocks may yield uncertain results due to the unknown nature of water insoluble fractions within them. Similarly, the water soluble fractions are meaningful only if the nature of the water insoluble

fraction is studied. This last point can best be addressed by detailed study of the clay-size (minus-two micron), authigenic minerals common to evaporites.

(1) Whole rocks: the water insoluble content of whole rocks varies from less than 1 percent to 32 percent, with a mean of 6.5 percent if sample Dv-4D (clay rich) is omitted. The basic mineralogy of these samples is a halite rich assemblage with some samples rich in sylvite and/or polyhalite as well. Langbeinite-rich samples are rare. The Rb-Sr isochron for eleven samples is shown in Figure 7.13. The date of 132 m.y. must be considered very approximate as nine of the eleven samples plot essentially on the ordinate. Of these last eleven, nine are used to yield a reasonable estimate of initial ratio = 0.7081 $\pm$ 0.0005 (in agreement with Tremba's 1973 value of 0.7077).

(2) Water soluble samples: in working with water soluble samples the assumption is made that ions released into solution will not be absorbed onto the surface of the insoluble material. This is probably true only if the insoluble material consists of allogenic quartz, feldspars, etc. but not clay minerals. An isochron for five water soluble samples yields an apparent date of 206 m.y. with R_o = 0.7084 (Figure 7.14). While this date is not unreasonable for the Permian-Triassic boundary, it is slightly low.

(3) Minus-two micron fraction: the authigenic clay minerals which one might predict for an evaporite sequence are present in this fraction (Table 7.26). Of interest is that this material is (a) authigenic as demonstrated by the x-ray diffraction work and (b) is also the dominant part of the water insoluble fraction. Thus the apparent

isochron date (Figure 7.15) of 325 m.y. needs
explanation. If one remembers that many of the clay
partings in the potash mines are interpreted as being of
aeolian origin, then it is very likely that such aeolian
clay minerals will, in part, reflect their provenance.
This has been noted before by Hurley et al. (1962) for
minus-two micron clay minerals from the Bermuda Rise.
Of interest here is that our 325 m.y. date (Figure 7.15)
is virtually identical with Tremba's (1973) 331 m.y.
date for total water-soluble material.

7.8.5 Discussion

There are several ways to treat the data gathered so far. First a
composite of whole rocks, water soluble and minus-two micron size clay
minerals yields an isochron date (Figure 7.16) of 165 $\pm$ 20 m.y. with R_o
= 0.7115. This date must be interpreted as a minimum due to the fact
that the best estimate of R_o is 0.7081 $\pm$ 0.0004 according to the data
presented in Table 7.24.

It is also apparent that the whole rocks by themselves are, in general,
too halite-rich and possess Rb/Sr ratios which are too low for isochron
work. When to this is added the uncertainty introduced by the insoluble
material mixed with possible pre-T_s (i.e. time of sedimentation)
material smaller than two microns, plus some detrital feldspar, quartz,
etc., then the whole rocks can be assumed to be unsuitable for the
isochron work.

If the clay minerals in the minus-two micron fraction are aeolian,
pre-T_s material may account for the pre-Permian date of 325 m.y.
(Figure 7.15). Similarly, since the clay mineralogy (Table 7.26) is very
typical of evaporite clay minerals, then an alternate explanation is that
these clay minerals have acted as local sinks for some ^{*87}Sr presumably
remobilized during and after lithification and diagenesis. A lower age
limit for this event is set by the 206 m.y. date from the water soluble
fraction.

When only the water soluble and minus-two micron clay mineral fractions are considered together, a 204 m.y isochron (Figure 7.17) results with R_o = 0.7137. This date is only somewhat lower than the Permian-Triassic boundary and can safely be interpreted as a minimum due to the high initial ratio (0.7137). This interpretation assumes, however, that the clay minerals equilibrated with the evaporite medium (i.e. salts plus brine plus remnant sea water) at the time of sedimentation and this point remains to be unequivocally demonstrated.

Many of the above mentioned uncertainties will almost certainly be resolved by additional samples now in various stages of analysis for Rb-Sr systematics plus additional samples not yet treated. Furthermore, scanning electron microscope studies are planned to help resolve the problems of aeolian versus non-aeolian authigenesis hypotheses regarding clay mineral occurrences. Finally, rare earth element (REE) data, when complete, will greatly enhance understanding of the evaporite-insoluble material systematics of the Los Medanos area.

7.8.6 Concluding Statements

These data are of importance to he WIPP in the Los Medanos area because: (1) Widespread recent rehomogenization of radiogenic ^{87}Sr would be obvious if consistently high $^{87}Sr/^{86}Sr$ ratios were determined either from Rb-poor phases or by extrapolation from all samples with high Rb/Sr to the ordinate (Figures 7.13-7.17). This is not the case, and in fact values for whole rocks yield a mean of 0.7081, and several isochrons yield extrapolated values from approximately 0.709 to 0.713. The entire set of data argues against large amounts of radiogenic ^{87}Sr-enriched brine, having been formed post-200 m.y. ago, subsequently leaving its imprint in the recrystallized minerals. (2) the Rb-Sr isochron based on water soluble fractions and clay minerals, Figure 7.17 yields a date of 204 m.y. This date, in view of R_o = 0.7137 (i.e. higher than 0.7084), must be interpreted as a minimum date pending further analyses. (3) The clay minerals (Table 7.26) are of special interest in that they are typical of evaporite clay minerals formed during evaporite diagenesis,

yet they have been interpreted as aeolian. If they are aeolian, then some mixture of kaolinite-montmorillonite-illite would be expected rather than the saponite-chlorite-montmorillonite-serpentine-talc-illite assemblage noted. Since the clay minerals yield (Figure 7.15) a pre-sedimentation apparent date of 325 m.y. with high R_o (0.7123), then it is possible that these clays acted as local sinks for radiogenic ^{87}Sr (and Rb?) released during early diagenesis from roughly 235 m.y to 204 m.y.; such an interpretation is consistent with the data obtained to date. Tremba (1973) has argued for some mid-Cretaceous "rehomogenization event" at about 120 m.y. ago but inspection of his data coupled with these data do not support such an hypothesis. (4) REE are especially sensitive as geochemical tracers and forthcoming data, coupled with continued Rb-Sr and other work, should permit resolution of some of the problems concerning alkali and alkaline earth retention/migration in the geologic past at the Los Medanos site.

7.9 URANIUM ISOTOPE DISEQUILIBRIUM IN GROUNDWATERS OF SOUTHEASTERN NEW MEXICO AND IMPLICATIONS REGARDING AGE-DATING OF WATERS

7.9.1 Introduction

History. Regional exploration of bedded salt deposits for a radioactive waste repository in the Delaware Basin (Permian, New Mexico) included boreholes into the evaporites and associated rocks. These rocks contained various amounts of fluids, already described (Lambert, 1978). Although the halite deposits of the Ochoan Epoch are the prime target of consideration for waste storage, the older rocks of the Guadalupian Epoch are included in the present study, because of the Capitan reef, a body of cavernous limestone which encircles the Basin. The Capitan not only is the dominant rock in the Carlsbad Caverns, but also supplies potable water to the city of Carlsbad. Therefore, it is appropriate to consider possible connections between the Capitan and accumulations of water found in pockets in the evaporites. Brine and gas pockets are known to occur in the Carlsbad district potash mines and in the Castile Formation (anhydrite and halite) underlying the Salado Formation.

One exploration hole, ERDA No. 6, drew national attention (Boffey, 1975), when it encountered an accumulation of saturated NaCl brine laced with Na_2SO_4, accompanied by H_2S-rich gas at 826 m below the surface. Discovery of this artesian fluid, together with bedding-plane dips in the host Castile Formation exceeding 70°, led to abandonment of that particular site. Geophysical investigations showed that this and other occurrences of brine and gas were associated with closed structure contours drawn for the Castile formation. These structures, restricted to a narrow strip of evaporites near the reef have been termed "salt anticlines" (Anderson and Powers, 1978). Core from the fluid-producing zone of ERDA No. 6 consisted of gray laminated anhydrite whose fractures were filled with massive crystalline white anhydrite (Plate 7.52). While isolated fluid accumulations are not rare in evaporites, the possible use of the region for radioactive waste disposal requires attention to the origin of this particular type of accumulation. In the extreme cases, the fluid originates directly from water from the Capitan Reef, or the water was entrapped in the Castile Formation at the time for evaporite deposition in the Permian. In the first case, the water would have an age little older than Capitan waters. In the second case, the water would be in excess of 230 million years old.

Implications. Indeed, the very presence of the ERDA No. 6 accumulation of fluid poses several questions:

1. How long has the water been confined in the pocket?

2. Does the time of the water's intrusion correspond to any significant known geologic events?

3. What is the source of the water?

4. How long has this pocket been disconnected from nearby aquifers such as the Capitan Reef, if it ever was connected?

5. What are the limits to rates of influx (if any) or recharge and discharge (if any) of this fluid pocket?

6. To what degree does the ERDA No. 6 occurrence (or any other in the area) represent a flowing system?

6. Which radiometric clock should be used to age-date the water and what should be taken as initial conditions for age-dating?

7.9.2 Analytical Approach

General Geochemistry of Groundwaters. A number of groundwaters from the Delaware Basin have been characterized in terms of their general geochemistry with respect to their host rocks (Lambert, 1978). In terms of solutes, all waters from below the fresh-saline interface in the Capitan were similar to each other. In addition all shallow (≤ 300 m depth) waters were similar to one another and all deep (≥ 1000 m depth) waters were similar to one another. The ERDA No. 6 water was unique in its solute content, indicative of profound disequilibrium between solution and host rock and also between solution and associated gas phase.

In terms of D/H and $^{18}O/^{16}O$ ratios, Capitan and shallow waters all are similar and are of meteoric origin. (Carlsbad Caverns waters are also of meteoric origin, but are not related to other waters in the Capitan.) Deep water stable isotope ratios are similar to one another, and are not characteristically meteoric. ERDA No. 6 has uniquely non-meteoric isotopic ratios among those of Delaware Basin waters. No waters were found which represent original evaporite mother-liquor.

Experimental Procedures. In spite of the evidence that this fluid has experienced profound interactions with rock (Lambert, 1978), radioisotopes were examined to establish that the ERDA No.6 fluid was not of relatively recent origin. Plutonium concentration was determined by isotope dilution employing a spike of ^{244}Pu. The actual measurement was made on a three-stage thermal emission solid source mass spectrometer equipped with pulse counting for ion detection. The instrument has a very high abundance sensitivity (10^7) and low background, allowing for the determination of precise isotopic ratios on small samples amounting to 0.1 to 1 nanograms of plutonium. The plutonium concentration of the ERDA No. 6 brine was found to be less than 10^{-15} grams per gram, corresponding to the lower limit of analytical detectability. The absence of plutonium suggests the brine has been isolated at least since 1945, a date corresponding to the first atmospheric detonation of nuclear weapons.

Carbon 14 was measured in the CO_2, which amounted to 55% of the total gas collected from ERDA No. 6. Carbon 14 content was counted in a gas proportional detector whose efficiency was calibrated with the NBS oxalate standard. The result was the same as the background, which was about 2 counts per minute in a 1.5 liter detector at 2 atmospheres pressure. From this it was concluded either that the brine is older than about 30,000 years or possibly that carbonates in the host rock have diluted the carbon in the system with non-radioactive carbon.

The disequilibrium of the activity of ^{234}U relative to ^{238}U in natural waters has been attractive as an indicator of the age of groundwaters (Osmond and Cowart, 1976). ^{234}U and ^{238}U are related by the decay scheme:

$$_{92}^{239}U \xrightarrow[4.5 \times 10^9 a]{\alpha} {}_{90}^{234}Th \xrightarrow[24d]{\beta-} {}_{91}^{234}Pa \xrightarrow[1\ min]{\beta} {}_{92}^{234}U \tag{1}$$
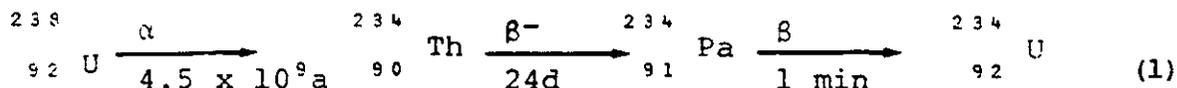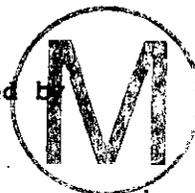
It has been proposed that excess ^{234}U builds up in confined waters as an aging effect as a result of the alpha-recoil of ^{234}Th, which ejects ^{234}Th out of the host rock crystal lattice into the water (Kigoshi, 1971; Kronfeld et al., 1975). From a knowledge of decay constants and initial activity ratio α_0 ($\alpha = \lambda_{234} N_{234} / \lambda_{238} N_{238}$), the time of confinement is calculated. It cannot be assumed, however, that the earth's natural abundance ratio, $\alpha = 1.00$, is a priori valid for a confined rock-water system. The water carried in with it an initial uranium concentration and original activity ratio, α_0. The water ultimately comes to thermodynamic equilibrium with its host rock and may leach or even deposit ^{234}U and ^{234}Th. Uranium concentrations and α-ratios of rocks and waters in this study were determined by isotope dilution mass spectrometry, described above. Figure 7.18 shows the locations of principal water samples of this study. Table 7.27 shows uranium conentrations and values of α for various waters.

7.9.3   Results and Discussion

The overleaf of Plate 7.52 shows the variations of U content and α in anhydrite of rock core taken from the zone which produced fluid in ERDA No. 6 (826 m, 2709 ft depth). Table 7.27 shows that in ERDA No. 6, both U concentration and α vary with time, until U concentration falls asymptotically to about 2 parts in 10^9, and α rises asymptotically to about 1.35. In the early part of a several-hour flow test, water samples were found to be contaminated with drill mud and spallations from metal pipe. By 1400 hours not only had the uranium reached steady state values, but the iron concentration had fallen from 260 parts in 10^6 (1130 hours) to a steady value of 5 parts in 10^6 (1400 hours), indicating the flushing out of drilling-introduced contaminants. Thus, the later samples are probably representative of the fluid accumulation.

The total variation in α among all water samples is relatively small (1.2 to 5.2). In contrast, absolute uranium content in the waters of Table 7.27 varies by more than two orders of magnitude. Similarly, rock material illustrated in Plate 7.52 shows a wide variation in U content: 1 to 2 parts in 10^6 for "original" laminated gray anhydrite down to 20 to 30 parts in 10^9 in the secondary white anhydrite fracture filling only a few centimeters away.

7.9.4   Applicaton of the Uranium Isotope Disequilibrium Model

If N_2 is the amount of ^{234}U present in a phase, and N_1 is the amount of ^{238}U, the change in ^{234}U content with time in the brine is

$$\left(\frac{dN_2}{dt}\right)_{brine} = \lambda_1 N_1 - \lambda_2 N_2 + Q_1 + Q_2, \tag{2}$$

in which Q_1 is the rate of release of ^{234}Th (the parent of ^{234}U) from the rock, Q_2 is the rate of release of ^{234}U from the rock and λ_1 and λ_2 are decay constants for ^{238}U and ^{234}U, respectively.

Release rates Q_1 and Q_2 can be modeled in the fashion of Kigoshi (1971), who studied the release of ^{234}Th from zircon powder. He gave the accumulated activity of ^{234}Th in solution after time t as

$$(\lambda_{Th} \, N_{Th})_{brine} = 1/4 \; L \; S\rho \; (N_{238} \; \lambda_1)_{rock} \; (1 - e^{-\lambda_{Th} t}),$$

$$(3)$$

in which λ_{Th} is for ^{234}Th, L is the recoil distance of ^{234}Th in decay scheme (1) above, S is the surface area of parent rock, ρ is its density, and N_{238} is expressed as the number of ^{238}U atoms per gram of rock. Thus, the activity of ^{234}Th in the brine is related to the activity of ^{238}U in the rock by a proportionality constant, and, of course, the time-dependent term. When t >> 24 days, (3) can be approximated as

$$(\lambda_{Th} \, N_{Th})_{brine} \approx f_1 \cdot (\lambda_1 \, N_1)_{rock},$$

$$(4)$$

in which f_1 is now the leach fraction of ^{234}Th, incorporating $1/4 \; L \; S \rho$ in (3). In general, ^{238}U activities in rock and coexisting brine will not be equal, but will be related by a distribution coefficient r, which is theoretically an equilibrium constant, neglecting the kinetics of dissolution and precipitation:

$$(\lambda_1 \, N_1)_{rock} = r \, (\lambda_1 \, N_1)_{brine}$$

$$(5)$$

In actual fact, the time required to achieve chemical equilibrium between rock and brine might be very long relative to the half-life of ^{234}Th. Q_1 now becomes

$$Q_1 = r \cdot f_1 \cdot (\lambda_1 \, N_1)_{brine}$$

$$(6)$$

Similarly, the amount of ^{234}U released is dependent on the decay of its precursor ^{238}U, and on the equilibrium ratio r, and on the leach fraction for ^{234}U, f_2:

$$Q_2 = r \cdot f_2 \cdot (\lambda_1 \, N_1)_{brine}$$

$$(7)$$

In addition, some fraction, f_3, of the ^{238}U will be leached from the rock,

$$\lambda_1 N_1 = r \cdot f_3 \cdot (\lambda_1 N_1)_{brine} + (\lambda_1 N_1)_{brine} \qquad (8)$$

Now, equation (2) becomes:

$$\left(\frac{dN_2}{dt}\right)_{brine} = (\lambda_1 N_1)_{brine} \left[1 + r (f_1 + f_2 + f_3)\right] - \lambda_2 N_2 \qquad (9)$$

If f is defined as a composite leach fraction $(f_1 + f_2 + f_3)$, the solution to (9) is:

$$N_2(t) = \frac{\lambda_1}{\lambda_2 - \lambda_1} (1+fr) N_1(t) + N_1(t=0) \frac{\lambda_2 N_2(t=0)}{\lambda_1 N_1(t=0)} \frac{\lambda_1}{\lambda_2} (1+fr) e^{-\lambda_2 t} \qquad (10)$$

which allows us to express the solution in terms of $\alpha = \frac{\lambda_2 N_2}{\lambda_1 N_1}$:

$$\alpha_{brine} = \frac{\lambda_2}{\lambda_2 - \lambda_1} (1 + fr) + \left[\alpha_0 - \frac{\lambda_2}{\lambda_2 - \lambda_1} (1 + fr)\right] e^{-(\lambda_2 - \lambda_1) t} \qquad (11)$$

and since $\lambda_2 \gg \lambda_1$

$$\alpha_{brine} \approx 1 + fr + \left[\alpha_0 - 1 + fr\right] e^{-\lambda_2 t} \approx \alpha_b \qquad (12)$$

The corresponding equation for the rock is:

$$\left(\frac{dN_2}{dt}\right)_{rock} = \lambda_1 (1 - f) (N_1)_{rock} - \lambda_2 (N_2)_{rock} \qquad (13)$$

Since for a closed system, the $^{234}U/^{238}U$ equilibrium activity ratio is 1.000, the solution to (13) is:

$$N_2(t)_{rock} = \frac{\lambda_1}{\lambda_2 - \lambda_1} (1 - f) N_1(t)_{rock} + \frac{\lambda_1}{\lambda_2} N_1(0)_{rock} e^{-\lambda_2 t} \qquad (14)$$

$$- \frac{\lambda_1}{\lambda_2 - \lambda_1} N_1(0)_{rock} (1 - f) e^{-\lambda_2 t}$$

which in terms of α is

$$\alpha_{rock} = \frac{\lambda_2}{\lambda_2 - \lambda_1} (1 - f) + e^{-(\lambda_2 - \lambda_1)t} - \frac{\lambda_2}{\lambda_2 - \lambda_1} (1 - f) e^{-(\lambda_2 - \lambda_1)t} \tag{15}$$

The approximation $\lambda_2 \gg \lambda_1$ reduces the equation (15) to

$$\alpha_{rock} \approx 1 - f + f e^{-\lambda_2 t} \approx \alpha_r \tag{16}$$

Let us now assume that the geochemical conditions (i.e. U content and α) observed in the ERDA No. 6 rock-fluid assemblage represent equilibrium conditions. This requires the mutual consistency of equations (12) and (16), and that

$$f = \frac{(\alpha_0 - 1)(\alpha_r - 1)}{\alpha_b - \alpha_0 + r(\alpha_r - 1)} . \tag{17}$$

Anhydrite found in the veins is the most recently formed phase in the core, and using the U values from 1709.4 white anhydrite (U = 33 parts in 10^9, α = 1.04); Plate 7.52 overleaf), and the averages of the last two ERDA No. 6 brines in Table 7.27, (U = 2.01 parts in 10^9, α = 1.35) equation (17) gives rise to the plot in Figure 7.19. Note the prominent singularity at α_0 = 2.01, and that $\alpha_0 \leq 1.971$ at f = 1 (corresponding to 100% leaching, and $\alpha_0 \geq 2.052$ at f = -1 (corresponding to all the uranium in the rock having precipitated from the brine).

Solving equation (12) for t, we obtain an expression for the age of the brine:

$$t = \frac{\ln\left(\frac{\alpha_b - 1 - fr}{\alpha_0 - 1 - fr}\right)}{-\lambda_2} . \tag{18}$$

For values of $\alpha_0 \leq 1.971$, negative ages result. Only for values of $\alpha_0 \geq 2.052$ are realistic ages obtained. This result implies that there has been minimal leaching from the rock. Furthermore, it suggests rather that precipitation of uranium has occured from brine to rock which is consistent with reducing conditions implied by the presence of H_2S.

Clearly, the amount of precipitation which has occurred (negative leaching) is related to the original α_0 at the time of closure of the rock fluid system.

Values of α for nearby waters in the Capitan limestone (Table 7.27) which by proximity afford a possible source of water for the ERDA No. 6 brine pocket, are mostly in excess of 1.35. In addition, the ERDA No. 6 brine is not saturated in $CaSO_4$ (Lambert, 1978), and is not likely to have been responsible for the precipitation of substantial amounts of vein anhydrite. Furthermore, the limited volume of the brine pocket (Griswold, 1977) could not realistically be expected to dissolve and reprecipitate anhydrite in veins to the extent observed in the core. Therefore, the α_0 of the ERDA No. 6 brine must have been larger than 2.052, with very little interaction with the reservoir rock.

7.9.5   Model Ages Based on No Leaching

Values of α and α_0 will in this model allow an age determination of a water to be made. The highest α value thus far determined is 14.2, the result of isotope dilution mass spectrometry performed on a sample from Israel supplied by J. Kronfeld, which gave an α value of 10.1 $\pm$ 1.6 by alpha-spectroscopy (Kronfeld et al., 1975). In addition, the occurrence of waters elsewhere in the Delaware Basin (Table 7.27 suggests that a reasonable α_0 value might be 5.14 (in the Capitan limestone), the highest thus far found in the Basin. If the ERDA No. 6 brine represents water escaped from the Capitan, and its α_0 was on the order of 5, Figure 7.19 shows that its interaction with the ERDA No.6 reservoir rock (fractured Castile anhydrite) precipitated less than 6% of the rock's uranium from the brine.

Neither total concentration nor isotopic composition of uranium in the ERDA No. 6 brine was inherited through interaction with the Capitan limestone, for the ERDA No. 6 brine contains substantially more uranium that the Capitan waters (Table 7.27) presently do. Likewise, uniformity in the stable isotope composition of Capitan waters (Lambert, 1978) shows

that the peculiar stable isotope composition of ERDA No. 6 water cannot have arisen by interaction with the Capitan limestone. Composition of stable and unstable isotopes in ERDA No. 6 brine might have arisen from interaction between water and rocks encountered by the water if it moved from the Capitan to its ERDA No. 6 environment.

In its simplest form, equation (18), under conditions of no interaction between ERDA No. 6 brine and its reservoir rock, reduces to:

$$t = \frac{\ln\left(\frac{\alpha_b - 1}{\alpha_0 - 1}\right)}{-\lambda_2} \tag{19}$$

which very nearly corresponds to the combination of the solutions to the equations

$$\frac{dN_1}{dt} = -\lambda_1 N_1$$

$$\frac{dN_2}{dt} = -\lambda_2 N_2 + \lambda_1 N_1$$

for which

$$t \approx \frac{\ln\left(\frac{\alpha_b - 1}{\alpha_0 - 1}\right)}{-\lambda_2 + \lambda_1} \tag{20}$$

The above conclusions allow limits to be assigned to the age of confinement of the ERDA No. 6 brine, and also to ages of waters in the Capitan. Equation (20) differs from equation (19) only by the approximation that

$$\frac{\lambda_2}{\lambda_2 - \lambda_1} \approx 1,$$

since $\lambda_2 = 2.806 \times 10^{-6}$ a^{-1} for ^{234}U
and $\lambda_1 = 1.537 \times 10^{-10}$ a^{-1} for ^{238}U.

Figure 7.20 shows the family of curves obtained from equation (20), using observed values of α from Table 7.29, and various values for α_0. The model ages indicated on Figure 7.19 for the ERDA No. 6 brine are less

than those in Figure 7.20 because 4 to 5 percent interaction between brine and rock (uranium precipitation) involves loss of uranium from solution by means other than radioactive decay. There is no evidence for any degree of chemical equilibrium between ERDA No. 6 rock and fluid. If we realistically limit f (Figure 7.19) to have a value between -0.02 and -0.50, the minimum age of the ERDA No. 6 occurrence is 570,000 years (α_0 = 6). In actual fact, as the data of Kronfeld et al. (1975) suggest, maximum α_0 values are universally in the range 10 to 15, and the age is between 800,000 and 1,000,000 years. According to the no-interaction model, (Figure 7.20), if water escaped from the Capitan (α_0 = 5.14) into the brine pocket, this must have occurred at least 880,000 years ago. The highest α_0 value (14.2) confirmed by isotope dilution mass spectrometry gives an age of 1,300,000 years.

If the Carlsbad area (near the Pecos River) is a major recharge area for much of the Capitan reef, and if Carlsbad water (α_0 = 5.14) is the basis for age-dating other waters in the Capitan, ages between 300,000 and 1,100,000 years are obtained. The maximum α_0 (14.2) would imply that Capitan waters are at least 400,000 years old.

7.9.6 Implications and Conclusions

A mathematical model based upon analytical data has showed that the ERDA No. 6 occurrence of brine can be age-dated by the uranium-disequilibrium method. Combinations of leach fractions and ages were derived, and the interaction between rock and fluid was indicated to be minimal. If the brine pocket was once connected to the Capitan Reef, the most productive aquifer in the region, such connection was severed at least 500,000 years ago, and probably more than 900,000 years ago. The brine pocket has been stagnant ever since, and there is little evidence to indicate that chemical equilibrium has been established among the solid, liquid and gaseous phases involved in the brine pocket.

Even though the α value of the ERDA No. 6 brine was close to those of nearby metoric waters taken from the northern apex of the Capitan Reef, these α values are far removed from those of more remote meteorically-derived saline Capitan waters from the east and west arms of the reef (Carlsbad No. 7 and Shell No. 28). In fact, the remote waters appear to be younger than apex waters (Hackberry and Middleton), implying the groundwater flow in the reef is indeed toward the apex and recharge is in the east and west part of the reef.

Fresh and saline Capitan Reef waters have retained their meteoric D/H and $^{18}O/^{16}O$ ratios, even though the ages of some of them are comparable to that of ERDA No. 6. Although reef apex waters and ERDA No. 6 brine are radiometrically similar, the solutes and stable isotopes of ERDA No. 6 reflect a more profound rock/fluid interaction than Capitan waters have experienced. This interaction, however, is more likely to have taken place in rocks between the Capitan and the brine pocket than in the brine pocket itself.

The ERDA No. 6 reservoir rock has not replenished ^{234}U to the brine in spite of long contact. Furthermore, uranium mobility into the white recrystallized anhydrite from the gray laminated anhydrite from the gray laminated anhydrite was shown to be very low in this anoxic environment.

Dating by the uranium-disequilibrium method is not necessarily dependent on a closed system, and bounds on ages can be assigned. Requirements for $^{234}U/^{238}U$ dating include: α values of fluid and rock, leach rate, and knowledge of a value for original activity ratio, α_0 . The α value for the rock is necessary to evaluate the degree of rock-fluid disequilibrium. The leach rate might be negligible even in a closed system. A unique solution to an age-dating problem, however, requires knowledge of initial conditions, just as in case of the well-established uranium-lead and carbon 14 age-dating techniques.

7.10   SUMMARY

Geochemical investigations of the WIPP site have been undertaken to
characterize and quantify the mineralogy and petrology of the Delaware
Basin evaporites and associated non-evaporites, volatile constituents and
fluid inclusions native to the evaporites, the geochemistry of
groundwaters native to the rocks, and the lengths of time that the
evaporites and groundwaters have existed in their present environments.
While these investigations have utilized a number of techniques of
analytical chemistry, the choice and analysis of samples, together with
interpretations of results, are carried out in the context of the WIPP
geology.

The most common mineral in the Permian (Ochoan) Salado Formation, which
is proposed for radioactive waste emplacement, is halite. Some of the
halite contains minor amounts of anhydrite, and traces of trioctahedral
clays and detrital minerals. Locally throughout the Salado Formation
marker beds of anhydrite and polyhalite occur at intervals of a few tens
of meters. Local accumulations of potassium and magnesium sulfates occur
in the McNutt potash zone in the upper part of the Salado.

The petrographic textures, geochronology, and the presence of minerals
which are not primary precipitates of sea water, such as sylvite and
polyhalite, indicate that much of the evaporite section last underwent
recrystallization more than 200 million years ago, shortly after Permian
deposition. The trace clay mineral fraction of the rock salt has
efficiently entrapped and held radiogenic strontium for at least the last
200 million years. The aqueous solutions involved in this
recrystallization were not in communication with fluids outside the
evaporite section.

Volatiles presently occur in the evaporite section as the
chemically-combined water of crystallization, hydroxyl-groups bound in
sheet silicates, short-lived seeps exposed in mines, and as
physically-entrapped inter- and intracrystalline fluid inclusions. The

total volatiles recovered from rock salt heated to $600^{\circ}C$ typically amount to less than 0.5 weight percent (about 1.5% by volume). In addition to water, traces of nitrogen, CO_2 and contaminants from the coring operation are recovered from subsurface evaporite cores taken from boreholes. The fluid inclusions appear to have been entrapped at 20 to $45^{\circ}C$, and contain $NaCl$, $MgCl_2$ and minor amounts of other solutes. Fluid inclusions not affected by recrystallization have not moved in the ambient geothermal gradient since the Permian deposition.

Isolated pockets of aqueous solutions now found in the evaporites have no geochemical relationship to surface-derived meteoric waters or to groundwaters above and below the evaporites; neither do they represent original evaporite mother liquors. Such pockets probably are relics of the post-depositional recrystallization which took place more than 200 million years ago, at which time they might have inherited their geochemically distinct solute assemblages and stable isotope compositons.

Stable isotope and solute content studies of meteorically-derived groundwaters west of the WIPP site and peripheral to the Delaware Basin indicate that simple uptake of solutes from rocks with which they have come in contact did not alter their meteoric isotope ratios. Thus, waters participating in active dissolution of salt, which has not occurred in the Salado Formation at the WIPP site, could be readily identified by their geochemistry.

The origin and age of an artesian brine pocket in the Castile Formation, northeast of the WIPP site was evaluated by a uranium isotope disequilibrium model. It was concluded that this accumulation (encountered in borehole ERDA No. 6) has no connection with any other known groundwaters, and has been in its present environment for at least 880,000 years.

7.11 REFERENCES

Adams, S. S., 1967, Bromine in the Salado Formation, Carlsbad potash district, New Mexico: Unpublished Ph.D. Dissertation, Harvard University, 202 pp.

Adams, S. S., 1969, Bromine in the Salado Formation, Carlsbad potash district, New Mexico: New Mexico Bur. Mines Min. Res. Bull. 93, 112 p.

American Public Health Association, 1971, Standard methods for the examination of water and wastewater (13th ed.): APHA, Am. Water Works Assn., Water Pollution Control Fed: Washington, D. C.

Anderson, R. Y., Dean, W. E., Kirkland, D. W., and Snider, H. I., 1972, Permian Castile varved evaporite sequence, West Texas and New Mexico: Bull. Geol. Soc. Amer., v. 83, p. 59-86.

Anderson, R. Y., and Powers, D. W., 1978, Salt anticlines in the Castile-Salado evaporite sequence, northern Delaware Basin, New Mexico: N. Mex. Bur. Mines Min. Res. Circ. 159, in press.

Anthony, T. R. and Cline, H. E., 1971a, Thermal migration of liquid droplets through solids: Jour. Applied Physics, v. 42, no. 9, p. 3380-3387.

Anthony, T. R. and Cline, H. E., 1971b, The interaction of liquid droplets with a grain boundary in large accelerational fields: Philosop. Mag., v. 24, no. 189, p. 695-703.

Anthony, T. R. and Cline, H. E., 1972, The thermomigration of biphase vapor-liquid droplets in solids: Acta Metallur., v. 20, p. 247-255.

Anthony, T. R. and Cline, H. E., 1973, The stability of migrating droplets in solids: Acta Metallur., v. 21, p. 117-122.

Anthony, T. R., and Cline, H. E., 1974, Thermomigration of liquid droplets in salt, in Fourth Symp. on Salt, v. 1, A. H. Cougan, ed.: Cleveland, Ohio, Northern Ohio Geol. Soc., p. 313-321.

Anthony, T. R. and Sigsbee, R. A., 1971, The thermomigration of spherical bubbles through a transparent polycrystalline solid: Acta Metallur., v. 19, p. 1029-1035.

Baar, C. A., 1977, Applied salt-rock mechanics 1; the in-situ behavior of salt rocks: Elsevier Sci. Pub. Co., Amsterdam, 283 pp.

Bathurst, R. G. C. 1975, Carbonate Sediments and their Diagenesis, 2nd ed. Elsevier Scientific Publishing Company, New York, N.Y., 658 pp.

Bernas, B., 1968, New method for decomposition and comprehensive analysis of silicates by atomic absorption spectrophotometry: Anal. Chem. v. 40, p. 1682-1686.

Bernas, B., 1973, Acid pressure decomposition device for interference-free AA analysis: Amer. Lab., v. 5, no. 8, p. 41.

Bigeleisen, J., Perlman, M.L., and Prosser, H.C., 1952, Conversion of hydrogenic materials to hydrogen for isotopic analysis: Anal. Chem., v. 24, p. 1356-1357.

Bodine, M. W., Jr. 1971, Alteration of basic volcanic rocks by marine hypersaline brines, Hallstatt, Upper Austria: (Abstract), Geol. Soc. Am. Abstr., v. 3, p. 509.

Bodine, M. W., Jr. and Fernalld, T. H. 1973, EDTA dissolution of gypsum, anhydrite, and Ca-Mg carbonates: J. Sediment. Petrol. v. 43, p. 1152-1156.

Bodine, M. W., Jr. and Standaert, R. R., 1977, Chlorite and illite compositions from Upper Silurian rock salts, Retsof, New York: Clays and Clay Minerals, v. 25, p. 57-71.

Boffey, Philip M., 1975, Radioactive waste site search gets into deep water: Science, v. 190, p. 361.

Braitsch, O., 1971, Salt deposits -- their origin and composition, trans. P. J. Bureck and A. E. M. Nairn: Springer-Verlag, Heidelberg, p. 1-297.

Brokaw, A. L., Jones, C. L., Cooley, M. E., and Hays, W. H., 1972, Geology and Hydrology of the Carlsbad Potash Area, Eddy and Lea Counties, New Mexico: U.S. Geologic Survey open-file report 4339-1, 86 pages.

Calzia, J. P., and Hiss, W. L., 1978, Petrographic character and extent of an Oligocene basaltic dike system, northern Delaware Basin, New Mexico: N. Mex. Bur. Mines Min. Res. Circ. 159, in press.

Chen, K. H., and Wilcox, W. R., 1972, Boiling and convection during movement of solvent inclusions in crystals: Indust. Eng. Chem. Fundamentals, v. 11, no. 4, p. 563-565.

Clayton, R. N., Friedman, I., Graf, D. L., Mayeda, T. K., Meents, W. F., and Shimp, N. F., 1966, The origin of saline formation waters, I. Isotopic Composition: Jour. Geophys. Res., v. 71, p. 3869-3882.

Cline, H. E., and Anthony, T. R., 1971, Vaporization of liquid inclusion (sic) in solids: Philosoph. Mag., v. 24, p. 1483-1494.

Collins, A. G., 1975, Geochemistry of oilfield waters: Elsevier Scientific Publishing Company, Amsterdam, p. 1-496.

Craig, Gordon, L. I., and Horibe, Y., 1963, Isotopic exchange effects in the evaporation of water, I. Low-temperature experimental results: Jour. Geophys. Res., v. 68, p. 5079-5087.

Craig, H., 1961a, Isotopic variations in meteoric waters: Science, v. 133, p. 1702-1703.

Craig, H., 1961b, Standard for reporting concentrations of deuterium and oxygen – 18 in natural waters: Science, v. 133, p. 1833-1834.

Dellwig, L. F., 1955, Origin of the Salina salt of Michigan: Jour. Sed. Petrology, v. 25, p. 83-110.

Epstein, S., and Mayeda, T., 1953, Variaton of ^{18}O content of waters from natural sources: Geochim. Cosmochim. Acta, v. 4., p. 213-244.

Epstein, Sharp, R. P., and Gow, A. J., 1965, Six-year record of oxygen and hydrogen isotope variations in South Pole firn: Jour. Geophys. Res., v. 70, p. 1809-1814.

Epstein, 1970, Antarctic ice sheet: Stable isotope analyses of Byrd station cores and interhemispheric climatic implications: Science, v. 168, p. 1570-1572.

Fallis, S. M., 1973, Mineral sources of water and their influence on the safe disposal of radioactive wastes in bedded salt deposits: Unpublished Master's Thesis, University of Tennessee, Knoxville, 61 pp.

Faure, G., and Powell, J. L., 1972, Strontium isotope geology: Springer-Verlag, New York, 188 p.

Faure, G., 1977, Principles of Isotope Geology: J. Wiley & Sons, Inc., New York, 464 p.

Folk, R. L., 1965, Some Aspects of Recrystallization in Ancient Limestones, in L. C. Pray and R. C. Murray (eds.): Soc. Econ. Paleontologists and Mineralogists, Spec. Pub. 13, p 14-48.

Folk, R. L., 1968, Petrology of sedimentary rocks: Hemphill's, Austin, Texas, 170 p.

Fontes, J., and Gonfiantini, R., 1967, Fractionment isotopique de l'hydrogene dans l'eau de cristallisation du gypse: C. R. Acad. So. Paris, Ser. D., v. 265, p. 4-6.

Fournier, R. O., 1961, Regular interlayered chlorite-vermiculite in evaporite of the Salado Formation, New Mexico: U.S.G.S., Prof. Paper 424-D, p. 323-327.

Fuchtbauer, H. and Goldschmidt, H., 1969, Die Tonminerale der Zechsteinformation: Beitr. Mineral. Petrogr. v. 6, p. 320-345.

Garrels, R. M., and Christ, C. L., 1965, Solutions, minerals, and equilibria: Harper and Row, New York, p. 1-450.

Geguzin, Ya. E., and Dzyuba, A. S., 1973, *Study of liquid inclusions in rock salt crystals in the entire range of their existence*: Kristallografiya, v. 18, no. 7, p. 800-807 (in Russian; English abstract in Fluid Inclusion Research -- Proceedings of COFFI, v. 7, p. 62).

Gerlach, Hansludwig, and Heller, Siegfried, 1966, Uber Kunstliche Flussigkeitseinschusse in Steinsalzkristallen: Deutsche Gesell. Geol. Wiss., Reihe B., Mineralogie und Lagerstattenforschungen, Bd. 11, Heft 2, p. 195-214.

Graf, D. L., Meents, W. F., Friedman, I., and Shimp, N. F., 1966, The *origin of saline formation waters, III. Calcium chloride waters*: Illinois State Geol. Surv. Circ. 397, p. 1-60.

Grim, R. E., 1968, Clay Mineralogy (Second Edition), McGraw-Hill Book Company, New York, p. 1-596.

Grim, R. E., Droste, J. B., and Bradley, W. F., 1961, Diffraction data of a regular mixed layered clay mineral in an evaporite, in Eighth Natl. Conference on Clay and Clay Minerals: Pergamon Press, Inc., New York, p. 228-236.

Griswold, G. B., 1977, *Site selection and evaluation studies of the Waste Isolation Pilot Plant (WIPP), Los Mendanos, Eddy County, New Mexico*: Sandia Laboratories, SAND77-0946.

Hiss, W.L., 1975, Stratigraphy and ground-water hydrology of the Capitan aquifer, southeastern New Mexico and west Texas: unpublished ph.D. thesis, University of Colorado, Boulder, 396 p.

Holdoway, K. A., 1974, Behavior of fluid inclusions in salt during heating and irradiation, in Fourth Symp. on salt, v. 1, A. H. Coogan, ed.: Northern Ohio Geol. Soc., Cleveland, Ohio, p. 303-312.

Hopkins, R. H., Seidensticker, R. G., and Stewart, A. M., 1976, Degradation of Czochralski silicate oxyapatite crystals by the thermomigration of liquid drops: Jour. Crystal Growth, v. 33, p. 223-231.

Holser, W. T., 1963, Chemistry of brine inclusions in Permian salt from Hutchison, Kansas in J. L. Rau (ed.), Symposium on salt: Northern Ohio Geological Society, Cleveland, Ohio, p. 86-103.

Holser, 1966, Bromide geochemistry of salt rocks in J. L. Rau (ed.), Second Symposium on Salt: Northern Ohio Geological Society, Cleveland, Ohio, p. 248-275.

Hurley, P. M., Heezen, B. C., Pinson, w. H., and Fairbairn, H. W., 1963, K-Ar age values in pelagic sediments of North Atlantic: Geochim. Cosmochim. Acta, v. 27, p. 393-399.

Jones, C. L., 1973, Salt Deposits of Los Medanos Area, Eddy and Lea Counties, New Mexico, with sections on Ground-water Hydrology, by M. E. Cooley, and Surficial Geology, by G. O. Bachman: U.S. Geological Survey open-file report 4339-7, 67 pages.

Jones, C. L., 1974a, Salt Deposits of the Clovis-Portales Area, East-Central New Mexico: U.S. Geological Survey open-file report 74-60, 22 pages.

Jones, C. L., 1974b, Salt Deposits of the Mescalero Plains Area, Chavez County, New Mexico: U.S. Geological Survey open-file report 74-190, 21 pages.

Jones, C. L., 1975, Potash Deposits in Part of Los Medanos Area of Eddy and Lea Counties, New Mexico: U.S. Geological Survey open-file report 75-407, 37 pages.

Khetchikov, L. N., and Samoilovich, L. A., 1970, The possibilities of the decrepitation method in mineral thermometry: Akad. Nauk S.S.S.R., Izvest., Ser. Geol., 1970, no. 7, p. 92-98 (in Russian; translated in Fluid Inclusion Research — Proceedings of COFFI, v. 3, 1970, p. 94-100).

Kigoshi, Kunihiko, 1971, Alpha-recoil thorium-234: dissolution into water and the uranium-234/uranium-238 disequilibrium in nature: Science, v. 173, p. 47.

Kronfeld, J., Gradsztajn, E., Muller, H.W., Raddin, J., Yaniv, A., Zach, R., 1975, Excess ^{234}U: an aging effect in confined waters: Earth Planetary Sci. Letters, v. 27, p. 342.

Kuznetsov, S. I., Ivanov, M. V., and Lyalikova, N. N., 1963, Introduction to geological microbiology (transl. P. T. Broneer): McGraw-Hill Book Company, New York, p. 1-245.

Lambert, S. J., 1978, The geochemistry of Delaware Basin groundwaters: New Mexico Bur. Mines and Min. Res. Circ. 159, in press.

O'Neil, J. R., and Kharaka, Y. K., 1976, Hydrogen and oxygen isotope exchange reactions between clay minerals and water: Geochim. Cosmochim. Acta, v. 40, p. 241-246.

Osmond, J.K., and Cowart, J.B., 1976, The theory and uses of natural uranium isotopic variations in hydrology: Atomic Energy Review, v. 14, p. 621.

Oxburgh, V. M., Segnit, R. E., and Holland, H. D., 1959, Coprecipitation of strontium with calcium carbonate from aqueous solutions (abstr.): Bull. Geol. Soc. Amer., v. 70, p. 1653.

Potter, R. W., II, 1977, Pressure corrections for fluid-inclusion homogenization temperatures based on the volumetric properties of the system NaCl-H_2O: J. Research U.S. Geol. Survey, v. 5, no. 5, p. 603-607.

Randall, M., and Failey, C. F., 1927, The activity coefficient of gases in aqueous salt solutions: Chem. Rev., v. 4, p. 271-284.

Reeves, C. C., Jr., 1963, Subterranean natural brines produce sodium sulphate in West Texas: Ground Water, v. 1, p. 35-36.

Roedder, E., 1965, Liquid CO_2 inclusions in olivine bearing nodules and phenocrysts from basalts: Amer. Min., v. 50, p. 1746-1782.

Savin, S. M., and Epstein, S., 1970, The oxygen and hydrogen isotope geochemistry of clay minerals: Geochim. Cosmochim. Acta, v. 34, p. 25-42.

Schaller, W. T. and E. P. Henderson, 1932, Mineralogy of drill cores from the potash field of New Mexico and Texas: U. S. Geol. Surv. Bull. No. 833, 124 pp.

Shell Exploration and Production Research Center, 1973, Potassium-Argon dates on Permian potash minerals from southeastern New Mexico: Isochron/West, No. 6, p. 37.

Tremba, E. L., 1973, Isotope geochemistry of strontium in carbonate and evaporite rocks of marine origin: unpub. Ph.D. dissertaton, Ohio State Univ., 185 p.

Vogel, A. I., 1961, A Textbook of Quantitative Inorganic Analysis: 3rd Ed., John Wiley and Sons, Inc., N.Y., p. 462.

Wilcox, W. R., 1968, Removing inclusions from crystals by gradient techniques: Indust. Eng. Chem., v. 60, no. 3, p. 13-23.

Wilcox, W. R., 1969, Anomalous gas-liquid inclusion movement: Indust. Eng. Chem., v. 61, no. 3, p. 76-77.

7.12 ACKNOWLEDGEMENTS

FIGURE 7.1

DISTRIBUTION OF MINERALS IN ERDA #9 CORE SAMPLES
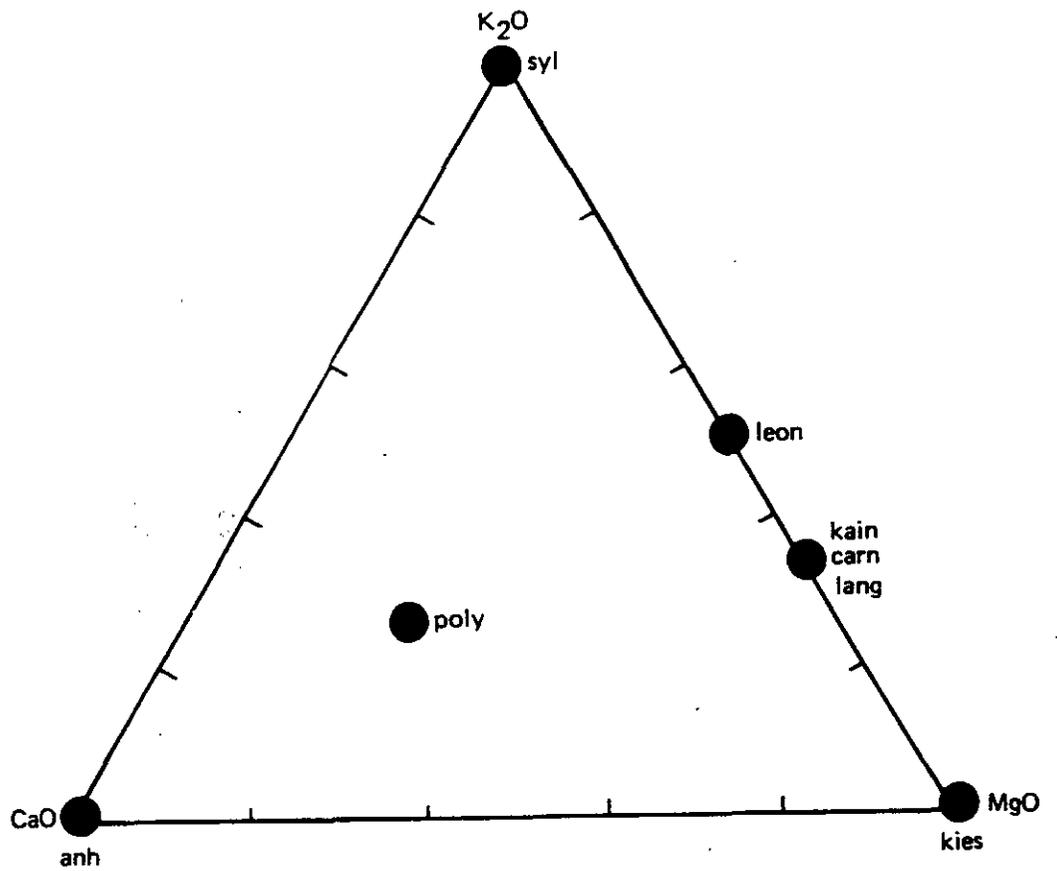
FIGURE 7.2

TRIANGULAR COMPOSITION DIAGRAM OF

SOLUBLE SULFATE-GROUP MINERALS
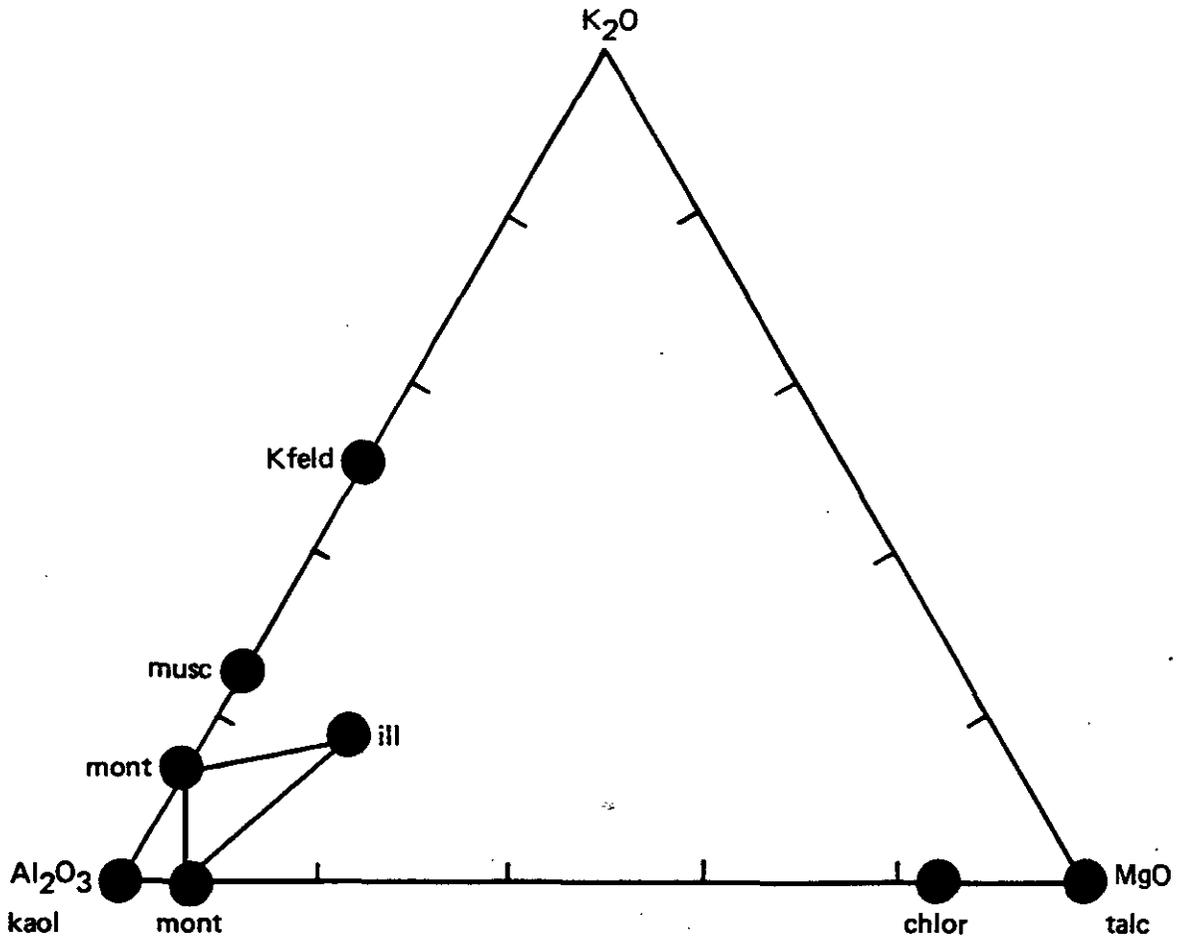
FIGURE 7.3

TRIANGULAR DIAGRAM OF

INSOLUBLE SILICATE-GROUP MINERALS
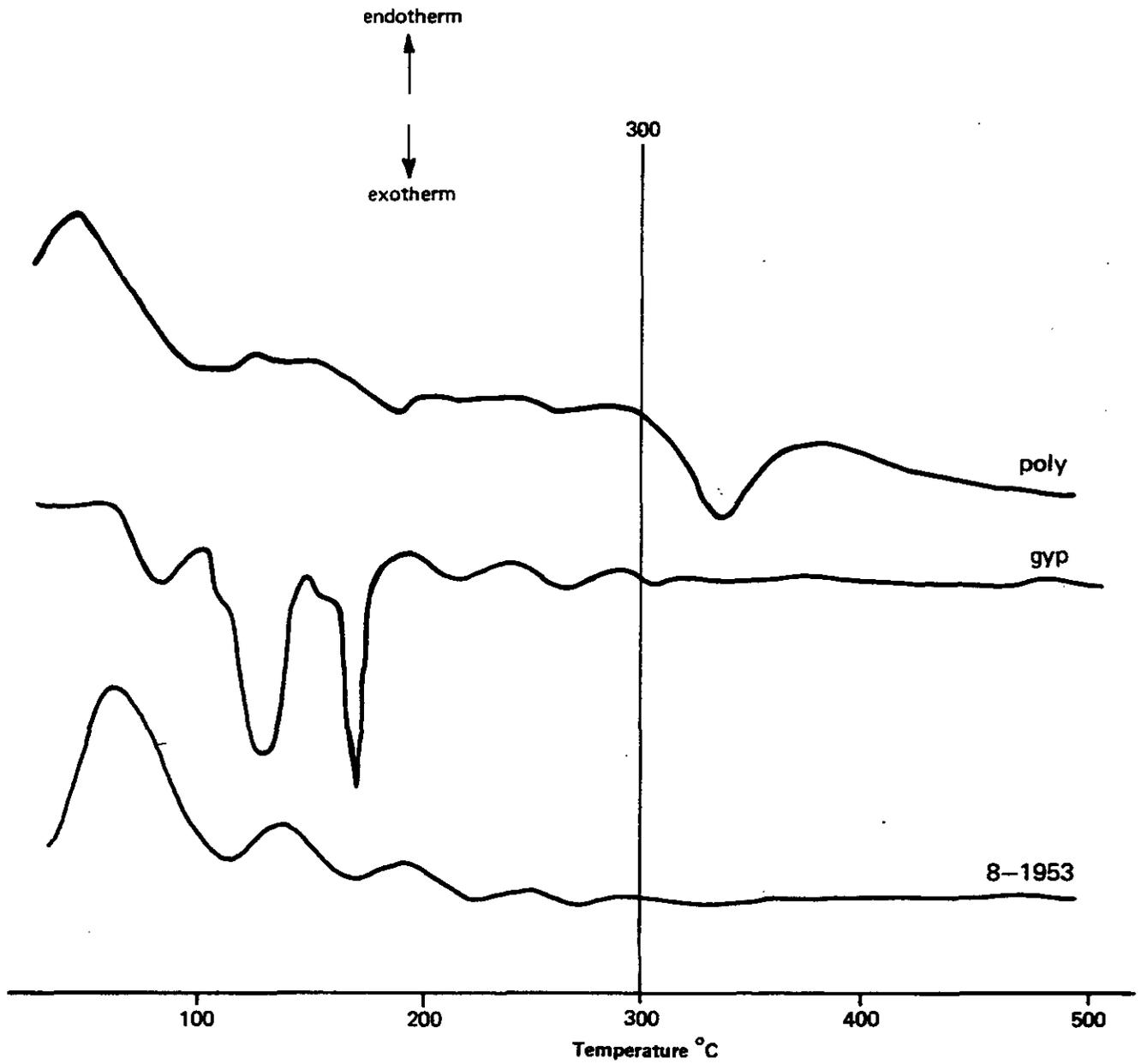
FIGURE 7.4

DIFFERENTIAL THERMAL ANALYSIS CURVES

FOR GYPSUM AND POLYHALITE
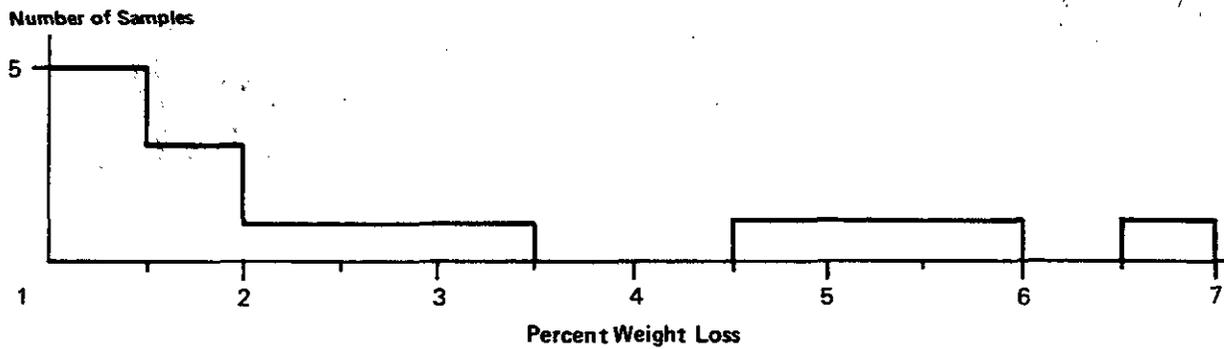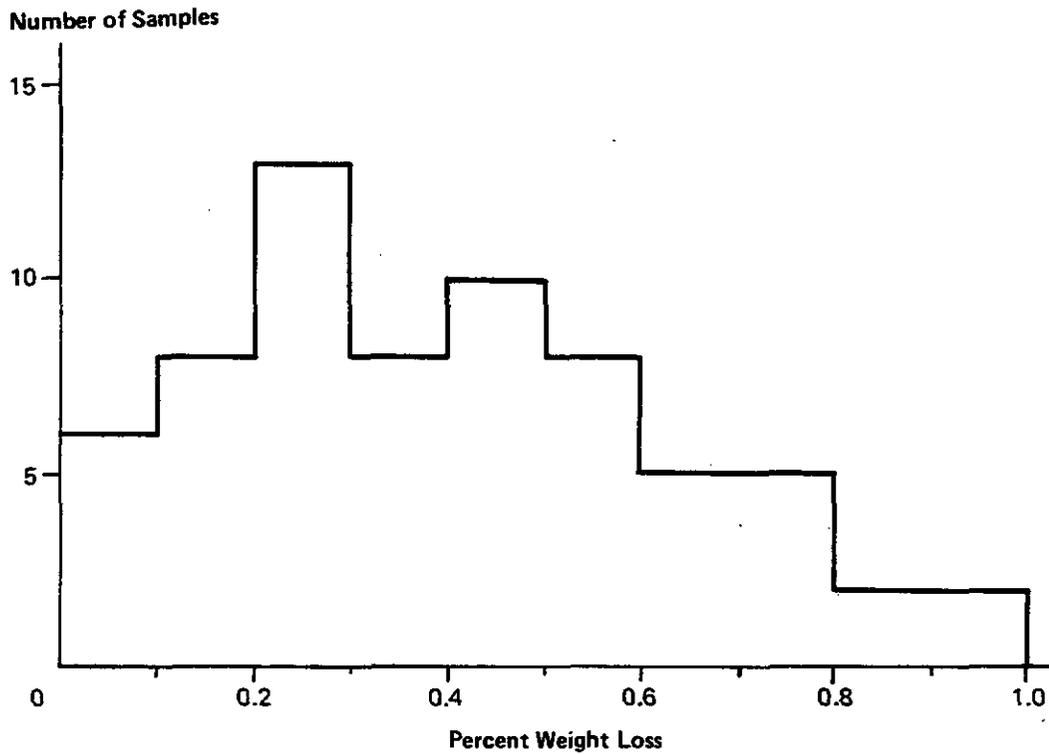
FIGURE 7.5

TOTAL WEIGHT LOSSES AT ELEVATED TEMPERATURES

(500°C) FOR CORES FROM AEC NOS. 7 AND 8
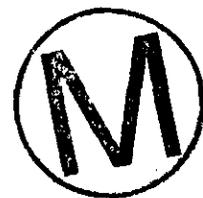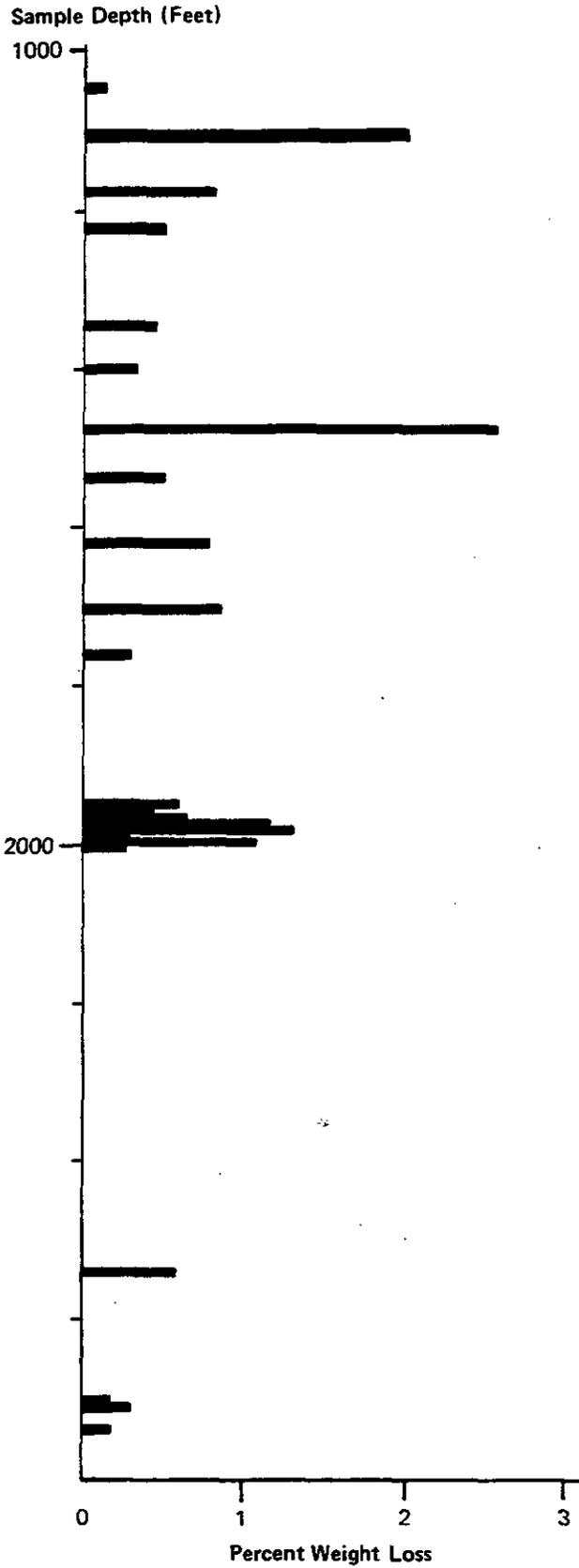
FIGURE 7.6A

AEC NO. 7 SAMPLE WEIGHT LOSSES VS. DEPTH

AT ELEVATED TEMPERATURES (500°C)

Sample Depth (Feet)

Percent Weight Loss

Off Scale
(6.84)
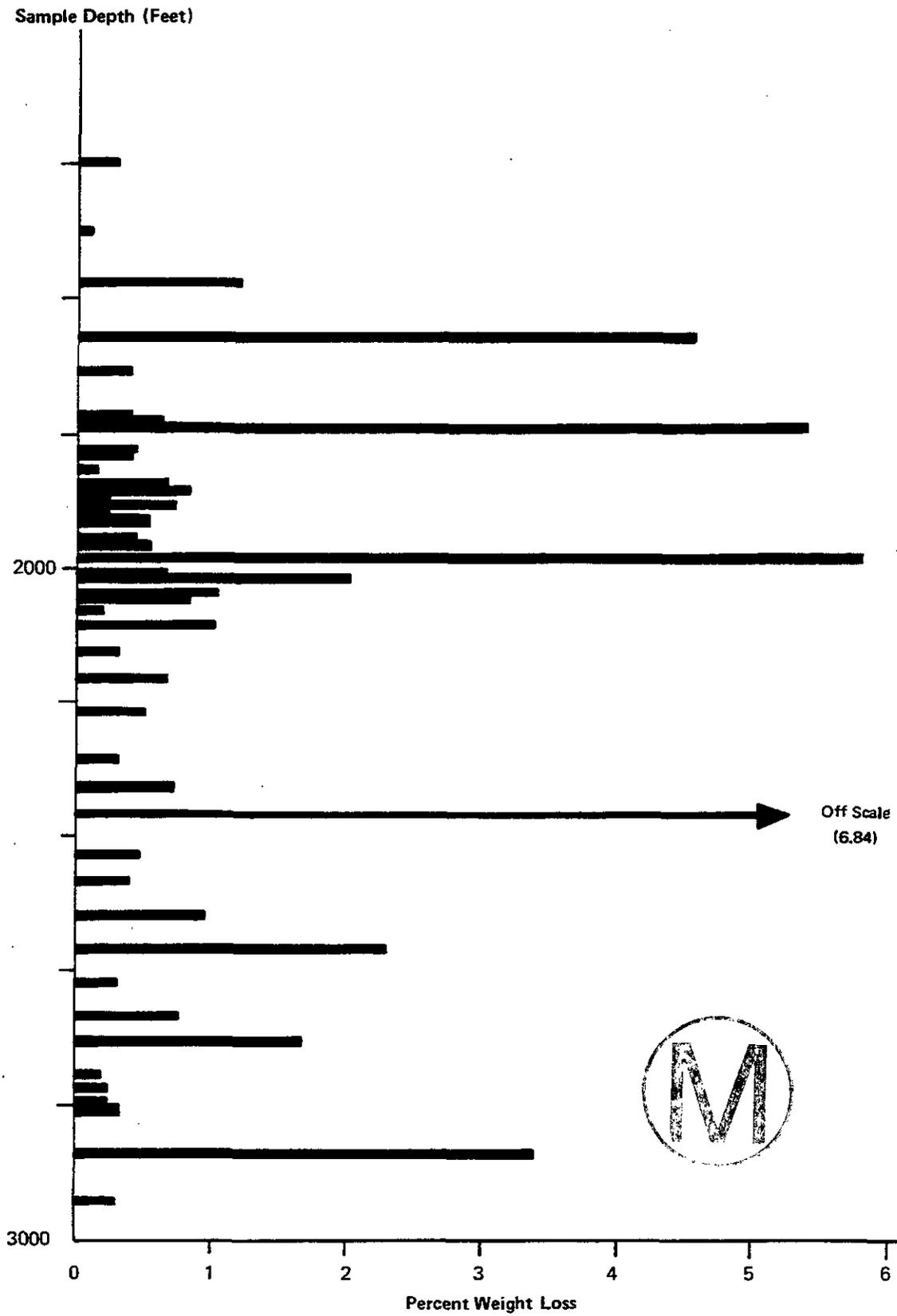
FIGURE 7.6B

AEC NO. 8 SAMPLE WEIGHT LOSSES VS. DEPTH

AT ELEVATED TEMPERATURES (500°C)
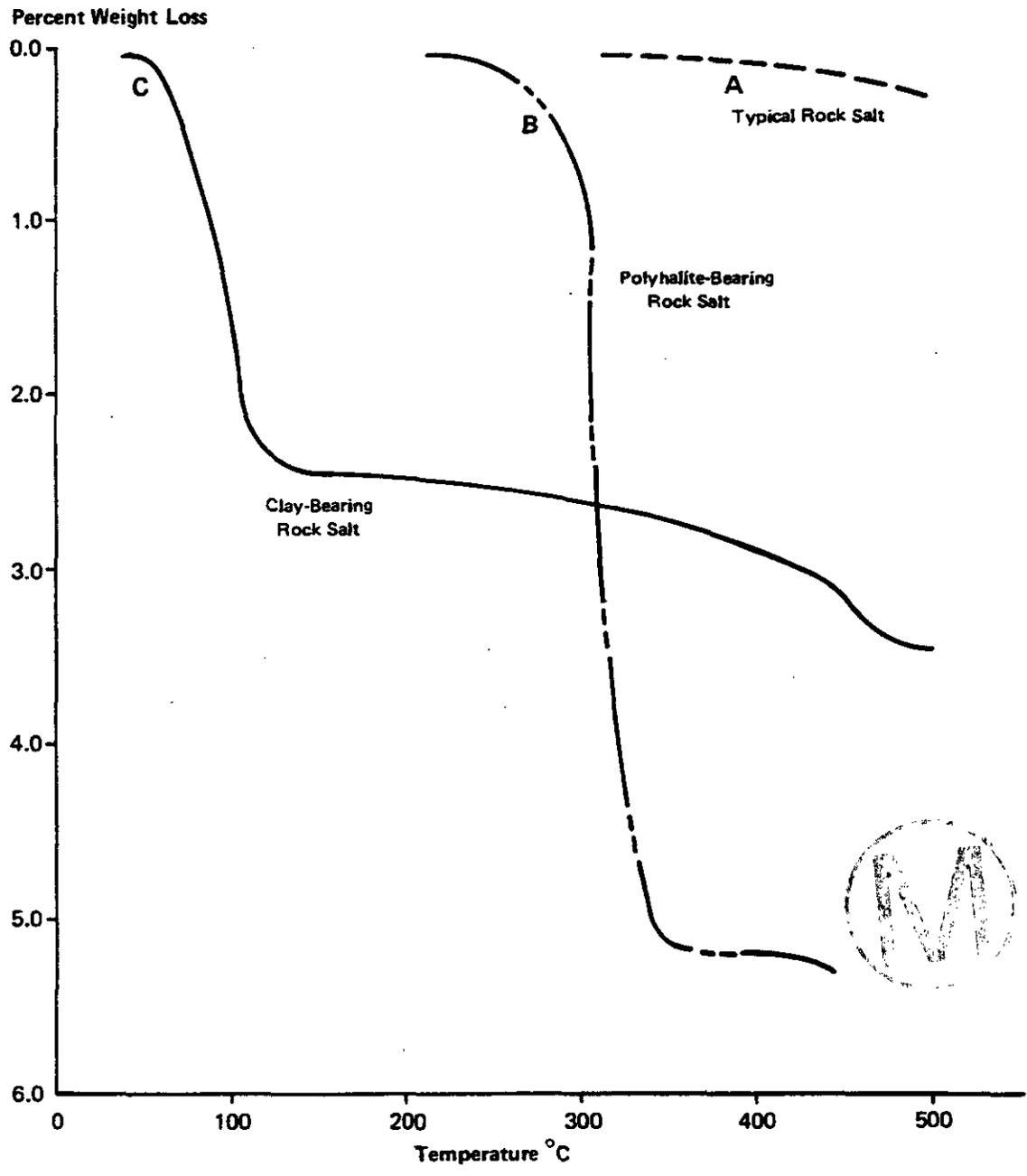
FIGURE 7.7

TYPICAL WEIGHT-LOSS CURVES FOR ERDA #9 EVAPORITE CORE

FIGURE 7.8 WEIGHT LOSS DATA FOR SAMPLES (102±5°C)

FROM CORES NO. 7 AND NO. 8 NEAR CARLSBAD, NEW MEXICO

Sample Depth (Feet)

LYONS

CARLSBAD

(NOTE: The Majority Of Samples From Carlsbad
Have Weight Losses Less Than 0.5%)

Percent Weight Loss
(Note Scale Change)
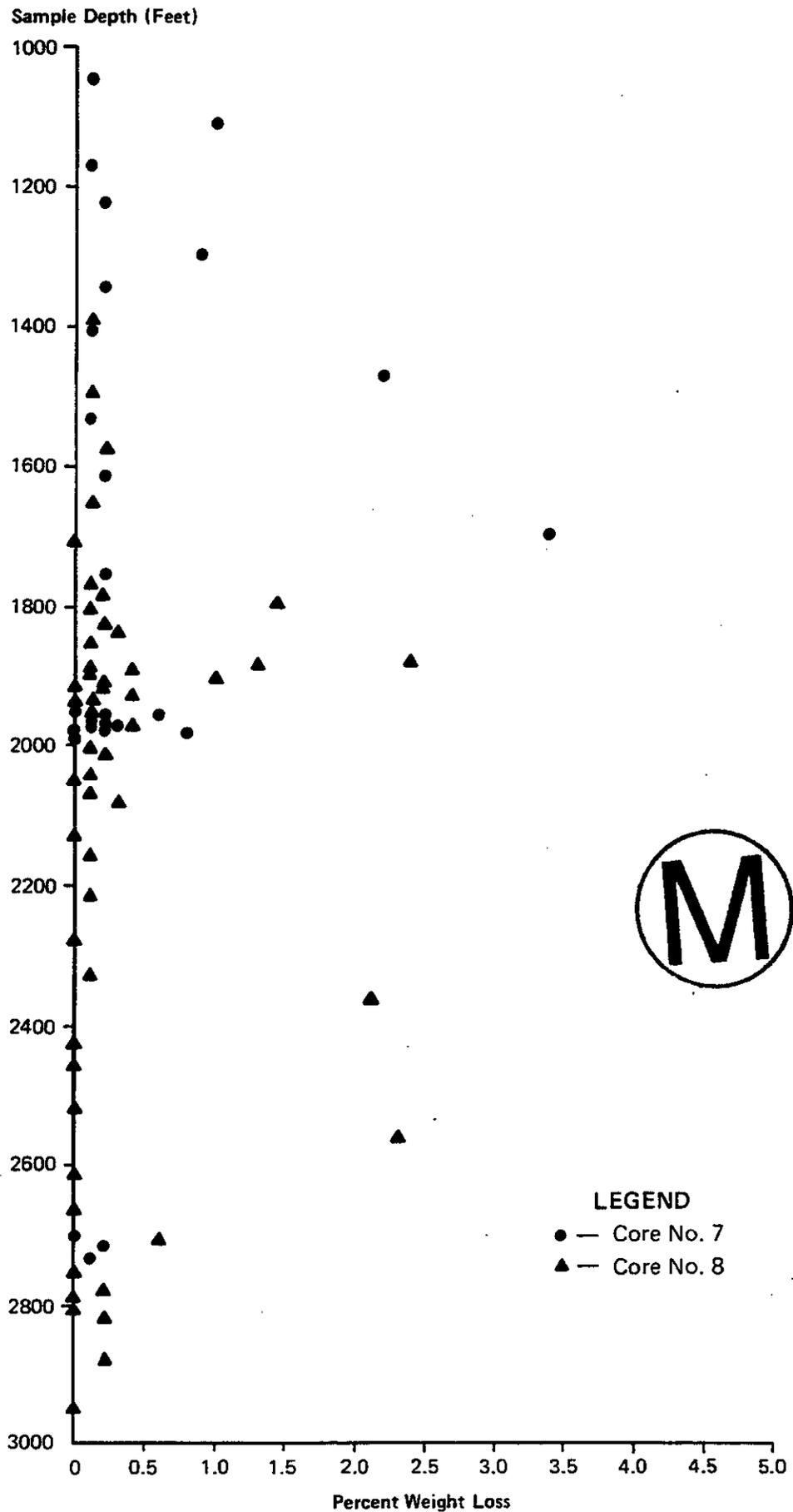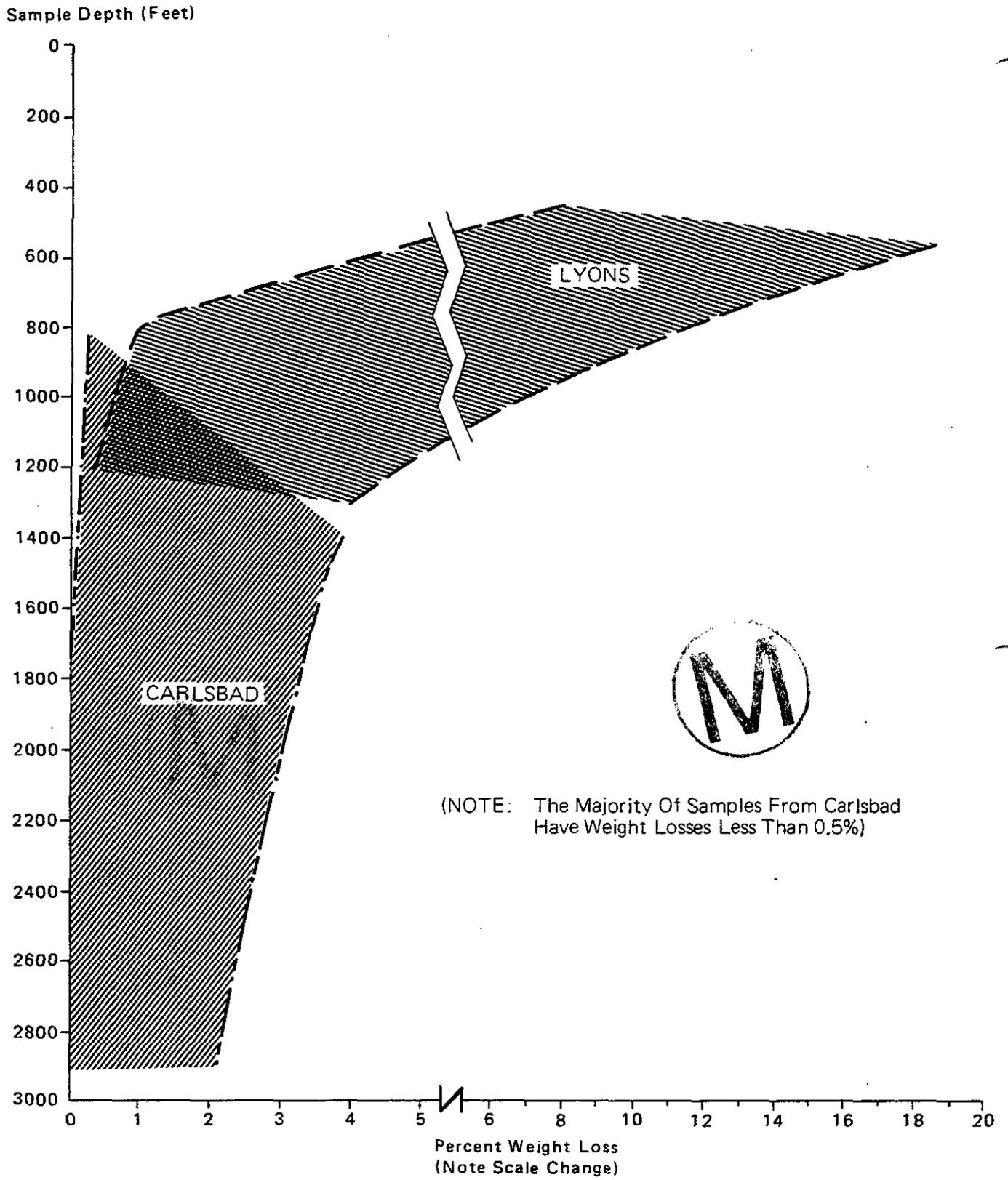
FIGURE 7.9 APPROXIMATE RANGE OF WEIGHT LOSS TO BE EXPECTED
At 102 + 5°C VS. DEPTH FOR SAMPLES FROM LYONS, KANSAS
AND CARLSBAD, NEW MEXICO
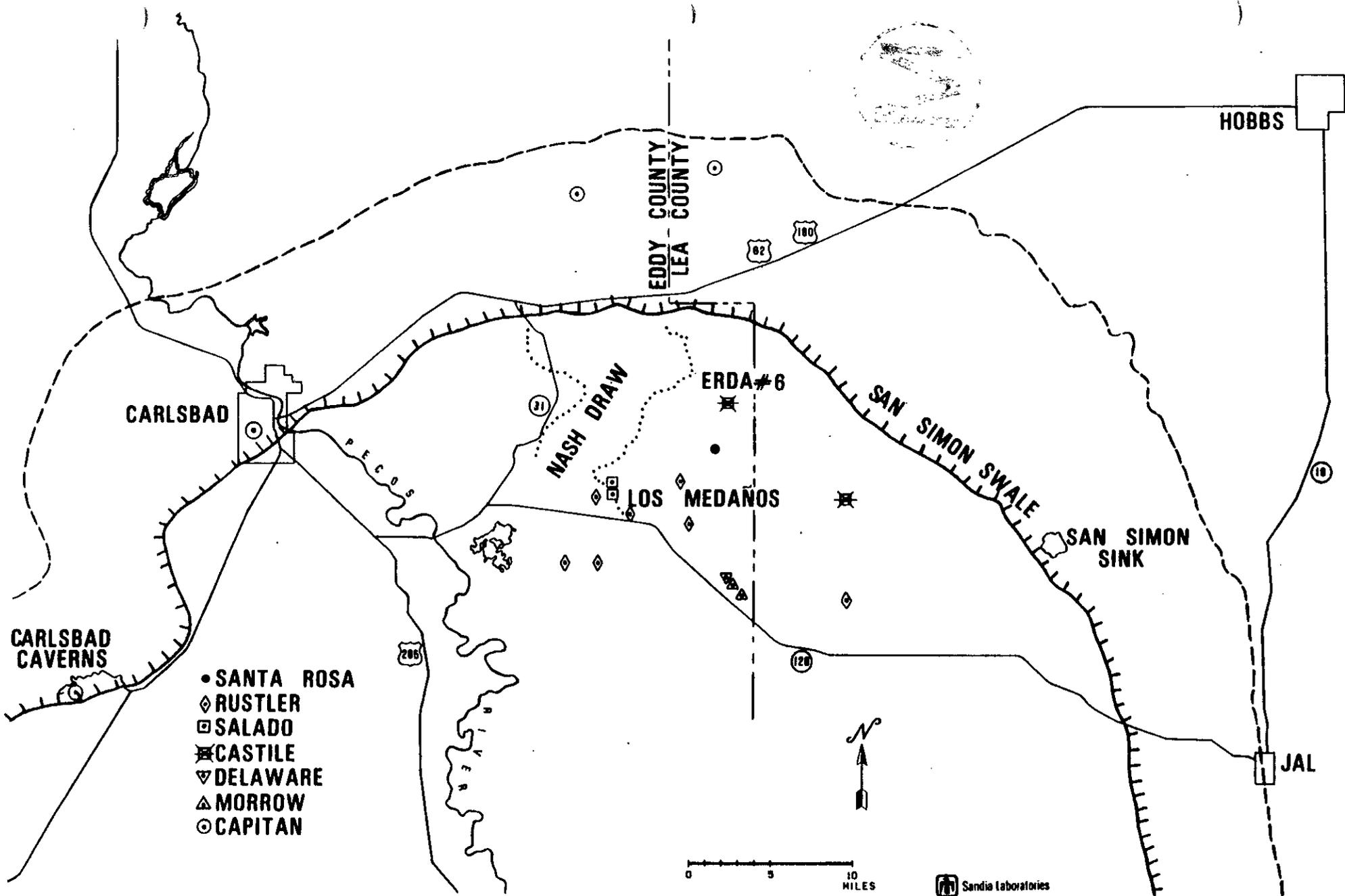
FIGURE 7.10 Map of the New Mexico portion of the Delaware Basin, showing locations of water sampling points in this study. The solid hachured line is the basinward margin of the Capitan Reef; the dashed line is the shelfward edge.

Legend:
- • SANTA ROSA
- ◇ RUSTLER
- ⊡ SALADO
- ✳ CASTILE
- ▽ DELAWARE
- △ MORROW
- ⊙ CAPITAN

Map labels: HOBBS, CARLSBAD, CARLSBAD CAVERNS, ERDA#6, NASH DRAW, LOS MEDAÑOS, SAN SIMON SWALE, SAN SIMON SINK, JAL, PECOS, EDDY COUNTY, LEA COUNTY, RIVER

Scale: 0 — 5 — 10 MILES

Sandia Laboratories
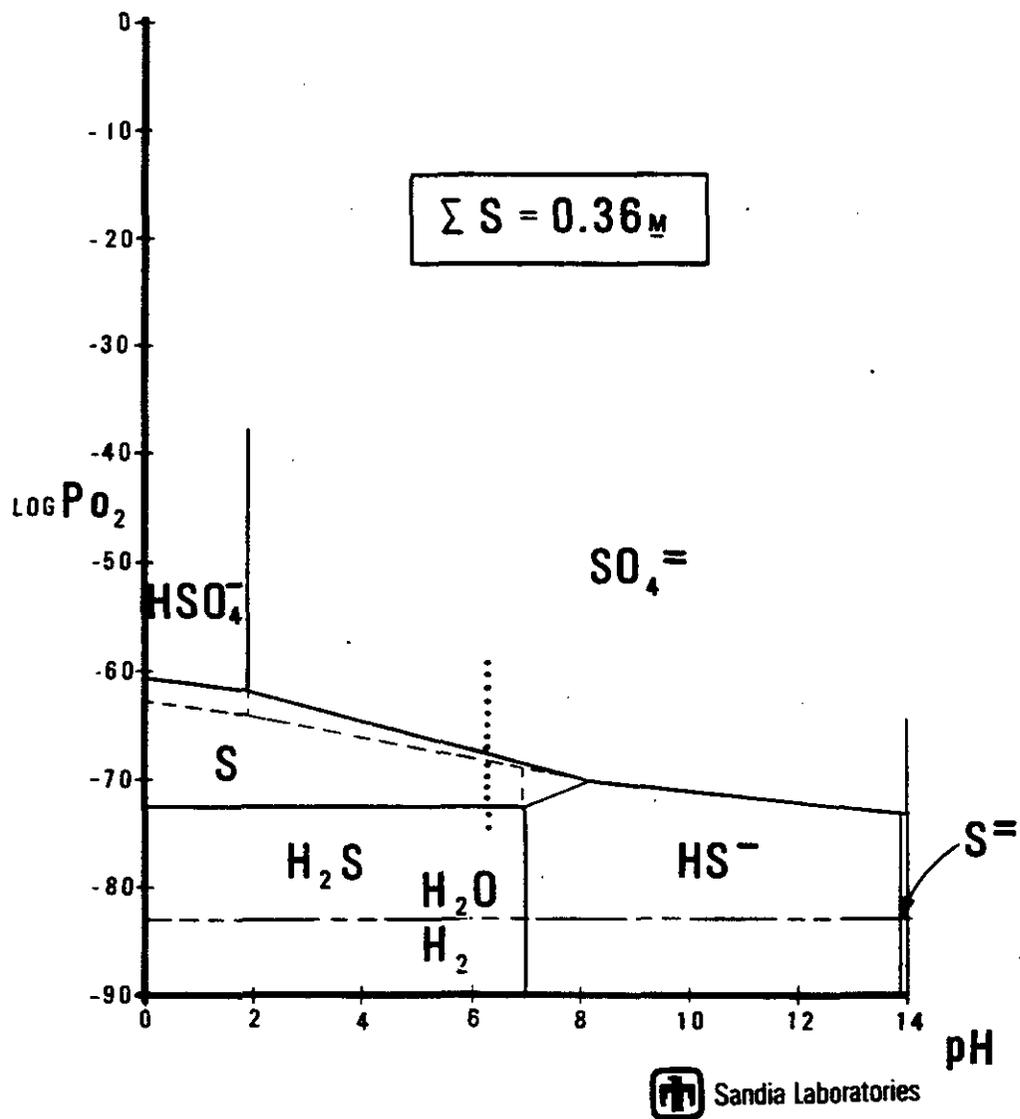
FIGURE 7.11 Predominance area diagram, oxygen partial pressure versus pH, for the System S-O-H at 25°C, 1 atmosphere and total sulfur concentration of 0.36m. Dashed lines are metastable extensions of boundaries. Dotted line represents the field-measured pH of ERDA No. 6, 6.3.
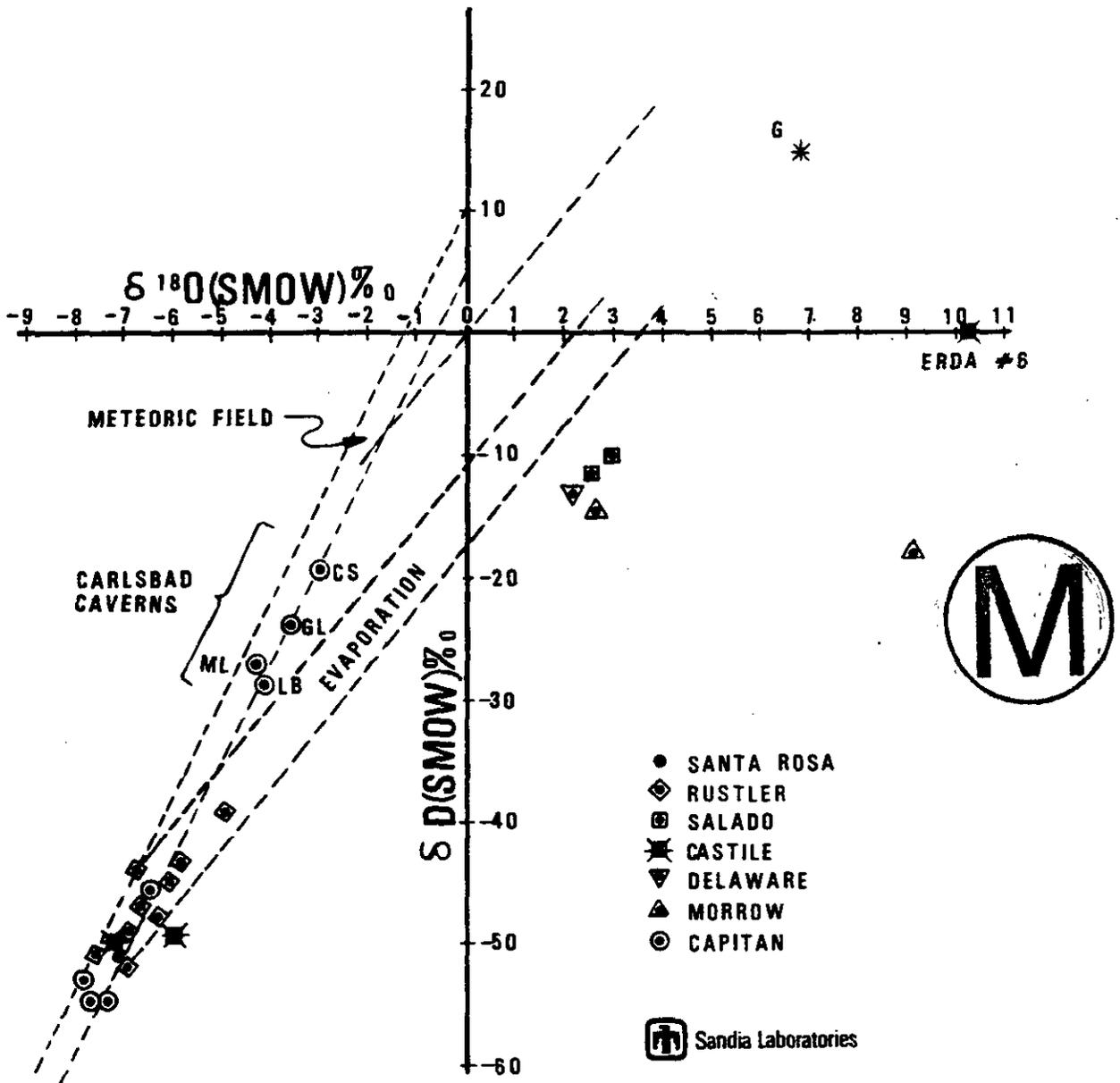
FIGURE 7.12 Stable isotope compositions, δD versus $\delta^{18}O$, for Delaware Basin groundwaters. Relationships are shown for meteoric waters, evaporating meteoric and sea waters. Hypothetical evaporite mother-liquor for gypsum (G) is shown for the case in which ERDA No. 6 is taken to be the water of crystallization for that gypsum.

FIGURE 7.13

Apparent Rb—Sr Isochron
Whole Rocks

T = 132 m.y.
R_0 = 0.7096

7 data

$^{87}Sr/^{86}Sr$

$^{87}Rb/^{86}Sr$

FIGURE 7.14

Apparent Rb–Sr Isochron
Water Soluble Fraction

$T = 206.1$ m.y.
$R_0 = 0.7084$

x-axis: $^{87}Rb/^{86}Sr$

y-axis: $^{87}Sr/^{86}Sr$
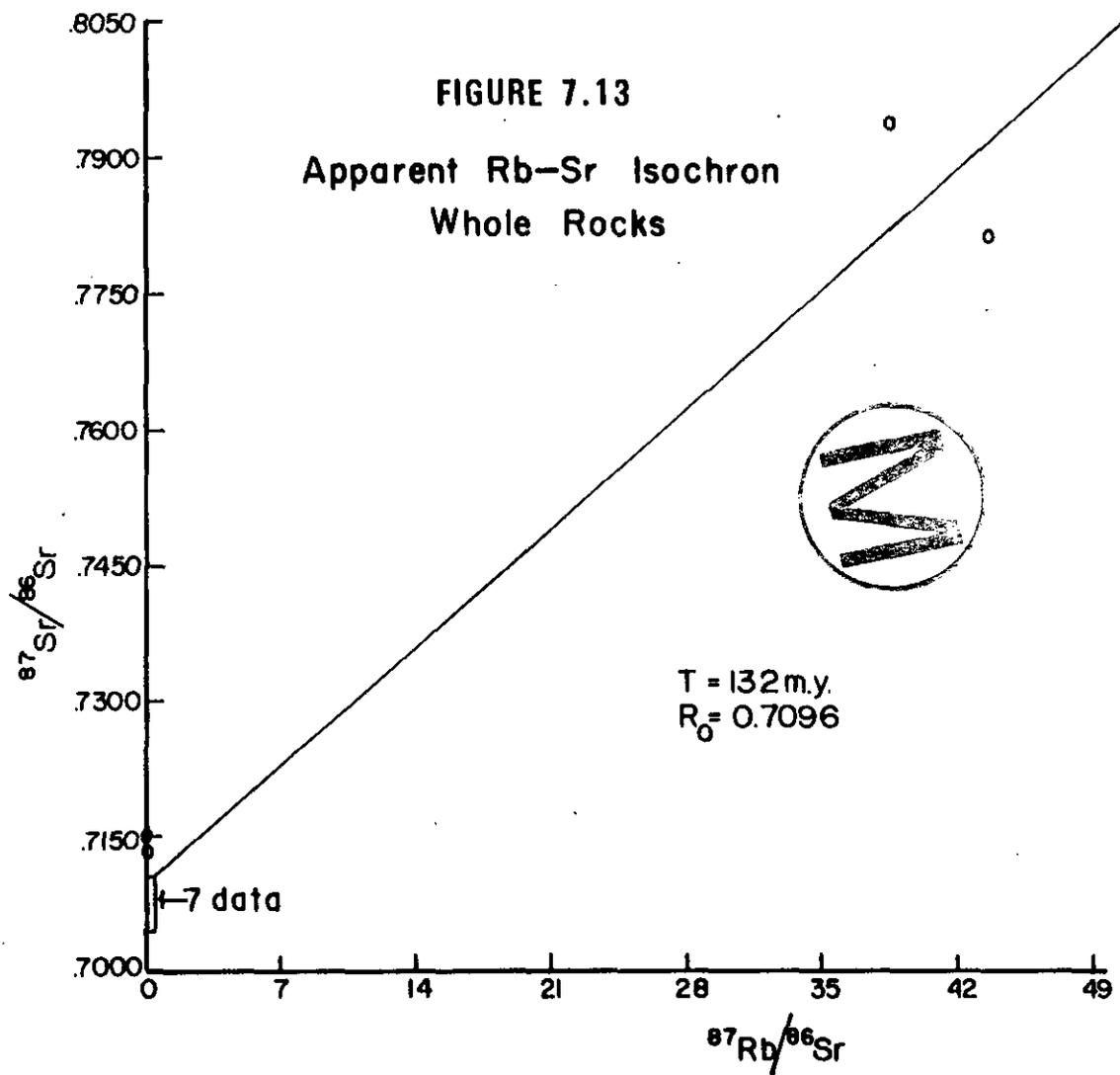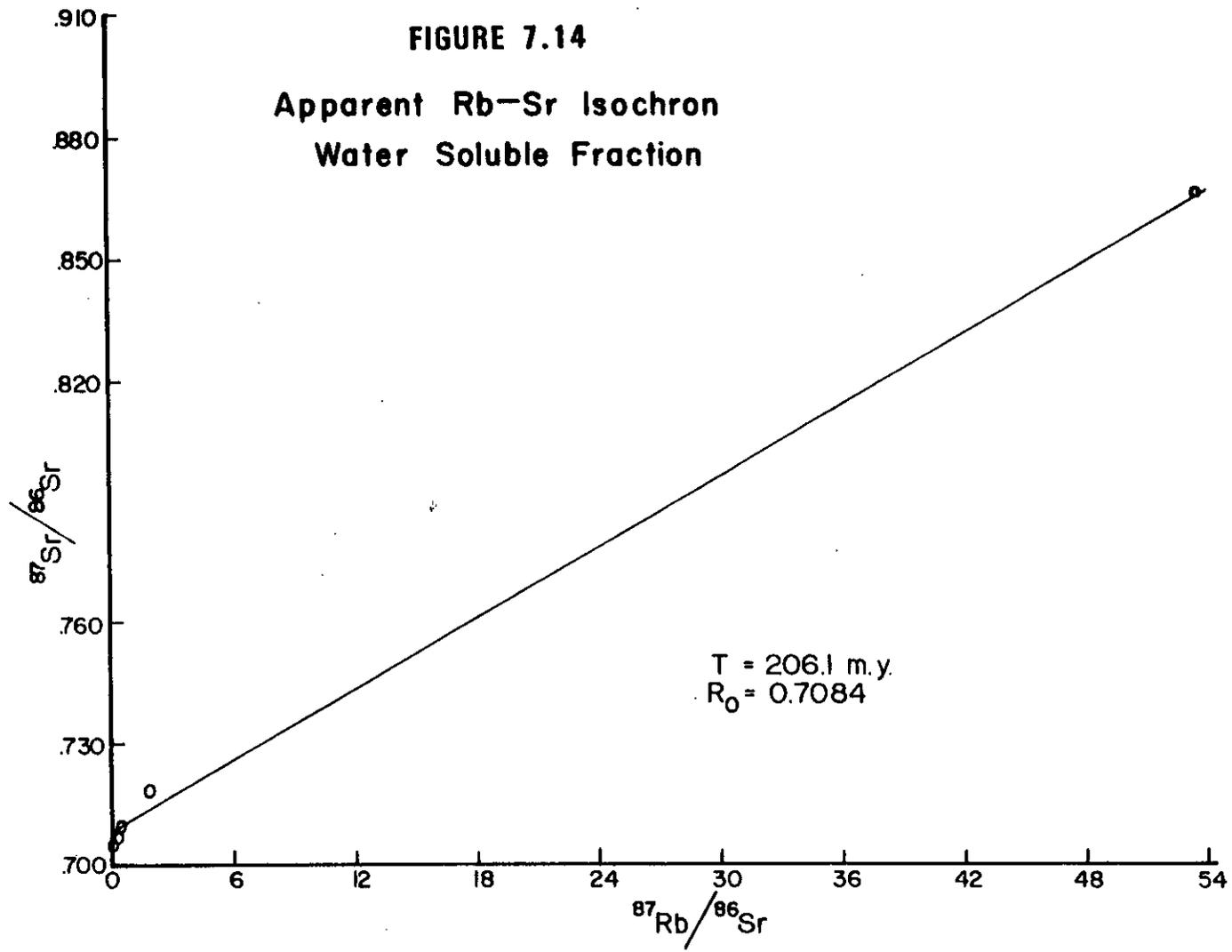
FIGURE 7.15

Apparent Rb—Sr Isochron
Clay Mineral (<2M) Fraction

$T = 325$ m.y.
$R_0 = 0.7123$

$^{87}Sr/^{86}Sr$

$^{87}Rb/^{86}Sr$
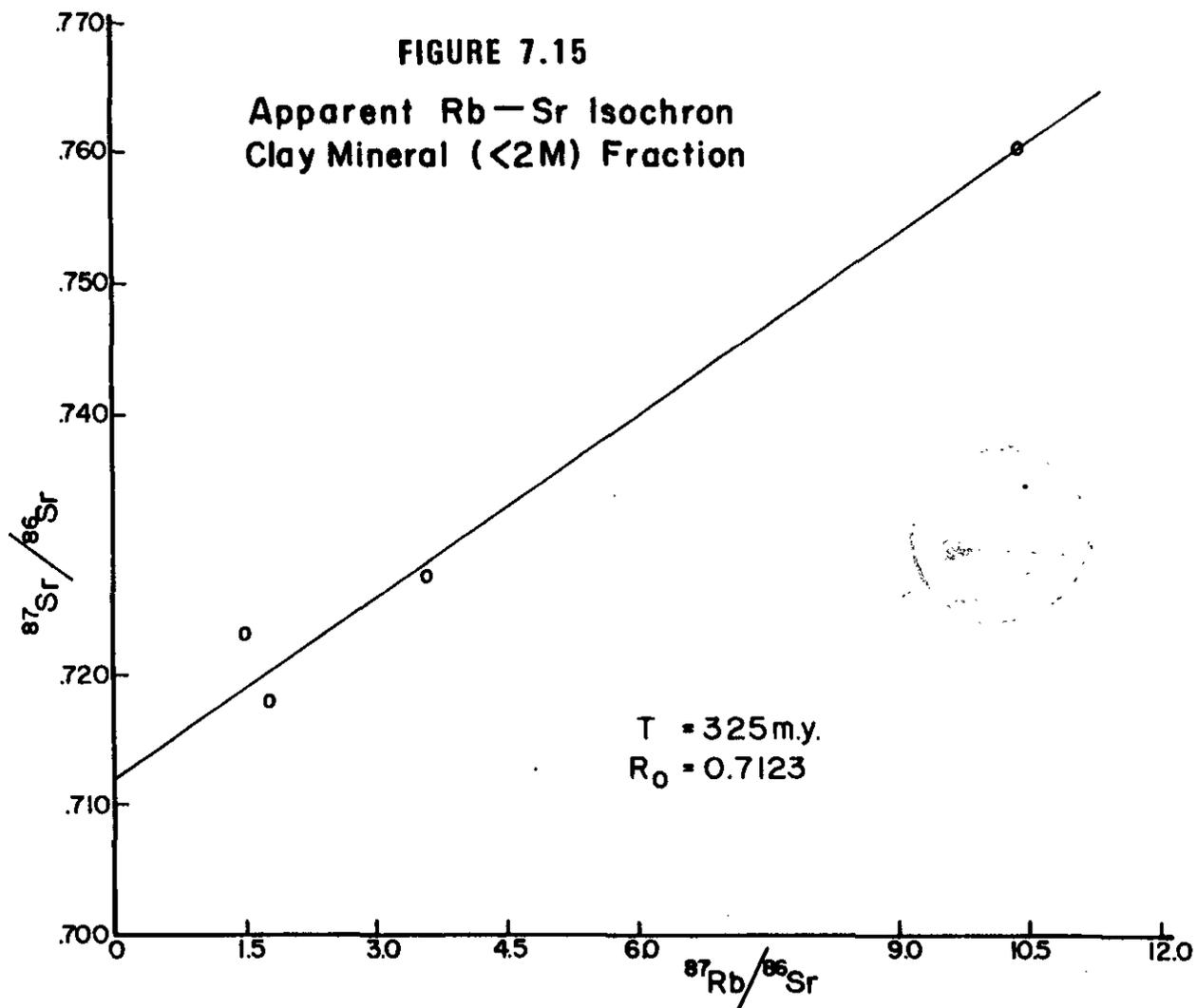
FIGURE 7.16

Apparent Rb–Sr Isochron
Composite of Whole Rock,
Water Soluble Fractions, and
Clay Minerals

$T = 165$ m.y.
$R_0 = 0.7115$

FIGURE 7.17

Apparent Rb—Sr Isochron
Water Soluble and Clay Mineral Fractions

$T = 204$ m.y.
$R_0 = 0.7137$

$^{87}Sr/^{86}Sr$

$^{87}Rb/^{86}Sr$
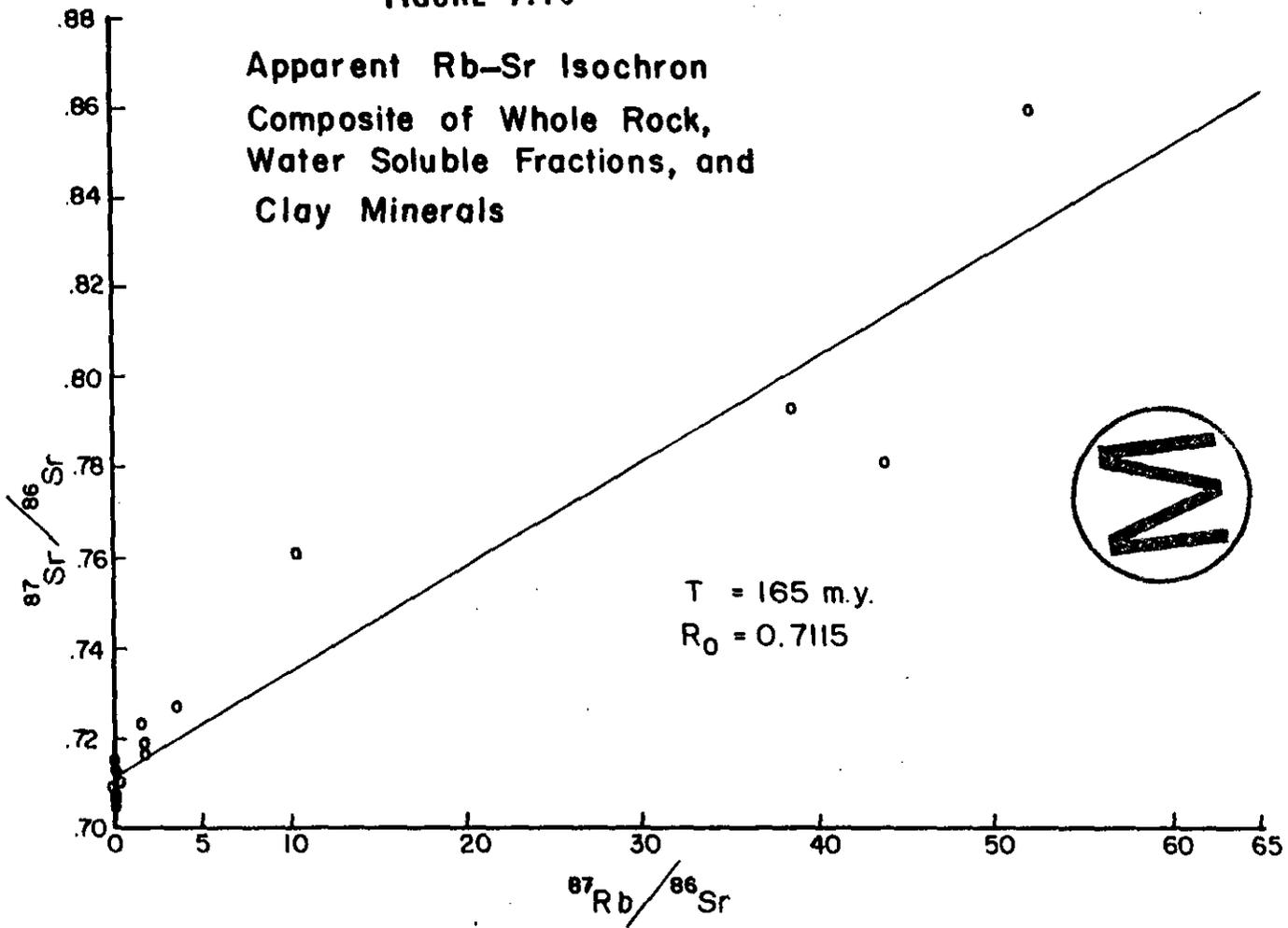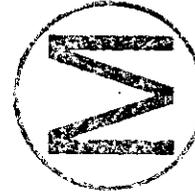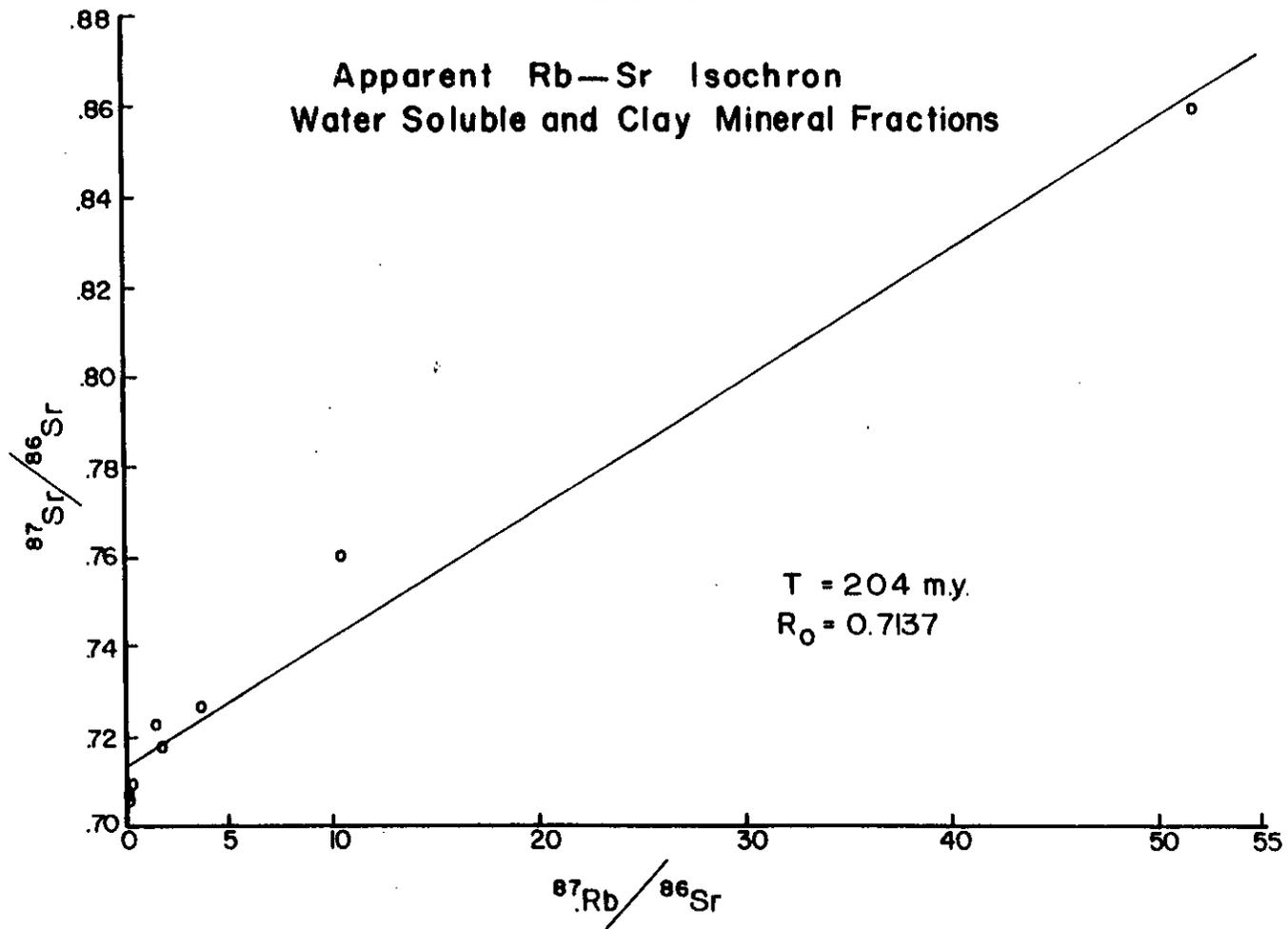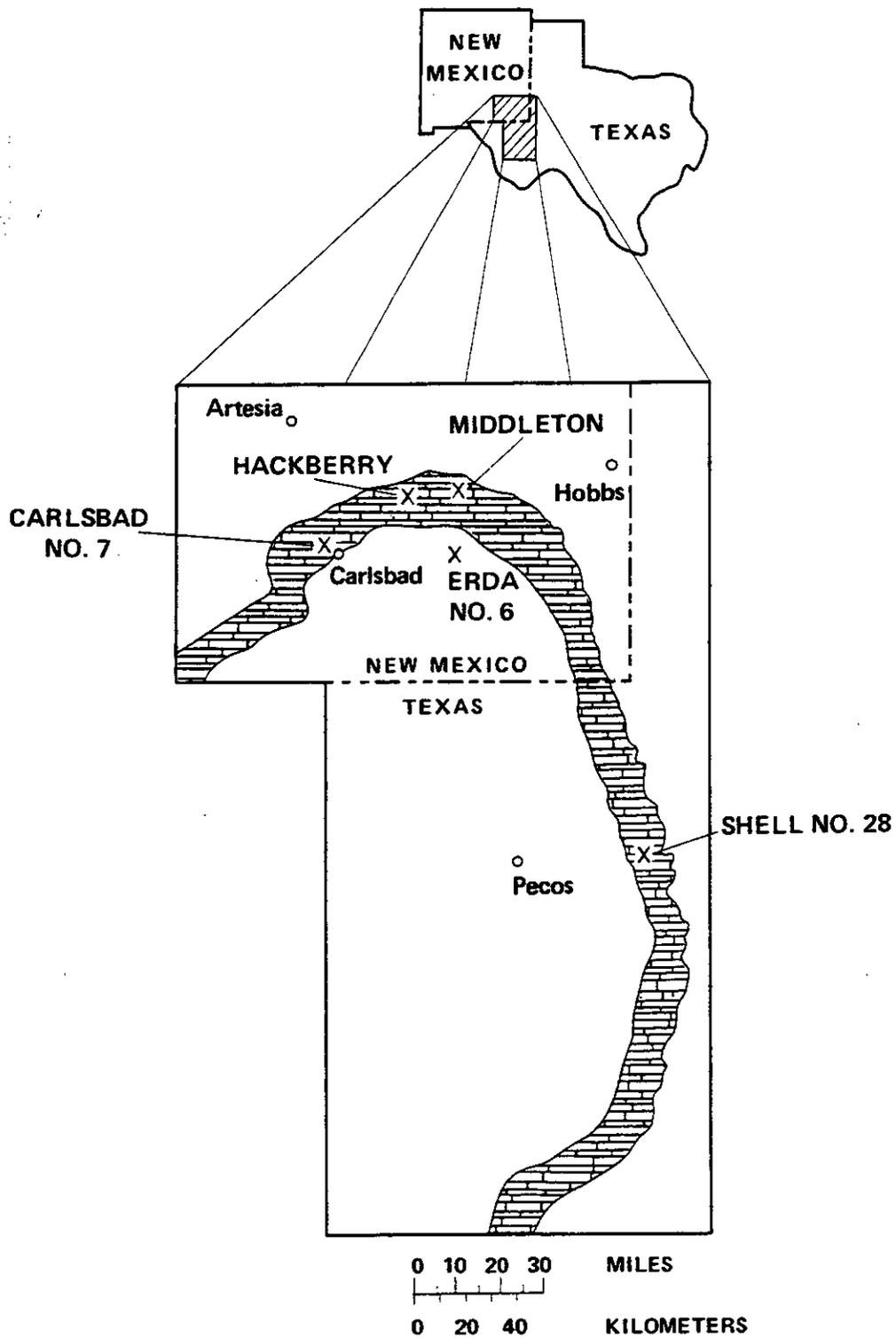
FIGURE 7.18   Map of a portion of the Delaware Basin (southeast New Mexico, west Texas) showing locations of holes whose fluids are sampled for $^{234}U/^{238}U$-disequilibrium age-dating. The brick-pattern shows the surface projection and outcrop of the capitan reef limestone. (from Hiss, 1975)

FIGURE 7.19 Graph of the equation $f = \dfrac{(\alpha_0 - 1)(\alpha_r - 1)}{\alpha_b - \alpha_0 + r (\alpha_r - 1)}$

for the ERDA No. 6 assemblage of rock and brine, in which $r = 16.42$, $\alpha_r = 1.04$, $\alpha_b = 1.35$.

Uranium disequilibrium ages for the brine are shown according to the equation

$$t = \frac{\ln\left(\dfrac{\alpha_b - 1 - fr}{\alpha_0 - 1 - fr}\right)}{-\lambda_2}$$

$a_0 = 1.971$
at $f = 1$

Uranium Leaching

5.7×10^5 yr.

7.8×10^5 yr.

9.4×10^5 yr.

Uranium Deposition

$a_0 = 2.052$
at $f = -1$
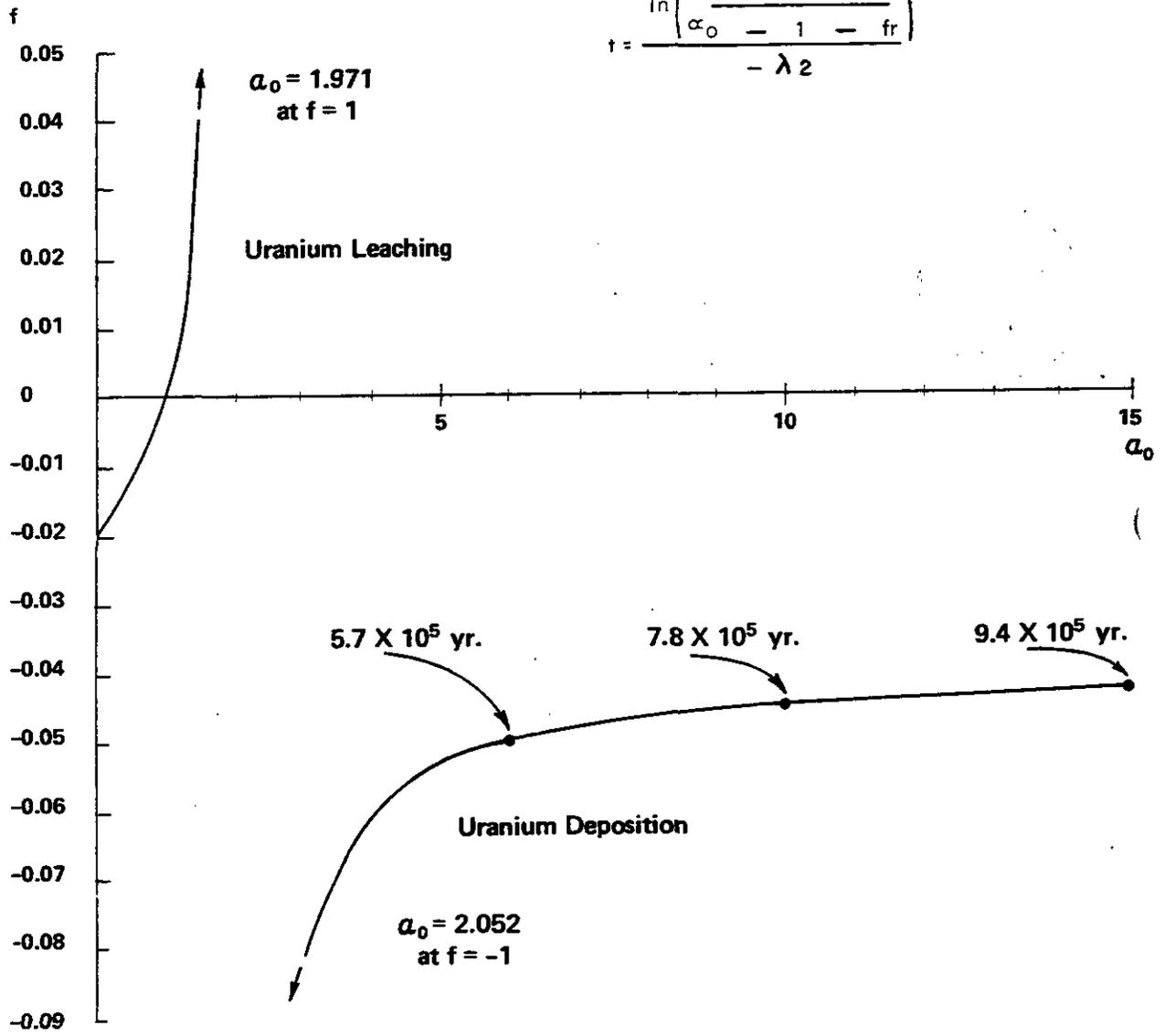
Note that the ERDA No. 6 assemblage is indicative of uranium deposition ($f < 0$) rather than uranium leaching.
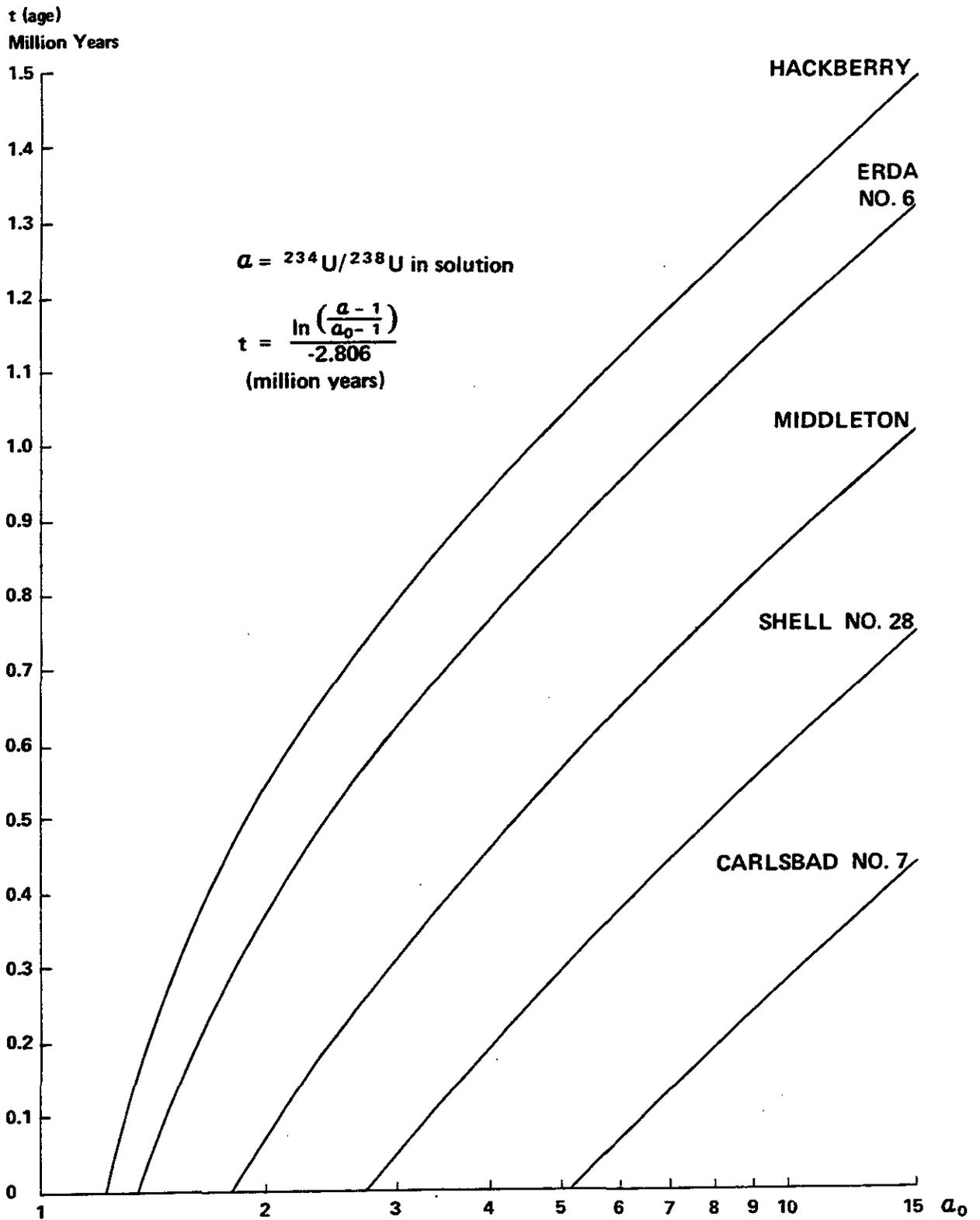
FIGURE 7.20 Uranium disequilibrium ages as a function of
original $^{234}U/^{238}U$ ratio, for Delaware Basin
groundwaters. These curves are derived from a
model involving no exchange or uranium between
rock and water.

TABLE 7.1. MINERAL CONTENT OF ERDA #9 CORE SAMPLES (M=MAJOR, T=TRACE).

ERDA 9
CORE #

(DEPTH IN FEET)	ANHYDRITE	CLAY	HALITE	LOEWEITE	MAGNESITE	POLYHALITE	QUARTZ	SYLVITE
1162.7	T		M					
1165.7	M		M					
1168.0	M		T					
1168.8			M					
1172.8			M			M		
1173.4	M				M		T	
1174.1			M			M		
1405.7			M		T			
1418.8						M		
1584.0			M					
1610.0			M					
1632.4	M				M			
1632.8						M		
1648.5			M	T				
2034.7	M		M				T	
2035.7	T		M					T
2036.3			M					
2065.0			M					
2067.5			M			T		
2302.6	M		T			M		
2413.7			M			M		
2414.2			M			M		
2415.6	M		M					
2512.0	M		M					
2516.3	M		M		T			
2518.8	M							
2528.7	M				T			
2529.0	M		T					
2538.5	M				T			

TABLE 7.1. MINERAL CONTENT OF ERDA #9 CORE SAMPLES (M=MAJOR, T=TRACE), continued

ERDA 9
CORE #

(DEPTH IN FEET)	ANHYDRITE	CLAY	HALITE	LOEWEITE	MAGNESITE	POLYHALITE	QUARTZ	SYLVITE
2541.0	•	•	M	•	•	•	•	•
2542.0	•	•	M	•	•	•	•	•
2593.2	M	•	•	•	•	•	•	•
2594.5	•	•	M	•	•	•	•	•
2597.0	T	•	M	•	•	•	•	•
2608.9	T	•	M	•	•	•	•	•
2614.7	•	•	M	•	•	•	•	•
2619.6	T	•	M	•	•	•	•	•
2658.5	M	•	M	•	•	•	•	•
2663.3	T	•	M	•	•	•	•	•
2696.4	M	•	M	•	T	•	•	•
2706.5	•	•	M	•	•	•	•	•
2711.9	T	•	M	•	T	•	•	•
2759.0	T	•	M	•	•	•	•	•
2768.5	M	T	M	•	•	•	•	•
2820.7	M	•	M	•	•	•	•	•
2820.6	T	•	M	•	•	•	•	•
2821.0	T	•	M	•	•	•	•	•
2826.5	T	•	M	•	•	•	•	•
2845.3	M	•	•	•	T	•	•	•
2848.8	M	•	•	•	•	•	•	•

TABLE 7.2

Size Distribution of Ground Samples

Mesh	% of Sample *
>20	5.2
20-28	8.8
28035	19.9
35-65	57.0
65-100	6.1
100-200	2.9
<200	0.2

*Total ≠ 100 due to rounding

TABLE 7.3

Listing of Minerals Named in Subsection 7.3

Mineral Name	Chemical Composition
Anhydrite	$CaSO_4$
Bloedite	$Na_2 Mg(SO_4)_2 \cdot 4H_2O$
Carnallite	$K\ Mg\ Cl_3 \cdot 6\ H_2O$
Chlorite	$Mg_5Al_2Si_3O_{10}(OH)_8$
Glaserite	$K_3Na(SO_4)_2$
Glauberite	$Na_2Ca(SO_4)_2$
Gypsum	$CaSO_4 \cdot 2H_2O$
Halite	$NaCl$
Illite	$K_{0.6}Mg_{0.25}Al_{2.3}Si_{3.5}O_{10}(OH)_2$
Iron Oxides (FEOX)	$Fe_2O_3 \cdot XH_2O$
Kainite	$KMgCl\ SO_4 \cdot 11/4\ H_2O$
K-Feldspar	$K\ Al\ Si_3O_8$
Kieserite	$MgSO_4 \cdot H_2O$
Langbeinite	$K_2Mg_2\ (SO_4)_3$
Leonite	$K_2Mg(SO_4)_2 \cdot 4\ H_2O$
Montmorillonite	$Mg_{0.16}\ Al_{2.33}\ Si_{3.67}\ O_{10}(OH)_2$
Polyhalite	$K_2Mg\ Ca(SO_4)_4 \cdot 2\ H_2O$
Quartz	SiO_2
Sylvite	KCl
Talc	$Mg_3\ Si_4\ O_{10}\ (OH)_2$
Thenardite	$Na_2\ SO_4$
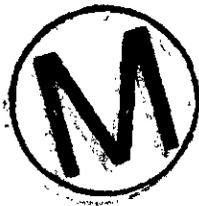
TABLE 7.4

ERDA No. 9 Samples Chosen for Silicate Mineralogy

Depth (ft)	Sample	Gross Lithology	Stratigraphic Position
1163.3-1163.6	MB-CS-18	Rock salt	SALADO Fm.
1165.1	MB-CS-16	Anhydrite	
1166.17	MB-CS-17	o Anhydrite	
1167.5	MB-CS-1	Anhydrite	
1168.31	MB-CS-6	Anhydrite w/ halite	
1169.4-1169.5	MB-CS-19	Rock salt	
1172.9	MB-CS-5	Polyhalite	
1173.7-1173.8	MB-CS-20	·Rock salt	
1242.5	JL-CS-24	Rock salt	
1242.9-1243.1	JL-CS-18	Polyhalite w/ halite	
1243.6-1243.7	JL-CS-27	Polyhalite w/ halite	
1244.2-1244.5	JL-CS-15	Rock salt w/ polyhalite	
1244.5-1244.8	JL-CS-16	Polyhalite w/ halite and clay	
1244.8	JL-CS-12	o Clay	
1245.0-1245.3	JL-CS-20	Rock Salt	
1246.7-1247.1	JL-CS-21	Rock Salt	
1247.1-1247.2	JL-CS-5	o Clay	
1325.2-1325.4	JL-CS-10	o Polyhalite w/ anhydrite veins	
1327.0-1327.2	JL-CS-23	Polyhalite	
1327.7-1327.8	JL-CS-26	Polyhalite w/ halite	
1328.2-1328.4	JL-CS-25	Polyhalite w/ halite and clay	
1328.6	JL-CS-3	o Clay	
1328.7-1329.8	JL-CS-17	Rock Salt	
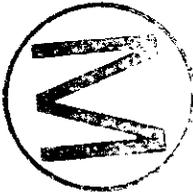
Depth (ft)	Sample	Gross Lithology	Stratigraphic Position
1404.6-1404.7	MB-CS-21	Rock Salt	11th ore zone
1418.2	MB-CS-7	Anhydrite with clay seam	
1418.6	MB-CS-8	Polyhalite	marker bed 117
1440.4-1440.6	JL-CS-2	o Polyhalite w/ halite	
1441.0-1441.3	JL-CS-6	o Polyhalite	
1441.7	JL-CS-4	o Clay	
1466.4-1466.6	JL-CS-11	o Polyhalite w/ clay	
1466.8-1467.1	JL-CS-9	o Polyhalite w/ clay	
1467.7-1468.1	JL-CS-22	Rock salt w/ clay	
1468.1	JL-CS-14	o Clay	
1535.6-1535.8	JL-CS-8	Polyhalite w/ anhydrite	
1536.5	JL-CS-7	Anhydrite	
1536.5-1536.6	JL-CS-19	Polyhalite w/ clay	
1537.8-1537.9	JL-CS-18	o Polyhalite w/ anhydrite	
1584.4-1584.5	MB-CS-22	Rock salt	near 5th ore zone
1609.5-1609.8	MB-CS-23	Rock salt	
1649.4-1649.6	MB-CS-24	Rock salt	near 4th ore zone
2034.5	MB-CS-14	Anhydrite	
2035.6-2035.9	MB-CS-25	Rock salt	
2036.5-2036.7	MB-CS-26	Rock salt	
2037.3	MB-CS-4	o Anhydrite	

Depth (ft)	Sample	Gross Lithology	Stratigraphic Position
2065.3-2065.4	MB-CS-29	Rock salt	
2066.1	MB-CS-28	Rock salt	
2067.0	MB-CS-27	o Rock salt	
2414.8	MB-CS-30	Rock salt	～16 ft above marker bed 143
2512.5	MB-CS-31	o Rock salt	
2517.9	MB-CS-12	Anhydrite)	
2518.3	MB-CS-13	o Anhydrite)	
		)	Cowden Anhydrite
2528.0	MB-CS-11	Anhydrite)	
2541.2-2541.9	MB-CS-32	o Rock salt	
2608.9-2609.5	MB-CS-33	Rock salt	
2615.9-2616.4	MB-CS-41	Rock salt	
2616.4-2616.8	MB-CS-34	Rock salt	
2617.2-2617.7	MB-CS-35	Rock salt	
2705.2-1705.6	MB-CS-37	Rock salt	
2705.8	MB-CS-10	o Rock salt	

Depth (ft)	Sample	Gross Lithology	Stratigraphic Position
2758.2-2758.6	MB-CS-36	o Rock salt	

2819.1-2819.6	MB-CS-39	o Rock salt	
2820.2	MB-CS-15	o Anhydrite	
2820.3	MB-CS-2	Anhydrite	
2821.1-2821.7	MB-CS-38	Rock salt	
2827.3-2827.5	MB-CS-40	o Rock salt	
			2829
2846.0	MB-CS-9	o Anhydrite	
2848.4	MB-CS-3	o Anhydrite	CASTILE Fm.
2867.4-2867.6	MB-CS-42	Anhydrite	

o Samples subjected to semi quantitative analysis (see Table 7.10).

TABLE 7.5

Core depths of samples selected for mineralogic-geochemical analysis.

Sample	Depth (ft)		Sample	Depth (ft)
MB-CS-1	1167.5		MC-CS-36	2758.2-2758.6
-2	2820.3		-37	2705.2-2705.6
-3	2848.4		-38	2821.1-2821.7
-4	2037.3		-39	2819.1-2818.6
-5	1172.9		-40	2827.3-2827.5
MB-CS-6	1168.3		MC-CS-41	2615.9-2616.4
-7	1418.2		-42	2867.4-2867.6
-8	1418.6			
-9	2846.0			
-10	2705.8			
MB-CS-11	2528.0		JL-CS-1	1441.5
-12	2517.9		-2	1440.4-1440.6
-13	2518.3		-3	1328.6
-14	2034.5		-4	1441.7
-15	2820.2		-5	1247.1-1247.3
MB-CS-16	1165.1		JL-CS-6	1441.0-1441.3
-17	1166.2		-7	1536.5
-18	1163.3-1163.6		-8	1535.6-1535.8
-19	1169.4-1169.5		-9	1466.8-1467.1
-20	1173.7-1173.8		-10	1325.2-1325.4
MB-CS-21	1404.6-1404.7		JL-CS-11	1466.4-1466.6
-22	1484.4-1584.5		-12	1244.8
-23	1609.5-1609.8		-13	1467.5
-24	1649.4-1649.6		-14	1468.1
-25	2035.6-2035.9		-15	1244.2-1244.5
MB-CS-26	2036.5-2036.7		JL-CS-16	1244.5-1244.8
-27	2067.0		-17	1328.7-1329.8
-28	2066.1		-18	1537.8-1537.9
-29	2065.3		-19	1536.5-1536.6
-30	2414.8		-20	1245.0-1245.3

TABLE 7.5, continued

Core depths of samples selected for mineralogic-geochemical analysis.

Sample	Depth (ft)	Sample	Depth (ft)
MB-CS-31	2512.5	JL-CS-21	1246.7-1247.1
-32	2541.2-2541.9	-22	1467.7-1468.1
-33	2608.9-2609.5	-23	1327.0-1327.2
-34	2616.4-2616.8	-24	1242.5-1242.8
-35	2617.2-2617.7	-25	1328.2-1328.4
		JL-CS-26	1327.7-1327.8
		-27	1343.6-1343.7
		-28	1242.9-1243.1
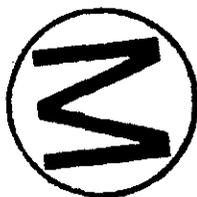
TABLE 7.6

Quantities of water-leach and EDTA-leach residues in samples from the ERDA-9 core. Sulfate lithologies (anhydrites and polyhalites) and salztons were not subjected to water leach.

Hole Depth (ft)	Sample Number	Bulk wt. (g)	LEACH RESIDUES (Percent of bulk) WATER	EDTA	EDTA Residue wt. (g)	Lithology
1163.5	MB-CS-18	1820	0.005	neg	neg+	rock salt
1165.1	MB-CS-16	40	>90	0.11	.043	anhydrite
1166.2	MB-CS-17	1229	>90	0.20	2.33	anhydrite
1167.5	MB-CS-1	38	>90	0.074	0.027	anhydrite
1168.3	MB-CS-6	358	>75	0.23	0.81	anhydrite
1169.4	MB-CS-19	209	0.36	0.005	0.011+√	rock salt
1172.9	MB-CS-5	40	>90	0.13	0.050	polyhalite
1173.7	MB-CS-20	259	0.012	neg	neg+	rock salt
1242.5	JL-CS-24	655	1.89	*	*	rock salt
1242.9	JL-CS-28	200	>75	0.76	1.52	polyhalite
1243.6	JL-CS-27	200	>75	0.60	1.21	polyhalite
1244.4	JL-CS-15	537	0.013	0.003	0.018	rock salt
1244.6	JL-CS-16	400	>75	1.13	4.51	polyhalite
1244.8	JL-CS-12	#	>90	>90	8.40	salzton
1245.1	JL-CS-20	400	6.18	1.15	4.60	rock salt
1246.8	JL-CS-21	747	0.21	*	*	rock salt
1247.2	JL-CS-5	#	>90	>90	2.70	salzton
1325.3	JL-CS-10	641	29.8	0.26	1.68	rock salt
1327.0	JL-CS-23	350	>75	0.25	0.89	polyhalite
1327.8	JL-CS-26	200	>75	0.30	0.61	polyhalite
1328.3	JL-CS-25	200	>75	1.13	2.26	polyhalite
1328.6	JL-CS-3	#	>90	>90	1.46	salzton
1328.7	JL-CS-17	1765	0.18 —	0.12	2.09	rock salt
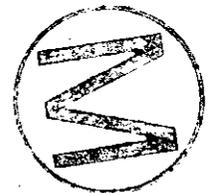
Hole Depth (ft)	Sample Number	Bulk wt. (g)	LEACH RESIDUES (Percent of bulk)		EDTA Residue wt. (g)	Lithology
			WATER	EDTA		
1404.6	MB-CS-21	244	2.5	1.0	2.43	rock salt
1418.2	MB-CS-7	40	>90	20.80	8.32	anhydrite
1418.6	MB-CS-8	1120	>90	0.62	6.94	polyhalite
1440.5	JL-CS-2	200	>75	0.83	1.66	polyhalite
1441.2	JL-CS-6	600	>75	0.13	0.80	polyhalite
1441.7	JL-CS-4	#	>90	>90	2.92	salzton
1466.5	JL-CS-11	400	>75	0.42	1.67	polyhalite
1466.9	JL-CS-9	200	>75	3.99	7.97	polyhalite
1467.9	JL-CS-22	860	4.17	1.22	10.5	rock salt.
1468.1	JL-CS014	#	>90	>90	3.30	saltzon
1535.7	JL-CS-8	400	>75	0.44	1.76	polyhalite
1536.5	JL-CS-7	320	>75	2.63	8.41	anhydrite
1536.6	JL-CS-19	360	>75	0.37	1.33	polyhalite
1537.8	JL-CS-18	400	>75	0.55	2.19	polyhalite
1584.4	MB-CS-22	248	0.53	0.42	1.20+✓	rock salt
1609.6	MB-CS-23	473	0.037	0.017	0.081 ✓	rock salt
1649.5	MB-CS-24	176	1.6	1.1	1.90+✓	rock salt
2034.5	MB-CS-14	104	>90	3.9	4.07	anhydrite
2035.7	MB-CS-25	891	0.23	0.009	0.078+✓	rock salt
2036.6	MB-CS-26	810	0.23	0.025	0.20+✓	rock salt
2073.3	MB-CS-4	145	>90	5.0	7.28	anhydrite
2065.3	MB-CS-29	1085	0.18	0.11	1.17+✓	rock salt
2066.1	MB-CS-28	220	3.3	1.5	3.38	rock salt
2067.0	MB-CS-27	229	2.8	0.83	1.90	rock salt
2414.8	MB-CS-30	421	36.3	0.049	0.21	rock salt

Hole Depth (ft)	Sample Number	Bulk wt. (g)	LEACH RESIDUES (Percent of bulk)		EDTA Residue wt. (g)	Lithology
			WATER	EDTA		
2512.5	MB-CS-31	1073	1.79	0.074	0.074	rock salt
2517.9	MB-CS-12	40	>90	0.024	0.010+	anhydrite
2518.3	MB-CS-13	586	>90	0.55	3.20	anhydrite
2528.0	MB-CS-11	40	>90	0.23	0.094	anhydrite
2541.5	MB-CS-32	891	0.70	0.21	1.83	rock salt
2609.2	MB-CS-33	901	0.043	0.015	0.14+✓	rock salt
2616.2	MB-CS-41	811	0.165	0.076	0.62+✓	rock salt
2616.6	MB-CS-34	660	0.071	0.004	0.027+✓	rock salt
2617.5	MB-CS-35	1015	1.17	0.18	1.83	rock salt
2705.4	MB-CS-37	638	13.3	0.65	4.14	rock salt
2705.8	MB-CS-10	450	>90	2.2	9.87	anhydrite
2758.4	MB-CS-36	421	6.6	0.77	3.25	rock salt
2819.3	MB-CS-39	982	2.2	0.27	2.65	rock salt
2820.2	MB-CS-15	520	>90	0.82	4.25	anhydrite
2820.3	MB-CS-2	640	>90	0.59	3.79	anhydrite
2821.4	MB-CS-38	916	1.25	0.039	0.36	rock salt
2828.7	MB-CS-40	920	1.22	0.13	1.17	rock salt
2846.0	MB-CS-9	200	>90	1.2	2.45	anhydrite
2848.4	MB-CS-3	656	>90	0.90	5.93	anhydrite
2867.5	MB-CS-42	240	>90	0.85	2.04	anhydrite

* Water-leach and EDTA-leach dissolutions of this sample not complete.
⨍ ample is hand-picked fragment of saltzto⌐
⌐ eported as containing "negligible insolu   residue" Table 7.7.
✓ A subsequent second dissolution of a substantially greater quantitiv of

TABLE 7.7

Relative Abundances of minerals in EDTA-insoluble residues.

Sample	Depth (ft)	EDTA-insoluble residue				$<2\ \mu m$ fraction of residue				
		qtz	feld	hem	clay	il	ch	serp	talc	exp
MB-CS-18	1163.5	Negligible insoluble residue								
MB-CS-16	1165.1	XX	--	--	X	X	a	--	--	XX
MB-CS-17	1166.2	XX	x	--	XX	x	a	--	--	XX
MB-CS-1	1167.5	--	--	--	XX	X	--	--	--	XX
MB-CS-6	1168.3	XX	x	--	XX	x	a	--	--	XX
MB-CS-19	1169.4	Negligible insoluble residue								
MB-CS-5	1172.9	XX	--	--	x	x	--	--	--	XX
MB-CS-20	1173.7	Negligible insoluble residue								
JL-CS-12	1244.8	XX	x	--	XX	X	X	--	--	X
JL-CS-5	1247.2	XX	x	--	XX	XX	X	--	--	X
JL-CS-10	1325.3	a	--	--	XX	--	--	--	--	XX
JL-CS-3	1328.6	XX	X	--	XX	X	X	--	--	X

Relative Abundances of minerals in EDTA-insoluble residues (cont'd).

Sample	Depth (ft)	EDTA-insoluble residue				$< 2 \mu$ m fraction of residue				
		qtz	feld	hem	clay	il	ch	serp	talc	exp
MB-CS-21	1404.6	XX	a	--	XX	x	x	--	X	XX
MB-CS-7	1418.2	--	x	--	XX	XX	X	--	--	X
MB-CS-8	1418.6	--	a	x	XX	x	x	--	--	XX
JL-CS-2	1440.5	X	XX	a	XX	a	a	--	--	XX
JL-CS-6	1441.2	X	XX	X	XX	XX	X	--	--	X
JL-CS-4	1441.7	--	X	--	XX	XX	X	--	--	X
JL-CS-11	1466.5	--	x	X	XX	XX	X	--	--	X
JL-CS-9	1466.9	XX	x	x	X	XX	X	--	--	XX
JL-CS-14	1468.1	X	X	--	XX	XX	X	--	--	XX

Relative Abundances of minerals in EDTA-insoluble residues (cont'd).

Sample	Depth (ft)	EDTA-insoluble residue				<2 μm fraction of residue				
		qtz	feld	hem	clay	il	ch	serp	talc	exp
JL-CS-8	1535.7	--	X	x	XX	XX	x	--	--	XX
JL-CS-7	1536.5	a	--	--	XX	--	--	--	--	XX
JL-CS-18	1537.8	X	--	x	XX·	XX	x	--	--	X
MB-CS-22	1584.4	Negligible insoluble residue								
MB-CS-23	1609.6	XX	X	x	XX	XX	X	--	--	XX
MB-CS-24	1649.5	Negligible insoluble residue								
MB-CS-14	2034.5	XX	--	--	x	x	x	--	--	XX
MB-CS-25	2035.7	Negligible insoluble residue								
MB-CS-26	2036.6	Negligible insoluble residue								
MB-CS-4	2037.3	XX	--	--	X	x	x	--	--	XX

Relative Abundances of minerals in EDTA-insoluble residues (cont'd).

		EDTA-insoluble residue				$< 2 \mu$ m fraction of residue				
Sample	Depth (ft)	qtz	feld	hem	clay	il	ch	serp	talc	exp
MB-CS-29	2065.3			Negligible insoluble residue						
MB-CS-28	2066.1	XX	a	--	XX	a	a	--	--	XX
MB-CS-27	2067.0	XX	X	x	XX	x	x	---	--	XX
MB-CS-30	2414.8	XX	X	--	X	a	x	--	--	XX
MB-CS-31	2512.5	X	--	a	XX	x	x	---	--	XX
MB-CS-13	2518.3	X	x	--	XX	a	a	--	--	XX
MB-CS-11	2528.0	--	--	--	XX	--	--	--	--	XX
MB-CS-32	2541.5	X	a	--	XX	X	X	--	--	XX

Relative Abundances of minerals in EDTA-insoluble residues (cont'd).

Sample	Depth (ft)	EDTA-insoluble residue				$< 2 \mu$ m fraction of residue				
		qtz	feld	hem	clay	il	ch	serp	talc	exp
MB-CS-33	2609.2				Negligible insoluble residue					
MB-CS-41	2616.2				Negligible insoluble residue					
MB-CS-34	2616.6				Negligible insoluble residue					
MB-CS-35	2617.5	XX	X	a	XX	XX	X	--	--	XX
MB-CS-37	2705.4	XX	X	a	X	XX	X	--	--	XX
MB-CS-10	2705.8	XX	X	a	X	X	x	--	--	XX
MB-CS-36	2758.4	XX	X	a	X	XX	X	--	--	XX

Relative Abundances of minerals in EDTA-insoluble residues (cont'd).

Sample	Depth (ft)	EDTA-insoluble residue				$< 2 \mu$ m fraction of residue				
		qtz	feld	hem	clay	il	ch	serp	talc	exp
MB-CS-39	2819.3	XX	X	--	X	XX	x	--	--	XX
MB-CS-15	2820.2	XX	--	--	XX	--	a	--	XX	X
MB-CS-2	2820.3	a	X	--	XX	XX	--	--	--	XX
MB-CS-38	2821.4	--	--	--	XX	--	--	XX	--	XX
MB-CS-40	2827.4	--	--	--	XX	--	--	XX	--	XX
MB-CS-9	2846.0	a	--	a	XX	--	--	XX	--	XX
MB-CS-3	2848.4	--	--	--	XX	--	--	X	--	XX

Relative Abundances of minerals in EDTA-insoluble residues (cont'd).

Sample	Depth (ft)	EDTA-insoluble residue				$< 2 \mu$ m fraction of residue				
		qtz	feld	hem	clay	il	ch	serp	talc	exp
MB-CS-42	2867.5	--	--	--	XX	--	x	X	--	X

Minerals: qtz = quartz; feld = feldspar; hem = hematite; il = illite; ch = chlorite; serp = serpentine; exp = expandable (smectite-bearing).

Relative abundances: XX = dominant constituent; X = major constituent; x = minor constituent; a = accessory constituent. All abundances based on relative intensities of major diffraction maxima.

TABLE 7.8

Low-angle diffraction maxima (Å) of expandable clays in the < 2 μ m fraction of the EDTA-insoluble residues.

Sample	Depth (ft)	Air-dried	Glycol-saturated	375°C (> 1hr)	500°C (> 1hr)
MB-CS-16	1165.1	14.5	n.d.	n.d.	n.d.
MB-CS-17	1166.2	13.8, 30.5	15.5, 32.7	13.8, (29.4)	13.6, (25.2)
MB-CS-1	1167.5	14.5	n.d.	n.d.	n.d.
MB-CS-6	1168.3	14.5, (25.2)	15.5, (35.3)	13.6, 31.6	13.2, 11.8, (27.6)
MB-CS-5	1172.9	14.3	n.d.	n.d.	n.d.
JL-CS-16	1244.6	13.8, 29.4	15.5, 11.2, 31.6	n.d.	n.d.
JL-CS-12	1244.8	13.6, 29.4	15.5, 31.5	13.6	13.2
JL-CS-20	1245.1	13.8, (30.5)	15.5, 34.0	n.d.	n.d.
JL-CS-5	1247.2	14.5, 30.5	15.5, 11.2, 31.6	14.3	13.6
JL-CS-10	1325.3	10.2	10.4, (12.1)	9.8	9.8, 11.0-11.9
JL-CS-3	1328.6	14.0, 30.5	15.5, 11.2, 31.6	14.5, (31.6)	12.6-14.7, (22.21)
MB-CS-21	1404.6	13.8, 31.6	15.8, 34.0	13.8, (32.7)	13.4, (29.4)
MB-CS-7	1418.2	13.8, (30.5)	n.d.	n.d.	n.d.
MB-CS-8	1418.6	13.4	15.5, (34.0)	13.6, (27.6)	11.6, (27.6)

Low-angle diffraction maxima ($\mathring{A}$) of expandable clays in the $< 2 \, \mu$ m fraction of the EDTA-insoluble residues (cont'd).

Sample	Depth (ft)	Air-dried	Glycol-saturated	375°C (> 1hr)	500°C (> 1hr)
JL-CS-2	1440.5	10.3	10.2, 11.8	9.8	n.d.
JL-CS-6	1441.2	10.7, 13.6, (29.4)	11.3, 15.5, (31.6)	10.2, 13.0-14.3	10.0
JL-CS-4	1441.7	13.8, 31.6	15.5, 31.6	13.8, (29.4)	13.2
JL-CS-11	1466.5	13.8, 11.2, (30.5)	15.2, (32.7)	13.6, (26.0)	n.d.
JL-CS-9	1466.9	14.7	16.1	13.8	13.8
JL-CS-22	1467.9	14.1, 31.6	15.5, 34.0	n.d.	n.d.
JL-CS-14	1468.1	13.6, 30.5	15.5, 32.7	13.6	13.2
JL-CS-8	1535.7	10.3, 13.6	9.4, 11.5, 16.1	9.8, 13.6	9.7
JL-CS-7	1536.5	10.3	9.3, 11.3	9.9	9.8
JL-CS-18	1537.8	14.3, 32.7	15.8, 34.0	n.d.	n.d.
MB-CS-23	1609.6	12.3	n.d.	n.d.	n.d.
MB-CS-14	2034.5	13.8, 30.5	15.2, 31.6	14.0, 11.9, (31.6)	11.9, 13.2, 29.4
MB-CS-4	2037.3	13.5	15.5, 31.6	13.2, (28.5)	13.0

Low-angle diffraction maxima (Å) of expandable clays in the < 2 μ m fraction of the EDTA-insoluble residues (cont'd).

Sample	Depth (ft)	Air-dried	Glycol-saturated	375°C (> 1hr)	500°C (> 1hr)
MB-CS-28	2066.1	14.5, 30.5	15.5, 31.6	14.0, (29.4)	13.6, (30.5, 22.1)
MB-CS-27	2067.0	14.7, 29.4	16.7, 32.7	14.0, (29.4)	12.6, (26.0)
MB-CS-30	2414.8	13.8, 11.8, (29.4)	15.8, 12.8, (31.6)	13.8, 11.6, (24.5)	11.6, (26.0)
MB-CS-31	2512.5	12.6	n.d.	n.d.	n.d.
MB-CS-12	2517.9	12.8, 31.6	15.5, 31.6	n.d.	n.d.
MB-CS-13	2518.3	12.6, 26.0	17.0, 25.2	13.2, (26.8)	12.3, 10.3, 26.0
MB-CS-11	2528.0	13.2	n.d.	n.d.	n.d.
MB-CS-32	2541.5	13.8, 29.4	15.5, 31.5	13.4, (26.8)	14.2, (31.6)
MB-CS-35	2617.5	13.8, (29.4)	16.7, 32.7	13.8, (26.8)	12.6, 27.6
MB-CS-37	2705.4	14.5, 30.5	16.4, 34.0	13.8, (29.4)	12.5
MB-CS-10	2705.8	13.4	16.7, (35.3)	14.3, (30.5)	14.3, 11.8, (27.6)
MB-CS-36	2758.4	14.0, 29.4	16.4, 32 7	13.8, (29.4)	12.5, (29.4)

Low-angle diffraction maxima ($\mathring{A}$) of expandable clays in the < 2 μm fraction of the EDTA-insoluble residues (cont'd).

Sample	Depth (ft)	Air-dried	Glycol-saturated	375°C (> 1hr)	500°C (> 1hr)
MB-CS-39	2819.3	14.5, 29.4	16.1, 31.6	14.5	13.6, (22.0)
MB-CS-15	2820.2	11.6, (26.8)	14.7, (27.6)	11.6, (24.5)	11.6, (26.8)
MB-CS-2	2820.3	14.5	----	10.4	9.8-17.7
MB-CS-38	2821.4	14.7	----	13.8	13.8
MB-CS-40	2827.4	14.7, 11.3	17.0	14.7	n.d.
MB-CS-9	2846.0	12.3, (24.5)	17.0, (28.5)	10.0 - 13.6, (29.4)	13.4
MB-CS-3	2848.4	12.3, (24.5)	17.3, (27.6)	12.63, (27.6)	11.6, (24.5)
MB-CS-42	2867.5	11.8	17.7	14.7	----

n.d. - data not yet determined

Values in parentheses, e.g. (30.5) represent diffraction maximum present only as shoulder.

TABLE 7.9

Mineralogy of Duval Mine Samples
4th Ore Zone

A. Evaporites

Mine Wall Samples	Halite	Sylvite	Polyhalite	Langbeinite
DV-1A	t	–	VA	–
DV-1B	VA	VA	–	–
DV-1C	VA	–	VA	t
DV-1D	VA	VA	t	–
DV-2A	A	VA	–	t
DV-2B	VA	–	A	–
DV-4A	A	–	VA	t
DV-4B	VA	–	–	–
DV-4C	VA	–	–	t
DV-4D	VA	–	–	t
DV-4E	t	t	–	VA
DV-5A	VA	–	–	–
DV-5B	VA	A	t	–

B. 2 Micron Fractions (Silicates)

Mine Wall Samples	Chlorite	Saponite	Chlorite-Saponite	Illite	Talc	Serpentine	Insoluble Residue (Wt. %)
DV-4B	t	–	VA	VA	t	A	15.7
DV-4C	–	–	VA	VA	t	A	12.3
DV-4D	t	t	VA	A	–	t	32.3
DV-5A	t	t	VA	A	t	A	10.3

VA : very abundant
A : abundant
t : tract
– : not detected

TABLE 7.10

Semiquantitive* chemical analysis of EDTA-insoluble fractions from ERDA-9 core.

	MB-CS-17	JL-CS-12	JL-CS-5	JL-CS-10	JL-CS-3	JL-CS-2	JL-CS-6	JL-CS-4
Depth (ft)	1166.2	1244.8	1247.1	1325.3	1328.6	1440.5	1441.2	1441.7
Lithology[+]	Anhydr.	Clay	Clay	Polyhal.	Clay	Polyhal.	Polyhal.	Clay

Weight Percent

	MB-CS-17	JL-CS-12	JL-CS-5	JL-CS-10	JL-CS-3	JL-CS-2	JL-CS-6	JL-CS-4
SiO_2	59.	50.	50.	59.	52.	56.	45.	38.
TiO_2	.8	.9	1.2	.2	1.4	.4	.7	1.4
Al_2O_3	12.	13.	15.	12.	15.	6.2	2.5	18.
FeO[@]	1.2	2.4	3.8	1.3	3.2	5.3	14.	4.5
MgO	20.	25.	20.	32.	18.	20.	15.	19.
CaO	.01	.01	.04	.002	.008	.02	.03	.06
Na_2O	1.2	1.2	1.0	1.0	.5	2.4	1.4	1.6
K_2O	1.8	2.3	3.0	.3	3.3	2.9	2.0	4.6

Semiquantitive* chemical analysis of EDTA-insoluble fractions from ERDA-9 core.

	MB-CS-17	JL-CS-12	JL-CS-5	JL-CS-10	JL-CS-3	JL-CS-2	JL-CS-6	JL-CS-4
Depth (ft)	1166.2	1244.8	1247.1	1325.3	1328.6	1440.5	1441.2	1441.7
Lithology[+]	Anhydr.	Clay	Clay	Polyhal.	Clay	Polyhal.	Polyhal.	Clay

Atom Proportions (al = 1.0)

	MB-CS-17	JL-CS-12	JL-CS-5	JL-CS-10	JL-CS-3	JL-CS-2	JL-CS-6	JL-CS-4
Si	4.2	3.2	2.9	4.3	3.0	7.6	15.	1.8
Ti	.04	.04	.05	.01	.06	.04	.2	.05
Al	1.0	1.0	1.0	1.0	1.0	1.0	1.0	1.0
Fe	.07	.13	.18	.08	.15	.61	4.0	.17
Mg	2.1	2.3	1.7	3.5	1.6	4.0	7.4	1.3
Na	.16	.15	.11	.14	.06	.64	92	.14
K	.16	.19	.22	.03	.24	.51	.87	.27

Semiquantitive* chemical analysis of EDTA-insoluble fractions from ERDA-9 core.

	JL-CS-11	JL-CS-9	JL-CS-14	JL-CS-18	MB-CS-4	MB-CS-27	MB-CS-31	MB-CS-13
Depth (ft)	1466.5	1467.0	1468.1	1537.8	2037.3	2067.0	2512.5	2518.3
Lithology[+]	Polyhal.	Polyhal.	Clay	Polyhal.	Anhydr.	Halite	Halite	Anhydr.

Weight Percent

SiO_2	34.	42.	41.	43.	54.	65.	41.	54.
TiO_2	.6	.6	1.2	.6	.8	1.0	.9	.4
Al_2O_3	10.	9.0	14.	8.8	12.	14.	14.	7.0
FeO[@]	23.	3.7	3.3	8.2	3.7	4.7	N.D.	2.1
MgO	19.	29.	22.	21.	21.	9.3	18.	22.
CaO	.005	.005	.001	.03	.002	.02	.02	.04
Na_2O	1.3	.4	1.6	1.2	1.0	3.9	2.2	2.7
K_2O	2.9	2.6	4.1	2.0	1.5	4.1	2.6	2.5

TABLE 7.10, continued

Semiquantitive* chemical analysis of EDTA-insoluble fractions from ERDA-9 core.

	JL-CS-11	JL-CS-9	JL-CS-14	JL-CS-18	MB-CS-4	MB-CS-27	MB-CS-31	MB-CS-13
Depth (ft)	1466.5	1467.0	1468.1	1537.8	2037.3	2067.0	2512.5	2518.3
Lithology[+]	Polyhal.	Polyhal.	Clay	Polyhal.	Anhydr.	Halite	Halite	Anhydr.

Atom proportions (Al = 1.0)

	JL-CS-11	JL-CS-9	JL-CS-14	JL-CS-18	MB-CS-4	MB-CS-27	MB-CS-31	MB-CS-13
Si	2.9	3.9	2.5	4.2	4.0	3.9	2.5	6.2
Ti	.04	.04	.05	.04	.04	.04	.04	.03
Al	1.0	1.0	1.0	1.0	1.0	1.0	1.0	1.0
Fe	1.7	.29	.17	.66	.23	.23	--	.20
Mg	2.4	4.0	2.0	3.1	2.3	.83	1.7	3.8
Na	.21	.07	.19	.22	.14	.45	.26	.60
K	.31	.31	.32	.25	.14	.31	.21	.37

Semiquantitive* chemical analysis of EDTA-insoluble fractions from ERDA-9 core.

	MB-CS-32	MB-CS-10	MB-CS-36	MB-CS-39	MB-CS-15	MB-CS-40	MB-CS-9	MB-CS-3
Depth (ft)	2541.5	2705.8	2758.4	2819.3	2820.2	2827.4	2846.0	2848.4
Lithology[+]	Halite	Halite	Halite	Halite	Anhydr.	Halite	Anhydr.	Anhydr.

Weight Percent

SiO_2	37.	61.	70.	67.	52.	33.	42.	44.
TiO_2	.8	.8	.8	.8	.1	.3	.2	.2
Al_2O_3	13.	12.	12.	12.	3.4	5.0	3.1	3.6
FeO[@]	3.4	4.4	3.4	3.3	.7	1.4	2.6	1.5
MgO	30.	17.	11.	13.	33.	29.	35.	37.
CaO	.002	.01	.1	.06	.007	1.0	.003	.003
Na_2O	1.0	2.9	2.3	2.1	1.6	.9	2.6	1.9
K_2O	1.7	1.8	1.4	1.8	.6	.9	3.3	.7

Semiquantitive* chemical analysis of EDTA-insoluble fractions from ERDA-9 core.

	MB-CS-32	MB-CS-10	MB-CS-36	MB-CS-39	MB-CS-15	MB-CS-40	MB-CS-9	MB-CS-3
Depth (ft)	2541.5	2705.8	2758.4	2819.3	2820.2	2827.4	2846.0	2848.4
Lithology[+]	Halite	Halite	Halite	Halite	Anhydr.	Halite	Anhydr.	Anhydr.

Atom proportions (Al = 1.0)

Si	2.5	4.5	5.1	4.7	13.	5.6	11.	10.
Ti	.04	.04	.04	.04	.02	.04	.04	.04
Al	1.0	1.0	1.0	1.0	1.0	1.0	1.0	1.0
Fe	.19	.27	.21	.19	.15	.20	.59	.30
Mg	2.8	1.8	1.2	1.3	12.	7.3	14.	13.
Na	.13	.41	.33	.29	.77	.30	1.4	.87
K	.15	.17	.13	.16	.19	.19	1.1	.21

* Calculated from 1:1 linear regression; matrix effects and other than unit regression slope not yet included.

+ Anhydr. = anhydrite; polyhal. = polyhalite.

@ Tc̄ l iron as FeO.

Mineralogy of Cores from ERDA No. 9

Core Footage	Gross Lithology (listed in decreasing order of abundance, lower case indicates (trace amount)	Bulk Mineralogy by X-ray Diffraction
1168.1	Anhydrite Halite Magnesite	Anhydrite Magnesite
1168.55	Anhydrite Halite Polyhalite	Anhydrite Halite Polyhalite
1173.5	Halite "Brown Material"	Halite Polyhalite trace 12A° (expandable) clay
1173.5	silty claystone or anhydrite	Anhydrite Polyhalite
1584.4	Halite "brown material" anhydrite	Halite polyhalite
1649.7	Halite polyhalite anhydrite	Halite polyhalite
2066.8	Halite '"brown material"	Halite Anhydrite quartz magnesite trace 10A° clay (illite) trace 14A° clay (chlorite)

Mineralogy of Cores from ERDA No. 9

Core Footage	Gross Lithology (listed in decreasing order of abundance, (trace	Bulk Mineralogy by X-ray Diffraction (listed in decreasing order of abundance, lower case indicates trace amount)
2067.4	see 2066.8	Halite polyhalite quartz? trace $12A^o$ (expandable) clay
2302	Polyhalite "White Material"	Anhydrite Polyhalite
2414.7	Polyhalite Halite Anhydrite	Halite Polyhalite
2415.0	see 2414.7	Polyhalite Anhydrite
2415.4	see 2414.7	Anhydrite
2529.5	Anhydrite magnesite?	Anhydrite Halite Magnesite
2538.5	Anhydrite Halite	Anhydrite Halite
2619.5	Halite anhydrite or magnesite	Halite Anhydrite
2820 B	Anhydrite Halite magnesite	Anhydrite Halite

Weight Losses Observed Upon Heating of ERDA No. 9 Cores

Specimen No. (depth)	Total Weight-Loss (%)	Mass-Loss (%) At Mean Temperature Ranges		
		100°C	300°C	450°
2034.7	1.60	0.70	0.36	.057
2035.7	0.20	----	----	----
2065.0	0.35	----	----	----
2067.5	0.52	----	----	----
2302.6	5.40	----	5.10	0.17
2413.7	1.38	----	1.00	----
2414.2	3.13	----	2.90	----
2415.6	0.10	----	----	----
2512.0	0.14	----	----	----
2516.3	2.15	----	----	1.55
2518.8	0.32	----	----	----
2528.7	2.12	----	----	1.52
2529.0	3.12	----	----	2.94
2538.5	1.55	----	----	1.20
2542.0	6.39	----	6.19	0.20
2593.2	1.47	----	----	1.20
2594.5	0.36	----	----	----
2597.0	0.37	----	----	----
2608.9	0.17	----	----	----
2614.4	0.13	----	----	----
2619.6	0.22	----	----	----
2658.5	0.48	----	0.10	0.17
2663.3	0.50	----	----	0.29
2696.4	1.12	----	----	0.80
2706.5	0.37	----	----	----
2711.9	0.47	----	----	0.21
2759.0	0.28	----	----	----
2786.5	3.64	2.27	----	0.90
2820.7A	0.36	----	----	0.17
2820.6B	0.35	----	----	0.12
2821.0	0.40	----	0.19	----
2826.5	0.36	----	0.27	----
2845.3	1.42	----	----	1.21
2848.8	0.86	----	----	0.53

TABLE 7.13

Data on the volume percent of fluid now present in the salt cores from ERDA No. 9.

Depth interval (feet)	Type Sampled	Volume sampled (mm^3)	Approx. grain size (mm)	Fraction of total slide	Fluid % by vol.	Total % by vol., whole slide
1799.0-1799.5	B	500	5 to 10	1/4	1.66	
	A	500	1 to 5	3/4	0.17	0.54
1902.0-1902.3	B	500	2 to 8	1/5	0.866	
	A	500	0.5 to 3	4/5	0.11	0.26
2065.0-2065.4	B	500	20 to 50	5/6	3.4	
	A	500	20 to 50	1/6	0.20	2.86
2095.1-2095.5	B	500	3 to 15	1/10	2.58	
	A	500	3 to 15	9.10	0.039	0.29
2274.4-2272.7	(B	470	10 to 15	1/2	2.29	
	(A	470	5	1/2	0.17	1.23
" "	(B	510	5 to 7	2/5	0.86	
	(A	510	1 to 3	3/5	0.02	0.36
" "	(B	520	5 to 7	1/3	0.55	
	(A	520	1 to 3	2/3	0.02	0.20
2391.0-2391.3	B	460	10 to 15	1/10	1.17	
	A	460	3 to 10	9/10	0.12	0.22
2611.5-2611.8	B	530	5 to 25	1/5	0.79	
	A	530	2 to 5	4/5	0.015	0.17
2658.7-2659.0	B	360	5 to 10	1/4	1.18	
	A	360	2 to 8	3/4	0.039	0.32

Data on the volume percent of fluid now present in the salt cores from ERDA No. 9.

Depth interval (feet)	Type Sampled	Volume sampled (mm^3)	Approx. grain size (mm)	Fraction of total slide	Fluid % by vol.	Total % by vol., whole slide
2760.0-2760.2	B	460	5 to 8	1/5	0.96	
	A	460	3 to 5	4/5	0.27	0.40
2820.8-2821.2	B	490	3 to 8	1/4	0.87	
	A	490	2 to 5	3/4	0.31	0.45

TABLE 7.14

Homogenization temperatures (°C) of two-phase liquid + gas inclusions from ERDA No. 9 core (numbers of inclusions run given in parentheses)

Depth interval	Homogenization temperatures
1799.0-1799.5	20.5(1), 21.0(1), 25(3)
1902.0-1902.3	25.1(1)
2065.0-2065.4	(none)
2095.1-2095.5	25.6(2), 34.5(1), 44.0(1), 45.5(2)
2272.4-2272.7	41.25(1), 42.5(1), 42.6(3)
2391.0-2391.3	23(4), 39(1)
2611.5-2611.8	(none)
2658.7-2659.0	43.0(1), 43.25(1), 43.5(1), 44(2), 45.0(1)
2760.0-2760.2	20.4(1), 21.6(1), 21.8(2)
2820.8-2821.2	22.5(1), 23.0(1), 25.5(1)

TABLE 7.15

Summary of freezing data (^{O}C), mainly on type B inclusion in samples from ERDA No. 9 core

Depth	First melting temp.	Freezing temp.	Notes
1799	< -31.9	> +10	~20% liquid at -31.9
1902	< -32	> +10	
2095	< -28.4	+15	~20-25% xls at 0°C
"	-32.2	"	
2272	< -32.8	+11.8	~50% xls at 0°C
2391	< -26.1	> +12.8	
2760	< -32	> +12.7	

TABLE 7.16

Test data and weight loss (in %) from decrepitation tests.
Roman numerals indicate amount of sample breakup after run:
I - unbroken; II - broken into 2 or 3 pieces;
III - broken into more than 3 pieces.

	Temperature, ^{o}C		
Core interval (ft)	150	200	250
2058.8 - 2059.0	0.16 II	0.23 II	0.76 III
2070.4 - 2070.6	0.16 II	0.12 I	0.35 III
2606.5 - 2606.9	0.02 I	0.24 II	0.95 III
2617.2 - 2617.7	0.06 I	0.30 I	0.62 II
2626.7 - 2627.0	0.19 I	0.28 I	1.04 III
2659.0 - 2659.2	0.14 I	0.13 I	0.59 III
2665.0 - 2665.1	0.19 I	0.18 I	0.75 III
2692.4 - 2692.6	0.06 I	0.26 I	0.83 III
2699.8 - 2700.0	0.19 I	0.24 II	0.65 III
Average	0.13	0.22	0.73

Heating schedule (hours)

Room T to run T	7	9.5	8
Hold at run T	79	95	79
Run T to room T	~9	~9	~10

TABLE 7.17

Temperature of homogenization and volume % vapor
of two-phase inclusions in salt of samples after
decrepitation tests.

Decrepitation run temp. (°C)	Homogenization temp. (°C)		Number of inclusions runs	Volume % vapor phase; avg. for ~25 inclusions
	Minimum	Maximum		
150	90	120	16	0.8
200	110	180	21	1.8
250	180	273	28	5.0

Note: Birefringent crystals, present in some of these inclusions, do not
disappear during homogenization runs.

TABLE 7.18

Temperature of homogenization of two-phase inclusions
in salt from near dike in Kerr-McGee mine,
Lea County, New Mexico.

Sample no.	Distance from dike (m)	Temp. of homogenization (^{O}C)		Number of inclusions run
		Minimum	Maximum	
MB-77-8	0.01 - 0.02	71	116	7
MB-76-3	0.2	60	110	6
MB-76-4	2.5	85	88*	9

* Two birefringent crystals remained unchanged, and a cubic crystal (KC] ?)
dissolved at 82°C. (See Plate 7-42 for a similar inclusion.)

TABLE 7.19

INVENTORY OF FLUIDS SAMPLED FOR GEOCHEMICAL STUDIES
OF DELAWARE BASIN GROUNDWATERS

Sample No.	Sample Name	Formation Sampled	Location	Solutes	Stable Isotopes	Solute *Analyst
1	Carlsbad City #7	Capitan	T22S-R26E-S1	X	X	M
2	Duval Mine/Collector Ring	Rustler	T22S-R30E-S33	X	X	M
3	Duval Mine/Seep-BT26	Salado	T22S-R30E-S33	X	X	S
4	Duval Mine/Seep-BT48	Salado	T22S-R30E-S33	X	X	M
5	Duval Mine/Seep-BT58	Salado	T22S-R30E-S33	X		M
6	James Ranch	Rustler	T23S-R31E-S5	X	X	M
7	Fairview	Rustler	T23S-R32E-S36	X	X	M
8	Todd State 36-1	Morrow	T23S-R31E-S36	X	X	M
9	Todd Federal 26-4	Bell Canyon	T23S-R31E-S26	X	X	M
10	Todd Federal 26-1	Morrow	T23S-R31E-S26	X	X	M
11	Shell No. 28	Capitan	PSL Blk 74-S34(Texas)	X	X	M
12	Middleton	Capitan	T19S-R32E-S21	X	X	M
13	Hackberry	Capitan	T19S-R31E-S31	X	X	M
14	ERDA #6	Castile	T21S-R31E-S35	X	X	S
15	Shell Bootleg	Castile	T22S-R32E-S36	X		Sh
16	Duval Mine/Vent Hole	Salado	T22S-R30E-S33	X		M
17	UNM Pokorny	Castile	PSL Blk 61-S3(Texas)	X	X	M
18	Smith Livingston Ridge	Santa Rosa	T22S-R31E-S15		X	
19	Indian	Rustler	T23S-R30E-S21		X	
20	Mobley	Rustler	T23S-R30E-S19		X	
21	Mobley #3	Rustler	T23S-R30E-S2		X	
22	H1-Magenta	Rustler	R22S-R31E-S29	X	X	U
23	H1-Culebra	Rustler	T22S-R31E-S29	X	X	U
24	H3-Magenta	Rustler	T22S-R31E-S29	X	X	U
25	H3-Culebra	Rustler	T22S-R31E-S29	X	X	U
26	Green Lake	Capitan	Carlsbad Caverns		X	
27	Mirror Lake	Capitan	Carlsbad Caverns		X	
28	Longfellow's Bathtub	Capitan	Carbsbad Caverns		X	
29	Celery Stalk Pool	Capitan	Carlsbad Caverns		X	

* Analysts: M – Martin Water Laboratories
                   S – Sandia
                   Sh – Shell
                   U – U.S. Geological Survey

TABLE 7.20

GEOCHEMICAL ANALYSES OF DELAWARE BASIN GROUNDWATERS
(Solutes in mg/l)

No.	pH	$\delta^{18}O$ $^o/_{oo}$	δD $^o/_{oo}$	Ca^{++}	Mg^{++}	Na^+	K^+	Cl^-	Br^-	SO_4^+	HCO_3^-	TDS	Other Information
T 1	7.2	− 7.9	−54	74	29	8	1	10	0	72	285	474	NO_3:5
2	7.4	− 6.4	−48	1100	280	3600	405	6400	0	2500	122	14380	Sr:30
3	5.5	+ 3.0	−10	640	55400	27500	3000	236500	305	3650	1090	355085	BO_3:660
4	5.4	+ 2.6	−12	500	62600	44400	30250	251500	530	3300	1170	395000	BO_3:840
5	5.5			520	62000	46300	30250	250000	582	3100	1170	395000	BO_3:990
6	7.6	− 5.0	−40	590	175	68	5	400	0	1570	190	3240	NO_3:225
7	7.6	− 7.1	−53	590	200	120	3	142	0	2140	130	3350	
8	6.4	+ 2.7	−15	1600	240	11300	500	20600	23	300	380	35600	
9	7.1	+ 2.2	−13	27600	6075	76700	1700	18500	410	210	215	295400	Sr:240
10	6.6	+ 9.2	−18	4880	920	28700	200	55400	90	30	300	92400	Sr:1750
11	7.1	− 7.7	−56	940	280	2280	57	3900	0	2400	550	11300	Sr:1750
12	7.4	− 7.5	−55	1100	570	10600	330	17050		3720	300	33800	Sr:64
13	6.0	− 6.5	−46	2200	1680	68700	2950	110808		5150	132	192000	Sr:140,Fe:312
14	7.3	+10.3	0	130	350	112000	5100	186100	240	16000	1310	321000	BO_3:650,Li:160
15	7.7			550	1860	124500		185000		16800	1480	330700	
16	5.8			1260	38500	49000	52500	241500	385	3600	700	388650	BO_3:1160
17	1.6	− 6.0	−50	190	100	200	18	2700	0	570	0	3800	
18		− 7.2	−52										
19		− 6.3	−46										
20		− 6.9	−44										
21		− 5.9	−44										
22	7.4	− 6.8	−48	890	270	5700	70	8000		3900	92	18922	
23	7.6	− 7.0	−50	780	280	9400	190	12000		7400	105	30155	
24	7.4	− 7.3	−53	760	190	4200	100	5800		2600	1150	14800	
25	7.4	− 7.0	−53	1500	720	19000	450	33000		5200	88	60000	
26		− 3.6	−24										
27		− 4.3	−28										
28		− 4.2	−29										
29		− 3.0	−20										

TABLE 7.21

DUVAL MINE VENT HOLE WATER #16

One liter of solution might be expressed as the
following amounts of common evaporite minerals:

0.006 moles	(1 gm)	$CaMg(CO_3)_2$	Dolomite
0.026 moles	(4 gm)	$CaSO_4$	Anhydrite
0.012 moles	(3 gm)	$KMgClSO_4 \cdot 11/4H_2O$	Kainite
1.343 moles	(370 gm)	$KMgCl_3 \cdot 6H_2O$	Carnallite
0.224 moles	(46 gm)	$MgCl_2 \cdot 6H_2O$	Bischofite
0.005 moles	(2 gm)	$Na_2B_4O_7 \cdot 10H_2O$	Borax
2.121 moles	(121 gm)	$NaCl$	Halite
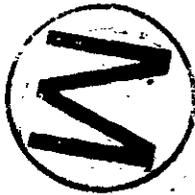
TABLE 7.22

TODD FEDERAL 26-4 WATER #9

One liter of solution might be expressed as the following
amounts of common evaporite minerals:

0.10 moles	(52 gm)	$CaMg_2Cl_6 \cdot 12H_2O$	Tachyhydrite
0.04 moles	(4 gm)	$KMgCl_3 \cdot 6H_2O$	Carnallite
0.59 moles	(129 gm)	$CaCl_2 \cdot 6H_2O$	Antarcticite
3.34 moles	(195 gm)	$NaCl$	Halite

TABLE 7.23

ERDA 6 WATER #14

One liter of solution might be expressed as the following
amounts of common evaporite minerals:

0.003 moles	(1 gm)	$CaMg(CO_3)_2$	Dolomite
0.009 moles	(1 gm)	$MgCO_3$	Magnesite
0.011 moles	(3 gm)	$KMgClSO_4 \cdot 11/4H_2O$	Kainite
0.130 moles	(9 gm)	KCl	Sylvite
0.155 moles	(22 gm)	Na_2SO_4	Thenardite
0.048 moles	(14 gm)	$LiCl$	?
4.521 moles	(265 gm)	$NaCl$	Halite

TABLE 7.24

Rb-Sr Data for Evaporites from the Salado Formation

A. Whole Rocks

Core hole Interval	$(^{87}Sr/^{86}Sr)_N$	Rb (ppm)	Sr (ppm)	$^{87}Rb/^{86}Sr$
AEC-8				
1622.4-1622.9	0.7056	5.0	112.4	0.13
1636.6-1637.1 (sylvite rich portion)	0.7816	120.1	8.0	43.77
1645.0-1645.3	0.7150	0.40	48.2	0.02
1671.2-1671.8	0.7097	5.6	39.8	0.41
1715.4-1715.7	0.7089	0.07	90.9	0.02
1762.0-1762.3	0.7099	1.3	37.9	0.10
1782.2-1782.4	0.7137	0.30	5.7	0.15
ERDA-9				
1404.8-1405.8	0.7934	67.1	5.1	38.41
1648.5-1649.0	0.7079	0.47	44.7	0.03
1759.1-1759.8 (polyhalite rich portion)	0.7064	4.9	793.5	0.02
ERDA-6				
1421.0-1421.7	0.7095	0.60	156.2	0.01

B. Water Soluble Portions

Core hole Interval	$(^{87}Sr/^{86}Sr)_N$	Rb (ppm)	Sr (ppm)	$^{87}Rb/^{86}Sr$
ERDA-8				
1607.0-1608.0	0.7173	26.7	44.7	1.73
ERDA-9				
1408.8-1405.8	0.8601	70.8	4.0	51.87
1709.0-1709.5	0.7094	0.99	8.5	0.34
1713.6-1714.0	0.7072	2.0	34.1	0.17
1772.0-1772.4	0.7067	1.5	57.7	0.07

C. < 2 Micron Fractions (Clays)

Core hole Interval	$(^{87}Sr/^{86}Sr)_N$	Rb (ppm)	Sr (ppm)	$^{87}Rb/^{86}Sr$
AEC-8				
1607.0-1608.0	0.7229	42.9	82.2	1.51
1671.2-1671.8	0.7273	43.9	35.2	3.62
ERDA-9				
1404.8-1405.8	0.7608	84.5	23.6	10.40
1772.0-1772.4	0.7181	29.4	48.1	1.76

TABLE 7.25

% Insoluble Residue in Whole Rock

Core hole Interval	Insoluble Residue (percent)
AEC-8	
1607.0-1608.0	9.0
1610.8-1611.3	9.0
1622.4-1622.9	2.0
1636.6-1637.1	3.7
1645.0-1645.3	0.8
1671.2-1671.8	11.3
1715.4-1715.7	1.1
1782.2-1782.4	12.5
ERDA-9	
1404.8-1405.8	7.2
1621.9-1622.2	0.8
1633.6-1634.1	0.4
1648.5-1649.0	2.1
1652.8-1653.1	0.3
1709.0-1709.5	1.1
1713.6-1714.0	18.2
1759.1-1759.8	0.7
1772.0-1772.4	12.6

TABLE 7.26

Mineralogical Data

Core hole Interval	Halite	Sylvite	Polyhalite	Langbeinite

A.   Whole Rocks (Evaporite Mineralogy by XRD)

AEC-8

1607.0-1608.0	VA	VA	–	–
1610-8-1611-3	VA	A	–	--
1622.4-1622.9	VA	A	–	–
1636.6-1637.1	VA	VA	t	–
1645.0-1645.3	VA	t	–	--
1671.2-1671.8	VA	t	t	--
1715.4-1715.7	VA	t	–	–
1762.0-1762.3	VA	t	-	–
1782.2-1782.4	A	A	A	t

ERDA-9

1404.8-1405.8	A	t	VA	VA
1621.9-1622.2	VA	t	–	–
1633.6-1634.1	VA	t	–	–
1648.5-1649.0	VA	A	--	–
1652.8-1653.1	VA	t	–	–
1709.0-1709.5	VA	A	--	--
1713.6-1714.0	VA	A	–	–
1759.1-1759.8	VA	A	t	--
1772.0-1772.4	VA	A	t	–

ERDA-6

1421.0-1421.7	VA	t	–	–

Mineralogical Data

Core hole Interval	Halite	Sylvite	Polyhalite	Langbeinite

B. 2 Micron Fractions (Clays, Minerals)

Core Hole Interval	Chlorite	Saponite	Chlorite/ Saponite	Illite	Talc	Serpentine
AEC-8						
1607.0-1608.0	-	-	VA	A	t	A
1610.8-1611.3	t	-	A	A	-	A
1622.4-1622.9	-	-	t	A	A	t
1636.6-1637.1	-	-	A	VA	t	t
1645.0-1645.3	t	-	A	A	t	A
1671.2-1671.8	-	-	VA	A	-	t
1715.4-1715.7	A	-	t	VA	-	VA
1762.0-1762.3	t	t	-	A	A	t
1782.2-1782.4	A	-	t	VA	VA	A
ERDA-9						
1404.8-1405.8	-	-	A	VA	t	A
1648.5-1649.0	A	-	A	VA	VA	VA
1713.6-1714.0	-	-	VA	A	A	VA
1772.0-1772.4	-	-	VA	A	t	A
ERDA-6						
1421.0-1421.7	-	-	t	t	VA	t

VA: very abundant
A: abundant
t: trace
-:   not detected

TABLE 7.27

URANIUM CONCENTRATIONS AND ISOTOPIC RATIOS IN DELAWARE BASIN WATERS

Sample	U Concentration	$\alpha(^{234}U/^{238}U)$	$\delta^{18}O$ (SMOW)‰	δD (SMOW)‰
Shell	0.60 parts in 10^9	2.75	−7.7	−56
Middleton	0.54 parts in 10^9	1.81	−7.5	−55
Hackberry	0.02 parts in 10^9	1.22±0.05	−6.5	−46
Carlsbad 7	0.05 parts in 10^9	5.14	−7.9	−54
ERDA 6 1140 hr.	89 parts in 10^9	1.11±0.04		
ERDA 6 1212 hr.	4.8 parts in 10^9	1.26±0.05		
ERDA 6 1445 hr.	2.14 parts in 10^9	1.37±0.07	+10.3	0
ERDA 6 1520 hr.	1.88 parts in 10^9	1.33±0.07		
ERDA 6 Drill Mud	67.2 parts in 10^9	1.19		
Brine Lake (Mud Ingredient)	56.3 parts in 10^9	2.04		
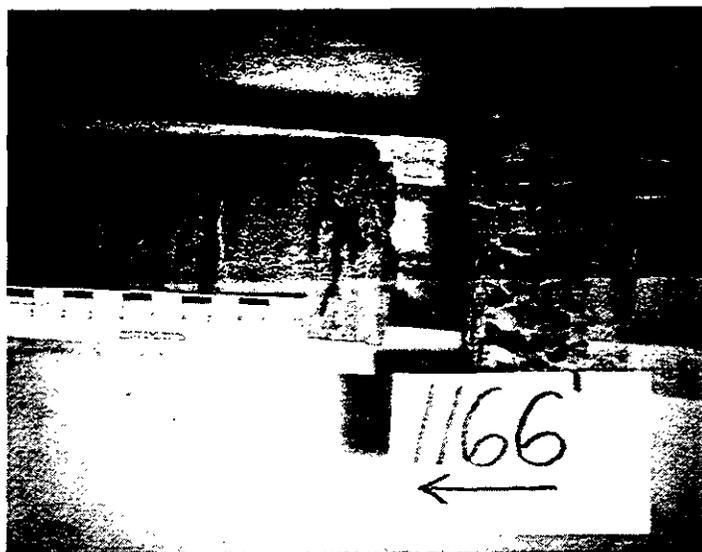
Plate 7.1. Core footage: 1165.4 to 1177.1 ft. (including 0.1 ft. gap) Brownish halite in gray anhydrite. Halite occurs as a thin bed at top of specimen, then as irregular lenses and thin laminae, finally as vertically elongate crystals, some with "swallow tail" form, near bottom of specimen. Locally horizontal laminae occur within the anhydrite due either to color change of the anhydrite or laminae of magnesite.
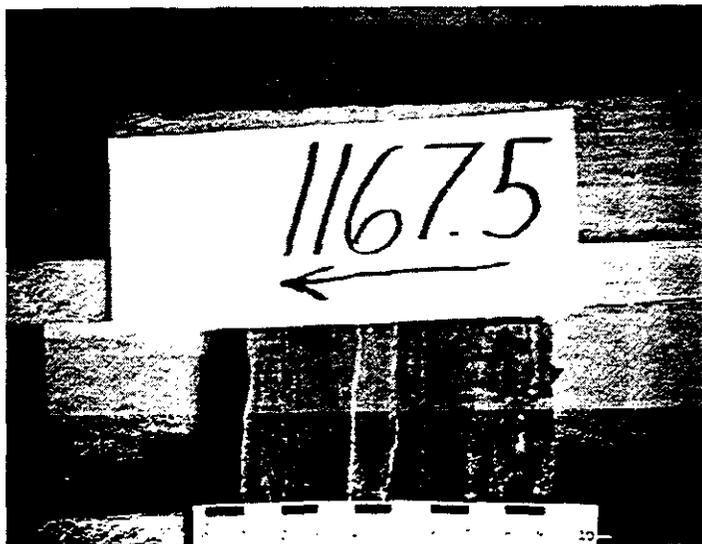
Plate 7.2. Core footage: 1167.5 ft. Dominantly light to dark gray, laminated anhydrite with thin, locally discontinuous, laminae of white magnesite and brownish, elongate halite oriented perpendicular to convex-upward, discontinuous laminae of light gray to white anhydrite.

Plate 7.3. Core footage: 2065.8 to 2066.6 ft.
Dominantly clear to milky white halite crystals, approx-
imately 10 mm in size, and reddish brown to pinkish brown
polyhalite. Note rectangular outline of polyhalite
body stratigraphically above the first 6 in 2066; but most
polyhalite occurs around halite crystal boundaries below
2066 label.
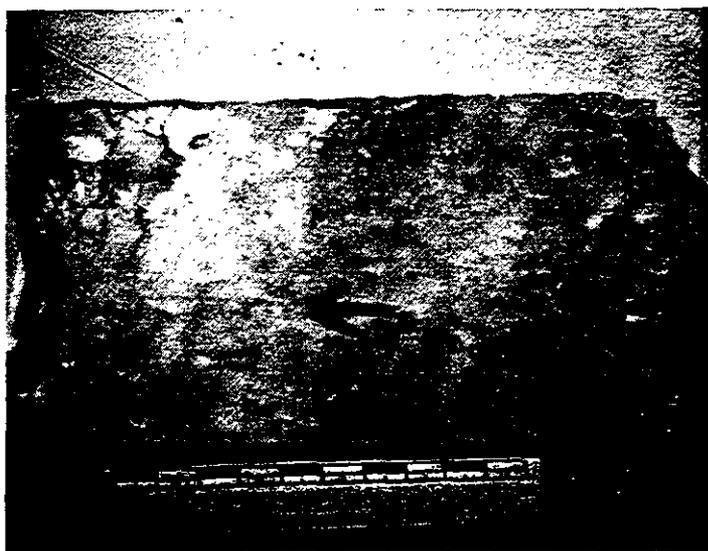
Plate 7.4. Core footage: 2615.0 to 2615.6 ft.
Dominantly coarse (ranging from 3 to 40, average 20 mm in
size) halite crystals, some with cubic form but most
anhedral, locally separated by microcrystalline white
anhydrite.

Plate 7.5. Core footage: 2705.8 ft. Coarse, ranging from 2 to 15 mm, light gray to black halite in white microcrystalline anhydrite and rare 1 to 2 mm bodies of pure white magnesite.
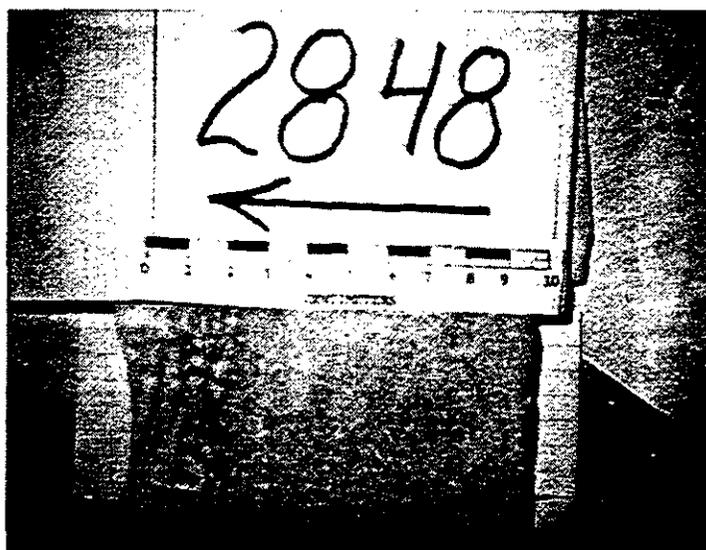
Plate 7.6. Core footage: 2848 ft. Varicolored (white and all shades of gray) anhydrite, some crystals near stratigraphic top of sample exhibit "swallow tail" form.

Plate 7.7. Photomicrograph (25X, plane light) of halite: many euhedral (cubic) to subhedral, relatively clear crystals locally containing fluid inclusions. Crystal size ranges from 0.5 to 1.5 mm. Compare with Plate 7.8.
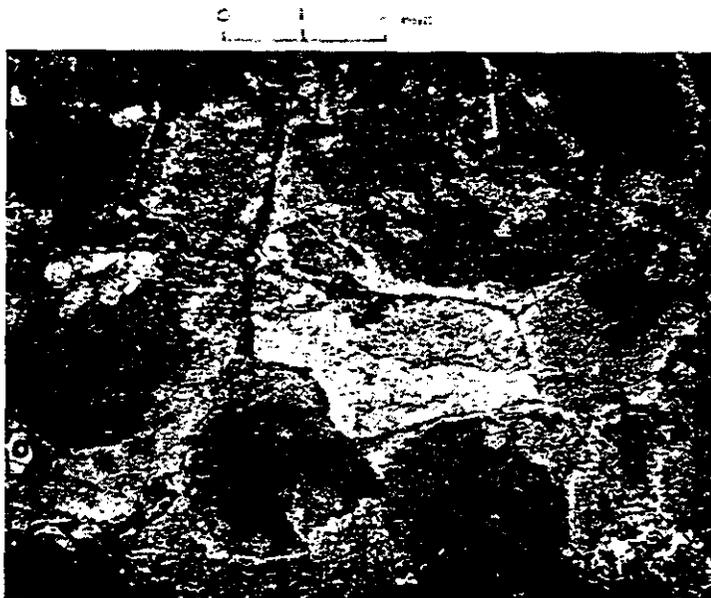
Plate 7.8. Photomicrograph (10X, plane light) of halite: subhedral to anhedral, cloudy crystals devoid of fluid inclusions. Crystal size ranges from 1.5 to 4.5 mm.

Plate 7.9. Photomicrograph (10X, plane light) of
sylvite (reddish, translucent to black, opaque in photo)
and halite: halite anhedra size ranges from 0.4 to 5 mm.
Two subhedra dominantly of sylvite occur within halite anhedra,
one subhedron/anhedron of mixed sylvite and halite occurs
within a coarse halite subhedron, but most sylvite occurs
as anastomosing bodies having gradational contacts with halite
between halite anhedra.
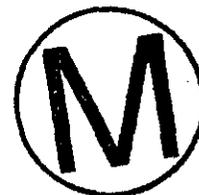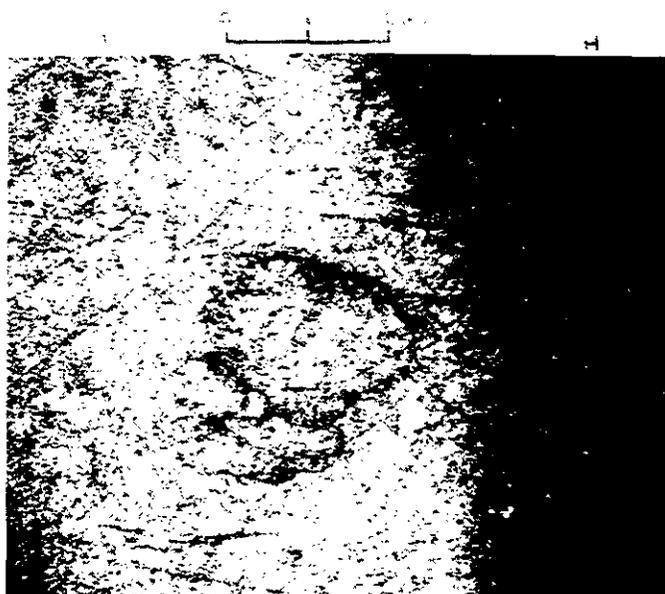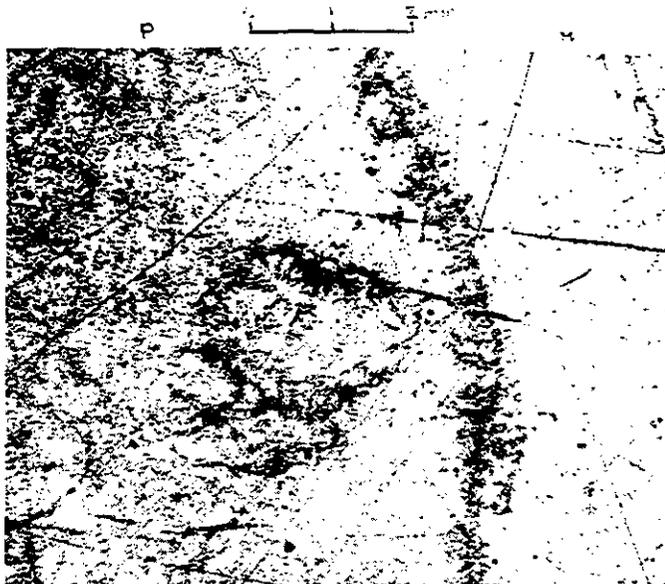
Plates 7.10A and 7.10B. Photomicrographs (10X, plane light in 7.10A, crossed nicols in 10B) of polyhalite (P) and halite (H): Polyhalite occurs as a cloudy anhedron (pinkish in hand specimen) locally containing smaller anhedra which are apparent due to concentrations of opaque (black in the photo, red under microscope reflected light) material, probably hematite. Concentrations of hematite also occur along the contact of polyhalite with halite which becomes extinct (black in 10B) under crossed nicols. The contact is irregular and gradational.
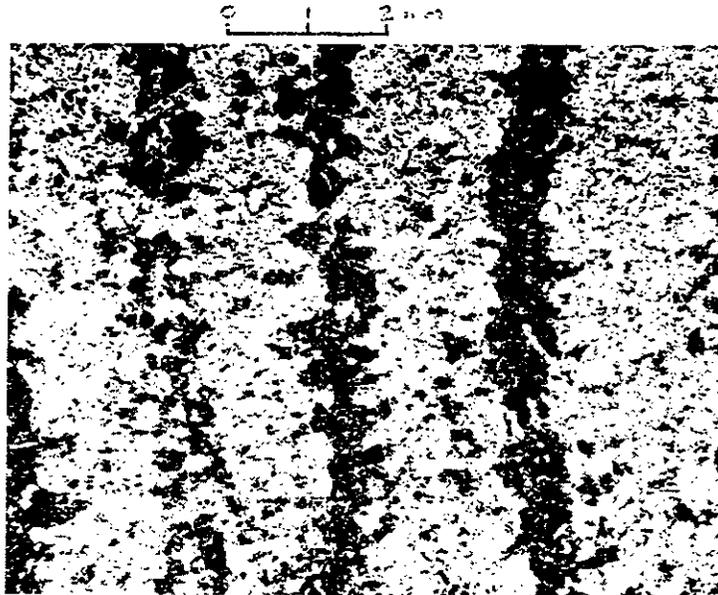
Plate 7.11. Photomicrograph (10X, plane light) of
laminated anhydrite and calcium or magnesium carbonate:
Dark thin laminae (approximately 1 mm thick) of dominantly
carbonate anhedra separate thin laminae (approximately
2 mm thick) of dominantly anhydrite anhedra.
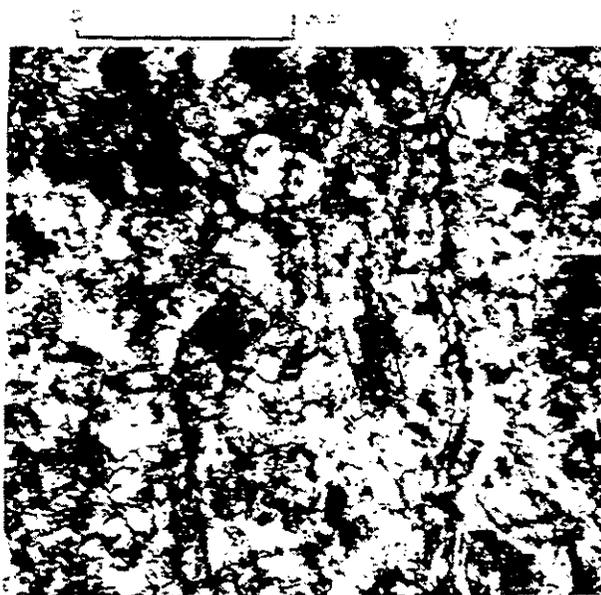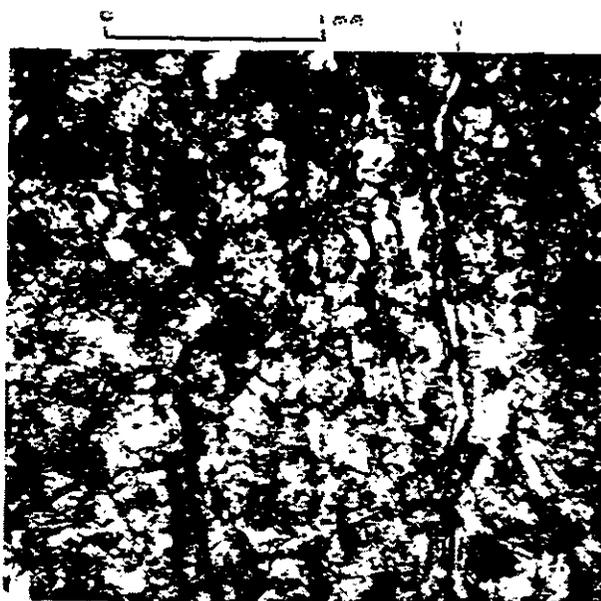
Plates 7.12A and 7.12B. Photomicrographs (25X, plane
light in Plate 7.12A, crossed nicols in Plate 7.12B)
of anhydrite with veinlet (V) of gypsum. Anhydrite occurs
as a mosaic of 0.04 to 0.4 mm anhedra and subhedra with
high order interference colors in 12B. Veinlet somewhat
discontinuous, is more apparent in 12A and consists of
very elongate irregular anhedra of relatively clear
gypsum with lower order interference colors than the
anhydrite in 12B. The veinlet is approximatedly strati-
graphically horizontal and is 0.06 mm thick, the width
of a single elongate gypsum anhedron.

_/mm_

Plate 7.13 Group of dark unrecrystallized zones in
essentially inclusion-free single crystal of halite of
sample 2065. For detail on central area see Plate 7.14.

_100μm_

Plate 7.14 Detail of area in Plate 7.13 showing sharp
crystallographically controlled boundaries of inclusion-rich
zones (type A). Such boundaries may represent primary
crystallization features rather than recrystallization fronts.
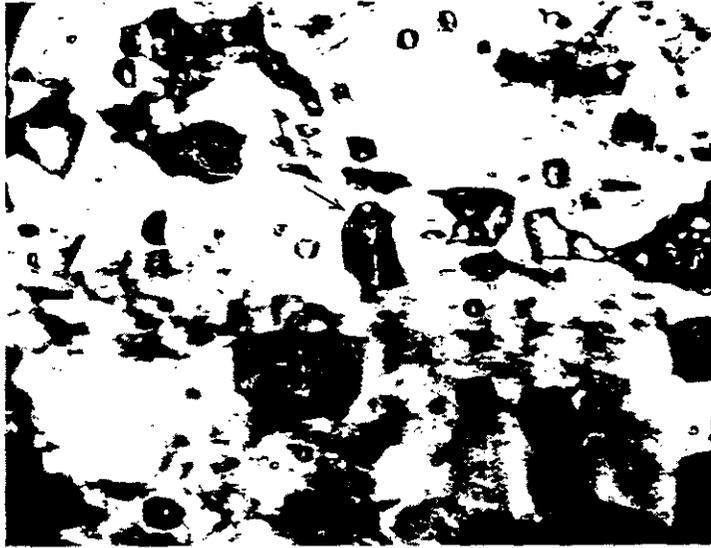
Plate 7.15 Recrystallized part of sample 2065 with large
numbers of type B inclusions with small bubbles (e.g., see
arrow) and some dark, cloudy unrecrystallized portions
(details in Plate 7.16).

Plate 7.16 One of the dark areas in Plate 7.15 showing
dense cloud of primary type A inclusions with some primary
banding (arrow), and sharp but curving (solution?) contact
with crystallographically parallel but almost inclusion-free
recrystallized salt (at top).

1mm
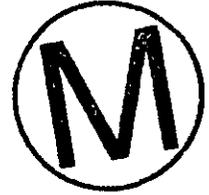
Plate 7.17 Coarsely recrystallized part of sample 2760,
with many large type B inclusions, each with bubbles
(arrows). Dark clouds are masses of unrecrystallized salt
with large numbers of tiny type A primary inclusions (see
Plates 7.18 and 7.19).

100µm

Plate 7.18 Detail of one of the cloudy areas in Plate 7.17,
showing high concentration of tiny type A inclusions. Most
of these inclusions are < 1µm (see Plate 7.19).

100 μm
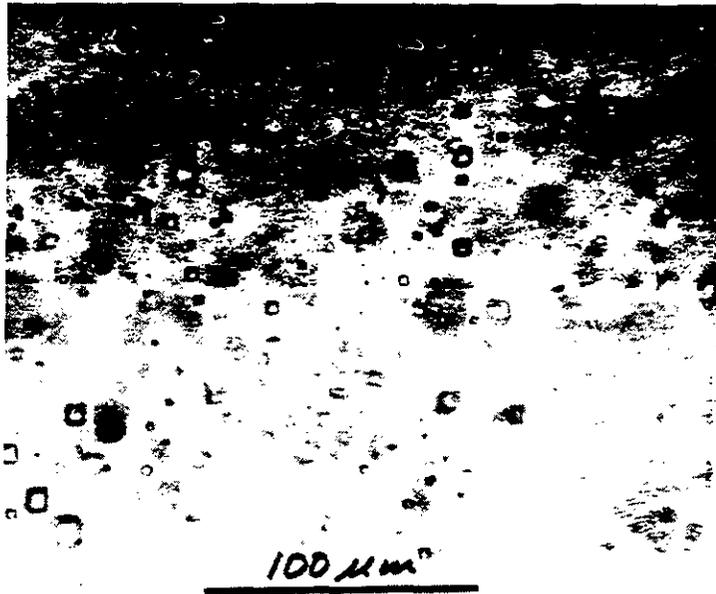
Plate 7.19 Detail of portion of Plate 7.18 that is relatively free of larger inclusions. The smallest inclusions are ≈ 0.5μm. All are type A. None of these inclusions contain a bubble.

50 μm
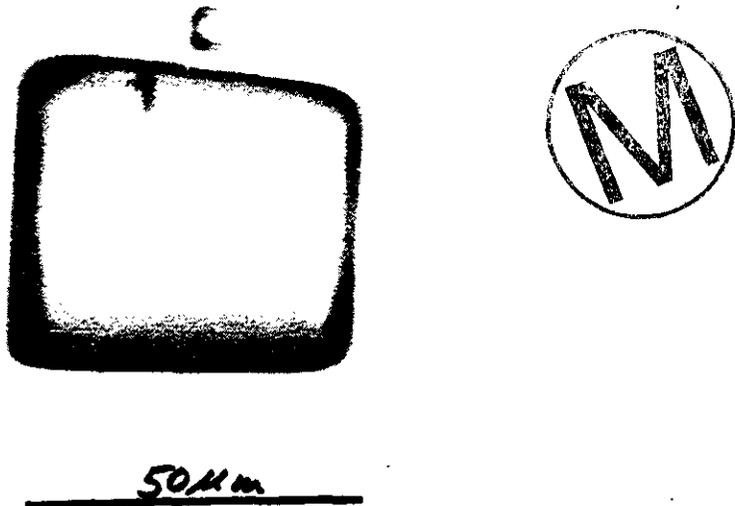
Plate 7.20 Inclusion in sample 2272.5 that contains only liquid, with no bubble, even though fairly large. Type B.
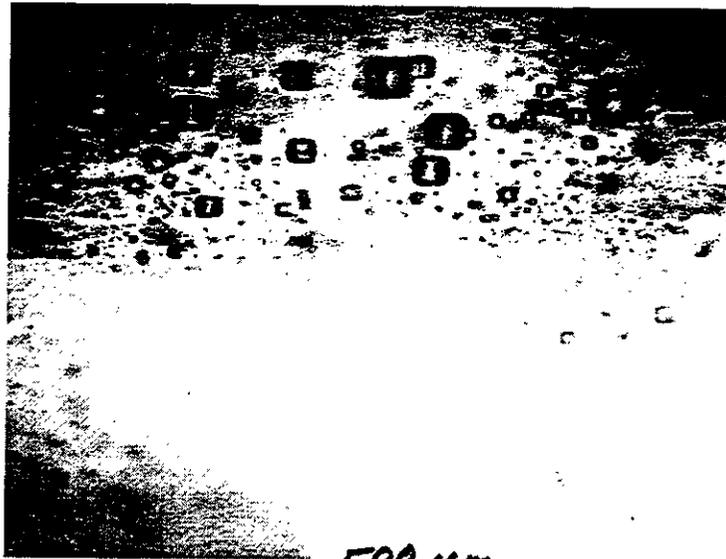
Plate 7.21 Unrecrystallized part of sample 1902 showing primary cubic growth zone feature, delineated by a cloud of tiny type A primary inclusions.

Plate 7.22 Unrecrystallized part of sample 1902 showing thin inclusion-free zone through dense cloud of tiny type A primary inclusions.

Plate 7.23 Oval grain of salt from sample 2760 containing unrecrystallized core with tiny type A primary inclusions. See Plate 7.24 for detail. Top of core is shown by arrow.
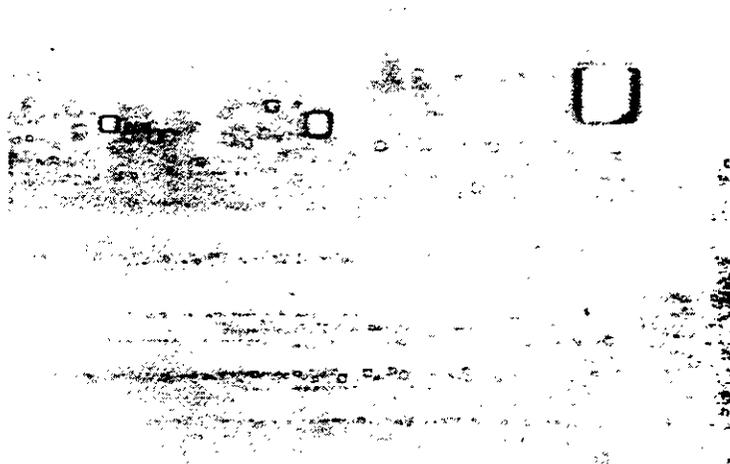
Plate 7.24 Enlgarged view of right central portion of Plate 7.23, showing extremely fine banding of primary type A inclusions, with inclusion-free zones between. Top of core is shown by arrow.
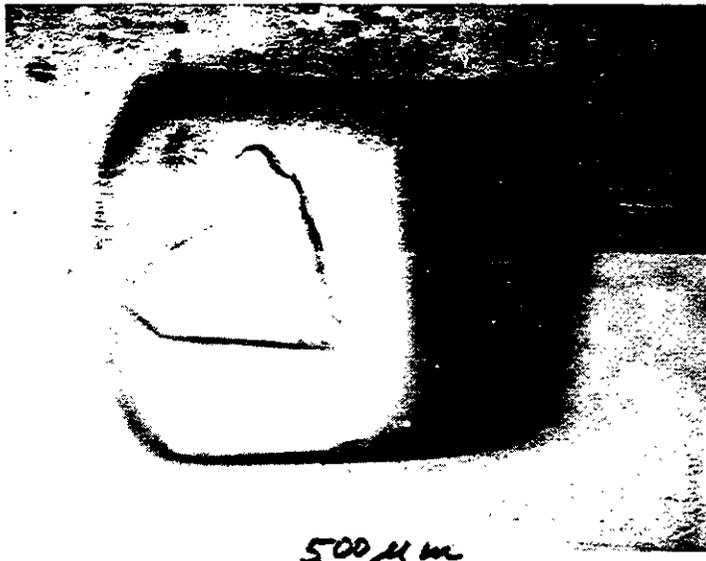
Plate 7.25 Inclusion (type B) in sample 1902 showing
twinned birefringent daughter crystal of unidentified
phase.
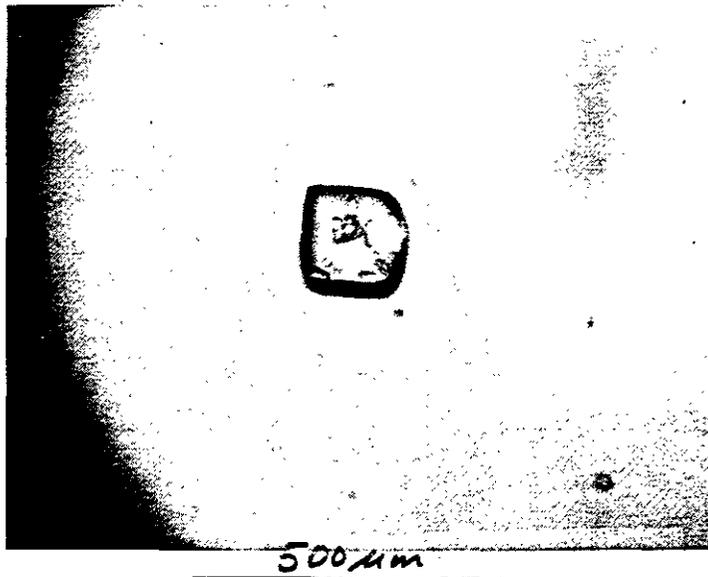
Plate 7.26 Daughter crystals of unidentified phase in
type B inclusion in sample 1902.2, with partly crossed
polarizers. Note twinning in largest crystal. Many inclusions
in this same sample have no daughter crystal or just a few tiny
crystals (see Plate 7.28).
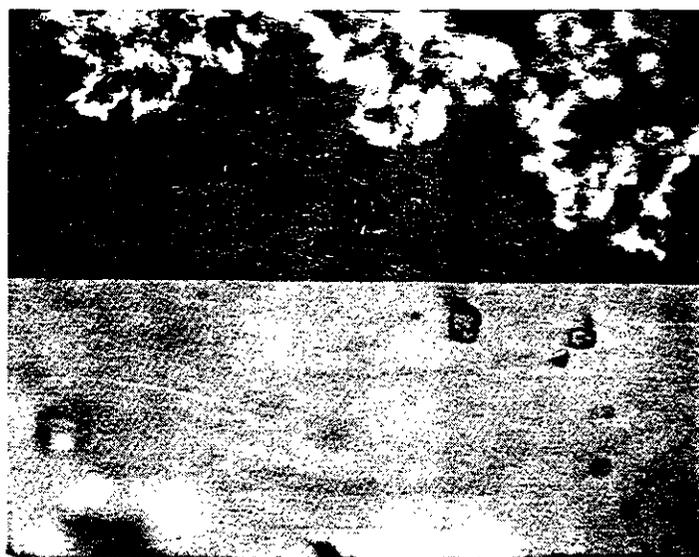
Plate 7.27   Plane of type B liquid inclusions each with
a large number of unidentified bladed birefringent daughter
crystals, just 400 µm below another plane of inclusions
with no daughter crystals (Plate 7.28).   Inclusion in
Plate 7.26 with daughter crystals is similar in phase ratio
but not in same plane (out of focus in lower left here).
Sample 1902.2 partly crossed polarizers; birefringent mass
embedded in salt crystal at top may be the same phase.

Plate 7.28   Plane of liquid type B inclusions, several with
bubble, but without daughter crystals, about 400 µm above a
plane of type B inclusions with a large number of unidentified
daughter crystals (Plate 7.27).   This lower plane is visible
but out of focus.   Sample 1902.2.   Inclusion of Plate 7.26 is
visible in lower left.

Plate 7.29 Large irregular type C inclusions in sample 2065 with "too large" bubbles.
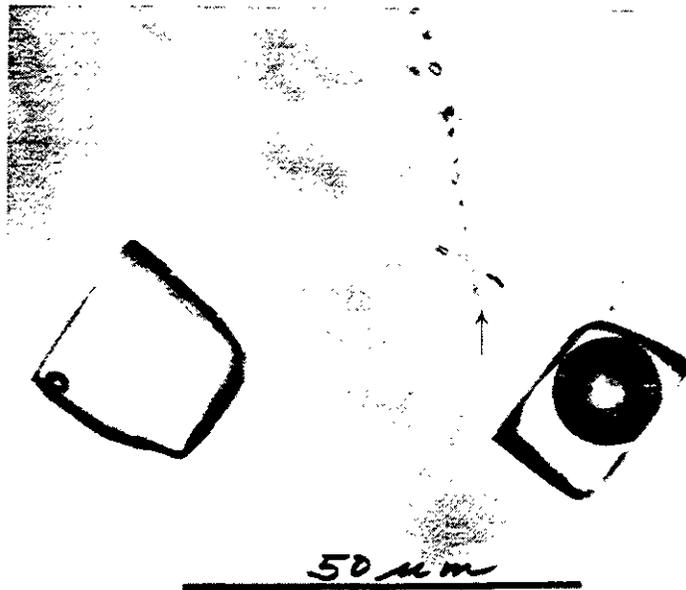
Plate 7.30 Pair of inclusions in sample 1902. The one on left (Type B) with small bubble is typical of those in this sample; that on right (Type C) is on a healed fracture (see arrow) and has apparently been opened and the original fluid replaced with a gas-rich mixture under pressure.
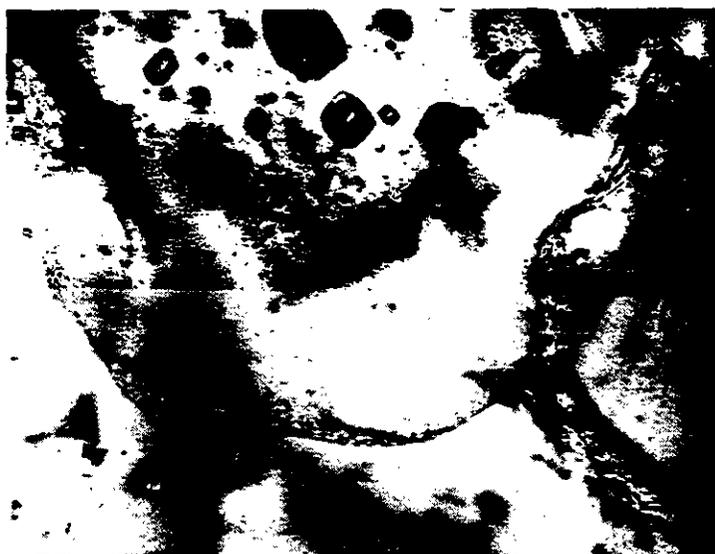
Plate 7.31 Single crystal of salt in sample 2760 with curving planes, outlined by type D inclusions, separating it from adjacent grains. Note also large type B inclusions and mass of tiny type A primary inclusions in central core of crystal. Sample has probably undergone two stages of recrystallization (see text). Top of core is shown by arrow.
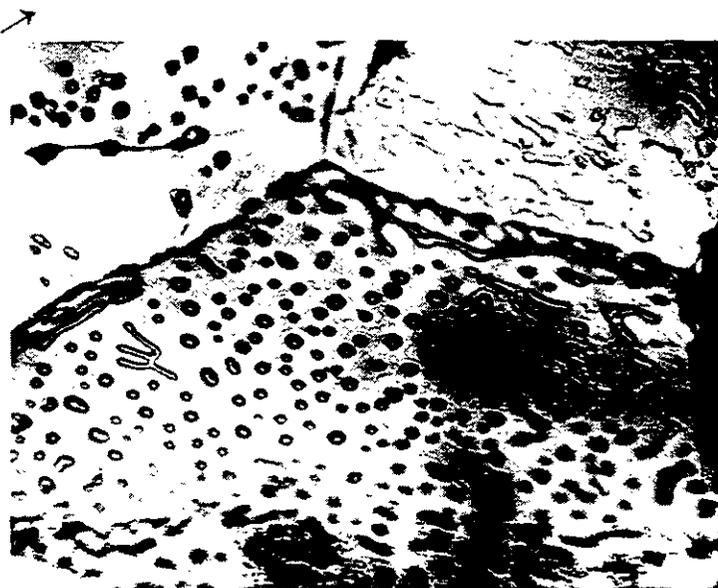
Plate 7.32 Fluid inclusions (gas; type D) on interface between recrystallized salt crystals in sample 2760. Note 120° junction. Top of core is shown by arrow.
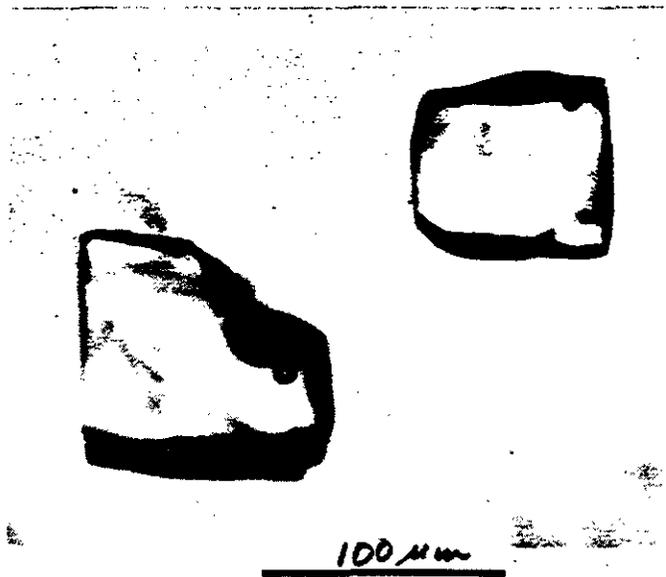
Plate 7.33 Large type B inclusions in sample 1799.1
homogenizing at 20.5^{o}C (lower left) and 21°C (upper right).
Photographed at $\approx$ 19°C.
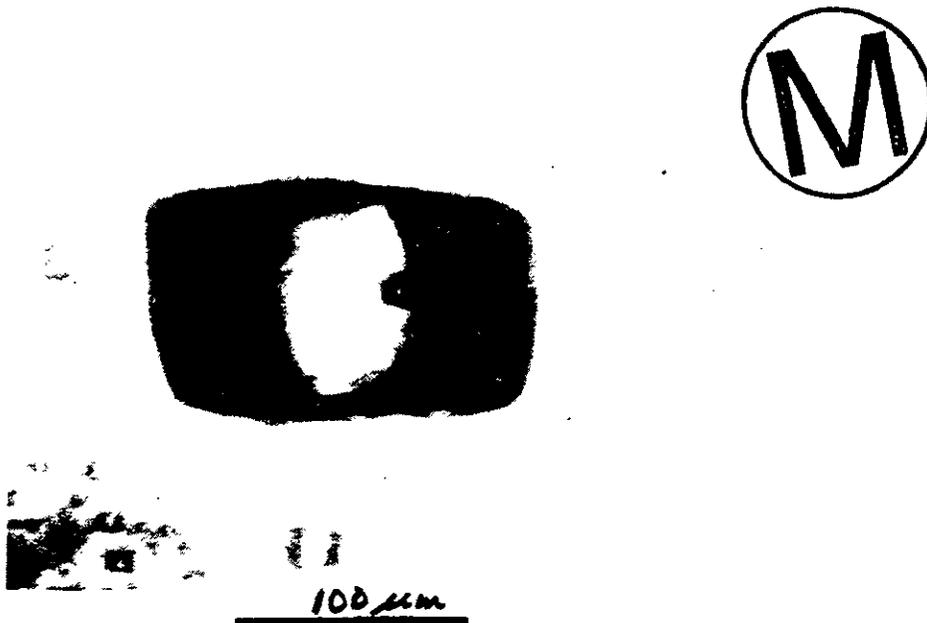
Plate 7.34 Large type B inclusion in sample 2760.1 homogeniz-
ing at 20.5^{o}C. Photographed at $\approx$ 19°C.
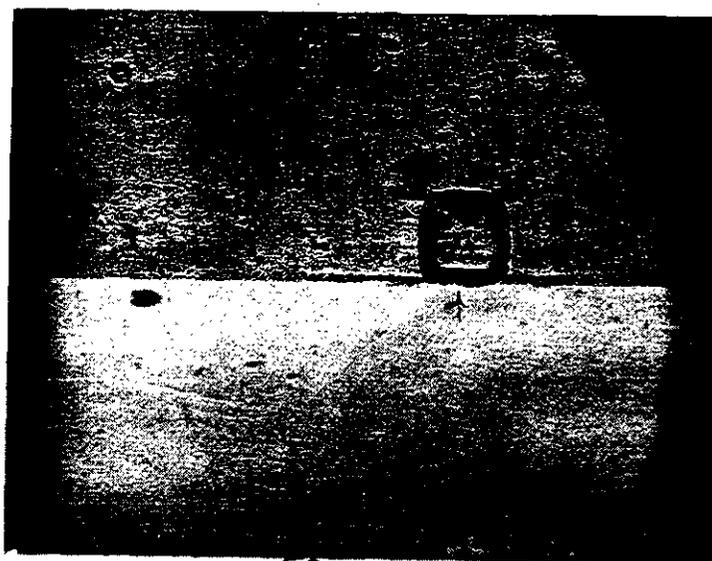
50 μm

Plate 7.35 Inclusion (type B) in sample 1902 after
freezing run, showing horizontal crack formed by expansion
on freezing, that is now a plane of tiny secondary fluid
inclusions; larger bubble than originally was present (due
to volume increase); and rounded halo of tiny inclusions
formed during freezing run (arrows), as a result of water
in inclusion reacting with halite of walls to form
$NaCl \cdot 2H_2O$, thus increasing inclusion volume. See text.
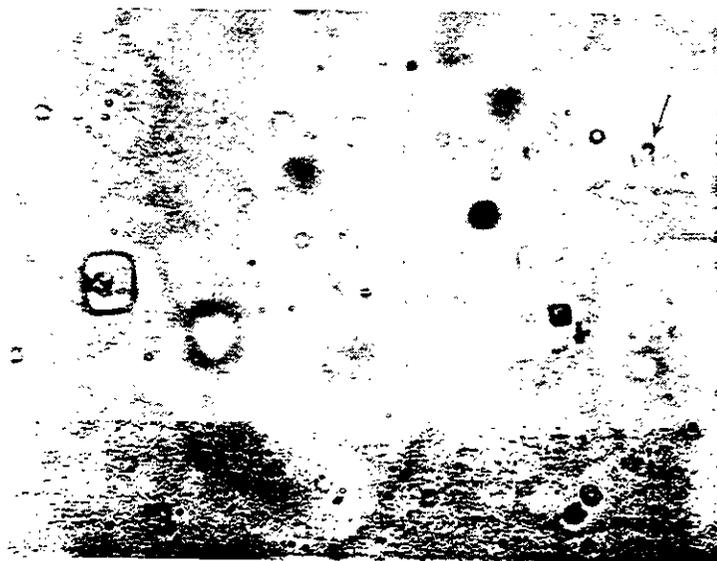
10 μm

Plate 7.36 Minute primary inclusion in unrecrystallized salt
from sample 1902 at high magnification (1560 X). The inclusion
in upper right is about 1.8 μm on an edge, and contains a
bubble of <0.5μm. Resolution of bubble is poor as it is
generally in rapid motion even with an IR filter in optical
system and exposures must be long. Many inclusions with no
bubble area are ≈ 0.5μm on an edge.

（M）
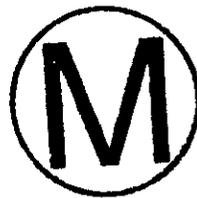
Plate 7.37 Sequence of photographs of type B inclusions in sample 2095.3 taken at the temperatures indicated during a freezing run. At $-75.5°C$ the inclusions contain a partly opaque mixture of solid grains of ice and salts. No change was visible on warming to $-34.5°C$, but at $-32.2°C$ the mixture suddenly became more translucent and the grain size started to increase, indicating first melting. Extensive melting occurred around $-4°C$, and the remaining crystals decreased to $\approx$ 20-25% at $0°C$. These were probably a hydrate but not all Nacl $2H_2O$, since a few were present at $+12°$, and the last dissolved at $+15°C$. The room temperature photo was taken after the run. The bubble size varies with phases present and temperature.

-34.5°   -32.2°   200μm   -4.°

0°   +20°   +12°
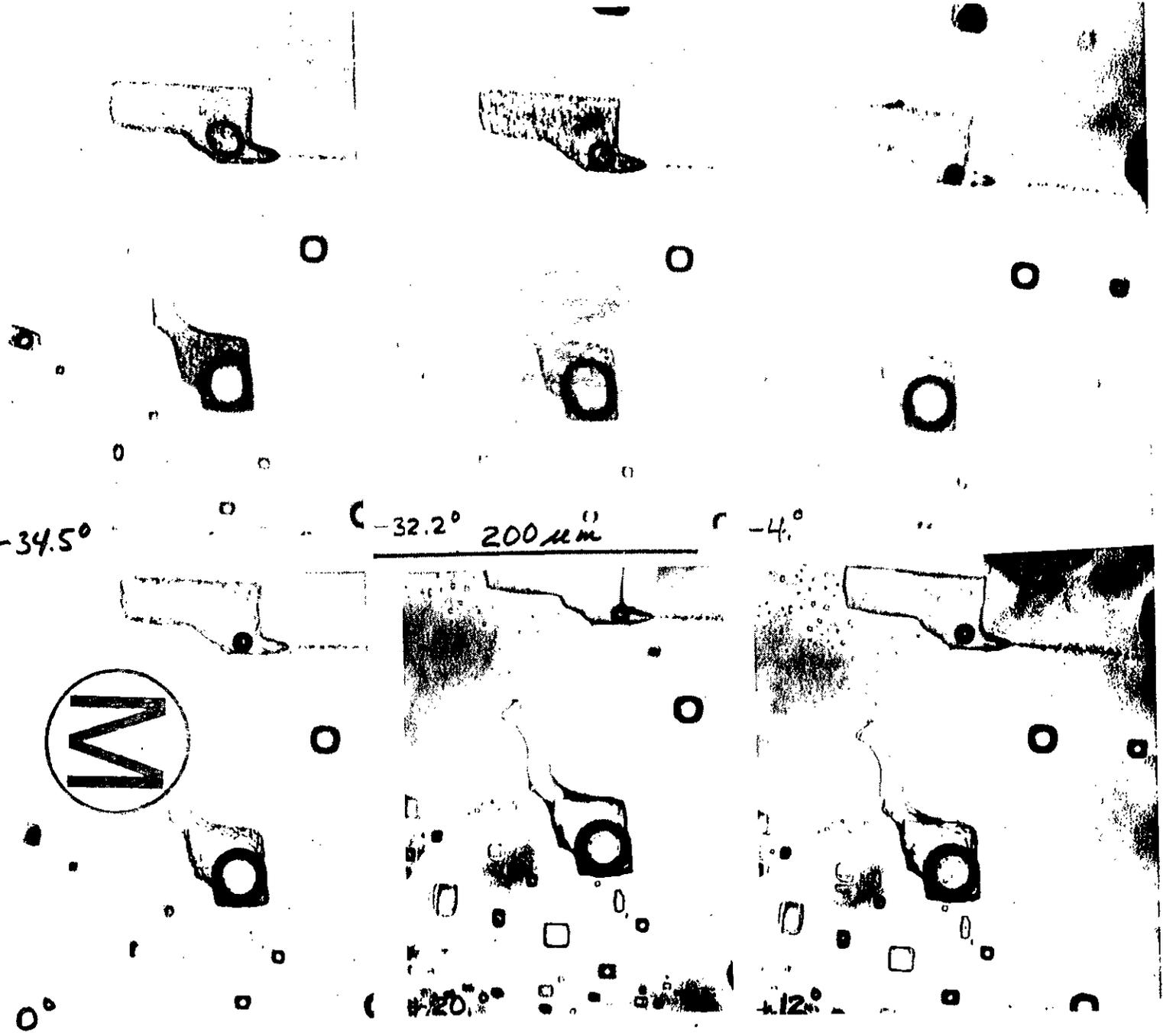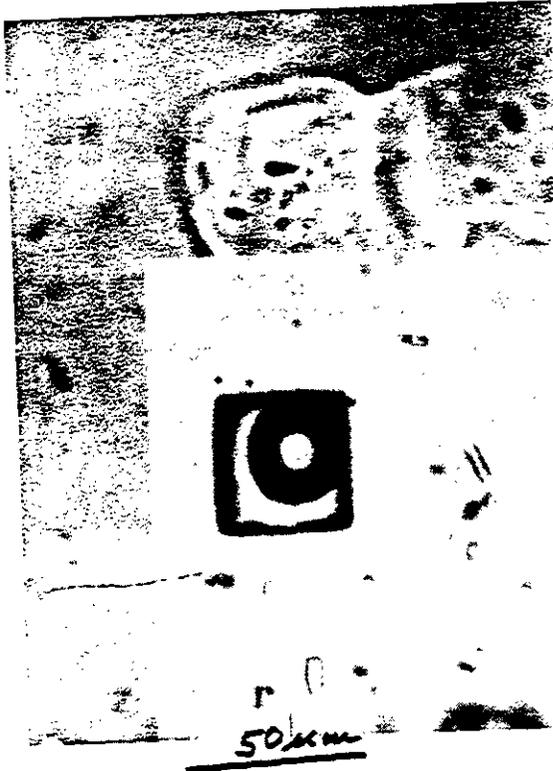
Plate 7.38 Inclusion from sample 2760, as found, with large bubble, viewed on crushing stage. The bubble contains gas under pressure (see Plate 7.39).

Plate 7.39 Same inclusion as seen in Plate 7.38, on crushing stage, after fracture has reached it. The bubble has expanded approximately 270% (vol) on pressure release.

A   50 μm   B

C   D
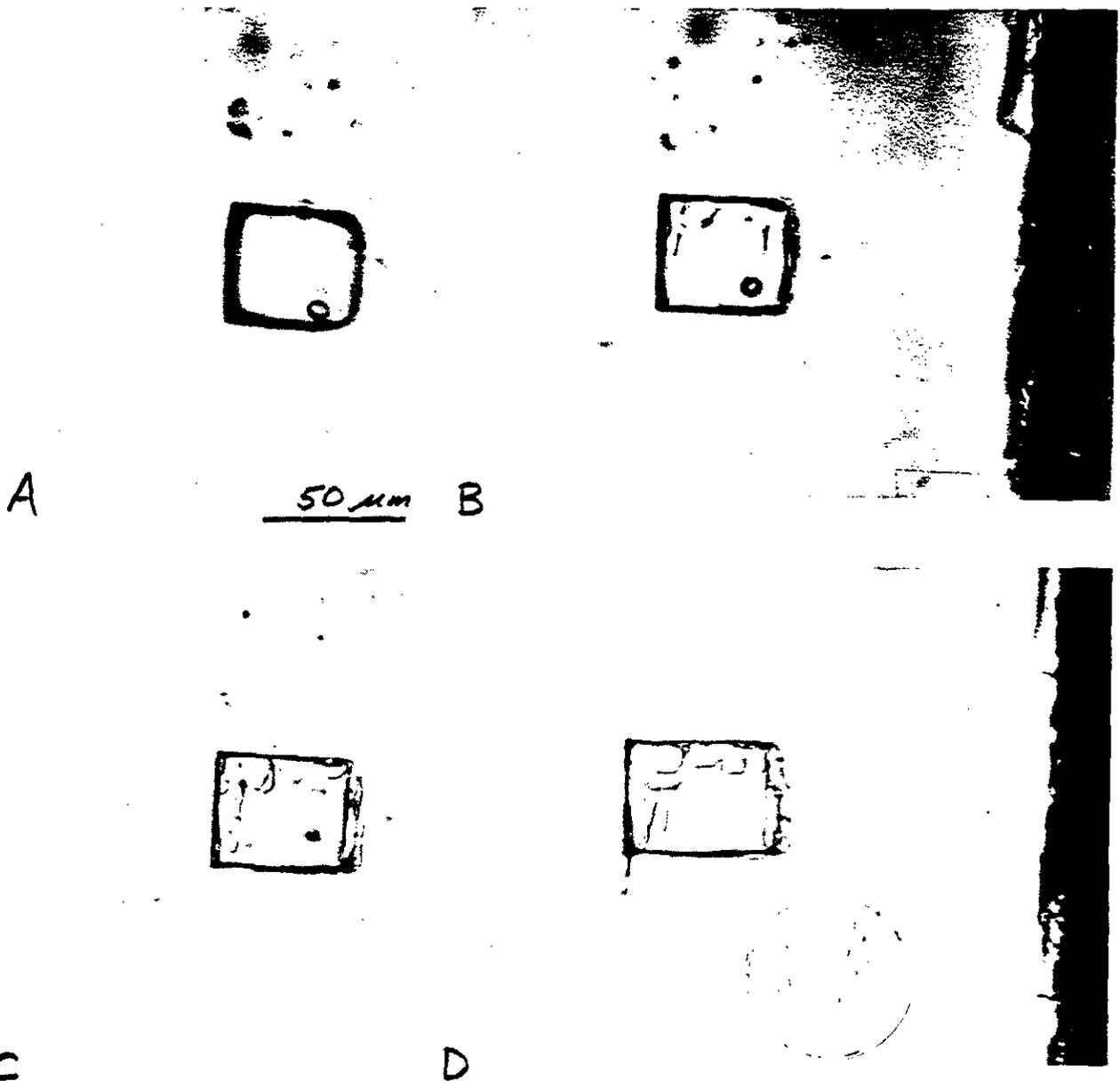
Plate 7.40   Sequence of photographs of inclusion in sample 2760 on crushing stage. A shows the inclusion as found. The sample was then stressed and immediately cracked (at right in B), but the area of inclusion was still under stress, since changes took place along edges of inclusion during next 10 minutes at constant stress (photo B). After 16 minutes at constant stress (C) changes are more pronounced and bubble is smaller; after 18 minutes bubble is gone (D).

In each of the following plates, the length of the scale bar is 100 μm.

Plate 7.41 (Photo 1) Group of small primary hopper-growth inclusions in ERDA-9 sample 2699.8-2700.0, after 250°C decrepitation run. These inclusions probably had no bubble originally, and now have one as a result of plastic deformation of the host salt. They now homogenize at temperatures as high as 273°C (Table 7.17).

Plate 7.42 (Photo 2) Solid phases (daughter crystals?) in inclusion in Kerr-McGee mine sample MB-76-4. The small rod-like crystal has parallel extinction, and the large cubic(?) crystal (KCl?) appears isotropic.

Plate 7.43 (Photo 3) Dense gas inclusion in Kerr-McGee mine sample MB-77-8, photographed at the approximate temperatures indicated (°C). See text, subchapter 7.5.

Plates 7.44 and 7.45 (Photos 4 and 5) Steam inclusions (arrows) in Kerr-McGee mine samples MB-76-3 (7.44) and MB-77-8 (7.45), now containing essentially vacuum, before (a) and after (b) being intersected by a fracture during crushing tests. The surrounding oil has filled the inclusions completely in (b).

Plates 7.46 and 7.47 (Photos 6 and 7) Gas inclusions in Kerr-McGee mine sample MB-77-8 containing gas at less than one atmosphere pressure, before (a) and after (b) being intersected by a fracture during crushing tests.

Plate 7.48 (Photo 8) High pressure gas inclusion in Kerr-McGee mine sample MB-76-4 before (a) and after (b) being intersected by a fracture during crushing.

Plates 7.49, 7.50 and 7.51 (Photos 9, 10, and 11) High pressure gas inclusions in Kerr-McGee mine samples MB-77-8 (7.49 and 7.51) and MB-76-3 (7.50), before (a) and after (b) being intersected by a fracture during crushing. The approximate volume expansion is 30-fold in 7.49, 40-fold in 7.50, and 100-fold in 7.51. Two bubbles formed in 7.49, and one in 7.50 (arrows).

1

2

a +22	d −56	a
b −21	e −68	
c −30	f −75	b

3

4

9   10   11

(M)
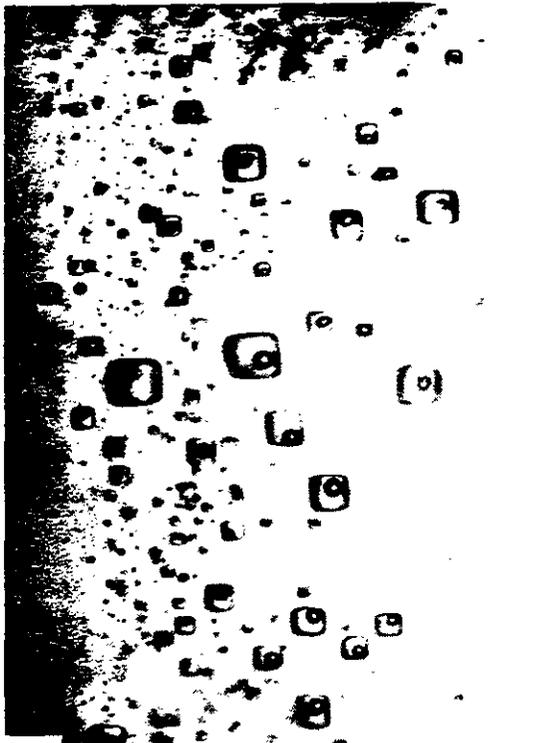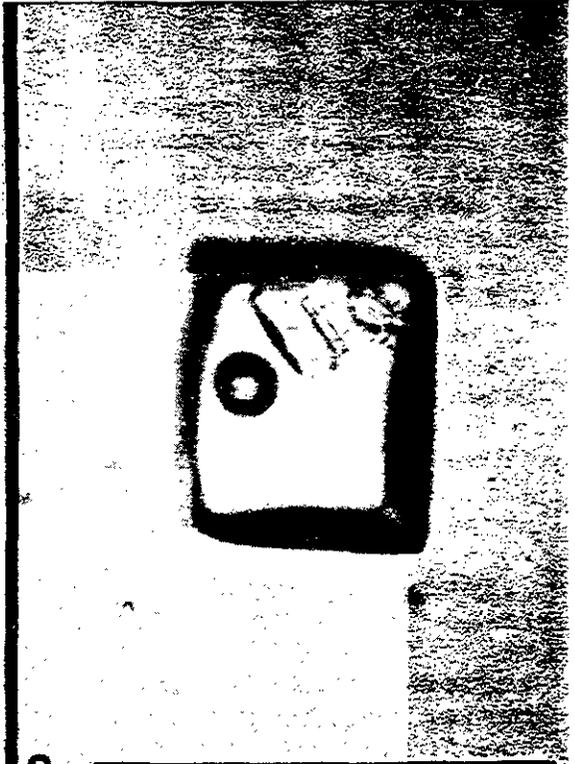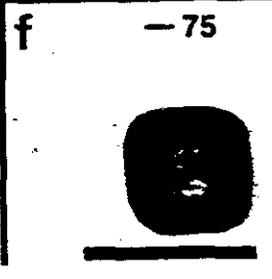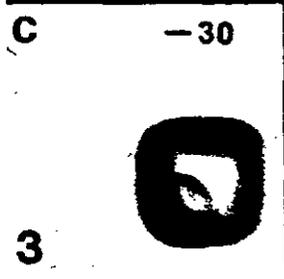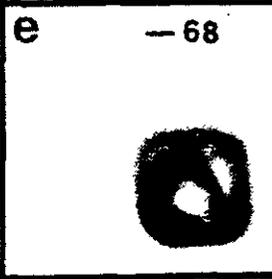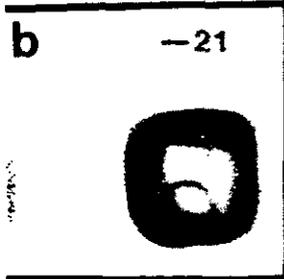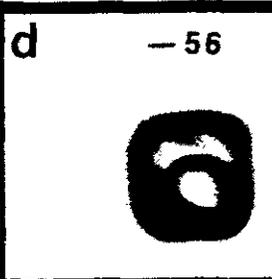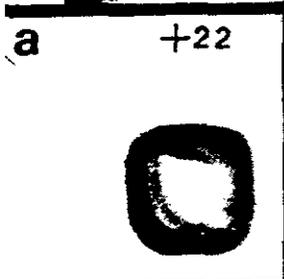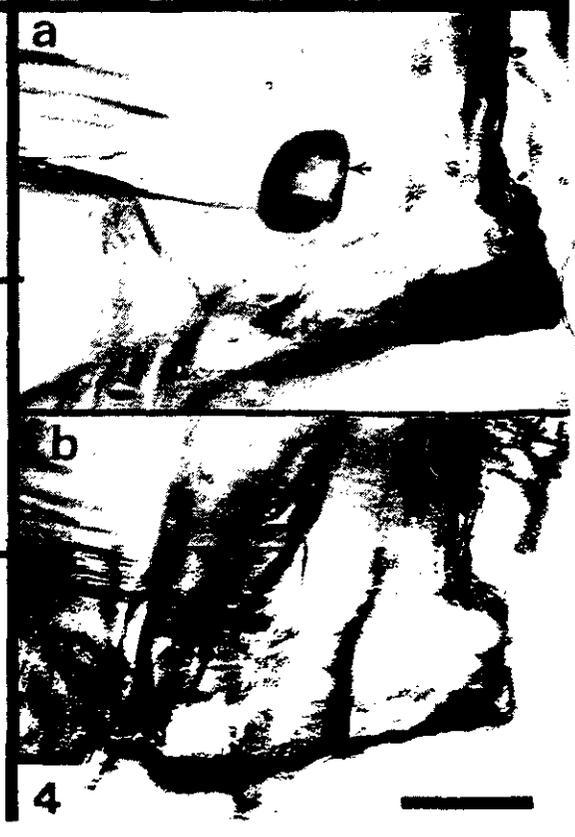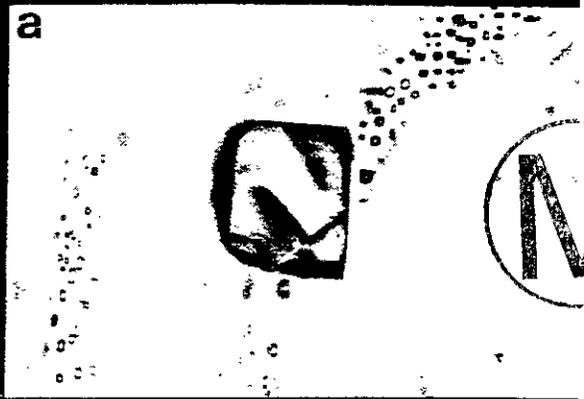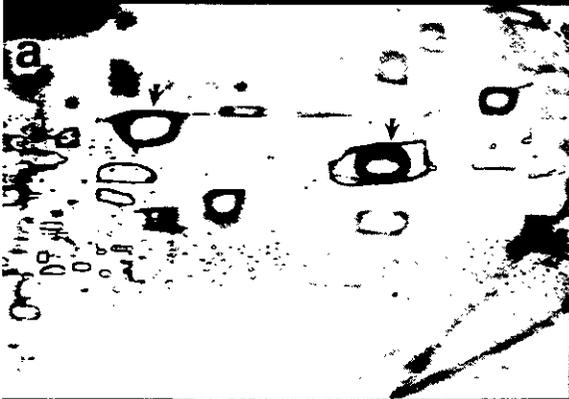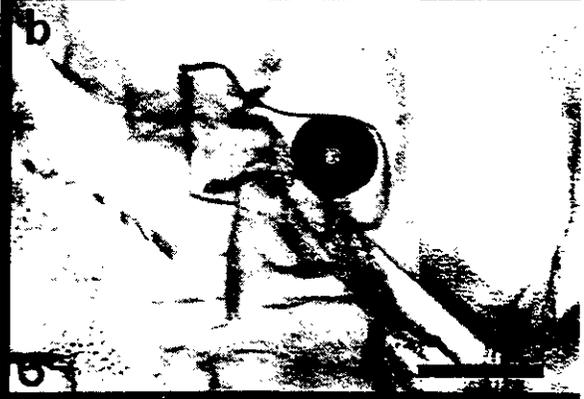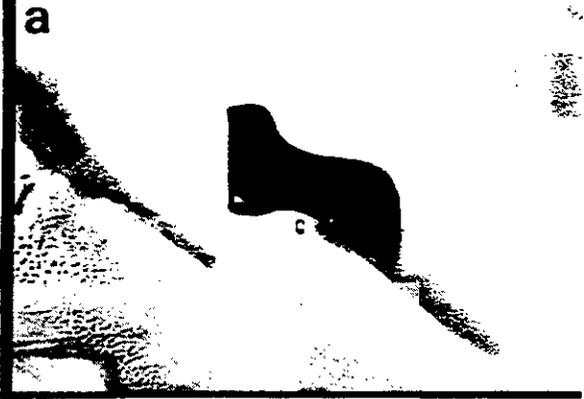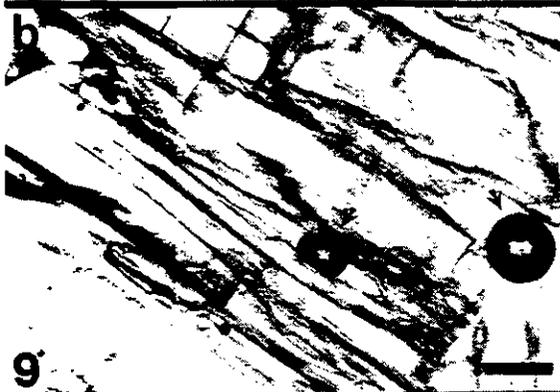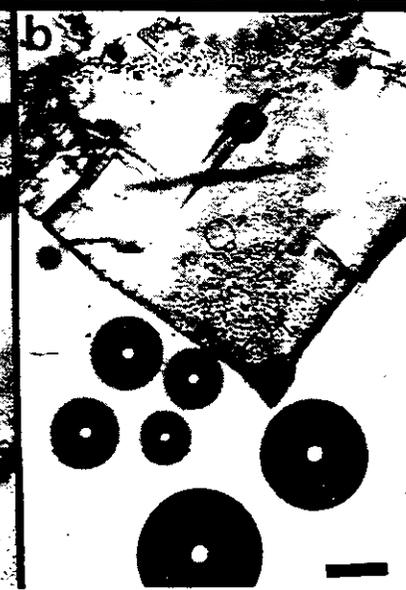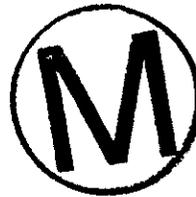
PLATE CAPTION

Plate 7.52 and Overleaf: Core fragments from Castile
anhydrite serving as host rock for the ERDA No. 6 brine
reservoir. Depths of origin, uranium contents and $^{234}U/^{238}U$
ratios are given in the overleaf for various parts of the core
fragments.

TOTAL U $\overline{a}$
$(^{234}U/^{238}U)$ <u>DEPTH (Ft.)</u>

2708

19.2 ppb   1.09

1.61 ppm   1.02

2709.4

33 ppb   1.04

coarsely
crystalline
anhydrite
(white)

laminated
calcite and
anhydrite
(gray)

2.17 ppm   1.04   2709.9
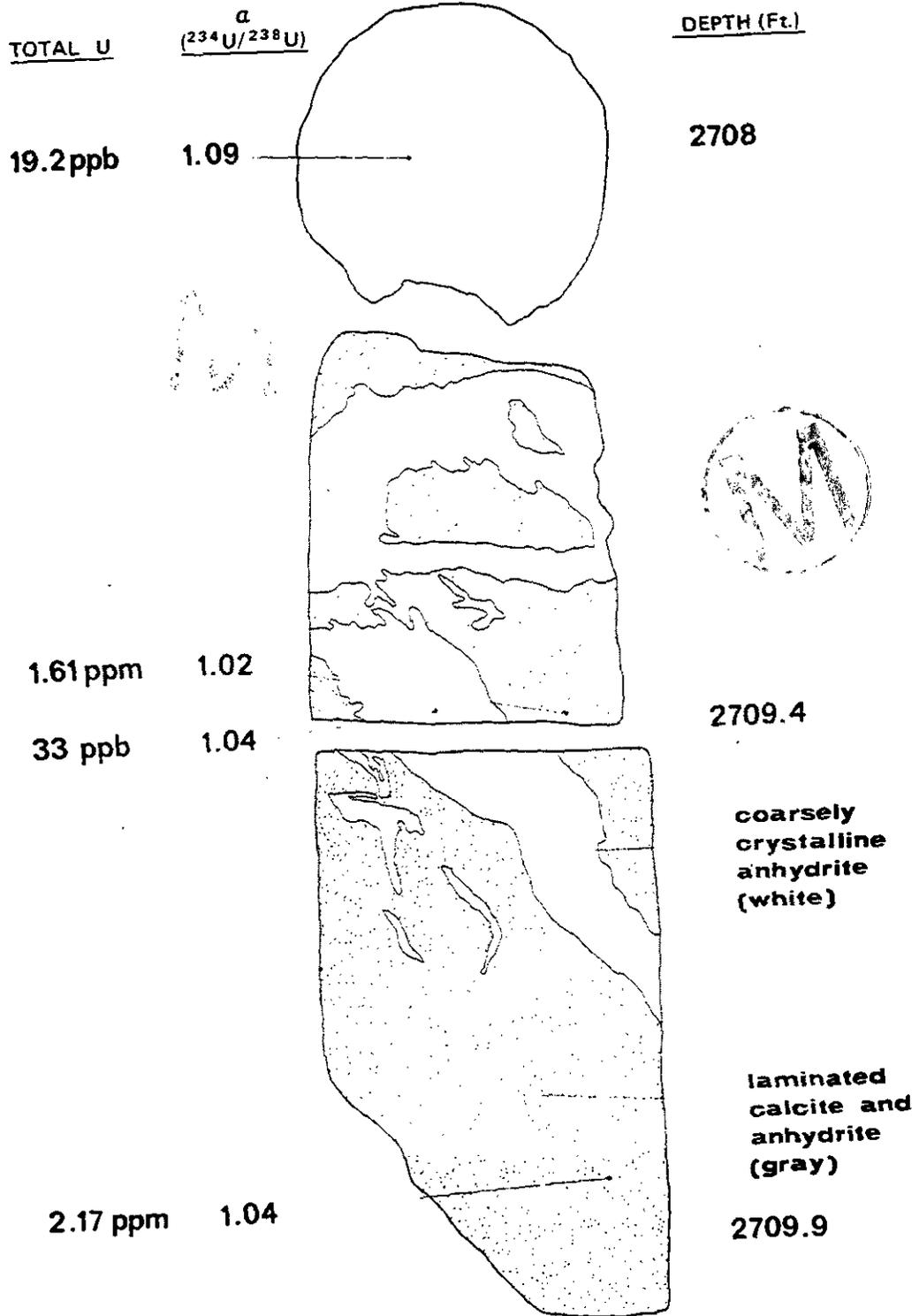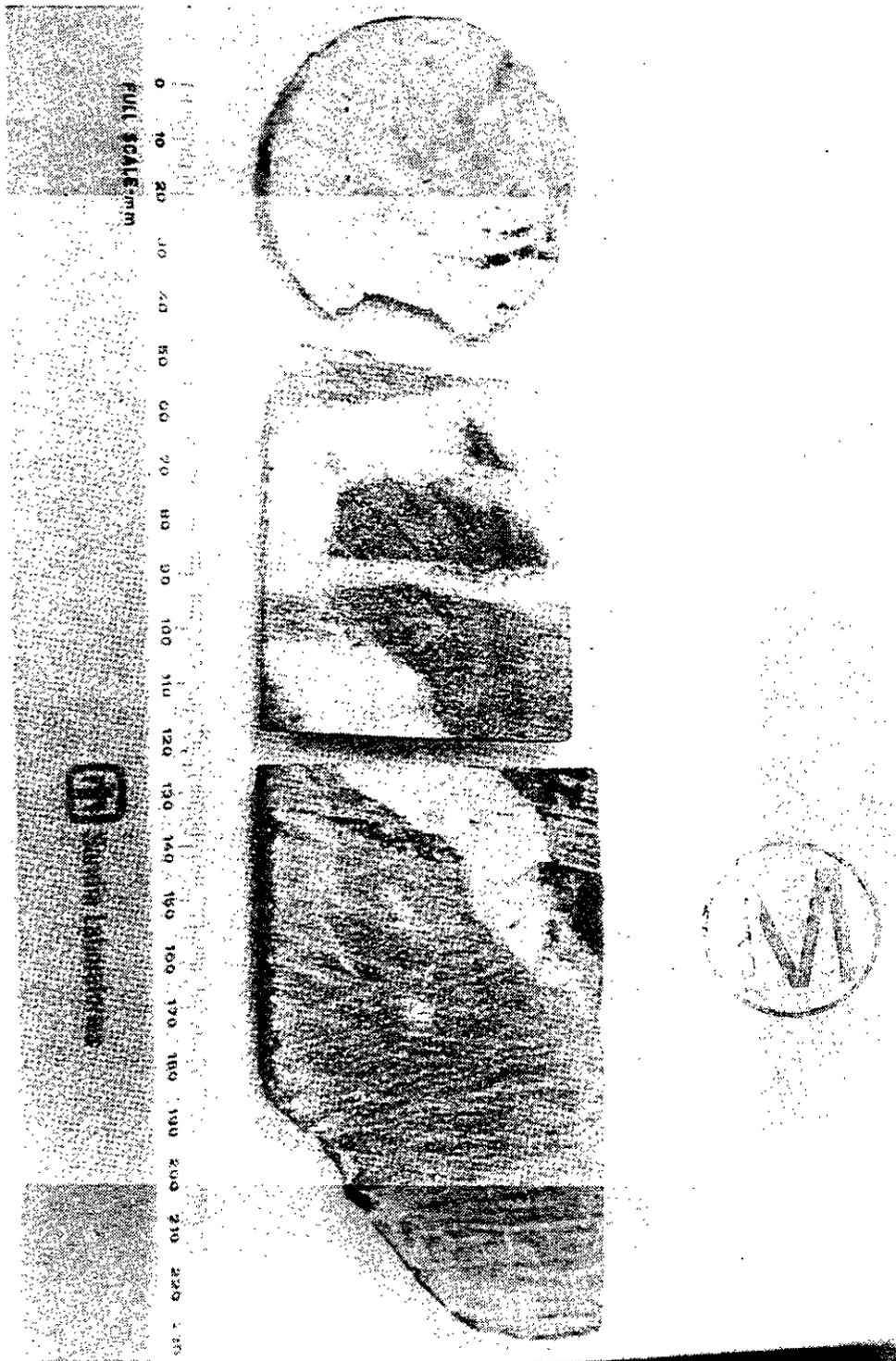
PLATE 7.52

8.1   INTRODUCTION

The northern portion of the Delaware Basin is known for production of
potassium salts and fluid hydrocarbons. An effort was made to select a
location for the WIPP that would minimize conflict with these resources.
It is likely, however, that some of these potash and hydrocarbon
resources underlie the site. The extent of potash mineralization has
been fairly well established because the potash mining industry has
released information concerning their exploratory drilling in the area.
Those findings were supplemented by information from 21 additional holes
drilled by the Department of Energy. Site selection criteria described
in Chapter 2 prescribe that the site be no closer than one mile from a
deep drill hole. This means that the potential hydrocarbon resource must
be evaluated by inference utilizing subsurface information from
surrounding areas. An investigation was also carried out to determine
the significance of other possible industrial minerals such as caliche,
gypsum, salt, uranium, sulfur, and lithium at or very near the WIPP
site. Table 8-1 summarizes the principal findings of resource studies.
Only potash and natural gas are considered to be significant exploitable
deposits as shown in Table 8-2. The economic resources denied in Zones
I-III are shown in Table 8-3.

8.2   ORGANIZATIONS INVOLVED IN RESOURCE EVALUATION, AND THEIR REPORTS

Numerous contractors representing both government and private companies
were engaged in the resource evaluation at the WIPP site. An outline of
work accomplished during this phase of the site characterization is given
in Table 8-4.

The listed studies quantify in-place resources and evaluate what portion
of those resources would be extractable. A legal determination is now
under way to establish values to the various mineral and oil and gas

lease holders within the site area. However, these studies deal with the present value of specific land tracts and as such are not pertinent to site chacterization.

8.3 POTENTIAL RESOURCES IN RELATIONSHIP TO STRATIGRAPHY AT THE WIPP SITE

Resource evaluation at the WIPP site took into consideration the existing stratigraphy of the site area. Each formation was evaluated for mineral deposits that were either known or that could exist based on the characteristics of the sediments present.

A stratigraphic column is given in Table 8-5 that indicates where in the geologic section specific types of deposits are considered to have a reasonable likelihood of occurrence. The table briefly describes the character, thickness, and median depth of each formation.

8.4 RESOURCE DESCRIPTION BY SPECIFIC COMMODITIES

The description of resources commences with the shallowest formation and proceeds down the stratigraphic column to the Precambrian.

8.4.1 Caliche

A thin layer of caliche (a whitish, calcium carbonate-rich material) underlies most of the site area. Exposures are normally obscured by dune sand, but it has been estimated that the caliche blanket covers approximately 80% of the site area. The average thickness is 4.3 feet, and the total resource has been estimated at 185 million tons (Siemers et al., 1978). The quality of caliche as determined by insoluble content (ranging from 21 to 69%) appears to be typical for caliche for this region.

Caliche is often used to surface dirt roads in southeast New Mexico. Small quarries dot the landscape, and several provided material for road construction to various drill locations within the WIPP site. This is the sole use for caliche in this region. Caliche is so extensive in this region that it can not be considered as either a limited resource or one that has significance to road construction of surrounding areas if land is withdrawn for the WIPP site.

8.4.2 Uranium

Uranium could occur in sediments such as those of the Gatuna, Santa Rosa or Dewey Lake Formations. However, no significant occurrence of uranium has been found within the Delaware Basin. Reducing environments favoring uranium deposition are absent as evidenced by the lack of organic debris, pyrite or humates in these formations. No signal indicative of economic or even marginal uranium concentrations was observed on gamma ray logs of the 36 holes drilled through these beds during site evaluation. The conclusion is that significant uranium deposits are most unlikely, even in beds which are considered to be the most favorable.

8.4.3 Gypsum

Dissolution of salt from the Rustler Formation has occurred over much of the site area. Waters accompanying this dissolution have caused partial conversion of anhydrite within the Rustler to gypsum. The conversion is not complete, however, and it is doubtful that high-quality gypsum would be persistent in any single bed. The maximum amount that could be present, assuming an aggregate thickness of 40 feet, amounts to 1.3 billion tons (Siemers et al., 1978). The quality and bed thickness are inferior to those in beds west of the WIPP site. Still farther west and south, extensive outcrops of high quality gypsum of the Castile Formation occur. The nearby availability of superior quality gypsum that can be mined by open pit methods leads to the conclusion that gypsum in the Rustler Formation can not be considered a likely economic resource.
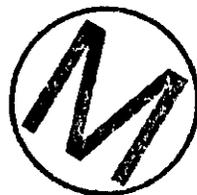
8.4.4 Halite (Salt)

Halite is the dominant constituent of the Ochoan evaporites. The
shallowest salt is in the Rustler, but dissolution of this formation has
removed much of the Rustler salt except in the southeast quadrant of the
WIPP site. On the other hand, salt beds persist under the site in the
Salado and Castile Formations. The thickest and purest salt beds in the
region are in the Castile. The State Bureau of Mines and Mineral
Resources estimated 118 billion tons of salt in the Salado within the
WIPP boundary (Siemers et al., 1978). The Castile Formation would add
approximately 80 billion tons of additional salt resource.

As with gypsum and caliche, the immense halite deposits are not
considered to have economic significance because of the prevalence of
these deposits throughout the general area and the existence of adequate
supplies closer to areas where salt is in demand.

8.4.5 Sulfur

A significant deposit of native sulfur is being exploited by the Frasch
process approximately 50 miles south of the WIPP site in northeastern
Culberson County, Texas. The occurrence is associated with brecciated
and carbonatized anhydrite beds of the Castile Formation. Considerable
exploration has been under way since discovery of the Culberson deposit,
but that exploration has been aligned along the southern and western
parts of the Delaware Basin where the Castile Formation either lacked
halite during deposition or the halite has been removed by dissolution.
The genesis of the deposits is believed to depend on a combination of
bacterial action, induced fracture permeability and a source of
hydrocarbons (presumably from upward escape of natural gas or crude oil
along fractures from the Delaware Mountain Group). The closest analogy
to such a setting in the northern part of the Delaware Basin and the
vicinity of the WIPP site would be either "breccia pipes" or H_2S-laden
brine reservoirs. Careful attention was given in selecting the WIPP site
to avoid such structures; further investigation has not revealed any such
structures, therefore, no sulfur deposits are expected.

8.4.6 Lithium

Lithium occurs in a concentration of 140 mg/L in a saturated brine reservoir that was encountered during the drilling of ERDA 6. The hole was located 2 miles northeast of the outer boundary of the WIPP site. A similar reservoir was found in the Belco Hudson Federal No.1 gas well 1/4 mile outside Zone IV on the southwest side of the site. No analyses were done for lithium in the latter well, but both reservoirs were at equivalent stratigraphic positions (middle Castile), contained H_2S, and were fully saturated brines. The concentration of 140 ppm lithium in ERDA 6 verges on being economically extractable if the reservoir is of sufficient size. Griswold (1977) estimated the reservoir volume at ERDA 6 to be on the order of 100,000 to 1 million bbl. If reservoirs are limited to this size, they would not warrant development. At current market price the in-place value of the lithium would not exceed $1 million.

There has been a deliberate attempt to locate the WIPP site in an area free of brine reservoirs in the Castile. Extensive seismic surveys have been run across the area to ensure that no anomalous structures occur in the Castile Formation. The occurrences at ERDA 6 and at the Belco well are associated with complex anticlinal structures and are easily recognizable on seismic survey traces.

8.4.7 Potash

Method of Evaluation. Sylvite (KCl) and langbeinite $(K_2Mg_2(SO_4)_3)$ exist under portions of the WIPP site (see Figures 8.2, 8.3, 8.4). Although an attempt was made to avoid such deposits during the site selection process, it was not possible to do so completely because other site selection factors such as avoiding deep oil and gas test wells and the desire for uniform and thick salt beds at reasonable depth took precedence.

The potash evaluation commenced in August, 1976, after the site was
chosen for detailed characterization.   When chosen, the site was located
mostly outside the Known Potash Area defined by the Conservation Division
of the U.S. Geological Survey. Considerable potash exploratory drilling
had been done on the flanks of the site area by private industry, but it
is a requirement that the results of that drilling be held in confidence
by the USGS. However, Sandia Laboratories contacted each mining company
that had drilled in the vicinity and was granted access to the drill
records on a private basis. These records indicated that deposits of
commercial quality probably extended into the site area. The Department
of Energy (then ERDA) authorized an exploratory drilling program to
evaluate the potash deposits within the WIPP site. Technical direction
of this exploratory drilling program was given to the USGS. The drilling
program commenced in August and was completed by the end of November,
1976.

The Roswell, New Mexico, office of the Conservation Division of the USGS
was given the task of determining potash resources by combining the
results of DOE-sponsored drilling with records of drilling in the
vicinity of the site. Findings have been reported by John et al. (1978).

The DOE also engaged the services of the U.S Bureau of Mines (USBM) to
evaluate the extent to which the resources defined by the USGS could be
produced at a profit using existing mining and beneficiation practices.
The results of the study have been reported by the USBM (1977). The
essential conclusion was that langbeinite in the 4th ore zone could be
profitably mined in the northeast quadrant of the WIPP site. A band of
sylvite, contained mostly within the 10th ore zone on the north and west
sides of the sites, verged on being economically exploitable. Profitable
mining of the sylvite would require a higher price for muriate (KCl) than
current market value ($52/ton versus a current price of $43/ton).

Description of the Potash Exploration Drilling Phase. Figure 8-1 is a
map showing a land block, centered on the WIPP site, that measures 8
miles on a side. This land block constitutes the area investigated by

the USGS and USBM. All locations of drill holes are shown from which information was available as to the depth, thickness, grade, and mineral suite of ore beds. Note that a different symbol is used to denote holes drilled by DOE from those drilled by mining companies. Examination of the distribution of hole locations reveals that the drilling plan directed by the USGS included testing the entire WIPP area on a spacing of not less than one hole per square mile. The objective was to completely cover the site area following industry practice for reconnaisance exploration. The density of the holes is judged to be quite adequate for resource appraisal.
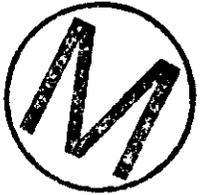
Drilling closely followed standard industry practices (Jones, 1978). Rotary techniques were used from the surface down to a point just above the uppermost ore zone. Drilling operations were then converted to coring using a brine saturated with potassium chloride as the drilling fluid. Core recovery was excellent in all 21 holes. The core recovered was examined, and zones of interest were "split" for chemical analysis. Routine check analyses were done by an independent laboratory. All cores, including the remaining half of sample splits and sample rejects (excess after assay), have been permanently stored.

The results of the analyses of the 21 exploratory holes are attached as Appendix 8A. Included in the list are hole AEC 8 (drilled at the old ORNL site) and 17 holes for which information is available for release either by permission of the mining company involved or because the lease or permit on which the hole was drilled has expired.

Calculation of Potash Resource Distribution, Volume and Grade. As previously stated, calculation of the in-place volume and grade was undertaken by the Roswell office of the Conservation Division of the USGS. Technical assistance was also provided by the Special Projects Branch of the USGS.

There are 61 exploratory holes in the 8 x 8 mile land block shown in Figure 8-1. Ore intercept information was available to the USGS on all

of these holes. Thus, while their calculations used all available data,
some specific information pertaining to 22 industry drilled holes is not
reported in Appendix 8A to protect proprietary information of individual
companies as they so requested.

The reserve calculation commenced with assigning depth intercepts to
significant mineralization within the various ore zones. There are 11
such ore zones within the McNutt member of the Salado Formation (see
Figure 4.3-3b). The next step consisted of extrapolating continuity of
individual ore zones between holes. The final step was to calculate the
volume and grade for continuous blocks of mineralization. In addition,
the Conservation Division utilized criteria they have established for
classifying resources as either measured, indicated, unevaluated, or
barren. The criteria are:

Measured potash reserves - Tonnage is computed from dimensions
revealed in workings and drill holes. The grade is computed from
the results of detailed sampling and analyses. A minimum of three
data points in any one ore zone meeting quality and thickness
standards, no more than 1 1/2 miles (2.4 km) apart, have been used
to delineate measured reserves.

Indicated potash reserves - Tonnage and grade are computed partly
from specific measurements, samples, or production data and partly
from projection for a reasonable distance on geologic evidence. The
sites available for inspection, measurement, and sampling are too
widely or inappropriately spaced to permit the mineral bodies to be
outlined completely or the grade established throughout.

Unevaluated potash areas - Tonnage and grade have not been computed
due to low density drilling and sampling, but are surrounded by
measured and (or) indicated reserves.

Barren and/or minor potash mineralization areas - Subeconomic
resources that would require a substantially higher market value or
a major cost-reducing technology for economical production.

Subeconomic resources also include other bittern minerals not presently being recovered.

Potash resources were then quantified at three minimum grade and thickness levels. Standard conditions for each class are shown in Table 8.6.

The intermediate conditions, termed "lease", conform with established policy of the Department of Interior that any area known to contain potash mineralization meeting or exceeding that standard and located on Federal land can be acquired only through competitive bid. The standard is based on judgment along with recognition that ores as low as these grades have been successfully treated from time to time at one or more of the potash refineries in the Carlsbad district. The conditions termed "high" are roughly equivalent to the grade of langbeinite and sylvite ores currently being mined in the district.

Results of the USGS Resource Estimate. The essential results of the USGS resource calculations are best shown by three consecutive maps (Figures 8-2, 3 and 4) which commence with the lowest resource grade standards and progress to the highest. For simplicity, measured and indicated resources were combined. The majority of the resource meets the criteria for "measured" because the entire WIPP site has been drilled on one mile centers. The resource maps do not segregate the several mineralized ore zones, and at times they are "stacked", e.g. the 4th and 10th may be mineralized in the same area in plan even though they are stratigraphically separated by about 180 feet.

Most of the WIPP site area is underlain by potash resources that meet the low standards. No significant planimetric change occurs on raising the standard to lease grades. However, at the high standard, which is roughly equivalent to the current standard of producing mines, the WIPP is nearly clear of potash deposits of interest (particularly Zones I-III). Mining operations may be allowed in Zone IV, the outer boundary of the WIPP site, under controlled conditions.

As grade standards are increased, the potash resources reduce, at more rapid rate on a mass weight basis than on a planimetric basis. Table 8-7 lists the tonnage of by ore zone, type, and location by Zone boundaries within the WIPP site.

For ease in interpretation, the data in Table 8-7 has been charted on Figures 8-5 and 8-6 for langbeinite and sylvite resources, respectively. The USGS recognized the 4th ore zone (langbeinite) and the 10th (mainly sylvite) as the two major mineralized ore zones in the WIPP site area (John et al., 1977). At lease grade, the 4th ore zone contains 115.4 million tons of langbeinite resource, of which only 24 million tons (21%) lies inside the outer boundary of Zone III. At the higher grade (8% K_2O as langbeinite) the tonnage under the WIPP reduces to 59 million tons, of which only 14.6 million tons (25%) lies inside the outer boundary of Zone III.

The 10th ore zone contains mostly sylvite, but a mixed assemblage containing both langbeinite and sylvite exists on the east side of the withdrawal area. At present only one operator in the Carlsbad district has a refinery capable of handling such ores. This operator is the leaseholder over part of this mixed ore zone. However, the langbeinite in the 10th ore zone would be difficult to beneficiate according to the USBM study (USBM, 1977, p.103). Therefore, the 10th ore zone is considered to be viable only for its sylvite content. With this restriction, the 10th ore zone contains 53.5 million tons of ore at lease standard under the entire WIPP site, of which 30.4 million tons (57%) are located within the outer boundary of Zone III. At the high standard, the total tonnage reduces to 38.8 million tons, of which only 9.8 million tons (25%) are inside Zone III.

Results of the USBM Valuation of Potash Resources. The USBM has performed an economic assessment of the potash resources that were defined by the USGS. The USBM study included beneficiation testing to determine the amenability of the various mineral assemblages to refining into marketable products. The USBM engineers visited most of the mines in the district to gather data concerning mining and refining techniques, power consumption, water use, etc. Then, knowing the location and grade

of potash deposits in the WIPP site area, they devised conceptual designs of various mining and processing facilities that would provide both the highest profit and efficient recovery of marketable products from the potash deposits. The approach followed what private industry would do in an evaluation of a potash prospect. No restriction was placed as to where physical mining could be done, or problems related to land acquisition or permitting. Resources adjacent to the WIPP site were considered in the mine development plans. In all, the USBM conceived 12 different conceptual plans for exploiting potash in this area. Each plan, called a mining unit, was evaluated leading to a conclusion that 8 were worthy of full cost analysis. The full findings have been reported by the USBM (1977).

The USBM concluded that only one mining unit (Unit B-1) could be considered economic under existing market conditions and technology (see Table 8.8).

Unit A-1 almost meets the economic requirement of 15% rate of return on invested capital set by the USBM. To make it viable one needs a price of $52.04 per ton of muriate without any increase in production costs. Muriate is currently selling at $43.40 for standard grade containing 62% K_2O (Source: July 1978 issue of Engineering and Mining Journal); however, the price for muriate has exceeded $60 per ton in the past.

Data within the USBM report indicate that the langbeinite resources associated with the Unit B-1 that lie within the boundary of WIPP amount to 48.46 million tons, of which only 13.33 million tons (27.5%) lie inside the outer boundary of Zone III. For Unit A-1 the corresponding numbers are 27.41 million and 0.9 million tons.

Summary of Conclusions Concerning Potash Resources in the WIPP Site. The site contains economically mineable reserves of langbeinite and possibly sylvite. If total rights withdrawal is a requirement to satisfy waste isolation, then the relevant quantities of potash resources are much greater than if mining is allowed in the Zone IV, the outer buffer zone. The relevant quantities are presented in Table 8-9.

The USGS has estimated that potash resources in southeast New Mexico
(excluding the WIPP site) that meet lease standards are on the order of
5000 million tons of combined sylvite and langbeinite ores. Therefore,
total withdrawal of potash lease rights at the WIPP site would account
for about 7% of those resources; withdrawal of Zone I, II, and III rights
would account for about 2%. No data are available for the Carlsbad
potash district regarding what percentage of these resources would meet
the standards deemed by the USBM to be mineable under today's
conditions. In addition, the principal potash resource at the WIPP site
consists of langbeinite. No estimates, either by USGS or USBM standards,
are available for this ore alone. The Carlsbad district is the only area
mining langbeinite in the free world. Langbeinite equivalent is produced
in quantity, however, by combining sulfates of potassium and magnesium
obtained from brine lakes. When the site was initially selected, most of
the WIPP lay outside the Known Potash Area, however the 21 hole drilling
program conducted as part of the WIPP potash evaluation resulted in
discoveries sufficient to warrant expansion of that boundary (see Figure
8-1). The expansion conforms with USGS policy that potash resources
meeting the lease standard must be placed within the enclave.

8.4.8   Hydrocarbons

Method of Evaluation. The WIPP site selection criteria dictated that
deep drill holes (defined as those that penetrate through the Ochoan) be
excluded from Zones I, II, and III. The objective was to maintain a one
mile buffer between deep holes and Zone II, the zone in which waste is to
be stored. This particular criterion is restrictive, because much of the
Delaware Basin has been penetrated by wildcat test holes with an average
density of about one hole per square mile. The present site is one of
the few remaining portions of the Delaware Basin in New Mexico which will
satisfy the criterion pertaining to deep holes. The absence of extensive
drilling is due in part to the great depth (greater than 10,000 feet) to
potentially favorable gas formations. In addition, potash deposits north
and west of the site area precluded oil and gas exploration in those
directions. Federal and State regulations have set aside potash

ineralized areas to protect underground mining operations from accidental entrance of methane gas. Therefore, most of the WIPP site is untested for deep reservoirs that might contain crude oil and natural gas. The evaluation must rely on projection of surrounding subsurface geologic information into the site area. There are four petroleum test holes in Zone IV of the WIPP site. Three holes tested the Delaware sands and were unproductive. The fourth was a deep gas test (15,000 feet) that was also unproductive.

The State Bureau of Mines and Mineral Resources performed a regional evaluation of the hydrocarbon resources in southeast New Mexico which was then used to further evaluate a four township area centered on the original ORNL site (Foster, 1974). This report is useful for the current WIPP site because, as indicated in Figure 8-7, the present site is still within the area studied.

Data contained in Foster's report provide a basis for estimating total hydrocarbon resources that might underlie the site area. By using a statistical approach, Foster arrived at a possible hydrocarbon content for each potential productive zone, commencing with the "Ramsey Sand," down to the top of the Precambrian basement. The Ramsey, the first potential pay zone, is located in the upper part of the Delaware Mountain Group. The lowest zones he considered to be potentially productive were dolomitic reservoirs in the Silurian/Devonian. His estimate was based on full development of any prospective area; therefore, total resources were estimated rather than the economics associated with their extraction. His resource estimate was based on the premise that geologic conditions beneath the site were as favorable as elsewhere in the study area and that each potential zone beneath an untested section would contain a proportionate share of the statistical average of hydrocarbons for that zone. The average was derived from success ratios and a conservative estimate of primary recovery of hydrocarbons as established by past exploration, development and production.

A consulting petroleum engineering firm, Sipes, Williamson and Aycock, Inc (SW&A), was engaged by Sandia Laboratories to conduct an economic evaluation of hydrocarbons in the site area. Based on known drilling costs and market conditions, they made a judgment as to what portion and which formations under the site were worthy of testing. The basic criterion was reasonable prospect for discovery with an economic reward to the operator of at least 10% return on his investment plus full recovery of costs. The essential conclusion of the SW&A study was that the Morrow unit has a high potential for successful discovery of natural gas. All other formations present were considered too high a risk to be the objective of a prudent wildcat test. Naturally, once a Morrow well was drilled it could encounter shallower productive pay zones, but the odds of such happening were deemed too speculative to be considered in the overall economics. The full findings of this study have been reported by Keesey (1976).

Structure maps of several horizons beneath the Ochoan evaporites have been compiled from seismic surveys that were either purchased from existing surveys or conducted as part of the WIPP site study. While the main purpose of these seismic surveys has been to understand the geologic aspects of the site area, they are also valuable for interpretation of potential hydrocarbon reservoirs. These structure maps were not available to Foster for his 1974 study, but they were to SW&A during their 1976 evaluation. The seismic studies have been reported by McMillan (1976) and G. J. Long & Associates (1976). Updated structural interpretations based on later seismic studies are now available. The recent changes have had little impact on the overall hydrocarbon evaluation.

Total Hydrocarbon Resources at the WIPP Site. The New Mexico Bureau of Mines study forms the basis of the evaluation of the total hydrocarbon resources in the site area (Foster, 1974). We assume there is a reasonable probability that Foster's estimated resources could exist under the site. However, this probably represents the upper bound of exploitable hydrocarbons.

The validity of the resource estimate rests on the subsurface geology and statistical probability. The geologic setting under the Ochoan evaporites is considered to be quite typical for this portion of the Delaware Basin; therefore the chance of finding oil or gas should approximate what has been found in similar areas near the site which have been more fully tested. However, since it is a regional statistical approach, it is possible that much more or much less than the average expected resource would be found if the site was actually drilled. The hydrocarbon evaluation is not as definitive as that for potash, which was actually confirmed by exploratory drilling. This would be self-defeating in the case of the deeper hydrocarbon resources since the area was selected to avoid such deep drill holes.

Foster's evaluation (Foster, 1974) took into account the occurrence of all known oil and gas accumulations in much of southeast New Mexico (Figure 8-7). The statistical base encompassed about 42 full townships equivalent to almost 1 million acres. The reserves for each oil pool or gas reservoir were estimated from the standpoint of actual or, where possible, projected production. Areas were then classed as developed or undeveloped based on the density and depth of drilling. From these data, Foster (1974) then determined the expected resource per section of land by assuming that the success of future drilling would have the same success ratio as in the past. A coincident assumption was that, while past wildcat drilling avoided the current WIPP site, the past economic incentive for drilling was low. Also, drilling restrictions pertaining to the Known Potash Enclave have prevented drilling, particularly on the west side of the WIPP area. There were more attractive areas available throughout the basin that satisfied the availability of private venture for exploration capital. These past constraints do not enter into the hydrocarbon potential estimates because the characterization of the site must take into consideration the long-term needs for mineral resources.

Figure 8-8 is taken from Foster (1974). Formations that he considered as potentially productive are shown opposite the stratigraphic column of sedimentary rocks underlying the Ochoan evaporites. Table 8-10 then

shows the potential resource he assigned to the various specific
intervals but which were composited to more gross intervals. Further
explanation is required pertaining to "wildcat" and "acreage" assignment
of reserves.

The acreage method tests the success ratio of producing acreage versus
the acreage considered to have been tested by wildcat drilling. The
wildcat method considered a field, regardless of the number of wells in
that field, as a single discovery. A success ratio was then determined
by dividing the number of wildcat discoveries by the number of dry holes
that were drilled to that formational depth. The acreage method normally
results in a higher success ratio and, therefore, higher reserve
estimates. In-place hydrocarbon resources for each zone within the WIPP
site can be readily calculated from Foster's data by combining his
estimate of in-place hydrocarbon resources per section (640 acres) with
the known area for each zone of the WIPP site. The acreage method was
used to prepare Table 8-11.

While the quantities given in Table 8-11 may appear large, they are
brought into perspective by stating that all of the nearby region, i.e.,
the area studied by Foster, would contain 51 times the resource quantity
under the WIPP site. The factor is simply the ratio of the total area
evaluated by Foster (1512 square miles) divided by the area of the WIPP
site (29.62 square miles). In addition, if hydrocarbon development is
allowed in Zone IV, e.g., by deviated drilling, then the resource that
would be withdrawn is reduced in proportion to the excluded area, i.e.,
from 29.62 square miles down to 12.73 square miles for a 43% reduction in
restricted resources. The hydrocarbon resources remaining in Zones I,
II, and III would account for only 0.84% of the total hydrocarbon
resources Foster has estimated in the area immediately surrounding the
WIPP site.

Estimate of the Economically Recoverable Hydrocarbon Resources. Sipes,
Williamson, and Aycock, Inc. (SW&A) estimated the potentially economic
hydrocarbon resources (Keesey, 1976). Their approach was to review the

existing geologic information pertaining to the area in and around the site and then to determine if the probability of oil and gas occurrences justified the risk of drilling and completing a well. The base area studied by SW&A consisted of a 20 x 20 mile block centered on the WIPP site (Figure 8-7). All available data were evaluated on each test that had been drilled within this 400 square mile area, with particular emphasis placed on deliverability and recoverable reserves.

SW&A found that 60 wells in this area were producing oil and/or gas from reservoirs in the Delaware Mountain, Bone Spring, Wolfcamp, Strawn, Atoka and Morrow. With the exception of the Atoka and Morrow, all other zones were considered as presenting too high a risk to justify the cost of wildcat drilling. Furthermore, even though an Atoka reservoir is being produced from a well located near the southwest corner of the WIPP site, SW&A concluded that that particular reservoir is being effectively drained by the single well. Offset drilling would enhance recovery rate but not total recovery.

The Morrow was considered to be worthy of testing, because of the high success ratio of wells drilled to that formation in the area around the site. Of 26 wells drilled to sufficient depth to test the Morrow, 23 were successfully completed as gas wells. A study of these wells revealed that the projected ultimate recovery ranged from insignificant to as much as 5.20 billion cubic feet (bcf) of natural gas. From the distribution of recoveries they concluded that the average successful Morrow well would recover 2.074 bcf of gas. This is in fair agreement with Foster's estimate for Pennsylvanian gas wells; he estimated 3.2 bcf per Morrow gas well if spaced at 320 acres per well.

Drilling and completion costs were then estimated for wells drilled to the Morrow (approximately 14,000 ft.). The estimate was $1.4 million. Using discounted cash flow analysis and the expected delivery rate and current gas price ($1.42 per 1,000 cu. ft. with 4% yearly escalation) they concluded that if a well produced 0.7 bcf over its lifetime it would

recover costs. Since the average well was more than twice this production, it was apparent that drilling in the site area could be justified.

Use was then made of the structure map on a limestone reflector horizon in the Morrow based on data from seismic surveys (Figure 8-9) (Long, 1976). Tentative drilling sites were picked with weight given to the flanks of anticlines because local experience indicates that productive sand lenses would more likely occur at such localities. A total of 20 drill sites was selected (Figure 8-9). In favorable structural areas wells were placed on a spacing of 320 acres per well. This spacing is standard practice for wells of this depth in New Mexico. Depending on proximity to producing wells and structural favorability, the 20 wells were ranked as proven, probable or possible. The proven category was limited to locations that would offset producing wells in the Los Medanos field. Two locations were designated as proven, nine as probable, and nine as possible.
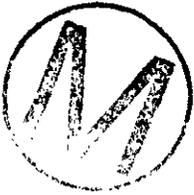
The ultimate recovery of wells was adjusted to take into account the risk factor associated with wildcat drilling. Proven wells were assigned production of 2.07 bcf, probable wells 1.64 bcf, and possible wells 1.33 bcf per well for the southwest quadrant of the WIPP site. The estimated reserves for locations in other parts were placed at 2.09 bcf for probable and 1.67 bcf for possible reserves. No locations could be considered as proven. The higher reserves assigned to these locations were considered justifiable because shallower pay zones may be discovered on the way down to the Morrow. This calculation yielded a total reserve of 36.85 bcf of natural gas under the WIPP site (Table 8-12). Some distillate would accompany this gas production. Foster (1974) estimated that Pennsylvanian gas is accompanied by 14,950 barrels of distillate per bcf of natural gas produced. Therefore, the 36.85 bcf of reserve under the site should be expected to be accompanied by 550,900 bbl distillate.

Of the 20 drilling sites selected, 7 lie in Zone IV, 2 of which are ranked as proven, 4 as probable, and 1 as possible. The aggregate

reserve of these 7 wells is 13.38 bcf of natural gas and 200,000 bbl of distillate. If drilling is allowed into Zone IV these hypothetical reserves could be recovered. The net balance that would be non-recoverable because of restrictions on drilling in Zones I, II, and III is 23.47 bcf of natural gas and 350,000 bbl of distillate.

Summary of Conclusion Concerning Hydrocarbon Resources. Table 8-13 summarizes the findings of the New Mexico Bureau of Mines resource study and the SW&A economic evaluation of the part of those resources considered attractive enough to be developed by the petroleum industry at 1977 prices and drilling costs.

The hydrocarbon resources remaining under the WIPP, if Zone IV is developed, amount to about 0.84% of that projected by Foster for the vicinity of the WIPP site. The total economic reserve, including Zone IV, amounts to approximately 90 days production of dry gas from southeast New Mexico.

8.4.9   Metalliferous Deposits in the Precambrian

Even the deepest oil/gas test near the WIPP site has not penetrated deep enough to encounter the Precambrian basement. A regional survey of test holes has been done by Foster and Stipp (1961). The basement may consist of slightly metamorphosed rhyolites and tuffs known as the Panhandle Volcanic Complex (Flawn, 1954). Such rocks hold potential for sulfide deposits. Geophysical techniques (induced polarization or electromagnetics) have a detection capability scarcely exceeding 1000 feet, while the Precambrian is at median depth of 18,000 feet beneath ground level at the WIPP site. No evaluation, therefore, is feasible for sulfide deposits. The depth is greater by a factor of almost two over the deepest mines in the world. Therefore, resources in the basement rocks, should they exist, are not likely to be attractive targets for exploitation.

8.5 SUMMARY

Potassium salts and fluid hydrocarbons are the only two resources thought
to be economically significant in the WIPP site area. The depth, volume
and richness of the deposits are the principal factors which will
determine when and if they might be exploited by a free-enterprise
system. Such economic evaluation has been conducted and reported in the
WIPP Environmental Impact Statement. Because economic aspects change,
they are not so relevant to site characterization as they are to
assessing the impacts of constructing the WIPP facility. Hence, in this
chapter, amounts and types of resources will be discussed rather than
their present economic value. The principal findings of resource studies
are summarized in Table 8-1.

If reasonable technologic and economic restraints are considered for
extracting, processing and marketing the resources then both the amounts
and types of exploitable deposits are greatly reduced. Only potash and
natural gas are considered to be significant in this respect (see Table
8.2). Even these reduced quantities should be considered as upper
estimates because of these assumptions: 1) complete mineral lease
ownership by a single company and 2) no conflict between the simultaneous
development of the shallow potash deposits and the deep gas reservoirs.

Economic resources are further reduced by allowing the mining of potash
and recovery of oil and gas by deviated drilling in Zone IV, the outer
buffer zone. If this is the case, then economic resources lying in the
inner zones are limited to those given in Table 8-3.

Caliche, salt, and gypsum are also present, but the abundance of these
minerals throughout the region leads to the conclusion that land
withdrawal for the WIPP will have little effect on present or future
requirements for them. Consideration was also given to the possible
presence of uranium in redbed-type sediments that overlie the
evaporites. The conclusion is that no significant uranium deposit
exists. Lithium occurs in a brine reservoir within the Castile Formation

northeast of the present site and may be present in a similar reservoir
to the southwest. However, care has been taken to avoid such brine
reservoirs within the site area. Consideration was also given to the
possible existence of metalliferous deposits in the Precambrian basement
under the site. However, the depth (about 18,000 feet below the ground
surface) to Precambrian rocks would preclude mining even if mineral
concentrations were present. No geologic or geophysical evidence exists
to suggest that deposits are any more likely in the basement rock of the
WIPP area than elsewhere in the region.

8.6 REFERENCES

Flawn, P. T., 1954, Summary of Southeast New Mexico Basement Rocks: Guidebook of Fifth Field Conference, New Mexico Geological Society, p 114-116.

Foster, R. W., 1974, Oil and Gas Potential of a Proposed Site for the Disposal of High-Level Radioactive Waste: Open-file report, New Mexico Bureau of Mines and Mineral Resources (work done under Contract No. AF(40-1)-4423 to ORNL).

Foster, R. W. and Stipp, T. F., 1961, Preliminary Geologic and Relief Map of the Precambrian Rocks of New Mexico: New Mexico Bureau of Mines and Mineral Resources, Circular 57.

Griswold, G. B., 1977, Site Selection and Evaluation Studies of The Waste Isolation Pilot Plant (WIPP), Los Medanos, Eddy County, New Mexico: SAND77-0946, Sandia Laboratories.

John, C. B., Cheeseman, R. J., Lorenz, J. C. and Millgate, M. L., 1978, Potash Ore Reserves in the Proposed Waste Isolation Pilot Plant Area, Eddy County, New Mexico: U. S. Geol. Surv. Open-file report 78-828.

Jones, C.L., 1978, Test Drilling for Potash Resources: Waste Isolation Pilot Plant Site, Eddy County, New Mexico: U.S. Geol. Surv. Open-file report 78-592.

Keesey, J. J., 1976, Hydrocarbon Evaluation Proposed Southeastern New Mexico Radioactive Material Storage Site, Eddy County, New Mexico: Sipes, Williamson and Aycock, Inc., Vols. I and II.

G. J. Long and Associates, Inc., 1976, Interpretation of Geophysical Data, Los Medanos and Vicinity: Report to Sandia Laboratories.

McMillan, C., 1976, Los Medanos Area: Permian Exploration Co., Report to Sandia Laboratories.

Siemers, W. T., Hawley, J. W., Rautman, C., and Austin, G., 1978, Evaluation of the Mineral Potential (excluding hydrocarbons, potash and water) of the Waste Isolation Pilot Plant Site, Eddy County, New Mexico: New Mexico Bureau of Mines and Mineral Resources, Report to Sandia Laboratories.

U. S. Bureau of Mines, 1977, Valuation of Potash Occurrences Within the Waste Isolation Pilot Plant Site in Southeastern New Mexico: Prepared for the ERDA.

LEGEND

○ Potash drill holes

⊗ ERDA potash drill holes

☐ Federal surface and mineral rights

▨ State surface and mineral rights

▨ Private surface and mineral rights

☐ Potash Enclave Boundary Extension, July, 1977

▨ Private surface, all mineral rights owned by Federal Government

▨ Private surface and mineral rights, except oil and gas federally owned

SCALE IN MILES

0   1/2   1   2   3

—N—

- - - - Proposed WIPP site outline

- - - - Zone boundaries and areas provided by ERDA

FIGURE 8-1

LOCATION OF POTASH EXPLORATION DRILL HOLES
IN THE VICINITY OF WIPP SITE

LEGEND

— — — Proposed WIPP site outline

— — — Zone boundaries and areas provided by ERDA

Measured and indicated mineralization

Measured and indicated mineralization are at a cut off
of 3% K_2O as langbeinite or 8.0% K_2O as sylvite
or equivalent grade of mixed langbeinite-sylvite
occurring in a minimum 4-foot interval

0   1/2   1   2   3

SCALE IN MILES

— N —
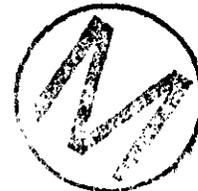
FIGURE 8-2   LOW STANDARD POTASH RESOURCES

FIGURE 8-3 LEASE STANDARD POTASH RESOURCES
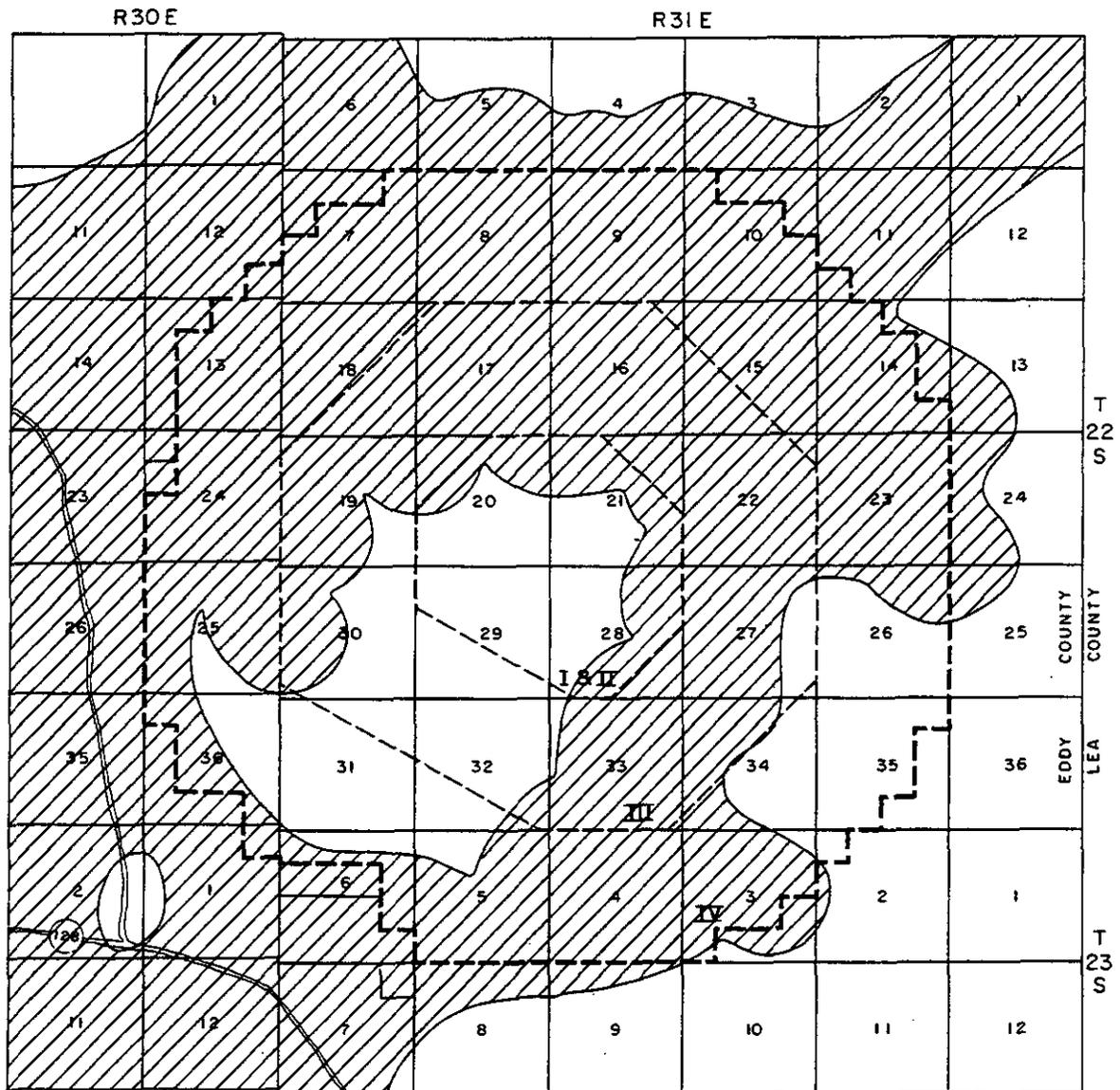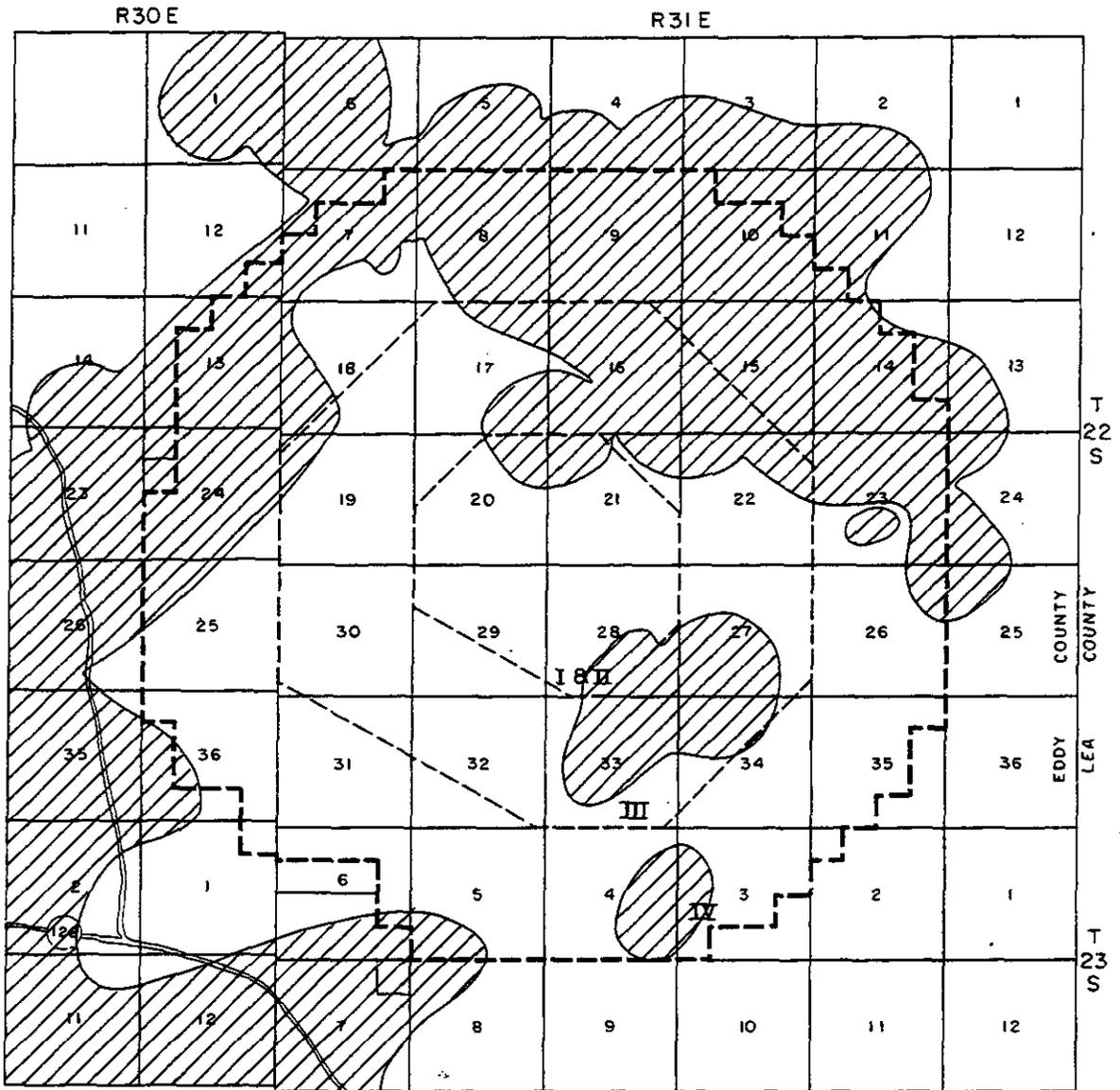
Data provided by USGS Conservation
Division and ERDA
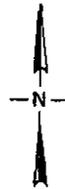
SCALE IN MILES

LEGEND

— — —   Proposed WIPP site outline

— — —   Zone boundaries and areas provided by ERDA

Measured and indicated mineralization

Measured and indicated mineralization are at a cutoff
of 8% K_2O as langbeinite or 14.0% K_2O as sylvite
or equivalent grade of mixed langbeinite-sylvite
occurring in a minimum 4-foot interval

FIGURE 8-4   HIGH STANDARD POTASH RESOURCES

MILLION TONS

350

300

200

.100

0

3   4   5   6   7   8   9   10

ALL LANGBEINITE ALL ZONES ORES

4th ORE BED ALL ZONES ORES

ALL LANGBEINITE ZONES I+II+III

4th ORE BED ZONES I+II+III
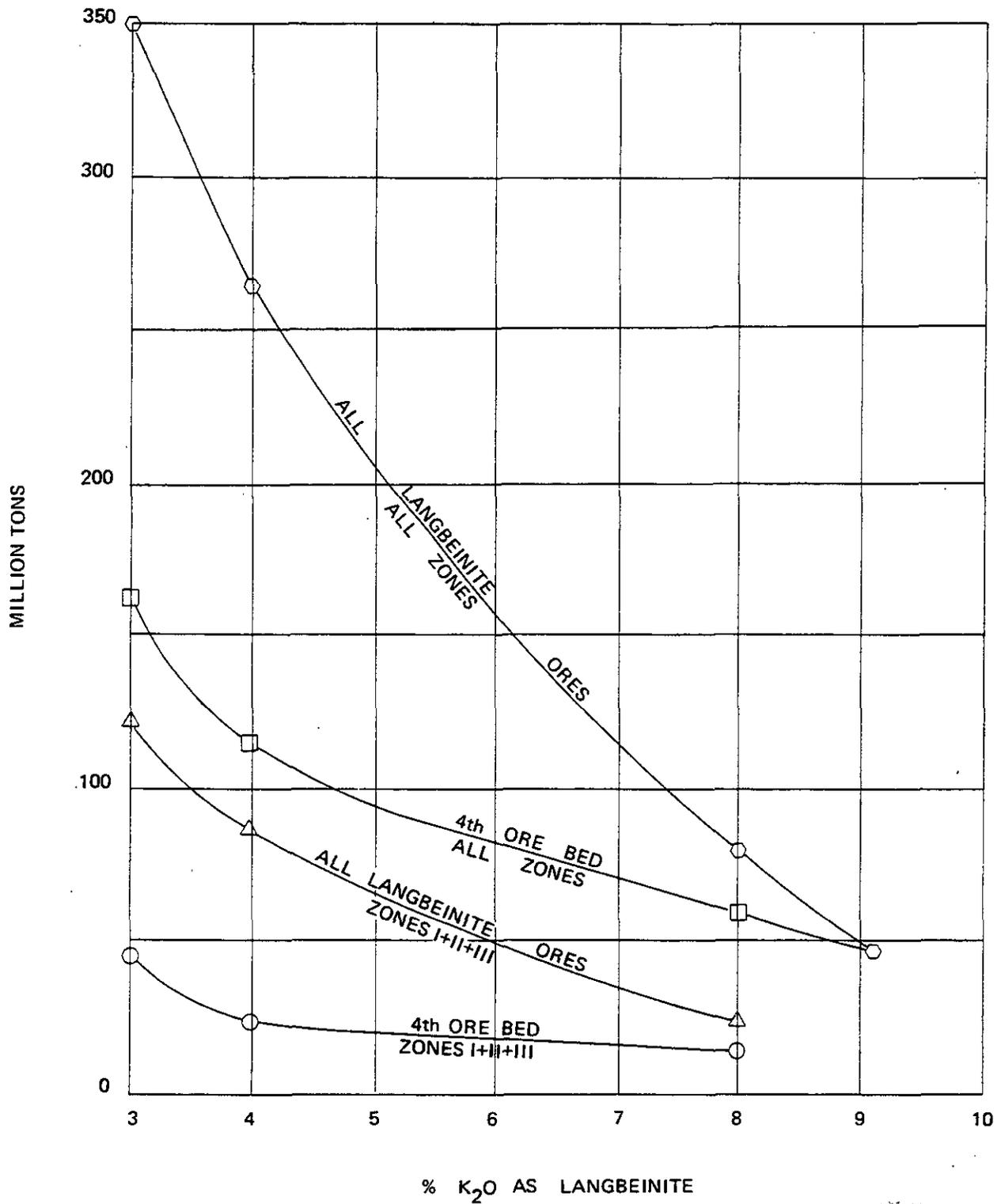
% K₂O AS LANGBEINITE

FIGURE 8-5.   LANGBEINITE RESOURCES
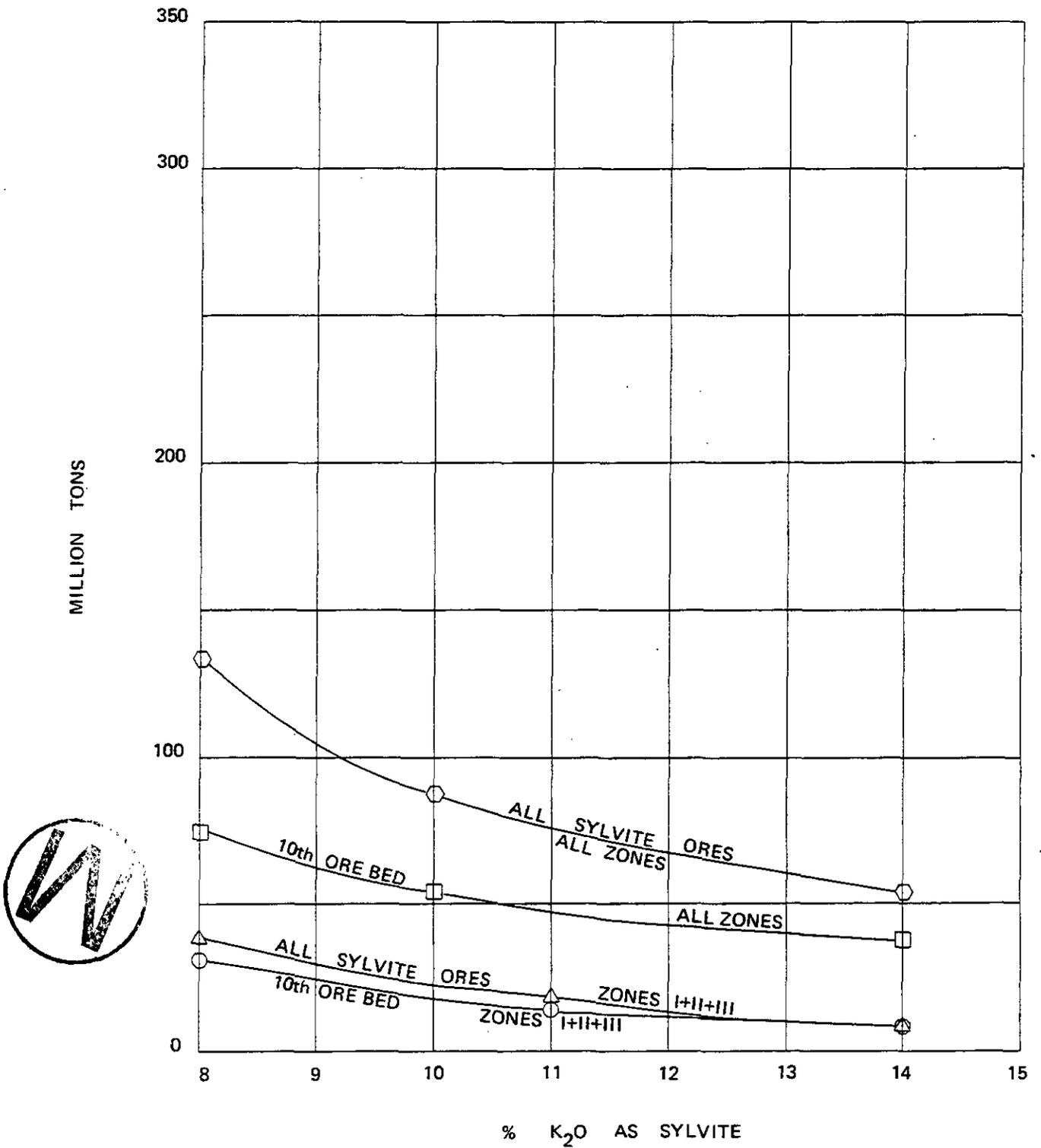
FIGURE 8-6. SYLVITE RESOURCES
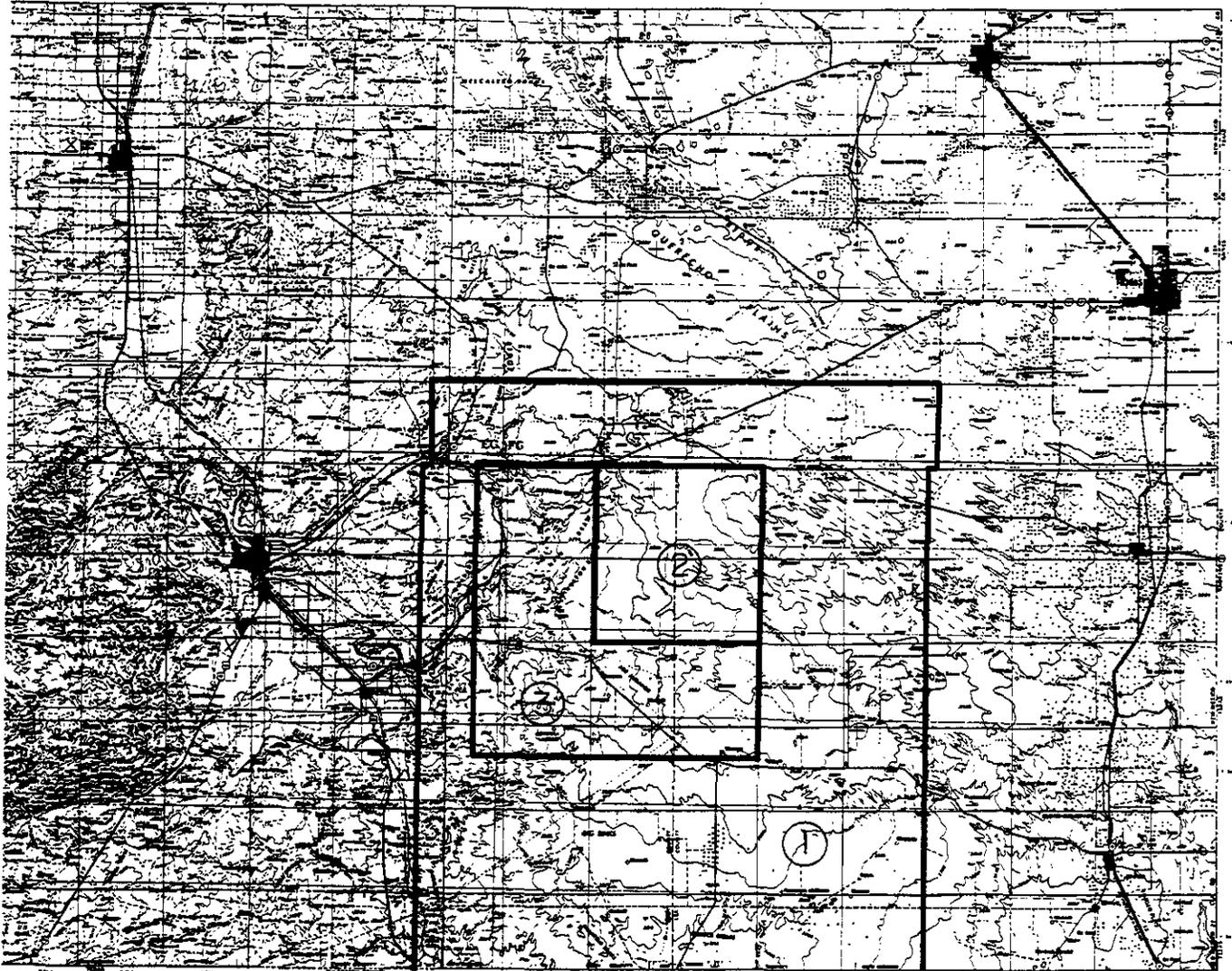
(1)   NEW MEXICO BUREAU OF MINES STUDY AREA

(2)   NEW MEXICO BUREAU OF MINES DETAILED STUDY CENTERED ON OLD ORNL SITE

(3)   SIPES, WILLIAMSON AND AYCOCK STUDY AREA CENTERED ON WIPP SITE

FIGURE 8-7

LOCATION OF HYDROCARBON RESOURCE STUDY AREAS

Elev. | Depth

3,000 — ⌇⌇⌇⌇⌇

Ochoan
Triassic &
Younger

4,000 —

-750 — — — — Ramsey Sand
Bell
Canyon

5,000 —

-2,000 — — — — Cherry
Canyon

6,000 —

Delaware Mountain Group
(2,900'-4,000')

-3,150 — — — —

7,000 — Brushy
Canyon

8,000 —

-4,750 — — — —

9,000 —

Bone
Spring
(2,900'-3,500')

10,000 —

11,000 —

-7,650 — — — —

Wolfcamp
(1,000'-1,500')

12,000 —

Permian

-9,100 — — — —

13,000 — Strawn

-9,700 — — —

Atoka

-10,200 — — —

14,000 — Morrow

Penn.
(1,800'-2,100')

-10,950 — — — Barnett
-11,100 — — — Mississippian
15,000 — Limestone
-11,600 — — — Woodford
-11,800 — — —

Miss.
(550')(750')

Silurian-
Devonian
Carbonate

16,000 —

Silurian-
Devonian
(1,250'-1,700')

-13,050 — — —

Montoya

17,000 —

-13,500 — — —

Simpson

-13,900 — — —

Ellenburger

-14,250 — — —

Ordo-
vician
(1,000'-1,4000')

18,000 — Precambrian

■ Potential pay zones.

┌ 5,000 ft.

├ 4,000

├ 3,000

├ 2,000

├ 1,000

├ 500

└ 0

FIGURE 8-8.   GEOLOGIC COLUMN AND POTENTIAL HYDROCARBON
RESERVOIRS (ADAPTED FROM FOSTER, 1974)
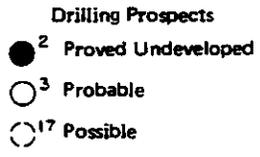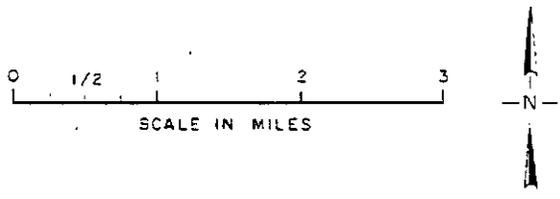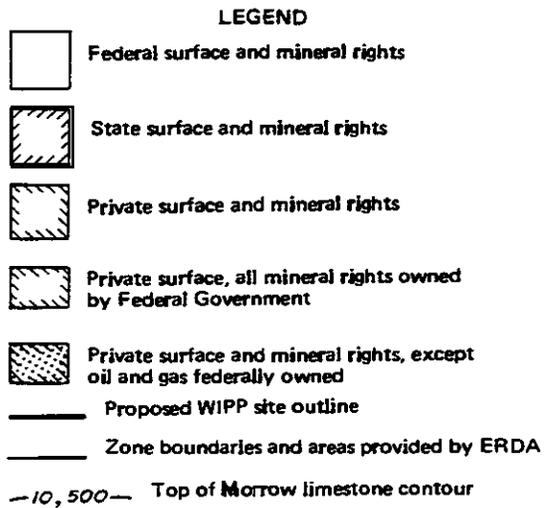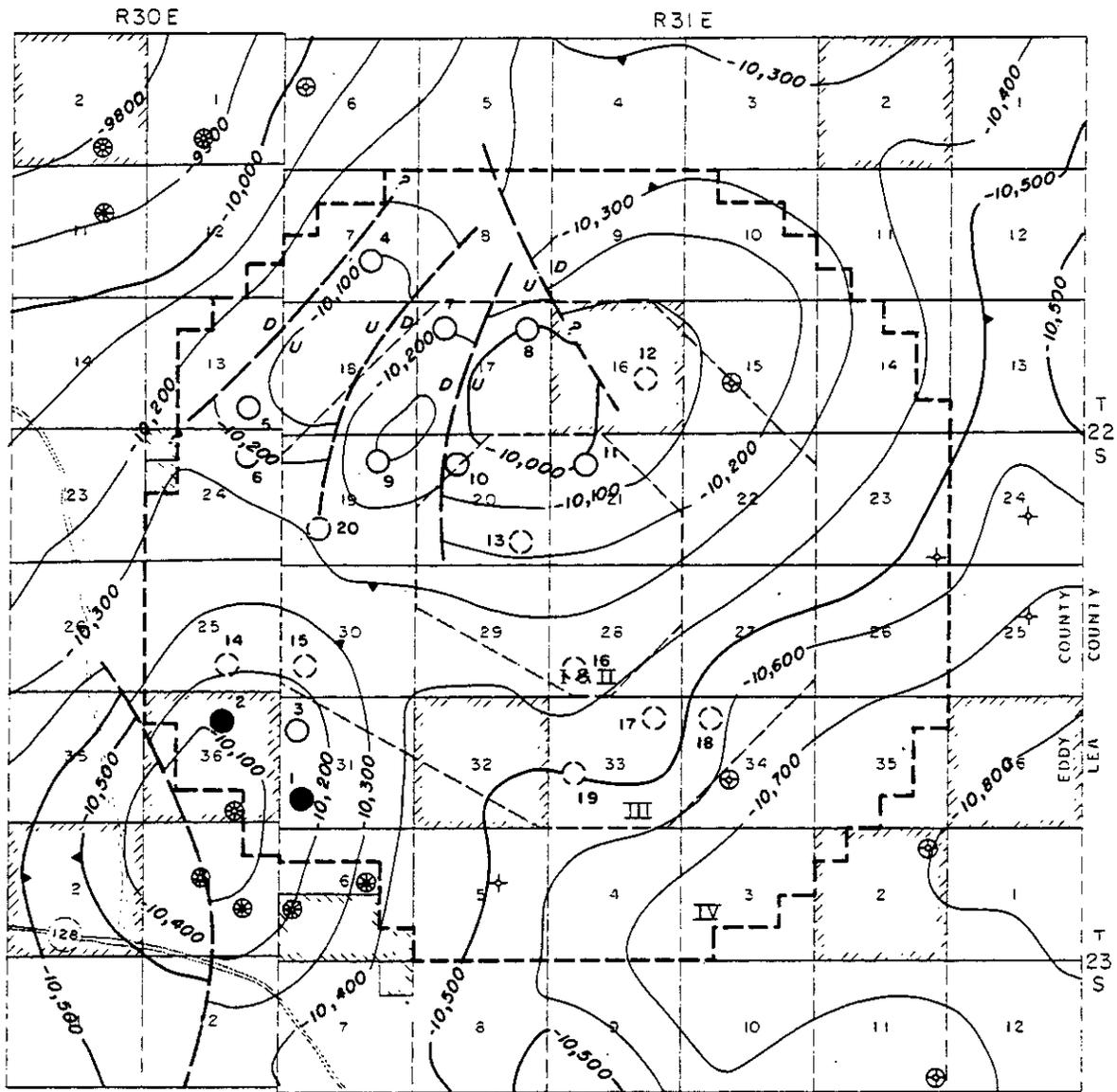
FIGURE 8-9

HYPOTHETICAL DRILLING SITES TO DEVELOP
POTENTIAL MORROW GAS RESERVOIRS
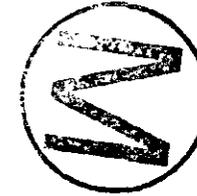
TABLE 8-1

TOTAL ESTIMATED RESOURCES AT WIPP SITE

Resource	Quantity	Depth	Richness
Caliche	185×10^6 tons	at surface	21-69% Insol.
Gypsum	1.3×10^9 tons	300-1,500 feet	Pure to mixed
Salt	198×10^9 tons	500-4,000 feet	Pure to mixed
Sylvite	88.5×10^6 tons	1600 feet	11.8 K_2O
Langbeinite	264.8×10^6 tons	1800 feet	6.10 K_2O
Crude Oil	37.7×10^6 bbls	4,000-20,000 feet	31-46° API
Natural Gas	490×10^9 cu. ft.	4,000-20,000 feet	1100 BTU/cu ft
Distillate	5.72×10^6 bbls	4,000-20,000 feet	53-56° API

)
)
)

TABLE 8-2

POTENTIAL ECONOMIC RESOURCES AT WIPP SITE

Resource	Quantity	Depth	Richness
Sylvite	27.43×10^6 tons	1,600 feet	13.33% K_2O
Langbeinite	48.46×10^6 tons	1,800 feet	9.11% K_2O
Natural Gas	36.85×10^9 cu ft	14,000 feet	1,100 BTU/cu ft
Distillate	0.55×10^6 bbls	14,000 feet	53° API

TABLE 8-3

ECONOMIC RESOURCES WITHIN ZONE I, II AND III AT WIPP SITE

Resource	Quality	Depth	Richness
Langbeinite	10×10^6 tons	1,800 feet	10% K_2O
Natural Gas	20×10^9 cu ft	14,000 feet	1,100 BTU/cu ft
Distillate	132×10^3 bbls	14,000 feet	53° API

TABLE 8-4

ORGANIZATIONS RESPONSIBLE FOR RESOURCE EVALUATION AND
KEY REPORTS CONCERNING RESOURCES

Organization	Responsibility	Reports
U.S. Geol Surv.	Potash Resources as related to ore grade and volume	John et al. (1978) Jones (1978)
U.S. Bur. of Mines	Determination as to what extent the potash resources reported by U.S.G.S could be economically mined and refined under today's technology and market	USBM (1977)
N.M. Bur. of Mines	Definition of resources and economics for caliche, salt, gypsum, brine, sulfur and uranium	Siemers et al. (1978)
N.M. Bur. of Mines	Oil and gas resources of a four township area which includes the WIPP site	Foster (1974)
Sipes, Williams and Aycock, Inc.	Determination of the economic viability of hydrocarbons under the WIPP site	Keesey (1976)
G.J. Long & Assoc. Inc., Permain Exploration Co.	Intrepretation of structure of Paleozoic sediments beneath Ochoan evaporites. These studies were useful in evaluation of hydrocarbons	Long (1976), McMillan (1976)
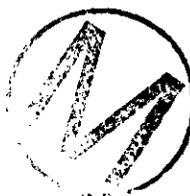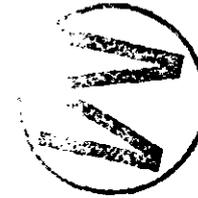
Table 8-5

POTENTIAL RESOURCES CORRELATED WITH STRATIGRAPHY

Formation	Thickness(ft)	General Character	Potential Resources	Evaluation
Mescalero Sand	0-15	Dune sand, fine grained	None	No resource
Caliche	0-5	Limestone, chalky	Caliche (in road construction)	Caliche is abundant throughout the area
Gatuna	0-375	Sandstone and siltstone	Uranium	Conditions apparently were oxidizing during deposition, and no uranium is apt to occur in the vicinity
Santa Rosa Sandstone		Sandstone	Uranium	Conditions apparently were oxidizing during deposition, and no uranium is apt to occur in this vicinity
Dewey Lake	487	Siltstone and sandstone some claystone	Uranium	Minor occurrences have been reported outside the WIPP site area. Gamma ray logs of 36 holes drilled within the site area showed no anomalies.
Rustler	310	Anhydrite and rock salt with subordinate dolomite, sandstone, claystone and polyhalite	Gypsum and salt	Abundant throughout the area, no advantage for site resources.
Salado	1976	Rock salt with subordinate anhydrite, polyhalite, potassium ores sandstone, and magnesite	Potassium salts, salt and gypsum	Langbeinite and sylvite occur in commercial quantities

)   )   )

Table 8-_ (Continued)

Formation	Thickness(ft)	General Character	Potential Resources	Evaluation
Castile	1400	Anhydrite and rock salt with subordinate limestone	Sulfur, salt, lithium in brine reservoirs	Salt is abundant throughout the area. Lithium concentration in brine is subeconomic today. Care has been taken to exclude brine reservoirs from site. Conditions and structures for sulfur deposits not known to exist at site.
Delaware Mtn. Group	3800	Fine grained sandstone (possibly a siltstone), shale, limestone, and dolomite	Oil and associated gas. Most favorable zone is the Ramsey sand	Reservoirs may exist, but small in comparison with the Morrow Formation
Bone Spring	3400	Limestone, fine-grained sandstone, and black shale	Oil and associated gas	Reservoirs may exist, but are small in comparison to the Morrow Formation
Wolfcamp (Hueco)	1480	Limestone, black shale, red or green shale, sandstone, and conglomerate	Oil and gas	Reservoirs may exist, but are small in comparison to the Morrow Formation
Strawn	300	Limestone, oolitic limestone and gray to black shale	Oil and associated gas	Reservoirs may exist, but are small in comparison to the Morrow Formation
Atoka	640	Limestone, oolitic limestone and gray to black shale	Natural gas	Commercial gas is being produced from near site. Atoka reservoirs are restricted in size, therefore, small likelihood of existence under the site
Morrow	1300	Limestone, oolitic limestone, gray to black shale, and sandstone	Natural	Commercial quantities of gas probably exist
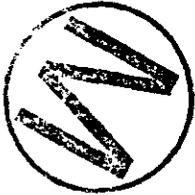
Table 8-5 (Continued)

Formation	Thickness(ft)	General Character	Potential Resources	Evaluation
Mississippian	740	Black, angillaceous shale, black calcareous shale or shaly limestone, some sandstone	None	None likely
Siluro Ordovician	2100	Limestone, dolomite, chert, shale, black shale with rounded quartz grain inclusions, and small amounts of sandstone	Oil and gas. Most favorable zone is beneath the Woodford Shale	Oil and gas may be present in anticlinal situations
Precambrian		Not tested with in the WIPP site locality. Regional inference is that it consists of acidic volcanics or metasediments	Sulfide deposits	Considered too deep to exploit.

References: Siemers et al., 1978; Foster, 1974.

)   )   )
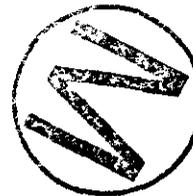
TABLE 8-6
STANDARD CONDITIONS FOR POTASH RESOURCES

Class	Type Ore	% K_2O	Thickness, ft
Low	Langbeinite	3	4
	Sylvite	8	4
Lease	Langbeinite	4	4
	Sylvite	10	4
High	Langbeinite	8	4
	Sylvite	14	4

Reference: John et al, 1978.
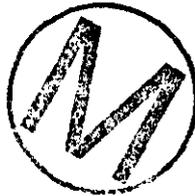
Table 8-7

POTASH RESOURCES, TONS x 10^6

I. Sylvite Ores

Ore Zone	Low Grade			Lease Grade			High Grade		
	I+II+III	IV	Total	I+II+III	IV	Total	I+II+III	IV	Total
10	30.4	44.4	74.8	16.5	37.2	53.7	9.8	28.9	38.7
9	3.7	6.6	10.3	1.2	4.8	6.0	--	0.7	0.7
8	5.0	43.1	48.1	1.0	27.8	28.8	--	13.7	13.7
Total	39.1	94.1	133.2	18.7	69.8	88.5	9.8	43.3	53.1

II. Langbeinite Ores

Ore Zone	Low Grade			Lease Grade			High Grade		
	I+II+III	IV	Total	I+II+III	IV	Total	I+II+III	IV	Total
10	25.0	30.6	55.6	24.6	24.8	49.4	9.7	0.9	8.8
5	11.6	14.6	26.2	10.9	13.3	24.2	--	1.6	1.6
4	46.5	114.5	161.0	24.0	91.4	115.4	14.6	44.4	59.0
3	14.6	19.9	34.5	9.6	16.0	25.6	--	--	--
2	24.2	49.5	73.7	18.7	31.5	50.2	1.9	7.9	9.8
Total	121.9	229.1	351.0	87.8	177.0	264.8	24.4	54.8	79.2

III. All Ores

Ore Zone	Low Grade			Lease Grade			High Grade		
	I+II+III	IV	Total	I+II+III	IV	Total	I+II+III	IV	Total
10	55.4	75.0	130.4	41.1	62.0	103.1	17.7	29.8	47.5
9	3.7	6.6	10.3	1.2	4.8	6.0	--	0.7	0.7
8	5.0	43.1	48.1	1.0	27.8	28.8	--	13.7	13.7
5	11.6	14.6	26.2	10.9	13.3	24.2	--	1.6	1.6
4	46.5	114.5	161.0	24.0	91.4	115.4	14.6	44.4	59.0
3	14.6	19.9	34.5	9.6	16.0	25.6	--	--	--
2	24.2	49.5	73.7	18.7	31.5	50.2	1.9	7.9	9.8
Total	161.0	323.2	484.2	106.5	246.8	353.3	34.2	98.1	132.3

Reference: John et al., 1978.

Table 8-8

ECONOMIC POTASH RESOURCES, TONS x 10^6

Mining Unit	Products	Recoverable Ore in Mining Unit	Recoverable Ore in WIPP Site	Percent in Zones I,II,III	Price[1] that Provides a 15 Percent ROR[2], $
B-1	Langbeinite	79.78	48.46	27.5	35.00
	Sulphate			27.5	88.50
A-1	Muriate	57.60	27.41	3.2	52.04
D-2	Langbeinite	87.93	23.57	0.7	36.51
	Sulphate			0.7	92.31
A-2	Muriate	98.32	51.80	7.6	61.73
C-2	Muriate	57.19	36.49	54.2	61.74
D-3	Langbeinite	140.27	42.45	23.5	42.26
	Sulphate			23.5	106.86
C-3	Muriate	70.64	52.87	57.5	67.52
A-3	Muriate	135.02	73.77	14.9	70.28

[1]Market price assuming no increase in production costs. Estimated weighted average annual price per ton of product, f.o.b., Carlsbad, New Mexico, used for evaluation.

[2]Rate of return

Reference: U.S. Bureau of Mines, 1977.

Table 8-9

SUMMARY OF POTASH RESOURCES, 10^6 TONS

| | In Place Resources (USGS Study) | | | | Mineable Today (USBM Study) | |
| | Lease Standard | | High Standard | | | |
	Langbeinite	Sylvite	Langbeinite	Sylvite	Langbeinite	Sylvite
Total Withdrawal	264.8	88.5	79.2	53.1	48.46	27.41*
Mining Permitted in Zone IV	87.8	18.7	24.4	9.8	13.35	0.9

*The USBM does not consider the sylvite contained in Unit A-1 to be mineable under today's market. To do so would require the price for muriate to be $52.04 per ton, or the investor must be willing to accept a rate of return less than 15%.
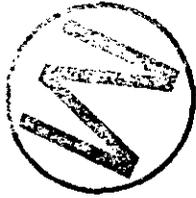
Table 8-10

POTENTIAL HYDROCARBON RESOURCES
EXPECTED IN VARIOUS FORMATIONS WITHIN THE DELAWARE BASIN

Stratigraphic Unit	Rating Geological Oil	Gas	Statistical Oil	Gas	P.O.F.	Oil (bbls)	Acreage Assoc. Gas (MCF)	Dist. (bbls)	Gas (MFC)	Oil (bbls)	Wildcat Assoc. Gas (MFC)	Dist. (bbls)	Gas (MCF)	Adjusted Rating Oil	Gas
Ramsey	IV		V		62	472,350	756,324			75,052	120,141			IV	
Delaware Mtn. Gp.	II		II		21	51,686	19,546			34,462	13,029			II	
Bone Spring	III		IV		39	193,952	379,738			88,170	172,610			III	
Wolfcamp	III	III	II	II	23	20,800	228,462	32,544	633,984	20,475	224,953	19,530	383,969	III	III
Pennsylvania	III	V	III	V	88	265,455				299,788	1,784,799	94,596	6,441,672	IV	IV
Mississippian	I	I	I	I	14										
Silurian/ Devonian	III	III	IV	IV	72	1,368,330	656,676	36,720	4,244,310	343,422	164,804	36,562	4,225,491	I	IV
Ordovician	I	II	I	III	63										

Production Estimate Section (640 Acres)

Table 8-10 (Continued)

Adjusted Production Estimate Section (640 Acres)

Stratigraphic Unit	Oil (bbls)	Assoc. Gas (MCF)	Dist. (bbls)	Gas (MFC)	Oil (bbls)	Wildcat Assoc. Gas (MFC)	Dist. (bbls)	Gas (MCF)
Ramsey	472,350	756,324			75,052	120,141		
Delaware Mtn. Gp.	25,843	9,773			17,231	6,515		
Bone Spring	145,464	284,804			66,128	129,458		
Wolfcamp	15,600	171,347	24,408	475,488	15,356	168,715	14,648	287,979
Pennsylvanian	265,455	1,580,826	132,440	8,857,200	299,788	1,784,799	118,245	8,052,090
Mississippian								
Silurian Devonian	342,083	164,169	36,720	4,244,310	85,856	41,201	36,562	4,225,495
Ordovician								
Total	1,266,795	2,967,243	193,568	13,576,998	559,411	2,250,829	169,455	12,565,558

Ratings		Calculated %
I:	Very low	25
II:	Low	50
III:	Moderate	75
IV:	High	100
V:	Very High	125

Taken from: R. W. Foster, 1974

Table 8-11

IN PLACE HYDROCARBON RESOURCES AT WIPP SITE*

Formation	Zone I+II+III			Zone IV			Total		
	Oil	Nat. Gas (C.F.)	Dist.	Oil	Nat. Gas (C.F.)	Dist.	Oil	Nat. Gas (C.F.)	Dist.
	(bbls)	$(x\ 10^9)$	(bbls)	(bbls)	$(x\ 10^9)$	(bbls)	(bbls)	$(x\ 10^9)$	(bbls)
Ramsey	6.0×10^6	9.6		8.0×10^6	12.8		14.0×10^6	22.4	
Delaware Group	3.3×10^5	0.1		4.4×10^5	0.2		7.7×10^5	0.3	
Bone Spring	1.9×10^6	3.6		2.5×10^6	4.8		4.4×10^6	8.4	
Wolfcamp	2.0×10^5	8.2	3.1×10^5	2.6×10^5	10.9	4.0×10^5	4.6×10^5	19.1	7.1×10^5
Pennsylvanian	3.4×10^6	132.9	1.7×10^6	4.5×10^6	176.3	2.2×10^6	7.9×10^6	309.2	3.9×10^6
Mississippian									
Silurian/ Devonian	4.4×10^6	56.1	4.7×10^5	5.8×10^6	74.5	6.3×10^5	10.2×10^6	130.6	1.1×10^6
Ordovician									
Total	16.2×10^6	210.5	2.5×10^6	21.5×10^6	279.5	3.2×10^6	37.7×10^6	490.0	5.7×10^6

* Based on Adjusted Production Estimate per Section (640 acres), Acreage method, Table 8-10.
  WIPP site contains 29.6 square miles or sections.

TABLE 8-12
ESTIMATE OF ECONOMIC HYDROCARBON RESOURCES AT WIPP SITE

Well Number	Natural Gas (BCF) Zone I, II, III			Natural Gas (BCF) Zone IV			Natural GAS (BCF) Total		
	Proven	Probable	Possible	Proven	Probable	Possible	Proven	Probable	Possible
1	---	---	---	2.07	---	---	2.07	---	---
2	---	---	---	2.07	---	---	2.07	---	---
3	---	---	---	---	1.64	---	---	1.64	---
4	---	---	---	---	2.09	---	---	2.09	---
5	---	---	---	---	2.09	---	---	2.09	---
6	---	---	---	---	2.09	---	---	2.09	---
7	---	2.09	---	---	---	---	---	2.09	---
8	---	2.09	---	---	---	---	---	2.09	---
9	---	2.09	---	---	---	---	---	2.09	---
10	---	2.09	---	---	---	---	---	2.09	---
11	---	2.09	---	---	---	---	---	2.09	---
12	---	---	1.67	---	---	---	---	---	1.67
13	---	---	1.67	---	---	---	---	---	1.67
14	---	---	---	---	---	1.33	---	---	1.33
15	---	---	1.33	---	---	---	---	---	1.33
16	---	---	1.67	---	---	---	---	---	1.67
17	---	---	1.67	---	---	---	---	---	1.67
18	---	---	1.67	---	---	---	---	---	1.67
19	---	---	1.67	---	---	---	---	---	1.67
20	---	---	1.67	---	---	---	---	---	1.67
	---	10.45	13.02	4.14	7.91	1.33	4.14	18.36	14.35
		Total	23.47		Total	13.38		Total	36.85

Plus Distillate 350,900 BBLS   Plus Distillate 200,000 BBLS   Plus Distillate 550,960 BBLS

Reference: Keesey, 1976.
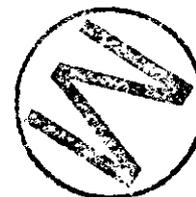
TABLE 8-13
SUMMARY OF IN-PLACE AND ECONOMIC HYDROCARBON RESOURCES AT THE WIPP

	IN PLACE RESOURCES (NMBM STUDY)			ECONOMIC RESOURCES (SW&A STUDY)		
	Zone I,II,III	Zone IV	Total	Zone I,II,III	Zone IV	Total
Crude Oil 10^6BBLS	16.2	21.5	37.7	---	---	---
Natural Gas 10^9CUFT	210.5	279.5	490	23.47	13.38	36.85
Distillate 10^6BBLS	2.5	3.2	5.7	0.35	0.20	0.55

SPECIAL STUDIES

9.1 INTRODUCTION

The special studies presented in Chapter 9 cover issues of particular
interest because the site is being characterized for radioactive waste
isolation (the WIPP). The first special study presented is that of
determining the thermophysical behavior of Southeastern New Mexico (SENM)
rocks for mine design and the effects of heat-producing wastes, if placed
in the WIPP. The second special study is to determine the site-specific
sorptive capacities of SENM rocks for radionuclides flowing with SENM
groundwaters. Characterization of the sorptive capacities of SENM rocks
is required for safety assessment analysis of hypothetical failure
events, not for site selection. Both of these studies are by no means
complete and are continuing. The information presented here is an
indication of the status of these studies in midyear 1978. Tabulations
of test data are left to the references and future reports on specific
subjects.

9.2 THERMOPHYSICAL PROPERTIES

9.2.1 Introduction

The thermophysical properties of New Mexico rock salt are being
investigated to support the structural mine design and to evaluate the
overall stability of bedded salt for the WIPP. A goal of this program is
to develop constitutive relations which can be used in design and
long-term stability calculations, commonly by finite element analyses
(Dawson and Tillerson, 1977). Specific concerns are the stability of the
facility during its life, the influence of ground motions on waste
retrieval capabilities, and the effect of waste emplacement on the long
term containment potential. The program was initiated in 1975.

Rock salts are weak, anelastic geological materials. They exhibit
nonlinear response under practically all loading conditions at
temperatures and pressures normally encountered in mining. Since salt

can experience large strains prior to failure, openings even at very
shallow depths have been known to completely close and heal (Baar, 1977).

In long-established active mining districts, careful in situ observations
and measurements have provided a basis for making reasonably reliable
predictions of room deformation and failure (Baar, 1977). Some of this
knowledge is applicable to the WIPP, although it cannot be directly
applied to the WIPP because the behavior of rock salt is dependent upon
the site, facility design, temperature and time involved. The rock
mechanics program considers the particular problems posed by the
longevity of the WIPP and by the unusual combination of mechanical and
thermal loading anticipated in the repository.

Laboratory experiments have been severely criticized by some for not
realistically representing in situ conditions, (Baar, 1977). However,
laboratory experiments on rock salt are a useful step in material
characterization, to establish limits of behavior. Ultimately,
laboratory and in-situ test data coupled with modeling should lead to
representative descriptions of material and structural behavior. As the
WIPP is developed, in situ monitoring should enhance the validity of
laboratory and modeling results.

The thermophysical behavior of rock salt has been modeled through various
approaches, (e.g., Bradshaw and McClain, 1975; Fossum, 1977; Langer,
1967; Mraz, 1978; St. John, 1978; Serata, 1966, 1968, 1970; Serata and
Cundey, 1978; Thompson and Ripperger, 1964; Thoms et al., 1973; Wahi et
al., 1978). A widely accepted model which can translate laboratory data
into a prediction of in situ salt behavior has not been developed.

Three broad areas were studied to identify the relative and site specific
importance of various southeast New Mexico rock salt thermophysical
properties. These three areas of study consist of: 1) petrography
relevant to physical and mechanical properties, 2) general physical
properties (density, moisture content, resistivity, etc.), and 3)
thermal-mechanical properties (quasi-static and creep parameters).

Petrographic studies were conducted on mineralogically characterized core from AEC 7, AEC 8 and ERDA 9 to investigate structural petrographic changes between natural and experimentally-deformed samples (Callender & Ingwell, 1977). Identification of failure mechanisms by petrographic analyses will assist in selecting models to describe rock behavior.

Physical properties being measured for selected core include density, moisture content, porosity, permeability, electrical resisitivity, ultrasonic velocity, and thermal conductivity. Additional gas and brine permeability measurements are in progress at Sandia both on experimentally undeformed and deformed samples.

The following mechanical properties are being measured: uniaxial compressive strength, indirect (Brazilian) tensile strength, stress-strain behavior and ultimate stress in quasi-static triaxial compression, elastic moduli, principal strain ratios, elastic limit ("yield" stress), and creep rates. Additional tests address the effects of specimen machining, specimen aging due to stress relief during and after core retrieval, and specimen size, all of which could limit the field applicability of laboratory-determined results. The influence of sample size may be partially inferred from published data (e.g., Uhlenbecker, 1968; Dreyer, 1972; Szeki, 1978).

The data base for physical and thermal properties determined from core from the WIPP study area is still being compiled, and tests are continuing. Moreover, most of the results obtained to date pertain to rock salt alone, as opposed to other members of the stratigraphic column above and below the proposed repository horizons.

9.2.2 Petrography

Approximately 35 samples of experimentally undeformed and deformed salt were macroscopically and microscopically examined for mineralogy, fabric, and induced structure by J.F. Callender and T. Ingwell of the University of New Mexico (1977). Mineralogy of rock salt from southeast New Mexico has been described in detail in Chapter 7.

Between the depths of 1,000 and 2,000 feet, the samples are predominantly
halite (NaCl) (range 47-98 percent) with lesser amounts of anhydrite
($CaSO_4$) (range 0-15 percent), polyhalite ($K_2MgCa_2(SO_4)_4.2H_2O$)
(range 0-18 percent), and clay and silt (range 0-44 percent). Halite is
usually present in the core, except in samples from anhydrite layers and
polyhalite seams. Anhydrite, clay and silt are generally present, while
polyhalite occurs less commonly. Detailed stratigraphy of the WIPP study
area is presented in the ERDA 9 corehole lithologic log, Figure 4.3.3.b.

Fabric   In general, the undeformed rock salt specimens do not show
well-developed linear or planar fabrics, aside from uncommonly-observed
bedding. Locally, however, halite crystals show a faint to strong
elongation, probably due to readjustment to local stresses. Certain
fabric features within the cores may presumably have important local
effects on salt deformation. These features include bubble trains,
hopper crystals, cleavage, glide planes, grain boundaries, and clay zones
(Callender and Ingwell, 1977).

Bubble trains are commonly aligned along cleaveage traces or grain
boundaries in halite. The bubbles generally contain fluid, although some
may also be gas or partially solid-filled (see section 7.6). Fracturing
in experimentally deformed cores locally follows the bubble trains, and
they are likely the site of small-scale structural weaknesses within
halite. Once such fractures heal, the zones they followed become
stronger than before (section 7.6) Hopper crystals, generally filled
with clay, also tend to grow and be aligned along halite cleavage
planes. In a number of samples, small-scale fracturing, induced by
sample preparation or by disturbance during the coring operation in the
field, is associated with zones of hopper crystals.

Cleavage, and fracture related to cleavage, is observed in halite. In
euhedral, generally recrystallized, halite, the cleavage direction and
grain boundary are coincident. In these cases, deformation along trends
parallel to grain boundaries should certainly be facilitated. Similar
relations, though less common, exist in subhedral halite. Translation

glide in halite is an important dislocation mechanism and has been described in the literature (c.f., Buerge, 1930; Clabaugh, 1962). Two glide planes, (110) and (001), have been recognized in both undeformed and deformed salt.

In summary, a local concentration of discrete fabric elements (e.g., hopper crystals, bubble trains) may be as statistically significant as planar or linear elements (such as bedding, cleavage alignment, or elongation) for the structural evaluation of the core, and local zones in deformed salt may play an important role in establishing fracture patterns.

Fracture. Analyses of fracture patterns in salt to date have been complicated by induced fracture during sample preparation and the field coring procedures used to obtain samples. The recognition of these induced fractures is generally fairly straightforward; however, the persistent question of local induced fracture arises during detailed study, and is a problem which cannot be easily resolved. Fortunately for the petrographer, many fractures are filled with clay, anhydrite, and polyhalite; these filled fractures give some insight into patterns in material before laboratory testing since they are clearly not a result of sample handling.
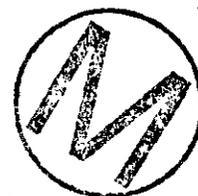
In general, fracture in undeformed salt core is relatively minor and is commonly associated with cleavage or grain boundary adjustments. It appears that fractures may have remained open at some stages of diagenesis for a sufficiently long period of time to be filled by sulfate or other solutions. A few unusual fracture geometries have been noted: en echelon fractures, generally with their major trend parallel to cleavage; circular fractures commonly around hopper crystals; fracture refraction across grain boundaries; jog and kink fractures; and fracture and local extension along glide planes. The number of fractures observed in the laboratory resulting from relief of the in situ confining stresses is unknown. Clay, anhydrite, and polyhalite have apparently flowed in some undeformed samples. Perhaps the best evidence for this statement is

local well-defined linear fabric in polyhalite and anhydrite, and the inclusion of halite in clay along grain boundaries.

In samples severely deformed by laboratory testing, fracture patterns are easily observed. In one sample a well-defined zone of cleavage and glide-plane fracture developed at about 40° to the compressional axis. Apparently, a network of interconnected fractures has been established in this zone which respects neither grain boundaries nor grain size. In contrast, another sample suggests that local fabric elements, particularly clay-rich zones, may affect fracture geometry and that planar fracture fabrics may not be as well-developed in clay-rich samples.

Fracturing of halite can be generated in the laboratory at relatively low confining pressures ($<$ 1500 psi) and moderately high strains (5 to 12 percent); this fracturing induces a fracture porosity in the material. At higher confining pressures, rock salt displays ductile behavior and it is difficult to induce fracturing. The position of the fracture pattern observed in the laboratory is related to both the stress direction and the local fabric elements. In addition, the crystal lattice of halite permits, through defects and crystallographic constraints (c.f., Hirth and Lothe, 1968), a complex dislocation system to develop.

9.2.3 Physical Properties

Measurements of physical properties of rock salt pertinent to the design of the WIPP have been conducted by several investigators. Some representative data are summarized in Table 9.2.3-1.

Density and Resistivity. Measurements were made on full dimension (4-1/2 inch diameter) core. The density determinations were performed following conventional laboratory procedures for determing bulk rock densities utilizing the buoyancy method. Commercial grade kerosene was used for buoyancy measurements. Direct current resistivity determinations were made using current densities of less than 0.20 microamperes per square centimeter (Elliot, 1976), and by downhole geophysical measurements (Griswold, 1977).

Volatile Mass Loss. Total volatiles, including water, were obtained by heating samples of Salado salt from the proposed repository levels to 300°C in several stages. Static weight loss determinations were made at each stage of heating (Kopp & Combs, 1975) and were reported in section 7.5.3.. In addition, thermogravimetric analyses were made by suspending powdered samples from a microbalance while dry nitrogen flowed over the sample. The samples were heated at 5°C/minute until the temperature reached 500°C and held there until gas evolution had ceased (see section 7.5.2 for details and data).

Permeability. Gas permeability of SENM rock salt has been measured for pressures up to 5000 psi and at room temperature to determine the tightness of the host rock to any gases evolved in the WIPP. The data developed by Sutherland (1978), are for argon gas at confining pressures to 2000 psi. A plot of permeability test results is shown on Figure 9.2.3-1. Sutherland's data demonstrate the influence of confining pressure (crack closure and healing) on permeability. Preloading of samples to near lithostatic confining pressures is required to obtain reproducible data in laboratory experiments. Other gases (air, nitrogen, argon) were measured by Core Labs (1977), Terra Tek (1978), and Shelby (1978). The Core Labs' tests followed API standards, however, they did not allow for crack healing. Shelby tested single crystal NaCl. The results of these measurements illustrate the following:

(1) There is no correlation between measured permeabilities for as-received (stress-relieved) core samples;

(2) Samples behave as if they are "healing" when subjected to a confining pressure on the order of their original in situ pressure (illustrated on Figure 9.2.3-1).

(3) After an initial "healing" or "consolidation" period, the polycrystalline samples tested by Sutherland (1978) and Terra Tek (1978) have measured permeabilities of less than 0.05 microdarcys (the limit of resolution of their permeability measurement systems);

(4) There is little or no gas flow through the salt single crystals (less than 1 picodarcy) in the single crystal test apparatus of Shelby (1978). Therefore, the preferred flow channels through a core sample are believed to be along crystalline boundaries.

Thermal Conductivity. The thermal conductivity of several rock salt samples from core of AEC 8 were determined by a longitudinal heat flow apparatus. This apparatus was designed specifically for use with geologic core sections. Constant power is supplied to a heater at one end of the specimen until thermal equilibrium is established. The heat flux transducer and thermocouple outputs are then recorded allowing the thermal conductivity to be calculated from the readings (Acton, 1977). A plot of test results is shown on Figure 9.2.3-2.

Sonic Pulse Velocity. Measurements of compressional wave velocity were made both on laboratory samples (Kent and Wawersik, 1976) and by down hole geophysical methods (Griswold, 1977). Laboratory measurements were made both parallel and perpendicular to the core axis. No signficant variations (less than 0.02 Km/sec) were observed between the axial and transverse values of twenty measurements. The laboratory data were within 15% of the downhole geophysical values.

Summary of Data. Some physical properties are summarized in Table 9.2.3-1. In addition, permeability data are plotted on Figure 9.2.3-1 and thermal properties are shown in Figure 9.2.3-2. The experimental data are presented in the referenced documents.

9.2.4 Thermomechanical Properties

Introduction. It is the goal of laboratory stress-strain tests to develop constitutive relations which can be used in structural calculations. As the program progresses, a combination of finite element calculations using data obtained in the laboratory, empirical mine design methods and in-situ validation studies will serve to evaluate, in detail, certain aspects of the final WIPP design.

To achieve a valid and practical description of the behavior of rock salt from experiments in the laboratory, several programs are being conducted. These are: (1) Measurement of the mechanical response of SENM rock salts and other nearby rocks (e.g., anhydrite) over the domain of stresses and temperatures which may be expected in the WIPP; (2) Development of general models based on test results that are applicable to differing stress deformation and/or temperature histories; (3) Determination of mechanisms governing salt response in sufficient detail to allow the extrapolation of laboratory measurement in time; and finally (4) Establishment of relationships between laboratory samples of rock salt and salt masses in-situ.

This report summarizes the first series of laboratory tests, consisting primarily of short term "quasi-static" tests. These tests served to compare the response of WIPP salt with rock salts from other horizons and locations and to effectively scope the rock behavior for planning the long term creep tests. It is recognized that short term test behavior may be only partially indicative of long term behavior. Not all of the data developed is presented, particularly where detailed information has been published elsewhere. Instead, test values have been selected which are felt to best represent the behavior of the WIPP rock salt. Too few repetitive tests have been performed thus far to determine statistical significance of the data. This is due to the long times required to perform tests and the limited amount of rock salt core available to this test program from specific horizons of interest to WIPP.

A deliberate attempt was made to encompass a broad range of parameter variations including confining pressure and principal stress difference, i.e., mean stress and deviator stress, as well as temperature, time, loading rate, loading path, handling history, and specimen size. These variations covered a wider spectrum than might ordinarily be required to support the design of conventional mines or solution cavities. The approach is predicated on the unusual combination of anticipated mechanical and thermal loadings associated with WIPP. The experimental program plan also tried to address specific questions, for example,

concerning the effect of loading path, which were raised by critics of conventional quasi-static experiments in the past (Baar, 1977).

Testing was primarily conducted on rock salt samples from three horizons in the Salado Formation. The two horizons at 2,100+ feet and 2,600 to 2,700 feet represent the relatively pure halite from the proposed contact-handling (CH) and remote-handling (RH) levels, while the third horizon at 1,900 feet was chosen for study because it is clay rich salt.

The testing program through the summer of 1978 was generally divided into two segments, quasi-static tests and creep tests. Quasi-static properties were generated over a range of loading rates from d/dt ($\sigma_1 - \sigma_3$) of 150 to 215 psi/min (RE/SPEC Inc. data, Gnirk et al., 1973, Hansen and Mellegard, 1977) to loading rates of 30 to 60 psi/min (Sandia data, Wawersik, 1977, 1978c). The 30 psi/min loading rate was chosen to match that of published data (Dreyer, 1972, Menzel and Schreiner, 1977). Creep tests were carried over a range of confining pressure $0 \leq \sigma_3 \leq$ 3,000 psi, deviator stresses $1,500 \leq (\sigma_1 - \sigma_3) \leq 6,000$ psi, and temperatures of $24^\circ \leq T \leq 100^\circ C$ with a duration of up to 70 days. These loading rates were arbitrarily chosen as a means of scoping the behavior of SENM rock salt under conditions that may be encountered in the WIPP.

Apparatus, Experiments, Capabilities, and Data Handling. To support the determination of material properties of WIPP site rocks, a new triaxial facility was developed (Wawersik et al., 1976). Based on earlier experience (Wawersik and Brown, 1973; Gnirk et al., 1973; Wawersik, 1975), the present apparatus has the following capabilities.

The apparatus accepts cylindrical specimens up to 4-1/4 inches diameter by 8.5 inches in length to accomodate the coarse grain size or rock salt.

The system has a pressure rating of 10,000 psi; this is adequate to perform variable load path tests, for example, in triaxial compression, in triaxial extension, at constant maximum compression, etc.

The equipment is suitable to conduct both quasi-static tests and creep experiments.

Specimens can be heated uniformly to approximately 250°C in short-term tests and to 200°C to 220°C in long-term experiments.

Controlled, known temperature gradients can be applied for studies of fluid migration.

The equipment provides access to both specimen ends for possible venting or for measurements of pore pressure and permeability and for application of pore pressure, etc.

It provides both axial and radial deformation measurements. For uniform lateral deformation, this combination of strain measurements yields shear and volumetric strains.

The apparatus is equipped with multiple feed-throughs for use of instrumentation inside the pressure vessel.

Normally, hydrostatic and deviatoric loading are decoupled so that the hydrostatic response of all specimens can be defined and, more importantly, so that linear and bulk thermal expansion measurements can be determined as a function of temperature and pressure.

The apparatus and procedures allow for large, relatively unrestrained sample deformation.

Details of the test equipment (ranges, calibration procedures and precisions) are discussed elsewhere (Wawersik, 1975; Wawersik et. al., 1977; Wawersik, 1978a).Material and Test Specimens - The rock salt studied was machined from 4-1/4 inch diameter core obtained from zones at depths of 1,900 feet, 2,100 feet and 2,600 to 2,700 feet. Sample machining consisted of cylindrical and flat-end grinding following documented procedures which were designed to minimize the thickness of any shatter zones at the specimen surfaces. Alternatively, specimens were obtained by means of standard coring tools. Final specimen dimensions were nominally 2 inches or 4 inches in diameter, with a

length-to-diameter ratio of at least two. After machining, the
cylindrical surfaces of all samples were coated with a protective layer
of RTV silastic.

Quasi-static Rock Salt Properties. Quasi-static testing was conducted on
WIPP salt under hydrostatic pressures to 5,000 psi. Deviatoric loading
tests were performed to 3000 psi confining pressure and to temperatures
of 200°C. Variables of interest were: pressure (confining pressure,
mean stress), principal stress difference (deviator stress), time
(loading rate), temperature and load path. A separate study of the role
of the intermediate principal stress will also be initiated. The
importance of the foregoing variables was suggested by prior mine
measurements and by existing laboratory data (for example Schmidt, 1937;
U.S. Corps of Engineers, 1963; Le Comte, 1965; Hofer and Thoms, 1968;
Schlichta, 1969; Carter and Heard, 1970; Bradshaw and McClain, 1971;
Dreyer, 1972; Heard, 1972, Serata et al., 1972; Kern, 1973; Menzel and
Schreiner, 1977; Baar, 1977).

The term quasi-static is used in the conventional sense to denote a fixed
slow rate of loading. To avoid misunderstandings and undue
generalizations of these data, it is emphasized that most quasi-static
experiments were carried out at particular loading rates, e.g., 30
psi/min. It is important to realize that any data concerning the
mechanical behavior of WIPP rock salt under different loading conditions
must be inferred with proper regard to the time-dependent nature of the
material (Wawersik and Hannum, 1978).

Quasi-static data available to date include approximately 75 uniaxial
compression and indirect Brazilian tension tests at ambient temperature
on core from drill holes AEC 7 and 8 (Hansen and Gnirk, 1975). These
experiments were performed under the direction of Oak Ridge National
Laboratory prior to June, 1975. They include approximately 20
experiments on anhydrite and 5 tests on polyhalite. More recent
quasi-static data include approximately 50 tests on selected specimens
from the potential WIPP repository horizons (Wawersik et al., 1976;

Hansen, 1977; Hansen and Mellegard, 1977, Wawersik and Hannum, 1978).
Samples were machined from core of drill holes AEC 7 and ERDA 9.
Emphasis was placed on the response of rock salt from the storage horizon
at 2600 feet because of the added complexities of elevated temperatures
if heat producing wastes are placed in WIPP.

Selected representative mechanical properties in uniaxial compression and
indirect tension are listed in Table 9.2.4-1.

Quasi-static Triaxial Properties - Representative triaxial data are
listed on Table 9.2.4-2 for a range of confining pressures and
temperatures. Note that both tables 9.2.4.1 and 9.2.4-2 list secant
moduli (stress/total strain) and principal strain ratios (ϵ_3/ϵ_1) rather
than the elastic constants, that is, Young's modulus, E, and Poisson's
ratio. To calculate the intrinsic elastic constants it is necessary to
separate the nonelastic portion from the total deformation or to move
through stress states where elastic response dominates. This was
accomplished for New Mexico rock salt recently during unload/reload
cycles.

The constants obtained were 4.55 x 10^6 $\leq \epsilon \leq$ 5.2 x 10^6 psi and
0.17 $\leq \nu \leq$ 0.24 (Wawersik and Hannum, 1978). These values agree to
within 15% with those which were determined from borehole geophysical
data.

During initial deviatoric loading in the laboratory, nearly all
deformation of WIPP salt was nonelastic (Wawersik and Hannum, 1978). The
actual magnitude of this nonelastic deformation is likely to be sensitive
to the magnitude of the deviatoric stress which the core experienced
during drilling (Wawersik and Hannum, 1978), associated core damage and
subsequent core "relaxation" during core storage and handling.
Combinations of these factors probably account for the variations in
secant moduli and principal strain ratios in tables 9.2.4-1 and 9.2.4-2.

It is common practice in engineering to plot triaxial test data in the
form of Mohr's circles at the ultimate stress. The plots are made in the

stress space (σ,T) where σ and T denote normal and shear stresses, and an envelope is drawn tangent to the circles representing the ultimate shear stress of any value of confining pressure.

When the data from Tables 9.2.4-1 and 9.2.4-2 are plotted, three Mohr's circles which are normal for SENM rock salt are obtained in Figure 9.2.4-2A in stress space (σ,T). The ultimate stresses can be approximated by a straight line (Coulomb) envelope of the form $T = C + \sigma \tan \phi$. In conventional engineering terminology, C is called the cohesion and ϕ, the angle of internal friction. In this case, at ambient temperatures, rock salt from the 2,700 foot level has an apparent cohesion of approximately 1,000 psi and an angle of internal friction of 33°. Similar data for other rocks are being used for mine pillar design. However, it should be recognized that the validity of these ultimate stress analyses rests on two assumptions: (1) failure is independent of the intermediate principal stress, and (2) failure is defined solely in terms of stresses and independent of strain, strain rate and time. Both of these assumptions are currently being evaluated for rock salt.

In contrast to other rocks, it is important to remember that rock salt undergoes large deformations long before the ultimate stress is reached. Since these deformations can exceed 15% even at ambient temperature, it is conceivable that a practial failure condition might incorporate a maximum deformation criterion. To illustrate this case, a Coulomb envelope was constructed (Figure 9.2.4-2B) which defines the stress magnitudes at an arbitrarily chosen constant value of strain $(\varepsilon_1 = 2.5\%)$. This value is the average strain at the ultimate stress of samples tested in uniaxial compression at ambient temperature and a loading rate of 30 psi/min. It can be seen that Figure 9.2.4-2B is different from the ultimate stress envelope in Figure 9.2.4-2A. Clearly, the shapes of the Mohr envelopes are highly dependent on failure criteria. The values obtained also depend on the manner in which the Mohr's envelope is drawn. In Figure 9.2.4-2A, a "best fit" straight line tangent to the circles was drawn; while in B, a parabola was drawn tangent to the circles.

Detailed Quasi-static Stress-Strain Relationships. Elastic constants, ultimate stresses, and stress or strain envelopes are useful for conventional failure stability analyses where rock is treated either as an elastic or as an elastic-plastic material. While such analyses have proven valuable in combination with careful engineering judgement, they are not always accurate. In view of the time-dependent nature of rock salt it is especially important that design calculations be based on a more comprehensive constitutive model. To initiate the development of such a model, detailed short-term quasi-static stress strain observations were made to identify the effects of pressure, deviatoric stress, (shear stress), temperature, and loading history. The influence of time as a discrete parameter is mainly considered in creep experiments.

Deviatoric Loading at Constant Confining Pressure. Deviatoric loading at constant confining pressure is the process of increasing the principal stress difference (deviator stress) from an initial state of hydrostatic compression. It is a necessary condition to induce substantial salt flow.

Typical quasi-static deviatoric loading data are shown in Figures 9.2.4-3 through 9.2.4-15. The key to these curves indicates sample depth in feet and (confining pressure in ksi and temperature in degree C). These stress strain curves depict complete continuous experimental records which indicate the manner in which all specimens were loaded. Deviator stress was applied incrementally rather than continuously. Actual force was raised quickly by some predetermined amount and then held constant for between 4 and 15 minutes while axial and lateral strains ε_1 and ε_2 (= ε_3) were monitored in time. The stepwise loading procedure made it relatively easy to control the mean applied loading rate while monitoring time dependent strains during load hold periods with a minimum of experimental error (Wawersik and Hannum, 1978). In most figures, these details of loading are omitted. As illustrated by the curve for sample 9-2601 in Figure 9.2.4-3, where smooth fits are made to the endpoints of each step in the actual stress strain record. Note that large changes in specimen cross sectional area at constant force during

all load hold intervals lead to considerable decreases in principal
stress difference with time (Wawersik et al., 1977, 1978c). Conventional
plots $(\sigma_1 - \sigma_3)$ versus ε_1 such as Figure 9.2.4-3 relate the present data
to virtually all similar results for rock salt in the literature (for
example, Schmidt, 1937; Heard, 1972; Dreyer, 1972, Menzel and Schreiner,
1977).

Considering Figures 9.2.4-3 through 9.2.4-6, three observations are
particularly noteworthy.

1. Laboratory specimens of New Mexico rock salt have an initial
elastic limit close to zero. Furthermore, this initial elastic
limit appears to be the same following all hydrostatic pressure
histories up to 5000 psi (Wawersik and Hannum, 1978).

2. Pressure appears to have a considerable effect on all properties
of New Mexico rock salt except the elastic constants (Wawersik and
Hannum, 1978). Specifically pressure controls the strain magnitudes,
the ultimate stress and the relationships between the principal
strain (Figures 9.2.4-5 and 9.2.4-6). Pressure effects are
particularly evident at $(\sigma_1 - \sigma_3)$ greater or equal 1200 psi.

3. New Mexico rock salt subjected to quasi-static laboratory
compression can undergo substantial dilatancy which is associated
with cataclasis, i.e., microfracturing. The magnitudes of the
observed volume changes were significant particularly at low
confining pressure and amounted to sizeable fractions of the
observed shear strains near the ultimate stress (Wawersik and
Hannum, 1978). Isovolumetric conditions of deformation are
approached only at 3000 psi confining pressure. However, data at
elevated temperature demonstrate that even comparatively minor
amounts of dilatancy can have a considerable effect on the rate at
which New Mexico rock salt deforms (Wawersik and Hannum, 1978).

Elevated Temperature Data. Elevated temperature experiments were carried out in two groups. First, the influence of temperature was considered at fixed confining pressures, for example, 500 psi (Figs. 9.2.4-7, 8 and 9). Then, the effect of pressure was evaluted at 200°C (Figs. 9.2.4-10, 11 and 12). As expected (Bradshaw and McClain, 1971; Heard, 1972: Dreyer, 1972), temperature reduced the ultimate stress and increased the ductility (Fig. 9.2.4-7). Increasing the temperature is qualitatively equivalent to increasing confining pressure at ambient temperature. Cataclastic effects with considerable dilatancy are suppressed in favor of deformation modes which proceed at constant, or nearly constant, volume (Figs. 9.2.4-8 and 9.2.4-9). (Wawersik and Hannum, 1978)

Influence of Loading History. Effects of loading history are noted in several studies in the literature (for example, Schmidt, 1937; Sereta et al., 1972; Baar, 1977). To consider such effects, three sets of experiments were performed early in the experimental program. First, the influence of differing hydrostatic loading histories was tested. The results indicated no measurable effects on the behavior of rock salt from southeastern New Mexico during subsequent deviatoric loading (Wawersik and Hannum, 1978).

In the second group of experiments, quasi-static strains were measured as a function of load path in a conscious effort to separate the influences of load path and loading history as much as possible. The load paths employed are shown in Figure 9.2.4-15. They consist of:

    1. Conventional triaxial tests at constant confining pressure (load path I).

    2. Triaxial loading at constant mean stress $(\sigma m = \frac{1}{3} (\sigma_1 + \sigma_2 + \sigma_3)$ load path II).

    3, Deviatoric loading at approximately constant maximum compression (load path III).

Figure 9.2.4-13 also identifies one test which combined load path III and I passing through points A, D, E, G, and H (Wawersik and Hannum, 1978). Table 9.2.4-3 provides a comparison of strains at several common stress states of Figure 9.2.4-13 with the strains ε_1 and ε_3 are numerically greatest along the path of constant confining pressure (load path I). The smallest ε_1 and ε_3 were obtained along the path of maximum pressure, either confining pressure or mean stress (load path III) (Wawersik and Hannum, 1978).

To evaluate load history even further, a third set of tests was performed. In these experiments, one sample was deformed in three successive stages at 3000, 500, and again at 3000 psi confining pressure. The response of this specimen was then compared with the strain behavior of individual samples which had been loaded deviatorically at 3000 psi and 500 psi confining pressure (Wawersik and Hannum, 1978). The results of the latter tests are shown in Figures 9.2.4-14 and 9.2.4-15. Notice particularly, that the stress strain record for the third load cycle of sample 7-2740.5 does not immediately converge to the stress strain records of specimens 7-2745 and 9-2601.5. Differences in results are obviously due to the influence of loading history (Wawersik and Hannum, 1978).

Interpretation of Quasi-static Data - In view of the quasi-static testing to date, as illustrated in the figures, the following observations were made repeatedly and establish broad guidelines which should be observed in modeling the thermomechanical behavior of New Mexico rock salt up to fracture and/or massive flow (ε_1 greater or equal 20%).

Rock salt from SENM in the laboratory is nonlinear under all loading conditions with an initial elastic limit ($\sigma_1 - \sigma_3$) approximately zero. Its intrinsic elastic properties can be evaluated accurately only in load/unload/reload cycles provided restrictions are imposed either on the loading (strain) rate or on the range of deviator stresses. However, given comparatively nonelastic strains, the intrinsic elastic behavior does not appear to be very important.

In the low confining pressure domain $\sigma_3 \leq 3000$ psi, rock salt behavior depends strongly on pressure and temperature. Both dependencies are reflected in ductility, ultimate stresses and in the variation between maximum and minimum principal strains or in the variations between volumetric strains and shear strains (Figures 9.2.4-4, 5, 8, 11, and 15).

A brittle mode of deformation (microfracturing) dominates rock salt deformation at ambient temperature, low confining pressure, and deviator stress in excess of approximately 1000 to 1500 psi. Accordingly, the overriding pressure effect under these conditions is pressure dependent dilatancy (Figures 9.2.4-4, 6 and 9). Brittle fracture, including creep fracture, i.e., macroscopic collapse and loss in load bearing ability are possible. At low (less than 1,000 to 1,500 psi) deviator stress, high temperature, and/or high pressure, salt deformation proceeds in a predominantly ductile manner at nearly constant volume. Particularly at high temperatures, pressure does not appear to further influence the nature of the governing deformation mechanisms. This is indicated by a pressure invariance (Figure 9.2.4-11) of the relationship between maximum and minimum compressive strains (shear and volumetric strains). However, observed differences in induced strain rate at a fixed loading rate but different confining pressures indicate that pressure influences the rate at which the governing deformation mechanisms, cataclastic or ductile flow, proceed.

It is recognized that available quasi-static stress strain data do not necessarily describe the properties of New Mexico rock salt over long periods of time. However, for lack of other information, quasi-static tests have been used to define the matrices of future creep experiments and to anticipate phenomena which might occur during creep. For example, emphasis is being placed on triaxial creep experiments as opposed to uniaxial tests. Simultaneous measurements are being made of both volumetric strains and shear strains in creep. Similar tests are not conducted routinely elsewhere and the apparatus to perform these tests is at the state-of-the-art in experimental rock mechanics.

Creep of Rock Salt   Creep tests on rock salt are continuing to evaluate
the long-term time-dependent behavior of New Mexico rock salt.   Since
August, 1977, two sets of triaxial creep tests have been performed on
core from drill holes AEC 7 and ERDA 9, emphasizing the interval of 2600
to 2800 feet depth.   Experiments were carried out over the range

$$0 \leq \sigma_3 \leq 3000 \text{ psi}, \; 1500 \leq (\sigma_1 - \sigma_3)$$
$$\leq 6000 \text{ psi, and } 24^{\circ} \leq T \leq 130^{\circ}\text{C}.$$

Results indicate that in principle WIPP salt can undergo both transient
and steady state creep.   Furthermore, limited data suggest that steady
state creep rates lie in the range from 10^{-10} sec^{-1} to 10^{-7}
sec^{-1}, depending strongly on stress state and temperature.   Steady
state creep may have to be considered in WIPP design calculations; it was
not included in earlier wastes repository analyses which were conducted
in conjunction with in situ experiments during Project Salt Vault, Kansas
(Bradshaw and McClain, 1971).

To evaluate the nature of transient creep of the WIPP salt, 34 tests were
carried out on NX sized (two inch nominal diameter) core.   Tests
durations vary between 0.5 and 500 hours (Hanson, 1977, and Hanson and
Mellegard, 1977).   Initial efforts served to evaluate the significance of
transient creep on the possible repository conditions, to establish upper
(conservative) bounds for steady state creep rates at relatively low
deviator stress and temperature, and to test the applicability of a
pillar creep formula which has been widely used (Bradshaw and McClain,
1971):

$$E(t) = A(\sigma_1 - \sigma_3)^a T^b t^c \qquad (9.1)$$

The results of present transient creep data demonstrate significant
pressure effects which are consistant with all quasi-static observations
but are not predicted by equation 9.1.

Beyond that, however, at least one block of data appears to support equation 9.1 which in its generalized form is:

$$\varepsilon = F_1(p)F_2(\sigma_1 - \sigma_3)F_3(T)F(\text{strain or time}) \quad (9.2)$$

Work is now in progress to estimate the error magnitudes which are associated with the use of equation 9.2 even under restricted conditions, e.g., $(\sigma_1 - \sigma_3) \leq 2{,}500$ psi and $\sigma_3 \leq 1{,}000$ psi. To accomplish this, numerical simulations are compared with the results of independent laboratory experiments which combine multiple creep runs with intermittent short-term stress variations at two different temperatures.

Time Dependent Fracture. To determine the long term strength of New Mexico rock salt, two approaches are being take. First, long-term laboratory creep tests are conducted to establish a relationship between strength and time. Obviously such tests are time consuming. Second, failure times may be calculated from creep flow and from estimates of the amount of nonelastic strain at the point of fracture. The nonelastic failure strain can be estimated by means of an empirical procedure which establishes a relationship between creep, time dependent fracture and quasi-static post failure characteristics (Wawersik, 1972). If this technique is applied to New Mexico rock salt, it appears that the range of stable creep prior to fracture at ambient temperature is:

$$\varepsilon_1 \leq 2.5 \text{ to } 6\% \text{ at } \sigma_3 = 0 \text{ psi}$$

$$\varepsilon_1 \leq 17 \text{ to } 20\% \text{ at } \sigma_3 = 500 \text{ psi}$$

Substantially greater stable creep occurs at $\sigma_3 = 3000$ psi confining pressure (Wawersik 1977). On Figure 9.2.4-18, photographs of core samples from ERDA #9 are shown that were deformed during triaxial testing (Hansen and Mellegard, 1977). Notice the large amount of strain test Numbers 6 and 7 have undergone without apparent major physical damage.

Applicability of Laboratory Measurements. Several investigations are underway to define the qualitative and quantitative applicability of laboratory experiments on WIPP salt to in-situ design predictions. Apart from numerical validation studies, measurements are in progress to determine the relaxation of core after drilling and to assess whether rock salt is damaged during field coring, recovery and storage. The latter efforts are supported by repeated tests on specimens with known laboratory stress histories to further define the effects of stress history, aging and specimen machine. In addition, numerical simulation are being conducted to balance the magnitude of deviatoric loading of salt core during drilling.

9.2.5 Summary and Conclusions

Data from the petrographic and physical properties studies show the WIPP horizon rock salt has low moisture content ($< 0.5\%$), is essentially impermeable ($< 5 \times 10^{-8}$ darcy) and has a high thermal conductivity ($\simeq 5.75$ watts/m^{o}k). These properties along with the studies of fabric and fracture indicate this rock salt is ideally suited from a physical standpoint for the storage of high temperature nuclear waste.

The initial elastic limit is close to zero for rock salt for any confining pressure. Although strengths for rock salt are substantial (unconfined compressive strength to 3700 psi and modulus to 2×10^{6} psi) the load bearing ability is dependent on time, temperature and confining pressure.

It has been shown that rock salt can experience large creep strains (25%) prior to loss of load bearing capacity. Gradual creep is an acceptable feature in the design of underground openings in rock salt as it allows the structure to close without a sizeable reduction in bearing strength and without the physical damage which is associated with fracture.

Laboratory testing is continuing to develop a constitutive model to
describe the behavior of SENM rocks. The model will be used in computer
codes to study the structural response of the geologic media to WIPP.

9.3 RADIONUCLIDE SORPTION ON WIPP ROCKS

9.3.1 Introduction

An important mechanism in retarding nuclide movement in groundwater is
sorption. In the following discussion, this term will be used to
encompass all mechanisms pertinent to interaction between nuclides and
geomedia which include ion exchange, adsorption, and precipitation.

The ability of rocks to adsorb radionuclides and hinder their migration
away from a geologic repository for radioactive waste is not a factor in
site selection criteria (Chapter 2). Also, since sorptive affinity is
not a fundamental invariant property of a rock sample, such as is
mineralogy or total volatile content, radionuclide sorption properties
were not discussed in Chapter 7 (Geochemistry). Nevertheless,
quantification of rocks' affinities for radionuclide sorption, however,
is NOT a generic problem which can be solved simply for all rocks. Since
the only rational approach to the problem is to conduct experiments to
determine radionuclide sorption properties for site-specific rocks and
site-specific aqueous solutions, preliminary results of such experiments
are reported as special studies. The results of special studies of
radionuclide sorption are entirely dependent upon experimental
conditions, just as in the measurement of quasistatic mechanical
properties.

In some safety assessment modeling scenarios described for the escape of
radionuclides from WIPP repository horizons, groundwters contact and
leach the waste form, and eventually find their way out of the salt
deposit into the surrounding rock and mineral strata. During this exit,
the nuclide-bearing liquid would contact clay-containing halite in the
repository horizon, polyhalite formations, anhydrite formations, and

finally the sandstone and dolomite formations which are the bounds of the evaporites. To a rough approximation, the concentration per unit mass of a given nuclide, sorbed on a solid mineral phase C_{solid} can be related to the concentration per unit volume, in the liquid phase C_{liquid}, by the relation:

$$C_{solid} = KC_{liquid}$$

where K is generally known as the distribution coefficient, Kd, with units of ml/g. The use of the term Kd implies an equilibrium condition for a given reaction which is both instantaneous and reversible. In the interaction of a nuclide with a complex mineral assemblage, neither condition may apply and the nuclide sorption observed can result from one or more sorption phenomena on one or more phases. To prevent confusion in nomenclature, the term Kd is used in this report, but with the understanding that what is being measured is a sorption coefficient which applies only to the system described and for the particular set of conditions used in making the measurement. Thus, the measurement of "Kd" does not reflect a fundamental thermodynamic property of rocks and/or solutions; it is rather a function of the experiment in which it is measured.

Ideally, sorptive affinities for radionuclides would be measured in situ in the geological formation of interest using long path lengths and available groundwater. This is not generally feasible and must be supplanted with data generated in a laboratory. Most of this section is an extract of SAND78-0297, "Interaction of Radionuclides with Geomedia Associated with the Waste Isolation Pilot Plant (WIPP) site in New Mexico" by R. G. Dosch and A. W. Lynch. It provides the results of a series of laboratory Kd measurements for various radionuclides and samples of different geological media from the vicinity of the WIPP site, and a discussion of the conditions used in making the measurements. The nuclides chosen for study have either a high potential for leaching and/or migration, a high radiotoxicity, or a chemistry similar to that of a nuclide with these properties. They included ^{137}Cs, ^{85}Sr, ^{131}I, ^{125}Sb, ^{144}Ce, ^{152}Eu, ^{153}Gd, ^{106}Ru, ^{243}Am, ^{244}Cm and ^{238}Pu.

A given set of conditions including pH, Eh, particle size, nuclide concentrations, and brine and/or groundwater simulant composition was defined prior to starting the work and maintained throughout. The Kd values reported are considered to be a set of preliminary baseline data for use in evaluating the effects of changes in those conditions which will undoubtedly be necessary as more information about the WIPP site itself and interactions of the waste forms with bedded salt become available.

The results of some parametric studies with lanthanide elements are also given. Significant differences in Kd's were observed as a result of varying pH and nuclide concentrations, and from the addition of trace quantities of organic contaminants to simulant solutions.

9.3.2 Geological Media

Sample Selection. The geological samples used in this work were taken from four inch diameter core samples from AEC #8 and ERDA #9 boreholes. (See Chapters 4 and 7 for descriptions of stratigraphy and mineralogy.) These include three samples from various rock formations (including the water-bearing rocks above and below the evaporites), four halite samples from the Salado Formation, and samples of polyhalite and Cowden anhydrite also from the Salado Formation.

The selection of the geological media for study was based on both the hydrology of the WIPP site and surrounding area and on a reasonable scenario for radionuclide transport from a bedded salt repository. The Magenta, Culebra, and Bell Canyon formations represent actual or potential aquifers.

Any path to the biosphere for water which may have contacted and leached a waste form would involve migration through halite formations, and also through anhydrite and polyhalite strata interspersed in the halite. Thus, these materials, along with the clay contained in the halite, are included in this study as they represent potential barriers to nuclide migration.

Sample Preparation. Culebra, Magenta, Bell Canyon, polyhalite, and anhydrite samples were reduced to a powder prior to use. Clays from the halite samples were obtained by dissolving core samples in deionized water, filtering and washing the insoluble residue, and drying at ambient temperature in air or vacuum.

9.3.3 Brine and Groundwater Simulants

The bulk of the Kd measurements reported herein were done using simulated brines and groundwater of the compositions given in Table 9.3-1. The Brine A composition is based on that expected in an aqueous solution in contact with potash deposits found in the vicinity of the WIPP site. The Brine B composition is typical of water in contact with halite deposits in the repository horizons. The groundwater Solution C composition is based on analyses of shallow groundwaters from the Los Medanos area (Lambert, 1978) above the evaporites and is intended to represent an "average" composition.

In determining Kd values for halite particles, saturated brines prepared from the particular core sample from which the halite had been taken were used as the liquid phase.

9.3.4 Solution Chemistry

Solutes. The use of simulated brines became necessary as both naturally occurring brines and core samples from repository horizons are currently available in very limited quantities. Simulants do offer the advantage of providing a reproducible matrix which allows for direct comparison of Kd data generated in different laboratories.

Potential problems in using simulants could arise from the absence of trace constituents which may be present in natural waters. If these are common inorganic species, the effect on Kd's would probably be negligible. However, trace quantities of organic compounds or dissolved gases such as hydrogen sulfide could produce significant changes in Kd

values should they tend to form stable complexes with some nuclides. The effect of trace quantities of organics which may be introduced into the repository as radwaste is being addressed and is discussed in Section 9.3.8.

Oxidation Potential. In aqueous migration from a deep geologic storage site, nuclides would most likely encounter both anoxic and aerobic conditions, in that order, as the biosphere is approached. The potential effect on Kd values could be many orders of magnitude; however, this should be limited to nuclides such as U, Np, and Pu which may undergo oxidation-reduction reactions in the potential range encountered.

Oxidizing conditions have been used to date as they are believed to produce the "worst case" with respect to migration, i.e., the higher valence states of the previously mentioned actinides tend to have lower Kd's, and they will be encountered in any scenario leading to contamination of the biosphere.

Hydrogen Ion Activity. The effect of the pH is believed to be extremely important in both the solution chemistry and the adsorption mechanism involved in the Kd for a given geological media. Problems encountered in determining Kd values in systems where solution pH is varying are discussed in Section 9.3.8. Changes in the adsorption characteristics of clays, oxides, and some zeolite materials as a function of pH are well documented (Amphlett, 1964).

The initial pH values of 6.5, 6.5 and 7.5 for Brine A, Brine B and solution C simulants, respectively, were chosen as being representative of field pH measurements of natural brines and groundwaters in the Los Medanos area.

Radionuclide Concentation. Ideally, a distribution coefficient should be independent of concentration. This condition usually exists only over a narrow concentration range and, therefore, nuclide concentrations should be chosen which are somewhat representative of those expected in a

repository. The problem lies in the fact that little or no data exists to aid in estimating leaching rates under conditions expected after closure of a repository. These include glass or other waste forms at elevated temperature (70-200°C) and lithostatic pressure (2000 psi) in contact with "wet" salt or brine. Another presently unknown variable is the effect of radiolysis on leaching mechanisms and rates. Available leaching data primarily result from laboratory leaching experiments with simulated waste in distilled water at ambient temperature.

In order to simplify both sampling and counting operations in the initial. work, an activity of approximately 1 μ Ci/ml was used for all determinations unless stated otherwise. The corresponding nuclide concentrations based on the suppliers' analyses of the isotopes used are listed in Table 9.3-2.

Unless otherwise stated, all distribution coefficient measurements were made using a single nuclide in the brines or groundwater to eliminate competing ion effects. The effect of the nuclide concentration on Kd's is of concern and some initial work in this regard is presented in Section 9.3.8.

9.3.5 Experimental Procedures

Apparatus, Sample Size and Sampling. Samples of rock, clay, anhydrite, polyhalite, or halite were weighed directly into polyethylene dropping bottles volumes of doped brine or groundwater were added. The ratio of liquid to solid was typically in the range of 30 to 35. Due to limited quantities of the clay samples, higher ratios (50-150) were used in experiments with clays.

The bottles were sealed by placing a piece of polyethylene film over the opening and replacing the bottle top. Agitation was provided by orbital, reciprocating, or wrist-action shakers. Samples for analysis were taken by replacing the polyethylene film with a 0.8 μ pore size Gelman filter, tightening the dropping bottle top down over the filter, and squeezing

the bottle to force 0.5 to 1.0 ml volumes into pre-weighed polyethylene vials. Quantitative volumes were determined from weight and density measurements. The filters were replaced with polyethylene film and the agitation continued.

Portions of all "feed" solutions were put in identical polyethylene dropping bottles, agitated, and sampled at the same time and in the same manner. The activity in the filtered "feed" samples were used as the initial solution activity in the Kd calculations.

<u>Analyses.</u> The activity in solutions containing ^{137}Cs, ^{85}Sr, ^{106}Ru, ^{131}I, ^{125}Sb, ^{152}Eu, ^{144}Ce, or ^{153}Gd was determined by x-ray spectroscopy. A Harshaw 3" x 3" NaI(Tl) scintillation crystal or an Ortec VIP Series Coaxial Ge(Li) solid state detector was used. Data was accumulated and processed by a PDP-11/20 computer system. ^{99}Tc beta activity was measured using a mica end-window Geiger tube or by liquid scintillation counting. Alpha activities were determined by liquid scintillation counting. Since only relative activities are needed to determine Kd's, units of cpm/ml were used in all calculations.

<u>Equilibration Time.</u> Samples of fission product nuclides were generally taken after 14-20 and 30-35 day equilibration periods. In some instances, more frequent sampling was done. Variation in Kd's between the two sampling times were generally within a factor of two and are believed to result from changes in concentration due to adsorption on container walls, filters, or pH changes in both the sample and feed solutions rather than from rock-nuclide sorption kinetics.

Equilibration times of 170 days were used in the actinide experiments. This extended period was dictated by delays in acquiring laboratory facilities rather than by experimental design.

9.3.6 Kd Data

The results of Kd measurements using the conditions described in previous sections are given in Tables 9.3-3 through 9.3-11. Each table represents a different geological sample and contains th Kd's determined for the various brine/groundwater-nuclide combinations listed and a pH range including the initial feed pH and final sample pH values. The Kd ranges given for the fission product nuclides include two or more measurements made during the course of the experiment. Error associated with these measurements is certainly the most significant at the high ($>10^4$) and low (<1) ends of the Kd range, where background to signal ratios are high or calculations are based on small differences in large numbers. Two-to-fivefold variations of Kd's between duplicate analyses in these regions were not uncommon. Another obvious source of uncertainty is sampling, both in picking a section of core to represent a geological formation and in taking small samples to represent the core. The magnitude of error due to heterogeneity in a given core sample is unknown, as multiple samples were not used in this survey.

9.3.7 Discussion of Kd Data

Cesium. Cesium adsorption from brines "A" and "B" on Culebra and Magenta samples, representing a potential aquifer region overlying the repository horizons, is minimal or non-existent with Kd's ranging from 0 to 2. Adsorption from groundwater C is slightly higher (Kd's from 4 to 10). In the potential aquifer underling the repository, the Bell Canyon Formation, Cs adsorption is significantly higher in the groundwater "C" simulant than in brine "B". This trend tends to support an ion exchange mechanism for Cs adsorption.

Similar results are observed on the samples associated with the repository horizons, with the exception of the polyhalite sample, which did not adsorb Cs from any of the solutions used.

Strontium. The adsorption of Sr on the rock samples from potential
aquifer regions was very low with a Kd of 5 being the highest value
observed in both brines and groundwater simulant.

Of the materials associated with the repository horizons, only the
polyhalite sample showed any appreciable adsorption of Sr from the brine
solutions that would be associated with the region.

The interstitial clay in the halite formation shows no tendency to adsorb
Sr from the brine solutions (Tables 9.3-6 and (.3-9), and this may be
attributed in part to the relatively high concentration of stable Sr used
in the simulants. However, the same behavior was observed in an
experiment where a brine prepared by dissolving a halite core and doped
with < 0.3 ppm ^{85}Sr was cycled through a column of the halite particles
from the same core (Tables 9.3-1 and 9.3-11). In this case, only a
slight reduction in Sr activity was observed (which may have resulted
from adsorption on the glass column or Tygon tubing used to circulate the
brine), while ^{144}Ce was quantitatively removed by the halite.

Europium, Gadolinium and Cerium. These nuclides have been grouped
together for discussion because their chemistries are very similar,
particularly with respect to hydrolysis, and secondly, because they
exhibited similar behavior in their interactions with the geomedia from
the WIPP site.

With the exception of polyhalite samples, Kd's of greater than 10^3 for
these nuclides were observed on all the geological samples with which
they were contacted. Any interpretation of these data with respect to
mechanism or comparison of the effects of different brines or geological
media is difficult because of the contribution of hydrolysis and
subsequent precipitation to the overall adsorption observed in the
experiments.

For example, the polyhalite sample which was singled out as having Kd's
of less than 10^3 for these nuclides (Table 9.3-7), also had final pH
values which were lower than the rock or clay samples. Thus, the

apparent difference in Kd's may be a hydrolysis effect rather than be related to the polyhalite. The effect of hydrolysis is further discussed in Section 9.3.8.

Technetium and Iodine. Both of these nuclides are expected to exist as anionic species in natural groundwaters or brines and were used in the form of pertechnetate, TcO_4, and iodide, I, in this work.

Natural ion exchangers typically exhibit extremely low anion capacities, particularly in neutral or basic solution. In this work, the only material which showed significant adsorption of pertechnetate and iodide was a clay sample taken from a halite core (Table 9.3-9). The adsorption was observed in Brine A and groundwater C, but neither species appeared to be adsorbed from Brine B. The relatively high concentration of Tc used may have far exceeded the anion exchange capacity of some or all of the samples and this possibility is being investigated.

Ruthenium and Antimony. Difficulty was encountered in preparing the doped "A", "B", and "C" solutions due to the high concentrations of stable Ru and acid (4NHCl) in the ^{106}Ru solution used. Adjustment of pH after doping resulted in precipitation of > 95% of the Ru. The final feed solutions were estimated to contain approximately 0.10 μCi/ml of ^{106}Ru in "B" and "C" or 25 ppm total Ru.

General trends observed in the Kd measurements include: 1) higher Kd's for the clay minerals than for the rock samples, 2) higher Kd's in simulants "B" and "C" than observed in "A". The latter effect may be the result of brine composition, but more likely is a hydrolysis effect as the final equilibrium pH of "B" and "C" is higher than that in the "A" brine.

Antimony was added to the group of nuclides being studied late in this work, and there are not sufficient data available on which to base any general statements.

Actinides. The actinides used in this work were supplied as Am(III), Cm(III), and Pu(IV) solutions and used at face value. No attempts were made to determine the Pu species present in the simulant solutions after doping. The nominal activity of the actinides in the solutions used in this work was 1 μCi/ml, however, the final activities in the "feed" solutions were lower. The doping was done by adding the isotope solutions to containers and evaporating to dryness at room temperature. The brines or groundwater solutions were then added to the containers and the solutions were set aside for several days. The amount of isotope used was sufficient to provide an activity of 1.0 μCi per milliliter of solution if the entire amount was dissolved.

In general, the actinide concentrations in groundwater "C" at a pH of 7.3-7.4 are greater than those in the brine solutions in the 6.9-7 pH range. This is particularly true for ^{244}Cm, where the concentrations are 2 to 3 orders of magnitude lower in the brine solutions.

Kd values for the actinides of 300 or greater are observed for all the geological samples if the halite Kd's are based on weight of insoluble material rather than the weight of the total halite sample. In general, the Kd values in the groundwater "C" are higher than in Brine "B" which could result from hydrolysis due to higher pH in the "C" solutions; however, there are some cases where this Kd order is reversed.

The reasonably good agreement between the Kd values for the clay samples (Table 9.3-6) and the halite containing interstitial clay particles (Tables 9.3-5 and 9.3-11) suggests that the halite in the vicinity of the repository can serve as a barrier to actinide migration.

9.3.8 Parametric Effects

pH and Nuclide Concentration Effects on Kd. The first investigation into the contribution of the pH of the aqueous phase and effect of nuclide concentration on the sorption coefficient involved ^{152}Eu sorption from brines A and B and groundwater C on samples from the Magenta and Culebra Formations.

The experimental procedure used was the same as that described
previously, except two blank samples of each feed solution were included
instead of one. At the end of a two week equilibration period, the pH of
the samples and feed solutions were measured. One of the feed B and C
solutions was then adjusted so that its pH was equal to that observed in
sample solutions containing that feed. A sodium carbonate solution was
used for the pH adjustment, which was done over a period of three days.
By the time analytical samples of the adjusted feeds were taken, the pH
of some of them had increased and was higher than the corresponding
sample. The pH of the Brine A feeds was not adjusted as the final values
were the same as those in the samples.

The pH of the adjusted feeds decreased significantly during the first
three months, probably due to adsorption of atmospheric carbon dioxide
(Garrels and Christ, 1965). The pH of the solutions contacting the rock
also varied with some increasing and others decreasing; however, the
change was consistent within a given set of samples containing the same
rock and solution.

Distribution coefficients calculated from both the feed activities and pH
adjusted feed activities after two week and three month periods are
listed in Table 9.3-12.

Europium is apparently more soluble in Brine A than in Brine B at the
same pH or in the C composition at higher pH. The effect of adjusting
the pH in B and C solutions definitely resulted in hydrolysis and
formation of some species which did not pass through a 0.8μ filter. It
is also of interest that significant decreases in activity in the
pH-adjusted feeds were observed for all Eu concentrations used.

The Effect of Trace Organic Contaminants of Kd's of ^{152}Eu, ^{153}Gd and
^{144}Ce. One of the concerns in estimating migration rates of
radionuclide in aqueous media is the ionic form of the nuclide of
interest. Experiments have shown that the simple ionic forms of most
polyvalent cations interact quite readily with geologic media from the

WIPP site via ion exchange or other sorption phenomena. These interactions serve to retard the movement of the ionic species relative to the aqueous matrix containing them.

The extent of the nuclide-geologic media interaction can be significantly altered by changes in the ionic form of the nuclide. Examples of such changes are redox reactions which may result in species of zero or negative charge types and reactions with available inorganic or organic ligands to form complex species with different chemical properties. One such change in properties might be enhanced mobility over that of the bare ion.

Investigations of the sorption changes due to complexation between organic ligands and radionuclides have been initiated by Robert T. Paine of the University of New Mexico. One source of organic ligands which may be present in large quantities in the repository is the plywood used in containers for shipping TRU waste. Samples of these containers are being refluxed in synthetic Brine B at $70^{o}C$, the maximum temperature expected in the transuranic (TRU) waste horizon in the repository. The initial samples of this brine, subsequently referred to as B*, were taken after 5 weeks of refluxing.

Although no significant physical degradation of the plywood was observed after this time period, chemical leaching did occur as evidenced by the coffee brown appearance of the brine. Gas chromatograph-mass spectrometer analysis of the brine indicated the presence of organic material, but identificaton was inconclusive. Infrared spectroscopy was used to examine carbon tetrachloride and benzene-acetone extracts from the brine. The extracted organic material fell into the general class of esterified rosin compounds, but no specific indentification was possible. Qualitative observation indicated that the brine contained extremely small amounts of organic material. Neither solvent system extracted the colored species from the brine.

The effect of plywood extract on lanthanide distribution coefficients (Kd's) was determind by measuring Kd's for ^{153}Gd, ^{144}Ce and ^{152}Eu between five geologic media from the WIPP site and the brine B* containing the plywood extract, and comparing these values with Kd's obtained in identical experiments using pure Brine B. The results are given in Table 9.3-13.

Although both the B and B* brines were doped initially with the same concentrations of tracers, there is a significant difference in the activity of the final samples taken. This could result from adsorption on the polyethylene containers or hydrolysis and subsequent filtration of hydrated oxides of the tracer elements through the 0.8 μ filters. In either case, the effect occurs to a significantly lesser extent in the brine B*, which is probably the result of interaction between the tracers and some ligand extracted from the plywood to form complexes which are less susceptible to hydrolysis.

The difference in Kd values could also result from complex formation. The complexing ligand may be a rosin derivative, many of which form very stable compounds with heavy metals. It may also be the species which causes the brown coloration of the brine. Observation of the analytical samples taken from the brine B* samples showed that the clay material had completely decolorized the brine. The other materials decolorized the B* samples to varying degrees, as given below in order of decreasing color intensity remaining in solution:

Feed > Magenta > Culebra ≈ Bell Canyon > Cowden > Clay solution

Similar work will be done using extracts which are being prepared from other organic materials expected to be associated with TRU waste such as rubber gloves, swipes, detergents, etc. Based on lanthanide results, an experimental matrix will be designed to study the actinide elements.

The Effect of Oxidation State on Radionuclide Sorption. An additional approach to understanding the behavior of actinides under site specific conditions in WIPP is the study of the behavior of various oxidation

states of the actinides (particularly plutonium) in the presence of various components of the WIPP strata. This work is being performed at Argonne National Laboratory by Sherman Fried and Arnold Friedman.

Relatively concentrated solutions of actinides (0.01 M) whose oxidation states were determined by inspection of their optical absorption spectra were prepared and allowed to react with saturated WIPP brines, and with rocks from the WIPP site. Since it was assumed that in the final stages of a WIPP repository oxygen might be absent in the rock salt, the preparations were made in vacuo to identify species present under such conditions.

Solutions of plutonium were prepared in such a way that samples sealed in optical absorption cells at approximately 10^{-6} atmosphere of O_2 could be examined from time to time to observe changes in absorption peaks (if any) and thus determine the stability of the particular oxidation state as a function of time.

In the case of plutonium preparations, the isotope ^{242}Pu was employed. This was done to minimize radiolysis effects (specific activity Pu^{242} = 4.5×10^3 d/m/µg vs. $1/15 \times 10^5$ d/m/µg for ^{239}Pu). It is felt that while the behavior of plutonium in these concentrated solutions may be substantially different than tracer Pu migrating in an aquifer where the radiation field will be much less, it is nevertheless a good approximation to the conditions immediately in the vicinity of the canister when an amount of radioactivity has just leached out.

The various oxidation states of Pu were prepared by electrolytic means or oxidation by ozone as the case required, in order to avoid the introduction of extraneous ions which might affect the results.

The solutions of Pu compounds ($PuCl_3$, $PuCl_4$, and PuO_2Cl_2) were prepared directly in the absorption cell. The concentrations were generally of the order of 0.01 M. In a typical case, 4 ml of saturated WIPP brine "A" (Table 9.6-1) was introduced into the optical cell and

evaporated to dryness in a stream of nitrogen. After this operation, the proper amount of Pu compound was pipetted in the cell and evaporated to dryness with the salts from the WIPP brine.

The cell was attached to the vacuum line and evacuated until the pressure was ~10^{-6} atm. De-aerated water was then distilled under vacuum until the amount of solution equals that which originally pipetted into the cell.

These samples of various Pu compounds were examined from time to time observing any changes in intensity or wavelength of absorption peaks corresponding to the oxidation state in question.

The resulting samples prepared for measurement of changes in intensity of the optical absorption spectra are Pu(III), Pu(IV) and Pu(VI) in water, and in saturated WIPP brine solution.

No definite changes in absorption peaks corresponding to changes in oxidation state were observed. The Pu(IV) solutions were so dilute, because of precipitation from the hydrolysis of Pu(IV), that little or no characteristic absorption peaks could be observed at all. The Pu(III) solutions, whose absorption peak is at about 6000 $\overset{\circ}{\mathrm{A}}$, also showed little or no detectable change over the time interval of the experiment (2-4 months).

The Pu(VI) as PuO_2Cl_2, surprisingly, is insoluble in saturated WIPP brine. The level of solubility is so small that no absorption peaks could be seen at all. In order to be sure that this case is not one of very slow rate of solution, the sealed absorption cells are being rotated with periodic abosorption spectrum determinations.

Some absorption studies have already been carried out with Pu(IV) and Am(III) on anhydrite and dolomite from the WIPP site (see previous sections).

Work is presently underway with the Argonne National Laboratory Analytical Chemistry Group to develop procedures for the determination of the oxidation potential of WIPP salt, dolomite and anhydrite slurries, particularly those employing oxidation-reduction indicators.

Crude reaction rates and K_D values of Pu(III) and Am(III) with Magenta and Culebra dolomites in waters that have been equilibrated with the individual rock are in the table.

Rock Type	Radionuclide	Reaction Time (hr)	K_D
Magenta (gypsiferous dolomite)	Pu	50	41
	Am	400	47
Culebra (silty dolomite	Pu	1	19
	Am	1	84

It should be understood that these reaction rates are crude and that the K_D values are somewhat indeterminable because of varying quantities of radionuclides "plating out" on the walls of the containers. These experiments will be repeated as a function of temperature. Since these determinations were made on tablets of rock of known dimensions, the surface absorption coefficients can be calculated, these perhaps being more applicable to migration along fissures and cracks, where the surface absorption coefficient is

$$S_c = \frac{\text{activity/ml liquid}}{\text{activity/cm}^2 \text{ solid}}$$

The installation of a controlled atmosphere box has made it possible to study the absorption of the various oxidation states of Pu without the perturbing effects of atmospheric oxygen.

9.3.9 Summary

A survey of the potential of geological media from the vicinity of the
Waste Isolation Pilot Plant site in Southeastern New Mexico for
retardation of radionuclide migration via an aqueous carrier has been
completed. Solution simulants representing water in equilibrium with
potash minerals or halite zones and a typical groundwater were spiked
with radionuclides and contacted with geological samples to obtain
sorption coefficients, Kd's. The samples were taken from potential
aquifers above and below the repository horizons and from bedded salt
deposits in the repository horizons. The nuclides chosen for study
represent those with a high potential for leaching and/or migration, high
radiotoxicity, or those with a chemistry similar to nuclides with the
aformentioned properties. They included ^{137}Cs, ^{85}Sr, ^{131}I, ^{99}Tc,
^{125}Sb, ^{144}Ce, ^{152}Eu, ^{153}Gd, ^{106}Ru, ^{243}Am, ^{244}Cm and
^{238}Pu.

A very general summation of the Kd results in brine simulants is as
follows: Anionic species, TcO_4^- and I^-, showed little or no
tendency to adsorb on any of the geological media (Kd's $\leq$ 1), with the
possible exception of a clay material from a halite stratum (Kd < 5). Cs
and Sr Kd's were also generally less than 1, but values in the range of
10-20 were observed on several minerals. Ru Kd's ranged from
25 to >10^3, depending on the brine and geological materials. The
lanthanide and actinide Kd's were typically > 10^3, with only polyhalite
showing significantly lower adsorption.

In the groundwater simulant, Tc and I showed the same behavior. The Kd's
of the other nuclides were slightly higher, particularly those of Cs and
Sr. This would be expected if the sorption were due to an ion exchange
mechanism, but, in the case of the lanthanides and actinides, may also
result from an increased contribution of hydrolysis to the Kd due to the
higher pH of the groundwater simulant.

Important parameters in Kd measurements include solid sample form, simulant compositon, Eh and pH, and radionuclide concentration. In the Kd survey measurements, an initial set of these parameters was selected and, wherever possible, was used throughout the work. Parametric studies with Eu involving pH, trace organic constituents in the simulant solutions, and radionuclide concentrations have shown that significant differences in Kd's can be observed by varying any of those parameters.

A general observation which can be made from data obtained to date is that a Kd represents an empirical value for nuclide adsorption, which includes the effects of physical adsorption, ion exchange, and hydrolysis or other precipitation processes. The utility of a given Kd value is unambiguous only for that set of conditions used in making the measurement. Kd information which is used in modeling radionuclide migration should be in the form of a range of values generated in parametric studies under the variety of conditions postulated for a specific repository site.

For the WIPP site, rock salt, anhydrite, polyhalite and water-bearing dolomites and sandstones show an affinity for radionuclide sorption. Sorptive capacity as measured by batch Kd experiments generally expressed Kd > 0. Even small values of Kd (0 <Kd< 1) are effective in retarding the movement of radionuclides in groundwater.

9.4 REFERENCES

Acton, R.V., 1977, Thermal conductivity of SE New Mexico rocksalt and anhydrite: unpublished Sandia Laboratories preliminary report.

Amphlett, C.B., 1964, Inorganic Ion Exchangers, Elsevier, Amsterdam.

Baar, C.A., 1977, Applied Salt-Rock Mechanics 1: Elsevier Scientific, New York.

Bradshaw, R.L. and McClain, W.C., 1971, Project Salt Vault, a demonstration of the disposal of high-activity solidified waste in underground salt mines: Oak Ridge National Laboratories #4555.

Buerger, M.J., 1930, Translation-gliding in crystals of the NaCl structural type: Am. Mineralogist, v. 15, p. 174-187; p. 226-238.

Callender, J.F. and Ingwell, T., 1977, Structural Petrology of Undeformed and Experimentally Deformed Halite samples from USERDA Site #7 and #9, Report, SAND78-7076, Department of Geology, University of New Mexico.

Carter, N.L. and Heard, H.C., 1970, Temperature and rate dependent deformation of halite: Amer. Jour. Sci. 269, 193.

Clabaugh, P.S., 1962, Petrofabric study of deformed salt: Science, v. 136, p. 389-391.

Core Laboratories, 1977, Special core analysis study for Sipes, Williamson and Aycock, unpubl. consulting report to Sandia Laboratories by Sipes, Williamson and Aycock, Inc.

Dawson, P.R. and Tillerson, J.R., 1977, Comparative evaluations of the thermomechanical responses for three high level waste canister emplacement alternatives: Report, SAND77-0388, Sandia Laboratories.

Dreyer, W.E., 1974, Results of recent studies on the stability of crude oil and gas storage in salt caverns. 4th Symp. on Salt, A. H. Coogan, Ed.

Dreyer, W., 1972, The Science of Rock Mechanics: Trans. Tech. Publ. Cleveland, Ohio.

Elliot Geophysical Company, 1976, A laboratory investigation of the density and resisitivity physical properties of drill core sample ERDA #9: consulting report to Sandia Laboratories.

Fossum, A.F., 1977, On the structural behavior of progressively mined solution cavities in salt, Journal of Applied Mechanics, v. 44, Series E, No. 4, p. 565-570.

Garrels, R.M. and Christ, C.L., 1965, "Solutions, Minerals and Equilibria," Freeman, Cooper & Co., San Francisco.

Gnirk, P.F., Pariseau, W.G., Russel, J.E., Wawersik, W.R., and Hovland, H.V., 1973, Analysis and evaluation of the rock mechanics aspects of the proposed salt mine repository: Report, RSI-005, RE/SPEC, Inc.

Griswold, G.B., 1977, Site selection and evaluation studies of the waste isolation pilot plant (WIPP), Los Medanos, Eddy County, New Mexico: Sandia Laboratories report 77-0946, Albuquerque, New Mexico.

Hansen, F.D. 1977, Triaxial Quasi-Static Compression and Creep Bahavior of Bedded Salt from Southeastern New Mexico: <u>Technical Memorandum Report RSI-0055</u>, For Sandia Laboratories, Albuquerque, New Mexico.

Hansen, F.D., and Gnirk, P.F., 1975, Design Aspects of Radioactive Waste Repository: III Uniaxial Quasi-static and Creep Properties of the Site Rock, Tech. Memorandum Report RSI-0029.

Hansen, F.D. and Mellegard, K.D., 1977, Creep behavior for bedded salt from southeastern New Mexico at elevated temperatures: Tech Memo to Sandia Laboratory, RSI-0062, Albuquerque, New Mexico.

Heard, H.C., 1972, Steady-state flow in polycrystalline halite at pressure of 2 Kb: Geophys. Monograph Series, p. 16, 191, 1972.

Hirth, J.P. and Lothe, H., 1968, Theory of dislocations: New York, McGraw-Hill, 780 p.

Hofer, K.H. and Thomas, K., 1968, Triaxial tests on rock salt: Int. J. Rock Mech. Min. Sci., 5, 195.

Kent, D., and Wawersik, W.R., 1976, Laboratory velocity measurements on rock salt core samples: Sandia Laboratories interoffice memo, Albuquerque, New Mexico.

Kopp, O.D., and Combs, D.W. 1975, Mineral sources of water in evaporite sequences, Report, ORNL subcontract No. 3670, Dept. of Geol. Sci., Univ. of Tennessee.

Lambert, S.J., 1977, "The Geochemistry of Delaware Basin Groundwaters," SAND77-0420.

Langer, M., 1969, Rheologie der Gesteine, Z deutsch. geol. Ges., 119.

Le Comte, P., 1965, Creep of rock salt: J. Geol., 73, 469.

Levy, H.B., 1972, "On Evaluating the Hazards of Groundwater Contamination by Radioactivity from An Underground Nuclear Explosion," Lawrence Livermore Laboratory Rept. UCRL-51278.

Menzel, W. and Schreiner, W., 1977, Zum Geomechanischen verhalten von steinsalz verschiedener lagerstatten der DDR, Teil II: das Verformungsverhalten: Neue Bergbautechnik, 7, 585.

Mraz, D., 1978, Theoretical predictions confirmed by in-situ rock behavior in a deep potash mine: in 19th U.S. Rock Mechanics Symp., ed Y.S. Kim, Reno, Nevada.

Russel, J.E., 1978, A Creep Model for Rock Salt, Fifth Int. Salt Symps., Hamburg, Germany.

Schlichta, P.J., 1969, Growth, deformation, and defect structure of salt crystals: Geol. Soc. Am., Sp. Paper 88, 598.

Schmidt, W., 1937, Festigkeit and Verfestigung von Steinsalz: Zeitschr. Angew. Min., 1., 1.

Serata, S., 1966, Continuum theory and model of rock salt structure: in second symposium on salt, ed Jon L. Rau, Cleveland, Ohio.

Serata, S., 1968, Application of continuum mechanics to design of deep potash mines in Canada: Int. J. Rock Mech. Min. Sci., 5:293-314.

Serata, S., 1970, Prerequisites for application of finite-element method to solution cavities and conventional mines: in Third Symposium on Salt, ed., J.L. Rau and L.F. Dellwig, Cleveland Ohio.

Serata, S., 1972, The Serata stress control method of stabilizing undergound openings: Proc. 7 Can. Rock Mech. Symp. Edmonton, March 1971, pp. 99-118.

Serata, S., and Cundey, T.E., 1978, Rheological method of salt county design for underground storage of solid liquid, and gaseous matters: in 19th U.S. Symp. on Rock Mech. ed. Y.S. Kim, Reno, Nevada.

Serata, S., Sakuri, S., and Adachi, T., 1972, Theory of aggregate rock behavior based on absolute three-dimensional testing (ATT) of rock salt: in Basic and Applied Rock mechanics, Proc. 10th U.S. Symp. Rock Mech., K.E. Gray (ed.), AIME.

Shelby, J.E., 1978, Permeability of Sodium Cloride: Sandia Laboratories interoffice memo, Albuquerque, New Mexico.

St. John, C.M., 1978, Computer models and the design of underground radioactive waste repositories, M.I.T. Special Summer Session on Rock Engineering, June 1978.

Sutherland, H.J., 1978, Permeability of SENM rock salt: Sandia interoffice memo, Albuquerque, New Mexico.

Szeki, A, 1978, Influence of Volume on Creep Behavior of Rocksalt Pillars, Fifth. Int. Salt Sympos., Hamburg, Germany.

Terra Tek Inc., 1978, Gas permeabilities of SENM salt: consulting memo to Sandia Laboratories, Albuquerque, New Mexico.

Thompson, E., and Ripperger, E.A., 1964, An Experimental Technique for the Investigation of the Flow of Halite and Sylvinite, Proc. 6th Symp. Rock Mech., E.M. Spokes and C.R. Christiansen, eds., AIME.

Thoms, R.L., Char, C.V., and Bergeron, W.J., 1973, Finite Element Analysis of Creep in Rock-Salt Pillar Models, Proc. 14th, Symp. Rock Mech., H.R. Hardy and R. Stefanko eds., AIME.

Uhlenbecker, F.W., 1968, Verformungsmessungen in der Grube und erganzende Laboruntersuchungen auf dem Kaliwerk Hattorf (Werra-Revier) im Hinblick auf eine optimale Festlegung des Abbauverlustes bei grobtmoglicher Sicherheit der Grubenbaue, PhD Thesis, TH Clausthal.

U.S. Corps. of Engineers, 1963, Project Dribble, Petrographic examination and physical tests of cores, Tatum Salt Dome, Mississippi: Army Engineers Waterway Experiment Station, Techn. Rep. No. 6-614.

Wahi, K.K., Maxwell, D.F., Hofmann, 1978, Explicit finite-difference simulations of Project Salt Vault: in 19th U.S. Rock Mech. Symp., ed. Y.S. Kim, Reno, Nevada.

Wawersik, W.R. and Brown, W.S., 1973, Creep Fracture of Rock, Techn. Report UTEC 73-197, Univ. of Utah,

Wawersik, W.R., 1975, Technique and apparatus for strain measurements on rock in constant confining pressure experiments. Rock Mech. v. 7, 231.

Wawersik, W.R., 1977, Sandia Laboratories Albuquerque, New Mexico, Inter office memos, August and November.

Wawersik, W.R., 1978a, Large specimen triaxial apparatus for rock testing to 70 MPa confining pressure and 225°C: to be published.

Wawersik, W.R., 1978b, Effects of pressure, deviator stress and temperature on transient creep of rock salt at low confining pressure: AGU, Vol 59 No. 4, Apr. 78 p. 376.

Wawersik, W.R., 1978c, Sandia Laboratories, Albuquerque, New Mexico, Inter Office Memo, January.

Wawersik, W.R., Callender, J.F., Weaver, R., and Dropek, R.K., 1976, Preliminary determination of mechanical properties on rock salt from southeastern New Mexico. Pre-Proc., 17th U.S. Symp. Rock Mech., Univ. Utah Exp. St..

Wawersik, W.R. and Hannum, D.W., 1978, Mechanical behavior of New Mexico rock salt in triaxial compression up to 200°C: 5th Int'l Salt Symp. Hamburg, Germany, June 1978.
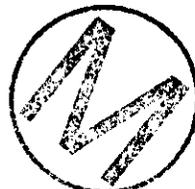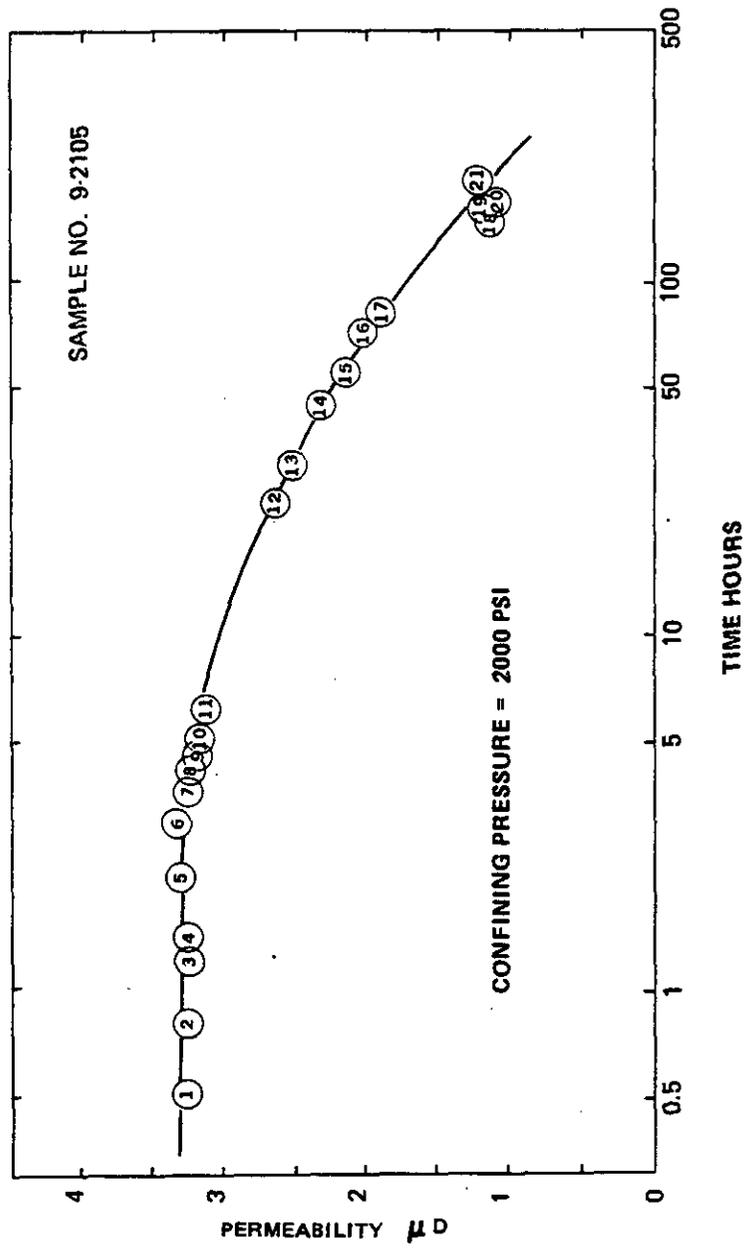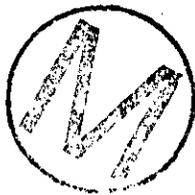
ARGON PERMEABILITY OF ROCK SALT SAMPLE AT 2000 PSI

CONFINING PRESSURE
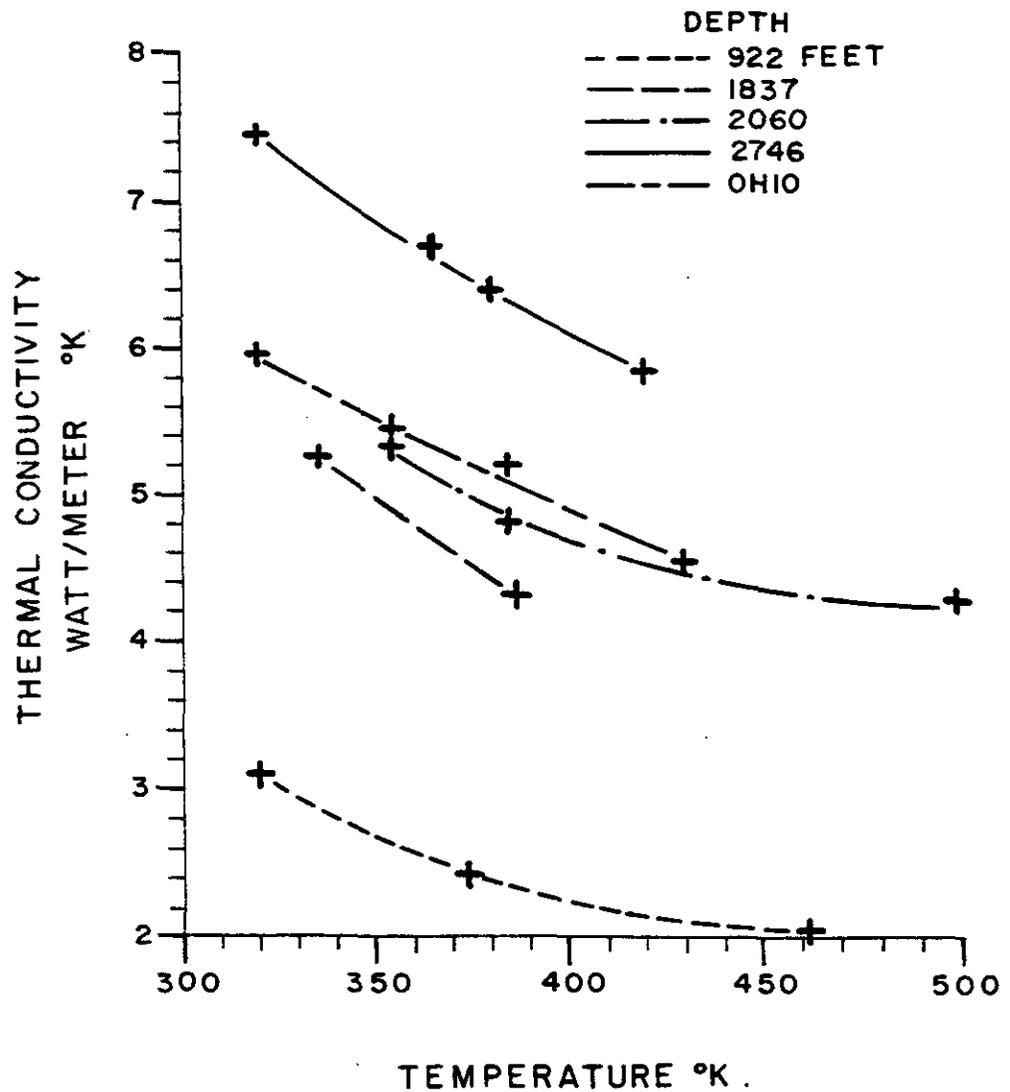
FIGURE 9.2.3-1

THERMAL CONDUCTIVITY OF ROCKSALT

CORE SECTIONS CONTAINING 50%

OR MORE HALITE, WELL AEC 8

From: Acton, 1977

FIGURE 9.2.3-2
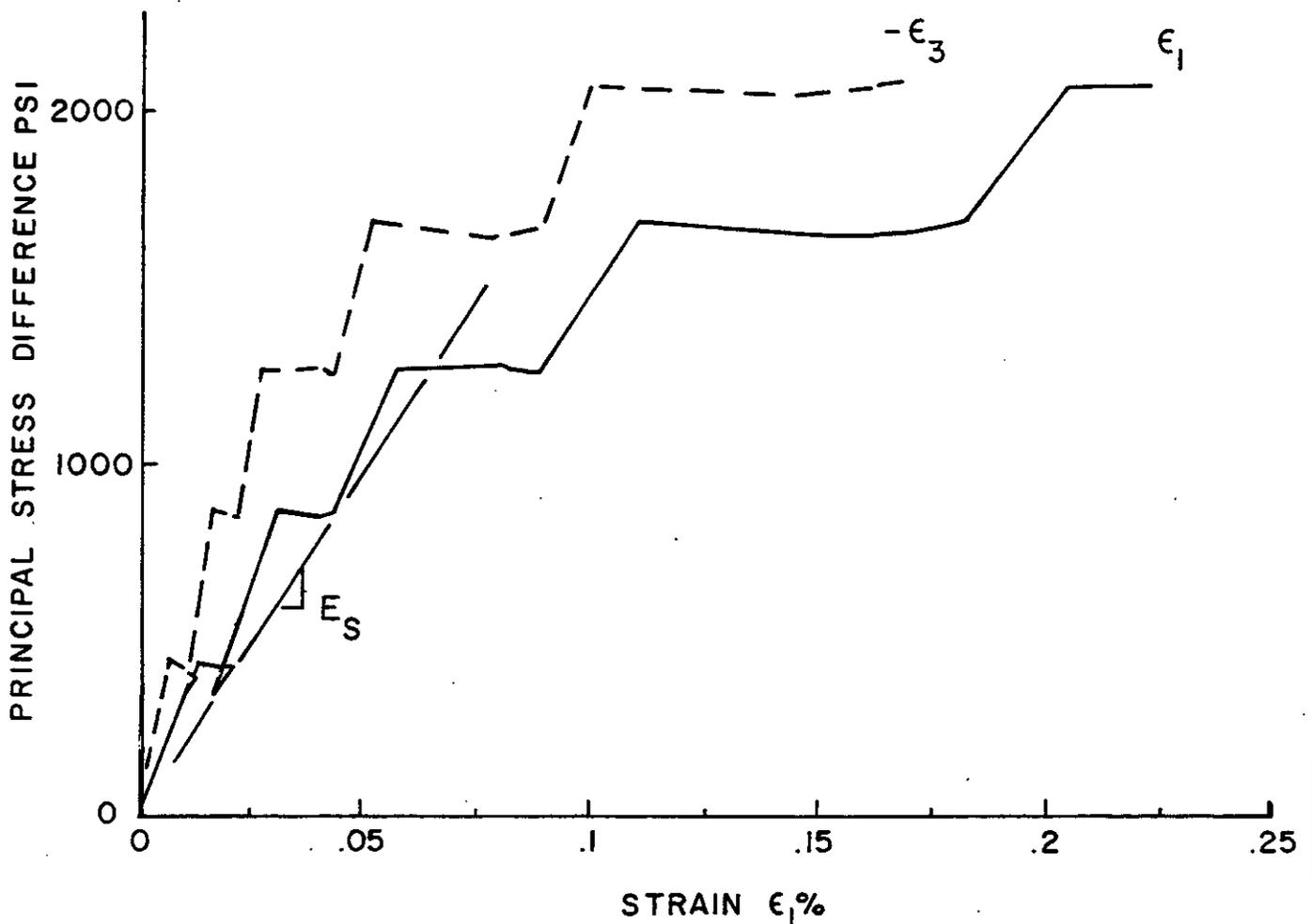
TRIAXIAL STRESS-STRAIN CURVES IN

REGIME OF SMALL PRINCIPAL STRESS DIFFERENCES

AND STRAIN

From: Wawersik and Hannum, 1978

FIGURE   9.2.4-1
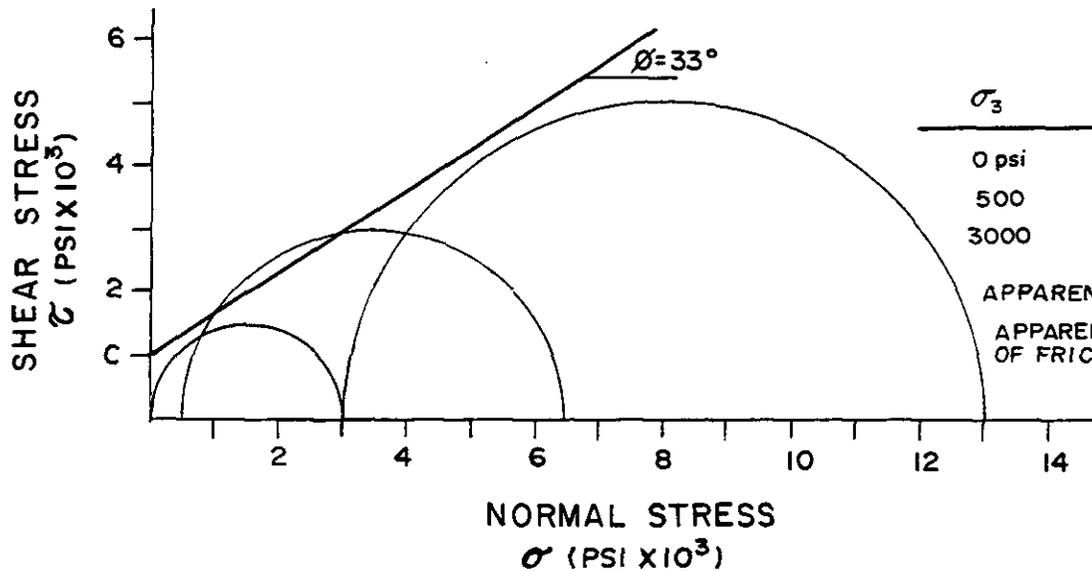
CONFINING PRESSURE	PRINCIPAL STRESS DIFFERENCE	AXIAL STRAIN AT FAILURE
σ_3	$(\sigma_1 - \sigma_3)$	ε_1
0 psi	3000 psi	2.5%
500	6000	15
3000	>10,000	>20

APPARENT COHESION C=1000 psi

APPARENT ANGLE OF FRICTION $\emptyset$ = 33°

T = 23°

A. MOHR'S ENVELOPE AT ULTIMATE STRENGTH
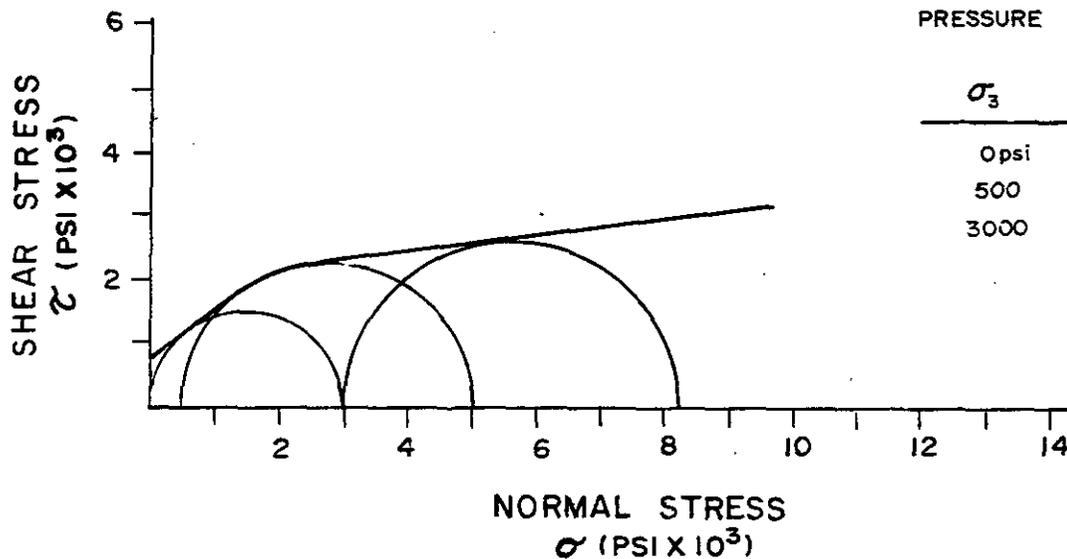
CONFINING PRESSURE	PRINCIPAL STRESS DIFFERENCE	AXIAL STRAIN
σ_3	$(\sigma_3 - \sigma_1)$	ε_1
0 psi	3000 psi	2.5%
500	4500	2.5
3000	5250	2.5

T = 23°

B. MOHR'S ENVELOPE AT CONSTANT STRAIN

NOTES:

1. THE SAME TEST DATA WERE USED TO GENERATE BOTH ENVELOPES. (TABLE 9 III, 9 IV ; WAWERSIK, 1977)

2. THESE QUASI-STATIC PROPERTIES DO NOT ACCOUNT FOR ANY STRENGTH DETERIORATION WITH TIME.

FIGURE   9.2.4-2
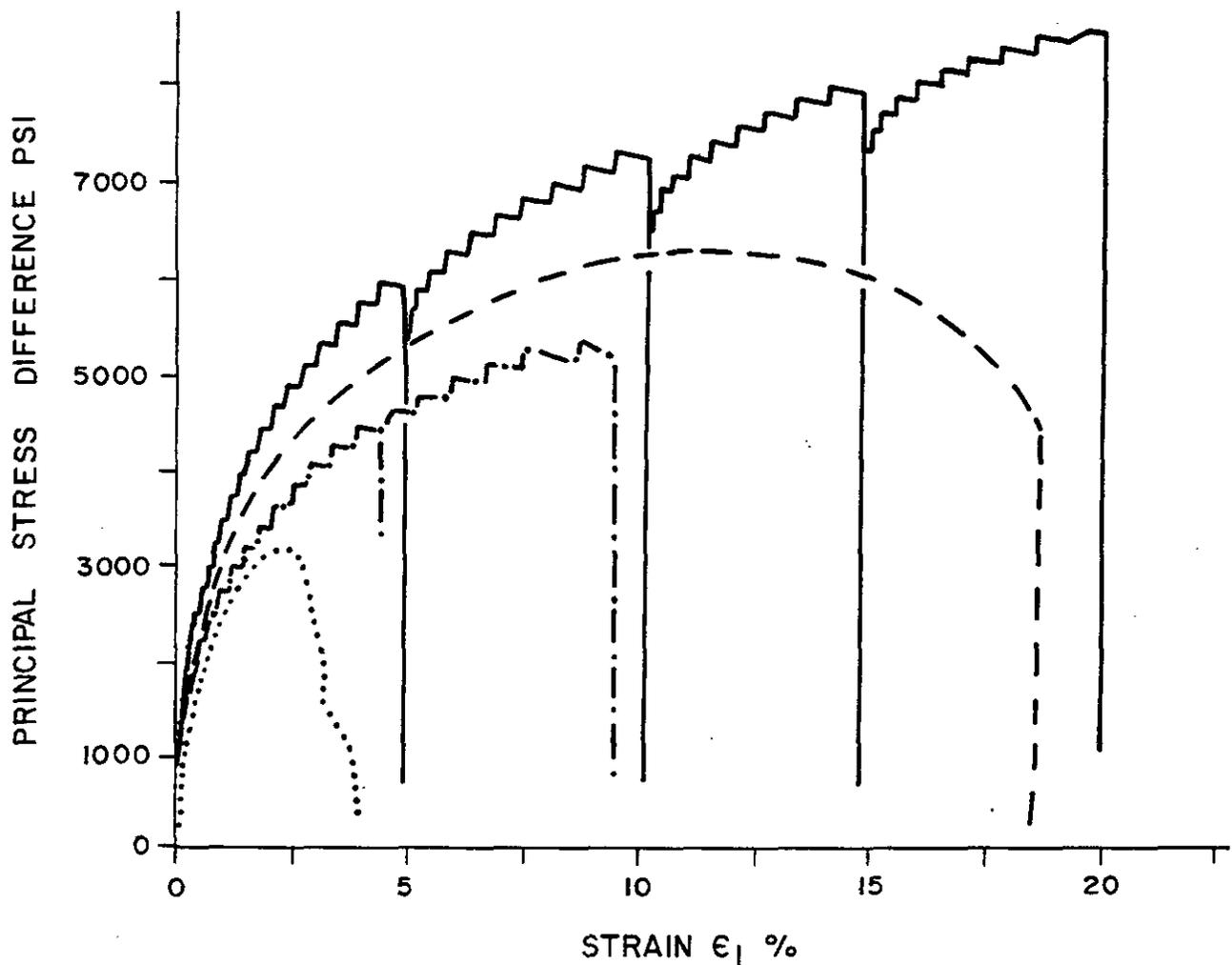
CONVENTIONAL QUASI-STATIC TRIAXIAL

STRESS-STRAIN DATA AT AMBIENT TEMPERATURE

EFFECT OF PRESSURE

From: Wawersik and Hannum, 1978
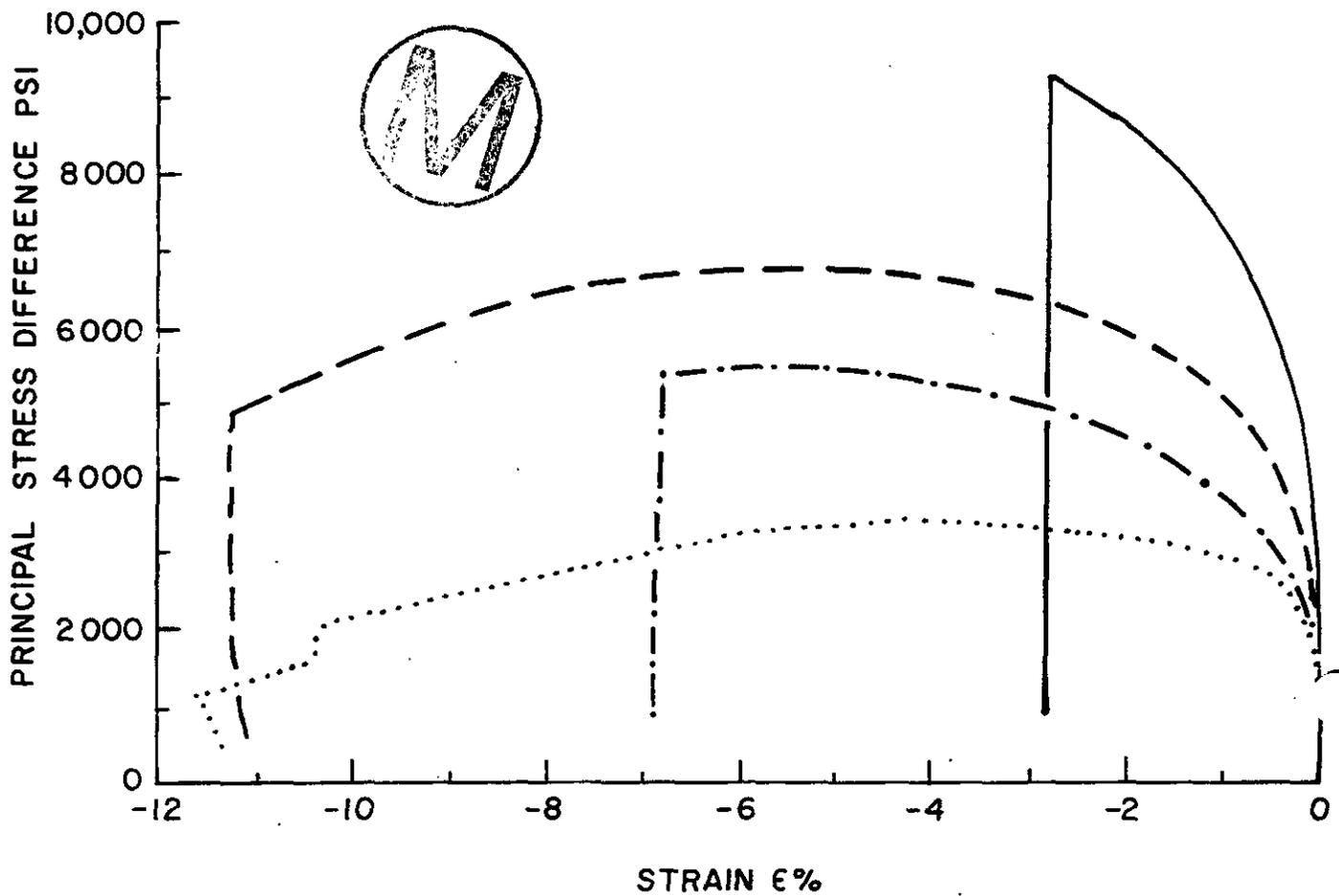
FIGURE 9.2.4-3

KEY

.... 9-2676 (0, 23)
    Hole No. — Sample depth in ft. (Conf. pressure in ksi, Temp. in °C)
— · — 7-2837 (.25, 23)
— — 9-2601 (.50, 23)
——— 9-2601.5 (3.0, 23)

PRINCIPAL STRESS DIFFERENCE VS. VOLUMETRIC

STRAIN FOR TEST OF FIGURE 9.2.4-3
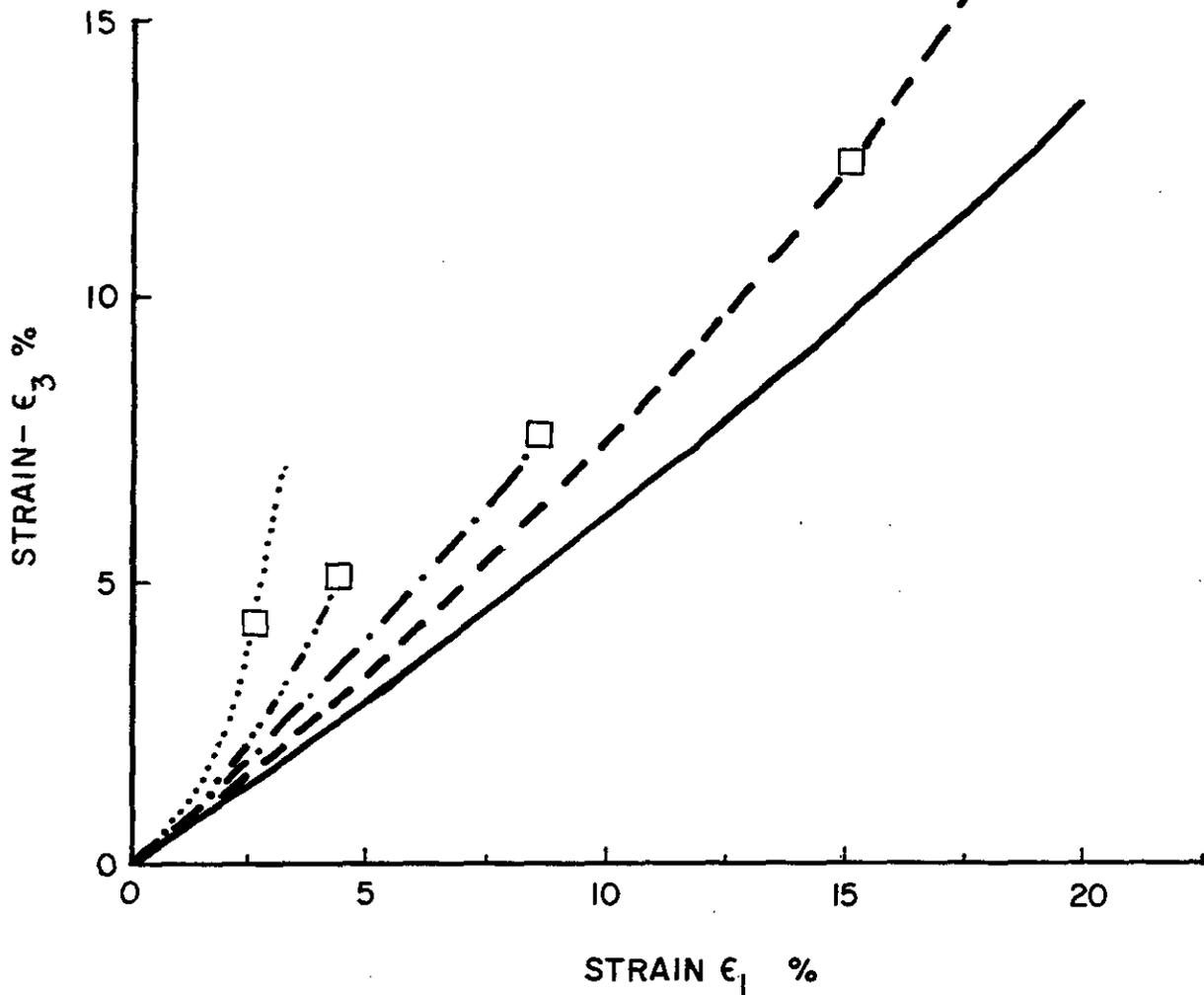
From: Wawersik and Hannum, 1978

FIGURE 9.2.4-4

KEY

.... 9-2676 (0, 23)
Hole No. — Sample depth in ft. (Conf. pressure in ksi, Temp. in °C)
— ··— 9-2689 (.10, 23)
— ·— 7-2837 (.25, 23)
— — 9-2601 (.50, 23)
——— 9-2601.5 (3.0, 23)

NOTE: Open squares identify approximate strains at ultimate stresses.

TRIAXIAL VARIATION OF LATERAL STRAIN VS. AXIAL
STRAIN FOR TEST OF FIGURE 9.2.4-3
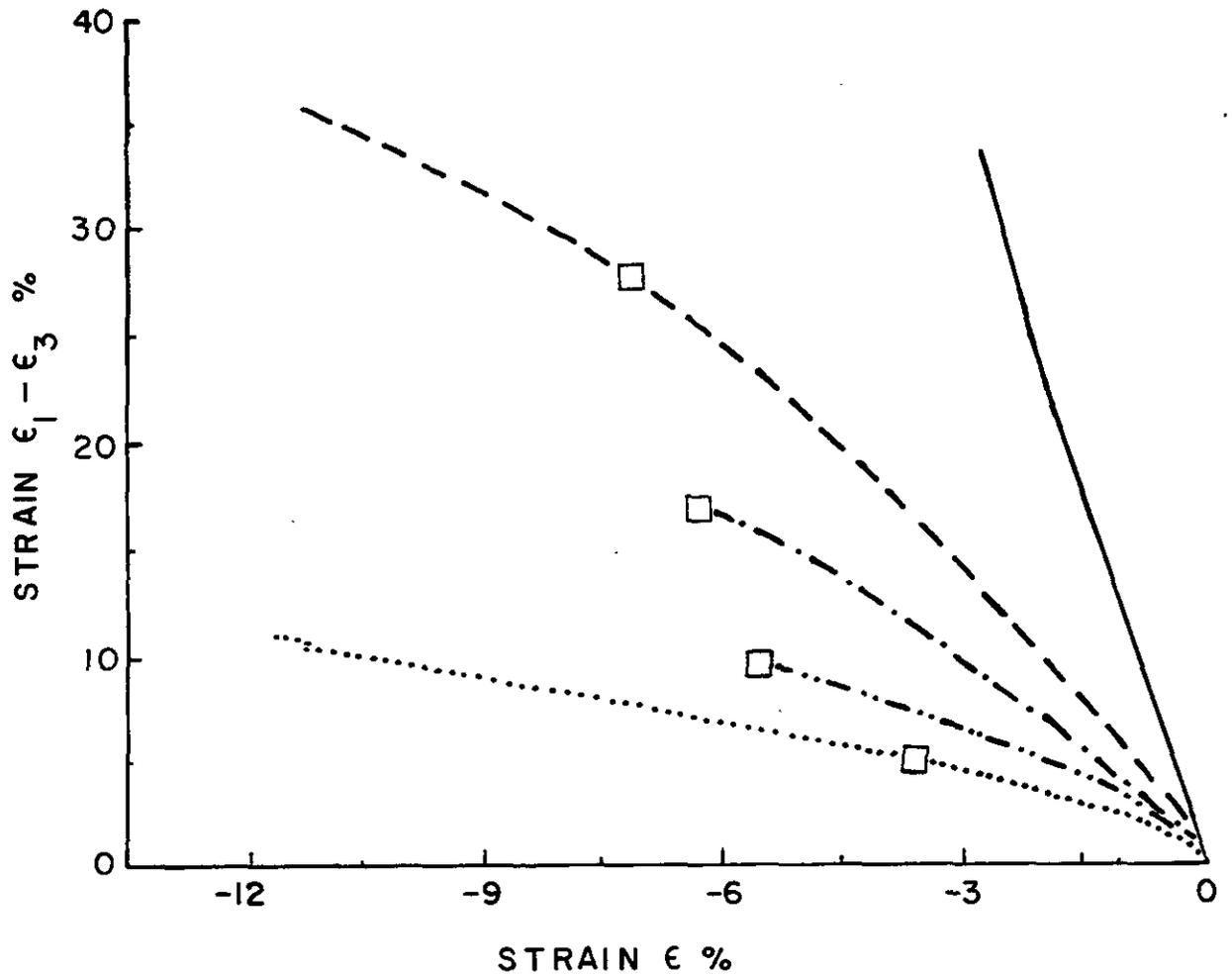
From : Wawersik and Hannum, 1978

FIGURE 9.2.4-5

KEY

········· 9-2676 (0, 23)
          Hole No. — Sample depth in ft. (Conf. pressure in ksi, Temp. in °C)

—··— 9-2689 (.10, 23)
—·— 7-2837 (.25, 23)
—— 9-2601 (.50, 23)
——— 9-2601.5 (3.0, 23)

NOTE: Open squares identify approximate strains at ultimate stresses.

TRIAXIAL VARIATION OF SHEAR STRAIN VS VOLUMETRIC STRAIN FOR TESTS OF FIGURE 9.2.4-3

From: Wawersik and Hannum, 1978

FIGURE 9.2.4-6

KEY
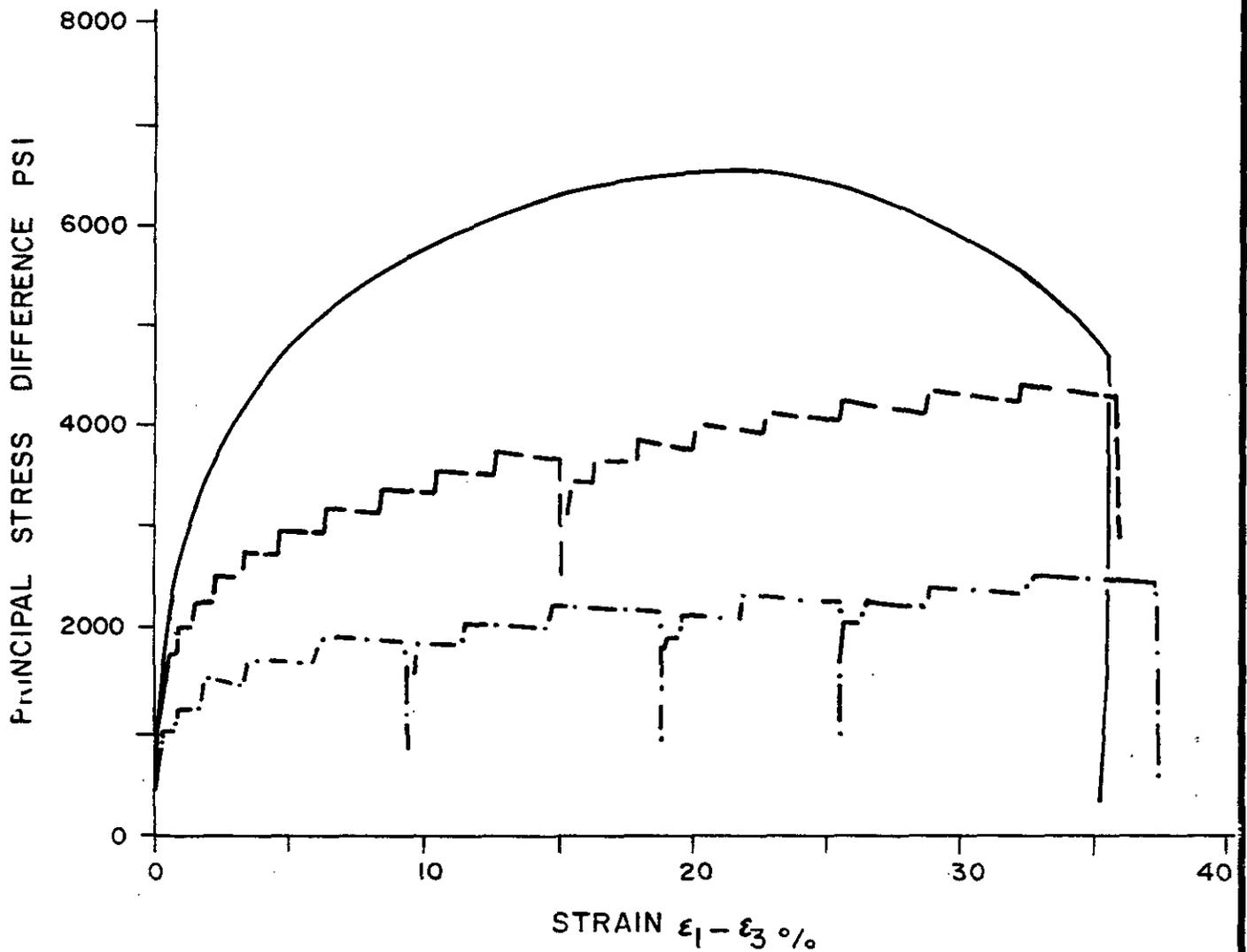
———	9-2601 (.50, 23)
	Hole No. — Sample depth in ft. (Conf. pressure in ksi, Temp. in °C)
— —	9-2673.4 (.50, 100)
—··—··—	9-2604 (.50, 200)

TRIAXIAL STRESS-STRAIN CURVES AS A FUNCTION OF TEMPERATURE AT CONSTANT CONFINING PRESSURE
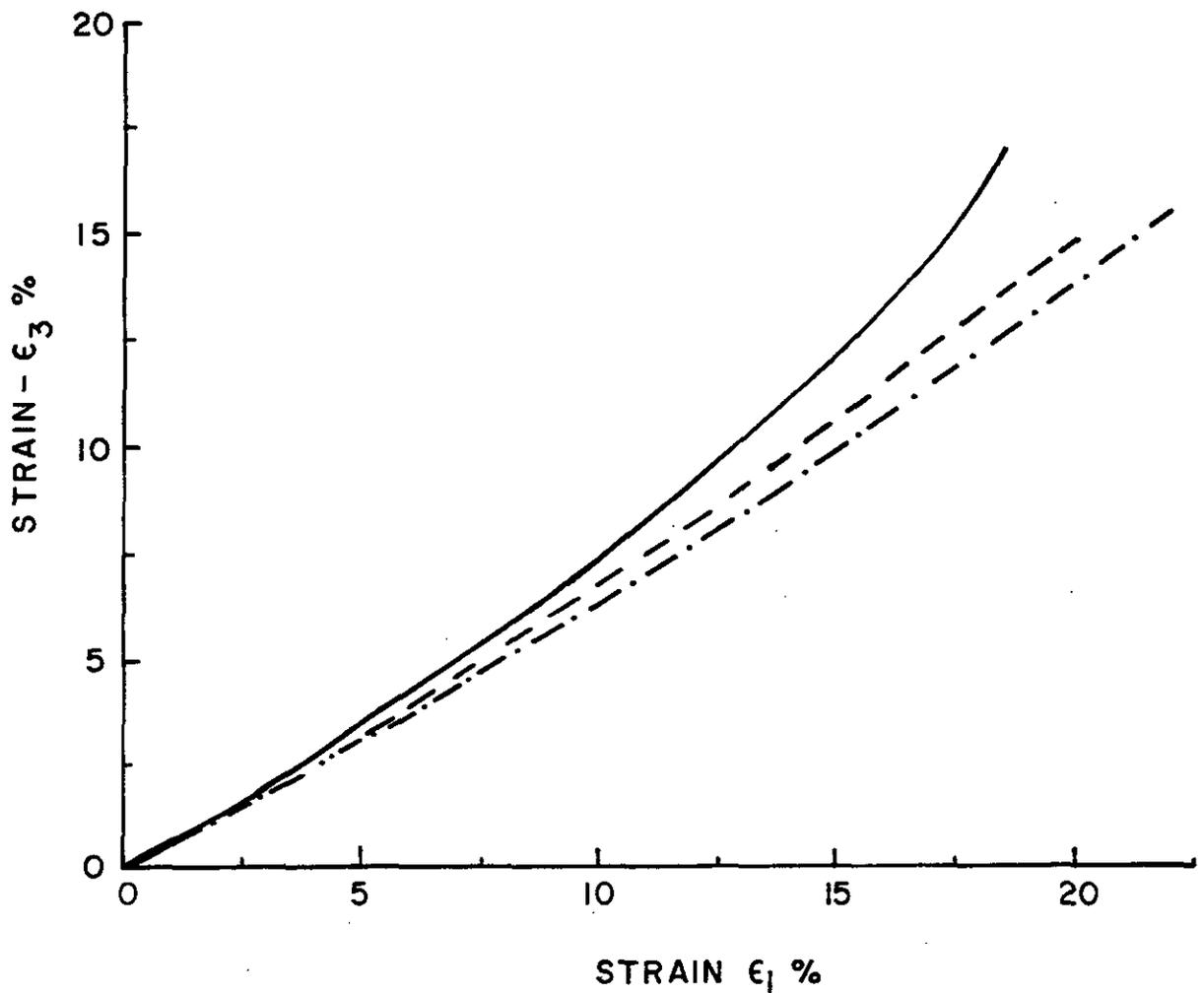
From : Wawersik and Hannum, 1978

FIGURE 9.2.4-7

KEY

———	9-2601 (.50, 23)
	Hole No. — Sample depth in ft. (Conf. pressure in ksi, Temp. in °C)
— —	9-2673.4 (.50, 100)
—·—	9-2604 (.50, 200)

VARIATION OF LATERAL VS. AXIAL STRESS

FOR TESTS OF FIGURE 9.2.4-7
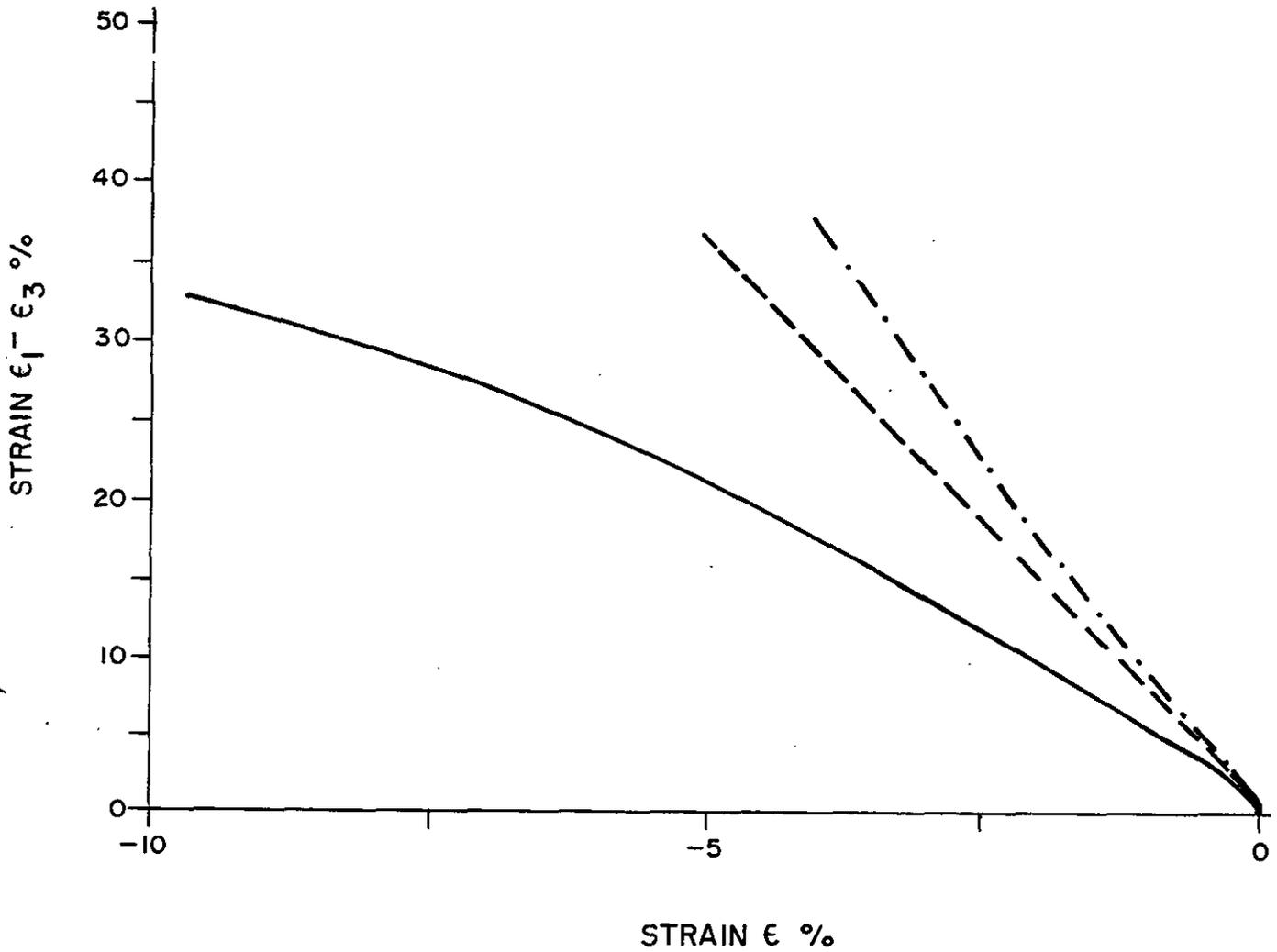
From: Wawersik and Hannum, 1978

FIGURE 9.2.4 - 8

KEY

————	9-2601 (.50, 23)
	Hole No. — Sample depth in ft. (Conf. pressure in ksi, Temp. in $^{\circ}$C)
— —	9-2673.4 (.50, 100)
—·—	9-2604 (.50, 200)

VARIATION OF SHEAR-STRAIN VS. VOLUMETRIC

STRAIN FOR TESTS OF FIGURE 9.2.4-7

From: Wawersik and Hannum, 1978

FIGURE 9.2.4-9
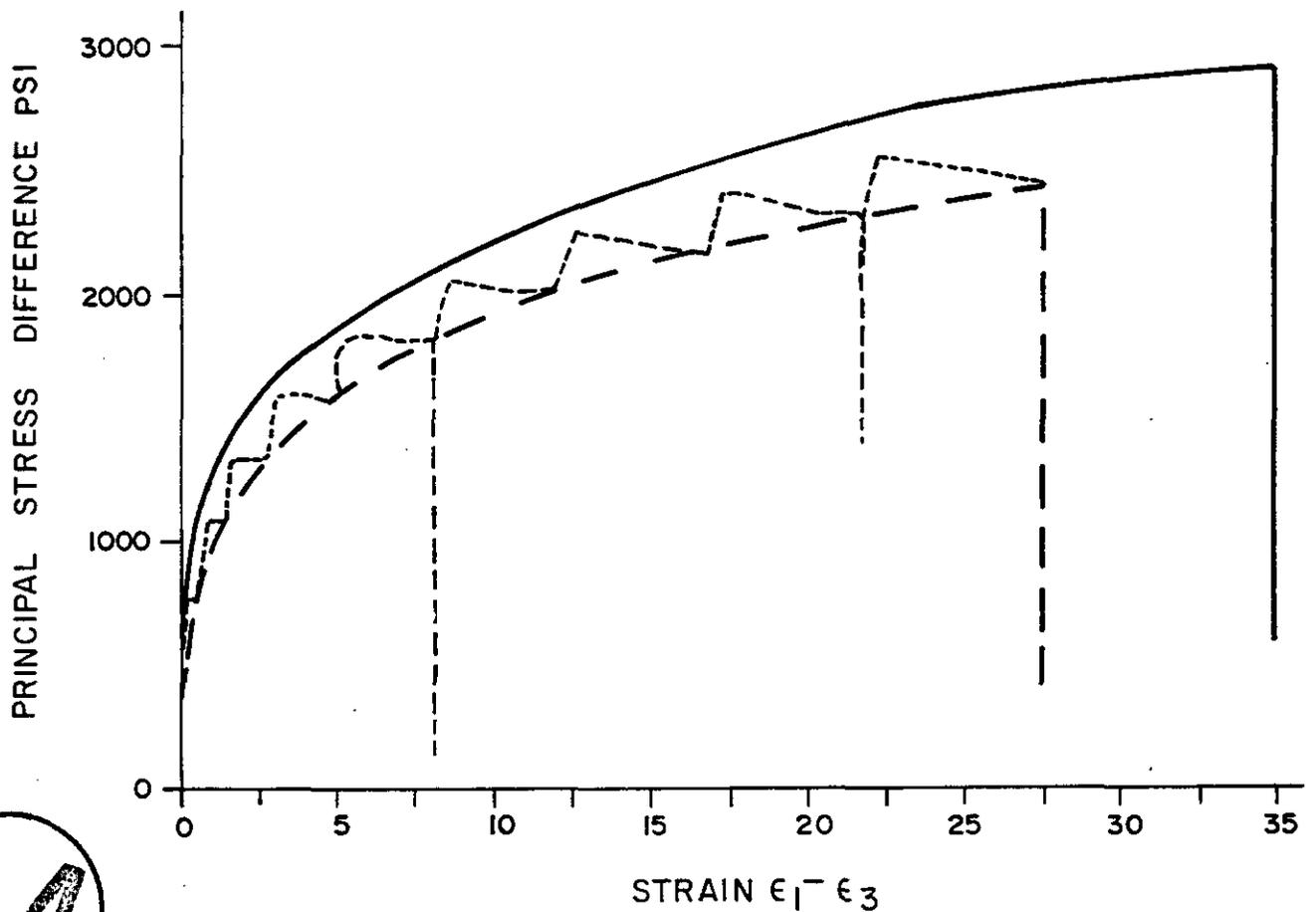
KEY

—————— 7-2740 (.50, 200)
Hole No. — Sample depth in ft. (Conf. pressure in ksi, Temp. in $^\circ$C)
— — — 7-2744 (3.0, 200)
------ Actual load path

TRIAXIAL STRESS STRAIN CURVES AS A

FUNCTION OF CONFINING PRESSURE AT

200°C
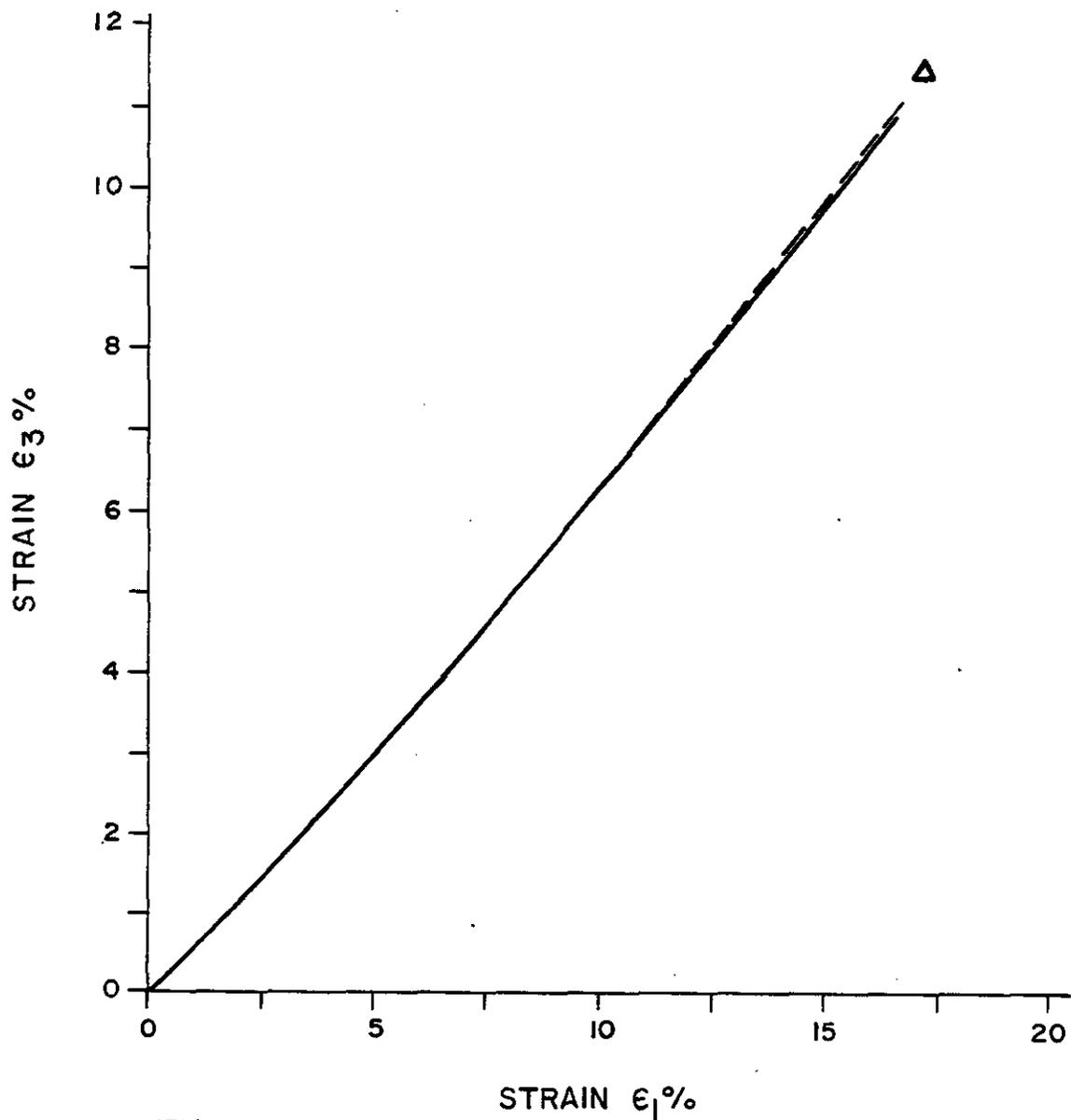
From : Wawersik and Hannum, 1978

FIGURE 9.2.4-10

KEY

△   7-2836 (0, 200)
        Hole No. — Sample depth in ft. (Conf. pressure in ksi, Temp. in °C)
——   7-2740 (.50, 200)
- - -   7-2744 (3.0, 200)

VARIATION OF LATERAL STRAIN VS. AXIAL STRAIN

FOR TESTS OF FIGURE 9.2.4-10

(PLUS ONE ADDITIONAL TEST
IN UNIAXIAL COMPRESSION)
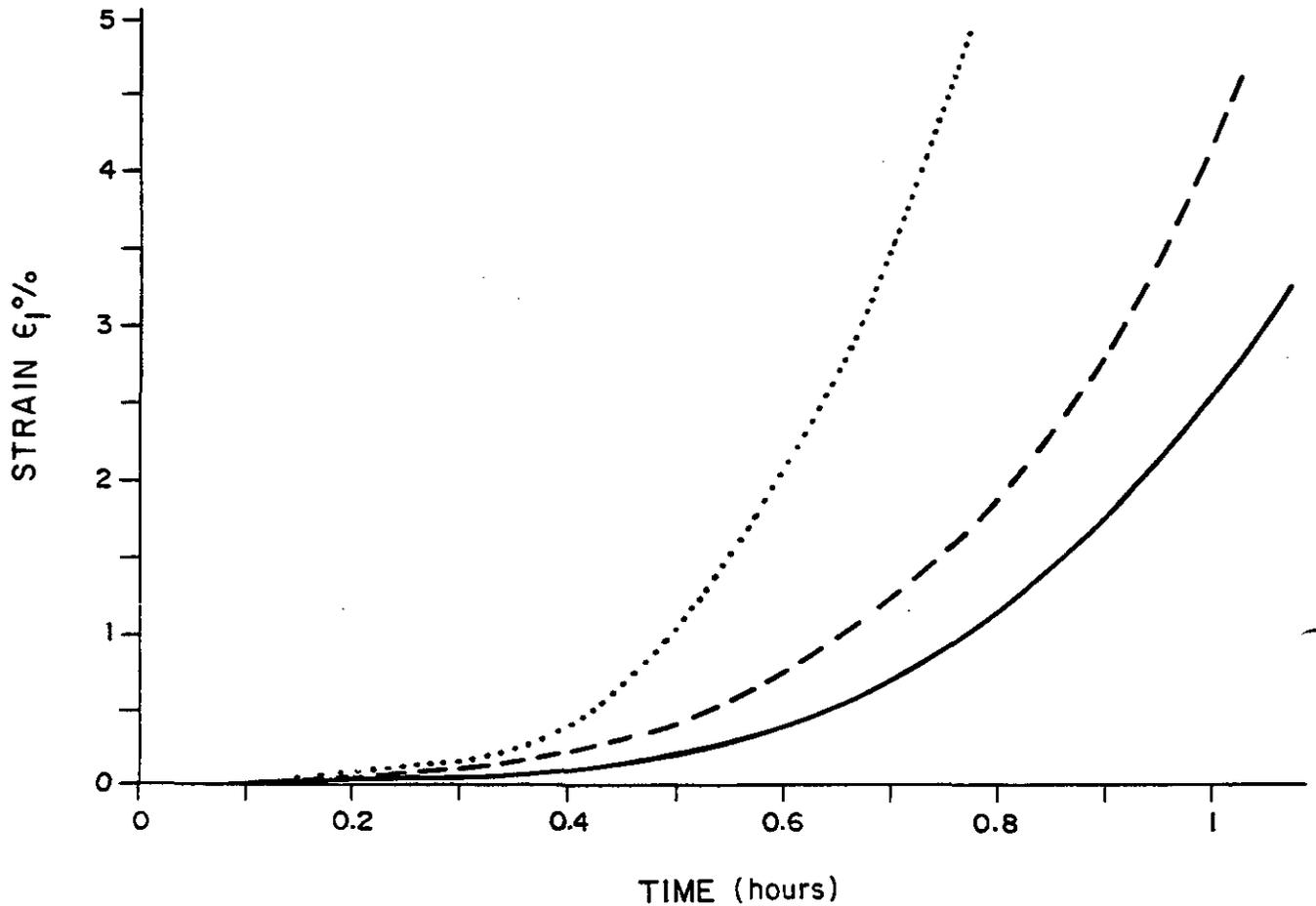
From: Wawersik and Hannum, 1978

FIGURE 9.2.4-11

KEY

.... 7-2836 (0, 200)
Hole No. — Sample depth in ft. (Conf. pressure in ksi, Temp. in °C)
- - - 7-2740 (.50, 200)
——— 7-2744 (3.0, 200)

AXIAL STRAIN VS. TIME FOR TEST OF

FIGURES 9.2.4-10 AND 9.2.4-11

From: Wawersik and Hannum, 1978

FIGURE 9.2.4-12
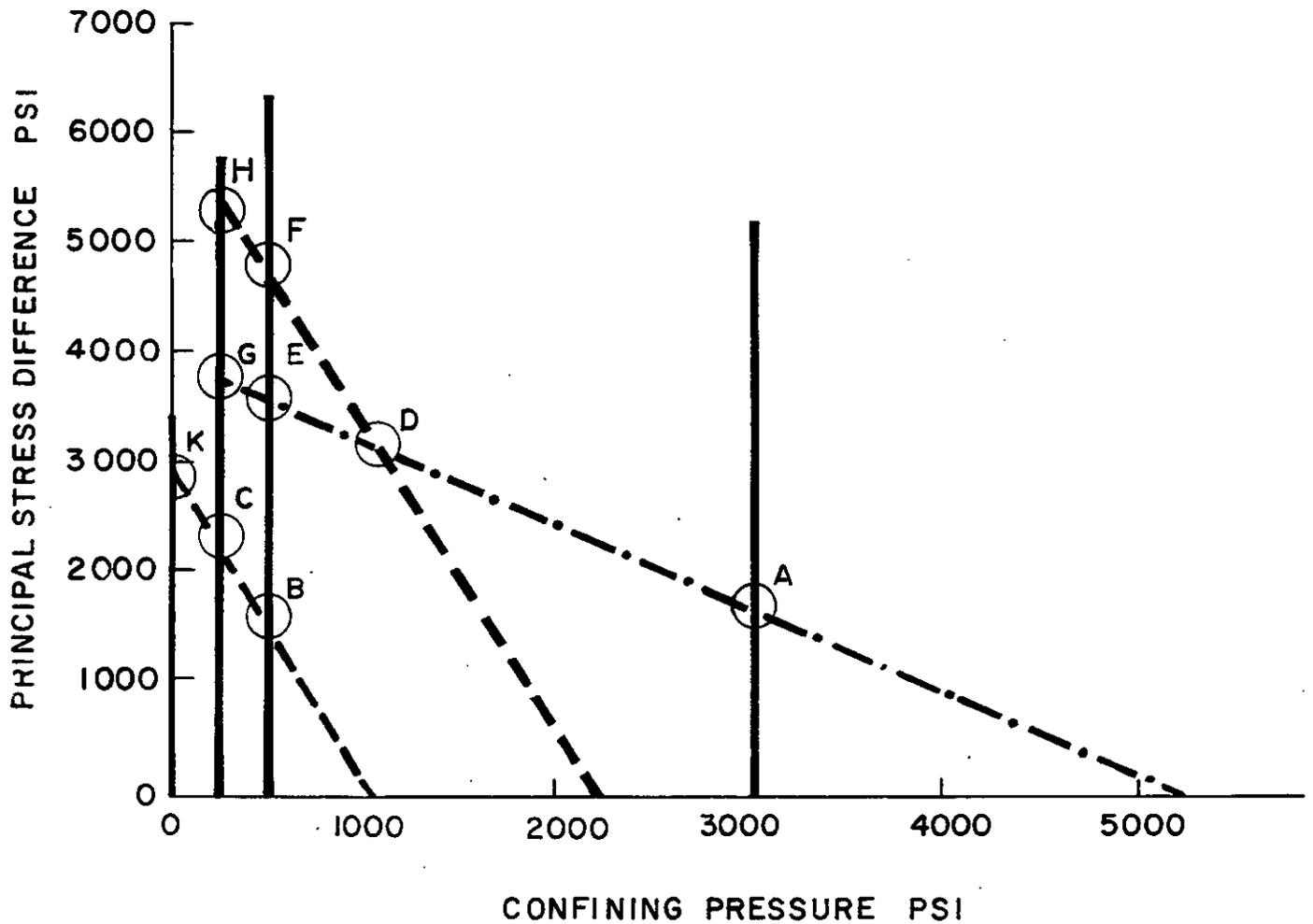
KEY

—— Load Path I ($\sigma_2 = \sigma_3 = $ const.)

– – – Load Path II ($\sigma_m = $ const.) $\sigma_m = \dfrac{\sigma_1 + \sigma_2 + \sigma_3}{3}$

—·—·— Load Path III ($\sigma_1 \approx $ const.)

NOTE: See table 9.2.4-3 for tabulated data.

MAP OF THREE NON-PROPORTIONAL LOAD PATHS

AND COMMON STRESS STATES

(POINTS A THROUGH K)

From : Wawersik and Hannum, 1978

FIGURE 9.2.4-13

STRESS-STRAIN CURVES

FOR SAMPLE SUBJECTED TO

ONE OR MORE CONFINING PRESSURES

From: Wawersik and Hannum, 1978

FIGURE 9.2.4-14

KEY
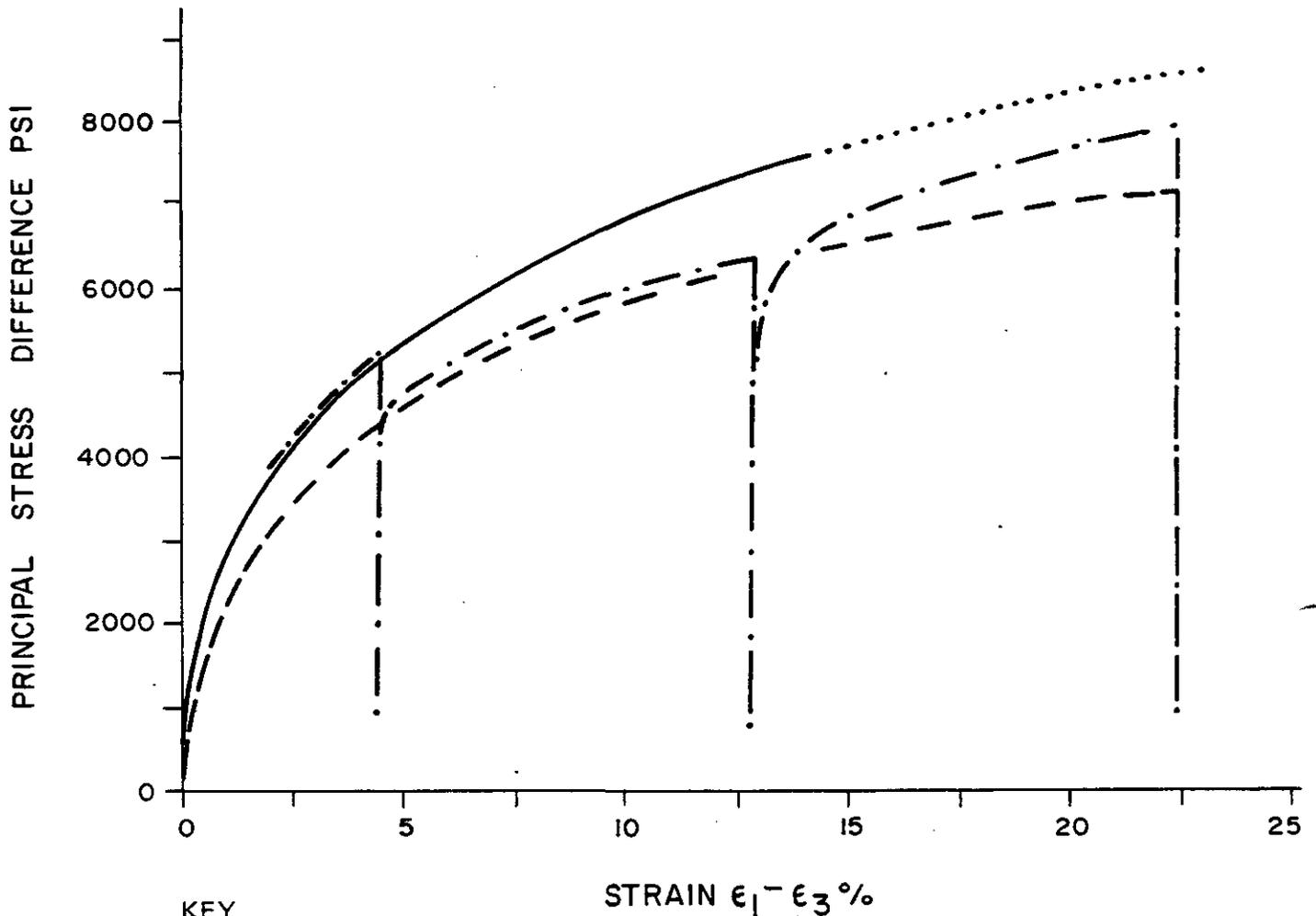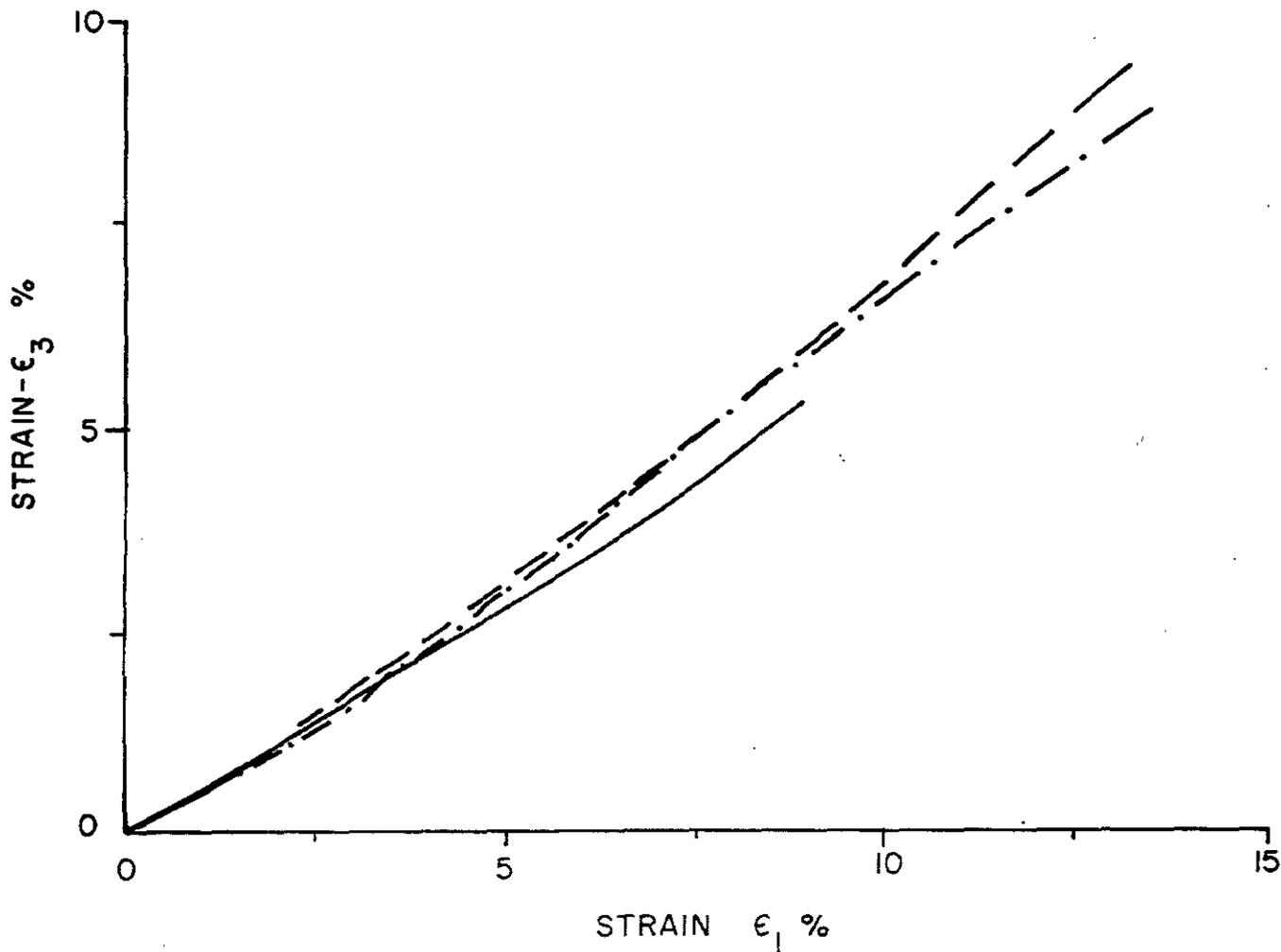
— — — 7-2725 (.50, 23)
Hole No. — Sample depth in ft. (Conf. pressure in ksi, Temp. in °C)
———— 7-2745 (3.0, 23)
—·—·— 7-2740.5 (3.0/.50/3.0, 23)

VARIATION OF LATERAL STRAIN VS.

AXIAL STRAIN FOR TESTS OF FIGURE 9.2.4-14

From : Wawersik and Hannum, 1978
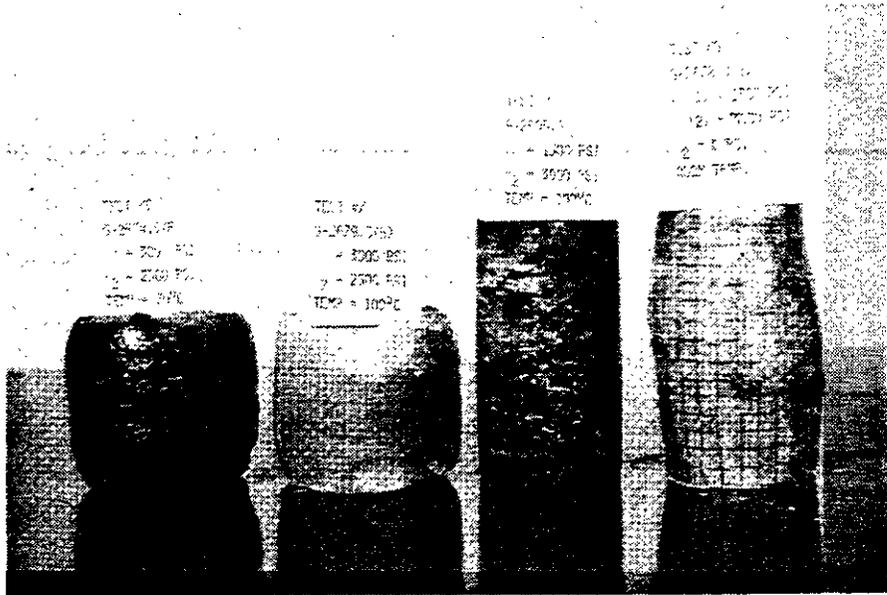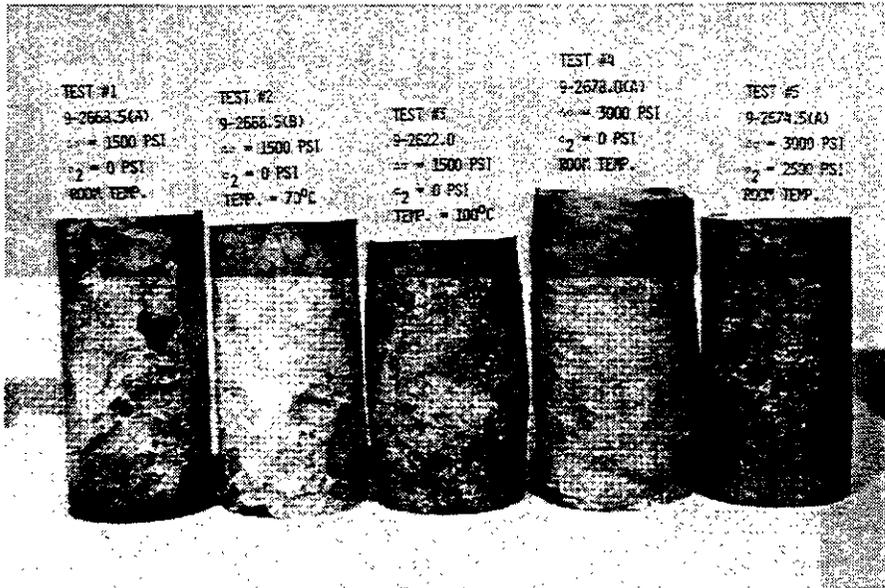
FIGURE 9.2.4-15

DEFORMED CORE SAMPLES OF ROCK SALT
FROM DRILL HOLE ERDA #9

FROM: HANSEN and MELLEGARD, 1977   FIGURE 9.2.4—16

Table 9.2.3-1: Physical properties of rock from WIPP study area

Material	Depth (ft)	Density (gm/cc)	Avg. Porosity (Range) (%)	Mass (Moisture) Loss (% to $\leq 300^\circ$C)	Resistivity in Ohm Meters	Avg. Air Permeability (Range) in (md)[2]	(P) Wave[3] Velocity (Km/sec)
Rock Salt	2000-2100	2.18	0.4 (0.1-0.8)	N[1] – 1.0	58,100	0.01 (0.0003-0.17)	(4.42-4.62)
Rock Salt	2600-2700	2.18	0.5 (0.3-0.7)	N – 0.4	(4,900-230,000)	–	–
Anhydrite		2.80	–	–	–	–	–
Polyhalite	–	2.70	–	–	–	–	–
Siltstone	–	2.26	–	–	–	–	–

[1] N – None Measured

[2] Core Labs Data; see also Figure 9.2.3-1

[3] Note: P Wave velocities determined in the lab agree to 15% with those measured downhole on borehole ERDA 9 (Griswold, 1977).

Table 9.2.4.-1 – Representative unconfined mechanical properties of rock salt from the WIPP study area

Material	Drillhole/ Approx. Depth (ft)	Uniax. Compr. Strength (psi)	Strain at failure percent	Brazilian Tensile Strength (psi)	Initial Elastic Limit $(\sigma_1 - \sigma_3)$ (psi)	Secant Modulus x10^6 (psi)	Principal Strain Ratio	Principal Strain Ratio, $\varepsilon_3/\varepsilon_1$ at Failure
Rock Salt	AEC 7,8/1900	2450	≥ 1.7	200	≤ 750	1.94	0.33	–
Rock Salt	AEC 7,8/2700	3700	3.6	240	≤ 750	1.94	0.34	–
Rock Salt	ERDA 9/2100	2400	1.6	–	< 200	–	–	1.6
Rock Salt	ERDA 9/2700	3300	2.9	–	< 200	–	–	2.1

Note: Loading rates – $30 \leq \dfrac{d}{dt} (\sigma_1 - \sigma_3) \leq 215$ psi/min

1 Megapascal (MPa) equals about 145 psi
Symbols < and > denote experimental uncertainty.

Table 9.2.4-2 – Representative triaxial compression data for rock salt from the WIPP study area

Drillhole/ Depth (ft)	Confining Pressure (psi)	Temp. (°C)	Ultimate (max) Princ. Stress Diff. (psi)	Ultimate (max) Strain, ε_1 Percent	Initial Elastic Limit $(\sigma_1 - \sigma_3)$ (psi)	Secant Modulus $\times 10^6$ (psi)	Principal Strain "Poissons'" Ratio	Max. Obs. Princ. Strain Ratio
ERDA 9/2100	500	23	6000	12	$\leq$100	2.7	0.20	- 0.72
ERDA 9/2100	3000	23	> 9000	>20	$\leq$100	2.7	0.20	- 0.65
ERDA 9/2600- 2700	500	23	6300	15	$\leq$100	2.7	0.20	- 0.80
ERDA 9/2600- 2700	3000	23	> 8900	>20	$\leq$100	2.7	0.20	- 0.67
AEC 7/2700- 2800	500	23	> 6200	>13	$\leq$100	2.7	0.21	- 0.71
AEC 7/2700- 2800	500	100	$\approx$ 4200	$\geq$18	$\leq$100	-	-	- 0.69
AEC 7/2700- 2800	500	200	$\approx$ 2400	>17	$\leq$100	2.4	-	- 0.68
AEC 7/2700- 2800	300	200	> 2750	>17	$\leq$100	-	-	-
ERDA 9/2600	500	200	> 2500	>22	$\leq$100	-	-	- 0.68

Note: Loading rate $d/dt\ (\sigma_1 - \sigma_3) = 30$ to 60 psi/min.

Table 9.2.4-3 Deviatoric Load Path Data For Figure 9.2.4-13

Reference Point In Figure 15	Load Path	$(\sigma_1 - \sigma_3)$ PSI	$\sigma_2 = \sigma_3$ PSI	σm PSI	ε_1 %	$-\varepsilon_3$ %
A	I	1600	2970	3550	0.17	0.07
	III	1640	3020	3570	0.075	0.05
B	I	1520	520	1015	0.357	0.175
	II	1500	520	1015	0.3	0.168
C	I	2200	260	1040	o.782	0.441
	II	2250	250	1015	0.769	0.476
D	II	3190	1120	2180	1.35	0.786
	III	3150	1120	2160	0.73	0.454
E	I	3540	520	1670	1.38	0.828
	II	3580	510	1700	1.12	0.705
F	I	4700	490	2090	4.04	2.434
	II	4740	510	2120	3.92	2.430
G	I	3840	250	1490	2.486	1.85
	III	3780	250	1500	1.49	1.01
H	I	5240	250	1990	8.58	7.81
	III & I	5140	260	2000	6.41	5.46
	II	5320	276	2070	5.71	3.79
K	I	2950	0	990	1.49	1.47
	II	2950	15	1000	1.58	1.19
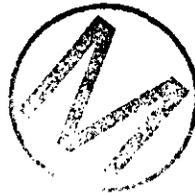
Table 9.3-1

REPRESENTATIVE BRINES/SOLUTIONS
FOR
WIPP EXPERIMENTATION

Ion	Brine "A" (mg/liter) (± 3%)	Brine "B" (mg/liter) (± 3%)	Solution "C" (mg/liter) (± 3%)
Na^+	42,000	115,000	100
K^+	30,000	15	5
Mg^{++}	35,000	10	200
Ca^{++}	600	900	600
Fe^{+++}	2	2	1
Sr^{++}	5	15	15
Li^+	20	-	-
Rb^+	20	1	1
Cs^+	1	1	1
Cl^-	190,000	175,000	200
SO_4^{--}	3,500	3,500	1,750
$B (BO_3^{---})$	1,200	10	-
HCO_3^-	700	10	100
NO_3^-	-	-	20
Br^-	400	400	-
I^-	10	10	-
pH (adjusted)	6.5	6.5	7.5
specific gravity	1.2	1.2	1.0

Table 9.3-2

Nominal Concentration of Nuclides Used in Kd Measurements

Nuclide	Concentration, ppm
^{137}Cs	0.012
Stable Cs	1.0
^{85}Sr	0.03 - 0.3
Stable Sr	5 - 15
^{106}Ru	2500
^{99}Tc	59
^{152}Eu	0.1 - 1.0
^{144}Ce	3×10^{-4}
^{131}I	5×10^{-5}
^{153}Gd	0.2 - 2.0
^{125}Sb	≤ 0.01
^{243}Am	5.4
^{244}Cm	0.012
^{238}Pu	0.058

Table 9.3-3

Distribution Coefficients on Samples From the Magenta Dolomite

Fission Product Distribution Coefficients

	pH range	Cs	Sr	I,Tc	Eu,Gd	Ru
Brine A	6.5 - 6.9	< 1	1	0 - 1.5	$> 5 \times 10^3$	40-50
Brine B	6.5 - 7.5	< 1	1	< 1	$> 5 \times 10^3$	500-600
Sol'n C	7.5 - 8.2	4	5	0 - 1.5	$> 10^4$	400-550

Actinide Distribution Coefficients

	pH range	Pu	Am	Cm
Brine B	6.5 - 7.8	5.4×10^3	3.1×10^2	1.3×10^3
Sol'n C	7.5 - 8.2	2.4×10^3	2.4×10^3	4.2×10^4

Table 9.3-4

Distribution Coefficients on Samples From the Culebra Dolomite

Fission Product
Distribution Coefficients

	pH range	Cs	Sr	I,Tc	Eu,Gd	Ru
Brine A	6.5 - 6.9	< 1	< 1	< 1	$> 10^4$	25 - 35
Brine B	6.5 - 7.6	1-2	1-2	< 1	$> 10^4$	640 - 660
Sol'n	7.5 - 8.2	7-10	4-5	< 1	$> 10^4$	240 - 400

Actinide
Distribution Coefficients

	pH range	Pu	Am	Cm
Brine B	6.5 - 7.8	2.1×10^3	2.6×10^3	1.2×10^4
Sol'n C	7.5 - 8.3	7.3×10^3	2.2×10^4	1.1×10^5

Table 9.3-5

Distribution Coefficients on Halite From The
2056' Horizon of ERDA #9 Borehole

Actinide Distribution
Coefficients [1]

pH range	Pu	Am	Cm
7.0 - 7.1	17	306	354
	(1.0×10^4)	(1.8×10^5)	(2.1×10^5)

1) The Kd values in parentheses were calculated
   from the weight of water insoluble material
   in the halite. The lower values are based on
   the total weight of halite taken.

Table 9.3-6

Distribution Coefficients on Samples of Clay From
The 2186.6' Horizon of AEC #8 Borehole

Fission Product
Distribution Coefficients

	pH range	Cs	Sr	I,Tc	Gd,Eu	Ru
Brine A	6.5 - 7.0	< 1	< 1	< 2	$> 2.5 \times 10^3$	150-180
Brine B	6.5 - 7.7	4-6	< 1	< 1	$> 10^4$	$> 2 \times 10^3$
Sol'n C	7.5 - 7.8	80-120	3-6	< 1	$> 10^4$	$> 1 \times 10^3$

Actinide
Distribution Coefficients

	pH range	Am	Pu	Cm
Brine B	6.5 - 8.0	1.1×10^3	4×10^4	1.9×10^4
Sol'n C	7.5 - 8.4	3.5×10^3	1.8×10^5	4.2×10^5

Table 9.3-7

Distribution Coefficients on Samples of Polyhalite
From the 2304' Horizon of ERDA #9 Borehole

Fission Product
Distribution Coefficients

	pH range	Cs	Sr	Eu,Ce [1]	Sb	Tc
Brine A	6.5 - 7.0	< 1	5-10	10-20	< 1	< 1
Brine B	6.5 - 7.2	< 1	19-22	430-700, 50-55	0.9-1.5	< 1
Sol'n C	7.5 - 7.6	< 1	35-40	100-200, 40-60	3-4	< 1

1) Where two ranges of values are given, the first refers to
Eu and the second to Ce.

Table 9.3-8

Distribution Coefficients on Sample of Cowden Anhydrite
From the 2562' Horizon of AEC #8 Borehole

Fission Product
Distribution Coefficients

	pH range	Gd,Eu,Ce
Brine B	6.5 - 7.9	$> 10^3$

Actinide Distribution
Coefficients

	pH range	Am	Pu	Cm
Brine B	6.5 - 7.9	2.9×10^2	6.7×10^3	4.2×10^3
Sol'n C	7.5 - 8.2	2.2×10^3	7.7×10^4	1.8×10^5

Table 9.3-9

Distribution Coefficients on Samples of Clay from the 2725' Horizon of AEC #8 Borehole

Fission Product Distribution Coefficients

	pH range	Cs	Sr	Eu,Gd [1]	Tc,I [1]	Ru
Brine A	6.6 - 7.0	4-9	< 1	$> 10^3$, $2.8-4 \times 10^2$	3.5-4.5, 0-3.5	90-120
Brine B	6.7 - 7.4	3-6	< 1	$> 10^4$	< 1	$> 10^3$
Sol'n C	7.5 - 8.0	34-40	30-45	$> 10^4$, $>3 \times 10^3$	0.7-1.5, 0.5-4	$> 10^3$

Actinide Distribution Coefficients

	pH range	Am	Pu	Cm
Brine B	6.5 - 7.8	310	7.2×10^4	2.7×10^3
Sol'n C	7.4 - 8.4	2.3×10^3	4.0×10^4	1.6×10^5

1) Where two ranges of values are given, the first refers to the first element listed and the second range is for the second element listed.

Table 9.3-10

Distribution Coefficients on Samples of Bell Canyon Formation

Fission Product Distribution Coefficients

	pH range	Cs	Sr	Eu	Sb	Tc
Brine B	6.5 - 7.4	14-16	< 1	$> 10^4$	5-8	< 1
Sol'n C	7.5 - 7.9	130-140	1-5	$> 10^4$	20-25	< 1
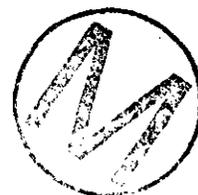
Table 9.3-11

Distribution Coefficients on Halite Samples From the
2611' Horizon of ERDA #9 Borehole

Column Experiment

Column Bed: 7.5 g of Halite in 1 cm diameter column

Solution: Saturated Halite Solution, 200 ml

Flow: 1 Bed volume/min.

| Time (days) | % of Initial Activity in Solution | |
	^{85}Sr	^{144}Ce
0	100	100
1	98.0	26.7
4	96.8	0.9
8	98.4	0

Actinide
Distribution Coefficients[1]

pH range	Am	Pu	Cm
7.0 - 7.3	11	59	56
	(3.8×10^3)	(2.11×10^4)	(2×10^4)

(1) The Kd values in parentheses were calculated using the weight of
water insoluble material in the clay. The lower values are based
on the weight of halite taken.

Table 9.3-12

^{152}Eu Distribution Coefficients (Kd's)

Rock	Simulant	Nominal ^{152}Eu(μCi/ml)	Kd(1) 2 week	Kd(1) 3 month	Kd(2) 2 week	Kd(2) 3 month
Culebra	A	0.01	1.7×10^4	1.5×10^4	--	--
"	A	0.1	3.6×10^4	2.1×10^4	--	--
"	A	1.0	1.8×10^4	4.3×10^4	--	--
"	B	0.01	3.4×10^3	1.6×10^3	--	7.6×10^3
"	B	0.1	1.1×10^4	3.6×10^3	--	1.3×10^3
"	B	1.0	3.7×10^3	3.9×10^3	8.8×10^2	1.4×10^3
"	C	0.01	2.8×10^4	1.3×10^4	--	1.1×10^4
"	C	0.1	2.7×10^4	2.6×10^4	--	1.9×10^4
"	C	1.0	2.0×10^4	1.4×10^4	1.2×10^3	9.6×10^3
Magenta	A	0.01	1.4×10^4	6×10^3	--	--
"	A	0.1	1.9×10^4	2.0×10^4	--	--
"	A	1.0	1.2×10^4	1.4×10^4	--	--
"	B	0.01	2.8×10^3	8.6×10^2	--	4×10^2
"	B	0.1	8.3×10^3	3.7×10^3	--	1.3×10^3
"	B	1.0	1.1×10^3	1.2×10^3	3.5×10^2	4.0×10^2
"	C	0.01	2.0×10^4	1.7×10^4	--	1.3×10^4
"	C	0.1	3.6×10^4	2.2×10^4	--	1.6×10^4
"	C	1.0	1.4×10^4	1.5×10^4	7.7×10^2	1.3×10^4

(1) Kd based on activity in feed solutions.

(2) Kd based on activity in pH adjusted feed solutions.

Table 9.3-13

Comparison of ^{153}Gd, ^{144}Ce, and ^{152}Eu Kd's in Brine B and Brine B* Containing Plywood Extract

14 Day Equilibration

Sample	Brine	^{153}Gd cpm/ml	^{153}Gd Kd	^{152}Eu cpm/ml	^{152}Eu Kd	^{144}Ce cpm/ml	^{144}Ce Kd
Feed	B	24,200	-	20,230	-	5,120	-
Feed	B*	38,090	-	38,090	-	7,080	-
Culebra	B		4.2×10^3		9.9×10^3		1.5×10^3
"	B*		6.3×10^2		6.6×10^2		6.0×10^2
Magenta	B		2.5×10^3		3.4×10^3		1.4×10^3
"	B*		6.5×10^1		7.0×10^1		1.1×10^2
Bell Canyon	B		3.4×10^3		3.4×10^3		3.2×10^3
"	B*		1.3×10^2		1.5×10^2		2.3×10^2
Cowden	B		2.6×10^3		2.2×10^4		2.2×10^3
"	B*		3.7×10^2		4.0×10^2		5.1×10^2
High Clay	B		6.8×10^3		8.5×10^4		1.2×10^3
"	B*		8.7×10^3		2.8×10^4		2.5×10^3

28 Day Equilibration

Sample	Brine	^{153}Gd cpm/ml	^{153}Gd Kd	^{152}Eu cpm/ml	^{152}Eu Kd	^{144}Ce cpm/ml	^{144}Ce Kd
Feed	B	23,260	-	20,170	-	4,800	-
Feed	B*	33,350	-	35,210	-	5,910	-
Culebra	B		4.3×10^3		8.3×10^3		3.3×10^3
"	B*		2.1×10^3		1.8×10^3		1.3×10^3
Magenta	B		3.5×10^3		2.5×10^3		$\geq 10^4$
"	B*		1.4×10^2		1.6×10^2		2.5×10^2
Bell Canyon	B		4.2×10^3		2.7×10^3		3.2×10^3
"	B*		1.5×10^2		1.7×10^3		3.2×10^2
Cowden	B		$\geq 10^5$		5.4×10^3		1.8×10^3
"	B*		4.7×10^2		4.8×10^2		5.3×10^2
Hi Clay	B		6.5×10^3		8.7×10^3		6.1×10^3
"	B*		1.9×10^4		3.2×10^4		5.9×10^3

10.1 INTRODUCTION

Continuing studies for the WIPP primarily encompass those geological processes that need to be understood in order to more quantitatively assess the safety of converting the WIPP to a repository. The processes of importance are tectonic, geochemical, hydrologic, and climatic. The studies indicated within this chapter generally relate to these major processes. In addition, a few studies indicated in this chapter relate to minor continuing efforts of site characterization. This chapter will serve to enumerate issues which remain to be addressed relevant to the safety of converting WIPP to a repository. It is not intended here that specific plans and schedules be presented.

The organization of Chapter 10 follows that of previous chapters.

10.2 SITE SELECTION

In line with the differentiation made in Chapter 2 between site selection, site characterization, and site confirmation, the activities of site selection and site characterization are nearly complete. The confirmation of the WIPP site for a repository will necessitate the continuing studies indicated in Sections 10.3 through 10.9.

10.3 REGIONAL GEOLOGY

Continuing studies of the regional geology focus mainly on the processes of tectonics and climate through studies of paleoclimates and various manifestations of past tectonic activity.

10.3.1 Paleoclimatology

The purpose of paleoclimatic studies in southeastern New Mexico is to develop the local timing and magnitude of past climatic changes and their relation to observed geology to help assess the possible effects of future changes on a repository.

The primary method of paleoclimatic study is to examine cores of Pleistocene or Recent sediments for fauna and flora which are indicative of past climatic conditions. In addition, organic matter or ash falls may, if suitable, be dated radiometrically to provide time control.

Studies of paleoclimate are underway with preliminary analysis of core taken in San Simon Sink from borehole WIPP 15. Fauna and flora are being separated from the sediment for paleontological analyses, and suitable organic material is being separated for radiocarbon analysis. These studies of the San Simon material will be completed in 1979 to yield an initial profile of climatic changes. Further coring in other locations may be undertaken at that time, if necessary, to supplement the record. The final stage of this study will be to integrate the local climatic. changes into the information about regional climates and to determine the relationship between climatic changes and related processes such as subsurface salt dissolution and resultant subsidence (see Section 10.6).

10.3.2 Regional Tectonic Studies

The purpose of various studies of regional tectonics is to assess the long-term effects of tectonic forces on a repository.

Several studies together contribute to information about regional tectonics and include the seismological studies discussed in Section 10.5.

LANDSAT. A preliminary examination of LANDSAT photos has been completed and is reported in Chapter 3. In addition, the WIPP site and surrounding regions will be re-examined in 1979 with more sophisticated image

enhancement to determine the presence and location of more subtle lineaments. Field evaluation of the interpretations will be undertaken as required.

Leveling Surveys. Releveling of some existing first-order vertical control lines was carried out in 1977, and about 300 km of new lines were established. These new lines, some of which traverse Nash Draw and the WIPP site, will be periodically releveled to establish a data base for separating regional tectonic effects from local effects perhaps due to dissolution (see Section 10.6).

West Texas Salt Flats Graben. Releveling and seismology studies indicate active tectonic displacement on the west Texas salt flats graben. Seismic reflection records will be examined and test coring conducted in 1979 to determine if the sediments will yield a record of tectonic disturbance that will contribute to information about the tectonic forces likely to affect a repository located in the Delaware Basin.

10.4 SITE GEOLOGY

The purpose of continuing studies of site geology are to refine the data base for assessment of the safety of a repository there, and to contribute some additional details of site characterization. The methods and studies as such are quite varied.

10.4.1 Geologic Mapping

Geologic mapping continues on the WIPP site and in the area, particularly under a study of the stability of the WIPP site. This study, being conducted by the USGS, is concerned with mapping caliche and related sediments to provide more conclusive data on the length of time the area has been stable, and the rates at which areas around the site have been disturbed.

10.4.2 Aeromagnetic Survey

A very high resolution aeromagnetic survey will be initiated during FY79
to examine the WIPP site and several special features. The survey of the
site will primarily be to determine if any dikes have intruded the
evaporites at the site since dikes might form a pathway for fluid flow.
Several of the domal features mentioned in Chapters 3, 4, and 6, two of
which are considered to be breccia pipes, will be examined to determine
if a magnetic signature is associated with disturbance of the magnetic
red beds. The tool, if proven applicable, might then be used for
prospecting to support continuing studies of breccia pipes as indicated
in 10.6.

10.5 SEISMOLOGY

The purpose of continuing seismological studies is to provide data for
facility design and to expand the data base contributing to an
understanding of tectonic processes affecting a repository in the
Delaware Basin. Seismological studies are supported by arrays of
stations near points of interest.

10.5.1 Near-Site Activity

The careful characterization of near-site background activity, as
indicated in Chapter 5, is the dominant seismic issue affecting the WIPP
site. Station CLN has been operating near the site since 1974, and
continues to operate. It is planned to augment this station so that at
least three stations will be operating at the site to better define
near-site seismicity.

10.5.2 Central Basin Platform

An array of stations has been operating near Kermit, Texas, since 1976 to
evaluate the seismic activity on the Central Basin Platform and to
explore the relationship, if any, between this activity and the massive

fluid injection for secondary oil recovery operations occurring in that area. This array will continue to operate both for this purpose and because the assessment of seismic activity at the WIPP site may partly depend on an understanding of the relationship between fluid injection and seismic activity should injection occur in oil fields near the site.

10.6 CONTINUING STUDIES IN HYDROLOGY

10.6.1 Introduction

Hydrology is a major consideration when examining the feasibility for locating a nuclear waste disposal site. Two factors are directly related to hydrology: (1) the geologic stability of the formation in which the waste products will be stored, and (2) the occurrence of water as a transport medium for radionuclides. Unsaturated waters migrating along the surfaces of the salt beds will dissolve salt; therefore, an examination of magnitude and direction of fluid flow and fluid chemistry in formations above and below the salt is necessary. Additionally, the direction and rate of fluid movement both above and below the storage horizon should be evaluated to predict the movement of radionuclides should they be accidentally discharged into the aquifers.

10.6.2 Purpose of Hydrologic Testing

Two hydrology-related questions are to be answered in evaluating the suitability of the proposed WIPP site.

1. What is the geologic stability of the Salado Formation?

2. Should the primary containment barrier (the salt) fail or an accident occur, where and how rapidly will radionuclides be transported by groundwater?

Three factors need to be investigated to examine the integrity of the Salado within the site: (1) the Rustler-Salado contact is to be examined

geophysically and petrologically within the WIPP area to determine if dissolution is presently occurring, (2) the dissolution front (as defined by the edge of the shallow dissolution zone in the Nash Draw) needs to be located more precisely, (3) the estimated rate of dissolution is to be refined.

The hydraulic gradients and rates of fluid movement in the series of fluid bearing zones that overlie the Salado require further definition. Estimates of concentrations of aqueous species (and when and where they might appear) may then be refined for specific safety-assessment modeling scenarios describing radionuclide escape into these groundwater systems and migration out of the area. In addition, formations which do not presently contain water but exhibit some degree of permeability are to be tested to see what rates of movement would be, should they contain water or other fluids at some later time.

10.6.3 Direction and Rate of Fluid Migration

If radionuclides were to reach fluid bearing zones in the Rustler, they would be transported away from the site by the groundwater system. To evaluate the impact of such an accident on the surrounding area, hydraulic gradients and hydraulic conductivities of fluid bearing zones overlying the salt beds will be determined or modified. Data for these determinations will be acquired by pumping tests on hydrologic test holes or measurements of the recovery time of fluid levels in bailed holes. Tracer tests will be conducted where they may contribute useful information.

A series of hydrologic tests is planned in holes placed near the periphery of the proposed land withdrawal area. After additional testing of some existing holes, control points for the potentiometric surfaces and for hydraulic conductivities will have been established for the periphery with a spacing of 2 to 3 miles. These data will allow construction of more detailed potentiometric surface maps for the site area. The potentiometric contours will be meshed with the results from

the Nash Draw program to the west. Consequently, the potentiometric
surface and hydraulic conductivity data required for modeling efforts of
long-term safety assessment will be obtained for an area extending from
the northeast part of the study area to Malaga Bend on the Pecos River
(an area of about 200 square miles).

The borehole plugging program requires data from both laboratory and in
situ permeability measurements. These permeability measurements, both in
the evaporites and in aquifers, will provide additional data for the
safety assessment work.

10.6.4 Dewey Lake Redbeds

The Rustler Formation and the shallow dissolution zone in Nash Draw have
demanded the attention of this program because they are fluid-bearing.
The Dewey Lake Redbeds are also of some significance since fluids are
present in sandstone lenses. Although the redbeds are only locally
saturated, two possibilities exist for additional water to enter the
formation: a climatic change to a high rainfall period, or migration of
fluids from below into the redbeds.

Tests in two types of holes are being considered: existing holes, and at
least one new hole specifically designed for Dewey Lake testing. The
casing in existing holes will be perforated opposite permeable zones as
identified from analyses of logging and drilling records.

The standard hydrologic testing procedures will allow calculation of the
transmissivity of fluid bearing strata in the Dewey Lake Redbeds or other
permeable zones that might be expected to contain fluids at some future
time.

10.6.5 Long-Term Monitoring

The peripheral hydrologic test holes, which now include four potash
holes, will be configured for long-term monitoring. This long-term

monitoring may show what changes are taking place in the hydraulic
gradients which in turn may indicate increased or decreased flow, and
variations in rates of recharge or discharge. Moreover, depending on the
extent of the monitoring system, a warning network for information on
fluid threats to the integrity of the repository is obtained.

The Dewey Lake Redbed hole(s) can be monitored to detect fluid movement
that may not be present except during high precipitation cycles of long
or short duration.

The test holes drilled in Nash Draw would be monitored to detect changes
in the hydrologic regime along the Rustler-Salado contact. Because the
Culebra is the main producer of water west and south of the WIPP area, it
is desirable to monitor this fluid-bearing strata to determine its
relationship with the shallow dissolution zone and to provide additional
data for modeling the safety assessment modeling scenarios.

10.6.6 Surface Hydrology

Surface hydrology must be examined climatologically with the aid of
surface mapping. Records of annual rainfall and intensity and duration
of storms (particularly high intensity, 24 hour, 50 and 100 year
recurring storms) are available. This information, in conjunction with
surface mapping (from aerial photographs, topographic maps, or both) of
contributory drainage will provide the basis to estimate amounts of
runoff and amounts of infiltration in the study area. Because of the
high evapotranspiration and the caliche layer below surficial sands,
infiltration estimates are expected to be only a small portion of the
calculated recharge.

Photogrammetric and field mapping is planned to locate and describe
springs which may issue from the Dewey Lake Redbeds or the shallow
dissolution zone. Several springs are suspected to be located west of
the site, and discharge measurements could aid in the identification of
the formations from which they issue. Geochemical monitoring of many

such springs, including the Malaga Bend seeps and the Pecos River salt load, will add to this overall understanding of hydrologic system dynamics.

10.6.7 Overview of Deep Hydrologic Testing

Three objectives for deep aquifer testing to complement the site-specific shallow aquifer investigations in the WIPP study area are:

(1) To obtain static bottom-hole pressure measurements in the deep aquifer zones, for the refinement of previous estimates of local potentiometric surfaces, hydraulic gradients, and hydraulic conductivities.

(2) To determine the bounds of the formational reservoirs.

(3) To obtain fluid samples for geochemical analyses.

Three wells suitable for hydrologic testing (Badger, Cabin-Baby, Cotton-Baby) are located within the site area. Each well will have to be re-entered and plugged, in accordance with methods now under study, or maintained as monitoring wells. Deep hydrologic data will be developed from these well to obtain site-specific information on the Delaware zones. Testing outside the study area involves two additional wells (AEC No. 8 and ERDA No. 6).

10.6.8 Long-Term Monitoring of Deep Wells

A number of wells could be equipped for long-term monitoring of the Delaware zone to show what changes, if any, are taking place in the hydraulic gradient, which in turn indicate fluid movement in the reservoir. Periodic fluid samples can be obtained to identify increased flow or chemical changes in the ground water system.

10.6.9 Continuing Studies in Salt Dissolution and Overburden Subsidence

Program Objectives. The program of investigation of dissolution and subsidence has four fundamental purposes, and one special-case consideration:

1. To correlate surficial collapse features and deposits with subsurface dissolution, in order to develop criteria for an evolutionary pattern of collapse.

2. To characterize subsurface dissolution products adjacent to the WIPP site.

3. To determine the behaviour of fluids in dissolution products adjacent to the WIPP site.

4. To analyze potential impacts of evolution of dissolution products at and near the WIPP site with respect to repository breachment and radionuclide transport.

The special case is to determine the nature of subsidence over mines in salt, and its effects on the overlying groundwater system.

An elaboration of these purposes follows.

Nash Draw Investigations. Nash Draw is believed to have originated by some combination of surface erosion and subsidence following subsurface dissolution. If the process of formation is overwhelmingly erosion, then the potential for removal of overburden at the WIPP site is probably about the same as it has been in Nash Draw. If, however, the process is overwhelmingly dissolution of salt and subsequent collapse of the overburden, the potential extension of Nash Draw toward the WIPP by dissolution will be more quantitatively described. At present, there is no conclusive way of defining an instantaneous rate of growth of Nash Draw toward the WIPP site; therefore, the only alternative is to

understand the processes which have resulted in Nash Draw, and incorporate their implications into the mathematical modeling efforts directed toward safety assessment involving the WIPP site in general, and radionuclide escape and migration in particular.

First, the Nash Draw program is a series of core holes, which will be geophysically logged. This operation will obtain data to serve three purposes: 1) reveal the subsurface of Nash Draw stratigraphy at carefully chosen points, 2) reveal the relationships between the subsurface structure and surface features and deposits, 3) reveal how much halite and anhydrite (or gypsum) has been removed by dissolution.

Second, the Nash Draw program is a source of geologic material for petrographic and geochemical examination. Examination of thin sections of recovered rock will allow the mineralogy of dissolution products to be determined, i.e. identification of what was dissolved and what remains. Mineralogy and textures of dissolution residues and cemented collapse fill can then be compared with those of dissolution features sampled in other programs, such as the one to investigate the cemented rubble chimneys (often called "karstic domal features" or "breccia pipes"). Geochemical analyses of core materials for trace constituents will reveal their degree of interaction with groundwaters, and possibly an age of formation. Also, permeabilities to fluids can be obtained from cores.

Third, the Nash Draw core holes will become a series of hydrology test holes. The brine flow underlying Nash Draw has been attributed responsibility for much of the dissolution and collapse observed today. The safety assessment scenarios for radionuclide escape and migration involve movement from WIPP into Rustler Formation waters into the shallow dissolution zone and out at Malaga bend on the Pecos River. It behooves us to understand the hydrologic relationships between the shallow dissolution zone and the Rustler water-bearing rocks in Nash Draw in order to verify that models of radionuclide transport are representative of the physical system.

Cemented Rubble Chimney Investigations. One of the "karstic domal features" described by J. D. Vine (called Hill "C") was encountered at the level of the McNutt potash zone by Mississippi Chemical Corporation. It was found to be a chimney in the Salado Formation filled with clay-cemented brecciated rock belonging to strata above the McNutt. Similarly a breccia-filled chimney was encountered in drilling near a circular hill near the Wills-Weaver Mine. There are numerous other erosion-breached domes such as Vine's Hill "C" in the vicinity of Nash Draw; the subsurface expression of them, if any, is virtually unknown. It is desirable that a hole be drilled to a depth at which no more brecciated rock is found. Hydrologic observation (including water sampling and static water-level measurements) in fluid-bearing zones of the structure itself and in "bedrock" and in nearby rocks will help to determine the degree of hydraulic connection of the structure with aquifers of regional extent.

Petrographic analyses of recovered core will allow comparisons to be made with dissolution products recovered from Nash Draw investigations, described previously. Such material also lends itself to geochemical analyses for the determination of rock-water interaction history and age. Similarly, fluid analyses will provide an indication of how the fluids have interacted with their host rocks, helping to determine the processes at work in such structures.

Since modeling of radionuclide escape and migration must take into account fluid movement, cemented rubble chimneys should be evaluated for their potential as paths for such movement. They should also be evaluated as members of the evolutionary pattern of dissolution and collapse features, and might be generically related to the development of Nash Draw. Consequently, it is desirable to measure in situ the permeability of the structure. In addition, the hydrologic relationships between the chimney and surrounding rocks should be understood in order to formulate a complete hydrologic model for risk assessment.

Mine Subsidence Investigations. The potash producers in southeastern New
Mexico mine in two stages -- the primary recovery which leaves rooms
separated by large pillars, and the secondary recovery in which they may
"rob the pillars" and ultimately remove almost 95% of the ore.
Second-mining requires abandonment almost immediately thereafter, because
there is no longer a large enough local pillar system to hold up the
roof. And so, the roof slowly sags, and subsidence is propagated to the
surface.

While investigations of subsidence over mines do not bear directly on the
four program objectives, mining is certainly a particular cause of
subsidence and perhaps an indirect agent for initiating dissolution. If
subsidence over a mine causes fracturing of water bearing rocks above,
locally increased permeability might allow circulation of groundwater to
underlying evaporites through the fractures to start dissolution.

The amount of subsidence and its potential for enhancement of salt
dissolution of the Salado Formation over the WIPP if the McNutt potash
zone were to be mined is unknown. If this subsidence program were to
lead to a satisfactory means to predict subsidence and its effects, in
particular dissolutioning, the control zone restrictions currently
prescribed around the WIPP could possibly be relaxed. It is possible
that minor subsidence will occur over the closed WIPP mine because it
will not be possible to backfill the repository to the same packing
density as original rock. Therefore, it is desirable to evaluate the
effect of mining and subsequent subsidence on the local groundwater
system in the subsiding overburden.

10.6.10 Modeling of Regional Hydrology

Hydrologic modeling has one basic objective, to support risk assessment
work by describing the movement of fluids in this region in as much
detail as possible. The movement of fluids affects the expected period
of integrity of the repository and the movement of radionuclides from the
repository. To fulfill this objective, the modeling emphasizes several

aspects. The first aspect is interpretation and explication of the data collected in field programs designed to delineate the regional flows. The second is to suggest where data are insufficient and more field or laboratory work is required. The third aspect is the simulation of experiments which cannot be performed in the field. Two examples for simulations are: consequences of perturbations to regional flow patterns caused by the existence of a repository, and consequences of changes in regional flow patterns due to alterations in rainfall patterns or due to man's activities.

The fourth aspect is prediction of the movement and concentrations of radionuclides consistent with fluid movement determined in part by the release scenarios developed for WIPP.

Implementation is based on the modification and use of certain 2-D and 3-D computer codes available for hydrologic modeling. Code verification based on field data already collected is in process. Supporting laboratory programs designed to provide parameters as absorption coefficients, permeabilities, etc., are already underway.

10.7   CONTINUING STUDIES IN GEOCHEMISTRY

10.7.1   Introduction

Detailed accounts of geochemical data reported in Chapter 7 have provided the pressing need of fundamental information for (1) conceptual design of WIPP operational facilities, and (2) formulation of site-specific process scenarios to be used in the consequence safety assessment effort. An evaluation of the available data has shown that the completed studies are not entirely sufficient to support WIPP experimental programs. These programs include borehole plugging, laboratory rock mechanics, in-mine rock mechanics, in-mine heater experiments, in-mine high-level waste emplacement experiments, laboratory waste-rock interaction experiments, radionuclide transport through rocks, and waste encapsulation studies.

In addition, the long-term safety assessment effort has lacked
information about geological processes associated with so-called
"geological anomalies" such as igneous dikes and cemented rubble chimneys.

10.7.2 Mineralogy and Petrology

The data concerning assemblages of evaporite minerals in the Salado
Formation which were presented in Chapter 7 have addressed the types of
minerals found and their relative (qualitative) abundances. While this
has been useful in selection of candidate horizons for waste emplacement,
it has been of limited use to the quantitative measurements of thermal
and physical properties of evaporite rocks (see Chapter 9).

It has been found that a small change in the quantitative mineralogical
proportions in a rock sample has a large non-linear effect on thermal
properties, for example. Chapter 7, together with its executive summary
in Chapter 1, has pointed out the variability in the mineralogical
composition of rocks in the Permian evaporite section.

In addition, quantitative mineralogy and petrology is required for
development of materials to be used in the plugging of shafts and
boreholes. The long-term thermodynamic stability of a grout plug, for
example, cannot be evaluated without an intimate knowledge of mineral
phases in both grout and rock, so that free energy calculations can be
made for degradation reactions which might occur between the two.
Compatibility of grout with rock and groundwater will be an essential
factor requiring thorough evaluation to provide confidence in the
long-term sealing of boreholes and shafts which penetrate from surface to
repository horizons.

10.7.3 Volatiles Characterization

Chapters 7 and 9 have alluded to the variability in volatile content of
evaporites and how the variation affects fundamental rock properties.
Chapter 7 has addressed the volatile component in detail mostly in view

of mass loss experienced by heated rock. The entire mass loss cannot be ascribed to water alone. Indeed, Chapter 7 briefly addressed the chemical species which were found in a few selected rock samples, and even so, considerable variation was observed. Experiments are planned to simulate high-level-waste-canister heat in a potash mine, in order to quantize the devolatilization products. Unambiguous interpretations of the experimental results derived therefrom require an understanding of the volatile components native to the rock before heating begins. Furthermore, the interpretations also require an understanding of the fundamental differences between potash ore zones and actual repository zones, since the results of devolatilization in one will certainly not be directly applicable to the other without taking into consideration the native differences.

10.7.4   Origins of Evaporite Assemblages

It was pointed out in Chapter 7 that many of the evaporite mineral assemblages observed in the Permian section cannot have precipitated from a seawater-like solution. Furthermore, the thermodynamic properties of some minerals, such as the almost ubiquitous polyhalite, are virtually unknown. Similarly its mode of origin is entirely unknown, and has been long regarded wholly as a product of recrystallization, commonly replacing anhydrite.

The present assemblages not only contain non-primary evaporite minerals, but also have a magnesium deficiency relative to other evaporites in the world. The sink for this magnesium presumably lost during recrystallization has not been identified. The observations of Chapter 7 urge that a thermodynamic understanding of the environments and processes of evaporite recrystallization be sought. In this way the water loss that the evaporites have experienced (during recrystallization) can be estimated, and confidence can be gained regarding what mineralogical changes (if any) are likely to take place in response to waste emplacement.

The techniques used in deducing the origins of evaporite assemblages include chemical quantitative analyses of minerals, petrographic paragenetic examination, and stable isotope, radioisotope and trace element analyses.

10.7.5   Igneous Dike

In Chapter 4, there was mention of a northeast-trending igneous dike intruding the evaporites on the west side of Nash Draw west of the WIPP study area. The characterization of the dike was based on the Yeso Hills and Kerr-McGee mine occurrences, together with an aeromagnetic survey. In order to come to an understanding of the marginal effects (i.e., dike-salt-fluid interactions), the following pursuits are recommended:

1.   Collection and study of additional samples from farther away from the Kerr-McGee dike occurrence.

2.   Determination of:

a.   K-Ar ages of the alteration micas in the dikes

b.   Drilling angle holes with coring at appropriate intervals, to sample the dike and the effects of the dike upon the host rock system.

The dike appears to be a natural laboratory experiment involving high-temperature interactions among salts, groundwaters, and "alien" mineralogies such as emplaced waste would also represent.

10.7.6   Trace Elements and Age-Dating

A continued effort is desirable in age-dating and trace element studies, in order to support investigative efforts contemplated for the so-called "geologic anomalies." The activities are, specifically:

1.   Chemical and isotopic study of exposed collapse structure in underground workings of Mississippi Chemical Mine.

a. If waters have percolated through this structure in very recent times then this may be reflected in oxygen isotopic study of grain coatings, etc. Rb-Sr studies of clay minerals should give an indication of Rb, Sr and ($^{87}Sr/^{86}Sr$) redistribution relative to clay minerals removed from the collapse structure.

b. Scanning electron microscope/microprobe study of grain boundaries: supplemented by instrumental neutron activation analysis (INAA) for adsorbed elements (alkalies, alkaline earths, rare earth elements).

c. Rare Earth Elements (REE) distribution in all primary and secondary phases most likely to have been affected by solutions.

2. REE (and other key trace element) abundance in major facies of drill core from WIPP site. At present trace element data are very sporadic and obtained by different techniques so that real differences due to analytical precision and accuracy are suspect. Detailed INAA study of various phases from the same stratigraphic horizons over a wide lateral extent are desirable to establish realistic background data for the REE (i.e. because the REE are commonly used as analogues for the transuranics) so that REE data from dike-salt contact zones and elsewhere can be proprly assessed. If the REE distribution is extremely variable then local variations due to solution, recrystallization, contact effects will be difficult to interpret; if the REE show a more or less uniform distribution pattern and abundance then such effects can be closely scrutinized.

3. Dike-evaporite contact effects. Samples from the lamprophyre dike (T = ~ 35 MYBP) which is observed in the underground workings of the Kerr-McGee Mine offers a unique chance to examine the effects of a local, high temperature source in contact with several evaporite phases.

10.7.7   Reef and Back-Reef Waters

There is at present some degree of confusion surrounding the source and
discharge of water in the Capitan Reef surrounding the Delaware Basin.
Chapter 7 has shown that the greater portion of the water in the Reef
cannot have come from direct infiltration into outcrops in the Guadalupe
and Glass Mountains, nor from rocks in the Basin. Therefore, the
relationships between the Reef and its lagoonal facies (back-reef)
stratigraphic equivalents are likely source and sink candidates. These
relationships are best deduced by combinations of stable isotope, uranium
isotope, and solute analyses of reef and back-reef waters. An extensive
water-sampling of these areas is required for this. The results of this
geochemical mapping of regional groundwater flow would be used in the
long-term safety assessment modelling effort and the final publication
of the regional groundwater mathematical model.

10.7.8   Future Work on Fluid Inclusions

In addition to the obvious necessity of making studies on samples from
the actual strata to be used for high level waste storage, a variety of
approaches need to be explored. Fluid inclusions near the waste
canisters might decrepitate in the thermal pulse; the conditions under
which this will occur can and should be explored experimentally.
(studies are continuing of inclusions in a suite of salt samples
collected at various distances from a dike penetrating the salt horizons;
this provides a natural analog.) The identification of the daughter
minerals in some inclusions, and their thermal behavior, as well as
bubble movement in a thermal gradient, will provide additional
compositional information. The gases released on crushing or heating
should be explored, as well as the leakage of gases (or water) out of
inclusions. This would be pertinent both for interpretation of K/Ar ages
and in corrosion problems. The actual chemical composition of the larger
inclusions and their isotopic composition (particularly H/D and
O^{16}/O^{18}) can be determined by existing methods. This would help in

understanding the complex sequence of interactions of pore (and inclusion) fluid with the original salt beds to yield the present mineralogy.

10.8 RESOURCES

Sandia Laboratories has no continuing studies of resources at the WIPP site.

10.9 SPECIAL STUDIES

10.9.1 Purpose. The objective of thermophysical and radionuclide sorption studies on SENM rocks is to determine their characteristics as required by the structural mine design, in situ experimental, and long-term safety analyses programs. As with other continuing studies, these special studies are a means to an end, not an end in themselves.

10.9.2 Thermophysical Properties

Scope. A continuing assessment of the thermophysical properties of SENM rocks is envisioned because of the broad range of questions posed about radioactive waste isolation. These problems range from the plasticity of salt to the migration of brine in salt; many are not answered by a cursory investigation. Establishing a data base, for instance, for the analyses of long-term creep, is time consuming. It is not anticipated that evaluation of physical rock properties will be pivotal in mine, experiment or repository design; however, that is intrinsically impossible to guarantee. Such evaluations may very well be pivotal in considerations of retrievability of high-level waste experiments, in which high temperatures tend to accelerate creep. Thus, physical rock property determinations, such as the micromechanics of rock deformation, are a prudent pursuit to provide additional confidence in geologic isolation.

Continuing Studies. The primary object of the continuing experimental rock mechanics program is to understand and model the thermomechanical behavior of the WIPP salt. This will be accomplished through studies of transient creep data at pressures exceeding 1500 psi and at a principal stress difference less than 2000 psi where there is a paucity of data. In addition, petrographic investigations will continue to identify the governing deformation mechanisms.

Other studies relevant to the long-term stability of the WIPP include measurements of gas and brine permeabilities on previously deformed core and measurements of gas permeabilities at elevated temperatures. Studies are also planned in the area of thermal expansion coefficients and brine migration in salt under thermal gradients. Migration of fluid inclusions is being given attention, because of the brine's corrosive potential and because the capacity of fluid inclusions to carry radionuclides through rock salt is not known.

Rock mechanic programs will also be initiated to determine the mechanical properties of the WIPP site rock other than rock salt. These studies will be directed toward the engineering performance and construction characteristics of the non-salt rock which will influence the design and construction of shafts to the repository levels.

Mineralogic and petrographic studies will be conducted on core to support the physical rock properties determinations as required. This information is required to determine the phase systems in the rocks being investigated. A similar set of studies support the geochemical analyses, Chapter 7. The variations in mineral assemblage, grain size, fluid inclusion content, and petrofabric which have been observed in evaporite rocks have also given rise to variations in physical properties, which could only qualitatively be taken into account in the investigations reported here.

The arbitrary separation of mineralogical and physical rock properties from geology and hydrology that has often occurred in other studies is
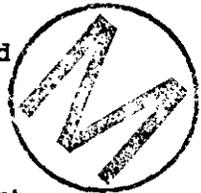
being avoided in the comprehensive studies being performed for the WIPP. The relations of rocks found at the proposed repository horizons to those found in an in situ test bed located elsewhere (e.g., nearby potash mine) are being evaluated. Quite possibly, mineralogic and fabric changes may cause discrepancies in results from one site to another.

10.9.3   Radionuclide Sorption Properties

Scope. A continuing assessment of WIPP rocks ability to inhibit the migration of radionuclides away from the repository is envisioned to augment the batch Kd determinations, which were used in preliminary calculations of radionuclide travel time in site-specific escape scenarios. A realistic approach to safety assessment requires data to be generated (mostly in the laboratory) under simulated physiochemical conditions anticipated in subsurface evaporites and related rocks of southeast New Mexico. The laboratory experiments in radionuclide migration would ultimately be evaluated by SENM field experiments involving the emplacement and observation of movement of non-radioactive tracers which are chemically analogous to radionuclides.

Continuing Studies. Whereas previous "Kd" measurements reflect the degree to which radionuclide soprtion on rocks takes place in static, closed systems, scenarios involving the entrainment of radionuclides in moving groundwater imply that a variety of physiochemical conditions will be encountered in the subsurface.

Now that the radionuclides of interest have been identified, different oxidation states of those radionuclides which might give rise to different mobilities in WIPP environments will next be identified. Investigations of effects on sorption of parameters such as pH, radionuclide concentration in solution, and oxidation potential will then proceed with the oxidation states of species of interest. These parameterization experiments will culminate in the simulation of radionuclide migration in flow-through experiments involving actual WIPP rocks and solutions, at the anticipated physiochemical conditions.

Appendix 7.A (Ref. sec. 7.3)

Whole Rock Chemical Analyses, Soluble-Insoluble

Fractions, Mineralogy, and Weight Losses

upon Heating.

TOTAL ANALYSIS

```
HOLE #   7
DEPTH = 1044.2  FEET

SOLUBLE =   99.72  %
INSOLUBLE =   0.28  %
```

COMPONENT	WT %
SO3	0.55
NA	38.56
NA2O	0.0
K	0.03
K2O	0.0
MGO	0.04
CAO	0.43
SIO2	0.0
FE2O3	0.0
AL2O3	0.0
CL	60.40
WEIGHT LOSS ON HEATING	
70	0.10
HI TEMP	0.0
TOTAL	100.39

```
MAJOR:   HAL
MINOR:   ANH
TRACE:   CARN
```

TOTAL ANALYSIS

```
HOLE #     7
DEPTH  =  1107.5  FEET

SOLUBLE   =   69.47  %
INSOLUBLE =   30.53  %
```

COMPONENT	WT %
SO3	20.88
NA	20.28
NA20	6.63
K	0.0
K20	4.48
MGO	4.57
CAO	1.84
SIO2	8.30
FE203	0.27
AL203	1.24
CL	30.78
WEIGHT LOSS ON HEATING	
70	0.12
125	0.10
200	0.40
350-400	1.37
TOTAL	101.26

```
MAJOR:  HAL
MINOR:  POLY, LANG, KFELD, TALC, QTZ
TRACE:  CHLOR, FEOX
```

TOTAL ANALYSIS

HOLE # = 7
DEPTH = 1171.5 FEET

SOLUBLE = 37.10 %
INSOLUBLE = 62.90 %

COMPONENT	WT %
SO3	39.73
NA	12.56
NA2O	0.88
K	1.91
K2O	0.0
MGO	0.70
CAO	25.13
SIO2	0.63
FE2O3	0.06
AL2O3	0.0
CL	18.87
WEIGHT LOSS ON HEATING	
70	0.14
300-400	0.58
425	0.08

TOTAL	101.27

MAJOR: HAL, ANH
MINOR: POLY
TRACE: SYL, BLOED, QTZ, FEOX

TOTAL ANALYSIS

```
HOLE #   7
DEPTH =  1221.0  FEET

SOLUBLE   =   99.51  %
INSOLUBLE =    0.49  %
```

COMPONENT	WT %
SO3	2.02
NA	38.79
NA2O	0.0
K	0.06
K2O	0.0
MGO	0.10
CAO	0.88
SIO2	0.01
FE2O3	0.0
AL2O3	0.0
CL	58.31
WEIGHT LOSS ON HEATING	
70	0.30
100-200	0.14
375-425	0.07
TOTAL	101.17

```
MAJOR:  HAL
MINOR:  ANH
TRACE:  POLY, LANG, QTZ
```

TOTAL ANALYSIS

HOLE # 7
DEPTH = 1343.0 FEET

SOLUBLE = 99.74 %
INSOLUBLE = 0.36 %

COMPONENT	WT %
SO3	0.99
NA	38.60
NA2O	0.0
K	0.35
K2O	0.0
MGO	0.15
CAO	0.66
SIO2	0.01
FE2O3	0.0
AL2O3	0.0
CL	59.40
WEIGHT LOSS ON HEATING	
70	0.27
300-350	0.16
TOTAL	100.95

MAJOR: HAL
MINOR: ANH, POLY
TRACE: QTZ

TOTAL ANALYSIS

```
HOLE #  = 7
DEPTH   = 1402.5  FEET

SOLUBLE   =  99.97  %
INSOLUBLE =   0.03  %
```

COMPONENT	WT %
SO3	0.11
NA	39.67
NA2O	0.0
K	0.06
K2O	0.0
MGO	0.06
CAO	0.02
SIO2	0.0
FE2O3	0.0
AL2O3	0.0
CL	59.78
WEIGHT LOSS ON HEATING	
70	0.19
400-500	0.12
TOTAL	100.04

```
MAJOR:  HAL
MINOR:
TRACE:  POLY
```

TOTAL ANALYSIS

HOLE # = 7
DEPTH = 1468.5 FEET

SOLUBLE = 93.66 %
INSOLUBLE = 6.34 %

COMPONENT	WT %
SO3	2.88
NA	34.44
NA2O	0.0
K.	0.37
K2O	0.07
MGO	1.85
CAO	0.19
SIO2	2.15
FE2O3	0.24
AL2O3	0.07
CL	53.61
WEIGHT LOSS ON HEATING	
70	1.27
100-150	0.36
175	0.10
250	0.07
375	0.34
400-500	0.45
TOTAL	98.46

MAJOR: HAL
MINOR: KAIN, KIES
TRACE: POLY, KFELD, TALC, QTZ

TOTAL ANALYSIS

HOLE # = 7
DEPTH = 1534.0 FEET

SOLUBLE = 99.86 %
INSOLUBLE = 0.14 %

COMPONENT	WT %
SO3	1.67
NA	36.10
NA2O	0.0
K	0.52
K2O	0.0
MGO	0.22
CAO	0.64
SIO2	0.01
FE2O3	0.0
AL2O3	0.0
CL	57.76
WEIGHT LOSS ON HEATING	
70	0.22
200	0.01
400-500	0.24
TOTAL	97.53

MAJOR: HAL
MINOR: POLY
TRACE: KAIN, QTZ

TOTAL ANALYSIS

HOLE # 7
DEPTH = 1615.0 FEET

SOLUBLE = 98.69 %
INSOLUBLE = 1.31 %

COMPONENT	WT %
SO3	4.56
NA	35.06
NA2O	0.0
K	1.05
K2O	0.0
MGO	0.71
CAO	1.47
SIO2	0.23
FE2O3	0.04
AL2O3	0.07
CL	55.95
WEIGHT LOSS ON HEATING	
70	0.34
100	0.09
350-400	0.37
TOTAL	99.94

MAJOR: HAL
MINOR: POLY, KAIN
TRACE: CHLOR, MONT

TOTAL ANALYSIS

HOLE # = 7
DEPTH = 1698.0 FEET

SOLUBLE = 95.35 %
INSOLUBLE = 4.65 %

COMPONENT	WT %
SO3	0.58
NA	36.47
NA2O	0.0
K	0.06
K2O	0.07
MGO	1.20
CAO	0.34
SIO2	2.07
FE2O3	0.25
AL2O3	0.61
CL	58.35
WEIGHT LOSS ON HEATING	
70	0.82
350	0.03
TOTAL	100.85
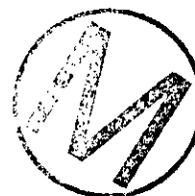
MAJOR: HAL
MINOR: ANH, CARN, KIES
TRACE: POLY, ILL, QTZ, FEOX

TOTAL ANALYSIS

HOLE #   7
DEPTH = 1755.0   FEET

SOLUBLE =   99.60 %
INSOLUBLE =   0.40 %

COMPONENT	WT %
SO3	0.65
NA	38.12
NA2O	0.0
K	0.23
K2O	0.0
MGO	0.13
CAO	0.08
SIO2	0.02
FE2O3	0.0
AL2O3	0.0
CL	59.54
WEIGHT LOSS ON HEATING	
70	0.19
200	0.04
300-400	0.05
TOTAL	99.45

MAJOR: HAL
MINOR:
TRACE: LEON, QTZ

TOTAL ANALYSIS

```
HOLE #    7
DEPTH =  1952.5  FEET

SOLUBLE =   99.30 %
INSOLUBLE =  0.70 %
```

COMPONENT	WT %
SO3	3.18
NA	37.14
NA2O	0.0
K	0.75
K2O	0.03
MGO	0.54
CAO	0.79
SIO2	0.34
FE2O3	0.03
AL2O3	0.05
CL	57.00
WEIGHT LOSS ON HEATING	
70	0.14
350-450	0.44

TOTAL	100.43

```
MAJOR:  HAL
MINOR:  POLY
TRACE:  LEON, CHLOR, KFELD, FEOX
```

TOTAL ANALYSIS

HOLE # 7
DEPTH = 1954.0 FEET

SOLUBLE = 97.46 %
INSOLUBLE = 2.54 %

COMPONENT	WT %
SO3	0.73
NA	37.94
NA2O	0.0
K	0.18
K2O	0.06
MGO	0.56
CAO	0.52
SIO2	1.34
FE2O3	0.09
AL2O3	0.23
CL	58.38
WEIGHT LOSS ON HEATING	
70	0.32
350-400	0.09
TOTAL	100.44

MAJOR: HAL
MINOR: POLY
TRACE: ANH, CHLOR, KFELD, TALC, FEOX

TOTAL ANALYSIS

HOLE #   7
DEPTH = 1957.5 FEET

SOLUBLE =   99.16 %
INSOLUBLE =   0.84 %

COMPONENT	WT %
SO3	1.72
NA	38.38
NA2O	0.0
K	0.36
K2O	0.01
MGO	0.41
CAO	2.18
SIO2	0.37
FE2O3	0.04
AL2O3	0.11
CL	59.00
WEIGHT LOSS ON HEATING	
70	0.20
300-400	0.12
TOTAL	102.90

MAJOR: HAL
MINOR: ANH
TRACE: POLY, CHLOR, KFELD, FEOX

TOTAL ANALYSIS

HOLE # = 7
DEPTH = 1961.0 FEET

SOLUBLE = 99.10 %
INSOLUBLE = 0.90 %

COMPONENT	WT %
SO3	0.49
NA	39.14
NA2O	0.0
K	0.21
K2O	0.01
MGO	0.25
CAO	0.19
SIO2	0.42
FE2O3	0.04
AL2O3	0.08
CL	58.83
WEIGHT LOSS ON HEATING	
70	0.07
100	0.16
150-200	0.16

TOTAL	100.05

MAJOR: HAL
MINOR: POLY
TRACE: CHLOR, KFELD, TALC, QTZ, FEOX

TOTAL ANALYSIS

HOLE # 7
DEPTH = 1967.0 FEET

SOLUBLE = 99.94 %
INSOLUBLE = 0.06 %

COMPONENT	WT %
SO3	3.03
NA	39.58
NA2O	0.0
K	0.90
K2O	0.0
MGO	0.23
CAO	0.94
SIO2	0.0
FE2O3	0.01
AL2O3	0.0
CL	58.74
WEIGHT LOSS ON HEATING	
70	0.20
300-350	0.28
450-500	0.65
TOTAL	104.62

MAJOR: HAL
MINOR: POLY
TRACE: FEOX

TOTAL ANALYSIS

HOLE # 7
DEPTH = 1969.0 FEET

SOLUBLE = 98.05 %
INSOLUBLE = 1.95 %

COMPONENT	WT %
SO3	0.32
NA	38.76
NA2O	0.0
K	0.08
K2O	0.0
MGO	0.22
CAO	0.08
SIO2	0.15
FE2O3	0.02
AL2O3	0.04
CL	60.60
WEIGHT LOSS ON HEATING	
70	0.43
100	0.08
400-500	0.20
TOTAL	100.98

MAJOR: HAL
MINOR:
TRACE: ANH, KAIN, CHLOR, TALC, QTZ, FEOX

TOTAL ANALYSIS

HOLE #   7
DEPTH =   1973.0   FEET

SOLUBLE =   98.63   %
INSOLUBLE =   1.37   %

COMPONENT	WT %
SO3	0.26
NA	38.46
NA2O	0.0
K	0.06
K2O	0.03
MGO	0.53
CAO	0.07
SIO2	0.66
FE2O3	0.01
AL2O3	0.13
CL	59.58
WEIGHT LOSS ON HEATING	
70	0.19
170	0.07
380	0.02
450+	0.12
TOTAL	100.19

MAJOR: HAL
MINOR: POLY, KIES
TRACE: KAIN, CHLOR, FKELD, TALC, QTZ, FEOX

TOTAL ANALYSIS

HOLE # 7
DEPTH = 1975.0 FEET

SOLUBLE = 99.93 %
INSOLUBLE = 0.07 %

COMPONENT	WT %
SO3	0.19
NA	38.93
NA2O	0.0
K	0.06
K2O	0.0
MGO	0.07
CAO	0.09
SIO2	0.0
FE2O3	0.0
AL2O3	0.0
CL	60.38
WEIGHT LOSS ON HEATING	
70	0.17
400-500	0.07
TOTAL	100.03

MAJOR: HAL
MINOR:
TRACE: ANH, KAIN

TOTAL ANALYSIS

```
HOLE #     7
DEPTH =  1978.5  FEET

SOLUBLE  =   91.07  %
INSOLUBLE =   8.93  %
```

COMPONENT	WT %
SO3	2.82
NA	32.52
NA2O	1.96
K	0.44
K2O	0.13
MGO	2.62
CAO	0.98
SIO2	2.89
FE2O3	0.37
AL2O3	1.06
CL	51.89
WEIGHT LOSS ON HEATING	
70	0.36
200	0.04
300-400	0.17
450-550	1.10
TOTAL	99.35

```
MAJOR:  HAL
MINOR:  POLY, CHLOR
TRACE:  ANH, LANG, BLOED, FEOX
```

TOTAL ANALYSIS

```
HOLE #   7
DEPTH = 1983.0  FEET

SOLUBLE =  100.00  %
INSOLUBLE =    0.0  %
```

COMPONENT	WT %
SO3	1.11
NA	36.00
NA2O	0.0
K	0.61
K2O	0.0
MGO	0.40
CAO	0.46
SIO2	0.01
FE2O3	0.0
AL2O3	0.0
CL	59.20
WEIGHT LOSS ON HEATING	
70	0.29
125	0.03
275	0.05
350-400	0.14
TOTAL	98.30

```
MAJOR:  HAL
MINOR:  DOLY, KAIN
TRACE:  QTZ
```

TOTAL ANALYSIS

HOLE #   7
DEPTH = 1986.5 FEET

SOLUBLE =   99.71 %
INSOLUBLE =   0.29 %

COMPONENT	WT %
SO3	0.17
NA	38.20
NA2O	0.0
K	0.04
K2O	0.0
MGO	0.03
CAO	0.21
SIO2	0.01
FE2O3	0.0
AL2O3	0.0
CL	60.66
WEIGHT LOSS ON HEATING	
70	0.10
TO 500	0.0
TOTAL	99.71

MAJOR: HAL
MINOR: ANH, POLY
TRACE: KAIN, QTZ
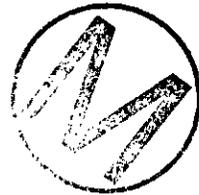
TOTAL ANALYSIS

HOLE # 7
DEPTH = 1993.5 FEET

SOLUBLE = 99.55 %
INSOLUBLE = 0.45 %

COMPONENT	WT %
SO_3	2.96
NA	38.25
NA_2O	0.0
K	1.68
K_2O	0.0
MGO	0.79
CAO	2.30
SIO_2	0.0
FE_2O_3	0.0
AL_2O_3	0.0
CL	53.81
WEIGHT LOSS ON HEATING	
70	0.19
100	0.05
350-400	0.80

TOTAL	101.28

MAJOR: HAL
MINOR: POLY
TRACE:

TOTAL ANALYSIS

HOLE #   7
DEPTH = 2537.0 FEET

SOLUBLE =   91.43 %
INSOLUBLE =   8.57 %

COMPONENT	WT %
SO3	46.62
NA	0.93
NA2O	4.93
K	0.90
K2O	0.0
MGO	13.02
CAO	4.37
SIO2	13.98
FE2O3	1.13
AL2O3	3.26
CL	2.63
WEIGHT LOSS ON HEATING	
70	0.47
100	0.09
TO 500	0.0
HI TEMP	8.68
TOTAL	109.56

MAJOR: ANH
MINOR: HAL, KIES
TRACE: BLOED, FEOX

TOTAL ANALYSIS

HOLE # 7
DEPTH = 2703.0 FEET

SOLUBLE = 98.97 %
INSOLUBLE = 1.03 %

COMPONENT	WT %
SO3	1.46
NA	38.36
NA2O	0.0
K	0.02
K2O	0.01
MGO	0.26
CAO	0.79
SIO2	0.25
FE2O3	0.06
AL2O3	0.05
CL	58.89
WEIGHT LOSS ON HEATING	
70	0.24
150	0.03
550	0.12
TOTAL	100.54

MAJOR: HAL
MINOR: ANH
TRACE: POLY, CHLOR, KFELD, TALC, FEOX

TOTAL ANALYSIS

HOLE # 7
DEPTH = 2716.3 FEET

SOLUBLE = 99.63 %
INSOLUBLE = 0.37 %

COMPONENT	WT %
SO3	0.44
NA	39.44
NA2O	0.0
K	0.01
K2O	0.0
MGO	0.01
CAO	0.18
SIO2	0.01
FE2O3	0.0
AL2O3	0.0
CL	61.00

WEIGHT LOSS
ON HEATING

70	0.22
350	0.04

TOTAL	101.72

MAJOR: HAL
MINOR: ANH
TRACE: POLY, TALC
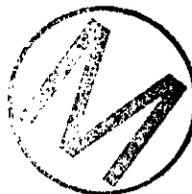
TOTAL ANALYSIS

HOLE #   7
DEPTH = 2736.0 FEET

SOLUBLE =   99.67 %
INSOLUBLE =   0.33 %

COMPONENT	WT %
SO3	0.42
NA	39.75
NA2O	0.0
K	0.01
K2O	0.0
MGO	0.06
CAO	0.51
SIO2	0.01
FE2O3	0.0
AL2O3	0.0
CL	59.88

WEIGHT LOSS
ON HEATING

70	0.08
TO 450	0.03
TOTAL	101.08

MAJOR: HAL
MINOR: ANH
TRACE:

TOTAL ANALYSIS

```
HOLE #   8
DEPTH = 1391.5  FEET

SOLUBLE   =   98.99  %
INSOLUBLE =    1.01  %
```

COMPONENT	WT %
SO3	1.14
NA	39.34
NA2O	0.0
K	0.31
K2O	0.02
MGO	0.27
CAO	0.53
SIO2	0.40
FE2O3	0.27
AL2O3	0.10
CL	58.07
WEIGHT LOSS ON HEATING	
70	0.04
110	0.03
350-400	0.19
TOTAL	100.71

```
MAJOR:  HAL
MINOR:  POLY
TRACE:  CHLOR, ILL, QTZ, FLUX
```

TOTAL ANALYSIS

```
HOLE #     8
DEPTH =  1495.3  FEET

SOLUBLE   =   99.83  %
INSOLUBLE =    0.17  %
```

COMPONENT	WT %
SO_3	1.12
NA	38.00
NA_2O	0.0
K	0.12
K_2O	0.0
MGO	0.13
CAO	1.62
SIO_2	0.01
FE_2O_3	0.0
AL_2O_3	0.0
CL	59.97
WEIGHT LOSS ON HEATING	
70	0.05
200	0.03
TOTAL	101.22

```
MAJOR:  HAL
MINOR:
TRACE:  CARN
```

TOTAL ANALYSIS

HOLE # 8
DEPTH = 1573.0 FEET

SOLUBLE = 97.72 %
INSOLUBLE = 2.28 %

COMPONENT	WT %
SO3	5.11
NA	34.63
NA2O	0.0
K	0.18
K2O	0.02
MGO	1.71
CAO	0.45
SIO2	0.02
FE2O3	0.0
AL2O3	0.01
CL	54.11
WEIGHT LOSS ON HEATING	
70	0.04
100	0.20
160	0.09
350-450	0.85
TOTAL	97.42

MAJOR: HAL
MINOR: (?) POLY, KIES
TRACE: (?) ILL
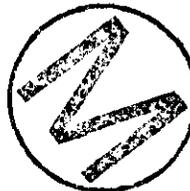
TOTAL ANALYSIS

HOLE #   8
DEPTH =   1652.0   FEET

SOLUBLE =   48.61 %
INSOLUBLE = 51.39 %

COMPONENT	WT %
SO3	51.04
NA	4.07
NA2O	4.24
K	18.59
K2O	0.99
MGO	4.58
CAO	3.93
SIO2	0.35
FE2O3	0.07
AL2O3	0.04
CL	7.35
WEIGHT LOSS ON HEATING	
70	0.09
300+	4.43
TOTAL	99.77
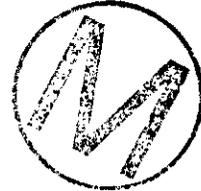
MAJOR: HAL
MINOR: POLY-(?) SYL, LEON, GLAS
TRACE: ILL, QTZ, FEOX

TOTAL ANALYSIS

HOLE # 8
DEPTH = 1705.0 FEET

SOLUBLE = 99.71 %
INSOLUBLE = 0.29 %

COMPONENT	WT %
SO3	1.18
NA	38.79
NA2O	0.0
K	0.35
K2O	0.0
MGO	0.17
CAO	0.44
SIO2	0.01
FE2O3	0.0
AL2O3	0.0
CL	58.64
WEIGHT LOSS ON HEATING	
70	0.15
170	0.02
400-500	0.15
TOTAL	100.19
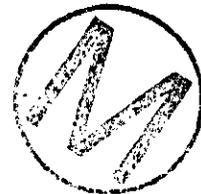
MAJOR: HAL
MINOR:
TRACE: POLY

TOTAL ANALYSIS

HOLE # 8
DEPTH = 1770.0 FEET

SOLUBLE = 98.79 %
INSOLUBLE = 1.21 %

COMPONENT	WT %
SO3	1.95
NA	35.75
NA2O	0.33
K	0.56
K2O	0.02
MGO	0.55
CAO	1.75
SIO2	0.48
FE2O3	0.0
AL2O3	0.12
CL	57.29
WEIGHT LOSS ON HEATING	
70	0.09
170	0.06
400	0.20
TOTAL	99.15
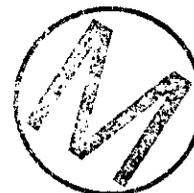
MAJOR: HAL
MINOR: ANH, KAIN
TRACE: ILL, QTZ

TOTAL ANALYSIS

HOLE #   8
DEPTH =   1787.0   FEET

SOLUBLE =   99.43 %
INSOLUBLE =   0.57 %

COMPONENT	WT %
SO3	3.01
NA	37.24
NA2O	0.0
K	0.69
K2O	0.01
MGO	0.54
CAO	0.70
SIO2	0.21
FE2O3	0.03
AL2O3	0.04
CL	58.00
WEIGHT LOSS ON HEATING	
70	0.32
100	0.04
300-400	0.23
TOTAL	101.06

MAJOR: HAL
MINOR: POLY, KAIN
TRACE: CHLOR, QTZ, FEOX
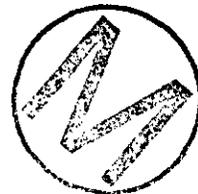
TOTAL ANALYSIS

HOLE #   8
DEPTH =   1794.5 FEET

SOLUBLE   =   75.34 %
INSOLUBLE =   24.66 %

COMPONENT	WT %
SO3	0.70
NA	29.75
NA2O	1.16
K	0.42
K2O	0.63
MGO	6.65
CAO	0.04
SIO2	7.80
FE2O3	0.46
AL2O3	1.91
CL	45.14
WEIGHT LOSS ON HEATING	
70	0.44
150	0.27
425+	4.70
TOTAL	100.07

MAJOR: HAL
MINOR: CARN, CHLOR, KFELD, TALC, QTZ
TRACE: POLY, FEOX

TOTAL ANALYSIS

HOLE #   8
DEPTH =   1804.0   FEET

SOLUBLE =   99.74   %
INSOLUBLE =   0.26   %

COMPONENT	WT %
SO_3	0.28
NA	39.43
NA_2O	0.0
K	0.06
K_2O	0.0
MGO	0.04
CAO	0.70
SIO_2	0.01
FE_2O_3	0.0
AL_2O_3	0.0
CL	59.94
WEIGHT LOSS ON HEATING	
70	0.02
200	0.05
TOTAL	100.79
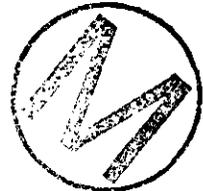
MAJOR: HAL
MINOR: ANH
TRACE: CARN

TOTAL ANALYSIS

HOLE # 8
DEPTH = 1829.0 FEET

SOLUBLE = 99.03 %
INSOLUBLE = 0.97 %

COMPONENT	WT %
SO3	0.02
NA	39.87
NA2O	0.0
K	0.05
K2O	0.02
MGO	0.29
CAO	0.01
SIO2	0.29
FE2O3	0.04
AL2O3	0.08
CL	58.81
WEIGHT LOSS ON HEATING	
70	0.16
200	0.23
TOTAL	99.87
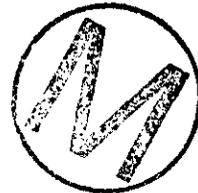
MAJOR: HAL
MINOR:
TRACE: ANH, CARN, CHLOR, KFELD, TALC, FEOX

TOTAL ANALYSIS

HOLE # 8
DEPTH = 1838.0 FEET

SOLUBLE = 97.53 %
INSOLUBLE = 2.47 %

COMPONENT	WT %
SO3	0.80
NA	37.58
NA2O	0.0
K	0.26
K2O	0.10
MGO	0.48
CAO	0.05
SIO2	0.13
FE2O3	0.16
AL2O3	0.27
CL	58.38
WEIGHT LOSS ON HEATING	
70	0.39
TO 500	0.0

TOTAL	98.60
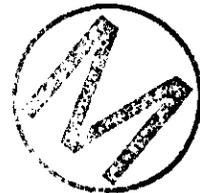
MAJOR: HAL
MINOR:
TRACE: POLY, SLY, LEON, CHLOR, KFELD, FEOX

TOTAL ANALYSIS

HOLE #   8
DEPTH = 1856.7 FEET

SOLUBLE =   99.96 %
INSOLUBLE =   0.04 %

COMPONENT	WT %
SO_3	2.70
NA	36.08
NA_2O	0.0
K	1.62
K_2O	0.0
MGO	0.03
CAO	1.56
SIO_2	0.0
FE_2O_3	0.0
AL_2O_3	0.0
CL	56.66
WEIGHT LOSS ON HEATING	
70	0.07
350	0.03

TOTAL	98.79

MAJOR: HAL
MINOR: ANH, SYL, POLY
TRACE:

TOTAL ANALYSIS

HOLE #   8
DEPTH = 1875.0 FEET

SOLUBLE =   70.94 %
INSOLUBLE =   29.06 %

COMPONENT	WT %
SO3	0.42
NA	25.64
NA2O	0.0
K	0.31
K2O	2.28
MGO	9.55
CAO	0.63
SIO2	15.30
FE2O3	1.23
AL2O3	3.00
CL	40.92
WEIGHT LOSS ON HEATING	
70	0.22
125-200	0.42
TOTAL	99.92

MAJOR: HAL
MINOR: CARN, KFELD, TALC
TRACE: POLY, CHLOR

```
                  TOTAL ANALYSIS
                  ---------------

            HOLE #    8
            DEPTH =  1884.0  FEET

            SOLUBLE  =   80.58  %
            INSOLUBLE =  19.42  %

            -----------------------


          COMPONENT            WT %
          ----------           ----

             SO3               3.76

             NA               27.10

             NA2O              0.0

             K                 6.98

             K2O               1.80

             MGO               5.09

             CAO               1.66

             SIO2              9.02

             FE2O3             0.60

             AL2O3             1.99

             CL               44.06
          WEIGHT LOSS
          ON HEATING

                 70            0.36

              350-400          0.44

                               ------

             TOTAL            102.86


     MAJOR:   HAL
     MINOR:   ANH, CARN, KFELD, TALC, FEOX
     TRACE:   CHLOR
```
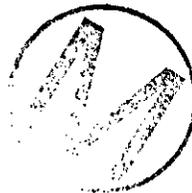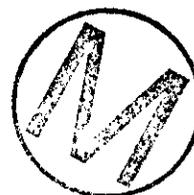
TOTAL ANALYSIS

HOLE #   8
DEPTH = 1890.0 FEET

SOLUBLE =   99.98 %
INSOLUBLE =   0.02 %

COMPONENT	WT %
SO3	0.77
NA	36.78
NA2O	0.0
K	0.10
K2O	0.0
MGO	0.10
CAO	0.95
SIO2	0.0
FE2O3	0.0
AL2O3	0.0
CL	59.33
WEIGHT LOSS ON HEATING	
70	0.05
300-400	0.08
TOTAL	100.18

MAJOR: HAL
MINOR:
TRACE: ANH, CARN

TOTAL ANALYSIS

HOLE #   8
DEPTH =   1894.3   FEET

SOLUBLE =   95.43   %
INSOLUBLE =   4.57   %

COMPONENT	WT %
SO3	0.12
NA	37.90
NA2O	0.0
K	0.06
K2O	0.13
MGO	0.74
CAO	0.03
SIO2	2.43
FE2O3	0.20
AL2O3	0.43
CL	57.78
WEIGHT LOSS ON HEATING	
70	0.30
TO 500	0.0
TOTAL	100.12

MAJOR: HAL
MINOR: QTZ
TRACE: ANH, CARN, CHLOR, KFELD, TALC, FEOX

TOTAL ANALYSIS

HOLE #   8
DEPTH =   1898.5 FEET

SOLUBLE =   98.53 %
INSOLUBLE =   1.47 %

COMPONENT	WT %
SO3	0.55
NA	38.81
NA2O	0.71
K	0.07
K2O	0.01
MGO	0.26
CAO	0.12
SIO2	0.45
FE2O3	0.02
AL2O3	0.07
CL	57.97
WEIGHT LOSS ON HEATING	
70	0.16
TO 500	0.0
TOTAL	99.20

MAJOR: HAL
MINOR:
TRACE: POLY, BLOED, CHLOR, TALC, FEOX
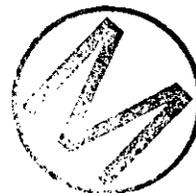
TOTAL ANALYSIS

HOLE #   8
DEPTH =   1900.0   FEET

SOLUBLE =   99.96   %
INSOLUBLE =   0.04   %

COMPONENT	WT %
SO3	3.20
NA	38.14
NA2O	0.0
K	0.98
K2O	0.0
MGO	0.47
CAO	0.39
SIO2	0.0
FE2O3	0.0
AL2O3	0.0
CL	57.60
WEIGHT LOSS ON HEATING	
70	0.17
300-400	0.64
TOTAL	101.63

MAJOR: HAL
MINOR: LEON
TRACE: POLY

TOTAL ANALYSIS

HOLE #   8
DEPTH =   1905.0   FEET

SOLUBLE =   96.98   %
INSOLUBLE =   3.02   %

COMPONENT	WT %
SO3	0.20
NA	38.67
NA2O	0.0
K	0.13
K2O	0.03
MGO	0.93
CAO	0.45
SIO2	0.91
FE2O3	0.14
AL2O3	0.25
CL	57.91
WEIGHT LOSS ON HEATING	
70	0.36
375	0.26

TOTAL	100.24

MAJOR: HAL
MINOR:
TRACE: POLY, CHLOR, KFELD, TALC

TOTAL ANALYSIS

```
HOLE #    8
DEPTH =  1910.0  FEET

SOLUBLE  =   99.02  %
INSOLUBLE =   0.98  %
```

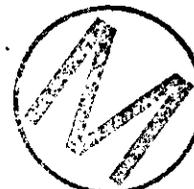| COMPONENT	WT %
SO3	0.53
NA	39.64
NA2O	0.0
K	0.0
K2O	0.30
MGO	0.31
CAO	0.44
SIO2	0.34
FE2O3	0.04
AL2O3	0.06
CL	59.04
WEIGHT LOSS ON HEATING	
70	0.06
375	0.04
TOTAL	100.82

```
MAJOR:  HAL
MINOR:  POLY
TRACE:  ANH, CHLOR, KFELD, TALC, QTZ, FEOX
```

TOTAL ANALYSIS

HOLE # 8
DEPTH = 1913.1 FEET

SOLUBLE = 97.71 %
INSOLUBLE = 2.29 %

COMPONENT	WT %
SO3	0.06
NA	38.48
NA2O	0.0
K	0.06
K2O	0.05
MGO	0.55
CAO	0.01
SIO2	0.91
FE2O3	0.13
AL2O3	0.21
CL	59.27
WEIGHT LOSS ON HEATING	
70	0.11
120	0.03
260	0.03
400+	0.04
TOTAL	99.94

MAJOR: HAL
MINOR:
TRACE: KAIN, CHLOR, KFELD, TALC, QTZ, FEOX

TOTAL ANALYSIS

HOLE # 8
DEPTH = 1916.2 FEET

SOLUBLE = 99.85 %
INSOLUBLE = 0.15 %

COMPONENT	WT %
SO3	0.92
NA	38.48
NA2O	0.0
K	0.21
K2O	0.0
MGO	0.13
CAO	0.44
SIO2	0.0
FE2O3	0.0
AL2O3	0.0
CL	57.71
WEIGHT LOSS ON HEATING	
70	0.13
250	0.02
350-400	0.10
TOTAL	98.29

MAJOR: HAL
MINOR: POLY
TRACE: ANH

TOTAL ANALYSIS

```
HOLE #    8
DEPTH =  1923.0  FEET

SOLUBLE  =   98.30  %
INSOLUBLE =   1.70  %
```

COMPONENT	WT %
SO3	1.06
NA	38.03
NA2O	0.0
K	0.05
K2O	0.08
MGO	0.09
CAO	0.20
SIO2	0.60
FE2O3	0.10
AL2O3	0.16
CL	58.43
WEIGHT LOSS ON HEATING	
70	0.19
300	0.06
450+	0.24
TOTAL	99.29

```
MAJOR:  HAL
MINOR:  POLY
TRACE:  KAIN, CHLOR, ILL, KFELD, QTZ, FEOX
```

TOTAL ANALYSIS

HOLE #   8
DEPTH = 1930.0 FEET

SOLUBLE =   98.99 %
INSOLUBLE = 1.01 %

COMPONENT	WT %
SO3	2.81
NA	35.71
NA2O	0.08
K	1.03
K2O	0.01
MGO	0.46
CAO	0.20
SIO2	0.18
FE2O3	0.07
AL2O3	0.04
CL	56.74
WEIGHT LOSS ON HEATING	
70	0.05
350-400	0.42
TOTAL	97.80

MAJOR: HAL
MINOR: POLY
TRACE: LEON, CHLOR, KFELD, TALC, FEOX

TOTAL ANALYSIS

```
HOLE #     8
DEPTH =   1933.0  FEET

SOLUBLE =     99.62   %
INSOLUBLE =    0.38   %
```

COMPONENT	WT %
SO3	0.78
NA	38.03
NA2O	0.0
K	0.15
K2O	0.0
MGO	0.09
CAO	0.65
SIO2	0.01
FE2O3	0.01
AL2O3	0.0
CL	59.61
WEIGHT LOSS ON HEATING	
70	0.19
200	0.09
TOTAL	100.19

```
MAJOR:  HAL
MINOR:  ANH, POLY, KAIN
TRACE:  QTZ, FEOX
```

TOTAL ANALYSIS

HOLE # 8
DEPTH = 1938.0 FEET

SOLUBLE = 99.86 %
INSOLUBLE = 0.14 %

COMPONENT	WT %
SO3	2.91
NA	35.63
NA2O	0.0
K	0.68
K2O	0.0
MGO	0.84
CAO	1.02
SIO2	0.0
FE2O3	0.0
AL2O3	0.0
CL	59.45
WEIGHT LOSS ON HEATING	
70	0.13
125	0.14
275	0.05
350-400	0.17
TOTAL	101.16
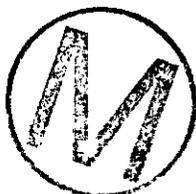
MAJOR: HAL
MINOR: POLY, KAIN
TRACE:

TOTAL ANALYSIS

HOLE #   8
DEPTH = 1953.2 FEET

SOLUBLE   =   99.91 %
INSOLUBLE =   0.09 %

COMPONENT	WT %
SO3	2.30
NA	39.50
NA2O	0.0
K	0.30
K2O	0.0
MGO	0.42
CAO	1.23
SIO2	0.01
FE2O3	0.0
AL2O3	0.0
CL	57.63
WEIGHT LOSS ON HEATING	
70	0.05
250	0.05
375	0.03
425	0.29
TOTAL	101.90

MAJOR: HAL
MINOR: ANH, POLY
TRACE: BLOED, TALC
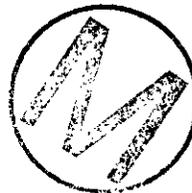
TOTAL ANALYSIS

HOLE #   8
DEPTH =   1967.0   FEET

SOLUBLE =   95.13   %
INSOLUBLE =   4.87   %

COMPONENT	WT %
SO3	1.25
NA	35.99
NA2O	2.73
K	0.57
K2O	0.09
MGO	1.21
CAO	0.41
SIO2	0.76
FE2O3	0.10
AL2O3	0.20
CL	57.52
WEIGHT LOSS ON HEATING	
70	0.28
190	0.04
ʰ00-500	0.20

TOTAL	101.35

MAJOR: HAL
MINOR: POLY, KAIN, TALC
TRACE: CHLOR, FEOX

TOTAL ANALYSIS

HOLE #   8
DEPTH = 1986.0 FEET

SOLUBLE =   36.72 %
INSOLUBLE =   63.28 %

COMPONENT	WT %
SO3	60.87
NA	0.36
NA2O	5.83
K	0.0
K2O	26.07
MGO	1.83
CAO	5.12
SIO2	0.54
FE2O3	0.17
AL2O3	0.85
CL	0.15
WEIGHT LOSS ON HEATING	
70	0.07
300-400	5.81
TOTAL	107.67

MAJOR: (?) GLAS, ANH, LEON
MINOR:
TRACE: HAL, FEOX

TOTAL ANALYSIS

HOLE # 8
DEPTH = 2006.0 FEET

SOLUBLE = 99.50 %
INSOLUBLE = 0.50 %

COMPONENT	WT %
SO3	2.37
NA	37.59
NA2O	0.0
K	1.03
K2O	0.0
MGO	0.31
CAO	0.06
SIO2	0.01
FE2O3	0.0
AL2O3	0.0
CL	57.17
WEIGHT LOSS ON HEATING	
70	0.20
350-400	0.29
450	0.13
475	0.04

TOTAL	99.70

MAJOR: HAL
MINOR: KAIN, BLOED
TRACE: POLY, QTZ

TOTAL ANALYSIS

HOLE # = 8
DEPTH = 2017.0 FEET

SOLUBLE = 95.20 %
INSOLUBLE = 4.80 %

COMPONENT	WT %
SO3	0.62
NA	35.66
NA2O	0.0
K	0.06
K2O	0.04
MGO	0.53
CAO	1.02
SIO2	2.02
FE2O3	0.28
AL2O3	0.70
CL	57.09
WEIGHT LOSS ON HEATING	
70	0.22
100	0.02
300-400	0.17
ORGANIC	1.59
TOTAL	100.02
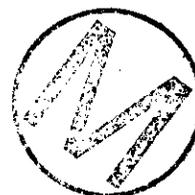
MAJOR: HAL
MINOR: ANH
TRACE: SYL, CAIN, CHLOR, FEOX, ILL

TOTAL ANALYSIS

HOLE #   8
DEPTH =   2039.0 FEET

SOLUBLE =   98.94 %
INSOLUBLE =   1.06 %
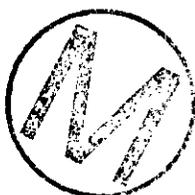
COMPONENT	WT %
SO3	5.50
NA	35.02
NA2O	0.0
K	1.56
K2O	0.03
MGO	0.70
CAO	1.58
SIO2	0.27
FE2O3	0.07
AL2O3	0.05
CL	54.01
WEIGHT LOSS ON HEATING	
70	0.21
100	0.05
300-400	0.49
425	0.27
TOTAL	99.81

MAJOR: HAL
MINOR: POLY, KAIN
TRACE: KFELD, TALC, FEOX

TOTAL ANALYSIS

HOLE #   8
DEPTH =   2050.0   FEET

SOLUBLE   =   28.61   %
INSOLUBLE =   71.39   %

COMPONENT	WT %
SO3	54.99
NA	8.00
NA20	4.90
K	0.05
K20	0.04
MGO	0.31
CAO	7.10
SI02	0.33
FE203	0.0
AL203	0.0
CL	12.44
WEIGHT LOSS ON HEATING	
70	0.11
475	0.68
TOTAL	88.95

MAJOR: ANH
MINOR: HAL
TRACE: QTZ
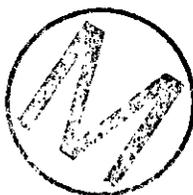
TOTAL ANALYSIS

```
HOLE #    8
DEPTH =  2068.0  FEET

SOLUBLE =   98.84  %
INSOLUBLE =   1.16  %
```

COMPONENT	WT %
SO3	2.49
NA	37.41
NA2O	0.0
K	0.08
K2O	0.01
MGO	0.31
CAO	0.89
SIO2	0.38
FE2O3	0.05
AL2O3	0.07
CL	55.99
WEIGHT LOSS ON HEATING	
70	0.04
250	0.10
TOTAL	97.82

```
MAJOR:  HAL
MINOR:  ANH, TALC, BLOED
TRACE:  POLY, CHLOR, FEOX
```

TOTAL ANALYSIS

HOLE #   8
DEPTH =   2084.0   FEET

SOLUBLE   =   92.00   %
INSOLUBLE =   8.00   %

COMPONENT	WT %
SO3	2.64
NA	34.46
NA2O	1.87
K	1.02
K2O	0.19
MGO	1.48
CAO	0.73
SIO2	2.07
FE2O3	0.25
AL2O3	0.37
CL	52.19
WEIGHT LOSS ON HEATING	
70	0.17
140	0.05
350-400	0.27
450-550	0.22

TOTAL	97.98

MAJOR: HAL
MINOR: CHLOR, TALC, QTZ
TRACE: KFELD, FEOX
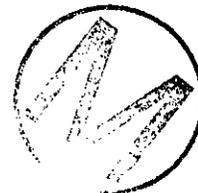
TOTAL ANALYSIS

HOLE #   8
DEPTH = 2130.0 FEET

SOLUBLE =   99.61 %
INSOLUBLE =   0.39 %

COMPONENT	WT %
SO3	2.31
NA	37.79
NA2O	0.0
K	0.42
K2O	0.0
MGO	0.25
CAO	0.75
SIO2	0.03
FE2O3	0.0
AL2O3	0.0
CL	57.16
WEIGHT LOSS ON HEATING	
70	0.11
125	0.07
350-400	0.10
TOTAL	99.38
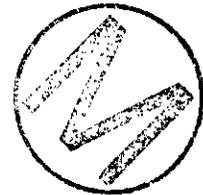
MAJOR: HAL
MINOR: POLY
TRACE: ANH, QTZ

TOTAL ANALYSIS

HOLE # 8
DEPTH = 2162.0 FEET

SOLUBLE = 98.90 %
INSOLUBLE = 1.10 %

COMPONENT	WT %
SO3	1.56
NA	36.77
NA2O	0.55
K	1.23
K2O	0.03
MGO	0.65
CAO	0.93
SIO2	0.23
FE2O3	0.06
AL2O3	0.05
CL	59.99
WEIGHT LOSS ON HEATING	
70	0.14
300-400	0.48
TOTAL	102.67

MAJOR: HAL
MINOR: ANH, POLY, SYL
TRACE: KFELD, TALC, FEOX
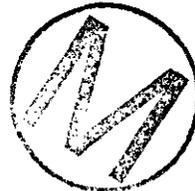
TOTAL ANALYSIS

HOLE #   8
DEPTH =   2217.0 FEET

SOLUBLE =   99.78 %
INSOLUBLE =   0.22 %

COMPONENT	WT %
SO3	0.0
NA	39.14
NA2O	0.0
K	0.07
K2O	0.0
MGO	0.02
CAO	0.12
SIO2	0.01
FE2O3	0.0
AL2O3	0.0
CL	59.75
WEIGHT LOSS ON HEATING	
70	0.04
300-400	0.40
TOTAL	99.77

MAJOR: HAL
MINOR:
TRACE: ANH, POLY, SLY, QTZ

TOTAL ANALYSIS

HOLE #   8
DEPTH =   2280.0   FEET

SOLUBLE =   100.00   %
INSOLUBLE =   0.0   %

COMPONENT	WT %
SO3	0.39
NA	37.91
NA2O	0.0
K	0.12
K2O	0.0
MGO	0.09
CAO	0.25
SIO2	0.02
FE2O3	0.0
AL2O3	0.0
CL	60.23
WEIGHT LOSS ON HEATING	
70	0.19
350	0.08
TOTAL	99.28

MAJOR: HAL
MINOR: ANH, CARN
TRACE: POLY, QTZ
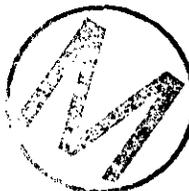
TOTAL ANALYSIS

HOLE #   8
DEPTH =   2326.0 FEET

SOLUBLE   =   95.44 %
INSOLUBLE =   4.56 %

COMPONENT	WT %
SO3	0.18
NA	37.83
NA2O	0.0
K	0.06
K2O	0.03
MGO	1.39
CAO	0.17
SIO2	1.15
FE2O3	0.12
AL2O3	0.25
CL	57.93
WEIGHT LOSS ON HEATING	
70	0.11
100-150	0.03
450+ MIN	0.56
TOTAL	99.81

MAJOR: HAL
MINOR: TALC
TRACE: HAL, CARN, CHLOR, FLOX

TOTAL ANALYSIS

HOLE # 8
DEPTH = 2366.3 FEET

SOLUBLE = 31.37 %
INSOLUBLE = 68.63 %

COMPONENT	WT %
SO_3	47.32
NA	0.62
NA_2O	3.76
K	0.0
K_2O	10.67
MGO	6.40
CAO	3.37
SIO_2	10.68
FE_2O_3	0.01
AL_2O_3	1.57
CL	1.17
WEIGHT LOSS ON HEATING	
70	0.43
200-375	4.81
375-500	1.60
TOTAL	92.41
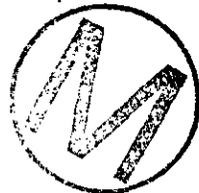
MAJOR:
MINOR: KAIN, KFELD, TALC, QTZ
TRACE: HAL, SYL

TOTAL ANALYSIS

HOLE #   8
DEPTH =   2427.5   FEET

SOLUBLE   =   99.36   %
INSOLUBLE =   0.64   %

COMPONENT	WT %
SO3	2.58
NA	39.42
NA2O	0.0
K	0.01
K2O	0.01
MGO	0.05
CAO	0.35
SIO2	0.10
FE2O3	0.01
AL2O3	0.01
CL	59.88
WEIGHT LOSS ON HEATING	
70	0.03
300-400	0.40
TOTAL	102.85
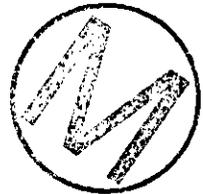
MAJOR: HAL
MINOR: ANH
TRACE: POLY, BLOED, KFELD, TALC, QTZ, FEOX

```
                    TOTAL ANALYSIS
                    --------------

             HOLE #    8
             DEPTH =  2460.0  FEET

             SOLUBLE =    99.21  %
             INSOLUBLE =    0.79  %

             --------------------


         COMPONENT           WT %
         ---------           ----

            SO3               1.14

            NA               38.75

            NA2O              0.0

            K                 0.03

            K2O               0.01

            MGO               0.20

            CAO               0.62

            SIO2              0.19

            FE2O3             0.03

            AL2O3             0.06

            CL               57.00
         WEIGHT LOSS
         ON HEATING

                  70          0.17

                 125          0.05

                 350          0.08

                 450          0.07

                            ------

            TOTAL            98.40


MAJOR:   HAL
MINOR:   ANH
TRACE:   KAIN, CHLOR, KFELD, TALC, FEOX
```
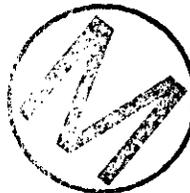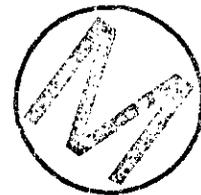
TOTAL ANALYSIS

```
HOLE #     8
DEPTH =  2519.6  FEET

SOLUBLE =    99.36  %
INSOLUBLE =   0.64  %
```

COMPONENT	WT %
SO3	0.17
NA	40.42
NA2O	0.0
K	0.02
K2O	0.0
MGO	0.01
CAO	0.03
SIO2	0.0
FE2O3	0.0
AL2O3	0.0
CL	60.31
WEIGHT LOSS ON HEATING	
70	0.08
480	0.06
TOTAL	101.74

```
MAJOR:  HAL
MINOR:
TRACE:  POLY
```

TOTAL ANALYSIS

HOLE #   8
DEPTH =   2563.0   FEET

SOLUBLE   =   7.11 %
INSOLUBLE =   92.89 %

COMPONENT	WT %
SO3	40.59
NA	1.47
NA2O	6.06
K	0.05
K2O	0.54
MGO	14.73
CAO	24.37
SIO2	6.25
FE2O3	0.96
AL2O3	1.86
CL	1.05
WEIGHT LOSS ON HEATING	
70	1.87
100-150	0.19
175	0.07
450+ MIN	0.11
TOTAL	100.17
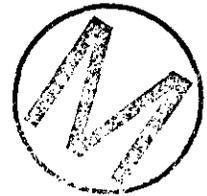
MAJOR: ANH
MINOR: CHLOR, KFELD, TALC, FEOX
TRACE: HAL, LANG

TOTAL ANALYSIS

HOLE # 8
DEPTH = 2615.5 FEET

SOLUBLE = 99.74 %
INSOLUBLE = 0.26 %

COMPONENT	WT %
SO3	0.86
NA	38.58
NA2O	0.0
K	0.05
K2O	0.0
MGO	0.02
CAO	0.58
SIO2	0.0
FE2O3	0.01
AL2O3	0.0
CL	59.37
WEIGHT LOSS ON HEATING	
70	0.21
300-350	0.06
TOTAL	100.00

MAJOR: HAL
MINOR: ANH
TRACE: POLY, FEOX

TOTAL ANALYSIS

HOLE # = 8
DEPTH = 2665.5 FEET

SOLUBLE = 99.08 %
INSOLUBLE = 0.92 %

COMPONENT	WT %
SO3	0.98
NA	38.68
NA2O	0.0
K	0.02
K2O	0.01
MGO	0.22
CAO	0.35
SIO2	0.23
FE2O3	0.04
AL2O3	0.06
CL	59.14
WEIGHT LOSS ON HEATING	
70	0.25
400-500	0.48
TOTAL	100.46

MAJOR: HAL
MINOR: ANH, CHLOR
TRACE: POLY, KFELD, TALC, FEOX

TOTAL ANALYSIS

HOLE #   8
DEPTH = 2706.0 FEET

SOLUBLE = 98.75 %
INSOLUBLE = 1.25 %

COMPONENT	WT %
SO3	1.13
NA	37.09
NA2O	0.64
K	0.03
K2O	0.03
MGO	0.19
CAO	0.68
SIO2	0.27
FE2O3	0.27
AL2O3	0.07
CL	58.60
WEIGHT LOSS ON HEATING	
70	0.16
300	0.05
380	0.75
400+	0.70
TOTAL	100.66
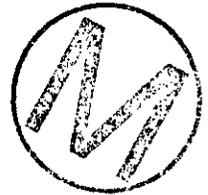
MAJOR: HAL
MINOR: ANH
TRACE: POLY, CHLOR, KFELD, TALC, FEOX

TOTAL ANALYSIS

HOLE # 8
DEPTH = 2758.0 FEET

SOLUBLE = 99.22 %
INSOLUBLE = 0.78 %

COMPONENT	WT %
SO3	1.70
NA	37.20
NA2O	0.83
K	0.08
K2O	0.01
MGO	0.18
CAO	1.14
SIO2	0.06
FE2O3	0.01
AL2O3	0.02
CL	58.07
WEIGHT LOSS ON HEATING	
70	0.11
250	0.05
TOTAL	99.46
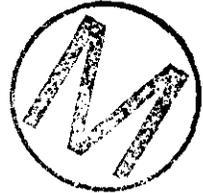
MAJOR: HAL
MINOR: ANH
TRACE: POLY, CHLOR, KFELD, TALC, FEOX

TOTAL ANALYSIS

HOLE # 8
DEPTH = 2779.0 FEET

SOLUBLE = 99.62 %
INSOLUBLE = 0.38 %

COMPONENT	WT %
SO3	1.09
NA	37.41
NA2O	0.0
K	0.01
K2O	0.0
MGO	0.03
CAO	1.80
SIO2	0.0
FE2O3	0.0
AL2O3	0.0
CL	58.53
WEIGHT LOSS ON HEATING	
70	0.21
HI TEMP	0.0
TOTAL	99.46

MAJOR: HAL
MINOR: CARN, ANH
TRACE:
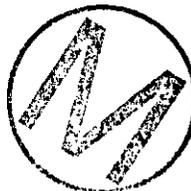
TOTAL ANALYSIS

HOLE # 8
DEPTH = 2794.0 FEET

SOLUBLE = 99.79 %
INSOLUBLE = 0.21 %

COMPONENT	WT %
SO3	0.99
NA	37.86
NA2O	0.0
K	0.02
K2O	0.0
MGO	0.01
CAO	0.68
SIO2	0.0
FE2O3	0.0
AL2O3	0.0
CL	60.58
WEIGHT LOSS ON HEATING	
70	0.18
HI TEMP	0.0
TOTAL	100.53

MAJOR: HAL
MINOR: ANH
TRACE: POLY
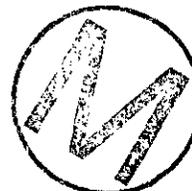
TOTAL ANALYSIS

HOLE # 8
DEPTH = 2802.5 FEET

SOLUBLE = 99.55 %
INSOLUBLE = 0.45 %

COMPONENT	WT %
SO3	1.76
NA	38.39
NA2O	0.0
K	0.02
K2O	0.0
MGO	0.01
CAO	0.22
SIO2	0.0
FE2O3	0.0
AL2O3	0.0
CL	58.19
WEIGHT LOSS ON HEATING	
70	0.10
170	0.02
375	0.02
TOTAL	99.18

MAJOR: HAL
MINOR: ANH
TRACE: BLOED, POLY
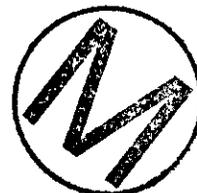
TOTAL ANALYSIS

HOLE # 8
DEPTH = 2809.0 FEET

SOLUBLE = 99.09 %
INSOLUBLE = 0.91 %

COMPONENT	WT %
SO3	2.02
NA	38.56
NA2O	0.0
K	0.01
K2O	0.01
MGO	0.04
CAO	1.09
SIO2	0.04
FE2O3	0.0
AL2O3	0.01
CL	59.70
WEIGHT LOSS ON HEATING	
70	0.15
150-200	0.09
400	0.24
TOTAL	101.96
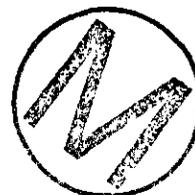
MAJOR: HAL
MINOR: ANH
TRACE: POLY, BLOED, POLY, KFELD, QTZ

TOTAL ANALYSIS

HOLE # 8
DEPTH = 2820.5 FEET

SOLUBLE = 99.46 %
INSOLUBLE = 0.54 %

COMPONENT	WT %
SO3	1.67
NA	38.42
NA2O	0.0
K	0.01
K2O	0.0
MGO	0.03
CAO	0.29
SIO2	0.06
FE2O3	0.0
AL2O3	0.0
CL	58.50
WEIGHT LOSS ON HEATING	
70	0.18
400+	0.18
TOTAL	99.34
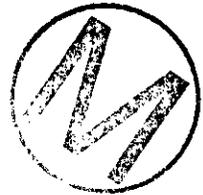
MAJOR: HAL
MINOR: THEN, ANH
TRACE: POLY, TALC

TOTAL ANALYSIS

HOLE #   8
DEPTH =   2879.0   FEET

SOLUBLE   =   96.41 %
INSOLUBLE =   3.59 %

COMPONENT	WT %
SO3	4.15
NA	32.65
NA2O	0.93
K	0.02
K2O	0.01
MGO	0.13
CAO	1.54
SIO2	0.13
FE2O3	0.01
AL2O3	0.01
CL	55.79
WEIGHT LOSS ON HEATING	
70	0.06
TO 500	0.0
500+	3.31
TOTAL	98.74
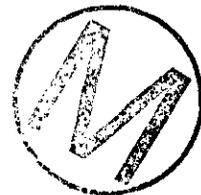
MAJOR: HAL
MINOR: GLAUB, ANH
TRACE: POLY, KFELD, TALC, FEOX

TOTAL ANALYSIS

HOLE #   8
DEPTH = 2948.0 FEET

SOLUBLE =   97.32 %
INSOLUBLE =   2.68 %

COMPONENT	WT %
SO3	5.34
NA	37.30
NA2O	0.0
K	0.01
K2O	0.01
MGO	0.03
CAO	0.79
SIO2	0.06
FE2O3	0.01
AL2O3	0.0
CL	55.51
WEIGHT LOSS ON HEATING	
70	0.20
150	0.02
450	0.02
500	0.02
TOTAL	99.32
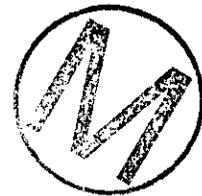
MAJOR: HAL
MINOR: GLAUB, ANH
TRACE: LANG, TALC, QTZ, FECX

Appendix 7.B (Ref. sec. 7.3)

Whole Rock Chemical Analyses in Soluble and

Insoluble Fractions & Moles times 1000

```
HOLE #    7
DEPTH =    1044.2  FEET
TOTAL
```

COMPONENT	WT %	MOLES
SO3	0.55	6.87
NA	38.56	1677.25
NA2O	0.0	0.0
K	0.03	0.77
K2O	0.0	0.0
MGO	0.04	0.99
CAO	0.43	7.67
SIO2	0.0	0.0
FE2O3	0.0	0.0
AL2O3	0.0	0.0
CL	60.40	1703.61

HOLE # 7
DEPTH = 1107.5 FEET

SOLUBLE
69.47 WT % OF TOTAL

COMPONENT	WT %	MOLES
SO3	9.24	115.41
NA	20.28	882.12
NA2O	0.0	0.0
K	0.0	0.0
K2O	3.70	39.28
MGO	2.24	55.57
CAO	1.61	28.71
SIO2	0.0	0.0
FE2O3	0.0	0.0
AL2O3	0.01	0.10
CL	30.78	868.26
SUBTOTAL	67.86 %	
MEASURED =	69.47	

HOLE # 7
DEPTH = 1107.5 FEET

INSOLUBLE
30.53 WT % OF TOTAL

WT %	MOLES
11.63	145.27
0.0	0.0
6.63	106.97
0.0	0.0
0.77	8.17
2.33	57.80
0.23	4.10
8.30	138.13
0.27	1.69
1.24	12.16
0.0	0.0
31.40 %	
30.53	

HOLE #   7
DEPTH =   1171.5   FEET

HOLE #   7
DEPTH =   1171.5   FEET

SOLUBLE
37.10 WT % OF TOTAL

INSOLUBLE
62.90 WT % OF TOTAL

COMPONENT	WT %	MOLES	WT %	MOLES
SO3	1.92	23.98	37.81	472.27
NA	12.56	546.32	0.0	0.0
NA2O	0.0	0.0	0.88	14.20
K.	1.91	48.85	0.0	0.0
K2O	0.0	0.0	0.0	0.0
MGO	0.47	11.66	0.23	5.71
CAO	1.65	29.42	23.48	418.69
SIO2	0.01	0.17	0.62	10.32
FE2O3	0.0	0.0	0.06	0.38
AL2O3	0.0	0.0	0.0	0.0
CL	18.87	532.30	0.0	0.0

SUBTOTAL	37.39 %		63.08 %	
MEASURED =	37.10		62.90	

HOLE # 7
DEPTH = 1221.0 FEET
TOTAL

COMPONENT	WT %	MOLES
SO3	2.02	25.23
NA	38.79	1687.26
NA2O	0.0	0.0
K	0.06	1.53
K2O	0.0	0.0
MGO	0.10	2.48
CAO	0.88	15.69
SIO2	0.01	0.17
FE2O3	0.0	0.0
AL2O3	0.0	0.0
CL	58.31	1644.85

HOLE # 7
DEPTH = 1343.0 FEET
TOTAL

COMPONENT	WT %	MOLES
SO3	0.99	12.37
NA	38.60	1678.99
NA2O	0.0	0.0
K	0.35	8.95
K2O	0.0	0.0
MGO	0.15	3.72
CAO	0.66	11.77
SIO2	0.01	0.17
FE2O3	0.0	0.0
AL2O3	0.0	0.0
CL	59.40	1675.60

HOLE # 7
DEPTH = 1402.5 FEET
TOTAL

COMPONENT	WT %	MOLES
SO3	0.11	1.37
NA	39.67	1725.53
NA2O	0.0	0.0
K	0.06	1.53
K2O	0.0	0.0
MGO	0.06	1.49
CAO	0.02	0.36
SIO2	0.0	0.0
FE2O3	0.0	0.0
AL2O3	0.0	0.0
CL	59.78	1686.32
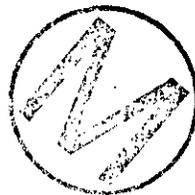
```
HOLE #    7                              HOLE #    7
DEPTH =    1468.5  FEET                  DEPTH =    1468.5  FEET

SOLUBLE                                  INSOLUBLE
   93.66 WT % OF TOTAL                      6.34 WT % OF TOTAL
```

COMPONENT	WT %	MOLES	WT %	MOLES
SO3	0.98	12.24	1.89	23.61
NA	34.44	1498.04	0.0	0.0
NA2O	0.0	0.0	0.0	0.0
K	0.37	9.46	0.0	0.0
K2O	0.0	0.0	0.07	0.74
MGO	0.52	12.90	1.32	32.75
CAO	0.18	3.21	0.01	0.18
SIO2	0.03	0.50	2.12	35.28
FE2O3	0.0	0.0	0.24	1.50
AL2O3	0.0	0.0	0.07	0.69
CL	53.61	1512.27	0.0	0.0
SUBTOTAL	90.13 %		5.72 %	
MEASURED =	93.66		6.34	

```
HOLE #    7
DEPTH =    1534.0  FEET
TOTAL


COMPONENT        WT %          MOLES
---------        ----          -----

  SO3           1.67          20.86

  NA           36.10        1570.25

  NA2O          0.0           0.0

  K             0.52          13.30

  K2O           0.0           0.0

  MGO           0.22          5.46

  CAO           0.64          11.41

  SIO2          0.01          0.17

  FE2O3         0.0           0.0

  AL2O3         0.0           0.0

  CL           57.76        1629.34
```
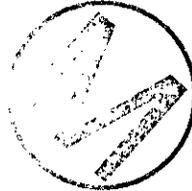
HOLE # 7
DEPTH = 1615.0 FEET
SOLUBLE
96.69 WT % OF TOTAL

HOLE # 7
DEPTH = 1615.0 FEET
INSOLUBLE
1.31 WT % OF TOTAL

COMPONENT	WT %	MOLES	WT %	MOLES
SO3	3.58	44.72	0.98	12.24
NA	35.06	1525.01	0.0	0.0
NA2O	0.0	0.0	0.0	0.0
K	1.05	26.85	0.0	0.0
K2O	0.0	0.0	0.0	0.0
MGO	0.69	17.12	0.02	0.50
CAO	1.39	24.79	0.08	1.43
SIO2	0.03	0.50	0.21	3.49
FE2O3	0.0	0.0	0.03	0.19
AL2O3	0.0	0.0	0.07	0.69
CL	55.95	1578.28	0.0	0.0
SUBTOTAL	97.75 %		1.39 %	
MEASURED =	98.69		1.31	

	HOLE # 7 DEPTH = 1698.0 FEET		HOLE # 7 DEPTH = 1698.0 FEET	
	SOLUBLE 95.35 WT % OF TOTAL		INSOLUBLE 4.65 WT % OF TOTAL	
COMPONENT	WT %	MOLES	WT %	MOLES
SO3	0.58	7.24	0.0	0.0
NA	36.47	1586.34	0.0	0.0
NA2O	0.0	0.0	0.0	0.0
K	0.06	1.53	0.0	0.0
K2O	0.0	0.0	0.07	0.74
MGO	0.28	6.95	0.92	22.82
CAO	0.33	5.88	0.01	0.18
SIO2	0.04	0.67	2.03	33.78
FE2O3	0.0	0.0	0.25	1.57
AL2O3	0.0	0.0	0.61	5.98
CL	58.35	1645.98	0.0	0.0
SUBTOTAL	96.11 %		3.89 %	
MEASURED =	95.35		4.65	

HOLE # 7
DEPTH = 1755.0 FEET
TOTAL

COMPONENT	WT %	MOLES
SO3	0.65	8.12
NA	38.12	1658.11
NA2O	0.0	0.0
K	0.23	5.88
K2O	0.0	0.0
MGO	0.13	3.23
CAO	0.08	1.43
SIO2	0.02	0.33
FE2O3	0.0	0.0
AL2O3	0.0	0.0
CL	59.54	1679.55

	HOLE # 7 DEPTH = 1952.5 FEET SOLUBLE 99.30 WT % OF TOTAL		HOLE # 7 DEPTH = 1952.5 FEET INSOLUBLE 0.70 WT % OF TOTAL	
COMPONENT	WT %	MOLES	WT %	MOLES
SO3	3.03	37.85	0.15	1.87
NA	37.14	1615.49	0.0	0.0
NA2O	0.0	0.0	0.0	0.0
K	0.75	19.18	0.0	0.0
K2O	0.0	0.0	0.03	0.32
MGO	0.42	10.42	0.12	2.98
CAO	0.78	13.91	0.01	0.18
SIO2	0.01	0.17	0.33	5.49
FE2O3	0.01	0.06	0.02	0.13
AL2O3	0.0	0.0	0.05	0.49
CL	57.00	1607.90	0.0	0.0
SUBTOTAL	99.14 %		0.71 %	
MEASURED =	99.30		0.70	
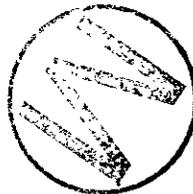
	HOLE # 7 DEPTH = 1954.0 FEET SOLUBLE 97.46 WT % OF TOTAL		HOLE # 7 DEPTH = 1954.0 FEET INSOLUBLE 2.54 WT % OF TOTAL	
COMPONENT	WT %	MOLES	WT %	MOLES
SO3	0.73	9.12	0.0	0.0
NA	37.94	1650.28	0.0	0.0
NA2O	0.0	0.0	0.0	0.0
K	0.18	4.60	0.0	0.0
K2O	0.0	0.0	0.06	0.64
MGO	0.17	4.22	0.39	9.68
CAO	0.51	9.09	0.01	0.18
SIO2	0.02	0.33	1.33	22.13
FE2O3	0.0	0.0	0.09	0.56
AL2O3	0.0	0.0	0.23	2.26
CL	58.38	1646.83	0.0	0.0
SUBTOTAL	97.93 %		2.11 %	
MEASURED =	97.46		2.54	

	HOLE # 7 DEPTH = 1957.5 FEET		HOLE # 7 DEPTH = 1957.5 FEET	
	SOLUBLE 99.16 WT % OF TOTAL		INSOLUBLE 0.84 WT % OF TOTAL	
COMPONENT	WT %	MOLES	WT %	MOLES
SO3	1.32	16.49	0.41	5.12
NA	38.38	1669.42	0.0	0.0
NA2O	0.0	0.0	0.0	0.0
K	0.36	9.21	0.0	0.0
K2O	0.0	0.0	0.01	0.11
MGO	0.24	5.95	0.17	4.22
CAO	2.18	38.87	0.0	0.0
SIO2	0.03	0.50	0.35	5.82
FE2O3	0.0	0.0	0.04	0.25
AL2O3	0.0	0.0	0.10	0.98
CL	59.00	1664.32	0.0	0.0
SUBTOTAL	101.51 %		1.08 %	
MEASURED =	99.16		0.84	
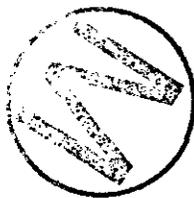
	HOLE # 7 DEPTH = 1961.0 FEET		HOLE # 7 DEPTH = 1961.0 FEET	
	SOLUBLE 99.10 WT % OF TOTAL		INSOLUBLE 0.90 WT % OF TOTAL	
COMPONENT	WT %	MOLES	WT %	MOLES
SO3	0.49	6.12	0.0	0.0
NA	39.14	1702.48	0.0	0.0
NA2O	0.0	0.0	0.0	0.0
K	0.21	5.37	0.0	0.0
K2O	0.01	0.11	0.01	0.11
MGO	0.07	1.74	0.18	4.47
CAO	0.19	3.39	0.0	0.0
SIO2	0.01	0.17	0.42	6.99
FE2O3	0.0	0.0	0.04	0.25
AL2O3	0.0	0.0	0.08	0.78
CL	58.83	1659.52	0.0	0.0
SUBTOTAL	98.95 %		0.73 %	
MEASURED =	99.10		0.90	

```
HOLE #    7
DEPTH =    1967.0  FEET

TOTAL


COMPONENT        WT %         MOLES
---------        -----        ------

   SO3           3.03         37.85

   NA           39.58        1721.62

   NA2O          0.0           0.0

   K             0.90         23.02

   K2O           0.0           0.0

   MGO           0.23          5.71

   CAO           0.94         16.76

   SIO2          0.0           0.0

   FE2O3         0.01          0.06

   AL2O3         0.0           0.0

   CL           58.74        1656.98
```

	HOLE # 7 DEPTH = 1969.0 FEET SOLUBLE 98.05 WT % OF TOTAL		HOLE # 7 DEPTH = 1969.0 FEET INSOLUBLE 1.95 WT % OF TOTAL	
COMPONENT	WT %	MOLES	WT %	MOLES
SO3	0.32	4.00	0.0	0.0
NA	38.76	1685.95	0.0	0.0
NA2O	0.0	0.0	0.0	0.0
K	0.08	2.05	0.0	0.0
K2O	0.0	0.0	0.0	0.0
MGO	0.11	2.73	0.11	2.73
CAO	0.08	1.43	0.0	0.0
SIO2	0.01	0.17	0.14	2.33
FE2O3	0.0	0.0	0.02	0.13
AL2O3	0.0	0.0	0.04	0.39
CL	60.60	1709.45	0.0	0.0
SUBTOTAL	99.96 %		0.31 %	
MEASURED =	98.05		1.95	

	HOLE # 7 DEPTH = 1973.0 FEET SOLUBLE 98.63 WT % OF TOTAL		HOLE # 7 DEPTH = 1973.0 FEET INSOLUBLE 1.37 WT % OF TOTAL	
COMPONENT	WT %	MOLES	WT %	MOLES
SO3	0.26	3.25	0.0	0.0
NA	38.46	1672.90	0.0	0.0
NA2O	0.0	0.0	0.0	0.0
K	0.06	1.53	0.0	0.0
K2O	0.0	0.0	0.03	0.32
MGO	0.13	3.23	0.40	9.92
CAO	0.06	1.07	0.01	0.18
SIO2	0.03	0.50	0.62	10.32
FE2O3	0.0	0.0	0.01	0.06
AL2O3	0.0	0.0	0.13	1.28
CL	59.58	1680.68	0.0	0.0
SUBTOTAL	98.58 %		1.20 %	
MEASURED =	98.63		1.37	
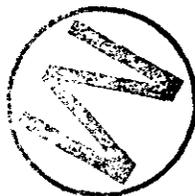
HOLE # 7

DEPTH = 1975.0 FEET

TOTAL

COMPONENT	WT %	MOLES
SO3	0.19	2.37
NA	38.93	1693.35
NA2O	0.0	0.0
K	0.06	1.53
K2O	0.0	0.0
MGO	0.07	1.74
CAO	0.09	1.60
SIO2	0.0	0.0
FE2O3	0.0	0.0
AL2O3	0.0	0.0
CL	60.38	1703.24

	HOLE # 7 DEPTH = 1978.5 FEET SOLUBLE 91.07 WT % OF TOTAL		HOLE # 7 DEPTH = 1978.5 FEET INSOLUBLE 8.93 WT % OF TOTAL	
COMPONENT	WT %	MOLES	WT %	MOLES
SO3	2.74	34.22	0.08	1.00
NA	32.52	1414.53	0.0	0.0
NA2O	0.0	0.0	1.96	31.62
K	0.44	11.25	0.0	0.0
K2O	0.0	0.0	0.13	1.38
MGO	0.37	9.18	2.25	55.82
CAO	0.96	17.12	0.02	0.36
SIO2	0.0	0.0	2.89	48.09
FE2O3	0.0	0.0	0.37	2.32
AL2O3	0.0	0.0	1.06	10.40
CL	51.89	1463.75	0.0	0.0
SUBTOTAL	88.92 %		8.76 %	
MEASURED =	91.07		8.93	

HOLE # 7
DEPTH = 1983.0 FEET
TOTAL

COMPONENT	WT %	MOLES
SO3	1.11	13.86
NA	36.00	1565.90
NA2O	0.0	0.0
K	0.61	15.60
K2O	0.0	0.0
MGO	0.40	9.92
CAO	0.46	8.20
SIO2	0.01	0.17
FE2O3	0.0	0.0
AL2O3	0.0	0.0
CL	59.20	1669.96
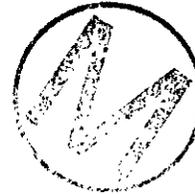
HOLE # 7
DEPTH = 1986.5 FEET

TOTAL

COMPONENT	WT %	MOLES
SO3	0.17	2.12
NA	38.20	1661.59
NA2O	0.0	0.0
K	0.04	1.02
K2O	0.0	0.0
MGO	0.03	0.74
CAO	0.21	3.74
SIO2	0.01	0.17
FE2O3	0.0	0.0
AL2O3	0.0	0.0
CL	60.66	1711.14

```
HOLE #   7
DEPTH =   1993.5  FEET

TOTAL


COMPONENT        WT %        MOLES
---------        ----        -----

  SO3            2.96        36.97

  NA            38.25      1663.77

  NA20           0.0         0.0

  K              1.68       42.97

  K20            0.0         0.0

  MGO            0.79       19.60

  CAO            2.30       41.01

  SIO2           0.0         0.0

  FE2O3          0.0         0.0

  AL2O3          0.0         0.0

  CL            53.81      1517.91
```
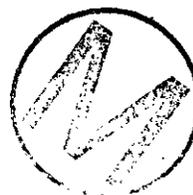
```
HOLE #     7
DEPTH =     2537.0  FEET

TOTAL


COMPONENT        WT %        MOLES
---------        ----        -----

  SO3           46.62       582.31
  NA             0.93        40.45
  NA2O           4.93        79.54
  K              0.90        23.02
  K2O            0.0          0.0
  MGO           13.02       323.00
  CAO            4.37        77.92
  SIO2          13.98       232.65
  FE2O3          1.13         7.08
  AL2O3          3.26        31.97
  CL             2.63        74.19
```

	HOLE # 7 DEPTH = 2703.0 FEET		HOLE # 7 DEPTH = 2703.0 FEET	
	SOLUBLE 98.97 WT % OF TOTAL		INSOLUBLE 1.03 WT % OF TOTAL	
COMPONENT	WT %	MOLES	WT %	MOLES
SO3	0.73	9.12	0.74	9.24
NA	38.36	1668.55	0.0	0.0
NA2O	0.0	0.0	0.0	0.0
K	0.02	0.51	0.0	0.0
K2O	0.0	0.0	0.01	0.11
MGO	0.06	1.49	0.20	4.96
CAO	0.78	13.91	0.01	0.18
SIO2	0.04	0.67	0.21	3.49
FE2O3	0.01	0.06	0.05	0.31
AL2O3	0.0	0.0	0.05	0.49
CL	58.89	1661.21	0.0	0.0
SUBTOTAL	98.89 %		1.27 %	
MEASURED =	98.97		1.03	

HOLE # 7
DEPTH = 2716.3 FEET

TOTAL

COMPONENT	WT %	MOLES
SO3	0.44	5.50
NA	39.44	1715.53
NA2O	0.0	0.0
K	0.01	0.26
K2O	0.0	0.0
MGO	0.01	0.25
CAO	0.18	3.21
SIO2	0.01	0.17
FE2O3	0.0	0.0
AL2O3	0.0	0.0
CL	61.00	1720.73
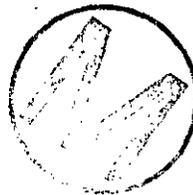
```
HOLE #    7
DEPTH =    2736.0  FEET
TOTAL
```

COMPONENT	WT %	MOLES
SO3	0.42	5.25
NA	39.75	1729.01
NA2O	0.0	0.0
K	0.01	0.26
K2O	0.0	0.0
MGO	0.06	1.49
CAO	0.51	9.09
SIO2	0.01	0.17
FE2O3	0.0	0.0
AL2O3	0.0	0.0
CL	59.88	1689.14

	HOLE # 8 DEPTH = 1391.5 FEET SOLUBLE 98.99 WT % OF TOTAL		HOLE # 8 DEPTH = 1391.5 FEET INSOLUBLE 1.01 WT % OF TOTAL	
COMPONENT	WT %	MOLES	WT %	MOLES
SO3	1.07	13.36	0.07	0.87
NA	39.34	1711.18	0.0	0.0
NA2O	0.0	0.0	0.0	0.0
K	0.31	7.93	0.0	0.0
K2O	0.0	0.0	0.02	0.21
MGO	0.21	5.21	0.06	1.49
CAO	0.52	9.27	0.01	0.18
SIO2	0.0	0.0	0.39	6.49
FE2O3	0.0	0.0	0.27	1.69
AL2O3	0.0	0.0	0.10	0.98
CL	58.07	1638.08	0.0	0.0
SUBTOTAL	99.52 %		0.92 %	
MEASURED =	98.99		1.01	

HOLE # 8
DEPTH = 1495.3 FEET
TOTAL

COMPONENT	WT %	MOLES
SO3	1.12	13.99
NA	38.00	1652.89
NA2O	0.0	0.0
K	0.12	3.07
K2O	0.0	0.0
MGO	0.13	3.23
CAO	1.62	28.89
SIO2	0.01	0.17
FE2O3	0.0	0.0
AL2O3	0.0	0.0
CL	59.97	1691.68

	HOLE # 8 DEPTH = 1573.0 FEET SOLUBLE 97.72 WT % OF TOTAL		HOLE # 8 DEPTH = 1573.0 FEET INSOLUBLE 2.28 WT % OF TOTAL	
COMPONENT	WT %	MOLES	WT %	MOLES
SO3	3.40	42.47	1.71	21.36
NA	34.63	1506.31	0.0	0.0
NA2O	0.0	0.0	0.0	0.0
K	0.18	4.60	0.0	0.0
K2O	0.0	0.0	0.02	0.21
MGO	1.65	40.93	0.06	1.49
CAO	0.29	5.17	0.16	2.85
SIO2	0.0	0.0	0.02	0.33
FE2O3	0.0	0.0	0.0	0.0
AL2O3	0.0	0.0	0.01	0.10
CL	54.11	1526.38	0.0	0.0
SUBTOTAL	94.26 %		1.98 %	
MEASURED =	97.72		2.28	

| | HOLE # 8 1652.0 FEET | | | HOLE # 8 1652.0 FEET | |
| | SOLUBLE 48.61 WT % OF TOTAL | | | INSOLUBLE 51.39 WT % OF TOTAL | |
COMPONENT	WT %	MOLES		WT %	MOLES
SO3	19.80	247.31		31.24	390.21
NA	4.07	177.03		0.0	0.0
NA2O	0.0	0.0		4.24	68.41
K	18.59	475.45		0.0	0.0
K2O	0.0	0.0		0.99	10.51
MGO	4.12	102.21		0.46	11.41
CAO	0.19	3.39		3.74	66.69
SIO2	0.0	0.0		0.34	5.66
FE2O3	0.0	0.0		0.07	0.44
AL2O3	0.0	0.0		0.04	0.39
CL	7.35	207.33		0.0	0.0
SUBTOTAL	54.12 %			41.12 %	
MEASURED =	48.61			51.39	
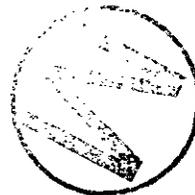
HOLE #   8
DEPTH =   1705.0   FEET

TOTAL

COMPONENT	WT %	MOLES
SO3	1.18	14.74
NA	38.79	1687.26
NA2O	0.0	0.0
K	0.35	8.95
K2O	0.0	0.0
MGO	0.17	4.22
CAO	0.44	7.85
SIO2	0.01	0.17
FE2O3	0.0	0.0
AL2O3	0.0	0.0
CL	58.64	1654.16

HOLE # 8
DEPTH = 1770.0 FEET

SOLUBLE
98.79 WT % OF TOTAL

COMPONENT	WT %	MOLES
SO3	1.78	22.23
NA	35.75	1555.02
NA2O	0.0	0.0
K	0.56	14.32
K2O	0.0	0.0
MGO	0.52	12.90
CAO	1.75	31.21
SIO2	0.01	0.17
FE2O3	0.0	0.0
AL2O3	0.0	0.0
CL	57.29	1616.08
SUBTOTAL	97.66 %	
MEASURED =	98.79	

HOLE # 8
DEPTH = 1770.0 FEET

INSOLUBLE
1.21 WT % OF TOTAL

	WT %	MOLES
SO3	0.17	2.12
NA	0.0	0.0
NA2O	0.33	5.32
K	0.0	0.0
K2O	0.02	0.21
MGO	0.03	0.74
CAO	0.0	0.0
SIO2	0.47	7.82
FE2O3	0.0	0.0
AL2O3	0.12	1.18
CL	0.0	0.0
SUBTOTAL	1.14 %	
MEASURED =	1.21	

COMPONENT	HOLE # 8 DEPTH = 1787.0 FEET SOLUBLE 99.43 WT % OF TOTAL WT %	MOLES	HOLE # 8 DEPTH = 1787.0 FEET INSOLUBLE 0.57 WT % OF TOTAL WT %	MOLES
SO3	3.01	37.60	0.0	0.0
NA	37.24	1619.84	0.0	0.0
NA2O	0.0	0.0	0.0	0.0
K	0.69	17.65	0.0	0.0
K2O	0.0	0.0	0.01	0.11
MGO	0.40	9.92	0.14	3.47
CAO	0.70	12.48	0.0	0.0
SIO2	0.01	0.17	0.21	3.49
FE2O3	0.0	0.0	0.03	0.19
AL2O3	0.0	0.0	0.04	0.39
CL	58.00	1636.11	0.0	0.0
SUBTOTAL	100.05 %		0.43 %	
MEASURED =	99.43		0.57	

```
HOLE #    8                              HOLE #    8
DEPTH =     1794.5  FEET                 DEPTH =     1794.5  FEET

SOLUBLE                                  INSOLUBLE
75.34 WT % OF TOTAL                      24.66 WT % OF TOTAL
```

COMPONENT	WT %	MOLES	WT %	MOLES
SO3	0.70	8.74	0.0	0.0
NA	29.75	1294.04	0.0	0.0
NA2O	0.0	0.0	1.16	18.72
K	0.42	10.74	0.0	0.0
K2O	0.0	0.0	0.63	6.69
MGO	0.44	10.92	6.20	153.81
CAO	0.03	0.53	0.01	0.18
SIO2	0.02	0.33	7.78	129.47
FE2O3	0.0	0.0	0.46	2.88
AL2O3	0.0	0.0	1.91	18.73
CL	45.14	1273.34	0.0	0.0

```
SUBTOTAL    76.50  %                     18.15  %

MEASURED =   75.34                       24.66
```

HOLE # 8
DEPTH = 1804.0 FEET
TOTAL

COMPONENT	WT %	MOLES
SO3	0.28	3.50
NA	39.43	1715.09
NA2O	0.0	0.0
K	0.06	1.53
K2O	0.0	0.0
MGO	0.04	0.99
CAO	0.70	12.48
SIO2	0.01	0.17
FE2O3	0.0	0.0
AL2O3	0.0	0.0
CL	59.94	1690.83

SOLUBLE
99.03 WT % OF TOTAL

INSOLUBLE
0.97 WT % OF TOTAL

COMPONENT	WT %	MOLES	WT %	MOLES
SO3	0.02	0.25	0.0	0.0
NA	39.87	1734.23	0.0	0.0
NA2O	0.0	0.0	0.0	0.0
K	0.05	1.28	0.0	0.0
K2O	0.0	0.0	0.02	0.21
MGO	0.06	1.49	0.23	5.71
CAO	0.01	0.18	0.01	0.18
SIO2	0.01	0.17	0.29	4.83
FE2O3	0.0	0.0	0.04	0.25
AL2O3	0.0	0.0	0.08	0.78
CL	58.81	1658.96	0.0	0.0
SUBTOTAL	98.83 %		0.67 %	
MEASURED =	99.03		0.97	

	HOLE #　8 DEPTH = 1838.0 FEET SOLUBLE 97.53 WT % OF TOTAL		HOLE #　8 DEPTH = 1838.0 FEET INSOLUBLE 2.47 WT % OF TOTAL	
COMPONENT	WT %	MOLES	WT %	MOLES
SO3	0.80	9.99	0.0	0.0
NA	37.58	1634.62	0.0	0.0
NA2O	0.0	0.0	0.0	0.0
K	0.26	6.65	0.0	0.0
K2O	0.0	0.0	0.10	1.06
MGO	0.11	2.73	0.37	9.18
CAO	0.05	0.89	0.0	0.0
SIO2	0.01	0.17	0.12	2.00
FE2O3	0.0	0.0	0.16	1.00
AL2O3	0.0	0.0	0.27	2.65
CL	58.38	1646.83	0.0	0.0
SUBTOTAL	97.19 %		1.02 %	
MEASURED =	97.53		2.47	

```
HOLE #    8
DEPTH =    1856.7  FEET
TOTAL
```

COMPONENT	WT %	MOLES
SO3	2.70	33.72
NA	36.08	1569.38
NA2O	0.0	0.0
K	1.62	41.43
K2O	0.0	0.0
MGO	0.03	0.74
CAO	1.56	27.82
SIO2	0.0	0.0
FE2O3	0.0	0.0
AL2O3	0.0	0.0
CL	56.66	1598.31
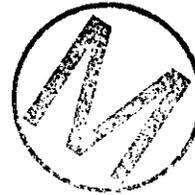
HOLE # 8
DEPTH = 1875.0 FEET

SOLUBLE
70.94 WT % OF TOTAL

COMPONENT	WT %	MOLES
SO3	0.42	5.25
NA	25.64	1115.27
NA2O	0.0	0.0
K	0.31	7.93
K2O	0.0	0.0
MGO	0.33	8.19
CAO	0.43	7.67
SIO2	0.01	0.17
FE2O3	0.0	0.0
AL2O3	0.0	0.0
CL	40.92	1154.30
SUBTOTAL	68.06 %	
MEASURED =	70.94	

HOLE # 8
DEPTH = 1875.0 FEET

INSOLUBLE
29.06 WT % OF TOTAL

WT %	MOLES
0.0	0.0
0.0	0.0
0.0	0.0
0.0	0.0
2.28	24.20
9.22	228.73
0.20	3.57
15.29	254.45
1.23	7.70
3.00	29.42
0.0	0.0
31.22 %	
29.06	
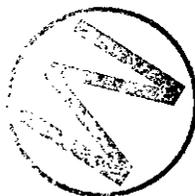
	HOLE # 8 DEPTH = 1884.0 FEET			HOLE # 8 DEPTH = 1884.0 FEET	
	SOLUBLE 80.58 WT % OF TOTAL			INSOLUBLE 19.42 WT % OF TOTAL	
COMPONENT	WT %	MOLES		WT %	MOLES
SO3	3.76	46.96		0.0	0.0
NA	27.10	1178.77		0.0	0.0
NA2O	0.0	0.0		0.0	0.0
K	6.98	178.52		0.0	0.0
K2O	0.0	0.0		1.80	19.11
MGO	1.44	35.72		3.65	90.55
CAO	1.65	29.42		0.01	0.18
SIO2	0.01	0.17		9.01	149.94
FE2O3	0.0	0.0		0.60	3.76
AL2O3	0.0	0.0		1.99	19.52
CL	44.06	1242.88		0.0	0.0
SUBTOTAL	85.00 %			17.06 %	
MEASURED =	80.58			19.42	
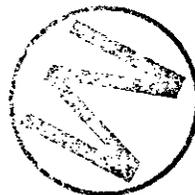
```
HOLE #      8
DEPTH =      1890.0  FEET

TOTAL


COMPONENT        WT %         MOLES
---------        ----         -----

  SO3           0.77          9.62
  NA           38.78       1686.82
  NA2O          0.0           0.0
  K             0.10          2.56
  K2O           0.0           0.0
  MGO           0.10          2.48
  CAO           0.95         16.94
  SIO2          0.0           0.0
  FE2O3         0.0           0.0
  AL2O3         0.0           0.0
  CL           59.33       1673.62
```
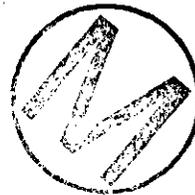
HOLE #   8
DEPTH =   1894.3   FEET

SOLUBLE
95.43 WT % OF TOTAL

COMPONENT	WT %	MOLES
SO3	0.12	1.50
NA	37.90	1648.54
NA2O	0.0	0.0
K	0.06	1.53
K2O	0.0	0.0
MGO	0.08	1.98
CAO	0.03	0.53
SIO2	0.0	0.0
FE2O3	0.0	0.0
AL2O3	0.0	0.0
CL	57.78	1629.90
SUBTOTAL	95.97 %	
MEASURED =	95.43	

WT %	MOLES
0.0	0.0
0.0	0.0
0.0	0.0
0.0	0.0
0.13	1.38
0.66	16.37
0.0	0.0
2.43	40.44
0.20	1.25
0.43	4.22
0.0	0.0
3.85 %	
4.57	

SOLUBLE
98.53 WT % OF TOTAL

HOLE # 8
DEPTH = 1898.5 FEET

INSOLUBLE
1.47 WT % OF TOTAL

COMPONENT	SOLUBLE WT %	SOLUBLE MOLES	INSOLUBLE WT %	INSOLUBLE MOLES
SO3	0.55	6.87	0.0	0.0
NA	38.81	1688.13	0.0	0.0
NA2O	0.0	0.0	0.71	11.46
K	0.07	1.79	0.0	0.0
K2O	0.0	0.0	0.01	0.11
MGO	0.08	1.98	0.18	4.47
CAO	0.11	1.96	0.01	0.18
SIO2	0.01	0.17	0.44	7.32
FE2O3	0.0	0.0	0.02	0.13
AL2O3	0.0	0.0	0.07	0.69
CL	57.97	1635.26	0.0	0.0

SUBTOTAL   97.60 %   1.44 %

MEASURED = 98.53   1.47
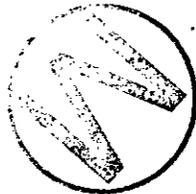
```
HOLE #    8
DEPTH =   1900.0   FEET
TOTAL
```

COMPONENT	WT %	MOLES
SO3	3.20	39.97
NA	38.14	1658.98
NA2O	0.0	0.0
K	0.98	25.06
K2O	0.0	0.0
MGO	0.47	11.66
CAO	0.39	6.95
SIO2	0.0	0.0
FE2O3	0.0	0.0
AL2O3	0.0	0.0
CL	57.60	1624.82

	HOLE # 8 DEPTH = 1905.0 FEET		HOLE # 8 DEPTH = 1905.0 FEET	
	SOLUBLE 96.98 WT % OF TOTAL		INSOLUBLE 3.02 WT % OF TOTAL	
COMPONENT	WT %	MOLES	WT %	MOLES
SO3	0.20	2.50	0.0	0.0
NA	38.67	1682.04	0.0	0.0
NA2O	0.0	0.0	0.0	0.0
K	0.13	3.32	0.0	0.0
K2O	0.0	0.0	0.03	0.32
MGO	0.10	2.48	0.83	20.59
CAO	0.44	7.85	0.01	0.18
SIO2	0.0	0.0	0.91	15.14
FE2O3	0.0	0.0	0.14	0.88
AL2O3	0.0	0.0	0.25	2.45
CL	57.91	1633.57	0.0	0.0
SUBTOTAL	97.45 %		2.17 %	
MEASURED =	96.98		3.02	

HOLE # 8
DEPTH = 1910.0 FEET

SOLUBLE
99.02 WT % OF TOTAL

COMPONENT	WT %	MOLES
SO3	0.53	6.62
NA	39.64	1724.23
NA2O	0.0	0.0
K	0.0	0.0
K2O	0.29	3.08
MGO	0.10	2.48
CAO	0.44	7.85
SIO2	0.01	0.17
FE2O3	0.0	0.0
AL2O3	0.0	0.0
CL	59.04	1665.44

SUBTOTAL   100.05 %

MEASURED =   99.02

HOLE # 8
DEPTH = 1910.0 FEET

INSOLUBLE
0.98 WT % OF TOTAL

WT %	MOLES
0.0	0.0
0.0	0.0
0.0	0.0
0.0	0.0
0.01	0.11
0.20	4.96
0.0	0.0
0.33	5.49
0.04	0.25
0.08	0.78
0.0	0.0

0.66 %

0.98

)   )   )
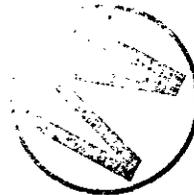
HOLE #   8
DEPTH =   1913.1   FEET

SOLUBLE
97.71 WT % OF TOTAL

COMPONENT	WT %	MOLES
SO3	0.06	0.75
NA	38.48	1673.77
NA2O	0.0	0.0
K	0.06	1.53
K2O	0.0	0.0
MGO	0.06	1.49
CAO	0.0	0.0
SIO2	0.01	0.17
FE2O3	0.0	0.0
AL2O3	0.0	0.0
CL	59.27	1671.93

SUBTOTAL   97.94 %

MEASURED =   97.71

INSOLUBLE
2.29 WT % OF TOTAL

WT %	MOLES
0.0	0.0
0.0	0.0
0.0	0.0
0.0	0.0
0.05	0.53
0.48	11.91
0.0	0.0
0.90	14.98
0.13	0.81
0.21	2.06
0.0	0.0

1.77 %

2.29
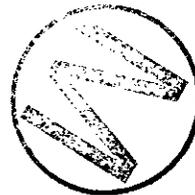
HOLE # = 8 1916.2 FEET
DEPTH =

TOTAL

COMPONENT	WT %	MOLES
SO3	0.92	11.49
NA	38.48	1673.77
NA2O	0.0	0.0
K	0.21	5.37
K2O	0.0	0.0
MGO	0.13	3.23
CAO	0.44	7.85
SIO2	0.0	0.0
FE2O3	0.0	0.0
AL2O3	0.0	0.0
CL	57.71	1627.93

	HOLE # 8 DEPTH = 1923.0 FEET SOLUBLE 98.30 WT % OF TOTAL		HOLE # 8 DEPTH = 1923.0 FEET INSOLUBLE 1.70 WT % OF TOTAL	
COMPONENT	WT %	MOLES	WT %	MOLES
SO3	0.10	1.25	0.95	11.87
NA	38.03	1654.20	0.0	0.0
NA2O	0.0	0.0	0.0	0.0
K	0.05	1.28	0.0	0.0
K2O	0.0	0.0	0.08	0.85
MGO	0.05	1.24	0.03	0.74
CAO	0.08	1.43	0.12	2.14
SIO2	0.01	0.17	0.59	9.82
FE2O3	0.0	0.0	0.10	0.63
AL2O3	0.0	0.0	0.16	1.57
CL	58.43	1648.24	0.0	0.0
SUBTOTAL	96.75 %		2.03 %	
MEASURED =	98.30		1.70	

HOLE # 8
DEPTH = 1930.0 FEET

SOLUBLE
98.99 WT % OF TOTAL

COMPONENT	WT %	MOLES
SO3	2.81	35.10
NA	35.71	1553.28
NA2O	0.0	0.0
K	1.03	26.34
K2O	0.0	0.0
MGO	0.33	8.19
CAO	0.19	3.39
SIO2	0.0	0.0
FE2O3	0.0	0.0
AL2O3	0.0	0.0
CL	56.74	1600.56

SUBTOTAL   96.81   %

MEASURED =   98.99

HOLE # 8
DEPTH = 1930.0 FEET

INSOLUBLE
1.01 WT % OF TOTAL

WT %	MOLES
0.0	0.0
0.0	0.0
0.08	1.29
0.0	0.0
0.01	0.11
0.13	3.23
0.01	0.18
0.18	3.00
0.07	0.44
0.04	0.39
0.0	0.0

0.52   %

1.01

HOLE # 8
DEPTH = 1933.0 FEET
TOTAL

COMPONENT	WT %	MOLES
SO3	0.78	9.74
NA	38.03	1654.20
NA2O	0.0	0.0
K	0.15	3.84
K2O	0.0	0.0
MGO	0.09	2.23
CAO	0.65	11.59
SIO2	0.01	0.17
FE2O3	0.01	0.06
AL2O3	0.0	0.0
CL	59.81	1687.17

```
HOLE #     8
DEPTH =    1938.0  FEET

TOTAL


COMPONENT        WT %          MOLES
---------        -----        -------

   SO3            2.91          36.35

   NA            35.63        1549.80

   NA20           0.0           0.0

   K              0.68          17.39

   K20            0.0           0.0

   MGO            0.84          20.84

   CAO            1.02          18.19

   SIO2           0.0           0.0

   FE2O3          0.0           0.0

   AL2O3          0.0           0.0

   CL            59.45        1677.01
```
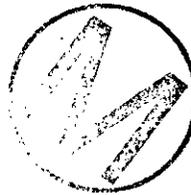
HOLE #   8
DEPTH =   1953.2   FEET

TOTAL

COMPONENT	WT %	MOLES
SO3	2.30	28.73
NA	39.50	1718.14
NA2O	0.0	0.0
K	0.30	7.67
K2O	0.0	0.0
MGO	0.42	10.42
CAO	1.23	21.93
SIO2	0.01	0.17
FE2O3	0.0	0.0
AL2O3	0.0	0.0
CL	57.63	1625.67

```
HOLE #    8                           HOLE #    8
DEPTH =    1967.0  FEET               DEPTH =    1967.0  FEET

SOLUBLE                               INSOLUBLE
  95.13 WT % OF TOTAL                   4.87 WT % OF TOTAL
```

COMPONENT	WT %	MOLES	WT %	MOLES
SO3	1.25	15.61	0.0	0.0
NA	35.99	1565.46	0.0	0.0
NA2O	0.0	0.0	2.73	44.05
K	0.57	14.58	0.0	0.0
K2O	0.0	0.0	0.09	0.96
MGO	0.23	5.71	0.98	24.31
CAO	0.40	7.13	0.0	0.0
SIO2	0.0	0.0	0.76	12.65
FE2O3	0.0	0.0	0.10	0.63
AL2O3	0.0	0.0	0.20	1.96
CL	57.52	1622.57	0.0	0.0

```
SUBTOTAL    95.96  %                   4.86  %

MEASURED =  95.13                      4.87
```

	HOLE # 8 DEPTH = 1986.0 FEET		HOLE # 8 DEPTH = 1986.0 FEET	
	SOLUBLE 36.72 WT % OF TOTAL		INSOLUBLE 63.28 WT % OF TOTAL	
COMPONENT	WT %	MOLES	WT %	MOLES
SO3	22.99	287.16	37.88	473.15
NA	0.36	15.66	0.0	0.0
NA2O	0.0	0.0	5.83	94.06
K	0.0	0.0	0.0	0.0
K2O	14.68	155.84	11.39	120.91
MGO	0.62	15.38	1.20	29.77
CAO	0.87	15.51	4.25	75.78
SIO2	0.0	0.0	0.54	8.99
FE2O3	0.0	0.0	0.17	1.06
AL2O3	0.0	0.0	0.85	8.34
CL	0.15	4.23	0.0	0.0
SUBTOTAL	39.67 %		62.11 %	
MEASURED =	36.72		63.28	
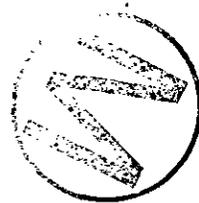
```
HOLE #      8
DEPTH =    2006.0   FEET

TOTAL


COMPONENT        WT %         MOLES
---------       ----        -------

   SO3          2.37         29.60

   NA          37.59       1635.06

   NA2O         0.0          0.0

   K            1.03         26.34

   K2O          0.0          0.0

   MGO          0.31         7.69

   CAO          0.06         1.07

   SIO2         0.01         0.17

   FE2O3        0.0          0.0

   AL2O3        0.0          0.0

   CL          57.17       1612.69
```

HOLE #   8
DEPTH =   2017.0 FEET

SOLUBLE
95.20 WT % OF TOTAL

COMPONENT	WT %	MOLES
SO3	0.55	6.87
NA	35.66	1551.11
NA2O	0.0	0.0
K	0.06	1.53
K2O	0.0	0.0
MGO	0.08	1.98
CAO	0.96	17.12
SIO2	0.02	0.33
FE2O3	0.0	0.0
AL2O3	0.0	0.0
CL	57.09	1610.44

SUBTOTAL   94.42 %

MEASURED =   95.20

HOLE #   8
DEPTH =   2017.0 FEET

INSOLUBLE
4.80 WT % OF TOTAL

WT %	MOLES
0.07	0.87
0.0	0.0
0.0	0.0
0.0	0.0
0.04	0.42
0.44	10.92
0.06	1.07
2.01	33.45
0.28	1.75
0.70	6.87
0.0	0.0

3.60 %

4.80
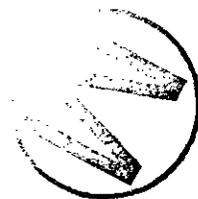
	HOLE # 8 DEPTH = 2039.0 FEET			HOLE # 8 DEPTH = 2039.0 FEET	
	SOLUBLE 98.94 WT % OF TOTAL			INSOLUBLE 1.06 WT % OF TOTAL	
COMPONENT	WT %	MOLES		WT %	MOLES
SO3	4.88	60.95		0.62	7.74
NA	35.02	1523.27		0.0	0.0
NA2O	0.0	0.0		0.0	0.0
K	1.56	39.90		0.0	0.0
K2O	0.0	0.0		0.03	0.32
MGO	0.50	12.40		0.21	5.21
CAO	1.57	28.00		0.01	0.18
SIO2	0.0	0.0		0.26	4.33
FE2O3	0.0	0.0		0.07	0.44
AL2O3	0.0	0.0		0.05	0.49
CL	54.01	1523.55		0.0	0.0
SUBTOTAL	97.54 %			1.25 %	
MEASURED =	98.94			1.06	

HOLE # 8
DEPTH = 2050.0 FEET

SOLUBLE
28.61 WT % OF TOTAL

COMPONENT	WT %	MOLES
SO3	3.92	48.96
NA	8.00	347.98
NA2O	0.0	0.0
K	0.05	1.29
K2O	0.0	0.0
MGO	0.02	0.50
CAO	0.55	9.81
SIO2	0.0	0.0
FE2O3	0.0	0.0
AL2O3	0.0	0.0
CL	12.44	350.92
SUBTOTAL	24.98 %	
MEASURED =	28.61	

HOLE # 8
DEPTH = 2050.0 FEET

INSOLUBLE
71.39 WT % OF TOTAL

	WT %	MOLES
	51.08	638.02
	0.0	0.0
	4.90	79.06
	0.0	0.0
	0.04	0.42
	0.29	7.19
	6.55	116.80
	0.33	5.49
	0.0	0.0
	0.0	0.0
	0.0	0.0
	63.19 %	
	71.39	

HOLE # 8
DEPTH = 2068.0 FEET

SOLUBLE
98.84 WT % OF TOTAL

HOLE # 8
DEPTH = 2068.0 FEET

INSOLUBLE
1.16 WT % OF TOTAL

COMPONENT	WT %	MOLES	WT %	MOLES
SO3	2.49	31.10	0.0	0.0
NA	37.41	1627.23	0.0	0.0
NA2O	0.0	0.0	0.0	0.0
K	0.08	2.05	0.0	0.0
K2O	0.0	0.0	0.01	0.11
MGO	0.03	0.74	0.28	6.95
CAO	0.87	15.51	0.02	0.36
SIO2	0.02	0.33	0.37	6.16
FE2O3	0.0	0.0	0.05	0.31
AL2O3	0.0	0.0	0.07	0.69
CL	55.99	1579.41	0.0	0.0
SUBTOTAL	96.89 %		0.80 %	
MEASURED =	98.84		1.16	

HOLE #   8
DEPTH =   2084.0 FEET

	SOLUBLE 92.00 WT % OF TOTAL		INSOLUBLE 8.00 WT % OF TOTAL	
COMPONENT	WT %	MOLES	WT %	MOLES
SO3	2.05	25.61	0.59	7.37
NA	34.46	1498.91	0.0	0.0
NA2O	0.0	0.0	1.87	30.17
K	1.02	26.09	0.0	0.0
K2O	0.0	0.0	0.19	2.02
MGO	0.35	8.68	1.13	28.03
CAO	0.72	12.84	0.01	0.18
SIO2	0.01	0.17	2.07	34.45
FE2O3	0.01	0.06	0.24	1.50
AL2O3	0.0	0.0	0.37	3.63
CL	52.19	1472.21	0.0	0.0
SUBTOTAL	90.81 %		6.47 %	
MEASURED =	92.00		8.00	

```
HOLE #    8
DEPTH =    2130.0   FEET
TOTAL
```

COMPONENT	WT %	MOLES
SO3	2.31	28.85
NA	37.79	1643.76
NA2O	0.0	0.0
K	0.42	10.74
K2O	0.0	0.0
MGO	0.25	6.20
CAO	0.75	13.37
S1O2	0.03	0.50
FE2O3	0.0	0.0
AL2O3	0.0	0.0
CL	57.16	1612.41
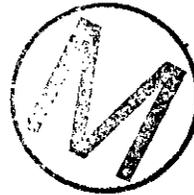
HOLE #   8
DEPTH =   2162.0   FEET

SOLUBLE
98.90 WT % OF TOTAL

COMPONENT	WT %	MOLES
SO3	1.31	16.36
NA	36.77	1599.39
NA2O	0.0	0.0
K	1.23	31.46
K2O	0.0	0.0
MGO	0.45	11.16
CAO	0.93	16.58
SIO2	0.0	0.0
FE2O3	0.0	0.0
AL2O3	0.0	0.0
CL	59.99	1692.24

SUBTOTAL   100.68   %

MEASURED =   98.90

HOLE #   8
DEPTH =   2162.0   FEET

INSOLUBLE
1.10 WT % OF TOTAL

WT %	MOLES
0.25	3.12
0.0	0.0
0.55	8.87
0.0	0.0
0.03	0.32
0.20	4.96
0.01	0.18
0.23	3.83
0.06	0.38
0.05	0.49
0.0	0.0

1.38   %

1.10

```
HOLE #    8
DEPTH =    2217.0  FEET

TOTAL
```

COMPONENT	WT %	MOLES
SO3	0.0	0.0
NA	39.14	1702.48
NA2O	0.0	0.0
K	0.07	1.79
K2O	0.0	0.0
MGO	0.02	0.50
CAO	0.12	2.14
SIO2	0.01	0.17
FE2O3	0.0	0.0
AL2O3	0.0	0.0
CL	59.75	1685.47

HOLE # 8
DEPTH = 2280.0 FEET
TOTAL

COMPONENT	WT %	MOLES
SO3	0.39	4.87
NA	37.91	1648.98
NA2O	0.0	0.0
K	0.12	3.07
K2O	0.0	0.0
MGO	0.09	2.23
CAO	0.25	4.46
SIO2	0.02	0.33
FE2O3	0.0	0.0
AL2O3	0.0	0.0
CL	60.23	1699.01
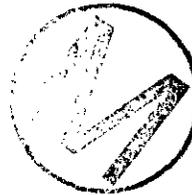
```
HOLE #    8
DEPTH =    2326.0  FEET

INSOLUBLE
   4.56 WT % OF TOTAL
```

COMPONENT	WT %	MOLES
SO3	0.0	0.0
NA	0.0	0.0
NA2O	0.0	0.0
K	0.0	0.0
K2O	0.03	0.32
MGO	1.31	32.50
CAO	0.03	0.53
SIO2	1.14	18.97
FE2O3	0.12	0.75
AL2O3	0.25	2.45
CL	0.0	0.0
SUBTOTAL	2.88 %	
MEASURED =	4.56	

```
HOLE #    8                        HOLE #    8
DEPTH =    2366.3  FEET            DEPTH =    2366.3  FEET

SOLUBLE                            INSOLUBLE
31.37 WT % OF TOTAL               68.63 WT % OF TOTAL
```

COMPONENT	WT %	MOLES	WT %	MOLES
SO3	16.19	202.22	31.13	388.83
NA	0.62	26.97	0.0	0.0
NA2O	0.0	0.0	3.76	60.66
K	0.0	0.0	0.0	0.0
K2O	7.47	79.30	3.19	33.86
MGO	2.77	68.72	3.63	90.05
CAO	0.16	2.85	3.21	57.24
SIO2	0.01	0.17	10.67	177.57
FE2O3	0.0	0.0	0.01	0.06
AL2O3	0.0	0.0	1.57	15.40
CL	1.17	33.00	0.0	0.0
SUBTOTAL	28.39 %		57.17 %	
MEASURED =	31.37		68.63	

HOLE # 8
DEPTH = 2427.5 FEET

	SOLUBLE 99.36 WT % OF TOTAL		INSOLUBLE 0.64 WT % OF TOTAL	
COMPONENT	WT %	MOLES	WT %	MOLES
SO3	2.22	27.73	0.36	4.50
NA	39.42	1714.66	0.0	0.0
NA2O	0.0	0.0	0.0	0.0
K	0.01	0.26	0.0	0.0
K2O	0.0	0.0	0.01	0.11
MGO	0.01	0.25	0.04	0.99
CAO	0.31	5.53	0.04	0.71
SIO2	0.0	0.0	0.09	1.50
FE2O3	0.0	0.0	0.01	0.06
AL2O3	0.0	0.0	0.01	0.10
CL	59.88	1689.14	0.0	0.0
SUBTOTAL	101.85 %		0.56 %	
MEASURED =	99.36		0.64	

	HOLE # 8 DEPTH = 2460.0 FEET		HOLE # 8 DEPTH = 2460.0 FEET	
	SOLUBLE 99.21 WT % OF TOTAL		INSOLUBLE 0.79 WT % OF TOTAL	
COMPONENT	WT %	MOLES	WT %	MOLES
SO3	1.14	14.24	0.0	0.0
NA	38.75	1685.52	0.0	0.0
NA2O	0.0	0.0	0.0	0.0
K	0.03	0.77	0.0	0.0
K2O	0.0	0.0	0.01	0.11
MGO	0.03	0.74	0.17	4.22
CAO	0.62	11.06	0.0	0.0
SIO2	0.0	0.0	0.19	3.16
FE2O3	0.0	0.0	0.03	0.19
AL2O3	0.0	0.0	0.06	0.59
CL	57.00	1607.90	0.0	0.0
SUBTOTAL	97.57 %		0.46 %	
MEASURED =	99.21		0.79	

HOLE # 8
DEPTH = 2519.6 FEET
TOTAL

COMPONENT	WT %	MOLES
SO3	0.17	2.12
NA	40.42	1758.16
NA2O	0.0	0.0
K	0.02	0.51
K2O	0.0	0.0
MGO	0.01	0.25
CAO	0.03	0.53
SIO2	0.0	0.0
FE2O3	0.0	0.0
AL2O3	0.0	0.0
CL	60.31	1701.27

```
HOLE #      8
DEPTH =       2563.0  FEET

SOLUBLE
     7.11  WT % OF TOTAL
```

COMPONENT	WT %	MOLES
SO3	1.49	18.61
NA	1.47	63.94
NA20	0.0	0.0
K	0.05	1.28
K20	0.0	0.0
MGO	0.07	1.74
CAO	0.60	10.70
SIO2	0.0	0.0
FE2O3	0.0	0.0
AL2O3	0.0	0.0
CL	1.05	29.62
SUBTOTAL	4.73 %	
MEASURED =	7.11	

```
HOLE #      8
DEPTH =       2563.0  FEET

INSOLUBLE
     92.89  WT % OF TOTAL
```

	WT %	MOLES
	39.10	488.38
	0.0	0.0
	6.06	97.77
	0.0	0.0
	0.54	5.73
	14.66	363.68
	23.77	423.86
	6.25	104.01
	0.96	6.01
	1.86	18.24
	0.0	0.0
	93.20 %	
	92.89	

HOLE # 8
DEPTH = 2615.5 FEET
TOTAL

COMPONENT	WT %	MOLES
SO3	0.86	10.74
NA	38.58	1678.12
NA2O	0.0	0.0
K	0.05	1.28
K2O	0.0	0.0
MGO	0.02	0.50
CAO	0.58	10.34
SIO2	0.0	0.0
FE2O3	0.01	0.06
AL2O3	0.0	0.0
CL	59.37	1674.75
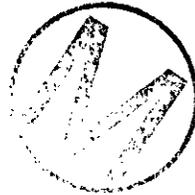
	HOLE # 8 DEPTH = 2665.5 FEET		HOLE # 8 DEPTH = 2665.5 FEET	
	SOLUBLE 99.08 WT % OF TOTAL		INSOLUBLE 0.92 WT % OF TOTAL	
COMPONENT	WT %	MOLES	WT %	MOLES
SO3	0.98	12.24	0.0	0.0
NA	38.68	1682.47	0.0	0.0
NA2O	0.0	0.0	0.0	0.0
K	0.02	0.51	0.0	0.0
K2O	0.0	0.0	0.01	0.11
MGO	0.01	0.25	0.21	5.21
CAO	0.35	6.24	0.01	0.18
SIO2	0.01	0.17	0.22	3.66
FE2O3	0.0	0.0	0.04	0.25
AL2O3	0.0	0.0	0.06	0.59
CL	59.14	1668.27	0.0	0.0
SUBTOTAL	99.19 %		0.55 %	
MEASURED =	99.08		0.92	

```
HOLE #   8
DEPTH =   2706.0  FEET              HOLE #   8
                                    DEPTH =   2706.0  FEET
SOLUBLE
98.75 WT % OF TOTAL                 INSOLUBLE
                                    1.25 WT % OF TOTAL
```

COMPONENT	WT %	MOLES	WT %	MOLES
SO3	1.12	13.99	0.01	0.12
NA	37.09	1613.31	0.0	0.0
NA2O	0.0	0.0	0.64	10.33
K	0.03	0.77	0.0	0.0
K2O	0.0	0.0	0.03	0.32
MGO	0.01	0.25	0.18	4.47
CAO	0.68	12.13	0.0	0.0
SIO2	0.01	0.17	0.27	4.49
FE2O3	0.0	0.0	0.27	1.69
AL2O3	0.0	0.0	0.07	0.69
CL	58.60	1653.03	0.0	0.0

```
SUBTOTAL    97.54 %                 1.47 %

MEASURED =  98.75                   1.25
```
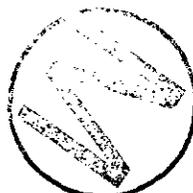
HOLE # 8
DEPTH = 2758.0 FEET

SOLUBLE
99.22 WT % OF TOTAL

COMPONENT	WT %	MOLES
SO3	1.70	21.23
NA	37.20	1618.10
NA2O	0.0	0.0
K	0.08	2.05
K2O	0.0	0.0
MGO	0.01	0.25
CAO	1.14	20.33
SIO2	0.0	0.0
FE2O3	0.0	0.0
AL2O3	0.0	0.0
CL	58.07	1638.08
SUBTOTAL	98.20 %	
MEASURED =	99.22	

HOLE # 8
DEPTH = 2758.0 FEET

INSOLUBLE
0.78 WT % OF TOTAL

WT %	MOLES
0.0	0.0
0.0	0.0
0.83	13.39
0.0	0.0
0.01	0.11
0.17	4.22
0.0	0.0
0.06	1.00
0.01	0.06
0.02	0.20
0.0	0.0
1.10 %	
0.78	
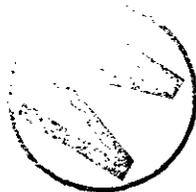
HOLE # 8
DEPTH = 2779.0 FEET
TOTAL

COMPONENT	WT %	MOLES
SO3	1.09	13.61
NA	37.41	1627.23
NA2O	0.0	0.0
K	0.01	0.26
K2O	0.0	0.0
MGO	0.03	0.74
CAO	1.80	32.10
SIO2	0.0	0.0
FE2O3	0.0	0.0
AL2O3	0.0	0.0
CL	58.53	1651.06

```
HOLE #     8
DEPTH =     2794.0  FEET
TOTAL
```

COMPONENT	WT %	MOLES
SO3	0.99	12.37
NA	37.86	1646.80
NA2O	0.0	0.0
K	0.02	0.51
K2O	0.0	0.0
MGO	0.01	0.25
CAO	0.68	12.13
SIO2	0.0	0.0
FE2O3	0.0	0.0
AL2O3	0.0	0.0
CL	60.58	1708.89

HOLE # 8
DEPTH = 2802.5 FEET
TOTAL

COMPONENT	WT %	MOLES
SO3	1.76	21.98
NA	38.39	1669.86
NA2O	0.0	0.0
K	0.02	0.51
K2O	0.0	0.0
MGO	0.01	0.25
CAO	0.22	3.92
SIO2	0.0	0.0
FE2O3	0.0	0.0
AL2O3	0.0	0.0
CL	58.19	1641.47

	HOLE # 8 DEPTH = 2809.0 FEET SOLUBLE 99.09 WT % OF TOTAL		HOLE # 8 DEPTH = 2809.0 FEET INSOLUBLE 0.91 WT % OF TOTAL	
COMPONENT	WT %	MOLES	WT %	MOLES
SO3	2.02	25.23	0.0	0.0
NA	38.56	1677.25	0.0	0.0
NA2O	0.0	0.0	0.0	0.0
K	0.01	0.26	0.0	0.0
K2O	0.0	0.0	0.01	0.11
MGO	0.01	0.25	0.03	0.74
CAO	0.96	17.12	0.13	2.32
SIO2	0.0	0.0	0.04	0.67
FE2O3	0.0	0.0	0.0	0.0
AL2O3	0.0	0.0	0.01	0.10
CL	59.70	1684.06	0.0	0.0
SUBTOTAL	101.26 %		0.22 %	
MEASURED =	99.09		0.91	

HOLE # 8
DEPTH = 2820.5 FEET

SOLUBLE
99.46 WT % OF TOTAL

COMPONENT	WT %	MOLES
SO3	1.30	16.24
NA	38.42	1671.16
NA2O	0.0	0.0
K	0.01	0.26
K2O	0.0	0.0
MGO	0.01	0.25
CAO	0.10	1.78
SIO2	0.03	0.50
FE2O3	0.0	0.0
AL2O3	0.0	0.0
CL	58.50	1650.21
SUBTOTAL	98.37 %	
MEASURED =	99.46	

INSOLUBLE
0.54 WT % OF TOTAL

WT %	MOLES
0.37	4.62
0.0	0.0
0.0	0.0
0.0	0.0
0.0	0.0
0.01	0.25
0.19	3.39
0.03	0.50
0.0	0.0
0.0	0.0
0.0	0.0
0.60 %	
0.54	

```
HOLE #    8                              HOLE #    8
DEPTH =    2879.0  FEET                   DEPTH =    2879.0  FEET

SOLUBLE                                   INSOLUBLE
   96.41 WT % OF TOTAL                      3.59 WT % OF TOTAL

COMPONENT    WT %        MOLES          WT %          MOLES

   SO3       2.17        27.10          1.97          24.61

   NA       32.65      1420.18          0.0           0.0

   NA2O      0.0         0.0            0.93          15.00

   K         0.02        0.51          0.0           0.0

   K2O       0.0         0.0            0.01          0.11

   MGO       0.01        0.25          0.12          2.98

   CAO       0.59        10.52          0.95          16.94

   SIO2      0.02        0.33          0.12          2.00

   FE2O3     0.0         0.0            0.01          0.06

   AL2O3     0.0         0.0            0.01          0.10

   CL       55.79      1573.77          0.0           0.0

SUBTOTAL    91.25   %                   4.12   %

MEASURED =  96.41                       3.59
```

HOLE # 8
DEPTH = 2948.0 FEET

SOLUBLE
97.32 WT % OF TOTAL

COMPONENT	WT %	MOLES
SO3	3.41	42.59
NA	37.30	1622.45
NA2O	0.0	0.0
K	0.01	0.26
K2O	0.0	0.0
MGO	0.01	0.25
CAO	0.54	9.63
SIO2	0.01	0.17
FE2O3	0.0	0.0
AL2O3	0.0	0.0
CL	55.51	1565.87

SUBTOTAL   96.79 %

MEASURED =   97.32

HOLE # 8
DEPTH = 2948.0 FEET

INSOLUBLE
2.68 WT % OF TOTAL

WT %	MOLES
1.92	23.98
0.0	0.0
0.0	0.0
0.0	0.0
0.01	0.11
0.02	0.50
0.25	4.46
0.05	0.83
0.01	0.06
0.0	0.0
0.0	0.0

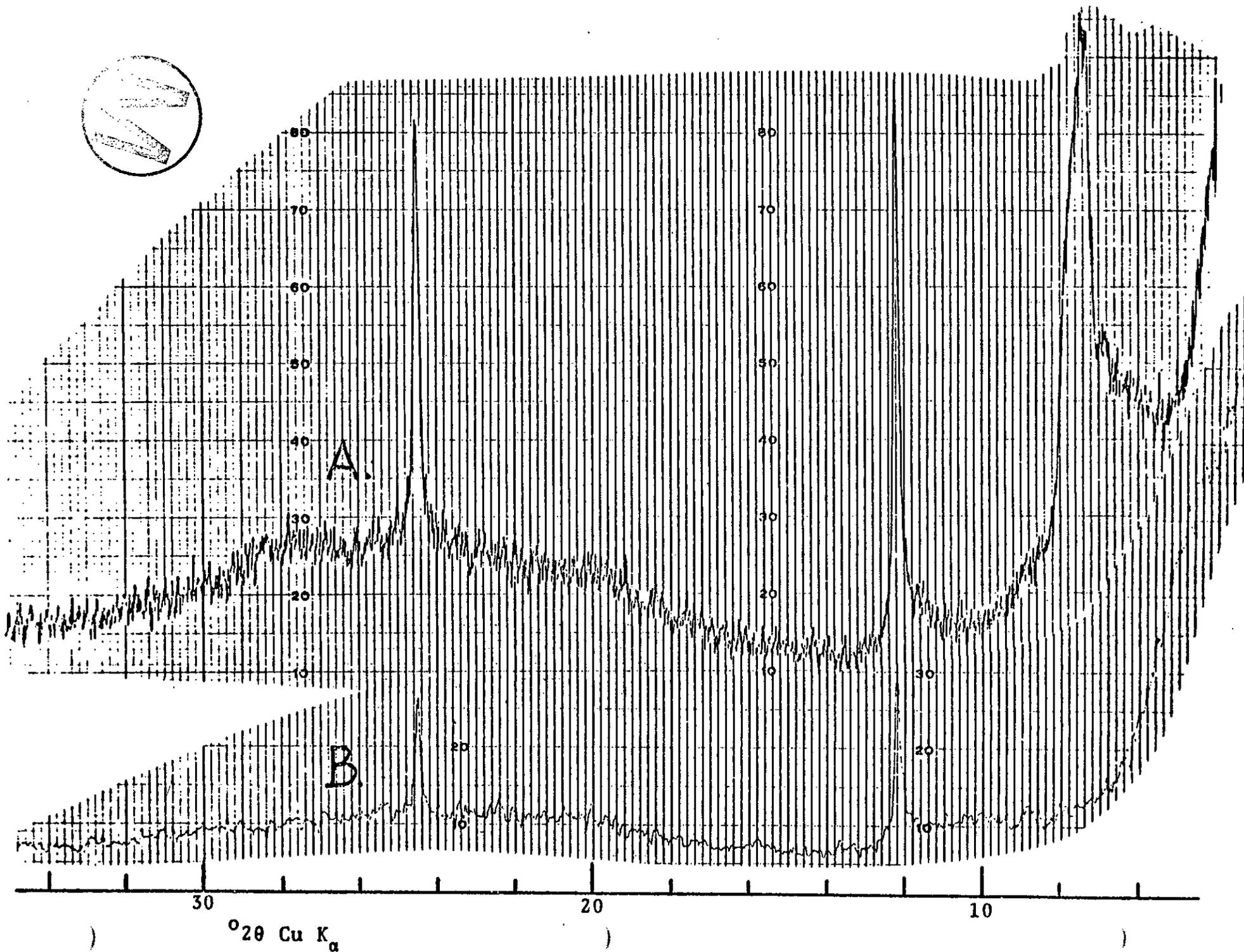2.26 %

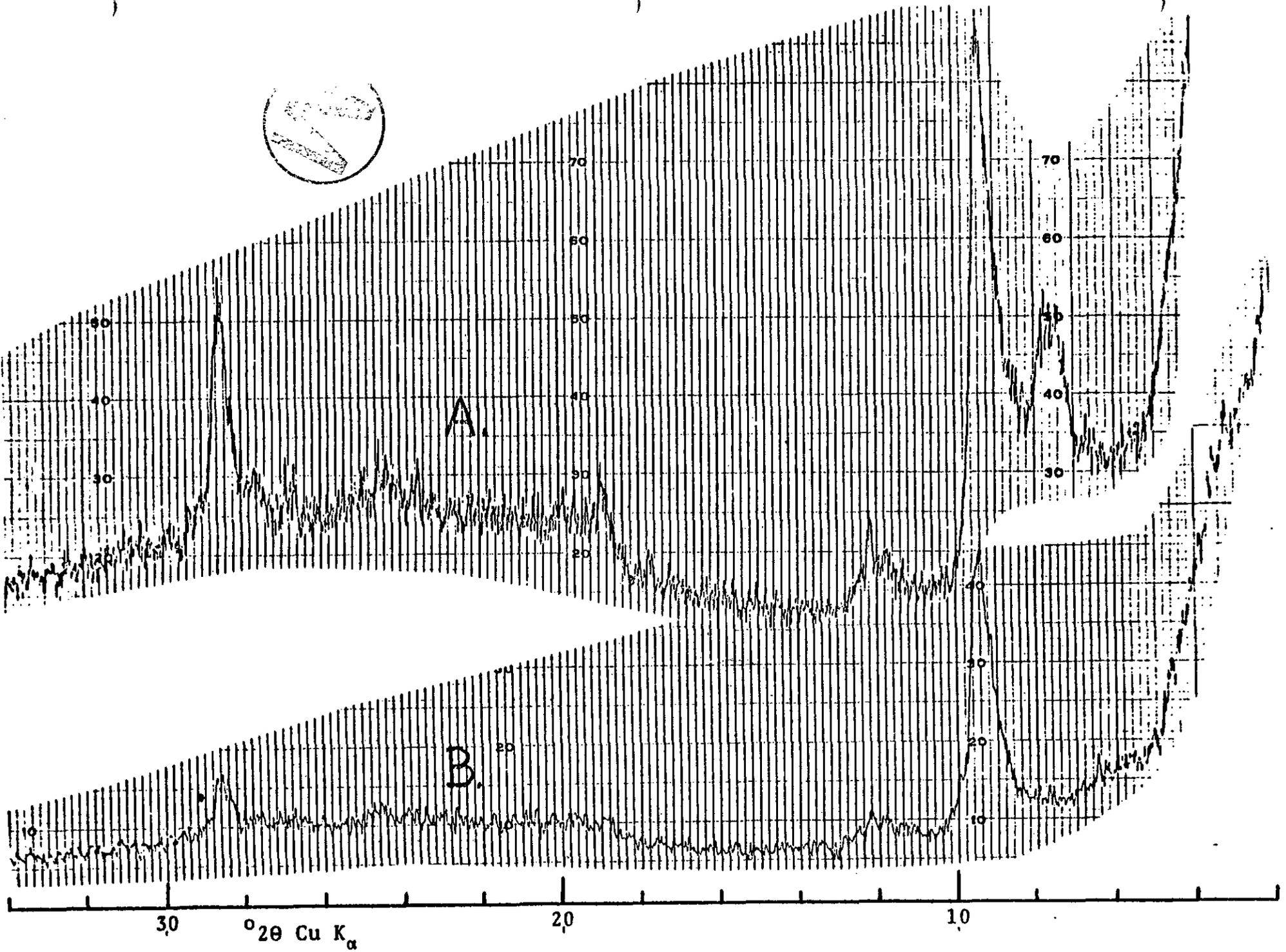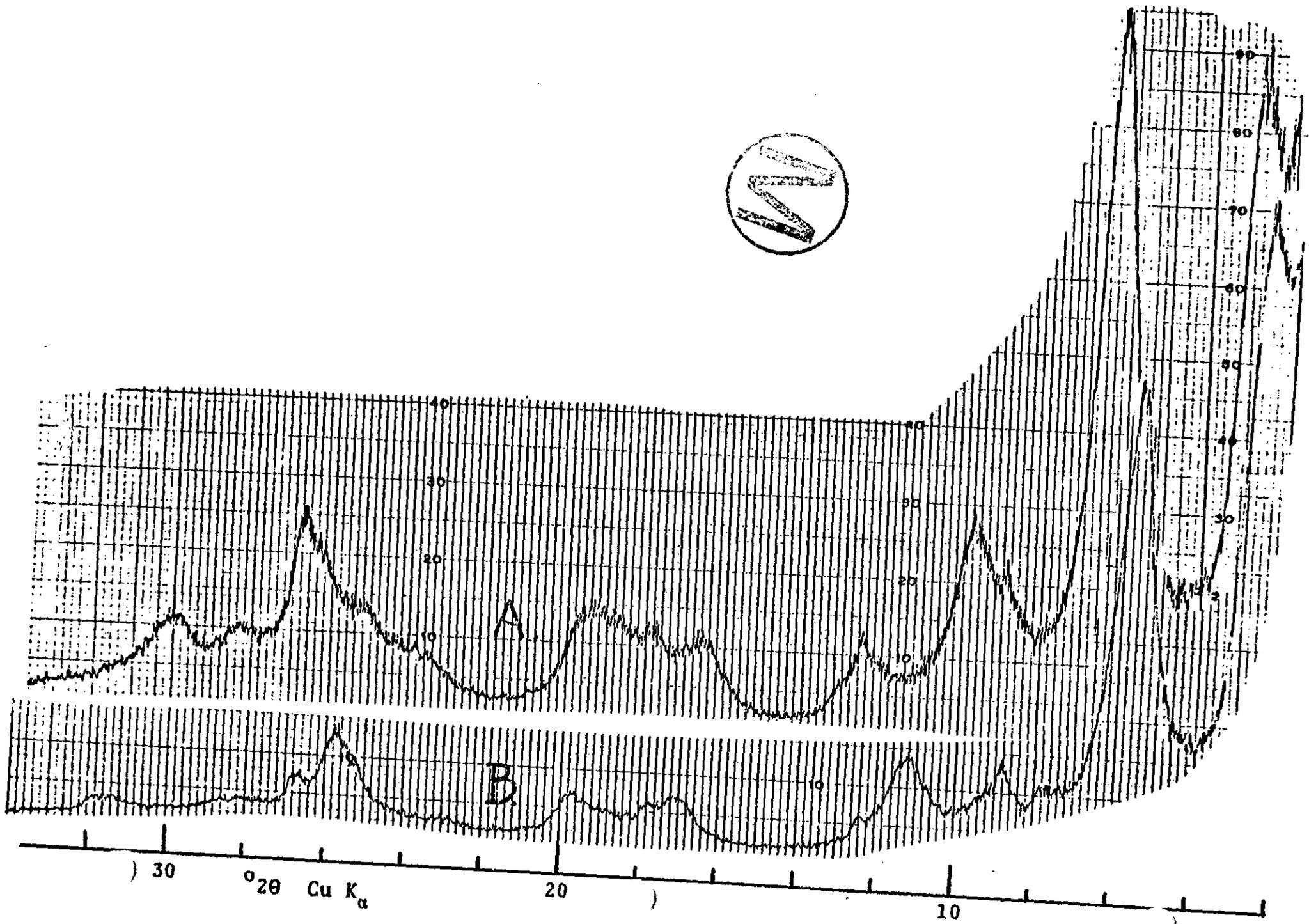2.68
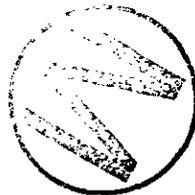
Selected x-ray diffraction traces of EDTA-insoluble residues from the ERDA-9 core.
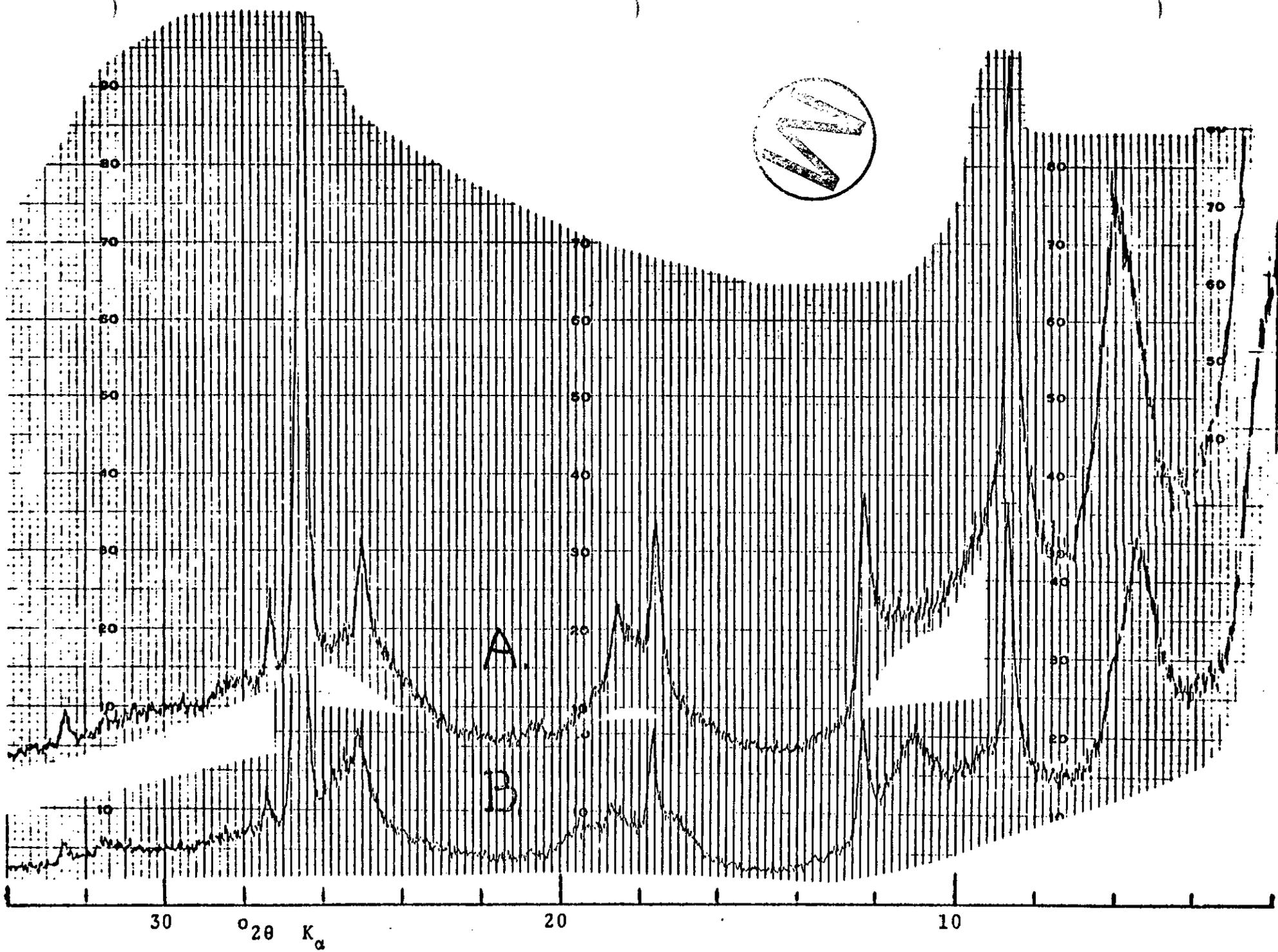
I-2. MB-CS-42: Serpentine and saponite; the sharp maxima at 12.2 and 24.5°2θ are basal spacings of serpentine's 7Å periodicity. The broad peak at 7.25°2θ (air-dried) becomes a broad weak shoulder at ~5°2θ upon glycol saturation and is saponite.

   A. <2µm EDTA-insoluble residue, air-dried.
   B. Bulk EDTA-insoluble residue, glycol-saturated.

I-3. MB-CS-15: Talc and smectite (saponite); sharp peaks at 9.5 and 28.5°2θ are basal spacings of talc's 9.5Å periodicity; they do not shift with glycol-saturation. The broad low-angle peak again is saponite; accessory amounts of serpentine also present.

   A. <2µm EDTA-insoluble residue, air-dried.
   B. Bulk EDTA-insoluble residue, glycol-saturated.

I-4. MB-CS-17: Regularly interstratified mixed-layer chlorite-saponite (corrensite); distinct strong superlattice reflection at 2.9°2θ (air-dried) which expands to 2.7°2θ with glycol-saturation. The peak at 6.4°2θ (air-dried) expands to 5.6°2θ.

   A. <2µm EDTA-insoluble residue, air-dried.
   B. <2µm EDTA-insoluble residue, glycol-saturated.

I-5. JL-CS-9: Randomly interstratified mixed-layer chlorite-saponite; air-dried peak at 6.1°2θ expands to 5.5°2θ with glycol saturation. Illite (8.7, 17.6, and 26.6°2θ), minor serpentine (12.3 and 13.1°2θ), and minor feldspar (27.4°2θ) also present.

   A. <2µm EDTA-insoluble residue, air-dried.
   B. <2µm EDTA-insoluble residue, glycol-saturated.

I-6. MB-CS-13: Saponite; reflections at 6.1 and 27.3°2θ which expand to 5.2° 2θ upon glycol saturation. A small quantity of a regularly interstratified mixed-layer clay (small superlattice peak at 2.4°2θ) also present.

   A. <2µm EDTA-insoluble residue, air-dried.
   B. <2µm EDTA-insoluble residue, glycol saturated.

I-7. JL-CS-2: Randomly interstratified mixed-layer clay, either talc-saponite or illite-saponite; single strong maximum at 8.6°2θ becomes pronounced doublet at 9.6 and 7.6°2θ with glycol saturation.

   A. <2µm EDTA-insoluble residue, air-dried.
   B. <2µm EDTA-insoluble residue, glycol-saturated.

A

B

$^{o}2\theta$ Cu K$_\alpha$

30   20   10

A.

B.

$^{\circ}2\theta$ Cu K$_\alpha$

30 20 10

30) $^{o}2\theta$ Cu K_{α} 20)   10)

A

B

$^{o}2\theta$ K$_{\alpha}$

30   20   10
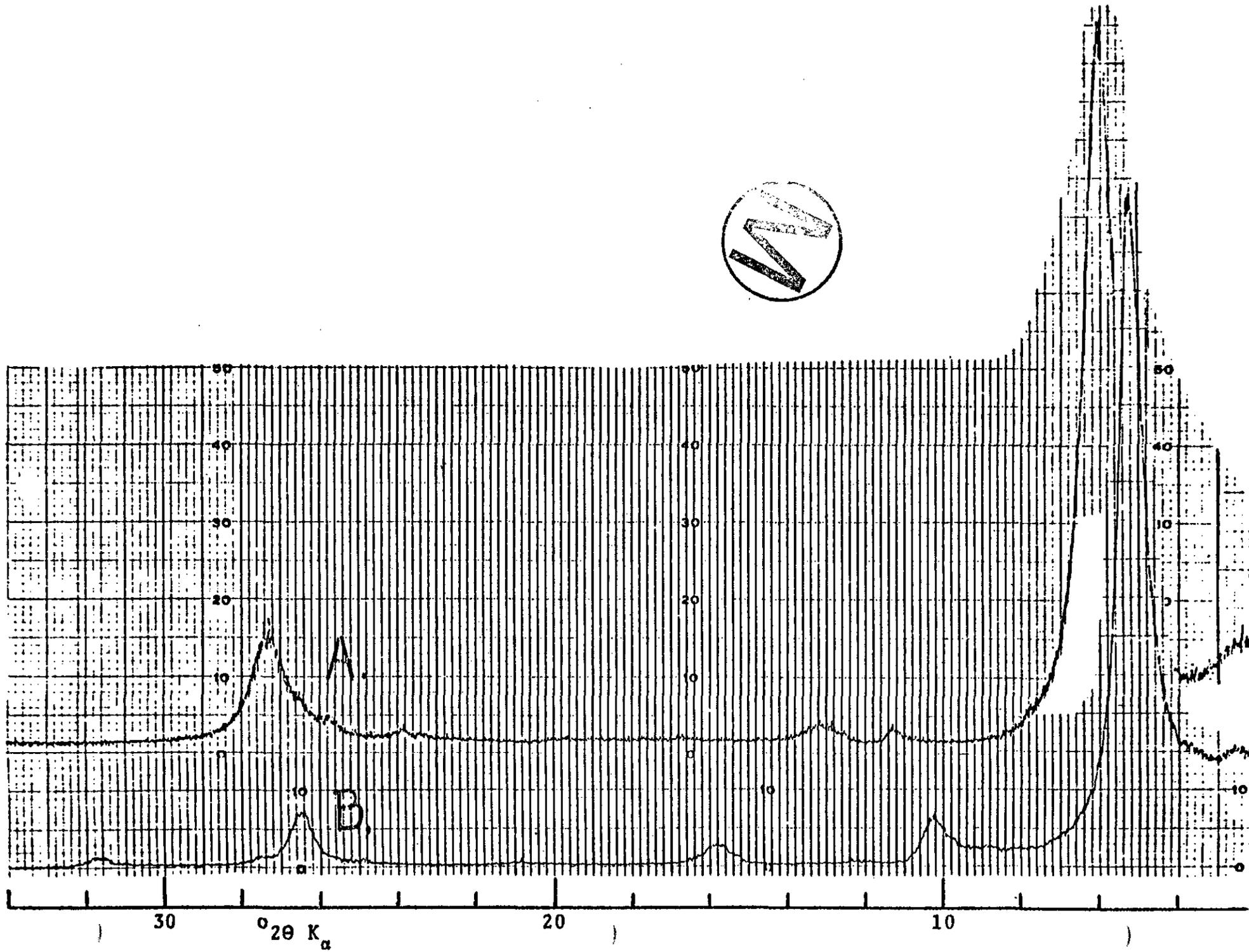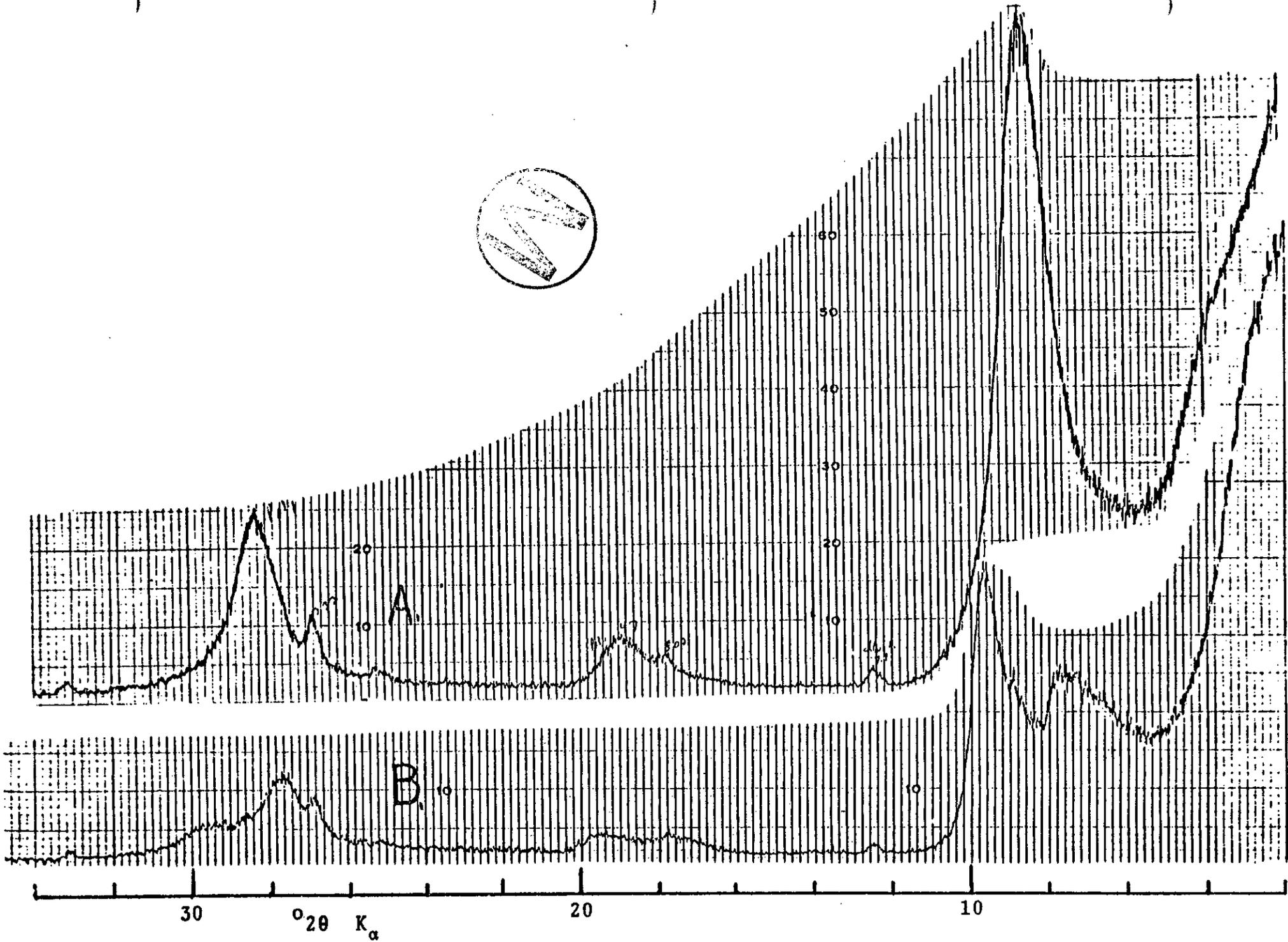
Core Footage (Sandia Core Photo #), Informal Lithology and Detailed Macroscopic Core Description

FI in left column indicates abundant fluid inclusions.

† just to left of right column indicates description incorporates stratigraphic variation within that interval.

Abbreviations and Meanings used in Core Description (right column)

anhy or anhyd	anhydrite
ave	average
brwn	brown
dom	dominant
fg	fine grained or finely crystalline
inc	increasing
irreg	irregular
L	length
lams	laminae or laminations
lite or lt	light
loc	local or locally
max	maximum
repl	replacement
struc	structure
thk	thick or thickness
W	Width
w/	with
Xtals or Xtalline	crystals or crystalline
µX	microcrystalline

Core Footage (Sandia Photo #)	Informal Lithology	Macroscopic (aided by binocular microscope) Core Description
1162.7 (27) 1163.7	Halite	lite brwn, clear, anhedral Xtals (1cm), sharp Xtal boundaries of halite minor 1-4mm thk, lenses of lite gray, µX, anhydrite rimmed with polyhalite
1165.2 (28) 1166.6	Anhydrite w/ halite "crystal growth"	dominantly gray, µX anhydrite w/ slight color banding (gray-lite gray) with: lenses (1/2 to 1 cm thk.) of brown, clear to opaque, poorly defined anhedral Xtals, of halite layers (1 to 4 cm thk) of vertically elongate (L/W=2 to 3, L=2mm to 3 1/2 cm), locally swallow-tail, Xtals of halite
1167.3 (28) 1168	Banded Anhydrite	banding of dominantly gray, µX anhydrite laminae (5-10mm thk) with white, thin (<1mm) laminae of µX magnesite locally a few anhedral (some swallow tail) Xtals of halite, locally vertically elongate or radiating
1168 (29) 1168.25	Anhydrite	similar to 1165.2 - 1166.6 but including laminae (~1mm thick) of magnesite
1168.25 (29) 1169.9	brick-red Polyhalite and Halite	dominantly anhedral (rare euhedral) 1/2 cm Xtals of halite, clear to cloudy with red, µX polyhalite between and in halite crystals
1172.6 (30) 1173.5	Banded Polyhalite	prominant banding but mineralogy obscure - "brown mineral" typically opaque, microcrystalline or massive halite, orange to orange brown poorly bounded anhedra -1/2 cm - silty claystone or anhydrite? locally contorted banding

Core Footage (Sandia Photo #)	Informal Lithology	Macroscopic (aided by binocular microscope) Core Description
1173.5 (31) 1174.7	Halite	halite - clear to red, anhedral Xtals (ave 1/2 cm, max 2 cm) red from polyhalite stain; minor anhydrite
1404.7 (103) 1405.7	11th ore zone (leonite, kainite?)	polyhalite (± halite?) white & cloudy to blood red, massive w/ irreg. patches of dark gray claystone and irreg patches of pale yellow mineral (kainite-leonite?) massive patches are both vertically and horizontally elongate
1418 (106-107) 1418.8	Marker Bed 117, polyhalite plus mud	dominantly massive red polyhalite (w/ microscopic granular texture) laminations 1/2 to 1 1/2 cm thk alternating w/ clay laminae (<2mm thk) which are black & wavy [near 1418 - claystone w/ poor horizontal fissility plus "brown mineral" which looks like halite but has bitter taste]
1584 (160) 1584.9	5th ore zone, very dirty	dominantly halite - clear anhedra ~1 cm (max 2 cm) locally stained by "brown mineral" µXtalline coatings & locally patches a few mm in size; minor patches of gray µX anhydrite
1609.1 (168) 1610.3	Clear Halite (~2 ft above polyhalite)	dominantly halite - brwn (due to polyhalite stain?) indistinct anhedral about 1 1/2 cm; minor evenly dispersed polyhalite stain, and patches (~2mm) of gray material (anhydrite or clay?)
1632 (175) 1632.8	Mudstone	near top: banded anhydrite - claystone; anhydrite dark gray, µX - laminae up to 2mm thk, locally vertically elongate masses or Xtals; claystone lite grey, laminae from 1/2mm to 1/2 cm (thk inc. upward) near base: polyhalite w/ gray clay

)   )   )

Core Footage (Sandia Photo #)	Informal Lithology	Macroscopic (aided by binocular microscope) Core Description
1648.5 (180-181) 1649.7	4th ore zone halite, bloedite, vanthoffite	dominantly halite - lite brown anhedra ~3/4 cm locally red, μXtal polyhalite as stain & repl. of halite - some lenses and Xtal coatings of gray μX anhydrite?
2034.3 2037.3	Halite	↑ dominantly halite: finely crystalline & clayey near top - coarsely crystalline & banded anhydrite &/or polyhalite near center - finely crystalline & banded ↑ w/ anhydrite near base
2065.2 2067.6	Halite	dominantly coarsely Xtalline (~2 cm) clear, anhedral halite w/ patches, lenses & stains of "brown material" (polyhalite, carnallite, glauberite?) loc w/ radiating acicular texture
2301.6 (384) 2302.7	lite colored Polyhalite	dominantly red, μX polyhalite - locally crinkly flakes & irreg. patches of white fg. material
2413.6 FI (418-419) 2415.7	pure & impure Polyhalite	↑ dominantly poorly thickly banded polyhalite w/ subequal lenses of anhydrite & halite polyhalite: pinkish brown to red, μX halite: med. to coarsely Xtal, usually anhedral but some euhedra, typically clear anhydrite: layers, lenses and interXtalline patches, ↑ gray, μX, locally brown
2512 (450) 2512.5	dirty Halite	dominantly halite-gray, clear to cloudy, anhedral, 1 cm Xtal; minor light gray anhydrite as interXtalline patches.
2515.6 (452+) 2519.2	typical massive Cowden Anhy.	↑ (halite above 2516.9) faintly banded gray, μX, anhydrite w/ wispy lenses of magnesite ↑ very minor halite

Core Footage (Sandia Photo #)		Informal Lithology	Macroscopic (aided by binocular microscope) Core Description
2527.7 (456+) 2529.2		typical laminated Cowden Anhy.	laminations of gray, µX, anhydrite - lam up to 1 1/2 cm (some needle like & loc radiating into magnesite) white, opaque µX magnesite lams, wavy, <1mm to 3mm thk
2538.5 (459) 2539.4		base of Cowden Anhy.	top: faintly banded (color) µX anhydrite, minor patches of halite ↑ dominantly coarsely Xtalline (~1 cm) clear, anhedral halite w/ lenses & interXtalline anhydrite base: similar to middle but halite Xtal size decreases to ~1mm
2541 (460) 2542.5		dirty halite just below Cowden	dominantly halite - gray, clear to cloudy, anhedral Xtals (ave 1 cm, <1mm to 3 cm) minor anhydrite (or magnesite?) - interXtalline patches (1 or 2 cm by 2mm)
2606.5 2608.8		Halite	dominantly halite - typically clear but some cloudy, white to gray anhedra typically ~1 cm but three 3 cm thk zones of ave size ~2mm which tend to be gray; minor anhydrite - interXtalline gray, µX
2614.7 2615.6		Halite	dom. halite - clear white euhedra & subhedra, most anhedra, ave 2 cm (<1mm to 4 cm); minor anhydrite - lt gray to white, µX, interXtalline
2615.9 FI 2619.5		Halite	↑ 15.9 - 16.5 dom halite - clear, white to gray, anhedra, ave 2 cm (1/2 - 6 cm) w/ v minor gray-white, µX, interXtalline anhyd or magnesite 16.5 - 18.4 dom halite - clear to cloudy, white to gray anhedra, ave 1 cm (<1mm - 2 cm) locally "chevron struc" within (& across) Xtals w/ minor gray-white, µX, interXtalline anhyd or magnesite ↑ 18.4 - 19.5 similar to 15.9 - 16.5

)   )   )

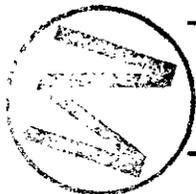| Core Footage (Sandia Photo #)	Informal Lithology	Macroscopic (aided by binocular microscope) Core Description
(2705.7) 2704.8 (509) (2706.8) 2706.5	mottled Anhy & Halite	dominantly halite - coarsely Xtalline (1 to 1 1/2 cm) anhedral, clear to white cloudy cut at ~45° by zones more finely Xtalline halite and mixed w/ up to 30% interXtalline gray, µX, anhydrite (w/ minor magnesite)
2758 (526) 2759.3	dirty Halite	dom halite - light to dk gray, anhedra, ave ~1 cm (<1mm to 3 cm) w/ minor anhydrite - dk gray, µX (but some microlites) as interXtall material
2819.1 (545) 2819.8	clean Halite, slightly banded	dom halite - cloudy, white to lt. gray, anhedral; faint banding by ave Xtal size variation from 1/2 to 1 cm, finer Xtalline tends to be whiter; minor thin horizontal lenses (rare patches), white, µX (rare microlites)
2819.9 (545) 2820.9A	see above	dom anhydrite - lt gray to dk gray (locally banded), µX; subordinate halite - irreg lenses & patches (frequently thin & horiz elongate) unusually sharp contacts between anhydrite & halite
2820 B (545-546) 2820.6B	see above	same as 19.9 - 20.9A except anhydrite locally brown and may contain magnesite
2820.6B (546) 2821.9	see above	dom halite - cloudy, white, anhedral, ave 1 cm (<1mm to 2 cm); very rare lense of wh to lt gray, µX anhydrite possibly w/ magnesite
2826.5 2827.5	dirty Halite	dom halite - poorly developed banding from clear, to cloudy white, to opaque dk gray, anhedral crystals ave 1/2 - 1 cm some magnesite (or anhydrite) - thin irreg seams & wavy lams (both horiz), white, µX

Core Footage (Sandia Photo #)	Informal Lithology	Macroscopic (aided by binocular microscope) Core Description
2845.6	massive light Anhydrite	dom anhydrite – mottled from clear to white & cloudy to gray to dk gray
2846.4	(in Castile)	sub. magnesite – thin seams and irreg patches, µX
2847.8	banded light	dom anhydrite – banded from clear, to white & cloudy, to gray to dk gray, to black; clear tends to occur
2849.1	Anhydrite	in laminae & lenses, locally "enterolithic" contortions and w/ smooth lower contacts & irreg "swallow-tail" upper contacts; subordinate magnesite

Appendix 7.E (Ref. sec. 7.5)

Gas Chromatograms and Mass Spectra
of Volatiles from Selected Samples
of Core from ERDA No. 9

Mass spectra are reported as intensity (normalized
to the highest mass peak) as a function of
mass/charge ratio (in atomic mass units).
Gas chromatograms are reported as intensity of
elution peaks (normalized to the highest elution peak)
as a function of relative elution time (in
arbitrary units).

SALT SAMPLE   2302.6
              TOTAL ION CHROMATOGRAM   X6
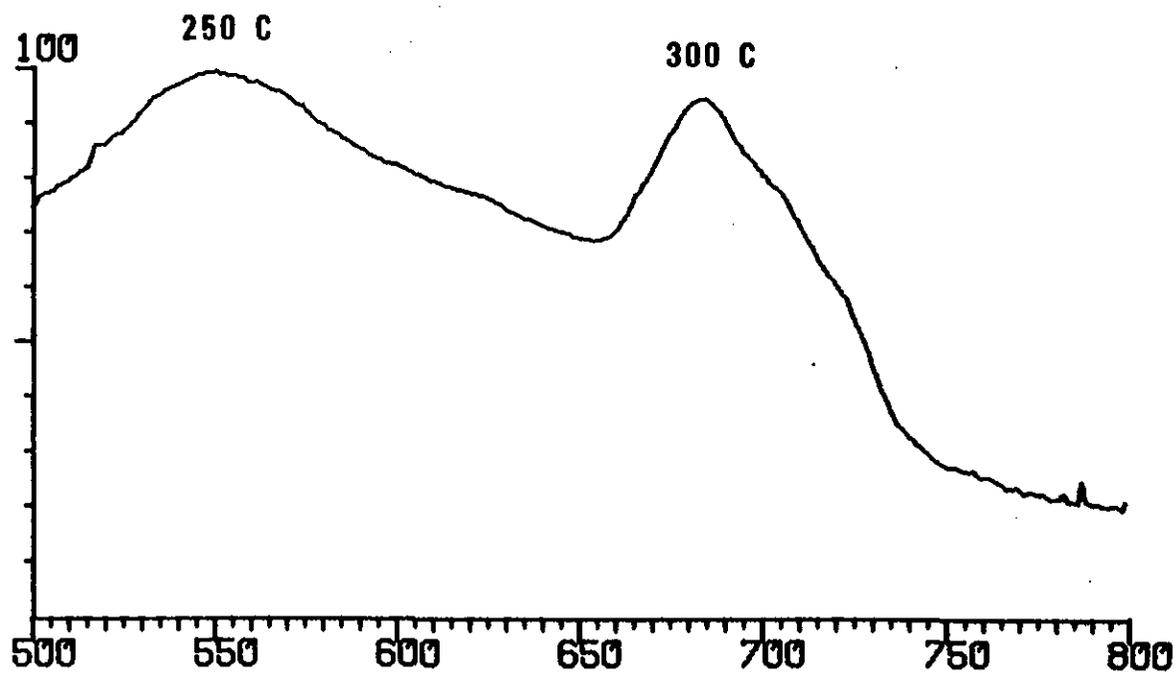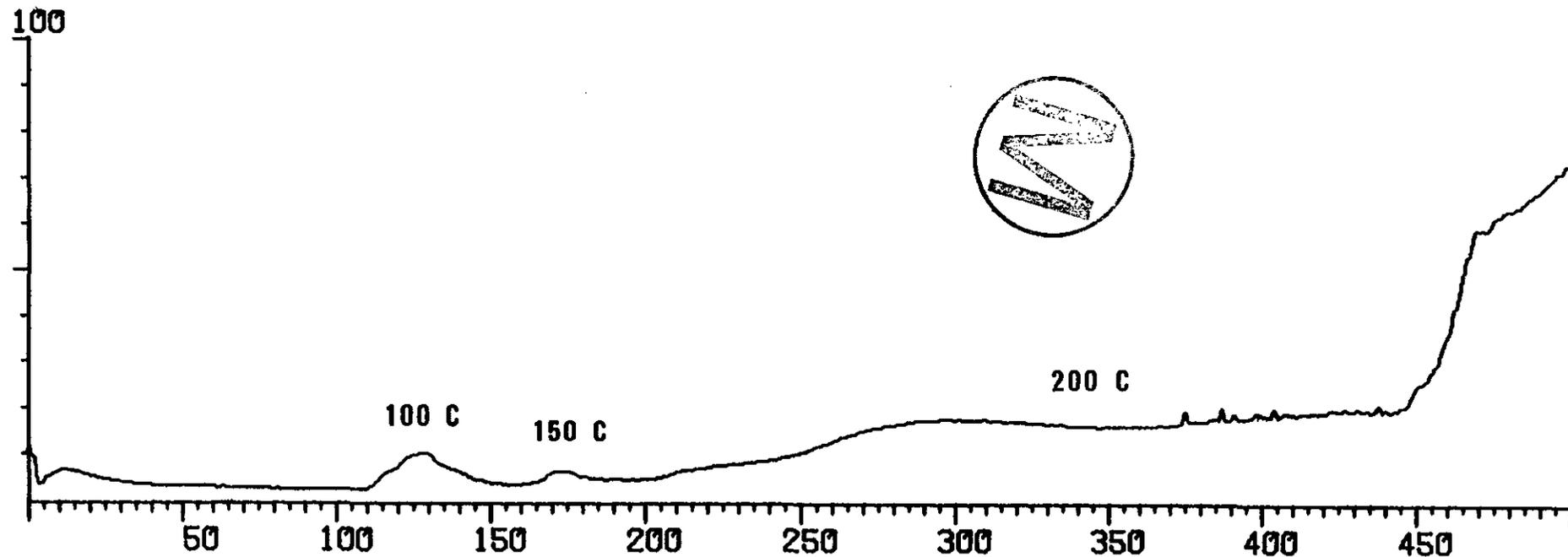
SALT SAMPLE   2302.6
12   MASS SPECTRA   50C X3

SALT SAMPLE   2302.6
128   MASS SPECTRA   100C X3
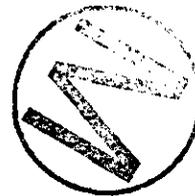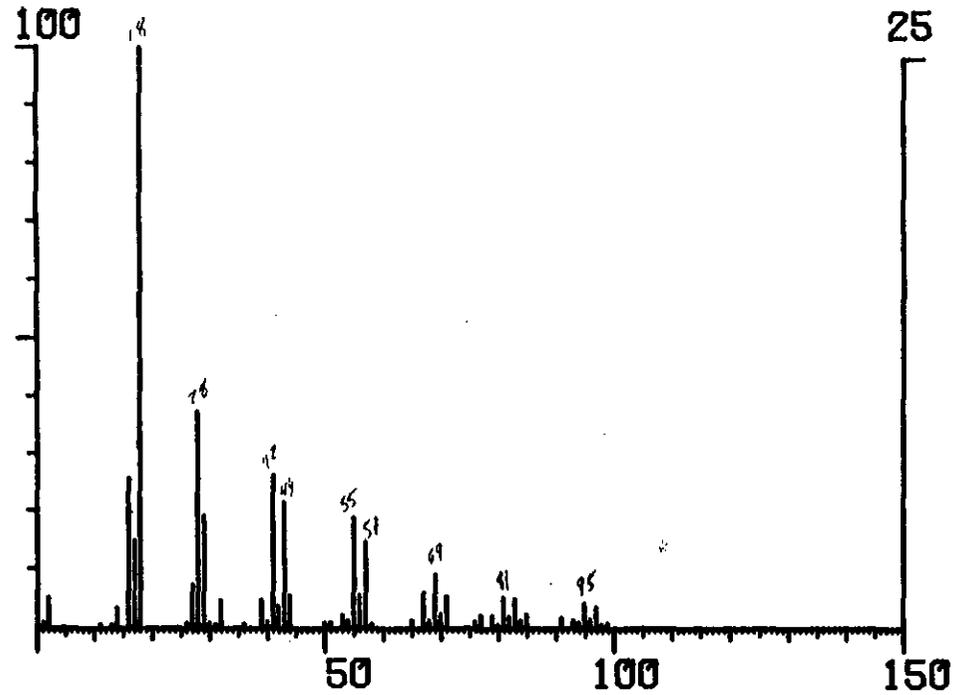
SALT SAMPLE   2302.6
174   MASS SPECTRA   150C X3
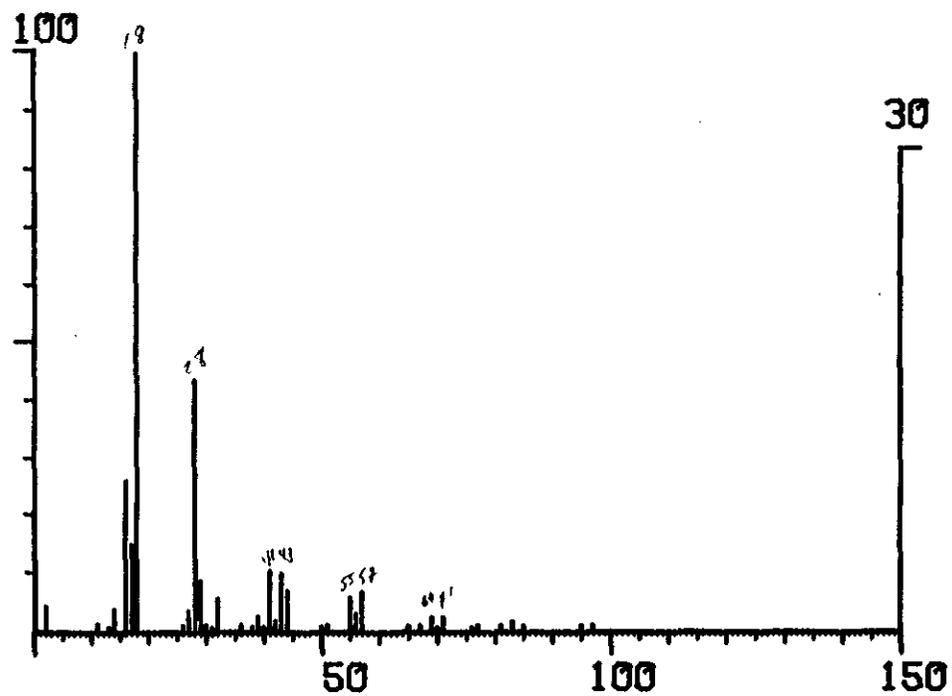
SALT SAMPLE   2302.6
297   MASS SPECTRA   200C X4

100   60

         50   100   150
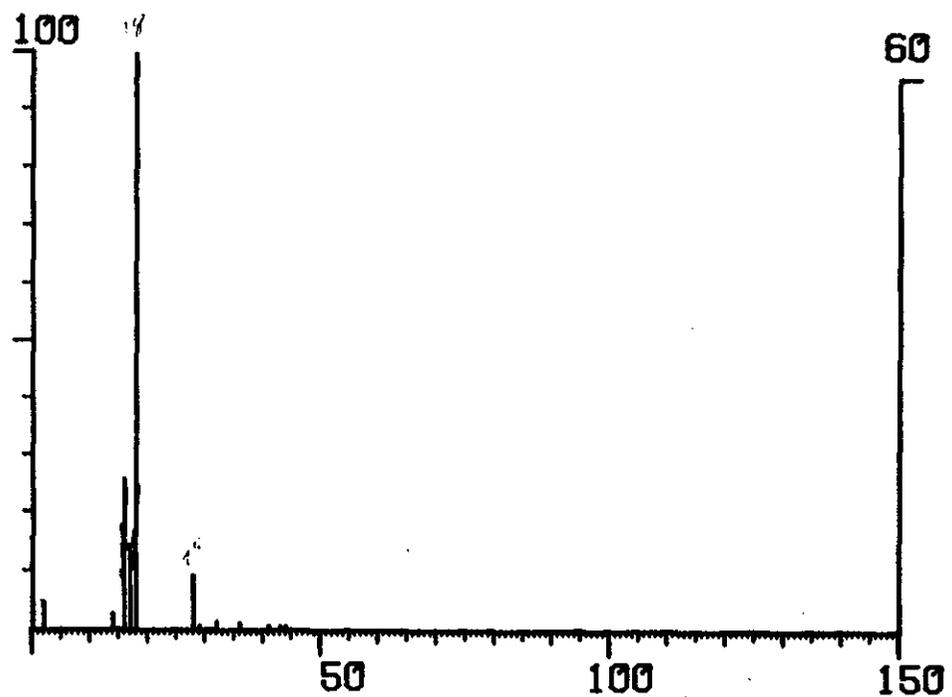
SALT SAMPLE   2302.6
550   MASS SPECTRA   250C X4

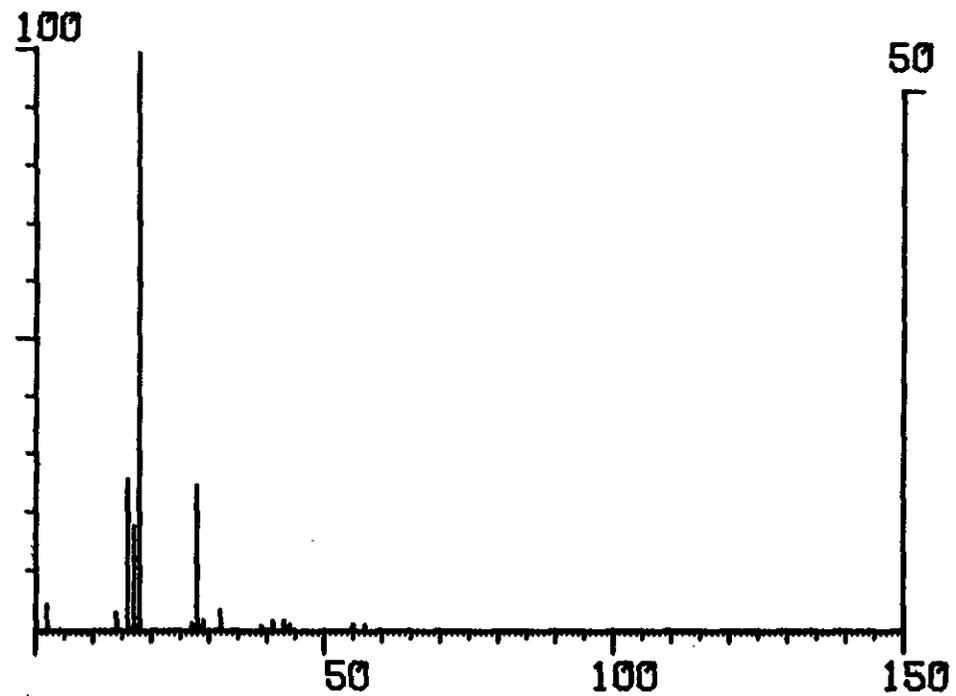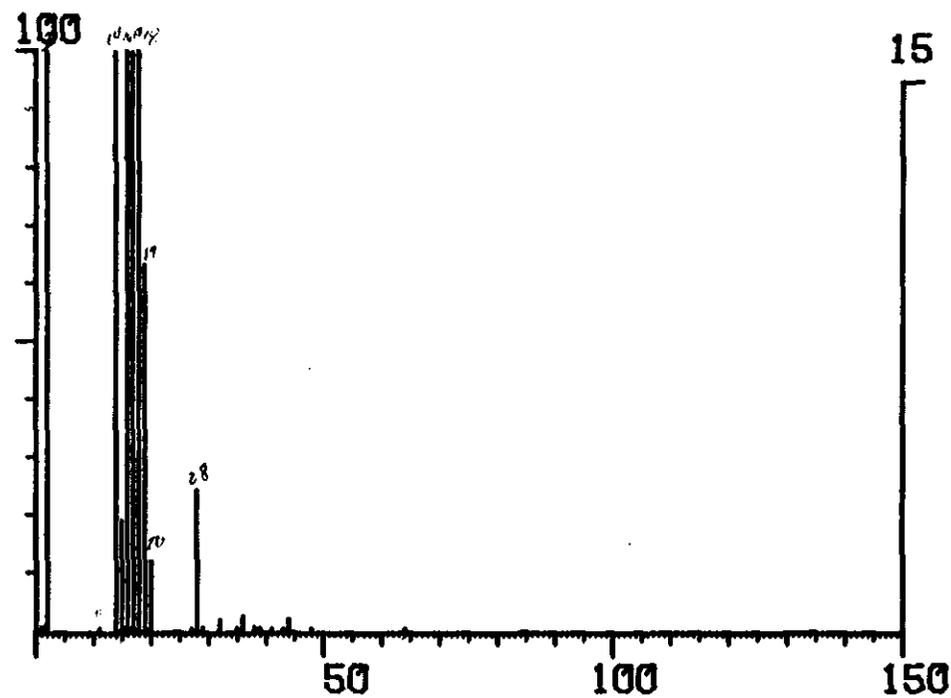SALT SAMPLE   2302.6
686   MASS SPECTRA   300C X4
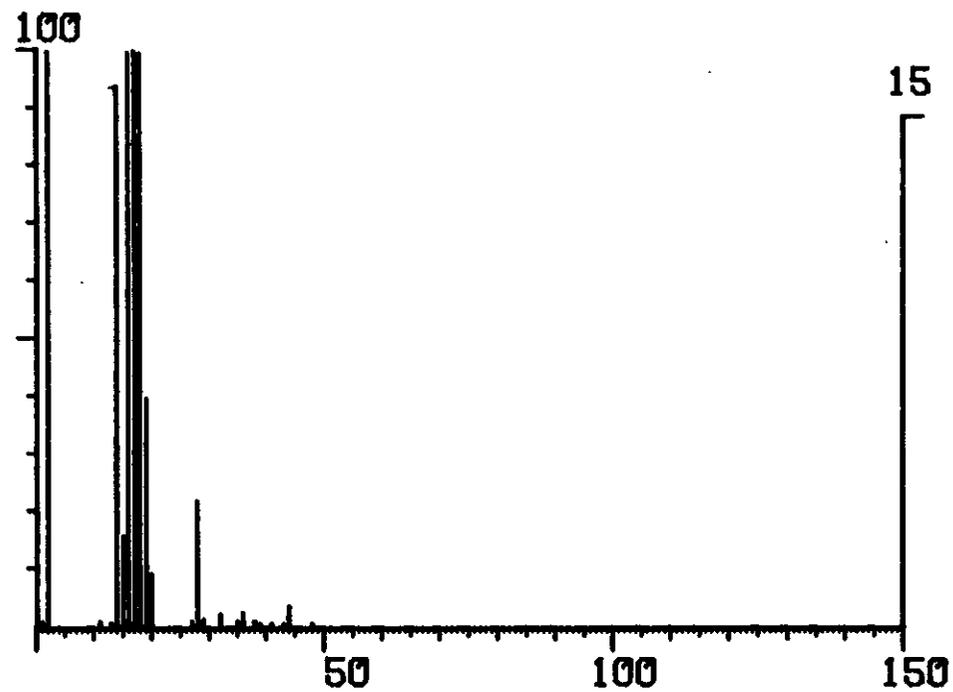
SALT SAMPLE   2302.6
        MASS 14 SEARCH X5
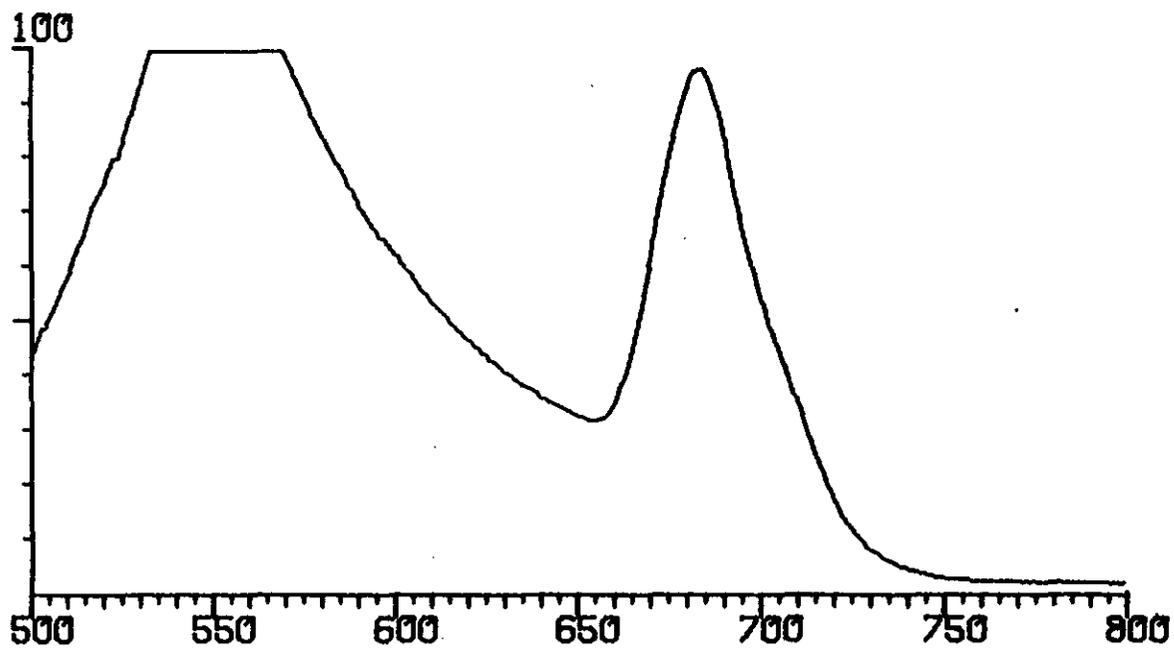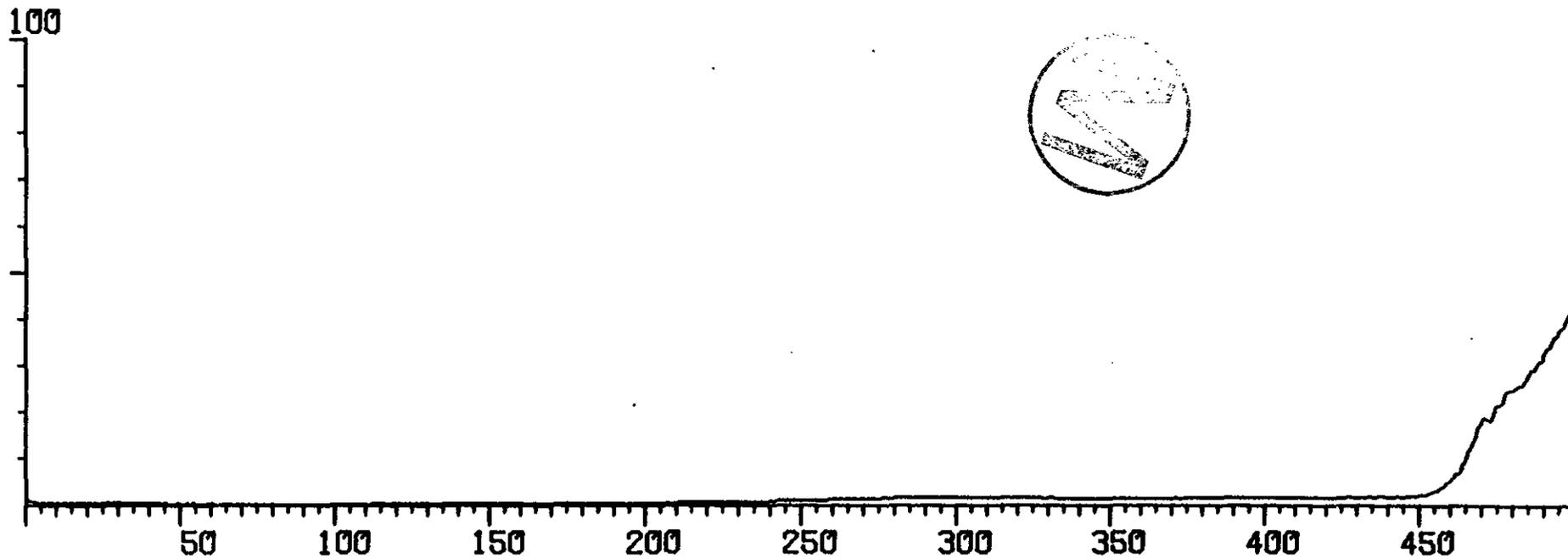
SALT SAMPLE

2302.6

MASS 18 SEARCH X4

SALT SAMPLE   2302.6
             MASS 19 SEARCH X4

SALT SAMPLE   2302.6
              MASS 20 SEARCH X3

SAL. SAMPLE   2302.8

MASS 32 SEARCH X2

100

50   100   150   200   250   300   350   400   450

100

500   550   600   650   700   750   800

SALT SAMPLE   2302.6
          MASS 36 SEARCH X2

SALT SAMPLE   2302.6
                MASS 44 SEARCH X2

SALT SAMPLE   2302.6
          MASS 48 SEARCH X1

100

         50   100   150   200   250   300   350   400   450

100

         500   550   600   650   700   750   800
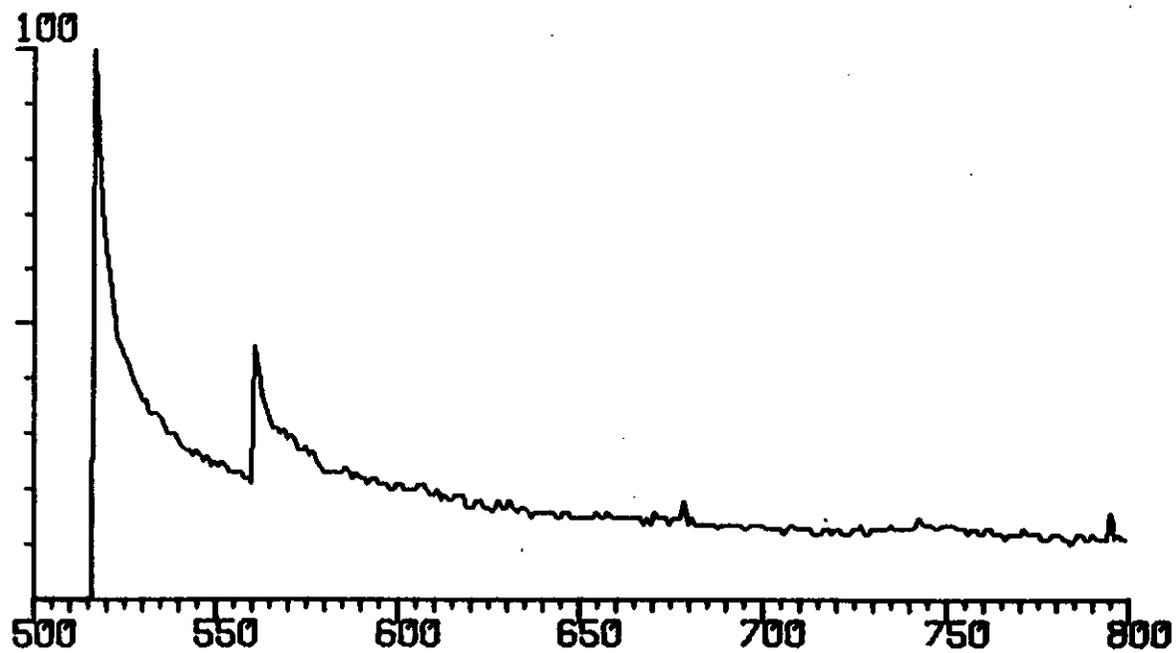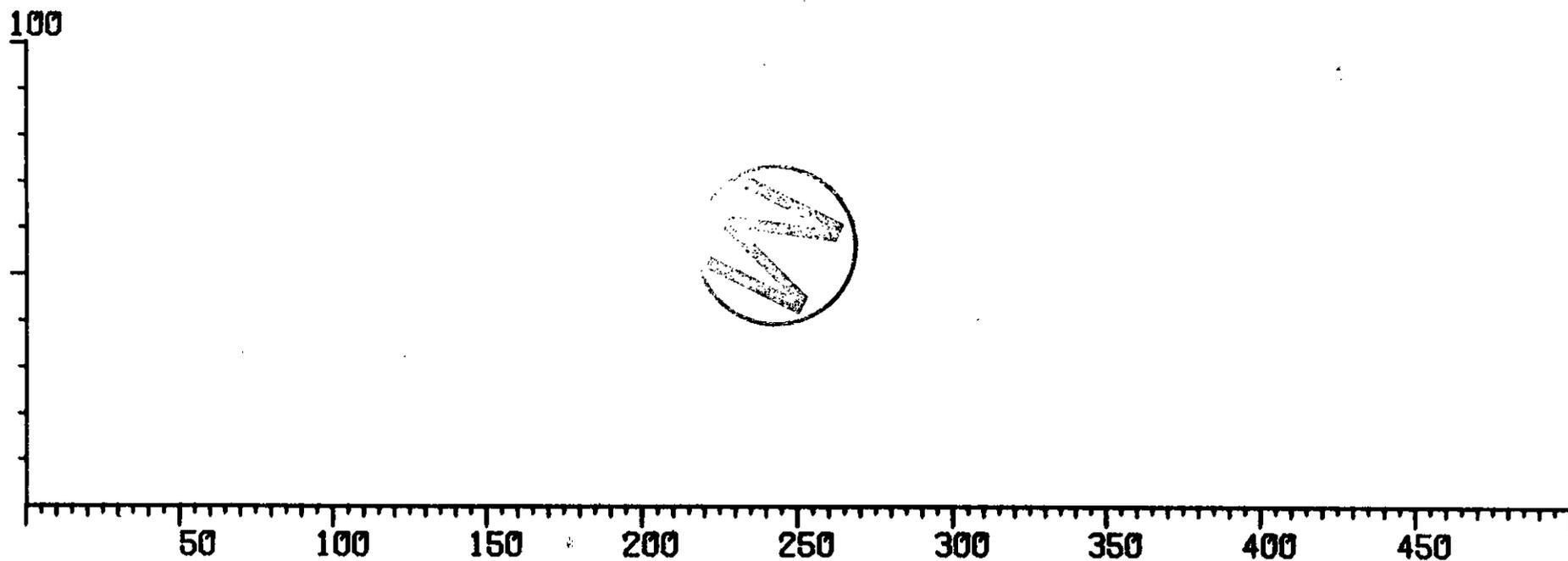
SALT SAMPLE   2302.6

MASS 80 SEARCH X1
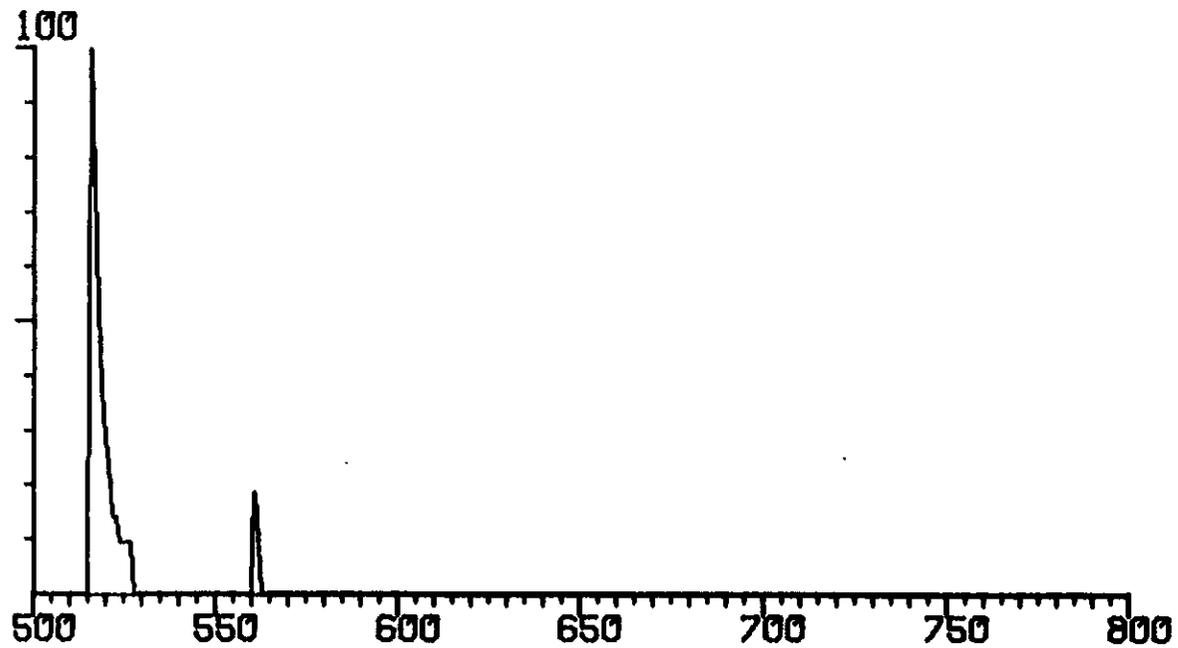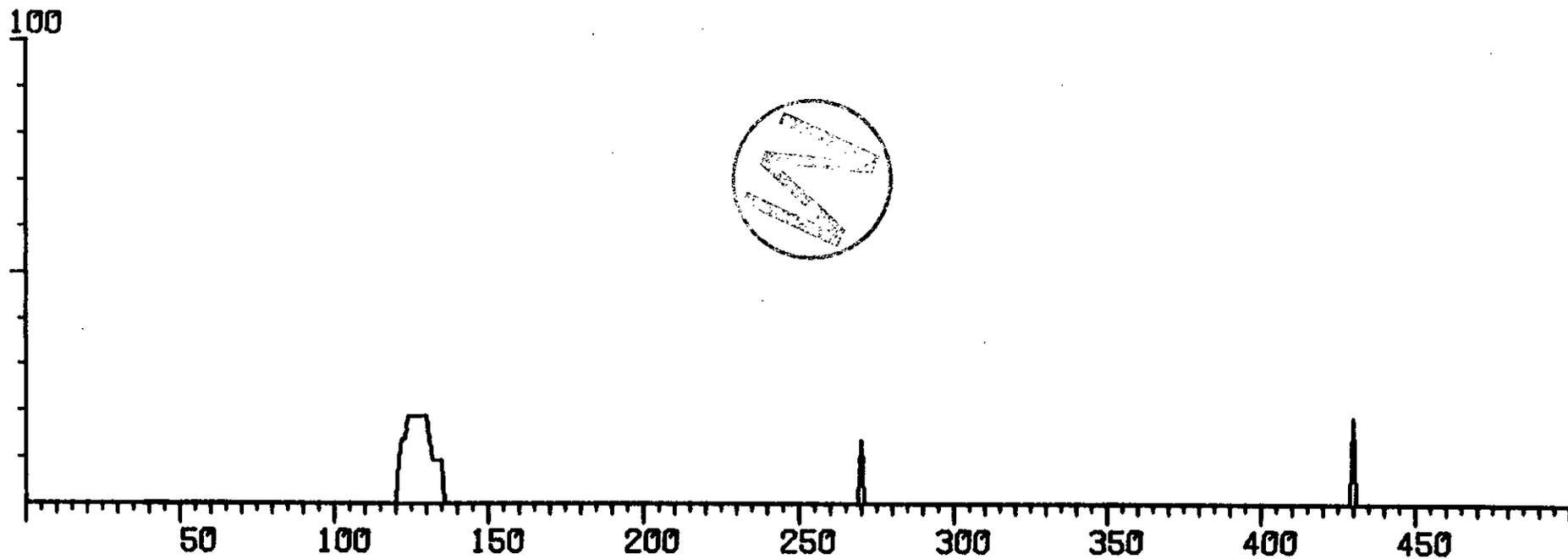
SALT SAMPLE   2302.6
          MASS 64 SEARCH X1
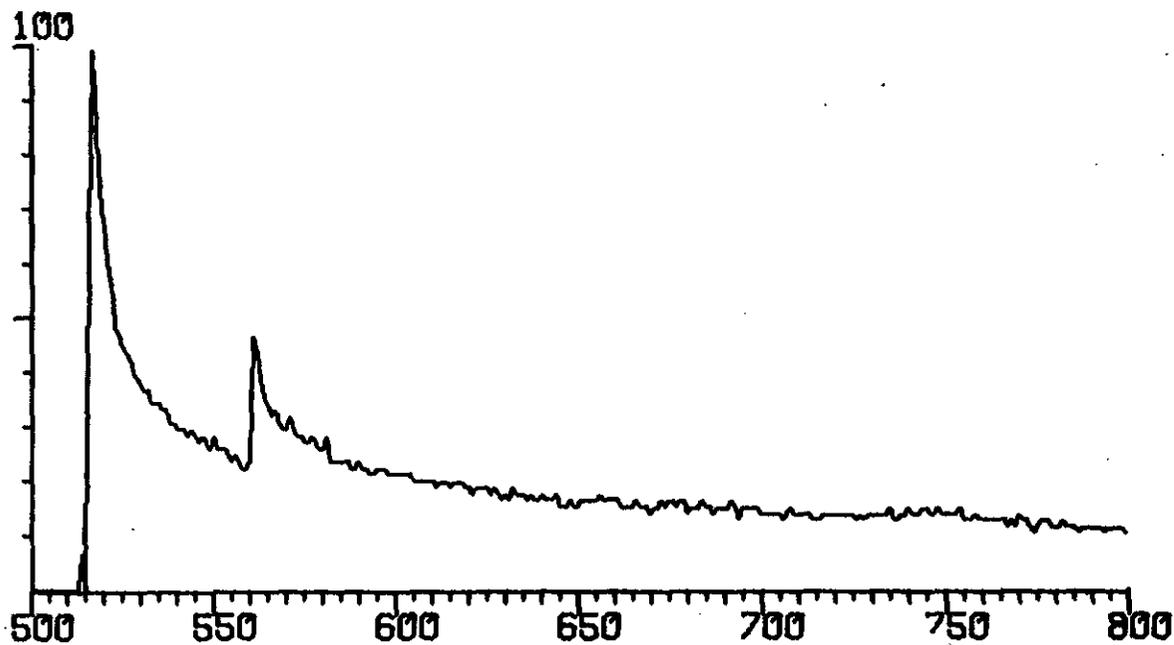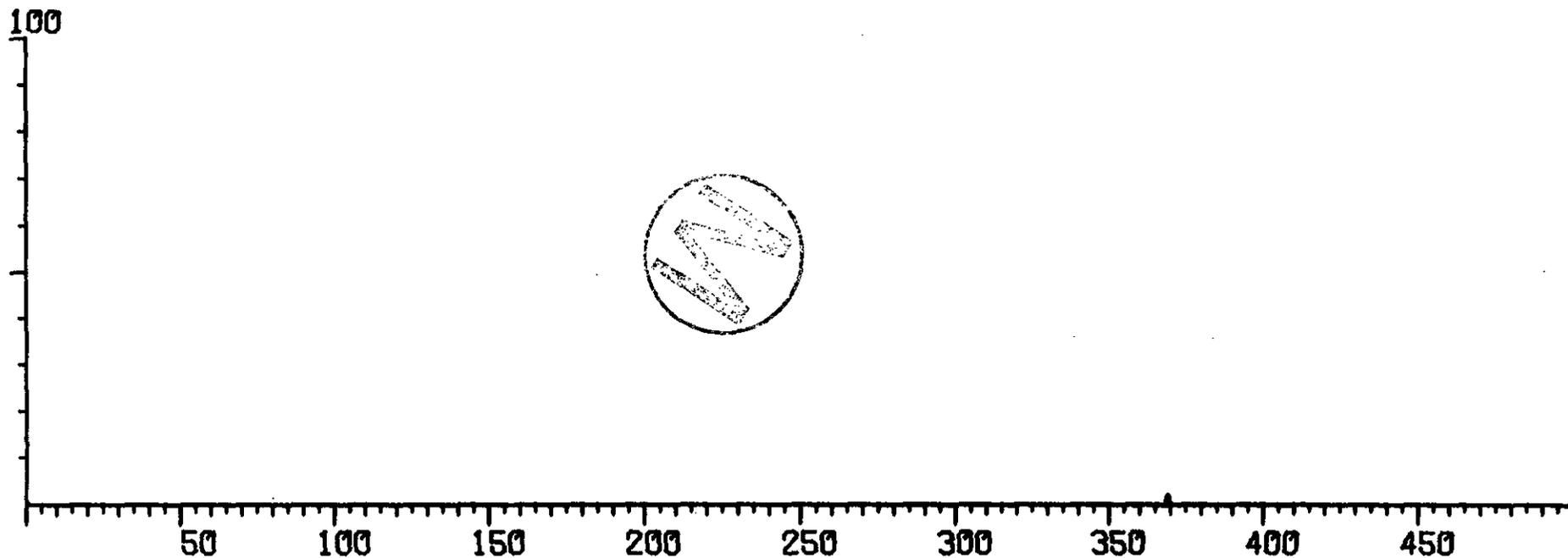
SALT SAMPLE   2516.3
      MASS 18 SEARCH X3
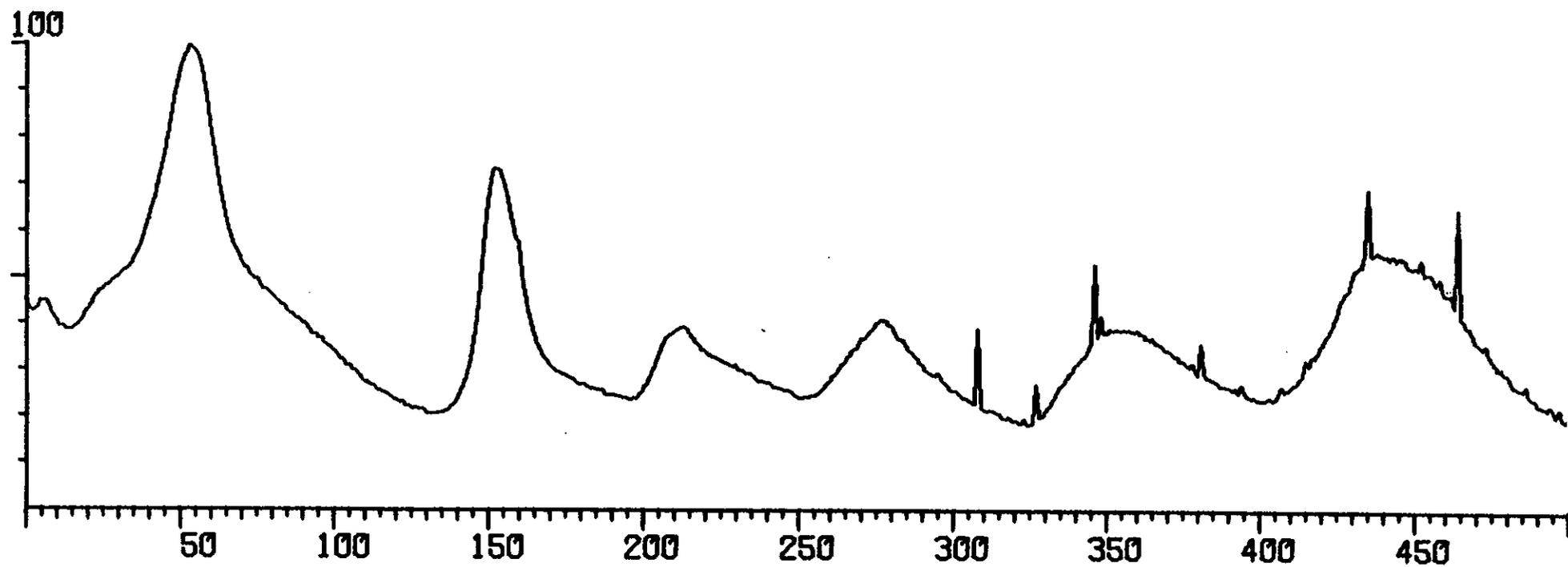
SALT SAMPLE   2516.3

MASS 28 SEARCH X3

100

50   100   150   200   250   300   350   400   450
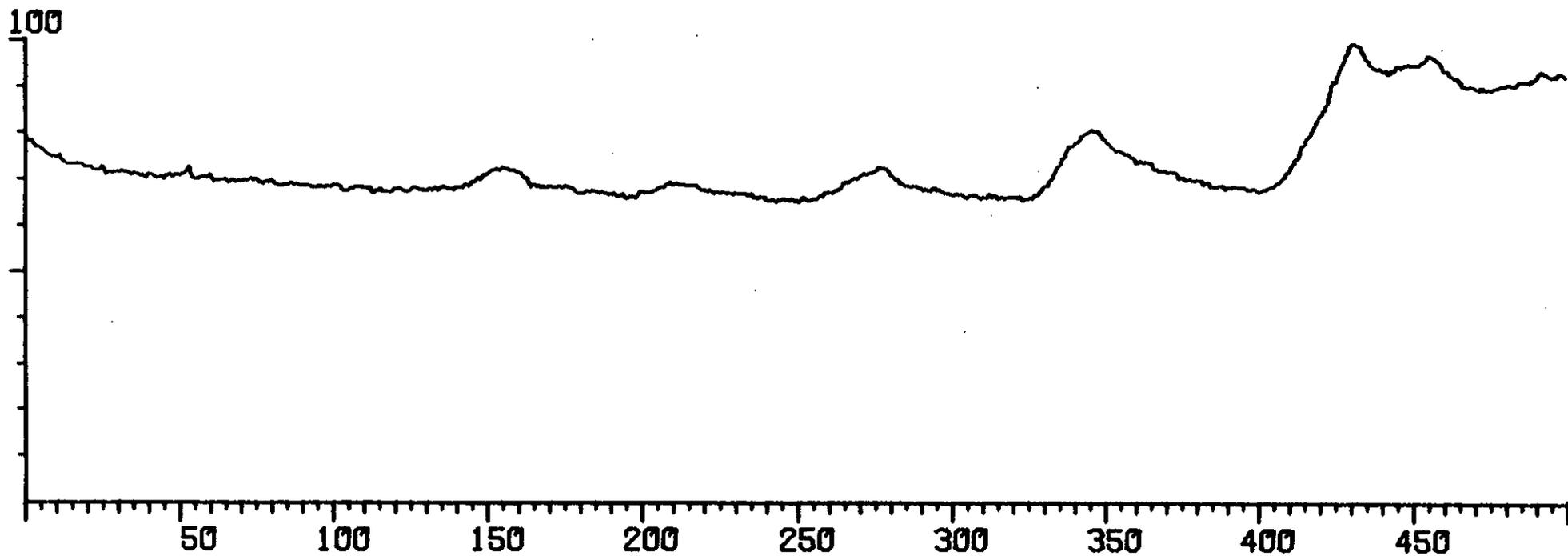
SALT SAMPLE   2302.6
517   CH 517 - CH 522 X1
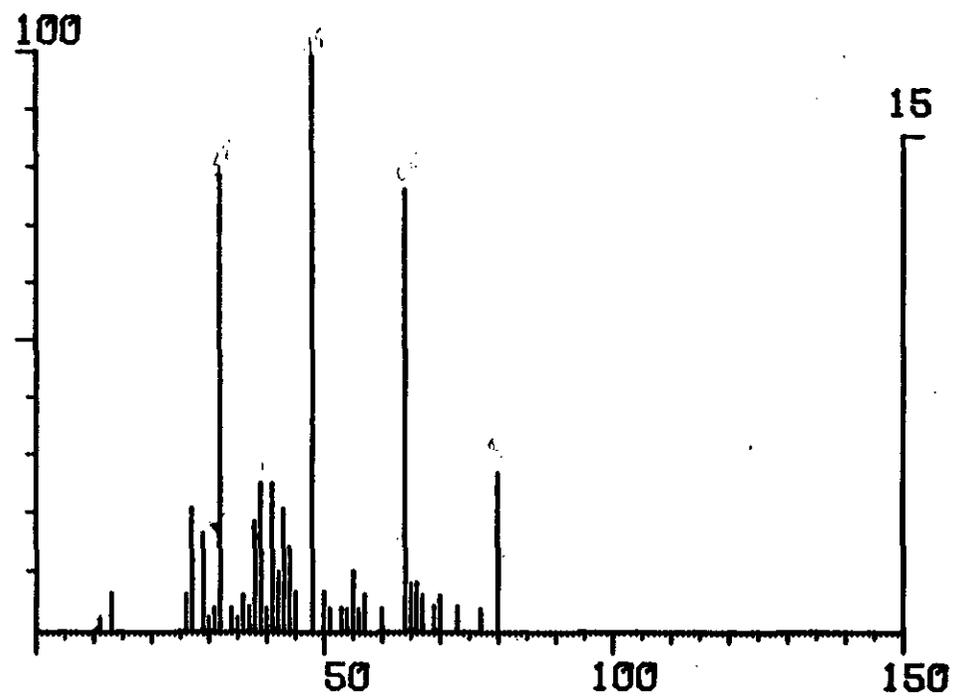
SALT SAMPLE   2516.3
          TOTAL ION CHROMATOGRAM

100
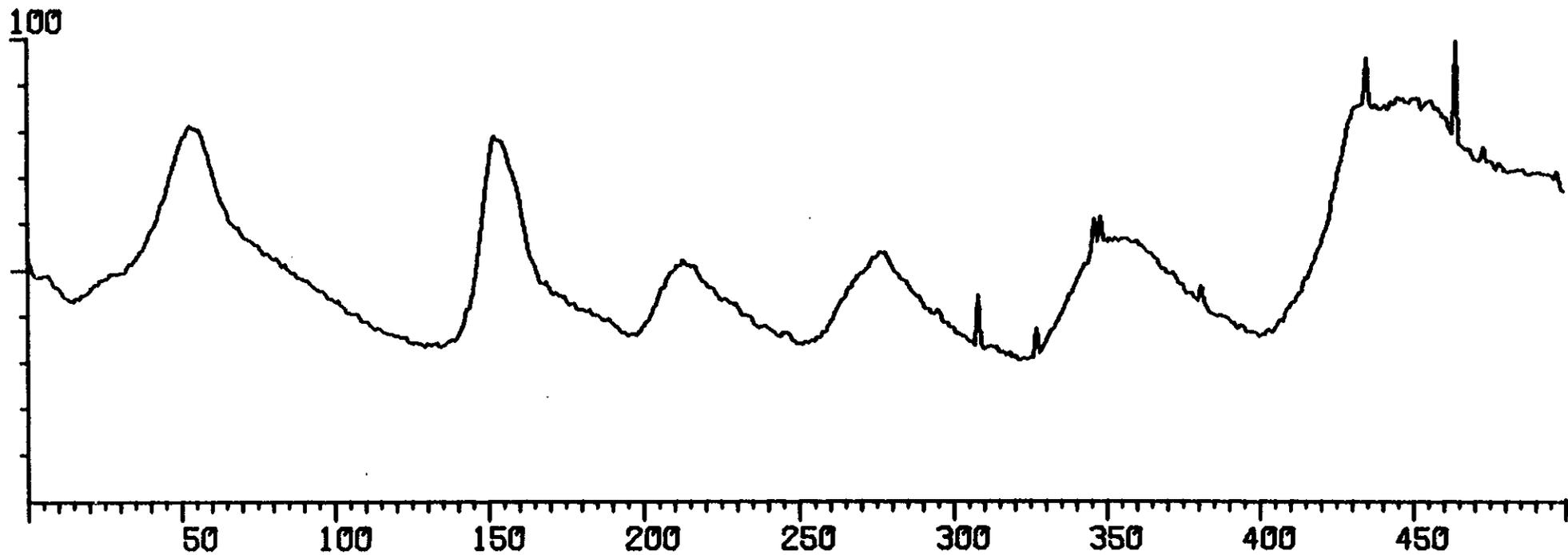
SALT SAMPLE   2516.3
        MASS 32 SEARCH X2
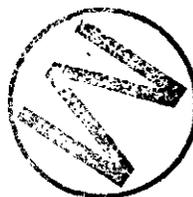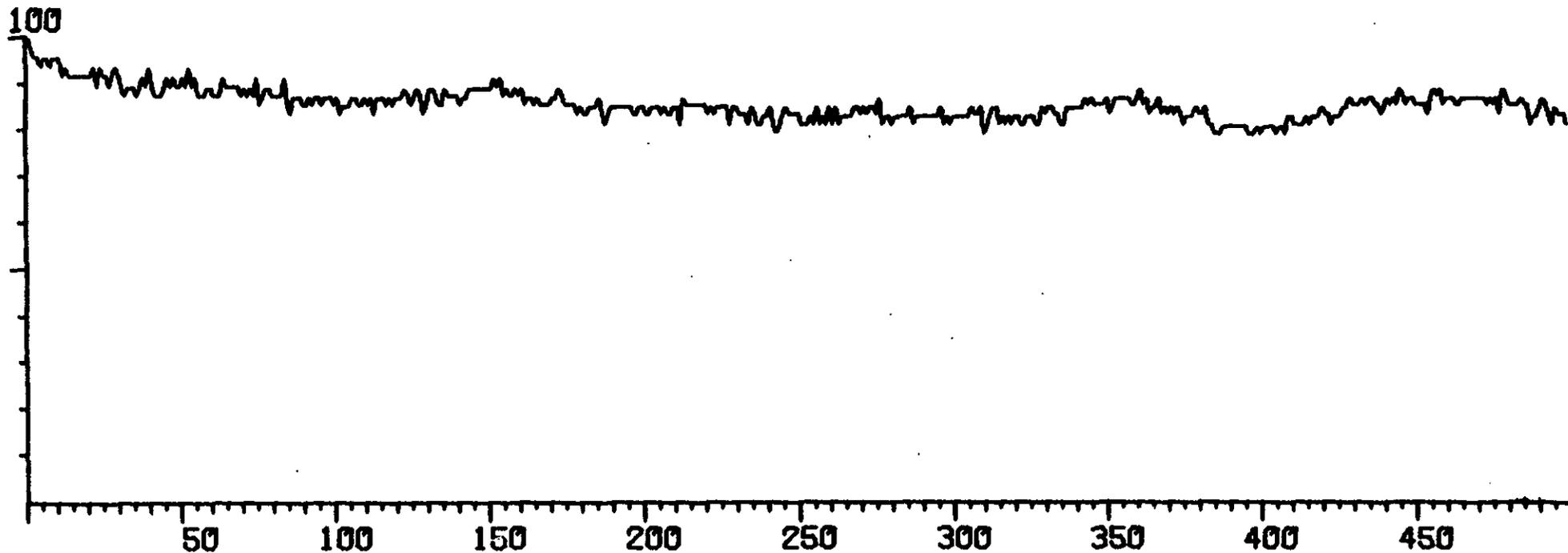
SALT SAMPLE   2516.3
            MASS 36 SEARCH X2
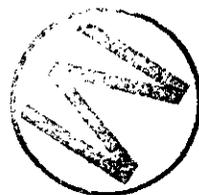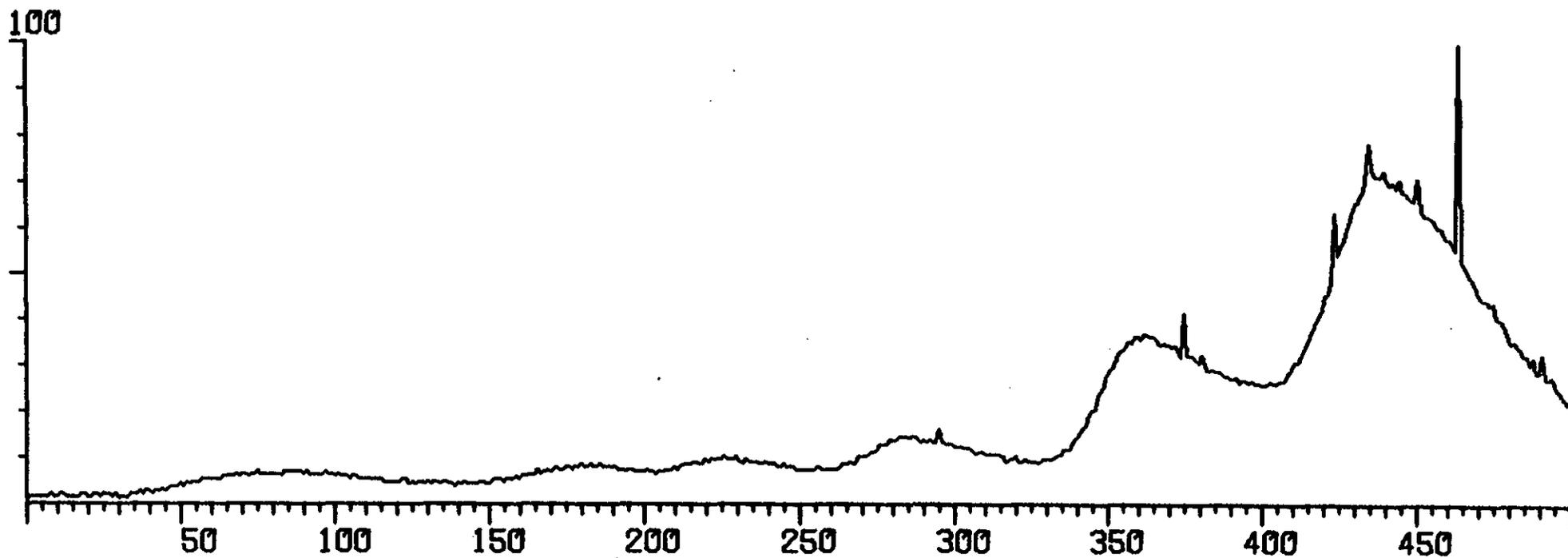
SALT SAMPLE   2516.3
        MASS 44 SEARCH X3
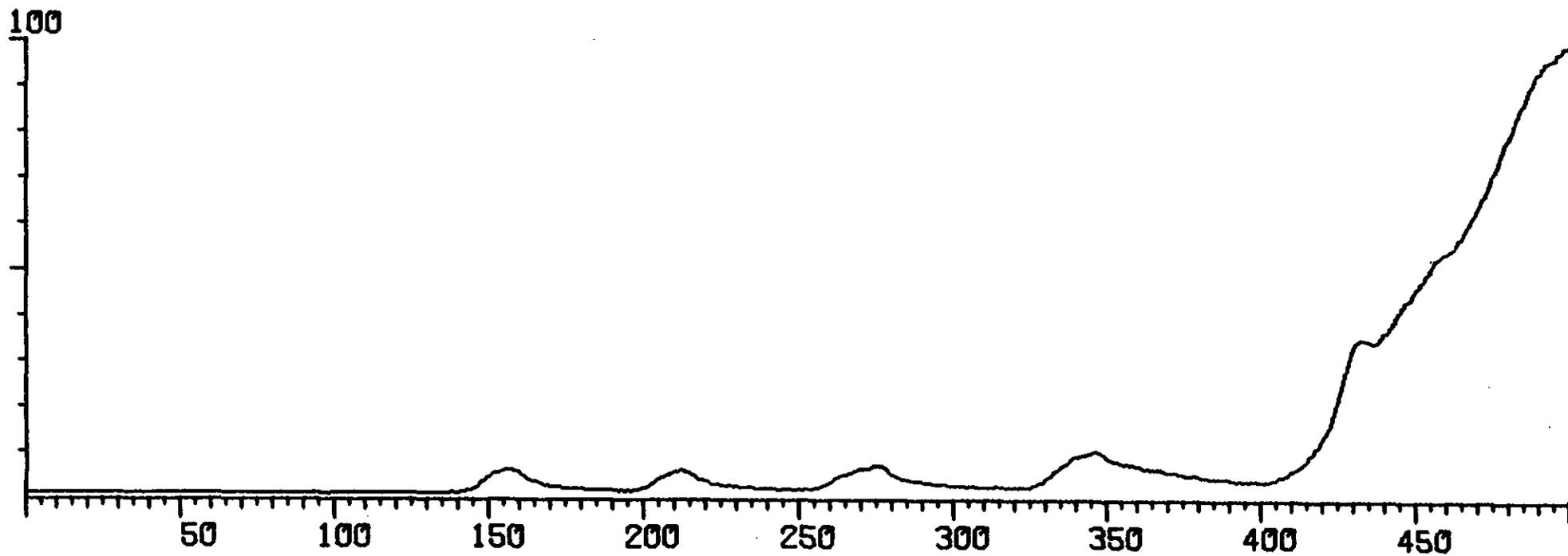
SALT SAMPLE   2516.3
          MASS 48 SEARCH X1
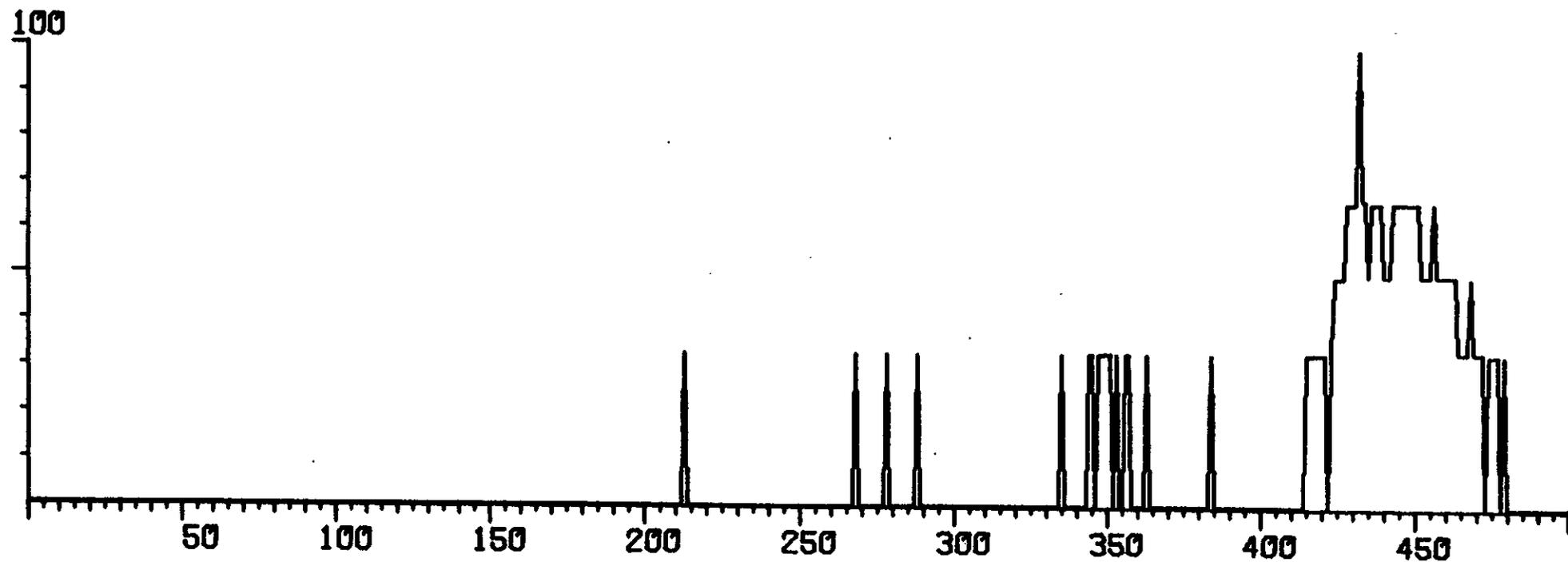
SALT SAMPLE   2658.5
        TOTAL ION CHROMATOGRAM
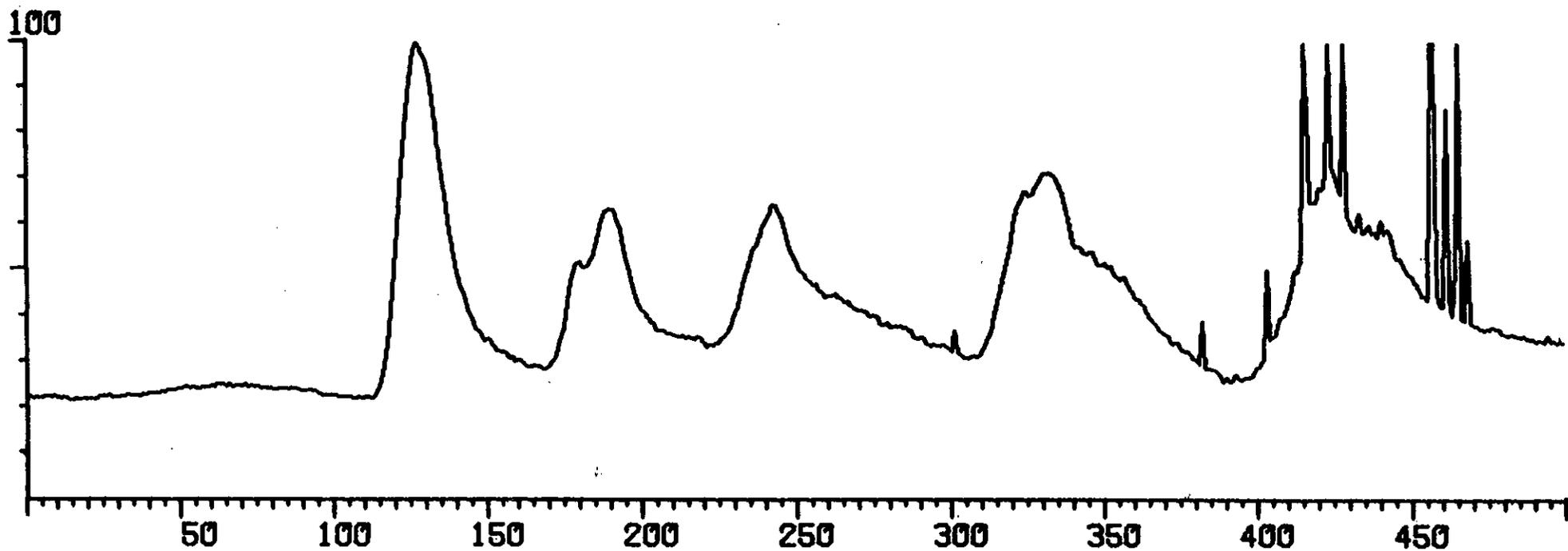
SALT SAMPLE   2658.5
                    MASS 14 SEARCH X1
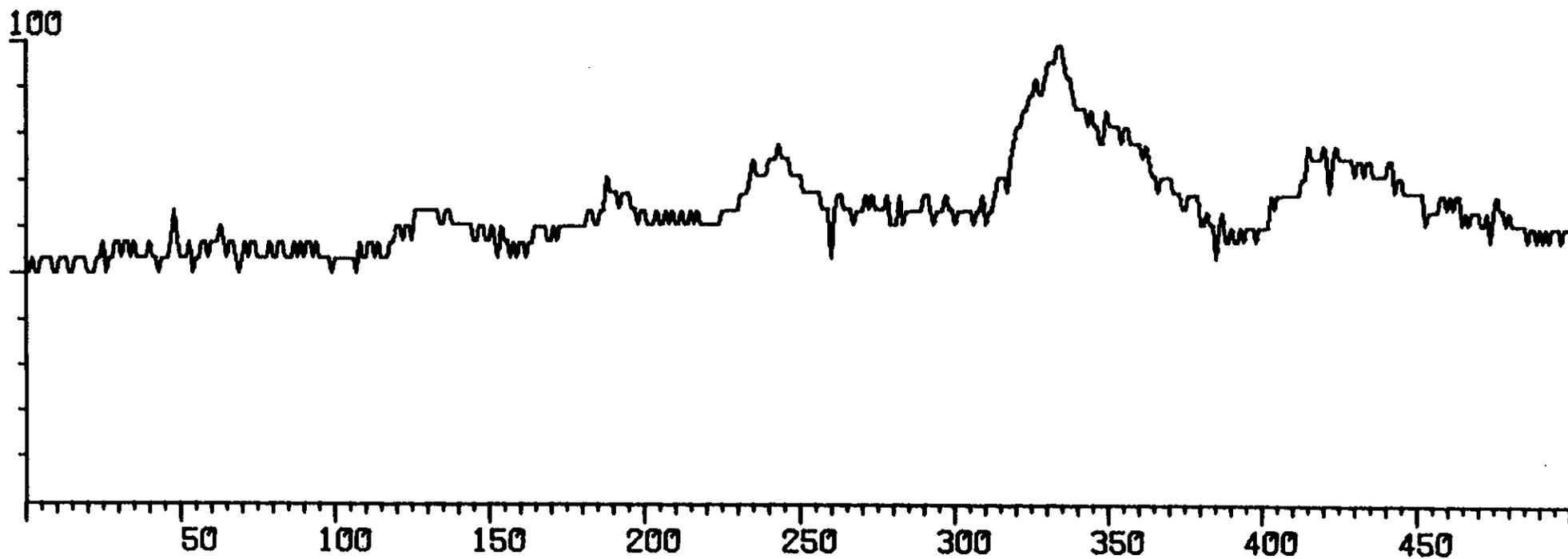
SALT SAMPLE   2658.5
        MASS 18 SEARCH X4 (CH 127 = 100%)

100
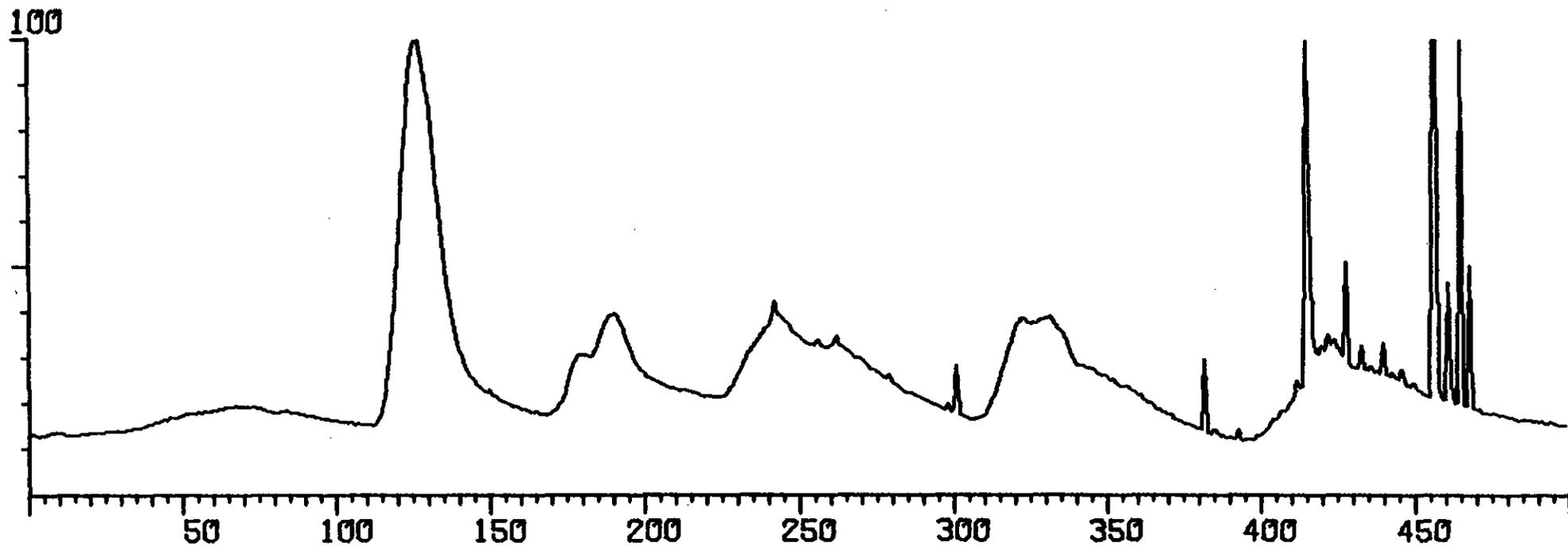
SALT SAMPLE   2658.5
        MASS 28 SEARCH X3

100

50   100   150   200   250   300   350   400   450
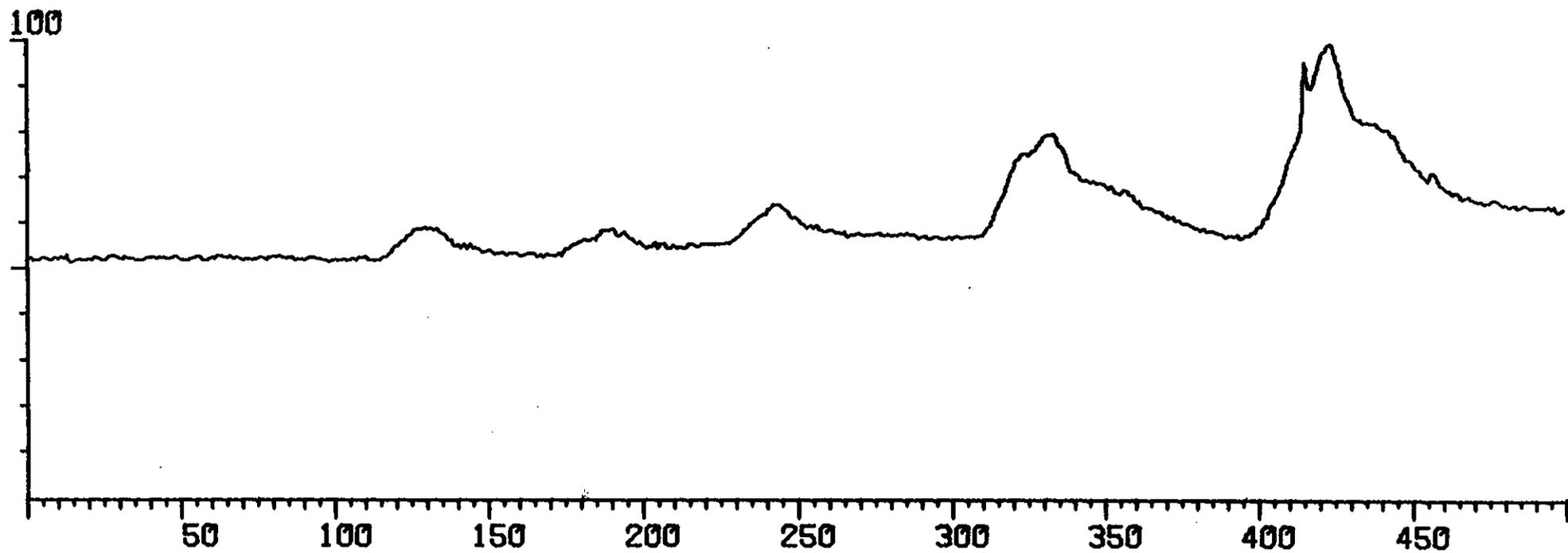
SALT SAMPLE   2658.5
         MASS 32 SEARCH X1
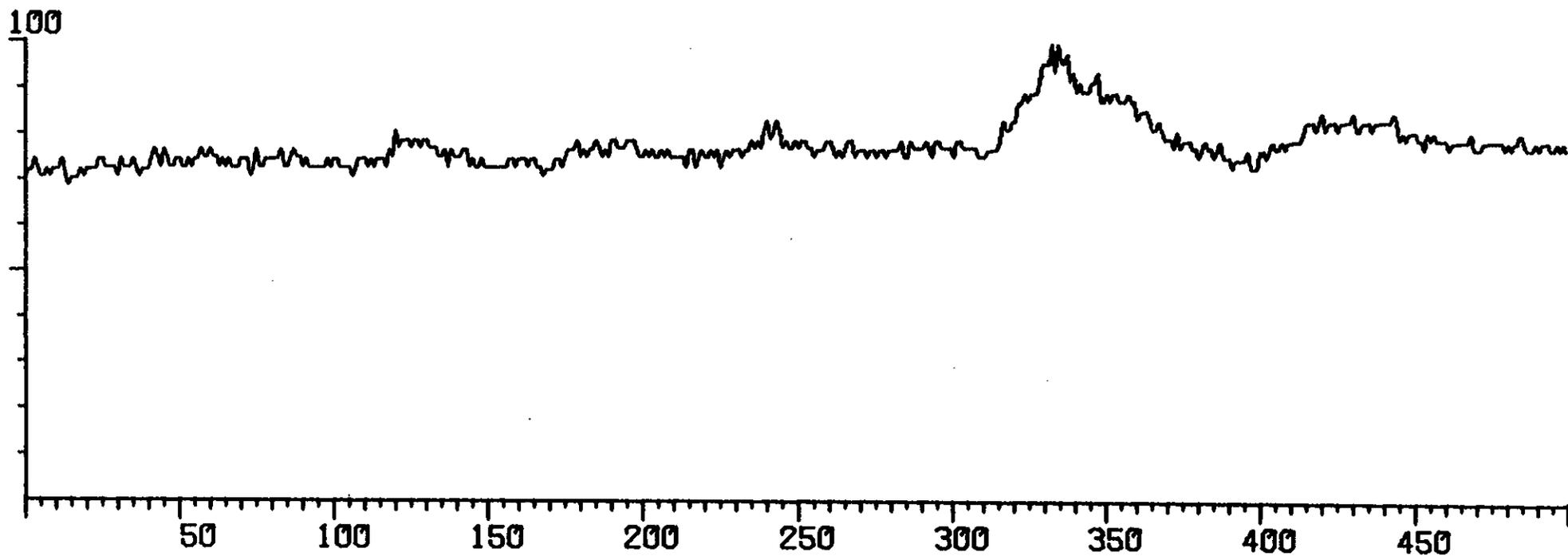
SALT SAMPLE   2658.5
        MASS 36 SEARCH X2 (CH 415 = 100%)
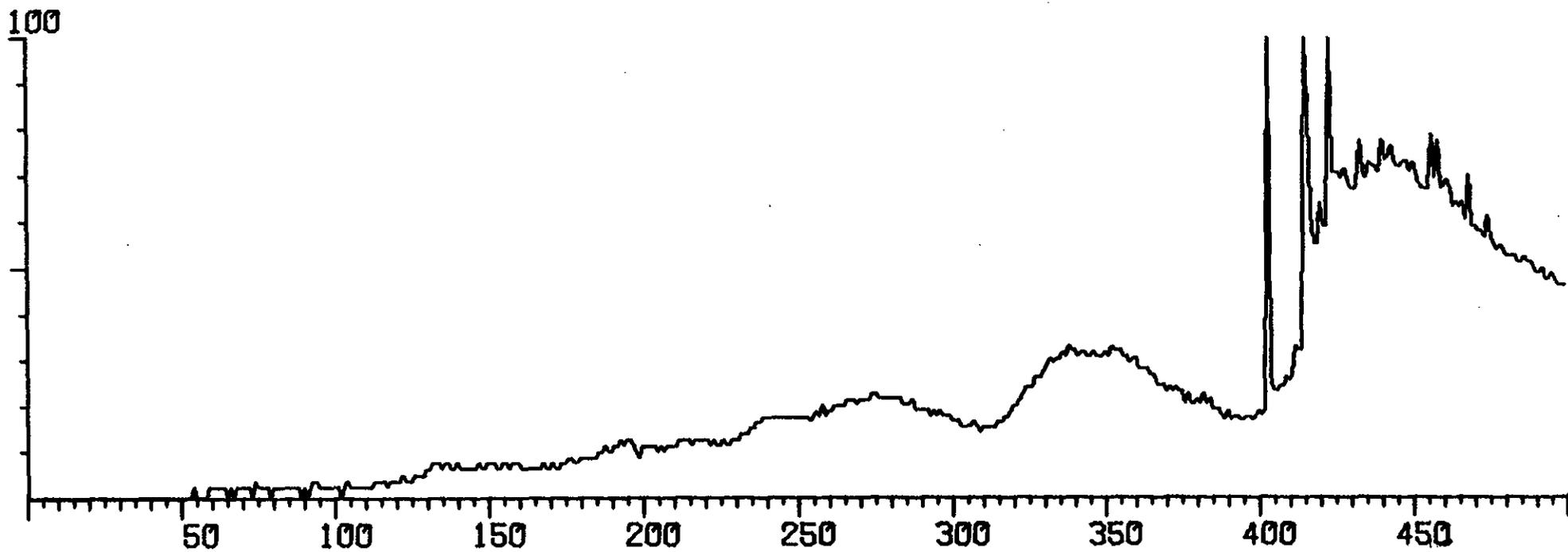
SALT SAMPLE   2658.5
            MASS 44 SEARCH X2
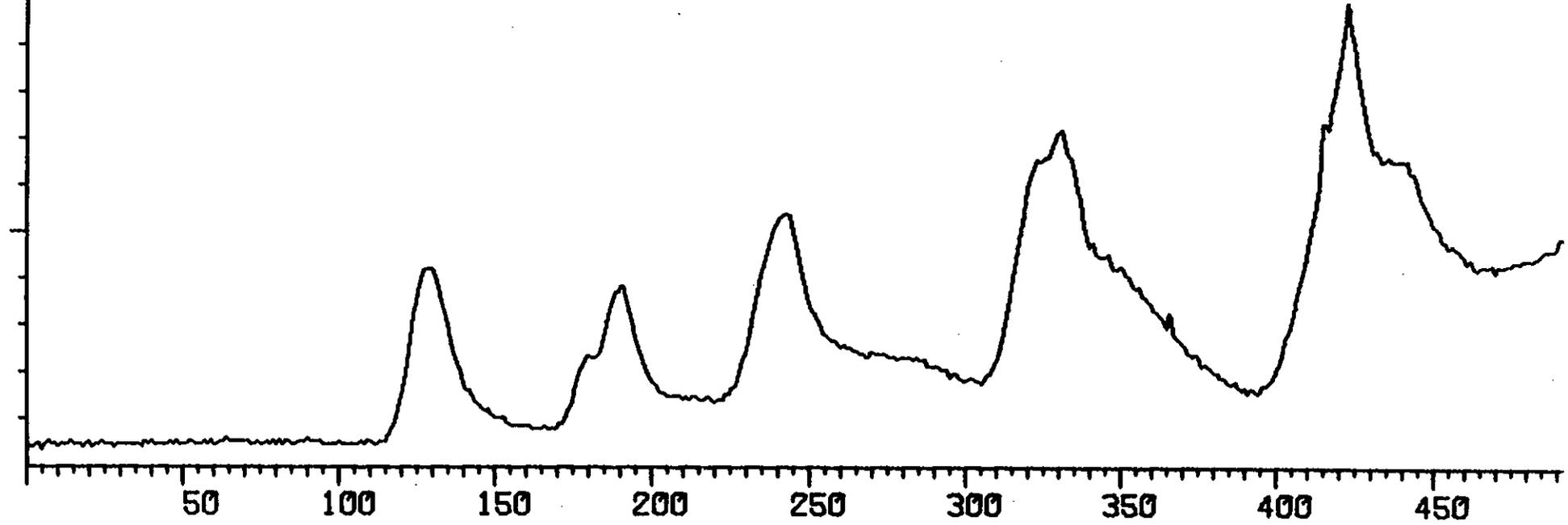
SALT SAMPLE   2658.5
        MASS 48 SEARCH X1
100
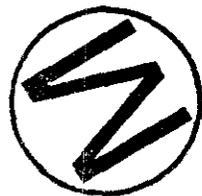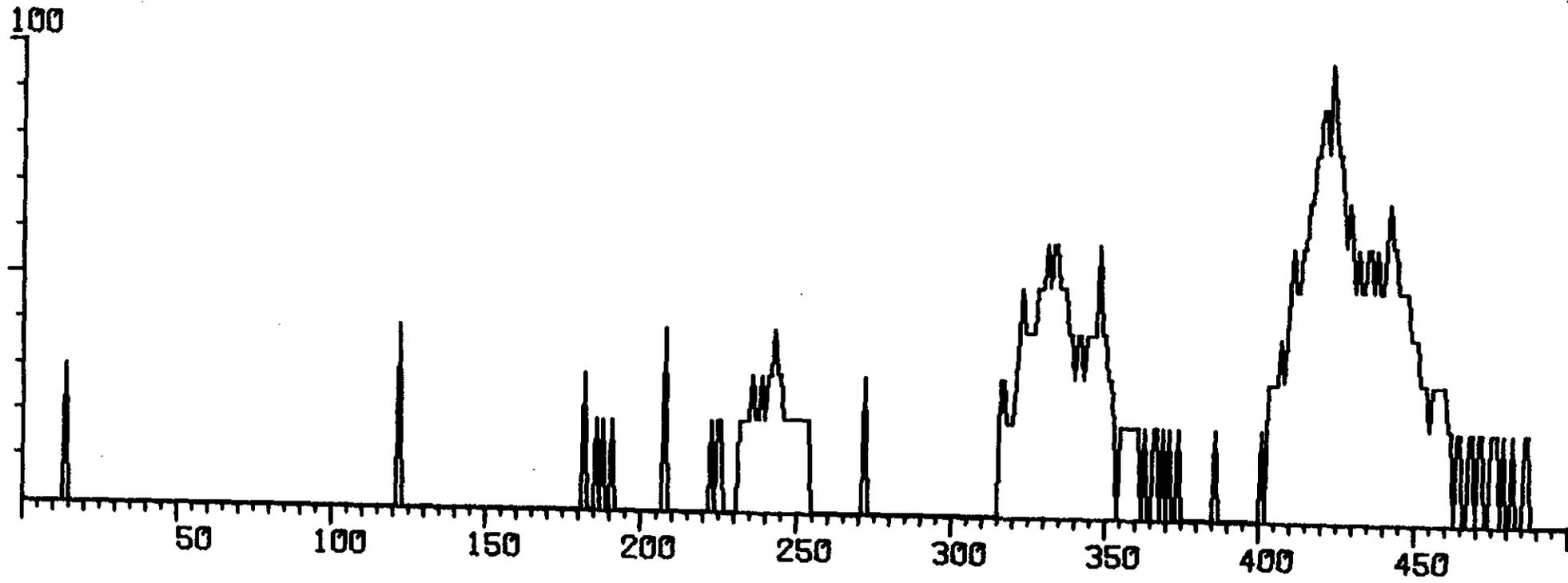
SALT SAMPLE   2786.5
             TOTAL ION CHROMATOGRAM
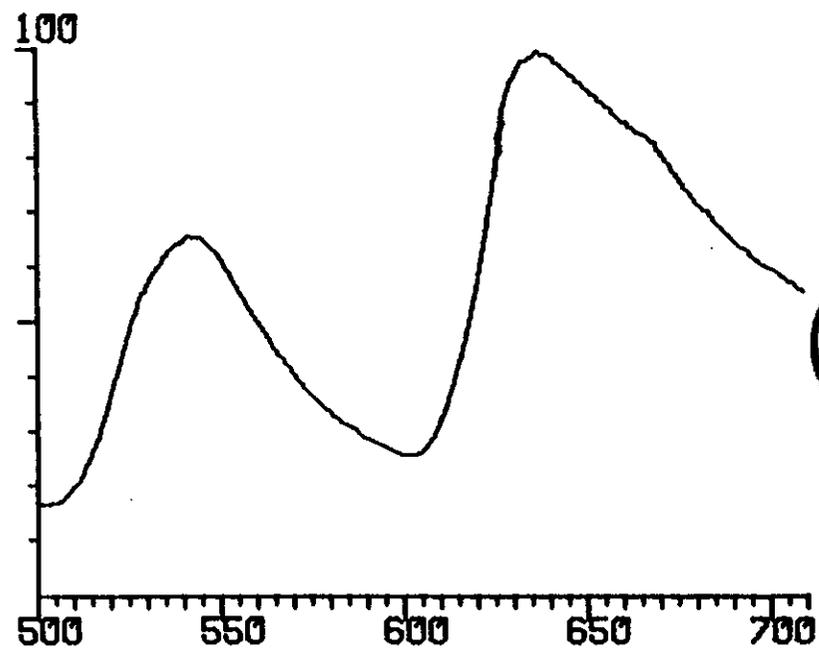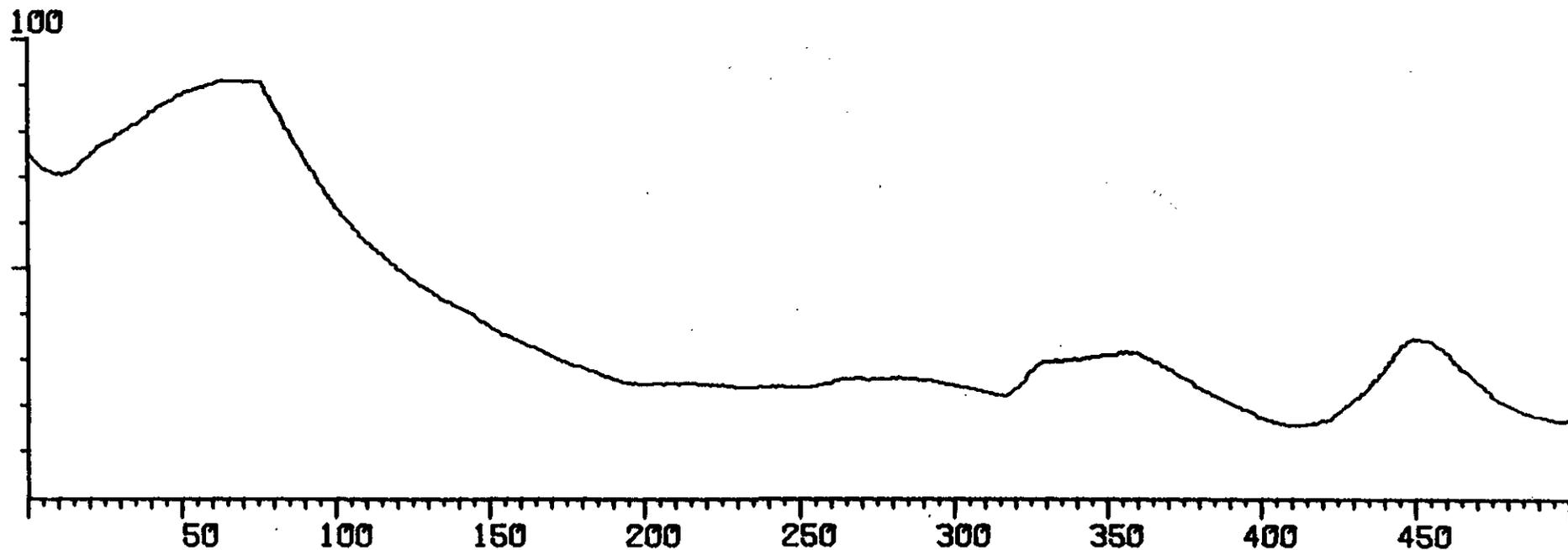
SALT SAMPLE   2786.5
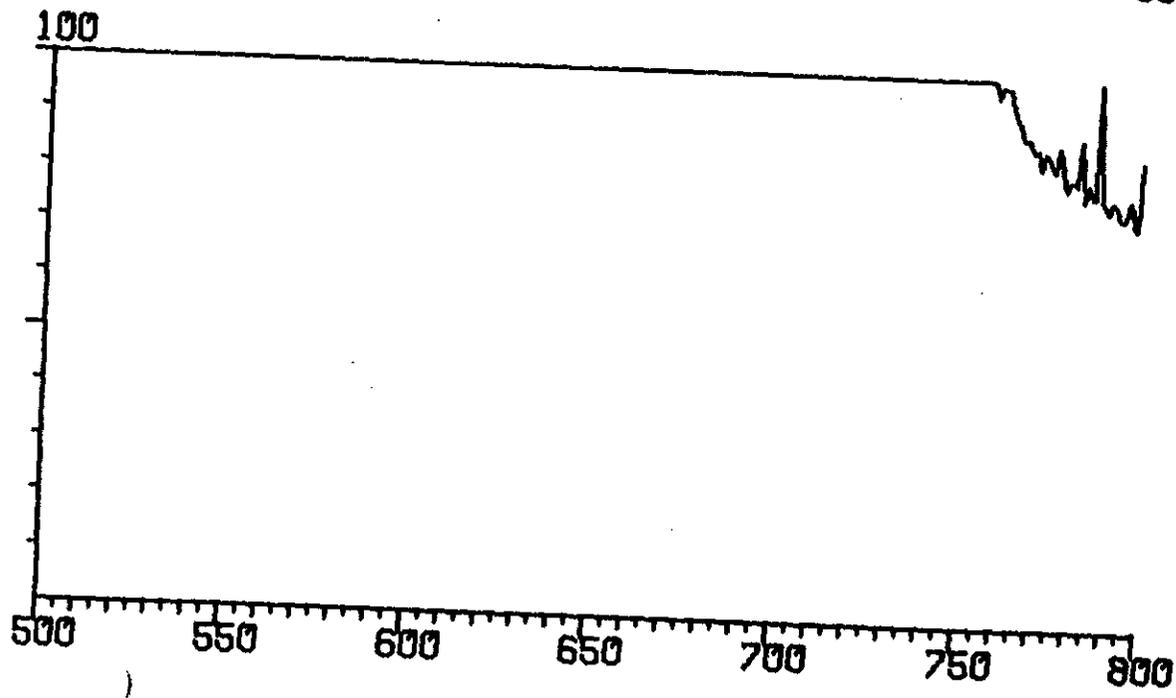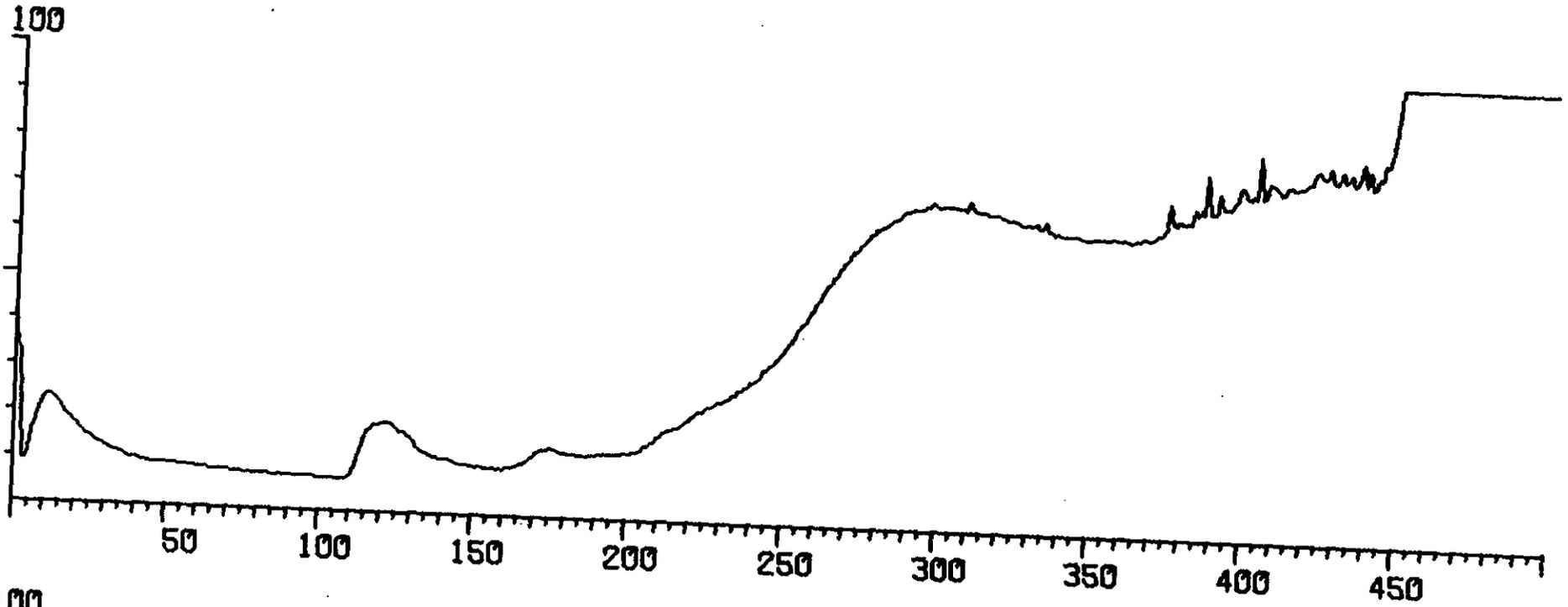   MASS 14 SEARCH X1
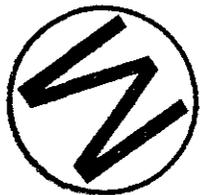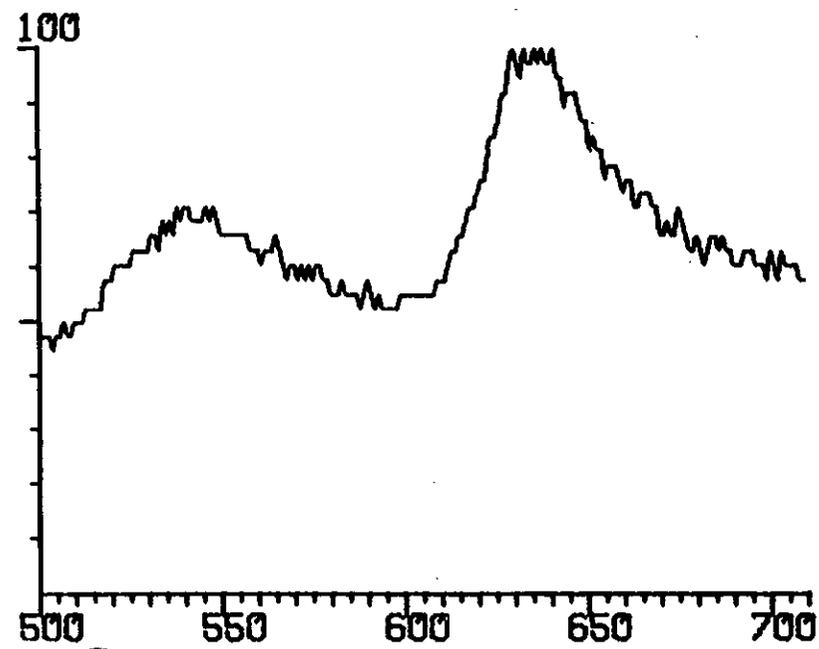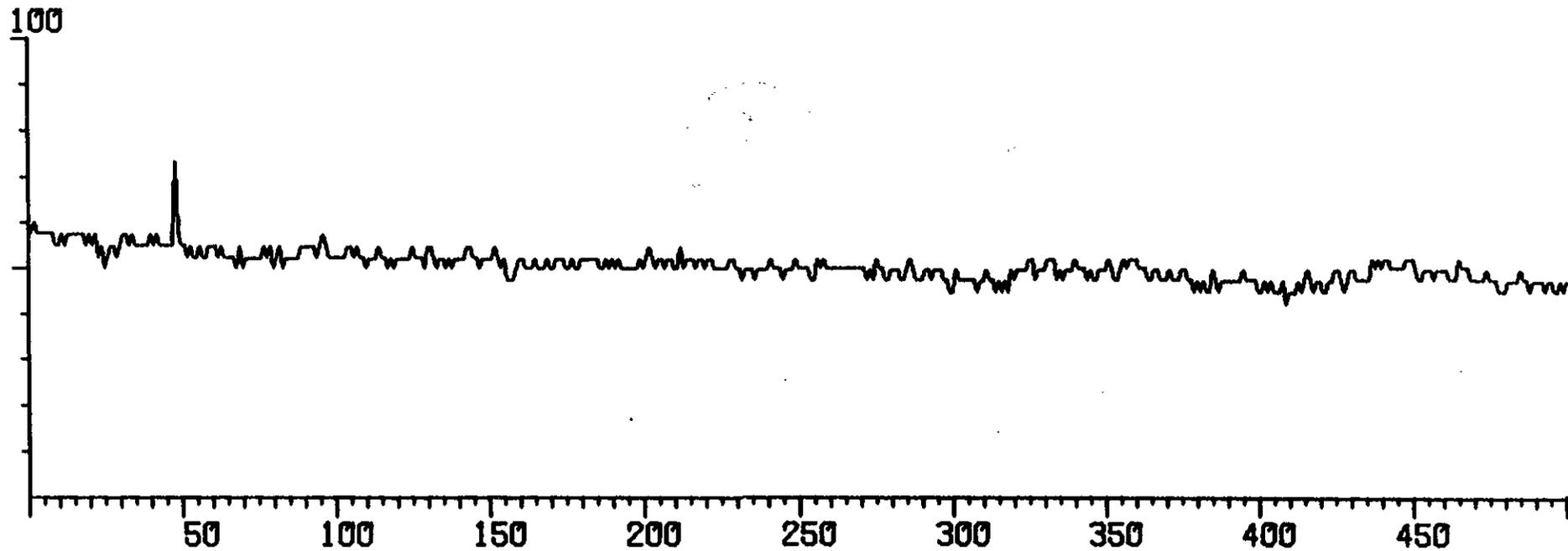
SALT SAMPLE   2786.5
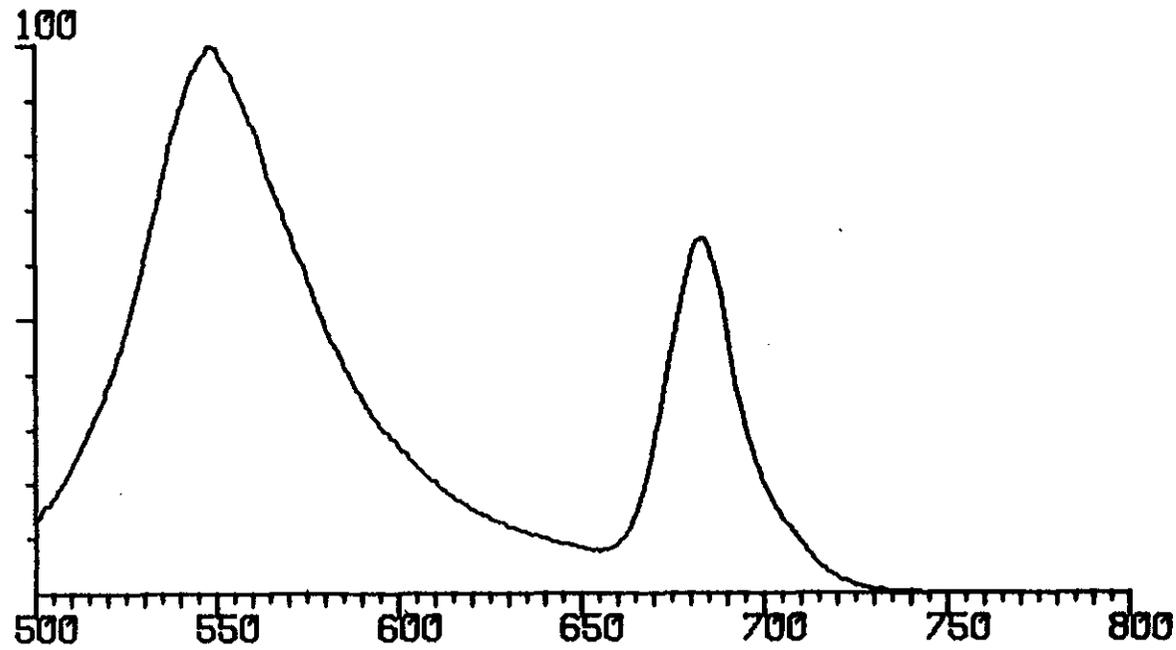   MASS 18 SEARCH X4
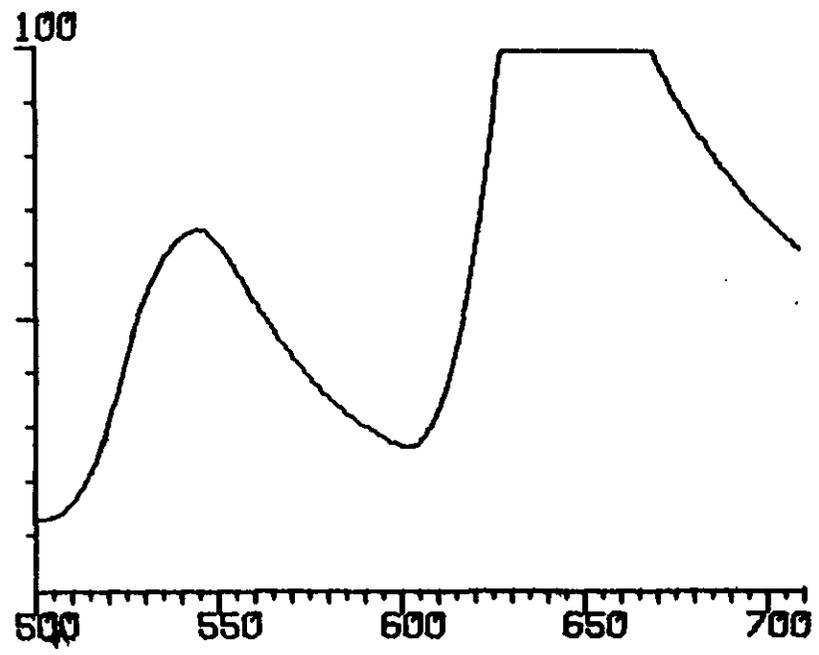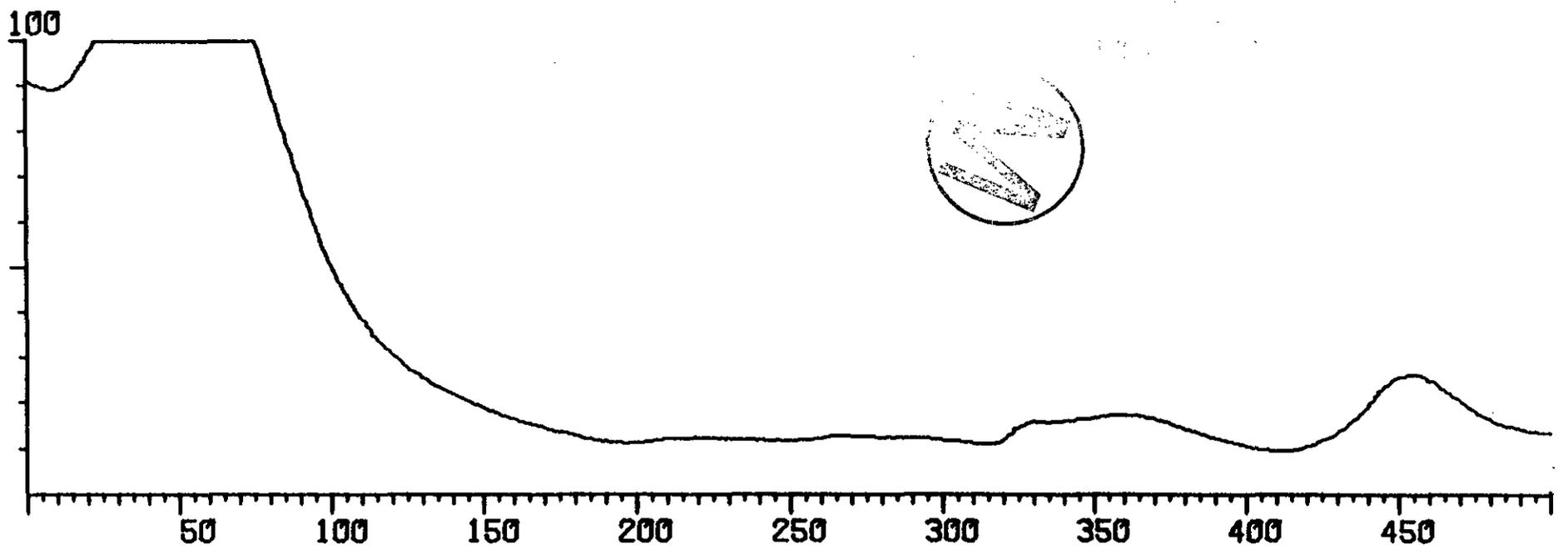
SALT SAMPLE   2786.5
                MASS 19 SEARCH X1
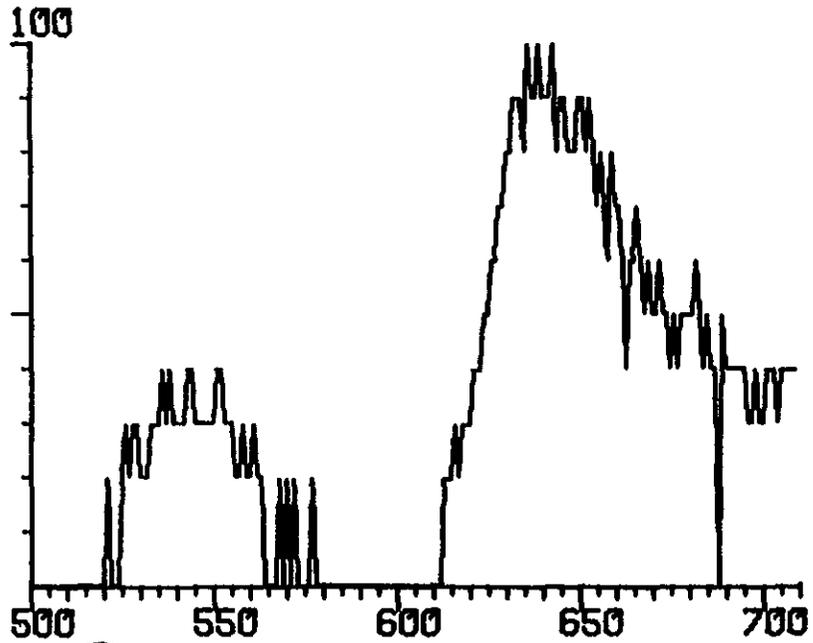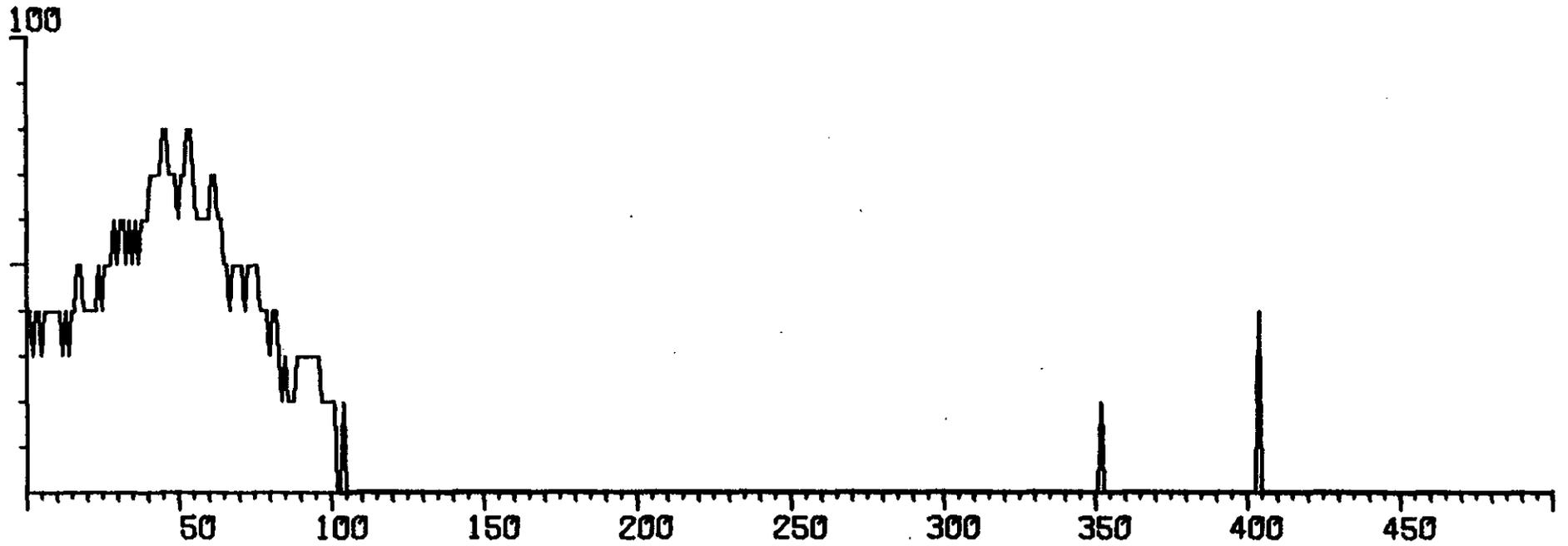
SALI SAMPLE   2786.5
        MASS 28 SEARCH X3
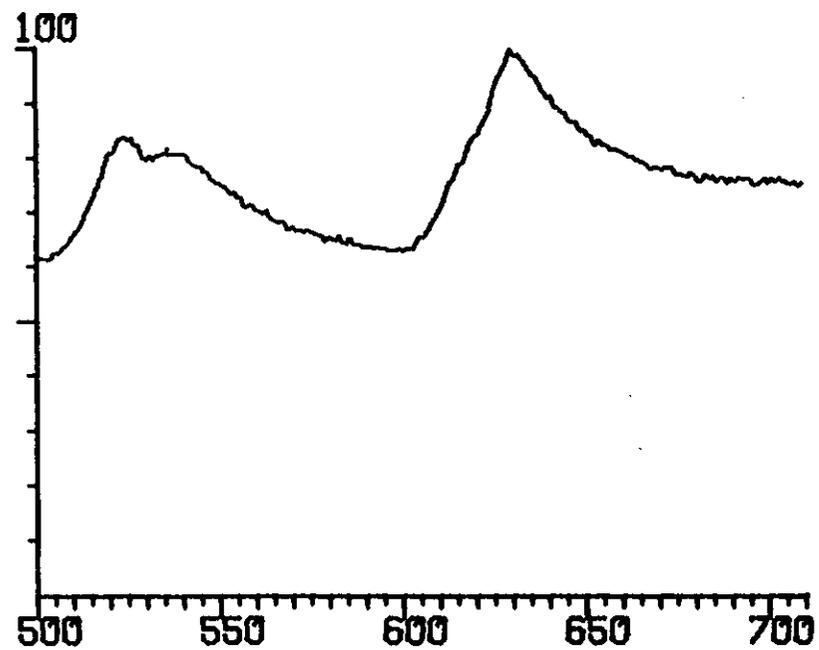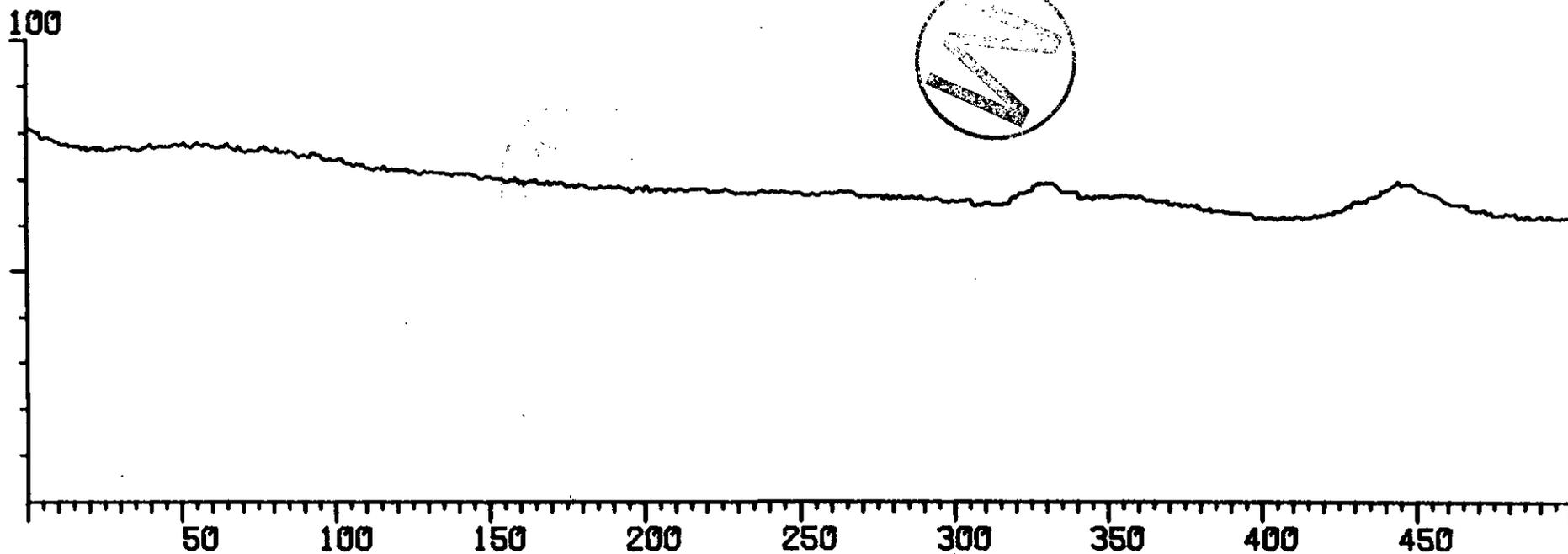
SALT SAMPLE   2786.5
          MASS 32 SEARCH X1
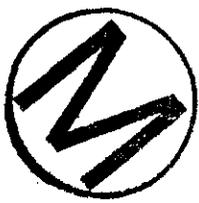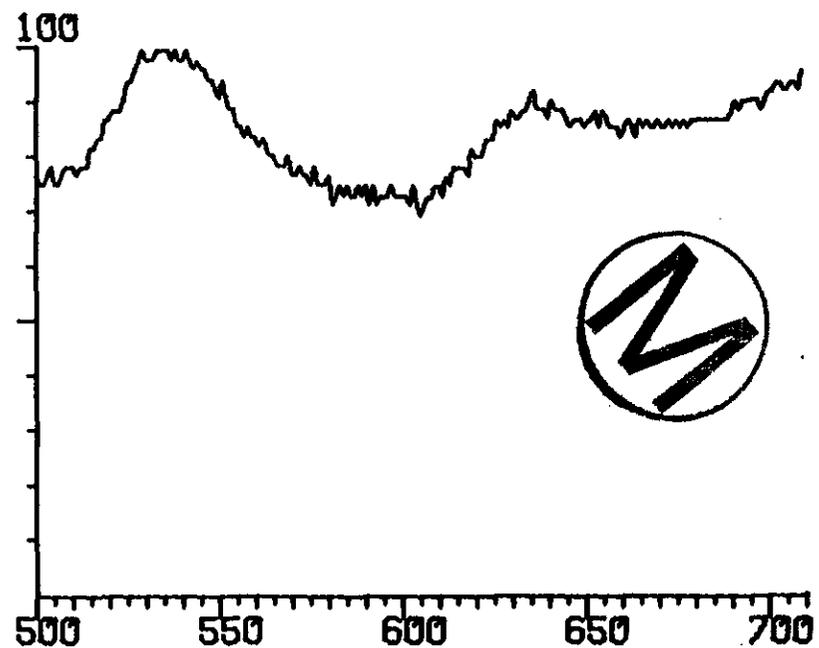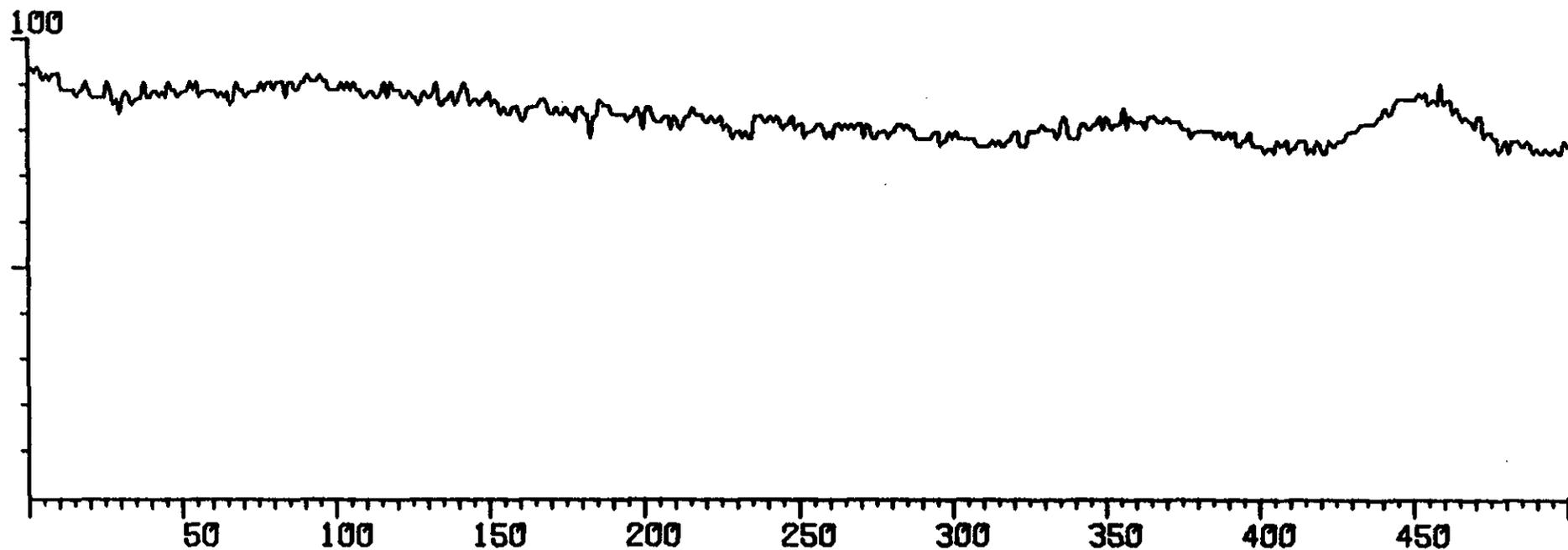
SALT SAMPLE   2786.5
          MASS 36 SEARCH X2

100

    50   100   150   200   250   300   350   400   450

100

500   550   600   650   700
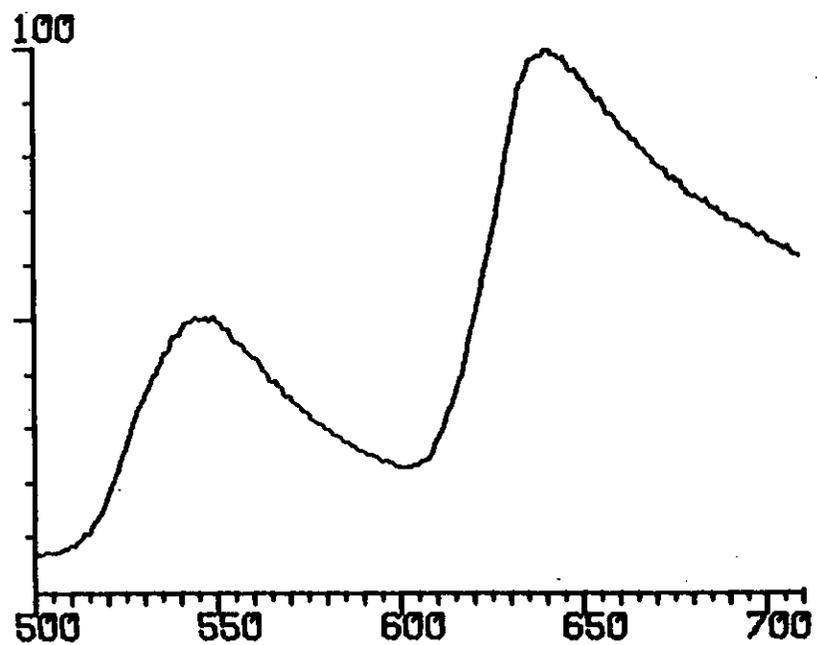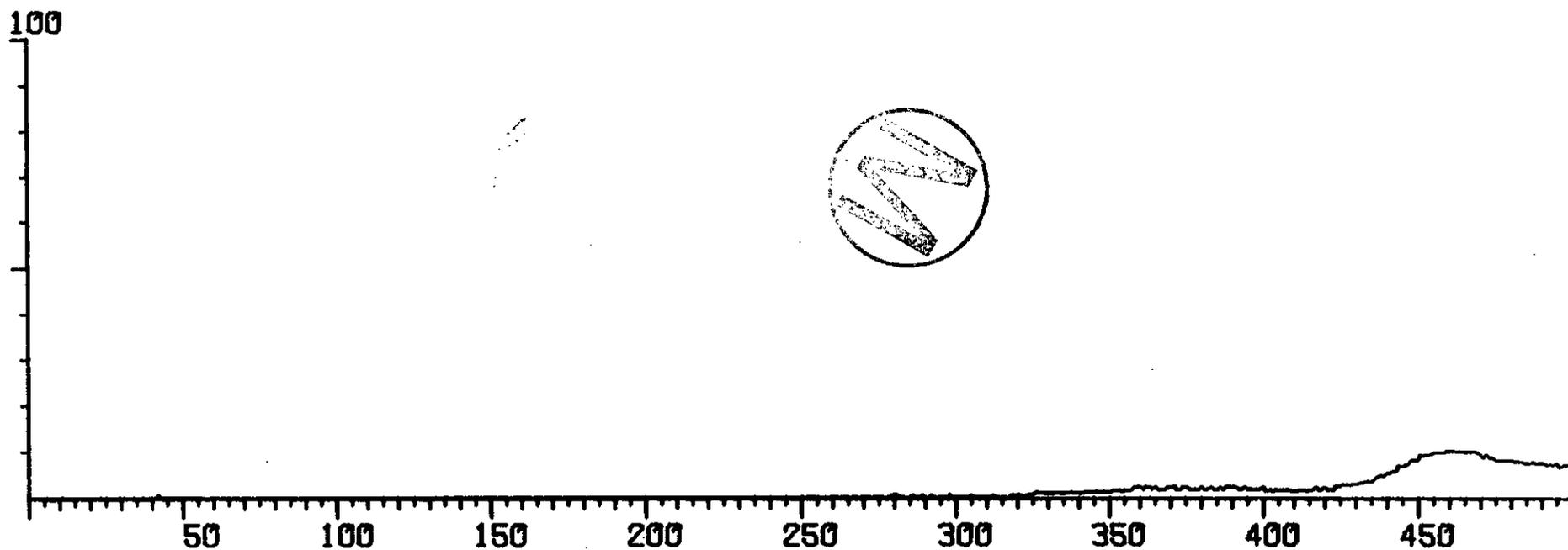
SALT SAMPLE   2786.5
MASS 44 SEARCH X2
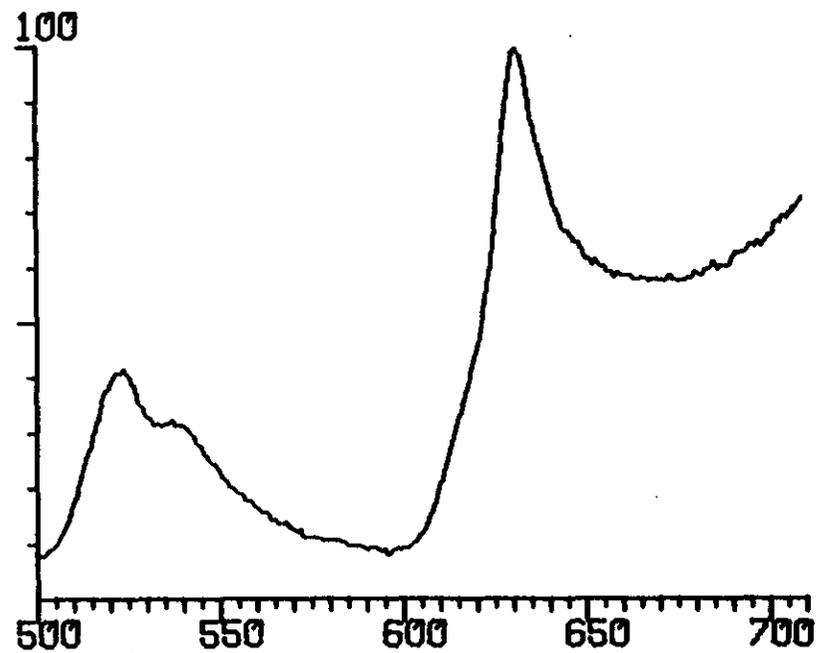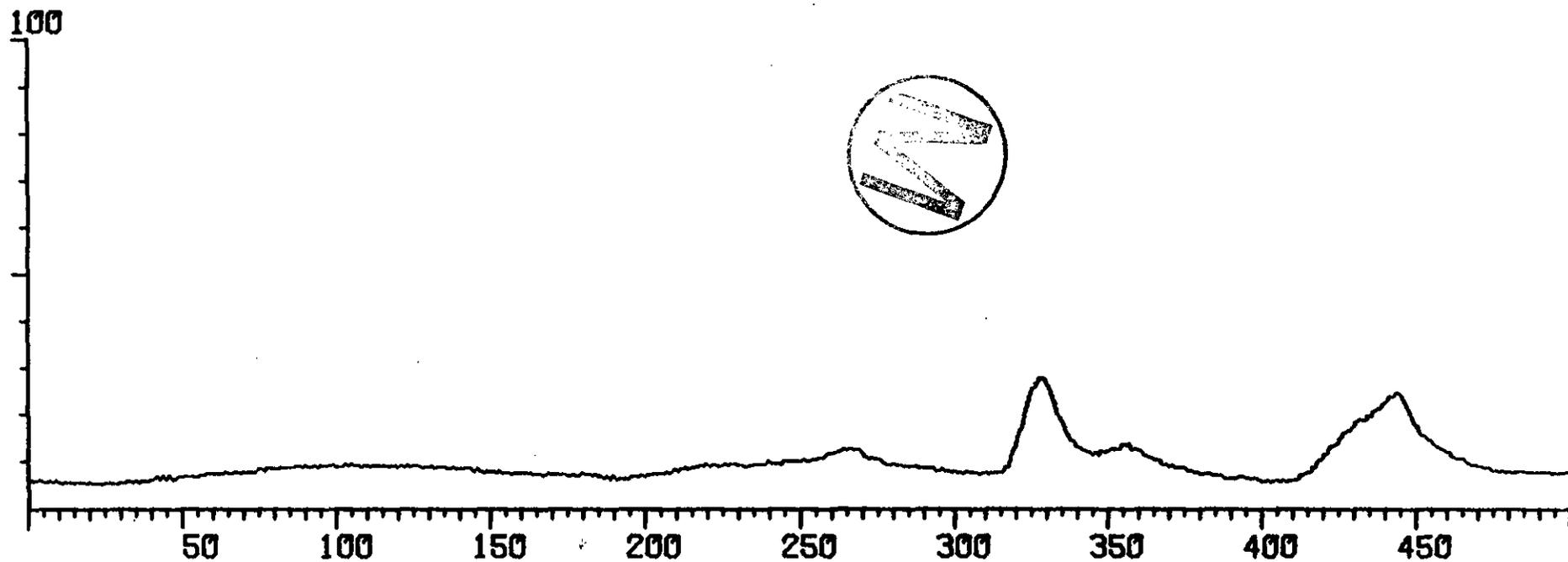
SALT SAMPLE   2786.5

MASS 48 SEARCH X1
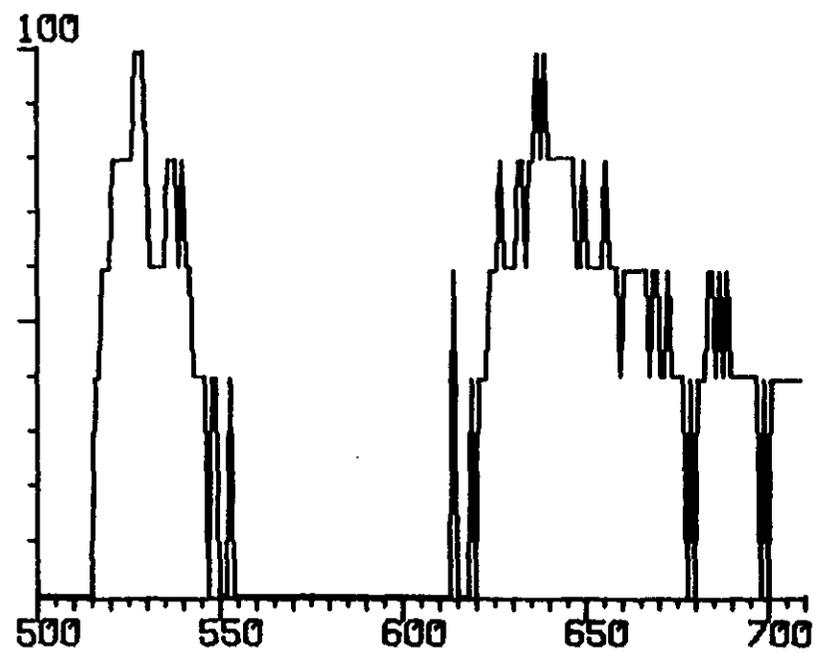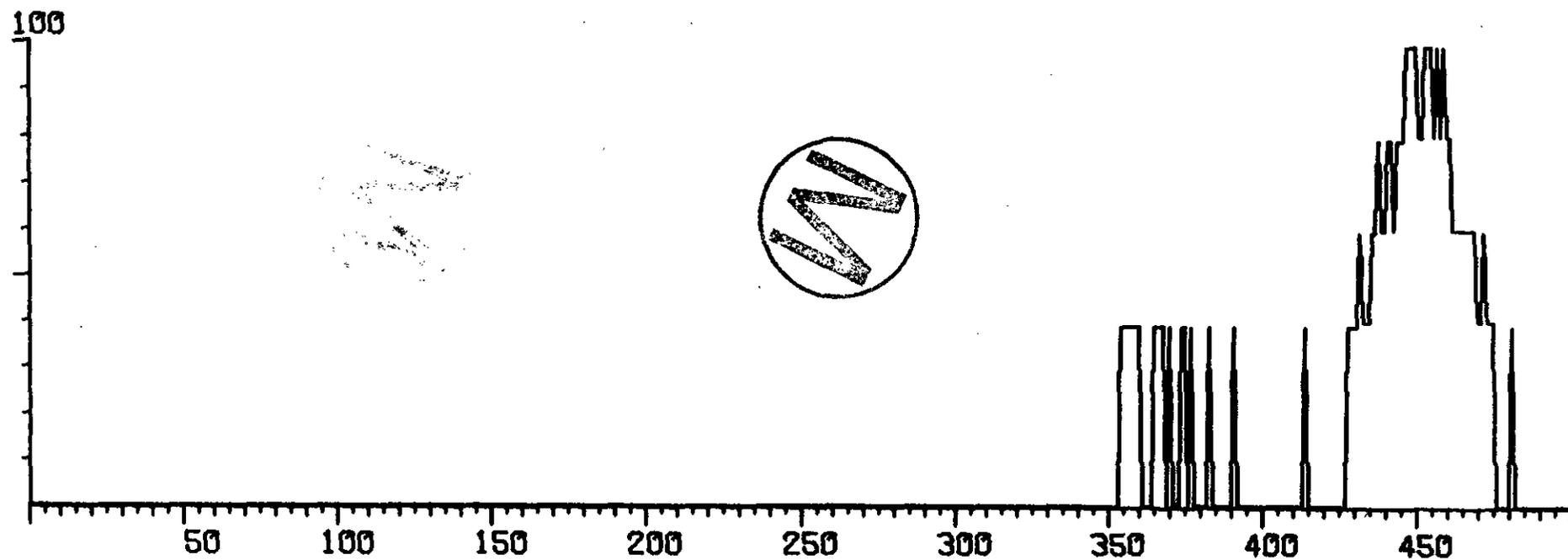
SALT SAMPLE   2821.0
            TOTAL ION CHROMATOGRAM
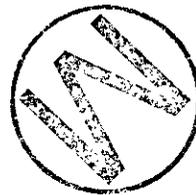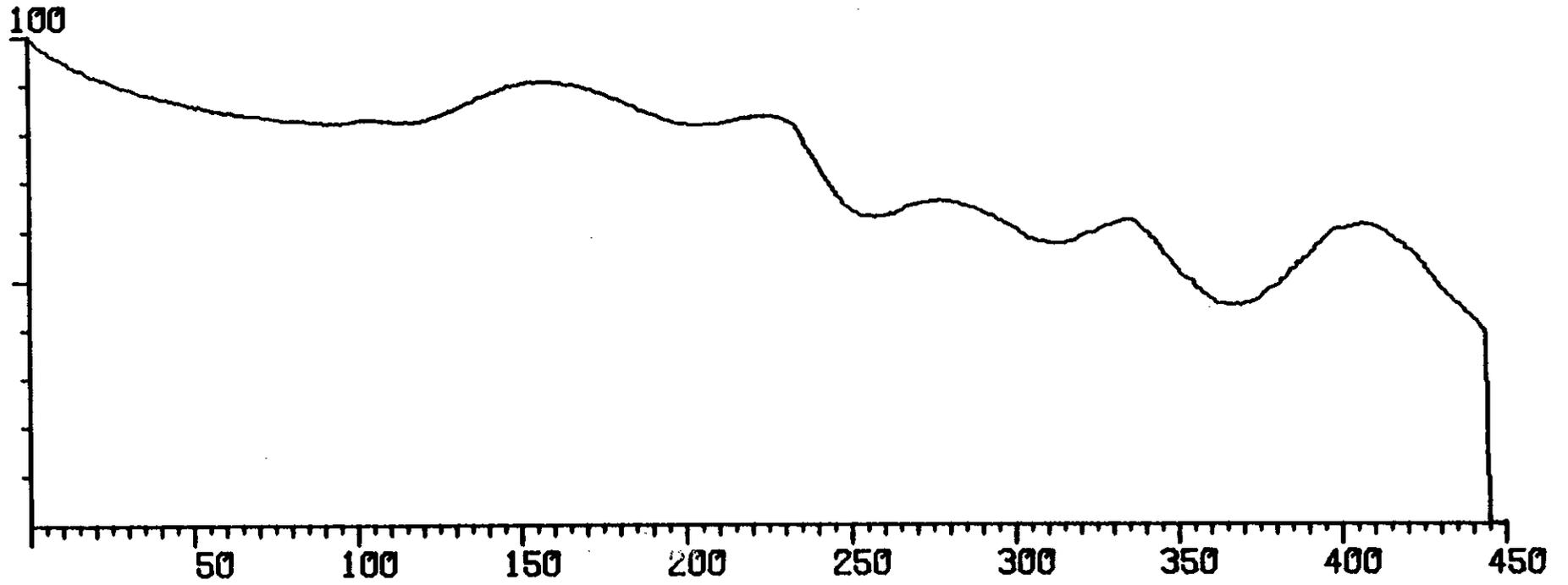
SALT SAMPLE   2821.0
            MASS 14 SEARCH X3
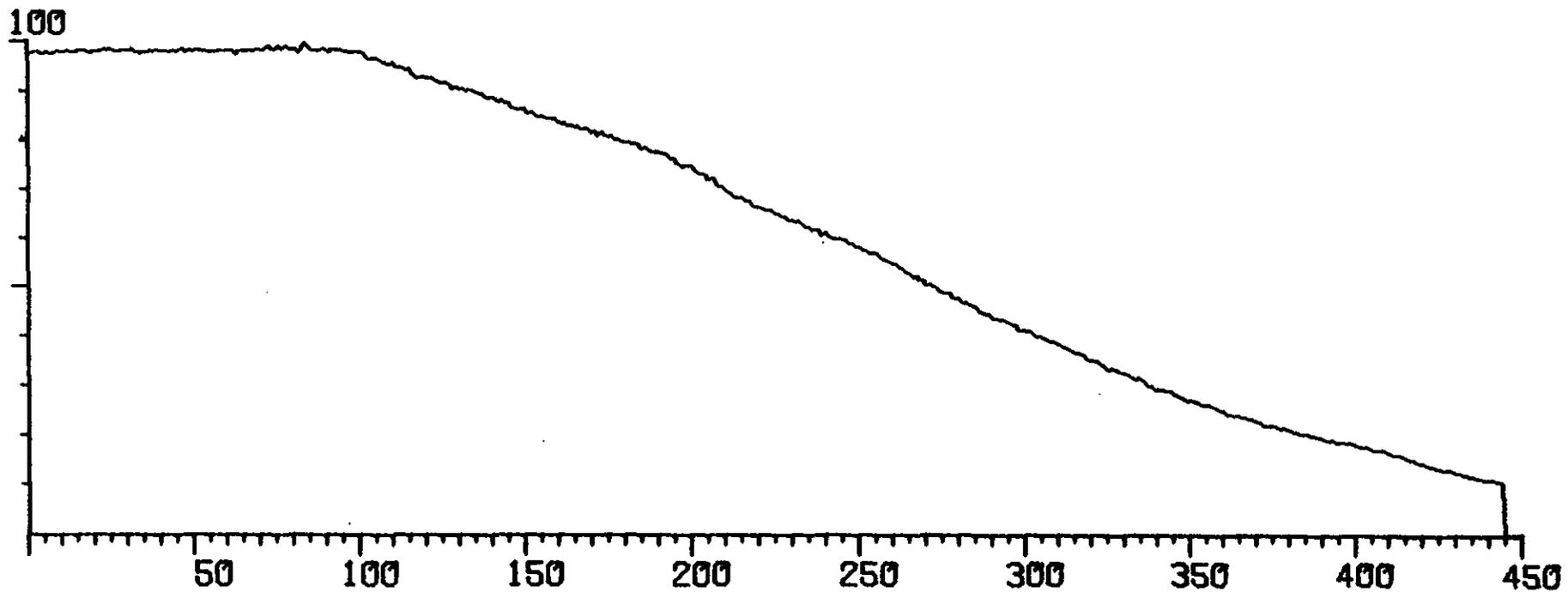
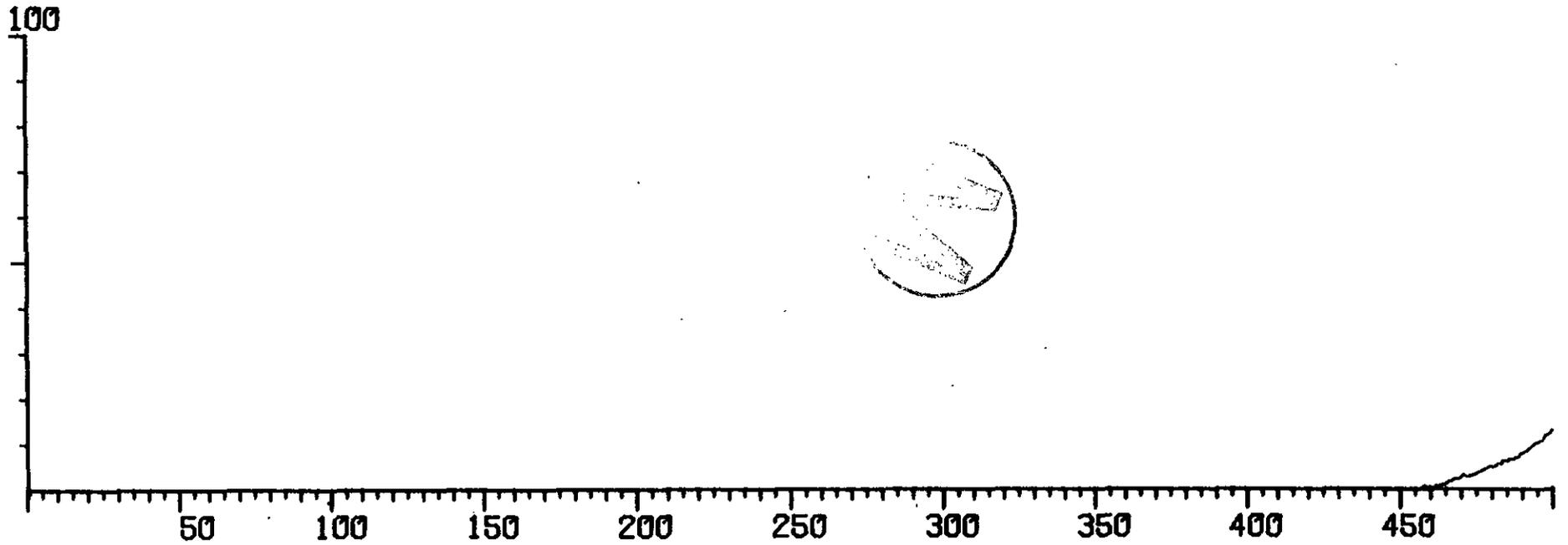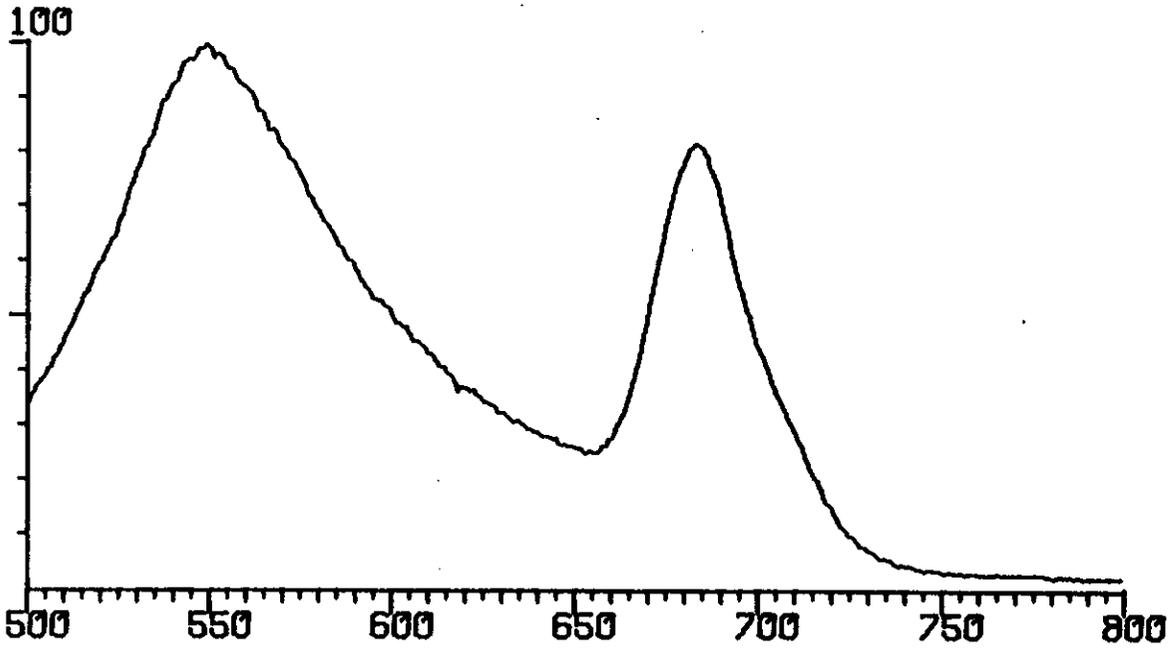SALT SAMPLE   2821.0
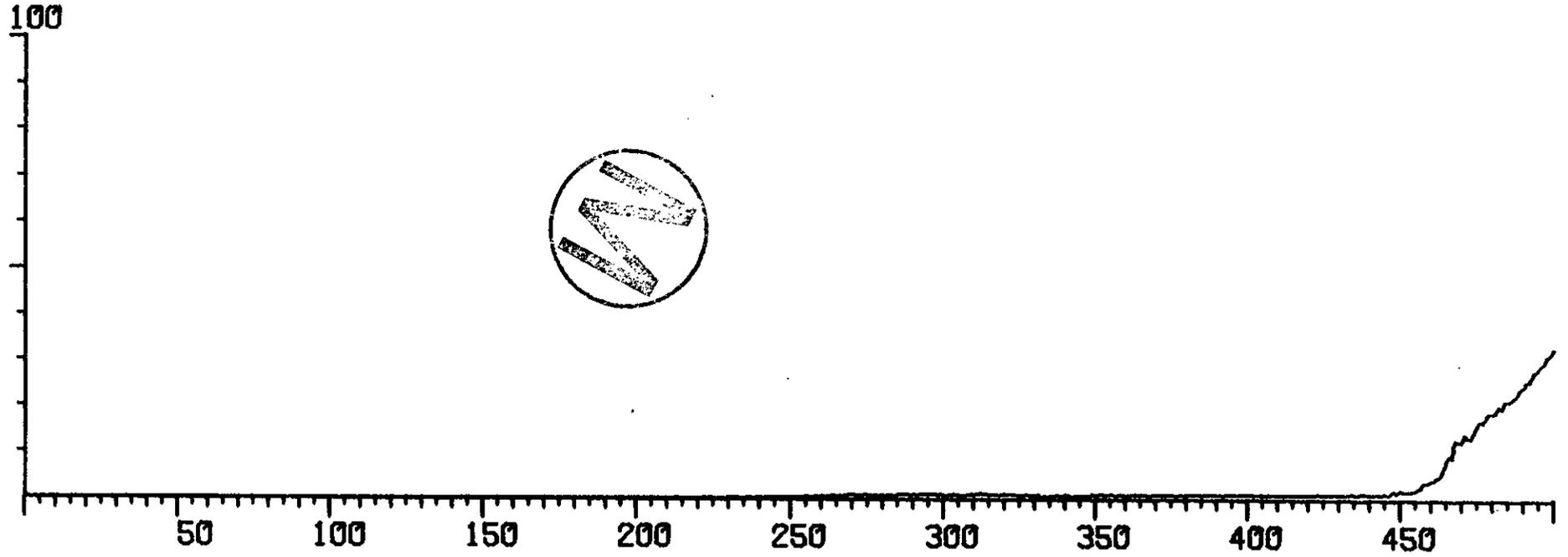
MASS 18 SEARCH X4
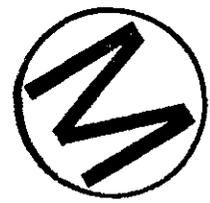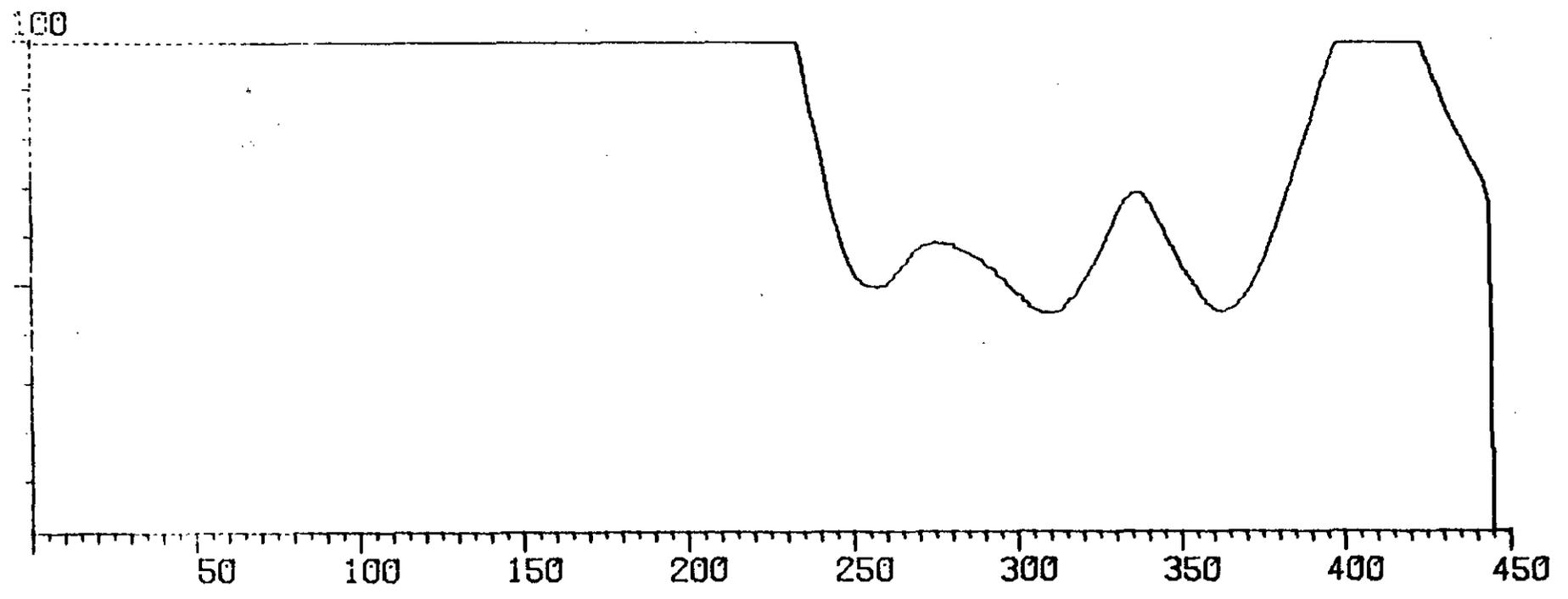
SALT SAMPLE   2821.0
        MASS 28 SEARCH X4
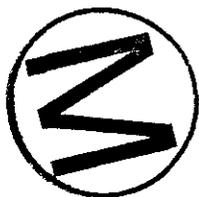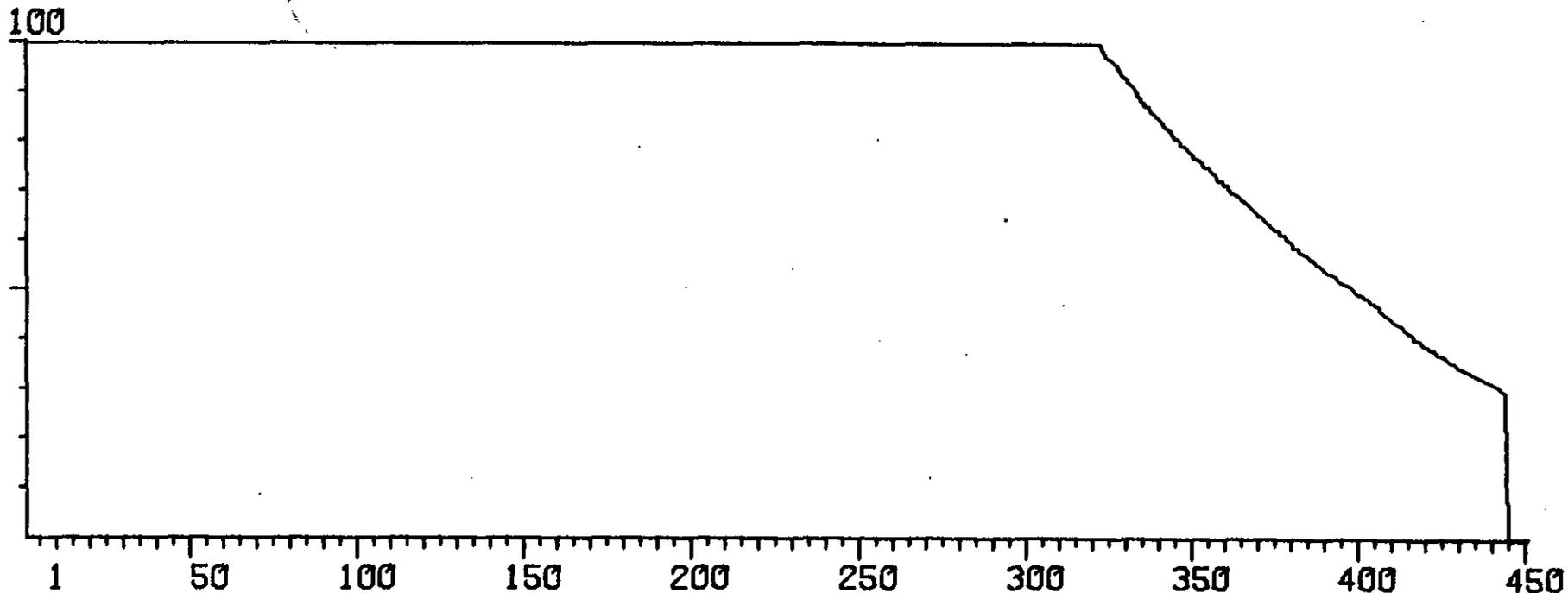
SALT SAMPLE   2821.0
        MASS 32 SEARCH X4
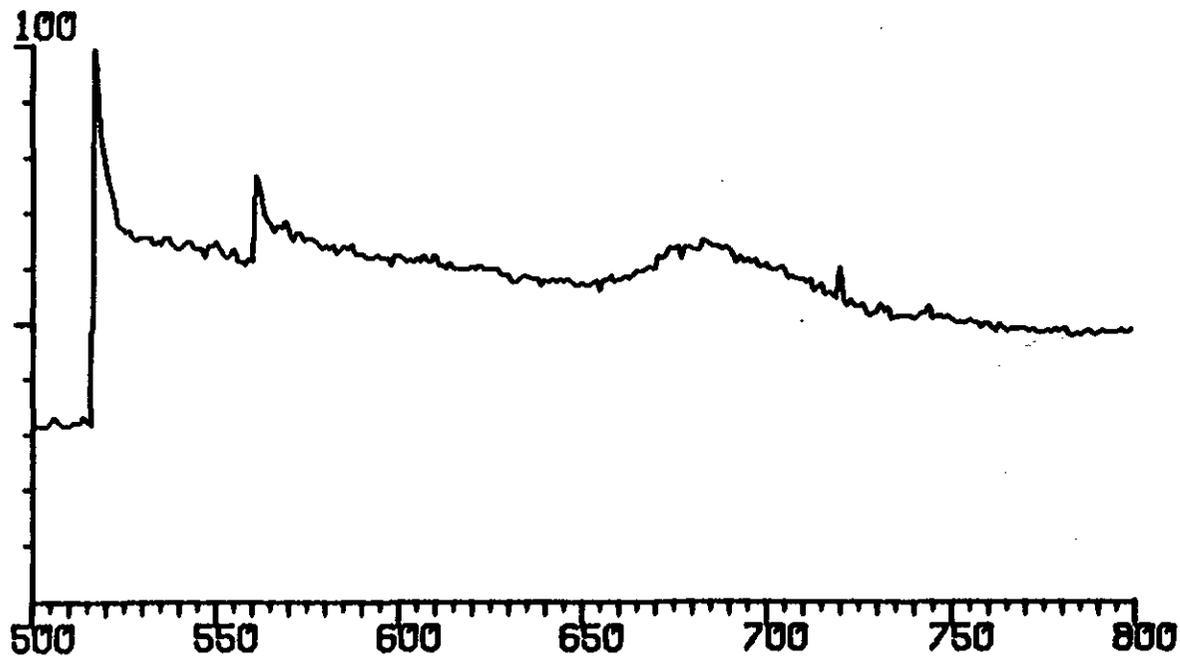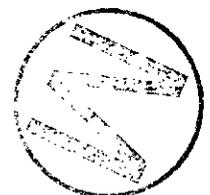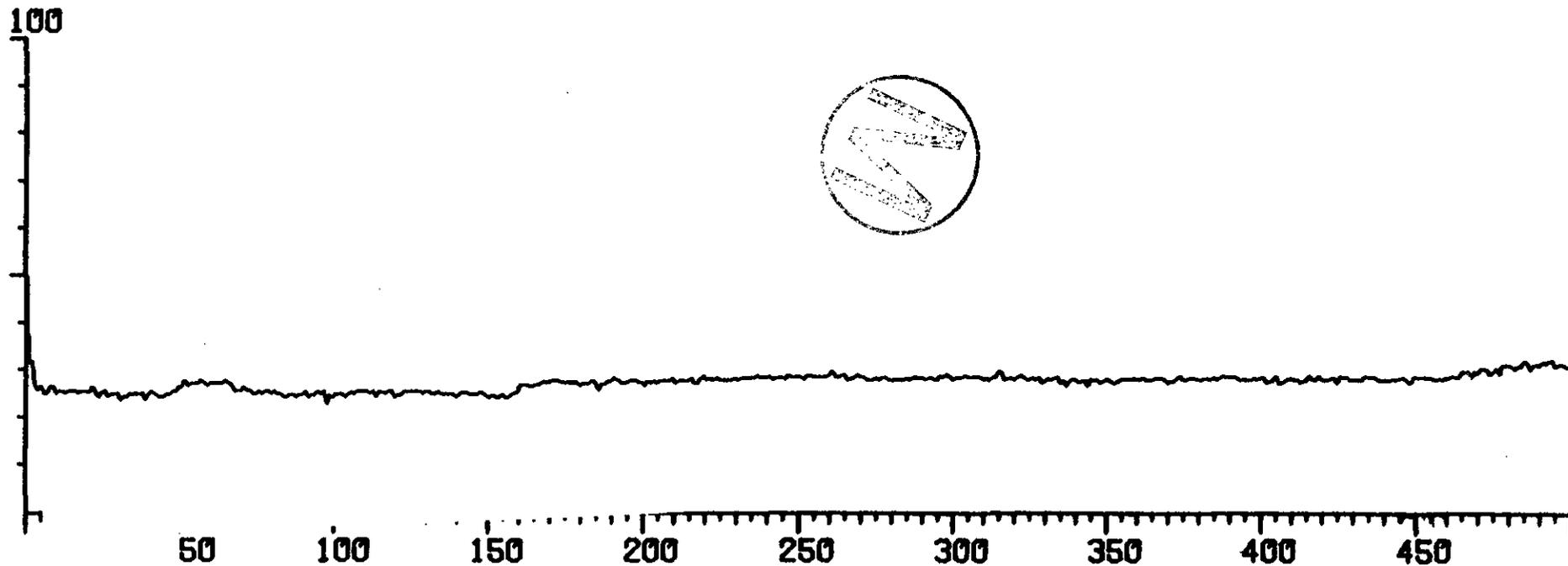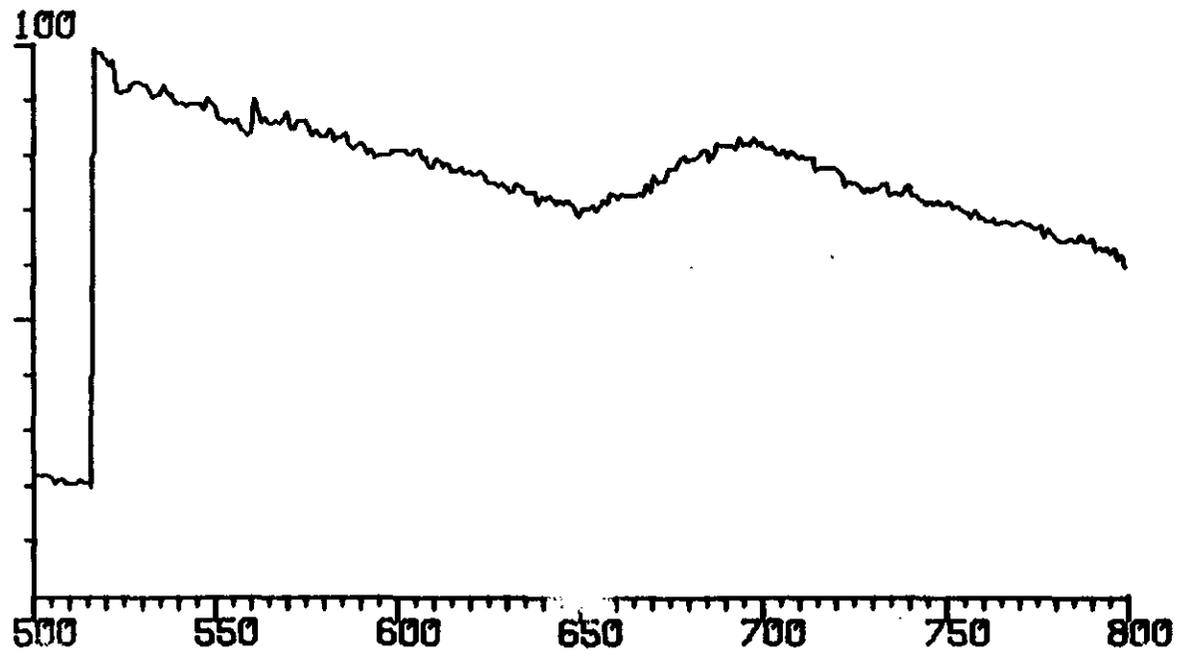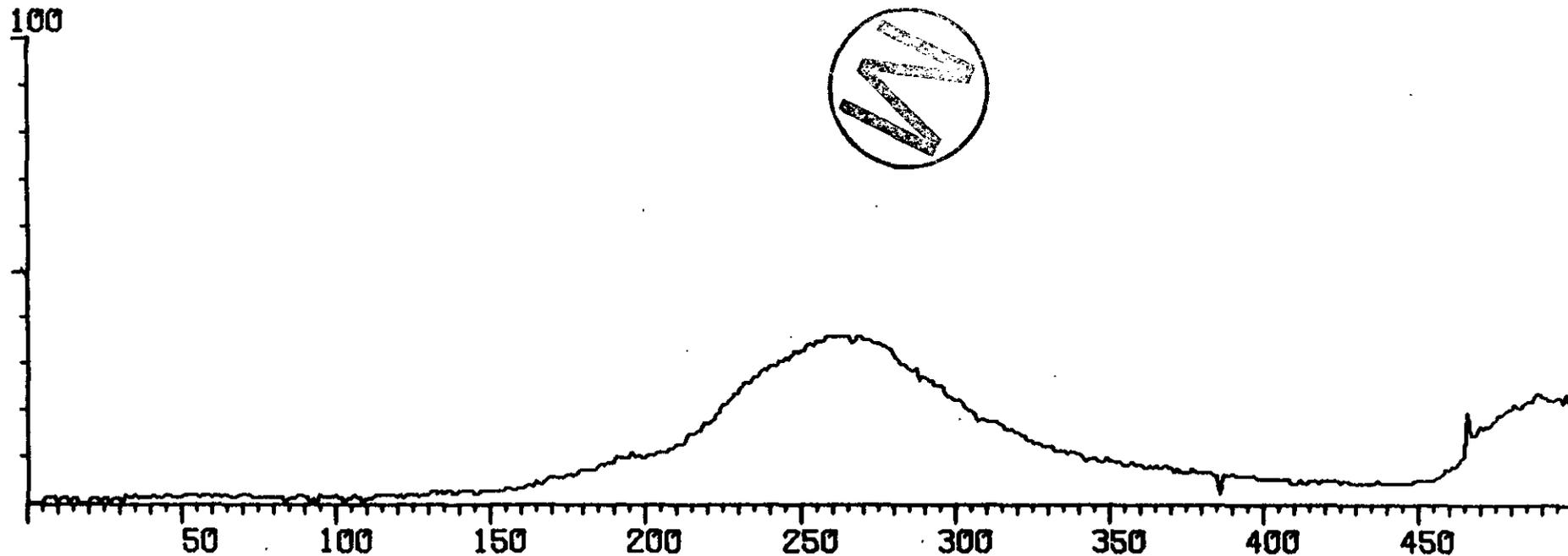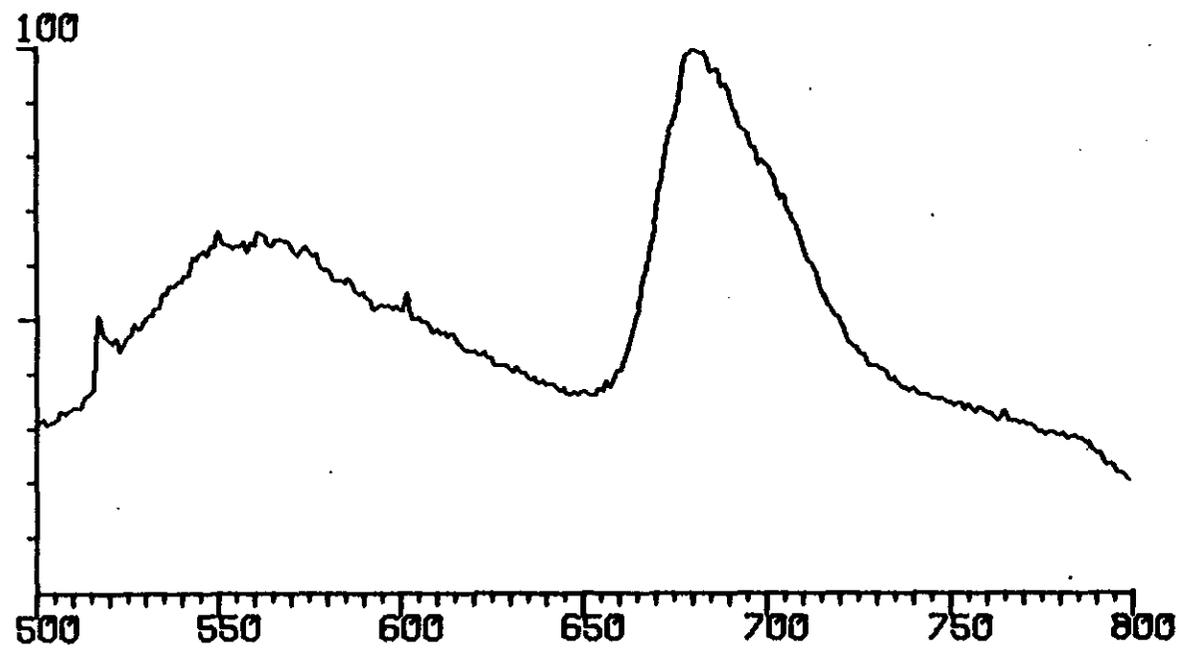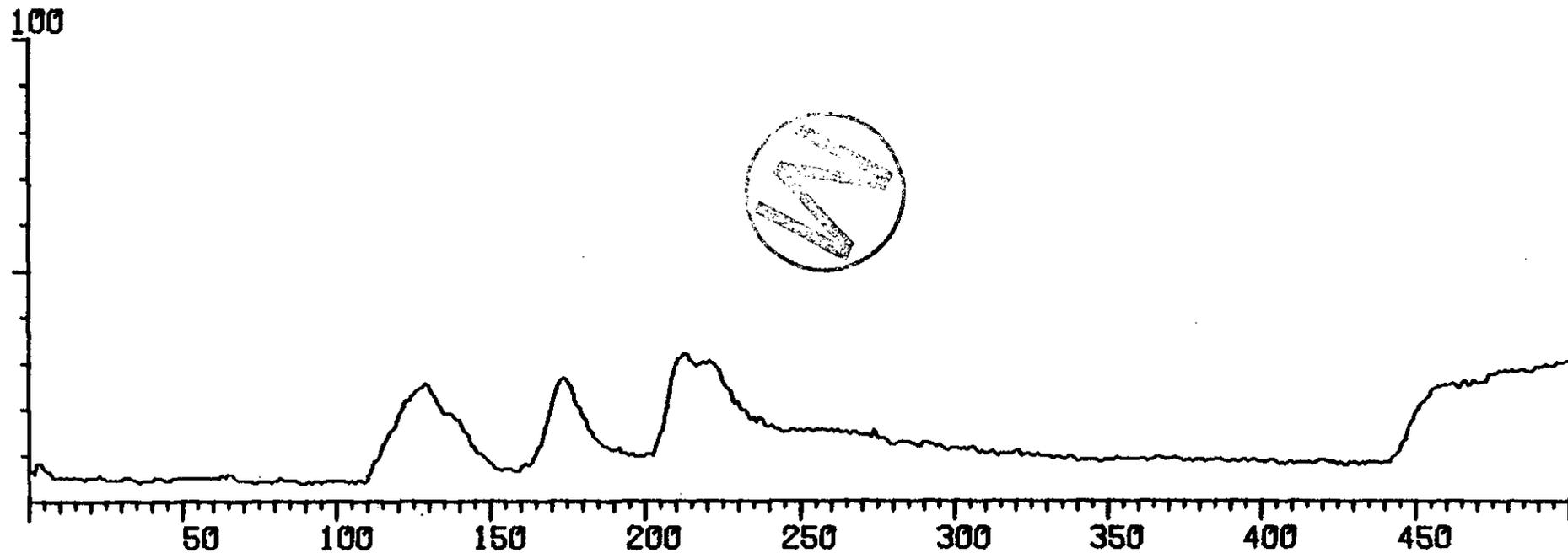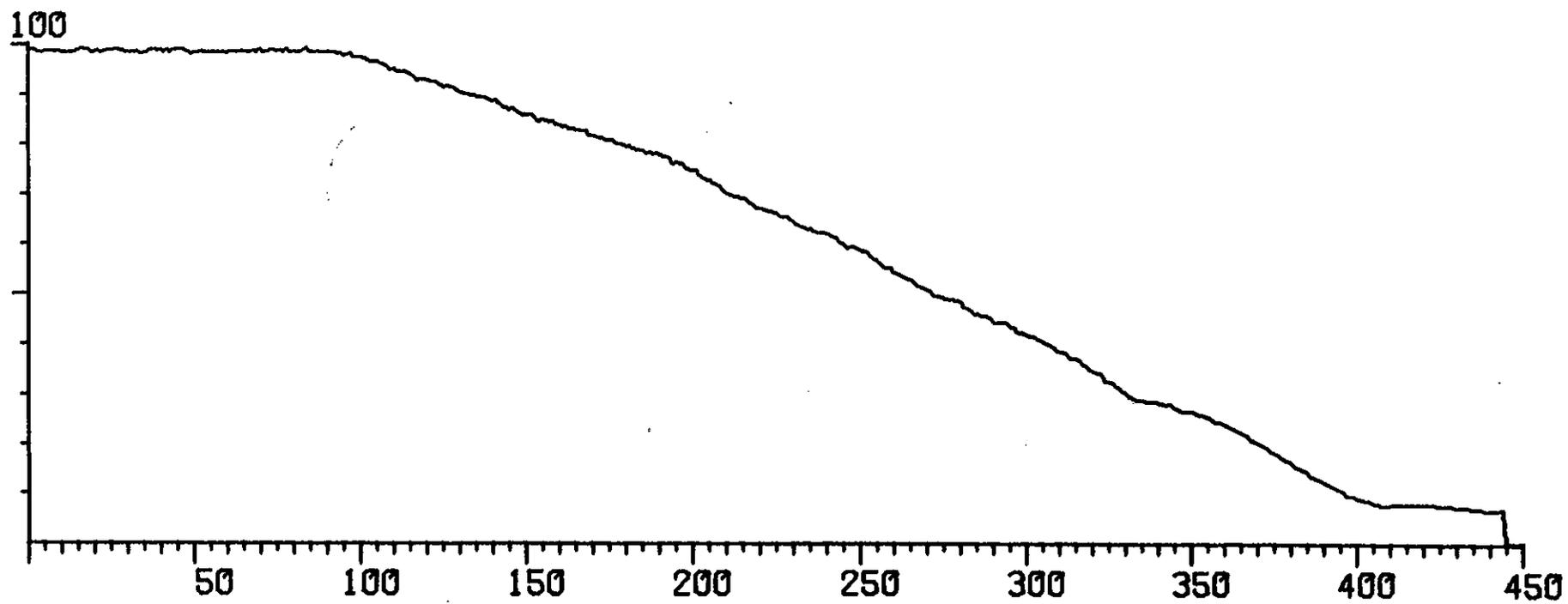
SALT SAMPLE   2821.0
                MASS 36 SEARCH X2
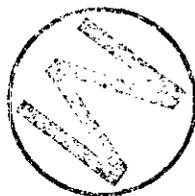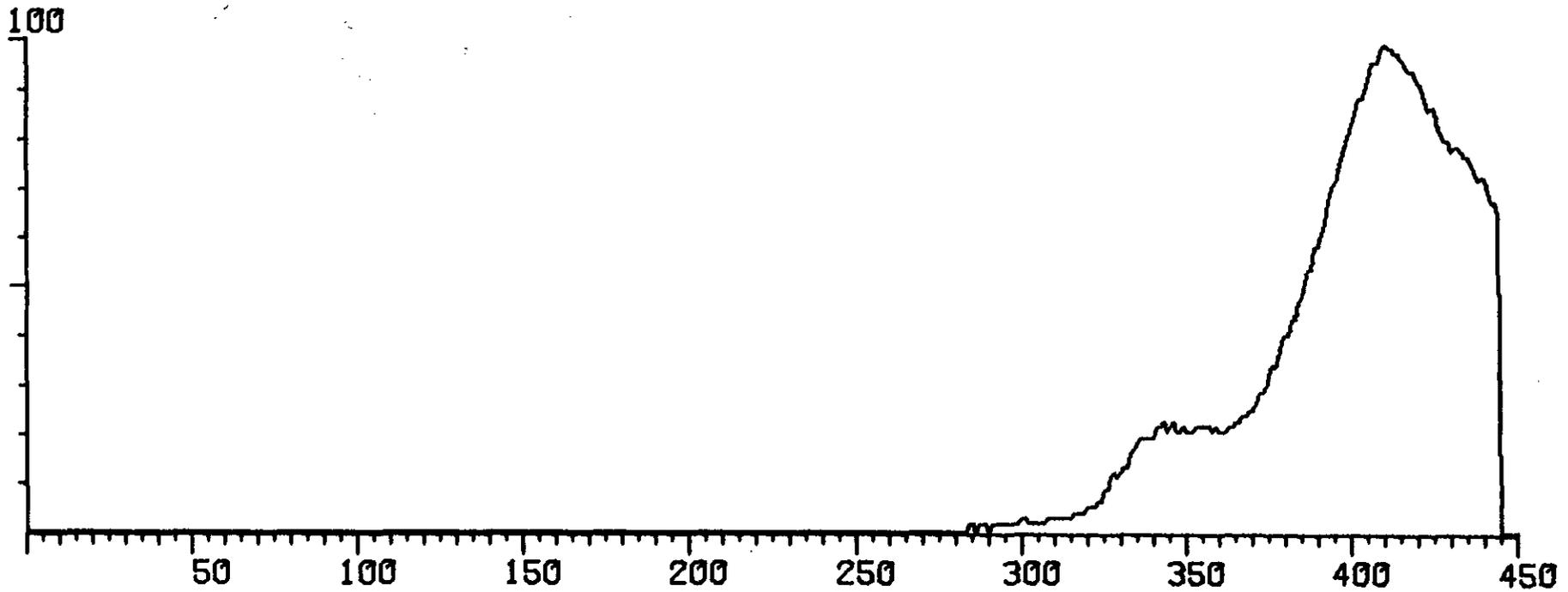
SALT SAMPLE   2821.0

MASS 44 SEARCH X2
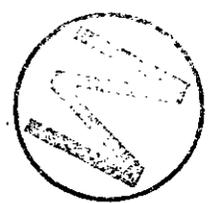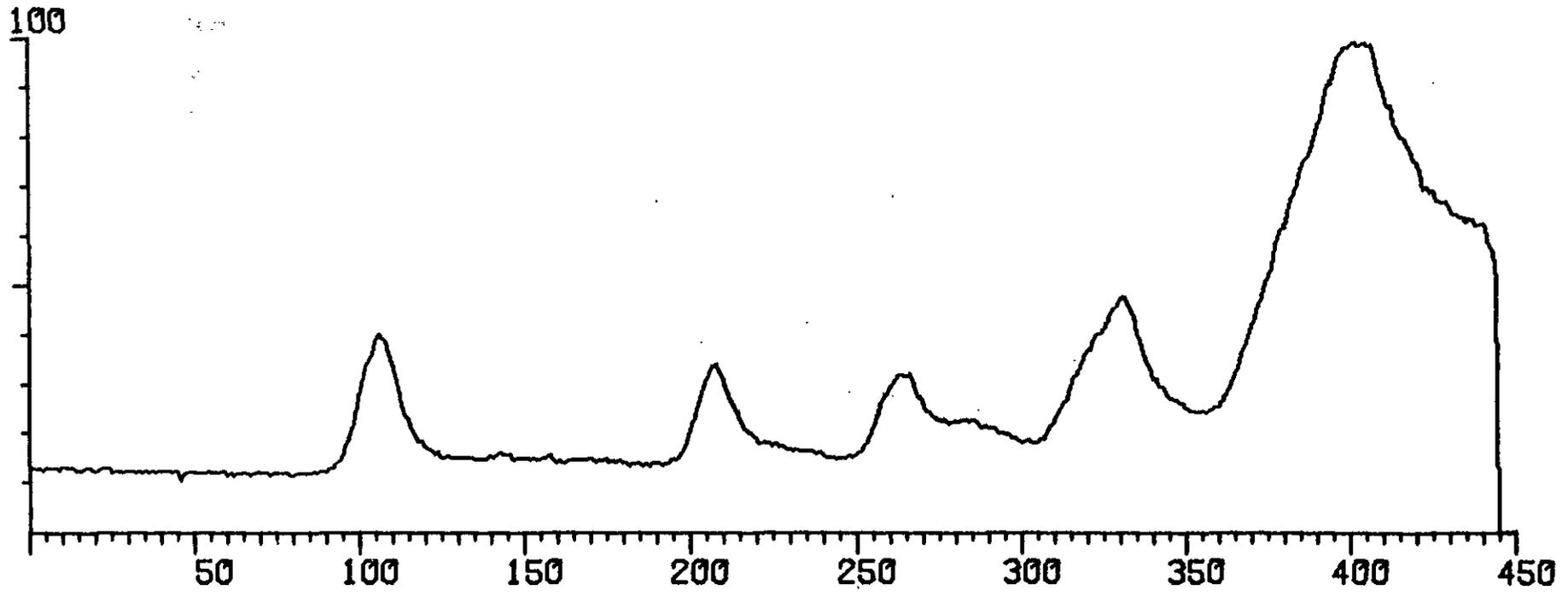
APPENDIX 7.F. Analytical Precision. (Ref. Sec. 7.5)

1. General statement concerning sample sizes, weighing errors, etc.

The sample weights used in this study ranged from approximately 0.5 to 2.5 grams, but typically were from 1.5 to 2.0 grams. The sample bottles were weighed before each new batch of samples was prepared, and both the sample bottles and the combined sample bottle and sample were weighed two times or more. Replicate weighings errors should result in a precision of no worse than $\pm$0.1 to 0.2 weight %.

2. Results of triplicate analyses on selected samples.

Triplicate analyses were performed on separate splits taken from the sample vial using different initial sample weights each time. The results are tabulated below:

Sample	Weight Losses Determined (Wt. %)			Mean to Nearest 0.1%
7-1044	0.1	0.1	0.3	0.2
7-1296	1.3	0.9	1.3	1.2
8-1794	1.2	1.4	1.2	1.3
8-1986	0.0	0.0	0.1	0.0
8-2563	2.0	2.3	1.9	2.1
8-2616	0.0	0.0	0.0	0.0

The results of these analyses indicate that most weight losses determined from replicate samples (taken from the same sample bottle) fall within ±0.2 to 0.3 of the mean value. Because of vertical and lateral variation in mineral content typical of sedimentary rocks the range anticipated for different samples of the same core would be larger, but it is not possible to estimate the precision under such non-reproducible conditions. In the case of relatively uniform samples (such as some halite or anhydrite beds) the precision might be anticipated to remain fairly good. On the other hand, samples which contain varying amounts of clays or other hydrous minerals might be expected to show much larger variations in their weight losses upon heating.
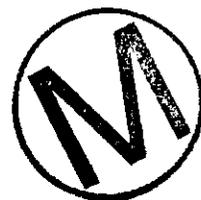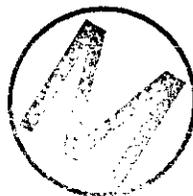
APPENDIX 7.G. Weight Loss Data for Cores #7 and #8, Carlsbad, New Mexico, Including Comparisons with the Data of Section 7.3. (Ref. Sec. 7.5)

1. Core #7.

Sample (ft)	Depth (m)	Weight Losses at 102 $\pm$ 5°C (Wt.%)	@70°C	Data from Section 7.3 To 200°C	To Above 400°C
1044	318.2	0.1	0.10	0.10	0.10
1107	337.4	1.0	0.12	0.22	1.99
1171	356.9	0.1	0.14	0.14	0.80
1221	372.2	0.2	0.30	0.44	0.51
1342	409.0	0.2	0.27	0.27	0.43
1402	427.3	0.1	0.19	0.19	0.31
1468	447.4	2.2	1.27	1.73	2.59
1533	467.3	0.1	0.22	0.23	0.47
1615	492.3	0.2	0.34	0.43	0.80
1697	517.2	3.4	0.82	0.82	0.85
1755	534.9	0.2	0.19	0.23	0.28
1952	595.0	0.0	0.14	0.14	0.58
1954	595.6	0.6	0.32	0.32	0.41
1958	596.8	0.2	0.20	0.20	0.32
1960	597.4	0.1	0.07	0.39	0.39
1967	599.5	0.1	0.20	0.20	1.13
1969	600.2	0.2	0.43	0.51	0.71
1973	601.4	0.3	0.19	0.26	0.40
1975	602.0	0.2	0.17	0.17	0.24
1978	602.9	0.8	0.36	0.40	1.67
1983	604.4	0.0	0.29	0.32	0.51
1986	605.3	0.0	0.10	0.10	0.10
1993	607.5	0.0	0.19	0.24	1.04
2702	823.6	0.0	0.24	0.27	0.39
2716	827.8	0.2	0.22	0.22	0.26
2736	833.9	0.1	0.08	0.08	0.11

APPENDIX 7.G. Weight Loss Data, Continued.

2. Core #8

Sample (ft)	Depth (m)	Weight Losses at 102 ± 5°C (Wt.%)	Data from Section 7.3		
			@70°C	To 200°C	To Above 400°C
1391	424.0	0.1	0.04	0.07	0.26
1495	455.7	0.1	0.05	0.08	0.08
1573	479.5	0.2	0.04	0.33	1.18
1652	503.5	0.1	0.09	0.09	4.52
1705	519.7	0.0	0.15	0.17	0.32
1769	539.2	0.1	0.09	0.15	0.35
1787	544.7	0.2	0.32	0.36	0.59
1794	546.8	1.4	0.44	0.71	5.41
1804	549.9	0.0	0.02	0.07	0.07
1829	557.5	0.1	0.16	0.39	0.39
1838	560.2	0.3	0.39	0.39	0.39
1857	566.0	0.1	0.07	0.07	0.10
1875	571.5	1.2	0.22	0.64	0.64
1884	574.2	0.9	0.36	0.36	0.80
1890	576.1	0.1	0.05	0.05	0.13
1894	577.3	0.4	0.30	0.30	0.30
1899	578.8	0.1	0.16	0.16	0.16
1900	579.1	0.1	0.17	0.17	0.81
1905	580.6	1.0	0.36	0.36	0.62
1911	582.5	0.2	0.06	0.06	0.10
1913	583.1	0.2	0.11	0.14	0.21
1916	584.0	0.0	0.13	0.13	0.25
1923	586.1	0.1	0.19	0.19	0.49
1930	588.3	0.4	0.05	0.05	0.47
1933	589.2	0.1	0.19	0.28	0.28
1938	590.7	0.0	0.13	0.27	0.49
1953	595.3	0.1	0.05	0.10	0.42
1967	599.5	0.5	0.28	0.32	0.52
1986	605.3	0.0	0.07	0.07	5.81

APPENDIX 7.G. Weight Loss Data, Continued.

2. Core #8

Sample (ft)	Depth (m)	Weight Losses at 102 ± 5°C (Wt.%)	@70°C	Data from Section 7.3 To 200°C	To Above 400°C
2006	611.4	0.1	0.20	0.20	0.66
2017	614.8	0.2	0.22	0.24	0.41
2039	621.5	0.1	0.21	0.26	1.02
2050	624.8	0.0	0.11	0.11	0.79
2068	630.3	0.1	0.04	0.04	0.14
2084	635.2	0.3	0.17	0.22	0.71
2130	649.2	0.0	0.11	0.18	0.28
2162	659.0	0.1	0.14	0.14	0.62
2217	675.7	0.1	0.04	0.04	0.44
2280	694.9	0.0	0.19	0.19	0.27
2326	709.0	0.1	0.11	0.14	0.70
2366	721.2	1.9	0.43	0.43	6.84
2427	739.7	0.0	0.03	0.03	0.43
2460	749.8	0.0	0.17	0.22	0.37
2519	767.8	0.0	0.08	0.08	0.14
2563	781.2	2.3	1.87	2.13	2.24
2616	797.4	0.0	0.21	0.21	0.27
2666	812.6	0.0	0.25	0.25	0.73
2707	825.1	0.6	0.16	0.16	1.66
2758	840.6	0.0	0.11	0.11	0.16
2779	847.0	0.2	0.21	0.21	0.21
2793	851.3	0.0	0.18	0.18	0.18
2803	854.4	0.0	0.10	0.12	0.14
2809	856.2	0.0	0.15	0.24	0.48
2821	859.8	0.2	0.18	0.18	0.36
2879	877.5	0.2	0.06	0.06	3.37
2948	898.6	0.1	0.20	0.22	0.26

APPENDIX 7.G. Weight Loss Data, Continued.

3. Weight losses determined at higher temperatures for selected samples from Core #8.

Sample (ft)	Depth (m)	Weight Losses 102 $\pm$ 5°C	($\pm$ 0.1 to 0.2 Weight %) 170 $\pm$ 5°C	300 $\pm$ 10°C
1804	549.9	0.0	0.0	0.2
1829	557.5	0.1	0.2	0.4
1875	571.5	1.2	1.8	2.2
1884	574.2	0.9	1.0	1.5
1923	586.1	0.1	0.1	0.2
1967	599.5	0.5	0.5	1.4
2050	624.8	0.0	0.0	0.7
2366	721.2	1.9	2.0	7.4
2948	898.6	0.1	0.0	0.2

Note: In this set of weight loss determinations, one split from each sample selected was heated to successively higher temperatures.

APPENDIX 7.H. Mineralogy and Petrology of Core #7 and #8.

I.   Abbreviations used.

Minerals   In the summaries which follow the approximate
amounts of the minerals present are indicated
by upper and lower case letters. AN + MAJOR
(> 25%); An + Minor (5 to 25%); an = trace
(< 5%. Often less than 1%)

AN	=	Anhydrite	HA	=	Halite
CAR	=	Carnallite	KAIN	=	Kainite
CEL	=	Celestite	PH	=	Polyhalite
CSSM	=	Clay and silt-sized	QTZ	=	Quartz
		minerals (often magnesitic)	SYL	=	Sylvite
FELD	=	Feldspar(s)			
GLAU	=	Glauconite			
GYP	=	Gypsum			

Grain Sizes

fg	=	Fine grained (< 1 mm)
mg	+	medium grained (1 mm to 1 mm)
cg	=	coarse grained (> 1 cm)

With the exception of halite, which shows a wide range of
grain sizes, most of the minerals observed are fine grained.

APPENDIX 7.H.   Mineralogy and Petrology, Continued.

2. Core #7
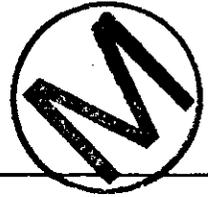
Depth (ft)	Description
1044	cg HA with An and cssm in patches and stringers. An also in isolated crystals and crystal clusters.
1107	fg to mg HA with mg gyp which is partially replaced by An. fg to mg ph in patches and stringers along with cssm.
1171	Appears macroscopically bedded. Primarily vuggy AN. Voids filled with radial ("starbursts") of ph and also with ha and cssm.
1221	cg HA. Patches and stringers filled with ph (radial in part) and an. Some evidence of ph replacing an.
1296	mg to cg HA with Cssm, ph and possibly some an in patches and stringers. Some of the Cssm appears intergranular among HA crystals. May represent subaerial deposition.
1342	mg to cg HA with ph and cssm in patches and stringers.
1402	mg HA. ph (radial in part) and an in patches and stringers and as crystal clusters.
1468	mg HA with much intergranular Cssm. Possibly represents subaerial deposition. Trace an and ph as isolated crystals and crystal clusters. Some authigenic quartz and feldspar.
1533	mg to cg HA with poorly preserved hoppers. Ph in patches and stringers, some possibly intergranular with HA. Trace Cssm associated with the Ph.
1615	mg to cg HA with hoppers. fg to mg An and ph in patches and stringers. ph appears to be replacing An, some of which may be psuedomorphic after gypsum.
1697	Appears to be macroscopically bedded. Large, nodular masses of AN (possibly pseudomorphic after gypsum nodules) with voids filled with Cssm, Ph, ha and syl. Ph associated with Cssm; syl associated with Ph.

APPENDIX 7.H. Mineralogy and Petrology, Continued.
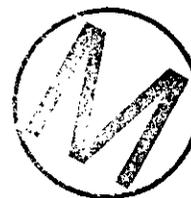
2. Core #7, continued

Depth (ft)	Description
1755	mg to cg Ha with poorly preserved hoppers. ph and an in patches and stringers. ph replaces an in part. Perhaps a little syl is present.
1952	Appears macroscopically bedded. mg to cg HA with hoppers. Ph and an in patches, stringers and as isolated crystals and clusters. Ph replacing an in part.
1954	mg to cg HA with Cssm in patches and stringers. Some Cssm is intergranular with HA. May represent subaerial deposition. Some isolated crystals and clusters of ph associated with Cssm.
1958	mg to cg HA. cssm in patches and stringers. (Some cssm may be intergranular). ph and possible an in patches and stringers associated with cssm and also in isolated crystals and clusters.
1960	Possibly macroscopically bedded. fg to cg HA with hoppers. Intergranular Cssm with associated authigenic qtz and feld. May represent suberial deposition. Some isolated crystals and clusters of ph and an.
1967	mg to cg HA with poorly preserved hoppers. ph in patches and stringers shows some evidence of flow or deformation. A few isolated crystals and clusters of an.
1969	fg to cg HA with poorly preserved hoppers. Intergranular Cssm with associated authigenic qtz and feld. Isolated crystals and clusters of an and lesser ph.
1973	cg HA with very few patches and stringers of cssm, ph and even some ha crystals.
1975	cg HA with ph, cssm and an in patches and stringers. ph appears to be replacing an. ph associated with cssm.
1978	mg to cg HA with intergranular Cssm and ph. May represent subaerial deposition. Some ph in patches and stringers and as isolated crystals and clusters. Some ph is mg. Isolated crystals of an are associated with the ph.

APPENDIX 7.H. Mineralogy and Petrology, Continued.

2. Core #7, continued

Depth (ft)	Description
1983	mg to cg HA with hoppers. Ph and an in patches and stringers Ph replacing an.
1986	mg to cg HA with small amounts of ph, an and cssm in patches and stringers.
1993	cg HA with hoppers. Ph and an in patches and stringers. (Some Ph and an may be intergranular). Ph appears to replace an.
2702	mg to cg HA with An and cssm in patches and stringers.
2716	mg to cg HA with hoppers. an and cssm in patches and stringers, some possibly intergranular with HA. May represent subaerial deposition.
2736	mg to cg HA with hoppers. An and cssm in patches and stringers, some possibly intergranular with HA. May represent subaerial deposition.
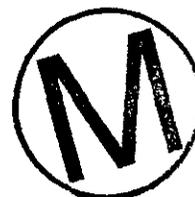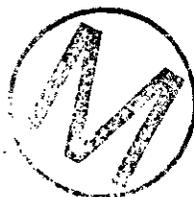
APPENDIX 7.H.   Mineralogy and Petrology, Continued.

3.   Core #8

Depth (ft)	Description
1391	cg HA with ph and possibly some an in patches and stringers.
1495	mg to cg HA with hoppers. Ph associated with cssm in patches and stringers. Some may be intergranular. Ph shows evidence of flowage or deformation.
1573	Appears macroscopically bedded. mg to cg HA with Ph and fg to mg An in large patches. Ph appers to be replacing An.
1652	Appears macroscopically bedded. fg to mg AN with Ph. mg Ha in patches or voids. Some syl associated with Ph. Algal laminations may be present in the An.
1705	fg to cg HA with hoppers. Ph in patches and stringers; some may be intergranular. Small amount of an associated with Ph.
1769	mg to cg HA with poorly preserved hoppers. fg to mg Ph in patches and stringers and intergranular with HA. In part, Ph appears to be replacing HA. Some gyp (?) may be present in very small amounts. There also may be trace amounts of cel (?).
1787	mg to cg HA with hoppers. Ph in patches and stringers and some intergranular with HA. Some mg, acicular an crystals and mg, acicular cel (?) crystals noted. There may be a small amount of gyp (?) present in this slide.
1794	Appears macroscopically bedded. fg to mg HA with hoppers. CSSM is intergranular with HA. May represent subaerial deposition. Also noted: a few isolated ph crystals, some authigenic qtz and feld, and a trace of glau (?).
1804	fg to cg HA with poorly presrved hoppers. CSSM is intergranular with HA. May represent subaerial deposition. ph in isolated crystals and cluters.
1829	cg HA with hoppers. Cssm in patches and stringers and some intergranular. Possible subaerial deposition. Trace of ph.

APPENDIX 7.H.   Mineralogy and Petrology, Continued.

3.   Core #8, continued

Depth (ft)	Description
1838	fg to mg HA with poorly preserved hoppers. Cssm intergranular with HA. Ph and An in patches and stringers and associated wtih the Cssm. May represent subaerial deposition.
1857	cg HA with poorly preserved hoppers. ph along stringers.
1875	Apperas macroscopically bedded. fg to mg HA intergranular with CSSM. May represent subaerial deposition. Isolated crystals and clusters of ph and fg to mg an. Traces of authigenic qtz and feld.
1884	fg to mg HA with hoppers, intergranular with CSSM. May represent subaerial deposition. Some isolated crystals and clusters of fg to mg an (some may be pseudomorphic after gyp). Possible trace of syl.
1890	mg to cg HA with hoppers. ph and an in patches and stringers.
1894	mg to cg HA with poorly preserved hoppers. ph and an in patches and stringers. cssm in patches and stringers with authigenic qtz and feld.
1900	fg to cg HA with hoppers. Ph, An and cssm in patches and stringers and some intergranular with HA. May represent subaerial deposition. Some Ph appears to be deformed or to have flowed.
1905	mg to cg HA with patches and stringers and some intergranular Cssm. (May represent subaerial deposition). Scattered, isolated crystals of ph and an.
1910	mg to cg HA with poorly preserved hoppers. Ph, an and cssm intergranular with HA and in patches and stringers. Ph apperas to be replacing an.
1911	mg to cg HA with hoppers. Ph, An and cssm in patches and stringers, some intergranular with HA. (May represent subaerial deposition). Ph appears to be replacing an.

APPENDIX 7.H. Mineralogy and Petrology, Continued.

3. Core #8, continued

Depth (ft)	Description
1913	fg to cg HA with intergranular Cssm. Inclusions of ha in Cssm. May represent subaerial deposition. Isolated crystals of ph. A few authigenic grains of qtz and feldspar.
1916	cg HA with poorly preserved hoppers. ph and an in patches and stringers.
1923	fg to cg HA with intergranular Cssm. May represent subaerial deposition. ph and an in patches and stringers and as isolated crystals. Trace authigenic feld.
1930	mg to cg HA with poorly presrved hoppers. Ph and an in patches and stringers, some as isolated crystals. cssm in patches and stringers. Possible trace gyp (?).
1933	cg HA with hoppers. cssm, ph and an in patches and stringers. Small amounts of authigenic qtz and feld (?).
1938	cg HA with poorly preserved hoppers. Ph and an in patches and stringers.
1953	fg to mg HA with hoppers. Cssm intergranular with HA and in patches and stringers. May represent subaerial deposition. Isolated crystals and clusters of ph and an.
1967	fg to cg HA with hoppers. Cssm intergranular with HA and in patches and stringers. May represent subaerial deposition. Isolated crystals and clusters of ph and an.
1986	Appears cross-bedded. PH with mg AN. Ph appeas to be replacing AN. Some fine laminations may be algal lamination or traces of cssm seams. ha in patches or filling void places.
2006	fg to cg HA with hoppers. Ph and an in patches and stringers. Trace of syl associated with Ph.

APPENDIX 7.H.   Mineralogy and Petrology, Continued.

3.   Core #8, continued
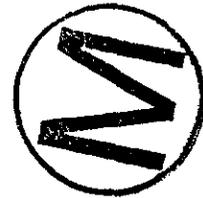
Depth (ft)	Description
2017	mg to cg HA with hoppers. Ph and an in patches and stringers. Ph appears to be replacing an. cssm in patches.
2039	mg to cg HA with hoppers. Ph and an with cssm in patches and stringers. Much of the Ph is radial. Ph appears to be replacing an.
2050	mg AN with numerous inclusions. AN apperas to be replacing ha with former cubic crystal outlines preserved.
2068	fg to cg HA. Patches and stringers and intergranular An, cssm and possible ph (?). May represent subaerial deposition.
2084	fg to cg HA with much intergranular Cssm, ph and poissible an (?). May represent subaerial deposition. Some Ha crystals appear to be growing in the Cssm.
2130	fg to mg HA with intergranular An and minor cssm. Some ph (?) may be replacing An.
2162	cg HA with intergranular Cssm and Ph. May represent subaerial deposition. Trace of an associated with Ph. Trace of syl associated with Ph.
2217	cg HA with patches and stringers of Ph and an. Some Ph radial and replacing an. Possible syl associated with Ph.
2280	fg to cg HA with patches and stringers of Ph and an. POssible trace of kain (?).
2326	fg to cg HA with poorly preserved hoppers. Cssm intergranular with HA. May represent subaerial deposition. Isolated crystals and clsuters of ph and an. Trace authigenic feld (?).
2366	Possibly macroscopically bedded. fg, radial PH with minor an. cssm scattered throughout.

APPENDIX 7.H. Mineralogy and Petrology, Continued.

3. Core #8, continued

Depth (ft)	Description
2427	fg to cg HA with poorly preserved hoppers. An and cssm in patchers, stringers, and intergranular with HA. May represent subaerial deposition, in part. Possible fossil (bryozoan) fragment.
2460	mg to cg HA with hoppers. Patches, stringers, and intergranular An and cssm. mg an in isolated crystals and clusters along the margins of the patches and stringers.
2519	mg to cg HA with poorly preserved hoppers. Patches, stringers and intergranular an ofter associated with cssm. May represent subaerial deposition.
2563	Possibly macroscopically bedded. Nodular AN with patches of Cssm. Possible mudcrack or burrow along one edge of slide normal to the bedding.
2616	fg to mg HA with poorly preserved hoppers. An intergranular with HA and as patches and stringers. May represent subaerial deposition.
2666	fg to cg HA with poorly preserved hoppers. Patches, stringers, and intergranular Cssm and an. May represent subaerial deposition.
2707	cg HA with hoppers. Patches and stringers of Cssm and an.
2758	fg to mg HA with poorly preserved hoppers. An associated wtih cssm in patches, stringers (some intergranular). May represent subaerial deposition. Some An in isolated crystals.
2779	fg to cg HA with hoppers. An and cssm in patches stringers and intergranular with HA. May represent subaerial deposition.
2793	fg to cg HA with trace evidence of hoppers. Intergranular AN and cssm. May represent subaerial deposition. Patches and stringers of An. Traces of ph and authigenic qtz (?).
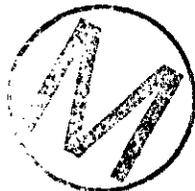
APPENDIX 7.H.   Mineralogy and Petrology, Continued.

3.   Core #8, continued

Depth (ft)	Description
2803	fg to cg HA with hoppers. Intergranular An and cssm. Some An in patches with possible ph (?). A few large, isolated crystals of An. May represent subaerial deposition.
2809	fg to mg HA with trace evidence of hoppers. An and cssm in patches, stringers and as intergranular material. May represent subaerial deposition.
2821	mg to cg HA with hoppers. Intergranular An and cssm. Some An in patches and stringers. May represent subaerial deposition.
2879	Possible macroscopic evidence of bedding. fg to mg HA with hoppers. Patches and stringers of An and cssm. POssible trance of ph (?). An unknown minerals with lower birefringence and positive relief was observed. Also present are some large, isolated crystals of An.
2948	Possible macroscopic evidence of bedding. mg to cg HA with hoppers. Some patches and stringers of An present. Some may be nodular (?) (possibly pseudomorphic after gyp). a few isolated crystals of ph (?) were noted.
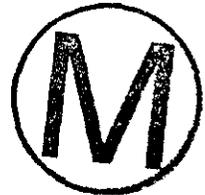
APPENDIX 8A

Analyses of Potash for Department of Energy
(then ERDA) and Industry Boreholes in the WIPP Area

Source is Table 3, John et al., 1978
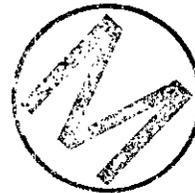
Table 3 - <u>Calculated mineral content of selected samples</u>
<u>from potassium-bearing intervals with summation</u>
<u>of percent K_2O as ore mineral</u>

[Drill-hole no.. Drill-hole designations. P. Energy Research and Development Administration:
FC. Farm Chemical Res. Dev. Corp: IMC, International Minerals and Chemical Corp:
NFU. Farmers Edu. and Coop. Union of America; D. Duval Sulphur and Potash Co.;
U. U.S. Potash Co., Inc. Arc, arcanite; Bs. bischofite. Bl, bloedite; C. carnallite;
Gl. glaserite: Gu. glauberite: Ka, kainite; Ki, kieserite; L, langbeinite; Le. leonite.
Lo. loewite. S, sylvite; Va. vanthoffite]

Drill-hole no.	Ore zone	Sample no.	Depths of interval (feet)	Thickness (feet)	Calculated minerals present (weight percent)					K_2O as ore minerals (percent)	Weighted average K_2O as ore mineral for all intervals in ore zone (feet and percent)
					Polyhalite	Halite	Sylvite	Langbeinite	Other minerals		
P-1	5	9	1440.47-1441.35	0.88	8	76	---	15.0	Tr/Ka[1]	3.4/L	
	5	10	1441.35-1442.30	0.95	9	86	---	4.4		1.0/L	
	5	11	1442.30-1443.50	1.20	---	79	---	---	14.0/Ka Tr/Bl[2]	---	
	5	12	1443.50-1444.35	0.85	---	95	---	2.34	---	0.53/L	
	5	13	1444.35-1445.30	0.95	1	79	---	17.07	---	3.87/L	4.83-1.67/L
P-2	10	14	1627.15-1628.35	1.20	1	39	---	39.9	1.9/Ka 5.0/Le	9.05/L	
	10	15	1628.35-1629.52	1.17	1	46	---	43.1	2.6/Ka 0.5/Le	9.78/L	2.37-9.41/L
	4	5	1802.70-1804.00	1.30	1	39	---	38.0	12.9/Ka	8.6/L	
	4	6	1804.00-1805.00	1.00	6	80	---	---	---	---	
	4	7	1805.00-1805.85	0.85	5	89	---	---	---	---	
	4	8	1805.85-1806.30	0.45	6	60	---	20.0	4.0/Ka 3.7/Le	4.54/L	3.60-3.67/L
	2	1	1833.08-1834.00	0.92	2	79	---	4.4	1.9/Ka	3.14/L	
	2	2	1834.00-1834.50	0.50	---	38	---	52.9	0.5/Ka	12.0/L	1.42-6.26/L
P-3	4	3	1596.30-1597.60	1.30	2	72	---	24.7	0.5/Ka	5.6/L	
	4	4	1597.60-1598.70	1.10	2	62	---	18.6	0.5/Ka	4.22/L	
	4	5	1598.70-1599.53	0.83	34	38	---	23.4	---	5.31/L	3.23-5.06/L
P-4	10	2	1572.60-1574.97	2.37	1	56	46.0	---	---	29.40/S	
	10	3	1574.97-1576.17	1.20	4	64	27.6	---	---	17.48/S	
	10	4	1576.17-1577.77	1.60	3	86	7.0	---	---	4.32/S	
	10	5	1577.77-1578.69	0.92	4	64	28.0	---	---	17.46/S	6.09-18.66/S
P-5	10	6	1546.69-1548.65	1.96	6	65	28.0	---	---	18.28/S	
	10	7	1548.65-1549.66	1.01	4	76	13.3	---	---	8.42/S	
	10	8	1549.66-1551.40	1.74	3	60	21.0	---	---	13.41/S	
	10	9	1551.40-1552.75	1.35	2	65	14.5	---	---	9.14/S	6.06-13.2/S
P-6	4	12	1476.00-1477.45	1.45	6	74	---	22.0	1.0/Ki	5.01/L	
	4	13	1477.45-1478.37	0.92	1	83	2.0	8.0	6.0/Ki	1.90/L 1.26/S	
	4	14	1478.37-1480.00	1.63	3	84	---	12.0	---	2.78/L	4.00-3.39/L
	2	18	1510.50-1511.32	0.82	1	37	2.0	54.0	6.0/Ki	12.31/L	
	2	19	1511.32-1512.10	0.78	---	53	---	42.0	---	9.65/L	
	2	20	1512.10-1513.05	0.95	7	79	3.0	1.0	8.6/Ka	0.19/L	2.55-6.18/L
P-7	4	2	1479.73-1481.20	1.47	2	65	1.0	29.0[4]	---	6.53/L[4]	
	4	3	1481.20-1483.00	1.80	---	89	2.0	3.0[4]	---	0.75/L[4]	
	4	4	1483.00-1483.43	0.48	3	69	2.0	3.8	5.7/Ka 1.0/Le 1.0/Bl	3.8/L	3.75-3.41/L
P-8	10	2	1363.70-1365.00	1.30	---	52	29.0	25.0	---	18.45/S 5.62/L	
	10	3	1365.00-1366.72	1.72	1	46	3.0	45.0	4.0/Ka 2.0/Le	10.3/L 1.65/S	
	10	4	1366.72-1368.05	1.33	1	86	---	14.0	---	8.23/L	4.35-6.74/L 4.35-6.17/S mixed ore equivalent: 4.35-9.2/L

32

Table 3 - <u>Calculated mineral content of selected samples</u>
<u>from potassium-bearing intervals with summation</u>
<u>of percent K$_2$O as ore mineral</u>--continued

Drill-hole no.	Ore zone	Sample no.	Depths of intervals (feet)	Thickness (feet)	Calculated minerals present (weight percent)					K$_2$O as ore minerals (percent)	Weighted average K$_2$O as ore mineral for all intervals in ore zone (feet and percent)
					Polyhalite	Halite	Sylvite	Langbeinite	Other minerals		
P-9	10	8	1522.56-1523.41	0.85	1	42	7.0	48.0	0.67/Ka	4.73/S 10.8/L	
	10	9	1523.41-1524.07	0.66	1	93	2.0	---	3.0/Ki	0.96/S	
	10	10	1524.07-1524.70	0.63	2	17	7.0	63.37	---	4.42/S 14.37/L	
	10	11	1524.70-1526.04	1.34	3	95	---	1.10	---	0.24/L	
	10	12	1526.04-1526.74	0.70	2	65	---	31.31	---	7.1/L	4.18-5.63/L 2.14-3.48/S mixed ore equivalent: 4.18-6.34/L
	4	17	1703.65-1705.23	1.58	2	70	---	28.70	---	6.51/L	
	4	18	1705.23-1705.65	0.42	1	89	---	6.80	3.0/Ka	1.55/L	2.00-5.47/L
P-10	11	1	1650.38-1651.22	0.84	6	89	1.8	---	1.0/Ka	1.13/S	
	11	2	1651.22-1652.03	0.81	7	81	6.1	---	2.0/Ki	3.83/S	
	11	3	1652.03-1653.83	1.80	5	85	7.7	---	1.0/Ki	4.85/S	3.45-3.70/S
	11	4	1653.83-1654.58	0.75	6	94	---	---	---	---	
P-11	11	2	1601.90-1603.56	1.66	---	56	5.0	---	3.60/Ki 1.0/C	3.34/S	
	11	3	1603.56-1604.64	1.08	3	61	2.0	---	31.0/Ka 3.0/C	1.48/S	
	11	4	1604.64-1605.38	0.74	4	84	3.0	---	7.0/Ka 2.0/C	2.20/S	3.48-2.52/S
	10	7	1670.70-1671.84	1.14	1	71	19.0	8.0	1.0/Ki	12.0/S 1.82/L	
	10	8	1671.84-1673.42	1.58	2	66	10.0	18.0	1.0/Ki	6.32/S 3.98/L	
	10	9	1673.42-1674.70	1.28	3	71	16.7	---	1.0/Ki	10.53/S	4.00-9.29/S 2.72-3.07/L mixed ore equivalent: 4.00-14.51/S
	9	14	1688.72-1689.60	0.88	3	76	22.0	---	---	13.74/S	
	9	15	1689.60-1690.89	1.29	1	84	36.9	---	---	23.30/S	
	9	16	1690.89-1691.95	1.06	1	71	21.3	---	2.0/C	13.43/S	
	9	17	1691.95-1693.28	1.33	2	92	2.0	---	1.0/C	1.24/S	4.56-12.73/S
	4	19	1840.60-1842.35	1.75	1	58	---	40.0	5.0/Ki	9.14/L	
	4	20	1842.35-1843.40	1.05	4	76	5.0	4.9	---	1.11/L 2.98/S	2.80-6.0/L
	2	22	1868.67-1870.28	1.61	1	38	2.0	60.0	2.0/Ki	13.65/L	
	2	23	1870.28-1871.10	0.82	---	54	5.0	45.0	1.0/Ki	13.53/L	
	2	24	1871.10-1872.30	1.20	---	27	---	58.3	8.0/Ka Tr/Bl&Lo[1]	13.24/L	3.63-13.49/L

Table 3 - Calculated mineral content of selected samples
from potassium-bearing intervals with summation
of percent K₂O as ore mineral--continued

| Drill-hole no.	Ore zone	Sample no.	Depths of interval (feet)	Thickness (feet)	Calculated minerals present (weight percent)					K₂O as ore minerals (percent)	Weighted average K₂O as ore mineral for all intervals in ore zone (feet and percent)
					Polyhalite	Halite	Sylvite	Langbeinite	Other minerals		
P-12	10	2a	1344.97-1345.27	0.3	4	36	62.3[2]	---	1.0/Ki	39.38/S	
	10	2b	1345.27-1345.90	0.63	---	10	24.0[2]	---	59.0/Ki	15.08/S	
	10	3	1345.90-1346.95	1.05	1	59	18.0	---	18.0/Ki	11.39/S	
	10	4	1346.95-1348.90	1.95	3	64	18.0	---	19.0/Ki	11.36/S	
	10	5	1348.90-1349.91	1.01	7	44	20.0	---	8.6/Ki 8.7/Ka	12.63/S	
	10	6	1349.91-1350.80	0.89	3	67	16.0[3]	---	2.0/Ka	10.42/S	5.83-13.29/S
	8	14	1390.19-1390.97	0.78	4	80	15.5	---	---	9.77/S	
	8	15	1390.97-1392.66	1.69	7	88	7.0	---	---	4.12/S	
	8	16	1392.66-1394.29	1.63	4	88	10.3	---	---	6.47/S	
	8	17	1394.29-1394.90	0.61	8	51	35.5	---	---	22.42/S	4.71-8.24/S
	4	21	1520.00-1521.55	1.55	1	22	23.0	45.0	9.0/Ki	14.47/S 10.13/L	2.39-7.08/L
	4	22	1521.55-1522.39	0.84	10	48	7.0	6.0	16.0/Ka 10.0/Le	1.44/L 4.42/S	2.39-10.94/S mixed ore equivalent: 4.00-8.23/L
	3	26	1533.50-1535.05	1.55	---	40	11.0	49.0	---	7.0/S 8.59/L	
	3	27	1535.05-1535.59	0.54	34	86	1.0	8.0	1.0/Ki	1.80/L 0.62/S	3.51-5.98/L
	3	28	1535.59-1537.01	1.42	2	47	10.0	21.0	---	4.72/L 6.32/S	3.51-5.74/S mixed ore equivalent: 3.51-8.27/L
	2	34	1549.79-1550.65	0.86	3	85	---[4]	11.0	2.42/L	0.54/L	
	2	35a	1550.65-1551.29	0.64	---	20	5.0	70.0	1.0/Ka Tr/Le[1]	15.93/L	
	2	35b	1551.29-1551.61	0.32	---	21	5.0	30.0	18.0/Ka 19.0/Le 17.0/Bl	12.48/L	1.82-8.05/L
P-13	10	29	1318.02-1319.00	0.98	1	46	49.5	---	---	31.32/S	
	10	30	1319.00-1320.22	1.22	1	62	17.0	2.0	15.0/Ki	10.92/S	
	10	31	1320.22-1320.88	0.66	3	97	---	---	---	---	
	10	32	1320.88-1321.87	0.99	1	30	20.0	10.0	30.0/Ki 10.0/Ka	12.6/S 2.27/L	3.85-14.67/S
	9	36	1334.82-1336.38	1.56	2	94	2.0	---	---	1.12/S	
	9	37	1336.38-1337.32	0.94	2	62	34.8	---	---	21.99/S	
	9	38	1337.32-1338.64	1.32	---	90	3.8	---	---	2.41/S	3.82-6.7/S
	8	21	1359.65-1360.63	0.98	2	67	30.2	---	---	19.13/S	
	8	22	1360.63-1361.70	1.07	8	80	9.14	---	---	4.97/S	2.05-11.74/S
	4	2	1480.20-1481.73	1.53	2	82	2.0	9.0	3.0/Ki	2.03/L	
	4	3	1481.73-1482.78	1.05	1	63	---	33.2	0.4/Le	7.53/L	3.53-4.06/L
	4	4	1482.78-1483.73	0.95	1	64	---	7.0	7.0/Bl	1.59/L	

Table 3 - Calculated mineral content of selected samples
from potassium-bearing intervals with summation
of percent K_2O as ore mineral--continued

Drill-hole no.	Ore zone	Sample no.	Depths of interval (feet)	Thickness (feet)	Calculated minerals present (weight percent)					K_2O as ore minerals (percent)	Weighted average K_2O as ore mineral for all intervals in ore zone (feet and percent)
					Polyhalite	Halite	Sylvite	Langbeinite	Other minerals		
	3	8	1493.23-1493.88	0.65	2	86	---	7.0	---	1.59/L	
	3	9	1493.88-1494.58	0.70	---	15	---	53.0	---	12.06/L	
	3	10	1494.58-1495.50	0.92	3	86	---	10.0	---	2.21/L	2.27-5.07/L[5] 4.00-2.88/L[5]
P-14	10	2	1255.24-1255.64	0.40	---	41	57.0	---	---	36.03/S	
	10	3	1255.64-1257.56	1.92	---	41	57.0	---	---	36.06/S 8.84/S	
	10	4	1257.56-1259.07	1.51	3	64	14.0	18.0	Tr/Ka[1]	3.99/L	
	10	5	1259.07-1260.15	1.08	4	74	7.0	22.0	---	4.36/S 4.88/L	
	10	6	1260.15-1261.05	0.90	2	55	12.0[6]	---	16.0/Ka	6.21/S	5.81-18.47/S 2.59-4.36/L mixed ore equivalent: 5.81-23.33/S
	5	10	1364.44-1366.11	1.67	5	74	5.0	15.0	1.0/Ka	3.35/L 3.00/S	
	5	11[6]	1366.11-1367.86	1.75	3	83	---	19.0	Tr/Ka[1]	4.3/L	
	5	12[6]	1367.86-1369.26	1.40	1	80	---	13.0	Tr/Ka[1]	3.03/L	4.82-3.60/L 1.67-3.0/S mixed ore equivalent: 4.82-4.02/L
	4	18	1440.79-1441.98	1.19	4	46	6.0	38.5	---	8.74/L 3.99/S	
	4	19	1441.98-1442.84	0.86	5	95	---	---	---	---	
	4	20	1442.84-1443.98	1.14	16	56	4.0	23.0	Tr/Le 2.0/Ka	5.22/L 2.53/S	
	4	21	1443.98-1444.61	0.63	3	88	---	11.0	---	2.50/L	3.82-4.69/L 3.19-2.39/S
P-15	4	7	1371.94-1372.81	0.87	6	76	---	25.0	---	5.59/L	
	4	8	1372.81-1374.77	1.96	8	89	---	4.0	---	1.00/L	
	4	9	1374.77-1375.80	1.03	9	64	---	28.0	---	6.30/L	3.86-3.45/L
	2	13	1399.66-1400.38	0.72	3	64	---	32.0	4.0/Ka	7.18/L	
	2	14	1400.38-1401.51	1.13	---	78	---	17.0	3.0/Ka 3.0/Le	4.28/L	1.85-5.41/L
P-16	10	4	1301.94-1302.57	0.63	3	93	0.7	4.0	---	0.47/S 0.89/L	
	10	5	1302.57-1303.91	1.34	3	79	---	21.0	---	4.77/L	
	10	6	1303.91-1304.39	0.48	---	61	---	34.0	8.1/Ka 8.0/Le Tr/Ki[1]	7.77/L	2.45-4.63/L
	4	10	1476.76-1478.40	1.64	---	36	2.0	53.0	Tr/Ka&Le[1]	12.01/L 1.26/S	
	4	11	1478.40-1478.95	0.55	2	86	---	8.7	---	1.98/L	2.19-9.49/L
	4	12	1490.12-1491.00	0.88	1	83	1.0	14.1[7]	---	4.94/L	
	4	13	1491.00-1491.56	0.56	0	39	7.0	19.7[7]	---	4.40/L 4.12/S	
	4	14	1491.56-1492.64	1.08	7	79	---	12.0	---	2.75/L	
	4	15	1492.64-1493.89	1.25	2	56	3.0	31.0	6.0/Le 2.0/Ka	7.05/L 2.09/S	3.77-4.93/L

Table 3 - Calculated mineral content of selected samples
from potassium-bearing intervals with summation
of percent K₂0 as ore mineral--continued

Drill-hole no.	Ore zone	Sample no.	Depths of interval (feet)	Thickness (feet)	Calculated minerals present (weight percent)					K_2O as ore minerals (percent)	Weighted average K_2O as ore mineral for all intervals in ore zone (feet and percent)
					Polyhalite	Halite	Sylvite	Langbeinite	Other minerals		
P-16	2	19	1526.90-1528.00	1.10	1	51	1.0	42.0	2.0/Ka	?.05/L	1.10-9.60/L
P-17	10	2	1365.60-1367.20	1.6	1	27	---	68.8	---	15.61/L	
	10	3	1367.20-1368.45	1 25	3	76	---	12.6	2.0/Ka	2.87/L	
	10	4	1368.45-1369.70	1.25	3	44	---	6.64	30.0/Le 9 0/Ka	1.51/L	4.10-7.43/L
	4	8	1542.90-1543.68	0.78	---	48	---	38.0	13.0/Le Tr/Ka[1]	8.62/L	
	4	9	1543.68-1544.46	0.78	---	43	---	53.0	3.0/Le	12.03/L	1.56-10.33/L
	2	18	1591.39-1592.71	1.32	1	44	---	46.0	1.0/Ka	10.46/L	
	2	19	1592.71-1594.21	1.50	4	83	---	2.4	2.0/Ka	0.53/L	2.82-5.18/L
P-18	10	3	1728.40-1728.78	0.38	1	41	33.0	35.0	---	22.83/S 7.94/L	
	10	4	1728.78-1730.45	1.67	3	86	9.0	---	---	5.61/S	
	10	5	1730.45-1731.49	1.04	6	80	0.72	---	---	0.45/S	
	10	6	1731.49-1732.29	0.80	4	74	0.81	---	---	0.51/S	3.89-4.86/S 0.38-7.94/L mixed ore equivalent: 3.89-6.8/S
P-19	10	7	1741.80-1742.35	0.55	1	55	6.70	36.0	---	4.23/S 8.24/L	
	10	8	1742.35-1743.72	1.37	1	26	2.0	59.0	---	1.20/S 13.39/L	
	10	9	1743.72-1745.09	1.37	4	81	1.0	15.0	---	0.62/S 3.40/L	
	10	10	1745.09-1746.00	0.91	2	53	---	30.0	8.4/Le 2.0/Ka	9.21/L	4.20-8.03/L
	4	21	1925.20-1925.90	0.70	1	74	---	11.0	12.0/Ki	2.50/L	
	4	22	1925.90-1926.70	0.80	1	27	---	57.0	2.0/Ka 9.0/Ki	12.93/L	
	4	23	1926.70-1927.94	1.24	2	62	---	3.6	5.0/Ka Tr/Le[1]	0.82/L	2.74-4.79/L
	2	26	1956.40-1957.36	0.96	6	64	1.0	16.0	15.0/Ki	3.74/L	
	2	27	1957.36-1958.71	1.35	1	29	---	65.0	Tr/Ka[1]	14.83/L	
	2	28	1958.71-1959.21	0.50	0.5	61	---	25.0	Tr/Ka[1]	5.72/L	2.81-9.42/L
P-20	10	2	1725.00-1726.15	1.15	2	72	21.2	Tr/L[4]	---	13.43/S	
	10	3	1726.15-1728.10	1.95	4	64	7.0	35.0	---	4.42/S 8.01/L	
	10	4	1728.10-1729.62	1.52	3	60	28.0[6]	---	6.0/Ka	17.69/S	1.95-8.01/L
	10	5	1729.62-1731.48	1.86	3	60	34.0	---	---	21.48/S	6.51-14.03/S mixed ore equivalent: 6.51-20.03/S
	4	10	1898.80-1900.45	1.65	5	53	1.0	37 0	5.0/Ka	8.35/L	
	4	11	1900.45-1901.77	1.32	16	85	---	1.3	---	0.30/L	
	4	12	1901.77-1903.35	1.58	10	74	---	17.7	---	4.0/L	4.55-4.5/L

Drill-hole no.	Ore zone	Sample no.	Depths of interval (feet)	Thickness (feet)	Calculated minerals present (weight percent)					K_2O as ore minerals (percent)	Weighted average K_2O as ore mineral for all intervals in ore zone (feet and percent)
					Polyhalite	Halite	Sylvite	Langbeinite	Other minerals		
P-20	2	14[4]	1925.08-1926.30	1.22	3	95	---	0.88	---	0.2/L	
	2	15	1926.30-1927.75	1.45	1	61	---	35.5	---	8.05/L	2.67-4.46/L
P-21	10	2	1644.03-1644.84	0.81	4	80	17.0	---	---	10.82/S	
	10	3	1644.84-1646.00	1.16	4	81	11.8[6]	---	2.0/Ki	7.46/S	
	10	4	1646.00-1646.33	0.33	1	28	20.2[6]	---	42.0/Ki	12.76/S	
	10	5	1646.33-1647.20	0.87	1	41	25.5[6]	---	18.0/Ki	16.14/S	
	10	6	1647.20-1648.22	1.02	.1	62	29.5[2]	---	1.0/Ki	18.66/S	
	10	7	1648.22-1649.23	1.01	3	64	31.3	---	---	19.81/S	5.20-14.37/S
	8	15	1685.17-1686.48	1.31	0	55	45.0[6]	---	---	28.4/S	
	8	16	1686.48-1687.20	0.72	4	83	6.0[6]	---	---	3.72/S	
	8	17	1687.20-1688.24	1.04	5	92	3.0	---	---	1.95/S	
	8	18	1688.24-1688.77	0.53	4	95	0.8	---	---	0.52/S	
	8	19	1688.77-1690.19	1.42	6	86	9.9	---	---	6.24/S	
	8	20	1690.19-1691.26	1.07	8	90	1.0	---	---	0.75/S	
	8	21	1691.26-1692.40	1.14	3	65	33.0	---	---	21.16/S	
	8	22	1692.40-1693.34	0.94	5	65	13.0	---	---	8.18/S	8.17-10.24/S
	4	24	1809.90-1811.50	1.60	0	31	3.0	64.0	2.5/Ka 3.9/Le	14.60/L	1.92-14.69/L
	4	25	1811.50-1811.82	0.32	0	18	5.0[2]	54.66	9.0/Ka 10.60/Le	15.12/L	4.00-7.05/L[5]
	4	30	1815.51-1816.10	0.59	11	51	5	27.0	9.0/Ki	6.08/L	
	4	31	1816.10-1817.25	1.15	3	42	5	44.0	8.0/Ka	9.95/L	1.74-8.64/L[5] 4.00-3/76/L[5]
AEC-8	10	10	1589.10-1589.70	0.60	1	85	5	---	5/Ki 2/An	2.97/S	
	10	11[6]	1589.70-1591.70	2.00	---	43	16	---	40/Ki	10.32/S	
	10	12[6]	1591.70-1592.20	0.50	---	37	24	---	6/C 30/Ki	15.16/S	
	10	13[6]	1592.20-1594.50	2.30	---	49	32	---	0.1/An 7/C 9/Ka 0.8/An	20.31/S	
	10	14	1594.50-1594.70	0.20	---	38	4	---	51/C 9/Ka 1/Ki 0.1/An	2.34/S	
	10	15[6]	1594.70-1595.50	0.80	2	85	3	---	4/C 2/Ki 9/Ka 0.9/An	2.18/S	6.4-12.33/S
	4	2	1752.70-1753.40	0.70	---	95	---	4	---	0.86/L	
	4	3	1753.40-1754.00	0.60	1	69	2	33	3/Ka	7.39/L	
	4	4	1754.00-1755.00	1.00	---	33	2	68	2/Ka	13.90/L	
	4	5	1755.00-1756.70	1.70	---	24	---	69	3/Le	15.38/L	4-11.27/L

Table 3 - Calculated mineral content of selected samples
from potassium-bearing intervals with summation
of percent K₂0 as ore mineral--continued

Drill-hole no.	Ore zone	Sample no.	Depths of interval (feet)	Thickness (feet)	Calculated minerals present (weight percent)					K₂0 as ore minerals (percent)	Weighted average K₂0 as ore mineral for all intervals in ore zone (feet and percent)
					Polyhalite	Halite	Sylvite	Langbeinite	Other minerals		
FC-70	10	2	1377.67-1379.00	1.33	2	65	11.2	---	20.0/Ki	7.11/S	
	10	3	1379.00-1381.00	2.00	2	51	39.1[6]	---	1.0/Ki	24.72/S	
	10	4	1381.00-1382.00	1.00	2	64	19.4[6]	---	3.0/C 3.0/Ki	12.29/S	4.33-16.44/S
	9	6	1391.50-1393.00	1.50	1	53	28.00	---	---	17.74	1.5-17.74/S
	8	7	1415.08-1415.75	0.67	2	70	25	---	Tr/Ki[1]	16.10/S	
	8	8	1415.75-1416.50	0.75	5	89	2	---	Tr/Ki[1]	1.35/S	
	8	9	1416.50-1418.00	1.50	2	97	1	---	1.0/Ka Tr/Ki[1]	0.57/S	
	8	10	1418.00-1419.50	1.50	3	91	3	---	---	1.62/S	
	8	11	1419.50-1420.42	0.92	2	80	16	---	1.0/Ka Tr/Ki[1]	10.04/S	
	8	12	1420.42-1421.50	1.08	1	71	16	---	1.0/Ka	20.21/S	6.42-5.5/S
	5	16	1466.00-1467.58	1.58	---	72	---	19.6	---	4.43/L	
	5	17	1467.58-1469.00	1.42	1	53	---	40.7	---	9.22/L	
	5	18	1469.00-1469.67	0.67	1	70	---	24.2	---	5.49/L	3.67-6.48/L
	4	19	1529.92-1531.42	1.50	1	36	---	52.6[6]	---	11.93/L	
	4	20	1531.42-1532.42	1.00	---	45	---	33.0[6]	---	7.42/L	2.5-10.13/L
FC-81	8	7	1564.17-1564.92[8]	0.75	2	58	36.6	---	2.0/C	23.16/S	
	8	8	1564.92-1566.13	1.21	2	79	15.3	---	4.0/C	9.71/S	
	8	9	1566.13-1567.38	1.25	5	66	8.9	6.1	10.0/C	5.62/S 1.38/L	3.21-11.26/S 3.21-0.54/L mixed ore equivalent: 3.21-12.61/S
	4	10	1687.00-1688.21	1.21	---	20	---	74.0	4.0/Ka Tr/Va[1]	16.71/L	
	4	11	1688.21-1689.46	1.25	1	25	---	67.0	Tr/Va[1]	15.31/L	2.46-16.0/L
	2	15	1712.88-1714.46	1.58	1	40	---	56.0	2.2/Le	12.7/L	
	2	16	1714.46-1715.46	1.00	---	65	---	30.3	3.0/Ka Tr/Le[1]	6.9/L	
	2	17	1715.46-1716.00	0.54	4	45	---	42.8	Tr/Le[1]	9.71/L	3.12-10.4/L
FC-82	5	1	1541.42-1541.79	0.37	---	17	---	72.2	2.0/Le 6.0/C	16.34/L	
	5	2	1541.79-1542.29	0.50	---	85	7.0	7.2	---	1.63/L	
	5	3	1542.29-1543.96	1.67	2	5	---	49.8	4.0/Lo 20.9/C	11.3/L	
	5	4	1543.96-1544.50	0.54	1	59	5.0	20.0	Tr/Le[1]	4.54/L	3.08-9.37/L
	4	5	1613.42-1615.08	1.66	---	17	---	63.0	9.3/Ki Tr/Lo[1]	14.3/L	
	4	6	1615.08-1615.92	0.84	1	48	0.7	12.8	17.7/Le 12.0/Ki	2.9/L	2.5-10.52/L

Table 3 - <u>Calculated mineral content of selected samples</u>
<u>from potassium-bearing intervals with summation</u>
<u>of percent K$_2$0 as ore mineral</u>--continued

Drill-hole no.	Ore zone	Sample no.	Depths of interval (feet)	Thickness (feet)	Calculated minerals present (weight percent)					K$_2$0 as ore minerals (percent)	Weighted average K$_2$0 as ore mineral for all intervals in ore zone (feet and percent)
					Polyhalite	Halite	Sylvite	Langbeinite	Other minerals		
FC-82	3	7	1624.33-1625.58	1.25	2	57	---	31.1	3.5/Bl 3.7/Ka	7.06/L	
	3	8	1625.58-1627.00	1.42	2	67	---	29.9	0.6/C	6.78/L	
	3	9	1627.00-1627.75	0.75	1	28	---	62.2	Tr/Bl 5.0/G1	14.11/L	3.42-8.49/L
FC-91	4	34	1712.25-1712.66	0.42	1	18	---	50.0	11.0/Ka 7.5/Le 6.0/Ki	11.35/L	
	4	35	1712.66-1713.08	0.42	---	62	---	---	5.0/Ki 3.4/Ki	---	
	4	36	1713.08-1714.17	1.08	1	25	---	64.6	5.0/Ki	14.66/L	
	4	37	1714.17-1714.75	0.58	2	32	---	58.7	5.0/Ka 1.3/Ki	13.32	
	4	38	1715.75-1715.75	1.00	20	38	---	47.0	5.0/Ka Tr/Gu	10.66	
	4	39	1715.75-1716.33	0.58	6	31	---	54.0	6.2/Ka 4.0/G1 1.2/Ki	12.25/L	4.08-11.3/L
	4	40	1718.66-1719.42	0.75	3	81	---	8.0	3.0/Ka 9.0/Bs	1.82/L	
	4	41	1719.42-1720.75	1.33	2	37	---	59.5	---	13.5/L	
	4	42	1720.75-1722.00	1.25	---	60	---	37.08	Tr/Gu 3.4/Bs	8.41/L	
	4	43	1722.00-1722.58	0.58	---	71	---	13.5	0.4/Ka 6.0/Bs Tr/Gu	3.06/L	3.91-8.08/L
	2	44	1742.75-1743.25	0.50	---	15	---	62.0	8.8/Ka Tr/Va	14.07/L	
	2	45	1743.25-1744.25	1.00	---	47	---	30.5	10.0/Ki 10.0/Va	6.92/L	
	2	46	1744.25-1745.00	0.75	---	61	---	1.0	3.2/Ka 10.1/Ki 24.0/Va Tr/Gu	0.73/L	2.25-6.44/L
FC-92[9]	8	5	1604.92-1606.04	1.12	1	51	47	Tr[1]	Tr/C[1]	29.0/S	
	8	6	1606.04-1606.50	0.46	---	50	49	Tr[1]	Tr/C[1]	31.0/S	
	8	7	1606.50-1606.75	0.25	---	60	29	1	5.7/C	18.5/S	1.83-28/S
	4	57	1740.66-1741.58	0.92	1	51	---	46.7	---	10.6/L	
	4	58	1741.58-1742.25	0.66	1	36	---	61.0	---	13.85/L	
	4	59	1742.25-1743.25	1.00	1	36	---	61.2	0.1/Ki	13.89/L	
	4	60	1743.25-1744.08	0.83	1	34	---	61.3	---	13.91/L	
	4	61	1744.08-1745.00	0.92	2	38	---	48.8	1.8/Ki	11.07/L	4.33-12.6/L
	2	62	1769.42-1770.08	0.66	1	42	---	55.4	3.0/Va	12.57/L	
	2	63	1770.08-1771.42	1.33	1	51	---	45.7	2.0/Va 1.0/Arc	10.37/L	
	2	64	1777.42-1772.08	0.66	---	39	---	33.0	17.0/Va 8.0/Ki 1.0/Gu	7.49/L	
	2	65	1772.08-1772.38	0.5	---	73	---	1.5	14.0/Va 1.0/Gu	0.34/L	3.16-8.64/L

39

Table 3 - Calculated mineral content of selected samples
from potassium-bearing intervals with summation
of percent K₂O as ore mineral--continued

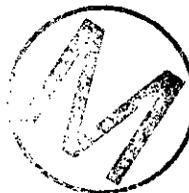| Drill-hole no.	Ore zone	Sample no.	Depths of interval (feet)	Thickness (feet)	Calculated minerals present (weight percent)					K_2O as ore minerals (percent)	Weighted average K_2O as ore mineral for all intervals in ore zone (feet and percent)
					Polyhalite	Halite	Sylvite	Langbeinite	Other minerals		
IMC-374	4	8	1430.70-1432.10	1.40	6	86	0.7	2.0	0.7/Ki 0.3/Ka	0.46/L 0.44/S	
	4	9	1432.10-1433.10	1.00	13	68	1.0	6.4	1.35/Le	1.46/L 0.63/S	2.4-0.88/L 2.4-0.51/S
IMC-375	4	7	1627.90-1629.00	1.10	2	78	---	6.6	2.0/Ka	1.50/L	
	4	8	1629.00-1630.50	1.50	4	70	2.0	13.2	2.0/Le 1.0/Ka	3.0/L 1.3/S	2.5-2.46/L 1.5-1.3/S
IMC-376	10	2	1427.00-1427.70	0.7	---	60	38.4	---	---	24.3/S	
	10	3	1427.70-1428.30	0.6	---	98	0.2	---	---	0.1/S	
	10	4	1428.30-1429.20	0.9	1	96	0.4	---	---	0.26/S	
	10	5	1429.20-1431.00	1.8	2	86	11.2	---	---	7.1/S	4.0-7.52/S
	5	13	1528.00-1528.90	0.9	2	89	1.0	2.8	---	0.63/L	
	5	14	1528.90-1530.90	2.0	0	45	---	51.3	1.0/Le	11.65/L	
	5	15	1530.90-1531.70	0.8	2	93	1.0	1.05	---	0.25/L	3.7-6.5/L (4.0-6.03/L)[5]
NFU-1[10]	8		1536.25-1540.17	3.92	---	---	---	---	---	19.67/S	3.92-19.67/S
	4		1646.75-1649.08	2.33	---	---	---	---	---	11.96/L	2.33-11.96/L
NFU[10]	10		1441.08-1445.17	4.08	---	---	---	---	---	0.8/S	4.08-0.8/S
	8		1479.80-1483.80	4.00	---	---	---	---	---	9.1/S	4.0-9.1/S
	4		1598.50-1602.70	4.20	---	---	---	---	---	13.1/L	4.2-13.1/L
D-120[10]	10		1248.30-1249.80	1.50	---	---	---	---	---	31.63/S	
	10		1249.80-1251.10	1.30	---	---	---	---	---	10.4/S	
	10		1251.10-1252.50	1.40	---	---	---	---	---	7.34/S	4.2-15.3/S
	4		1419.60-1421.30	1.70	---	---	---	---	---	13.8/S	2.2-10.7/S
	4		1421.30-1421.80	0.50	---	---	---	---	---	0.5/S	2.2-7.5/L mixed ore equivalent: 2.2-29.45/S
D-48[10]	10		1236.60-1240.60	4.00	---	---	---	---	---	---	4.0-11/S 4.0-2.1/L (visual estimate)
	8		1280.52-1289.78	9.26	---	---	---	---	---	---	9.26-17.37/S
	4		1414.20-1416.20	2.00	---	---	---	---	---	---	2.0-8.8/L (visual estimate)

Table 3 - Calculated mineral content of selected samples
from potassium-bearing intervals with summation
of percent K₂O as ore mineral--continued

Drill-hole no.	Ore zone	Sample no.	Depths of interval (feet)	Thickness (feet)	Calculated minerals present (weight percent)					K₂O as ore minerals (percent)	Weighted average K₂O as ore mineral for all intervals in ore zone (feet and percent)
					Polyhalite	Halite	Sylvite	Langbeinite	Other minerals		
D-207	10	24	1358.60-1359.60	1.00	4	87	5	---	2/Ka	3.34/S	
	10	25	1359.60-1360.20	0.60	4	89	5	1	2/Ka	3.34/S 0.25/L	
	10	26	1360.20-1360.60	0.40	1	75	4	1	6/Ka	0.31/L	
	10	27[4]	1360.60-1361.20	0.60	1	47	6	16	5/Ka	3.79/S 3.70/L	
	10	28	1361.20-1361.80	0.60	2	69	2	9	2/Ka	2.04/L	
	10	29	1361.80-1362.30	0.50	7	62	5	10	7/Ka	3.34/S 2.31/L	
	10	30	1362.30-1363.10	0.80	6	83	4	---	1/C 3/Ka	2.66/S	4.5-2.54/S 2.7-1.8/L mixed ore equivalent: 4.5-5.24/S
	4	33	1533.10-1533.50	0.40	2	53	36	7	---	1.51/L 22.74/S	
	4	34	1533.50-1533.80	0.30	4	86	2	11	---	2.43/L	
	4	35	1533.80-1534.40	0.60	2	85	1	2	---	0.50/L	
	4	36	1534.40-1534.70	0.30	3	95	---	4	---	0.85/L	
	4	37	1534.70-1535.00	0.30	2	74	4	1	3.0/Ki	0.14/L	
	4	38	1535.00-1539.80	4.80	6	87	2	4	---	0.85/L	6.7-0.90/L 0.4-22.74/S mixed ore equivalent: 6.7-1.44/L
	3	44	1545.90-1546.30	0.40	1	66	---	32.0	0.74/Le	7.2/L	
	3	45	1546.30-1546.66	0.30	1	11	---	73.2	9.0/Ki	16.6/L	
	3	46	1546.66-1548.00	1.40	2	62	---	30.3	3.8/Le	6.89/L	
	3	47	1548.00-1548.60	0.60	1	43	---	54.7	---	12.4/L	2.7-9.24/L
	2	52	1552.20-1553.00	0.80	11	83	---	5.0	---	1.05/L	
	2	53	1553.00-1553.20	0.20	11	45	---	41.5	2.0/Le	9.41/L	
	2	54	1553.20-1553.60	0.40	4	81	---	15.8	---	3.59/L	
	2	55	1553.60-1554.00	0.40	1	47	---	49.4	1.32/Le	11.19/L	
	2	56	1554.00-1554.80	0.80	18	86	1.4	8.8	---	2.0/L 0.9/S	2.6-3,94/L Tr/S[4]
D-104[10]	10		1340.40-1341.70	1.30	---	---	---	---	---	---	
	10		1341.70-1343.20	1.50	---	---	---	---	---	---	
	10		1343.20-1344.00	0.80	---	---	---	---	---	---	
	10		1344.00-1344.70	0.70	---	---	---	---	---	---	
	10		1344.70-1346.40	1.70	---	---	---	---	---	---	6.0-5.5/S 3.2-4.71/L mixed ore equivalent: 6.0-11.78/S
	8		1391.10-1392.00	0.90	---	---	---	---	---	---	
	8		1392.00-1395.30	3.30	---	---	---	---	---	---	
	8		1395.30-1396.30	1.00	---	---	---	---	---	---	5.2-10.8/S
	4		1519.90-1522.80	2.90	---	---	---	---	---	---	2.9-9.4/L

41

Drill-hole no.	Ore zone	Sample no.	Depths of interval (feet)	Thickness (feet)	Calculated minerals present (weight percent)					K₂O as ore minerals (percent)	Weighted average K₂O as ore mineral for all intervals in ore zone (feet and percent)
					Polyhalite	Halite	Sylvite	Langbeinite	Other minerals		
D-104[10]	3		1527.50-1528.90	1.40	---	---	---	---	---	---	1.4-5.0/L
	3		1528.90-1530.50	1.60	. .	---	---	---	---	---	2.9-11.4/S mixed ore equivalent: 2.9-6.66/L
	2		1539.50-1540.20	1.20	---	---	---	---	---	---	1.2-15.0/L
U-134[10]	10		1319.58-1321.25	1.69	3	---	6.0	---	2.0/Ka 0.7/C	3.79/S	
			1321.25-1322.83	1.58	2	---	---	---	12.5/Ka	17.22/S	3.27-10.28/S
	8		1361.10-1362.17	1.08	---	---	---	---	---	---	
	8		1362.17-1364.50	2.33	---	---	---	---	---	---	
	8		1364.50-1366.50	2.00	---	---	---	---	---	---	6.33-7.89/S
	8		1366.50-1367.42	0.92	---	---	---	---	---	---	(4.0-12.5/S)[5]
	5		1406.75-1409.42	2.66	---	---	---	---	---	14.44/L	
	5		1409.42-1410.00	0.58	---	---	---	---	---	8.03/L	
	5		1410.00-1411.66	1.66	---	---	---	---	---	7.05/L	4.9-11.2/L
	4		1471.66-1474.00	2.33	---	---	---	---	---	8.54/L	2.33-8.54/L
	3		1484.91-1487.33	2.42	---	---	---	---	---	3.6/L	
	3		1487.33-1490.25	2.92	---	---	---	---	---	1.86/L	
	3		1490.25-1491.33	1.08	---	---	---	---	---	8.7/L	6.42-3.7/L[3]

*Values in table for percent mineral and K₂O equivalent are not consistent owing to independent rounding of assays and conversion factors by numerous authors and investigators.

[1] Trace amount; equals 0 to 2.0 percent
[2] Incomplete dissolution of sample
[3] 5.9 percent insolubles, by weight
[4] Incomplete or unreliable assay
[5] Grade adjusted to 4-foot interval
[6] High insoluble content
[7] 7.1 percent potassium assay used
[8] Outside of the ERDA area by 300 feet, included due to influence
[9] Raw data unavailable; these are company figures
[10] Company interval data; raw data unavailable; no sample numbers assigned

42